

JETC 2013

**PROCEEDINGS OF THE
12TH JOINT EUROPEAN
THERMODYNAMICS
CONFERENCE**



BRESCIA, ITALY, JULY 1-5, 2013



UNIVERSITÀ DEGLI STUDI DI BRESCIA

JETC 2013

**PROCEEDINGS OF THE
12TH JOINT EUROPEAN
THERMODYNAMICS
CONFERENCE**

BRESCIA, ITALY, JULY 1-5, 2013

EDITORS:

M. PILOTELLI AND G.P. BERETTA



UNIVERSITÀ DEGLI STUDI DI BRESCIA

Publisher

Cartolibreria SNOOPY s.n.c. - via Bligny n.27
25133 Brescia - Tel. e Fax 0302006331
E-mail: cartolibreriasnoopy@numerica.it

Editors

Mariagrazia Pilotelli and Gian Paolo Beretta
Dipartimento di Ingegneria Meccanica e Industriale
Università degli Studi di Brescia
Via Branze 38, 25123 Brescia, Italy
E-mail: mariagrazia.pilotelli@ing.unibs.it
E-mail: beretta@ing.unibs.it

Proceedings of the 12th Joint European Thermodynamics Conference, JETC 2013

Printed in Brescia, Italy, June 2013

ISBN: 978-88-89252-22-2

E' vietata la riproduzione, anche parziale con qualsiasi mezzo effettuata, compresa la fotocopia, anche a uso didattico, se non autorizzata da parte dell'editore e dell'autore.

Permission is granted to quote from this book with the customary acknowledgement of the source:

A. Author(s), Title of Article, in Proceedings of the 12th Joint European Thermodynamics Conference, JETC 2013, Eds. M. Pilotelli and G.P. Beretta (ISBN 978-88-89252-22-2, Snoopy, Brescia, Italy, 2013), pp. xxx-xxx.

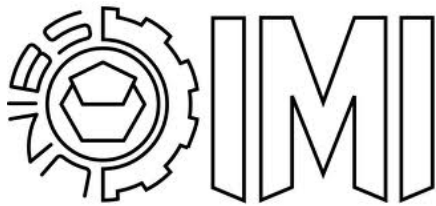
In copertina: Faustino Joli (1818-1876)

“Il Popolo Radunato in Piazza Vecchia (Piazza della Loggia) il 23 marzo 1849”

Brescia, Museo del Risorgimento

Su concessione del Servizio Collezioni d'Arte e Storia del Comune di Brescia

ORGANIZED BY:



Dipartimento di Ingegneria
Meccanica e Industriale



of the Università degli Studi
di Brescia

WITH THE PATRONAGE OF:



the Brescia Municipality

AND CONTRIBUTIONS FROM:



WWW.FONDAZIONECARIPLO.IT



a group company of  MITSUBISHI HEAVY INDUSTRIES, LTD.

WWW.TURBODEN.EU



WWW.MDPI.COM/JOURNAL/ENTROPY

SCIENTIFIC COMMITTEE

Sumiyoshi ABE	Mie U, Mie	Japan
Bjarne ANDRESEN	Niels Bohr Inst, Copenhagen	Denmark
Gian Paolo BERETTA (Chair)	U Brescia	Italy
Subhash CHATURVEDI	U Hyderabad	India
Vito Antonio CIMMELLI	U Basilicata	Italy
Daniel FAVRAT	EPFL Lausanne	Switzerland
Pierre GASPARD	UL Bruxelles	Belgium
Ahmed GHONIEM	MIT, Cambridge, MA	USA
Alexander GORBAN	U Leicester	UK
Karl-Heinz HOFFMANN	U Chemnitz	Germany
David JOU	AU Barcelona	Spain
Signe KJELSTRUP	NTNU, Trondheim	Norway
Ronnie KOSLOFF	The Hebrew U, Jerusalem	Israel
Michal KURZYNSKI	U Adam Mickiewicz, Poznan	Poland
Hameed METGHALCHI	Northeastern U, Boston, MA	USA
Robert NIVEN	U New South Wales at ADFA, Canberra	Australia
Marc ROSEN	U Ontario IT, Oshawa	Canada
Leonard SAGIS	U Wageningen	Netherlands
Altug SISMAN	TU Istanbul	Turkey
Doros THEODOROU	National TU, Athens	Greece
Daniel TONDEUR	CNRS, Nancy	France
Peter VÁN	Budapest U	Hungary
Michael VON SPAKOVSKY	Virginia Tech, Blacksburg, VA	USA
Qiang YANG	Tsinghua U, Beijing	China
Jakob YNGVASON	U Wien	Austria
Enzo ZANCHINI	U Bologna	Italy
Pasko ZUPANOVIC	U Split	Croatia

ORGANIZING COMMITTEE

Gian Paolo Beretta (Chair)

Mariagrazia Pilotelli (Secretary and co-editor of the conference proceedings)

Adriano M. Lezzi

Pietro Poesio

Stefano Farisè

Alessandro Garbellini

Andriy Gordiychuk

Marco Lorini

Davide Luscietti

Anna Marchesini

Gian Pietro Marena

Paola Milani

Manuela Neri

Domenico Petrocelli

Candida Petrogalli

Davide Picchi

Talieh Rajabloo

Matteo Rocco (PoliMI)

Fernando Sala

Roberto Sandrini



DIPARTIMENTO DI INGEGNERIA MECCANICA E INDUSTRIALE

UNIVERSITÀ DEGLI STUDI DI BRESCIA

TABLE OF CONTENTS

PANEL A:

ENTROPY PRODUCTION MINIMIZATION, CONSTRUCTAL LAW, AND OTHER OPTIMIZATION TECHNIQUES IN ENERGY AND OTHER TECHNOLOGIES

Andresen B., Essex C.

PRINCIPAL EQUATIONS OF STATE AND THEIR RELATION TO THE SECOND LAW AND TO THERMODYNAMIC GEOMETRY OPTIMIZATION 2

Bejan A.

CONSTRUCTAL LAW: DESIGN AS PHYSICS 4

Favrat D.

THERMODYNAMICS AND THE OPTIMIZATION OF ENERGY SYSTEMS: STRENGTHS AND LIMITS 10

Feidt M.

DOES MINIMUM ENTROPY GENERATION RATE CORRESPOND TO MAXIMUM POWER OR OTHER OBJECTIVES ? 16

Ghoniem A.F.

FROM MACROSCOPIC OBSERVATIONS TO MICRO-KINETIC MODELS OF SURFACE REACTIONS 21

Hoffmann K.H., Fischer A., Getzlaff J., Lambert T., Mehnert J.

APPLYING ENDOREVERSIBLE THERMODYNAMICS: THE OPTIVENT METHOD FOR SI-ENGINES 22

Wilhelmsen Ø., Johannessen E., Kjelstrup S.

ENERGY EFFICIENT REACTOR DESIGN SIMPLIFIED BY APPLICATION OF THE SECOND LAW OF THERMODYNAMICS 24

Kowalski G.J., Zenouzi M., Modaresifar M.

ENTROPY PRODUCTION: INTEGRATING RENEWABLE ENERGY SOURCES INTO SUSTAINABLE ENERGY SOLUTIONS 25

PANEL B:

NON-EQUILIBRIUM THERMODYNAMICS: THE VARIOUS APPROACHES AND THEIR REASONS

Bedeaux D., Kjelstrup S.

MESOSCOPIC NON-EQUILIBRIUM THERMODYNAMICS 34

Daivis P. J.

STUDYING NON-EQUILIBRIUM THERMODYNAMICS USING NON-EQUILIBRIUM MOLECULAR DYNAMICS SIMULATIONS 35

Evans D.J., Searles D.J., Williams S.R.

DISSIPATION AND THE FOUNDATIONS OF STATISTICAL THERMODYNAMICS 40

Grmela M.

MULTISCALE MESOSCOPIC DYNAMICS AND THERMODYNAMICS 41

Naudts J. THERMODYNAMICS FROM THE PERSPECTIVE OF INFORMATION GEOMETRY	42
Jou D., Restuccia L. NON-EQUILIBRIUM TEMPERATURES IN SYSTEMS WITH INTERNAL VARIABLES	43
Rubi J.M. MESOSCOPIC NON-EQUILIBRIUM THERMODYNAMICS FOR THE STOCHASTIC DYNAMICS OF SMALL-SCALE SYSTEMS	49

PANEL C:

BIOLOGY AND THERMODYNAMICS: WHERE DO WE STAND?

Bresme F., Lervik A. HEAT TRANSFER AND DISSIPATION IN BIOMOLECULES: COMPUTATIONAL STUDIES	54
Demirel Y. FLUCTUATION THEOREM, INFORMATION AND BIOLOGICAL SYSTEMS	55
Kleidon A. UNDERSTANDING LIFE FROM A THERMODYNAMIC EARTH SYSTEM PERSPECTIVE	61
Kurzynski M. STOCHASTIC DYNAMICS OF PROTEINS AND THE ACTION OF BIOLOGICAL MOLECULAR MACHINES	67
Mavelli F., Caputo M., Altamura E., Stano P. STOCHASTIC SIMULATIONS OF MINIMAL CELL MODEL SYSTEMS	73
Moroz A., Chong S. ACCELERATION OF ENERGY DISSIPATION BY BIOLOGICAL SYSTEMS	82
Wollrab E., Scherer S., Worst E., Zimmer P., Kruse K., Ott A. DRIVEN CHEMISTRY AND INCREASINGLY COMPLEX FORMS OF DYNAMIC ORDER	91
Salamon P., Andresen B., Hoffmann K.H. NEARLY PERPETUAL MOTION MACHINES OF THE THIRD KIND	93
Županović P., Juretić D. THE RELEVANCE OF MAXIMUM ENTROPY PRODUCTION PRINCIPLE AND MAXIMUM INFORMATION ENTROPY PRINCIPLE IN BIOLOGY	94

PANEL D:

MAXIMUM ENTROPY PRODUCTION, STEEPEST ENTROPY ASCENT, DISSIPATION POTENTIALS, AND VARIATIONAL PRINCIPLES: HOW UNIVERSAL AND INTERRELATED?

Beretta G.P. STEEPEST-ENTROPY-ASCENT AND MAXIMAL-ENTROPY-PRODUCTION DYNAMICAL MODELS OF IRREVERSIBLE RELAXATION TO STABLE EQUILIBRIUM FROM ANY NON-EQUILIBRIUM STATE. UNIFIED TREATMENT FOR SIX NON-EQUILIBRIUM FRAMEWORKS	100
Cafaro C. INFORMATION GEOMETRIC COMPLEXITY OF ENTROPIC MOTION ON CURVED STATISTICAL MANIFOLDS	110
Niven R.K., Noack B.R. MINIMUM FLOW POTENTIAL (MASSIEU FUNCTION) IN FLOW SYSTEMS AND CONNECTION TO ENTROPY PRODUCTION EXTREMA	119

Ozawa H., Shimokawa S. GENERAL CHARACTERISTICS OF ENTROPY PRODUCTION IN NONLINEAR DYNAMIC SYSTEMS	121
Verhás J. GYARMATI'S VARIATIONAL PRINCIPLE OF DISSIPATIVE PROCESSES	127
Yang Q., Leng K., Liu Y. ON THE STRUCTURE OF MAXIMUM ENTROPY PRODUCTION PRINCIPLE: FROM NEAR TO FAR-FROM EQUILIBRIUM	133

PANEL E:

THERMODYNAMIC ENTROPY: THE VARIOUS DEFINITIONS AND THEIR REASONS

Lezzi A.M., Niro A., Pilotelli M. "DEFINING ENTROPY BEFORE HEAT, NOT VICEVERSA" IN INTRODUCTORY THERMODYNAMICS: TWENTYFIVE-YEAR TEACHING EXPERIENCE IN ENGINEERING PROGRAMS	140
Thess A. INTRODUCING THE LIEB-YNGVASON ENTROPY-DEFINITION INTO UNDERGRADUATE ENGINEERING THERMODYNAMICS EDUCATION: A CASE STUDY AT ILMENAU UNIVERSITY OF TECHNOLOGY	148
Tondeur D. ENTROPY-LIKE FUNCTIONS IN MULTI-SCALE HIERARCHICAL ORGANIZATION	149
Yngvason J. COMPARABILITY OF STATES AND THE DEFINITION OF ENTROPY	151
Zanchini E., Beretta G.P. RIGOROUS OPERATIONAL DEFINITION OF ENTROPY NOT BASED ON THE CONCEPTS OF HEAT AND OF EMPIRICAL TEMPERATURE	152

PANEL F:

THERMODYNAMICS OF INTERFACIAL PHENOMENA: SURFACE TENSION AND NON-EQUILIBRIUM EFFECTS OF KORTEWEG CAPILLARY FORCES

Glavatskiy K., Bedeaux D. HEAT AND MASS TRANSFER DURING NUCLEATION	162
Llovel F., Vilaseca O., Vega L.F. INHOMOGENEOUS DENSITY THEORIES COUPLED INTO A MOLECULAR EQUATION OF STATE FOR THE DESCRIPTION OF THE FLUID-FLUID INTERFACE	169
Mauri R. PHASE FIELD MODELING OF MULTIPHASE SYSTEMS	175
Plapp M. GRAND-CANONICAL FORMULATION OF PHASE-FIELD MODELS FOR ALLOY SOLIDIFICATION	176
Sagis L.M.C. DYNAMICS OF COMPLEX FLUID-FLUID INTERFACES	177
Schneider W. SURFACES AS NON-AUTONOMOUS THERMODYNAMIC SYSTEMS	178

PANEL G:

EQUILIBRIUM AND NON-EQUILIBRIUM THERMODYNAMICS OF SMALL SYSTEMS, MULTISCALE METHODS, AND ENERGY HARVESTING FROM FLUCTUATIONS

Fasano M., Bozorg Bigdeli M., Vaziri Sereshk M.R., Chiavazzo E., Asinari P. MOLECULAR DYNAMICS SIMULATION OF CARBON NANO-BINDERS INTO ZEOLITE THERMAL STORAGE	188
Chamberlin R.V. NANOTHERMODYNAMICS: SMALL-SYSTEM THERMODYNAMICS APPLIED TO LARGE SYSTEMS	189
Gammaitoni L. ENERGY HARVESTING AT MICRO AND NANOSCALE	190
Gaspard P. THE FLUCTUATION THEOREM FOR CURRENTS AND NONEQUILIBRIUM THERMODYNAMICS	191
Pérez-Madrid A., Santamaria-Holek I. THE IMPLICATIONS OF THE BREAKDOWN OF THERMODYNAMIC STABILITY IN ENERGY GENERATION AND CONVERSION NANODEVICES	200
Issa K.M., Poesio P. HYBRID ATOMISTIC-CONTINUUM APPROACH TO DESCRIBE INTERFACIAL PROPERTIES BETWEEN IMMISCIBLE LIQUIDS	201
Searles D.J., Reid J.C., Johnston B.M., Evans D.J., Rondoni L., Michel G. FLUCTUATION RELATIONS FOR THE DISSIPATION	206

PANEL H:

CONCEPTUAL ANALYSIS OF THE ENTROPY PRINCIPLE IN CONTINUUM PHYSICS

Cimmelli V.A. CONCEPTUAL ANALYSIS OF THE ENTROPY PRINCIPLE IN CONTINUUM PHYSICS: AN OVERVIEW	208
Hütter M., Svendsen B. NON-NEGATIVE ENTROPY PRODUCTION BY QUASI-LINEAR OR POTENTIAL-BASED FORCE- FLUX RELATIONS	210
Jou D. ENTROPY, ENTROPY FLUX, TEMPERATURE, AND SECOND LAW IN EXTENDED IRREVERSIBLE THERMODYNAMICS	211
Camiola V.D., Mascali G., Romano V. ON THE FORMULATION OF ENTROPY FOR A PARTIALLY QUANTIZED ELECTRON SYSTEM IN SEMICONDUCTORS	217
Ruggeri T. RECENT RESULTS IN RATIONAL EXTENDED THERMODYNAMICS: MACROSCOPIC APPROACH AND MAXIMUM ENTROPY PRINCIPLE FOR DENSE AND RAREFIED POLYATOMIC GASES	218
Trovato M., Reggiani L. A PROPER NONLOCAL FORMULATION OF QUANTUM MAXIMUM ENTROPY PRINCIPLE FOR FERMI, BOSE AND FRACTIONAL EXCLUSION STATISTICS	219
Ván P. THERMODYNAMICS OF CONTINUA: THE CHALLENGE OF UNIVERSALITY	228

PANEL I:

CONNECTING SECOND LAW ANALYSIS WITH ECONOMICS, ECOLOGY, FLUID MECHANICS, AND MORE

Gaggioli R.A. RELEVANCE OF THE DEAD STATE TO ECOLOGICAL AND ECONOMIC ANALYSES	236
Lazzaretto A. FUEL AND PRODUCT DEFINITIONS IN COST ACCOUNTING EVALUATIONS: IS IT A SOLVED PROBLEM?	244
Reini M., Daniotti S. ENERGY/EXERGY BASED COST ACCOUNTING IN LARGE ECOLOGICAL-TECHNOLOGICAL ENERGY SYSTEMS	251
Rosen M.A. CORRELATING THERMODYNAMICS AND ECONOMIC INVESTMENTS TO IMPROVE THE RATIONALE FOR ENERGY RESEARCH	259
Sciubba E. USE OF EXERGY ANALYSIS TO COMPUTE THE RESOURCE INTENSITY OF BIOLOGICAL SYSTEMS AND HUMAN SOCIETIES	268
Tsatsaronis G. ADVANCED EXERGY-BASED METHODS	276
Valero An., Valero Al. THERMODYNAMIC ACCOUNTING OF THE GLOBAL DEPLETION OF THE MINERAL CAPITAL ON EARTH. A PROPOSAL TO THE U.N.	277
Verda V., Caccin M., Kona A. THERMOECONOMICS AS A REGULATION TOOL IN FUTURE DISTRICT HEATING NETWORKS	284

PANEL J:

MODEL ORDER REDUCTION OF COMPLEX COMBUSTION THERMODYNAMICS AND KINETICS

Gorban A.N., Zinovyev A., Radulescu O. DOMINANT PATHS AND SYSTEMS IN MULTISCALE REACTION NETWORKS	292
Klimenko A.Y., Maas U. CPT INVARIANCE AND ITS IMPLICATIONS FOR THERMODYNAMICS AND KINETICS	294
Maas U., Klimenko A.Y. HIERARCHICAL CONCEPTS FOR MODEL REDUCTION FOR REACTING FLOWS BASED ON LOW-DIMENSIONAL MANIFOLDS	304
Nicolas G., Janbozorgi M., Metghalchi H. THE RATE-CONTROLLED CONSTRAINED-EQUILIBRIUM (RCCE) METHOD: A REDUCTION TECHNIQUE FOR COMPLEX KINETIC MODELS	313
Najm H.N. MODEL REDUCTION IN REACTING FLOW	319
Valorani M., Paolucci S. ENTROPY PRODUCTION AND THE G-SCHEME	323
Yablonsky G.S., Constales D., Marin G.B. GRASPING COMPLEXITY IN CHEMICAL KINETICS: TOP-DOWN, BOTTOM-UP AND SOME MORE	330

PANEL K:

QUANTUM THERMODYNAMICS: WHAT IS IT AND WHAT CAN BE DONE WITH IT

Abe S. QUANTUM-MECHANICAL ANALOG OF THE CARNOT CYCLE: GENERAL FORMULA FOR EFFICIENCY AND MAXIMUM-POWER OUTPUT	334
Chaturvedi S. MICROSCOPIC BROWNIAN HEAT ENGINES: A QUANTUM DYNAMICAL FRAMEWORK	337
Gemmer J. TYPICALITY APPROACH TO QUANTUM THERMODYNAMICS	338
Kosloff R., Levi A. QUANTUM REFRIGERATORS AND THE III-LAW OF THERMODYNAMICS	344
Sisman A., Ozturk F., Firat C., Babac G. THERMODYNAMICS UNDER QUANTUM SIZE EFFECTS	353
von Spakovsky M.R. INTRINSIC QUANTUM THERMODYNAMICS: WHAT IT IS AND WHAT CAN BE DONE WITH IT	359

PANEL L:

COMPUTATION OF THERMODYNAMIC PROPERTIES, PHASE EQUILIBRIA, AND MIXING AND SEPARATION DYNAMICS OF INDUSTRIAL BLENDS AND NANOSTRUCTURED FLUIDS

Brauner N., Shacham M. COMBINING CONSTANT PROPERTY PREDICTION TECHNIQUES FOR WIDER APPLICABILITY AND IMPROVED ACCURACY	370
Correra S. ASPHALTENE OR HOW AND WHY I BECAME A FAN OF THE REGULAR SOLUTIONS THEORY	377
Deiters U.K. THERMODYNAMICS—OLD SCIENCE AND NEW CHALLENGES	383
Jaubert J.-N., Privat R. USE OF A UNIQUE SET OF TEMPERATURE-DEPENDENT BINARY INTERACTION PARAMETERS TO SIMULTANEOUSLY DESCRIBE EXCESS PROPERTIES AND FLUID-PHASE EQUILIBRIUM WITH A CUBIC EQUATION OF STATE	388
Rousseau B. COARSE-GRAINED SIMULATIONS OF OIL-WATER-SURFACTANT MIXTURES	394
Theodorou D.N. STATISTICAL THERMODYNAMICS-BASED SIMULATION METHODS FOR THE PREDICTION OF POLYMER PROPERTIES	396
Zvelindovsky A.V., Pinna M. BLOCK COPOLYMERS IN CONFINEMENTS AND UNDER EXTERNAL FIELDS	402

ORAL PRESENTATIONS BY A PHD STUDENT OR POSTDOC AUTHOR OR COAUTHOR

Polettini M., Vedovato F. OF DICE AND MEN. SUBJECTIVE PRIORS, GAUGE INVARIANCE, AND NONEQUILIBRIUM THERMODYNAMICS	404
Gielen R., Baelmans M. THE INFEASIBILITY OF REVERSIBILITY AND ITS CONSEQUENCES FOR ENGINEERING DESIGN	410
Karabetoglu S., Sisman A. DIMENSIONAL TRANSITIONS IN THERMODYNAMIC PROPERTIES	416
Babac G., Sisman A., Ozturk Z.F. QUANTUM SIZE AND DEGENERACY EFFECTS ON THERMAL SELF-DIFFUSION UNDER FREE MOLECULAR TRANSPORT REGIME	421
Aydin A., Sisman A. DISCRETE NATURE OF THERMODYNAMIC PROPERTIES	425
Cano-Andrade S., Beretta G.P., von Spakovsky M.R. NON-EQUILIBRIUM THERMODYNAMIC MODELING OF AN ATOM-FIELD STATE EVOLUTION WITH COMPARISONS TO PUBLISHED EXPERIMENTAL DATA	430
Langenbach K., Browarzik D., Browarzik C., Enders S. THERMODYNAMIC DESCRIPTION OF BRANCHED MOLECULES	436
Latella I., Pérez-Madrid A. LONG-RANGE INTERACTING SYSTEMS AND THE GIBBS-DUHEM EQUATION	437
Malgaretti P., Pagonabarraga I., Rubi J.M. DEBYE LENGTH MATCHES CHANNEL BOTTLENECK: CORRUGATION-GOVERNED REGIME IN TRACER DIFFUSION THROUGH A VARYING-SECTION CHANNEL	442
De Luca S., Todd B.D., Hansen J.S., Daivis P.J. PUMPING OF WATER WITH ROTATING ELECTRIC FIELDS AT THE NANOSCALE	447
Neri M., Luscietti D., Pilotelli M. COMPUTING THE EXERGY OF SOLAR RADIATION FROM REAL RADIATION DATA ON THE ITALIAN AREA	452
Pavelka M., Maršik F. DETAILED THERMODYNAMIC ANALYSIS OF FUEL CELL EFFICIENCY	458
Rocco M., Toro C. EXERGY BASED METHODS FOR ECONOMIC AND ENVIRONMENTAL ANALYSIS APPLIED TO A 320 MW COMBINED CYCLE POWER PLANT	464
Wilhelmsen Ø., Bedeaux D., Kjelstrup S., Reguera D. PHASE TRANSITIONS IN MULTICOMPONENT SYSTEMS AT THE NANO-SCALE: THE EXISTENCE OF A MINIMAL BUBBLE SIZE	470
Shvab I., Sadus R. STRUCTURAL AND POLARIZATION PROPERTIES OF AQUEOUS NONPOLAR SOLUTE MIXTURES	476
Válu O.S., Beneš O., Konings R.J.M. HIGH TEMPERATURE THERMODYNAMIC PROPERTIES OF THE (U, AM)O ₂ SOLID SOLUTIONS	477
Glavatskiy K.S., Waage M.H., Vlught T.J.H., van Erp T.S., Kjelstrup S. THERMODYNAMIC STABILITY AND KINETIC ASPECTS OF CH ₄ - CO ₂ HYDRATE EXCHANGE	478

Meddah C., Sabeur S.A., Hammou A.B. STUDY OF THERMODYNAMIC AND STRUCTURAL PROPERTIES OF A FLEXIBLE HOMOPOLYMER CHAIN USING MULTICANONICAL MONTE CARLO METHOD	479
Ziólkowski P., Zakrzewski W., Badur J. INNOVATIVE THERMODYNAMICAL CYCLES BASED ON ENHANCEMENT MASS, MOMENTUM, ENTROPY AND ELECTRICITY TRANSPORT DUE TO SLIP, MOBILITY, TRANSPIRATION, ENTROPY AND ELECTRIC JUMPS AS WELL AS OTHER NANO-FLOWS PHENOMENA	482
POSTER PRESENTATIONS	489
González-Narváez R.E., Sánchez-Salas N., Calvo Hernández A., Barranco-Jiménez M.A. OPTIMIZATION CRITERIA AND EFFICIENCIES OF ISOTHERMAL MOLECULAR MACHINES	490
Okumura H. FREE-ENERGY CALCULATION OF A PROTEIN AS A FUNCTION OF TEMPERATURE AND PRESSURE: MULTIBARIC-MULTITHERMAL MOLECULAR DYNAMICS SIMULATIONS	494
Zamora-Gómez M., Páez-Hernández R., Portillo-Díaz P., Ladino-Luna D. A POSSIBLE APPLICATION OF THE MECHANICS OF FLUIDS AND THE NONLINEAR DYNAMICS OF BEHAVIOR OF THE HEART	499
Páez-Hernández R., Portillo-Díaz P., Ladino-Luna D. EFFECTS OF THE TIME DELAYS IN AN ENDOREVERSIBLE AND NONENDOREVERSIBLE THERMAL ENGINES WORKING AT DIFFERENT REGIMES	504
Županović P., Sorić I., Sorić T. STIRLING ENGINE AS SIMPLE AS POSSIBLE	510
Trinh T.T., Vlught T.J.H., Hägg M.-B., Bedeaux D., Kjelstrup S. SIMULATING CO ₂ ADSORPTION AND DIFFUSION ON A GRAPHITE SURFACE	514
Ván P., Czél B., Fülöp T., Gróf Gy., Gyenis Á., Verhás J. EXPERIMENTAL ASPECTS OF HEAT CONDUCTION BEYOND FOURIER	519
Fülöp T., Ván P., Csatár A. ELASTICITY, PLASTICITY, RHEOLOGY AND THERMAL STRESS— AN IRREVERSIBLE THERMODYNAMICAL THEORY	525
Ivashnyov O., Ivashneva M. MAXIMUM ENTROPY PRODUCTION IN BOILING SHOCKS	531
Loimer T. THE THERMODYNAMIC STATES OF A FLUID IN A JOULE-THOMSON PROCESS INVOLVING PHASE CHANGES AT INTERFACES WITH LARGE CURVATURE	537
Serdyukov S.I. ON THE LAGRANGE MULTIPLIERS METHOD IN ENTENDED THERMODYNAMICS OF IRREVERSIBLE PROCESSES	542
Cimmelli V.A., Sellitto A., Jou D. MULTITEMPERATURE MIXTURE OF PHONONS AND ELECTRONS AND NONLOCAL THERMOELECTRIC TRANSPORT IN NANOSYSTEMS	545
Ván P., Biró T.S. DISSIPATION FLOW-FRAMES: PARTICLE, ENERGY, THERMOMETER	546

Celenk D., Ozelik Z., Senocak S. ADVANCED EXERGY ANALYSIS OF THE STEAM TURBINE OPERATIONS OPTIMISATION	558
Dzuban A.V., Voskov A.L. CALCULATION OF POLYTHERMAL SECTIONS OF TERNARY PHASE DIAGRAMS BY THE CONVEX HULL METHOD	563
Ozturk Z.F., Sisman A., Karabetoglu S. QUANTUM CONFINEMENT EFFECTS ON SEEBECK COEFFICIENT	567
Sellitto A., Cimmelli V.A., Jou D. THERMOELECTRIC EFFECTS AND SIZE DEPENDENCY OF THE FIGURE-OF-MERIT IN CYLINDRICAL NANOWIRES	571
Shvab I., Sadus R. HEAT CAPACITIES AND TRANSPORT PROPERTIES OF AQUEOUS NONPOLAR SOLUTE MIXTURES	572
Al-Abbasi O., Beretta G.P., von Spakovsky M.R. INTRINSIC QUANTUM THERMODYNAMIC PREDICTION OF THE NON-EQUILIBRIUM ATOMISTIC-LEVEL BEHAVIOUR OF CHEMICALLY REACTIVE SYSTEMS	573
Ható Z., Makó É., Kristóf T. MOLECULAR SIMULATION STUDY OF KAOLINITE INTERCALATION	579
Ható Z., Gillespie D., Kristóf T., Boda D. COMPUTER SIMULATION OF A RECTIFYING ION CHANNEL	580
Badur J., Ziolkowski P. FURTHER REMARKS ON THE SURFACE VIS IMPRESSA CAUSED BY A FLUID-SOLID CONTACT	581
AUTHOR INDEX	587

PANEL A

**ENTROPY PRODUCTION MINIMIZATION,
CONSTRUCTAL LAW, AND OTHER OPTIMIZATION
TECHNIQUES IN ENERGY AND OTHER
TECHNOLOGIES**

PRINCIPAL EQUATIONS OF STATE AND THEIR RELATION TO THE SECOND LAW AND TO THERMODYNAMIC GEOMETRY OPTIMIZATION

Bjarne Andresen* and Christopher Essex†

* Niels Bohr Institute, University of Copenhagen
Universitetsparken 5, DK-2100 Copenhagen Ø, Denmark

† Department of Applied Mathematics, The University of Western Ontario
London, Ontario N6A 5B7, Canada

EXTENDED ABSTRACT

Functions, not dynamical equations, are the definitive mathematical objects in equilibrium thermodynamics. However, more than one function is often described as “the” equation of state for any one physical system. Usually these so named equations only capture incomplete physical content in the relationships between thermodynamic variables, while other equations, no less worthy of the name equation of state, go inconsistently by other names. While this approach to terminology can be bewildering to newcomers, it also obscures crucial properties of thermodynamic systems generally. We introduce specific principal equations of state and their complements for ideal gases, photons, and neutrinos that have the complete thermodynamic content from which all other forms can be easily deduced. The Gibbs equation and the Gibbs-Duhem equation,

$$dU = TdS - PdV + \sum_i \mu_i dN_i$$

$$0 = SdT - VdP + \sum_i \mu_i N_i d\mu_i$$

can be solved to yield these principal and complementary principal equations of state,

$$U = f(S, V, N_1, N_2, \dots)$$

$$0 = g(T, P, \mu_1, \mu_2, \dots).$$

These principal equations of state make properties like the second law of thermodynamics and local thermodynamic equilibrium completely visual (see the figure). The second law requires that the principal equation of state function is convex (bandshell-like surface) and that it scales linearly with the amount of material (green rays). This requirement must obviously also be satisfied by approximate equations of state. Superposition of states ($S(\mathbf{r}_1) + S(\mathbf{r}_2)$) along with the convexity provides the entropy generation resulting from equilibration of the states (short thick vertical red line).

Further, these principal equations of state are the foundation of thermodynamic geometry from which bounds on the exergy lost in a process or the entropy generated in the process can be derived. These bounds, e.g.

$$\Delta A \geq \frac{L^2 \varepsilon}{\tau}$$

are stronger than the conventional bounds stating that the losses must be non-negative, $\Delta A \geq 0$, and they factor nicely into a thermodynamic distance L from initial to final state based on equilibrium quantities, a factor ε describing the relaxation time when the system is disturbed, and finally the duration τ allowed for the process. This is possible only when the complete set of independent extensive variables is used.

Whereas the principal equation of state is given in terms of all the extensive variables of the system, the complementary principal equation of state is formulated in the set of intensive variables only. One loses the property of system scale in these variables, but that makes them naturally suited for envisioning the distinction between global and local thermodynamic equilibrium. All local equilibria of a system would occur at a single point for a particular physical system in global thermodynamic equilibrium. But out of equilibrium, when local equilibrium still makes sense, the local equilibria spread out to become a cloud of points. The extent of that cloud naturally defines a quality for global equilibrium in any system purported to be in equilibrium overall.

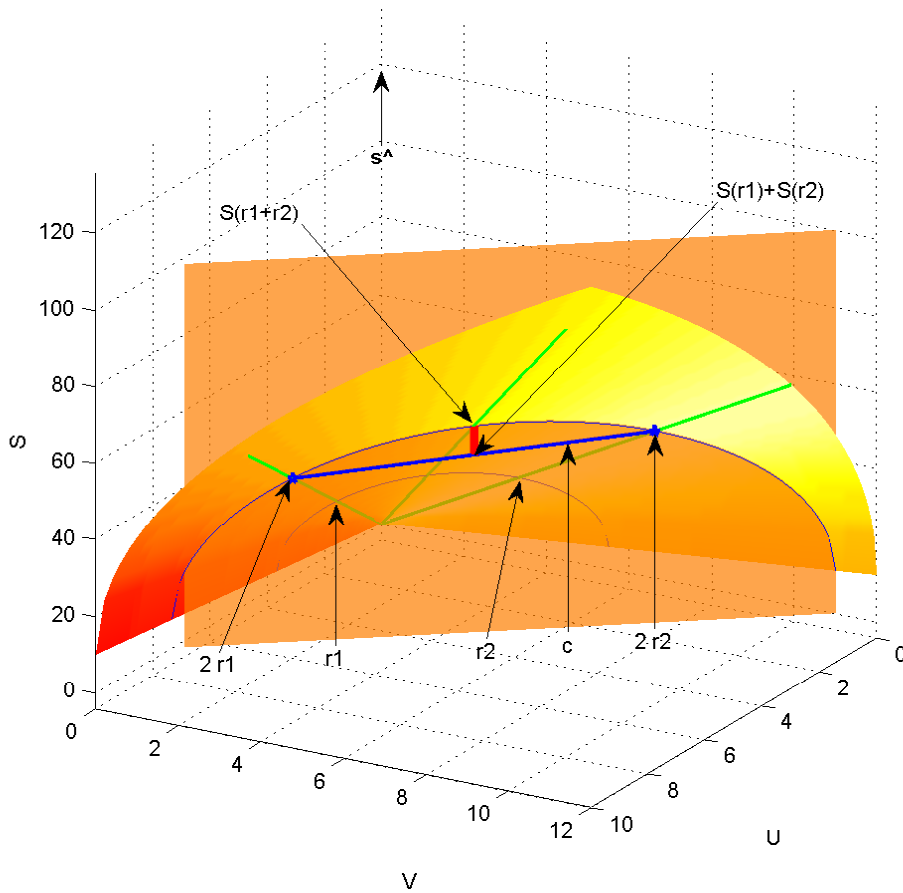


Figure. Equilibrium surface $S(U, V)$ (shaded bandshell-like surface). The green rays emanating from the origin represent equivalent equilibrium states, differing only in magnitude, e.g. states \mathbf{r}_1 and $2\mathbf{r}_1$. The vector \mathbf{c} (thick blue line) is a chord connecting the two equilibrium points $2\mathbf{r}_1$ and $2\mathbf{r}_2$ on the equilibrium surface but otherwise being under the surface and thus passing through non-equilibrium states. The equilibrated mixture of \mathbf{r}_1 and \mathbf{r}_2 is indicated as $S(\mathbf{r}_1 + \mathbf{r}_2)$ and the entropy produced in the equilibration is shown as the thick red line.

CONSTRUCTAL LAW: DESIGN AS PHYSICS

Adrian Bejan

Duke University, Department of Mechanical Engineering and Materials Science
Durham, North Carolina 27708-0300, USA

ABSTRACT

A law of physics is a concise statement that summarizes a phenomenon that occurs everywhere in nature. A phenomenon is a fact, circumstance or experience that is apparent to the human senses and can be described. The phenomenon summarized by the constructal law is the occurrence and evolution of designs in nature. The phenomenon is the time direction of the movie of design evolution. The direction is universal, toward configurations and rhythms (designs) that flow and move more easily, for greater access, over time. Based on its record, the constructal law accounts for the design phenomenon and also for all the phenomena associated ad-hoc with final-design (destiny) statements of “optimality” (min, max) that have been proposed. Most notably, the constructal law accounts for the contradictory final-design statements of minimum entropy production and maximum entropy production, and minimum flow resistance and maximum flow resistance. On the earth’s surface, the design in nature phenomenon facilitates access for everything that flows, spreads and is collected: river basins, atmospheric and ocean currents, animal life and migration, and our civilization (the evolution of the “human and machine species”).

DESIGN AS SCIENCE

Design in nature is the main theme in science today. It began with geometry and mechanics, which are about designs (configurations), their principles, and the contrivances made based on designs and principles. Science has always been about the human urge to make sense out of what we discern: numerous observations that we tend to store compactly as “phenomena” and, later, as much more compact “laws” that account for the phenomena.

To see the position of design in nature as a subject in physics, it is necessary to recall that thermodynamics rests on two laws that are both “first principles”. The first law commands the conservation of energy in any system. The second law commands the presence of irreversibility (i.e. the generation of entropy) in any system. The permanence and extreme generality of the two laws are consequences of the fact that in thermodynamics the “any system” is a black box. It is a region of space, or a collection of matter without specified shape and structure. The two laws are global statements about the balance or imbalance of the flows (mass, heat, work) that flow into and out of the black box.

Nature is not made of boxes without configuration. The systems that we identify in nature have shape and structure. They are resoundingly macroscopic, finite size, and recognizable as sharp lines drawn on a different background. They have patterns, maps, rhythms and sounds. The very fact that they have names (river basins, blood vessels, trees) indicates that they have unmistakable appearances.

In my 1997 thermodynamics book [1], I pointed out that the laws of thermodynamics do not account *completely* for the systems of nature, even though scientists have built thermodynamics into thick books in which the two laws are just the introduction. The body of doctrine is devoted to describing, designing and “improving” things that seem to

correspond to systems found in nature, or can be used by humans to make life easier. Nowhere is this more evident than in the method of Entropy Generation Minimization [2, 3] where design is recognized as “thermodynamics”, even though neither of the two laws accounts for the natural occurrence of “design” and “design evolution” phenomena.

If physics is to account for the systems of nature, then thermodynamics must be strengthened with an additional self-standing law (i.e., with another first principle) that covers all phenomena of design occurrence and evolution. To achieve this, I added to physics the constructal law [1, 4], which states briefly that

“For a finite-size system to persist in time (to live) its configuration must change such that it provides easier access to its currents” [1, 4].

The constructal law is a definition of life in the broadest possible sense: to be alive, a system must be able to flow and to morph in time so that its currents flow more and more easily. Live are the water streams in the river basins and the streams of animal mass flowing on the landscape, which are better known as animal locomotion and migration. Live are the animate and the inanimate systems that flow, move, and change configuration. The constructal law commands that the changes in configuration must occur in a particular *direction* in time (toward designs that allow currents to flow more easily). The constructal law places the concepts of “design” and “evolution” centrally in physics.

The Constructal Law is a field that is expanding rapidly in physics, biology, technology and social sciences. The field was reviewed in 2006 [5, 6], and now it is expanding even more rapidly. No less than 13 books have been published on the Constructal Law since 2006 [5-19]. In April 2013, the entry “constructal” on ISI revealed an h index of 39 and a

total number of 7000 citations. On Google Scholar, the word “constructal” yielded more than 2,300 titles.

DESIGN AND EVOLUTION: ANIMATE AND INANIMATE

The constructal law of design in nature constitutes a unified view of design evolution. It predicts evolution in all the domains in which evolutionary phenomena are observed, recorded and studied scientifically: animal design, river basins, turbulent flow, dendritic crystals, animal movement, athletics, technology evolution and global design. Some of the most common animate and inanimate systems that we predicted with the constructal law are sketched in Fig. 1.

Evolution means design modifications, in time. How these changes are happening are *mechanisms*, and *mechanism* should not be confused with *law*. In the evolution of biological design, the mechanism is mutations, biological selection and survival. In geophysical design, the mechanism is soil erosion, rock dynamics, water-vegetation interaction, and wind drag. In sports evolution, the mechanism is training, recruitment, mentoring, selection, and rewards. In technology evolution, the mechanism is liberty, freedom to question, innovation, education, trade, theft and emigration.

What flows through a design that evolves is not nearly as special in physics as how the flow system generates its configuration in time. The “how” is the physics principle—the constructal law. The “what” are the mechanisms, and they are as diverse as the flow systems themselves. The “what” are many, and the “how” is one.

Having “impact” on the environment is synonymous with having design in nature. To flow means to get the surroundings out of the way. There is no part of nature that does not resist the flows and movements that attempt to get through it. Movement means penetration, and its name differs depending on the direction from which the phenomenon is observed. To the observer of river basins, the phenomenon is the emergence and evolution of the dendritic vasculature. To the observer of the landscape, the phenomenon is erosion and the reshaping of the earth’s crust.

This mental viewing of design generation and environmental impact as a unitary design in nature is universally applicable. Think of the paths of animals, versus the river-like paths and burrows dug into the ground. Think of the migration of elephants, versus the toppling of trees. The patterns of social dynamics go hand-in-glove with impact on the environment.

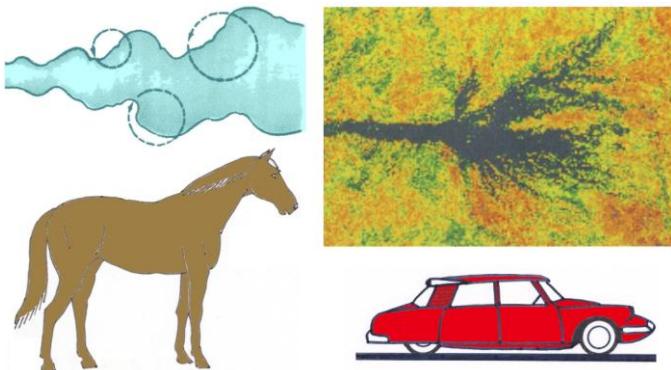


Figure 1 The larger are more efficient, faster, live longer and travel farther lifetime: vehicles, animals, rivers and the winds.

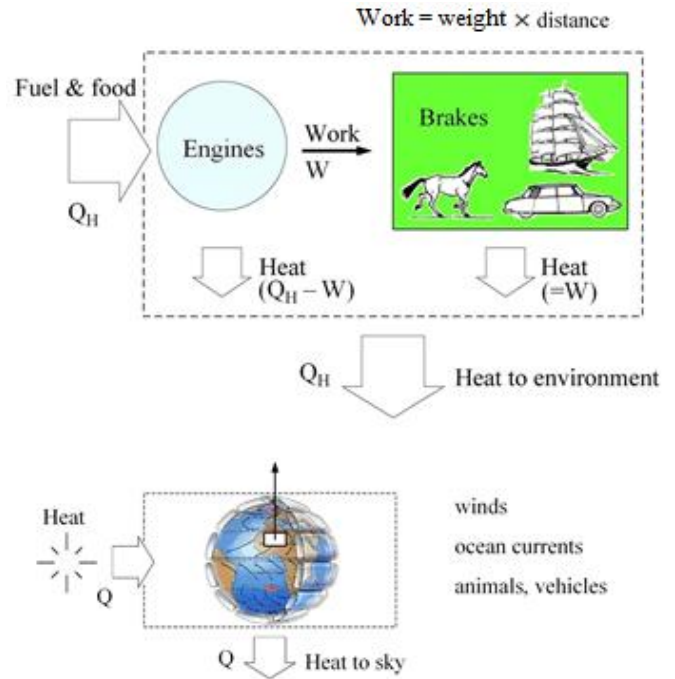


Figure 2 Everything that moves on earth is driven. It moves because an engine dissipates its work output into a brake.

Animal locomotion is “guided locomotion”, with design—it is efficient, economical, safe, fast and purposefully straight. This is the constructal design of animal and human locomotion, and it is the complete opposite of Brownian motion. The constructal design of animal locomotion is much more complicated and perfected than the thermodynamics of balancing two work efforts, one on the vertical (lifting weight) and the other on the horizontal (getting the environment out of the way), which led to the discovery of the allometric relation between all animal speeds, body frequencies and body mass [20-24].

The movement of the body weight on alternating legs is equivalent to the view of walking and running as falling-forward locomotion. The legs are the two spokes of the human wheel [25] from which the other spokes are missing, and which make the animal wheel the lightest wheel.

The constructal design of all urban movement is such that, at all length scales, *the time needed to travel short and slow is roughly the same as the time needed to travel long and fast*. The need to “travel short and long” to move on a territory (area, volume) was the example with which the constructal theory of design in nature began in 1996 [4]. This continued with explaining why the design of the Atlanta airport is efficient, and why the designs of new airports are evolving toward the Atlanta design [26, 27].

In the Atlanta design, the short and slow is walking along the concourse, and the long and fast is riding on the train. In the city design, at the smallest scale the time balance is between walking from the house to the car and riding on the small street. At the next scale, the balance is between riding on streets (short, slow) and avenues (long, fast), and so on to larger scales: avenues and highways, highways and intercity train and air travel, short flights and long flights, all the way to the scale of the globe. We have applied this principle to the design of the infrastructure (inhabited spaces) for fastest and safest evacuation of pedestrians, from crowded areas and

volumes [28, 29].

The slow and short are many, and the fast and long are few. The design of all movement on earth, animate and inanimate (river basins, eddies of turbulence, animal life, trucks on the roads, airplanes in the air, streets in the city) is one design: *few large and many small* [20, 30].

The effect of life is *measurable* in terms of the mass moved over distances during the life time of the flow system (Fig. 2). The work required to move any mass on earth (vehicle, river water, animal mass) scales as the weight of that mass time the distance to which it is moved horizontally, on the landscape. It is this way with the life of the river basin and the animal, and it is the same with the life of man, family, country and empire. The economic activity of a country is all this movement—mass (people, goods) moved to distances. Because every movement is proportional to the amount of fuel burned in order to drive it, the entire economic activity on a territory must be proportional to the amount of fuel consumed on that territory. This view predicts that the annual GDP of a country should be proportional to the amount of fuel burned in the country (i.e. the useful energy generated and destroyed) [31]. This is confirmed by the economics data plotted in Fig. 3.

Animals have been spreading in space, in this unmistakable time direction dictated by the constructal law: from sea to land, and later from land to air [32]. The movement of the human & machine species evolved in the same direction, from small boats with oars on rivers and along the sea shore, to the wheel and vehicles on land, and most recently to aircraft.

The same movie (because this is what the occurrence and evolution of design is, a time sequence of images) shows that speeds have been increasing in time, and will continue to increase. For the same body mass, the runners are faster than

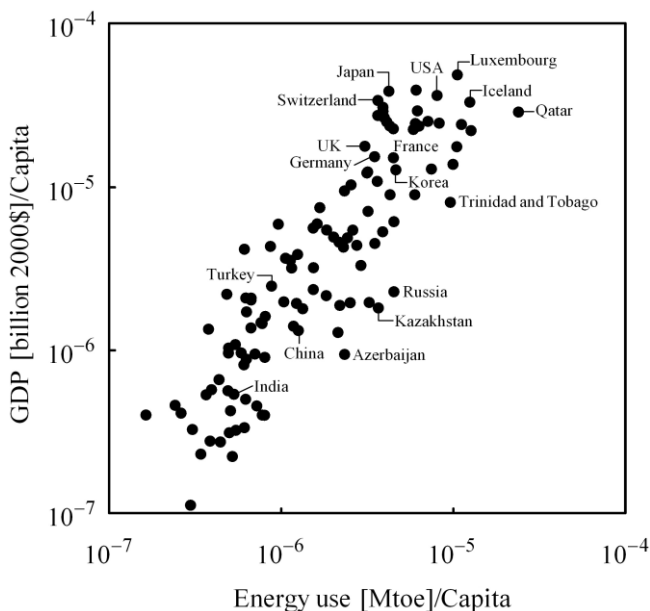


Figure 3 Economic activity means movement, which comes from the burning of fuel for human needs. This is demonstrated by the annual GDP of countries all over the globe, which is proportional to the fuel burned in those countries (data from International Energy Agency. Key World Energy Statistics, 2006). In time, all the countries are moving up and to the right, on the bisector.

the swimmers, and the fliers are faster than the runners. This movie is the same as the evolution of inanimate mass flows, for example, the river basins. Under the persisting rain, all the channels morph constantly, to flow more easily.

Spreading and collecting flows occupy areas and volumes that have S-shaped history curves predicted with the constructal law [33-35]. Design is the speed governor of nature. None of the changes observed in politics, history, sociology, animal speed and river speed are spinning out of control. None of the expansions feared in geography, economics and urbanism are slamming into a brick wall.

CONSTRUCTAL LAW VERSUS FINAL DESIGN

The constructal law is not a statement of optimization, maximization, minimization, or any other mental image of “final design” or “destiny”. The constructal law is about the direction of evolution in time, and the fact that design in nature is not static: it is dynamic, ever changing, like the images in a movie at the cinema. This is what design and evolution are in nature, and the constructal law captures them completely. Evolution never ends.

There have been many proposals of final-design in science, but each addresses a narrow domain, and, as a consequence, the body of optimality statements that have emerged is self-contradictory, and the claim that each is a general principle is easy to refute. Here are the best known statements:

- (i) Minimum entropy generation and maximum efficiency are used commonly in engineering.
- (ii) Maximum entropy generation is being invoked in geophysics.
- (iii) Maximum “fitness” and “adaptability” (robustness, resilience) are used in biology.
- (iv) Minimum flow resistance (fluid flow, heat transfer, mass transfer) is invoked in engineering, river mechanics and physiology.
- (v) Maximum flow resistance is used regularly in physiology and engineering, e.g. maximum resistance to loss of body heat through animal hair and fur, or through the insulation of power and refrigeration plants, the minimization of fluid leaks through the walls of ducts, etc.
- (vi) Minimum travel time is used in urban design, traffic, transportation.
- (vii) Minimum effort and cost is a core idea in social dynamics and animal design.
- (viii) Maximum profit and utility is used in economics.
- (ix) Maximum territory is used for rationalizing the spreading of living species, deltas in the desert, and empires.
- (x) Uniform distribution of maximum stresses is used as an “axiom” in rationalizing the design of botanical trees and animal bones.
- (xi) Maximum growth rate of flow disturbances (deformations) is invoked in the study of fluid flow disturbances and turbulence.
- (xii) Maximum power was proposed in biology and is used in physics and engineering.

This list is incomplete. Even though the optimality

statements are contradictory, local, and disunited on the map of design in nature, they demonstrate that the interest in placing design phenomena deterministically in science is old, broad and thriving. One example is flow of stresses phenomenon [36] that accounts for the emergence of solid shape and structure in vegetation, skeleton design, and technology. The flow of stresses is an integral part of the design-generation phenomenon of moving mass more and more easily on the landscape [11, 30].

Another example is the contradiction between minimum and maximum of entropy generation [see (i) and (ii) above], which was resolved based on the constructal law in 2006 [26]. The flowing nature is composed of systems that move as engines connected to brakes. In time, the “engines” of nature acquire configurations that flow more easily, and this means that they evolve toward less entropy generation, and more production of motive power per unit of useful energy (exergy) used. At the same time the “brakes” of nature destroy the produced power, and this translates into their evolution toward configurations that dissipate more and more power. The principle is not the maximum or the minimum, or the fact that the “engine + brake” constitution of nature (Fig. 2) brings them together. The principle is the design evolution of “engine” configurations in the time direction dictated by the constructal law and the design evolution of “brake” configurations in the same direction over time.

To think that design evolution means “evolution toward patterns of least resistance” is, at best, a metaphor. What “resistance” when walking in total freedom alone on the beach? What “resistance” when sitting down on the train in the Atlanta airport, and wanting to arrive at your gate faster? What “resistance” when searching for a cheaper ticket between Atlanta and Hong Kong? What “resistance” when the lucky animal finds food and we find oil? What “resistance” when the snowflake grows freely as a daisy wheel of trees? Furthermore, what is “least” (or maximum, minimum) about any design? Who is to know that the urge to have an even better design has reached the end? Who is the to know that a final design exists?

Resistance is a concept from electricity (voltage divided by current), which was introduced subsequently in fluid mechanics (pressure difference divided by mass flow rate) and heat transfer (temperature difference divided by heat current). In pedestrian and animal movement the current is obvious: it is the flow rate of human mass through a plane perpendicular to the flow path. Not obvious is the “difference” (voltage, pressure, temperature) that drives the pedestrian flow.

I faced these questions squarely when I composed the constructal law in 1996 [1, 4], and this is why I summarized the design-in-nature phenomenon with a statement of all physics that is universally applicable, without words and such as resistance and static end-design (optimum, min, max), cf. Section 1. Yet, in our morphing movement (i.e., life) on earth, we rely on thoughts such as greater access, more freedom, go with the flow, shorter path, less resistance, longer life, less expensive and greater wealth. These ideas guide us, like the innate urges to have comfort, beauty and pleasure.

The constructal law empowers the mind to fast-forward the design evolution process. This is in fact what the human mind does with any law of physics—the mind uses the law to predict features of future phenomena. Knowing ahead is also an expression of the constructal law [32], because all animal

design is about moving more and more easily on the landscape, and this includes the phenomenon of cognition – the urge to get smarter, understand and remember faster, so that the animal can get going and place itself out of danger. Relying on the constructal-law direction to fast-forward the design is useful.

CONSTRUCTAL LAW VERSUS SECOND LAW

The constructal law, the first law, and the second law are first principles. The constructal law is a useful reminder of not only what is missing in thermodynamics (the design & evolution principle) but also of what is present.

For example, we often read that the second law states that “entropy must increase”, and that the “classical” laws of thermodynamics pertain to “equilibrium states”. Many even teach that thermodynamics should be called thermo“statics”. Such statements are unrecognizable from a point of view rooted in thermodynamics. Here is the correct statement of the second law, made by two of its three original proponents in 1851-1852 (the other was Rankine) [26]:

Clausius: No process is possible whose sole result is the transfer of heat from a body of lower temperature to a body of higher temperature.

Kelvin: Spontaneously, heat cannot flow from cold regions to hot regions without external work being performed on the system.

Note that the second law says absolutely nothing about “equilibrium states”, “entropy”, “classical”, and “statics”.

Like any other law of physics, the second law of thermodynamics is a concise summary of observed facts. A law unifies phenomena (the observed facts). The second-law phenomenon is irreversibility. The correct summary of the phenomenon of irreversibility is due to Clausius and Kelvin above, and to others who made demonstrably *equivalent* statements (for a review, see Ref. [1]). The only relevant question about the second law statement is whether it is correct. The evidence is massively in support of answering “yes”, based on all the machines that have been built by engineers successfully because they relied on the second law of thermodynamics of Rankine, Clausius, and Kelvin. These machines are every day futuristic (not “classical”), they are full of life and motion (not in “equilibrium”), and are dynamic (not “static”).

The constructal-law phenomenon is the occurrence of design and evolution in nature. The constructal law recognizes the natural tendency of evolution toward “easier access in time”. The word “access” means the opportunity to enter and move through a confined space such as a crowded room. This mental viewing covers all the flow design and evolution phenomena, animate and inanimate, because they all morph to enter and to flow better, more easily, while the flow space is constrained. This is why “finite-size” is mentioned in the statement of the constructal law (Section 1). See also the comments on flow resistance, at the end of Section 3.

If the reader has a particular flow system in mind, say, air flow in lungs or electricity in lightning, then the reader can express the evolutionary design toward easier access in terms of locally appropriate variables and units. Yet, the fluid flow terminology of the lungs has no place in the analysis of the

flow of electricity as a lightning tree, and vice versa. What is the same in both examples is the first principle: the evolution of design toward easier access, through changes in flow configuration in a finite-size system.

CONSTRUCTAL THERMODYNAMICS: PHYSICS AND BIOLOGY

The constructal law is universally valid, as physics, precisely because it is not a statement of optimality and final design [all the optimization statements have failed: see again (i) – (xii) in Section 1]. A new law does not have to be stated in mathematical terms (e.g., thermodynamic variables, units). For example, the second law of thermodynamics was stated in words, as a mental viewing, not as a mathematical formula (see the Clausius and Kelvin statements). The mathematization of the second law statement (and of thermodynamics) came later. The same evolution occurred in constructal theory. The 1996 statement of the constructal law was followed in 2004 by a complete mathematical formulation of *constructal-law thermodynamics* [37], Fig. 4.

The constructal law is a contribution to physics and evolutionary biology because it simplifies and clarifies the terminology that is in use, and because it unifies it with the biology-inspired terminology that is in use in many other fields such as geophysics, economics, technology, education and science, books and libraries [38]. This unifying power is both useful and potentially controversial because it runs against current dogma.

For example, the constructal designs of the river basin, the tree distribution in the forest, the animal distribution and “animal flow” on the landscape, and all the other “few large and many small” designs such as the food chain, demography and transportation are viewed as *whole* architectures in which what matters is the better and better flow over the global system. In all such architectures, the few large and many small flow together. They collaborate, adjust, and collaborate again toward a better flowing whole, which is better for each subsystem of the whole. This holistic view of design phenomena represents two new steps:

First, the concept of “better” is defined in physics terms, along with direction, design and evolution (cf. the constructal law). In biology, this step unveils the concept of random events and mutations (“changes”, from this to that, from here to there) as a *mechanism* akin to river bed erosion, periodic food scarcity, plagues, scientific discovery, etc., which make possible running sequences of changes that are recognized widely as evolution. This step places in physics the biology

terms of natural selection, freedom to change and adapt, survival, and the idea that *there are* better designs.

Second, the constructal view of design and evolution runs against the negative tone of biology-inspired terms that have invaded the scientific landscape, for example, winners and losers, zero sum game, competition, hierarchy, food chain, limits to growth, etc. No, in the big picture, the few large and many small evolve together, in order to survive and to be able to move more mass on the landscape together. The few large do not and cannot eliminate the many small. Their balanced multiscale design gets better and better, for the benefit of the whole flowing system. Contrary to this apparent conflict with standard interpretations of evolutionary biology, what is “good” in biology is good in constructal theory and all the domains of design science that the constructal law covers.

The constructal law is predictive, not descriptive. This is the big difference between the constructal law and other views of design in nature. Previous attempts to explain design in nature are based on empiricism: observing first, and explaining after. They are backward looking, static, descriptive and at best explanatory. They are not predictive theories even though some are called “theory”, e.g., complexity theory, network theory, chaos theory, power laws (allometric scaling rules), “general models”, and optimality statements (minimum, maximum, optimum).

With the constructal law, complexity and scaling rules are discovered, not observed. Complexity is finite (modest), and is part of the description of the constructal design that emerges. If the flows are between points and areas or volumes, the constructal designs that are discovered are tree-shaped networks. The “networks” are discovered, not observed, and not postulated. Networks, scaling rules and complexity are part of the description of the world of constructal design that emerges predictively from the constructal law.

Constructal “theory” is not the same as constructal “law”. Constructal *theory* is the view that the constructal *law* is correct and reliable in a predictive sense in a particular flow system. For example, reliance on the constructal law to predict the evolving architecture of the snowflake is the constructal theory of rapid solidification. Using the constructal law to predict the architecture of the lung and the rhythm of inhaling and exhaling is the constructal theory of respiration.

The law is one, and the theories are many—as many as the phenomena that the thinker wishes to predict by invoking the law.

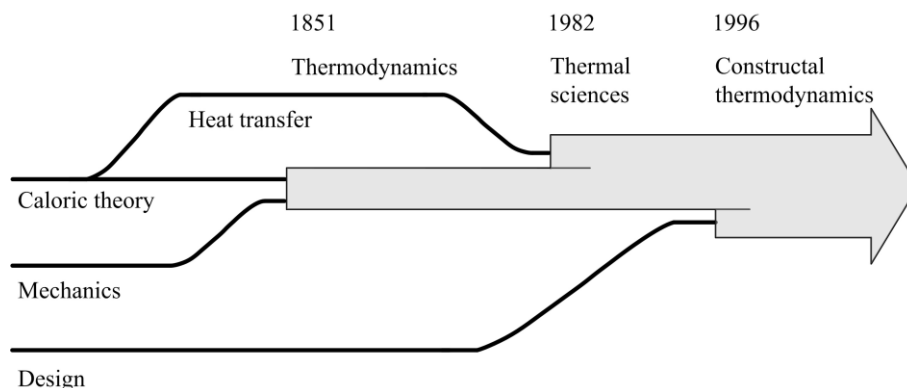


Figure 4 The evolution and spreading of thermodynamics during the past two centuries (after Ref. 2, Diagram 1, p. viii).

REFERENCES

- [1] A. Bejan, *Advanced Engineering Thermodynamics*. 2nd ed., Wiley, New York, 1997.
- [2] A. Bejan, *Entropy Generation Through Heat and Fluid Flow*, Wiley, New York, 1982.
- [3] A. Bejan, *Entropy Generation Minimization*, CRC Press, Boca Raton, 1996.
- [4] A. Bejan, Constructal-theory network of conducting paths for cooling a heat generating volume, *Int. J. Heat Mass Transfer*, vol. 40, pp. 799-816, 1997 (published on 1 Nov. 1996).
- [5] A. Bejan and S. Lorente, Constructal theory of generation of configuration in nature and engineering, *J. Appl. Phys.*, vol. 100, pp. 041301, 2006.
- [6] A. H. Reis, Constructal theory: from engineering to physics, and how flow systems develop shape and structure, *Appl. Mech. Rev.*, vol. 59, pp. 269-282, 2006.
- [7] A. Kremer-Marietti and J. Dhombres, *L'Épistémologie*, Ellipses, Paris, 2006.
- [8] A. Bejan and G. W. Merks, Eds, *Constructal Theory of Social Dynamics* New York: Springer; 2007.
- [9] P. Kalason, *Le Grimoire des Rois: Théorie Constructale du Changement*, L'Harmattan, Paris, 2007.
- [10] P. Kalason, *Épistémologie Constructale du Lien Culturel*, L'Harmattan, Paris, 2007.
- [11] A. Bejan and S. Lorente, *Design with Constructal Theory*, Wiley, Hoboken, 2008.
- [12] D. Queiros-Conde and M. Feidt, Eds., *Constructal Theory and Multi-scale Geometries: Theory and Applications in Energetics, Chemical Engineering and Materials* (Les Presses de L'ENSTA, Paris, 2009).
- [13] L. Rocha, *Convection in Channels and Porous Media. Analysis, Optimization, and Constructal Design*, VDM Verlag, Saarbrücken, 2009.
- [14] A. Bejan, S. Lorente, A. F. Miguel and A. H. Reis, Eds. *Constructal Human Dynamics, Security and Sustainability*. Amsterdam: IOS Press; 2009.
- [15] G. Lorenzini, S. Moretti and A. Conti, *Fin Shape Optimization Using Bejan's Constructal Theory*, Morgan & Claypool Publishers, San Francisco, 2011.
- [16] A. Bachta, J. Dhombres and A. Kremer-Marietti, *Trois Études sur la Loi Constructale d'Adrian Bejan*, L'Harmattan, Paris, 2008.
- [17] A. Bejan and J. P. Zane, *Design in Nature. How the Constructal Law Governs Evolution in Biology, Physics, Technology, and Social Organization*, Doubleday, New York, 2012.
- [18] N. Acuña, *Mindshare. Igniting Creativity and Innovation Through Design Intelligence* (Motion, Henderson, Nevada 2012).
- [19] L. A. O. Rocha, S. Lorente and A. Bejan, *Constructal Law and the Unifying Principle of Design*, Springer, New York, 2012.
- [20] A. Bejan, Why the bigger live longer and travel farther: animals, vehicles, rivers and the wind. *Nature Scientific Reports*, vol. 2, pp. 594, DOI: 10.1038/srep00598, 2012.
- [21] A. Bejan and S. Lorente, The constructal law of design and evolution: physics, biology, technology and society. *J. Appl. Phys.*, vol. 113, 151301, 2013.
- [22] A. Bejan, *Shape and Structure, from Engineering to Nature*, Cambridge University Press, Cambridge, UK, 2000.
- [23] A. Bejan and J. H. Marden, Unifying constructal theory for scale effects in running, swimming and flying. *J. Exp. Biol.* vol. 209, pp. 238-248, 2006.
- [24] J. D. Charles and A. Bejan, The evolution of speed, size and shape in modern athletics. *J. Exp. Biol.*, vol. 212, pp. 2419-2425, 2009.
- [25] A. Bejan, The constructal-law origin of the wheel, size, and skeleton in animal design, *Am. J. Phys.* vol. 78, pp. 692-699, 2010.
- [26] A. Bejan, *Advanced Engineering Thermodynamics*, 3rd ed., Wiley, Hoboken, 2006.
- [27] A. Bejan and S. Lorente, Thermodynamic optimization of flow geometry in mechanical and civil engineering, *J. Non-Equilib. Thermodyn.*, vol. 26, pp. 305-354, 2001.
- [28] C. H. Lui, N. K. Fong, S. Lorente, A. Bejan and W. K. Chow, Constructal design for pedestrian movement in living spaces: Evacuation configurations, *J. Appl. Phys.* vol. 111, 054903, 2012.
- [29] C. H. Lui, N. K. Fong, S. Lorente, A. Bejan and W. K. Chow, Constructal design of pedestrian evacuation from an area, *J. Appl. Phys.* vol. 113, 034904, 2013.
- [30] S. Lorente and A. Bejan, Few large and many small: hierarchy in movement on Earth, *Int. J. Design & Nature Ecodyn.*, vol. 5, pp. 254-267, 2010.
- [31] A. Bejan and S. Lorente, The constructal law and the evolution of design in nature, *Phys. Life Reviews*, vol. 8, pp. 209-240, 2011.
- [32] A. Bejan, The golden ratio predicted: Vision, cognition and locomotion as a single design in nature, *Int. J. Design & Nature Ecodyn.*, vol. 4, pp. 97-104, 2009.
- [33] A. Bejan and S. Lorente, The constructal law origin of the logistics S curve, *J. Appl. Phys.*, vol. 110, 024901, 2011.
- [34] E. Cetkin, S. Lorente and A. Bejan, The steepest S curve of spreading and collecting: discovering the invading tree, not assuming it, *J. Appl. Phys.*, vol. 111, 114903, 2012.
- [35] A. Bejan and S. Lorente, The physics of spreading ideas. *Int. J. Heat Mass Transfer*, vol. 55, pp. 802-807, 2012.
- [36] A. Bejan, S. Lorente, J. Lee, Unifying constructal theory of tree roots, canopies and forests, *J. Theor. Biol.*, vol. 254, pp. 529-540, 2008.
- [37] A. Bejan and S. Lorente, The constructal law and the thermodynamics of flow systems with configuration, *Int. J. Heat Mass Transfer*, vol. 47, pp. 3203-3214, 2004.
- [38] A. Bejan, Science and technology as evolving flow architectures, *Int. J. Energy Res.*, vol. 33, pp. 112-125, 2009.

THERMODYNAMICS AND THE OPTIMISATION OF ENERGY SYSTEMS: STRENGTHS AND LIMITS

Daniel Favrat*

*Ecole Polytechnique Federale de Lausanne, EPFL, Station 9, CH1015 Lausanne

ABSTRACT

The Second Law of thermodynamics is known to be an essential guide for the improvement of energy conversion systems. Throughout the years it has been applied to various engineering methods in particular in methods based on exergy [1] including the 2nd Law, thermoeconomics and exergoeconomics. It has also been used in graphically attractive energy integration techniques such as pinch technology and its derivatives. Apart from economic considerations, the emissions and the overall life cycle impacts have become of growing importance, exceeding the scope of pure thermodynamics. The latter point is related to the fact that there is no direct link between the entropy of local pollutants and their impacts on health. An appropriate combination between thermodynamics and advanced optimisation techniques allows to overcome the inherent limits of thermodynamic approaches and provides meaningful results on real systems. Examples of thermoeconomic, extended exergy analysis and environomic optimisation problems including Life cycle considerations are also considered. Drying processes, power plants, fuel cell systems and storage systems are dealt with.

INTRODUCTION

Energy systems play a crucial role in the development of our societies, by providing some of the essential services, going from electricity generation to comfort conditioning and transport. Gradual awareness of the global environmental impacts, and concerns for resources with the fast growing world population reinforce the need for increased efficiency and cleaner systems. This can be achieved not only by improving individual processes but also by an increased use of systems integrating several complementary technologies and simultaneously providing several different services. Combined cycles, energy integration as well as co- or tri-generation or post-treatment have become fairly common terms. Furthermore the optimisation of these complex systems during the operation is often not sufficient anymore and life cycle analysis, including the fabrication and the dismantling or the recycling of components, is more and more requested. The increased number of parameters and constraints exceed the human capabilities if the significant potential of modern information technology is not better exploited. Thermodynamics as the key engineering science, in this highly technological energy era, is to account for this development in order to contribute to more sustainable energy solutions.

ENTROPY AND EXERGY IN A LIFE CYCLE PERSPECTIVE

Basic approaches

From the early major contributions of the 19th century key players like Carnot, Clausius and later Gouy, the quest to reduce the entropy creation in energy conversion systems has been a constant concern. Accounting for the physical

environment in which these systems are embedded has been further acknowledged by the development of the exergy theory in its various forms. Bejan [1] and Reistad et al. [2] emphasized the need for a trade-off between the irreversibilities of heat transfer, friction and, for the latter, of the embedded energy of components like heat exchangers in particular. This was later illustrated by Staine [3] for the case of shell-in-tube heat exchangers as can be seen in Fig 1. In this case the designer is faced with the option of increasing the heat exchange area and to distribute the heat exchange area so as to reduce the pressure drop for a given duty.

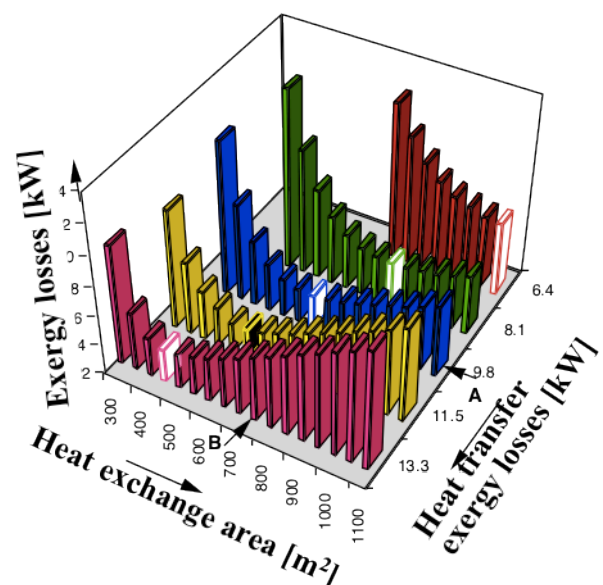


Fig.1 Extended exergy optimisation of a heat exchanger

The black block of the second row of Fig. 1 corresponds with the minimum of the overall exergy losses. This can then

be applied to all heat exchangers of an integrated energy system.

Linnhof et al. [4] simplified the 2nd Law practical application to account for economic factors by developing clever graphical representations and systematic rules for the energy targeting and design of integrated industrial processes. The so-called pinch technology, often wrongly opposed to exergy or mathematical programming approaches, did bring efficient tools to the engineers. An example of composites applied to a plaster panel drying process is shown in Fig. 2.

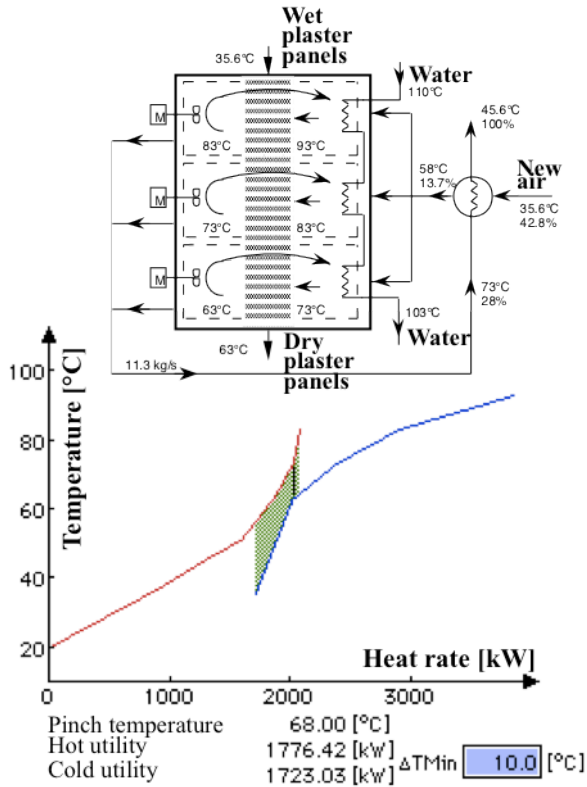


Fig. 2 Composites of a plaster drying process [3, 5]

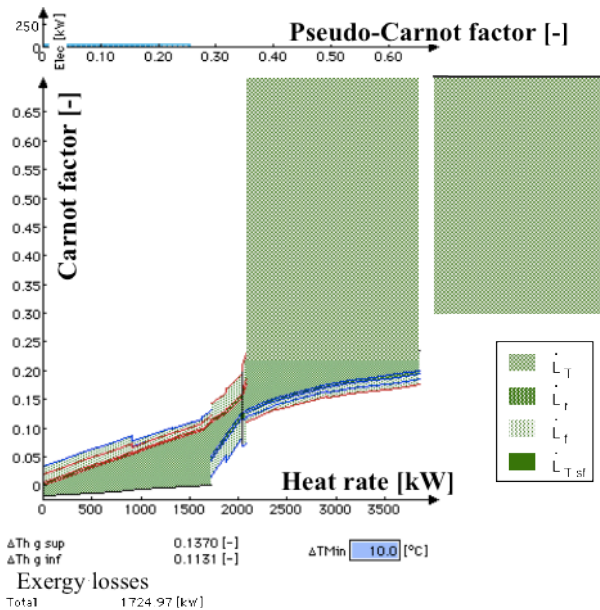


Fig. 3 Extended composite representation including the 3 main exergy losses (heat transfer T, friction r, fabrication f and heat transfer to the cold utility T_{st})

Staine [3, 6] proposed an extension of the latter to simultaneously consider the three main irreversibilities (heat transfer, friction and fabrication losses) as shown in Fig. 3.

He also introduced a formalism and a graphical representation highlighting the electrical balance of the process or site considered. Fabrication losses can be expressed in terms of power (Watts) by using the ratio of the total embedded energy divided by the expected lifetime of the equipment. This method allows to approach the thermodynamic optimum. In this representation the total area of the coloured zones is proportional to the exergy losses.

Fig. 2 and Fig. 3 show the composites corresponding to the present situation with a gas boiler satisfying the heating energy needs for drying. As can be observed there is little overlap of the curves, so the potential for energy recovery within the process is minimal. In Fig. 3 the coloured areas are increased compared to Fig. 2 since they include the exergy losses of the gas boiler that were not shown in Fig. 2. Moreover the topping diagram illustrates the electricity consumption of the auxiliaries (fan, pump) and the corresponding exergy losses. In this representation the pseudo Carnot factor is adapted so that the coloured areas represent those losses.

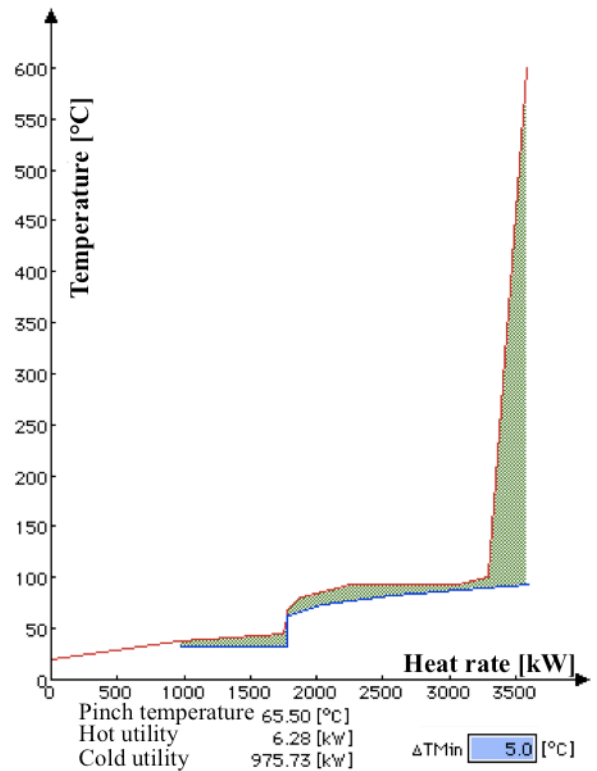


Fig. 4 Composites of the plaster drying process retrofitted with a heat pump and a gas cogeneration engine.

Fig. 4 and Fig. 5 show the result of the proposed retrofit consisting of replacing the boiler by a cogeneration gas engine and an industrial heat pump. As shown by the coloured areas of Fig. 5, the exergy losses of the retrofitted system could be reduced by 40%. The topping diagram of Fig. 5 shows the increased electricity consumption of the electrical heat pump with its corresponding area of exergy losses. The right part beyond a pseudo-Carnot of 1 represents the exergy losses of the gas engine. The empty box on the left of a pseudo-Carnot of 1 indicates the power supplied by the engine, which balances the electrical needs of the plant.

The power of this thermodynamic approach, which accounts for the exergy of fabrication, is its capability to identify a meaningful lower bound of the optimum pinch. This lower bound is more realistic than the bound, which would result from an ideal reversible approach. Taking into account the embedded exergy is not entirely sufficient and the economic optimised solution accounting for all factors such as transport, marketing cost and so on, will be different. However, the thermodynamic optimum, including the embedded exergy, is more robust in function of time, since it does not depend on the variable economic conditions. With that approach the decision maker has a narrower range of optima. He knows that, in case of an increase of energy costs, the real optimum will move closer to the thermodynamic one.

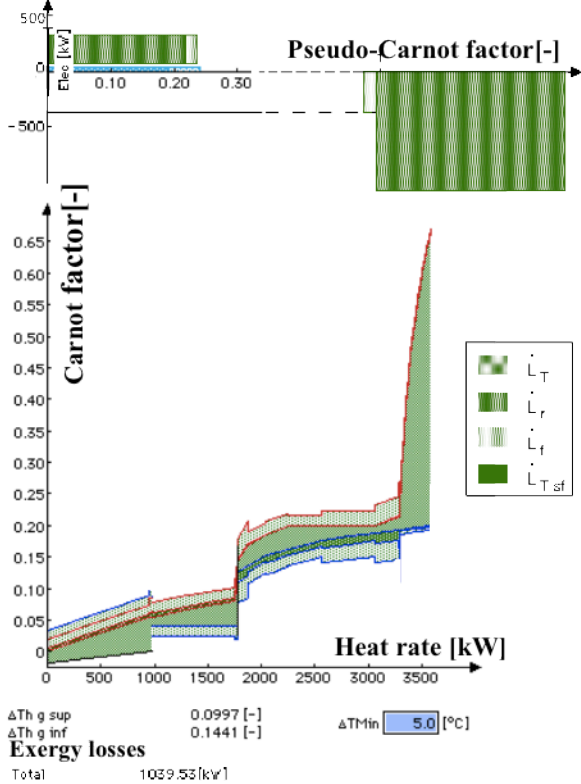


Fig. 5 Extended composite view of the drying process retrofitted with a heat pump and a cogeneration engine

The embedded exergy is becoming more important when analysing the true potential of many concepts proposed recently to recover the exergy of waste heat. Some of these concepts claim the possibility to recover energy from streams with temperature differences as low as a few tens of °C. This remark is related in particular to thermoelectric devices, or to osmotic concepts not based on natural fluids.

The power of thermodynamics should also be used to clearly rank future energy conversion paths, as shown by Agrawal and Singh [7] for the conversion from solar energy to biofuels.

Emissions and their impacts are more difficult to account for by thermodynamics alone. While there usually is a direct link between efficiency and global warming emissions for fossil based systems, it is less obvious for local pollutants. This is due to the fact that there is no direct link between the entropy of a substance, like NO_x, and the effects that these pollutants have on health. Moreover the existing level of the local pollution at a given implementation site has a role to play on the conditions imposed on the implementation of new energy systems. This can be accounted for by pollution

factors as proposed by Curti [8]. However, such local pollution factors cannot be visualized in a thermodynamic diagram such as the extended composite diagram. Therefore optimisation tools have to come into play.

Many attempts have been made to apply gradient based linear mixed integer algorithm to complex integrated energy systems, including economic and environmental factors as shown, for example, in the papers of von Spakovsky [9] and Valero et al. [10]. For solution spaces highly non linear and potentially non contiguous, such approaches had difficulties to identify and distinguish the global optimum from the local optima. Fortunately progress made in the late 90ies in the so-called non deterministic approaches, like those based on genetic algorithms, did provide a significant step forward to deal with these problems. Moreover, the gradual availability of cheap clusters of processors reinforced the possibilities of treating large integrated system problems. It became possible to do it without having to rely on the decomposition in sub-problems, with the associated difficulties of energy or exergy costing in order to keep the coherence of the system. Thermodynamics had reached limits, which progresses in information technology helped to bypass. The results from superstructure based mono-objective optimisation like used by Curti et al.[8], or Pelster et al. [11] demonstrated the power of these combined approaches for district heating as well as for power plants with or without CO₂ separation. Olsommer et al. [12] extended the scope by also including reliability factors with the passive and/or active redundancy that often have to be accounted for in real projects. For these studies, thermodynamics, including pinch analysis, was still a vital tool. But it was used, at first to build a coherent superstructure, and lateron for the interpretation of the results. Some genetic algorithms proved to be so powerful that no complex decomposition was needed anymore. Cost functions, which could also deal with the step functions of a library of real component of different scale could be used.

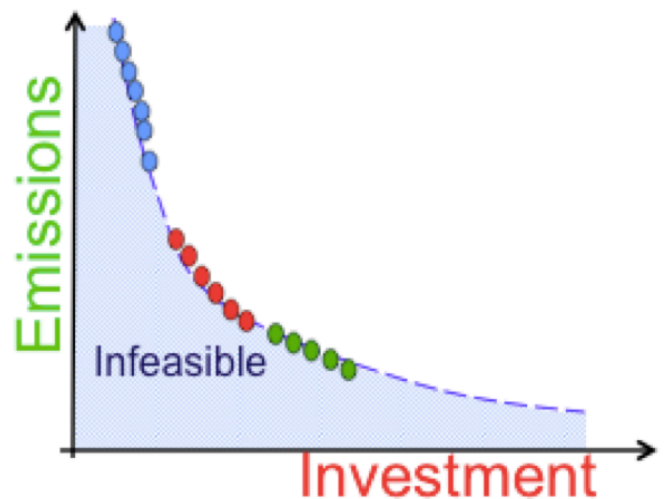


Fig. 6 Concept of Pareto curves applied to energy systems (the dotted points correspond to optimal solutions)

Mono-objective optimisation with genetic algorithm was a lengthy and inefficient process. This was corrected by the emergence of multi-objective algorithm of practical relevance for the engineering of energy systems, such as the algorithm QMOO briefly described in Molyneaux et al. [13]. Knowledge gained during the computer search is kept and the results can be expressed by the optima distributed along a

Pareto curve in function of two main decision parameters, like efficiency and costs. The thermodynamicist is then better equipped to discuss the relevant trade-offs with the stakeholders.

Another way to structure the information, essentially for a faster numerical treatment, is to work with pre-optimised functions of technologies by using the concept of performance typification of those technologies that can be considered in a superstructure. This was illustrated by Li et al. [14,15] in examples of power plants, with or without cogeneration. Thus the knowledge of the purely thermodynamic performances that do not depend on economics, could be saved without repeating the calculation for each change of economic conditions.

Multi-objective optimisation was also applied by Pelet et al. [16] and coupled with a LCA data basis to optimize the retrofit of the energy system of a remote community. Here again thermodynamics was used to better define the superstructure of the integrated system including Diesel generators, Organic Rankine Cycles with thermal storage, solar thermal or Photovoltaic panels.

Accounting for reactive phenomena

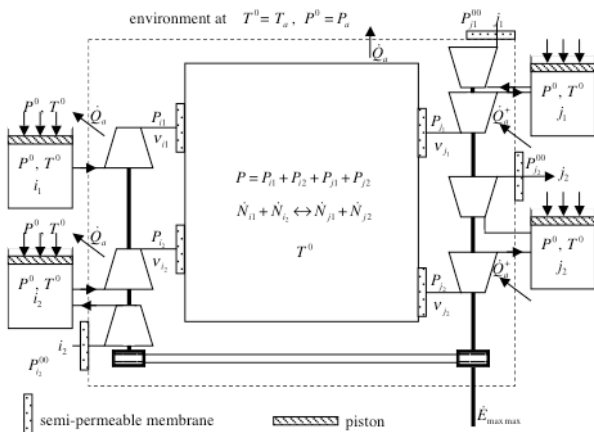


Fig. 7 Representation of the irreversible oxidation using a van't Hoff box and a mechanistic model [17]

Present energy conversion from fuel is mainly done through reactive phenomena with quasi-complete oxidation, like in the boilers or combustion chambers of power plants or of engines, without CO₂ separation. Among new concepts aiming at efficiency improvement let us cite the partial oxidation (gasification) and/or the electrochemical conversion that take place in fuel cells. CO₂ separation can be reached by either conditioning the combustible mixture directly upstream, or in the system through mass transfer in a membrane, or downstream in the tail pipe through sorption techniques. In such cases, a proper account of the exergy terms is essential to be able to define appropriate performance factors.

The representation of the reversible combustion using the van't Hoff box and turbomachines, as shown in Borel and Favrat [17], is useful (Fig. 7). Thanks to the specific semi-permeable membranes, both the components of the reactive mixture and of the oxidation products can be separated. Small changes on one side of the box could induce the change of direction of the flows, hence the reversible feature of this setup made for one fuel and one oxidizer and resulting in two products.

One additional compressor illustrates the diffusion exergy involved in the uptake of oxygen diluted in the atmosphere. Two additional turbines (or expanders), one for each oxidation product, illustrate the diffusion exergy, which could be recovered by expanding the gases to the same partial pressure they have in the atmosphere.

The cartoon representation of Fig. 8 illustrates the exergy pit showing the specific coenergy ($j = u + P_a v - T_a s$) of substances. The thermo-mechanical equilibrium dead state relative to the environment (P_a, T_a) is shown at the bottom of the pit. The physico-chemical equilibrium with the environment is represented by the lower sub-pits (physico-chemical dead states) corresponding to each of the oxidation products (here CO₂ and H₂O). Some of the different technologies for house heating are represented as well and the small characters represent the units of mass. The significant drop of exergy level of the direct electrical heating or of the simple boiler heating are clearly shown. Cogeneration and electrical heat pumps are also represented. These various representations are useful, in particular for the education of students, but also as a reminder for engineers in the practice, who too often consider exergy with scepticism.

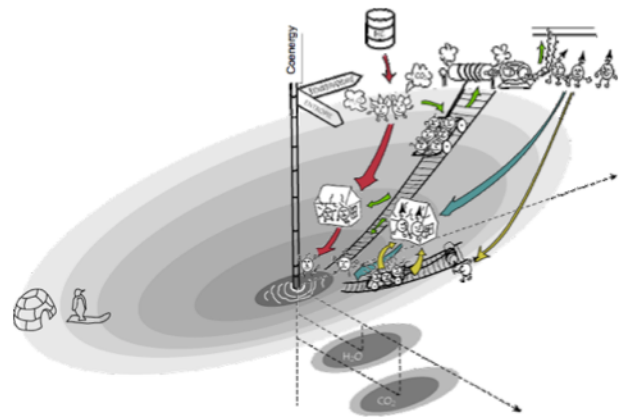


Fig. 8 Schematic representation of the exergy pit with the illustration of some technologies for heating

ANALYSIS OF ADVANCED ENERGY CONVERSION SYSTEMS

Trying to stay in the upper part of the exergy pit is partly made possible by direct electricity conversion using electrochemical phenomena. The solid oxide fuel cell (SOFC) is a good example since the solid electrolyte is also inherently a separator of the oxygen and nitrogen from the air. This feature is fully exploited in the concept developed by Facchinetti et al. [18] in which CO₂ is finally separated without exergy penalty.

The so-called SOFC-GT hybrid cycle used couples an atmospheric pressure SOFC with a sub-atmospheric Brayton cycle in which the water vapor is condensed at the lower pressure level (Fig. 9). This allows not only a lower compressor power for the compressor of the Brayton cycle, but also an easy separation of the CO₂. In such a concept, energy integration with optimized heat exchangers is a key to reaching electrical efficiencies in decentralized plants higher than 70%, which is higher than those of centralized power plants. In such a case the definition of the effectiveness (First Law efficiency) is not obvious when pure O₂ is supplied to the burner to facilitate CO₂ separation. In Equation (1) we propose a hybrid approach where the exergy of diffusion of

oxygen in air is added to the denominator instead of trying to introduce an effectiveness of separation in the sense of the First Law.

$$\varepsilon = \frac{\dot{E}_{FC}^- + \dot{E}_{GT}^-}{\dot{M}_F^+ \Delta h_i^0 + \dot{M}_{O_2}^+ e_{dO_2}^0} \quad (1)$$

The definition of the exergy efficiency is more straightforward as follows:

$$\eta = \frac{\dot{E}_{FC}^- + \dot{E}_{GT}^- + \dot{M}_{CO_2}^- e_{dCO_2}^0}{\dot{M}_F^+ \Delta h_i^0 + \dot{M}_{O_2}^+ e_{dO_2}^0} \quad (2)$$

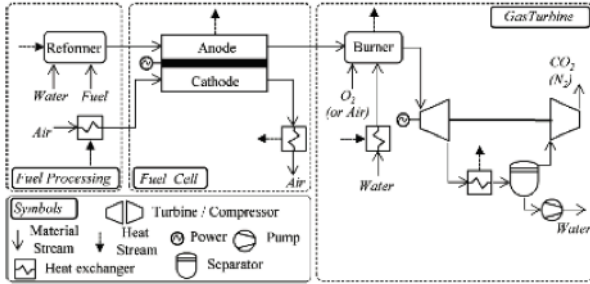


Fig.9 Concept of hybrid SOFC-GT with CO₂ separation [18]

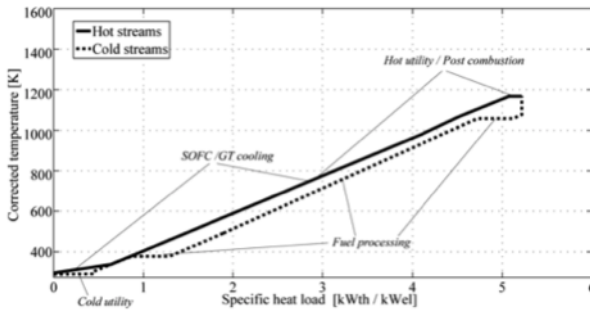


Fig.10 Composite curves corresponding to the integration of a hybrid SOF-GT unit

Energy storage

Thermodynamics is important for evaluating and optimising energy storage systems. Powertrains of vehicles concepts, including compressed air or liquid nitrogen, have been explored in recent years. Often, thermodynamics, and in particular exergy analysis, allows to quickly evaluate the potential from these forms of storage, independently from the details of the mechanical device or thermodynamic cycles used. The difference between the coenergy of the fluid contained in the tanks and the coenergy of the environment (atmosphere) gives an indication of the maximum work, which can be extracted by the drivetrains. Using this criterion Iglesias et al. [20] compare, on an exergy basis, different drive trains and storage systems. They show how difficult and challenging it is to meet some of the claims of autonomy of compressed air or liquid nitrogen cars. However, the global picture, when comparing with standard gasoline or Diesel vehicles, should include the emissions. Then, the so-called environomic optimisation for given duties should be made using advanced algorithm.

Stationary electricity storage systems are more and more needed with the growth of wind and solar power. This application is less demanding in terms of power density and weight. Compressed air storage, often coupled with thermal storage or fossil fuel use, can be considered and have been analysed by Kim et al. [21]. The same paper also compares these concepts with concepts using thermodynamic cycles

that can be operated in power mode when electricity is needed and in heat pump mode when cheap or excess electricity needs to be stored. Once again, detailed thermoeconomic optimisation for superstructure defined by thermodynamics, allows the identification of better designs as shown by Morandin et al. [22].

CONCLUSION

Thermodynamics is essential for the design and the operation of more sustainable systems. However, it is important to realize its limitations. The recent advent of powerful MINLP optimisation algorithms based on evolutionary algorithm provides the necessary complement to tackle the more holistic considerations needed for modern energy systems. The main challenge is to combine detailed thermodynamic models of processes with full system integration.

NOMENCLATURE

Symbol	Quantity	SI Unit
\dot{E}^-	Exiting exergy rate (mechanical or electrical power)	W
e	Specific exergy	J/kg
J	Coenergy (exergy of a substance)	J
j	Specific coenergy	J/kg
\dot{M}^-	Exiting mass flow rate	kg/s
\dot{M}^+	Entering mass flow rate	kg/s
Δh_i^0	Lower heating value	J/kg _F
Δk^0	Exergy value	J/kg _F
GT	Gas turbine	
$SOFC$	Solid Oxide Fuel Cell	

REFERENCES

- [1] A. Bejan, Thermodynamics of heat transfer devices, *Proc. Of the IVth Int. Symposium on the 2nd Law analysis of thermal systems*, pp. 1-15, ASME, 1987.
- [2] S. Aceves-Saborio, J. Ranasinghe, GM. Reistadt, An extension to the irreversibility minimization analysis applied to heat exchangers, *J. of heat transfer*, vol. 111 (2), pp. 29-36, 1989.
- [3] F. Staine, Intégration énergétique des procédés industriels par la méthode du pincement étendue aux facteurs exergétiques, EPFL Thesis no 1318, Lausanne, Switzerland, 1994.
- [4] B. Linnhof et al., A user guide on process integration for the efficient use of energy, Institution of Chemical Engineers, England, 1982
- [5] F. Staine, D. Favrat, Evaluation des économies d'énergie par la méthode du pincement dans une usine de fabrication de panneaux de plâtre, *Entropie*, vol.27, pp.164-165, 1991

- [6] F. Staine and D. Favrat, Energy integration of industrial processes based on pinch technology extended to include exergy factors, *J. of applied thermal engineering*, vol. 16, pp. 497-507, 1996.
- [7] R. Agrawal and N.R. Singh, Solar energy to biofuels, *Annu. Rev. Chem. Biomol. Eng.*, vol. 1, pp. 343-364, 2010.
- [8] V. Curti, MR. von Spakovsky and D. Favrat, An environomic approach for the modeling and optimisation of a district heating network based on centralized and decentralized heat pumps, cogeneration and/or gas furnace, *Int. J of Thermal Sciences*, vol. 39 (7), pp. , 2000.
- [9] MR. von Spakovsky, Application of functional analysis to the analysis and optimisation of the CGAM problem, *Energy*, vol 19(3),pp343-364,1994
- [10] A.Valero, MA Lozano et al, CGAM problem-Definition and conventional solution, *Energy*, vol.19 (3), pp 279-286,1994.
- [11] S. Pelster, MR.von Spakovsky, and D. Favrat, The thermodynamic and environomic modeling and optimisation of the synthesis, design and operation of combined cycles with advanced options, *Int.J. of Applied Thermodynamics*, vol. 2 (4), pp. , 1999.
- [12] B. Olsommer, MR. von Spakovsky, and D. Favrat, An approach for the Time-dependent Thermoeconomic Modeling and Optimisation of energy system Synthesis, Design and Operation (Part II: Reliability and Availability), *J. of Engineering for Gas Turbine and Power*, vol. 123 (4), pp. 717-726, 2001.
- [13] A. Molyneaux, G. Leyland and D. Favrat, Environomic Multi-Objective Optimisation of a District Heating Network considering Centralized and Decentralized heat pumps, *Energy*, vol. 35 (2), pp. 751-758, 2010.
- [14] HT. Li, F. Marechal and D. Favrat, Power and Cogeneration Environomic Performance Technology Typification in the context of CO₂ abatement (Part 1: Power generation), *Energy*, vol 35 (8),pp 3143-3154,2010
- [15] HT. Li, F. Marechal and D. Favrat, Power and Cogeneration Environomic Performance Technology Typification in the context of CO₂ abatement (Part II: Combined Heat and Power cogeneration), *Energy*, vol 35 (9), pp 3517-3123, 2010
- [16] X. Pelet, D. Favrat and G. Leyland, Multi-objective optimisation of integrated energy systems for remote communities considering economics and CO₂ emissions, *Int. J. of thermal sciences*, vol. 44 (12), pp. 1180-1189, 2005.
- [17] L. Borel and D. Favrat, Thermodynamics and energy systems analysis, EPFL Press, Lausanne, Switzerland, 2010.
- [18] E. Facchinetti, Integrated Solid Oxide Fuel Cell-Gas Turbine Hybrid System with or without CO₂ Separation, *EPFL thesis 5323*, Lausanne, 2012
- [19] E. Facchinetti, M. Gassner, M. D'Amelio, F. Marechal, and D. Favrat, Process integration and optimisation of a solid oxide fuel cell-gas turbine hybrid cycle fuelled with hydrothermally gasified waste biomass, *Energy*, vol. 41 (1), pp. 408-419, 2012.
- [20] A. Iglesias and D. Favrat, Comparative exergy analysis of compressed, liquid nitrogen and classical thermal power cycles for urban vehicles, *Proc. of ECOS 2013*, Guilin, China, 2013.
- [21] YM. Kim, DG. Shin, SY. Li and D. Favrat, Potential and evolution of compressed air energy storage: Energy and exergy analyses, *Energy*, vol. 49 (1), pp. 484-501, 2013.
- [22] M. Morandin, F. Marechal, M. Mercangöz and F. Buchter, Conceptual design of a thermo-electrical energy storage system based on heat integration of thermodynamic cycles, *Energy*, vol. 45 (1), pp. 375-385, 2012.

DOES MINIMUM ENTROPY GENERATION RATE CORRESPOND TO MAXIMUM POWER OR OTHER OBJECTIVES ?

FEIDT Michel

Professeur, Université de Lorraine – LEMTA 2, avenue de la Forêt de Haye, TSA 60604, 54518
VANDOEUVRE Cedex, France

ABSTRACT

In a recent book, A. Bejan has reconsidered the important problem of maximization of power with heat engine models associated to heat transfer irreversibilities (endoreversible models).

He explains that for these models maximum power is equivalent to minimum entropy generation rate (corresponding to Gouy-Stodola theorem). He also stresses that the method is well known in the engineering literature [4], if new one for physicist [5, 6, 7]. More precisely, he points out, that in these last papers [5, 6, 7], maximum power and minimum entropy generation rate are two distinct optimization criteria for power plants.

An example was given in [2] for coincidence of these two objectives. We propose here to reconsider these two approaches and try to enlighten on simple Chambadal power plant model, but irreversible one, the conditions of equivalence between the two objectives, maximum of power, and minimum of entropy generation.

Influence of various system configurations are analyzed. Consequences are discussed, and generalization of the proposed method allows to clarify the subject and to precise the equivalence conditions or not regarding other important objectives.

1 INTRODUCTION

Since the eighties, optimization of energy systems, mainly engine and reverse cycle machines, has been reconsidered starting with the paper of F. Curzon and L. Ahlborn [1].

In a recent book [2], A. BEJAN has reconsidered the important problem of maximization of power with heat engine models associated to heat transfer irreversibilities (endoreversible models).

He explains that for these models maximum power is equivalent to minimum entropy generation rate (corresponding to GOUY-STODOLA) theorem [3]. He also stresses that the method is well known in the engineering literature [4], if new one for physicist [5, 6, 7].

More precisely he points out, that in these last papers [5, 6, 7], maximum power and minimum entropy generation rate are two distinct optimization criteria for power plants. An example was given in [2] for coincidence of these two objectives.

We propose here to reconsider these two approaches and try to enlighten on simple model of power plants, but irreversible one, the conditions of equivalence between the two objectives, maximum of power, and minimum of entropy generation.

Influence of various system configurations are analyzed. Consequences are discussed, and generalization of the proposed method allows to clarify the subject and to precise the equivalence conditions regarding other important objectives. The results illustrated here from a simple pedagogical point of view, can be completed regarding recent published papers [8 - 10]. Paper [8] is a general review, that can be particularized to reverse cycle machines [9, 10]. Reference [11] reports on the energy and exergy optimization of combined heat and power systems. Reference [12]

considers two examples of Exergy Optimization too including "Thermofrigopump".

The two papers [13, 14] are more fundamental and are related to new upperbounds of what we named Optimal Thermodynamics, as well as on reconsideration of criteria in order to optimize irreversible thermomechanical heat systems.

2 CHAMBADAL MODEL OF POWER PLANT

This model from 1957 is the first one proposed, and it uses a sensible heat source. This source is a finite size one, due to the fact that heat is transferred through an imposed mass flux

\dot{m}_H , with a constant calorific C_{PH} value, so that :

$$\dot{C}_H = \dot{m}_H C_{PH} \quad (1)$$

Regarding figure 1 and the converter, we use thermodynamics convention $\left(\dot{W} < 0 ; \dot{Q}_{HC} > 0 \right)$. The studied case is focused on steady states.

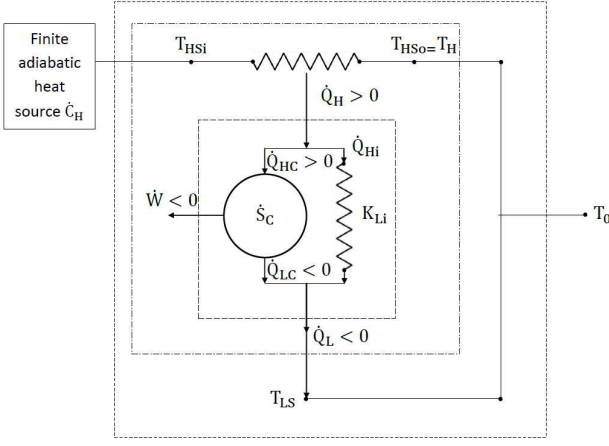


Figure 1. Chambadal power plant model

2.1 Characterization of the converter

The method of heat transfer used for heat exchangers HEX is the (ε, NTU) method, in the reported cases. The proposed model is an extended one of the model reported by A. Bejan [2], but with internal irreversibilities of the converter.

These irreversibilities are mainly represented by the created dissipation rates inside the converter \dot{S}_C . This rate is the sum of all dissipation rates appearing in the converter. For Novikov, it is only related to expander irreversibilities. More generally, the prevailing irreversibilities are related to mechanical losses in the converter (associated to fluid flow and solid friction). For others it is related to heat short circuit between hot and cold side of the converter. If \dot{Q}_{Hi} represents this rate, for a linear law it comes :

$$\dot{Q}_{Hi} = L_{li}(T_H - T_{LS}) \quad (2)$$

The corresponding created entropy rate is :

$$\dot{S}_{Hi} = K_{li} \frac{(T_H - T_{LS})^2}{T_H T_{LS}} \quad (3)$$

It is to be noted that \dot{S}_{Hi} depends on T_H and T_{LS}

The energy and entropy balances of the converter are :

$$\dot{W} + \dot{Q}_{HC} + \dot{Q}_{LC} = 0 \quad (4)$$

$$\frac{\dot{Q}_{HC}}{T_H} + \frac{\dot{Q}_{LC}}{T_{LS}} + \dot{S}_C = 0 \quad (5)$$

$$\text{with } \dot{Q}_{HC} = \dot{Q}_H - \dot{Q}_{Hi} \quad (6)$$

$$\dot{Q}_{LC} = \dot{Q}_L - \dot{Q}_{Hi} \quad (7)$$

Accordingly to Chambadal hypothesis, we suppose perfect heat transfer at the source side such that :

$$\dot{Q}_H = \dot{C}_H (T_{HSi} - T_H) \quad (8)$$

It means that $T_{HS0} = T_H$, $\varepsilon = 1$ (consequently hot side heat transfer area becomes infinite). This equilibrium hypothesis is adopted for simplicity and pedagogical purpose.

Combining (4 to 8) it is easy to get the general relation of the power of the plant to maximize :

$$\text{MAX}(-\dot{W}) = \text{MAX} \left[\left(1 - \frac{T_{LS}}{T_H} \right) \left(\dot{C}_H (T_{SHi} - T_H) - \dot{Q}_{Hi} \right) - T_{LS} \dot{S}_C \right] \quad (9)$$

It is to be precised here that \dot{S}_C could depend on the temperature difference across the converter (as \dot{S}_{Hi} , (3)), so that we note it $\dot{S}_C(T_H)$.

$\text{MAX}(-\dot{W})$ is obtained for a T_H variable value satisfying :

$$\frac{1}{T_H^2} \left(\dot{C}_H T_{LS} T_{HSi} + K_{li} T_{LS}^2 \right) - T_{LS} \frac{\partial \dot{S}_C}{\partial T_H} - \left(\dot{C}_H + K_{li} \right) = 0 \quad (10)$$

The same methodology is applied to the total internal entropy created inside the converter \dot{S}_i , according to :

$$\frac{\dot{Q}_H}{T_H} + \frac{\dot{Q}_L}{T_{LS}} + \dot{S}_i = 0 \quad (11)$$

By combination of (5-7) with (11) it comes :

$$\dot{S}_i = k_{li} (T_H - T_{LS}) \left(\frac{1}{T_{LS}} - \frac{1}{T_H} \right) + \dot{S}_C(T_H) \quad (12)$$

The minimum of \dot{S}_i , $\min(\dot{S}_i)$, must consequently satisfy :

$$K_{li} \left(\frac{1}{T_{LS}} - \frac{T_{LS}}{T_H^2} \right) + \frac{\partial \dot{S}_C}{\partial T_H} = 0 \quad (13)$$

The only physical solution of equation (13) is $T_H = T_{LS}$, and \dot{S}_C constant. It means that the converter does not deliver

power, and \dot{S}_C must be nul. Consequently minimum entropy created in the converter does not provide maximum power, obtained through condition (10).

If \dot{S}_C is a constant (or for the endoreversible case), the following optimal temperature condition T_H^* is obtained regarding the maximum of power :

$$T_H^* = \sqrt{T_{LS} \frac{\dot{C}_H T_{HSi} + K_{li} T_{LS}}{\dot{C}_H + K_{li}}} \quad (14)$$

We retrieve the nice radical, if $K_{li} = 0$

2.2 Characterization of the system

As can be seen on Figure 1, the system consist of the converter, and the hot heat exchanger (boiler in the case of the power plant). The external fluid is the flue gas, whose energy comes from external adiabatic hot heat source (nuclear ; combustion ; solar). The sensible heat of the flue gas is partly transferred to the converter as was indicated before (section 2.1).

The energy and entropy balances of the system are :

$$\dot{W} + \dot{Q}_H + \dot{Q}_L = 0 \quad (15)$$

$$\dot{C}_H \ln \frac{T_{HSi}}{T_H} + \frac{\dot{Q}_L}{T_{LS}} + \dot{S}_S = 0 \quad (16)$$

Relation (15) is identical to relation (4). Equation (5) remains too as a constraint. So $MAX(-\dot{W})$ does not change, nor the first law efficiency (or others) for the system.

Simply the created entropy inside the system comprises now the entropy due to the heat transfer between the source hot fluid and the converter. Combining (5-11) with (16) it comes :

$$\begin{aligned} \dot{S}_S = & \dot{C}_H \left(\frac{T_{HSi} - T_H}{T_H} - \ln \frac{T_{HSi}}{T_H} \right) \\ & + K_{li} (T_H - T_{LS}) \left(\frac{1}{T_{LS}} - \frac{1}{T_H} \right) + \dot{S}_C \end{aligned} \quad (17)$$

$\min(\dot{S}_S)$ is obtained for T_H satisfying :

$$-\frac{\dot{C}_H T_{HSi} + K_{li} T_{LS}}{T_H^2} + \frac{\dot{C}_H}{T_H} + \frac{\partial \dot{S}_C}{\partial T_H} + \frac{K_{li}}{T_{LS}} = 0 \quad (18)$$

This equation differs from (10). Consequently the maximum of power of the system does not correspond to min of entropy generated inside the system.

It is relatively easy to show, that this result is not affected, if we add direct external linear heat loss between the hot source and heat sink of the system.

2.3 Characterization of the system in the environnement

Referring again to Figure 1, and supposing adiabaticity between the finite heat source and the environment, it appears a transiting heat rate \dot{Q}_{H0} such that :

$$\dot{Q}_{H0} = \dot{C}_H (T_H - T_0) \quad (19)$$

This heat rate could be used for combined heat and power (CHP), eventually in organic Rankine Cycle (ORC) or others [12].

It corresponds the following exergy rate :

$$\dot{E}_{x0} = \dot{C}_H \left[(T_H - T_0) - T_0 \ln \frac{T_H}{T_0} \right] \quad (20)$$

Hot fluid as reference.

The energy and entropy balances of the system in the environment becomes from the hot fluid point of view :

$$\dot{W} + \dot{Q}_{HS} + \dot{Q}_{LS} = 0 \quad (21)$$

$$\dot{C}_H \ln \frac{T_{HSi}}{T_0} + \frac{\dot{Q}_{LS}}{T_0} + \dot{S}_0 = 0 \quad (22)$$

$$\text{with } \dot{Q}_{HS} = \dot{Q}_H + \dot{Q}_{H0}$$

$$\dot{Q}_{LS} = \dot{Q}_L - \dot{Q}_{H0}$$

We renew here that if \dot{Q}_{H0} could be valorized, it is the same for \dot{Q}_L , if T_{LS} differs from T_0 . \dot{Q}_{HS} corresponds to the imposed heat rate consumption (constraint related to the fluid mass rate and T_{HSi} , T_0).

The $MAX(-\dot{W})$ is always furnished by the equation corresponding to (10), but the value of the efficiency at maximum power differs, due to change in energy expanses

$$\dot{Q}_{HS}.$$

To simplify, we suppose that T_{LS} is identical to T_0 , the ambient temperature. This hypothesis remains consistent with the Chambadal model of power plant.

Using (5-8, 22) it comes after some calculations the condition for $\min \dot{S}_0$:

$$\begin{aligned} \frac{1}{T_H^2} \left[\dot{C}_H T_0 T_{HSi} + K_{li} T_0^2 \right] - T_0 \frac{\partial \dot{S}_C(T_H)}{\partial T_H} \\ - \left(\dot{C}_H + K_{li} \right) = 0 \end{aligned} \quad (23)$$

This equation is identical to (10) due to the fact that $T_{LS} = T_0$. In that case $MAX(-\dot{W})$ corresponds to $min(\dot{S}_0)$, created entropy rate for the system hot fluid in the environment.

Heat source as reference

The energy and entropy balance of the system in contact with the heat source at T_{Hsi} (thermostat) and the ambient cold sink at $T_{LS} = T_0$ becomes now (21) and (24).

$$\frac{\dot{Q}_{HS}}{T_{Hsi}} + \frac{\dot{Q}_{LS}}{T_0} + \dot{S}_{00} = 0 \quad (24)$$

We have always

$$\dot{Q}_{HS} = \dot{Q}_H + \dot{Q}_{H0}$$

$$\dot{Q}_{LS} = \dot{Q}_L - \dot{Q}_{H0}$$

Using (5-8, 24) it comes after calculations, the condition for $min(\dot{S}_{00})$. We obtain again the equation (23), identical to (10) with $T_{LS} = T_0$. $MAX(-\dot{W})$ corresponds too to $min(\dot{S}_{00})$, created entropy rate between the thermostat T_{Hsi} , necessary to produce the hot fluid, and the environment at T_0 .

3 DISCUSSION AND CONCLUSIONS

This paper has reconsidered the optimizations regarding maximum power of a thermomechanical engine, and minimum entropy generation rate for steady state configurations.

The convenient model of Chambadal power plant has been chosen, but extended, taking particularly account of internal irreversibilities of the converter (Carnot engine).

It has been proved that these internal irreversibilities depend on T_H temperature. An example has been developed regarding heat losses between hot (T_H) and cold (T_{LS}) side of the converter.

3.1 Comparison of $MAX(-\dot{W})$ condition with $min(\dot{S}_i)$, total internal entropy created inside the converter

These two conditions differ. $min(\dot{S}_i)$ occurs for a plant that does not deliver power ($T_H = T_{LS}$).

The maximum power condition leads to T_H^* for the endoreversible converter

$$T_H^* = \sqrt{T_{LS} \frac{\dot{C}_H T_{Hsi} + K_{li} T_{LS}}{\dot{C}_H + K_{li}}}$$

This value gives a generalized form of the nice radical.

3.2 Comparison of $MAX(-\dot{W})$ condition with $min(\dot{S}_S)$, total entropy created within the system

The condition for $min(\dot{S}_S)$ (18) differs from the one corresponding to $MAX(-\dot{W})$ (10), even for endoreversible

system, where $min(\dot{S}_S)$ corresponds to the thermodynamic equilibrium situation ($T_H = T_{Hsi}$).

3.3 Comparison of $MAX(-\dot{W})$ condition with the minimum of total entropy created for the system in the environment

In that case, it appears a transiting heat rate \dot{Q}_{H0} . This heat rate, as the one rejected at the cold sink (\dot{Q}_L at T_{LS}) is supposed degraded, as done by A. Bejan. But in fact, it could be valorized (through CHP system, ORC system or others).

If not, it contributes effectively to entropy generation for both heat fluxes (\dot{Q}_{H0} from T_H , to T_0 ; \dot{Q}_L from T_{LS} , to T_0).

Reported calculations are relative to the common case where T_{LS} equal T_0 .

It has been shown that, whatever is the reference (hot fluid, or heat source), $MAX(-\dot{W})$ is associated to the min of generated entropy rate. It comes for the endoreversible converter, the same relation as in a section (3.1) with $T_{LS} = T_0$.

3.4 Conclusions

Maximization of power, or minimization of entropy generation are equivalent, if we consider the system in his environment. This is confirmation of the Gouy Stodola theorem. But it supposes that all rejected heat are not valuable. This must be reconsidered and is an actual challenge [11, 12].

Regarding the converter and the system in itself, the two objectives are not identical.

If maximization of power is a clear objective function, regarding entropy is not so easy. We have shown here that results differ, if considering entropy of the converter, or system in the environment (including hot fluid, or hot source).

Preceding results obtained in the literature have been precized and extended, clarifying the existing controversy. These results remains to combine, to existing ones [8, 14].

REFERENCES

- [1] F. Curzon, B. Ahlborn, Efficiency of a Carnot Engine at maximum power output, Am. J. Phys., 1, p 22-24, 1975.
- [2] A. Bejan, Entropy Generation Minimization, The method of Thermodynamic Optimization of Finite Size Systems and Finite Time Processes, CRC Press, Boca Raton, USA, 1996.
- [3] M. Gouy, Sur l'énergie Utilisable, J. de Physique, 2ème série, t. VIII, p 501-518, Nov. 1889.
- [4] A. Bejan, Engineering advances on Finite Time Thermodynamics, Am. J. of Phys., 62, p 11-12, 1994.
- [5] P. Salomon, A. Nitzan, Finite Time optimization of a Newton's law Carnot cycle, J. Chem. Phys., 74, p 3546-3560, 1989.
- [6] B. Andresen et al, Thermodynamics in finite time. Phys. Today, Sept., p 62-70, 1984.
- [7] B. Andresen, Finite Time Thermodynamics, in Finite Time Thermodynamics and Thermoconomics, S.

- Sieniutycz and P. Salomon Eds, Taylor and Francis, New York, p 66-94, 1990.
- [8] M. Feidt, Thermodynamics of Energy Systems and Processes : a review and perspectives, *J. of Applied Fluid Mechanics*, vol. 5, n° 2, p 85-98, 2012.
- [9] M. Feidt, Thermodynamics applied to reverse cycle machines, a review, *Int. J. Refrigeration*, 33, p 1327-1342, 2010.
- [10] M. Feidt, Evolution of thermodynamic modelling for 3 and 4 heat reservoirs machines : a review and new trends. *Int. J. of Refrigeration*, 36, p. 8-23, 2013.
- [11] M. Feidt, M. Costea, Energy and Exergy analysis and optimization of Combined Heat and Power Systems. Comparison of various systems, *Energies*, 5, p 3701-3722, 2012.
- [12] M. Feidt, Two examples of Exergy Optimization regarding the "Thermofrigopump" and Combined heat and Power systems, *Entropy*, 15, p 544-558, 2013.
- [13] M. Feidt, Optimal Thermodynamics, new upperbounds, *Entropy*, 11, p 529-547, 2009.
- [14] M. Feidt, Reconsideration of criteria and modelling in order to optimize the efficiency of irreversible thermomechanical heat engines, *Entropy*, 12, p 2470-2484, 2010.

FROM MACROSCOPIC OBSERVATIONS TO MICRO-KINETIC MODELS OF SURFACE REACTIONS

Ahmed F Ghoniem

Massachusetts Institute of Technology

EXTENDED ABSTRACT

Surface chemistry, both thermal and electrochemical, is very important in many energy applications including catalysis, fuel cells, membrane reactors, reformers, etc. However, accurate mechanisms describing its kinetics have not been widely developed. *In situ* spectroscopic measurements to determine the reacting species and reaction rates are often rare and incomplete. Frequently one must rely on macroscopic measurements (permeation fluxes) or device performance (I-V curve in fuel cells) in which surface processes play an important role. Models relating the device performance to the surface chemistry are formulated in terms of partial differential equations describing the interaction between different modes of transport and chemistry in both the homogeneous and heterogeneous phases using the mean-field approximation. The source terms are assembled using multistep reaction kinetics (microkinetics) often involving adsorption/desorption, charge transfer, incorporation into bulk and the corresponding species. The choice of the intermediate molecules in the microkinetics mechanism, and the corresponding reaction steps, is often guided by prior knowledge or some *ab initio* calculations. Individual reactions (forward and backward) must satisfy thermodynamic consistency (although this is not always done). Estimating the unknown kinetics parameters is done by matching the solution to the available data over a reasonable range of operating conditions. I will discuss couple of recent examples from our work on solid oxide fuel cell [1,4,5] and ion-transport membranes [2,3].

REFERENCES

- [1] Lee, Won Yong, Wee, D.H., and Ghoniem, A.F. Membrane Electrode Assemble Model of Solid Oxide Fuel Cells, Journal of Power Sources, 186, 2009, pp. 417-427.
- [2] Hong, JS, Kirchen, P. and Ghoniem, A.F., Interaction between oxygen permeation and homogeneous-phase fuel conversion on the sweep side of an ion transport membrane, J. Membrane Sci., 428, Feb 2013, 309-322.
- [3] Hong, JS, Kirchen, P. and Ghoniem, A.F., Estimating the kinetics data for oxygen exchange and fuel oxidation on the surface of pervoskite membranes, for publication J. Membrane Sci., 2013.
- [4] Hanna, J., She, Y., Lee, WY, and Ghoniem, A.F., Fundamentals of electro and thermochemistry in the anode of solid-oxide fuel cells with hydrocarbon and syngas fuels, a review, for publication Prog. Energy Combust. Sci., 2013.
- [5] Hanna, J., Lee, WY, and Ghoniem, A.F., Electrochemical kinetics models for CO oxidation in Ni-YZS anodes, for publication J. Electrochem. Soc., 2013.

APPLYING ENDOREVERSIBLE THERMODYNAMICS: THE OPTIVENT METHOD FOR SI-ENGINES

K. H. Hoffmann^{1,*}, A. Fischer¹, J. Getzlaff², T. Lambert² and J. Mehnert²

*Corresponding Author: hoffmann@physik.tu-chemnitz.de

¹Institut für Physik, Technische Universität Chemnitz, Chemnitz, Germany

²Institut für Fahrzeug- und Antriebstechnik, Westsächsische Hochschule Zwickau, Zwickau, Germany

EXTENDED ABSTRACT

All energy transformation processes occurring in reality are irreversible and in many cases these irreversibilities must be included in a realistic description of such processes. Especially the quantification of the losses occurring in technologically relevant processes is an important goal. Endoreversible thermodynamics provides a non-equilibrium approach towards this goal by viewing a system as a network of internally reversible (endoreversible) subsystems exchanging energy in an irreversible fashion. All irreversibilities are confined to the interaction between the subsystems.

Although the performance limits of reversible processes like the Carnot efficiency provide upper bounds for real irreversible processes they are usually not good enough to be a useful guide in the improvement of real processes. Real heat engines, for example, seldom attain more than a fraction of the reversible Carnot efficiency.

The concept of ‘endoreversibility’ has proven to be a powerful tool for the construction of models with the desired qualities. Endoreversible systems basically are composed of internally reversible subsystems with (irreversible) interactions between them. The losses due to the finite times or rates of processes are located in the interactions alone. A proper modelling of the transport equations between the subsystems allows to quantify the dissipation associated with the energy exchange. The hypothesis of endoreversibility simplifies the expenditure for the analysis essentially. This concept of ‘endoreversibility’ has been successfully applied to a wide variety of thermodynamic systems and led to remarkable results [1, 2].

An important problem in the analysis of endoreversible systems is how to deal with the time dependence of process variables and parameters, i.e. how the dynamics of a system evolves during a process. This problem has first been investigated in relatively simple models, which lacked the richness in technological detail of sophisticated engine models. However, while it was this approach which made insights into thermodynamic path optimization feasible, endoreversible thermodynamics as a general theory provides a framework to deal with thermodynamical systems *at all levels of detail* and is thus a universal approach also ranging to very elaborate and complex models [3].

We here present an example of such a treatment. It is the analysis of a SI (spark ignition) engine, which is optimized in efficiency under the constraints given by CO₂-emission commitments and legislation all over the world. The goal is to improve the efficiency of the SI engine significantly, while of course the exhaust emissions must not become worse.

One known approach is to reduce the gas exchange losses using fully variable valve trains on the intake side of the combustion engine. OptiVent is another approach [4]. It is a patented new way controlling the mass air flow in the cylinder of a combustion engine using opening valves during the *compression phase* of a four stroke engine, see fig. 1. This technology requires a wider range of variability on the valve train components of the engine especially for opening the valves more than one time during a cycle. In addition it is necessary to combine this technology with direct injection to avoid fuel losses in the exhaust system of the engine. Chemnitz University of Technology and the West Saxon University of Applied Sciences in Zwickau performed numerical investigations on the potential of the OptiVent engine control and combustion system, using a fully variable valve train on the exhaust valves of the engine. We present results from numerical simulations based on the endoreversible description of the OptiVent principle, see figs. 2 and 3. These simulations show the potential of the new OptiVent-way of air mass control, thus enabling us to progress towards developing a running engine and putting it on a test bench.

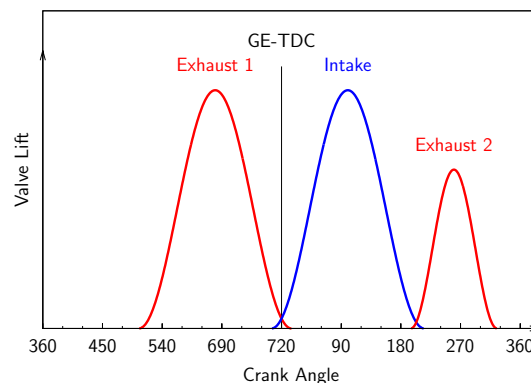


Figure 1. The OptiVent method makes use of adjusting the amount of compressed air in the cylinder by a second opening of the exhaust valve, here shown as “Exhaust2”.

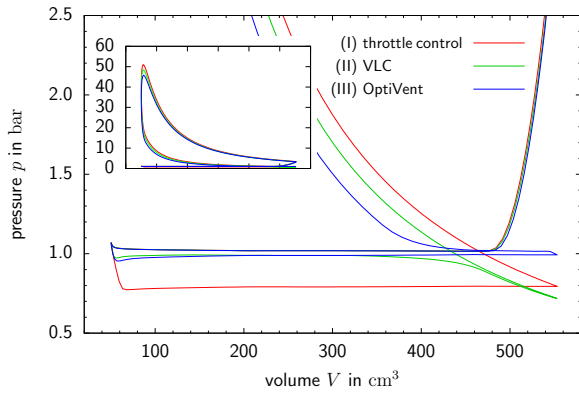


Figure 2. The pressure in the cylinder of a SI engine is shown as a function of the cylinder volume. The lower loops show the exhaust and the intake stroke. The pressure difference is a measure for the so called load exchange losses.

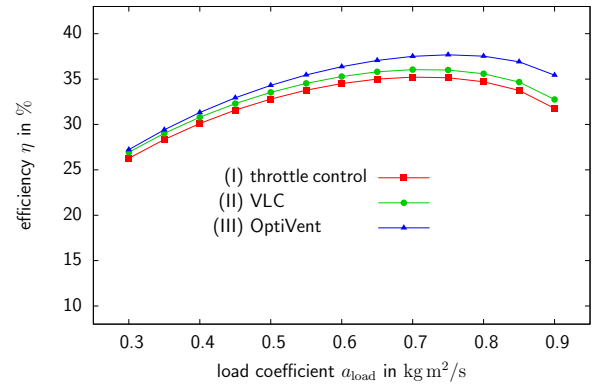


Figure 3. The engines' efficiency as function of the load coefficient at constant (intermediate) accelerator position. Note the efficiency gain of the OptiVent method.

References

- [1] K. H. Hoffmann, J. M. Burzler, and S. Schubert. Endoreversible thermodynamics. *J. Non-Equilib. Thermodyn.*, 22(4):311–355, 1997.
- [2] K. H. Hoffmann, J. Burzler, A. Fischer, M. Schaller, and S. Schubert. Optimal process paths for endoreversible systems. *J. Non-Equilib. Thermodyn.*, 28(3):233–268, 2003.
- [3] A. Fischer and K. H. Hoffmann. Can a quantitative simulation of an Otto engine be accurately rendered by a simple Novikov model with heat leak? *J. Non-Equilib. Thermodyn.*, 29(1):9–28, 2004.
- [4] Jörn Getzlaff, Thomas Lambert, Karl Heinz Hoffmann, and Andreas Fischer. “OptiVent” – A new approach for controlling mass air flow and combustion in direct injection SI-engines. SAE Technical Paper 2013-01-0592, 2013.

ENERGY EFFICIENT REACTOR DESIGN SIMPLIFIED BY APPLICATION OF THE SECOND LAW OF THERMODYNAMICS

Ø. Wilhelmsen¹, E. Johannessen², S. Kjelstrup^{1*}

¹Department of Chemistry, Norwegian University of Science and Technology, 7491 Trondheim, Norway,
and Process and Energy Laboratory, Delft University of Technology, Leeghwaterstraat 44, 2628CA Delft, The Netherlands

²Statoil Research Centrem N-7005 Trondheim, Norway

*Corresponding author: signe.kjelstrup@ntnu.no

EXTENDED ABSTRACT

Gas heated reformers of length L which all produce the same amount of hydrogen have been investigated, for varying inlet temperature T_0 . By analysing various stationary states of operation formulated by optimal control theory, we find numerical support for the hypothesis of minimum entropy production, namely that the state of operation with constant entropy production, and also in some cases constant thermal driving force, are good approximations to this most energy efficient state of operation [1], see Fig. 1.

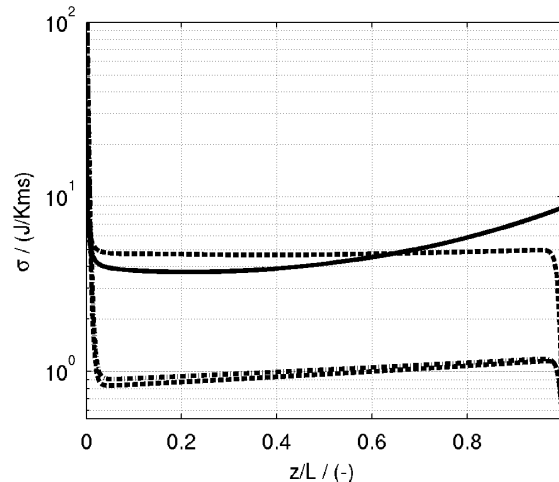


Figure 1: The local entropy production for the reference gas heated reformer (solid line), the optimal cases with fixed T_0 and L (upper dashed line), free T_0 and fixed L (dash-dotted line) and free T_0 and L (lower dashed line). All cases have heat transfer by convection, radiation and conduction.

This result applies for non-linear transport equations and conditions for which there exist no rigorous mathematical description of the most energy efficient state [2]. Clearly there is a need for an extended mathematical analysis. Based on the theoretical and numerical results we proceed to formulate a set of guidelines to aid in energy efficient reactor design, which can be used once the best available heat transfer coefficients have been obtained. The optimal reactor design depends on the relative size of the heat transfer coefficient for heat transfer across the tubular reactor wall and typical heat transfer coefficients in heat exchangers. Very efficient heat transfer across the reactor tube wall favours a design consisting of an adiabatic pre-reactor followed by a tubular reactor section exchanging heat. Very poor heat transfer across the reactor tube wall favours a design consisting of one or more adiabatic reactor stages with interstage heating/cooling in dedicated heat exchangers. We discuss how the guidelines add to proposals in the literature and help define central optimization variables and boundary conditions.

REFERENCES

- [1] Ø. Wilhelmsen, E. Johannessen, S. Kjelstrup, *Int. J. Hydrogen Energy*, 2010, 34, 13219.
- [2] E. Johannessen, S. Kjelstrup, *Chem. Eng. Sci.* 2005, 60, 3347.

ENTROPY PRODUCTION: INTEGRATING RENEWABLE ENERGY SOURCES INTO SUSTAINABLE ENERGY SOLUTIONS

Gregory J. Kowalski^{*}, Mansour Zenouzi[°], Masoud Modaresifar^{*}

^{*} Northeastern University, Boston, MA 02115, USA

[°] Wentworth Institute of Technology, Boston, MA 02115, USA

ABSTRACT

An investigation of the transient entropy property term, entropy storage, for a solar thermal and desalination device was performed. It was illustrated that entropy production rates provide a means of comparing alternative energy solutions and a measure of their sustainability. To satisfy these objectives one needs accurate calculation of entropy production rates. It was confirmed that neglecting the energy storage terms is a valid approximation for the first law analysis, but not for the second law analysis where entropy storage terms are significant. For a generalized solar thermal system neglecting the entropy storage terms introduced a maximum difference in the entropy production rate of 7.4% and a difference of 7.3% in the daily average. Similar differences for the solar desalination process were observed. In the solar desalination process the second law performance is greater than that for the reverse osmosis process, the chief competitor, when the entropy storage are correctly included in the analysis. The results demonstrate that for variable energy sources such as renewable energy systems, the second law analysis provides a measure of the sustainability of competing system and that the entropy storage terms should be included in the analysis.

INTRODUCTION

Entropy production analysis has been promoted as being an important tool for identifying where major losses in a system occur, as a design tool to identify system improvements and as a measure of sustainability. The process with the lower entropy production rate is the more sustainable one because it converts one form of energy into another useful form more efficiently. However, use of this second law based tool is not widespread at a practical level because of its complexity and subtleties. There are numerous examples of reporting entropy production rates as part of energy analysis of a system performance in the literature [1-7], but there are few instances where decisions to implement design modifications are based on reducing entropy production rates [8,9]. In these reported investigations, the developments of the entropy production analysis of a particular device or process are the key outcomes of the investigation. However, in most cases issues related to heat flows and the associated entropy flows are not described. The system boundaries are not defined to allow the total entropy production of the delivered product to be identified. For example, [5] provide a complete and thorough second law analysis of a reverse osmosis desalination plant starting with the power input to the pumps. They do not include the entropy production associated with the production of this power that would allow a direct comparison with competing renewable energy desalination technologies. This inconsistency in system definition prevents a direct comparison of the entropy production with other competing technologies and of its use as a measure of sustainability.

The examples discussed in this presentation are intended to highlight cases involving renewable energy sources, specifically solar energy, where including entropy production into the analysis leads to a better understanding and potential

improvements of the system. They also illustrate the fundamental information misconceptions by practitioners that are limiting the accurate and productive use of the second law, especially as a means of integrating energy system solutions and addressing sustainability concerns. These examples include formulating the entropy production analysis for renewable energy systems, their integration with traditional systems and comparing them to nonrenewable or fuel driven resources.

The transient entropy term is one feature of the entropy production analysis that is neglected in most of the previous reported studies. Renewable energy sources are variable in nature and systems involving them usually include an energy storage device such as thermal storage device or batteries as well as energy stored in the energy collection device itself. Neglecting the transient entropy term leads to erroneous predictions of entropy production during the startup and time immediately after the renewable energy source has ended when the stored energy in the system continues to produce useful output. For example, Modaresifar [8,9] demonstrates that fresh water is produced in a solar desalination device after sunset due to the stored thermal energy in the device.

The quasi-steady state analysis, which is commonly used in solar thermal energy simulations, especially in the first law analysis, may not be accurate in the second law analysis. Using daily simulations to avoid these transient effects [9] may not lead to an accurate prediction of the entropy production in these systems and its use as a measure of the sustainability. Additionally, one has also lost the opportunity to fully understand the device process and to possibly improve it when using the daily integrated results.

A generalized system with the same physical characteristics as that of a solar thermal collector will be used to investigate the effects of the transient entropy property changes and energy storage on its performance. The system

will be simplified and the incident solar radiation will be represented by a parabolic function so that a closed form solution can be developed to investigate the second law characteristics. A quasi-steady state and transient solution will be obtained to measure of the accuracy of the quasi-steady state solution. The subtleties of describing the heat flows associated with this type of analysis are discussed during this development. The results of this demonstration will be extended to a more complex problem involving a solution, salt and water that is involved in the solar desalination process. This demonstration emphasizes the use of entropy production rates as a measure of the sustainability of competing systems.

DEVELOPMENT:

Generalized Solar System

The generalized system used to investigate the effect of the transient entropy property term is shown in Figure 1 and includes the energy storage terms for the device, E_{Sr} and the working fluid, E_{Swf} . The absorbed incident solar radiation entering the system and the heat loss from the solar thermal device is shown.

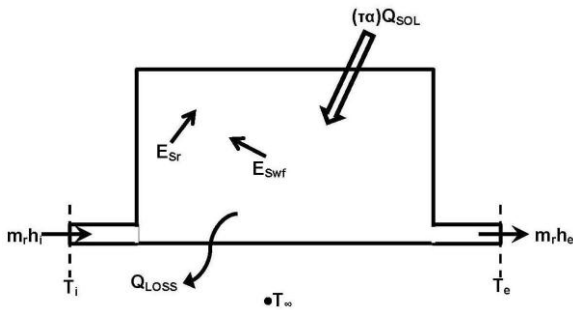


Figure 1 System sketch for the generalized solar thermal device and its associated energy flows.

The energy for the system shown in Figure 1 is:

$$m_r h_i + (\tau\alpha)Q_{SOL} = E_{Sr} + E_{Swf} + Q_{LOSS} + m_r h_e \quad (1)$$

The heat loss, Q_{LOSS} , and energy storage terms for the device, E_{Sr} , and the working fluid, E_{Swf} , are related to the average temperature of the system. For the purpose of this analysis, it is assumed that the mass flow rate, m_r , is sufficiently large that the spatial variation of the temperature through the system is a linear function and equals the arithmetic average of the inlet and outlet temperatures, T_i and T_e , respectively. Introducing the equation of state and the definition of the energy storage terms and rearranging Eq. (1) yields:

$$(1/2)(m_D c_D + m_{wf} c_{wf}) \frac{dT_e}{dt} = - (m_r c_{wf} + C_L/2)(T_e - T_i) + (\tau\alpha)Q_{SOL} \quad (2)$$

Where $T_i = T_\infty =$ ambient temperature = constant.

The generalized function for the incident solar radiation is a parabola with the maximum value at solar noon and zero

value at sunrise and sunset. The function is normalized with respect to day length, t_d .

$$Q_{SOL} = 4Q_{s,peak}[(t/t_d) - (t/t_d)^2] \quad (3)$$

$Q_{s,peak}$ equals the peak incident solar radiation for the day, W/m^2 , and t_d equals the day length, hours. Eq. (3) applies for time between sunrise and sunset.

The solution to Eq. (2) for the time period between sunrise and sunset when the initial condition is that the device and enclosed fluid are at the ambient temperature is:

$$T_e = T_i + C_3 \exp[-C_2 t] + b_0 + b_1 t + b_2 t^2 \quad (4)$$

Where:

$$C_1 = \frac{(\tau\alpha)Q_{s,peak}}{(1/2)(m_D c_D + m_{wf} c_{wf})} \quad (5)$$

$$C_2 = \frac{(m_r c_{wf} + C_L/2)}{(1/2)(m_D c_D + m_{wf} c_{wf})} \quad (6)$$

$$C_3 = -b_0 = \frac{[4C_1/t_d + 8C_1/(C_2 t_d^2)]}{C_2^2} \quad (7)$$

$$b_1 = \frac{[4C_1/t_d + 8C_1/(C_2 t_d^2)]}{C_2} \quad (8)$$

$$b_2 = \frac{-4C_1}{C_2 t_d^2} \quad (9)$$

At sunset, the exit temperature is above the ambient and inlet temperature even though there is no incident solar radiation. The transient response continues under this condition until the solar device cools to the ambient temperature. Modifying Eq. (2) for zero incident solar radiation and solving for the exit temperature yields the following:

$$T_e = T_i + (T_e(t_d) - T_i) \exp[-C_2(t - t_d)] \quad (10)$$

Where $T_e(t_d)$ is the exit temperature calculated from Eq. (3) at time equal to the day length, sunset.

The collected useful energy rate for the device is related to the change in the enthalpy of the working fluid mass flow rate.

$$q_{use} = (m_r c_{wf})(T_e - T_i) \quad (11)$$

The Transient simulation model is described above using Eqs. (3-11) and represents a closed form solution for the behavior of the system. The quasi-steady state simulation model is based on the same system definition. However, the energy storage terms are neglected. This is equivalent to setting the first time derivative in Eq. (2) to zero. The exit

temperature based on the quasi-steady state model is determined from resulting equation.

$$T_e|_{QS} = T_i + \frac{(\tau\alpha)Q_{SOL}}{(m_r c_{wf} + C_L/2)} \quad (12)$$

The collected useful energy rate for the quasi-steady state model is determined using Eq. (11) with the exit temperature calculated with Eq. (12).

Entropy Production Rate for Generalized Solar System

The system definition for the entropy balance for the generalized solar energy system is shown in Figure 2. This system is modified from that shown in Figure 1 to reflect the entropy flow associated with the heat flows. This modification also reflects a basic second law question that is not commonly mentioned when new practitioners are introduced to the second law and entropy production rate. That question is “Is the heat flow used in another process to produce a useful energy output or is it allowed to reach equilibrium with the surroundings without doing useful work?” The location of the system boundary and what devices are included in it are determined based on the answer to this question. In the present case, the heat flow input from the sun should be viewed as coming from the sun and the system boundary for this energy flow should be at the temperature of the sun. This feature is shown in Figure 2 as the dotted line extension the original system definition. Using this approach includes the irreversibility of this thermal transport to the defined system. For the entropy flow associated with the heat loss from the solar thermal device the system boundary is defined at the ambient temperature because no attempt is made to use this energy flow in another process. By defining the system in this manner one avoids the complicated integral involved in evaluating the entropy flow of a heat flow at a variable temperature and it insures that all sources of entropy production related to the process are included in the analysis.

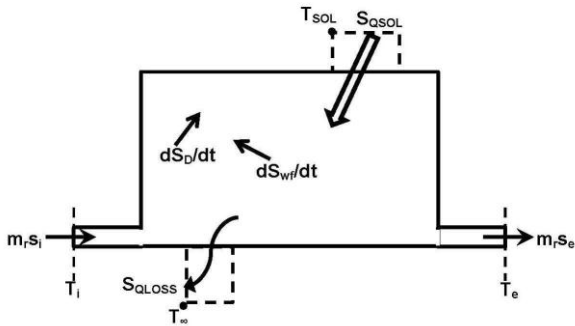


Figure 2 System sketch for the generalized solar thermal device and its associated entropy flows. The system definition has been modified from that shown in Figure 1.

The entropy balance for this system is:

$$\dot{\sigma}_p = m_r (s_e - s_i) + \frac{dS_D}{dt} + \frac{dS_{wf}}{dt} + C_L \frac{(T_{ave} - T_i)}{T_{ave}} - \frac{Q_{SOL}}{T_{SUN}} \quad (13)$$

Introducing the T-ds equation to relate the entropy change to the temperatures for an incompressible working fluid and for a constant pressure process yields:

$$\dot{\sigma}_p = m_r c_{wf} \ln \left[\frac{T_e}{T_i} \right] + \left[\frac{(m_D c_D + m_{wf} c_{wf})}{T_{ave}} \right] \frac{dT_{ave}}{dt} + C_L \frac{(T_{ave} - T_i)}{T_{ave}} - \frac{Q_{SOL}}{T_{SUN}} \quad (14)$$

The entropy production rate for the quasi-steady state model neglects the transient entropy property terms.

$$\dot{\sigma}_p = m_r c_{wf} \ln \left[\frac{T_e}{T_i} \right] + C_L \frac{(T_{ave} - T_i)}{T_{ave}} - \frac{Q_{SOL}}{T_{SUN}} \quad (15)$$

The above developments were used to calculate the exit temperature, collected useful energy rate and entropy production rate for a typical day in July for the Boston, Massachusetts, USA region. The peak solar energy for the day was 918.5 w/m² and the day length was 15 hours with sunrise at 430 hours. The results are discussed later.

Solar Desalination Process Model

The system shown in Figure 3 illustrates schematically a tray design solar desalination. The system description and the model development are described in detail in [8, 9] and is not repeat here. In this tray design, a film of salty water is placed in thermal contact with absorber plate using trays mounted to its rear surface and the condensing surface is placed in a shaded region to minimize its temperature. The condensing surface is inclined at an angle of 40° in order to allow the condensed water vapor to flow down into the fresh water trough. In this solar distillation design, an absorber plate is thermally isolated from the environment using a glazing surface that is transparent to the incident solar radiation. Water trays are in contact with the rear surface of the absorber plate and are inclined to provide gravity flow through the collector. The trays have a fin efficiency of 0.97 and a combined surface area greater than the absorber plate area. In this configuration, the glazing surface is separated from condensing surface that is the common configuration of most solar distillation units.

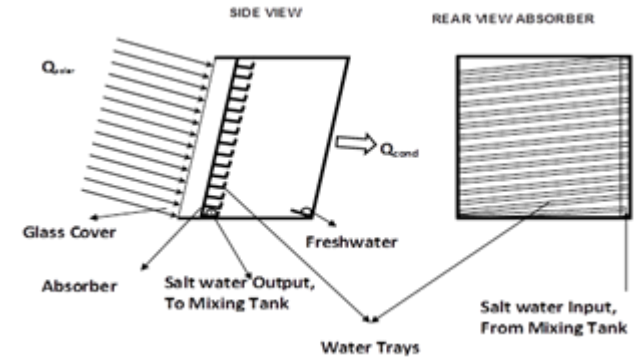


Figure 3 schematic diagram of the solar still analyzed in this work. The incident solar radiation is absorbed on the absorber plate. The evaporated water vapor is condensed on the shaded rear surface where the freshwater is collected.

In addition to minimizing the condensing surface temperature, this configuration also avoids reducing the solar

energy incident on the absorber surface due to condensation or frost formation in the winter months on the glazing surface. The brackish water inlet is to the side of the collector and feeds the water trays as shown in the rear view section of Figure 3. The volume surrounding the water trays and bounded by the condensing plate is defined as the chamber. Fresh water is condensed by maintaining the chamber above its dew point temperature and the condensing plate below it. The fresh water accumulates on the condensing plate and is collected at the outlet as shown. The heated, concentrated salty water flows out of the trays as shown.

The amount of fresh water produced is calculated using the condensation rate that is based on the condensation heat flow. The set of coupled equations based on the energy balance on the absorber plate, water in the trays, chamber and condensation plate are solved using an explicit integration procedure. The evaporation and condensing process are included in this model and require the determination of the chamber's relative humidity and partial pressure of the water vapor. The energy balance equations for the water in the trays, plate and condensing surface are recast into a temporal finite difference form and are solved over the day length in time steps of 1 sec. to allow a stable solution. The mass flow rate of the fresh water produced equals the condensation mass flow rate. The mass of freshwater produced is calculated by integrating the condensation flow over time. A Matlab program was written using these relationships to calculate the temperatures of the absorber plate, water, chamber, and glass surface as a function of the incident solar radiation and ambient air temperature [8,9].

The second law analysis of the tray design solar distillation device performed by Modaresifar [9] was an exergy analysis. Modaresifar [9] based his analysis on two system definitions that are summarized in Figure 4. Using his exergy destruction term and the defined dead state temperature allows his analysis to be restated in terms of the entropy production rate.

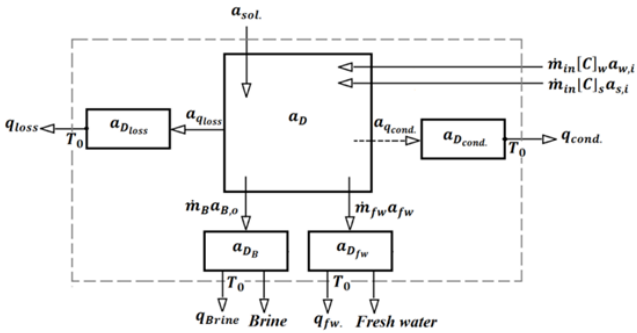


Figure 4 Schematic diagram of exergy balance for a solar distillation system. The dashed line boundary defines a system in which all inflows and outflows all occur at the dead state. The “product approach” system is the central block with the exergy destruction, $e_{x|D}$, indicated.

The second law exergy balance for the system defined by the dashed line in Figure 4:

$$e_{x|D} = \sigma_p T_0 = e_{x,QSOL} - e_{x,q_{loss}} - e_{x,q_{cond}} - \frac{de_{x,sys}}{dt} - (m_w + m_{salt})(e_{x,B} - e_{x,in}) - m_f(e_{x,f} - e_{x,B}) \quad (16)$$

Where the inflow (brine) and the outflows are treated as a solution of salt and water. This approach is taken to accurately describe the irreversibility of the separation process to obtain the freshwater. The details of this development are given in [8,9] and are not repeated here. The primary focus of this work is the transient exergy term and its effect on the calculated entropy production rate. In [9] the daily average exergy destruction and second law efficient were determined and it was argued that over the course of the day the transient system exergy term would go to zero because the device returned to its original state. As will be seen in the result section this is not true, for this system and for the generalized solar thermal system. Modaresifar [9] also illustrates the difference between the dashed line system in Figure 4 and the “product approach” which neglects the exergy destroyed when the hot outflows are allowed to reach equilibrium with the dead state without attempting to use them for other purposes. The large difference between the second law efficiency of these two system is an effective argument for introducing a waste heat recovery heat exchanger. The addition of the heat exchanger does significantly improve the performance and is discussed below.

RESULTS

Generalized Solar System

The prediction of the exit temperature from the solar thermal device, the entropy production rate and the useful collected energy rates are determined for a typical day in July for the Boston, Massachusetts, USA location using the formulations described above are discussed below. The calculations were based on a parabolic description of the incident solar radiation with a peak incident solar radiation of 981.5 w/m^2 and a day length of 15 hours. A comparison of the parabolic function used in this analysis and the predicted incident solar radiation using the method of Masters [10] is given in Figure 5. The idealized parabolic function is in general agreement with the functional trend of the incident solar radiation, but yields slightly large values. These differences are acceptable for the purpose of the present

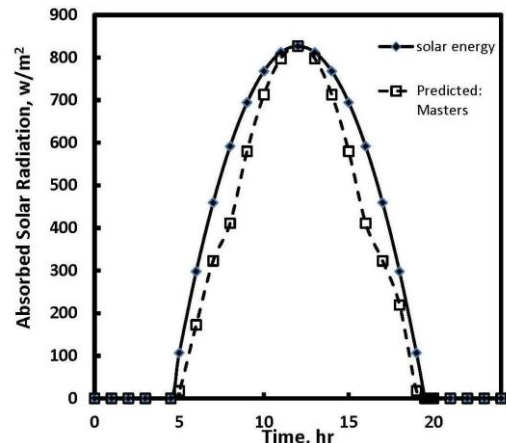


Figure 5 The comparison of the idealized parabolic function used to describe the incident absorbed solar radiation to that predicted for July 15 in the Boston, Massachusetts, USA region.

analysis in order to take advantage of the closed form solution and it is the relative comparison of simulation models that is discussed.

The idealized daily incident solar radiation model was introduced into the quasi-steady state and Transient simulation to calculate the collected useful energy rate shown in Figure 6. The first observation is that there is little difference in the collected useful energy rate between the two models which is consistent with the commonly used Frist law models. The total collected useful energy over the day for the quasi-steady state simulation is 55.6 MJ while that for the Transient simulation is 55.7 MJ, a 0.12% increase. This graph is included because the results are those commonly desired and are the basis of most economical, reduced fuel consumption and carbon emission calculations.

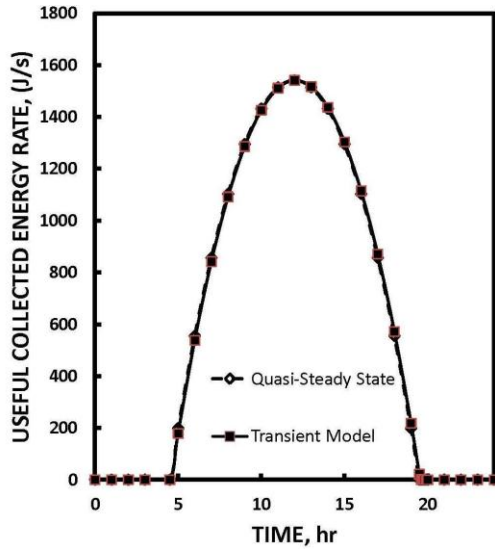


Figure 6 The comparison of the collected useful energy rate as a function of time of day between the quasi-steady state and transient simulations.

The fluid exit temperature for the quasi-steady state and transient simulations are compared in Figure 7. As expected there is little difference between the models and the

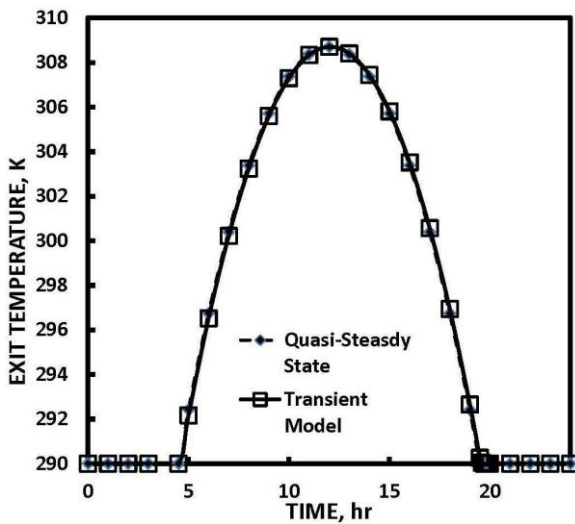


Figure 7 The comparison of the fluid exit temperature from the solar thermal collector as a function of time of day between the quasi-steady state and transient simulations.

commonly used approximation of neglecting the device's energy storage term is supported. One can discern a slight difference where the quasi-steady state simulation predicts a slightly higher exit temperature during the time before solar noon (12 hrs) and a slightly lower exit temperature for the time between solar noon and sunset. However, these differences are not significant and are well within the uncertainty of the simulation accuracy.

In Figures 8 and 9 details of the fluid exit temperature near solar noon and at sunset are illustrated. In Figure 8 the slight difference from the quasi-steady state simulation predicting a higher value than that of the transient simulation before solar noon and then reversing the trend is more easily observed. The more significant difference between the two simulations occurs at sunset where the transient model predicts an exponential type temperature response to the ambient temperature while the quasi-steady state model abruptly reaches the ambient temperature at sunset (Figure 9). The increased fluid exit temperature predicted by the transient model is a result of converting the energy stored in the device to useful energy collected. A similar energy conversion

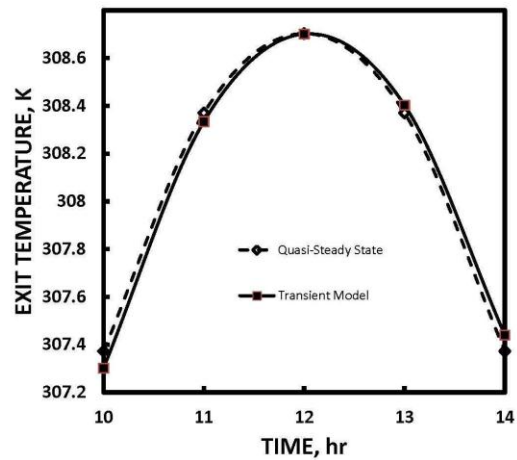


Figure 8 The comparison of the fluid exit temperature from the solar thermal collector as a function of time of day between the quasi-steady state and transient simulations near the time of solar noon.

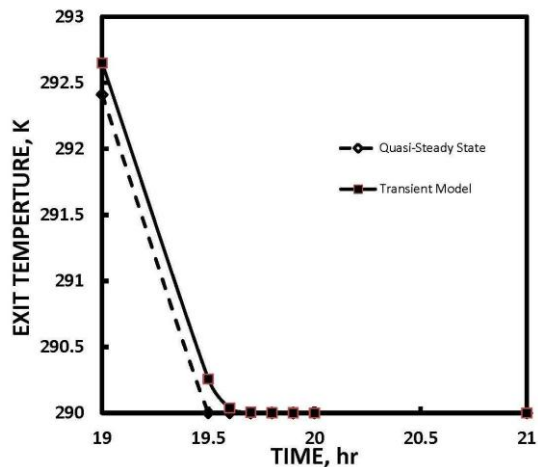


Figure 9 The comparison of the fluid exit temperature from the solar thermal collector as a function of time of day between the quasi-steady state and transient simulations near the time of sunset.

is not included in the quasi-steady state model. Again, the differences between these first law simulations are not significant and the results are consistent with the common approach used in the field.

In Figure 10 the entropy production rate as a function of the time of day are compared for the two simulations. These results are significantly different and illustrate that the quasi-steady state simulation predicts a larger entropy production rate than that for the transient model by a maximum of 7.4%. The integrated daily entropy production for the quasi-steady state simulation is 0.20 MJ while that for the transient simulation is 0.18 MJ, a 7.3% decrease. These results suggest that if one is comparing entropy production rates between two competing solar thermal designs or solar radiation collection devices (solar thermal vs photovoltaics) one should include the transient entropy property term. In the present comparison, Figure 10, the shown difference suggests that the commonly used approximation to neglect the energy storage term that is justifiable for the first law analysis is not justifiable for the second law analysis. The inherent transient nature of renewable energy sources suggests that daily analysis and simulation of its second law performance should use the transient model.

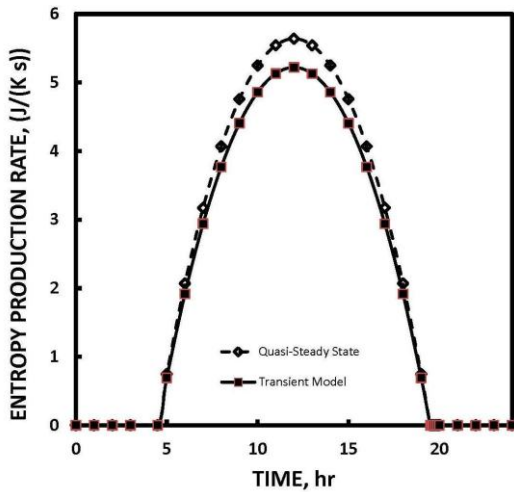


Figure 10 The comparison of the entropy production rate as a function of time day between the quasi-steady state and Transient simulations.

The reason for this difference has to do with the entropy flow out of the system with the heat loss term. In the actual device and the transient simulation model the heat loss term is lower during a larger part of the day because part of the incident solar radiation is converted into internal energy of the device and is later converted to useful collected energy in the working fluid. This energy conversion path is ignored in the quasi-steady state results. The second law analysis should be used to compare different devices or systems for sustainability in order to determine the best use of the energy resource. The change in the system definition between the first and second law analysis described in the development section serves two purposes. First, it reflects that the heat loss term is not converted into a useful energy output and, second, it simplifies the heat transfer analysis. The heat flow into the system at the high temperature of the sun incorporates its high energy quality and simplifies the analysis. The need to define the ultimate use of an energy outflow from the system, especially a heat flow, is an inherent feature of the system redefinition procedure is a subtlety that needs to be discussed

when practitioners are first introduced to these second law concepts. It is also important to use this procedure when energy systems are discussed for their sustainability or for means to improve their performance.

Solar Desalination Process

The impact of assuming a quasi-steady state approximation for the second law for a solar desalination device is investigated in this section. As discussed in the Development section the production of freshwater is usually modeled using a transient first law analysis because of the nonlinear relationships between the temperature of the device and the evaporation and condensation rates. However, as mention previously most of the reported second law analyses of the solar desalination process use an effective parameter approach and not the salt and water solution, a brine solution, approach reported for the reverse osmosis or MFS processes [5,11,12,13]. Modaresifar [9] follows the brine solution approach to describe properly the irreversibility associated with separating the salt from the water. However, [9] does not include the transient entropy property term in the analysis and uses a daily average to describe the irreversibility and exergy destruction because the system returns to its initial condition over the course of the day and the integrated transient entropy production term is assumed to be zero. As seen from the previous section, this is not necessarily true since there is a difference in the daily entropy production between the quasi-steady state and transient simulations. The need for an accurate second law analysis in Modaresifar's [9] investigation was to determine design improvements and to compare the sustainability as measured by the second law of the solar and reverse osmosis desalination processes.

The transient effect of the First law simulation of the solar desalination devices reported are clearly illustrated in Figure 11, which is a plot of the brine temperature as a function of the time of day [9]. The functional form of the incident solar radiation for this analysis is similar to that reported in Figure 5 and one has a peak solar radiation at solar noon, 12.0 hours and zero incident solar radiation at sunset, 20.0 hours. In Figure 11 the maximum temperatures occur well after solar noon and there is an elevated temperature after sunset.

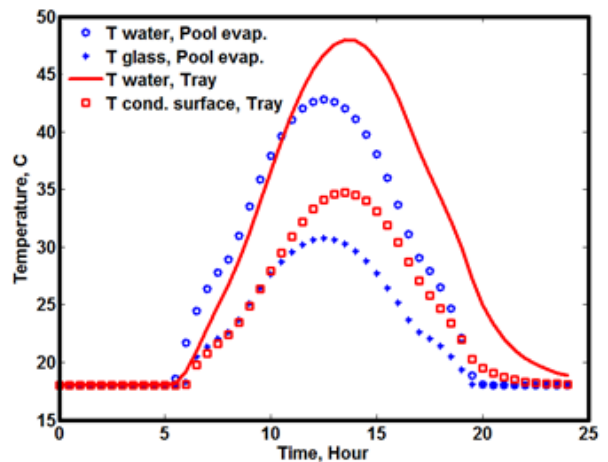


Figure 11. Comparison of the water and condensing temperatures between the pool evaporation and tray design solar desalination units. The performance for the July design days are shown. Taken from [9].

In Table 1 the results of the second law analysis for the Tray Design desalination device are summarized for the waste heat recovery and no recovery system configuration. The performance for the different system definitions are also summarized.

Table 1 Comparison of the Summary of second law performance measures of the Tray Design solar desalination device for the quasi-steady state and transient simulations.

Tray Design: July				
	Quasi-Steady State No Recovery	Transient No Recovery	Quasi-Steady State Recovery	Transient Recovery
Daily Fresh water Production, kg	2.81	2.81	6.05	6.05
Daily Entropy Production, KJ/K	88.5	87.6	86.54	83.40
Daily Entropy Production, (Product Approach),KJ/K	83.1	79.1	NA	NA
Second Law efficiency (Product Approach), %	6.65	11.1	NA	NA
Second Law efficiency, %	0.63	1.63	2.79	6.33
Mass flow rate, kg/s	0.003	0.003	0.007	0.007
Area of Incidence, m ²	1.0	1.0	1.0	1.0

In the second row, the simulation approach for the second law analysis is identified for the two different solar desalination processes under consideration, the waste heat recovery and no recovery designs. The first process is the no recovery process in which the hot, concentrated brine is discharged into the water source and the inlet is from the large available brine source, usually the ocean. The second process is the recovery process that includes a heat exchanger that uses the hot concentrated brine to preheat the entering cold brine. Both processes are transient simulations using the first law, but a quasi-steady state and a transient model are used to calculate the daily entropy production parameter and the results are reported in the marked separate columns.

Two system definitions are used to report the second law efficiency. In the fourth row, the “product approach” corresponds to the system defined at the exit of the solar desalination unit as shown in Figure 4 in the Development section. Using the “product approach” system definition one is neglecting the availability flow carried by the hot brine and fresh water. This is not a rigorous application of the second law because one is not asking the question “what can I do with this outflow” and one is not following the entropy and availability flows to their final equilibrium states. This is a common mistake because from a first law design perspective this system definition is perfectly adequate. It should be noted that the second law efficiency predicted for this system is greater than that reported for the correct second law definition where all outflows are tracked to their final equilibrium state as reported in the fifth row. Modaresifar, [9] used this system to identify the potential gain if the hot brine were used to preheat the entering cold brine.

The second process, the recovery process, introduces the heat exchanger and follows all the outflows to equilibrium with the surroundings. This complete system definition was used and is the reason that the “product approach” cells are left unreported, “NA”.

From the table it is clear that neglecting the transient entropy property term leads to under estimating the second law performance in all cases. Modaresifar [9] uses these results to argue that the second law performance can identify the sources of entropy production and indicate means of reducing it. However, this argue is valid in this case because

the same assumption, neglecting the transient entropy property term, was made in both simulation models. The more accurate estimate using the transient simulation model indicates that the performance measured by both the second law efficiency and the daily entropy production are higher than that predicted by quasi-steady state model. This difference becomes important when one wants to compare the predicted performance of a solar desalination process to competing operations such as reverse osmosis or MSF plants.

In the reverse osmosis (RO) plants reported in the literature the second law efficiencies are in the range of 4% to 4.5%. Aljundi [5] reported 4.1% for a plant in Jordan, Cerci has the 4.3 % for the second law efficiency in a plant in California [6] and Y.Cengel reported 4.2 % for a MSF desalination plant [7]. The second law efficiency is calculated from the exergy of products divided by the input power exergy. When one compares the calculated performance of the solar desalination process using the transient model one finds that it is higher than for these other processes.

This comparison is not a valid because the second law calculations in literature use the input exergy as the power input that is needed for the pumps, not at the primary energy input point. The entropy production in producing the input power is not included in the reported second law efficiency calculations for the (RO) process. The comparison between the solar and (RO) processes is not consistent because the input energy source for the (RO) process is not the primary energy input source as it is for the solar processes. A. Rashad [14] showed that a thermal power plant has a second law efficiency of less than 50% in all conditions of loading. The performance of the primary power source must be taken into account to calculate equivalent second law parameters in order to get accurate comparison, especially when using the entropy production or second law efficiency as a measure of the sustainability of the processes.

CONCLUSION

An investigation of the transient system entropy property term, entropy storage, for a solar thermal and desalination device was performed. The objective was to illustrate the use of entropy production rates as a means of comparing alternative energy solutions and as a measure of their sustainability. The solar thermal analysis was based on a generalized system with a functionally correct form of the incident solar energy that yielded a closed form solution. To satisfy the above objectives one needs accurate calculation of entropy production rates. It was confirmed that neglecting the energy storage terms is a valid approximation for the first law analysis, but not for the second law analysis where entropy storage terms are significant for both systems investigated. For a generalized solar thermal system neglecting the entropy storage terms introduced a maximum difference in the entropy production rate of 7.4% and a difference of 7.3% in the daily average. Similar differences were observed for the solar desalination process. It was shown that by adding a waste heat recovery device the desalination system’s entropy production rate decreased for the same energy input and resulted in a better performing system. In the solar desalination process the difference between including the entropy storage terms leads to a second law performance that is greater than that for the reverse osmosis process, the chief competitor. It was also demonstrated that modifying the system definition between the first and second law analysis simplifies the analysis and provides the practitioner a

framework to include all entropy production parameters associated with the process. This framework also provides design insight as to means of improving the system performance and sustainability. The results demonstrate that for variable energy sources such as renewable energy systems, the second law analysis provides a measure of the sustainability of competing system and that the entropy storage terms should be included in the analysis.

ACKNOWLEDGMENT

The authors thank the College of Engineering at Northeastern University and the College of Engineering and Technology at Wentworth Institute of Technology for supporting this research.

NOMENCLATURE

b_0, b_1, b_2	Solution parameters defined by Eqs.(7-9)	
C_1, C_2	Constant defined by Eqs, (5) and (6)	
C_3	Integration Constant	K
c_D	Specific heat of device	J/(Kg K)
C_L	Overall heat transfer factor	W/K
C_{wf}	Specific heat of working fluid	J/(Kg K)
$e_{x,D}$	Exergy destroyed	W
$e_{x,B}$	Exergy of brine at outlet	J/Kg
$e_{x,f}$	Exergy of freshwater produced	J/Kg
$e_{x,in}$	Exergy of brine at inlet	J/Kg
$e_{x,qcond}$	Exergy carried by condensation heat flow	W
$e_{x,qloss}$	Exergy carried by heat loss	W
$e_{x,QSOL}$	Exergy of incident solar radiation	W
$e_{x,sys}$	Exergy of device and working fluid	J/Kg
$e_{x,B}$	Exergy of brine at inlet	J/Kg
E_{Sr}	Energy Storage term for the device	J/s
E_{Swf}	Energy Storage term for the working fluid	J/s
h_i	Enthalpy at device inlet	J/Kg
h_e	Enthalpy at device exit	J/Kg
m_r	Mass flow rate of working fluid	Kg/s
m_D	Mass of device	Kg
m_{wf}	Mass of working fluid in device	Kg
Q_{LOSS}	Heat loss from device	W
Q_{SOL}	Incident solar radiation on device	W
$Q_{s,peak}$	Peak incident solar radiation on device	W
q_{use}	Collected useful energy rate	W
s_e	Entropy at device exit	J/(Kg K)
s_i	Entropy at device inlet	J/(Kg K)
S_D	Entropy of device	J/K
S_{wf}	Entropy of working fluid in device	J/K
T_{ave}	Average temperature of device	K
T_e	Exit temperature from device	K
T_i	Inlet temperature to device	K
T_{SUN}	Temperature of the sun	K
t_d	Daylength	hr
$(\tau\alpha)$	Transmission-absorption coefficient for solar collector	
σ_P	Entropy production rate	J/s

REFERENCES

[1] Hepbasli, A., A key review on exergetic analysis and assessment of renewable energy resources for a sustainable future, *Renewable and Sustainable Energy Reviews* 12, pp. 593–661, 2008.

- [2] Romero-Ternero, V., Garcia-rodriguez, L. & Gomez-Camacho, C., Thermoeconomic analysis of Wind Powered Seawater Reverse Osmosis Desalination in the Canary Islands, *Desalination*, Vol. 186, pp. 291-298, Elsevier, 2005 .
- [3] Garcia-Rodriguez and Gomez-Camacho, Exergy analysis of the SOL-14 Plant, *Desalination* 137, pp. 251-258, 2001.
- [4] Tiwari, G.N., Dimri, V., Chel, A., 2009, Parametric study of an active and passive solar distillation system: Energy and exergy analysis, *Desalination* 242, pp.1-8, 2009.
- [5] Aljundi, I.H., Second-law analysis of a reverse osmosis plant in Jordan, *Desalination*, vol. 239, pp. 207-215, , 2009.
- [6] Cerci, Y., Exergy analysis of a reverse osmosis desalination plant in California, *Desalination*, vol. 142, pp. 257-266, 2002.
- [7] Kahraman, N. and Cengel, Y., Exergy analysis of a MSF distillation plant, *Energy Conv. Mgmt*, Vol. 46, pp. 2625-2636, 2005.
- [8] Modaresifar, M., Zenouzi, M. & Kowalski, G.J., Exergetic Performance Comparisons of Solar Desalination Devices and Reverse Osmosis Processes, *Proceedings of the ASME-ESFuelCell2012 Conference in San Diego*, July 23-26, 2012 (ESFuelCell2012-91517) , 2012.
- [9] Modaresifar, M., Zenouzi, M. & Kowalski, G.J. Exergy Analysis for Solar Desalination Devices and Processes, To be presented at *Proceedings of the ASME 2013 7th International Conference on Energy Sustainability & 11th Fuel Cell Science, (Engineering and Technology Conference ESFuelCell2013)*, July 14-19, 2013.
- [10] Masters, G.M., *Renewable and Efficient Electric Power Systems*, Wiley, Hoboken, NJ, 2004.
- [11] Sharqawy, M.H., Lienhard V, J.H., Zubair, S.M., Formulation of Seawater Flow Exergy using Accurate Thermodynamic Data, *Proceedings of the ASME-IMECE2010*, November pp12-18, Vancouver, British Columbia, Canada, IMECE2010-40915, 2010.
- [12] Sharqawy, M.H., Lienhard V, J.H., Zubair, S.M., On Exergy Calculations of Seawater with Applications in Desalination Systems, *International Journal of Thermal Sciences*, vol 50, pp187-196, 2011.
- [13] Nafiz Kahraman, Yunus A.Cengel, Exergy analysis of a MSF distillation plant, *Energy Convers Management*, Vol. 16, Issues 15-16, pp. 2625-63, 2005.
- [14] A. Rashad and A.EI Maihy, Energy and Exergy Analysis of a Steam Power Plant in Egypt, *13th International Conference on Aerospace Sciences & Aviation Technology, ASAT- 13*, May 26 – 28, 2009.

PANEL B

NON-EQUILIBRIUM THERMODYNAMICS: THE VARIOUS APPROACHES AND THEIR REASONS

MESOSCOPIC NON-EQUILIBRIUM THERMODYNAMICS

Dick Bedeaux, Signe Kjelstrup

Department of Chemistry, NTNU, 7491 Trondheim, Norway

EXTENDED ABSTRACT

Classical thermodynamics is a theory for a collection of molecules in equilibrium. What happens if the number of molecules in the system becomes smaller and smaller, and the system boundaries reflect conditions further and further away from equilibrium? Can we still use thermodynamics? In our work we have found that the answer is yes. The field of non-equilibrium thermodynamics can be extended to mesoscopic systems and describe in a systematic manner even molecular behavior far from equilibrium conditions. Using the concept of internal variables along the reaction coordinate we derive the law of mass action. This shows that the mesoscopic analysis gives a natural explanation of the fact that the reaction rate is a nonlinear function of the Gibbs energy of the reaction. The theory can be applied to RNA stretching experiments. This application shows why stretching RNA leads to different results when one uses a constant force to stretch or when one stretches to a constant length. This relates to the fact that for small systems the results differ for different ensembles. Important work was done on this issue by Hill who wrote a book in the sixties of the last century on equilibrium thermodynamics of small systems. Furthermore the mesoscopic analysis can be applied to active transport by the Ca-ATPase. We were able to explain how temperature differences feature in this phenomenon. This understanding is relevant for instance to understand thermogenesis. In conclusion we find that mesoscopic non-equilibrium thermodynamic theory can be used, also on a molecular level.

REFERENCES

- [1] S. Kjelstrup, D. Bedeaux, Isabella Inzoli, Jean-Marc Simon, Criteria for validity of thermodynamic equations from non-equilibrium molecular dynamics simulations, *Energy*, 33 (2008) 1185-1196
- [2] D. Bedeaux, J. Ortiz de Zárate, I. Pagonabarraga, J.V. Sengers and S. Kjelstrup, Concentration fluctuations in non-isothermal reaction-diffusion systems. II. The nonlinear case, *J. Chem. Phys.* 135 (2011) 124516
- [3] J.M. Rubi, D. Bedeaux and S. Kjelstrup, Thermodynamics for small molecule stretching experiments, *J. Phys. Chem. B*, 110 (2006) 12733-12737
- [4] T.L. Hill, *Thermodynamics of small systems*, Benjamin Inc. 1963; Dover, 1994
- [5] D. Bedeaux and S. Kjelstrup, The measurable heat flux that accompanies active transport by Ca-ATPase, *Phys. Chem. Chem. Phys.* 48 (2008) 7304-7317
- [6] A. Lervik, D. Bedeaux, and S. Kjelstrup, Kinetic and mesoscopic non-equilibrium description of the Ca²⁺-pump: a comparison, *Eur. Biophys. J.* 41 (2012) 437-448.

STUDYING NON-EQUILIBRIUM THERMODYNAMICS USING NON-EQUILIBRIUM MOLECULAR DYNAMICS SIMULATIONS

Peter J. Daivis

School of Applied Sciences, RMIT University
GPO Box 2476, Melbourne Vic 3001, Australia
E-mail: peter.daivis@rmit.edu.au

ABSTRACT

One of the greatest hindrances to the development of theories of non-equilibrium thermodynamics beyond the local equilibrium approximation is the difficulty of formulating definitive experimental tests of the basic concepts. For example, the existence and definition of quantities such as temperature and entropy in far-from-equilibrium systems are extremely difficult questions to directly address by experiment. Of course, this is partially due to the extraordinary success and great range of validity of non-equilibrium thermodynamics in the local-equilibrium approximation. It is usually necessary to create systems under extreme conditions such as shock waves, if we want to see deviations from the local equilibrium approximation, although non-Newtonian fluids also provide some opportunities. Even in these situations, gaining direct experimental access to measurable quantities that can be related to the theory is not simple. Alternatively, non-equilibrium molecular dynamics simulations are an ideal test environment for many concepts in non-equilibrium thermodynamics. Many quantities of interest can be directly computed in molecular dynamics simulations. In this paper, I would like to discuss several ways in which non-equilibrium molecular dynamics simulations can be used to extract detailed information that can contribute to a deeper understanding of non-equilibrium thermodynamics. I will also describe some of the pitfalls of this approach.

INTRODUCTION

Classical non-equilibrium thermodynamics as presented by de Groot and Mazur [1] and others, has been incredibly successful in providing a unified description of an enormous breadth of non-equilibrium phenomena. However, there still remain many non-equilibrium processes that do not fit within the realm of the classical treatment. Some examples include extremely rapid heating and deformation of simple fluids (as found in shock waves, for example), and the deformation of complex materials with large relaxation times (rheology) [2]. Although many successful thermodynamically oriented theories have been developed to describe these phenomena, they are often quite specific to particular materials or processes. Furthermore, there is still disagreement about the basic assumptions underlying these extensions to classical non-equilibrium thermodynamics. Direct comparisons between experimental results and theories often lack the detail needed to test these basic assumptions. For example the concepts of temperature and entropy, which are so important in equilibrium thermodynamics, become controversial when the local equilibrium assumption is violated, but it is very difficult to delineate the range of validity of the local equilibrium assumption experimentally.

Computer simulation methods offer the opportunity to escape some of the constraints of experimental studies. Non-equilibrium molecular dynamics simulation methods have developed rapidly since the late 1970's to the point where the techniques and the theory behind them are now fairly well understood [3]. In molecular dynamics simulations, we have the opportunity to calculate almost all properties of interest while subjecting the sample to a wide variety of different perturbations, some of which could never be achieved in a controlled

way in the laboratory. However, the new pathways opened up by non-equilibrium molecular dynamics simulation techniques also lead us into unknown thermodynamic territory.

In this paper, I will first very briefly summarise the main assumptions of classical non-equilibrium thermodynamics and the ways that they can be generalised. In the second half of the paper, I will discuss two different types of non-equilibrium molecular dynamics simulations in which extensions to classical non-equilibrium thermodynamics are required.

NON-EQUILIBRIUM THERMODYNAMICS

Any brief discussion of non-equilibrium thermodynamics will be necessarily and inevitably incomplete. However, I hope that this will be sufficient to serve as a theoretical framework for the second part of the paper.

Classical non-equilibrium thermodynamics

The two major assumptions made in classical non-equilibrium thermodynamics are the local equilibrium assumption and the assumption that linear (algebraic) constitutive equations are sufficient. The local equilibrium assumption essentially postulates that the local values of fields such as the internal energy, pressure, density and entropy can be expressed entirely in terms of their equations of state using the local values of their independent variables. Thus, we can assume that the local internal energy density is a function of the local entropy, temperature, pressure and mass densities use the first and

second laws of equilibrium thermodynamics to write

$$\rho \frac{du}{dt} = \rho T \frac{ds}{dt} + \frac{p}{\rho} \frac{d\rho}{dt}. \quad (1)$$

This says that the time dependence of the internal energy is due entirely due to the time dependence of the (independent variables i.e. the specific entropy and the density) appearing in the Gibbs equation (combined first and second laws of thermodynamics). From energy conservation, we also have

$$\rho \frac{du}{dt} = -\nabla \cdot \mathbf{J}_q - \mathbf{P}^T : \nabla \mathbf{v} \quad (2)$$

and equating eq(1) with eq(2) also using the assumption that the rate of change of the local entropy density is given by

$$\rho \frac{ds}{dt} = -\nabla \cdot \mathbf{J}_s + \sigma \quad (3)$$

we obtain the usual expression for the entropy production (for details, see [1]),

$$\sigma = -\frac{1}{T} (\mathbf{P}^T - p\mathbf{1}) : \nabla \mathbf{v} - \frac{1}{T^2} \mathbf{J}_q \cdot \nabla T \quad (4)$$

where $\mathbf{P}^T - p\mathbf{1}$ is the non-equilibrium part of the pressure tensor. When the part of the entropy production due to stresses is decomposed into its irreducible components, we obtain terms due to the scalar, traceless symmetric and antisymmetric components of the pressure and velocity gradient tensors. At this point in the classical treatment of non-equilibrium thermodynamics, the assumption of linear algebraic constitutive equations is made. The fluxes are assumed to be linear algebraic functions of the thermodynamic forces and we have

$$\Pi = -\eta_V \nabla \cdot \mathbf{v}, \quad \mathbf{P}^{ts} = -2\eta (\nabla \mathbf{v})^{ts}, \quad \mathbf{J}_q = -\lambda \nabla T \quad (5)$$

These equations are valid for isotropic materials in the linear response regime and in the absence of memory and spatial non-locality. In this sense, they are quite restrictive, but they nevertheless describe a wide range of phenomena.

Deviations from local equilibrium

Classical non-equilibrium thermodynamics cannot correctly describe the behaviour of viscoelastic materials, even in a steady state. This is because, even though the viscoelastic constitutive equation (for a Maxwell model material, for example) reduces to Newton's law of viscosity in a steady state, the Gibbs equation must also be modified to account for elastic stored energy. In this sense, the local equilibrium assumption is violated. To account for the stored energy, the work done by stresses must be broken into elastic and viscous components. The decomposition of the work into elastic and viscous components for a general linear viscoelastic material has been discussed in detail previously [4; 5]. Here we will just consider the particularly simple case of a Maxwell model fluid in steady shear.

For a Maxwell model fluid, the shear stress is given by

$$P_{yx} + \tau \frac{dP_{yx}}{dt} = -\eta \dot{\gamma} \quad (6)$$

where $\tau = \eta/G$ is the viscoelastic relaxation time and the work done by the shear stress is

$$\frac{1}{\eta} P_{yx}^2 + \frac{1}{G} P_{yx} \frac{dP_{yx}}{dt} = -\dot{\gamma} P_{yx} \quad (7)$$

where η is the steady shear viscosity and G is the infinite frequency shear modulus. The terms involving these two coefficients naturally separate the work into purely viscous (irreversible) and purely elastic (reversible) contributions. When the system is taken from an equilibrium state into a thermostatted shearing steady state, the integral of the viscous term continues to increase with time, but the integral of the elastic term reaches a value depending on the shear rate (or stress) in the steady state, which becomes constant. Then the change in the total internal energy of the system can be written as the integral of eq(2) over the volume of the system and over time,

$$\Delta U = Q - W_I - W_R = Q_R - W_R \quad (8)$$

where we have defined $Q_R = Q - W_I$ as the reversible heat. This is reminiscent of the "compensated heat" of Clausius, recently discussed in detail again by Eu [6]. In a steady state, the irreversible part of the work is exactly matched by the heat removed from the system by the thermostat, and for this reason, it has been called the "housekeeping heat" [7; 8]. It is interesting to note that since the internal energy is a state function, we expect that the internal energy difference between an equilibrium state and a given shearing steady state should be independent of the path taken. Also, since we are free to take any path into the steady state (provided that it does end in the steady state), we can choose one for which $Q_R = 0$. This is analogous to an adiabatic process in equilibrium thermodynamics, but in this case, it requires a specially tuned thermostat rather than complete thermal insulation.

For the Maxwell model, we can write the reversible work in the steady state as

$$W_R = -\frac{V}{2G} P_{yx}^2 = -\frac{\dot{\gamma}^2 V \eta \tau}{2} \quad (9)$$

This can be expressed in terms of an extensive variable related to the shear rate as

$$W_R = -\frac{\dot{\gamma}^2 V \eta \tau}{2} = -\frac{(\dot{\gamma} V)^2 \eta \tau}{2V} = -\frac{\Gamma^2 \eta \tau}{2V} \quad (10)$$

where the velocity difference Δv is an external macroscopic variable

$$\Gamma = \dot{\gamma} V = \frac{\Delta v}{L} LA = \Delta v A \quad (11)$$

This is similar to the choice made by Sasa [9]. Jou et al. [2] have proposed an extensive variable based on the stress as an alternative macroscopic variable. Choosing a path to the steady state for which the reversible heat and the change in the volume are both zero, we find that the internal energy in the steady state is given by

$$U(S, V, \Gamma) = U(S, V, \Gamma = 0) + \frac{\Gamma^2 \eta \tau}{2V} \quad (12)$$

then we have

$$dU = TdS - pdV + \zeta d\Gamma \quad (13)$$

with

$$T = T_0 + \frac{\Gamma^2}{2V} \frac{\partial(\eta\tau)}{\partial S} \quad (14)$$

$$p = p_0 + \frac{\Gamma^2}{2V} \left(\frac{\eta\tau}{V} - \frac{\partial(\eta\tau)}{\partial V} \right) \quad (15)$$

$$\zeta = \frac{\eta\tau\Gamma}{V} \quad (16)$$

These equations show that the thermodynamic temperature and pressure in a shearing steady state must include strain rate dependent corrections. The same conclusion was reached by Jou et al. [2] from a completely different point of view. The resultant Gibbs equation shows that there is a rich set of Maxwell relations that it should be possible to investigate either experimentally or by computer simulation. In fact, some work in this direction has already been carried out, although the treatment in [4; 5] was slightly different from the one presented here.

Another way that local equilibrium can be violated is when certain degrees of freedom are heated and others are cooled, creating an relaxation of internal energy between different degrees of freedom. This immediately violates the assumption of local equilibrium, because at equilibrium, the temperatures of all degrees of freedom are equal. Internal thermal relaxation can be accounted for by proposing separate Gibbs equations for each of the internal energy reservoirs corresponding to the different degrees of freedom. Each of these is assumed to be at equilibrium internally but out of equilibrium with other degrees of freedom. Similar models have been investigated before in the context of plasma physics and NMR for example. They may at first seem unfamiliar, but they are not too different from the local thermodynamic equilibrium models in the sense that the standard local equilibrium models assume that we have spatially separated subsystems that are locally at equilibrium but at different temperatures. This idea has been developed in greater detail in the context of thermostats for non-equilibrium molecular dynamics simulations in [12]. From this, it is found that an additional term in the entropy production due to internal thermal relaxation appears.

Non-equilibrium molecular dynamics (NEMD) simulations exhibit both types of deviation from local equilibrium. Due to the extremely high shear rates generated in these simulations, viscoelastic effects (and also non-linear rheology) are easily observed, even for simple fluids. Also, the homogeneous thermostats that are applied in NEMD simulations remove heat specifically from some degrees of freedom while the dissipation occurs in others. This means that there are internal energy fluxes from the degrees of freedom where dissipation appears to those that are thermostatted. This will be described in more detail in the following section.

NON-EQUILIBRIUM MOLECULAR DYNAMICS SIMULATIONS

There are many different varieties of non-equilibrium molecular dynamics simulation. Some of them are designed to faithfully reproduce experimental conditions by incorporating explicit molecular boundaries by which thermodynamic driving

forces such as velocity and temperature gradients are applied to the fluid between them. These explicit boundary simulations are restricted in size due to computational limitations, making surface effects and inhomogeneity more apparent than they would be for macroscopic systems. In cases where these effects are the main focus of attention, this is an advantage. However, if the bulk macroscopic properties are the focus of interest, it is more convenient to use homogeneous simulations with periodic boundary conditions. In this case, the absence of explicit boundaries means that the thermodynamic forces must be applied through specially formulated external forces which generate the desired thermodynamic fluxes. The details of these homogeneous NEMD algorithms can be found in the literature [3; 11]. Because there are no explicit walls in homogeneous NEMD simulations, dissipated heat cannot be removed from the system by thermal conduction. Instead, additional forces in the equations of motion that do a type of work to remove heat have been developed. These thermostat terms are designed to control the value of a chosen quantity, which may be the internal energy, the kinetic temperature or some other measure of temperature. This raises the important question of the microscopic definition of temperature. At equilibrium, we can derive generalised statistical-mechanical expressions for the temperature directly from the thermodynamic definition of the temperature, but far less is known about the microscopic measures of temperature in far from equilibrium states.

Homogeneous shear

The equations of motion that are commonly used to generate a homogeneous velocity gradient are called the SLLOD equations of motion

$$\dot{\mathbf{r}}_i = \frac{\mathbf{p}_i}{m_i} + \mathbf{r}_i \cdot \nabla \mathbf{v} \quad (17)$$

$$\dot{\mathbf{p}}_i = \mathbf{F}_i - \mathbf{p}_i \cdot \nabla \mathbf{v} - \alpha \mathbf{p}_i \quad (18)$$

which generate shear flow when we set the velocity gradient as

$$\nabla \mathbf{v} = \begin{bmatrix} 0 & 0 & 0 \\ \dot{\gamma} & 0 & 0 \\ 0 & 0 & 0 \end{bmatrix} \quad (19)$$

where $\dot{\gamma}$ is the shear rate. The work done by stresses calculated from the microscopic expression for the rate of change of the internal energy exactly matches eq(2) when these equations are applied. These equations of motion include a thermostat through the last term of the momentum equation of motion. The thermostat coefficient α in this case acts to keeps the kinetic temperature fixed, where the kinetic temperature is given by

$$T_K = \frac{1}{(3N - N_C) k_B} \left\langle \sum_{i=1}^N \frac{\mathbf{p}_i^2}{m_i} \right\rangle. \quad (20)$$

N is the number of particles in the system and N_C is the number of constrained degrees of freedom. Note that the momentum appearing in this expression is the thermal part of the momentum, as defined by the position equation of motion, eq(17). Then we

have

$$\alpha = \frac{\sum_{i=1}^N \mathbf{p}_i \cdot (\mathbf{F}_i - \mathbf{p}_i \cdot \nabla \mathbf{v}) / m_i}{\sum_{i=1}^N \mathbf{p}_i^2 / m_i} \quad (21)$$

Eq(20) is not the only microscopic expression for the temperature that is available to us. For example, the configurational temperature, which only depends on the positions of the particles, is given by

$$k_B T_C = \frac{\left\langle \sum_{i=1}^N \left(\frac{\partial \Phi}{\partial \mathbf{r}_i} \right)^2 \right\rangle}{\left\langle \sum_{i=1}^N \frac{\partial^2 \Phi}{\partial \mathbf{r}_i^2} \right\rangle}. \quad (22)$$

where Φ is the total intermolecular potential energy of the system. At equilibrium the kinetic and configurational temperatures are equal.

We have used the SLLOD equations of motion to calculate the viscosity and first normal stress coefficient of a simple liquid undergoing shear flow in the presence of different types of thermostat [12]. Previous work has shown that as the strain rate is increased, the kinetic and configurational temperatures diverge from each other. Furthermore, it is also observed that the kinetic temperatures calculated from the different cartesian components of the thermal momentum diverge from each other as the strain rate is increased. Similarly, the configurational temperatures calculated from the different cartesian components of the force also begin to differ as the shear rate increases. This difference can be eliminated by constraining each independent cartesian kinetic and configurational temperature to the same set value with thermostats of increasing complexity (for details see [12]). It is interesting to observe that in each case, the limiting zero shear rate viscosity of the system (a linear transport coefficient) was the same within the statistical uncertainty. But the first normal stress coefficient, which is a second order property, changed dramatically under the influence of different thermostats. The value obtained also differed from the value found from the stress relaxation function evaluated at equilibrium, using the Coleman-Markovitz equation

$$\Psi_{1,0} = 2 \int_0^\infty t G(t) dt. \quad (23)$$

It has previously been shown that the first normal stress coefficient is related to the elastic energy stored in a shearing fluid [5].

The limiting zero shear rate values of viscosity and first normal stress coefficient for different thermostats are shown in Table 1. All of the values for the first normal stress coefficient differ from the value obtained from eq(23), which is evaluated at equilibrium. This provides strong evidence that the thermodynamic considerations discussed in the first section of this paper must be taken into account when analysing non-equilibrium molecular dynamics simulation results. In particular, we must question the use of microscopic expressions for temperature derived from the equilibrium distribution function to describe the state of systems that are in shearing steady states, particularly

Table 1. Zero shear rate viscosities and first normal stress coefficients calculated by NEMD for various thermostats.

temperatures fixed	η_0	error	$\Psi_{1,0}$	error
T_K	2.119	0.001	0.206	0.004
T_C	2.118	0.002	0.193	0.009
$T_{K\alpha}, \alpha = x, y, z$	2.124	0.006	0.27	0.03
$T_{C\alpha}, \alpha = x, y, z$	2.115	0.002	0.205	0.009
$T_{K\alpha}, T_{C\alpha}, \alpha = x, y, z$	2.120	0.003	0.24	0.02

when we consider non-linear properties such as the first normal stress coefficient. We must also account for temperature inhomogeneity between different degrees of freedom due to the action of the homogeneous thermostats employed in NEMD simulations. Work in this direction is currently under way.

Inhomogeneous shear

Extensions to classical non-equilibrium thermodynamics are also required for the analysis of results from inhomogeneous NEMD simulations. As an example, we will consider simulations that model the flow of a nanoparticle suspension through a narrow slit pore [13]. In these simulations, a binary solution of simple spherical particles is sandwiched between two planar molecular walls and an external field is applied to the fluid to generate Poiseuille flow. The equations of motion for the fluid are

$$\dot{\mathbf{r}}_i = \frac{\mathbf{p}_i}{m_i} \quad (24)$$

$$\dot{\mathbf{p}}_i = \mathbf{F}_i - \mathbf{F}_e m_i \quad (25)$$

where \mathbf{F}_e is the external field. Here, \mathbf{p}_i represents the laboratory frame momentum, not the thermal momentum. More details of the simulation technique can be found in [13; 14]. When a sufficiently low external field is applied to the fluid, we obtain a quadratic velocity profile, as predicted by the classical Navier-Stokes equations. Fig. 1 shows the velocity profile for a model colloidal fluid with an external field of $F_e = 0.0001$. The fluid consists of a solution of larger particles in an explicit solvent. The solute to solvent mass ratio is 10, the solute to solvent diameter ratio is 2.2254 and the mass fraction of colloid is 0.2939. The reduced temperature is equal to 1.0. The predicted velocity profile, using the viscosity calculated from independent homogeneous simulations at equilibrium using the Green-Kubo relation, is in excellent agreement with the simulation results within the error bars which are approximately the size of the plot symbols. In a similar way, we can calculate the kinetic temperature profile for the shearing fluid, as shown in Fig. 2. The surprising result here is that, even though the flow is slow enough for the Navier-Stokes equation for the velocity profile to apply very precisely, the temperature profile cannot be predicted using Fourier's law of heat conduction. It might be thought that by using Fourier's law, we have neglected the coupling of the heat flux to the concentration gradient (in other words, the Dufour effect). However, we have calculated all of the relevant transport coefficients and find that this term is negligible in comparison to the other effects. On the other hand, we do find that the additional quadratic term in the temperature

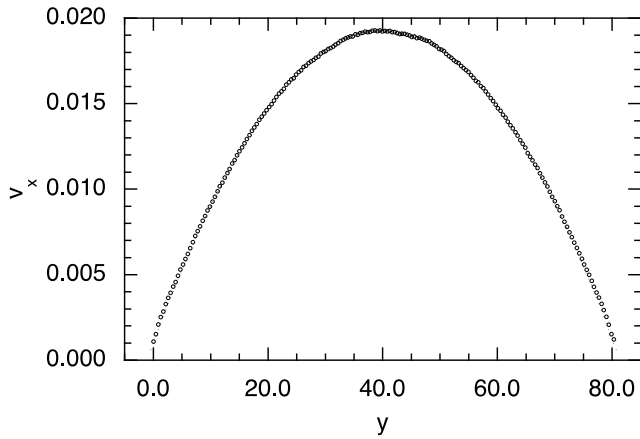


Figure 1. Velocity profile for a model colloid in planar Poiseuille flow.

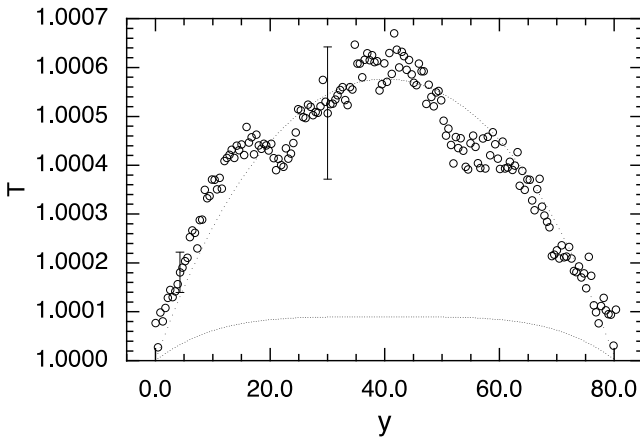


Figure 2. Temperature profile for a model colloid in planar Poiseuille flow. The solid line is the prediction of Fourier's Law and the dashed line is Fourier's Law supplemented with a nonlinear coupling to the strain rate.

profile is consistent with coupling to the strain rate. The heat flux is then given by

$$J_{qy} = -\lambda \frac{\partial T}{\partial y} - \xi \dot{\gamma} \frac{\partial \dot{\gamma}}{\partial y} \quad (26)$$

This coupling has been observed before in simulations of single component fluids [15; 16]. Further analysis of the coupling shows that it is only observable for very narrow channels - exactly the case that our non-equilibrium molecular dynamics simulations are restricted to, by computational limitations on the system size.

CONCLUSION

In this paper, we have shown how two quite different types of non-equilibrium molecular dynamics simulation cannot be described by classical non-equilibrium thermodynamics. It seems that the extensions that are required in order to have a consistent thermodynamic explanation of non-equilibrium molecular dynamics simulation results include the modification of the Gibbs equation to include a term due to the storage of elastic energy for viscoelastic fluids, a microscopic definition of temperature that can be used for shearing steady states, a proper account of

the effects of homogeneous thermostats in producing thermal relaxation between different degrees of freedom, and allowance for non-linear strain rate coupling in the constitutive equation for the heat flux. Clearly, non-equilibrium molecular dynamics simulations provide a fertile testing ground for extended theories of non-equilibrium thermodynamics.

ACKNOWLEDGMENT

I would like to thank Nicholas Miller for providing the data from his thesis [13].

REFERENCES

- [1] S.R. de Groot and P. Mazur, *Non-Equilibrium Thermodynamics*, Dover, London, 1984.
- [2] D. Jou, J. Casas-Vazquez and G. Lebon, *Extended Irreversible Thermodynamics*, Springer, Berlin, 2001.
- [3] D.J. Evans and G.P. Morriss, *Statistical Mechanics of Non-Equilibrium Liquids, 2nd Ed.*, Cambridge University Press, London, 2008.
- [4] P.J. Daivis and M.L. Matin, Steady-state thermodynamics of shearing linear viscoelastic fluids, *J. Chem. Phys.*, vol. 118, pp. 11111-11119, 2003.
- [5] P.J. Daivis, Thermodynamic relationships for shearing linear viscoelastic fluids, *J. Non-Newtonian Fluid Mech.*, vol. 152, pp. 120-128, 2008.
- [6] B.C. Eu, *Generalized Thermodynamics: The thermodynamics of Irreversible Processes and Generalized Hydrodynamics*, Kluwer, Dordrecht, 2002.
- [7] Y. Oono and M. Paniconi, Steady-state thermodynamics, *Prog. Theor. Phys. Suppl.*, vol. 130, pp. 29-44, 1998.
- [8] T. Hatano and S. Sasa, Steady-state thermodynamics of Langevin systems, *Phys. Rev. Lett.*, vol. 86, pp. 3463-3466, 2001.
- [9] S. Sasa and H. Tasaki, Steady-state thermodynamics, *J. Stat. Phys.*, vol. 125, pp. 125-227, 2006.
- [10] P.J. Daivis and D. Jou, Thermodynamic considerations on thermostats and Maxwell relations in steady sheared fluids, *Continuum Mech. Thermodyn.*, vol. 24, pp. 37-48, 2012.
- [11] B.D. Todd and P.J. Daivis, Homogeneous non-equilibrium molecular dynamics simulations of viscous flow: techniques and applications, *Molec. Sim.*, vol. 33, pp. 189-229, 2007.
- [12] P.J. Daivis, B.A. Dalton and T. Morishita, Effect of kinetic and configurational thermostats on calculations of the first normal stress coefficient in non equilibrium molecular dynamics simulations, *Phys. Rev. E*, vol. 86, art. no. 056707, 2012.
- [13] N.A.T. Miller, Heat and Mass Transport in Nanoconfined Colloidal Fluids, Ph.D. thesis (under examination), RMIT University, Melbourne, Vic., Australia 2013.
- [14] I. Snook, P. Daivis and T. Kairn, The flow of colloids and polymers in channels simulated using non-equilibrium molecular dynamics, *J. Pys. Condens. Matter*, vol. 20, art. no. 404211, 2008.
- [15] A. Baranyai, D.J. Evans and P.J. Daivis, Isothermal shear-induced heat flow, *Phys. Rev. E*, vol. 46, pp. 7593-7600, 1992.
- [16] B.D. Todd, and D.J. Evans, Temperature profile for Poiseuille flow, *Phys. Rev. E*, vol. 55, pp. 2800-2807, 1997.

DISSIPATION AND THE FOUNDATIONS OF STATISTICAL THERMODYNAMICS

Denis J Evans*, Debra J. Searles^o, S.R. Williams*

*Research School of Chemistry, Australian National University, Canberra, ACT 0200, Australia

^oAustralian Institute of Bioengineering and Nanotechnology and School of Chemistry and Molecular Biosciences,
The University of Queensland, Brisbane, Qld 4072, Australia

ABSTRACT

The argument of the Evans Searles Fluctuation Theorem [1], namely the dissipation function [2] is also the key quantity in all linear and nonlinear response theory [3]. It is also the key quantity in the proof of the newly discovered equilibrium relaxation theorems. For the first time we have, subject to certain simple assumptions, a proof of thermal relaxation to the canonical distribution function [4] postulated by J. Willard Gibbs.

REFERENCES

- [1] D.J. Evans and D.J. Searles, Phys. Rev. E 50,1645(1994).
- [2] D.J. Searles and D.J. Evans, J.Chem. Phys., 113,3503(2000).
- [3] D.J. Evans, D.J. Searles and S.R. Williams, J. Chem. Phys., 128, 014504(2008), *ibid*, 128, 249901(2008).
- [4] D.J. Evans, D.J. Searles and S.R. Williams, J. Stat Mech.,P07029(2009).

MULTISCALE MESOSCOPIC DYNAMICS AND THERMODYNAMICS

Miroslav Grmela

École Polytechnique de Montréal, C.P.6079 suc. Centre-ville, Montréal, H3C 3A7, Québec, Canada
E-mail: miroslav.grmela@polymtl.ca

EXTENDED ABSTRACT

Dynamics is primary and statics secondary in investigations of macroscopic systems. It is in the time evolution where explanations for their behavior, both static and dynamics, have to be searched. By the time evolution we mean either the microscopic time evolution of $\sim 10^{23}$ microscopic particles composing them or a multiscale mesoscopic time evolution. In this investigation we concentrate on the latter.

Different types of observations of macroscopic systems have led to different experiences that in turn have led to different theoretical frameworks providing settings for their organization and understanding. As an example we mention fluid mechanics (FM) and kinetic theory (KT), both involving the time evolution, and a static theory known as classical equilibrium thermodynamics (CET). We recall that all these three theories (we shall call them levels of description) have arisen (recall their well known history) independently one of the other and all three are completely self-contained (i.e. they do not need others to be applied). Depending on the amount of details involved on the levels, a hierarchical order can be established. We say that KT is more microscopic (i.e. involving more details) than FM and CET and that FM is more microscopic than CET. Instead of saying that KT is more microscopic than FM we can also equivalently say that FM is more macroscopic than KT. Formally, we shall denote the levels by the symbol \mathcal{L} and we shall say that a level \mathcal{L}_j is more microscopic than \mathcal{L}_i if $j > i$.

Having a family of levels (that are initially completely independent and unrelated) equipped with the hierarchical order, we can attempt to recognize a level \mathcal{L}_i as a pattern emerging in an analysis of the time evolution on a more microscopic level $\mathcal{L}_j; j > i$. I make now the following proposition: **Passages from \mathcal{L}_j to $\mathcal{L}_i; i < j$ share a universal structure that I will call Multiscale Mesoscopic Dynamics (MMD)**. This abstract dynamics encompasses both classical as well as mesoscopic equilibrium and nonequilibrium thermodynamics. Below, I will make a few comments about MMD. A more detailed presentation can be found for instance in [1],[2],[3],[4].

We begin with CET. Its essence is maximization of entropy known as MaxEnt principle. The entropy is a potential (a real valued function of state variables satisfying certain requirements). Its specification is called a fundamental thermodynamic relation. Two questions arise: Where does the fundamental thermodynamic relation come from, and why is the entropy maximized. For answers we turn to the time evolution taking place on a more microscopic level (e.g. KT). The entropy is a potential (or one of the potentials) generating the (fast) time evolution bringing the macroscopic system under consideration to states at which the more macroscopic level (e.g. CET) applies. The maximization of the entropy during the fast time evolution is a manifestation of the approach to the more macroscopic level on which either no time evolution takes place (as it is in the case of CET) or a slow time evolution takes place (as it is for example in the case of the passage $\text{KT} \rightarrow \text{FM}$).

The main challenge in the mathematical formulation of the abstract thermodynamics is to identify a geometry in which the Hamiltonian (i.e. time reversible and nondissipative) dynamics (formulated in the setting of *symplectic geometry*) naturally coexists with the gradient (i.e. time irreversible and dissipative) dynamics (formulated in the setting of *Riemannian geometry*). Such geometry appears to be a *contact structure geometry*. This conclusion arises also from the following argument. We ask the question of what is the group of transformations playing a dominant role in thermodynamics. The answer is: it is a group of Legendre transformations (since these are the transformations arising in MaxEnt). It is then well known that the contact structure geometry provides a natural setting for Legendre transformations.

REFERENCES

- [1] M. Grmela, "Multiscale Equilibrium and Nonequilibrium Thermodynamics in Chemical Engineering: Adv. Chem. Engineering **39**, 75-128 (2010)
- [2] M. Grmela, "Fluctuations in Extended Mass-Action-Law Dynamics", Physica D, **241**, 976-986 (2012)
- [3] M. Grmela, "Role of Thermodynamics in Multiscale Physics", Computers and Mathematics with Appl. DOI. org/10.1016/j.camwa.2012.11.019 (2013).
- [4] M. Grmela, "Extensions of Nondissipative Continuum Mechanics Toward Complex Fluids and Complex Solids" Cont.Mech.Themod. **25**, 55-57 (2013)

THERMODYNAMICS FROM THE PERSPECTIVE OF INFORMATION GEOMETRY

Jan Naudts

Physics Department, Universiteit Antwerpen,
Universiteitsplein 1, 2610 Antwerpen Belgium,
E-mail: Jan.Naudts@ua.ac.be

EXTENDED ABSTRACT

The statistical foundation of equilibrium thermodynamics relies heavily on the Gibbs distribution and its dependence on a few intensive variables such as the inverse temperature β and the chemical potential μ . In mathematical statistics these probability distributions are said to belong to the exponential family of models. In systems out of equilibrium the rationale for Gibbs distributions disappears. Other types of modeling, such as those tried out in the area of complex systems, are indicated.

My approach is based on generalizing the concept of an exponential family [1]. In the simplest case this is the q -exponential family as found in non-extensive statistical physics [2]. Here q is a deformation parameter. It equals 1 in the standard case. The same family is known in the domain of information geometry as Amari's alpha-family [3]. The concept has been further generalized in [4; 5] and applies in the context of both classical and quantum systems.

An essential characteristic of these generalized theories is that the dual structure of thermodynamics survives. The model states satisfy the maximum entropy principle. The dual of the inverse temperature β is the energy U . A Massieu function $\Phi(\beta)$ replaces the logarithm of the partition sum. Its contact transform is the thermodynamic entropy $S(U)$.

The main tool of the geometric formalism is a divergence function, which is the relative entropy functional of the physics literature. It is used as a distance measure. Arbitrary states are projected onto the manifold of model states by minimizing the divergence. The projection can be claimed to be orthogonal because a Pythagorean relation holds.

A nice example of the geometric approach is found in a study of the porous medium equation [6]. There it is proved that the projection of an arbitrary solution onto the statistical manifold of q -Gaussian distributions follows a geodesic. This suggests that it suffices to study the dynamics of the model states to capture the essence of non-equilibrium thermodynamics.

REFERENCES

- [1] J. Naudts, *Generalised Thermostatistics* (Springer Verlag, 2011).
- [2] C. Tsallis, *Introduction to nonextensive statistical mechanics* (Springer Verlag, 2009).
- [3] S. Amari and H. Nagaoka, *Methods of Information Geometry*, Translations of Mathematical Monographs (Oxford University Press, Oxford, UK, 2000) (originally in Japanese (Iwanami Shoten, Tokyo, 1993)).
- [4] J. Naudts, *Estimators, escort probabilities, and phi-exponential families in statistical physics*, *J. Ineq. Pure Appl. Math.* **5** (2004) 102.
- [5] J. Naudts, B. Anthonis, *The exponential family in abstract information theory*, arXiv:1302.5205 [cs.IT].
- [6] A. Ohara, *Geometric study for the Legendre duality of generalized entropies and its application to the porous medium equation*, *Eur. Phys. J.* **B70** (2009) 15–28.

NON-EQUILIBRIUM TEMPERATURES IN SYSTEMS WITH INTERNAL VARIABLES

David Jou *, Liliana Restuccia**

* Universitat Autònoma de Barcelona, Grup de Física Estadística,
08193 Bellaterra, Catalonia, Spain, E-mail: David.Jou@uab.cat

** University of Messina, Department of Mathematics, Viale F. Stagno D'Alcontres 31,
98166 Messina, Italy, E-mail: lrestuccia@unime.it

ABSTRACT

We discuss different definitions of non-equilibrium temperature in systems with internal variables. In equilibrium states, all the different definitions of temperature (caloric, entropic, kinetic, vibrational, configurational, fluctuational, and so on) lead to the same value, but in non-equilibrium they lead to different values. Out of equilibrium, equipartition is not to be expected and therefore the "temperatures" of the different degrees of freedom will be different from each other. Here, we focus our attention on the caloric temperature, based on the internal energy corresponding to the internal variable, the entropic temperature, based on the entropy, and several thermometric or empirical temperatures, based on the zeroth law. We illustrate the difference and the connections between them in some simple systems with a heat flux (two-level and three-level systems, ideal gases), and we also consider a solid system with internal variables. These variables may be measured, but not controlled, and they appear in the Gibbs equation like the classical thermodynamic variables. As an example, we consider a crystal with dislocations submitted to an external flux of energy (like a wall of a fusion reactor bombarded by energetic particles).

INTRODUCTION

Temperature is a concept common to all thermodynamic approaches. However, the meaning and measurement of temperature in non-equilibrium steady states beyond the local-equilibrium approximation is one of the fundamental problems in advanced non-equilibrium thermodynamics. Thus, it is logical that different approaches may consider temperature from different perspectives. For instance, in rational thermodynamics, it is considered as a primitive quantity. In theories with internal variables, each variable could have in principle its own temperature. In extended thermodynamics, temperature is assumed to depend also on the fluxes. In statistical theories, temperature may be related to the form of the distribution functions. Thus, a comparative discussion of the several thermodynamic approaches requires as a preliminary condition to compare and clarify the role of temperature.

Wide surveys of this topic are in [1]-[5]. Out of equilibrium, energy equipartition is not expected and, therefore, different measurements of temperature, sensitive to different sets of degrees of freedom, will yield different values for the temperature. From the theoretical perspective as well, different definitions of temperature will also lead to different values of this quantity.

For instance, in a system composed of matter and radiation, a thermometer with purely reflecting walls will give the temperature of matter, as it will be insensitive to radiation. In contrast, a thermometer with perfectly black walls will yield a temperature related both to matter and radiation. In equilibrium, both thermometers will give the same temperature, but in a non-equilibrium steady state (for instance, with photons transmitting heat and colliding against the particles of a gas) these thermometers will give different temperatures.

Another situation with several -or many-temperatures arises

in mixtures of gases with internal degrees of freedom and at high temperatures, as in the entry of spaceships into a planetary atmosphere. In such a case, one may have different kinetic temperatures for different gases, and different electronic temperatures (related to the relative occupancy of electrons at the several energy levels), and different vibrational and rotational temperatures. All these temperatures may be experimentally obtained by means of spectrometric methods, by measuring the intensity of the spectral lines emitted by the gases.

As it was pointed out in [1], instead of trying to attribute to some of the mentioned temperatures a more relevant role than to others (this will be indeed the case, but for different kinds of temperatures depending on the problem being addressed to), one should try to obtain the relations between them when the conditions on the system (total energy, energy flux, and so on) are specified. In fact, the ensemble of these different temperatures yields a very rich information about the system: about their internal energy transfers and their internal energy contents for the several degrees of freedom.

Here, we will discuss in detail the thermometric, caloric and entropic temperatures for systems with internal variables, the first one related to the zeroth law, the second one being based on the internal energy of the variable, and the third one related to its entropy.

TEMPERATURE DEFINITIONS IN EQUILIBRIUM THERMODYNAMICS

In equilibrium thermodynamics there are several definitions of temperature: empirical (based on the zeroth law), caloric (based on the first law), and entropic (based on the second law). Here, we remind the reader these definitions.

Empirical definition:

Empirical (or thermometric) temperature is defined by the zeroth law, which states the transitive character of thermal equilibrium. In particular, it states that if a state A of a system is in equilibrium with state B of another system, and state B is in equilibrium with state C of a third system, states A and C are in mutual thermal equilibrium.

Entropic definition:

The most fundamental definition of temperature in equilibrium thermodynamics is that appearing in the Gibbs equation.

$$\frac{1}{T} \equiv \left(\frac{\partial S}{\partial U} \right)_{\text{all other extensive variables}}, \quad (1)$$

where the subscript "all other extensive variables" means that the derivative must be carried out keeping constant all the other extensive variables appearing in the entropy, as for instance the volume V , the number of particles N_i of the species i and so on.

Caloric definition:

Another definition of temperature - we will call it the caloric definition, because it uses the so-called caloric equation of state relating internal energy and temperature - is obtained from the internal energy of the different degrees of freedom. For instance

$$U = U(T, V, N_i). \quad (2)$$

Since U is defined by the first principle, this definition is related to this principle.

TEMPERATURE DEFINITIONS IN STEADY STATE NON-EQUILIBRIUM THERMODYNAMICS

Our aim is to explore in a few simple situations how the temperatures defined by (1) and (2) differ in non-equilibrium steady states. Non-equilibrium steady states are different than equilibrium states because in them the system is crossed by fluxes of energy, matter, electric current and so on. Thus, it is interesting to investigate the influence of such fluxes on the thermodynamics of the system. The presence of fluxes is related to inhomogeneities in the system: the presence of a gradient of temperature, concentration, electrical potential or barycentric velocity.

Illustration 1: caloric and entropic temperatures in two-level system with an energy flux

First, we present an example related to a statistical description [6]. We illustrate the mentioned concepts of temperature with a two-level system, with N_1 particles at level 1 (with energy E_1) and N_2 particles at level 2 (with energy E_2). For instance, this could refer to electrons in two electronic levels, or to spins under an external magnetic field, or some other situations. The total internal energy will be $U = N_1 E_1 + N_2 E_2$; from here, one may define a caloric temperature T as

$$k_B T \equiv \frac{N_1}{N} E_1 + \frac{N_2}{N} E_2, \quad (3)$$

with N the total number of particles $N = N_1 + N_2$, and k_B the Boltzmann constant. On the other side, in equilibrium situations following the canonical distribution function, the temperature

will be defined as

$$k_B T \equiv \frac{E_2 - E_1}{\ln(N_1/N_2)}. \quad (4)$$

Assume now that the system is submitted to an energy flow q (energy per unit time), in such a way that the relative proportion of particles in states 1 and 2 is modified (for instance, the higher energy level 2 becomes more populated than in equilibrium, and the lowest level, which is receiving the external energy, becomes less populated).

Assume that the dynamics of the populations N_1 and N_2 is given by

$$\frac{dN_1}{dt} = -\frac{dN_2}{dt} = -\alpha N_1 + \beta N_2 - \gamma q N_1, \quad (5)$$

where α and β are the transition rates from 1 to 2 and from 2 to 1 respectively, and γ is a coefficient related to efficiency of energy absorption by particles in the lower level 1 bringing them to the higher level 2. The steady state solution of (5) is

$$\frac{N_1}{N_2} = \frac{\beta}{\alpha + \gamma q}. \quad (6)$$

For $q = 0$, one has

$$\frac{N_1}{N_2} = \frac{\beta}{\alpha} = \exp \left[-\frac{E_1 - E_2}{k_B T} \right]. \quad (7)$$

This is the detailed-balance relation amongst the rates. By keeping the definitions (3) and (4) but related to the non-equilibrium populations, one gets the following expressions for the non-equilibrium caloric temperature

$$T_{\text{neq,cal}} = T \frac{\alpha + \beta}{\alpha + \beta + \gamma q} \frac{E_1 + (\alpha + \gamma q)\beta^{-1}E_2}{E_1 + \alpha\beta^{-1}E_2}. \quad (8)$$

The entropy is

$$S = -k \left[\frac{N_1}{N} \ln N_1/N + \frac{N_2}{N} \ln N_2/N \right], \quad (9)$$

which in presence of q takes the form

$$S = S_{\text{eq}} - k_B \frac{\gamma^2}{\beta^2} \left[\frac{N}{N_1} + \frac{N}{N_2} \right] q^2. \quad (10)$$

This leads to

$$\frac{1}{T_{\text{neq,ent}}} = \frac{1}{T_{\text{cal}}} + k_B \frac{\gamma^2}{\beta^2} \frac{1}{(E_1 - E_2)N} \left[\frac{N^2}{N_1^2} - \frac{N^2}{N_2^2} \right] q^2. \quad (11)$$

Finally, the non-equilibrium thermometric temperature from (4) and (6) will be

$$T_{\text{neq,th}} = T \frac{1}{1 - \frac{\ln[1+(\gamma/\alpha)q]}{E_2 - E_1} k_B T}. \quad (12)$$

It is seen that these temperatures are different from each other when $q \neq 0$. Here, T is the equilibrium temperature, which is equal to the temperature of a thermal bath in which these systems are in contact. Note that in the extreme situations that the higher-level population 2 becomes higher than the lower level population 1, namely, for q higher than $(\beta - \alpha)/\gamma$, the entropic temperature becomes negative, whereas the caloric temperature remains positive. Note that a thermometer in equilibrium in contact with the system will measure temperature (12), rather than temperature (8) or (11). From temperature (12) it would be possible measure γ . Spectrometric methods allow to measure temperature (12) through the intensity of spectral emission line corresponding to $2 \rightarrow 1$.

Illustration 2: thermometric temperature in three-level system with an energy flux

To discuss the problems related to zeroth law and thermometric temperature we consider a three-level system, with energies $E_1 < E_2 < E_3$, and assume, for the sake of simplicity, the simplest triangular scheme for its possible internal transitions, namely $1 \rightarrow 2 \rightarrow 3 \rightarrow 1$. More realistic schemes are possible, but here we want to stick to the simplest illustrations. The evolution of the atomic populations N_1, N_2 and N_3 will be given by

$$\begin{aligned} \frac{dN_1}{dt} &= -\alpha_1 N_1 + \beta N_3 - \gamma_1 q N_1, \\ \frac{dN_2}{dt} &= -\alpha_2 N_2 - \gamma_2 q N_2 + \alpha_1 N_1 + \gamma_1 q N_1, \\ \frac{dN_3}{dt} &= -\frac{dN_1}{dt} - \frac{dN_2}{dt}, \end{aligned} \quad (13)$$

where α_1, α_2 and β stand for the rate transitions coefficients; in particular, γ_1 and γ_2 stand for the part of the energy flux which interacts with particles in state 1 and in state 2. The steady state populations will be

$$\begin{aligned} \frac{N_1}{N_2} &= \frac{\alpha_2 + \gamma_2 q}{\alpha_1 + \gamma_1 q}, \\ \frac{N_1}{N_3} &= \frac{\beta}{\alpha_1 + \gamma_1 q}. \end{aligned} \quad (14)$$

The equilibrium temperature will be

$$k_B T = \frac{E_2 - E_1}{\ln(N_1/N_2)} = \frac{E_3 - E_1}{\ln(N_1/N_3)}. \quad (15)$$

The thermometric temperatures related to populations 1 and 2, as 1 and 3, will be the following non-equilibrium temperatures

$$T_{neq,12} = T \frac{1}{1 - \frac{\ln[1 + (\gamma_1/\alpha_1)q]}{E_2 - E_1} / \frac{\ln[1 + (\gamma_2/\alpha_2)q]}{E_3 - E_1}},$$

$$T_{neq,13} = T \frac{1}{1 - \frac{\ln[1 + (\gamma_1/\beta_1)q]}{E_3 - E_1}}. \quad (16)$$

A thermometer in contact with levels 1 and 2 would measure T_{12} , and a thermometer in contact with 1 and 3 would measure T_{13} ; analogously, a thermometer in contact with 2 and 3 would measure a temperature T_{23} defined in analogy with (16)_a and (16)_b. Of course, in equilibrium all these temperatures would be the same. It is not clear, instead, what would measure a thermometer in contact with 1, 2 and 3. From expressions (16) it would be possible to obtain γ_1 and γ_2 . Note, therefore, that the zeroth-principle of equilibrium thermodynamics cannot be applied to non-equilibrium steady states.

Illustration 3: caloric and entropic temperatures in non-equilibrium ideal gas

Ideal gases are a system for conceptual discussion of thermodynamic concepts [7], [8]. In kinetic theory, the temperature of a gas is usually defined as the kinetic temperature, which is a form of caloric temperature, through the relation

$$\frac{3}{2} k_B T = \langle \frac{1}{2} m C^2 \rangle, \quad (17)$$

where m and C are the mass and the velocity intensity of a gas particle, respectively. This relation has nothing to do with the special form of the distribution function. In non-equilibrium states, the distribution function may be written as

$$f(\mathbf{r}, C, t) = f_{eq}(\mathbf{r}, C, t) [1 + \Phi], \quad (18)$$

with f_{eq} the equilibrium distribution function characterized by the local values of the thermodynamic parameters, and Φ a non-equilibrium contribution. Up to the second order in Φ , the "entropy" s obtained from the H -function has the form

$$s = s_{eq} - \frac{1}{2} k_B \int f_{eq} \Phi^2 dC, \quad (19)$$

with s the entropy per unit volume. It is seen that, in principle, s will be different from the local-equilibrium entropy s_{eq} . Then one may define the entropic temperature as

$$\frac{1}{T_{neq,ent}} = \frac{\partial s}{\partial u} = \frac{1}{T} - \frac{k_B}{2c} \frac{\partial}{\partial T} \int f_{eq} \Phi^2 dC. \quad (20)$$

In a system submitted to a heat flux, the entropy (19) has the form, up to the second order in the heat flux,

$$s = s_{eq} - \frac{\tau}{2\lambda T^2} \mathbf{q} \cdot \mathbf{q}, \quad (21)$$

where τ is the collision time and λ the thermal conductivity. In more explicit terms, taking into account that

$$\lambda = \frac{5}{2} k_B \frac{p}{m} \tau, \quad (22)$$

the general expression (21) combined with definition (20) yields

$$\frac{1}{T_{neq,ent}} = \frac{1}{T} + \frac{2}{5} \frac{nm}{p^3 T} \mathbf{q} \cdot \mathbf{q}. \quad (23)$$

This temperature would be merely formal unless a method of measurement of it may be specified. It has been shown that this non-equilibrium temperature corresponds to the kinetic temperature in the plane perpendicular to the heat flux. Thus, if the heat flux is in the z direction, one has

$$\left\langle \frac{1}{2} m C_x^2 \right\rangle = \left\langle \frac{1}{2} m C_y^2 \right\rangle = \frac{1}{2} k_B T_{neq,ent} < \frac{1}{2} k_B T$$

and

$$\left\langle \frac{1}{2} m C_x^2 \right\rangle = \frac{1}{2} k_B (3T_{neq,ent} - 2T) > \frac{1}{2} k_B T \quad (24)$$

in such a way that the usual definition of T given in (18) is satisfied. Thus, the concept of the entropic definition of temperature is not in contradiction with that of the kinetic definition.

NON-EQUILIBRIUM TEMPERATURES IN CONTINUUM THERMODYNAMICS

Here, we formulate the problem in the framework of continuum thermodynamics and we consider non-equilibrium steady states, different than equilibrium states because in them the system is crossed by fluxes of energy, matter, electric current or so on. In classical irreversible thermodynamics it is assumed the local equilibrium hypothesis, that states that the fluxes have not an essential influence on the thermodynamics of the system. It assumes that a continuous system out of equilibrium may be decomposed in many small subsystems, each of which behaves, from a thermodynamic point of view, as if it was in local equilibrium.

Non-equilibrium steady states are the natural generalization of equilibrium states: in them, the values of the variables do not depend on time but, in contrast to equilibrium states, a continuous flux of energy - or matter, or momentum, or charge - must be supplied and extracted from the system. We recall the well-known Fourier's transport equation for heat flow \mathbf{q}

$$\mathbf{q} = -\lambda \nabla T, \quad (25)$$

with λ the thermal conductivity.

Beyond local equilibrium, for an ideal monoatomic gas, the entropy takes the form (21), which writes as

$$s(u, \mathbf{q}) = s_{eq}(u) - \alpha(u) \mathbf{q} \cdot \mathbf{q}, \quad (26)$$

where s and u are the entropy and the internal energy, respectively, per unit volume and $\alpha = -\tau(2\lambda T^2)^{-1}$. Using definition (1) we have for the entropic temperature θ

$$\frac{1}{\theta} = \left(\frac{\partial s}{\partial u} \right)_{\mathbf{q}} = \frac{1}{T} - \left(\frac{\partial \alpha(u)}{\partial u} \right) \mathbf{q} \cdot \mathbf{q}, \quad (27)$$

with T the caloric temperature. In a steady state we can use $\mathbf{q} = -\lambda \nabla T$ and rewrite relation (27) in the form

$$s(u, \mathbf{q}) = s_{eq}(u) - \frac{\tau \lambda}{2T^2} \nabla T \cdot \nabla T. \quad (28)$$

Non-equilibrium temperatures in solid systems with internal variables

In this section we will discuss the caloric and entropic non-equilibrium temperatures in a crystal with dislocations, submitted to a given energy flux. We have in mind, for instance, the walls of a fusion nuclear reactor, which are submitted to an intense neutron flux supplied by the nuclear reaction or an electronic device with hot electrons. The neutron flux has two effects on the walls: a thermal effect (it heats them), and a mechanical effect (it produces dislocations in the walls). The second effect is unwanted, because it may reduce the mechanical resistance of the wall.

We assume that in the considered medium we have following fields [9]-[11]: *the elastic field* described by the total stress tensor t_{ij} and the small-strain tensor ϵ_{ij} , defined by $\epsilon_{ij} = \frac{1}{2}(u_{i,j} + u_{j,i})$ (being u_i the components of the displacement vector), *the thermal field* described by the local temperature θ , and the heat flux q_i . However, we assume that the description of the evolution of the system requires the introduction of further dynamical variables in the thermodynamic state space like, for instance, an internal variable. But, whereas the classical variables may be measured and controlled, the internal variables cannot be controlled. In solid media they can describe internal defects like dislocation lines, point defects, porous channels, disclinations and so on. They appear in the Gibbs equation like the classical thermodynamical variables. The evolution of internal variables is described by rate equations, different from the constitutive relations, the transport equation of heat, the balance equations of mass, momentum, momentum of momentum and energy. The whole set of these equations describe the evolution of the system.

Thus, we introduce in the thermodynamic state space the internal variable a_{ij} and its flux V_{ijk} .

We assume that the *evolution equation* for the tensorial internal variable is the following

$$\frac{da_{ij}}{dt} + V_{ijk,k} = A_{ij}, \quad (29)$$

where a_{ij} is the dislocation core tensor, V_{ijk} is its flux and A_{ij} is a field source. The tensor a_{ij} , introduced by Maruszewski [12], describes the local structure of dislocations lines, which form a network of very thin lines disturbing the otherwise perfect periodicity of the crystal lattice. Since these very thin channels, in general, are not distributed isotropically, it is natural to describe them by a tensor, taking into account the local density of the dislocation channels along several directions

The tensor A_{ij} represents the source-like term describing the net effects of formation and annihilation of dislocation lines, which may be a function of temperature T , the strain tensor ϵ_{ij} , the energy flux \mathbf{q} , or the stress tensor t_{ij} . Equation (29) could be simplified, for instance, by assuming for the dislocation flux $V_{ijk} = -D \frac{\partial a_{ij}}{\partial x_k}$, with D being a diffusion coefficient for dislocations. On the other hand, the production term may be seen as the

combination of a dislocation-formation term and a dislocation-destruction term, namely, $A_{ij} = A_{ij}$ (formation) $-A_{ij}$ (destruction).

Then, we consider for the evolution equation for the internal variables the simple form

$$\frac{da_{ij}}{dt} - D\nabla^2 a_{ij} = A_{ij,eq} + \tilde{\alpha} q_i q_j. \quad (30)$$

Here, $A_{ij,eq}$ is the net formation tensor in the absence of an external energy flux ($\mathbf{q} = 0$), and we have added to it a tensor depending on the energy flux.

This form does not pretend to be especially realistic, but only to illustrate that thermal stresses related to $q_i q_j$ could influence the evolution of dislocation lines. More realistic than a simple energy flux, would be to consider, for instance, an energy flux due to the bombardment of the crystal with particles having relatively high energy, which could produce new defects or modify the structure of the dislocation lines.

Non-equilibrium entropic temperature

The entropic definition of absolute temperature is related to the Gibbs equation which, for the system we are considering, has the form

$$ds = \theta^{-1} dU + \theta^{-1} \sigma_{ij} d\varepsilon_{ij} - \theta^{-1} \pi_{ij} da_{ij} - \theta^{-1} \pi dq_i, \quad (31)$$

with π_{ij} the corresponding thermodynamic potential conjugate of the dislocation tensor a_{ij} and π the corresponding thermodynamic potential conjugate of the heat flux q_i . Here, u is the total internal energy of all the degrees of freedom, and we call θ the entropic (absolute) temperature to distinguish it from the T related to the caloric definition.

We have assumed that only the internal variable under consideration is modified by the presence of an external energy flow. Of course the classical variables, like U and ε_{ij} will also be modified by the flux, but here we refer to the modification of temperature for given values of the classical variables.

The thermodynamic absolute temperature is given by (1). In particular, for given values of the classical variable ε_{ij} and in steady states, the equilibrium temperature and the non-equilibrium temperature are defined by

$$\theta_{eq}^{-1} \equiv \left(\frac{\partial s}{\partial u} \right)_{\mathbf{q}=0}; \quad \theta_{neq}^{-1} \equiv \left(\frac{\partial s}{\partial u} \right)_{\mathbf{q} \neq 0}. \quad (32)$$

The quantity θ_{neq}^{-1} can be expanded around its equilibrium counterpart obtaining

$$\theta_{neq}^{-1} = \theta_{eq}^{-1} - \theta_{eq}^{-2} \frac{\partial \theta_{eq}}{\partial a_{ij}} \Delta a_{ij}, \quad (33)$$

where in steady states

$$\Delta a_{ij} = a_{ij}(\mathbf{q} \neq 0) - a_{ij}(\mathbf{q} = 0). \quad (34)$$

Then, in the first approximation, the non-equilibrium temperature θ_{neq} will be related to the equilibrium temperature corre-

sponding to a_{ij} ($\mathbf{q} = 0$) as

$$\theta_{neq} = \frac{\theta_{eq}}{1 - \theta_{eq}^{-1} \frac{\partial \theta_{eq}}{\partial a_{ij}} \Delta a_{ij}} \approx T \left(1 + T^{-1} \left(\frac{\partial T}{\partial a_{ij}} \right) \Delta a_{ij} \right) =$$

$$T + \left(\frac{\partial T}{\partial a_{ij}} \right) \Delta a_{ij}, \quad (35)$$

where we have taken into account that in equilibrium (or local-equilibrium) all the definitions of temperature coincide, therefore $\theta_{eq} = T$, and we have used the approximation $(1-x)^{-1} \approx 1+x$, for $x \ll 1$.

Non-equilibrium caloric temperature

To define the caloric definition of temperature first we consider the caloric equation of state at the equilibrium of the system for given values of ε_{kl} and for vanishing values of the external flux \mathbf{q} : $U_{dis} = U(a_{ij}(T, \varepsilon_{kl}), T, \varepsilon_{kl})$, where we have taken in consideration that at equilibrium the internal variable depends on temperature and the stress tensor. Then, we define the caloric non-equilibrium temperature field T_{neq} related to a_{ij} in a steady state in the following way

$$U_{dis}(a_{ij}(T_{neq}, \varepsilon_{kl}, \mathbf{q} = 0), T_{neq}, \varepsilon_{kl}) \equiv U_{dis}(a_{ij}(T, \varepsilon_{kl}, \mathbf{q}), T, \varepsilon_{kl}). \quad (36)$$

Then, to define the caloric non-equilibrium temperature assume that the formal expression of the relation between internal energy and temperature keeps, out of equilibrium, the same form as in equilibrium ($U_{dis} = U(a_{ij}(T, \varepsilon_{kl}), T, \varepsilon_{kl})$), where $\mathbf{q} = 0$, and we equate it to the value of internal energy in non-equilibrium, where $\mathbf{q} \neq 0$. Thus, we define the temperature in non-equilibrium state as that temperature which, introduced in the caloric state equation would give for the internal energy the actual value corresponding to the non-equilibrium state. Namely, we will have

$$T_{neq} = T + \left(\frac{\partial T}{\partial U_{dis}} \right) \Delta U_{dis} = T + \left(\frac{1}{c_{dis}} \right) \Delta U_{dis}, \quad (37)$$

where $\left(\frac{\partial T}{\partial U_{dis}} \right) \Delta U_{dis}$ is the non-equilibrium contribution due to the presence of $\mathbf{q} \neq 0$, and c_{dis} is the specific heat associated to the changes of the internal energy of dislocation lines, per unit volume, namely $c_{vdis} = \frac{\partial U_{dis}}{\partial T}$. The specific heat plays thus an important role in the caloric definition of temperature.

Entropic flux in the definition of non-equilibrium temperature

In [1] it was seen that in the case of a crystal with dislocations, the entropy flux has the form

$$J_k^s = \theta^{-1} q_k - \pi_{ij} \theta^{-1} V_{ijk}. \quad (38)$$

Here, the variable π_{ij} is the conjugate to a_{ij} as introduced in (31). It has been proposed that a convenient definition of a non-equilibrium contribution could be based on this expression (38),

taking as the reciprocal of thermodynamic temperature the coefficient linking the heat flux \mathbf{q} with the entropy flux \mathbf{J}^S . Based on the idea of perfect interfaces between systems, in which both the heat flux and the entropy flux would be continuous, Muller gave the definition of the so-called "coldness", namely, of the reciprocal of absolute temperature.

Considering the entropy flux and the heat flux through an interface between two systems (let us say, a thermometer and a system) is convenient, because this reminds us the importance of the contact between the system and the thermometer in measuring temperature.

In this aspect, problematic questions arise. In first place, the existence of ideal interfaces is a nice theoretical concept, but in general the interfaces between different materials are not ideal, but exhibit the so-called "thermal boundary resistance", which implies a discontinuity of temperature through the surface, and a corresponding discontinuity of the entropy flux, due to entropy production across the wall, due to the fact that heat is flowing between two different temperatures.

FINAL COMMENTS

In this presentation we have emphasized that one of the aims of non-equilibrium thermodynamics should be to find the transformation laws relating several thermometric, entropic, caloric and other temperatures in systems submitted to given energy flux.

This program has been partially carried out in [1] for forced harmonic oscillators in a thermal bath, in which case kinetic and vibrational temperatures play a special role, and for ideal gases in Couette flow [13], for kinetic temperatures along the three spatial axes, thermodynamic absolute temperature, local-equilibrium temperature, and fluctuation dissipation temperature, or the relation among some non-equilibrium temperatures in heat transport along nanowires [14].

Here, we have tried to be more general, both by the use of simple illustrations of two-level, three-level systems and ideal gases, as by the statement of this problem in the context of a more difficult and demanding situation of solids systems with dislocations.

REFERENCES

- [1] J. Casas-Vazquez and D. Jou, *Rep. Prog. Phys.* 66bb, p. 1937, 2003.
- [2] J. G. Powles, S. G. Rickayzen and D. M. Heyes, Temperatures: Old, New and Middle Aged, *Mol. Phys.*, vol. 103, pp.1361-1373, 2005.
- [3] W. G. Hoover and C. G. Hoover, Non-Equilibrium Temperature and Thermometry in Heat-Conducting Models, *Phys. Rev. E*, vol. 77, 041104, 2008.
- [4] E. Bertin, K. Martens, O. Dauchot and M. Droz, Intensive Thermodynamic Parameters in Non-Equilibrium Systems, *Phys. Rev. E*, vol. 75, 031120, 2007.
- [5] R. S. Johal, Quantum Heat Engines and Non-Equilibrium Temperature, *Phys. Rev. E*, vol. 80, 041119, 2009.
- [6] L. E. Reichl, *A Modern Course in Statistical Physics*, University Texas Press, Austin, 1998.
- [7] D. Jou, J. Casas-Vazquez and G. Lebon, *Extended Irreversible Thermodynamics*, Springer, Berlin, fourth edition, 2010.
- [8] D. Jou and L. Restuccia, Mesoscopic Transport Equations and Contemporary Thermodynamics: an Introduction, *Contemporary Physics*, vol. 52, 5, pp. 465-474, 2011.
- [9] W. Muschik, *Non-Equilibrium Thermodynamics with Applications to Solids*, Springer, Wien-New York, vol. 336, 1993.
- [10] L. Restuccia, Thermomechanics of Porous Solids Filled by Fluid Flow, in E. De Bernardis, R. Spigler and V. Valente (ed.), Series on Advances in Mathematics for Applied Sciences, *Applied and Industrial Mathematics in Italy III*, vol. 82, pp. 485-495, World Scientific, Singapore, 2010.
- [11] L. Restuccia, On a Non-conventional Thermodynamical Model of a Crystal with Defects of Dislocation, *to be published*.
- [12] B. T. Maruszewski, On a Dislocation Core Tensor, *Phys. Stat. Sol.(b)*, vol. 168, p.59, 1991.
- [13] M. Criado-Sancho, D. Jou and J. Casas-Vazquez, Non-equilibrium Kinetic Temperature in Flowing Gases, *Phys. Lett. A*, vol.350, pp. 339-341, 2006.
- [14] D. Jou, V. A. Cimmelli and A. Sellitto, Non-Equilibrium Temperatures and Second-Sound Propagation along Nanowires and Thin Wires, *Phys. Lett. A*, vol. 373, pp. 4386-4392, 2009.

MESOSCOPIC NON-EQUILIBRIUM THERMODYNAMICS FOR THE STOCHASTIC DYNAMICS OF SMALL-SCALE SYSTEMS

J. Miguel Rubi

Departament de Física Fonamental, Facultat de Física, Universitat de Barcelona, Martí i Franques, 1,
E-08028 Barcelona, Spain, E-mail: mrubi@ub.edu, Web: <http://www.ffn.ub.edu/webmrubi>

ABSTRACT

We show how to extend the use of thermodynamic concepts into the mesoscopic domain where fluctuations and nonlinearities play an important role. The theory presented: mesoscopic nonequilibrium thermodynamics, provides a new interpretation of local equilibrium that is formulated at small scales. From it one derives kinetic equations and nonlinear transport equation for the study of small-scale systems outside equilibrium.

1. INTRODUCTION

Systems in equilibrium strictly follow the laws of thermodynamics [1]. Despite the disordered motion of large numbers of molecules, the system can be characterized by a few variables accounting for average properties. Thermodynamics also applies to systems outside equilibrium, in the local equilibrium regime in which the volume elements are considered small thermodynamic systems in equilibrium. This hypothesis is fundamental in the formulation of non-equilibrium thermodynamics [2].

Non-equilibrium thermodynamics is restricted to the linear response domain in which the response of the system is linear in the perturbation exerted to remove it from equilibrium. Moreover, this theory performs a macroscopic description in terms of average values not accounting for the presence of fluctuations. Whereas the linear approximation holds for transport processes such as heat conduction and mass diffusion, even in the presence of large gradients [3], it is not appropriate for describing activated processes in which the system immediately enters the nonlinear domain. Small systems [4], such as single molecules in a thermal bath, in which fluctuations and nonlinearities can be very important, are beyond the scope of this theory.

We show that a probabilistic interpretation of non-equilibrium thermodynamics which uses the concept of local equilibrium at the mesoscale [5] sets the basis of a theory able to analyze irreversible processes in the presence of fluctuations. The theory (Mesoscopic Non-equilibrium Thermodynamics [6], [7]) obtains the Fokker–Planck equation as a diffusion equation for the probability and the nonlinear relationships between activation rates and proper affinities of activated processes. The situations that can be studied with this formalism include, among others, slow relaxation processes, barrier crossing dynamics, chemical and biochemical reactions (see Fig. 1), entropic transport, active transport, dissipative self-assembly and single molecules and molecular motors [7].

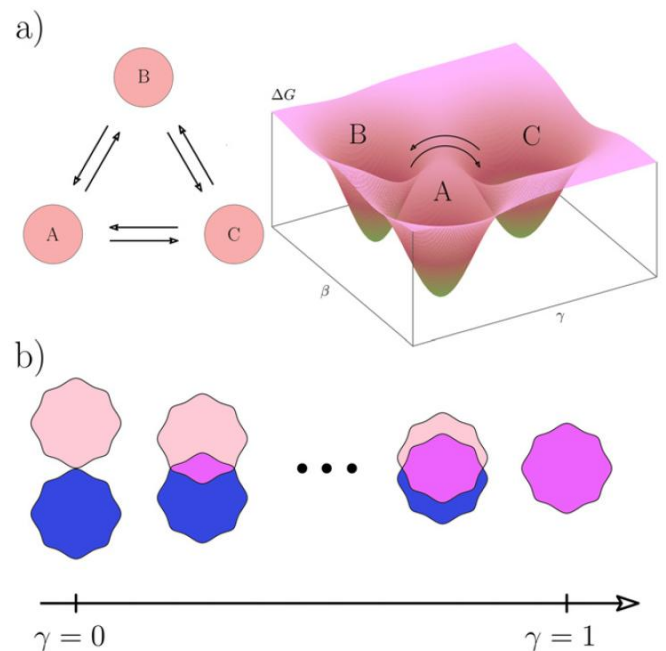


Figure 1: A chemical reaction can be treated as a diffusion process through a potential barrier that separates the initial and final states of the reaction which correspond to the minima of the potential. (a) Transformations of the molecules of a biochemical cycle viewed as a diffusion process in a free energy landscape. The configurations are described by means of two reaction coordinates γ and β . (b) In each reaction, the molecular structure of a substance transforms progressively until it reaches its final conformation.

These processes are, in general, nonlinear and influenced by the presence of fluctuations.

2. THERMODYNAMICS AND MESOSCOPIC DYNAMICS OF SMALL-SCALE SYSTEMS

A reduction of the observational time and length scales of a system usually implies an increase in the number of degrees of freedom which have not yet equilibrated and that therefore exert an influence in the overall dynamics of the system. The nonequilibrated degrees of freedom could be the velocity of a particle, the orientation of a spin, the size of a macromolecule or any coordinate or order parameter whose values define the state of the system in a phase space. The will be denoted by means of the set of coordinates γ ($\equiv \{\gamma_i\}$).

At the mesoscopic level, the characterization of the state of the system is performed through the knowledge of the probability density. The statistical expression of the entropy of the system in terms of this probability can be expressed by the Gibbs entropy postulate [2, 6]

$$S = S_{eq} - k_B \int P(\gamma, t) \ln \frac{P(\gamma, t)}{P_{eq}(\gamma)} d\gamma, \quad (1)$$

where S_{eq} denotes the entropy when the degrees of freedom γ are in equilibrium. The equilibrium probability density $P_{eq}(\gamma)$ can be related to the minimum reversible work required to create that state [4] through the expression

$$P_{eq} \sim \exp\left(\frac{-\Delta W(\gamma)}{k_B T}\right) \quad (2)$$

Here k_B is Boltzmann's constant, and T is the temperature of the heat bath. The minimum work can in general be expressed as

$$\Delta W = y\Delta Y \quad (3)$$

where y is an intensive parameter and Y its conjugated extensive variable. This general form stands for mechanical, electrical, magnetic, surface work, etc., performed on the system [4].

The expression of the minimum reversible work (3) reduces to the different thermodynamic potentials. For instance, for the case of constant temperature, volume and number of particles, the minimum work coincides with the Helmholtz free energy. The statistical mechanics definition of the entropy is therefore crucial to connect thermodynamics with the mesoscopic description in terms of the probability distribution $P(\gamma, t)$.

The dynamics of the mesoscopic degrees of freedom can be analyzed from the statistical mechanics definition of the entropy. Taking variations in Eq. (1), one obtains

$$\delta S = -k_B \int \delta P(\gamma, t) \ln \frac{P(\gamma, t)}{P_{eq}(\gamma)} d\gamma. \quad (4)$$

Conservation of the probability density in γ -space implies that it obeys the continuity equation

$$\frac{\partial P}{\partial t} = -\frac{\partial J}{\partial \gamma}, \quad (5)$$

where $J(\gamma, t)$ is a current in the space of mesoscopic coordinates.

To derive the expression of this current, we take the time derivative in equation (4) and use the continuity equation (5) to eliminate the probability time derivative. After a partial integration, one then arrives at the expression of the mesoscopic entropy production [6]

$$\sigma = -k_B \int J(\gamma, t) \frac{\partial}{\partial \gamma} \left(\ln \frac{P(\gamma, t)}{P_{eq}(\gamma)} \right) d\gamma, \quad (6)$$

This quantity expresses in the form of current-force pairs, the latter being the gradients in the space of mesoscopic variables. We will now assume a linear dependence between current and force and establish the linear relationship

$$J(\gamma, t) = -k_B L(\gamma, P(\gamma)) \frac{\partial}{\partial \gamma} \left(\ln \frac{P(\gamma, t)}{P_{eq}(\gamma)} \right), \quad (7)$$

where $L(\gamma, P(\gamma))$ is an Onsager coefficient [2], which in general depends on the probability $P(\gamma)$ interpreted as a state variable in the thermodynamic sense and on the mesoscopic coordinates γ .

The kinetic equation follows by substituting Eq. (7) into the continuity equation (5):

$$\frac{\partial P}{\partial t} = \frac{\partial}{\partial \gamma} \left(D P_{eq} \frac{\partial P}{\partial \gamma} \right), \quad (8)$$

where the diffusion coefficient is defined as

$$D(\gamma) \equiv \frac{k_B L(\gamma, P)}{P}. \quad (9)$$

This equation, which in view of Eq. (2) can also be written as

$$\frac{\partial P}{\partial t} = \frac{\partial}{\partial \gamma} \left(D \frac{\partial P}{\partial \gamma} + \frac{D}{k_B T} \frac{\partial \Delta W}{\partial \gamma} P \right), \quad (10)$$

is the Fokker-Planck equation for the evolution of the probability density in γ -space.

Under the conditions for which the minimum work is given by the Gibbs free energy G , $\Delta W \equiv \Delta G = \Delta H - T\Delta S$, where H is the enthalpy, this equation transforms into the Fokker-Planck equation for a system in the presence of a free energy barrier:

$$\frac{\partial P}{\partial t} = \frac{\partial}{\partial \gamma} \cdot \left(D \frac{\partial P}{\partial \gamma} + \frac{D}{k_B T} \frac{\partial \Delta G}{\partial \gamma} P \right). \quad (11)$$

A particularly interesting situation which will be discussed in more detail in Section 3, is the case of a purely entropic barrier, often encountered in soft-condensed matter and biophysics.

Mesoscopic nonequilibrium thermodynamics provides a general formalism able to analyze the dynamics of systems away from equilibrium from the knowledge of the equilibrium probability. In this way, by knowing the equilibrium thermodynamic potential of a system, one could derive the kinetic equation.

The mesoscopic entropy production can also be obtained from a generalized chemical potential that account for the additional mesoscopic variables. We may then assume that the evolution of these degrees of freedom is described by a diffusion process and formulate the corresponding Gibbs equation

$$\delta S = -\frac{1}{T} \int \mu(\gamma) \delta P(\gamma, t) d\gamma, \quad (12)$$

which resembles the corresponding law proposed in nonequilibrium thermodynamics for a diffusion process in terms of the mass density of particles. Here $\mu(\gamma)$ plays the role of a generalized chemical potential conjugated to the distribution function $P(\gamma, t)$. Comparison of the Gibbs equation (12) with Eq. (4), where the variations of the equilibrium entropy are given by

$$\delta S_{eq} = -\frac{1}{T} \int \mu_{eq} \delta P(\gamma, t) d\gamma, \quad (13)$$

and μ_{eq} is the value of the chemical potential at equilibrium, yields the expression of the generalized chemical potential

$$\mu(\gamma, t) = k_B T \ln \frac{P(\gamma, t)}{P_{eq}(\gamma)} + \mu_{eq}, \quad (14)$$

or alternatively, using Eq. (2),

$$\mu(\gamma, t) = k_B T \ln P(\gamma, t) + \Delta W. \quad (15)$$

In this reformulation, the ‘‘thermodynamic force’’ driving this general diffusion process is $T^{-1} \partial \mu / \partial \gamma$, and the entropy production is given by

$$\sigma = -\frac{1}{T} \int J \frac{\partial \mu}{\partial \gamma} d\gamma \quad (16)$$

This expression coincides with the entropy production of a diffusion process over a potential landscape in the space of the mesoscopic coordinates. This landscape is conformed by the values of the equilibrium energy associated to each configuration γ . The treatment of a diffusion process in the framework of nonequilibrium thermodynamics can then be extended to the case in which the relevant quantity is a probability density instead of a mass density. This fact shows the close connection between entropy and stochastic dynamics.

3. AN EXAMPLE: ACTIVATED PROCESSES

In this Section, we will apply our general formalism to the study of the kinetics of activated processes. We will show how

the Fokker-Planck equation can be obtained from a diffusion process of the probability compatible with the statistical formulation of the second law. We will also illustrate how to derive the nonlinear equations for the activation rate in terms of the affinity of the process.

Activated processes are frequently modeled by a particle crossing a free energy barrier that separates two well-differentiated states located at the minima at each side of the barrier. Processes such as chemical reactions, adsorption, nucleation, thermal emission in semiconductors, and active transport through biological membranes, share these features and, therefore, are generically referred to as activated processes.

These processes are essentially different from the linear transport processes described by nonequilibrium thermodynamics. The latter constitute the instantaneous response to an applied external force or gradient and may take place even at very low values of the force. Since activated processes need of a minimum of energy to proceed, the regime in which they may be observed is essentially nonlinear. This difference becomes even more evident when we contrast the form of Fourier, Fick, or Ohm laws, in which the corresponding currents are proportional to the conjugated thermodynamic forces or gradients, with the exponential Arrhenius laws for the rates in activated processes.

To better illustrate this point, let us consider a general process for which a system passes from state 1 to state 2 via activation. Instances of this process can be a chemical reaction in which a substance transforms into another, an adsorption process in which the adsorbing particle goes from the physisorbed to the chemisorbed state, or a nucleation process in which the metastable liquid transforms into a crystal phase. Nonequilibrium thermodynamics describes the process only in terms of the initial and final positions, obtaining a linear behaviour of the current in terms of the affinity which only agrees with the law of mass action for small values of the affinity. If we consider the process at shorter time scales, the state of the system instead of jumping from 1 to 2, progressively transforms by passing through successive molecular configurations. These configurations can be characterized by a reaction coordinate γ . At these time scales, one may assume that the reaction coordinate undergoes a diffusion process through a potential barrier separating the initial from the final states (see Fig. 1).

At the time scales of interest, the system is mostly found in the states 1 and 2, which correspond to the minima at γ_1 and γ_2 , respectively. In the quasi-stationary limit, when the energy barrier is much higher than the thermal energy and intra-well relaxation has already taken place, the probability distribution is strongly peaked at these values and almost zero everywhere else. Under these conditions, the Fokker-Planck description, leads to a kinetic equation in which the net reaction rate satisfies the mass action law.

The current obtained from the mesoscopic entropy production (16) can be rewritten in terms of the local fugacity defined along the reaction coordinate $z(\gamma) \equiv \exp \mu(\gamma) / k_B T$ as

$$J = -k_B L \frac{1}{z} \frac{\partial z}{\partial \gamma}, \quad (17)$$

which can be expressed as

$$J = -D \frac{\partial z}{\partial \gamma}, \quad (18)$$

where $D = k_B L / z$ is the diffusion coefficient. We now assume that D is constant and integrate from 1 to 2 to obtain the nonlinear kinetic law for the averaged current

$$\bar{J} \equiv \int_1^2 J d\gamma = -D(z_2 - z_1) = -D \left(\exp \frac{\mu_2}{k_B T} - \exp \frac{\mu_1}{k_B T} \right). \quad (19)$$

This equation can also be expressed as

$$\bar{J} = J_0 \left(1 - e^{A/k_B T} \right),$$

where \bar{J} is the averaged rate, $J_0 = D \exp(\mu_1/k_B T)$ and $A = \mu_1 - \mu_2$ is the corresponding affinity. We have then shown that a Fokker-Planck equation, linear in probabilities and in the gradient of $\mu[\gamma, P(\gamma)]$, accounts for a non-linear dependence in the affinity. The scheme presented has been successfully applied to different classical activated processes, like chemical reactions, nucleation, active transport in ion channels, and molecular motors, to obtain the corresponding kinetic laws.

4. CONCLUSIONS

In this article, we have shown how to extend the use of thermodynamic concepts into the mesoscopic domain where fluctuations and nonlinearities play an important role. The probabilistic interpretation of thermodynamics together with

probability conservation laws can be used to obtain kinetic equations for the mesoscopic degrees of freedom.

The approach we have presented starts from the mesoscopic equilibrium behavior and adds all the dynamic details compatible with the second principle of thermodynamics and with the conservation laws and symmetries of the system. From the knowledge of the equilibrium properties of a system, it is straightforward to obtain Fokker-Planck equations for its dynamics. The coefficients entering the dynamic equations can be obtained from experiments or microscopic theories.

We have shown explicitly the applicability of the mesoscopic nonequilibrium thermodynamics to study the kinetics of activated processes showing that the formulation of local equilibrium at small scales leads to the nonlinear kinetic equations that govern those processes.

REFERENCES

- [1] Callen H B 1985, *Thermodynamics and an Introduction to Thermostatistics* (New York: Wiley)
- [2] de Groot S R and Mazur P 1984, *Non-Equilibrium Thermodynamics* (New York: Dover)
- [3] Romer F, Bresme F, Muscatello J, Bedeaux D and Rubi J M 2012, *Phys. Rev. Lett.* 108 105901
- [4] Hill T L 1994, *Thermodynamics of Small Systems* (New York: Dover)
- [5] Vilar J M G and Rubi J M 2001, *Proc. Natl Acad. Sci. USA* 98 11081
- [6] Reguera D, Rubi J M and Vilar J M G 2005, *J. Phys. Chem. B* 109 21502
- [7] Rubi J M 2012, *Phys. Scr.* T151 014027

PANEL C

**BIOLOGY AND THERMODYNAMICS:
WHERE DO WE STAND?**

HEAT TRANSFER AND DISSIPATION IN BIOMOLECULES: COMPUTATIONAL STUDIES

Fernando Bresme*^o, Anders Lervik*

*Department of Chemistry, Imperial College London, SW7 2AZ, United Kingdom

^oDepartment of Chemistry, Norwegian University of Science and Technology, Norway

EXTENDED ABSTRACT

Non-equilibrium phenomena play an essential role in many processes of relevance in biology, physics and material science. One of such non-equilibrium processes is thermoelectricity, in which a temperature gradient applied to a circuit made from different metals induces an electric current. Temperature measuring devices, and some refrigerators rely on these thermoelectric effects. One major application of this principle in material sciences is the synthesis of materials that can efficiently convert waste heat into electricity. It has been suggested that thermoelectricity can represent a physical mechanism used by some fish to sense temperature gradients.

Recent work indicates the possibility of generating large thermal gradients in nanoscale assemblies. Such large thermal gradients have been inferred from theoretical analyses of systems involving metal nanoparticles heated with electromagnetic radiation, a notion that is being used in cancer therapy treatments. Similarly experimental studies of molecular motors, such as Ca^{2+} -ATPase, indicate that significant thermal gradients can develop during the ion transport process. Quantifying thermal relaxation as well as the microscopic mechanisms operating at thermolecular scales characteristic of these nanomotors is therefore a very important objective. The environment, namely, the bilayer structure supporting these proteins, is expected to play a role in determining the relaxation. In fact, recent work has shown that the thermodynamic efficiency associated to ion transport reaches a maximum value at specific bilayer compositions, showing the relevance of the environment in regulating biological activity.

Recent developments on fluorescent thermometry have revealed the existence of thermal gradients inside the cell too. These results indicate important correlations between local temperature and organelle function and raise interesting questions on how the resulting thermal gradients can influence biochemical reactions or transport of solutes inside biological structures. We are interested in developing computational approaches to quantify thermal transport in biological structures, including the transport of proteins and other biomolecules driven by thermal gradients. Also, for small systems, nanomaterials, e.g., nanofluids, and in particular biomolecules, interfacial effects become relevant as compared with bulk effects. In order to understand processes of relevance in biophysics, it is necessary to quantify the resistivity of the interfaces to heat transfer. The relevant structures in biological system involve aqueous interfaces. We are currently investigating the response of aqueous solutions and interfacial water to thermal perturbations. Our work suggests that water does not behave as a passive medium that transports heat only. We have recently described a novel phenomenon whereby water molecules reorient as a response to the thermal gradient, and polarize along the direction of the gradient. This polarization can result in electrostatic fields for thermal gradients that are achievable in biological processes. Thermoelectric effects are well known in semiconductors, but we find that related mechanisms can arise in polar fluids.

REFERENCES

- [1] A. Lervik, F. Bresme, S. Kjelstrup and J.M. Rubi, *Biophys. J.*, vol. 103, p. 1218, 2012.
- [2] F. Romer, A. Lervik and F. Bresme, *J. Chem. Phys.*, vol. 137, art n. 074503, 2012.
- [3] F. Romer, F. Bresme, J. Muscatello, D. Bedeaux and J.M. Rubi, *Phys. Rev. Lett.*, vol. 108, art n. 105901, 2012.
- [4] A. Lervik, F. Bresme and S. Kjelstrup, *Phys. Chem. Chem. Phys.*, vol. 14, p. 3543, 2012.
- [5] J. Muscatello, F. Romer, J. Sala and F. Bresme, *Phys. Chem. Chem. Phys.*, vol. 13, art n. 19970, 2011.

FLUCTUATION THEOREM, INFORMATION AND BIOLOGICAL SYSTEMS

Yaşar Demirel

Department of Chemical and Biomolecular Engineering, University of Nebraska Lincoln, Lincoln, NE 68588

ABSTRACT

Fluctuation theorems in the presence of information as well as the definition and quantification of information have created broad discussions and are constantly evolving. The fluctuation theorem can quantify the hysteresis observed in the amount of the irreversible work of unfolding and refolding of a macromolecule in nonequilibrium regimes. It also describes how the probability of violations of the second law of thermodynamics becomes exponentially small as the time or the system size increases. Functional information may lead to self-organizing capabilities of living systems, while instructional information is a physical array. The informational entropy is applicable to describe of objects of any nature. Developed dissipative structures are capable of degrading more energy, and of processing complex information through developmental and environmental constraints. Within this trend, control information is defined as the capacity to control the acquisition, disposition, and utilization of matter, energy, and information flows in purposive processes. On the other hand, maximum entropy production and the fluctuation theorem are seen as the properties of maximum entropy distributions.. This review brings out some critical turning points in describing living systems with the help of fluctuation and information theories.

INTRODUCTION

For a system in contact with a heat bath, symmetry of the probability distribution of entropy production in the steady state is known as the fluctuation theorem. Crook's fluctuation theorem compares probability distributions for the work required in the original process with the time-reversed one. The probabilistic approach reached the broader appeal due to advances in experimental techniques for tracking and manipulation of single particles and molecules [1-7].

An overdamped motion $x(\tau)$ of a system in contact with a heat bath and a single continuous degree of freedom can be described by the Langevin equation: $\dot{x} = \mu F(x, \lambda) + \zeta$. The systematic force $F(x, \lambda)$ can arise from a conservative potential and/or be applied to the system directly as a nonconservative force, while ζ is the stochastic force, which is not affected by a time-dependent force, and μ is a positive constant. The Langevin dynamics generates trajectories $x(\tau)$ starting at x_0 . For an arbitrary number of degrees of freedom, x and F become vectors. The Langevin equation is the generic equation of motion for a single fluctuating thermodynamic quantity such as the concentrations of the chemical species in the vicinity of equilibrium [6-8].

Definition and quantification of information have created broad discussions. 'Information system' with its role in living systems is a constantly evolving field [2,6]. This short review addresses some critical discussions on the association of information theory with fluctuation theorem and entropy production in living systems.

FLUCTUATION THEOREM

The fluctuation theorem relates the probability $p(\sigma_\tau)$ of observing a phase-space trajectory with entropy production rate of σ_τ over time interval τ , to that of observing a trajectory with entropy production rate of $-\sigma_\tau$

$$\frac{p(\sigma_\tau)}{p(-\sigma_\tau)} = \exp(\tau\sigma_\tau / k_B) \quad (1)$$

where k_B is the Boltzmann constant. This result describes how the probability of violations of the second law of thermodynamics becomes exponentially small as τ or the system size increases. FT relates the work along nonequilibrium trajectories to the thermodynamic free energy differences, and applicable to single molecule force measurements. The FT depends on the following assumptions. The system is finite and in contact with a thermal bath. The dynamics are required to be stochastic, Markovian, and microscopically reversible. The probabilities of the time-reversed paths decay faster than the probabilities of the paths themselves and the thermodynamic entropy production arises from the breaking of the time-reversal symmetry of the dynamical randomness. Since the statistics of fluctuations will be different in different statistical ensembles.

Crook's FT can be used to determine free energies of folding and unfolding processes occurring in nonequilibrium systems. For that, the unfolding and refolding process need to be related by time-reversal symmetry, i.e. the optical trap used to manipulate the molecule must be moved at the same speed during unfolding and refolding [3,5,6].

In processes that are microscopically reversible, Crook's FT predicts a symmetry relation in the work fluctuations for forward and reverse changes a system undergoes as it is driven away from thermal equilibrium by the action of an external perturbation. A consequence of Crook's FT is Jarzynski's equality: $\exp(-\Delta G / k_B T) = \langle \exp(-W / k_B T) \rangle$.

However, for processes that occur far from equilibrium the applicability of Jarzynski equality is hampered by large statistical uncertainty arising from the sensitivity of the exponential average to rare events [3].

In the absence of the initial or final correlations, entropy production satisfies the integral of FT (or the Jarzynski

equality): $\langle \exp(-\sigma) \rangle = 1$ where $\langle \dots \rangle$ is the ensemble average over all microscopic trajectories. In the presence of information (I) processing with initial and final correlations, the integral FT with energy dissipation and energy cost of information exchange becomes [5]

$$\langle \exp(-\sigma + \Delta I) \rangle = 1 \quad (2)$$

where ΔI is the change in the mutual information. Convexity of $\exp\langle x \rangle \leq \langle \exp(x) \rangle$ leads to $\langle \sigma \rangle \geq \langle \Delta I \rangle$ [5]. With the correlation remaining after a feedback control (I_{rem}) by Y on X , Eq. (2) becomes

$$\langle \exp(-\sigma - (I - I_{\text{rem}})) \rangle = 1 \text{ so } \langle \sigma \rangle \geq -\langle I - I_{\text{fb}} \rangle \quad (3)$$

where $\langle I - I_{\text{rem}} \rangle$ may be an upper bound of the correlation that can be used.

The detailed FT in the presence of information processing is

$$\frac{p_b[X_b, y]}{p_f[X_f, y]} = \exp(-\sigma + \Delta I) \quad (4)$$

with the constraint $p[x, y] \neq 0$ (x and y are initial phase-space points), p_b and p_f are the joint probability distributions of the backward and forward processes, respectively, and $(-\sigma + \Delta I)$ shows the total entropy production of the composite system XY and the baths. Here system x evolves from x to x' along a path x_f in such a manner that depends on the information about y , which does not evolve in time [5].

FT allows a general orthogonality property of maximum information entropy (MIE) to be extended to entropy production (EP). Maximum entropy production (MEP) and the FT are generic properties of MIE probability distributions. Physically, MEP applies to those macroscopic fluxes that are free to vary under the imposed constraints, and corresponds to the selection of the most probable macroscopic flux configuration [9,10]. The constrained maximization of Shannon information entropy (H) is an algorithm for constructing probability distributions from partial information. MIE is a universal method for constructing the microscopic probability distributions of equilibrium and non-equilibrium statistical mechanics. The distribution of the microscopic phase space trajectories over a time τ satisfies $p_\alpha \propto \exp(\tau\sigma/2k_B)$.

INFORMATION THEORY

Information may be defined as the capacity to reduce statistical uncertainty in the communication of messages between a sender and a receiver. Consider the number of ways in which N distinguishable entities can be assigned to M distinguishable states such that there are n_i entities in state i

$$W = \frac{N!}{n_1! n_2! \dots n_M!} \quad (5)$$

Maximum probability is related to maximum entropy in the limit of large N and n_i and the asymptotic result from Stirling's approximation ($\ln N! \approx N \ln N$) yields

$$\frac{1}{N} \ln W = -\sum_i^M p_i \ln p_i = H \quad (6)$$

where the occupation frequency of state i is: $p_i = n_i/N$ [10].

In Shannon's theory, entropy represents the amount of uncertainty one particular observer has about the state of this system [11]. This uncertainty is not information. For a variable X with the x_1, x_2, \dots, x_N of its N possible states, the probability of finding X in state x_i would be p_i and the Shannon's entropy H of X is $H(X) = -\sum_i^N p_i \ln p_i$. If nothing is known about X , we have $H(X) = \ln N$, which is the maximum value that $H(X)$ can be; this occurs if all the states are equally likely $p_i = 1/N$. However, for example, if $X = x_5$ then the uncertainty about X becomes smaller, and therefore $H(X)$ represents the quantity of the closest description of X . The probability distribution using prior knowledge or measurements can teach us something about a system. The difference between the maximal and the actual entropy after our measurements or analysis is the amount of information we have for the system. As it measures the difference of uncertainty, information is a relative quantity [11].

If we define another random variable Y with its states y_1, y_2, \dots, y_M and probabilities p_1, p_2, \dots, p_M , then the joint entropy $H(X, Y)$ measures our uncertainty about the joint system XY in $N \cdot M$ states. If X and Y are somehow connected, such as two molecules that can bind to each other, the information that one molecule has about the other is

$$I(X : Y) = H(X) + H(Y) - H(XY) \quad (7)$$

Here ':' shows that information is symmetric; X and Y equally know each other. If the state of Y is known, then the so called 'conditional entropy' becomes

$$H(X/Y) = H(XY) - H(Y) \quad (8)$$

For independent variables: $H(XY) = H(X) + H(Y)$. With the conditional entropy, Eq. (7) becomes

$$I(X : Y) = H(X) - H(X/Y) \quad (9)$$

Eq. (9) shows that information measures deviation from independence that is the amount by which the entropy of X or Y is reduced by knowing the other (Y or X) [11].

Maximization of the information entropy (IE) determines the probability of a particular state of the system. This leads to the relation between the probability of a nonequilibrium process and the number of microscopic trajectories [12,13].

Information and Thermodynamics

Maximum entropy and maximum entropy production are two essential properties in equilibrium and nonequilibrium thermodynamics, respectively. MEP may be an organizational principle applicable to physical and biological systems. Various derivations of MEP by using the MIE procedure by Jaynes [14] exist in the literature [2]. In these derivations the IE is not defined by a probability measure on phase space, but on path space for the stationary nonequilibrium systems [10].

Consider M sites with a variable $n_i(t)$ ($i = 1, 2, \dots, M$) at each site with $t = 0, 1, \dots, \tau$. The flux (time asymmetric) occurring

randomly at every time step, $J_{ij} = -J_{ji}$ from i to j depends on a parameter $c_{ij} = c_{ji}$, such that $J_{ij}(t) = \pm c_{ij}$ with stochastic sign. A microscopic path a is a set of values $\pm c_{ij}$ so that: $n_{i,a}(t+1) - n_{i,a}(t) = -\sum_j J_{ij,a}(t)$. The path dependent time average is $\bar{J}_{ij,a} = (1/\tau) \sum_t J_{ij,a}(t)$ and $n_i(0)$ does not depend on the complete path. With the microscopic path dependent probability p_a , the path ensemble averages are $\langle \bar{J}_{ij} \rangle = \sum_a p_a \bar{J}_{ij,a}$. By using Jayne's information theory and maximizing path information entropy

$$S_I = -\sum_a p_a \ln p_a \quad (10)$$

with the constraints

$$1 = \sum_a p_a \quad (11)$$

$$\langle n_i(0) \rangle = \sum_a p_a n_{i,a}(0) \quad (12)$$

$$N_{ij} = -\sum_a p_a \bar{J}_{ij,a} \quad (13)$$

the most likely probability on path space is estimated as

$$p_a = \frac{1}{Z} \exp A_a \quad (14)$$

where N_{ij} is the numerical value of the time and path ensemble average of the flux J_{ij} , A_a the path action: $A_a = -\sum_{ij} \lambda_i n_{i,a}(0) + \sum_i n_{ij} \bar{J}_{ij,a}$ in which λ_i and $n_{ij} = -n_{ji}$ are the Lagrange multipliers of constraints (12) and (13), respectively, and Z is the partition function [2,9,14].

However, a trajectory of a quantity possessed by a system may fluctuate wildly (far from equilibrium) or weakly; than they would not have the same probabilities as long as they have the same initial and final states. Here a path trajectory is a sequence of p over some time interval:

$$a \equiv [p(0), p(dt), p(2dt), \dots, p(Mdt)] \quad (15)$$

where $M = \tau/dt$. And dt is the coarse graining corresponding to the time scale of experimental observations [8].

The partition and constitutive (phenomenological) equation of motion have the relations

$$\frac{\partial \ln Z}{\partial n_{ij}} = N_{ij} \quad (16)$$

$$X_{ij} = \frac{n_{ij}}{\tau} \quad (17)$$

The forward and backward components of the time and ensemble averaged fluxes are

$$N_{ij} = N_{ij}^f - N_{ij}^b = \frac{c_{ij} e^m}{e^m + e^{-m}} - \frac{c_{ij} e^{-m}}{e^m + e^{-m}} \quad (18)$$

where $m = X_{ij} c_{ij}$ and $2c_{ij} X_{ij} = \ln(N_{ij}^f / N_{ij}^b)$.

The entropy production of a microscopic path a is [2]

$$\sigma_a = \sum_a p_a \sigma_a = \sum_{ij} X_{ij} N_{ij} \quad (19)$$

By using Eq. (14) in Eq. (10), the maximum information entropy as a function of the forces becomes

$$S_{I,\max}(X) = \ln Z(X) - \langle A(X) \rangle \approx \ln W(\langle A(X) \rangle) \quad (20)$$

where $W(\langle A(X) \rangle)$ is the density of paths.

The entropy curvature (response) matrix is

$$A_{ij,kl}(N) = \frac{\partial X_{ij}}{\partial N_{kl}} = -\frac{\partial^2 S_{I,\max}(X(N))}{\tau \partial N_{ij} \partial N_{kl}} \quad (21)$$

The probability distribution for the time averaged flux is

$$p(\bar{J}) \propto \exp\left(-\frac{\tau}{2} \sum_{ij,kl} [\bar{J}_{ij} - N_{ij}] A_{ij,kl}(N) [\bar{J}_{ij} - N_{kl}]\right) \quad (22)$$

Combining the equation above with the FT yields [2]

$$\frac{p(\bar{J})}{p(-\bar{J})} = \exp(2\tau\sigma(\bar{J})) \quad (23)$$

In near equilibrium regime, the maximum path information is

$$S_{I,\max}(X) = \ln(W) \approx \ln 2^{\tau(M^2 - M)} + \tau\sigma / 2 \quad (24)$$

The first part on the right side of the equation above is the logarithm of the total number of paths for uniform probability distribution, while the second term is the entropy production. In the MEP, the assumption was that the number of paths W should be an increasing function of the averaged action [10]. Here for higher entropy production, the SI is minimum [2].

MEP principle states that if thermodynamic forces X_i are preset, then the true thermodynamic flows J_i satisfying the condition $\sigma = \sum_i J_i X_i \geq 0$ yield the maximum value of the $\sigma(J)$. This can be written using the Lagrange multiplier λ

$$\delta_j [\sigma(J_k) - \lambda(\sigma(J_k) - \sum_i J_i X_i)]_X = 0 \quad (25)$$

and at fixed forces, the relationship between the fluxes and forces become

$$X_i = \frac{\sigma(J)}{\sum_i J_i (\partial \sigma / \partial J_i)} (\partial \sigma / \partial J_i) \quad (26)$$

and indicates that the relationship between the thermodynamic forces and fluxes can be both linear and nonlinear [12].

The same entropy production can be both maximum and minimum depending on the constraints used in the entropy production variation. However, it is widely published that the MEP principle may be a critical link in the explanation of the direction of the biological evolution under the imposed constraints of the environment [9,10,12,13]. If X is fixed, the MEP leads to maximum J that is the selection of fastest process. MEP principle has proved to be valuable for understanding and describing of various nonequilibrium processes in physics, biology, and environment. The local equilibrium of a nonequilibrium system and the representation of the EP as a bilinear form of flows and forces are a

mandatory condition for the use of MEP principle [11,14].

In the cortex, populations of neurons continuously receive input from other neurons, interpret their ongoing activity, and generate output destined for other neurons. This information processing and transmission is limited by the repertoire of different activated configurations available to the population. The extent of this repertoire may be quantified by its entropy H characterizing the information capacity as the upper limit on aspects of information processing of the population. When the information transmitted from the input to the output by a population that has only two states in its repertoire ($H = 1$ bit), then regardless the information the input contains, the output information content cannot exceed 1 bit. Therefore, a network with low entropy population may limit information transmission. Activity in the cortex depends on the ratio of fast excitatory E to inhibitory I synaptic signals to neurons. This E/I ratio remains fixed at an average in various events during highly fluctuating activity levels, yet a small E/I ratio, caused by weak excitation drive, may reduce the correlations as well as the overall level of activity [16].

For a number of unique binary patterns, p_i the probability that pattern i occurs, the entropy of the set of patterns is

$$H = -\sum_{i=1}^n p_i \log_2 p_i \quad (27)$$

Eq. (27) estimates the occurrence probability for each pattern. Maximization of entropy may be an organizing principle of neural information processing systems [16].

The information capacity I_C in binary units may be expressed as a function of the probability p

$$I_C = \frac{1}{\ln 2} \left(\sum_{j=1}^{\Omega} p_j \ln p_j - \sum_{j=1}^{\Omega} p_j^o \ln p_j^o \right) \quad (29)$$

where Ω is the number of possibilities, p^o is the probability at equilibrium (i.e., no knowledge), and p is the probability when some information are available about the system. Information here is used as a measure of structure [1,7].

BIOLOGICAL SYSTEMS

Ribonucleic acid (RNA) translates the genetic codes in the nucleic acids of deoxyribonucleic acid (DNA). The codes consisting of four different bases (nucleotides) are adenine (A), guanine (G), cytosine (C) and thymine (T, DNA only) or uracil (U, RNA only). During the gene expression, RNA serves as the template for the translation of genes into proteins by transferring amino acids to the ribosome to form proteins, which may undergo posttranslational conformational changes, folding, and association with other polypeptide chains. All these steps can be regulated, therefore, the dynamical object of a gene is to produce functional, folded, and chemically modified protein [17].

Information and Biological Systems

DNA is a code, and codes from sequence alone do not reveal information. The nonconditional entropy for DNA sequence or proteins is about two bits per base; a random protein would have $\log_2(20) = 4.32$ bits of entropy per site. Due to repetitions, pair, and triplet correlations the actual entropy would be lower [11]. This entropy per symbol only allows us to quantify our uncertainty about the sequence

identity; it will not reveal the ‘function’ of the genes.

In equilibrium thermodynamics, isolated systems have the maximum entropy and there are no correlations; hence there is no information. The information as the amount of correlations between two systems stored in living system (biological genomes) points out that they are far away from equilibrium. Consequently, information theory becomes a part of nonequilibrium thermodynamics in living cells. Information measures the amount of entropy shared between two systems; so it is the information that one system has about the other. If it cannot be specified what the information is about, then it would be entropy. Also information enables us to make predictions about other systems; only in reference to another ensemble entropy can become information. Therefore, what is described by the correlations between the sequences stores information not the sequence itself. On the other hand, what information a genomic sequence represents depends on the interpreter environment. If a sequence means something it can create a function necessary for its environment [11,17].

The information theory introduced ‘functional information’ that leads to self-organizing capabilities of living systems, and ‘instructional information’ that is a physical array. However, linkages with the field of semiotics established a much more compatible approach to biological information [17]. Within this trend ‘control information’ is defined as the capacity to control the acquisition, disposition, and utilization of matter, energy, and information flows functionally.

Each position on the genome is four-base code and the uncertainty at each position is two bits; then the maximum entropy becomes

$$H_{\max} = - \sum_{i=G,C,A,T} p(i) \log_2 p(i) = \log_2(4) = 2 \text{ bits} \quad (30)$$

since $p(i) = 1/4$. The actual entropy is obtained from the actual probabilities $p_j(i)$ for each position j on the sequence. In N sequences, we have $p_j(i) = n_j(i) / N$ by counting the number of $n_j(i)$ occurrences of nucleotide i at position j (this will be done for all positions $j = 1, \dots, M$ on the sequence length M). When we ignore correlations between positions j , the information stored in the sequence becomes

$$I = H_{\max} - H = 2M - H \text{ bits} \quad (31)$$

where

$$H = - \sum_{j=1}^M \sum_{i=G,C,A,T} p_j(i) \log_2 p_j(i)$$

The thermodynamics of protein structures implies that sequence and structure are related. If a structural entropy of proteins $H(\text{str})$ is obtained for a given chain length and for a given environment, the mutual entropy between structure and sequence becomes [11]

$$I(\text{seq};\text{str}) = H(\text{seq}) - H(\text{seq}/\text{str}) \quad (32)$$

where $H(\text{seq})$ is the entropy of sequences of length M and $H(\text{seq}/\text{str})$ is the entropy of sequences given the structure. If the environment requires a certain structure that will be functional in that environment then $H(\text{seq}/\text{str}) \approx H(\text{seq}/\text{env})$. Then $I(\text{seq};\text{str})$ is approximately equal to the physical complexity. Assuming that any given sequence produces an exact structure: $H(\text{str}/\text{seq}) = 0$, and Eq. (32) becomes

$$I(\text{seq:env}) \approx I(\text{seq:str}) = H(\text{str}) \quad (33)$$

Therefore, thermodynamic entropy of a protein structure is limited by the amount of information about the environment coded by the sequence. This may imply that sequences that encode more information about the environment may be more functional.

One of the consequences of the Human Genome project has proved that 'biology is an informational science' [16,17]. The communication in living cells is based on the signals, such as electromagnetic-light, mechanical-touch, and chemical, received. In the signal-transduction pathway, a signal on a cell surface converted into a specific cellular response in a series of functional steps [16]. This suggests that information is conceived as the communication of a form from object to interpreter through the sign. The evolution of ways of storing, transmitting, and interpreting information can be seen a major step in the increased capacity for collective behavior and robustness in living systems [4,6,7].

In semiotic understanding of living systems, interpreters of signs and information will often be an interpreter-dependent objective process. Genes should be regarded as signs in DNA, which can only have any effect on a cell function through a triadic-dependent process. The object of sign in DNA is a functional, folded, and chemically configured protein production; when a particular gene product is necessary, a signal from the environment activates the expression of a certain gene. The cell as an interpreter alters its internal states triggered by a collective signal transduction pathway to establish the boundary conditions to processes and perform something functional with the genetic material [17].

Coupled Biological Systems and Information

Biochemical reactions coupled with diffusion of species can lead to molecular pumps and biochemical cycles in living systems. Here, the coupling refers that a flux occurs without its primary thermodynamic driving force, or opposite to the direction imposed by its primary driving force. This is possible only if a process is coupled with another spontaneous process and is consistent with the second law that states that a finite amount of organization may be obtained at the expense of a greater amount of disorganization in a series of coupled spontaneous processes. An example to that is the adenosine triphosphate (ATP) synthesis coupled to the respiratory electron transport. The ATP synthesis, in turn, is matched and synchronized to cellular ATP utilization. This shows a functional process leading to organized structures where the ATP synthesis ($\sigma < 0$) has been made possible and the whole coupled processes satisfy the condition $\sigma > 0$ [7,19-21].

The general approach for incorporating thermodynamics into the information theory has been to derive probability distributions for nonequilibrium steady states by employing the variational approach. However, composing the appropriate constraints to be used in the variational principle is not clear, since there is no definite extremum quantity to characterize the state space of such steady nonequilibrium states. In the vicinity of equilibrium only, the linear phenomenological laws may be useful in that respect [8]. Therefore a natural question is that how useful such an approach would be to describe the information processing in functionally coupled and self-organized biochemical cycles of living systems that are mainly far from equilibrium. The probabilistic measure of

information derived from Jaynes information theory formalism of statistical mechanics is mainly indifferent to meaning [10].

The unified theory of evolution attempts to explain the origin of biological order as a manifestation of the flows of energy and information on various spatial and temporal scales. Genes originates the information to form the required enzymes, regulatory and structural proteins. The genome is the source of cellular codes; also any cellular structure such as lipids and polysaccharides may store and transmit information. Beside these, thermodynamic forces in the form of transmembrane gradients of H^+ , Na^+ , K^+ , Ca^{2+} and consequent electric potential cause significant displacements from equilibrium, and are therefore, potential sources of information. Genome-protein system may be a component of a large ensemble of cellular structures, which store, encode, and transmit the information [6,7,17].

The use of maximum entropy formalism in biology is growing [4,18] in detecting expression patterns in signal transduction. At the maximum entropy, the probabilities of the different proteins are not equal; each protein will be present in proportion to its partition function, which is the effective thermodynamic weight of a species at thermal equilibrium.

Le Chatelier principle may be applied to analyze how a protein-signalling networks at equilibrium returns to its equilibrium state after being slightly perturbed. For a single cell or small cell colony, cell to cell perturbations are small, while the unperturbed state of a single cell may be unstable in the presence of many other cells. Experiments permits observations of the covariance in the fluctuations and evolution of these fluctuations of different proteins when a single cell is perturbed in the presence of other cells. The information theory helps analyze these covariances to understand the network of interacting proteins [18].

The composite immediate object of a protein coding gene is the sequence of amino acids of a polypeptide, which can be folded in different ways in different cellular contexts and represents dynamical objects. So sign that is a sequence of nucleotides in DNA determines object that is a sequence of amino acids in a polypeptide through interpretant that is a range of possibilities of reconstruction of sequence of amino acids required by the environment (cell).

Dewar [4] suggests that MEP is the unifying optimization for living systems and ecosystem function, in which entropy production might be a general objective function. When a system is away from equilibrium, the nonequilibrium state of MEP is the most probable as it can be realized microscopically in a greater number of ways than any other nonequilibrium state. In this sense, MEP is a statistical principle, rather than a physical principle open to experimental validation. MEP may predict optimal plant behavior from the perspective of natural selection as well as offers a novel statistical reinterpretation of that behavior that is the survival of the likeliest.

For a multicomponent fluid system under mechanical equilibrium with n species and N_r number of chemical reactions and diffusion, the rate of energy dissipation due to local rate of entropy production is [19,20]

$$T\sigma = \int_V \left(-\sum_i \mathbf{J}_i \cdot (\nabla \mu_i)_{T,P} + \sum_{i,j} \mu_i \nu_{ij} J_{rj} \right) dV \geq 0 \quad (34)$$

where \mathbf{J}_i the vector of mass fluxes, μ_i the chemical potential of species i , and A the affinity $A = -\sum \nu_i \mu_i$. The local mass

balance of chemical species i from the continuity equation

$$\rho \frac{\partial w_i}{\partial t} = -\nabla \cdot \mathbf{j}_i + \sum_{i,r} \nu_{ir} J_r \quad (35)$$

For a steady state system, we have $\nabla \cdot \mathbf{j}_i = \sum_{i,j} \nu_{ij} J_{r_j}$ allowing the dissipation to be expressed in terms of affinity

Assuming that we have N number of linear flux-force system expressed in matrix form: $-\mathbf{J} = \mathbf{L}\mathbf{X}$, Onsager's reciprocal relations states that the coefficient matrix \mathbf{L} is symmetrical. The \mathbf{L} will have $N \times N$ elements and the number of cross coefficients would be $(N^2 - N)/2$, which may be on and off based on the biochemical path and its environment. In the absence of pertinent symmetries or invariances, all types of cross-couplings are possible and lead to nonvanishing cross coefficients. If the structure of the system is invariant with respect to some or all of the orthogonal transformations, then the invariance will eliminate certain cross-couplings and their cross-coefficients will vanish.

Thermodynamic coupling may lead to self organized and $(N^2 - N)/2$ number of possibility of coupled-uncoupled structures with N biochemical reactions depending on the environmental interpretations. This, in turn, brings out the challenge of implementing the trajectories belonging two or much more coupled processes (recognizing each other) with different initial and end nonequilibrium states into the fluctuating and information theory.

CONCLUSIONS

Shannon's theory can define both entropy and information and should be used to quantify the information content of sequences by distinguishing information-coding parts from random parts in ensemble of genomes. It can also be used in investigating protein-protein interactions and the association of enzymes and proteins with their binding sites. Also, information theory based biomolecule design may maximize the information shared between the target and biomolecule, such as drug, ensembles. The use of information and entropy in thermodynamically coupled processes in fluctuation theory may be helpful further understanding the concept of functionality in dissipative and self-organized structures of living systems.

REFERENCES

- [1] Y. Demirel, Energy Coupling, in Information and Living Systems in Philosophical and Scientific Perspectives, eds. G. Terzis and R. Arp, MIT Press, Cambridge, 2011.
- [2] S. Bruers, A Discussion on Maximum Entropy Production and Information Theory, *J. Phys. A*, vol. 40, pp. 7441-7450, 2007.
- [3] D. Collin, F. Ritort, C. Jarzynski, S.B. Smith, I. Tinoco Jr and C. Bustamante, Verification of the Crooks Fluctuation Theorem and Recovery of RNA Folding Free Energies, *Nature*, vol.437, pp. 231-234, 2005.
- [4] R.C. Dewar, Maximum Entropy Production and Plant Optimization Theories, *Phil. Trans. R. Soc. B* vol. 363, pp. 1429-1435, 2010.
- [5] T. Sagawa and M. Ueda, Fluctuation Theorem with Information Exchange: Role of Correlations in Stochastic Thermodynamics, *Phys. Rev. Lett.*, vol. 109, pp. 180602-1-5, 2012.
- [6] Y. Demirel, Nonequilibrium Thermodynamics Modeling of Coupled Biochemical Cycles in Living Cells, *J. Non-Newtonian Fluid Mech.*, vol. 165, pp. 953-972, 2010.
- [7] Y. Demirel, Nonequilibrium Thermodynamics: Transport and Rate Processes in Physical, Chemical and Biological Systems, 3rd ed., Elsevier, Amsterdam, 2013 (in print).
- [8] G.C. Paquette, Comment on the Information Theoretic Approach to the Study of Non-equilibrium Steady States, *J. Phys. A* vol. 44, pp. 368001-6, 2011.
- [9] L.M. Martyushev, The Maximum Entropy Production Principle: Two Basic Questions, *Phil. Trans. R. Soc. B* vol. 365, pp. 1333-1334, 2010.
- [10] R.C. Dewar, Maximum Entropy Production as an Inference Algorithm that Translates Physical Assumption into Macroscopic Predictions: Don't Shoot the Messenger, *Entropy*, vol. 11, 931-944, 2009.
- [11] C. Adami, Information Theory in Molecular Biology, *Phys. Life Rev.*, vol. 1, pp. 3-22, 2004.
- [12] V.D. Seleznev and L.M. Martyushev, Fluctuations, Trajectory Entropy, and Ziegler's Maximum Entropy Production, [arXiv:1112.2848](https://arxiv.org/abs/1112.2848), pp. 1-19, 2012
- [13] L.M. Martyushev, Entropy and Entropy Production: Old Misconception and New Breakthroughs, *Entropy*, vol. 15, pp. 1152-1170, 2013.
- [14] E.T. Jaynes, Probability Theory: The Logic of Science. Ed. G.L. Brentthorst, Cambridge Univ. Pres., Cambridge, 2003.
- [15] P. Zupanović, D. Kulic, D. Juretić and A. Dobovisek, On the Problem of Formulating Principles in Nonequilibrium Thermodynamics, *Entropy*, vol. 12, pp. 926-931, 2010.
- [16] W.L. Shew, H. Yang, S. Yu, R. Roy and D. Plenz, Information Capacity and Transmission are Maximized in Balanced Cortical Networks with Neuronal Avalanches, *J. Neurosci.*, vol. 31, pp. 55-63, 2011.
- [17] C.N El-Hani, J. Queiroz and C Emmeche, A Semiotic Analysis of the Genetic Information System, *Semiotica*, vol. 160, pp. 1-68, 2006.
- [18] Y.S. Shin, F. Remacle, R. Fan, K. Hwang, W. Wei, H. Ahmad and R.D. Levine, Protein Signalling Networks, from Single Cell fluctuations and Information Theory Profiling, *Biophys. J.*, vol. 100, pp. 2378-2386, 2011.
- [19] Y. Demirel, Thermodynamically Coupled Heat and Mass Flows in a Reaction-Transport System with External Resistances, *Int. J. Heat Mass Transfer*, vol. 52, pp. 2018-2025, 2009.
- [20] Y. Demirel and S.I. Sandler, Linear-Nonequilibrium Thermodynamics Theory for Coupled Heat and Mass Transport, *Int. J. Heat Mass Transfer*, vol. 44, pp. 2439-2451, 2001.
- [21] R.C. Dewar, D. Juretić and P. Zupanović, The Functional Design of the Rotary Enzyme ATP Synthase is Consistent with Maximum Entropy Production. *Chem. Phys.*, vol. 30, pp. 177-182, 2006.

UNDERSTANDING LIFE FROM A THERMODYNAMIC EARTH SYSTEM PERSPECTIVE

Axel Kleidon

Biospheric Theory and Modelling Group
Max-Planck-Institute for Biogeochemistry, Hans-Knöll-Str. 10, 07745 Jena, Germany
E-mail: akleidon@bgc-jena.mpg.de

ABSTRACT

The Earth's biosphere – the sum of all life – as well as the Earth system itself are two highly dissipative, thermodynamic systems that are driven by low entropy solar radiation and that produce high entropy "waste". Their dissipative activities are constrained by the exchange of energy of different entropies, but also by the material transport processes within these systems. The strength of material transport links the dissipative activity of the Earth system as a whole with the material exchange of the biosphere, such as the exchange of carbon dioxide that is critical to maintain life. Here, I show how the thermodynamic limit of material transport within the Earth's atmosphere imposes a limit to the exchange of carbon dioxide for terrestrial photosynthesis. This limit is not fixed, but is modulated by the biosphere through its effects on surface absorption and on the atmospheric composition. These effects are illustrated by a simple model of atmospheric transport and biotic activity. This tight interplay between the limits of physical transport on biotic activity and the effects of biotic activity on the Earth system emphasizes the need to approach and understand life in its Earth system context in which thermodynamics defines the limits of the overall dissipative activities of both systems.

THERMODYNAMICS OF LIFE ON EARTH

It is well recognized that life can be seen as a thermodynamic dissipative process that is fueled by low entropy energy and produces high entropy waste [1; 2]. Boltzmann [1] already described in the late 19th century that the

general struggle for existence of living organisms is therefore not a struggle for the basic materials – these materials are abundantly available for organisms in air, water and soil – ... but a struggle for entropy, which through the transformations of energy from the hot sun to the cold Earth becomes available.

Likewise, the Earth system as a whole is a thermodynamic, dissipative system that is fueled by the absorption of low entropy solar radiation and produces high entropy terrestrial radiation. This correspondence was noted by Lovelock [3; 4], who popularized the notion that the Earth is like a living organism. This comparison was not made on the basis of a biological definition of life, but rather from the recognition that both, life and the Earth system are highly dissipative systems that are maintained in states far from thermodynamic equilibrium.

Yet, the notion that life and the Earth system are dissipative systems by itself does not provide a constraint on how dissipative these systems are. Yet, thermodynamics provides information about limits as well and the factors that shape these limits. A prime example for such a limit is the Carnot limit of a heat engine, which describes how much heat can be converted into mechanical work by the engine which can later be dissipated. To evaluate such limits for life and for the Earth system, we need to view these systems in terms of their environmental setting. The Earth system is driven by radiative exchange,

so the question regarding the limit of dissipative activity of the Earth system relates to the thermodynamic limit of how much free energy can be generated from the radiative forcing. Life is embedded within the functioning of the Earth system, and it is subjected to thermodynamic limits regarding the conversion of sunlight into chemical energy, but also to limits regarding the transport and exchange of the basic materials that are required during the process of chemical energy generation and that are taken up from (and released to) the abiotic environment. The chemical transformation associated with life leaves an imprint in the environment, most notably in terms of the atmospheric composition, which has likely changed drastically during the history of the Earth system due to life [5; 6] and which would affect the radiative exchanges within the system. Hence, we gain a view of life and the Earth system as two, closely connected thermodynamic systems with reciprocal roles, with Earth system functioning shaping a habitable environment that favors life and with the effects of life shaping the Earth's environment.

This interplay between the Earth system and the biosphere – the sum of all life – is illustrated in Fig. 1. Both, the abiotic processes of the Earth system as well as the biosphere are driven mostly by the absorption of low entropy solar radiation. Solar radiation is absorbed at the Earth's surface, and differences in absorption and emission provide the gradients to drive abiotic processes, such as the generation of motion or the evaporation of water which represent the dissipative activity of the Earth system (arrow A in Fig. 1). Most of the biotic activity is driven directly or indirectly by photosynthesis, which utilizes a fraction of the absorbed solar radiation in converting carbon dioxide into carbohydrates (arrow B in Fig. 1). In both cases, the absorbed solar energy is eventually reemitted to space, but it is emitted at a much lower radiative temperature, so that the emitted ra-

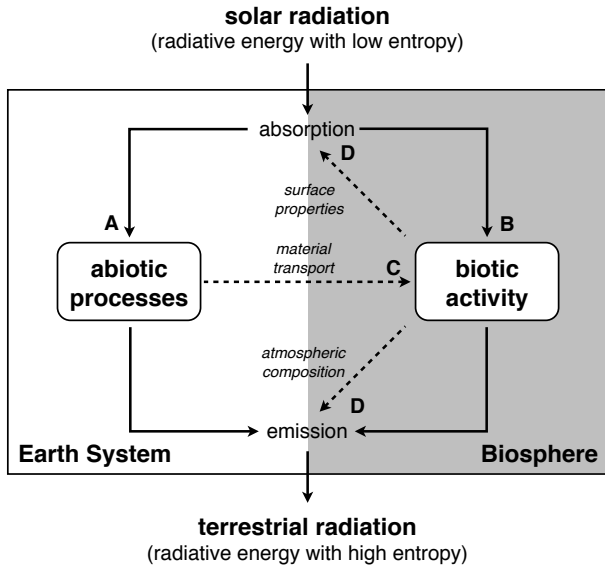


Figure 1. Schematic diagram to understand life in the thermodynamic context of the whole Earth system.

diation has a much higher radiative entropy. This difference in radiative temperatures between the absorbed solar radiation and the emitted terrestrial radiation provides the difference in entropy that fuels both, the Earth system and its biosphere.

To link biotic activity and Earth system functioning, we first note that biotic activity also requires basic building materials, particularly carbon dioxide from which organic biomass is being formed from. Carbon dioxide is taken up from the atmosphere (for the terrestrial biosphere, which I will focus on here), or from the ocean (for the marine biosphere), and in both cases the physical environment provides the means to transport carbon dioxide to the biosphere (arrow C). The ability to transport depends on the intensity by which motion can be generated within the Earth system from the planetary forcing of solar radiation, and this generation rate is thermodynamically constrained. Hence, the material supply for biotic activity is one factor by which the Earth system imposes a constraint on biotic activity (among other factors, such as temperature or water availability on land).

The arrows D in Fig. 1 describe the effects of biotic activity on the Earth system by the mass exchange of basic materials (as mentioned above). Two aspects of this modification directly relate to the radiative forcing of the Earth system. The first aspect relates to the presence of photosynthetic tissues that typically increase the absorption of solar radiation at the surface, which can, for instance, easily be noted on land where the presence of vegetation darkens the surface. The second aspect is more subtle and involves alterations of the atmospheric composition, for instance in terms of the concentration of carbon dioxide, methane, and molecular oxygen. The atmospheric composition alters the radiative properties of the atmosphere in terms of the concentration of greenhouse gases and thereby affects the transfer of terrestrial radiation and the ability of the system to emit radiation. Hence, the two effects associated with arrows D have quite profound effects for the physical functioning of the Earth system.

The goal of this contribution is to illustrate the interplay between life and Earth shown in Fig. 1 with a simple, yet quantitative model of the Earth system and biotic activity and to quantify the thermodynamic limits of both systems as well as their

coupling. I first illustrate the thermodynamic limit on mass exchange between the surface and the atmosphere associated with convection. This intensity of mass exchange is then related to the limitation imposed by the environment on the transport of basic materials for photosynthesis. The consequences of biotic activity are then discussed in terms of altering the atmospheric composition, which in turn affects the strength of the atmospheric greenhouse effect and the thermodynamic limits. The implications for the understanding of life in a thermodynamic Earth system context are then summarized.

TRANSPORT LIMITS IN THE EARTH SYSTEM

The transport and exchange of mass within the Earth system is strongly constrained by thermodynamic limits. To demonstrate these limits, I set up a simple model of atmospheric convection in the following, which is based on [7; 8]. This model considers the Earth's surface with a temperature T_s and the atmosphere with a temperature T_a as a thermodynamic system made up of two heat reservoirs. The system is forced by the heating associated with the absorption of solar radiation at the surface, J_{sw} , and by the cooling associated with the emission of terrestrial radiation from the atmosphere, J_{lw} . Its steady state is considered in which $J_{sw} = J_{lw}$. The surface and the atmosphere are coupled by a flux of radiative exchange, $J_{s,a}$, as well as the sensible and latent heat fluxes, J_{sh} and J_{lh} . These latter fluxes are directly linked to atmospheric motion and thus to the ability of the atmosphere to transport mass, with the latent heat flux linked to the strength of the hydrologic cycle.

To derive the thermodynamic constraints of material transport, we consider the limit to the rate by which kinetic energy can be generated within the atmosphere. This rate, G , is set by the Carnot limit for dry convection which is associated with the sensible heat flux, J_{sh} , and the temperature difference, $T_s - T_a$:

$$G = J_{sh} \cdot \frac{T_s - T_a}{T_s} \quad (1)$$

The two terms, J_{sh} and $T_s - T_a$, are constrained by the energy balances of the system, with a greater flux J_{sh} corresponding to a smaller temperature difference $T_s - T_a$. This trade-off is derived from the explicit consideration of the energy balances. Using this energy balance constraint then yields a maximum power limit G_{max} that is associated with an optimum mass exchange between the surface and the atmosphere that is characterized by an optimum vertical exchange velocity w_{opt} .

In the following, several simplifying assumptions are being made to derive a relatively simple, but realistic analytical solution. A wet surface is considered, i.e. that the evaporation rate is not limited by water availability. The atmosphere is assumed to absorb all of the emitted terrestrial radiation from the surface. As will be seen below, these considerations are quite reasonable for present-day conditions and yield estimates by the model that compare well with observations.

Energy balance constraints

The surface energy balance of the system is given by

$$0 = J_{sw} - J_{s,a} - J_{sh} - J_{lh} \quad (2)$$

The corresponding energy balance of the atmosphere is given by

$$0 = J_{s,a} + J_{sh} + J_{lh} - J_{lw} \quad (3)$$

In these equations, J_{sw} represents the forcing of the system, and the steady state requires that $J_{lw} = J_{sw}$. Since the radiative temperature is fixed by the global energy balance, $J_{sw} = \sigma T_a^4$ (with σ being the Stefan-Boltzmann constant), the atmospheric temperature is fixed at $T_a = (J_{sw}/\sigma)^{1/4}$. The radiative exchange flux between the surface and the atmosphere is expressed in a linearized approximation by $J_{s,a} = k_r(T_s - T_a)$ with $k_r = 4\sigma T_s^3/(1 + 0.75\tau)$ and τ being the longwave optical depth of the atmosphere. The sensible heat flux is expressed as $J_{sh} = c_p \rho w (T_s - T_a)$ with heat capacity c_p and air density ρ . The latent heat flux for an open water surface is written as $J_{lh} = \lambda w (q_s - q_a) \approx s/\gamma \cdot J_{sh}$ with λ being the latent heat of vaporization, q_s and q_a being the specific humidities of near surface and atmospheric air, $s = de_{sat}/dT \approx s_0 \exp[19.83 - 5417/T_s]/T_s^2$ is the slope of the saturation vapor pressure evaluated at the reference temperature T_s (with $s_0 \approx 3.3 \cdot 10^6$ Pa K), and γ is the psychrometric constant. These formulations are typical formulations of atmospheric heat fluxes in meteorology, and the details of the formulations can be found in [8].

Maximum power limit

The expression for the Carnot limit with these formulations of the heat fluxes depends on the forcing, J_{sw} , a series of physical and radiative parameters (such as heat capacity, air density, the psychrometric constant, the slope of the saturation vapor pressure curve, and optical thickness), and on the vertical exchange velocity within the atmosphere, w , which is a yet unconstrained variable:

$$G = \frac{c_p \rho w}{T_s (k_r + c_p \rho w (\gamma + s) / \gamma)^2} \cdot J_{sw}^2 \quad (4)$$

We can constrain the value of w by assuming that the generation rate G is maximized with respect to w , that is, that the generation of motion is maximized and operates at the thermodynamic limit within the system. When we neglect the slight dependence of T_s (because variations in T_s are relatively small compared to the mean), we can derive an analytic expression for the maximum generation rate, G_{max} :

$$G_{max} = \frac{\gamma}{\gamma + s} \cdot \frac{J_{sw}^2}{2k_r T_s} \quad (5)$$

with associated partitioning of heat fluxes of

$$J_{s,a,opt} = \frac{J_{sw}}{2} \quad J_{sh,opt} = \frac{\gamma}{\gamma + s} \cdot \frac{J_{sw}}{2} \quad J_{lh,opt} = \frac{s}{\gamma + s} \cdot \frac{J_{sw}}{2} \quad (6)$$

Note that this state of maximum power associated with convection is closely related to a state of Maximum Entropy Production (MEP), which is a general hypothesis that complex thermodynamic systems are maintained in steady states at which entropy production is maximized ([9; 10; 11; 12; 13; 14; 15]). The generation of kinetic energy equals its frictional dissipation

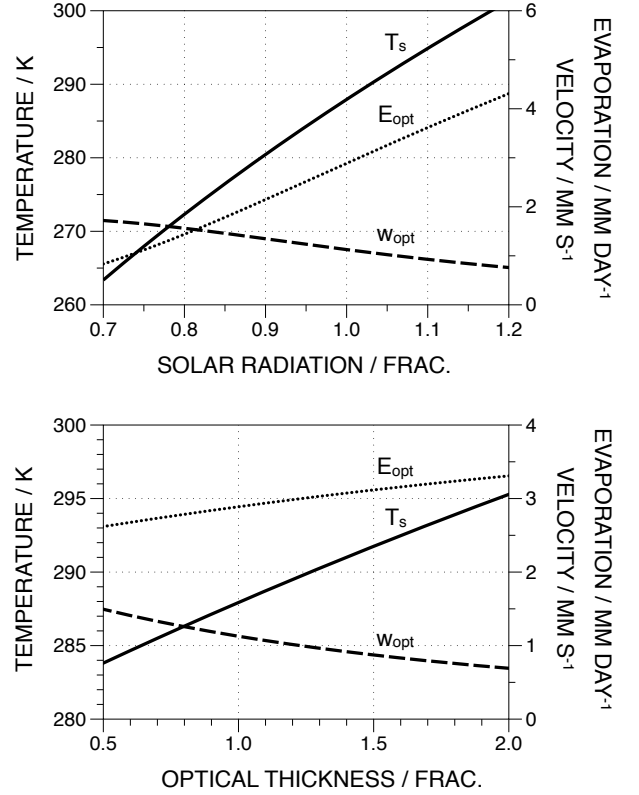


Figure 2. Sensitivity of the thermodynamic limit of convective exchange within the atmosphere, represented by the optimum exchange velocity w_{opt} , to radiative forcing and the associated surface climate in terms of surface temperature T_s and evaporation E_{opt} . The panels show the sensitivities to (top) solar radiative heating, J_{sw} , and (bottom) optical thickness, τ , both expressed as a fraction of today's reference value.

in steady state, i.e. $G = D$, so that a maximization of the generation rate then corresponds to a maximization of dissipation. If this dissipation occurs at the cold, atmospheric temperature, T_a , then the entropy production, σ_{sh} , associated with this frictional dissipation is given by:

$$\sigma_{sh} = \frac{G}{T_a} = J_{sh} \cdot \left(\frac{1}{T_a} - \frac{1}{T_s} \right) \quad (7)$$

using $G = D$ and eqn. 1 from above. Since T_a is fixed by the planetary energy balance with $T_a = (J_{sw}/\sigma)^{1/4}$, the maximization of G corresponds to a maximization of σ_{sh} .

This state of maximum power (and maximum dissipation) relates back to the motivation of this contribution (arrow A in Fig. 1) in that it is this state which characterizes the maximum dissipative activity of the Earth system in terms of atmospheric motion.

Climate sensitivity at maximum power

The properties at a state of maximum convective power can now be associated with climatic conditions at the surface. The above maximization is associated with an optimum vertical exchange velocity w_{opt} at the surface-atmosphere interface of

$$w_{opt} = \frac{\gamma}{\gamma + s} \cdot \frac{k_r}{c_p \rho} \quad (8)$$

With this maximization, the temperature difference is set, so that the surface temperature, T_s , is obtained from the energy balance and the atmospheric temperature, T_a :

$$T_{s,opt} = T_a + \frac{J_{sw}}{2k_r} = \left(\frac{J_{sw}}{\sigma} \right)^{1/4} + \frac{J_{sw}}{2k_r} \quad (9)$$

The associated strength of the hydrologic cycle, expressed by the flux of evaporation E (or precipitation, since $P = E$) is given by:

$$E_{opt} = \frac{s}{\gamma + s} \cdot \frac{J_{sw}}{2\lambda} \quad (10)$$

When these properties are evaluated for present-day conditions with $J_{sw} = 240 \text{ W m}^{-2}$ and $\tau = 0.65$, these expressions yield values of $T_s = 288 \text{ K}$, $w_{opt} = 1.1 \text{ mm s}^{-1}$, and $E_{opt} = 2.9 \text{ mm d}^{-1}$, which are very close to observed magnitudes of $w_{obs} \approx 1 \text{ mm s}^{-1}$ [16] and $E_{obs} \approx 2.7 \text{ mm d}^{-1}$ [17].

The sensitivity of these estimates to changes in the radiative forcing is shown in Fig. 2. The upper plot in the figure shows the sensitivity to absorbed solar radiation, J_{sw} , which characterizes the strength of the forcing of the system. This forcing is affected by the luminosity of the Sun, but also to some extent by the reflectivity of the Earth's atmosphere (e.g. clouds) and the surface (e.g. ice, vegetation, water), with the latter aspects not dealt with here. The lower plot in Fig. 2 shows the sensitivity to the optical thickness, τ , which describes the strength of the atmospheric greenhouse effect. This property does not affect the rate of surface heating, but rather the rate by which the surface cools through emission of terrestrial radiation.

The sensitivities of the estimates to these two radiative properties are qualitatively similar and consistent with sensitivities derived from complex climate models. Greater values of J_{sw} and τ both result in warmer surface temperatures, T_s , but for different reasons. In the first case, the warmer temperature results from a stronger solar forcing, while in the latter case, it results from a reduced cooling rate due to a stronger atmospheric greenhouse effect. Greater values of J_{sw} and τ also result in enhanced evaporation, E_{opt} , and lower values of the optimum vertical exchange velocity, w_{opt} . This lower value of w_{opt} results from the fact that at higher temperatures, s obtains a greater value, so that less vertical motion is needed to accomplish the turbulent heat exchange.

To summarize this section, we derived a Carnot-type limit for convective motion within the atmosphere from the radiative forcing and evaluated the climatic conditions associated with this maximum convective transport state. The maximum results from the strong interaction between the convective heat fluxes of sensible and latent heat, $J_{sh} + J_{lh}$, and the driving temperature difference, $T_s - T_a$, which decreases with greater convective heat fluxes due to the energy balance constraints. This trade-off is the same trade-off that is involved in studies of Maximum Entropy Production (MEP), although here this limit is interpreted by more conventional means in terms of the Carnot limit to mechanical power. This maximum convection state yields a realistic representation of the climate and characterizes the upper thermodynamic limit on mass exchange between the surface and the atmosphere. Next, this limit is evaluated regarding its implication for biotic activity at the surface.

TRANSPORT LIMITS AND BIOTIC ACTIVITY

The environmental limits on the photosynthetic rate are now being considered, as photosynthesis acts as the main driver for biotic activity on Earth. Two environmental limits are considered that directly relate to the processes considered in the previous section: the availability of light at the surface to drive the photochemistry associated with photosynthesis (arrow B in Fig. 1), and the ability of the atmosphere to transport carbon dioxide to the surface at which photosynthesis takes place (arrow C in Fig. 1). These two constraints are formulated in terms of a light-limited rate, $J_{bio,sw}$, and a flux-limited rate, J_{bio,CO_2} , of photosynthesis.

The light-limited rate, $J_{bio,sw}$, is linked to the absorption of solar radiation at the surface and is expressed as

$$J_{bio,sw} = \varepsilon \cdot J_{sw} \quad (11)$$

where ε is the light use efficiency. Since about 55% of solar radiation is photosynthetically active radiation, and it requires about 10 photons of wavelengths of 580 and 600nm to fix one molecule of carbon, the value of ε should be around $\varepsilon = 3.910^{-6} \text{ gC J}^{-1}$. For present-day conditions with $J_{sw} = 240 \text{ W m}^{-2}$, this yields a light-limited rate of about $J_{bio,sw} = 77 \mu\text{mol m}^{-2} \text{ s}^{-1}$. This rate is quite a bit higher than the observed maximum photosynthetic rate of around $50 \mu\text{mol m}^{-2} \text{ s}^{-1}$ [18] so that, overall, it is not the availability of light that limits biotic activity.

The flux-limited rate, J_{bio,CO_2} , reflects the limitation due to the atmospheric exchange of carbon dioxide between the atmosphere and the surface. It is expressed in terms of the vertical exchange velocity, w_{opt} , as well as the difference in carbon dioxide concentration

$$J_{bio,CO_2} = \rho w_{opt} \cdot (pCO_{2,a} - pCO_{2,s}) \quad (12)$$

where $\rho = 1.2 \text{ kg m}^{-3}$ is the air density and $pCO_{2,a}$ and $pCO_{2,s}$ are the mixing ratios of carbon dioxide within the atmosphere and at the surface. Since the CO_2 mixing ratio within the air space of leaves is about 70% of the atmospheric concentration, a value of $pCO_{2,s} = 0.7 pCO_{2,a}$ is used here, with a value of $pCO_{2,a} \approx 390 \text{ ppmv}$. With $w_{opt} = 1.1 \text{ mm s}^{-1}$, this yields a value of J_{bio,CO_2} for present day conditions of about $20 \mu\text{mol m}^{-2} \text{ s}^{-1}$. This is noticeably smaller than the observed maximum photosynthetic rate stated above, emphasizing the importance of this transport limitation to photosynthesis.

The sensitivity of both limitations to the radiative properties of absorbed solar radiation, J_{sw} , and longwave optical thickness, τ , are shown in Fig. 3. The light-limited rate increases with absorbed solar radiation, while it is insensitive to changes in τ . In contrast, the flux-limited rate decreases with both, J_{sw} and τ , due to the lower value of w_{opt} .

This example is, of course, formulated in a highly simplified way. There are several ways by which the biota, particularly vegetation on land, can alter the transport limit to some extent, thereby alleviating this constraint. For instance, vegetation can reduce the rate of transpiration by stomatal control, which would enhance the vertical exchange velocity by reducing the effect of s in the expression of w_{opt} (not shown here). A greater value of w_{opt} would then raise the flux-limited rate and allow for a greater rate of photosynthesis.

Nevertheless, the example demonstrates that atmospheric transport and the associated flux limitation for photosynthesis

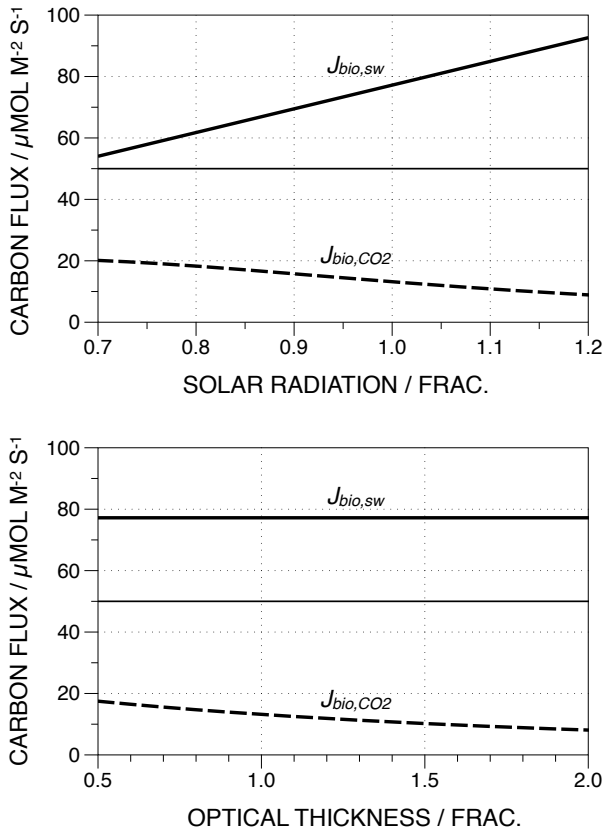


Figure 3. Sensitivity of the light-limited and flux-limited rates of photosynthesis ($J_{bio,sw}$, solid line and $J_{bio,CO2}$, dashed line) to (top) solar radiative absorption, J_{sw} , and (bottom) optical thickness, τ , both expressed as a fraction of today's reference value. The thin horizontal line indicates roughly the maximum observed rate of photosynthesis.

is more limiting than the availability of light. This limitation forms one aspect of the coupling between the dynamics within the abiotic part of the Earth system and the activity of the biosphere, as represented by arrow C in Fig. 1.

BIOTIC EFFECTS ON THE EARTH SYSTEM

The effects of biotic activity on the Earth system as shown by arrows D in Fig. 1 affect the values of J_{sw} through enhanced absorption by biomass and of τ through changes in atmospheric composition. Even though the first effect plays a large role on land, its global effect is relatively small, so that it is not considered here. The following scenario focuses on the second effect that involves changes in τ that are taken here as a result of biotic activity.

The scenario that is considered here is placed in the context of Earth system history. Geological indicators suggest that the Earth maintained an ice-free state and maintained surface temperatures within a relatively narrow range through most of its history although the sun was a lot fainter in the past, with about 70% of today's luminosity at 4.5 billion years ago. One common "solution" to this discrepancy is that the concentration of greenhouse gases may have been substantially higher in the past [19; 20], with changes in greenhouse gas concentrations being attributed to changes in biotic activity.

We now consider such a scenario in the context of the simple model developed here. The surface temperature T_s is prescribed to its present-day value, and this condition is used to derive the value of τ under the assumption of maximized convective

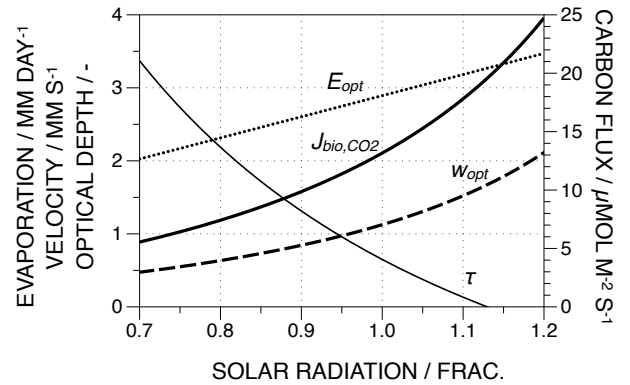


Figure 4. Implied changes in optical depth τ (thin solid line), evaporation E_{opt} (dotted line), vertical exchange velocity w_{opt} (dashed line), and flux-limited rate of carbon exchange, $J_{bio,CO2}$ (solid line) when a fixed surface temperature of $T_s = 288$ K is prescribed for the given variation in absorbed solar radiation, J_{sw} .

exchange. The sensitivity of this setting is then evaluated to changes in J_{sw} , which is shown in Fig. 4. The figure shows the decrease in τ with an increase in J_{sw} , which is consistent with the previous studies that argued for a stronger greenhouse effect to compensate for the lower values of solar luminosity in the past. The figure also shows a strengthening of the hydrologic cycle, shown by E_{opt} , and a stronger vertical exchange, w_{opt} , with greater values of J_{sw} , which result in a less-limiting rate $J_{bio,CO2}$.

This sensitivity shown in Fig. 4 can directly be related to the equations described above. The prescribed surface temperature of $T_s = 288$ K requires a smaller value of k_r for lower values of J_{sw} , which can be seen in eqn. 9. This smaller value of k_r is achieved by a greater value of τ . Hence, the value of τ is reduced with increased values of J_{sw} under the constraint of the prescribed surface temperature. The evaporation rate, E_{opt} , is directly proportional to J_{sw} (eqn. 10), so that the strength of the hydrologic cycle increases proportionally with the rate of absorption of solar radiation, J_{sw} . The increase in w_{opt} with J_{sw} reflects the increased value of k_r (cf. eqn. 8), which is due to the lower values of τ that are needed to maintain the prescribed surface temperature. This increase in w_{opt} then leads to the increase in $J_{bio,CO2}$ with J_{sw} .

Even though the sensitivity and the model considered here is highly simplified, it illustrates the important point that the dissipative activities of the Earth system and of the biosphere are not externally determined, but merely constrained. In the model, this constraint is represented by the magnitude of absorption of solar radiation, J_{sw} . Furthermore, these two systems strongly interact, with the radiative forcing and the value of τ affecting the flux-limited rate of photosynthesis, while greater values of biotic activity could result in a reduction of greenhouse gases, which could reduce τ . Hence, the interaction between life and the Earth system is likely to affect the magnitudes of their respective dissipative behaviors.

CONCLUSIONS

To conclude this study, the results presented here suggest that it is not primarily the struggle for light that limits the dissipative activity of the Earth's biosphere, but rather the ability to exchange materials. To formulate the essence of this contribution in a similar way to Boltzmann's quote that was presented at

the beginning of this paper, this study would suggest that the

general struggle for existence of living organisms is therefore not a struggle for light – this is abundantly available at the surface – but a struggle for transport of the basic materials, which through the transformations of energy from the hot sun to the cold Earth becomes available.

This perspective intimately links the abiotic transport characteristics of the Earth system to the essential resource requirements for life. If we want to better understand the role of life, we would need to view it as a component of the Earth system that is deeply embedded in its function and that is subjected to limits that are not just related to direct energy conversions, but also to environmental transport limitations. These limits are, however, not fixed, but are ameliorated by the consequences of life. Hence, this would seem to require a thermodynamic Earth system perspective to understand the role and consequences of life on Earth.

REFERENCES

- [1] L. Boltzmann, “Der zweite Hauptsatz der mechanischen Wärmetheorie,” *Almanach der kaiserlichen Akademie der Wissenschaften*, vol. 36, pp. 225–259, 1886.
- [2] E. Schrödinger, *What is Life? The physical aspect of the living cell*. Cambridge, UK: Cambridge University Press, 1944.
- [3] J. E. Lovelock, “Gaia as seen through the atmosphere,” *Atmos. Environ.*, vol. 6, pp. 579–580, 1972.
- [4] J. E. Lovelock, *Gaia: A New Look at Life on Earth*. Oxford, UK: Oxford University Press, 1972.
- [5] J. F. Kasting and D. Catling, “Evolution of a habitable planet,” *Annu. Rev. Astron. Astrophys.*, vol. 41, pp. 429–463, 2003.
- [6] E. Nisbet and C. M. R. Fowler, “The evolution of the atmosphere in the archaean and early proterozoic,” *Chinese Science Bulletin*, vol. 56, pp. 4–13, 2011.
- [7] A. Kleidon, “Beyond Gaia: Thermodynamics of life and Earth system functioning,” *Clim. Ch.*, vol. 66, pp. 271–319, 2004.
- [8] A. Kleidon and M. Renner, “Thermodynamic limits of hydrologic cycling within the earth system: concepts, estimates and implications,” *Hydrol. Earth Syst. Sci. Discuss.*, vol. 10, pp. 3187–3236, 2013.
- [9] G. W. Paltridge, “The steady-state format of global climate,” *Q. J. Roy. Meteorol. Soc.*, vol. 104, pp. 927–945, 1978.
- [10] H. Ozawa and A. Ohmura, “Thermodynamics of a global-mean state of the atmosphere – a state of maximum entropy increase,” *J. Clim.*, vol. 10, pp. 441–445, 1997.
- [11] R. D. Lorenz, J. I. Lunine, P. G. Withers, and C. P. McKay, “Titan, mars and earth: Entropy production by latitudinal heat transport,” *Geophys. Res. Lett.*, vol. 28, pp. 415–418, 2001.
- [12] H. Ozawa, A. Ohmura, R. D. Lorenz, and T. Pujol, “The second law of thermodynamics and the global climate system – a review of the Maximum Entropy Production principle,” *Rev. Geophys.*, vol. 41, p. 1018, 2003.
- [13] L. M. Martyushev and V. D. Seleznev, “Maximum entropy production principle in physics, chemistry, and biology,” *Physics Reports*, vol. 426, pp. 1–45, 2006.
- [14] A. Kleidon, Y. Malhi, and P. M. Cox, “Maximum entropy production in environmental and ecological systems,” *Phil. Trans. R. Soc. B*, vol. 365, pp. 1297–1302, 2010.
- [15] A. Kleidon, “How does the earth system generate and maintain thermodynamic disequilibrium and what does it imply for the future of the planet?,” *Phil. Trans. R. Soc. A*, vol. 370, pp. 1012–1040, 2012.
- [16] J. P. Peixoto and A. H. Oort, *Physics of Climate*. New York, NY: American Institute of Physics, 1992.
- [17] T. Oki and S. Kanae, “Global hydrological cycle and world water resources,” *Science*, vol. 313, pp. 1068–1072, 2006.
- [18] J. R. Ehleringer, “Photosynthesis: physiological and ecological considerations,” in *Plant Physiology* (L. Taiz and E. Zeiger, eds.), Sinauer Associates, Sutherland, MA, USA, 2006.
- [19] C. Sagan and G. Mullen, “Earth and mars: Evolution of atmospheres and surface temperatures,” *Science*, vol. 177, pp. 52–56, 1972.
- [20] J. F. Kasting, “Earth’s early atmosphere,” *Science*, vol. 259, pp. 920–926, 1993.

STOCHASTIC DYNAMICS OF PROTEINS AND THE ACTION OF BIOLOGICAL MOLECULAR MACHINES

Michal Kurzynski

Faculty of Physics, Adam Mickiewicz University, Umultowska 85, 61-614 Poznan, Poland, E-mail: kurzphys@amu.edu.pl

ABSTRACT

Biological molecular machines are proteins that operate under isothermal conditions hence are referred to as free energy transducers. They can be formally considered as enzymes that simultaneously catalyze two chemical reactions: the free energy-donating (input) reaction and the free energy-accepting (output) one. It is now well established that most if not all enzymatic proteins display a slow stochastic dynamics of transitions between a variety of conformational substates composing their native state. A hypothesis is stated that, like higher level biological networks: the protein interaction network and the metabolic network, the protein conformational transition networks have evolved in a process of self-organized criticality. All three classes of networks are scale-free and, probably, display a transition from the fractal organization in a small length scale to the small-world organization in the large length scale. Good mathematical models of such networks are stochastic critical branching trees extended by long-range shortcuts. The degree of coupling between the output and the input reaction fluxes have been studied both theoretically and by means of the Monte Carlo simulations on model networks. For single input and output gates the degree of coupling values cannot exceed unity. Study simulations of random walks on several model networks involving more extended gates indicate that the case of the degree of coupling with the value higher than one is realized on the mentioned above critical branching trees extended by long-range shortcuts.

ENZYMATIC PROTEINS – CHANGE OF THE FUNDAMENTAL PARADIGM

Proteins are linear polymers of amino acids arranged in a sequence determined by genes. Since the origin of molecular biology in the 1950s, a paradigm has been commonly accepted, expressed shortly in two successive implications:

sequence \rightarrow structure \rightarrow function.

It assumes implicitly that the dynamics of native proteins reduces to simple normal vibrations about a single well defined conformational state referred to as the 'tertiary structure' of the protein. For at least two decades, however, it becomes more and more clear that not only structure but also more complex dynamics determine the function of proteins thus the paradigm has to be changed onto [1]

sequence \rightarrow structure & dynamics \rightarrow function.

Two classes of experiments imply directly that besides fast vibrations enzymatic proteins display also a much slower stochastic dynamics of transitions between a variety of conformational substates composing their native state. The first class includes observations of the non-exponential initial stages of reactions after special preparation of an initial microscopic state in a statistical ensemble of biomolecules by, e.g., the laser pulse [2; 3]. The second class concerns statistics of the dichotomous noise generated by single biomolecules in various processes, which often displays a non-exponential time course [4; 5]. The even more convincing proof of the conformational transition dynamics of simple native proteins has been afforded by early molecular dynamics simulations [6; 7]. Research of biomolecular dynamics is being developed faster and faster and today, even in the case of small, water-soluble proteins, one speaks about the

'native state ensemble' rather than a single native state, and for very small proteins or protein fragments trials to reconstruct the actual networks of conformational transitions are realized [8].

Because of the slow character of the conformational dynamics, both chemical and conformational transitions in an enzymatic protein have to be treated on an equal footing [9] and jointly described by a system of coupled master equations

$$\dot{p}_l(t) = \sum_{l'} [w_{ll'} p_{l'}(t) - w_{l'l} p_l(t)], \quad (1)$$

determining time variation of the occupation probabilities $p_l(t)$ of the individual protein's substates (Fig. 1). In Eq. (1), $w_{l'l}$ is the transition probability per unit time from the substate l to l' and the dot denotes the time derivative. The conformational transition probabilities satisfy the detailed balance condition which, however, can be broken for the chemical transition probabilities controlled by concentrations of the enzyme substrates. Eqs. (1) are to be treated as a model of microscopic dynamics in the stochastic theory of reaction rates [10; 11] the origins of which go back to the Smoluchowski theory of diffusion-controlled coagulation and the Kramers one-dimensional theory of reactions in the overdamped limit. It is the stochastic theory of reaction rates and not the conventional transition state theory that has to be applied in the description and interpretation of biochemical processes [9; 12].

Contrary to the transition state theory the stochastic theory of reaction rates takes seriously into account the very process of reaching the partial thermodynamic equilibrium in non-chemical degrees of freedom of the system described. In the closed reactor, a possibility of a subsequent chemical transformation of an enzyme to proceed before the conformational equilibrium have been reached in the actual chemical state re-

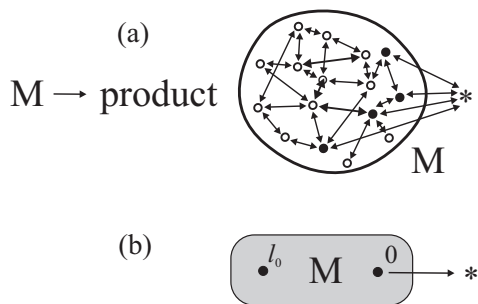


Figure 1. (a) Exemplifying realization of the model intramolecular dynamics underlying the irreversible reaction $M \rightarrow \text{product}$. Chemical state M is composed of many substates (the white and black circles) and the dynamics involves purely stochastic transitions between these states (the arrows). Chemical state product is represented by a single, totally absorbing 'limbo' state $*$. The reaction is realized through transitions between distinguished substates in M , jointly forming what is called the transition state R^\ddagger (the black circles) and the limbo $*$. (b) Particular case of the irreversible reaction when the transition state is reduced to a single 'gate' substate 0 . The shaded box represents a network of an arbitrary number of sites and the direct transitions between them.

sults in the presence of a transient non-exponential stage of the process and in an essential dynamical correction to the reaction rate constant describing the following exponential stage. In the open reactor under stationary conditions (the concentrations of reactants and products of the reaction kept constant), the general situation is more complex but for reactions gated by single transition conformational substates (Fig. 1(b)) a simple analytical theory was proposed [9; 13]. A consequence of the slow conformational transition dynamics is that the steady-state kinetics, like the transient stage kinetics, cannot be described in terms of the usual rate constants. This possibility was suggested forty years ago by Blumenfeld [14]. More later on, we have shown that adequate physical quantities that should be used are the mean first-passage times between distinguished transition substates [9; 13]. The subject of the present paper is an application of this formalism to elucidate the action of biological molecular machines.

BIOLOGICAL MACHINES AS CHEMO-CHEMICAL FREE ENERGY TRANSDUCERS

The primary purpose of thermodynamics, born in the first half of the 19th century, was to explain the action of heat engines. The processes they are involved in are practically reversible and proceed in varying temperatures. As a consequence, thermodynamics being the subject of the school and academic teaching, still deals mainly with equilibrium processes and changes of temperature. Meanwhile, biological machines as well as many other contemporary machines act irreversibly, with considerable dissipation, but at constant temperature. Machines that operate under the condition $T = \text{const.}$ are free energy transducers [12]. A good example are enzymes kinases that catalyze simultaneously two reactions, the ATP hydrolysis and a substrate phosphorylation.

From a theoretical point of view, it is convenient to treat all biomolecular machines, also pumps and motors, as chemo-chemical machines [12], enzymes that simultaneously catalyze two chemical reactions: the free energy-donating reaction and the free energy-accepting one. Under isothermal conditions, all

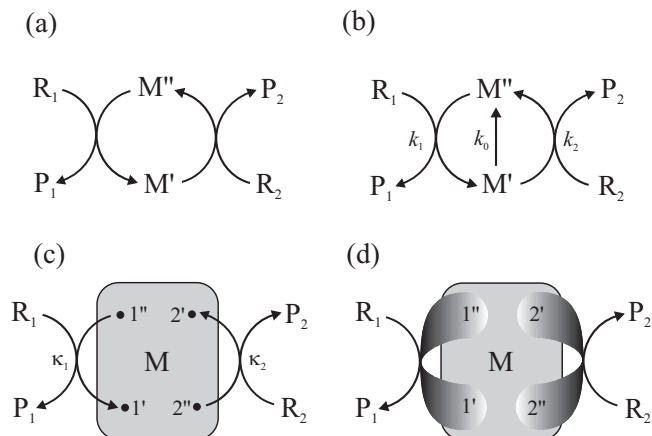


Figure 2. Development of kinetic schemes of the chemo-chemical machine. (a) Principle of the chemo-chemical free energy transduction. Due to proceeding on the same enzyme, reaction $R_1 \leftrightarrow P_1$ drives reaction $R_2 \leftrightarrow P_2$ against its conjugate force determined by steady state concentrations of the reactant and the product. (b) Assumption of a possible short circuit or slippage of the input vs. output reaction. (c) Assumption of both the free energy-donating and the free energy-accepting reaction to participate in a kinetic scheme like the one shown in Fig. 1(b). (d) Further generalization of the kinetic scheme to involve many input and output of gates.

chemical reactions proceed due to thermal fluctuations: a free energy needed for their realization is borrowed from the environment and then returned to it. In fact, the biological molecular machines are biased Maxwell's demons: their mechanical or electrical elements are 'soft' and perform work at the expense of thermal fluctuations [15; 16; 17]. Of course, Maxwell's demon can operate only out of equilibrium and it is a task of the free energy-donating reaction to secure such conditions.

The principle of action of the chemo-chemical machine is simple [18]. It is a protein enzyme that catalyzes simultaneously two chemical reactions (Fig. 2(a)). Separately, each reaction takes place in the direction determined by the second law of thermodynamics, i.e., the condition that energy dissipated, determined by the product of flux and force, is positive. However, if both reactions take place simultaneously in a common cycle, they must proceed in the same direction and the direction of the first reaction can force a change of direction of the second. As a consequence, the first reaction transfers a part of its free energy recovered from dissipation performing work on the second reaction.

In formal terms, the chemo-chemical machine couples two unimolecular reactions: the free energy-donating reaction $R_1 \leftrightarrow P_1$ and the free energy-accepting reaction $R_2 \leftrightarrow P_2$. Bimolecular reactions can be considered as effective unimolecular reactions on assuming a constant concentration of one of the reagents, e.g. ADP in the case of ATP hydrolysis. The input and output fluxes J_i ($i = 1$ and 2 , respectively) and the conjugate thermodynamic forces A_i are defined as [18]

$$J_i = \frac{d[P_i]/dt}{[E]_0} \quad (2)$$

and

$$\beta A_i = \ln K_i \frac{[R_i]}{[P_i]}, \quad K_i \equiv \frac{[P_i]_{\text{eq}}}{[R_i]_{\text{eq}}}. \quad (3)$$

Here, symbols of the chemical compounds in the square brackets denote the molar concentrations in the steady state (no superscript) or in the equilibrium (the superscript eq). $[E]_0$ is the total concentration of the enzyme and β is proportional to the reciprocal temperature, $\beta \equiv (k_B T)^{-1}$, where k_B is the Boltzmann constant. The flux-force dependence is one-to-one only if some constraints are put on the concentrations $[R_i]$ and $[P_i]$ for each i . There are two possibilities. Either the concentration of one species, say R_i , in the open reactor under consideration is kept constant: $[R_i] = \text{const.}$, or is such the total concentration of the enzyme substrate: $[R_i] + [P_i] = \text{const.}$

The free energy transduction is realized if the product $J_2 A_2$, representing the output power, is negative. The efficiency of the machine is the ratio

$$\eta = -J_2 A_2 / J_1 A_1 \quad (4)$$

of the output power to the input power. In general, the degree of coupling

$$\varepsilon = J_2 / J_1, \quad (5)$$

being itself a function of the forces A_1 and A_2 , can be both positive and negative.

Usually, the assumption of tight coupling between the both reactions is made (Fig. 2(a)). It states that the flux of the first reaction equals the flux of the second, $J_1 = J_2$ thus $\varepsilon = 1$. However, an additional reaction can take place between the two states M' and M'' of the enzyme-substrates complex (Fig. 2(b)). The latter reaction can be considered either as a short circuit, the non-productive realization of the first reaction not driving the second reaction, or a slippage, the realization of the second reaction in the direction dictated by its conjugate force.

The multiconformational counterpart of the scheme in Fig. 2(b) is shown in Fig. 2(c). Here, like in the scheme in Fig. 1(b), a network of conformational transitions within the enzyme-substrates complex is represented by the gray box and the assumption of gating by single pairs of transition conformational substates is made. In Ref. [13], using a technique of summing up the directional diagrams proposed by Terrell L. Hill [18] who formalized an old idea of Gustav Kirchhoff, we shown how the input and the output reaction fluxes are related to the mean first-passage times between the distinguished substates.

For all the schemes shown in Figs. 2(a-c), the flux-force dependence for the two coupled reactions has a general functional form [13]:

$$J_i = \frac{1 - e^{-\beta(A_i - A_i^{\text{st}})}}{J_{+i}^{-1} + J_{-i}^{-1} e^{-\beta(A_i - A_i^{\text{st}})} + J_{0i}^{-1} (K_i + e^{\beta A_i})^{-1}}. \quad (6)$$

The parameters J_{+i} , J_{-i} , J_{0i} and A_i^{st} depend on the other force and are determined by a particular kinetic scheme. A_i^{st} have the meaning of stalling forces for which the fluxes J_i vanish: $J_i(A_i^{\text{st}}) = 0$. The dependence $J_i(A_i)$ is strictly increasing with an inflection point, determined by J_{0i} , and two asymptotes, J_{+i} and J_{-i} (Fig. 3). The asymptotic fluxes J_{+i} and J_{-i} display the Michaelis-Menten dependence on the substrate concentrations. Because of high complexity, we refrained from giving any formulas for the turnover numbers and the apparent dissociation constants, but simpler formulas for the degree of coupling ε and the stalling forces A_i^{st} are given and discussed in Ref. [8].

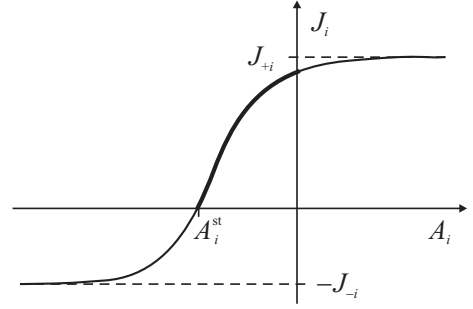


Figure 3. Character of the functional dependence of the output flux J_i versus force A_i determined by Eq. (6). Only when the stalling force A_i^{st} is negative does free energy transduction take place. The $J_i(A_i)$ dependence in this range is marked with a bold line.

In Ref. [8], we have compared theoretical results with Monte Carlo simulations on several model networks. Fig. 4 shows an example for 5-dimensional hypercube. It is seen that even for such simple and small network of 32 nodes large fluctuations make determination of the input and the output fluxes in 10^4 iteration steps impossible. Only the increase of the number of the iteration steps to 10^9 enables one to determine the fluxes with the error lower than 0.3%. Preliminary estimations indicate that the result is in a good agreement with the Gallavotti-Cohen

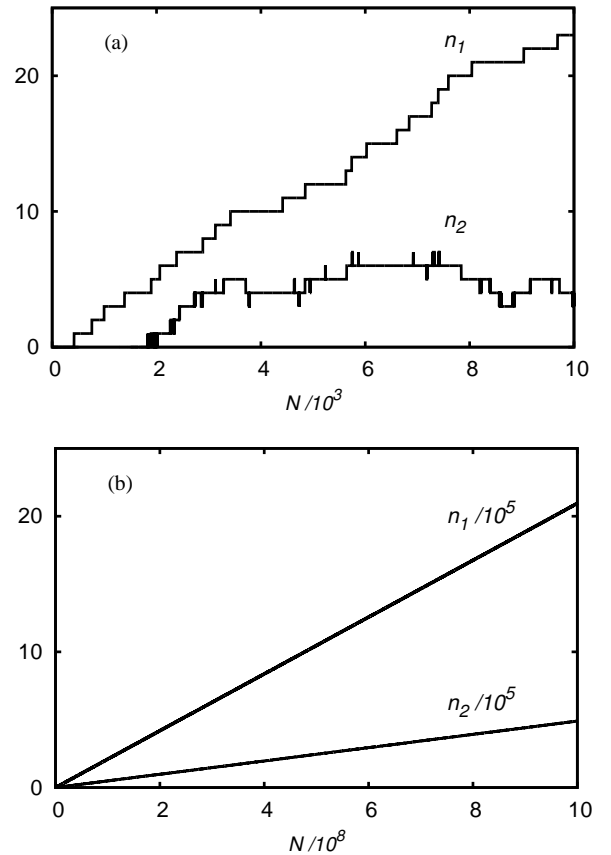


Figure 4. Simulated time course of the net number of the input ($R_1 \leftrightarrow P_1$) and the output ($R_2 \leftrightarrow P_2$) external transitions for the 5-dimensional hypercube with gates and parameters described in text. (a) Snapshots made every step. (b) Snapshots made every 10^5 steps.

fluctuation theorem [19]

$$\frac{p(\sum_i \beta A_i j_i^+)}{p(-\sum_i \beta A_i j_i^-)} = \exp(-\sum_i \beta A_i j_i t), \quad (7)$$

which can be equivalently rewritten as

$$\langle \exp(-\sum_i \beta A_i j_i t) \rangle = 1. \quad (8)$$

Above, $j_i = j_i^+ - j_i^-$ denotes the random variable of the i -th net flux being the difference of the forward and backward components j_i^+ and j_i^- , respectively, and $j_i = j_i^+ - j_i^-$ is the value of that flux.

NETWORKS OF CONFORMATIONAL TRANSITIONS AND CRITICAL BRANCHING TREES

The essential motive of our studies is a trial to answer the intriguing question whether is it possible for the degree of coupling to have a value higher than unity. A dogma in the physical theory of, e.g., biological molecular motors is the assumption that for making a single step along its track the motor molecule has to hydrolyze at least one molecule of ATP [20]. Several years ago this assumption has been questioned by a group of Japanese biophysicists from the Yanagida laboratory who, joining a specific nanometry technique with the microscopy fluorescence spectroscopy, shown that the myosin II head can make several steps along the actin filament per ATP molecule hydrolyzed [21; 22]. The structure of myosin II is similar to that of small G proteins, e.g., protein Ras (rat sarcoma) p21, both proteins having a common ancestor [23]. After the bounded nucleotide triphosphate hydrolysis, both in the G proteins [24] and in the myosin II [25; 26] one of the α helices unwinds in part what makes the neighboring region partly disordered, highly flexible, thus fluctuating. Also for the transcription factor p53 a DNA binding core domain is partly disordered [27]. The commonly assumed model of facilitated, alternating 3- and 1-dimensional passive diffusion, does not explain all the known facts concerning the search for a proper binding site on DNA [28], so a hypothesis that this search can be active, using multiply the free energy of a single ATP molecule hydrolysis seems reasonable.

No conventional chemical kinetics approach is able to explain such behaviors. In Refs. [13] and [12], basing on approximations carried too far, we suggested that the degree of coupling can exceed unity already for reactions proceeding through single pairs of transition substates. In Ref. [8] we proved the theorem that the value of the degree of coupling should be lower or at the most equal to unity, but only in the case when the input and output reactions proceed through single pairs of transition conformational substates. It is reasonable to suppose that a possibility of higher degree of coupling is realized if the output gate is extended to two or more pairs of the transition substates. In fact, it is obvious that replacing the single output gate in the scheme in Fig. 2(a) by n gates succeeding each other, we get the degree of coupling $\epsilon = n$. Such reasoning has been proposed in order to explain multiple stepping of the myosin molecule along the actin filament [22]. One can also imagine an incorporation of a system of additional nonreactive transitions what was for the first time considered by Terada and coworkers [29]. In

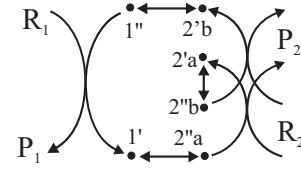


Figure 5. Extension of the kinetic scheme in Fig. 2 (c) to one input and two output gates. Obligatory transitions are drawn by arrows. If no other transitions are realized, the degree of coupling between second and first reaction equals two. Otherwise, it is lower than two but possibly higher than one.

Fig. 5 a scheme is shown with one input and two output gates, being an extension of the kinetic scheme in Fig. 2(c). Unfortunately, even in the case of only two output gates the analytical formulas are so complex and not transparent that serious approximations are needed to be made from the very beginning. Being not able to formulate presently such approximations, we decided to apply computer experiment for a preliminary study of the problem.

Since the formulation by Bak and Sneppen a cellular automaton model of the Eldredge and Gould punctuated equilibriums [30], the biological evolution is more and more often considered as a self-organized criticality phenomenon [31; 32]. There are grounds to suppose that the conformational transition networks, like two networks of the systems biology: the protein interaction network and the metabolic network, have evolved to reach a scale-free structure [8]. A controversy emerges if this structure is simultaneously small-world or fractal. The former feature is suggested by results of molecular dynamics simulations for small atomic clusters [33] and by a specific spatial organization of proteins [34]. The latter has been shown already in the pioneer papers from the Hans Frauenfelder laboratory [3] and confirmed in early molecular dynamics simulations for the very proteins [6; 7]. Only recently, an apparent contradiction between fractality and small-worldness have been explained by application of the renormalization group technique [35]. It appears that on adding to an original fractal network shortcuts with the distance r distribution following the power law $r^{-\alpha}$, a transition to the small world network occurs below some critical value of the exponent α . Close to this critical value the network can be fractal in a small length-scale, simultaneously having the small-world features in the large length-scale and this is the case of the protein interaction network, the metabolic network and, probably, the protein conformational transition network as well.

The topological structure of the flow (of probability, metabolites, energy or information) through a network is characterized by a spatial spanning tree composed of the most conducting links not involved in cycles. It is referred to as the skeleton [36] or the backbone [37] of the network, all the rejected links being considered as shortcuts. The skeleton of the scale-free and fractal network is also scale-free and fractal. For the scale-free fractal trees a criticality feature appears important that denotes the presence of a plateau equal to unity in the mean branching number dependence on the distance from the skeleton root. The critical trees can be completed to self-similar scale-free networks and such is the case of the protein interaction and metabolic networks [36; 38].

Fig. 6(a) shows a scale-free fractal tree with $N = 200$ nodes constructed following the algorithm described in Ref. [36], and Fig. 6(b) shows an extension of this tree by 200 shortcuts with

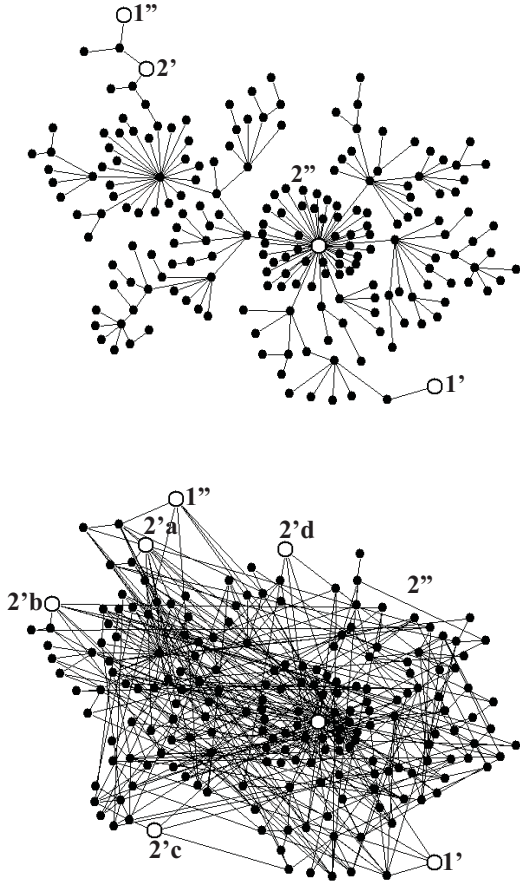


Figure 6. (a) Exemplifying realization of a scale-free fractal tree with $N = 200$ nodes constructed following the algorithm described in Ref. [36]. The single input and output gates are distinguished, chosen for the Monte Carlo simulations. (b) Tree from the upper figure extended by 200 shortcuts with the distance distribution following the power law r^{-2} what makes the network a scale free small world. Four output gates are distinguished, chosen for the Monte Carlo simulations; the unlabeled largest hub is the fourfold degenerated complement gate $2''$.

the distance distribution following the power law r^{-2} , with negative α , what makes the network a scale free small world. To provide the network with a stochastic dynamics described by Eq. (1), we assume the probability of changing a node to any of its neighbors to be the same in each random walk step. Consequently, the transition probability from the node l to the neighboring node l' per computer step

$$w_{l'l} = 1/k_l, \quad (9)$$

where k_l is the number of links (the degree) of the node l . The network with such a dynamics cannot be isoenergetic and following the detailed balance principle the equilibrium occupation probability of the node l ,

$$p_l^{\text{eq}} = k_l / \sum_{l'} k_{l'}. \quad (10)$$

To complete Ref. [8], for the system of gates shown in Fig. 6(a) we performed a series of Monte Carlo simulations and

found $\epsilon = 0.99$ for mean times of external transitions $\tau_1 = \tau_2 = 40$, those times being the order of magnitude shorter than the internal relaxation time $\tau_{\text{rx}} = 400$, and $\epsilon = 0.88$ for $\tau_1 = \tau_2 = 400$. In the latter case of the comparable external and internal transition rates, there is some little slippage, but the output reaction proceeds backward relatively rarely. The case of multiple output gates needs more systematic studies. For the system of gates shown in Fig. 6(b) and $\tau_1 = \tau_2 = 40$ we found $\epsilon = 1.40$, larger than unity. Random search for more optimal configuration of gates indicates a possibility of obtaining much higher value of the degree of coupling.

SUMMARY

It is now well established that most if not all enzymatic proteins display a slow stochastic dynamics of transitions between a variety of conformational substates composing their native state. This makes a possibility of chemical transformations to proceed before the conformational equilibrium has been reached in the actual chemical state. In the closed reactor, it results in the presence of transient, non-exponential stages of the reactions. In the open reactor, a consequence is the necessity of determining the steady-state reaction fluxes by mean first-passage times between transition conformational substates of the reactions rather than by conventional reaction rate constants. A hypothesis is stated that, like higher level biological networks: the protein interaction network and the metabolic network, the protein conformational transition networks have evolved in a process of self-organized criticality. All three classes of networks are scale-free and, probably, display a transition from the fractal organization in a small length scale to the small-world organization in the large length scale. Good mathematical models of such networks are stochastic critical branching trees extended by long-range shortcuts.

Biological molecular machines are proteins that operate under isothermal conditions hence are referred to as free energy transducers. They can be formally considered as enzymes that simultaneously catalyze two chemical reactions: the free energy-donating (input) reaction and the free energy-accepting (output) one. The degree of coupling between the output and the input reaction fluxes have been studied both theoretically and by means of the Monte Carlo simulations on model networks. In the steady state, on taking advantage of the assumption that each reaction proceeds through a single pair (the gate) of transition conformational substates of the enzyme-substrates complex, the degree of coupling between the output and the input reaction fluxes has been expressed in terms of the mean first-passage times between the distinguished substates. The theory has been confronted with the results of random walk simulations on various model networks.

For single input and output gates the degree of coupling values cannot exceed unity. As some experiments for the myosin II and the dynein motors suggest such exceeding, looking for conditions of increasing the degree of coupling value over unity (realization of a 'molecular gear') challenges the theory. Probably it holds also for the G-proteins and transcription factors, mutations of which can result in the cancerogenesis. Study simulations of random walks on several model networks involving more extended gates indicate that the case of the degree of coupling with the value higher than one is realized in a natural way on the mentioned above critical branching trees extended by long-range shortcuts. For short-range shortcuts, the networks are scale-free and fractal, and represent an ideal model for the

biomolecular machines with the tight coupling, i.e., with the degree of coupling value equal exactly to unity.

ACKNOWLEDGMENT

The study has been supported in part by the Polish Ministry of Science and Higher Education (project N N202 180038).

REFERENCES

- [1] T. Chouard, Breaking the protein rules, *Nature*, vol. 471, pp. 151-153, 2011.
- [2] R. H. Austin, K. W. Beeson, L. Eisenstein, H. Frauenfelder and I. C. Gunsalus, Dynamics of ligand binding to myoglobin, *Biochemistry*, vol. 14, pp. 5355-5373, 1975.
- [3] H. Frauenfelder, S. G. Sligar and F. G. Wolynes, The energy landscapes and motions of proteins, *Science*, vol. 254, 1598-1602, 1991.
- [4] M. P. S. Sansom et al., Markov, fractal, diffusion, and related models of ion channel gating. A comparison with experimental data from two ion channels, *Biophys. J.* vol. 56, 1229-1243, 1989.
- [5] M. Kurzynski, Statistical properties of the dichotomous noise generated in biochemical processes, *Cell. Mol. Biol. Lett.* vol. 13, pp. 502-513, 2008.
- [6] A. E. Garcia, R. Blumenfeld, G. Hummer and J. A. Krumhansl, Multi-basin dynamics of a protein in a crystal environment, *Physica D*, vol. 107, pp. 225-239, 1997.
- [7] A. Kitao, S. Hayward and N. Gö, Energy landscape of a native protein: Jumping-among-minima model, *Proteins*, vol. 33, pp. 496-517, 1998.
- [8] M. Kurzynski, M. Torchala and P. Chelminiak, Output-input coupling in thermally fluctuating biomolecular machines, *arXiv:1106.4961v1*, pp. 1-13, 2011.
- [9] M. Kurzyński, A synthetic picture of intramolecular dynamics of proteins. Towards a contemporary statistical theory of biochemical processes, *Progr. Biophys. Molec. Biol.* vol. 69, pp. 23-82, 1998.
- [10] B. Widom, Molecular transitions and chemical reaction rates, *Science*, vol. 148, pp. 1555-1560, 1965.
- [11] S. H. Northrup and J. T. Hynes, The stable states picture of chemical reactions, *J. Chem. Phys.* vol. 73, pp. 2700-2714, 1980.
- [12] M. Kurzynski, *The Thermodynamic Machinery of Life*, Springer, Berlin, 2006.
- [13] M. Kurzyński and P. Chelminiak, Mean first-passage time in stochastic theory of biochemical processes. Application to actomyosin molecular motor, *J. Stat. Phys.* vol. 110, pp. 137-181, 2003.
- [14] L. A. Blumenfeld, *Problems of Biological Physics*, Nauka, Moscow, 1974; English translation, Springer, Berlin, 1982.
- [15] R. D. Vale and F. Oosawa, Protein motors and Maxwell's demons: Does mechanochemical transduction involve a thermal ratchet?, *Adv. Biophys.* vol. 26, pp. 97-134, 1990.
- [16] R. A. L. Jones, *Soft Machines, Nanotechnology and Life*, Oxford University Press, Oxford, 2004.
- [17] T. Yanagida, M. Ueda, T. Murata, S. Esaki and Y. Ishii, Brownian motion, fluctuation and life, *BioSystems*, vol. 88, pp. 228-242, 2007.
- [18] T. L. Hill, *Free Energy Transduction and Biochemical Cycle Kinetics*, Springer, New York, 1989.
- [19] G. Gallavotti and E. G. D. Cohen, Dynamical ensembles in non-equilibrium statistical mechanics, *Phys. Rev. Lett.* vol. 74, 2694-2697, 1995.
- [20] J. Howard, *Mechanics of Motor Proteins and the Cytoskeleton*, Sinauer, Sunderland, 2001.
- [21] K. Kitamura, M. Tokunaga, A. H. Iwane and T. Yanagida, A single myosin head moves along an actin filament with regular steps of 5.3 nanometers, *Nature*, vol. 397, pp. 129-134, 1997.
- [22] K. Kitamura, M. Tokunaga, S. Esaki, A. H. Iwane and T. Yanagida, Mechanism of muscle contraction based on stochastic properties of single actomyosin motors observed in vitro, *Biophysics*, vol. 1, pp. 1-19, 2005.
- [23] F. J. Kull, R. D. Vale and R. J. Fletterick, The case for a common ancestor: kinesin and myosin motor proteins and G proteins, *J. Muscle Res. Cell Motil.*, vol. 19, pp. 877-886, 1998.
- [24] I. Kosztin, R. Bruinsma, P. O'Lague and K. Schulten, Mechanical force generation by G proteins, *Proc. Natl. Acad. Sci. USA*, vol. 99, pp. 3575-3580, 2002.
- [25] J. Xu and D. D. Root, Conformational selection during weak binding of the actin and myosin interface, *Biophys. J.* vol. 79, pp. 1498-1510, 2000.
- [26] A. Houdusse and H. L. Sweeney, Myosin motors: Missing structures and hidden springs, *Curr. Res. Struct. Biol.* vol. 11, pp. 182-194, 2001.
- [27] A. C. Joerger and A. R. Fersht, Structural biology of the tumor suppressor p53, *Annu. Rev. Biochem.* vol. 77, pp. 557-582, 2008.
- [28] A. B. Kolomeisky, Physics of protein-DNA interactions: mechanisms of facilitated target search, *Phys. Chem. Chem. Sol.* vol. 13, pp. 2088, 2011.
- [29] T. P. Terada, M. Sasai and T. Yomo, Conformational change of the actomyosin complex drives the multiple stepping movement, *Proc. Natl. Acad. Sci. USA*, vol. 99, pp. 9202-9206, 2002.
- [30] P. Bak and K. Sneppen, Punctuated equilibrium and criticality in simple model of evolution, *Phys. Rev. Lett.* vol. 71, pp. 4083-4086, 1993.
- [31] P. Bak, *How Nature Works: The Science of Self-Organized Criticality*, Copernicus Press, New York, 1996.
- [32] K. Sneppen and G. Zocchi, *Physics in Molecular Biology*, Cambridge University Press, New York, 2005.
- [33] J. P. K. Doye, Network topology of a potential energy landscape: A static scale-free network, *Phys. Rev. Lett.* vol. 88, p. 238701, 2002.
- [34] I. A. Kovacs, M. S. Szalay and P. Csermely, Water and molecular chaperones act as weak links of protein folding networks, *FEBS Letts.* vol. 579, pp. 2254-2260, 2005.
- [35] H. D. Rozenfeld, C. Song and H. A. Makse, Small-world to fractal transition in complex networks: A renormalization group approach, *Phys. Rev. Lett.* vol. 104, p. 025701, 2010.
- [36] K. I. Goh, G. Salvi, B. Kahng and D. Kim, Skeleton and fractal scaling in complex networks, *Phys. Rev. Lett.* vol. 96, p. 018701, 2006.
- [37] L. K. Gallos, C. Song, S. Havlin and H. A. Maxe, Scaling theory of transport in complex biological networks, *Proc. Natl. Acad. Sci. USA*, vol. 104, pp. 7746-7751, 2007.
- [38] J. S. Kim, K. I. Goh, G. Salvi, E. Oh, B. Kahng and D. Kim, Fractality in complex networks: Critical and supercritical skeletons, *Phys. Rev. E*, vol. 75, p. 016110, 2007.

STOCHASTIC SIMULATIONS OF MINIMAL CELL MODEL SYSTEMS

Mavelli Fabio*, Margherita Caputo*, Altamura Emiliano*, Stano Pasquale°

*Chemistry Department, University Aldo Moro, Via Orabona 4 – 70125 Bari

° Science Department, University Roma Tre, V.le Marconi 446 - 00146 Roma

ABSTRACT

The construction of artificial cells based on the encapsulation of chemical reacting systems inside lipid vesicles is rapidly progressing in recent years. Several groups are currently interested in synthesizing such simple cell models for biotechnological purposes or for investigating origin of life scenarios. Within this context, the properties of lipid vesicles (e.g., their stability, permeability, growth dynamics, potential to host reactions or undergo division processes...) play a central role, in combination with the dynamics of the encapsulated chemical or biochemical networks. Thus, from a theoretical standpoint, it is very important to develop deterministic equations in order to explore first - and specify later - the conditions that allow the robust implementation of these complex chemically reacting systems, as well as their controlled reproduction. Due to their intrinsic compartmentalized nature, the population of reacting molecules can be very low in terms of number of molecules so that their behaviour can be highly affected by stochastic effects both in the time course of their reactions and in their occupancy distribution among the vesicle population. In this contribution we report our mathematical approaches to model artificial cell systems in this complex scenario, with emphasis on the issue of primitive cell (protocell) systems.

INTRODUCTION

The chemical implementation of diverse proto-cellular model systems is gathering the interest of a growing number of researchers in the fields of synthetic biology and origins of life [1]-[6], who are becoming aware of the potential of micro-compartments and lipid vesicle technologies to uncover biologically relevant phenomena, as well as prebiotically plausible processes and evolutionary transitions. Protocells are lipid micro-compartments (generally lipid vesicles, but other compartments have been also used) which contain a minimal number of (bio)chemicals in order to generate typical cellular behavior, like self-maintenance and self-reproduction.

Lipid vesicles consist in a closed, spherical, semi-permeable membrane formed by the spontaneous self-assembly of lipid molecules. The membrane is a highly organized molecular bilayer that separates the molecules trapped inside the vesicle (i.e., in the inner aqueous vesicle core) from the environment.

A variety of chemical and biochemical reactions have been implemented inside protocells, from RNA synthesis to gene expression, from DNA amplification to lipid synthesis (for a review, see [7]). The latter reaction is particularly important because it allows the growth of vesicles thanks to the enlargement of vesicle membrane. Division might also follow vesicle growth, so that two ‘daughter’ vesicles are obtained from a parent one (i.e., self-reproduction).

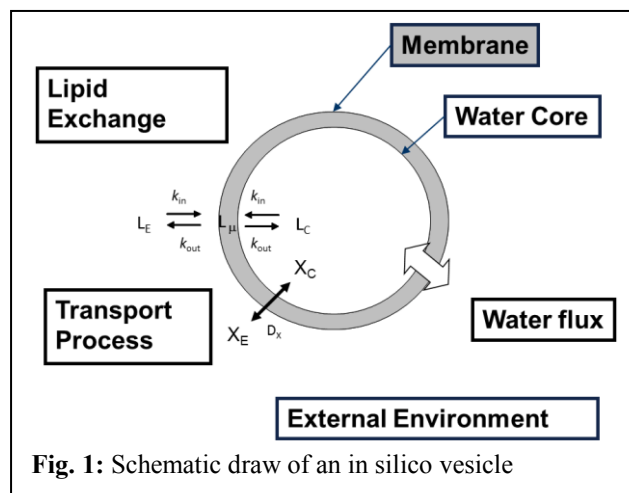
The aim of this contribution is to introduce the mathematical framework used to describe the time behaviour of reacting protocells in terms of the deterministic versus the stochastic approach [8] and to review and discuss some recent results obtained by our research group, focusing on the interplay between internalized reactions, vesicle growth and self-reproduction.

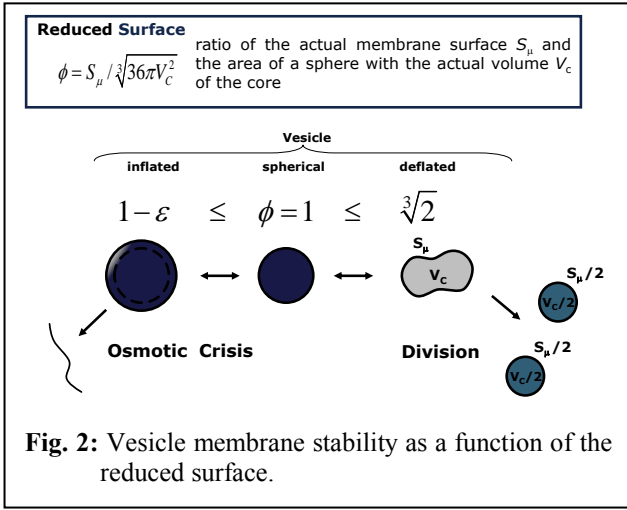
MATHEMATICAL BACKGROUND

In Silico Protocell Model

According to the schematic draw of a lipid vesicle reported in Fig. 1, reacting vesicles are described as compartmentalized systems made of two different homogeneous domains: the membrane and the water core [9]. Lipids can be exchanged between the membrane and water core and between the membrane and the external environment while transport processes can also occur, exchanging molecules directly from the external environment to the internal water pool. The vesicle membrane surface S_μ can be determined by its composition:

$$S_\mu = \sum_i^{\text{Lipids}} \frac{\alpha_i n_{\mu,i}}{2} \quad (1)$$



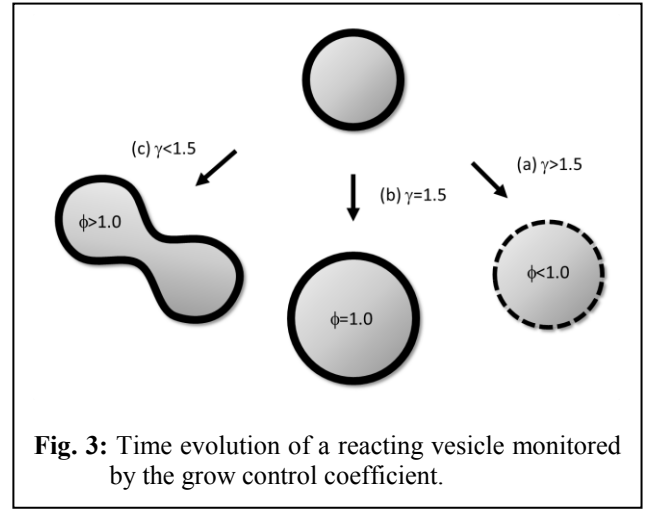


according to the hydrophilic head area α_i of different lipids, while the internal aqueous volume core V_C is affected by a water flux due to osmotic pressure unbalance. In the rest of this paper we will deal with a vesicle membrane made of one lipid molecule so the previous equation simplifies $S_\mu = \alpha_i n_i^u / 2$. The membrane stability can be monitored by introducing the reduced surface ratio ϕ , that equals 1.0 for spherical vesicles, while it will be less than 1.0 or greater than 1.0 for inflated or deflated vesicles respectively. In fact, a flux of water can take place across the lipid membrane driven by an osmotic pressure unbalance. Therefore, inflated vesicles can undergo an osmotic crisis when the internal volume grows to much bringing the membrane to rupture when $\phi < (1 - \varepsilon)$, ε being the osmotic tolerance. On the other hand, in the present model deflated vesicles are assumed to divide when the membrane surface is large enough to form two twin spherical daughters: $\phi = \sqrt[3]{2}$. This event has been observed in some experimental conditions [10] nevertheless the dynamics of a deflated membrane is a much more complex process.

Since the aqueous core volume V_C and the membrane surface S_μ may follow independent time trends, in order to describe the various possible behaviors of the system, it is convenient to introduce the *growth control coefficient* γ [11]:

$$\gamma = \left(\frac{1}{V_C} \frac{dV}{dt} \right) \bigg/ \left(\frac{1}{S_\mu} \frac{dS}{dt} \right) = \frac{S_\mu}{V_C} \frac{dV}{dS} \quad (2)$$

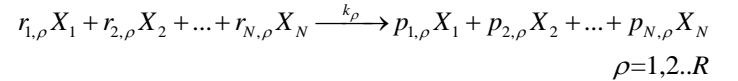
This dimensionless observable is defined as the ratio between the relative velocities of variation of volume and surface, respectively: In presence of an endogenous (biosynthetic or proto-metabolic) production of lipid results $dS > 0$ thanks to the spontaneous uptake of fresh lipid by the membrane and, in these conditions, $\gamma > 0$ indicates a real growth regime. Therefore, just by applying some straightforward geometry rules for a growing sphere: $d(\ln V)/3 = d(\ln S)/2 = d(\ln R)$, three different scenarios among all possible growth regimes may be distinguished: (a) $\gamma = 3/2$ *continuous spherical growth*, i.e. a spherical vesicle will increase its size without any change of shape ($\phi = 1$); (b) $\gamma > 3/2$ *osmotically-stressed growth*, i.e. the volume increases faster than it will reach an elastic tension condition and, above the limit of elasticity of the membrane, this will lead the vesicle to osmotic burst ($\phi < 1 - \varepsilon$); (c) $\gamma < 3/2$ *reproductive growth*, i.e. the surface increases faster than the two previous cases, the



growing vesicle will turn deflated, changing to some other closed but non-spherical shape (ellipsoidal, elongated or, generally speaking, a prolate shape) and the energy of the membrane will be higher due to a bending tension.

Deterministic Approach

If in the internal core of the compartment, N species X_i ($i=1,2,\dots,N$) react according to R chemical elementary reactions:



then the average time evolution of the reacting vesicles can be described by the deterministic approach [8] solving the following ordinary differential equation set (ODES):

$$\begin{cases} \frac{dx_i}{dt} = N_A V_C \sum_{\rho=1}^R (p_{i,\rho} - r_{i,\rho}) v_\rho + N_A \phi_i S_\mu \left([X_i]_{Ex} - \frac{x_i}{N_A V_C} \right) & i = 1, 2, \dots, N, \\ & i \neq L \\ \frac{dx_L}{dt} = N_A V_C \sum_{\rho=1}^R (p_{i,\rho} - r_{i,\rho}) v_\rho - k_{in} S_\mu \frac{x_L}{N_A V_C} + k_{out} x_L^u \\ \frac{dx_L^u}{dt} = k_{in} S_\mu \frac{x_L}{N_A V_C} - k_{out} x_L^u \\ \frac{dV_C}{dt} = \omega_{aq} \phi_{aq} S_\mu (C_C - C_{Ex}) \end{cases} \quad (3)$$

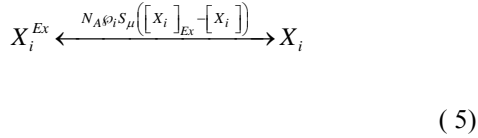
where v_ρ are the reaction rates given by the mass action law:

$$v_\rho = k_\rho \prod_{n=1}^N \left(\frac{x_n}{V_C N_A} \right)^{r_{n,\rho}} \quad (4)$$

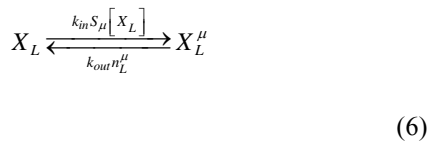
The solution of the ODES gives the average time behavior of the vesicle solution in terms of the number of molecules x_i of internal aqueous species X_i ($i=1,2,\dots,N$, $i \neq L$), the lipid molecules x_L in the water core, the lipid molecules in membrane x_L^u and core volume V_C . Moreover, it has been written for the case of aggregates formed by a single lipid X_L . Others simplifying assumptions are to neglect the specie diffusion in the internal core and in the external environment as well, and assuming the external concentration $[X_i]_{Ex}$ to be

constant in time, i.e. the environment is considered as an infinity source of external compounds.

Going into details, the mole number rate change of each aqueous species dx_i/dt is due to the internal metabolic reaction and to the transport process from the outside. The transport across the membrane is driven by a concentration gradient as shown by the following scheme:



where ϕ_i is the membrane permeability of i -species and N_A is Avogadro's number. Instead, the rate change of the lipid in the core dx_L/dt takes into account the exchange between the aqueous internal phase and the membrane described as follows:



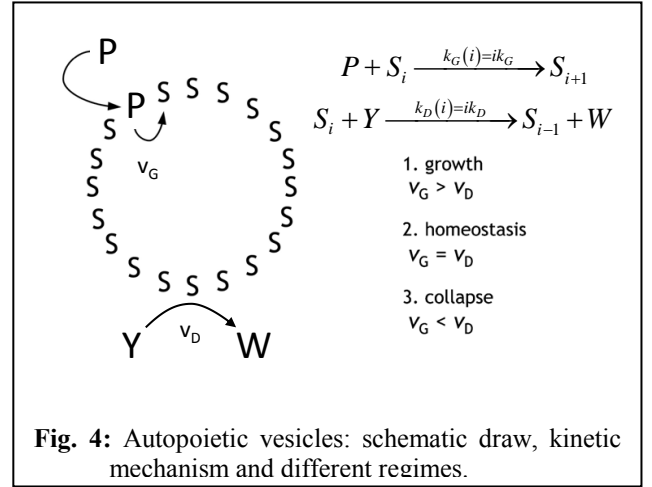
while the lipid exchange towards the outside is not explicitly considered in rate change of membrane lipids dx_L^μ/dt since the external lipid concentration is assumed to be constantly equal to the equilibrium value $[X_i]_{Ex} = \alpha_L k_{out}/(2k_{in})$. The last equation in the ODES (3) describes the core volume rate change due to a flux of water driven by the difference of the total osmolite concentration, i.e. an osmotic pressure unbalance, being ϕ_{aq} the water permeability and ω_{aq} the water molecular volume. It is important to remark that the deterministic approach gives the time evolution of the vesicle solution as the average time course calculated over the vesicle ensemble, so that x_i and x_L^μ are not positive integer numbers but they are positive real values nevertheless; they represent amount of molecules, Therefore the vesicle state is represent by the array $\mathbf{X}=(x_1, x_2, \dots, x_N)^\top$ and the core volume V_C . When the condition for division is satisfied ($\phi = \sqrt[3]{2}$), then the vesicle divides in two twin daughters with volume equal to $V_C/2$ and all the elements of the state array are accordingly divided by 2.

Stochastic Simulations

The stochastic kinetic approach explicitly takes into account the discrete nature of molecules and the intrinsic randomness of reacting events. Therefore, the state of a reacting vesicle is defined by an array of integer molecular numbers n_i : $\mathbf{N}=(n_1, n_2, \dots, n_N, n_L^\mu)^\top$ and the core volume V_C . Moreover, for each elementary reacting event a propensity density probability $a_\rho(\mathbf{N})$ is introduced instead of the deterministic reaction rate so that $a_\rho(\mathbf{N})dt$ gives the probability ρ -th reaction will take place in the next infinitesimal time interval dt [8]:

$$a_\rho(\mathbf{N}) = \frac{k_\rho}{(N_A V_C) \left(\sum_j r_{j,\rho} \right)^{-1}} \prod_j \binom{n_j}{r_{j,\rho}} \quad (7)$$

while the propensity density probabilities for transport processes and lipid exchange can be predicted according to



eqs. (5) and (6) [12]. The stochastic time evolution of a well stirred chemically reacting system can be then obtained by solving the Master Equation (ME) [8]:

$$\frac{\partial P(\mathbf{N}, t | \mathbf{N}_0, t_0)}{\partial t} = \sum_{\rho=1}^R a_\rho(\mathbf{N} - \Delta \mathbf{N}_\rho) P(\mathbf{N} - \Delta \mathbf{N}_\rho, t | \mathbf{N}_0, t_0) + P(\mathbf{N}, t | \mathbf{N}_0, t_0) \sum_{\rho=1}^R a_\rho(\mathbf{N}) \quad (8)$$

that expresses the change rate of the Markov Density function $P(\mathbf{N}, t | \mathbf{N}_0, t_0)$, i.e. the density probability to find the system in the state \mathbf{N} in the time interval $[t, t+dt)$ given the system in the state \mathbf{N}_0 at time t_0 . $\Delta \mathbf{N}_\rho$ is the jump array, that is the stoichiometric variation of the number of molecules due to the ρ -th reaction. By solving analytically the ME, the average time behavior of the reacting system can be obtained along with displacements from the average species time trend due to random fluctuations that can bring the system towards regimes unpredictable by the deterministic approach [8]. ME is very difficult to solve analytically, but it can be exactly simulated by the well know Monte Carlo direct methods introduced by Gillespie [16]. Based on this method we developed a software platform [12] suitable to simulate the stochastic time evolution of a collections of reacting vesicles assuming that diffusion processes can be neglected and the concentration gradients take place only across the lipid membrane. This program allows also to study the case of vesicle self-reproduction since it is able to follow a collection reacting compartment that increases in number. For further details the reader is address to references [12]-[15]. What we want to remark here is this program is suitable to study also the influence of extrinsic stochasticity. In fact, reacting molecules can be distributed randomly among compartments at the starting time or between daughters at the division time ($\phi = \sqrt[3]{2}$), simulating how this source of randomness affects the system time behavior.

RESULTS AND DISCUSSION

Autopoietic vesicles in homeostatic regime

Autopoiesis, as developed by Maturana and Varela in the seventies [17], is a theoretical description of the 'blue print' of cellular life. It poses as a main feature the self-maintenance of the cell, as due to a process of components' self-generation from within the cellular boundary—a boundary which is itself

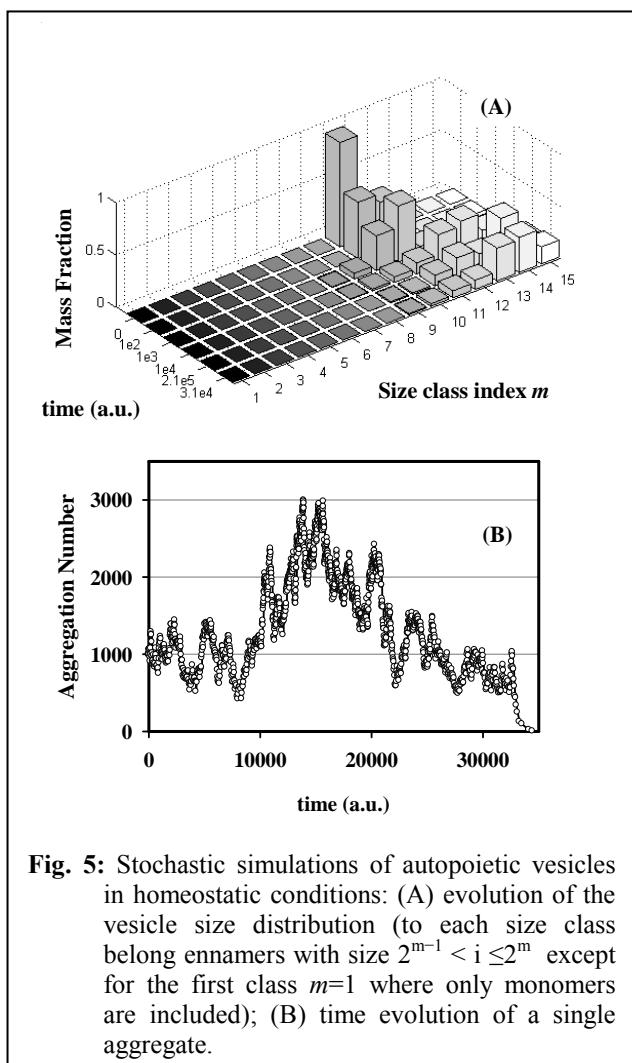


Fig. 5: Stochastic simulations of autopoietic vesicles in homeostatic conditions: (A) evolution of the vesicle size distribution (to each size class belong ennamers with size $2^{m-1} < i \leq 2^m$ except for the first class $m=1$ where only monomers are included); (B) time evolution of a single aggregate.

one of the products. From the chemical point of view, the fertility of autopoiesis theory allowed the design and the experimental achievement of some autopoietic chemical systems all based on surfactant self-assembling structures, such as micelles, reverse micelles and vesicles [18]. In Fig. 4, the schematic representation of an autopoietic vesicle is shown along with the kinetic conditions for experimentally observing different regimes in the time course of total surfactant concentration depending on the rates of amphiphiles production v_G and decay v_D respectively. These three scenarios have been really implemented and investigated by Zepik et al. [19]. In particular, the chemical system consists in a solution of oleic acid/oleate vesicles (S_i , i being the aggregation number), buffered at pH 8.8, fed with a surfactant precursor and with a reactant capable of destroying oleic acid. The surfactant precursor (P) is oleic anhydride, a hydrophobic substrate rapidly taken up by oleate vesicles at their membranous interface. Thanks to the high pH value, P is converted to oleate by alkaline hydrolysis that takes place on the membrane of vesicles. Oleate vesicles also undergo a decay process due to the simultaneous transformation of oleate molecules into 9, 10-dihydroxystearate (W) by osmium tetroxide/potassium ferrocyanide oxidation (Y). The dihydroxylated compound P does not form vesicles; therefore, the consequence of the latter conversion is a stepwise vesicle collapse (death). Due to the two competitive reactions, the overall oleate concentration increases, remains approximately constant, or decreases, depending on the magnitude of the P and Y flux rates [19]. In order to reproduce the experimental

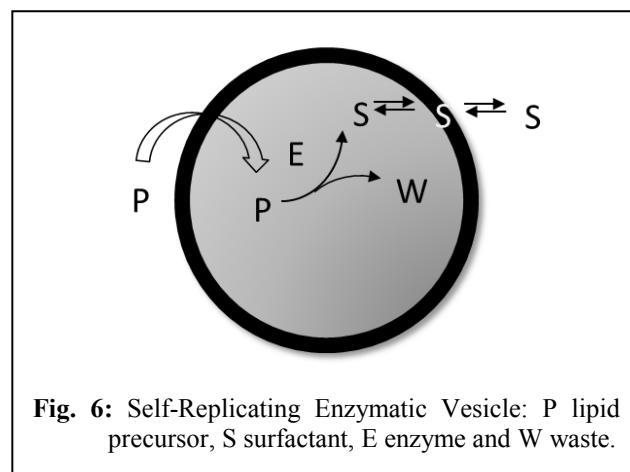


Fig. 6: Self-Replicating Enzymatic Vesicle: P lipid precursor, S surfactant, E enzyme and W waste.

observed behavior we proposed the simple mechanism reported on the right of Fig. 4 and we were able to obtain the time course of the overall oleic acid concentration [15]:

$$[S] = [S]_0 e^{(k_G[P]_0 - k_D[Y]_0)t} \quad (9)$$

This equation accounts for the three regimes by explicitly expressing the rates of amphiphiles production $v_G = k_G[P]_0$ and decay $v_D = k_D[Y]_0$, as a function of the aqueous concentration of the anhydride $[P]_0$ and of the oxidant $[Y]_0$ kept constant by the external fluxes. Stochastic simulations performed in homeostatic conditions ($k_G[P]_0 = k_D[Y]_0$) have been then done in order to elucidate the evolution of the vesicle size distribution.

Starting from a size monodispersed ennamers solution, what emerges from simulations is that stochasticity selects ennamers with aggregation numbers in the range 10^3 – 10^4 (Fig. 5A). This effect can be ascribed to the presence of random fluctuations in the growth and decay specific rates, which in real (chemical) reacting systems are due to the intrinsic stochasticity of reacting events but they can also be enlarged by natural changes of physical parameters such as temperature, molecular fluxes, etc. In fact, stochastic simulations starting from a single aggregate have shown how random fluctuations at the steady state can drive the evolution of the aggregate towards a growth or a decrease in size (Fig. 5B). Therefore, when autopoietic ennamers of different sizes are present in a system in stationary conditions, fluctuations can act as a selection rule that leads to the perpetuation of those aggregates large enough to overcome large deviations.

In conclusion, stochastic simulations have shown that, in this landscape, random and driven fluctuations can represent the driving force for ennamer evolution, growth or decay, and at the same time they can act as a selection rule for the fittest, i.e. the most robust, aggregates in a prebiotic environment.

Protocell stationary self-reproduction

In a recent work, a phenomenological law that predicts when a *stationary self-reproduction* takes place for minimal self-producing vesicles have been derived. By 'stationary self-reproduction' we mean a dynamic regime where the condition for division is reached at a constant, characteristic period of time, giving as a result two vesicles or *protocells* with the same (initial) size, lifetime and metabolite concentration profile as the progenitor.

In terms of the *growth control coefficient* the steady condition takes place when $\gamma=1$. Then, two general

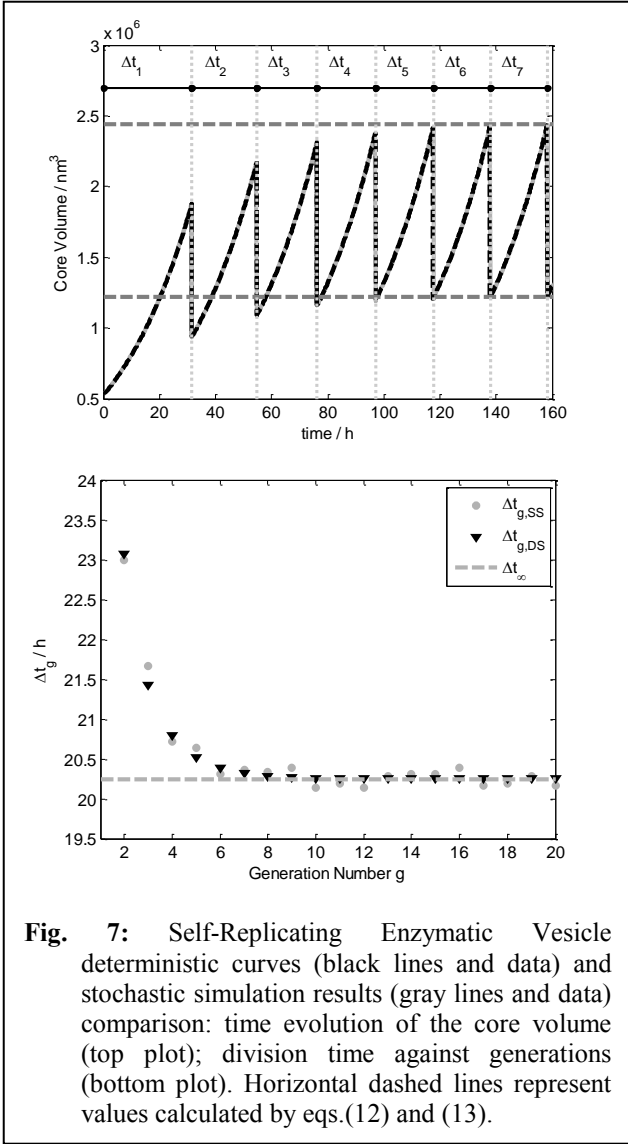


Fig. 7: Self-Replicating Enzymatic Vesicle deterministic curves (black lines and data) and stochastic simulation results (gray lines and data) comparison: time evolution of the core volume (top plot); division time against generations (bottom plot). Horizontal dashed lines represent values calculated by eqs.(12) and (13).

expressions for the temporal behavior of the protocell surface and the protocell core volume have been independently derived [11] and an explicit relationship among different molecular and kinetic parameters (e.g., reaction rates v_p , permeability coefficients ϕ_i , metabolite concentrations $[X_i]$) have been analytically derived for the protocell stationary reproduction:

$$\sum_{\rho}^{\text{Reactions}} \Delta m_{\rho} v_{\rho} + \frac{S_{\mu}}{V_C} \sum_i^{\text{Species}} \phi_i ([X_i]_{\text{Env}} - [X_i]) - v_L = \frac{C_C \alpha_L N_A V_C}{2} \frac{v_L}{S_{\mu}} \quad (10)$$

where v_L is the rate of lipid production, C_C is the total internal concentration and Δm_{ρ} is total variation of the number of molecules due to the ρ -th reaction:

$$\Delta m_{\rho} = \sum_i (p_{i,\rho} - r_{i,\rho}) \quad (11)$$

Eq.(10) shows the deterministic condition for a stationary reproduction regime that results from the *osmotic synchronization* between membrane and core volume growth, i.e.: a spontaneous ‘self-regulation’ driven by the osmotic balance across the protocell lipid bilayer. Eq.(10) links metabolic kinetic constants and membrane permeabilities with the external and internal concentrations of the system constituents. Therefore, it represents a constraint for the possible sizes and division periods of stationary self-reproducing protocells. We have applied the general eq. (10)

to the simplest case of a self-producing enzymatic vesicle (SPEV) represented in Fig. 6. SPEV is a hypothetical protocell model where the production of lipid S takes place through the chemical transformation of a precursor molecule P, assumed to occur only in the presence of an additional compound E encapsulated in the core volume. The S production generates also the waste W so that $\Delta m=1$ and the osmotic synchronization can in principle takes place. Moreover W is accumulated in the core volume since it is assumed not to be transported across the membrane, i.e. $\phi_W=0$. It is worthwhile to note that this model is very close to some experimental approaches based on giant vesicles that produce internally (with the help of a synthetic catalyst) the main membrane component and eventually undergo self-reproduction [20].

SPEV is not a real autopoietic vesicle since the catalytic specie E is not synthesized by the internal metabolism. Therefore after each vesicle division the number of E molecules will decrease until just one copy of these molecules will be present in the internal core. As a consequence, whenever a division occurs only one of the two daughter vesicles will be able to encapsulate the catalyst molecule and, therefore, will keep the potential to continue growing, producing S and, eventually, reproducing as a protocell. The vesicle that contains that single molecule E, by default, will be taken as the mother vesicle, whereas the daughter (and all possible granddaughters) will be ‘sterile’ vesicles. Thus, by handling eq. (10) it was possible to predict [11] for the mother SPEV, i.e. the vesicle containing only one E molecule, its stationary radius R_{∞} :

$$R_{\infty} = \frac{6}{\alpha_S N_A C_C} \quad (12)$$

and the division time Δt_{∞} :

$$\Delta t_{\infty} = \frac{2}{\alpha_S [P]_{\text{Ex}}} \left(\frac{\ln 2}{N_A \phi_P} + \frac{4\pi R_{\infty}^2}{k} \right) \quad (13)$$

where C_C is the overall internal osmolite concentration, $[P]_{\text{Ex}}$ and ϕ_X are the external concentration and the membrane permeability of the lipid precursor respectively, while k is the kinetic constant of the lipid production: $v_L = k[E][P] = k[P]/(N_A V_C)$.

Fig. 7 shows in the upper plot the core volume time trend for the first 7 generations, i.e. vesicle divisions, obtained both by ODES integration (black line) and by stochastic simulations (gray lines). Vertical gray dotted lines represent the time of division that takes place when the reduced surface satisfied the splitting conditions: $\phi = \sqrt[3]{2}$. Generation by generation the mother protocell tends to the stationary growth and division as illustrated by the upper plot where the core volume values before $2V_{\infty}$ end after the division $V_{\infty} = 4\pi R_{\infty}^3/3$ can be calculated with eq.(12). In the lower plot it is reported the division time Δt_g against the generation number, showing that generation by generation it tends to Δt_{∞} as predicted theoretically.

An important aspect to remark is that eq.(10), strictly speaking, only captures the condition for stationary reproduction in the sense of a global synchronization process between membrane and volume growth. In other words, it does not guarantee that when a vesicle reaches the division threshold the number of each internal constituent gets effectively doubled (with regard to their initial state in the

procell cycle). This becomes manifest in the case of SPEV, where the single enzyme/catalyst present in the mother is not doubled and, therefore cannot be transferred but to one of the offspring vesicles (i.e.: the only one that will remain fertile). Therefore, eq.(10) states a necessary but not sufficient condition for reliable reproduction of proto-cellular systems. In a more complex scenario, which will be introduced in the next section and where the metabolic reaction network included the synthesis of the enzymatic/catalytic compound, a more complete reproduction of the protocell could be achieved. But the synchronization among lipid production, enzyme duplication and membrane division would emerge in that system only if the new metabolic pathway(s) lead to effective internal chemical synthesis (i.e. $\Delta m > 0$), since the mechanism that drives the synchronization is the osmotic balance across the lipid bilayer. Moreover in this complex scenario also stochastic fluctuations can effect much more the time behavior of each single protocell and in particular the random distribution of enzymatic species between daughter vesicles.

A minimal cell model: the Ribocell

The so-called Ribocell (RNA-based cell) is a theoretical minimal cell model based on a self-replicating minimum RNA genome coupled with a self-reproducing lipid vesicle compartment that has been recently hypothesized [21]. This model suppose the existence of two ribozymes, one (the lipid synthase R_L) able to catalyse the conversion of molecular precursors (P) into lipids (S) and the second (the polymerase R_p) able to replicate RNA strands by a template driven elongation. Therefore, in an environment rich in both lipid precursors (P) and activated nucleotides (NTP), the Ribocell can self-reproduce if both processes, i.e. genome self-replication and membrane reproduction (growth and division), are somehow synchronized. Recently we have explored the feasibility of this hypothetical minimal cell [14] by determining the best external conditions to observe synchronization between genome self-replication and vesicle membrane reproduction, thanks to a deterministic kinetic analysis, while the Ribocell robustness to random fluctuations has been tested by stochastic simulations. The proposed metabolic mechanism is reported in Fig. 8. Both pairs of RNA strands reversibly associate (A) and these processes are shifted towards the dimer formation and are strongly dependent on temperature. The replication of any RNA strand is catalysed by the polymerase R_p according to the steps in bracket (B). This process is described as a catalytic template-directed addition of mononucleotides with high fidelity and processivity. It starts with R_p binding any of the monomeric template T ($T=R_p, {}_cR_p, R_L$ and ${}_cR_L$) to form the complex $R@T$. This complex will then initiate the polymerization of the conjugate strand ${}_cT$, by coupling and iteratively binding the complementary bases and releasing the by-product W. When the strand ${}_cT$ has been completely formed, the polymerase ribozyme releases the new dimer. Finally, the ribozyme R_L catalyzes the conversion of the precursor P into the lipid S (C). All the kinetic constants have been estimated by experimental values reported in literature and are listed in Table 1 along with references.

Thanks to a deterministic analysis [28][29], we showed that if the kinetic constant for lipid formation k_L is in the range: $1.7 \cdot 10^3 s^{-1} M^{-1} \leq k_L \leq 1.7 \cdot 10^5 s^{-1} M^{-1}$ then synchronization between vesicle reproduction and genome replication can

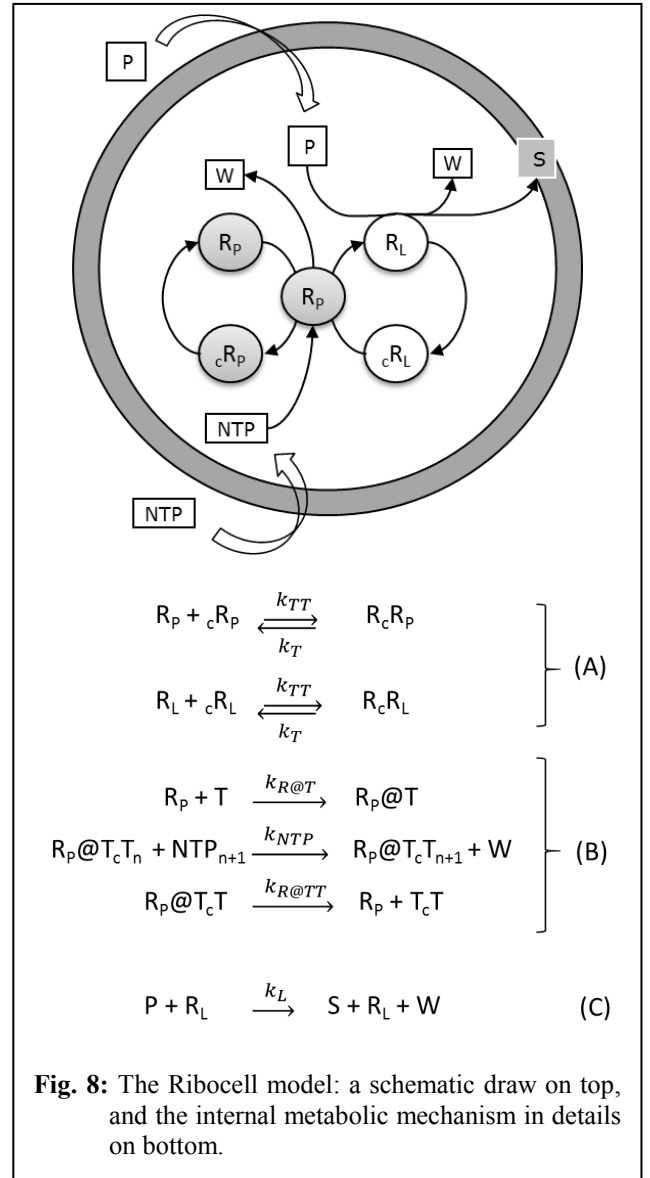


Fig. 8: The Ribocell model: a schematic draw on top, and the internal metabolic mechanism in details on bottom.

spontaneously emerge under the model assumptions and kinetic parameters reported in Table 1. Deterministic calculations were performed for two ribozymes 20 bases long and showed that the Ribocell reaches a stationary growth and division regime ($\gamma=1$), where the cell size remains constant after each division along with the amount of genetic material. Although the observed cell life time stabilizes after the first 10 generations, it remains very high, at over 80 days for all the k_L values in the synchronization range, making the Ribocell very hard to implement and study experimentally. Therefore, we investigated the robustness of the stationary growth and division regime of the Ribocell in terms of the external substrate concentrations, vesicle size and initial ribozyme amount in order to define optimal external conditions for Ribocell self-reproduction [14]. The influence of ribozyme length will also be explored in the optimal external conditions by ranging strand size from 20 to 200 bases in length and keeping all the other kinetic parameters constant. 20 bases is in fact the minimum length required to observe a folded RNA structures, i.e. a structure that can reasonably exhibit catalytic action. On the other hand, entities of about 200 nucleotides have been suggested as plausible ancient proto-ribosomes [30] even though, more recently, smaller subunits of 60 nucleotides have also been considered as plausible candidates [31]. This analysis shows that starting from external concentrations

Table 1: Kinetic Parameters for the in silico Ribocell model at room temperature.

Kinetic Parameters	Values	Ref.
$K_{TT}[s^{-1}M^{-1}]$	$8.8 \cdot 10^6$	[22]
$K_T[s^{-1}]$	$2.2 \cdot 10^{-6}$	[22]
$k_{R@T}[s^{-1}M^{-1}]$	$5.32 \cdot 10^5$	[23]
$k_{R@TT}[s^{-1}]$	$9.9 \cdot 10^{-3}$	[23]
$k_{NTP}[s^{-1}M^{-1}]$	0.113	[25][26]
$k_L[s^{-1}M^{-1}]$	$1.7 \cdot 10^3$	[24]
$k_{in}[dm^2s^{-1}]$	$7.6 \cdot 10^{19}$	[12]
$k_{out}[dm^2s^{-1}]$	$7.6 \cdot 10^{-2}$	[12]
$\phi_P[cm \cdot s^{-1}]$	$4.2 \cdot 10^{-9}$	
$\phi_{NTP}[cm \cdot s^{-1}]$	$1.9 \cdot 10^{-11}$	[25][26]
$\phi_w = \phi_T$	0.0	
$\phi_{aq}[cm \cdot s^{-1}]$	$1.0 \cdot 10^{-3}$	[27]

* k_L is 10^5 times larger than the value of the splicing reaction, catalyzed by the hammerhead ribozyme.

$[NTP]_{Ex}=[P]_{Ex}=10^{-2}M$ at the stationary regime the Ribocell radius is 113.0 nm and the division time reduces to 68.2 days. The total number of RNA strands is 258 and the genome composition is quite uniform 25.2% (R_L), 25.2% (cR_L) 25.6% (R_P), 24.0% (cR_P). The stationary division regime can be reached starting from initial genome composition ranging from 1 to 100 dimers of R_cR_L and R_cR_P . In Fig. 9, the deterministic time behavior of the Ribocell in optimal external conditions is reported.

Finally, the dependence of Δt_{25} (division time after 25 generations) on the kinetic constants for RNA dimer formation k_{TT} and dissociation k_T has been also studied. What emerged is the Ribocell life cycle at stationary regimes does not depend explicitly on the kinetic constant single values k_{SS} and k_S but on their ratio: k_{SS}/k_S , that is on the thermodynamic constant of RNA dimerization. The more thermodynamically stable the RNA dimers, the longer it takes to observe Ribocell self-reproduction. For instance, if k_{SS}/k_S is decreased by two orders of magnitude, the Ribocell life time reduces from 68.2 days to 11.8-6.4 days.

Stochastic simulations have been then performed in order to test the robustness of the ribocell base on 100-base length ribozymes in optimal external conditions, with the aim of elucidating the role of intrinsic and extrinsic stochasticity on the time behavior of a protocell population. Simulations were executed by means of the parallel version of ENVIRONMENT [12], running 32 statistically equivalent simulations of a 10-ribocell solution on different CPUs. Therefore, the outcomes were obtained as averages from a population of 320 vesicles. Kinetic parameters used for simulations are those reported in Table 1. At each cell division, only one of the two offspring was kept while the other was discarded in order to reduce computation time, thus keeping the number of monitored vesicles constant. This is in agreement with the assumption that the external concentrations of all substrates are fixed due to an incoming flux of material, i.e. the substrates cannot ever be exhausted. The simulation outcomes are reported on the left of Fig. 10 where the composition of the Ribocell population is reported against time. In fact, during simulations at each division the genetic material is randomly distributed between the daughters. If the amount of genetic material is very low, then this can result in a separation of R_P from the other RNA

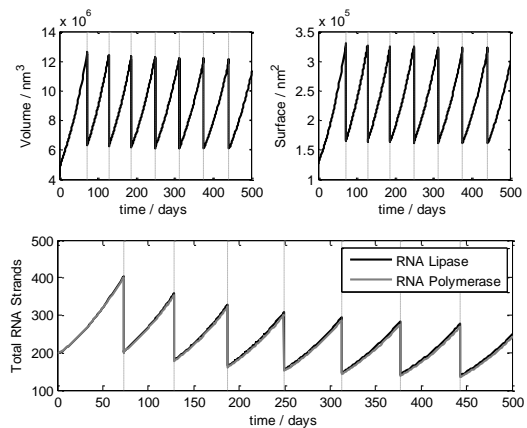


Fig. 9: Deterministic time behavior of the Ribocell in optimal external conditions: $[NTP]_{Ex}=[P]_{Ex}=0.01M$. At the starting time the genome was composed by 100 dimers of R_cR_L and R_cR_P and the radius was 100nm and the core volume $4.2 \times 10^6 nm^3$.

strands. In fact, the Ribocell must contain a minimum genetic kit of three RNA filaments in order to be capable of self-replicating its entire genome: one R_P that catalyzes the RNA base pair transcription, one (R_L or cR_L) and one (R_P or cR_P) that work as templates for the transcription. Moreover, since R_L is necessary to catalyze lipid precursor conversion, the optimal minimum 3-ribozyme kit must be made up of $2R_P$ and one R_L . This minimum kit should be at least doubled before cell division, in order to have a chance that both daughters continue to be active. Therefore, if a random distribution of RNA filaments takes place after vesicle division, ribozyme segregation between the two daughters might occur. Different scenarios can be envisaged: *death by segregation* is reached if vesicles are produced without any ribozymes (*empty vesicles*) or containing one lone R_P or many filaments of cR_P and/or cR_L (*inert vesicles*). Vesicles that encapsulate R_L strands are *self-producing*: they are able to synthesize lipids and then can grow and divide producing in turn self-producing and/or empty vesicles. On the other hand, vesicles containing more than one molecule of R_P or both R_P and cR_P filaments are able to self-replicate this reduced genome (*self-replicating genome vesicles*) but they cannot self-reproduce the membrane. So they are destined for an osmotic burst due to an unbalanced increase in waste concentration. Finally, a reduced version of the Ribocell consists in a lipid aggregate that contains one R_P filament and R_L/cR_L strands. As a consequence of this, *reduced ribocells* are able to replicate the R_L/cR_L genetic stuff, and at the same time to synthesize lipids. Therefore, they can grow and divide, producing in turn at least one reduced ribocell and/or self-replicating, inert and empty vesicle.

On the left of Fig. 10 a schematic draw of the different types of protocells is reported. At the end of the simulation, the composition of the protocell population are obtained with low percentages of real ribocells (6.7%) while the most populated fractions are those of empty (40.0%) self-producing (33.3%) and broken (20.0%) vesicles, respectively. Reduced ribocells are present only in the first generations since they very soon decay into self-producing and empty vesicles. Inert vesicles, i.e. vesicles entrapping free chains of cRP and/or cRL or a single RP , are not formed and this can be ascribed to the high stability of RNA dimers and complexes so that the chance of finding free RNA monomers at the time of vesicle division is extremely improbable. Indeed, the stochastic time

trend presents a very irregular time behaviour compared to the deterministic one that describes a highly synchronized oscillating regime of growth and division. In contrast, stochastic simulations highlight the alternation of dormant phases, where the reduced surface remains practically constant, both the core volume and the membrane surface being constant (data not shown), to very active steps where protocell growth takes place very fast, leading to a division event. The fast growth and division step corresponds to the presence in the vesicle core of a free R_L chain while, in the dormant phase, ribozymes are all coupled in the form of dimers or complexes. As a consequence, self-producing vesicles with a genome made up only of R_L monomers can reproduce very efficiently since no dormant phase can occur, given that the formation of R_cR_L dimers is impossible. This protocells could then self-produce very efficiently, with a Δt less than one day.

In conclusion, the simulation outcomes show that ribocells are not enough robust to survive to random fluctuations. In fact only about the 5-7% of the initial population survive as genuine ribocells after 15-25 generations and on a longer time window they are destined for extinction. Furthermore, the time course of each single protocell is also greatly influenced by intrinsic stochasticity in particular by the time fluctuations of the RNA dimer dissociation. In fact, when all the RNA strands are associated in dimers, protocells remain in a lazy phase, whereas free R_L monomers induce fast growth and division steps and free R_p cause the fast RNA replication without changing the vesicle size appreciably. Therefore these two processes are synchronized only by chance and this also represents a reason of weakness of this model protocell. Further details can be found in papers [14], [28] and [29]

CONCLUSIONS

In this short article we have shown some aspects of

theoretical modelling in micro-compartmentalized systems, and in particular in the research on self-reproducing protocells. The occurrence of compartmentalized synthetic reactions coupled with the membrane dynamics in terms of growth and division plays a major role in determining the evolution of the system. In particular, we have firstly compared the deterministic and stochastic approach for modelling such systems, and applied these methodologies to describe (1) homeostatic autopoietic systems, (2) the stationary conditions for protocell self-reproduction, and (3) the more complex case of the “ribocell”, i.e., a protocell based on catalytic function encoded in self-reproducing ribozymes (RNA enzymes).

Here we would like to emphasize the common aspects of analysis and modeling of these (and other) systems, namely the need of a systemic approach that integrates (and couple) the internal reactions, the membrane dynamics, and the environment. This is perhaps the most important scientific message that emerges from numerical simulations of these complex systems. Since numerical modeling is carried out by using true physical constants for all elementary molecular steps, it follows that genuine outcomes from modeling might actually help the experimentalists to design and construct protocell models or artificial cells for nanotechnological applications. Moreover, flanking stochastic modeling to deterministic approaches uniquely reveals intriguing dynamics in microcompartmentalized complex multimolecular systems and greatly helps to evaluate and understand basic mechanisms at the roots of biological behaviour.

ACKNOWLEDGMENT

We are very grateful to Kepa Ruiz-Mirazo for his collaboration in the past years.

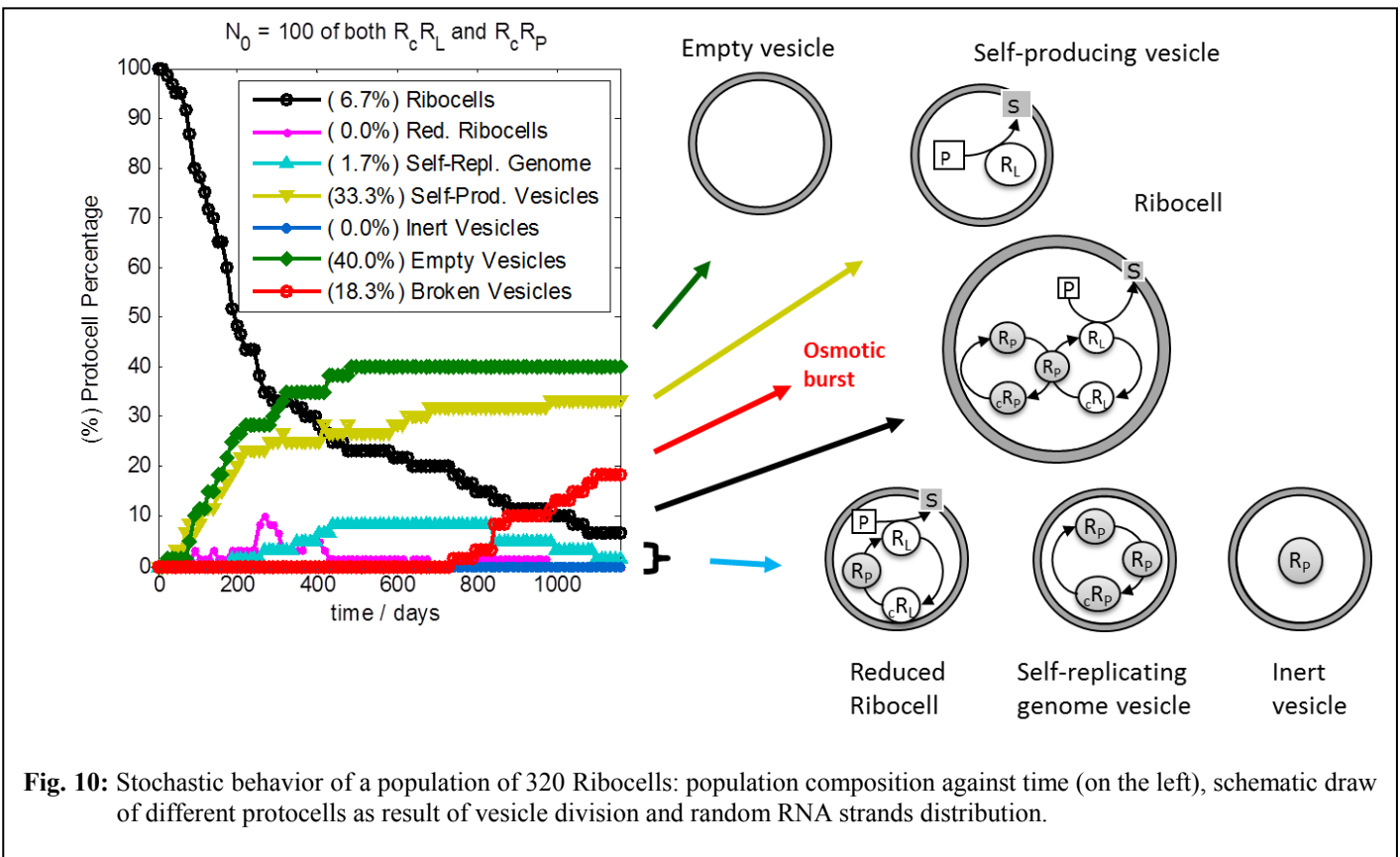


Fig. 10: Stochastic behavior of a population of 320 Ribocells: population composition against time (on the left), schematic draw of different protocells as result of vesicle division and random RNA strands distribution.

REFERENCES

- [1] Walde, P. (ed.) 2005 *Prebiotic Chemistry from Simple Amphiphiles to Model protocells. Topics in Current Chemistry*. Berlin:Springer.
- [2] Chen, I. and Walde, P. (2010) From Self-Assembled Vesicles to Protocells. *Cold Spring Harb Perspect Biol* 2, a002170
- [3] Luisi, P.L., Ferri, F. & Stano, P. 2006 Approaches to semi-synthetic minimal cells a review. *Naturwissenschaften* 93, 1-13.
- [4] Luisi, P.L. and Stano, P. (2011) *The minimal cell. The biophysics of cell compartment and the origin of cell functionality*. Berlin: Springer.
- [5] Noireaux, V. Maeda, Y.T. Libchaber A. (2011) Development of an artificial cell, from self-organization to computation and self-reproduction. *PNAS* 108, 3473
- [6] Solé RV, Munteanu A, Rodriguez-Caso C and Macía J (2007) Synthetic protocell biology from reproduction to computation *Phil. Trans. R. Soc. B* 362, 1727-39.
- [7] Stano, P.; Carrara, P.; Kuruma, Y.; Souza, T.; Luisi, P. L. (2011) Compartmentalized reactions as a case of soft-matter biotechnology: Synthesis of proteins and nucleic acids inside lipid vesicles. *J. Mat. Chem.* 21, 18887-902.
- [8] Mavelli F. and Piotto S. (2006) Stochastic simulations of homogeneous chemically reacting systems. *J. Mol. Struct* 771, 55-64.
- [9] Mavelli F. and Ruiz-Mirazo K. (2007) Stochastic simulations of minimal self-reproducing cellular systems, *Phil. Trans. R. Soc. B* 362, 1789-802.
- [10] Stano, P., Wehrli, E. & Luisi P.L. 2006 Insights into the self-reproduction of oleate vesicles. *J. Phys: Condens. Matter* 18, 2231-2238.
- [11] Mavelli F. and Ruiz-Mirazo K. (2013) Theoretical conditions for the stationary reproduction of model protocells. *Int. Biol.* 5 324-341.
- [12] Mavelli F. and Ruiz-Mirazo K. (2011) ENVIRONMENT: a computational platform to stochastically simulate reacting and self-reproducing lipid compartments, *Phys. Biol.* 7, 036002.
- [13] Ruiz-Mirazo K. and Mavelli F. (2008) On the way towards 'basic autonomous agents' stochastic simulations of minimal lipid-peptide cells. *BioSystems* 91, 374-87.
- [14] Mavelli F. (2012) Stochastic simulations of minimal cells: the Ribocell model. *BMC Bioinformatics* 13(4), S10.
- [15] Mavelli F. and Stano P. (2010) Kinetic models for autopoietic chemical systems role of fluctuations in homeostatic regime, *Phys Biol* 7, 016010.
- [16] Gillespie DT (2007) Stochastic simulation of chemical kinetics. *Annu Rev Phys Chem*, 58, 35-55.
- [17] Varela F J, Maturana H R and Uribe R (1974) Autopoiesis: the organization of living systems, its characterization and a model. *Biosystems* 5, 187-96.
- [18] Luisi P. L. and Varela F. J. (1990) Self-replicating micelles. A chemical version of minimal autopoietic systems, *Orig. Life Evol. Biosph.* 19, 633-43
- [19] Zepik HH, Blöchliger E and Luisi P L 2001 A chemical model of homeostasis. *Angew. Chem., Int. Ed. Engl.* 40, 199-202.
- [20] Takakura, K., Toyota, T. & Sugawara T. (2003) A Novel System of Self-Reproducing Giant Vesicles. *JACS* 125, 8134-8140
- [21] Szostak J.W., Bartel D.P. and Luisi P.L., (2001) Synthesizing life. *Nature* 409, 387-90.
- [22] Christensen U, (2007) Thermodynamic and kinetic characterization of duplex formation between 2'-O, 4'-C-Methylene-modified oligoribonucleotides, DNA and RNA. *Bioscience Reports*, 27:327-333
- [23] Tsoi PY, Yang M, (2002) Kinetic study of various binding modes between human DNA polymerase α and different DNA substrates by surface-plasmon-resonance biosensor. *Biochem. J.* 361: 317-325.
- [24] Stage-Zimmermann T.K., Uhlenbeck O.C., (1998) Hammerhead ribozyme kinetics. *RNA*, 4: 875
- [25] De Frenza A., (2009) Internal Technical Report, Chemistry Department University of Bari.
- [26] Mansy S.S., Schrum J.P., Krishnamurthy M., Tobé S., Treco D.A., Szostak J.W., (2008) Template-directed synthesis of a genetic polymer in a model protocell. *Nature*, 454: 122-U10.
- [27] Sacerdote M.G., Szostak J.W. (2005) Semipermeable lipid bilayers exhibit diastereoselectivity favoring ribose. *PNAS* 102, 6004-6008.
- [28] Mavelli F., Della Gatta P., Cassidei G., Luisi P.L. (2010) Could the Ribocell be a Feasible Proto-cell Model? *OLEB* 40, 459-464.
- [29] Mavelli F., (2011) Theoretical Approaches to Ribocell Modeling. In: *Minimal Cell*. Luisi P.L. and Stano P. (eds.), Dordrecht, Springer, 255-273.
- [30] Smith T.F., Lee J.C., Gutell R.R., Hartman H. (2008) The origin and evolution of the ribosome. *Biol. Direct.* 3, 16-24.
- [31] Agmon I. (2009) The Dimeric Proto-Ribosome: Structural Details and Possible Implications on the Origin of Life. *Int. J. Mol. Sci.* 10, 2921-2934.

ACCELERATION OF ENERGY DISSIPATION BY BIOLOGICAL SYSTEMS

Adam Moroz, Seng Chong

De Montfort University, Leicester, UK

ABSTRACT

A general scheme of evolution from autocatalytic processes to socio-technological system is discussed from the perspective of maximum energy dissipation principle. The scheme treats the emergence of biological systems as an initial stage in the acceleration of global free energy dissipation. The sequential emergence of qualitatively new levels of organisation (biological cell, multicellular organism, social system) has been proposed, the levels are suggested as the results of cooperation (symbiosis) of the dissipative systems at the previous levels. The cooperation/symbiosis provides sufficient complexity for development of the next, essentially a new level of energy dissipation, leading to a new form of free energy utilization and a new form of information mapping. From a thermodynamic perspective, every qualitatively new level of biological organisation provides an additional step to increase the rate of energy dissipation from qualitatively new sources, essentially widening the number of these sources involved in the utilization.

INTRODUCTION

The maximum energy dissipation (MED) principle, together with related maximum entropy production principle [1-4], has been discussed in various fields [3-10]. The maximum energy dissipation principle has been shown to be a good basis for consideration of kinetic non-linearities (cooperativity, autocatalytic growth) in chemical and biochemical reactions and variational description of dissipative processes [11-15]. As it has been considered in these works, the nonlinearities in processes of energy dissipation are naturally incorporated into the MED principle. This principle can be treated as the general case of the least action (LA) principle, has also the evolutionary implications [15]. On this ground it is reasonable to suggest that the MED and the LA principles are different forms of a principle of least instability, where the free energy can be treated as a quantitative measure of instability.

One can see that in such a way, as illustrated in Figure 1, chemical nonlinear and biological pathways utilise free energy more effectively, so the emergence of the nonlinear pathways satisfy the maximum energy dissipation/least action principle. Evolutionary, in a very complex system, having a planetary scale, when the richness of molecular primordial organic soup (diversity of molecular substances) allows, such nonlinear processes can take place. Therefore the overall “dissipative” action (dissipated free energy multiplied by time) is smaller comparably to the linear physical dissipative processes or linear chemical dissipative processes (Figure 1). Then in such interpretation, biological processes are the most effective in sense of the least action (dotted line, Figure 1).

In this work we will discuss some evolutionary and organisational implication of the maximum energy dissipation principle.

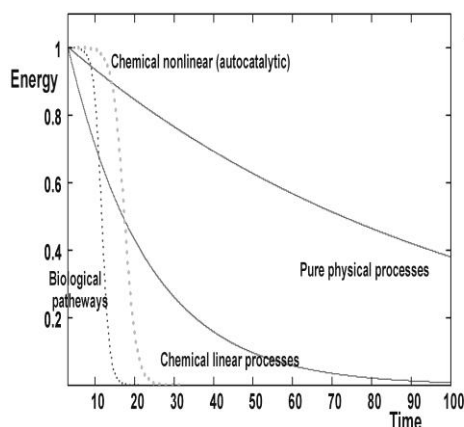


Figure 1. Schematic presentation of the linear and nonlinear dissipative pathways in free energy dissipation. Adopted from [11].

MOLECULAR, PREBIOTIC AND PURE BIOTICAL ORGANISATIONAL-EVOLUTIONAL LEVELS OF BIOLOGICAL DISSIPATIVE PATHWAYS

Considering the molecular level of organisation of biotical processes, it is also reasonable to link them evolutionary to the stage known as molecular evolution. Interpreting molecular organisation in such a way, we have to note that there are two approaches to molecular evolution, in some sense alternative. In a number of works, Russell and coauthors [16] have described an approach when a network of chemical reactions, located and created by a complex environment on the surface of prebiotic Earth, was able to develop a level of complexity, sufficient to generate prebiotic molecular life. Such a molecular network was located nearby the surface and was not separated from the environment [16]. Alternative concept - the Eigen theory of molecular evolution [17-18] is based on known autocatalytic properties of organic polymers (proto-

RNA and proto-enzymes). These, in the catalytic sense, are two opposite approaches, which might be combined in the way when at the first, initial stage, the catalytic role of surface prevails to develop a variety of organic substances and later these substances can independently support a hypercyclic network and evolve into proto-cell in a sort of symbiosis with the coacervates. One should note that a biochemical network [19] is a coupled network [20], as of any self-reproductive biological cycle. Particularly in an autocatalytic molecular network, free energy utilization is necessary for synthesis and can be proportional to the rate constants of replication of molecular subspecies involved in such an autocatalytic dissipative processes. The growth of molecular autocatalytic networks is accompanied by utilization of energy rich molecules [17-19] and, therefore, is dissipative. Later in evolution, cellular living organisms, once emerged, had consumed/utilised all resources of free energy reach primordial organic soup, and had developed a spectrum of heterotrophs (mono- and multi-cellular ones) which successfully terminate this soup and everything which was organic which was unprotected and less competitive [21-26].

Evolution of unicellular biological systems went through a number of stages. According to the Margulis endo-symbiosis theory (see, for example, [27]), a proto-eukaryotic cell at certain stage has integrated a chloroplastic cell and proto-mitochondrion. Mitochondrion is known as a semi-autonomic subcellular organelle with its own two-strand cyclic DNA, indicating the bacterial origin and similar to bacterial mechanism of transcription/translation.

Based on the assumption that cooperation of the same level biosystems, as sort “dissipative autonomic agents” of similar level of organisation (cellular systems) can provide additional adoptivity for the species and opportunity to develop a new dissipative degrees of freedom, necessary for surviving, an evolutionary transition from the single cell organisation to the social pinnacle can be built as in [15].

Then the overall scheme can be expected as a series of levels with a superordination, superinclusion and coevolution. The qualitative evolutionary transitions, as are seen from this scheme, can be characterized by the following qualitative transitions [15]:

- +compartmentalisation of macromolecules with hypercyclically-like auto-catalytic properties which evolved into a proto-cell developing a number of catalytic and informational molecular processes;

- +forming a symbiosis of some proto-eukaryotic cells and their subsequent evolution into proto-multicellular organism;

- +formation of social super-organisms by some biological species;

- +emergence in the framework of social systems, a symbiotic relationship within some nonbiotic things that essentially extends functional and adaptive abilities.

The organisational structure, related to the evolution of the free energy consumption/dissipation by biological processes can be schematically represented by modifying so-called trophic pyramid illustrating the organisational hierarchy of biological systems (Figure 2).

Molecular autocatalytic networks can be considered as a first stage, an initial level of organisation of dissipative processes (Figure 2). However, just those molecular subspecies survived (and gave the life for a protocell) which were capable to develop a protection from environment coacervate-like encapsulation – membrane and cellular wall. So the second stage, second level can be linked to the organisation forming a prokaryotic-like cell (Figure 2).

The third level in the scheme (Figure 2), is introduced as a whole spectrum of eukaryotic cells, more precisely, spectrum of unicellular species. Evolutionary just a certain part of these species (designated as “cellular species capable to form multicellular organisation”) were able to form a multicellular form of organisation. Not all unicellular species had the capability to develop the next level of biological organisation by cooperation. One can note that the multicellular organism has been developed as a result of a long evolutionary process.

The fourth level can be represented as a level of multicellular organisation, where the cells are forming an organism characterised by the integration and specialization of the activity of all cells. This resulting integral activity cannot be considered in terms of a single cell. Even for prokaryotic cells, the cooperation between cells is widely observed [28]. Modern multicellular organisms represent the biosystems evolved throughout millions years. These organisms formed a different from the cellular metabolism, regulation, cognition and can be considered as next level in Figure 2. This organisational level can be represented by a number of multicellular species, which have developed an essentially new degree of freedom of competition as, for example, the locomotions (running, swimming, jumping, flying). The ability to move fast provided multicellular organisms with an important method to find food, to escape danger, to develop also the new integrative for this level informational cognition – eye-seeing, hearing, brain.

The fifth level can be considered as a level of those multicellular systems which were capable of forming so-called superorganisms – sometimes also referred to as communities or families of individuals. Such a known species as ants, bees, termites can be good examples of social species [29-30], organised in colonies, superorganisms. This kind of biological organisation can be characterised by the mode when the needs of superorganism/colony have a priority comparably to the individual needs. Such a sort of organisation provided an adaptive and competitive advantages for these species. Their social organisation is characterised by partial usage in their activity of things of non-biotal origin, which extends functional abilities of individuals and adaptation of the superorganism.

However, from the spectrum of social species just *Homo sapience* (HS) was capable to “spin-off” the non-biotic origin means of production to the stage that they achieved self-reproductive-like properties. In biological terms, HS was able to form symbiotic-like relations by means of production, see also next sections. This provided to the HS social system tremendous opportunity to explore a wide number of free energy sources not accessible or fragmentary accessed by other species. The sixth level can be considered as the level of social organisation widely exploring technology.

Following proposed scheme, the bioevolution is a result of the demand of maximal free energy dissipation: the emergence of every qualitatively new level of bio-organisation is due to capability to acceleration of dissipation of essentially new qualitatively sources of free energy.

The scheme in Figure 2 incorporates the minimal evolutionary mechanism: throughout the cooperation of (in cybernetic terms) dissipative autonomic agents to the formation of essentially new form of organisation, which allows utilization of new free energy from formerly inaccessible free energy sources; which can be seen at every evolutionary change on every level of hierarchy - cellular, organismic and social.

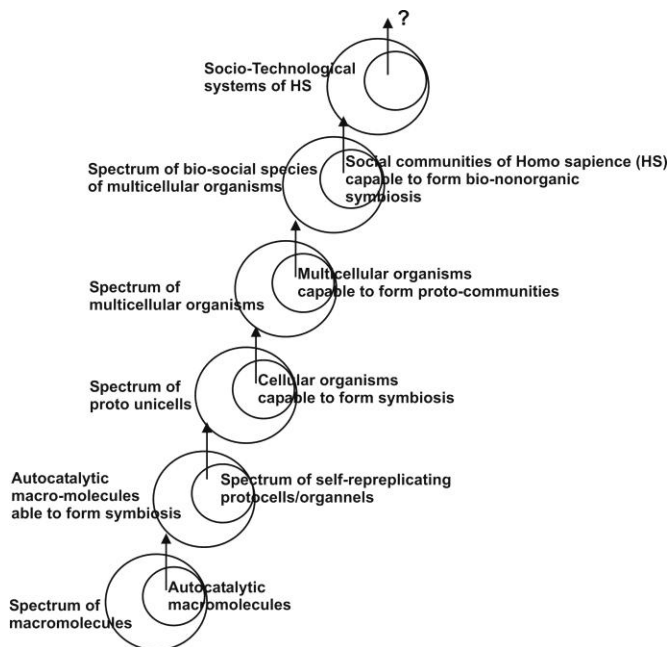


Figure 2 Evolutional ladder of dissipative systems. Schematic levelled representation of the organisation and evolution of dissipative cycles: from molecular Hypercycle to technological Supercycle (adapted from [15]). The role of symbiosis/cooperation during qualitative transitions in the trophic pyramid of dissipative systems, including bio- and biosocial-systems. The ability to utilise essentially new forms of free energy is related to the transition to the next step of the cooperative interaction of the biological systems at every level. The main outcome of symbiotic interaction is the formation of a qualitatively new type of integration and differentiation of the functions in the formed cooperative system, and also the formation of a qualitatively new form of the information mapping and a qualitatively new way of dissipative transformation of free energy.

An important note is that the cooperation between the autonomic dissipative agent of any bio-level provides not just better ability in competition, but also a potential to develop a qualitatively new level of organisation, qualitatively new level free energy consumption (dissipation) and qualitatively new level of information processes (cognitive), supporting dissipation.

From a thermodynamic perspective, bioevolution is a dissipative coupled process accelerating overall utilization/dissipation of free energy. From this perspective the reasons of emergence of biotical dissipative pathways - biological systems are purely physical - so physics and MED principle demand emergence and evolution of biosystems. Biosystems cooperate for the increase of adaptivity and from the thermodynamic perspective it helps to develop consumption of different sources of free energy, not accessible from the previous level of organisation. The utilization of new energy sources initiates a divergent phase in the development of species.

Thus, biological phenomena are the extreme phenomena in the sense of energy dissipation, they utilize free energy from sources where somehow usual physical mechanisms do not work or work insufficiently fast. Since the maximum energy dissipation principle demands fastest possible dissipation, biological and socio-technological phenomena satisfy this demand, and their emergence and existence are consistent with MED/LA principles and whole physics.

Previously [15] it has been concluded that each qualitatively new level of biological organisation becomes possible due to the cooperation/symbiosis of structures of the previous level, further specialization and integration of these structures within the framework of the association emerged, which developed essentially new form of substance-and free energy utilization and essentially new form of information cognition.

However, it can be seen that every level of biological organisation has its own limitations. These limitations are set up by nature and the scale of free energy utilization and material consumption as well as in the nature informational support of metabolism, which characterizes the particular level [15].

The level of pre-biotical processes (which has vanished in early stages of evolution and in modern biotical world can be thought as molecular network level) was limited to utilization of free energy-rich chemical substances available in a primordial organic soup. The metabolic processes obviously were limited by utilization of the limited range of energy rich molecular substances.

Emerged from autocatalytic networks/cycles the unicellular organisms in a long evolution accompanied by few symbiotic events explored a wider number of free energy sources. However, the unicellular level of biological organisation is limited in scale and nature of energy sources utilizing [26].

One can also see that the biomass, in fact free energy in a biotic material form, produced by multicellular biological systems, has the scale of billions tones, but still is limited and has a order much less than 1% of solar radiation in energy equivalent. Therefore, one can conclude that all biological levels and as we will illustrate below, the socio-technological processes, are limited in the scale of free energy consumption [15].

ACCELERATING DISSIPATION BY SOCIO-TECHNOLOGICAL CYCLE

Above, the hypothetical scheme, Figure 2, of the emergence of biological systems, their organisation and evolution as the dissipative systems, based on MED principle has been discussed, following [15]. The result of their evolution is the sort of organisational ladder from biopolymer macromolecules through their networks and cellular and multicellular organisms to the top level - social superorganisms. The key points of these formations are the cooperation between the system of same level to constitute initially nonintegrated associations and later to develop and evolve to a new level of systems, with essentially/qualitatively new levels of free energy processing and informational mapping.

Such a sort of cooperation (e.g. social form of cooperation, social symbiosis) widens the adaptivity of such a community (local population), increases the territorial competitiveness for food, and such a community has improved chances to survive. This trophic aspect can be interpreted in the thermodynamic sense, because biomass is a type of free energy and its consumption therefore is a dissipative process. Thus, from a thermodynamic perspective biological species are just specific dissipative processes (generalized biological flows) that overshoot, overtake, develop and compete with each other for free energy resources. In that sense the considerations from the maximum energy dissipation can be applied [15].

At the top level of these organisational developments, the cooperation produces the social level of organisation, known for a part of HS for several other species. Classical examples are superorganisms - formed by ants, bees, termites. However a long organisational distance divides them from humans. Would be it possible to explain this distance from the perspective of energy dissipation and the main mechanism of developing such a new level of organisation – cooperation or, biologically speaking, – symbiosis?

Let us note the important observable difference: the cooperation between the biosystems at the same level of biological organisation (macromolecules/networks, cells, individuals) always was carried out within the systems of biological nature exclusively. The observation of the humans' cooperation can be considered as the cooperation between biological individuals (humans) and the tools/means of production, having *non-biological* nature [15]. This in fact can be pointed out as the key difference between the social system, formed by HS and all others pure biotical social systems: one can say that humans invented technology.

Starting from a simple use of primitive tools, humans developed very complicated technological processes, which, one can see, indicate the self replicating-like properties. This helped humans (in the framework of developed new form of superorganism –society with technology) in thermodynamic terms to extend the overall process of energy dissipation to a very wide number of non-biological sources of free energy.

From the perspective of dissipation, only socio-technological system has jumped from the utilization of only biotical free energy sources, characteristic for bio-systems, as well as for known social species, known in the biological world. Only HS socio-technological system expanded usage free energy to qualitatively new sources and developed an essentially new level of organisation of free energy processing pathways. This utilization of free energy obtained a global character. Also, the essentially new form of informational support/cognition has been evolved in the process of evolution of the HS free energy processing and the development of the means of production accelerating pathway. These new pathways nowadays are dominating in energy consumption (dissipation) by the HS socio-technological system, Figure 6.

The self-reproductive-like, symbiotic interaction starts as pre-historical usage by HS individuals of the non-biotical origin tools which were able to develop more and more complex and useful ones. Throughout thousand years these tools have been successfully modified. One can see that from a self-organisational perspective, a minimal scheme of this evolutionary mechanism can be similar as for cells, which cooperate into a cell colony and evolve into a multicellular organism, [15].

As a result of such a “bio-nonbio” symbiosis, both components- biotical (biomass, the overall population of HS) and non-biotical (the means of production) grow tremendously. One can note that for the growth of biotical component a few critical stages observed. They can be linked to few key developments in exploration of new resources or the development of non-biotical “means of production” component (see, for example [15]). The first can be related to agricultural phase and another one in linked to technological phase.

The nonlinear growth of the nonbiotic component (means of production), having self-reproductive-like properties in biological terms, is rather characteristic of the industrial age; its self-reproductive-like growth is discussed in [15]. The main indices/parameters of technological, non-biological components also indicate the exponential growth (see the

statistical data from US Census [37] or data from the Angus Maddison's site and works [38-40]), which is similar to self-reproductive growth kinetics of biological systems [15]. One can conclude that this sort of growth supports the suggestion of indirect self-reproductivity. This sort of growth especially is characteristic for different types of energy produced in different economies. The various economic data indicate exponential growth for many indices. This proves the acceleration of the energy usage and dissipation by the socio-technological system, which can be illustrated as additional impact into global energy dissipation rate, Figure 4.

So, one can also note, as in [15], that every level in the trophic pyramid organisation, Figure 2, can be characterized by the limitations in the value of involved and consumed free energy. Single cell and multicellular organism are limited by quantitative and qualitative variety of free energy utilised. The socio-technological system is as well limited in the utilization of free energy.

Thus, one can see also the energy utilization limitations both - in purely biotical and bio-socio-technological parts of the global trophic pyramid (Figure 3). As a summary, in biological trophic (dissipative) pyramid one can observe several qualitatively essentially different levels of organisation of structural-energy dissipative transformation of the free energy flow from different sources (see also [15]):

- +level of pure physical dissipative processes
- +level of prebiotic, molecular evolution processes,
- +level of purely biological processes with unicellular organisation,
- +level of organismic organisation or multicellular organisms,
- +level of social species organisation evolving to socio-technological system of HS.

These levels are also limited in their information mapping/cognition of the environment and information, necessary for self-replication in a wide sense.

ON POSSIBLE POST-SOCIAL STAGES OF DISSIPATIVE SYSTEMS EVOLUTION

The scheme in Figure 4 and related considerations imply that the development of hierarchy of biological global dissipative processes expands toward the exploration of new resources of free energy, employing the cooperation and further specialisation and integration of processes at every level. As the result, the essentially new levels of processing of structural-and-material forms of free energy and the essentially new levels of information processing are formed and evolved, which make the hierarchy of biological processes completed and then the essentially new technological level emerged. Then, it is reasonable to suggest from observed biological and socio-technological parts of global free energy dissipative pyramid, that a next level of cooperation between technological systems has to be considered. As a possible result of forming such a new level of energy processing/dissipation and evolution, as one can suggest, can be a space/cosmic organisation of human-like socio-technological systems, which is continuing forming their technological activities at solar system toward to an unseeable scale. Then the human socio-technology can be considered as an elementary subsystem in an organized super technological system, similar to a single cell in a multicellular organism or an individual organism in the biotical societies.

SOME GENERALISATIONS

Presented above scheme of evolution of organisation of biological systems is based on the suggestion that driving force of the chemical, probiotic, biological and socio-technological evolution is the maximum energy dissipation principle, which can be treated as a partial case of the least action principle.

We expect that an evolutionary role for this fundamental principle for all physics: maximum energy dissipation/least action principle can be considered as an evolutionary principle, stating that those dissipative processes win in evolutionary competition, which could provide the highest possible rate of free energy dissipation. Kinetically, the maximum energy dissipation principle is a principle that employs nonlinearities.

Indeed, the maximum energy dissipation principle in combination with the maximum entropy production principle is probably the only physical principle that can explain the emergence of biological systems as the complex acceleration forms of free energy utilization. The relationship of the maximum energy dissipation principle to the least action principle unites, connects the biological processes to physical processes. In fact, these principles make the biological processes so universal, as physical processes. Thus, unified LA/MED principle can explain the emergence of biological pathways of dissipation. Moreover this unified principle can explain also the stages of the biological evolution and its transition to socio-technological evolution.

In the energy transformation performing by biosystems, one can note few key limitations, which can be linked to the thermodynamics properties and MED principle. First one is related to the variety and scale of the structural/material forms of free energy utilization/dissipation. Second limitation is linked to information (negentropy generation): the informational support of maintaining/providing the free energy utilization by biological systems is essentially limited in the mapping capability because of a material nature of informational subsystem.

Thus, the MED principle implies that the emergence of biological systems is a physical process. Indeed, the thermodynamic perspective can play a vital role in consideration any endogenous way of life emergence on our planet. Particularly the MED principle welcomes the emergence of the autocatalysis from the huge spectrum of catalytic processes.

Due to the diversity of chemical processes, the number of possible chemical dissipative pathways over-exceeds the number of several physical processes of energy dissipation by the number of decimal orders. Among them there is a number known of different catalytic processes. From MED perspective is not particularly important how the self-replicative molecular structures initially emerges, where they were synthesized - on the surface of the prebiotic planet (Russell and coauthors [16]), or they emerged as the result of self-polymerization in a complex network, proposed by Eigen and coauthors [17-18]. Important is that they bring the nonlinear, faster way of free energy dissipation, as illustrated in Figure 1. Significant is that they are capable to nonlinear acceleration of free energy dissipation - free energy in a form of various molecular compounds/structures. Certainly, that the physical and chemical processes of energy dissipation coexist.

Their competitiveness has an indirect form and is rather related to their existence.

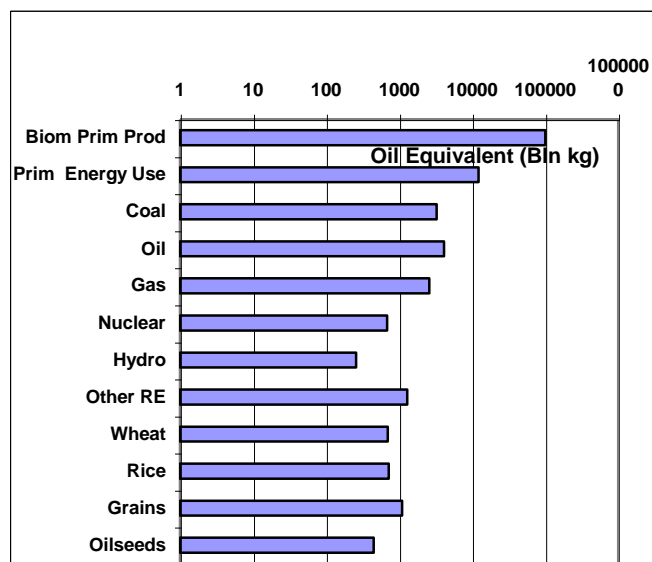
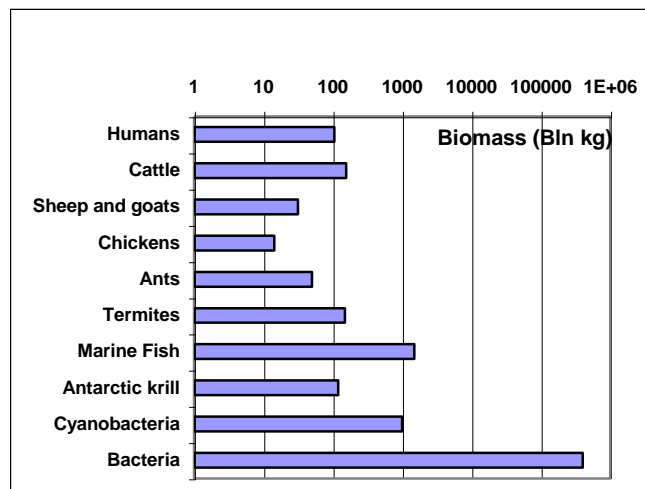


Figure 3. Global scales of energy utilization by some biospecies and socio-technological system, based on [31-40].

On the other hand, the gain, the acceleration of free energy dissipation by nonlinear autocatalytic processes can be considered as the emergence of non-pure-physical degrees of dissipations. The pure physical nonlinear dissipative processes can be observed in stimulated emission of the gain medium in the lasers. The nonlinear relaxation takes place and it has a pure physical nature. In more natural environment, the MED principle welcomes the non-linear processes of chemical nature, which may occur at the surfaces, e.g. catalytic processes. Kinetically, all these processes can be nonlinear, having at initial stage an exponential growth. In a spectrum of macromolecules, which can be initially randomly synthesized on the surface of prebiotic Earth, later the autocatalytic macromolecular structures emerged. Particularly these molecular structures can start the emergence of molecular networks and the hierarchy, which can lead to the emergence of prebiotic Eigen hypercycles-like molecular networks, having self-replication properties and RNA-based informational molecular cognition.

The cooperation in different forms has taken place in earlier stages of the emergence of biological systems. It has taken place in the form of molecular symbiosis. In the framework of this cooperation/symbiosis, further developments of molecular forms of informational

accumulation for more effective metabolic networks or primary structure of macromolecules, secondary structure, enzyme activity, informational control of functionality, functional/enzymic support of spatial separation from the environment have taken place and led to the formation of prokaryotic-like proto-cell.

The overall trend and qualitative transitions in the evolutionary process of biological systems can be explained by the complexity increasing based on symbiosis/cooperation as a universal mechanism to develop a new qualitative level of free energy consumption/dissipation. The emergence and formation of these symbiotic associations opened the capability to expand to a new dissipation level. New functions are gained by the capability of such a symbiotic organism to further develop the qualitatively new organisational structures and the exploration of qualitatively new sources of free energy.

The hypothetical general scheme in Figure 2 illustrates an overall trend in the biological hierarchical organisation. In some sense these levels of organisation are also the evolutionary levels, levels of major transition in the form of dissipative relations with the environment as a source of free energy. According to the maximum energy dissipation principle the key characteristic of biological evolution can be considered as in [15]:

- * every new level of organisation/evolution (cellular, multicellular, biosocial) emerges as a result of cooperative, symbiotic relationships, further specialisation and integration in associations/communities formed by previous level of organisation biological systems;

- * every major level of the organisation can be characterized by essentially new level of dissipation of the forms of free energy resources which are not possible to utilise at the previous organisational levels of free energy dissipation. This includes also new biological resources which appeared as a result of the process of evolution. Overall acceleration of dissipation can be schematically illustrated in Figure 4. Every transition in organisation indicated in Figure 2, is accompanied by increase of global rate of energy dissipation.

- * the initial phase of the emergence of a new possible dissipative level is accomplished by divergent phase of the spectrum development, when emerged new structures develop various forms of organisation and the overall number of species significantly increases;

- * the competition between different dissipative pathways increases when the total dissipation rate reaches the scale of free energy inflow into the system. Then, in biological terms, the integrative functionality of biosystems becomes crucial for the competition, specialisation of the constituent subsystem becomes very important and, as the final result, the essentially new level of integrative functionality and development of a new form of informational/cognitive support finally leads a new level of organisation;

- * the cooperation between the same level of organisation biosystems in the whole spectrum of species provides a capability to develop new level of symbiotic structures as an essentially new manner to adapt and survive. From a dissipative perspective, that lets to final development of a new way to dissipate free energy in an accelerated way, including exploring the new forms of it. Indeed, the cooperation, plays a crucial role in the emergence of new organisation, new biological systems;

- * at every level of biological organisation, there are qualitatively different informational sub-systems providing informational/cognitive support for the optimization of energy

use/exploration and overall competitiveness of the biological structures at this level.

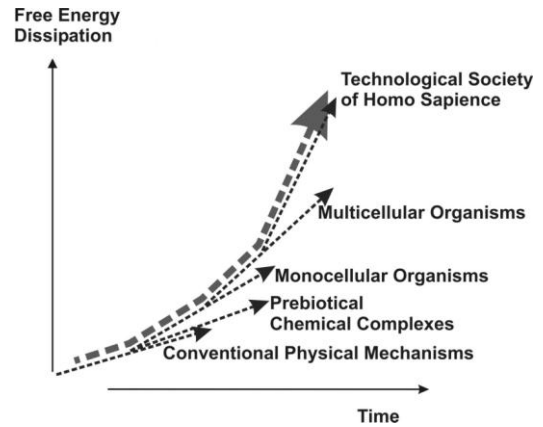


Figure 4. Schematic presentation of acceleration of energy dissipation at every stage of evolution of biosystems.

Finally, one can also suggest that by forming certain basic and minimal evolutionary step-unit, Figure 5, discussed also formerly in [15] can be considered:

- *cooperation (symbiosis) of the dissipative processes at level-down (previous level)

- *development of a qualitatively and essentially new form of organisational processes in the framework of new type of cooperation/symbiosis,

- *extension/exploration and utilization (or faster utilization than at previous organisational levels) of new free energy sources as a result from dissipative perspective.

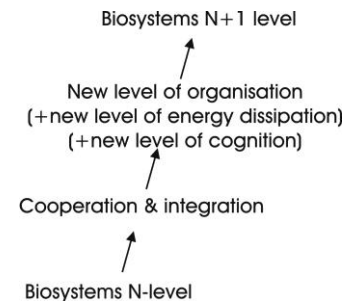


Figure 5. Principal evolutionary step, characteristic for "evolutionary ladder", see Figure 2.

Using this minimal evolutionary mechanism/step, Figure 5, it is possible to explain the transitions/evolution of biosystems at every qualitatively new level of biological hierarchy – cellular, organismic, social and even socio-technological. In this way, the biological life, its emergence as a phenomenon characterising by its low probability, is a very robust and probabilistic process, and its emergence, robustness and evolution towards complexity is provided by MED principle.

Taking into account discussed above, can be concluded that the emergence and evolution of socio-technological dissipative pathway can be seen as a result of evolutionary aspect of the MED principle. As it is shown in the general scheme, Figure 2, the socio-technological level of organisation predictably emerges/evolves from biosociality, which is characteristic of a number of biological species. However, just HS species developed a global socio-system, which has complex organisation in any aspect - social, energy and substance processing and informational processing. As we

have noticed above, the socio-technological system is the unique product of cooperation of biological component (individuals and the labour) with non-biological component - the means of production, having non-biological nature. In terms of energy dissipation, socio-technological system of HS considerably expands the pure biological scale of free energy exploration. Its emergence and evolution corresponds to the maximum energy dissipation demand or the least action principle.

This socio-technological level can be considered as a top of the biological trophic pyramid. It is essentially a new bio-socio-technological level of organisation which can be treated as a symbolically-like related to certain non-biological functional objects having a non-biological origin and characteristics (which usually called as the means of production). This is a key difference of HS "social organism" comparably to other known biological social species, like ants or termites. The data on biomass of these social species is indicated in Figure 3. One can note that the biomass of these species is very big, which can indicate the powerful role of social way of organisation in the adaptation of biological species to environment. However, only the HS social system was able to develop symbiosis-like relations with a non-biological means (later in evolution- the means of production), having self-reproductive-like properties. Due to these symbiotic interactions of Homo sapiens with nonbiological structures, the Homo sapiens social system was able to extend energy-structural consumption of qualitatively new energy resources of non-biological origin [15], and has developed qualitatively new mechanisms of energy processing and qualitatively new information processing (cognition). In this way, the socio-economic evolution appears as a continuation of bio-social evolution.

In Figure 6, the approximate scales of informational mapping, which can be considered as more sophisticated at a higher level of biosystems (like multicellular or social), as are indicated. One can see the expansion of this mapping with the increase of organisational complexity in direction to socio-technological system. However, one can expect also the limitations at every level of biological organisation [15].

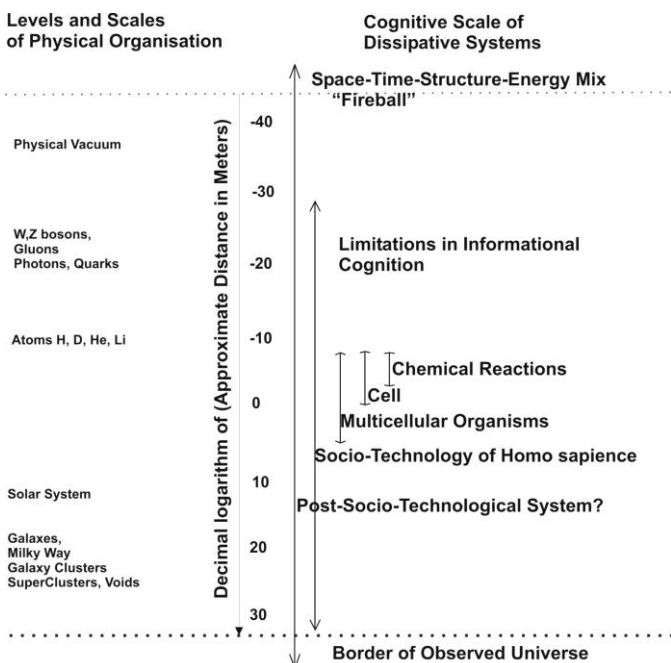


Figure 6. Schematic presentation of scales of informational cognition of the systems of different levels of organisation (adapted from [15]).

However, it is expected, that free energy processing scale and informational support in socio-technological system indicate their fundamental limitations [15]. First limitation is directly linked to the scale of exploration and processing of energy, which is limited by technological capability. Second limitation – is linked to socio-informational mapping/cognition – that part of technology which deal with the investigation of new energy sources (for example, nuclear fusion) and develop the processes of energy production in conventional forms suitable for standard usage in technology and for effective and qualitative consumer goods production.

Based on evolutionary trend, proposed in Figure 2, a post-socio-technological organisational level of dissipative processes can be expected as a next organisational level after the socio-technological organisation systems. This new level can be characterized by qualitatively new level of energy consumption and linked to it dissipative process carried out, and also a qualitatively new level of information mapping/cognition. Taking into account cognitive limitations at every biological level [15], illustrated in Figure 6, one can state a question: to what extent is it possible to predict the characteristics of this new post-socio-technological level. Is it possible to forecast within the framework of limited socio-technological and informative-scientific mapping of Homo sapiens?

Taking into account that in proposed evolutionary mechanism, every qualitative new level of dissipative systems organisation always emerges as a result of cooperativity of the systems of lower/previous level, one can suggest that a higher to socio-technological level can be the level when number of socio-technological systems cooperate, interact, specialize and form even more complex organisation, [15]. One can expect that the scale of this organisation can be enormously large. Then such extra-terrestrial expansion of HS-like technological systems can be considered as a first stage in the emergence of this post-socio-technological level of organisation. However, an expansion of post-socio-technological system into the small distances of physical world can also take place, see Figure 6. This is expected to be a combined expansion in both super-large and super-small, plank-scale physical worlds.

SUMMARY

It is suggested that the driving force for the molecular, prebiotic, biological and socio-technological evolution can be explained on the basis of the maximum energy dissipation principle, which can be treated as a partial case of the least action principle.

On this basis, a general scheme of evolution from autocatalytic molecular processes to socio-technological system can be built from the perspective of maximum energy dissipation. This scheme also reflects the organisational structure of biological world. The scheme treats the emergence of biological systems as an initial stage in the acceleration of global free energy dissipation. The sequential emergence of qualitatively new levels of dissipation (biological cell, multicellular organism, social and socio-technological systems) has been discussed, and the levels are suggested as evolved in the results of cooperation/symbiosis of the dissipative systems at the previous levels. The cooperation/symbiosis provides the basis for the development of every next, essentially new level of energy dissipation, leading to a new form of free energy utilization and a new

form of informational mapping/cognition. From a thermodynamic perspective, every qualitatively new level of biological organisation provides additional step to increase the global rate of energy dissipation from qualitatively new sources, essentially widening the number of these sources involved in the utilization. In the sense of maximum energy dissipation/least action principle, the emergence and existence of biological and post-biological (socio-technological) systems are the direct requirement of this united principle, which makes the existence of the biological world in agreement with physics as a whole.

Post-socio-technological level can be considered as the cooperative, symbiotic-like organisation of socio-technological systems as the subsystems, elements. This level can be characterized by significantly new level of energetical and substance/matter utilization, and qualitatively (and quantitatively) new level of informational supporting processes. Some observed in processes have to be analysed from the perspective to be considered as a super-socio-technological system's activity. Therefore some reservations can be taken into account with respect to the existence of post-socio-technological level of dissipative processes organisation.

REFERENCES

- [1] H. Ziegler, Chemical Reactions and the Principle of Maximal Rate of Entropy Production, *ZAMP, Journ. Appl. Math. Phys.*, vol. 34, pp. 832-844, 1983.
- [2] G.W. Paltridge, The Steady-State Format of Global Climate, *Q. J. R. Meteorol. Soc.*, vol.104, pp. 927-945, 1978.
- [3] G.W. Paltridge, Climate and Thermodynamic Systems of Maximum Dissipation, *Nature*, vol. 279, pp. 630-631, 1979.
- [4] G.W. Paltridge, Thermodynamic Dissipation and the Global Climate System, *Q. J. R. Meteorol. Soc.*, vol. 107, pp. 531-547, 1981.
- [5] H. Ozawa, A. Ohmura, R.D. Lorenz, T. Pujol, The Second Law of Thermodynamics and the Global Climate System: a Review of the Maximum Entropy Production Principle, *Rev. Geophys.*, vol 41, pp. 1018-1041, 2003.
- [6] D. Juretic, P. Županovic, Photosynthetic Models with Maximum Entropy Production in Irreversible Charge Transfer Steps, *Comp. Bio. Chem.*, vol. 27, pp. 541-553, 2003.
- [7] A. Kleidon, K. Fraedrich, T. Kunz, F. Lunkeit, The Atmospheric Circulation and States of Maximum Entropy Production, *Geophys. Res. Lett.*, vol. 30, pp. 2223, 2003.
- [8] R.C. Dewar, Information Theoretic Explanation of Maximum Entropy Production, the Fluctuation Theorem and Self-Organized Criticality in Non-Equilibrium Stationary States, *J. Phys. A*, vol. 36, pp. 631-641, 2003.
- [9] R.C. Dewar, Maximum Entropy Production and the Fluctuation Theorem, *J. Phys. A: Math. Gen.*, vol. 38, L371-L381, 2005.
- [10] L.M. Martyushev and V.D. Seleznev, Maximum Entropy Production Principle in Physics, Chemistry and Biology, *Physics Reports*, vol. 426, pp. 1-45, 2006.
- [11] A. Moroz, On a Variational Formulation of the Maximum Energy Dissipation Principle for Nonequilibrium Chemical Thermodynamics. *Chem Phys Lett*, vol. 427, pp. 448-452, 2008.
- [12] A. Moroz, A Variational Framework for Nonlinear Chemical Thermodynamics Employing the Maximum Energy Dissipation Principle, *J. Phys. Chem. B*, vol. 113, pp. 8086-8090, 2009.
- [13] A. Moroz, Cooperative and Collective Effects in Light of the Maximum Energy Dissipation Principle, *Phys. Letters A*, vol. 374, pp. 2005-2010, 2010.
- [14] A. Moroz and D.I. Wimpenny, On the Variational Framework Employing Optimal Control for Biochemical Thermodynamics, *Chem. Physics*, vol. 380, pp. 77-85, 2011.
- [15] A. Moroz, The Common Extremalities in Biology and Physics, Second Edition, Elsevier Insights, New York, NY, 2011.
- [16] W. Martin and M.J. Russell, On the Origins of Cells: a Hypothesis for the Evolutionary Transitions from Abiotic Geochemistry to Chemoautotrophic Prokaryotes, and from Prokaryotes to Nucleated Cells. *Philos. Trans. R Soc. Lond. B Biol. Sci.*, vol. 358(1429), pp. 59-85, 2003.
- [17] M. Eigen, Self-Organisation of Matter and the Evolution of Biological Macromolecules, Springer-Verlag, Heidelberg, 1971.
- [18] M.Eigen, P. Schuster, The Hypercycle. A principle of Natural Self- Organisation, Springer-Verlag, Berlin, Heidelberg, NY, 1979.
- [19] L. Orgel, Self-organizing Biochemical Cycles. *Proc. Natl. Acad. Sci. USA*, vol. 97, pp. 12503-12507, 2000.
- [20] Y. Demirel, Nonequilibrium Thermodynamics Modelling of Coupled Biochemical Cycles in Living Cells, *J. of Non-Newton. Fluid Mechanics*, vol. 165, pp. 953-972, 2010.
- [21] A.I. Oparin, Proiskhozhdenie Zhizni. Moskovskij Rabochij, Moscow, 1924.
- [22] A.I. Oparin, The Origin of Life (Translation1953), Dover Publishers, NY, 1938.
- [23] A.I. Oparin, The Chemical Origin of Life. Trans. Ann Synge. Charles C. Thomas Publisher, Illinois, USA, 1964.
- [24] J.B.S. Haldane, The Origins of Life, *New Biol.* Vol. 16, pp. 12-27, 1954.
- [25] S.W., Fox, K. Dose, Molecular Evolution and the Origin of Life. Marcel Decker Inc., 1977.
- [26] E. Broda, The Evolution of the Bioenergetic Processes. Pergamon Press, Oxford, 1978.
- [27] L. Margulis, Symbiosis in Cell Evolution: Microbial Communities in the Archean and Proterozoic Eons. W.H. Freeman, 1992.
- [28] J.A. Shapiro, M. Dworkin (eds.) Bacteria as Multicellular Organisms." Oxford Univ. Press. Oxford, 1997.
- [29] Animal Social Complexity: Intelligence, Culture, and Individualized Societies, Ed.by Frans de Waal and Peter L. Tyack, Harvard University Press, CT, 2003.
- [30] V.B. Sapurov, Global Dynamics of Termite Population: Modelling, Control and Role in Green House Effect, *Proc. of the Sixth International Conference on Urban Pests*, vol. 1, pp. 389-393, 2008.
- [31] M.M. Камшилов, Эволюция биосферы, Наука, Moscow, 1979.
- [32] B.W. Whitman, D.C. Coleman, W.J. Wiebe, Prokaryotes: the Unseen Majority, *Proc. Nat. Acad. Sci. of the United States of America*, vol. 95, pp. 6578-83, 1998.

- [33] F. Garcia-Pichel, J. Belnap, S. Neuer, F. Schanz, Estimates of Global Cyanobacterial Biomass and its Distribution, *Algol. Studies*, vol. 109, pp. 213–217, 2003.
- [34] R.W. Wilson, F.J. Millero, J.R. Taylor, P.J. Walsh, V. Christensen, S. Jennings, M. Grosell, Contribution of Fish to the Marine Inorganic Carbon Cycle" *Science*, vol. 323, pp. 359-362, 2009.
- [35] A. Atkinson, V. Siegel, E.A. Pakhomov, M.J. Jessopp, V. Loeb, A Re-appraisal of the Total Biomass and Annual Production of Antarctic Krill, *Deep-Sea Research I*, vol. 56, pp. 727–740, 2009.
- [36] S.C. Walpole, D. Prieto-Merino, P. Edwards, J. Cleland, G. Stevens, I. Roberts, The Weight of Nations: an Estimation of Adult Human Biomass, *BMC Public Health*, vol. 12, pp. 439, 2012.
- [37] Historical Estimates of World Population, U.S.Census Bureau (USCB), 2010. <http://www.census.gov/ipc/www/worldhis.html>.
- [38] A. Maddison, *Contours of the World Economy 1–2030AD: Essays in Macro-Economic History*, Oxford University Press. Oxford, 2007.
- [39] A. Maddison, *Statistics on World Population, GDP and Per Capita GDP, 1-2008 AD*, <http://www.ggdc.net/MADDISON/oriindex.htm> .
- [40] A. Maddison, *Contours of the World Economy 1–2030AD: Essays in Macro-Economic History*, Oxford University Press. Oxford, 2007.

DRIVEN CHEMISTRY AND INCREASINGLY COMPLEX FORMS OF DYNAMIC ORDER

Eva Wollrab, Sabrina Scherer, Emanuel Worst, Philipp Zimmer, Karsten Kruse and Albrecht Ott

Dept. of Physics, Universität des Saarlandes, Germany

ABSTRACT

We review some of the main advances in our understanding of the living state of matter as well as its stability. We cite some of the main ideas related to the production of self-organizing chemical order. We present preliminary, experimental results on two topics. In the first part we discuss prebiotic broths, following the ideas of Miller Urey. We show that by studying the dynamics of their molecular organization, temporal patterning emerges as a coherent feature of driven, random organic soups. In the second part, we consider coexisting self-reproducing agents. We ask how the self-reproducing agents attain a robust evolution towards increased complexity, rather than getting stuck by producing a single "winner". By simplifying the system to one dimension, we show that the system may escape from getting stuck by generating new configurations. We find, however, that the theoretical construct is difficult to realize experimentally, without detailed tuning of the parameters by hand. This may well explain why, to our knowledge, a one dimensional molecular ecosystem did not emerge as a result of evolution.

BACKGROUND

In his famous lecture series "What is Life?"[1], Erwin Schrödinger asked how the events in space and time that take place within the spatial boundary of a living organism, can be accounted for by physics and chemistry. Among many interesting and far-reaching reflections, Schrödinger insisted that living matter creates order from disorder. Living matter evades the decay to thermodynamic equilibrium by feeding: it gains 'negentropy' in an open system.

Chemical pattern formation: the Turing mechanism

More than 10 years later Turing was the first to propose a basic mechanism of order generating chemical pattern formation[2], in non-equilibrium conditions. He realized that two substances, which he termed morphogens, an activator (a) and an inhibitor (h), were needed to create a chemical pattern. Reaction-Diffusion (RD) equations of the type

$$\frac{\partial a}{\partial t} = D_a \nabla^2 a + S_a(a, h) - Q_a(a, h)$$
$$\frac{\partial h}{\partial t} = D_h \nabla^2 h + S_h(a, h) - Q_h(a, h)$$

can lead to chemical patterning if there are sufficiently strong non-linearities in the source (S) terms (in fact, stronger self-activation than simple autocatalysis is required). To observe pattern formation, it is also necessary that the diffusion constants D be sufficiently different (or the morphogen decay rates, given by Q). Alain Turing suggested that the reaction diffusion mechanism may explain patterning in developmental biology. In spite of its seducing simplicity,

even today there are only a limited number of cases in Biology where molecules/morphogens that follow an RD scheme have been clearly determined. Turing suggested that the organism Hydra, a 1cm tall polyp, could follow an RD scheme. Hydra can regrow lost body parts, it can even reform from a random cluster of its own cells. The work of Hans Meinhardt discusses this phenomenon at length, showing that almost any experiment can be explained based on an RD mechanism. In spite of an intense experimental search, the morphogens could not be isolated, suggesting a different pattern generating mechanism on the molecular scale. We have shown that next-neighbour signalling among the participating cells can explain the symmetry breaking and axis formation very well [3]. In order to comply to experiments, we borrow a mechanism from self organized critical systems. Although pattern forming systems are a major part of biology and the same applies to chemical oscillators, in the organism these phenomena remain poorly understood from a reductionist point of view.

In chemistry the realization of pattern forming reactions has been the subject of intense research. The first self-organizing periodic reaction in homogeneous solution was discovered by Bray in 1926, while studying the reduction and oxidation properties of H₂O₂ [4]. However, even today only few examples of pattern forming chemical systems exist. The Belousov-Zhabotinsky reaction [5] is the famous realization of a reaction diffusion mechanism that leads to colorful waves in an initial homogeneous solution. Initially this type of reaction was considered impossible to realize experimentally. The Briggs Rauscher reaction [6] was inspired from BZ. It is another classic of the few examples of a spontaneously oscillating chemical reaction. The detailed reaction mechanisms of both reactions are rather involved. Complexity could be a characteristic feature of this type of behaviour. Autocatalysis is the essential element in generating the required non-linearities for the phenomenon. Often the non-linearity is enhanced through the use of metal or

halogenide compounds with a strong and broad oxidation potential.

In physics it has long been known that the state space of a nonlinear system contracts if the system dissipates: the system becomes more ordered when driven. Among well-known examples of pattern forming phenomena is the Rayleigh Bénard convection, where rising liquid, due to heating at the bottom, will produce regular convection roles. Many other examples exist: cloud formation, dunes, turbulent fluids, mode selection in a laser. The patterns occur as a result of competition of 'modes' of the nonlinear system. The strongest among them wins and creates a pattern by starving the others in terms of energy.

The hypercycle

It has been proposed that self-reproduction is the strongly growing chemical "mode" that necessarily "wins" and dominates the dynamic behaviour of biochemistry. Manfred Eigen and Peter Schuster theoretically considered simple systems of reproducing molecular information carriers in competition [7]. In simple situations they could show that the selection process is governed by the same equation as mode selection in a laser. They also addressed a more complex situation: the evolution, in competition, of multiple, self-reproducing, cyclic, mostly deterministic reactions of information carriers and enzymes, so called hypercycles. In this case, a molecule like RNA contains the information for the production of enzymes, which in turn multiply the RNA and, at the same time, read the stored information to produce more enzyme. In the system, Schuster and Eigen introduced molecular self-reproduction by hand, and the molecular pathways have reduced complexity compared to real chemistry. As a result the hypercycles do not produce evolution, although they undergo mutations. In most cases, it is the hypercycle with the largest number of elements that wins the competition and the evolution remains stuck.

However, chemistry is different from systems that physicists usually investigate, including the system studied by Eigen and Schuster. Chemistry includes the transformation of matter, and the rules of chemistry evolve with changing concentrations, and with new molecules or molecular scaffolds that appear. No satisfying statistical characterization of (organic) chemistry has been achieved so far. Experimentally it is not clear, how chemical systems can be supplied with energy so that they self-organize in a non-trivial way. Even, theoretically, a system that compares to living matter has not yet been suggested.

With their reflections on hypercycles, Eigen and Schuster revealed one of the challenging problems that have not been solved: how can a number of reproducing entities coexist in an ecosystem and undergo Darwinian evolution without one species dominating the system and ultimately halting the process?

EXPERIMENTAL AND RESULTS

We study the time evolution of a Miller Urey type random prebiotic broth [8] using mass spectroscopy. We show [9] that the system produces polymerized substances as sudden bursts. They tend to disappear and the process restarts. Thus

reversibly assembling and disabling biodynamers emerge spontaneously as a result of driving chemical reactions.

We study the evolution of template based reproducing DNA strands that are allowed to double their length[10] We show that the experiment can produce filaments with increasing length only if it is helped by the experimentalist, in a narrow range of parameters. This is in contrast to theory, where a situation with several coexisting filaments lengths easily occurs as a stable dynamic result.

REFERENCES

- [1] E. Schrödinger, *What is life : the physical aspect of the living cell*, Cambridge University Press, New York, 1992.
- [2] A. Turing, The Chemical Basis of Morphogenesis, *Phil. Trans. Royal Soc. London*, vol. 641, pp. 37-72, 1952.
- [3] A. Gamba, M Nicodemi, J. Soriano, A. Ott, Critical Behavior and Axis Defining Symmetry Breaking in Hydra Embryonic Development, *Phys. Rev. Lett.*, vol 108, pp. 158103, 2012.
- [4] W. C. Bray: A Periodic Reaction in Homogeneous Solution and Its Relation to Catalysis. *J. Am. Chem. Soc.* vol43, Nr. 6, pp. 1262–1267, 1921, .
- [5] B. P. Belousov, A Periodic Reaction and Its Mechanism, *Sbornik Referatov po Radiatsionni Meditsine*, Medgiz, Moscow, p. 145 (1958).
- [6] T. S. Briggs, W. C. Rauscher , An Oscillating Iodine Clock, *J. Chem. Educ.* vol 50, pp. 496, 1973.
- [7] M. Eigen, P. Schuster: *The Hypercycle -A Principle of Natural Self-Organization*, Springer-Verlag, Berlin, 1979.
- [8] S. L. Miller, H. C. Urey *Organic Compound Synthesis on the Primitive Earth. Science.* vol 130 (3370), pp. 245–251, 1959
- [9] E. Wollrab, S. Scherer, A. Ott, to be published
- [10] E. Worst, P. Zimmer, A. Ott, K. Kruse, to be published

NEARLY PERPETUAL MOTION MACHINES OF THE THIRD KIND

Peter Salamon*, Bjarne Andresen^o, Karl Heinz Hoffmann**

*Department of Mathematics and Statistics, San Diego State University, San Diego CA 92182 USA
^oNiels Bohr Institute, University of Copenhagen, Universitetsparken 5, DK-2100 Copenhagen Ø, Denmark
** Institute of Physics, Chemnitz University of Technology, D-09107 Chemnitz, Germany

EXTENDED ABSTRACT

It has been stated that certain chains of biological reactions can go to near completion in both directions as needed without any exterior driving force. This claim represents a thermodynamic impossibility. Yet, this impossibility is of a new type not covered by the traditional list of impossibility devices known as perpetual motion machines. Rather, it represents a perpetual motion machine of the third kind (PM3) that becomes impossible only in finite time [1]. At non-vanishing rate the chain of biological reactions above would constitute a finite-time perpetual motion machine.

It turns out however that coexistent equilibrium degrees of freedom represent very low dissipation and can come surprisingly close to PM3 operation. Exactly how this fact is exploited in biological systems will be the subject of the talk.

Many biological processes seem to operate near the PM3 limit. In many cases the location where the free energy dissipation occurs is not even clear. Thus claims of the reversibility of such processes are not surprising. Below we present a number of processes for which the energy dissipation is indeed surprisingly low.

- The molecular motor ATP synthase operates very nearly reversibly [2, 3].
- Myriad crista shapes of the inner mitochondrial membrane are isoergic and interconvert freely [4].
- Lipid composition of *E. coli* adjusts to ambient temperature so the sol-gel phase transition temperature is just below ambient [5]. This brings the sol-gel transition within reach of many local fluctuations, e.g. in pressure or charge.
- Twisting and untwisting DNA mediated by DNA-binding proteins that perform extensive DNA remodeling or distortion are frequent processes. The isothermal enthalpy / entropy compensation that keeps these reactions nearly isoergic is well documented [6,7].

In each of these examples a degree of freedom is kept near equilibrium thereby lowering the associated dissipation needed in changing that degree of freedom. Moving along such neutral degrees of freedom is a nice trick for any control minimizing dissipation. As illustrated in Figure 1, to get the rolling pin from one end of the table to the other, we need only lift one end of the table a bit as the table is flat. General bounds on dissipation in finite time relate such dissipation to the thermodynamic distance traversed [8]. This distance is zero along exactly such equilibrium modes! Our list above serves as a partial argument that living systems sometimes exploit these degrees of freedom to achieve their control of the scenarios needed for life.



Figure 1: An illustration of the energetics along a neutral degree of freedom: the horizontal table. Note that only a very small elevation suffices to make the process go in one direction or the other.

REFERENCES

- [1] P. Salamon, B. Andresen, K.H. Hoffmann, J.D. Nulton, A.M. Segall, and F.L. Rohwer, "Free energies of staging a scenario and perpetual motion machines of the third kind," In Aaron Dinner, editor, *Advances in Chemical Physics*, Wiley, 2013.
- [2] G. Oster, and H. Wang, "Why Is the Mechanical Efficiency of F1-ATPase So High?," *J. Bioenerg. Biomembr.*, 32, 459 (2000).
- [3] T. Elston, H. Wang, and G. Oster, "Energy transduction in ATP synthase," *Nature*, 391, 510 (1998).
- [4] M. Ghochani, J.D. Nulton, P. Salamon, T.G. Frey, A. Rabinovitch, and A.R.C. Baljon, "Tensile Forces and Shape Entropy Explain Observed Crista Structure in Mitochondria," *Biophys. J.*, 99, 3244 (2010).
- [5] T. Heimburg, *Thermal Biophysics of Membranes*, Wiley-VCH Verlag, Berlin, 2007.
- [6] L. Jen-Jacobson, L.E. Engler, and L.A. Jacobson, "Structural and thermodynamic strategies for site-specific DNA binding proteins," *Structure*, 8, 1015 (2000).
- [7] M.S. Searle, and D.H. Williams, "On the stability of nucleic acid structures in solution: enthalpy-entropy compensations, internal rotations and reversibility," *Nucleic Acids Res.*, 21, 2051 (1993).
- [8] P. Salamon, and R. S. Berry, "Thermodynamic length and dissipated availability," *Phys. Rev. Lett.*, 51, 1127 (1983).

THE RELEVANCE OF MAXIMUM ENTROPY PRODUCTION PRINCIPLE AND MAXIMUM INFORMATION ENTROPY PRINCIPLE IN BIOLOGY

P. Županović, D. Juretić

*University of Split, Faculty of Science, Teslina 12, 21000 Split, Croatia

ABSTRACT

Prigogine and Wiame noticed correctly that biological processes are irreversible and as such should be described within irreversible thermodynamics. They took the entropy production as the basic quantity for the description of biological processes. In contrast to Prigogine, who suggests the principle of minimum entropy production as a relevant principle for the biology, we take maximum entropy production principle as a relevant one. We argue here that maximum entropy production principle is more suitable than minimum entropy production principle for a description of energy transduction in biological systems. Our basic assumption is that the biological evolution through enzyme catalysis, is accompanied by an entropy production increase in internal transitions and with the Shannon's information entropy increase of all enzyme states. In such a way the increase of entropy production is understood as being tightly coupled to biological evolution. Fully evolved enzymes are characterized by maximum possible entropy production in internal transitions.

INTRODUCTION

In this paper we examine whether the distribution of optimal rate constant values for transitions among functionally important states in enzymes can be predicted by maximum entropy production (MaxEP) principle, by maximum of Shannon information entropy (MaxEnt) or as the combination of these two principles.

The MaxEP and MaxEnt principles applied to Michaelis-Menten kinetics of β -Lactamase enzymes [1,2] give a good agreement of optimal rate constant values for internal transition $ES \rightarrow EP$ with experimentally determined values. We also found that the functional design of rotary enzyme ATP synthase is consistent with the MaxEP and MaxEnt principle applied in combination [3] to the extent that predicted optimal angular position for the ATP-binding transition agrees within experimental error with the experimental value.

In the Discussion section we maintain that the MaxEP principle is much more relevant than Prigogine's principle [4,5]. Furthermore, the successful application of the MaxEP and MaxEnt principle, reviewed in this paper, argues for the point of view that physical and biological evolution cannot be considered separately one from another.

ENTROPY PRODUCTION FOR MICHAELIS-MENTEN KINETICS

In often used three state model for enzyme kinetics (Michaelis-Menten kinetics, Fig. 1), the internal transition $ES \leftrightarrow EP$ is the only one not directly connected with a substrate or product concentration. Our conjecture here is that biological evolution, within fixed concentrations of substrate and product molecules, is accompanied with an increase of the entropy production in the internal transition. For fully

evolved enzyme (the "perfect enzyme" concept of Albery and Knowles [6]) maximum entropy production is expected to be associated with that transition. We also propose that biological evolution is accompanied with an increase in Shannon information entropy of the entire cyclic reaction scheme. The perfect, fully evolved enzymes, are rare in nature, if they exist at all, and we do not expect to find more than approximate correspondence among predicted optimal rate constants by using the MaxEP or MaxEnt principle and measured rate constants for enzymes considered to be highly evolved. The MaxEP principle can be used as a test whether the enzyme has approached a fully evolved state or not, but cannot be considered as an alternative to the biological selection and evolution.

Enzyme reactions involve metabolic fluxes (J) and thermodynamic forces (X) that govern these fluxes. The associated entropy production rate is defined as the product of the metabolic flux and the corresponding thermodynamic force, divided by absolute temperature

$$\sigma = \frac{JX}{T}. \quad (1)$$

For the three-state model (Fig. 1), J is the net flux of any given transition, because there is only one cycle and only one flux (which must be the same for all transitions in accordance with Kirchhoff's junction rule). For given substrate and product concentrations, the total thermodynamic force of the overall reaction is a constant. The sum of the affinities (i.e. thermodynamic forces) associated with chosen transitions equals the total thermodynamic force X (in accordance with Kirchhoff's loop rule). One of our basic results from previous research [1] shows that there is a unique maximum for the entropy production of any given transition with respect to variation in its forward rate constant. This is because the

associated transition flux and affinity are, respectively, monotonically increasing and decreasing functions of the forward rate constant. In other words, there is a simple trade-off between thermodynamic flux and force.

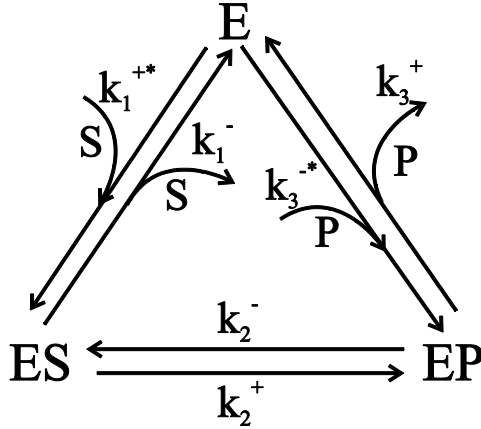


Figure 1. Michaelis-Menten reversible kinetic scheme.

Here we calculate the entropy production of the internal enzyme transition $ES \leftrightarrow EP$, and the Shannon entropy of the entire reaction, as functions of the forward rate constant k_2^+ . The net metabolic flux for $ES \leftrightarrow EP$ is

$$J \equiv \frac{d[P]}{dt} = k_2^+[ES] - k_2^-[EP], \quad (2)$$

where $[P]$, $[ES]$ and $[EP]$ are the concentrations of product and complex states ES and EP, respectively. Thermodynamic force (or affinity) is the difference in chemical potentials between states ES and EP,

$$A_{23} = RT \ln \left(K_2 \frac{[ES]}{[EP]} \right), \quad (3)$$

where R is the gas constant and K_2 is the equilibrium constant for $ES \leftrightarrow EP$. The affinity (3) is a function of the complex concentrations $[ES]$ and $[EP]$.

After lengthily, but otherwise straightforward calculation, we get entropy production as a function of forward kinetic constant in the internal transition,

$$\sigma(k_2^+) = R[E]_t \frac{k_2^+(DK_2 - F)}{K_2(Gk_2^+ + H)} \ln \left(K_2 \frac{Ck_2^+ + D}{Ek_2^+ + F} \right), \quad (4)$$

Here $A = k_3^+ + k_1^-/K_2$, $B = k_3^+k_1^-$, $C = (k_1^+[S] + k_3^-[P])/K_2$, $D = k_3^+k_1^+[S]$, $E = CK_2$, $F = k_1^-k_3^-[P]$, $G = A + C + E$, $H = B + D + F$.

SHANNON INFORMATION ENTROPY FOR MICHAELIS-MENTEN KINETICS

The Shannon information entropy of the enzyme model in Fig. 1 is defined as

$$H = -\sum_{i=1}^3 p_i \ln(p_i), \quad (5)$$

where p_i ($i=1,2,3$) are probabilities that the enzyme is found in one of its functional states (E, ES or EP, respectively). These probabilities are given by:

$$p_i = \frac{[X_i]}{[E]_t}, \quad (6)$$

where $[E]_t$ is the total enzyme concentration and $[X_i]$ are the concentrations of the enzyme species E, ES or EP (for $i=1,2,3$, respectively).

Similarly to entropy production we get the Shannon information entropy as a function of k_2^+

$$H(k_2^+) = -\left(\frac{1}{k_2^+G + H} \right) \left[(k_2^+A + B) \ln \left(\frac{k_2^+A + B}{k_2^+G + H} \right) + (k_2^+C + D) \ln \left(\frac{k_2^+C + D}{k_2^+G + H} \right) + (k_2^+E + F) \ln \left(\frac{k_2^+E + F}{k_2^+G + H} \right) \right] \quad (7)$$

COMPARISON OF PREDICTED OPTIMAL VALUES OF FORWARD KINETIC CONSTANT WITH EXPERIMENTAL RESULTS

Optimal values of the forward rate constant k_2^+ predicted by MaxEP and MaxEnt are then obtained from the conditions

$$\frac{d\sigma}{dk_2^+} = 0, \quad (8)$$

$$\frac{dH}{dk_2^+} = 0. \quad (9)$$

The predicted and observed value of forward kinetic constants for three types of β -Lactamase enzymes are shown in Table. 1.

Table 1. The comparison of experimental and predicted values of the forward rate constants k_2^+ for three types of β -Lactamase enzymes.

Enzyme	k_2^+ [s ⁻¹] (MaxEP)	k_2^+ [s ⁻¹] (MaxEnt)	k_2^+ [s ⁻¹] (Observed)
PC1 - β Lactamase	281	94.5	173
RTEM β Lactamase	4034	1091	2800
β Lactamase I	6669	3548	4090

The values of k_2^+ predicted by MaxEP and MaxEnt are of the same order of magnitude as the observed values.

MAXENT AND MAXEP RELEVANCE FOR THE FUNCTIONAL DESIGN OF THE ROTARY ENZYME ATP

ATP synthase is an important biomolecular nanomotor. From an evolutionary viewpoint it is a very ancient secondary proton pump, which exploits the proton motive force created by respiration or photosynthesis to drive the synthesis of adenosine triphosphate (ATP), the most commonly used "energy currency" in living cells. ATP synthase is embedded in the inner membrane of mitochondria or in the thylakoid membrane of chloroplasts. ATP is formed from adenosine diphosphate (ADP) and inorganic phosphate (P), assuming that activation energy is available. This activation energy is stored and released as elastic energy in the stalk-like axle of the ATP synthase nanomotor. The rotary mechanism is well understood [7]. The stator is an ensemble of three structural subunits. Translocation of protons through this protein, driven by the transmembrane proton gradient, is accompanied by a stepped rotation of the stalk-like axle. Each 120° clockwise (or counter-clockwise) rotation is accompanied by the synthesis (or hydrolysis) of ATP. Here we will consider only the ATP synthase of chloroplast thylakoid membranes.

The number of protons translocated through the thylakoid membrane that is necessary for the synthesis of one ATP molecule is called the gearing ratio, $g \equiv H^+ / ATP$. The gearing ratio g is related to the free energy input E per revolution,

$$E = 3g\Delta\mu_{H^+} \quad (10)$$

where

$$\Delta\mu_{H^+} = 2.3RT\Delta pH - F\Delta\Psi, \quad (11)$$

is the transthylakoid proton motive force. F is the Faraday constant, while ΔpH and $\Delta\Psi$ are the transmembrane differences in pH and electric potentials, respectively. The 120° stalk rotation has a short ($\approx 2ms$) pause, called the catalytic dwell, at a certain relative angular position of stalk, denoted by κ (with $0 \leq \kappa \leq 1$). The catalytic dwell is so-called because it is associated with the internal transition (synthesis or hydrolysis of ATP) of ATP synthase. In accordance with our starting assumption this internal transition is most sensitive to evolution. Therefore we take κ as the variable that is optimized during evolution. The free energy (E) partly depends on external conditions (the difference between pH factors outside and inside of the membrane), and we take this to be an adjustable parameter as explained below.

We describe the synthesis and hydrolysis of ATP using the five-state kinetic model shown in Fig.4. The problem can be solved analytically, either by solving the steady-state rate equations directly [8] or by using Hill's diagram method [9]. Using experimental data obtained by Pänke and Rumberg [8, 10], we calculated the state probabilities $p_E(i|\kappa)$, the forward fluxes,

$$J_{E+}(\kappa) = k_{E_{syn}}(\kappa)p(O^*P^*ADP|\kappa)_E \quad (12)$$

and the backward fluxes

$$J_{E-}(\kappa) = k_{E_{hyd}}(\kappa)p(O^*ATP|\kappa)_E. \quad (13)$$

Rate coefficients $k_{E_{syn}}(\kappa)$ and $k_{E_{hyd}}(\kappa)$ are calculated within the transition state theory [11] and are given by

$$k_{E_{syn}}(\kappa) = k_{syn}^0 \exp(\kappa E / 3RT), \quad (14)$$

$$k_{E_{hyd}}(\kappa) = k_{hyd}^0 \exp(-(1-\kappa)E / 3RT). \quad (15)$$

The values of specific binding change constants $k_{syn}^0(\kappa) = 1.15 \cdot 10^{-3} s^{-1}$ $k_{hyd}^0(\kappa) = 4.5 \cdot 10^5 s^{-1}$ are taken from [8, 10]. Under controlled experimental conditions, the enzyme was illuminated in the presence of 1mM ADP, 1 mM P and 10 μ M ATP at $T=300K$ [8, 10]. Fixed kinetic rate constants are given in the legend of Fig. 4.

The number of ATP molecules produced per enzyme p per second is then

$$J_E(\kappa) = J_{E+}(\kappa) - J_{E-}(\kappa). \quad (16)$$

The Shannon information entropy of state probabilities, and entropy production of the internal enzymatic transitions, are

$$H_E(\kappa) = -\sum_1^5 p_E(i|\kappa) \log p_E(i|\kappa), \quad (17)$$

$$\sigma_E(\kappa) = RJ_E(\kappa) \log \frac{J_{E+}(\kappa)}{J_{E-}(\kappa)}, \quad (18)$$

respectively.

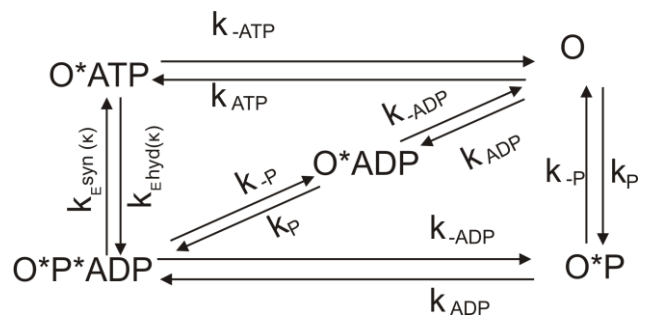


Figure 4. Kinetic model of ATP synthase cycle for transitions between enzyme open (O) states. O*P, O*ADP, O*ATP and O*P*ADP are states which bind P, ADP, ATP, and ADP respectively. Rate constants are expressed in same units when second-order rate constants are multiplied by substrate concentrations: $k_{ATP}=20.8s^{-1}$, $k_{-ATP}=270s^{-1}$, $k_{ADP}=8900s^{-1}$, $k_{-ADP}=490s^{-1}$, $k_P=810s^{-1}$ and $k_{-P}=2030s^{-1}$.

Our hypothesis is that the information entropy $H_E(\kappa)$ and entropy production $\sigma(\kappa)$ of a fully evolved enzyme are maximized at a common value of κ , the relative angular position of the catalytic dwell. That is,

$$\frac{\partial H_E(\kappa)}{\partial \kappa} = 0, \quad (19)$$

$$\frac{\partial \sigma_E(\kappa)}{\partial \kappa} = 0. \quad (20)$$

In order to obtain a solution, we adjust the free energy input E until there is a common value of κ that satisfies both equations (19) and (20). In other words, we are simultaneously optimizing κ and E .

The numerical calculations are shown in Fig. 5. The solution yields optimal values $\kappa_{opt} = 0.598$ and $E_{opt} = 161.4$ kJ/mol. The former value is very close to the empirical estimate $\kappa_{opt} = 0.6$ [8]. From equation (10), the optimal proton motive force $\Delta\mu_H = 13.4$ kJ/mol and calculated free energy $E_{opt} = 161.4$ kJ/mol corresponds to the gearing ratio $g=4$ observed in chloroplasts [12].

In summary, our calculations show that ATP synthase is a fully evolved enzyme in the sense of MaxEnt and MaxEP. It is also interesting that the optimal solution of MaxEnt and MaxEP coincides with an inflection point of the curve of ATP synthesis rate (J_E) versus proton motive force (Fig. 5); this feature allows fast metabolic control with respect to short-term changes in proton motive force, as well as a high optimal output/input free energy ratio of 69% [9].

CONCLUSIONS

Energy transduction is the central concept in physics, from the energy conservation principle to thermodynamics. One of the better known results from non-equilibrium thermodynamics is Prigogine's theorem of minimal entropy production [6]. It is valid close to thermodynamic equilibrium. The theorem defines a non-equilibrium stationary state, called the static head state. Non-equilibrium stationary states are the main interest to us here. Free-energy transduction and efficiency are zero in the static head stationary state, which can be considered as the closest non-equilibrium relative of the equilibrium state. Coupling downhill and uphill free energy changes is essential for all life, but this is impossible in the static head state. Life must look to other non-equilibrium steady states with a non-vanishing efficiency of free-energy transduction.

In contrast to static head state, which is the steady state with zero efficiency of free-energy transduction, MaxEP principle applied to β -lactamase enzymes and ATP synthase has predicted good order of magnitude relevant kinetic constants and reasonable efficiency of energy conversion.

Beside MaxEP we use MaxEnt principle and apply it to predict the probabilities of biomolecular states. It is a powerful inference algorithm for solving problems with incomplete available information. In physics, the whole of equilibrium statistical physics can be derived from this principle [13, 14]. At first sight, it might seem that biological evolution, by building ever more structurally complex macromolecules (i.e. of low configurational entropy), has proceeded in the direction of entropy decrease rather than

entropy increase. But when we look at the kinetics of β -lactamase enzymes and functional design of ATP synthase, as we have done here, we find that biological evolution is consistent with MaxEnt. There is no contradiction with the second law. The evolutionary optimization of β -lactamase enzymes and ATP synthase can be interpreted as selection of the most probable functional design within the constraints considered here.

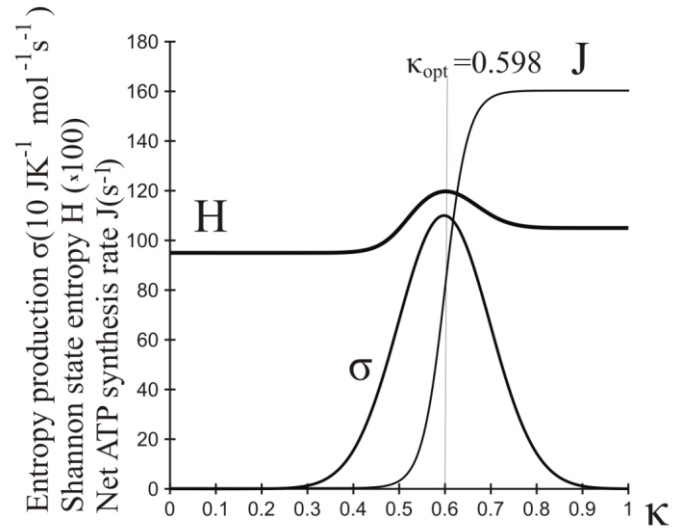


Figure 5. Information entropy of state probabilities, entropy production and net ATP synthesis rate as a function of relative angular position of catalytic dwell at optimal input free energy $E_{opt}=161.4$ kJmol⁻¹.

NOMENCLATURE

Symbol	Quantity	SI Unit
σ	Entropy production	$JK^{-1}s^{-1}$
J	Flux	s^{-1}
X	Thermodynamic force	J
$[E]$	Concentration of E species	m^{-3}
$k_i^{+(-)}$	Forward (backward) kinetic constant of i^{th} transition	s^{-1}
A	Affinity	J
H	Information entropy	
p_i	Probability	
E	Free energy	J
g	Gearing ratio	
$\Delta\mu_{H^+}$	Proton motive force	J
F	Faraday constant	$C\ mol^{-1}$
κ	Relative angular position of catalytic dwell	

REFERENCES

- [1] A. Dobovišek, P. Županović, M. Brumen, Ž. Bonačić-Lošić, D. Kuić and D. Juretić, Enzyme kinetics and the maximum entropy production principle. *Biophys. Chem.*, vol. 154, pp.49-55, 2011.
- [2] A. Dobovišek, P. Županović, M. Brumen and D. Juretić, Maximum entropy production and maximum Shannon entropy as germane principles for the evolution of enzyme, in R. Dewar, R. Niven and K. Regenauer (eds.), *Beyond the Second Law: Entropy Production and Non-Equilibrium Systems*, Springer Verlag, to be published.
- [3] R.C. Dewar, D. Juretić and P. Županović, The functional design of the rotary enzyme ATP synthase is consistent with maximum entropy production. *Chem. Phys. Lett.*, vol 430, pp. 177–182, 2006.
- [4] P. Glansdorff and I. Prigogine, *Thermodynamic theory of structure, stability and fluctuations*. John Wiley & Sons, New York, 1971.
- [5] L.M. Martyushev and V.D. Seleznev, Maximum entropy production principle in physics, chemistry and biology, *Phys. Rep.*, vol 426, pp. 1-45, 2006.
- [6] W.J. Albery and J.R. Knowles, Evolution of enzyme function and the development of catalytic efficiency *Biochemistry*, vol 15, pp. 5631–5640, 1976.
- [7] P.D. Boyer, The ATP synthase –a splendid molecular machine. *Ann. Rev. Biochem.*, vol 66, pp. 717-749, 1997
- [8] O. Pänke and B. Rumberg, Kinetic modeling of rotary CF0F1-ATP synthase: storage of elastic energy during energy transduction. *Biochim. Biophys. Acta*, vol 1412, pp. 118-128, 1999.
- [9] T. Hill, *Free Energy Transduction and Biochemical Cycle Kinetics*, Dover Publications, Inc. New York, 2005.
- [10] O. Pänke and B. Rumberg, Kinetic modelling of the proton translocating CF0CF1-ATP synthase from spinach. *FEBS Lett.*, vol 383, pp. 196-200, 1996.
- [11] R.C. Dewar, D. Juretić and P. Županović, The functional design of the rotary enzyme ATP synthase is consistent with maximum entropy production. *Chem. Phys. Lett.*, vol 430, pp. 177–182, 2006.
- [12] P. Turina, D. Samoray and P. Graeber, H⁺/ATP ratio of proton transport-coupled ATP synthesis and hydrolysis catalysed by CF0F1-liposomes. *Eur. Mol. Biol. Org. J.*, vol 22, pp. 418-426, 2003.
- [13] E.T. Jaynes, Information theory and statistical mechanics. *Phys. Rev.*, vol 106, p. 620–630, 1957.
- [14] E.T. Jaynes, Information theory and statistical mechanics II. *Phys. Rev.*, vol 108, pp. 171–190, 1957.

PANEL D

**MAXIMUM ENTROPY PRODUCTION, STEEPEST
ENTROPY ASCENT, DISSIPATION POTENTIALS,
AND VARIATIONAL PRINCIPLES:
HOW UNIVERSAL AND INTERRELATED?**

STEEPEST-ENTROPY-ASCENT AND MAXIMAL-ENTROPY-PRODUCTION DYNAMICAL MODELS OF IRREVERSIBLE RELAXATION TO STABLE EQUILIBRIUM FROM ANY NON-EQUILIBRIUM STATE. UNIFIED TREATMENT FOR SIX NON-EQUILIBRIUM FRAMEWORKS

Gian Paolo Beretta

Università di Brescia, via Branze 38, 25123 Brescia, Italy, Email: beretta@ing.unibs.it

ABSTRACT

By suitable reformulations, we review the mathematical frameworks of six different approaches to the description of non-equilibrium dynamics with the purpose to set up a unified formulation of the Maximum Entropy Production (MEP) principle valid in all these contexts. In this way, we extend to such frameworks the concept of Steepest Entropy Ascent dynamics introduced by the present author in previous work on quantum thermodynamics. Actually, the present formulation constitutes a generalization also in the quantum thermodynamics framework. The analysis emphasizes that in the SEA-inspired implementation of the MEP principle, a key role is played by the geometrical metric with respect to which to measure the length of a trajectory in state space. The metric tensor turns out to be directly related to the inverse of the Onsager's generalized conductivity tensor. We conclude that in most of the existing theories of non-equilibrium the time evolution of the state representative can be seen to actually follow in state space the path of SEA with respect to a suitable metric connected with the generalized conductivities. The resulting unified family of SAE/MEP dynamical models are all intrinsically consistent with the second law of thermodynamics. The nonnegativity of the entropy production is a general and readily proved feature of SEA dynamics. In several of the different approaches to non-equilibrium description we consider here, the SEA concept has not been investigated before. Therefore, it is hoped that the present unifying approach may prove useful in providing a fresh basis for effective, thermodynamically consistent, numerical models and theoretical treatments of irreversible conservative relaxation towards equilibrium from far non-equilibrium states. The six mathematical frameworks are: A) Classical Statistical Mechanics; B) Small-Scale and Rarefied Gases Dynamics (i.e., kinetic models for the Boltzmann equation); C) Statistical or Information Theoretic Models of Relaxation; D) Rational Extended Thermodynamics, Macroscopic Non-Equilibrium Thermodynamics, and Chemical Kinetics; E) Mesoscopic Irreversible Thermodynamics; F) Quantum Statistical Mechanics, Quantum Thermodynamics, Mesoscopic Non-Equilibrium Quantum Thermodynamics, and Intrinsic Quantum Thermodynamics.

INTRODUCTION

The problem of understanding entropy and irreversibility has been tackled by a large number of preeminent scientists during the past century. Schools of thought have formed and flourished around different perspectives of the problem. Several modeling approaches have been developed in various frameworks to deal with the many facets of non-equilibrium.

In this paper, we show how to construct Steepest Entropy Ascent (SEA) and Maximum Entropy Production (MEP) models of non-equilibrium dynamics by adopting a unified mathematical formulation that allows us to do it at once in several different well-known frameworks of non-equilibrium description.

To avoid doing inevitable injustices to the many pioneers of all these approaches and to the many and growing fields of their application, here we skip a generic introduction and given no references nor a review of previous work. Rather, we dig immediately into the mathematical reformulations of the different frameworks in such a way that then the construction of the proposed SEA dynamics becomes formally a single geometrical problem that can be treated at once.

Our reformulations here not only allow a unified treatment of the MEP principle (for a recent review see [1]) in the various frameworks, but also extends to all frameworks an observation that we have been developing in the quantum thermodynamics

framework for the last three decades [2; 3; 4; 5]. In doing so, we introduce an important generalization also in the quantum thermodynamics framework.

The observation is that we cannot simply maximize the entropy production subject to a set of conservation constraints or boundary conditions, but in order to identify a SEA path in state space we must equip it with a metric with respect to which to compute the distance traveled in state space during the time evolution.

The generalization is as follows. In our previous work, we adopted the proper uniform metric for probability distributions, namely, the Fisher-Rao metric, because in quantum thermodynamics the state representative, the density operator, is essentially a generalized probability distribution. In other frameworks, however, the state representative not always is a probability distribution. Moreover, the present application to the framework of Mesoscopic Non-Equilibrium Thermodynamics [6; 7] shows that standard results such as the Fokker-Planck equation and Onsager theory emerge as straightforward results of SEA/MEP dynamics with respect to a metric characterized by a generalized metric tensor that is directly related to the inverse of the generalized conductivity tensor. Since the generalized conductivities represent, at least in the near-equilibrium regime, the strength of the system's reaction when pulled out of equilibrium, it appears that their inverse, i.e., the generalized resistivity

tensor, represents the metric with respect to which the time evolution, at least in the near equilibrium, is locally SEA/MEP.

But the local SEA/MEP construction does much more, because it offers a strongly thermodynamically consistent way to extend the well-known near-equilibrium theories to the treatment of non-equilibrium states.

An investigation of the interrelations between the SEA and MEP concepts and Ziegler's [8] and Edelen's [9] formulations for the study of highly non-equilibrium dynamics in the nonlinear domain is under way and will be communicated elsewhere.

The unified formulation of the local SAE/MEP variational problem is as follows and it is not restricted to near equilibrium: *the time evolution and transport equations advance the local state representative in the direction of maximal entropy production per unit of distance traveled in state space compatible with the conservation constraints.* The measure of distance traveled in state space requires the choice of a metric defined over the state space. The standard near-equilibrium results obtain when the local metric tensor is proportional to the inverse of the local matrix of generalized conductivities.

In the next six sections we introduce slightly nonstandard notations in several non-equilibrium contexts with the purpose to formulating, in the seventh section, a unified construction and implementation of the SAE/MEP concept.

FRAMEWORK A: CLASSICAL STATISTICAL MECHANICS

Let Ω be the classical position-momentum q - p phase space, and \mathcal{L} the set of real, square-integrable functions A, B, \dots on Ω , equipped with the inner product $(\cdot|\cdot)$ defined by

$$(A|B) = \text{Tr}(AB) = \int_{\Omega} AB \, d\Omega \quad (1)$$

where $\text{Tr}(\cdot)$ in this framework denotes $\int_{\Omega} \cdot \, d\Omega$, with $d\Omega = d\mathbf{q} \, d\mathbf{p}$.

In Classical Statistical Mechanics, the index of statistics from a generally heterogeneous ensemble of identical systems (with associated phase space Ω) distributed over a range of possible classical mechanical states is represented by a nonnegative (Gibbs) density-of-phase distribution function $f_G = f_G(\mathbf{q}, \mathbf{p}, t)$ in \mathcal{L} .

Borrowing from the formalism we originally developed for the quantum framework [2; 3] (later introduced also in [4; 10]), in order to easily impose the constraint of preservation of the nonnegativity of f_G during its time evolution, we adopt as state representative not f_G itself but its square root, that we assume is a function in \mathcal{L} that denote by $\gamma = \gamma(\mathbf{q}, \mathbf{p}, t)$. Normalization is not imposed at this stage but later as one of the constraints. Therefore, we clearly have

$$f_G = \gamma^2, \quad \frac{\partial f_G}{\partial t} = 2\gamma \frac{\partial \gamma}{\partial t} \quad (2)$$

$$\frac{\partial f_G}{\partial \mathbf{q}} = 2\gamma \frac{\partial \gamma}{\partial \mathbf{q}}, \quad \frac{\partial f_G}{\partial \mathbf{p}} = 2\gamma \frac{\partial \gamma}{\partial \mathbf{p}}, \quad \{H, f_G\} = 2\gamma \{H, \gamma\} \quad (3)$$

where $\{\cdot, \cdot\}$ denotes the Poisson bracket.

Among the phase-space functions that represent physical observables we focus on the conserved ones that we denote synthetically by the set

$$\{C_i\} = \{H, M_x, M_y, M_z, N_1, \dots, N_r, I\} \quad (4)$$

where H is the classical Hamiltonian function, M_j the momentum function for the j -th component, N_i the number-of-particle function for particles of type i , and $I = 1$ is the constant unity function, so that $\text{Tr}(\gamma^2 H)$ represents the mean energy, $\text{Tr}(\gamma^2 \mathbf{M})$

the mean momentum vector, $\text{Tr}(\gamma^2 N_i)$ the mean number of particles of type i , and $\text{Tr}(\gamma^2 I)$ the normalization condition on f_G .

The description of an irreversible diffusion-relaxation process in this framework can be done by assuming a evolution equation for the state f_G given by

$$\frac{d\gamma}{dt} = \Pi_{\gamma} \quad \text{where} \quad \frac{d}{dt} = \frac{\partial}{\partial t} - \{H, \cdot\} \quad (5)$$

It is easy to verify that for $\Pi_{\gamma} = 0$ Eq. (5) reduces to Liouville's equation of classical reversible evolution. We do not make this assumption because we are interested in modeling irreversible evolution with energy, momentum, and particle numbers redistribution towards equilibrium, subject to the overall conservation of energy, momentum, number of particles of each kind, and normalization

$$\Pi_{C_i} = \frac{d}{dt} \text{Tr}(\gamma^2 C_i) = (2\gamma C_i | \Pi_{\gamma}) = 0 \quad (6)$$

The entropy state functional in this context is represented by

$$S(\gamma) = -k \text{Tr}(f_G \ln f_G) = (-k\gamma \ln \gamma^2 | \gamma) \quad (7)$$

so that the rate of entropy production under a time evolution that preserves the normalization of f_G is given by

$$\Pi_S = -k \frac{d}{dt} \text{Tr}(f_G \ln f_G) = (-2k\gamma \ln \gamma^2 | \Pi_{\gamma}) \quad (8)$$

Below, in the section on SAE/MEP dynamics, we construct an equation of motion for the square-root-of-density-of-phase distribution γ such that Π_S is maximal subject to the conservation constraints $\Pi_{C_i} = 0$ and a suitable additional constraint we discuss therein.

FRAMEWORK B: SMALL-SCALE AND RAREFIED GASES DYNAMICS

Let Ω_c be the classical one-particle velocity space, and \mathcal{L} the set of real, square-integrable functions A, B, \dots on Ω_c , equipped with the inner product $(\cdot|\cdot)$ defined by

$$(A|B) = \text{Tr}(AB) = \int_{\Omega_c} AB \, d\Omega_c \quad (9)$$

where $\text{Tr}(\cdot)$ in this framework denotes $\int_{\Omega_c} \cdot \, d\Omega_c$, with $d\Omega_c = dc_x \, dc_y \, dc_z$.

In the Kinetic Theory of Rarefied Gases and Small-Scale Hydrodynamics [11], the probability to find a particle at position \mathbf{x} with velocity between \mathbf{c} and $\mathbf{c} + d\mathbf{c}$ [where of course $\mathbf{c} = (c_x, c_y, c_z)$] is given by $f(\mathbf{x}, \mathbf{c}, t) \, d\Omega_c / \int_{\Omega_c} f \, d\Omega_c$ where $f(\mathbf{x}, \mathbf{c}, t)$ is the local phase-density distribution which for every position \mathbf{x} and time instant t is a function in \mathcal{L} .

Also in this framework, in order to easily impose the constraint of preservation of the nonnegativity of f during its time evolution, we introduce the local one-particle state representation not by f itself but by its square root, that we assume is a function in \mathcal{L} that we denote by $\gamma = \gamma(\mathbf{x}, \mathbf{c}, t)$. Therefore, we have

$$f = \gamma^2, \quad \frac{\partial f}{\partial t} = 2\gamma \frac{\partial \gamma}{\partial t}, \quad \frac{\partial f}{\partial \mathbf{x}} = 2\gamma \frac{\partial \gamma}{\partial \mathbf{x}}, \quad \frac{\partial f}{\partial \mathbf{c}} = 2\gamma \frac{\partial \gamma}{\partial \mathbf{c}} \quad (10)$$

Again, among the velocity-space functions that represent physical observables we focus on the conserved ones that we denote synthetically by the set

$$\{C_i\} = \{H = \frac{1}{2} m \mathbf{c} \cdot \mathbf{c}, M_x = m c_x, M_y = m c_y, M_z = m c_z, m\} \quad (11)$$

of functions in \mathcal{L}_c where H is the local kinetic energy function, M_x, M_y, M_z the components of the local momentum function, and m the particle mass, so that $\text{Tr}(\gamma^2 H)$ represents the local kinetic energy density, $\text{Tr}(\gamma^2 M_i)$ the i -th component of the local momentum density, and $\text{Tr}(\gamma^2 m)$ the local mass density.

The time evolution of the distribution function f is given by the Boltzmann equation or some equivalent simplified kinetic model equation, which in terms of the square-root distribution may be written in the form

$$\frac{D\gamma}{Dt} = \Pi_\gamma \quad \text{where} \quad \frac{D}{Dt} = \frac{\partial}{\partial t} + \mathbf{c} \cdot \frac{\partial}{\partial \mathbf{x}} + \mathbf{a} \cdot \frac{\partial}{\partial \mathbf{c}} \quad (12)$$

and \mathbf{a} denotes the particle acceleration due to external body forces.

In order to satisfy the constraints of energy, momentum, and mass conservation the collision term Π_γ must be such that

$$\Pi_{C_i} = \frac{\partial \text{Tr}(f C_i)}{\partial t} + \nabla \cdot \text{Tr}(f \mathbf{c} C_i) = (2\gamma C_i | \Pi_\gamma) = 0 \quad (13)$$

The local entropy density functional in this context is represented by

$$S(\mathbf{x}, t) = -k \text{Tr}(f \ln f) = (-k\gamma \ln \gamma^2 | \gamma) \quad (14)$$

so that the rate of entropy production under a time evolution that preserves the normalization of f is given by

$$\Pi_S = -k \frac{\partial \text{Tr}(f \ln f)}{\partial t} - k \nabla \cdot \text{Tr}(f \mathbf{c} \ln f) = (-2k\gamma \ln \gamma^2 | \Pi_\gamma) \quad (15)$$

Below, in the section on SAE/MEP dynamics, we construct a new family of models for the collision term Π_γ such that Π_S is maximal subject to the conservation constraints $\Pi_{C_i} = 0$ and a suitable additional constraint we discuss therein.

The resulting new family of SEA kinetic models of the collision integral in the Boltzmann equation is currently under investigation by comparing it with standard models such as the well-known BGK model as well as with Monte Carlo simulations of the original Boltzmann equation for hard spheres [12]. In addition to the strong thermodynamics consistency even far from stable equilibrium, Ref. [12] gives a proof that in the near-equilibrium limit the SEA model reduces to the BGK model.

FRAMEWORK C: STATISTICAL OR INFORMATION THEORETIC MODELS OF RELAXATION TO EQUILIBRIUM

Let \mathcal{L} be the set of all $n \times n$ real, diagonal matrixes $A = \text{diag}(a_j)$, $B = \text{diag}(b_j)$, \dots ($n \leq \infty$), equipped with the inner product $(\cdot | \cdot)$ defined by

$$(A|B) = \text{Tr}(AB) = \sum_{j=1}^n a_j b_j \quad (16)$$

In Information Theory [13], the probability assignment to a set of n events, p_j being the probability of occurrence of the j -th event is represented by $\rho = \text{diag}(p_j)$. Again, in order to easily impose the constraint of preservation of the nonnegativity of the probabilities during their time evolution, we adopt the description in terms of the square-root of ρ that we denote by

$$\gamma = \text{diag}(\sqrt{p_j}) \quad (17)$$

Typically we consider a set of conserved features of the process

$$\{C_i\} = \{H, N_1, \dots, N_r, I\} \quad (18)$$

of diagonal matrixes $H = \text{diag}(e_j)$, $N_1 = \text{diag}(n_{1j})$, \dots , $N_r = \text{diag}(n_{rj})$, $I = \text{diag}(1)$ in \mathcal{L} representing characteristic features of the events in the set, which for the j -th event take on respectively the values e_j , n_{1j} , \dots , n_{rj} . The corresponding expectation values are $\text{Tr}(\rho H) = \sum_{j=1}^n p_j e_j$, $\text{Tr}(\rho N_1) = \sum_{j=1}^n p_j n_{1j}$, \dots , $\text{Tr}(\rho N_r) = \sum_{j=1}^n p_j n_{rj}$, and $\text{Tr}(\rho I) = \sum_{j=1}^n p_j = 1$ thus providing the normalization condition on ρ .

The time evolution of the square-root probability distribution γ is the solution of the rate equation

$$\frac{d\gamma}{dt} = \Pi_\gamma \quad (19)$$

where in order to satisfy the constraints of conservation of the expectation values $\text{Tr}(\rho C_i)$ the term Π_γ must be such that

$$\Pi_{C_i} = \frac{d}{dt} \text{Tr}(\rho C_i) = (2\gamma C_i | \Pi_\gamma) = 0 \quad (20)$$

The entropy functional in this context is represented by

$$S(\gamma) = -k \text{Tr}(\rho \ln \rho) = (-k\gamma \ln \gamma^2 | \gamma) \quad (21)$$

so that the rate of entropy production under a time evolution that preserves the normalization of ρ is given by

$$\Pi_S = -k \frac{d}{dt} \text{Tr}(\rho \ln \rho) = (-2k\gamma \ln \gamma^2 | \Pi_\gamma) \quad (22)$$

Below, in the section on SAE/MEP dynamics, we construct a model for the rate term Π_γ such that Π_S is maximal subject to the conservation constraints $\Pi_{C_i} = 0$ and a suitable additional constraint we discuss therein.

An attempt along the same lines has been presented in [14].

FRAMEWORK D: RATIONAL EXTENDED THERMODYNAMICS, MACROSCOPIC NON-EQUILIBRIUM THERMODYNAMICS, AND CHEMICAL KINETICS

Let \mathcal{L} be the set of all $n \times n$ real, diagonal matrixes $A = \text{diag}(a_j)$, $B = \text{diag}(b_j)$, \dots ($n \leq \infty$), equipped with the inner product $(\cdot | \cdot)$ defined by

$$(A|B) = \text{Tr}(AB) = \sum_{j=1}^n a_j b_j \quad (23)$$

In Rational Extended Thermodynamics [15], the local state at position \mathbf{x} and time t of the continuum under study is represented by an element γ in \mathcal{L} , i.e.,

$$\gamma(\mathbf{x}, t) = \text{diag}[\alpha(\mathbf{x}, t)] \quad (24)$$

Thus, $\gamma(\mathbf{x}, t)$ represents the set of fields which represent the instantaneous spatial distributions within the continuum of the local densities that define all its other local properties. In particular, for the conserved properties energy, momentum, and mass it is assumed that their local densities and their local fluxes are all given by particular functions of γ that we denote synthetically by

$$\{C_i(\gamma)\} = \{E(\gamma), M_x(\gamma), M_y(\gamma), M_z(\gamma), m(\gamma)\} \quad (25)$$

$$\{\mathbf{J}_{C_i}(\gamma)\} = \{\mathbf{J}_E(\gamma), \mathbf{J}_{M_x}(\gamma), \mathbf{J}_{M_y}(\gamma), \mathbf{J}_{M_z}(\gamma), \mathbf{J}_m(\gamma)\} \quad (26)$$

so that the energy, momentum, and mass balance equations take the form

$$\frac{DC_i}{Dt} = \frac{\partial C_i}{\partial t} + \nabla \cdot \mathbf{J}_{C_i} = \Pi_{C_i} = 0 \quad (27)$$

Moreover, also for the local entropy density and the local entropy flux it is assumed that they are given by particular functions of γ that we denote respectively by

$$S(\gamma) \quad \text{and} \quad \mathbf{J}_S(\gamma) \quad (28)$$

so that the entropy balance equation takes the form

$$\frac{DS}{Dt} = \frac{\partial S}{\partial t} + \nabla \cdot \mathbf{J}_S = \Pi_S \quad (29)$$

where Π_S is the local production density.

In general the balance equation for each of the underlying field properties is

$$\frac{D\alpha_j}{Dt} = \frac{\partial \alpha_j}{\partial t} + \nabla \cdot \mathbf{J}_{\alpha_j} = \Pi_{\alpha_j} \quad (30)$$

where \mathbf{J}_{α_j} and Π_{α_j} are the corresponding flux and production density, respectively. Equivalently, this set of balance equations may be written synthetically as

$$\frac{D\gamma}{Dt} = \frac{\partial \gamma}{\partial t} + \nabla \cdot \mathbf{J}_\gamma = \Pi_\gamma \quad (31)$$

where $\mathbf{J}_\gamma = \text{diag}[\mathbf{J}_{\alpha_j}]$ and $\Pi_\gamma = \text{diag}[\Pi_{\alpha_j}]$.

It is then further assumed that there exist functions $\Phi_{\alpha_j}(\gamma)$ (Liu's Lagrange multipliers [16]) that we denote here in matrix form by

$$\Phi = \text{diag}(\Phi_{\alpha_j}) \quad (32)$$

such that the local entropy production density can be written as

$$\Pi_S = \sum_{j=1}^n \Phi_{\alpha_j} \Pi_{\alpha_j} = (\Phi | \Pi_\gamma) \quad (33)$$

and must be nonnegative everywhere.

For our development in this paper we shall additionally assume that there also exist functions $\Psi_{i\alpha_j}(\gamma)$ that we denote in vector form by

$$\Psi_i = \text{diag}(\Psi_{i\alpha_j}) \quad (34)$$

such that the production density of each conserved property C_i can be written as

$$\Pi_{C_i} = \sum_{j=1}^n \Psi_{i\alpha_j} \Pi_{\alpha_j} = (\Psi_i | \Pi_\gamma) \quad (35)$$

Typically, but not necessarily, the first five underlying fields $\alpha_j(\mathbf{x}, t)$ for $j = 1, \dots, 5$ are conveniently chosen to coincide with the energy, momentum, and mass densities, so that Eqs. (30) for $j = 1, \dots, 5$ coincide with Eqs. (27) because $\Pi_{\alpha_j} = 0$ for this subset of conserved fields.

The above framework reduces to the traditional Onsager theory of macroscopic Non-Equilibrium Thermodynamics (NET) [6] if the α_j 's are taken to represent the local deviations of the underlying fields from their equilibrium values. In this context, the usual notation calls the functions $X_{\alpha_j} = -\Phi_{\alpha_j}$ the "thermodynamic forces" and Π_{α_j} the "thermodynamic currents".

The same framework reduces to the standard scheme of Chemical Kinetics (CK) if the α_j 's are taken to represent the local reaction coordinates, Π_{α_j} the local rate of advancement of reaction j , Φ_{α_j} its entropic affinity, C_i the local concentration of atomic elements of kind i , $\Pi_{C_i} = 0$ their local production density.

Below, in the section on SAE/MEP dynamics, we construct an equation of motion for γ such that Π_S is maximal subject to the conservation constraints $\Pi_{C_i} = 0$ and a suitable additional constraint we discuss therein.

FRAMEWORK E. MESOSCOPIC NON-EQUILIBRIUM THERMODYNAMICS

Let \mathcal{L} be the set of all $n \times n$ diagonal matrixes $A = \text{diag}(a_j(\gamma))$, $B = \text{diag}(b_j(\gamma))$, ... whose entries $a_j(\gamma)$, $b_j(\gamma)$, ... are real, square-integrable functions of a set of mesoscopic properties usually denoted by $\alpha_1, \dots, \alpha_m$ that here we denote synthetically by defining the matrix

$$\gamma = \text{diag}(\alpha_1, \dots, \alpha_m) \quad (36)$$

and denoting its m -dimensional range by Ω_γ , usually called the α -space. Let \mathcal{L} be equipped with the inner product $(\cdot | \cdot)$ defined by

$$(A | B) = \sum_{i=1}^n \text{Tr}(a_i b_i) = \sum_{i=1}^n \int_{\Omega_\gamma} a_i(\gamma) b_i(\gamma) d\Omega_\gamma \quad (37)$$

where $\text{Tr}(\cdot)$ in this framework denotes $\int_{\Omega_\gamma} \cdot d\Omega_\gamma$, with $d\Omega_\gamma = d\alpha_1 \cdots d\alpha_m$.

In Mesoscopic Non-Equilibrium Thermodynamics (MNET) (see, e.g., [6]) the α_j 's are the set of mesoscopic (coarse grained) local extensive properties assumed to represent the local non-equilibrium state of the portion of continuum under

study. The mesoscopic description of the local state at position \mathbf{x} and time t is in terms of a probability density on the α -space Ω_γ , that we denote by $P(\gamma; \mathbf{x}, t)$. $P(\gamma; \mathbf{x}, t) d\Omega_\gamma$ represents the probability that the values of the underlying fields are between γ and $\gamma + d\gamma$.

It is assumed that the probability density P obeys a continuity equation that we may write as follows

$$\frac{DP}{Dt} = \frac{\partial P}{\partial t} + \mathbf{c} \cdot \nabla P = -\nabla_\gamma \cdot \Pi_\gamma \quad (38)$$

where $\mathbf{c} = \mathbf{c}(\gamma)$ is the particle velocity expressed in terms of the underlying fields (usually it is convenient to take the first three α_j 's to coincide with the velocity components) and we define for shorthand

$$\Pi_\gamma = \text{diag}(\Pi_{\alpha_j}) \quad \text{and} \quad \nabla_\gamma = \text{diag} \left(\frac{\partial}{\partial \alpha_j} \right) \quad (39)$$

where the Π_{α_j} 's are interpreted as the components of a streaming flux in Ω_γ , i.e., a current in the space of mesoscopic coordinates.

The conserved fields $C_i(\mathbf{x}, t)$ have an associated underlying extensive property which can be expressed in terms of the mesoscopic coordinates as $\psi_i(\gamma)$. They obey the balance equation

$$\frac{DC_i}{Dt} = \frac{\partial C_i}{\partial t} + \nabla \cdot \mathbf{J}_{C_i} = \Pi_{C_i} = 0 \quad (40)$$

where local density $C_i(\mathbf{x}, t)$, the local flux $\mathbf{J}_{C_i}(\mathbf{x}, t)$ and the local production density $\Pi_{C_i}(\mathbf{x}, t)$ are defined as follows

$$\begin{aligned} C_i(\mathbf{x}, t) &= \int_{\Omega_\gamma} \psi_i(\gamma) P(\gamma; \mathbf{x}, t) d\Omega_\gamma \\ \mathbf{J}_{C_i}(\mathbf{x}, t) &= \int_{\Omega_\gamma} \psi_i(\gamma) \mathbf{c}(\gamma) P(\gamma; \mathbf{x}, t) d\Omega_\gamma \\ \Pi_{C_i}(\mathbf{x}, t) &= \int_{\Omega_\gamma} \psi_i(\gamma) \frac{DP}{Dt}(\gamma; \mathbf{x}, t) d\Omega_\gamma \\ &= - \int_{\Omega_\gamma} \psi_i(\gamma) \nabla_\gamma \cdot \Pi_\gamma d\Omega_\gamma \\ &= \int_{\Omega_\gamma} \Pi_\gamma \cdot \nabla_\gamma \psi_i(\gamma) d\Omega_\gamma \\ &= (\Psi_i | \Pi_\gamma) \end{aligned} \quad (41)$$

where in the next to the last equation we integrated by parts and assumed that currents in α -space decay sufficiently fast to zero as the γ_j 's $\rightarrow \infty$, and we defined

$$\Psi_i = \nabla_\gamma \psi_i(\gamma) \quad (42)$$

The entropy balance equation takes the form

$$\frac{DS}{Dt} = \frac{\partial S}{\partial t} + \nabla \cdot \mathbf{J}_S = \Pi_S \quad (43)$$

where the local density $S(\mathbf{x}, t)$, the local flux $\mathbf{J}_S(\mathbf{x}, t)$ and the local production density $\Pi_S(\mathbf{x}, t)$ are defined in terms of the associated extensive property expressed in terms of the mesoscopic coordinates as

$$\phi(\gamma) = -k \ln P(\gamma) \quad (44)$$

as follows

$$\begin{aligned} S(\mathbf{x}, t) &= \int_{\Omega_\gamma} \phi(\gamma) P(\gamma; \mathbf{x}, t) d\Omega_\gamma \\ \mathbf{J}_S(\mathbf{x}, t) &= \int_{\Omega_\gamma} \phi(\gamma) \mathbf{c}(\gamma) P(\gamma; \mathbf{x}, t) d\Omega_\gamma \\ \Pi_S(\mathbf{x}, t) &= \int_{\Omega_\gamma} \phi(\gamma) \frac{DP}{Dt}(\gamma; \mathbf{x}, t) d\Omega_\gamma \\ &= - \int_{\Omega_\gamma} \phi(\gamma) \nabla_\gamma \cdot \Pi_\gamma d\Omega_\gamma \\ &= \int_{\Omega_\gamma} \Pi_\gamma \cdot \nabla_\gamma \phi(\gamma) d\Omega_\gamma \\ &= (\Phi | \Pi_\gamma) \end{aligned} \quad (45)$$

where again in the next to the last equation we integrated by parts and we defined

$$\Phi = \nabla_\gamma \phi(\gamma) \quad (46)$$

Below, in the section on SAE/MEP dynamics, we construct an equation of motion for γ such that Π_S is maximal subject to the conservation constraints $\Pi_{C_i} = 0$ and a suitable additional constraint we discuss therein. The result, when introduced in Eq. (38) will yield the Fokker-Planck equation for $P(\gamma; \mathbf{x}, t)$ which is also related (see, e.g., [17]) to the GENERIC structure [18]. The formalism can also be readily extended to the family of Tsallis [19] entropies in the frameworks of non-extensive thermodynamic models [20].

FRAMEWORK F: QUANTUM STATISTICAL MECHANICS, QUANTUM INFORMATION THEORY, QUANTUM THERMODYNAMICS, MESOSCOPIC NON-EQUILIBRIUM QUANTUM THERMODYNAMICS, AND INTRINSIC QUANTUM THERMODYNAMICS

Let \mathcal{H} be the Hilbert space ($\dim \mathcal{H} \leq \infty$) associated with the physical system, and \mathcal{L} the set of all linear operators A, B, \dots on \mathcal{H} , equipped with the real inner product $(\cdot | \cdot)$ defined by

$$(A|B) = \text{Tr}(A^\dagger B + B^\dagger A) / 2 \quad (47)$$

where A^\dagger denotes the adjoint of operator A and $\text{Tr}(\cdot)$ the trace functional.

In the quantum frameworks that we consider in this section, the state representative is the density operator ρ , i.e., a unit-trace, self-adjoint, and nonnegative-definite element of \mathcal{L} .

Instead, also here we will adopt the state representation in terms of the generalized square root of the density operator, that we developed in this context [2; 3; 4; 5] in order to easily impose the constraints of preservation of both the nonnegativity and the self-adjointness of ρ during its time evolution. Therefore, we assume that the state representative is an element γ in \mathcal{L} from which we can compute the density operator as follows

$$\rho = \gamma \gamma^\dagger \quad (48)$$

In other words, we adopt as state representative not the density operator ρ itself but its generalized square root γ . Therefore, we clearly have

$$\frac{d\rho}{dt} = \gamma \frac{d\gamma^\dagger}{dt} + \frac{d\gamma}{dt} \gamma^\dagger \quad (49)$$

We then consider the set of operators corresponding to the conserved properties, denoted synthetically as

$$\{C_i\} = \{H, M_x, M_y, M_z, N_1, \dots, N_r, I\} \quad (50)$$

Here we assume that these are self-adjoint operators in \mathcal{L} , that each M_j and N_i commutes with H , i.e., $HM_j = M_jH$ for $j = x, y, z$ and $HN_i = N_iH$ for $i = 1, \dots, r$, and that I is the identity operator.¹

¹In simplified models, the set $\{C_i\}$ is often restricted to only $\{H, I\}$. Operators M_x, M_y, M_z are the components of the momentum operator. Operator N_i , for $i = 1, \dots, r$, is the number operator for particles of type i in the system. If the system is closed to particle exchange, it has a fixed number n_i of particles of type i , then $N_i = n_i I$, i.e., it is a c-number operator, where I is the identity operator on \mathcal{H} . If the system is open to particle exchange, then the Hilbert space \mathcal{H} is a Fock space, i.e.,

$$\mathcal{H} = \bigoplus_{j_1=0}^{\infty} \dots \bigoplus_{j_r=0}^{\infty} \mathcal{H}_{j_1 j_2 \dots j_r} \text{ and } N_i = \sum_{j_1=0}^{\infty} \dots \sum_{j_r=0}^{\infty} j_i I_{j_1 j_2 \dots j_r}$$

where $I_{j_1 j_2 \dots j_r}$ is the projector operator onto the subspace $\mathcal{H}_{j_1 j_2 \dots j_r}$ belonging to the composition with j_1 particles of type 1, j_2 particles of type 2, and so on.

The semi-empirical description of an irreversible relaxation process is done in this framework by assuming an evolution equation for the state γ given by the equations

$$\frac{d\gamma}{dt} + \frac{i}{\hbar} H \gamma = \Pi_\gamma \quad (51)$$

$$\frac{d\gamma^\dagger}{dt} - \frac{i}{\hbar} \gamma^\dagger H = \Pi_{\gamma^\dagger} \quad (52)$$

As a result, it is easy to verify that for the density operator the dynamical equation is

$$\frac{d\rho}{dt} + \frac{i}{\hbar} [H, \rho] = \Pi_\gamma \gamma^\dagger + \gamma \Pi_{\gamma^\dagger} \quad (53)$$

where $[\cdot, \cdot]$ denotes the commutator. From this we see that in order to preserve hermiticity of ρ the dissipative terms Π_γ and Π_{γ^\dagger} must satisfy the conditions

$$\Pi_{\gamma^\dagger} = \Pi_\gamma^\dagger \quad \text{and} \quad \Pi_\gamma = \Pi_{\gamma^\dagger}^\dagger \quad (54)$$

In order to satisfy the constraints of conservation of the expectation values $\text{Tr}(\rho C_i)$, recalling that each C_i commutes with H , the term Π_γ must be such that

$$\Pi_{C_i} = \frac{d}{dt} \text{Tr}(\rho C_i) = \text{Tr}(C_i \Pi_\gamma \gamma^\dagger + \gamma \Pi_{\gamma^\dagger} C_i) = (2C_i \gamma | \Pi_\gamma) = 0 \quad (55)$$

The entropy functional in this context is represented by

$$S(\gamma) = -k \text{Tr}(\rho \ln \rho) = (-k (\ln \gamma \gamma^\dagger) | \gamma | \gamma) \quad (56)$$

so that the rate of entropy production under a time evolution that preserves the normalization of ρ is given by

$$\Pi_S = -k \frac{d}{dt} \text{Tr}(\rho \ln \rho) = (-2k (\ln \gamma \gamma^\dagger) | \gamma | \Pi_\gamma) \quad (57)$$

In Quantum Statistical Mechanics (QSM) and Quantum Information Theory (QIT), ρ is the von Neumann statistical or density operator which represents the index of statistics from a generally heterogeneous ensemble of identical systems (same Hilbert space \mathcal{H} and operators $\{H, N_1, \dots, N_r\}$) distributed over a range of generally different quantum mechanical states. If each individual member of the ensemble is isolated and uncorrelated from the rest of the universe, its state is described according to Quantum Mechanics by an idempotent density operator ($\rho^2 = \rho = P_{|\psi\rangle} = \frac{|\psi\rangle\langle\psi|}{\langle\psi|\psi\rangle}$), i.e., a projection operator onto the span of some vector $|\psi\rangle$ in \mathcal{H} . If the ensemble is heterogeneous, its individual member systems may be in different states, $P_{|\psi_1\rangle}, P_{|\psi_2\rangle}$, and so on, and the ensemble statistics is captured by the von Neumann statistical operator $\rho = \sum_j w_j P_{|\psi_j\rangle}$. The entropy functional here represents a measure of the informational uncertainty as to which homogeneous subensemble the next system will be drawn from, i.e., as to which will be the actual pure quantum state among those present in the heterogeneous ensemble.

In this framework, unless the statistical weights w_j change for some extrinsic reason, the quantum evolution of the ensemble is given by Eq. (53) with $\Pi_\gamma = 0$ so that Eq. (53) reduces to von Neumann's equation of quantum reversible evolution, corresponding to $\rho(t) = \sum_j w_j P_{|\psi_j(t)\rangle}$ where the underlying pure states $|\psi_j(t)\rangle$ evolve according to the Schrödinger equation $d|\psi_j\rangle/dt = -iH|\psi_j\rangle/\hbar$.

In the framework of QSM and QIT, the SEA equation of motion we construct in the next sections for ρ represents a model for the rates of change of statistical weights w_j in such a way that Π_S is maximal subject to the conservation constraints $\Pi_{C_i} = 0$ (and a suitable additional constraint, see below), thus essentially extends to the quantum landscape the same statistical or information theoretic non-equilibrium problem we defined above as Framework C.

In Quantum Thermodynamics (QT), instead, the density operator takes on a more fundamental physical meaning. It is not any longer related to the heterogeneity of the ensemble, and it is not any longer assumed that the individual member systems of the ensemble are in pure states.

The prevailing interpretation of QT is the so-called open-system model whereby the quantum system under study (each individual system of a homogeneous ensemble) is always viewed as in contact (weak or strong) with a thermal reservoir or 'heat bath', and its not being in a pure state is an indication of its being correlated with the reservoir. The overall system-plus-bath composite is assumed to be in a pure quantum mechanical state $\mathcal{H} \otimes \mathcal{H}_R$ and reduces to the density operator ρ on the system's space \mathcal{H} when we partial trace over the bath's space \mathcal{H}_R .

The semi-empirical description of an irreversible relaxation process is done in this framework by assuming for Π_ρ in Eq. (53) the Lindblad-Gorini-Kossakowski-Sudarshan (LGKS) [21; 22]

$$\Pi_\rho = \sum_j \left(V_j \rho V_j^\dagger - \frac{1}{2} \{V_j^\dagger V_j, \rho\} \right) \quad (58)$$

where $\{\cdot, \cdot\}$ denotes the anticommutator and operators V_j are to be chosen so as to properly model the system-bath interaction. The justification and modeling assumptions that lead to the general form of Eq. (58) are well known.

In the framework of QT the SEA equation of motion we construct in the next sections for ρ represents an alternative model for Π_ρ (or for a term additional to the LGKS term) such that Π_S is maximal subject to the conservation constraints $\Pi_{C_i} = 0$ (and a suitable additional constraint, see below). In some cases this could be simpler than the LGKS model and it has the advantage of a strong built-in thermodynamics consistency.

Mesoscopic Non-Equilibrium Quantum Thermodynamics (MNEQT) [7] starts from the formalism of QSM but attempts to extend the Onsager NET theory and MNET to the quantum realm. We will show elsewhere that the present SEA formulation reduces to MNEQT in the near-equilibrium limit, and can therefore be viewed as the natural extension of MNEQT. The essential elements of this proof have actually already been given [4], but only for the particular case corresponding to Eq. (62) below (Fisher-Rao metric).

An even more fundamental physical meaning is assumed within the theory that we originally called Quantum Thermodynamics [2; 3; 23; 24; 25; 26] but more recently renamed Intrinsic Quantum Thermodynamics (IQT) to avoid confusion with the QT model just outlined.

IQT assumes that the second law of thermodynamics should complement the laws of mechanics even at the single particle level [23]. This can be done if we accept that the true individual quantum state of a system, even if fully isolated and uncorrelated from the rest of the universe, requires density operators ρ that are not necessarily idempotent. Over the set of idempotent ρ 's, QT coincides with Quantum Mechanics (QM), but it differs fundamentally from QM because it assumes a broader set of possible states, corresponding to the set of non-idempotent ρ 's. This way, the entropy functional $S(\rho)$ becomes in IQT an intrinsic fundamental property.²

In the framework of IQT the SEA equation of motion (53)

for ρ which results from the expression for Π_γ we construct in the next section represents a strong implementation of the MEP principle at the fundamental quantum level and generalizes the original framework in which we developed the SEA formalism about 30 years ago by making it compatible, at least in the near-equilibrium limit with MNEQT.

Even the brief discussion above shows clearly that the differences between QSM, QIT, QT, and IQT are important on the interpretational and conceptual levels. Nevertheless, it is also clear that they all share the same basic mathematical framework. Hence, we believe that the SEA dynamical model, which they share on the mathematical basis, can find in the different theories different physical interpretations and applications.

STEEPEST-ENTROPY-ASCENT/MAXIMAL-ENTROPY-PRODUCTION DYNAMICS. UNIFIED VARIATIONAL FORMULATION FOR FRAMEWORKS A TO F

In the preceding sections we formulated the non-equilibrium problem in various different frameworks in a unifying way that allows us to represent their dissipative parts in a single formal way. In essence, the state is represented by an element γ of a suitable vector space \mathcal{L} equipped with an inner product $(\cdot|\cdot)$. The term in the dynamical equation for γ which is responsible for dissipative irreversible relaxation and hence entropy generation is another element Π_γ of \mathcal{L} which determines the rate of entropy production according to the relation

$$\Pi_S = (\Phi|\Pi_\gamma) \quad (59)$$

and the rates of production of the conserved properties C_i according to the relation

$$\Pi_{C_i} = (\Psi_i|\Pi_\gamma) \quad (60)$$

Except for the RET Framework D, where we have no explicit expressions for Φ and Ψ_i , in Frameworks A, B, C we found that $\Phi = -k(\ln \gamma^2) \gamma$ and $\Psi_i = 2C_i \gamma$, in Framework F we found that $\Phi = -k(\ln \gamma \gamma^\dagger) \gamma$ and $\Psi_i = 2C_i \gamma$.

The formulation in terms of square roots of probabilities in Framework C, of the phase density in Frameworks A and B, of the density operator in Framework F takes care of the important condition that for the evolution law to be well defined it must conserve the nonnegativity of probabilities, phase densities and density operators (which must also remain self adjoint).

Our next objective is to implement the MEP principle. We do this by assuming that the time evolution of the state γ follows the path of steepest entropy ascent in \mathcal{L} . So, for any given state γ , we must find the Π_γ which maximizes the entropy production Π_S subject to the constraints $\Pi_{C_i} = 0$. But in order to identify the SEA path we are not interested in the unconditional increase in Π_S that we can trivially obtain by simply increasing the "norm" of Π_γ while keeping its direction fixed. Rather, the SEA path is identified by the direction of Π_γ which maximizes Π_S subject to the constraints, regardless of norm of Π_γ . Hence, we must do the maximization at constant norm of Π_γ .

The norm of Π_γ represents the square of the distance $d\ell$ traveled by γ in the state space \mathcal{L} in the time interval dt , the square of the "length" of the infinitesimal bit of path traveled in state space in the interval dt . The variational problem that identifies the SAE/MEP direction at each state γ looks at all possible

²In a sense it accomplishes the conceptual program, so intensely sought for also by Ilya Prigogine and coworkers [27], of answering the following questions [2]: *What if entropy, rather than a statistical, information theoretic, macroscopic or phenomenological concept, were an intrinsic property of matter in the same sense as energy is universally understood to be an intrinsic property of matter? What if irreversibility were an intrinsic feature of the fundamental*

dynamical laws obeyed by all physical objects, macroscopic and microscopic, complex and simple, large and small? What if the second law of thermodynamics, in the hierarchy of physical laws, were at the same level as the fundamental laws of mechanics, such as the great conservation principles? When viewed from such extreme perspective, the IQT conceptual scheme remains today as "adventurous" as it was acutely perceived by John Maddox in 1985 [28].

paths through γ , each characterized by a possible choice for Π_γ . Among all these paths it selects the one with the highest entropy produced in the interval dt , $\Pi_S dt$ per unit of distance $d\ell$ traveled by γ .

It is therefore apparent that we cannot identify a SAE/MEP path until we equip the space \mathcal{L} with a metric with respect to which to compute the distance $d\ell$ traveled and the norm of Π_γ .

In our previous work [5], we selected the Fisher-Rao metric based on the inner product $(\cdot|\cdot)$ defined on \mathcal{L} . Indeed, in dealing with probability distributions it has been argued by several authors that the Fisher-Rao metric is the proper unique metric for the purpose of computing the distance between two probability distributions (see e.g. [29; 30; 31]). According to this metric, the distance between two states γ_1 and γ_2 is given by

$$d(\gamma_1, \gamma_2) = \sqrt{2} \arccos(\gamma_1|\gamma_2) \quad (61)$$

which implies that the distance traveled along a trajectory in state space is

$$d\ell = 2\sqrt{(\Pi_\gamma|\Pi_\gamma)} dt \quad (62)$$

As a result, for Framework F the SEA dynamics we have originally proposed is most straightforward.

However, here we will adopt a more general metric, which in Framework F generalizes our previous work and in the other frameworks provides a most general formulation. We assume the following expression for the distance traveled along a trajectory in state space

$$d\ell = \sqrt{(\Pi_\gamma|\hat{G}|\Pi_\gamma)} dt \quad (63)$$

where \hat{G} is a real, symmetric, and positive-definite operator on \mathcal{L} that we call the metric tensor, (super)matrix, or (super)operator depending on the framework. In Framework F, since \mathcal{L} is the space of operators on the Hilbert space \mathcal{H} of the quantum system, \hat{G} is a superoperator on \mathcal{H} . However, a simple case is when $\hat{G}|A\rangle = |GA\rangle$ with G some self-adjoint positive-definite operator in \mathcal{L} .

We may now finally state **the SAE/MEP variational problem** and solve it. The problem is to **find the instantaneous “direction” of Π_γ which maximizes the entropy production rate Π_S subject to the constraints $\Pi_{C_i} = 0$** . We solve it by maximizing the entropy production rate Π_S subject to the constraints $\Pi_{C_i} = 0$ and the additional constraint $(d\ell/dt)^2 = \dot{\epsilon}^2 = \text{prescribed}$. The last constraint keeps the norm of Π_γ constant so that we maximize only with respect to its direction. From Eq. (63) it amounts to keeping fixed the value of $(\Pi_\gamma|\hat{G}|\Pi_\gamma)$ at some small positive constant $\dot{\epsilon}^2$. The solution is easily obtained by the method of Lagrange multipliers. We seek the unconstrained maximum, with respect to Π_γ , of the Lagrangian

$$\Upsilon = \Pi_S - \sum_i \beta_i \Pi_{C_i} - \tau [(\Pi_\gamma|\hat{G}|\Pi_\gamma) - \dot{\epsilon}^2] \quad (64)$$

where β_i and τ are the Lagrange multipliers. They must be independent of Π_γ but can be functions of the state γ . Using Eqs. (59) and (60), we rewrite (64) as follows

$$\Upsilon = (\Phi|\Pi_\gamma) - \sum_i \beta_i (\Psi_i|\Pi_\gamma) - \tau [(\Pi_\gamma|\hat{G}|\Pi_\gamma) - \dot{\epsilon}^2] \quad (65)$$

Taking the variational derivative of Υ with respect to $|\Pi_\gamma\rangle$ and setting it equal to zero we obtain

$$\frac{\delta\Upsilon}{\delta|\Pi_\gamma\rangle} = |\Phi\rangle - \sum_i \beta_i |\Psi_i\rangle - \tau \hat{G}|\Pi_\gamma\rangle = 0 \quad (66)$$

Thus, we obtain the SEA/MEP general evolution equation (the main result of this paper)

$$|\Pi_\gamma\rangle = \hat{L}|\Phi\rangle - \sum_j \beta_j |\Psi_j\rangle \quad (67)$$

where we define for convenience

$$\hat{L} = \frac{1}{\tau} \hat{G}^{-1} \quad (68)$$

Since in the various frameworks \hat{L} can be connected with the generalized Onsager conductivity (super)matrix in the near equilibrium regime, we see here that $\tau\hat{L}$ is the inverse of the metric (super)matrix \hat{G} with respect to which the dynamics is SEA/MEP. In other words, denoting the generalized Onsager resistivity (super)matrix by \hat{R} we have: $\hat{R} = \tau\hat{G}$. Since, \hat{G} is positive definite and symmetric, so are \hat{L} and \hat{R} . In other words, the SEA assumption entails Onsager reciprocity.

Inserting Eq. (67) into the conservation constraints (60) yields the important system of equations which defines the values of the Lagrange multipliers β_j ,

$$\sum_j (\Psi_i|\hat{L}|\Psi_j) \beta_j = (\Psi_i|\hat{L}|\Phi) \quad (69)$$

This system can be readily solved for the β_j 's (for example by Cramer's rule) because the functionals $(\Psi_i|\hat{L}|\Psi_j)$ and $(\Psi_i|\hat{L}|\Phi)$ are readily computable for the current state γ . When Cramer's rule is worked out explicitly, the SEA equation (67) takes the form of a ratio of determinants with which we presented it in the IQT framework [24; 25; 26; 5].

We can now immediately prove the general consistence with the thermodynamic principle of entropy non-decrease (H -theorem in Framework B). Indeed, subtracting Eqs. (60) each multiplied by the corresponding β_j 's from Eq. (59) and then inserting Eq. (67) yields the following explicit expression for rate of entropy production

$$\begin{aligned} \Pi_S &= (\Phi|\Pi_\gamma) = (\Phi - \sum_j \beta_j \Psi_j|\Pi_\gamma) \\ &= (\Phi - \sum_i \beta_i \Psi_i|\hat{L}|\Phi - \sum_j \beta_j \Psi_j) \geq 0 \end{aligned} \quad (70)$$

which is clearly nonnegative-definite by virtue, again, of the nonnegativity that must be assumed for a well defined metric superoperator \hat{G} .

It is interesting to write the expression for the (prescribed) speed $d\ell/dt$ at which the state γ evolves along the SEA/MEP path. This amounts to inserting Eq. (67) into the additional constraint $(d\ell/dt)^2 = \dot{\epsilon}^2 = \text{prescribed}$. We readily find

$$\begin{aligned} \frac{d\ell^2}{dt^2} &= (\Pi_\gamma|\hat{G}|\Pi_\gamma) \\ &= \frac{1}{\tau^2} (\Phi - \sum_i \beta_i \Psi_i|\hat{G}^{-1}\hat{G}\hat{G}^{-1}|\Phi - \sum_j \beta_j \Psi_j) \end{aligned} \quad (71)$$

$$= \frac{1}{\tau} \Pi_S = \dot{\epsilon}^2 \quad (72)$$

from which we see that the Lagrange multiplier τ is related to the entropy production rate and the speed $d\ell/dt$. In other words, through τ we may specify either the speed at which γ evolves along the SEA/MEP trajectory in state space or the instantaneous rate of entropy production. Indeed, using Eq. (71), we obtain

$$\tau = \frac{\sqrt{(\Phi - \sum_i \beta_i \Psi_i|\hat{G}^{-1}|\Phi - \sum_j \beta_j \Psi_j)}}{d\ell/dt} \quad (73)$$

$$= \frac{(\Phi - \sum_i \beta_i \Psi_i|\hat{G}^{-1}|\Phi - \sum_j \beta_j \Psi_j)}{\Pi_S} \quad (74)$$

Hence, using τ given by Eq. (74) the evolution equation Eq. (67) will produce a SEA/MEP trajectory in state space with the prescribed entropy production Π_S . Eq. (74) also clearly supports the interpretation of τ as the “overall relaxation time”.

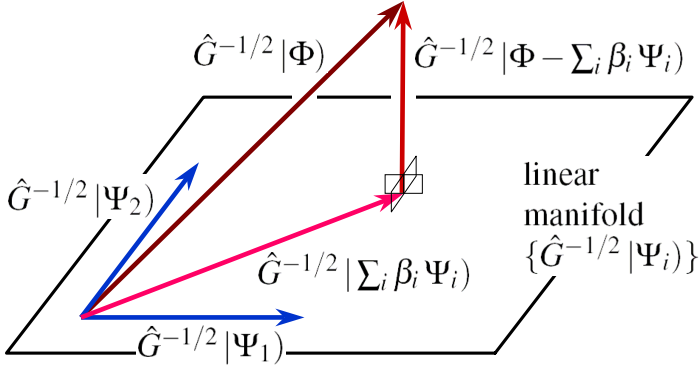


Figure 3. Pictorial representation of the linear manifold spanned by the vectors $\hat{G}^{-1/2} |\Psi_i\rangle$ and the orthogonal projection of $\hat{G}^{-1/2} |\Phi\rangle$ onto this manifold which defines the Lagrange multipliers β_i in the case of a non-uniform metric \hat{G} . The construction defines also the generalized affinity vector $|\Lambda\rangle = \hat{G}^{-1/2} |\Phi - \sum_i \beta_i \Psi_i\rangle$.

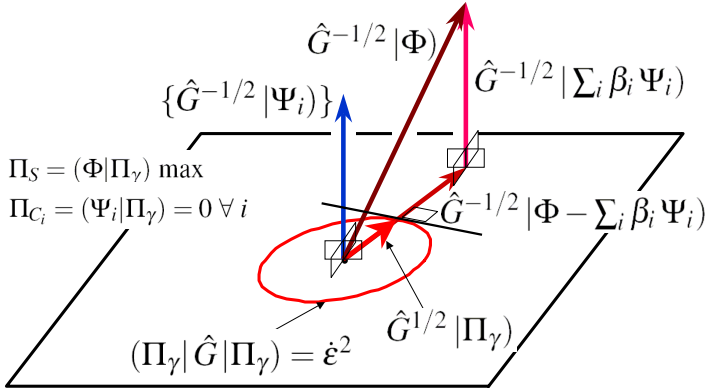


Figure 4. Pictorial representation of the SEA/MEP variational construction in the case of a non-uniform metric \hat{G} . The circle represents the condition $(\Pi_\gamma|\hat{G}|\Pi_\gamma) = \dot{\epsilon}^2$, corresponding to the norm of vector $\hat{G}^{1/2} |\Pi_\gamma\rangle$. This vector must be orthogonal to the $\hat{G}^{-1/2} |\Psi_i\rangle$'s in order to satisfy the conservation constraints $\Pi_{C_i} = (\Psi_i|\Pi_\gamma) = 0$. In order to maximize the scalar product $\Pi_S = (\Phi|\Pi_\gamma) = (\Phi - \sum_i \beta_i \Psi_i|\Pi_\gamma)$, vector $\hat{G}^{1/2} |\Pi_\gamma\rangle$ must have the same direction as $|\Lambda\rangle = \hat{G}^{-1/2} |\Phi - \sum_i \beta_i \Psi_i\rangle$.

and the orthogonal projection of $\hat{G}^{-1/2} |\Phi\rangle$ which defines the Lagrange multipliers β_i in the case of non-uniform metric \hat{G} , where the orthogonality conditions that define the β_i 's are $(\Psi_j|\hat{G}^{-1} |\Phi - \sum_i \beta_i \Psi_i\rangle) = 0$ for every j , which is Eq. (69). The construction defines also the generalized affinity vector $|\Lambda\rangle = \hat{G}^{-1/2} |\Phi - \sum_i \beta_i \Psi_i\rangle$ which is orthogonal to the linear manifold spanned by the vectors $\hat{G}^{-1/2} |\Psi_i\rangle$'s.

Figure 4 gives a pictorial representation of the subspace orthogonal to the linear manifold spanned by the $\hat{G}^{-1/2} |\Psi_i\rangle$'s that here we denote for simplicity by $\{\hat{G}^{-1/2} |\Psi_i\rangle\}$. The vector $\hat{G}^{-1/2} |\Phi\rangle$ is decomposed into its component $\hat{G}^{-1/2} |\sum_i \beta_i \Psi_i\rangle$ which lies in $\{\hat{G}^{-1/2} |\Psi_i\rangle\}$ and its component $|\Lambda\rangle = \hat{G}^{-1/2} |\Phi - \sum_i \beta_i \Psi_i\rangle$ which lies in the orthogonal subspace.

The circle in Figure 4 represents the more general condition $(\Pi_\gamma|\hat{G}|\Pi_\gamma) = \dot{\epsilon}^2$ corresponding in the non-uniform metric to the prescribed rate of advancement in state space, $\dot{\epsilon}^2 = (d\ell/dt)^2$. It is clear that the direction of $\hat{G}^{1/2} |\Pi_\gamma\rangle$ which maximizes the scalar product $(\Phi - \sum_i \beta_i \Psi_i|\Pi_\gamma)$, is when $|\Pi_\gamma\rangle$ is in the direction of the point of tangency between the ellipse and a

line orthogonal to $|\Phi - \sum_i \beta_i \Psi_i\rangle$.

The compatibility with the conservation constraints $\Pi_{C_i} = (\Psi_i|\Pi_\gamma) = 0$ requires that $\hat{G}^{1/2} |\Pi_\gamma\rangle$ lies in subspace orthogonal to the $\hat{G}^{-1/2} |\Psi_i\rangle$'s. To take the SEA/MEP direction, the vector $\hat{G}^{1/2} |\Pi_\gamma\rangle$ must maximize the scalar product $(\Phi - \sum_i \beta_i \Psi_i|\Pi_\gamma)$, which is equal to the entropy production $\Pi_S = (\Phi|\Pi_\gamma)$ since $(\Psi_i|\Pi_\gamma) = 0$. This clearly happens when $|\Pi_\gamma\rangle$ has the same direction as the generalized affinity vector $|\Lambda\rangle = \hat{G}^{-1/2} |\Phi - \sum_i \beta_i \Psi_i\rangle$.

CONCLUSIONS

In this paper, we review the essential mathematical elements of the formulations of six different approaches to the description of non-equilibrium dynamics. At the price of casting some of them in a somewhat unusual notation, we gain the possibility to set up a unified formulation, which allows us to investigate the locally Maximum Entropy Production (MEP) principle in all these contexts. It is a generalization to non-homogeneous cases of the local Steepest Entropy Ascent (SEA) concept whereby the time evolution the state is assumed to follow a path in state space which, with respect to an underlying metric, is always tangent to the direction of maximal entropy production compatible with the conservation constraints.

The present SEA/MEP unified formulation allows us to extend at once to all these frameworks the SEA concept which has so far been considered only in the framework of quantum thermodynamics. Actually, the present formulation constitutes a generalization even in the quantum thermodynamics framework and constitutes a natural generalization to the far-nonequilibrium domain of Mesoscopic Non-Equilibrium Quantum Thermodynamics.

The analysis emphasizes that in the SEA/MEP implementation of the MEP principle, a key role is played by the geometrical metric with respect to which to measure the length of a trajectory in state space. The metric tensor turns out to be directly related to the inverse of the Onsager's generalized conductivity tensor.

We conclude that in most of the existing theories of non-equilibrium the time evolution of the state representative can be seen to actually follow in state space the path of SEA with respect to a suitable metric connected with the generalized conductivities. This is true in the near-equilibrium limit, where in all frameworks it is possible to show that the traditional assumption of linear relaxation coincides with the SEA/MEP result. Since the generalized conductivities represent, at least in the near-equilibrium regime, the strength of the system's reaction when pulled out of equilibrium, it appears that their inverse, i.e., the generalized resistivity tensor, represents the metric with respect to which the time evolution, at least in the near equilibrium, is SEA/MEP.

Far from equilibrium the resulting unified family of SAE/MEP dynamical models is a very fundamental as well as practical starting point because it features an intrinsic consistency with the second law of thermodynamics. The proof of nonnegativity of the local entropy production density is a general and straightforward regardless of the details of the underlying metric tensor. In a variety of fields of application, the present unifying approach may prove useful in providing a new basis for effective numerical and theoretical models of irreversible, conservative relaxation towards equilibrium from far non-equilibrium states.

ACKNOWLEDGMENTS

The author gratefully acknowledges the Cariplo–UniBS–MIT–MechE faculty exchange program co-sponsored by UniBS and the CARIPO Foundation, Italy under grant 2008-2290. This work is part of EOARD (European Office of Aerospace R&D) grant FA8655-11-1-3068 and Italian MIUR PRIN-2009-3JPM5Z-002.

REFERENCES

- [1] L.M. Martyushev and V.D. Seleznev, “Maximum entropy production principle in physics, chemistry and biology”, *Physics Reports* **426**, 1- 45 (2006).
- [2] G.P. Beretta, “A General Nonlinear Evolution Equation for Irreversible Conservative Approach to Stable Equilibrium” and “Intrinsic Entropy and Intrinsic Irreversibility for a Single Isolated Constituent of Matter: Broader Kinematics and Generalized Nonlinear Dynamics”, in *Frontiers of Nonequilibrium Statistical Physics*, Proc. NATO ASI, Santa Fe, 1984, G.T. Moore, G.T. and M.O. Scully, Editors, NATO ASI Series B: Physics **135**, Plenum Press, New York, 1986, pp. 193-204 and 205-212.
- [3] G.P. Beretta, “Steepest Entropy Ascent in Quantum Thermodynamics”, in *The Physics of Phase Space*, Y.S. Kim and W.W. Zachary, Editors; Lecture Notes in Physics, **278**, Springer-Verlag, pp. 441-443 (1986).
- [4] S. Gheorghiu-Svirschevski, “Nonlinear Quantum Evolution with Maximal Entropy Production”, *Phys. Rev. A* **63**, 022105 (2001); “Addendum to: Nonlinear Quantum Evolution with Maximal Entropy Production”, *ibid*, **63**, 054102 (2001).
- [5] G.P. Beretta, “Nonlinear Quantum Evolution Equations to Model Irreversible Adiabatic Relaxation with Maximal Entropy Production and Other Nonunitary Processes”, *Reports on Mathematical Physics* **64**, 139-168 (2009).
- [6] P. Mazur, “Mesoscopic nonequilibrium thermodynamics; irreversible processes and fluctuations”, *Physica A* **274**, 491-504 (1999).
- [7] D. Bedeaux and P. Mazur, “Mesoscopic non-equilibrium thermodynamics for quantum systems”, *Physica A* **298**, 81-100 (2001).
- [8] H. Ziegler, “A Possible Generalization of Onsager’s Theory”, in *Irreversible Aspects of Continuum Mechanics and Transfer of Physical Characteristics in Moving Fluids*, Symposia Vienna, June 22-28, 1966 Editors H. Parkus and L. I. Sedov, Springer-Verlag, New York, 411-423 (1968).
- [9] D.G.B. Edelen, “A Thermodynamics with Internal Degrees Of Freedom and Nonconservative Forces”, *Int. J. Engng. Sci.*, **14**, 1013-1032 (1976).
- [10] B. Reznik, “Unitary Evolution between Pure and Mixed States”, *Phys. Rev. Lett.* **96**, 1192-1195 (1996).
- [11] N.G. Hadjiconstantinou, “The limits of Navier-Stokes theory and kinetic extensions for describing small-scale gaseous hydrodynamics”, *Phys. Fluids*, **18**, 111301 (2006).
- [12] G.P. Beretta and N.G. Hadjiconstantinou, “Steepest Entropy Ascent Models of the Boltzmann Equation. Comparisons with Hard-Sphere Dynamics and Relaxation-Time Models for Homogeneous Relaxation from Highly Non-Equilibrium States”, Proceedings of the ASME 2013 International Mechanical Engineering Congress and Exposition, IMECE2013, November 15-21, 2013, San Diego, USA, paper IMECE2013-64905.
- [13] E.T. Jaynes, “The Minimum Entropy Production Principle”, *Ann. Rev. Phys. Chem.* **31**, 579-601 (1980).
- [14] M. Lemanska, Z. Jaeger and R. Englman, A nonlinear model for relaxation in excited closed physical systems, *Physica D* **170**, 7286 (2002).
- [15] I. Müller and T. Ruggeri, “Rational Extended Thermodynamics”, Springer, New York, 1998.
- [16] I-Shih Liu, “Method of Lagrange multipliers for exploitation of the entropy principle”, *Arch. Rational Mechanics and Analysis*, **46**, 131-148 (1972).
- [17] A.N. Gorban, I.V. Karlin, and A.Y. Zinovyev, “Constructive methods of invariant manifolds for kinetic problems”, *Phys. Rep.* **396**, 197-403 (2004).
- [18] M. Grmela and H.C. Oettinger, “Dynamics and thermodynamics of complex fluids. I. Development of a general formalism”, *Phys. Rev. E* **56**, 66206632 (1997). H.C. Oettinger and M. Grmela, “Dynamics and thermodynamics of complex fluids. II. Illustrations of a general formalism”, *Phys. Rev. E* **56**, 66336655 (1997).
- [19] C. Tsallis, “Possible Generalization of Boltzmann-Gibbs Statistics”, *J. Stat. Phys.* **52**, 479487 (1988).
- [20] P. Gorban, “Monotonically equivalent entropies and solution of additivity equation”, *Physica A* **328**, 380390 (2003).
- [21] G. Lindblad, “On the generators of quantum dynamical semigroups”, *Commun. Math. Phys.* **48**, 119-130 (1976).
- [22] V. Gorini, A. Kossakowski and E.C.G. Sudarshan, “Completely positive dynamical semigroups of N-level systems”, *J. Math. Phys.* **17**, 821-825 (1976).
- [23] G.N. Hatsopoulos and E.P. Gyftopoulos, A Unified Quantum Theory of Mechanics and Thermodynamics, *Found. Phys.* **6**, 15, 127, 439, 561 (1976).
- [24] G.P. Beretta, “On the General Equation of Motion of Quantum Thermodynamics and the Distinction Between Quantal and Nonquantal Uncertainties”, Sc.D. thesis, MIT, Cambridge, MA, 1981; arXiv:quant-ph/0509116.
- [25] G.P. Beretta, E.P. Gyftopoulos, J.L. Park, and G.N. Hatsopoulos, “Quantum Thermodynamics. A New Equation of Motion for a Single Constituent of Matter”, *Nuovo Cimento B* **82**, 169 (1984).
- [26] G.P. Beretta, E.P. Gyftopoulos, and J.L. Park, “Quantum Thermodynamics. A New Equation of Motion for a General Quantum System”, *Nuovo Cimento B* **87**, 77 (1985).
- [27] M. Courbage and I. Prigogine, “Intrinsic randomness and intrinsic irreversibility in classical dynamical systems”, *Proc. Natl. Acad. Sci. USA*, **80**, 2412-2416 (1983).
- [28] J. Maddox, “Uniting Mechanics and Statistics. An Adventurous Scheme which Seeks to Incorporate Thermodynamics into the Quantum Laws of Motion May End Arguments About the Arrow of Time – But Only if it Works”, *Nature*, **316**, 11 (1985).
- [29] W.K. Wootters, “Statistical distance and Hilbert space”, *Phys. Rev. D* **23**, 357-362 (1981).
- [30] P. Salamon, J.D. Nulton, and R.S. Berry, “Length in Statistical Thermodynamics”, *J. Chem. Phys.* **82**, 2433-2436 (1985).
- [31] S.L. Braunstein and C.M. Caves, “Statistical Distance and the Geometry of Quantum States”, *Phys. Rev. Lett.* **72**, 3439-3443 (1994).

INFORMATION GEOMETRIC COMPLEXITY OF ENTROPIC MOTION ON CURVED STATISTICAL MANIFOLDS

Carlo Cafaro

Max-Planck Institute for the Science of Light, 91058 Erlangen, Germany
Institute of Theoretical Physics, University of Erlangen-Nurnberg, 91058 Erlangen, Germany
Institute of Physics, Johannes Gutenberg University Mainz, 55128 Mainz, Germany

ABSTRACT

Physical systems behave according to their underlying dynamical equations which, in turn, can be identified from experimental data. Explaining data requires selecting mathematical models that best capture the data regularities. Identifying dynamical equations from the available data and statistical model selection are both very difficult tasks. Motivated by these fundamental links among physical systems, dynamical equations, experimental data and statistical modeling, we discuss in this invited Contribution our information geometric measure of complexity of geodesic paths on curved statistical manifolds underlying the entropic dynamics of classical physical systems described by probability distributions. We also provide several illustrative examples of entropic dynamical models used to infer macroscopic predictions when only partial knowledge of the microscopic nature of the system is available. Finally, we present entropic arguments to briefly address complexity softening effects due to statistical embedding procedures.

INTRODUCTION

The intimate connection between dynamics, on the one hand, and modeling, prediction, and complexity, on the other, is quite remarkable in science [1]. In real-world experiments, we usually gather data of the state of a physical system at various points in space and time. Then, to achieve some comprehension of the physics behind the behaviour of the system, we must reconstruct the underlying dynamical equations from the data. Deducing dynamics from experimental observations (data) is a fundamental part of science [2], [3]. We observe the trajectories of planets to deduce the laws of celestial mechanics; we consider monetary parameters to determine economic laws; we observe atoms to deduce quantum mechanics. A current challenge is the analysis of data gathered from networks of interferometric gravitational-wave detectors to search for a stochastic gravitational-wave background [4].

A very recent and extremely interesting work shows that deducing the underlying dynamical equations from experimental data is NP hard (the NP complexity class denotes a class of problems that have solutions which can be quickly checked on a classical computer) and is computationally intractable [5]. This hardness result holds true for both classical and quantum systems, and regardless of how much experimental data we gather about the system. These results imply that various closely related problems, such as finding the dynamical equation that best approximates the data, or testing a dynamical model against experimental data, are intractable in general.

By analyzing the available data about a system of interest, it is possible to identify classes of regularities of the system itself. It is generally agreed that something almost entirely random, with practically no regularities, would have an effective complexity near zero [6]. Instead, structured systems (where correlations among system's constituents arise) can be very complex. Structure and correlation are not completely independent

of randomness. Indeed, both maximally random and perfectly ordered systems possess no structure [7], [8]. What then is the meaning of complexity? It appears that:

- A good measure of complexity is best justified through utility in further application [9];
- A good measure of complexity is most useful for comparison between things, at least one of which, has high complexity by that measure [6];
- A good measure of complexity for many-body systems ought to obey the so-called slow law growth [10]: complexity ought not to increase quickly, except with low probability, but can increase slowly;
- A good measure of complexity is one for which the motivations for its introduction and the features it is intended to capture are stated in a clear manner [7].

In general, good measures of complexity are introduced within formulations that deal with the whole sequence of events that lead to the object whose complexity is being described [9]. For such measures, that which is reached only through a difficult path is complex. For instance, when defining the complexity of a noisy quantum channel, the concept of pattern plays a role, in some sense [11]. The thermodynamic and the logical depths are two such measures as well. The thermodynamic depth is the measure of complexity proposed by Lloyd and Pagels and it represents the amount of entropy produced during a state's actual evolution [12]. The logical depth is a measure of complexity proposed by Bennett and it represents the execution time required for a universal Turing machine to run the minimal program that reproduces (say) a system's configuration [13].

Since the path leading to an object (or, state) is central when defining a measure of complexity, simple thermodynamic criteria applied to the states to be compared are inadequate. Thermodynamic potentials measure a system's capacity for irreversible

change, but do not agree with intuitive notions of complexity [10]. For instance, the thermodynamic entropy, a measure of randomness, is a monotonic function of temperature where high (low) temperature corresponds to high (low) randomness. However, given that there are many functions that vanish in the extreme ordered and disordered limits, it is clear that requiring this property does not sufficiently restrict a complexity measure of statistical nature (statistical complexity [8] is a quantity that measures the amount of memory needed, on average, to statistically reproduce a given configuration). Despite these facts, it is undisputable that thermodynamics does play a key role when investigating qualitative differences in the complexity of reversible and dissipative systems [13].

The difficulty of constructing a good theory from a data set can be roughly identified with cripticity while the difficulty of making predictions from the theory can be regarded as a rough interpretation of logical depth. Both cripticity and logical depth are intimately related to the concept of complexity. Making predictions can be very difficult in general, especially in composite systems where interactions between subsystems are introduced. The introduction of interactions leads to fluctuation growth which, in turn, can cause the dynamics to become nonlinear and chaotic. Such phenomena are very common and can occur in both natural (cluster of stars) and artificial (financial network) complex dynamical systems [14]. A fundamental problem in the physics of complex systems is model reduction, that is finding a low-dimensional model that captures the gross features of a high-dimensional system [15]. Sometimes, to make reliable macroscopic predictions, considering the dynamics alone may not be sufficient and entropic arguments should be taken into account as well [16].

As stated earlier, one of the major goals of physics is modelling and predicting natural phenomena using relevant information about the system of interest. Taking this statement seriously, it is reasonable to expect that the laws of physics should reflect the methods for manipulating information. This point of view constitutes quite a departure from the conventional line of thinking where laws of physics are used to manipulate information. For instance, in quantum information science, information is manipulated using the laws of quantum mechanics. This alternative perspective is best represented in the so-called Entropic Dynamics (ED) [17], a theoretical framework built on both maximum relative entropy (MrE) methods [18] and information geometric techniques [19]. The most intriguing question being pursued in ED stems from the possibility of deriving dynamics from purely entropic arguments. Indeed, the ED approach has already been applied for the derivation of Newton's dynamics [20] and aspects of quantum theory [21].

In this invited Contribution, inspired by the ED approach to physics and motivated by these fundamental links among physical systems, dynamical equations, experimental data and statistical modeling, we present our information geometric measure of complexity of geodesic paths on curved statistical manifolds underlying the entropic dynamics of classical physical systems described by probability distributions. We also provide several illustrative examples of entropic dynamical models used to infer macroscopic predictions when only partial knowledge of the microscopic nature of the system is available. Finally, we emphasize the relevance of entropic arguments in addressing complexity softening effects due to statistical embedding procedures.

COMPLEXITY

In [22], the so-called Information Geometric Approach to Chaos (IGAC) was presented. The IGAC uses the ED formalism to study the complexity of informational geodesic flows on curved statistical manifolds underlying the entropic dynamics of classical physical systems described by probability distributions.

A geodesic on a curved statistical manifold \mathcal{M}_S represents the maximum probability path a complex dynamical system explores in its evolution between initial and final macrostates. Each point of the geodesic is parametrized by the macroscopic dynamical variables $\{\theta\}$ defining the macrostate of the system. Furthermore, each macrostate is in a one-to-one correspondence with the probability distribution $\{p(x|\theta)\}$ representing the maximally probable description of the system being considered. The quantity x is a microstate of the microspace \mathcal{X} . The set of macrostates forms the parameter space \mathcal{D}_θ while the set of probability distributions forms the statistical manifold \mathcal{M}_S .

The IGAC is the information geometric analogue of conventional geometrodynamical approaches [23], [24] where the classical configuration space is being replaced by a statistical manifold with the additional possibility of considering chaotic dynamics arising from non conformally flat metrics (the Jacobi metric is always conformally flat, instead). It is an information geometric extension of the Jacobi geometrodynamics (the geometrization of a Hamiltonian system by transforming it to a geodesic flow [25]).

The reformulation of dynamics in terms of a geodesic problem allows the application of a wide range of well-known geometrical techniques in the investigation of the solution space and properties of the equation of motion. The power of the Jacobi reformulation is that all of the dynamical information is collected into a single geometric object in which all the available manifest symmetries are retained- the manifold on which geodesic flow is induced. For example, integrability of the system is connected with existence of Killing vectors and tensors on this manifold. The sensitive dependence of trajectories on initial conditions, which is a key ingredient of chaos, can be investigated from the equation of geodesic deviation. In the Riemannian [23] and Finslerian [24] (a Finsler metric is obtained from a Riemannian metric by relaxing the requirement that the metric be quadratic on each tangent space) geometrodynamical approach to chaos in classical Hamiltonian systems, a very challenging problem is finding a rigorous relation among sectional curvatures, Lyapunov exponents, and the Kolmogorov-Sinai dynamical entropy [26].

Information metric

An n -dimensional \mathbb{C}^∞ differentiable manifold is a set of points \mathcal{M} admitting coordinate systems $\mathcal{C}_\mathcal{M}$ and satisfies the following two conditions: 1) each element $c \in \mathcal{C}_\mathcal{M}$ is a one-to-one mapping from \mathcal{M} to some open subset of \mathbb{R}^n ; 2) For all $c \in \mathcal{C}_\mathcal{M}$, given any one-to-one mapping ξ from \mathcal{M} to \mathbb{R}^n , we have that $\xi \in \mathcal{C}_\mathcal{M} \Leftrightarrow \xi \circ c^{-1}$ is a \mathbb{C}^∞ diffeomorphism. In this article, the points of \mathcal{M} are probability distributions. Furthermore, we consider Riemannian manifolds (\mathcal{M}, g) . The Riemannian metric g is not naturally determined by the structure of \mathcal{M} as a manifold. In principle, it is possible to consider an infinite number of Riemannian metrics on \mathcal{M} . A fundamental assumption in the information geometric framework is the choice of the Fisher-Rao information metric as the metric that underlies the Riemannian

geometry of probability distributions [19], [27], [28], namely

$$g_{\mu\nu}(\theta) \stackrel{\text{def}}{=} \int dx p(x|\theta) \partial_\mu \log p(x|\theta) \partial_\nu \log p(x|\theta), \quad (1)$$

with $\mu, \nu = 1, \dots, n$ for an n -dimensional manifold and $\partial_\mu \stackrel{\text{def}}{=} \frac{\partial}{\partial \theta^\mu}$. The quantity x labels the microstates of the system. The choice of the information metric can be motivated in several ways, the strongest of which is Cencov's characterization theorem [29]. In this theorem, Cencov proves that the information metric is the only Riemannian metric (except for a constant scale factor) that is invariant under a family of probabilistically meaningful mappings termed congruent embeddings by Markov morphism [29], [30].

Given a statistical manifold \mathcal{M}_S with a metric $g_{\mu\nu}$, the ED is concerned with the following issue [17]: given the initial and final states, what trajectory is the system expected to follow? The answer turns out to be that the expected trajectory is the geodesic that passes through the given initial and final states. Furthermore, the trajectory follows from a principle of inference, the MrE method [18]. The objective of the MrE method is to update from a prior distribution q to a posterior distribution $P(x)$ given the information that the posterior lies within a certain family of distributions p . The selected posterior $P(x)$ is that which maximizes the logarithm relative entropy $\mathcal{S}[p|q]$,

$$\mathcal{S}[p|q] \stackrel{\text{def}}{=} - \int dx p(x) \log \frac{p(x)}{q(x)}. \quad (2)$$

Since prior information is valuable, the functional $\mathcal{S}[p|q]$ has been chosen so that rational beliefs are updated only to the extent required by the new information. We emphasize that ED is formally similar to other generally covariant theories: the dynamics is reversible, the trajectories are geodesics, the system supplies its own notion of an intrinsic time, the motion can be derived from a variational principle of the form of Jacobi's action principle rather than the more familiar principle of Hamilton. In short, the canonical Hamiltonian formulation of ED is an example of a constrained information-dynamics where the information-constraints play the role of generators of evolution. For more details on the ED, we refer to [17].

A geodesic on a n -dimensional curved statistical manifold \mathcal{M}_S represents the maximum probability path a complex dynamical system explores in its evolution between initial and final macrostates θ_{initial} and θ_{final} , respectively. Each point of the geodesic represents a macrostate parametrized by the macroscopic dynamical variables $\theta \equiv (\theta^1, \dots, \theta^n)$ defining the macrostate of the system. Each component θ^k with $k = 1, \dots, n$ is a solution of the geodesic equation [17],

$$\frac{d^2 \theta^k}{d\tau^2} + \Gamma_{lm}^k \frac{d\theta^l}{d\tau} \frac{d\theta^m}{d\tau} = 0. \quad (3)$$

Furthermore, as stated earlier, each macrostate θ is in a one-to-one correspondence with the probability distribution $p(x|\theta)$. This is a distribution of the microstates x .

Entropic motion

The main objective of ED is to derive the expected trajectory of a system, assuming it evolves from a known initial state θ_i to

a known final state θ_f . The ED framework implicitly assumes there exists a trajectory, in the sense that, large changes are the result of a continuous succession of very many small changes. Therefore, the problem of studying large changes is reduced to the much simpler problem of studying small changes. Focusing on small changes and assuming that the change in going from the initial state θ_i to the final state $\theta_f = \theta_i + \Delta\theta$ is sufficiently small, the distance Δl between such states becomes,

$$\Delta l^2 \stackrel{\text{def}}{=} g_{\mu\nu}(\theta) \Delta\theta^\mu \Delta\theta^\nu. \quad (4)$$

Following Caticha's work in [17], we explain how to determine which states are expected to lie on the expected trajectory between θ_i and θ_f . First, in going from the initial to the final state the system must pass through a halfway point, that is, a state θ that is equidistant from θ_i and θ_f . Upon choosing the halfway state, the expected trajectory of the system can be determined. Indeed, there is nothing special about halfway states. For instance, we could have similarly argued that in going from the initial to the final state the system must first traverse a third of the way, that is, it must pass through a state that is twice as distant from θ_f as it is from θ_i . In general, the system must pass through an intermediate states θ_ξ such that, having already moved a distance $d l$ away from the initial θ_i , there remains a distance $\xi d l$ to be covered to reach the final θ_f . Halfway states have $\xi = 1$, third of the way states have $\xi = 2$, and so on. Each different value of ξ provides a different criterion to select the trajectory. If there are several ways to determine a trajectory, consistency requires that all these ways should agree. The selected trajectory must be independent of ξ . Therefore, the main ED problem becomes the following: initially, the system is in state $p(x|\theta_i)$ and new information in the form of constraints is given to us; the system has moved to one of the neighboring states in the family $p(x|\theta_\xi)$; the problem becomes that of selecting the proper $p(x|\theta_\xi)$. This new formulation of the ED problem is precisely the kind of problem to be addressed using the MrE method. We recall that the MrE method is a method for processing information. It allows us to go from an old set of rational beliefs, described by the prior probability distribution, to a new set of rational beliefs, described by the posterior distribution, when the available information is just a specification of the family of distributions from which the posterior must be selected. Usually, this family of posteriors is defined by the known expected values of some relevant variables. It should be noted however, that it is not strictly necessary for the family of posteriors to be defined via expectation values, nor does the information-constraints need to be linear functionals. In ED, constraints are defined geometrically. Whenever one contemplates using the MrE method, it is important to specify which entropy should be maximized. The selection of a distribution $p(x|\theta)$ requires that the entropies to be considered must be of the form,

$$\mathcal{S}[p|q] \stackrel{\text{def}}{=} - \int dx p(x|\theta) \log \left(\frac{p(x|\theta)}{q(x)} \right). \quad (5)$$

Equation (5) defines the entropy of $p(x|\theta)$ relative to the prior $q(x)$. The interpretation of $q(x)$ as the prior follows from the logic behind the MrE method itself. The selected posterior distribution should coincide with the prior distribution when there are no constraints. Since the distribution that maximizes $\mathcal{S}[p|q]$

subject to no constraints is $p \propto q$, we must set $q(x)$ equal to the prior. That said, let us return to our ED problem. Assuming we know that the system is initially in state $p(x|\theta_i)$ but have obtained no information reflecting that the system has moved. We therefore have no reason to believe that any change has occurred. The prior $q(x)$ should be chosen so that the maximization of $S[p|q]$ subject to no constraints leads to the posterior $p = p(x|\theta_i)$. The correct choice is $q(x) = p(x|\theta_i)$. If on the other hand we know that the system is initially in state $p(x|\theta_i)$ and furthermore, we obtain information that the system has moved to one of the neighboring states in the family $p(x|\theta_\xi)$, then the correct selection of the posterior probability distribution is obtained by maximizing the entropy,

$$S[\theta|\theta_i] \stackrel{\text{def}}{=} - \int dx p(x|\theta) \log \left(\frac{p(x|\theta)}{p(x|\theta_i)} \right), \quad (6)$$

subject to the constraint $\theta = \theta_\xi$. For the sake of reasoning, let us assume that the system evolves from a known initial state θ_i to a known final state $\theta_f = \theta_i + \Delta\theta$. Furthermore, let us denote with $\theta_\xi = \theta_i + d\theta$ ($\xi \in \mathbb{R}_0^+$) an arbitrary intermediate state infinitesimally close to θ_i . Thus, the distance $d(\theta_i, \theta_f) \stackrel{\text{def}}{=} dl_{i \rightarrow f}^2$ between θ_i to and θ_f is given by,

$$dl_{i \rightarrow f}^2 \stackrel{\text{def}}{=} g_{\mu\nu}(\theta) \Delta\theta^\mu \Delta\theta^\nu, \quad (7)$$

while the distance between θ_i to and θ_ξ reads,

$$dl_{i \rightarrow \xi}^2 \stackrel{\text{def}}{=} g_{\mu\nu}(\theta) d\theta^\mu d\theta^\nu. \quad (8)$$

Finally, the distance between θ_ξ and θ_f becomes,

$$dl_{\xi \rightarrow f}^2 \stackrel{\text{def}}{=} g_{\mu\nu}(\theta) (\Delta\theta^\mu - d\theta^\mu) (\Delta\theta^\nu - d\theta^\nu). \quad (9)$$

The MrE maximization problem is to maximize $S[\theta_\xi|\theta_i] = S[\theta_i + d\theta|\theta_i]$,

$$S[\theta_i + d\theta|\theta_i] \stackrel{\text{def}}{=} -\frac{1}{2} g_{\mu\nu}(\theta) d\theta^\mu d\theta^\nu = -\frac{1}{2} dl_{i \rightarrow \xi}^2, \quad (10)$$

under variations of $d\theta$ subject to the geometric constraint,

$$\xi dl_{i \rightarrow \xi} = dl_{\xi \rightarrow f}, \quad (11)$$

or equivalently, $\xi^2 dl_{i \rightarrow \xi}^2 - dl_{\xi \rightarrow f}^2 = 0$. It must then be true that,

$$\delta \left[-\frac{1}{2} g_{\mu\nu}(\theta) d\theta^\mu d\theta^\nu - \lambda \left(\xi^2 dl_{i \rightarrow \xi}^2 - dl_{\xi \rightarrow f}^2 \right) \right] = 0, \quad (12)$$

where λ denotes a Lagrangian multiplier. Substituting Eqs. (8) and (9) into Eq. (12), we obtain

$$\{ [1 + 2\lambda(\xi^2 - 1)] d\theta_\mu + 2\lambda\Delta\theta_\mu \} \delta(d\theta^\mu) = 0. \quad (13)$$

Since (13) must hold for any $\delta(d\theta^\mu)$, it must be the case that

$$\{ [1 + 2\lambda(\xi^2 - 1)] d\theta_\mu + 2\lambda\Delta\theta_\mu \} = 0, \quad (14)$$

that is,

$$d\theta_\mu = \chi \Delta\theta_\mu, \quad (15)$$

where $\chi = \chi(\xi, \lambda)$ is defined as,

$$\chi(\xi, \lambda) \stackrel{\text{def}}{=} \frac{1}{(1 - \xi^2) - \frac{1}{2\lambda}}. \quad (16)$$

To find the value of the Lagrange multiplier λ , observe that the geometric constraint in Eq. (11) can be rewritten as, $\xi^2 dl_{i \rightarrow \xi}^2 - dl_{\xi \rightarrow f}^2 = 0$. Then, using Eqs. (8), (9) and (15), we obtain

$$\left[\xi^2 \chi^2 - (1 - \chi)^2 \right] g_{\mu\nu}(\theta) \Delta\theta^\mu \Delta\theta^\nu = 0, \quad (17)$$

thus,

$$\xi^2 \chi^2 - (1 - \chi)^2 = 0. \quad (18)$$

Combining Eqs. (16) and (18), we find

$$\chi(\xi) \stackrel{\text{def}}{=} \frac{1}{1 + \xi} \text{ and } \lambda(\xi) \stackrel{\text{def}}{=} -\frac{1}{2\xi(1 + \xi)}. \quad (19)$$

In conclusion, it has been determined that

$$dl_{i \rightarrow \xi}^2 \stackrel{\text{def}}{=} \frac{1}{(1 + \xi)^2} \Delta\theta^2, \quad (20)$$

and,

$$dl_{\xi \rightarrow f}^2 \stackrel{\text{def}}{=} \frac{\xi^2}{(1 + \xi)^2} \Delta\theta^2. \quad (21)$$

From Eqs. (20) and (21), it follows that

$$dl_{i \rightarrow \xi} + dl_{\xi \rightarrow f} = \frac{1}{1 + \xi} \Delta\theta + \frac{\xi}{1 + \xi} \Delta\theta = \Delta\theta. \quad (22)$$

However, recall that $dl_{i \rightarrow f}^2 \stackrel{\text{def}}{=} g_{\mu\nu}(\theta) \Delta\theta^\mu \Delta\theta^\nu = \Delta\theta^2$, that is

$$dl_{i \rightarrow f} = \Delta\theta. \quad (23)$$

Combining Eqs. (22) and (23), we arrive at

$$dl_{i \rightarrow f} = dl_{i \rightarrow \xi} + dl_{\xi \rightarrow f}. \quad (24)$$

In other words, given

$$\Delta\theta \stackrel{\text{def}}{=} d\theta + (\Delta\theta - d\theta), \quad (25)$$

we have shown by means of entropic arguments that,

$$\|\Delta\theta\| = \|d\theta\| + \|\Delta\theta - d\theta\|, \quad (26)$$

where $\|\Delta\theta\| \stackrel{\text{def}}{=} \sqrt{dl_{i \rightarrow f}^2}$, $\|d\theta\| \stackrel{\text{def}}{=} \sqrt{dl_{i \rightarrow \xi}^2}$ and, $\|\Delta\theta - d\theta\| \stackrel{\text{def}}{=} \sqrt{dl_{\xi \rightarrow f}^2}$. Given Eq. (25), Eq. (26) holds true iff $d\theta$ and $\Delta\theta - d\theta$ are collinear. Therefore, the expected trajectory is a straight line: the triangle defined by the points θ_i , θ_ξ , and θ_f degenerates into a straight line. This is sufficient to determine a short segment of the trajectory: all intermediate states lie on the straight line between θ_i and θ_f . The generalization beyond short trajectories is immediate: if any three nearby points along a curve lie on a straight line the curve is a *geodesic*. This result is independent of the arbitrarily chosen value ξ so the potential consistency problem we mentioned before does not arise. Summarizing, the answer to the ED problem is the following: *the expected trajectory between a known initial and final state is the geodesic that passes through them*. However, the question of whether the actual trajectory is the expected trajectory remains unanswered and depends on whether the information encoded in the initial state is sufficient for prediction.

Volumes in curved statistical manifolds

Once the distances among probability distributions have been assigned using the Fisher-Rao information metric tensor $g_{\mu\nu}(\theta)$, a natural next step is to obtain measures for extended regions in the space of distributions. Consider an n -dimensional volume of the statistical manifold \mathcal{M}_s of distributions $p(x|\theta)$ labelled by parameters θ^μ with $\mu = 1, \dots, n$. The parameters θ^μ are coordinates for the point p and in these coordinates it may not be obvious how to write an expression for a volume element $d\mathcal{V}_{\mathcal{M}_s}$. However, within a sufficiently small region any curved space looks flat. That is to say, curved spaces are locally flat. The idea then is rather simple: within that very small region, we should use Cartesian coordinates wherein the metric takes a very simple form, namely the identity matrix $\delta_{\mu\nu}$. In locally Cartesian coordinates χ^α the volume element is given by the product $d\mathcal{V}_{\mathcal{M}_s} \stackrel{\text{def}}{=} d\chi^1 d\chi^2 \dots d\chi^n$, which in terms of the old coordinates reads,

$$d\mathcal{V}_{\mathcal{M}_s} \stackrel{\text{def}}{=} \left| \frac{\partial \chi}{\partial \theta} \right| d\theta^1 d\theta^2 \dots d\theta^n. \quad (27)$$

The problem at hand then is the calculation of the Jacobian $\left| \frac{\partial \chi}{\partial \theta} \right|$ of the transformation that takes the metric $g_{\mu\nu}$ into its Euclidean form $\delta_{\mu\nu}$. Let the new coordinates be defined by $\chi^\mu \stackrel{\text{def}}{=} \Xi^\mu(\theta^1, \dots, \theta^n)$ where Ξ denotes a coordinates transformation map. A small change $d\theta$ corresponds to a small change $d\chi$,

$$d\chi^\mu \stackrel{\text{def}}{=} X_m^\mu d\theta^m \text{ where } X_m^\mu \stackrel{\text{def}}{=} \frac{\partial \chi^\mu}{\partial \theta^m}, \quad (28)$$

and the Jacobian is given by the determinant of the matrix X_m^μ , $\left| \frac{\partial \chi}{\partial \theta} \right| \stackrel{\text{def}}{=} |\det(X_m^\mu)|$. The distance between two neighboring points is the same whether we compute it in terms of the old or the new coordinates, $dl^2 = g_{\mu\nu} d\theta^\mu d\theta^\nu = \delta_{\alpha\beta} d\chi^\alpha d\chi^\beta$.

Therefore the relation between the old and the new metric is $g_{\mu\nu} = \delta_{\alpha\beta} X_\mu^\alpha X_\nu^\beta$. Taking the determinant of $g_{\mu\nu}$, we obtain $g \stackrel{\text{def}}{=} \det(g_{\mu\nu}) = [\det(X_\mu^\alpha)]^2$ and therefore $|\det(X_\mu^\alpha)| = \sqrt{g}$. Finally, we have succeeded in expressing the volume element totally in terms of the coordinates θ and the known metric $g_{\mu\nu}(\theta)$, $d\mathcal{V}_{\mathcal{M}_s} \stackrel{\text{def}}{=} \sqrt{g} d^n \theta$. Thus, the volume of any extended region on the manifold is given by,

$$\mathcal{V}_{\mathcal{M}_s} \stackrel{\text{def}}{=} \int d\mathcal{V}_{\mathcal{M}_s} = \int \sqrt{g} d^n \theta. \quad (29)$$

Observe that $\sqrt{g} d^n \theta$ is a scalar quantity and is therefore invariant under orientation preserving general coordinate transformations $\theta \rightarrow \theta'$. The square root of the determinant $g(\theta)$ of the metric tensor $g_{\mu\nu}(\theta)$ and the flat infinitesimal volume element $d^n \theta$ transform as,

$$\sqrt{g(\theta)} \xrightarrow{\theta \rightarrow \theta'} \left| \frac{\partial \theta'}{\partial \theta} \right| \sqrt{g(\theta')}, \quad d^n \theta \xrightarrow{\theta \rightarrow \theta'} \left| \frac{\partial \theta}{\partial \theta'} \right| d^n \theta', \quad (30)$$

respectively. Therefore, it follows that

$$\sqrt{g(\theta)} d^n \theta \xrightarrow{\theta \rightarrow \theta'} \sqrt{g(\theta')} d^n \theta'. \quad (31)$$

Equation (31) implies that the infinitesimal statistical volume element is invariant under general coordinate transformations that preserve orientation (that is, with positive Jacobian). For more details on these aspects, we suggest Caticha's 2012 tutorial [31].

Information geometric complexity

The elements (or points) $\{p(x|\theta)\}$ of an n -dimensional curved statistical manifold \mathcal{M}_s are parametrized using n real valued variables $(\theta^1, \dots, \theta^n)$,

$$\mathcal{M}_s \stackrel{\text{def}}{=} \left\{ p(x|\theta) : \theta = (\theta^1, \dots, \theta^n) \in \mathcal{D}_\theta^{(\text{tot})} \right\}. \quad (32)$$

The set $\mathcal{D}_\theta^{(\text{tot})}$ is the entire parameter space (available to the system) and is a subset of \mathbb{R}^n ,

$$\mathcal{D}_\theta^{(\text{tot})} \stackrel{\text{def}}{=} \bigotimes_{k=1}^n I_{\theta^k} = (I_{\theta^1} \otimes I_{\theta^2} \dots \otimes I_{\theta^n}) \subseteq \mathbb{R}^n \quad (33)$$

where I_{θ^k} is a subset of \mathbb{R} and represents the entire range of allowable values for the macrovariable θ^k . For example, considering the statistical manifold of one-dimensional Gaussian probability distributions parametrized in terms of $\theta = (\mu, \sigma)$, we obtain

$$\mathcal{D}_\theta^{(\text{tot})} \stackrel{\text{def}}{=} I_\mu \otimes I_\sigma = [(-\infty, +\infty) \otimes (0, +\infty)], \quad (34)$$

with $I_\mu \otimes I_\sigma \subseteq \mathbb{R}^2$. In the IGAC, we are interested in a probabilistic description of the evolution of a given system in terms of its corresponding probability distribution on \mathcal{M}_s which is homeomorphic to $\mathcal{D}_\theta^{(\text{tot})}$. Assume we are interested in the evolution

from τ_{initial} to τ_{final} . Within the present probabilistic description, this is equivalent to studying the shortest path (or, in terms of the MrE methods [18], the maximally probable path) leading from $\theta(\tau_{\text{initial}})$ to $\theta(\tau_{\text{final}})$.

Is there a way to quantify the complexity of such path? We propose the so-called information geometric entropy (IGE) $S_{\mathcal{M}_s}(\tau)$ as a good complexity quantifier [32]. In what follows, we highlight the key-points leading to the construction of this quantity.

The IGE, an indicator of temporal complexity of geodesic paths within the IGAC framework, is defined as [32],

$$S_{\mathcal{M}_s}(\tau) \stackrel{\text{def}}{=} \log \widetilde{\text{vol}}[\mathcal{D}_\theta(\tau)], \quad (35)$$

where the average dynamical statistical volume $\widetilde{\text{vol}}[\mathcal{D}_\theta(\tau)]$ (which we also choose to name the information geometric complexity (IGC)) is given by,

$$\widetilde{\text{vol}}[\mathcal{D}_\theta(\tau)] \stackrel{\text{def}}{=} \frac{1}{\tau} \int_0^\tau d\tau' \text{vol}[\mathcal{D}_\theta(\tau')]. \quad (36)$$

Note that the tilde symbol in (36) denotes the operation of temporal average. The volume $\text{vol}[\mathcal{D}_\theta(\tau')]$ in the RHS of (36) is given by,

$$\text{vol}[\mathcal{D}_\theta(\tau')] \stackrel{\text{def}}{=} \int_{\mathcal{D}_\theta(\tau')} \rho_{(\mathcal{M}_s, g)}(\theta^1, \dots, \theta^n) d^n \theta, \quad (37)$$

where $\rho_{(\mathcal{M}_s, g)}(\theta^1, \dots, \theta^n)$ is the so-called Fisher density and equals the square root of the determinant of the metric tensor $g_{\mu\nu}(\theta)$ with $\theta \equiv (\theta^1, \dots, \theta^n)$,

$$\rho_{(\mathcal{M}_s, g)}(\theta^1, \dots, \theta^n) \stackrel{\text{def}}{=} \sqrt{g(\theta)}. \quad (38)$$

The integration space $\mathcal{D}_\theta(\tau')$ in (37) is defined as follows,

$$\mathcal{D}_\theta(\tau') \stackrel{\text{def}}{=} \left\{ \theta : \theta^k(0) \leq \theta^k \leq \theta^k(\tau') \right\}, \quad (39)$$

where $k = 1, \dots, n$ and $\theta^k \equiv \theta^k(s)$ with $0 \leq s \leq \tau'$ such that,

$$\frac{d^2 \theta^k(s)}{ds^2} + \Gamma_{lm}^k \frac{d\theta^l}{ds} \frac{d\theta^m}{ds} = 0. \quad (40)$$

The integration space $\mathcal{D}_\theta(\tau')$ in (39) is an n -dimensional subspace of the whole (permitted) parameter space $\mathcal{D}_\theta^{\text{(tot)}}$. The elements of $\mathcal{D}_\theta(\tau')$ are the n -dimensional macrovariables $\{\theta\}$ whose components θ^k are bounded by specified limits of integration $\theta^k(0)$ and $\theta^k(\tau')$ with $k = 1, \dots, n$. The limits of integration are obtained via integration of the n -dimensional set of coupled nonlinear second order ordinary differential equations characterizing the geodesic equations. Formally, the IGE is defined in terms of a averaged parametric $(n+1)$ -fold integral (τ is the parameter) over the multidimensional geodesic paths connecting $\theta(0)$ to $\theta(\tau)$. Further conceptual details about the IGE and the IGC can be found in [33].

APPLICATIONS

In the following, we outline several selected applications concerning the complexity characterization of geodesic paths on curved statistical manifolds within the IGAC framework.

Gaussian statistical models

In [32], [34], we apply the IGAC to study the dynamics of a system with l degrees of freedom, each one described by two pieces of relevant information, its mean expected value and its variance (Gaussian statistical macrostates). This leads to consider a statistical model on a non-maximally symmetric $2l$ -dimensional statistical manifold \mathcal{M}_s . It is shown that \mathcal{M}_s possesses a constant negative scalar curvature proportional to the number of degrees of freedom of the system, $\mathcal{R}_{\mathcal{M}_s} = -l$. It is found that the system explores statistical volume elements on \mathcal{M}_s at an exponential rate. The information geometric entropy $S_{\mathcal{M}_s}$ increases linearly in time (statistical evolution parameter) and, moreover, is proportional to the number of degrees of freedom of the system, $S_{\mathcal{M}_s} \stackrel{\tau \rightarrow \infty}{\sim} l\lambda\tau$ where λ is the maximum positive Lyapunov exponent characterizing the model. The geodesics on \mathcal{M}_s are hyperbolic trajectories. Using the Jacobi-Levi-Civita (JLC) equation for geodesic spread, we show that the Jacobi vector field intensity $J_{\mathcal{M}_s}$ diverges exponentially and is proportional to the number of degrees of freedom of the system, $J_{\mathcal{M}_s} \stackrel{\tau \rightarrow \infty}{\sim} l \exp(\lambda\tau)$. The exponential divergence of the Jacobi vector field intensity $J_{\mathcal{M}_s}$ is a *classical* feature of chaos. Therefore, we conclude that $\mathcal{R}_{\mathcal{M}_s} = -l$, $J_{\mathcal{M}_s} \stackrel{\tau \rightarrow \infty}{\sim} l \exp(\lambda\tau)$ and $S_{\mathcal{M}_s} \stackrel{\tau \rightarrow \infty}{\sim} l\lambda\tau$. Thus, $\mathcal{R}_{\mathcal{M}_s}$, $S_{\mathcal{M}_s}$ and $J_{\mathcal{M}_s}$ behave as proper indicators of chaoticity and are proportional to the number of Gaussian-distributed microstates of the system. This proportionality, even though proven in a very special case, leads to conclude there may be a substantial link among these information geometric indicators of chaoticity.

Gaussian statistical models and correlations

In [35], we apply the IGAC to study the information constrained dynamics of a system with $l = 2$ microscopic degrees of freedom. As working hypothesis, we assume that such degrees of freedom are represented by two correlated Gaussian-distributed microvariables characterized by the same variance. We show that the presence of microcorrelations lead to the emergence of an asymptotic information geometric compression of the statistical macrostates explored by the system at a faster rate than that observed in absence of microcorrelations. This result constitutes an important and explicit connection between micro-correlations and macro-complexity in statistical dynamical systems. The relevance of our finding is twofold: first, it provides a neat description of the effect of information encoded in microscopic variables on experimentally observable quantities defined in terms of dynamical macroscopic variables; second, it clearly shows the change in behavior of the macroscopic complexity of a statistical model caused by the existence of correlations at the underlying microscopic level.

Random frequency macroscopic IHOs

The problem of General Relativity is twofold: one is how geometry evolves, and the other is how particles move in a given geometry. The IGAC focuses on how particles move in a given

geometry and neglects the other problem, the evolution of the geometry. The realization that there exist two separate and distinct problems was a turning point in our research and lead to an unexpected result. In [20], we explore the possibility of using well established principles of inference to derive Newtonian dynamics from relevant prior information codified into an appropriate statistical manifold. The basic assumption is that there is an irreducible uncertainty in the location of particles so that the state of a particle is defined by a probability distribution. The corresponding configuration space is a statistical manifold the geometry of which is defined by the Fisher-Rao information metric. The trajectory follows from a principle of inference, the MrE method. There is no need for additional physical postulates such as an action principle or equation of motion, nor for the concept of mass, momentum and of phase space, not even the notion of time. The resulting entropic dynamics reproduces Newton's mechanics for any number of particles interacting among themselves and with external fields. Both the mass of the particles and their interactions are explained as a consequence of the underlying statistical manifold.

Following this line of reasoning, in [36], [37] we present an information geometric analogue of the Zurek-Paz quantum chaos criterion in the *classical reversible limit*. This analogy is illustrated by applying the IGAC to a set of n -uncoupled three-dimensional anisotropic inverted harmonic oscillators (IHOs) characterized by a Ohmic distributed frequency spectrum.

Regular and chaotic quantum spin chains

In [38], [39], we study the entropic dynamics on curved statistical manifolds induced by classical probability distributions of common use in the study of regular and chaotic quantum energy level statistics. Specifically, we propose an information geometric characterization of chaotic (integrable) energy level statistics of a quantum antiferromagnetic Ising spin chain in a tilted (transverse) external magnetic field. We consider the IGAC of a Poisson distribution coupled to an Exponential bath (spin chain in a *transverse* magnetic field, regular case) and that of a Wigner-Dyson distribution coupled to a Gaussian bath (spin chain in a *tilted* magnetic field, chaotic case). Remarkably, we show that in the former case the IGE exhibits asymptotic logarithmic growth while in the latter case the IGE exhibits asymptotic linear growth. In view of these findings, we conjecture our IGAC might find some potential physical applications in quantum energy level statistics as well.

Complexity reduction and statistical embedding

In [40], we characterize the complexity of geodesic paths on a curved statistical manifold \mathcal{M}_s through the asymptotic computation of the IGC and the Jacobi vector field intensity $J_{\mathcal{M}_s}$. The manifold \mathcal{M}_s is a $2l$ -dimensional Gaussian model reproduced by an appropriate embedding in a larger $4l$ -dimensional Gaussian manifold and endowed with a Fisher-Rao information metric $g_{\mu\nu}(\theta)$ with non-trivial off diagonal terms. These terms emerge due to the presence of a correlational structure (embedding constraints) among the statistical variables on the larger manifold and are characterized by macroscopic correlational coefficients r_k . First, we observe a power law decay of the information geometric complexity at a rate determined by the coefficients r_k and conclude that the non-trivial off diagonal terms lead to the emergence of an asymptotic information geometric compression of the explored macrostates on \mathcal{M}_s . Finally, we also observe that

the presence of such embedding constraints leads to an attenuation of the asymptotic exponential divergence of the Jacobi vector field intensity. We are confident the work presented in [40] constitutes a further non-trivial step towards the characterization of the complexity of microscopically correlated multi-dimensional Gaussian statistical models, and other models of relevance in realistic physical systems.

Scattering induced quantum entanglement

In [41], [42], we present an information geometric analysis of entanglement generated by s -wave scattering between two Gaussian wave packets. We conjecture that the pre and post-collisional quantum dynamical scenarios related to an elastic head-on collision are macroscopic manifestations emerging from microscopic statistical structures. We then describe them by uncorrelated and correlated Gaussian statistical models, respectively. This allows us to express the entanglement strength in terms of scattering potential and incident particle energies. Furthermore, we show how the entanglement duration can be related to the scattering potential and incident particle energies. Finally, we discuss the connection between entanglement and complexity of motion. We are confident that the work presented in [41], [42] represents significant progress toward the goal of understanding the relationship between statistical microcorrelations and quantum entanglement on the one hand and the effect of microcorrelations on the complexity of informational geodesic flows on the other. It is also our hope to build upon the techniques employed in this work to ultimately establish a sound information geometric interpretation of quantum entanglement together with its connection to complexity of motion in more general physical scenarios.

Suppression of classical chaos and quantization

In [43], we study the information geometry and the entropic dynamics of a $3d$ Gaussian statistical model. We then compare our analysis to that of a $2d$ Gaussian statistical model obtained from the higher-dimensional model via introduction of an additional information constraint that resembles the quantum mechanical canonical minimum uncertainty relation. We show that the chaoticity (temporal complexity) of the $2d$ Gaussian statistical model, quantified by means of the IGE and the Jacobi vector field intensity, is softened with respect to the chaoticity of the $3d$ Gaussian statistical model. In view of the similarity between the information constraint on the variances and the phase-space coarse-graining imposed by the Heisenberg uncertainty relations, we suggest that our work provides a possible way of explaining the phenomenon of suppression of classical chaos operated by quantization.

In the same vein of our work in [43], a recent investigation claims that quantum mechanics can reduce the statistical complexity of classical models [44]. Specifically, it was shown that mathematical models featuring quantum effects can be as predictive as classical models although implemented by simulators that require less memory, that is, less statistical complexity. Of course, these two works use different definitions of complexity and their ultimate goal is definitively not the same. However, it is remarkable that both of them exploit some quantum feature, Heisenberg's uncertainty principle in [43] and the quantum state discrimination (information storage) method in [44], to exhibit the complexity softening effects.

Is there any link between Heisenberg's uncertainty princi-

ple and quantum state discrimination? Recently, it was shown that any violation of uncertainty relations in quantum mechanics also leads to a violation of the second law of thermodynamics [45]. In addition, it was reported in [46] that a violation of Heisenberg's uncertainty principle allows perfect state discrimination of nonorthogonal states which, in turn, violates the second law of thermodynamics [47]. The possibility of distinguishing nonorthogonal states is directly related to the question of how much information we can store in a quantum state. Information storage and memory are key quantities for the characterization of statistical complexity. In view of these considerations, it would be worthwhile exploring the possible thermodynamic link underlying these two different complexity measures.

CLOSING REMARKS

In this Contribution, we presented our information geometric measure of complexity of geodesic paths on curved statistical manifolds underlying the entropic dynamics of classical physical systems described by probability distributions within the IGAC framework. We also provided several illustrative examples of entropic dynamical models used to infer macroscopic predictions when only partial knowledge of the microscopic nature of the system is available. Finally, among other things, we also presented entropic arguments to briefly address complexity softening effects due to statistical embedding procedures.

All too often that which is correct is not new and that which is new is not correct. Being moderately conservative people, we hope that what we presented satisfies at least of one these two sub-optimal situations. We are aware that several issues remain unsolved within the IGAC framework and much more work remains to be done. However, we are immensely gratified that our scientific vision is gaining more attention and is becoming a source of inspiration for other researchers [48].

To conclude, we would like to outline the three possible lines of research for future investigations:

- Extend the IGAC to a fully quantum setting where density matrices play the analogous role of the classical probability distributions: since quantum computation can be viewed as geometry [49], [50] and computational tasks have, in general, a thermodynamic cost [51], we might envision a *thermodynamics of quantum information geometric flows on manifolds of density operators* whose ultimate internal consistency check forbids the prediction of the impossible thermodynamic machine.
- Understand the role of thermodynamics as the possible bridge among different complexity measures: softening effects in the classical-to-quantum transitions can occur provided that the various quantum effects being exploited by the different complexity measures do not violate the second law of thermodynamics;
- Describe and understand the role of thermodynamics within the IGAC: thermodynamics plays a prominent role in the entropic analysis of chaotic dynamics [52]. Chaoticity and entropic arguments are the bread and butter of the IGAC. Furthermore, inspired by [53], we could investigate the possible connection between thermodynamics inefficiency measured by dissipation and ineffectiveness of entropic dynamical models in making reliable macroscopic predictions.

ACKNOWLEDGMENT

I acknowledge that this work reflects my academic interaction with the following scientists: Erik Bollt (Potsdam-NY, USA), Carlo Bradaschia (Pisa, Italy), Ariel Caticha (Albany-NY, USA), Giancarlo Cella (Pisa, Italy), Stefano Mancini (Camerino, Italy), Jie Sun (Potsdam-NY, USA), Peter van Loock (Erlangen and Mainz, Germany). I also thank Sean Alan Ali and Adom Giffin whose careful reviews strengthened this Contribution and Denis Gonta for technical assistance. Finally, special thanks go to Gianpaolo Beretta for inviting me as an Invited Speaker at *The 12th Biannual Joint European Thermodynamics Conference* in Brescia, Italy.

REFERENCES

- [1] J. P. Crutchfield and B. S. McNamara, *Equations of motions from a data series*, *Complex Systems* **1**, 417 (1987).
- [2] I. J. Myung, V. Balasubramanian, and M. A. Pitt, *Counting probability distributions: differential geometry and model selection*, *Proc. Natl Acad. Sci.* **97**, 11170 (2000).
- [3] V. Balasubramanian, *Statistical inference, Occam's razor and statistical mechanics on the space of probability distributions*, *Neural Computation* **9**, 268 (1997).
- [4] G. Cella, C. N. Colacino, E. Cuoco, A. Di Virgilio, T. Regimbau, E. L. Robinson, and J. T. Whelan, *Prospects for stochastic background searches using VIRGO and LSC interferometers*, *Class. Quant. Grav.* **24**, S639 (2007).
- [5] T. S. Cubitt, J. Eisert, and M. W. Wolf, *Extracting dynamical equations from experimental data is NP hard*, *Phys. Rev. Lett.* **108**, 120503 (2012).
- [6] M. Gell-Mann, *What is complexity?*, *Complexity* **1**, 1 (1995).
- [7] D. P. Feldman and J. P. Crutchfield, *Measures of complexity: Why?*, *Phys. Lett.* **A238**, 244 (1998).
- [8] J. P. Crutchfield and K. Young, *Inferring statistical complexity*, *Phys. Rev. Lett.* **63**, 105 (1989).
- [9] R. Landauer, *A simple measure of complexity*, *Nature* **336**, 306 (1988).
- [10] C. H. Bennett, *How to define complexity in physics and why*, in *Complexity, Entropy, and the Physics of Information: Proceedings of the Santa Fe Institute Workshop*, ed. by W. H. Zurek (1989).
- [11] R. Romano and P. van Loock, *Quantum control of noisy channels*, arXiv:quant-ph/0811.3014 (2008).
- [12] S. Lloyd and H. Pagels, *Complexity as thermodynamic depth*, *Ann. Phys.* **188**, 186 (1988).
- [13] C. H. Bennett, *On the nature and origin of complexity in discrete, homogeneous, locally-interacting systems*, *Foundations of Physics* **16**, 585 (1986).
- [14] S. Lloyd, *Core-halo instability in dynamical systems*, arXiv:nlin.CD/1302.3199 (2013).
- [15] J. Sun, E. M. Bollt, and T. Nishikawa, *Judging model reduction of complex systems*, *Phys. Rev.* **E83**, 046125 (2011).
- [16] E. T. Jaynes, *Macroscopic prediction*, in *Complex Systems and Operational Approaches in Neurobiology, Physics, and Computers*, ed. by H. Haken, Springer, Berlin (1985).
- [17] A. Caticha, *Entropic dynamics*, *AIP Conf. Proc.* **617**, 302 (2002).
- [18] A. Caticha and A. Giffin, *Updating probabilities*, *AIP*

- Conf. Proc. **872**, 31 (2006).
- [19] S. Amari and H. Nagaoka, *Methods of Information Geometry*, Oxford University Press (2000).
- [20] A. Caticha and C. Cafaro, *From information geometry to Newtonian dynamics*, AIP Conf. Proc. **954**, 165 (2007).
- [21] A. Caticha, *Entropic dynamics, time and quantum theory*, J. Phys. A: Math. Theor. **44**, 225303 (2011).
- [22] C. Cafaro, *The Information Geometry of Chaos*, PhD Thesis, State University of New York at Albany, Albany-NY, USA (2008).
- [23] L. Casetti, C. Clementi, and M. Pettini, *Riemannian theory of Hamiltonian chaos and Lyapunov exponents*, Phys. Rev. **E54**, 5969 (1996).
- [24] M. Di Bari and P. Cipriani, *Geometry and chaos on Riemann and Finsler manifolds*, Planet. Space Sci. **46**, 1543 (1998).
- [25] C. G. J. Jacobi, *Vorlesungen uber dynamik*, Reimer, Berlin (1866).
- [26] T. Kawabe, *Indicator of chaos based on the Riemannian geometric approach*, Phys. Rev. **E71**, 017201 (2005).
- [27] R.A. Fisher, *Theory of statistical estimation*, Proc. Cambridge Philos. Soc. **122**, 700 (1925).
- [28] C.R. Rao, *Information and accuracy attainable in the estimation of statistical parameters*, Bull. Calcutta Math. Soc. **37**, 81 (1945).
- [29] N. N. Cencov, *Statistical decision rules and optimal inference*, Transl. Math. Monographs, vol. **53**, Amer. Math. Soc., Providence-RI (1981).
- [30] L. L. Campbell, *An extended Cencov characterization of the information metric*, Proc. Am. Math. Soc. **98**, 135 (1986).
- [31] A. Caticha, *Tutorial: Entropic Inference and The Foundations of Physics*, presented at the 11th Brazilian Statistical Bayesian Meeting, Amparo-SP-Brazil (2012).
- [32] C. Cafaro and S. A. Ali, *Jacobi fields on statistical manifolds of negative curvature*, Physica **D234**, 70 (2007).
- [33] C. Cafaro, A. Giffin, S. A. Ali, and D.-H. Kim, *Reexamination of an information geometric construction of entropic indicators of complexity*, Appl. Math. Comput. **217**, 2944 (2010).
- [34] C. Cafaro, *Information-geometric indicators of chaos in Gaussian models on statistical manifolds of negative Ricci curvature*, Int. J. Theor. Phys. **47**, 2924 (2008).
- [35] S. A. Ali, C. Cafaro, D.-H. Kim, and S. Mancini, *The effect of microscopic correlations on the information geometric complexity of Gaussian statistical models*, Physica **A389**, 3117 (2010).
- [36] C. Cafaro, *Works on an information geometrodynamical approach to chaos*, Chaos, Solitons & Fractals **41**, 886 (2009).
- [37] C. Cafaro and S. A. Ali, *Geometrodynamics of information on curved statistical manifolds and its applications to chaos*, EJTP **5**, 139 (2008).
- [38] C. Cafaro, *Information geometry, inference methods and chaotic energy levels statistics*, Mod. Phys. Lett. **B22**, 1879 (2008).
- [39] C. Cafaro and S. A. Ali, *Can chaotic quantum energy levels statistics be characterized using information geometry and inference methods?*, Physica **A387**, 6876 (2008).
- [40] C. Cafaro and S. Mancini, *Quantifying the complexity of geodesic paths on curved statistical manifolds through information geometric entropies and Jacobi fields*, Physica **D240**, 607 (2011).
- [41] D.-H. Kim, S. A. Ali, C. Cafaro, and S. Mancini, *Information geometric modeling of scattering induced quantum entanglement*, Phys. Lett. **A375**, 2868 (2011).
- [42] D.-H. Kim, S. A. Ali, C. Cafaro, and S. Mancini, *Information geometry of quantum entangled Gaussian wavepackets*, Physica **A391**, 4517 (2012).
- [43] C. Cafaro, A. Giffin, C. Lupo, and S. Mancini, *Softening the complexity of entropic motion on curved statistical manifolds*, Open Syst. & Inf. Dyn. **19**, 1250001 (2012).
- [44] M. Gu, K. Wiesner, E. Rieper, and V. Vedral, *Quantum mechanics can reduce the complexity of classical models*, Nature Commun. **3**, 1 (2012).
- [45] E. Hanggi and S. Wehner, *A violation of the uncertainty principle implies a violation of the second law of thermodynamics*, arXiv:quant-ph/1205.6894 (2012).
- [46] J. L. Pienaar, T. C. Ralph, and C. R. Myers, *Open time-like curves violate Heisenberg's uncertainty principle*, arXiv:quant-ph/1206.5485 (2012).
- [47] A. Peres, *Quantum Theory: Concepts and Methods*, Kluwer Academic Publishers (1995).
- [48] L. Peng, H. Sun, and G. Xu, *Information geometric characterization of the complexity of fractional Brownian motion*, J. Math. Phys. **53**, 123305 (2012).
- [49] M. A. Nielsen, M. R. Dowling, M. Gu, and A. C. Doherty, *Quantum computation as geometry*, Science **311**, 1133 (2006).
- [50] H. E. Brandt, *Riemannian geometry of quantum computation*, in Quantum Information and Its Contribution to Mathematics, edited by S. J. Lomonaco, AMS Proceedings of Symposia in Applied Mathematics, Vol. **68**, pp. 61, American Mathematical Society, Providence, RI, USA (2010).
- [51] C. H. Bennett, *The thermodynamics of computation-a review*, Int. J. Theor. Phys. **21**, 905 (1982).
- [52] C. Beck and F. Schlogl, *Thermodynamic Analysis of Chaotic Systems: An Introduction*, Cambridge University Press (1995).
- [53] S. Still, D. A. Sivak, A. J. Bell, and G. E. Crooks, *Thermodynamics of prediction*, Phys. Rev. Lett. **109**, 120604 (2012).

MINIMUM FLOW POTENTIAL (MASSIEU FUNCTION) IN FLOW SYSTEMS AND CONNECTION TO ENTROPY PRODUCTION EXTREMA

Robert K. Niven*, Bernd R. Noack^o

*School of Engineering and IT, UNSW at ADFA, Canberra, ACT 2600, Australia, r.niven@adfa.edu.au
^oInstitut PPrime, CNRS – Université de Poitiers – ENSMA, Poitiers, France, Bernd.Noack@univ-poitier.fr

EXTENDED ABSTRACT

Recently, the first author presented a new formulation of non-equilibrium thermodynamics, based on Jaynes' maximum entropy (MaxEnt) method, for the analysis of dissipative flow systems [1,2,3,4]. The analysis employs a *flux entropy* concept, representing the uncertainty associated with the set of instantaneous fluxes through the boundary of a fluid control volume, as well as the instantaneous rates of spontaneous chemical reactions within the control volume. Applying MaxEnt, these are constrained by mean values of the fluxes through and rates within the element. For an open system, this yields a new nonequilibrium thermodynamic potential (Massieu function), which can be termed the *flux potential*, which is minimised at steady-state flow. This minimum then reduces, in different circumstances, to a minimum or maximum in the rate of entropy production, suggestive of the respective extremum principles advocated by Prigogine [5] or Paltridge and Zeigler [6, 7]. The implications of the analysis for dissipative flow systems have subsequently been explored [1,2,3,4,8]. The analysis leads naturally to a thermodynamics-inspired mathematical formulation of flow systems, with conjugate extensive and intensive parameters (flows and gradients), first-order and second-order derivatives (giving susceptibilities, fluctuations and Maxwell reciprocal relations), a Legendre transformation between entropy- and potential-based representations, and a Riemannian geometric representation of the manifold of steady states [1,2,3,4,8]. This framework provides a new technique for prediction of the steady state of a flow system, subject only to summary information about the dynamics (e.g. without requiring the full, time-varying Navier-Stokes or energy equations).

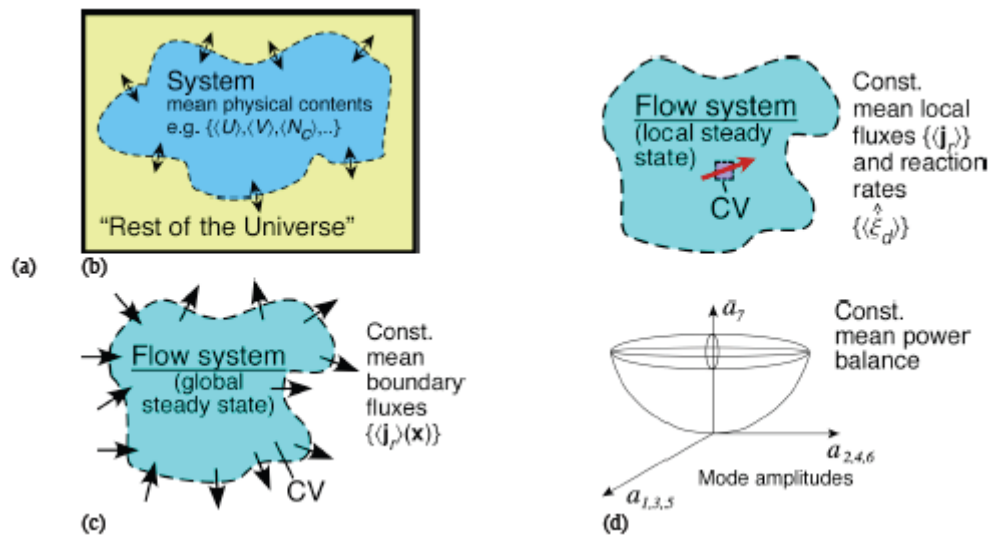


Figure 1: Types of systems amenable to analysis by MaxEnt: (a) equilibrium systems, (b) local and (c) global steady-state flowsystems [1,2,3,4] and (d) Galerkin reduced-order model [9,10,11].

In this study, a generic version of the derivation is first provided, encompassing four seemingly disparate formulations of (a) equilibrium thermodynamics; (b) local and (c) global steady-state flow in physical space; and (d) a Galerkin spectral model, based on a principal orthogonal decomposition of the flow field [9,10,11]. These are represented in Figure 1. The local and global flow system representations require careful control volume analysis [4], and lead into a discussion of scale effects, the definition of steady state, analysis by compartments and the effect of radiative transfer. In the Galerkin decomposition, the MaxEnt closure is applied to a seven-mode Galerkin model of an incompressible periodic cylinder wake at $Re=100$. The MaxEnt prediction of mean amplitude values is shown to be in close agreement with Direct Navier-Stokes simulations, at much lower computation cost. For all four representations, the choice of prior probabilities is critical to the analysis, and is examined in detail.

REFERENCES

- [1] R.K. Niven, Physical Review E 80(2): 021113 (2009).
- [2] R.K. Niven, Philosophical Transactions B, 365: 1323-1331 (2010).
- [3] R.K. Niven, Journal of Non-Equilibrium Thermodynamics, 35: 347-378 (2010).

- [4] R.K. Niven and B.R. Noack, in submission to Dewar R.C., Lineweaver C., Niven R.K., Regenauer-Lieb K. (eds), *Beyond the Second Law: Entropy Production and Non-Equilibrium Systems*, Springer, NY.
- [5] I. Prigogine, *Introduction to Thermodynamics of Irreversible Processes*, 3rd ed., Interscience Publ., NY (1967).
- [6] G.W. Paltridge, *Quart. J. Royal Meteorol. Soc.* 101, 475 (1975); 104, 927 (1978).
- [7] H. Ziegler, *An Introduction to Thermomechanics*, North-Holland (1983).
- [8] R.K. Niven, B. Andresen, in Dewar, R.L., Detering, F. (eds) *Complex Physical, Biophysical and Econophysical Systems*, World Scientific, Hackensack, NJ. ISBN: 978-981-4277-31-0, pp 283-318 (2009).
- [9] B.R. Noack & R.K. Niven, *Journal of Fluid Mechanics*, 700: 187-213, (2012).
- [10] B.R. Noack & R.K. Niven. (in press), *Computers and Mathematics with Applications*, accepted 17 February 2013.
- [11] B.R. Noack & R.K. Niven (2011), *APS Division of Fluid Dynamics (DFD11)*, Baltimore, Maryland, 20–22 Nov. 2011.

GENERAL CHARACTERISTICS OF ENTROPY PRODUCTION IN NONLINEAR DYNAMIC SYSTEMS

Hisashi Ozawa*, Shinya Shimokawa^o

*Hiroshima University, Higashi-Hiroshima, Japan

^oNational Research Institute for Earth Science and Disaster Prevention, Tsukuba, Japan

ABSTRACT

A basic expression for entropy production due to irreversible flux of heat or momentum is formulated together with balance equations for energy and momentum in a fluid system. It is shown that entropy production always decreases with time when the system is of a pure diffusion type without advection of heat or momentum. The minimum entropy production (MinEP) property is thus intrinsic to a pure diffusion-type system. However, this MinEP property disappears when the system is subject to advection of heat or momentum. When the rate of advection exceeds the rate of diffusion, entropy production tends to increase over time. A simple stability analysis shows that the rate of change of entropy production is proportional to the growth rate of an arbitrary external perturbation. The entropy production increases when the perturbation grows in the system under a dynamically unstable state, whereas it decreases when the perturbation is damped in the system in a stable state. The maximum entropy production (MaxEP) can therefore be understood as a characteristic feature of systems with dynamic instability. Implications of the result for time evolution of nonlinear dynamic phenomena under different external conditions are discussed from this thermodynamic viewpoint.

INTRODUCTION

Since an early investigation by Ziegler [1], maximum entropy production (MaxEP) has been suggested as a general thermodynamic property of nonlinear non-equilibrium phenomena, with later studies showing that the MaxEP state is consistent with steady states of a variety of nonlinear phenomena. These include the general circulation of the atmosphere and oceans [2–4], thermal convection [5], turbulent shear flow [6], climates of other planets [7], oceanic general circulation [8, 9], crystal growth morphology [10] and granular flows [11]. While the underlying physical mechanism is still debated, the MaxEP state is shown to be identical to a state of maximum generation of available energy [12, 13]. Moreover, recent theoretical studies suggest that the MaxEP state is the most probable state that is realized by non-equilibrium systems [14, 15].

It is known, however, that entropy production in a linear process tends to decrease with time and reach a minimum in a final steady state when a thermodynamic intensive variable (such as temperature) is fixed at the system boundary. This tendency was first suggested for a linear chemical process in a discontinuous system by Prigogine [16], and then extended to the case of a linear diffusion process in a continuous system [17]. Since then, this minimum entropy production (MinEP) principle has become widely known in the field of non-equilibrium thermodynamics. Although a number of attempts have been made to extend this MinEP principle to a general one including nonlinear processes, the results remain controversial and inconclusive (e.g. [18, 19]). In fact, Prigogine [20] noted that “it came as a great surprise when it was shown that in systems far from equilibrium the thermodynamic behavior could be quite different — in fact, even *directly opposite* that predicted by the theorem of minimum entropy production”.

Sawada [21] pointed out the limitations of the MinEP principle, and instead proposed the MaxEP principle as a general variational principle for nonlinear systems that are far from equilibrium. Dewar and Maritan [22] showed using Jaynes’s maximum entropy method that a state of minimum dissipation (MinEP) is selected for a system without dynamic instability, whereas that of maximum dissipation (MaxEP) is selected for a system with dynamic instability. It seems therefore that the existence of dynamic instability plays a key role in determining the behavior of entropy production in nonlinear non-equilibrium systems. However, the nature of the dynamic instability as well as its relation to nonlinearity remains unclear. Moreover, until now, we do not have a reasonable specification of the dynamic conditions under which the MinEP or MaxEP state is realized.

In order to clarify the issues in the phenomena mentioned above, we have investigated the behavior of time evolution of entropy production in a fluid system. Based on a general expression of entropy production and balance equations of energy and momentum, we present a condition under which the MinEP state is realized in the course of time in a system of linear diffusion. We then add nonlinear advection terms in the balance equations, and examine the condition under which the MinEP state becomes unstable and the MaxEP state is realized in the system. We show that the rate of advection of heat or momentum plays an important role in the enhancement of entropy production in a fluid system that possesses dynamic instability. Results obtained from this study are summarized, and a few remarks are presented concerning time evolution of nonlinear dynamic phenomena under different external conditions. This study is an extension of our previous work on thermodynamic properties of dynamic fluid systems by Ozawa and Shimokawa [23].

LINEAR DIFFUSION

Let us consider a fluid system in which several irreversible processes take place. These processes can be molecular diffusion of heat under a temperature gradient, molecular diffusion of momentum under a velocity gradient, or diffusion of a chemical component under a gradient of density of the chemical component. All these diffusion processes contribute to an increase in entropy of the total system consisting of the fluid system and its surroundings. A general expression for the rate of entropy production per unit time by these irreversible processes is given by

$$\dot{\sigma} = \int_V \sum_i \mathbf{J}_i \cdot \mathbf{X}_i dV, \quad (1)$$

where $\dot{\sigma}$ is the rate of entropy production, \mathbf{J}_i is the i -th diffusive flux density, \mathbf{X}_i is the gradient in the corresponding intensive variable that drives the flux, and the integration is taken over the whole volume of the system (e.g. [18]). If the flux density is heat, momentum, or a chemical component, the corresponding intensive variable is temperature ($1/T$), velocity ($-\mathbf{v}/T$), or chemical potential ($-\mu/T$) respectively. It should be noted that the diffusive flux \mathbf{J}_i does not, in principle, include a flux due to advection (i.e. coherent motion of fluid), which is intrinsically a reversible process¹. However, advection significantly enhances the local gradient of the intensive variable at the moving front, and hence entropy production is also enhanced. We will see how entropy production can change with and without advection.

Heat Diffusion

As the simplest example, let us discuss diffusion of heat under temperature gradient in a fluid system. In this case, Eq. (1) is

$$\dot{\sigma}_h = \int_V \mathbf{J}_h \cdot \nabla \left(\frac{1}{T} \right) dV = \int_V L_h \left[\nabla \left(\frac{1}{T} \right) \right]^2 dV, \quad (2)$$

where \mathbf{J}_h is the diffusive heat flux density due to heat conduction, T is the temperature and L_h is the kinetic coefficient relating the diffusive heat flux and the temperature gradient: $\mathbf{J}_h = L_h \nabla(1/T) = -\lambda \nabla T$, with $\lambda = L_h/T^2$ being the thermal conductivity in Fourier's law. In Eq. (2) we have assumed linearity between the diffusive heat flux and the temperature gradient.

We can show that the entropy production due to heat diffusion [Eq. (2)] is a monotonically decreasing function of time when the intensive variable (T) is fixed at the boundary of the system and when there is no advective heat transport in the system. Taking the time derivative of Eq. (2), and assuming a constancy of L_h in the temperature range of the system ($dL_h/dt = 0$), we get

$$\frac{d\dot{\sigma}_h}{dt} = 2 \int_V \mathbf{J}_h \cdot \nabla \left[\frac{\partial}{\partial t} \left(\frac{1}{T} \right) \right] dV. \quad (3)$$

¹ One can include a reversible flux due to advection in the balance equation of entropy, but it results in no contribution to entropy production after the integration over the whole volume of a fluid system (see, e.g., [24], Sec. 49; [13], Sec. 2.4).

This expression leads, with integration by parts, to

$$\frac{d\dot{\sigma}_h}{dt} = 2 \int_A \left[\frac{\partial}{\partial t} \left(\frac{1}{T} \right) \right] \mathbf{J}_h \cdot \mathbf{n} dA - 2 \int_V \left[\frac{\partial}{\partial t} \left(\frac{1}{T} \right) \right] \nabla \cdot \mathbf{J}_h dV, \quad (4)$$

where \mathbf{n} is the unit vector normal to the system boundary and directed to outward, and A is the surface bounding the system. The first surface integral vanishes when the temperature is fixed at the boundary (i.e. $\partial T/\partial t = 0$). Using Fourier's law ($\mathbf{J}_h = -\lambda \nabla T$) and assuming the uniformity of λ in the system ($\nabla \lambda = 0$), the second volume integral leads to

$$\frac{d\dot{\sigma}_h}{dt} = 2 \int_V \lambda \nabla^2 T \frac{\partial}{\partial t} \left(\frac{1}{T} \right) dV. \quad (5)$$

Equation (5) shows that the rate of change of entropy production is a function of the heat diffusion rate ($\lambda \nabla^2 T$) and the rate of change of temperature ($\partial T/\partial t$). The heat diffusion rate is related to the balance equation for internal energy (e.g. [25]) as

$$\rho \frac{\partial}{\partial t} (c_v T) = -\rho \mathbf{v} \cdot \nabla (c_v T) + \lambda \nabla^2 T - p \nabla \cdot \mathbf{v} + \mathbf{\Pi} : \nabla \mathbf{v}, \quad (6)$$

where ρ is the fluid density, c_v is the specific heat at constant volume, \mathbf{v} is the fluid velocity, p is the pressure and $\mathbf{\Pi}$ is the viscous stress. This equation shows that the rate of temperature increase is caused by the sum of the rates of heat advection, heat diffusion, cooling by volume expansion and viscous heating. Substituting $\lambda \nabla^2 T$ from Eq. (6) into Eq. (5), and assuming a constancy of c_v in the fluid system ($dc_v/dt = 0$), we get

$$\frac{d\dot{\sigma}_h}{dt} = 2 \int_V \left[\rho c_v \frac{\partial T}{\partial t} + \rho c_v \mathbf{v} \cdot \nabla T + p \nabla \cdot \mathbf{v} - \mathbf{\Pi} : \nabla \mathbf{v} \right] \frac{\partial}{\partial t} \left(\frac{1}{T} \right) dV. \quad (7)$$

If we consider a situation with no convective motion ($\mathbf{v} = 0$), Eq. (7) reduces to

$$\frac{d\dot{\sigma}_{h,\text{stat}}}{dt} = -2 \int_V \frac{\rho c_v}{T^2} \left(\frac{\partial T}{\partial t} \right)^2 dV \leq 0, \quad (8)$$

where the suffix stat denotes the static state with no motion. The rate of change of entropy production is negative in this static case, because ρ and c_v are positive definite. Equation (8) shows that entropy production due to pure heat conduction tends to decrease with time, and reaches a minimum in the final steady state ($\partial T/\partial t = 0$) provided there is no convective motion in the fluid. This tendency was first suggested by Prigogine [16], and is called the minimum entropy production (MinEP) principle. While several attempts have been made to extend this principle to a general one including dynamic motion, the results remain controversial and inconclusive [17, 18]. As we shall see in a later section, when advection due to dynamic motion is nonzero, the local rate of entropy production can either increase or decrease, depending on the rate of heat advection ($\mathbf{v} \cdot \nabla T$); the sign of $d\dot{\sigma}_h/dt$ becomes indefinite and even positive in some cases.

Momentum Diffusion

A similar result can be obtained for the diffusion of momentum due to viscosity under a velocity gradient. Suppose that a viscous fluid with a uniform viscosity is flowing in a system with a constant temperature T . In this case, entropy production due to momentum diffusion is given by

$$\dot{\sigma}_m = \int_V \frac{\mathbf{\Pi} : \nabla \mathbf{v}}{T} dV. \quad (9)$$

Here, the numerator represents the scalar product of the viscous stress tensor and the velocity gradient, and is identical to the heating rate due to viscosity per unit volume per unit time in the fluid. Assuming a linear relation between the viscous stress and the velocity gradient, we can drive the time derivative of the rate of entropy production after a few manipulations²:

$$\frac{d\dot{\sigma}_m}{dt} = \int_V \frac{\partial}{\partial t} \left(\frac{\mathbf{\Pi} : \nabla \mathbf{v}}{T} \right) dV = 2 \int_V \frac{1}{T} \left[\mathbf{\Pi} : \nabla \left(\frac{\partial \mathbf{v}}{\partial t} \right) \right] dV. \quad (10)$$

By a sequence of transformations similar to those from Eq. (3) to Eq. (5), we get

$$\frac{d\dot{\sigma}_m}{dt} = -2 \int_V \frac{1}{T} \left[\mu \nabla^2 \mathbf{v} + \frac{\mu}{3} \nabla (\nabla \cdot \mathbf{v}) \right] \cdot \left(\frac{\partial \mathbf{v}}{\partial t} \right) dV, \quad (11)$$

where μ is the viscosity of the fluid. Here we have assumed that velocity is fixed at the boundary ($\partial \mathbf{v} / \partial t = 0$). The diffusion rate of momentum [$\mu \nabla^2 \mathbf{v} + \mu \nabla (\nabla \cdot \mathbf{v}) / 3$] is related to the balance equation of momentum — the Navier–Stokes equation — as

$$\rho \frac{\partial \mathbf{v}}{\partial t} = -\rho (\mathbf{v} \cdot \nabla) \mathbf{v} - \nabla p + \mu \nabla^2 \mathbf{v} + \frac{\mu}{3} \nabla (\nabla \cdot \mathbf{v}). \quad (12)$$

Substituting Eq. (12) into Eq. (11) and eliminating the momentum diffusion rate, we get after a few transformations

$$\begin{aligned} \frac{d\dot{\sigma}_m}{dt} &= -2 \int_V \frac{1}{T} \left[\left(\rho \frac{\partial \mathbf{v}}{\partial t} + \rho (\mathbf{v} \cdot \nabla) \mathbf{v} \right) \cdot \left(\frac{\partial \mathbf{v}}{\partial t} \right) - p \frac{\partial}{\partial t} (\nabla \cdot \mathbf{v}) \right] dV \\ &\approx -2 \int_V \frac{1}{T} \left(\rho \frac{\partial \mathbf{v}}{\partial t} + \rho (\mathbf{v} \cdot \nabla) \mathbf{v} \right) \cdot \left(\frac{\partial \mathbf{v}}{\partial t} \right) dV. \end{aligned} \quad (13)$$

Here we have assumed incompressibility ($\nabla \cdot \mathbf{v} = 0$) in Eq. (13). If we further assume a situation with no advection of momentum, then $(\mathbf{v} \cdot \nabla) \mathbf{v} = 0$; that is, there is no velocity gradient along the flow direction, corresponding to a laminar flow in the Stokes approximation. In this specific laminar flow case, we get

$$\frac{d\dot{\sigma}_{m,\text{lam}}}{dt} = -2 \int_V \frac{\rho}{T} \left| \frac{\partial \mathbf{v}}{\partial t} \right|^2 dV \leq 0, \quad (14)$$

² Assuming linearity, $\mathbf{\Pi} : \nabla \mathbf{v} = [2\mu (\nabla \mathbf{v})^s - (2/3)\mu (\nabla \cdot \mathbf{v}) \mathbf{\delta}] : [(\nabla \mathbf{v})^s + (\nabla \mathbf{v})^a] = 2\mu (\nabla \mathbf{v})^s : (\nabla \mathbf{v})^s - (2/3)\mu (\nabla \cdot \mathbf{v})^2$, with $\mathbf{\delta}$ denoting the unit tensor, and \mathbf{T}^s and \mathbf{T}^a denoting symmetric and asymmetric parts of a tensor \mathbf{T} . Then, $\partial(\mathbf{\Pi} : \nabla \mathbf{v}) / \partial t = 2[2\mu (\nabla \mathbf{v})^s - (2/3)\mu (\nabla \cdot \mathbf{v}) \mathbf{\delta}] : [\nabla (\partial \mathbf{v} / \partial t)]^s = 2 \mathbf{\Pi} : \nabla (\partial \mathbf{v} / \partial t)$.

where the suffix lam denotes the laminar flow with no momentum advection. The rate of entropy production in an incompressible laminar flow tends to decrease with time and reach a minimum in the final steady state ($\partial \mathbf{v} / \partial t = 0$). This result shows another aspect of MinEP for a laminar flow. In an isothermal condition, this tendency is akin to that of minimum dissipation of kinetic energy in a slow incompressible steady flow suggested by Helmholtz [26] and Rayleigh [27]. However, as we shall see in the next section, when advection of momentum is nonzero (i.e. turbulent flow), the sign of $d\dot{\sigma}_m / dt$ becomes indefinite, and the entropy production can either decrease or increase depending on the rate of advection determined by the flow pattern produced in the fluid system.

NONLINEAR ADVECTION

We now discuss the effect of advection of heat or momentum on entropy production in a fluid system. The advection process is a typical nonlinear process since it is described as the product of the velocity and gradient of an intensive variable, which is also a function of the velocity. A fundamental difficulty arises from the presence of this nonlinear term in solving the balance equation of energy or momentum [Eq. (6) or (12)]. Exactly the same difficulty arises from this advection term in solving the equation of entropy production. We do not know, in a deterministic sense, how the rate of entropy production will change once advection becomes a dominant process in the transport of heat or momentum. However, advection of heat or momentum generally increases the local gradient of temperature or velocity at the moving front, which results in an enhancement of entropy production. Here we discuss the conditions under which advection enhances entropy production, using the general equations of entropy production [Eqs. (5) and (11)] as follows.

Heat Advection

Let us go back to the example of entropy production due to heat diffusion. With the presence of convective motion, the MinEP condition [Eq. (8)] cannot be justified since it requires $\mathbf{v} = 0$. Even in this case, Eq. (5) for the rate of change of entropy production remains valid. Assuming a constancy of c_v ($dc_v / dt = 0$) in Eq. (6), and substituting the rate of change of temperature ($\partial T / \partial t$) into Eq. (5), we get

$$\begin{aligned} \frac{d\dot{\sigma}_{h,\text{adv}}}{dt} &= -2 \int_V \frac{\rho c_v}{T^2} \kappa \nabla^2 T \left(\kappa \nabla^2 T - \mathbf{v} \cdot \nabla T - \frac{p \nabla \cdot \mathbf{v}}{\rho c_v} + \frac{\mathbf{\Pi} : \nabla \mathbf{v}}{\rho c_v} \right) dV \\ &\approx -2 \int_V \frac{\rho c_v}{T^2} \kappa \nabla^2 T (\kappa \nabla^2 T - \mathbf{v} \cdot \nabla T) dV, \end{aligned} \quad (15)$$

where the suffix adv denotes the presence of heat advection and $\kappa = \lambda / \rho c_v$ is the thermal diffusivity. The approximation in Eq. (15) corresponds to an assumption that the cooling rate by volume expansion ($\nabla \cdot \mathbf{v}$) and the heating rate by viscous dissipation ($\mathbf{\Pi} : \nabla \mathbf{v}$) are negligibly small compared with diffusive heating ($\kappa \nabla^2 T$) and advective cooling ($\mathbf{v} \cdot \nabla T$). Under this assumption, we can get a sufficient condition for the increase of entropy production ($d\dot{\sigma}_{h,\text{adv}} / dt \geq 0$) as

$$\mathbf{v} \cdot \nabla T \geq \kappa \nabla^2 T \geq 0 \text{ or } \mathbf{v} \cdot \nabla T \leq \kappa \nabla^2 T \leq 0 \Rightarrow \frac{d\dot{\sigma}_{h,adv}}{dt} \geq 0. \quad (16)$$

Condition (16) means that, when advective cooling ($\mathbf{v} \cdot \nabla T$) is greater than diffusive heating ($\kappa \nabla^2 T$), the local temperature decreases further ($\partial T / \partial t \leq 0$) because of Eq. (6), and thus entropy production increases because of Eq. (5). Alternatively, when advective heating ($-\mathbf{v} \cdot \nabla T > 0$) is greater than diffusive cooling ($-\kappa \nabla^2 T > 0$), the local temperature increases further ($\partial T / \partial t \geq 0$) because of Eq. (6), and thus entropy production increases because of Eq. (5). These conditions generally hold true during the development of convective motion ($\partial \mathbf{v} / \partial t > 0$) in a fluid system whose Rayleigh number is larger than the critical value for the onset of convection. The rate of entropy production thus tends to increase with time and reaches a maximum value through the development of convective motion, as suggested from previous studies [5, 6]. Moreover, it is known from numerical simulations that a state of convection tends to move to a state with higher rate of entropy production when the system has multiple steady states and the system is subject to external perturbations [8, 9, 28]. These results are consistent with condition (16) under which entropy production increases with time through the development of convective motion in a system with dynamic instability.

One can see from condition (16) that entropy production can decrease with time when the heat advection rate is smaller than the heat diffusion rate, i.e., $|\mathbf{v} \cdot \nabla T| \leq |\kappa \nabla^2 T|$. Such a situation can be realized in the relaxation period of a convection system towards a steady state, or in a convection system whose boundary temperature is unbounded so that the mean temperature gradient becomes smaller through the development of convective motion. One such example is thermal convection of a fluid system under fixed heat flux at the boundary. Entropy production as well as the overall temperature contrast at the boundary decreases with the onset of convection in this case (e.g. [29]). A quantitative analysis on the reduction of entropy production using Eq. (16) would therefore be attractive. Here it should be noted that the decrease of entropy production in this case is not in direct contradiction to the stability criterion of MaxEP, because relative stability of each steady state should be compared under the same boundary forcing condition, i.e., the same temperature contrast at the boundary characterized by the same Rayleigh number.

Momentum Advection

We can obtain a similar result for entropy production due to momentum diffusion. With the presence of advection of momentum $[(\mathbf{v} \cdot \nabla) \mathbf{v} \neq 0]$, the MinEP condition [Eq. (14)] cannot be justified. Even in this case, Eq. (11) for the rate of change of entropy production remains valid. Assuming incompressibility of fluid and substituting the rate of change of velocity from Eq. (12) into Eq. (11), we get

$$\frac{d\dot{\sigma}_{m,adv}}{dt} = -2 \int_V \frac{\rho}{T} (\nu \nabla^2 \mathbf{v}) \cdot \left(\nu \nabla^2 \mathbf{v} - (\mathbf{v} \cdot \nabla) \mathbf{v} - \frac{\nabla p}{\rho} \right) dV, \quad (17)$$

where the suffix adv denotes the presence of momentum advection and $\nu = \mu / \rho$ is the kinematic viscosity. We can then

find a sufficient condition for the increase of entropy production ($d\dot{\sigma}_{h,adv} / dt \geq 0$) as

$$\left[(\mathbf{v} \cdot \nabla) \mathbf{v} + \frac{\nabla p}{\rho} \right] \cdot \mathbf{e} \geq |\nu \nabla^2 \mathbf{v}| \Rightarrow \frac{d\dot{\sigma}_{m,adv}}{dt} \geq 0, \quad (18)$$

where $\mathbf{e} = \nabla^2 \mathbf{v} / |\nabla^2 \mathbf{v}|$ is the unit vector in the direction of $\nabla^2 \mathbf{v}$. Condition (18) means that, when advective export of momentum $[(\mathbf{v} \cdot \nabla) \mathbf{v}]$ plus pressure deceleration $[\nabla p / \rho]$ in the \mathbf{e} direction is greater than diffusive import of momentum $|\nu \nabla^2 \mathbf{v}|$, the local velocity in that direction decreases further because of Eq. (12), and thus entropy production increases because of Eq. (11). Alternatively, when advective import of momentum $[-(\mathbf{v} \cdot \nabla) \mathbf{v}]$ plus pressure acceleration $[-\nabla p / \rho]$ in the $-\mathbf{e}$ direction is larger than diffusive export of momentum $|\nu \nabla^2 \mathbf{v}|$, the local velocity increases further because of Eq. (12), and thus entropy production increases because of Eq. (11). It is known that advection of momentum is negligibly small in laminar flows whereas it is considerably large in turbulent flows. Thus, this condition generally holds true during the development of turbulent motion in a fluid system whose Reynolds number is larger than the critical value for the onset of turbulence. The rate of entropy production thus tends to increase to a maximum value through the development of turbulent motion [5]. Malkus [30] and Busse [31] suggested that the observed mean state of turbulent shear flow corresponds to the state with the maximum rate of momentum transport by turbulent motion. Malkus [32] also showed that velocity profiles estimated from maximum dissipation of kinetic energy due to the mean velocity field and a smallest scale of motion at the system boundary resemble those of observations. Since the dissipation rate is proportional to the entropy production rate, these results are consistent with condition (18) under which entropy production increases with time towards a maximum value when the system is in a state of dynamic instability.

One can also see from this condition (18) that entropy production can decrease with time when the momentum advection is less than the rates of diffusion and acceleration by the pressure gradient: $[(\mathbf{v} \cdot \nabla) \mathbf{v} + \nabla p / \rho] \cdot \mathbf{e} \leq |\nu \nabla^2 \mathbf{v}|$. Such a condition can be realized in the relaxation period of a turbulent fluid system, or in a fluid system whose boundary velocity is unbounded so that the momentum advection becomes less significant than the sum of momentum diffusion and pressure acceleration. Examples include turbulent shear flow under a fixed shear stress and turbulent pipe flow under a fixed pressure gradient. Entropy production as well as the overall velocity gradient is known to decrease with the onset of turbulence in these cases [33, 34]. Again, the decrease of entropy production in these cases is not in direct contradiction to the stability criterion of MaxEP, because relative stability of each steady state should be compared under the same boundary forcing condition, i.e., the same velocity contrast applied to the entire system characterized by the same Reynolds number.

It should be noted that the condition [(16) or (18)] is a *sufficient* condition rather than a *necessary and sufficient* condition for $d\dot{\sigma}_{adv} / dt \geq 0$ — entropy production for the total system can increase even if local entropy production decreases in some places. In order to get the exact condition for $d\dot{\sigma}_{adv} / dt \geq 0$, we need to treat the integral equation [(5) or (11)]. In what follows we shall deal with the integral equation based on the concept of linear stability analysis.

Stability Analysis

Suppose that a fluid system is subjected to a small disturbance. The disturbance is considered to be so small that its decomposition into spatial and temporal contributions may be possible. In this case, arbitrary small disturbances of temperature and velocity can be expanded into infinite Fourier series, whose components take the general forms:

$$\delta T = \delta T_0 \exp[i(k_x x + k_y y + k_z z) + p_k t], \quad (19)$$

$$\delta \mathbf{v} = \delta \mathbf{v}_0 \exp[i(k_x x + k_y y + k_z z) + p_k t], \quad (20)$$

where δT and $\delta \mathbf{v}$ are the disturbances of temperature and velocity, δT_0 and $\delta \mathbf{v}_0$ are their amplitudes, $k = \sqrt{k_x^2 + k_y^2 + k_z^2}$ is the wave number, and p_k is the complex growth rate of the disturbance of the wave number k . When the real part of p_k is negative for all k , the fluid system is stable with respect to the perturbation. The onset of instability is characterized by a critical condition beyond which the real part of p_k becomes larger than zero ($p_k^{(r)} > 0$) at a particular wave number (k_c). The critical condition must be determined by solving the governing equations [(6) and (12)] with appropriate boundary conditions. For a fluid layer heated from below, the critical condition is expressed by the Rayleigh number: $Ra > Ra^*$, where Ra^* is the critical value beyond which instability is manifested [35]. In the case of a fluid layer (thickness d) between two rigid boundary surfaces, it is known that $Ra^* \approx 1708$ and $k_c \approx 3.12/d$ (cf. [24, 25]), as illustrated in Fig. 1.

We shall then examine the behavior of entropy production at the onset of convective instability. Substituting the temperature disturbance Eq. (19) into Eq. (5), we get

$$\frac{d\dot{\sigma}_{h, \text{dis}(k)}}{dt} \approx 2k^2 p_k \int_V \lambda \left(\frac{\delta T}{T} \right)^2 dV, \quad (21)$$

where the suffix $\text{dis}(k)$ denotes the presence of a disturbance with the wave number k . One can see from Eq. (21) that the rate of change of entropy production by the disturbance is proportional to the growth rate p_k because all other factors [k^2 , λ , $(\delta T/T)^2$] are positive definite. If $p_k^{(r)}$ is negative, then the disturbance is damped and entropy production thereby decreases³. This condition corresponds to the stable state with $Ra < Ra^*$ (Fig. 1). By contrast, when Ra exceeds the critical value Ra^* , $p_k^{(r)}$ becomes larger than zero at the certain wave number k_c , and entropy production starts to increase at the onset of convective instability. A similar result can be obtained for entropy production due to momentum diffusion under velocity gradient. By substituting Eq. (20) into Eq. (11), the rate of change of entropy production is shown to be proportional to p_k . It is generally known that the onset of instability of such a system is determined by the Reynolds number: Re [36]. When Re becomes larger than a critical value ($Re > Re^*$), $p_k^{(r)}$ of a certain wave number becomes positive and entropy production starts to increase. These results are consistent with the findings in the preceding sections that entropy production tends to increase when the system is in a state of dynamic instability.

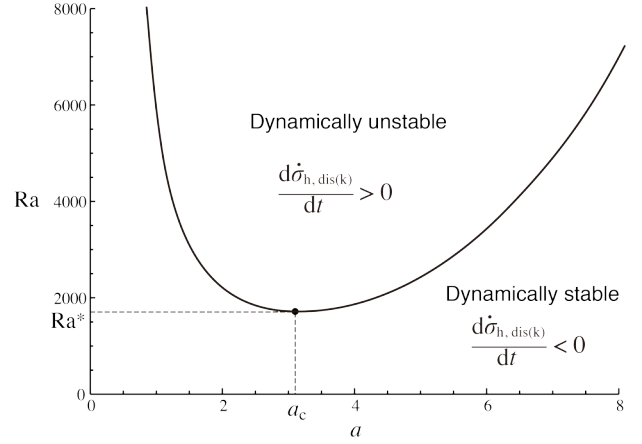


Fig. 1. Relation between the Rayleigh number Ra and the dimensionless wave number $a \equiv kd$. The solid line corresponds to the marginal state for the onset of instability (cf. [24, 25]). Entropy production tends to decrease with time when Ra is less than the critical value: $Ra < Ra^*$. Entropy production starts to increase at the onset of instability when $Ra > Ra^*$.

SUMMARY

In this paper, we have discussed some general characteristics of entropy production in a fluid system. We have shown that entropy production always decreases with time when the system is of a pure diffusion type without advection of heat or momentum. Thus, the minimum entropy production (MinEP) property is intrinsic to a system of a pure diffusion type; e.g., heat conduction in a static fluid or momentum diffusion in laminar flow. However, this MinEP property is no longer guaranteed when the system is in a dynamically unstable state. In this state, entropy production tends to increase by the growth of the advection rate over the diffusion rate of the corresponding extensive quantity. The hypothesis of maximum entropy production (MaxEP) suggested as a selection principle for multiple steady states of nonlinear non-equilibrium systems [1, 6, 13–15, 21–23] can therefore be seen to be a characteristic feature of systems with nonlinear dynamic instability.

ACKNOWLEDGMENT

The authors would like to thank Robert Niven and Roderick Dewar for valuable discussions on thermodynamics of fluid systems. This work was partly supported by a research grant (No. 25400465) from the Japan Society for the Promotion of Science.

REFERENCES

- [1] H. Ziegler, Zwei Extremalprinzipien der irreversiblen Thermodynamik, *Ing. Arch.* 30, 410–416, 1961.
- [2] G.W. Paltridge, Global dynamics and climate—A system of minimum entropy exchange, *Q. J. Roy. Meteorol. Soc.* 101, 475–484, 1975.
- [3] G.W. Paltridge, The steady-state format of global climate, *Q. J. Roy. Meteorol. Soc.* 104, 927–945, 1978.
- [4] H. Ozawa, A. Ohmura, Thermodynamics of a global-mean state of the atmosphere—A state of maximum entropy increase, *J. Clim.* 10, 441–445, 1997.

³ The imaginary part of p_k is zero when $Ra > 0$ in this case (cf. [24, 25]).

- [5] E.D. Schneider, J.J. Kay, Life as a manifestation of the second law of thermodynamics, *Mathematical and Computer Modelling*, 19, 25–48, 1994.
- [6] H. Ozawa, H., S. Shimokawa, H. Sakuma, Thermodynamics of fluid turbulence: A unified approach to the maximum transport properties, *Phys. Rev. E* 64, 026303, 2001.
- [7] R.D. Lorenz, J.I. Lunine, P.G. Withers, C.P. McKay, Titan, Mars and Earth: Entropy production by latitudinal heat transport, *Geophys. Res. Lett.* 28, 415–418, 2001.
- [8] S. Shimokawa, H. Ozawa, On the thermodynamics of the oceanic general circulation: Irreversible transition to a state with higher rate of entropy production, *Q. J. Roy. Meteorol. Soc.* 128, 2115–2128, 2002.
- [9] S. Shimokawa, H. Ozawa, Thermodynamics of irreversible transitions in the oceanic general circulation, *Geophys. Res. Lett.* 34, L12606, 2007. [doi: 10.1029/2007GL030208]
- [10] A. Hill, Entropy production as the selection rule between different growth morphologies, *Nature* 348, 426–348, 1990.
- [11] Y. Nohguchi, H. Ozawa, On the vortex formation at the moving front of lightweight granular particles, *Physica D* 238, 20–26, 2009.
- [12] E.N. Lorenz, Generation of available potential energy and the intensity of the general circulation, in R.L. Pfeffer, (ed.), *Dynamics of Climate*, pp. 86–92. Pergamon, Oxford, 1960.
- [13] H. Ozawa, A. Ohmura, R.D. Lorenz, T. Pujol, The second law of thermodynamics and the global climate system: A review of the maximum entropy production principle, *Rev. Geophys.* 41, 1018, 2003. [doi: 10.1029/2002RG000113]
- [14] R. Dewar, Information theory explanation of the fluctuation theorem, maximum entropy production and self-organized criticality in non-equilibrium stationary states, *J. Phys. A* 36, 631–641, 2003.
- [15] R.K. Niven, Steady state of a dissipative flow-controlled system and the maximum entropy production principle, *Phys. Rev. E* 80, 021113, 2009.
- [16] I. Prigogine, Modération et transformations irréversibles des systèmes ouverts, *Bulletin de la Classe des Sciences, Académie Royale de Belgique* 31, 600–606, 1945.
- [17] P. Glansdorff, I. Prigogine, Sur les propriétés différentielles de la production d'entropie. *Physica* 20, 773–780, 1954.
- [18] S.R. de Groot, P. Mazur, Non-equilibrium Thermodynamics, North-Holland Publ., Amsterdam, 1962.
- [19] I. Gyarmati, Non-equilibrium Thermodynamics, Field Theory and Variational Principles, Springer, Berlin, 1970. [First published in Hungarian, 1967]
- [20] I. Prigogine, From Being to Becoming, Time and Complexity in the Physical Sciences, Freeman, San Francisco, 1970.
- [21] Y. Sawada, A thermodynamic variational principle in nonlinear non-equilibrium phenomena, *Prog. Theor. Phys.* 66, 68–76, 1981.
- [22] R.C. Dewar, A. Maritan, A theoretical basis for maximum entropy production, in R.C. Dewar, C.H. Lineweaver, R.K. Niven, K. Regenauer-Lieb (eds.), *Beyond the Second Law: Entropy Production and Non-equilibrium Systems*, Springer, Berlin, 2013 (in press).
- [23] H. Ozawa, S. Shimokawa, The time evolution of entropy production in nonlinear dynamic systems, in R.C. Dewar, C.H. Lineweaver, R.K. Niven, K. Regenauer-Lieb (eds.), *Beyond the Second Law: Entropy Production and Non-equilibrium Systems*, Springer, Berlin, 2013 (in press).
- [24] L.D. Landau, E.M. Lifshitz, Fluid Mechanics, 2nd ed. Pergamon Press, Oxford, 1987. [First published in Russian, 1944]
- [25] S. Chandrasekhar, Hydrodynamic and Hydromagnetic Stability, Oxford Univ. Press, Oxford, 1961.
- [26] H. Helmholtz, Zur Theorie der stationären Ströme in reibenden Flüssigkeiten, *Verhandlungen des naturhistorisch-medicinischen Vereins zu Heidelberg* 5, 1–7, 1869.
- [27] Lord Rayleigh, On the motion of a viscous fluid, *Phil. Mag.* 26, 776–786, 1913.
- [28] M. Suzuki, Y. Sawada, Relative stabilities of metastable states of convecting charged-fluid systems by computer simulation, *Phys. Rev. A* 27, 478–489, 1983.
- [29] Y. Kawazura, Z. Yoshida, Entropy production rate in a flux-driven self-organizing system, *Phys. Rev. E* 82, 066403, 2010.
- [30] W.V.R. Malkus, Outline of a theory of turbulent shear flow, *J. Fluid Mech.* 1, 521–539, 1956.
- [31] F.H. Busse, Bounds for turbulent shear flow, *J. Fluid Mech.* 41, 219–240, 1970.
- [32] W.V.R. Malkus, Borders of disorder: in turbulent shear flow, *J. Fluid Mech.* 489, 185–198, 2003.
- [33] D.M. Paulus Jr., R.A. Gaggioli, Some observations of entropy extrema in fluid flow, *Energy* 29, 2487–2500, 2004.
- [34] R.K. Niven, Simultaneous extrema in the entropy production for steady-state fluid flow in parallel pipes, *J. Non-Equilib. Thermodyn.* 35, 347–378, 2010.
- [35] Lord Rayleigh, On convection currents in a horizontal layer of fluid, when the higher temperature is on the under side, *Philos. Mag.* 32, 529–546, 1916.
- [36] O. Reynolds, On the dynamical theory of incompressible viscous fluids and the determination of the criterion, *Philos. Trans. Roy. Soc. London* 186, 123–164, 1895.

GYARMATI'S VARIATIONAL PRINCIPLE OF DISSIPATIVE PROCESSES.

József Verhás

Budapest University of Technology and Economy, H-1521, E-mail: verhas@phy.bme.hu

ABSTRACT

Like mechanics and electrodynamics, the fundamental laws of the thermodynamics of dissipative processes can be compressed into a variational principle. This variational principle both in its differential (local) and in integral (global) forms was formulated by Gyarmati helped by the present author in 1965. This principle was applied to several fields of irreversible processes: first of all, his colleagues (Verhás [1], Böröcz [2], Farkas [3,4], Sándor [5], Vincze [6–8], Stark [9,10]); but also many others (Singh [11,12], Bhattacharya [13,14], Dickel [15,16] etc.). Consistent application of both the local and the global forms of Gyarmati's principle provides all the advantages throughout explicating the theory of irreversible thermodynamics that are provided in the study of mechanics and electrodynamics by the corresponding classical variational principles, e.g., Gauss' differential principle of least constraint, or Hamilton's integral principle.

THE GOVERNING PRINCIPLE OF DISSIPATIVE PROCESSES (GPDP)

Gyarmati's principle is based on the fact that the generalization of the dissipation functions — that were introduced by Rayleigh and Onsager for special cases — always exist locally in continua [17–22]. In linear theory these functions are defined as:

$$\Psi(X) = \frac{1}{2} \sum_{i,k} L_{ik} X_i X_k \quad (1)$$

and

$$\Phi(J) = \frac{1}{2} \sum_{i,k} R_{ik} J_i J_k. \quad (2)$$

The R_{ik} coefficients (general resistivities) are the components of the inverse of the conductivity matrix (L_{ik}).

The most important property of the dissipation function is that it is a homogeneous quadratic function of the X_i forces in the strictly linear theory, while in the quasi-linear theory it depends also on the state variables. The other fundamental property of Ψ is that its partial derivative with respect to X_k is equal to the current J_k conjugate to the force X_k in the entropy production density:

$$J_k = \frac{\partial \Psi}{\partial X_k} \quad (3)$$

Finally, the equality of the mixed second derivatives of Ψ with respect to the forces are equivalent to Onsager's reciprocal relations:

$$\frac{\partial^2 \Psi}{\partial X_i \partial X_k} = \frac{\partial J_i}{\partial X_k} = L_{ik} = L_{ki} = \frac{\partial J_k}{\partial X_i} = \frac{\partial^2 \Psi}{\partial X_k \partial X_i}. \quad (4)$$

Because of the above properties, the function Ψ is called a dissipation potential, more precisely: it is the flux-potential (see (3)).

The function Φ has similar properties. In the strictly linear theory the function Φ is a homogeneous quadratic function of the currents J , while in the quasi-linear case it depends also on the local state variables (through the coefficients). The partial derivative of the function Φ with respect to J_k equals X_k :

$$X_k = \frac{\partial \Phi}{\partial J_k} \quad (5)$$

Due to this relation the function Φ is also a dissipation potential, more exactly: it is the force potential.

The equality of the mixed second derivatives of Φ with respect to the J -s are equivalent to the Onsager relations, now expressed in terms of the R_{ik} resistances

$$\frac{\partial^2 \Phi}{\partial J_i \partial J_k} = \frac{\partial X_i}{\partial J_k} = R_{ik} = R_{ki} = \frac{\partial X_k}{\partial J_i} = \frac{\partial^2 \Phi}{\partial J_k \partial J_i} \quad (6)$$

Hence, it can be seen that the necessary and sufficient condition of the existence of the dissipation potentials Ψ and Φ is the existence of the Onsager reciprocal relations.

Some weighted potentials Ψ^G and Φ^G can be defined, too. They show all the essential properties of Ψ and Φ , but correspond to the weighted entropy production $G\sigma_s$. (G is any always positive state function.)

The dynamic laws can be formulated in different forms by the help of so-called representations and pictures which give mathematically equivalent formulae. The general theory of the "pictures" was worked out and applied by Gyarmati [23] and Farkas [3] (see also [5, 13, 14, 24–27]). Different pictures are obtained by multiplying both sides of the bilinear expression of the entropy production by an always positive state function, G , i.e.

$$G\sigma_s = \sum_j J_j X_j G. \quad (7)$$

The quantity $G\sigma_s$ is evidently non-negative, taking a zero value in equilibrium only. The coefficients of the current, J_j , namely,

$$X_j^G = X_j G \quad (8)$$

regarded as forces, and substituted into the original form give the linear laws in the “ G -picture”:

$$J_i = \sum_k \frac{1}{G} L_{ik} X_k^G = \sum_k L_{ik}^G X_k^G. \quad (9)$$

The coefficients obey the Onsager-Casimir reciprocal relations. By choosing various functions for G , various pictures for the description of dissipative processes are obtained [3, 28, 29].

Making use of equations (8) and (9), we obtain the forms of the dissipation potentials in the general G -picture:

$$\Psi^G = G\Psi, \quad \Phi^G = G\Phi. \quad (10)$$

Finally we note another essential property of the functions Ψ and Φ ; namely, that they are invariant scalar quantities with respect to the linear transformations of the currents and forces.

THE LOCAL FORMS OF GYARMATI'S PRINCIPLE

Gyarmati's variational principle of non-equilibrium thermodynamics can be derived from the properties (3) and (5) of the functions Ψ and Φ . We mention that this derivation does not make use of the homogeneous quadratic forms of the functions Ψ and Φ given in (1) and (2); thus the variational principle is applicable to strictly non-linear phenomena that cannot be described by the linear laws, yet the currents are uniquely determined by the forces and the local variables of state. This is the situation with all the phenomena the Gyarmati-Li generalization

$$\frac{\partial J_i}{\partial X_k} = \frac{\partial J_k}{\partial X_i} \quad (11)$$

of the Onsager relations corresponds to. These relations are necessary and sufficient conditions of the existence of dissipation potentials, obeying equations (3) and (5).

Notice, that equation (5) can be written in the form

$$\frac{\partial}{\partial J_k} (\sigma_s - \Phi) = 0, \quad (12)$$

where, in executing the partial differentiation, the currents must be regarded variables independent of the forces and local state variables. It means that the constitutive relations given by equation (5) are equivalent to the following statement: those currents correspond to a given set of forces and state variables, at which the function

$$\mathcal{L}_J = \sigma_s - \Phi \quad (13)$$

has a stationary point in the space of the currents. This form of the principle, which stands nearest to Onsager's principle for small fluctuations around an equilibrium in an adiabatically

closed discontinuous system, is called the flux representation of Gyarmati's principle [30].

The force representation of Gyarmati's principle is obtained by putting the relation (3) in the form

$$\frac{\partial}{\partial X_k} (\sigma_s - \Psi) = 0. \quad (14)$$

During partial differentiation the forces and the fluxes must be regarded again as independent variables. Thus, those forces correspond to a given set of currents and state variables at which the function

$$\mathcal{L}_X = \sigma_s - \Psi \quad (15)$$

has a stationary point in the space of the forces.

It is easily seen that the functions \mathcal{L}_J and \mathcal{L}_X in (13) and (15) can be put in the same form, as the subtraction of function independent of the J -s from \mathcal{L}_J has no influence on equation (12). The function Ψ just fits the purpose. On the other hand, Φ can be subtracted from \mathcal{L}_X (due to the same reasons). Now a universal Lagrange density of Gyarmati's principle has been obtained:

$$\mathcal{L} = \mathcal{L}_J - \Psi = \mathcal{L}_X - \Phi = \sigma_s - \Psi - \Phi, \quad (16)$$

by which the extremum properties (12) and (14) can be expressed universally.

It can be said, quite generally, that if a sufficient number of the currents and forces is known — that is either every force or every current, or even one part of the currents and the other part of the forces — then the remaining variables must be chosen so that the universal Lagrangian (16) is stationary. This is a necessary and sufficient condition for the set of the currents and forces describe a real process. In other words, the variation of the universal Lagrangian in Gyarmati's principle is zero around the real forces and fluxes, with respect to the simultaneous variation of the currents and forces.

In the quasi-linear theory the functions Ψ and Φ depend on the state variables through the conductivities L_{ik} and resistivities R_{ik} due to (1) and (2). The matrices of the conductivities L_{ik} and resistivities R_{ik} are reciprocal matrices:

$$\sum_r L_{ir} R_{rk} = \delta_{ik}. \quad (17)$$

Let us calculate the partial derivative of the \mathcal{L} Lagrange density with respect to a local state variable denoted by Γ :

$$\frac{\partial \mathcal{L}}{\partial \Gamma} = -\frac{1}{2} \sum_{i,k} \frac{\partial L_{ik}}{\partial \Gamma} X_i X_k - \frac{1}{2} \sum_{i,k} \frac{\partial R_{ik}}{\partial \Gamma} J_i J_k. \quad (18)$$

The partial derivatives $\partial R_{ik} / \partial \Gamma$, making use of (17), are expressed by the coefficients R_{ik} and the derivatives $\partial L_{ik} / \partial \Gamma$ as

$$\frac{\partial R_{ik}}{\partial \Gamma} = -\sum_{r,s} R_{ir} \frac{\partial L_{rs}}{\partial \Gamma} R_{sk}. \quad (19)$$

Substituting this in (18) and applying the reciprocal relations, the form

$$\frac{\partial \mathcal{L}}{\partial \Gamma} = -\frac{1}{2} \sum_{i,k} \frac{\partial L_{ik}}{\partial \Gamma} (X_i - \sum_s R_{is} J_s)(X_k + \sum_s R_{ks} J_s). \quad (20)$$

is obtained. Hence it is seen that the partial derivatives of the universal Lagrangian with respect to the local state variables, at real processes, are zero. So the parameters Γ can also be varied independently.

This theorem is Gyarmati's supplementary theorem [31], which guarantees the validity of the universal local form of the variational principle to the quasi-linear case, too.

The universal form of the local Gyarmati principle states, consistently with the supplementary theorem, that the Lagrangian $\mathcal{L} = \sigma_s - \Psi - \Phi$ has an extremum in all points that describe a real process in the unified space of forces, currents and state variables.

In examining the type of the extremum, instead of considering second variations, we had better use another form of the Lagrangian which is advantageous in other respects, as well. This form is

$$\mathcal{L} = -\frac{1}{2} \sum_{i,k} R_{ik} (J_i - \sum_s L_{is} X_s)(J_k - \sum_s L_{ks} X_s). \quad (21)$$

Executing the multiplications the form (16) of the universal Lagrange density is obtained again. This very form, however, clearly shows that the extremum for real processes is always a maximum and the value of this maximum is zero if no constraint is maintained; in other cases the Lagrangian is always negative, since the R_{ik} -s are the coefficients of a positive definite quadratic form and the variables of this quadratic form are $(J_i - \sum_s L_{is} X_s)$. This form of the local principle is considerably similar to Gauss' principle of least constraint, so this form is often called the Gaussian form of Gyarmati's principle. As the value of (21) is zero only in the absence of local constraints, while in other cases the value of this maximum depends on the constraints, the Gauss type local principle is an excellent tool for introducing the notion of thermodynamic constraint forces; consequently it is of great help in discussing problems with local constraints (Verhás [32], Gyarmati [29], Dickel [15]).

The local Gyarmati principle of irreversible thermodynamics is of universal validity, yet its primary importance is that it is the ground the integral principles are built on. Before the discussion of integral principles, however, the place of the local principle in the frame-work of the theory should be examined. To this end, the local principle is resumed more explicitly.

The essence of the local principle is that it replaces the set of linear laws by a single scalar function. If either the function Ψ or the function Φ is known, the constitutive equations can be obtained by the variational principle. Actually, it is sufficient to know only one of the dissipation potentials Ψ or Φ , since the matrix of the coefficients can be read from one of them, and the other potential is determined by the elements of the reciprocal matrix.. This calculation can be executed via a more elegant method. Let us regard, for example, the function Ψ as the given one. Then the Legendre-transformation of the function Ψ leads to the function $\Phi \left(\frac{\partial \Psi}{\partial X} \right)$. Putting J in the place of $\frac{\partial \Psi}{\partial X}$ the function Φ is obtained. The function Ψ is got from Φ in the same way, ([30,31]).

The advantage of the method of Legendre transformation lies in the fact that its formulation and application is independent of the linear or quasi-linear character of the theory; thus it is applicable to dissipation potentials of entirely different character. From the fact that the dissipation potentials Ψ and Φ are the Legendre transforms of each other, it is also seen that the validity of Gyarmati's supplementary theorem is not restricted to the quasi-linear case, but holds to any strictly non-linear theory, subject to the Gyarmati-Li generalized reciprocal relations (and where the higher order coefficients also depend on the variables of state). This, at the same time, means that the Lagrangian $\mathcal{L} = \sigma_s - \Psi - \Phi$ must be stationary at every point of space in every instant of time in the case of any non-linear theory, provided that dissipation potentials exist at all.

The next question is how a dissipation potential can be constructed from the constitutive equations. The potential character of the functions Ψ and Φ is defined by equations (3) and (5). The condition to the existence of such functions with potential character to a given (say: empirically proven) set of constitutive equations is that they be subjected to the Gyarmati-Li generalized reciprocal relations. It is rather inconvenient that no general physical law, or exact proof based on such laws, is known which would guarantee the fulfillment of the Gyarmati-Li generalized reciprocal relations, or of other equivalent conditions, for all possible constitutive equations. If, however, the reciprocal relations (11) hold in a particular case or approximation, then the dissipation potentials can be given and the Gyarmati principle can be applied. Dissipation potentials for non-linear cases were given first (and independently) by Verhás [33], Edele [34–37] and Presnov [38].

The function Ψ can be obtained from the bilinear form of the entropy production with introducing equations (3); we get

$$\sigma_s = \sum_i X_i \frac{\partial \Psi}{\partial X_i} = \sum_i X_i J_i(X) = \sigma_s(X) \quad (22)$$

for the entropy production. This expression can be regarded as a quasi-linear inhomogeneous first order partial differential equation. Its only solution subject to the condition $\Psi(0) = 0$ is the function

$$\Psi(X) = \int_0^1 \frac{1}{t} \sigma_s(tX) dt \quad (23)$$

A similar formula is obtained for $\Phi(J)$:

$$\Phi(J) = \int_0^1 \frac{1}{t} \sigma_s(tJ) dt \quad (24)$$

The knowledge of the function Ψ or Φ defined so, is equivalent to the knowledge of the original constitutive equations.

THE GOVERNING PRINCIPLE OF DISSIPATIVE PROCESSES

Though the local form of Gyarmati's principle is indispensable for the description of local constraints, an integral form of

the principle is of much greater importance in practical calculations. The integral forms are obtained by the integration of the universal Lagrange density with respect to space or space and time coordinates. The universal (global) principle, obtained so, is called the governing principle of dissipative processes [31].

Since the universal Lagrange density is everywhere and always stationary, it is also true that

$$\delta \int_V (\sigma_s - \Psi - \Phi) dV = 0, \quad (25)$$

and

$$\delta \int_{t_1}^{t_2} \int_V (\sigma_s - \Psi - \Phi) dV dt = 0. \quad (26)$$

The governing principle of dissipative processes given by Gyarmati can be regarded the most widely valid and the most widely applied integral principle of irreversible thermodynamics. From this principle the parabolic transport equations of irreversible transport processes can be derived both in the linear and quasi-linear case, as well as in all those non-linear cases where dissipation potentials can be determined by (23) and (24) due to the validity of the generalized reciprocal relations (11), [3, 5, 7, 9, 10, 26–29, 34, 35, 39].

The application of the governing principle can be understood through the properties of the local principle. The variational principle alone does not contain sufficient information about the system, the functional takes its absolute maximum in several points of the (Γ, X, J) space; but if the Γ and X values are given, then J can be determined. Obviously, not only the knowledge of Γ and X is suitable but any other restrictive circumstance denoting an equivalent hypersurface in the (Γ, X, J) space. Such a restrictive condition is the ensemble of the balance equations and the definition of the forces together with the equation of state.

Hence it follows that the variational principles (25) and (26) are to be understood with the above subsidiary conditions, and thus the processes occurring in the system are uniquely described.

The extraordinary importance of the formula (25) arises from the fact that the Euler-Lagrange equations are identical to the parabolic transport equations. Its use has the greatest advantage in the entropy picture, since the substitution of Γ with the entropy balance gives a particular form. The corresponding Euler-Lagrange equations have a separable subsystem of differential equations (viz. independently solvable) for the Γ parameters, and neither the consideration of the balance equations as subsidiary conditions nor the determination of the J currents is necessary [29].

The situation with the time integrated form in equation (26) is a bit different. The Euler-Lagrange equations do not display the set of transport equations directly. The latter can be calculated from transversality conditions and is obtained after a first integration of the Euler-Lagrange equations [40]. The other method introduces some potential functions the Euler-Lagrange equations concern to and the customary transport equations results after eliminating them [18, 19, 41, 42].

The governing principle of dissipative processes — like any other integral principle of physics — contains information on

the boundary conditions, too. They have to be given so as the absolute maximum be provided, viz. any further weakening of the proper boundary conditions may not increase the value of the maximum.

We mention that for strictly linear problems there are two partial forms also valid:

$$\delta \int_V (\sigma_s - \Psi) dV = 0, \quad \delta J = 0, \quad (27)$$

and

$$\delta \int_V (\sigma_s - \Phi) dV = 0, \quad \delta X = 0. \quad (28)$$

The first of these is called force, and the second is called flux representation. Both representations were widely applied to the solution of several practical problems. [9–11, 26, 27, 43]. It is also well known that the force representation of Gyarmati's governing principle is equivalent to the local potential method of Prigogine and Glansdorff [44], while the flux representation is the equivalent of the variational methods of Biot [45, 46]. (For details see references [11, 12, 31, 47–52].)

Here a more or less "classical" framework of Gyarmati's variational principle has been surveyed but life does not stop; new fields of applications and new aspects emerge. The unification of the different approaches is a permanent task. I mention only some works of P. Ván here [53–57].

ACKNOWLEDGMENT

This work has been supported by the Hungarian National Scientific Research Funds, OTKA (62278 and K81161).

NOMENCLATURE

G	Any positive state function [variant]
i, j, k, r, s	Runing indices [integer, no unite]
J_i	the j -th of the generalized currents [variant]
J	any of the generalized currents [variant]
J_i^G	the j -th of the generalized currents in "G" picture [variant]
J^G	any of the generalized currents in "G" picture [variant]
L_{ik}	a conductivity coefficient [variant]
L	any of the conductivity coefficients [variant]
L_{ik}^G	a conductivity coefficient in "G" picture [variant]
L^G	any of the conductivity coefficient in "G" picture [variant]
R_{ik}	a resistivity coefficient [variant]
R	any of the resistivity coefficient [variant]
R_{ik}^G	a resistivity coefficient in "G" picture [variant]
R^G	any of the resistivity coefficient in "G" picture [variant]
t	runing integration variable [real number, no unite]
X_i	the i -th thermodynamic force [variant]
X	any of the thermodynamic forces [variant]
X_i^G	the i -th thermodynamic force in "G" picture [variant]
X^G	any of the thermodynamic force in "G" picture [variant]
$\mathcal{L}, \mathcal{L}_J, \mathcal{L}_X$	Lagrangian [W/K m ³]
Γ	a state variable [variant]
σ_s	entropy production density [W/K m ³]
Φ	force-potential [W/K m ³]
Φ^G	force-potential [variant]
Ψ	flux-potential [W/K m ³]
Ψ^G	flux-potential [variant]

REFERENCES

- [1] József Verhás. *Thermodynamics and Rheology*. Akadémiai Kiadó and Kluwer Academic Publishers, Budapest and Dordrecht, 1997.
- [2] Sz. Böröcz. An example for Gyarmati's integral principle of thermodynamics. *Z. Phys. Chem.*, 234:26–32, 1967.
- [3] H. Farkas. The reformulation of the Gyarmati principle in a generalized Γ picture. *Z. f. Phys. Chemie*, 239:124–132, 1968.
- [4] H. Farkas and Z. Noszticzius. On the non-linear generalization of the Gyarmati principle and theorem. *Ann. d. Phys.*, 27:341–348, 1971.
- [5] J. Sándor. The treatment of non-isothermal multicomponent diffusion in electrostatic fields on the basis of Gyarmati's variational principle. *Electrochimica Acta*, 17:673–782, 1972.
- [6] Gy. Vincze. Deduction of the quasi-linear transport equations of hydro-thermodynamics from the Gyarmati principle. *Ann. d. Phys.*, 27:225–136, 1971.
- [7] Gy. Vincze. Deduction of the Reynolds equations of turbulence from the Gyarmati principle. *Acta Chim. Hung.*, 75:33–43, 1972.
- [8] Gy. Vincze. On the treatment of thermo-electrodynamical processes by Gyarmati's principle. *Ann. d. Phys.*, 30:50–61, 1973.
- [9] A. Stark. Approximation methods for the solution of heat conduction problems using Gyarmati's principle. *Ann. d. Phys.*, 7/31:53–75, 1974.
- [10] A. Stark. Variational properties of irreversible processes. *Ann. d. Phys.*, 5:481–490, 1975.
- [11] P. Singh. An approximate technique to thermodynamic stability problems on the basis of the governing principle of dissipative processes. *J. Non-Equilib. Thermodyn.*, 1:105–116, 1976.
- [12] P. Singh and K. K. Srivastava. Variational solution of heat convection in the channel flow with the help of G. P. D. P. *Acta Physica Hungarica*, 45:201–211, 1978.
- [13] D. K. Bhattacharya. *The Application of Governing Principle of Dissipative Processes to Incompressible Fluid Flow and Heat Transfer*. PhD thesis, Kharagpur, (India), 1978.
- [14] D. K. Bhattacharya. A variational principle for thermodynamical waves. *Ann. d. Phys.*, 7.39:325–332, 1983.
- [15] G. Dickel. Electro-mechanical equilibrium in membranes. In G. Milazzo, editor, *Topics in Bioelectrochemistry and Bioenergetics*, volume 4. John Wiley and Sons, New York, 1981.
- [16] G. Dickel, U. Baelz, and B. Piteza. Investigation of electromechanical equilibrium in ion exchange membranes. *Soc. Faraday Trans.*, 77/2:451–458, 1981.
- [17] F. Márkus and K. Gambár. Comments “on the relationship between extended thermodynamics and the wave approach to thermodynamics”. *J. Non-Equilib. Thermodyn.*, 14:355–362, 1989.
- [18] F. Márkus and K. Gambár. A variational principle in thermodynamics. *J. Non-Equilib. Thermodyn.*, 16:27–32, 1991.
- [19] F. Márkus and K. Gambár. Hamilton's canonical equations and the entropy production. *J. Non-Equilib. Thermodyn.*, 18:288–292, 1993.
- [20] L. Onsager. Reciprocal relations in irreversible processes. I. *Phys. Rev.*, 37:405–426, 1931.
- [21] L. Onsager. Reciprocal relations in irreversible processes. II. *Phys. Rev.*, 38:2265–2279, 1931.
- [22] L. Onsager and S. Maclup. Fluctuations and irreversible processes. *Phys. Rev.*, 91:1505–1512, 1953.
- [23] I. Gyarmati. *A termodinamika elveiről (in Hungarian)*. PhD thesis, Hungarian Academy of Sciences, Budapest, 1958.
- [24] D. K. Bhattacharya. On the problem of evolution criterion for thermodynamical waves. *Acta Mechanica*, 47:87–94, 1983.
- [25] D. Fekete. A systematic application of Gyarmati's wave theory of thermodynamics to thermal waves in solids. *Phys. Stat. Sol. (b)*, 105:161–174, 1981.
- [26] P. Singh and D. K. Bhattacharya. Application of G. P. D. P. to heat conduction problem. *Indian J. Pure Appl. Math.*, 9:407–416, 1978.
- [27] P. Singh and D. K. Bhattacharya. Application of Gyarmati principle to boundary layer flow. *Acta Mechanica*, 30:137–144, 1978.
- [28] H. Farkas. On the phenomenological theory of heat conduction. *Int. J. Engng. Sci.*, 13:1035–1053, 1975.
- [29] I. Gyarmati. *Non-Equilibrium Thermodynamics*. Springer, Berlin, 1970.
- [30] I. Gyarmati. On the relation between Onsager's and Prigogine's principles. *Z. Phys. Chemie*, 234:371–378, 1967.
- [31] I. Gyarmati. On the “governing principle of dissipative processes” and its extension to non-linear problems. *Ann. d. Phys.*, 23:353–378, 1969.
- [32] József Verhás. Application of the Prigogine-Gyarmati form of the principle of least dissipation of energy to thermodynamical constraint problems. In *Conference on Some Aspects of Physical Chemistry*, Budapest, 1966.
- [33] J. Verhás. The construction of dissipation potentials for non-linear problems and the application of Gyarmati's principle to plastic flow. *Z. f. Phys. Chemie*, 249:119–122, 1972.
- [34] D. G. B. Edelen. On the characterization of fluxes in nonlinear irreversible thermodynamics. *Int. J. Engng. Sci.*, 12:397–411, 1974.
- [35] D. G. B. Edelen. A thermodynamics with internal degrees of freedom and nonconservative forces. *Int. J. Engng. Sci.*, 14:1013–1032, 1976.
- [36] D. G. B. Edelen. A thermodynamic derivation of non-history dependent constitutive relation for elastic, viscoelastic, fluid and perfectly plastic bodies. *Arch. of Mech.*, 26:251–261, 1974.
- [37] D. G. B. Edelen. Generalized Onsager fluxes and forces. a nonlinear phenomenological theory. *Z. Phys. Chem. (Neue Folge)*, 80:37–53, 1974.
- [38] E. V. Presnov. Potencialnij kharakter kriterija evolucii termodinamiki neobratimih processov. (in russian). *Zh. Fiz. Himii.*, 47:2902–2904, 1973.
- [39] I. Gyarmati. Generalization of the governing principle of dissipative processes to complex scalar fields. *Ann. d. Phys.*, 7/31:18–32, 1974.
- [40] József Verhás. On the time integration of Gyarmati's variational principle. In *III. Szárítási Konferencia*, Budapest, 1971.
- [41] K. Gambár, F. Márkus, and B. Nyíri. A variational principle for the balance and constitutive equations in convective systems. *J. Non-Equilib. Thermodyn.*, 16:217–224, 1991.
- [42] K. Gambár and F. Márkus. On the global symmetry of

- thermodynamics and onsager's reciprocity relations. *J. Non-Equilib. Thermodyn.*, 18:51–57, 1993.
- [43] P. Singh. Non-equilibrium theory of unsteady heat conduction. *Acta Physica Hungarica*, 43:59–63, 1977.
- [44] P. Glansdorff and I. Prigogine. *Thermodynamic Theory of Structure, Stability and Fluctuations*. Wiley–Interscience, London, 1971.
- [45] M. A. Biot. Variational principles in irreversible thermodynamics with application to viscoelasticity. *Phys. Rev.*, 97:1463–1469, 1955.
- [46] M. A. Biot. *Variational Principles in Heat Transfer*. Oxford Univ. Press, London, 1970.
- [47] J. Keizer. Variational principles in nonequilibrium thermodynamics. *Biosystems*, 8:219–226, 1977.
- [48] J. A. del Rio, M. Lopez de Haro, and F. Vazquez. The non-equilibrium thermodynamics of the solid-water system: a variational approach. *J. Non-Equilib. Thermodyn.*, 17:67–76, 1992.
- [49] S. Sieniutycz and R. S. Berry. Conservation laws from Hamilton's principle for nonlocal thermodynamic equilibrium fluids with heat flow. *Phys. Rev. A.*, 40:348–361, 1989.
- [50] S. Sieniutycz and R. S. Berry. Canonical formalism, fundamental equation, and generalized thermodynamics for irreversible fluids with heat transfer. *Phys. Rev. E.*, 47:1765–1783, 1993.
- [51] S. Sieniutycz and R. S. Berry. Least-entropy generation: Variational principle of Onsager's type for transient, hyperbolic heat and mass transfer. *Phys. Rev. A.*, 46:6359–6370, 1992.
- [52] G. Vojta. Hamiltonian formalisms in the thermodynamic theory of irreversible processes in continuous systems. *Acta Chim. Hung.*, 54:55–64, 1967.
- [53] P. Ván and W. Muschik. The structure of variational principles in non-equilibrium thermodynamics. *Physical Review E*, 52/4:3584–3590, 1995.
- [54] P. Ván and B. Nyíri. Hamilton formalism and variational principle construction. *Annalen der Physik (Leipzig)*, 8:331–354, 1999.
- [55] P. Ván. Weakly nonlocal irreversible thermodynamics—the guyer–krumhansl and the cahn–hilliard equations. *Physics Letters A*, 290:(1–2):88–92, 2001.
- [56] P. Ván, A. Berezovski, and J. Engelbrecht. Internal variables and dynamic degrees of freedom. *Journal of Non-Equilibrium Thermodynamics*, 33/3:235, 2008.
- [57] P. Ván. Weakly nonlocal non-equilibrium thermodynamics—variational principles and second law. In Ewald Quak and Tarmo Soomere, editors, *Applied Wave Mathematics, Selected Topics in Solids, Fluids, and Mathematical Methods*, pages Ch. III. 153–186, Berlin-Heidelberg, 2009. Springer.

ON THE STRUCTURE OF MAXIMUM ENTROPY PRODUCTION PRINCIPLE: FROM NEAR TO FAR-FROM EQUILIBRIUM

Qiang Yang, Kuangdai Leng, Yaoru Liu

State Key Laboratory of Hydrosience and Engineering, Tsinghua University, Beijing 100084, China

ABSTRACT

In this paper, we investigate the microscopic structure of the maximum entropy production principle (MEPP) from a mathematical point of view. It is shown that a MEPP-governed thermodynamic flux or a Ziegler flux is a subclass of the non-linear Onsager flux that is potential or non-rotational in the constrained affinity space, which means MEPP conditionally holds for near-equilibrium processes. A non-linear Onsager flux can be represented in Maclaurin series of which each term is a Ziegler flux. For a far-from-equilibrium process whose thermodynamic flux is non-potential or rotational, the flux can be represented by a series of weighted non-linear Onsager fluxes using the Darboux theorem. The two levels of representation indicate that Ziegler fluxes can serve as the basic elements to construct any complex thermodynamic flux from near to far-from equilibrium. In other words, any complex phenomena can be described elementally by MEPP.

INTRODUCTION

The maximum entropy production principle (MEPP) is a thermodynamic postulate developed by Ziegler [1], which uniquely determines the “easiest and most accessible” [2] evolution path of a non-equilibrium thermodynamic system. Extensive applications of MEPP have been reported in different sciences (see, e.g., recent reviews by Kleidon & Lorenz [3] and Martyushev & Seleznev [4]), however, in the absence of compelling evidence to support its applicability, whether experimental or theoretical [2, 4]. Martyushev [2] left us with two essential questions around MEPP, “(i) can this principle claim to be the basis of all non-equilibrium physics? and (ii) is it possible to prove MEPP?” In this paper, we make an effort to answer question (i) from a mathematical point of view.

The relationship between MEPP and the second law of thermodynamics has been an issue of long-standing interests. Ziegler [1] and Ziegler & Wehrli [5] suggested that the second law of thermodynamics be covered by MEPP, which gives a positive answer to question (i). However, such idea has not yet been well accepted, because, when applied to different sciences, MEPP definitely involves constrains more than the second law of thermodynamics [4, 6-8]. Thus, the principle should be identified as a postulate, or a reasonable classification of behavior for certain non-equilibrium systems instead of a general thermodynamic law. To have a better understanding of MEPP and its scope of application, we may first “divide” the space of non-equilibrium states into several significant subspaces based on their distance with respect to equilibrium.

Figure 1 shows a sketch of the space of possible non-equilibrium states for a given thermodynamic system. The origin represents the equilibrium point. When the state of the system is infinitely close to equilibrium, the irreversible processes are governed by the well-known Onsager reciprocal

relation (Onsager flux in Fig. 1) [9], which is the defining characteristic of the linear subspace. The linear subspace is subsumed in the near-equilibrium subspace, which is characterized in definition by the non-linear Onsager reciprocal relation (non-linear Onsager flux in Fig. 1) by Edelen [10, 11]. The reason why the subspace is labelled “near-equilibrium” will be explained later. In a series of studies by Yang et al. [12-15], it has been proved that MEPP (Ziegler flux in Fig. 1) is a sufficient condition of the non-linear Onsager reciprocal relation, which means MEPP conditionally holds for near-equilibrium processes and thus its scope is not as broad as Ziegler [1] supposed. However, we shall show it in this paper that MEPP can still work as a basic element to describe any near- and far-from-equilibrium processes that do not satisfy the principle itself. The conclusions may help to understand the way MEPP acts in complex phenomena.

From a mathematical point of view, the thermodynamic theories mentioned above including MEPP focus on the dependences of the thermodynamic fluxes on their conjugate thermodynamic forces. To embody rigorous definitions of the thermodynamic flux and force, the theoretical context is formulated in the framework of normality structure. As an internal variable approach, the normality structure proposed by Rice [16, 17] has been an appealing constitutive framework for solids undergoing irreversible thermodynamic processes. Nevertheless, the conclusions might be extended to any well-defined non-equilibrium systems because we do not refer to any special properties of solids at the level of thermodynamic flux and force.

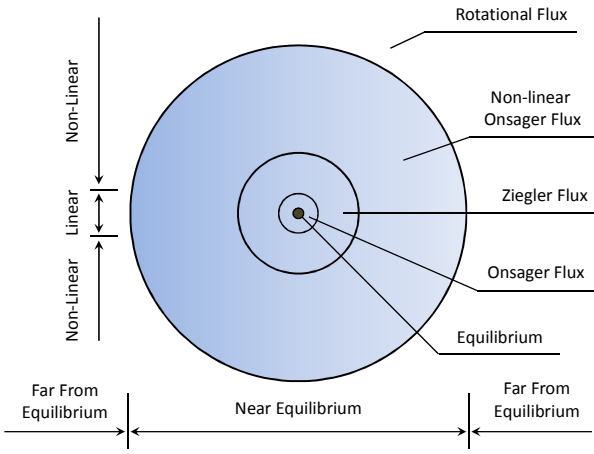


Figure 1 A sketch of the space of non-equilibrium states and its division

PRELIMINARIES

Internal variable approach for solids

Consider a material sample of size V . Introduce the specific free energy ϕ and its Legendre transform ψ with respect to strain,

$$\begin{aligned}\phi &= \phi(\boldsymbol{\varepsilon}, \vartheta, H) \\ \psi &= \psi(\boldsymbol{\sigma}, \vartheta, H) = \boldsymbol{\varepsilon} : \frac{\partial \phi}{\partial \boldsymbol{\varepsilon}} - \phi\end{aligned}\quad (1)$$

where ϑ denotes temperature; $\boldsymbol{\varepsilon}$ denotes any strain tensor, objective and symmetric, that measures deformation from an arbitrary reference state; $\boldsymbol{\sigma}$ denotes the symmetric conjugate stress such that $\boldsymbol{\sigma} : \delta \boldsymbol{\varepsilon}$ is the work per unit volume of the adopted reference state in any virtual deformation $\delta \boldsymbol{\varepsilon}$; H denotes symbolically the current pattern of microstructural rearrangement of constituent elements of the materials. At fixed H , variations of $\boldsymbol{\sigma}$ and ϑ necessarily induce a purely elastic response. Then the first law of thermodynamics leads to the stress-strain relations,

$$\boldsymbol{\sigma} = \frac{\partial \phi(\boldsymbol{\varepsilon}, \vartheta, H)}{\partial \boldsymbol{\varepsilon}}, \quad \boldsymbol{\varepsilon} = \frac{\partial \psi(\boldsymbol{\sigma}, \vartheta, H)}{\partial \boldsymbol{\sigma}} \quad (2)$$

Consider two neighbouring patterns of microstructural rearrangement denoted by H and $H + dH$, respectively. It is assumed that a set of incremental scalar internal variables $d\boldsymbol{\xi} = \{d\xi_1, d\xi_2, \dots, d\xi_n\}$ characterizes the specific local rearrangements, which is represented collectively by dH , at sites throughout the material sample. The $d\boldsymbol{\xi}$ and dH are related by

$$\frac{1}{V} f_\alpha d\xi_\alpha = \frac{1}{V} \mathbf{f} \cdot d\boldsymbol{\xi} = -d^p \phi = d^p \psi \quad (3)$$

where

$$\begin{aligned}d^p \phi &= \phi(\boldsymbol{\varepsilon}, \vartheta, H + dH) - \phi(\boldsymbol{\varepsilon}, \vartheta, H) \\ d^p \psi &= \psi(\boldsymbol{\sigma}, \vartheta, H + dH) - \psi(\boldsymbol{\sigma}, \vartheta, H)\end{aligned}\quad (4)$$

Equation (3) also defines a set of scalar thermodynamic forces $\mathbf{f} = \{f_1, f_2, \dots, f_n\}$ conjugate to the internal variables,

$$\mathbf{f} = \mathbf{f}(\boldsymbol{\varepsilon}, \vartheta, H) \text{ or } \mathbf{f} = \mathbf{f}(\boldsymbol{\sigma}, \vartheta, H) \quad (5)$$

The corresponding set of total internal variables,

$$\boldsymbol{\xi} = \{\xi_1, \xi_2, \dots, \xi_n\} \quad (6)$$

generally are not state variables in the sense that thermodynamic state functions are not direct functions of $\boldsymbol{\xi}$, but instead depend on the path history of $\boldsymbol{\xi}$. Only if the $\boldsymbol{\xi}$ is one set of explicit state variables, the conjugate forces can be determined as

$$\mathbf{f} = -V \frac{\partial \phi(\boldsymbol{\varepsilon}, \vartheta, \boldsymbol{\xi})}{\partial \boldsymbol{\xi}} = V \frac{\partial \psi(\boldsymbol{\sigma}, \vartheta, \boldsymbol{\xi})}{\partial \boldsymbol{\xi}} \quad (7)$$

Kinetic rate law

This paper focuses on the kinetic rate law of the internal variable set $\boldsymbol{\xi}$, namely, the dependence of the thermodynamic flux $\dot{\boldsymbol{\xi}}$ on the thermodynamic force \mathbf{f} . In the constrained affinity space \mathcal{A}^n coordinated by \mathbf{f} with fixed external variables, the general kinetic rate law can be written as

$$\dot{\boldsymbol{\xi}} = \dot{\boldsymbol{\xi}}(\mathbf{f}) \quad (8)$$

The kinetic rate law Eq. (8) is constrained only by the second law of thermodynamics, which leads to the *dissipation inequality*, i.e., the entropy production rate σ should be always non-negative,

$$\sigma = \frac{1}{\vartheta V} \mathbf{f} \cdot \dot{\boldsymbol{\xi}} \geq 0 \quad (9)$$

The most fundamental form of the kinetic rate law is the well-known Onsager reciprocal relation [9], that is, $\dot{\boldsymbol{\xi}}$ depends linearly on \mathbf{f} ,

$$\dot{\boldsymbol{\xi}} = \mathbf{L} \cdot \mathbf{f}, \quad \mathbf{L} = \mathbf{L}^T \quad (10)$$

where \mathbf{L} is the second order tensor of kinetic coefficients in \mathcal{A}^n that is symmetric and independent of $\dot{\boldsymbol{\xi}}$ and \mathbf{f} . As required by the dissipation inequality Eq. (9), \mathbf{L} should be positive semidefinite. A thermodynamic flux is termed an *Onsager flux* if it satisfies Eq. (10).

The number of degrees of freedom (DOFs) of a thermodynamic flux is defined as the number of independent scalar functions in \mathcal{A}^n to determine all its components. Thus, the number of DOFs of a general thermodynamic flux given by Eq. (8) is n . And the number of DOFs of an Onsager flux is 1 because all its components can be derived from a quadratic potential function Q ,

$$\dot{\boldsymbol{\xi}} = \nabla_{\mathbf{f}} Q, \quad Q = Q(\mathbf{f}) = \frac{1}{2} \mathbf{f} \cdot \mathbf{L} \cdot \mathbf{f} \quad (11)$$

where $\nabla_{\mathbf{f}}$ denotes the gradient operator in \mathcal{A}^n , $\nabla_{\mathbf{f}} = \partial / \partial \mathbf{f}$.

NON-LINEAR ONSAGER FLUX AND NEAR-EQUILIBRIUM

Rice flux and normality structure

The theory of normality structure is proposed by Rice [16, 17], who simplified Eq. (8) by assuming that each flux component depends only on its own conjugate force component, as termed the *Rice flux*,

$$\dot{\xi}_\alpha = \dot{\xi}_\alpha(f_\alpha), \quad (\alpha = 1, 2, \dots, n) \quad (12)$$

As a result, the number of DOFs is reduced from n to 1 because a flow potential Q exists such that the flux components are related in the following form

$$\dot{\xi} = \nabla_f Q, \quad Q = Q(\mathbf{f}) = \int_0^{\mathbf{f}} \dot{\xi}_\alpha df_\alpha \quad (13)$$

With the kinetic rate law given by Eq.(13), the normality structure for solids can be easily shown,

$$\frac{d^p \boldsymbol{\varepsilon}}{dt} = \frac{1}{V} \frac{\partial Q}{\partial \boldsymbol{\sigma}} \quad (14)$$

where $d^p \boldsymbol{\varepsilon}$ denotes the inelastic part of strain, because, known from Eq. (2) and Eq. (3),

$$\frac{d^p \boldsymbol{\varepsilon}}{dt} = \frac{1}{V} \frac{\partial \psi}{\partial \boldsymbol{\sigma}} = \frac{1}{V} \frac{\partial \mathbf{f}}{\partial \boldsymbol{\sigma}} \cdot \dot{\xi} = \frac{1}{V} \frac{\partial Q}{\partial \boldsymbol{\sigma}} \quad (15)$$

The Rice flux Eq. (12) is a very strong restriction because the flux components are required to be fully decoupled in \mathcal{A}^n . It is only a sufficient condition for the normality structure or the existence of a flow potential Q .

Non-linear Onsager flux

As discussed by Yang et al. [12-15], the sufficient and necessary condition for normality structure is the non-linear Onsager reciprocal relation proposed by Edelen [10, 11],

$$\frac{\partial \dot{\xi}_\alpha}{\partial f_\beta} = \frac{\partial \dot{\xi}_\beta}{\partial f_\alpha} \quad \text{or} \quad \nabla_f \dot{\xi} = \dot{\xi} \nabla_f \quad (16)$$

A thermodynamic flux is termed a *non-linear Onsager flux* if it satisfies Eq. (16), which encompasses both Rice flux and Onsager flux as subclasses. Know from the Green theorem and Stokes theorem, the following four statements are equivalent:

- the thermodynamic flux is a non-linear Onsager flux as defined by Eq. (16);
- the flux components can be derived from a flow potential Q ,

$$\dot{\xi} = \nabla_f Q, \quad Q = Q(\mathbf{f}) = \int_0^{\mathbf{f}} \dot{\xi} \cdot d\mathbf{f} \quad (17)$$

which means the number of DOFs of $\dot{\xi}$ is 1 and the normality structure Eq. (14) holds;

- the thermodynamic flux is potential or non-rotational,

$$\oint \dot{\xi} \cdot d\mathbf{f} = 0 \quad \text{or} \quad \nabla_f \wedge \dot{\xi} = \mathbf{0} \quad (18)$$

where \wedge denotes the exterior product in \mathcal{A}^n ;

- $\dot{\xi} \cdot d\mathbf{f}$ is a total differential or a differential 1-form of Class 1,

$$\dot{\xi} \cdot d\mathbf{f} = dQ \quad (19)$$

The non-linear Onsager flux is employed in this paper as the criterion to distinguish between near- and far-from equilibrium processes. That is to say, the behavior of a thermodynamic system in states near equilibrium is dominated by the thermodynamic flux that is potential or non-rotational in a sufficiently small neighborhood of an equilibrium state. The criterion can be formulated by anyone of the conditions from Eq. (16) to Eq. (19). Such criterion was suggested by Edelen [11] who put stress on the existence of a potential function (Eq. (17) or Eq. (19)) that characterizes near-equilibrium states:

“Thermostatistics is based on the assumption that the system under study is always at or sufficiently close to an equilibrium state that the thermodynamic potential functions (internal energy, free energy, etc.) can be defined as functions of the state variables, which are independent of the time and independent of the history of the system.”

In a few studies, the Onsager flux Eq. (10) was taken as the criterion, which, however, is somewhat narrow because Onsager fluxes occur only in an infinitesimal neighborhood of equilibrium and thus it is not convincing to conclude that a process violating Eq. (10) is far from equilibrium. Figure 1 shows a clearer vision: the linear subspace is subsumed in the near-equilibrium subspace.

MEPP NEAR EQUILIBRIUM

Ziegler flux and its scope

Let $\dot{\xi}$ be continuously differentiable with respect to \mathbf{f} , the MEPP can be written in the form of orthogonality condition [1, 5],

$$\dot{\xi} = \lambda \nabla_f \sigma \quad (20)$$

where σ denotes the entropy production rate and λ is a Lagrangian multiplier required by MEPP. Substituted with Eq. (9), Eq. (20) becomes

$$\nabla_f \dot{\xi} \cdot \mathbf{f} = q \dot{\xi} \quad (21)$$

where

$$q = \frac{1}{\lambda \theta V} - 1 \quad (22)$$

Known from the Euler's homogeneous function theorem, Eq. (21) shows that $\dot{\xi}$ should be a homogeneous function of degree q in its conjugate force \mathbf{f} . A thermodynamic flux satisfying Eq. (21) is termed a *Ziegler flux*. Obviously, Onsager flux is a subclass of Ziegler flux when $q = 1$.

Taking the derivative of Eq. (21) with respect to \mathbf{f} , one obtains

$$\xi \nabla_{\mathbf{f}} + \nabla_{\mathbf{f}}^2 \xi \cdot \mathbf{f} = q \nabla_{\mathbf{f}} \xi \quad (23)$$

Noting that the second order tensor $\nabla_{\mathbf{f}}^2 \xi \cdot \mathbf{f}$ is symmetric, Eq. (23) minus its transpose yields

$$\nabla_{\mathbf{f}} \xi = \xi \nabla_{\mathbf{f}} \quad (24)$$

Equation (24) means Ziegler flux is a subclass of non-linear Onsager flux, as indicated by Fig. 1. Therefore, the scope of application of MEPP is limited to near equilibrium processes.

Representation of a Non-linear Onsager flux in a series of Ziegler fluxes

Consider a generic non-linear Onsager flux ξ that is determined by the flow potential Q in the form of Eq. (17). Let Q be expanded in Maclaurin series at the equilibrium point $Q(\mathbf{0}) = 0$,

$$Q(\mathbf{f}) = \sum_{i=0}^{\infty} \frac{1}{i!} \mathbf{f}^i \circ \nabla_{\mathbf{f}}^i Q(\mathbf{0}) \quad (25)$$

where \circ denotes the complete inner product and the i -th order tensor $\nabla_{\mathbf{f}}^i Q(\mathbf{0})$ is full symmetric and constant. Note that the zeroth and the first terms vanish, i.e.,

$$\begin{aligned} \frac{1}{0!} \mathbf{f}^0 \circ \nabla_{\mathbf{f}}^0 Q(\mathbf{0}) &= Q(\mathbf{0}) = 0 \\ \frac{1}{1!} \mathbf{f}^1 \circ \nabla_{\mathbf{f}}^1 Q(\mathbf{0}) &= \mathbf{f} \cdot \left. \frac{\partial Q}{\partial \mathbf{f}} \right|_{\mathbf{f}=\mathbf{0}} = \mathbf{f} \cdot \xi(\mathbf{0}) = 0 \end{aligned} \quad (26)$$

Substituting Eq. (25) to Eq. (17), ξ is represented as

$$\xi = \nabla_{\mathbf{f}} Q = \xi^{(2)} + \xi^{(3)} + \dots = \sum_{i=2}^{\infty} \xi^{(i)} \quad (27)$$

where $\xi^{(i)}$ is the i -th term of the Maclaurin series,

$$\xi^{(i)} = \frac{1}{(i-1)!} \mathbf{f}^{i-1} \circ \nabla_{\mathbf{f}}^i Q(\mathbf{0}) \quad (28)$$

Obviously, $\xi^{(i)}$ ($i = 2, 3, \dots, n$) is a series of Ziegler fluxes of degree $i - 1$, because

$$\nabla_{\mathbf{f}} \xi^{(i)} \cdot \mathbf{f} = (i-1) \xi \quad (29)$$

And the first term $\xi^{(2)}$ is an Onsager flux,

$$\xi^{(2)} = \mathbf{L} \cdot \mathbf{f}, \quad \mathbf{L} = \left. \frac{\partial^2 Q}{\partial \mathbf{f}^2} \right|_{\mathbf{f}=\mathbf{0}} = \mathbf{L}^T \quad (30)$$

Equation (27) shows that, any non-linear Onsager flux can be represented in a series of Ziegler fluxes and the classical Onsager reciprocal relation holds strictly when and only when the current state is in an infinitesimal neighborhood of equilibrium. Therefore, any near-equilibrium processes can be approximately described using such representation, where the number of the terms can be arbitrary and determined by the required accuracy of the description.

Prigogine's minimum entropy production principle

One may refer to Martyushev & Seleznev [4] and Rajagopal & Srinivasa [7] for thorough discussions on the significance of the Prigogine's minimum entropy production principle [18] and its relationship between MEPP. Here we simply prove that the Prigogine's principle is an inevitable result of the second law of thermodynamics for a given Ziegler flux with $q \geq 0$.

The Prigogine's principle states that, if some of the thermodynamic forces are fixed at zero, i.e.,

$$f_{\alpha} = 0, \quad \alpha = 1, 2, \dots, \chi \quad (\chi < n) \quad (31)$$

the entropy production reaches the minimum if and only if the remained thermodynamic fluxes vanish, namely,

$$\xi_{\alpha} = 0, \quad \alpha = \chi + 1, \chi + 2, \dots, n \quad (32)$$

is the sufficient and necessary condition of

$$\sigma = \frac{1}{\partial V} \mathbf{f} \cdot \xi \rightarrow \min \quad (33)$$

The proof goes as follows. Equation (33) equals to

$$\nabla_{\mathbf{f}}(\sigma) = \frac{1}{\partial V} (\xi + \nabla_{\mathbf{f}} \xi \cdot \mathbf{f}) = \frac{1+q}{\partial V} \xi = \mathbf{0} \quad (34)$$

$$\mathbf{f} \cdot \nabla_{\mathbf{f}}^2(\sigma) \cdot \mathbf{f} = \frac{1+q}{\partial V} \mathbf{f} \cdot \nabla_{\mathbf{f}} \xi \cdot \mathbf{f} = (1+q)q\sigma \geq 0$$

Obviously, Eq. (34a) is exactly Eq. (32) and Eq. (34b) is the second law of thermodynamics as long as the degree q is positive.

MEPP FAR FROM EQUILIBRIUM

Representation of a rotational flux in a series of non-linear Onsager fluxes

In this section, we consider thermodynamic fluxes far away from equilibrium. The fluxes are rotational and cannot be derived from a potential function. Let $\xi(\mathbf{f})$ be a generic rotational flux. Using the n -dimensional generalization of the Helmholtz representation theorem [19], ξ can be decomposed into two parts,

$$\xi(\mathbf{f}) = \xi_p(\mathbf{f}) + \xi_r(\mathbf{f}) \quad (35)$$

where $\xi_p(\mathbf{f})$ is the potential part that is curl free and can be determined by the potential function Q ,

$$\xi_p = \nabla_{\mathbf{f}} Q, \quad Q = Q(\mathbf{f}) = \int_0^1 \xi(\tau \mathbf{f}) \cdot \mathbf{f} d\tau \quad (36)$$

and $\xi_r(\mathbf{f})$ is the purely rotational part

$$\xi_r = \int_0^1 \tau (\nabla_{\mathbf{f}} \xi(\tau \mathbf{f}) - \xi(\tau \mathbf{f}) \nabla_{\mathbf{f}}) \cdot \mathbf{f} d\tau \quad (37)$$

which also satisfies

$$\xi_r \cdot \mathbf{f} = 0 \quad (38)$$

The properties of ξ_p have been discussed in the previous two sections and here we only have to focus on ξ_r .

Consider the differential 1-form $\xi_r(\mathbf{f}) \cdot d\mathbf{f}$. Known from the Darboux theorem [19], it should be of Class $2m$ with $m \geq 1$ and can be represented as

$$\xi_r(\mathbf{f}) \cdot d\mathbf{f} = \sum_{i=1}^m P^{(i)}(\mathbf{f}) dQ^{(i)}(\mathbf{f}) \quad (39)$$

where $P^{(i)}$ and $Q^{(i)}$ are independent scalar functions of total number $2m$. Thus, the ξ_r is determined as

$$\xi_r = \sum_{i=1}^m P^{(i)}(\mathbf{f}) \nabla_{\mathbf{f}} Q^{(i)}(\mathbf{f}) \quad (40)$$

which indicates that the number of DOFs of ξ_r is $2m$. It should be noted that the representation of ξ_r by Darboux theorem is totally different from the representation of ξ_p in Maclaurin series as given by Eq. (27). First, the number of terms of Eq. (27) is arbitrary while in Eq. (40) m is a nature of the given flux: m increases as the flux removes from equilibrium. Second, in Eq. (27), each term is a high-level minimal of its preceding term, but in Eq. (40) all terms are of equal status.

Combining Eq. (40) with Eq. (35), a generic flux $\xi(\mathbf{f})$ that is far from equilibrium can be represent by a series of weighted non-linear Onsager fluxes in the following form

$$\xi = \xi_p + P^{(1)}\xi_p^{(1)} + P^{(2)}\xi_p^{(2)} + \dots + P^{(m)}\xi_p^{(m)} \quad (41)$$

where $\xi_p^{(i)}$ ($i = 1, 2, \dots, m$) denote m non-linear Onsager fluxes determined by the potential $Q^{(i)}(\mathbf{f})$ and weight functions are force-dependent, $P^{(i)} = P^{(i)}(\mathbf{f})$. On the other hand, any non-linear Onsager flux can be represented by a series of Ziegler fluxes, so we can conclude that any flux far from equilibrium can be finally represented by a series of weighted Ziegler fluxes through the two levels of representation. This might be the way MEPP acts in far-from-equilibrium processes. Finally, we may answer the question (i) proposed by Martyushev [2]: MEPP could be a basis of all non-equilibrium physics, but not in a straightforward way.

An example: the non-Darcy flow

Take the Darcy's law for example, which is a constitutive equation for the flow of a fluid through a porous medium. The Darcy's law establishes the linear relation between the pressure gradient and the velocity. For one-dimensional flow, it can be written as

$$-\nabla p = \frac{\mu}{K} v \quad (42)$$

where ∇p denotes the pressure gradient, v the velocity, μ the fluid viscosity and K the permeability of the porous medium. A well-known non-linear extension of the Darcy's law is the Forchheimer equation [20], which is quadratic,

$$-\nabla p = \frac{\mu}{K} v + \rho \beta v^2 \quad (43)$$

where ρ and β denote respectively the fluid density and the non-Darcy coefficient. In general, the non-Darcy effect can be presented in the polynomial form [21],

$$-\frac{K}{\mu} \nabla p = v + \frac{1}{v} f(v, v) + \frac{1}{v^2} g(v, v, v) + \dots \quad (44)$$

where f and g are bilinear and trilinear functions, respectively. The nonlinear extensions can be supported in thermodynamics with the proposed representation theorems.

CONCLUSIONS

In this paper, a non-equilibrium process is considered as near equilibrium if there exists a potential function from which all components of the thermodynamic flux can be derived. Such flux is termed non-linear Onsager flux. By contrast, a process is considered as far from equilibrium if the flux is non-potential or rotational.

The maximum entropy production principle (MEPP) by Ziegler is a reasonable classification of behavior for certain non-equilibrium systems instead of a general thermodynamic law. A MEPP-governed thermodynamic flux or a Ziegler flux is actually a homogenous non-linear Onsager flux. Thus, the scope of application of MEPP is not universe but limited to near-equilibrium processes.

Any non-linear Onsager flux can be represented in Maclaurin series of which each term is a Ziegler flux. Therefore, any near-equilibrium processes can be approximately described using such representation, where the number of the terms of the representation can be arbitrary and determined by the required accuracy of the description.

For a far-from-equilibrium process, the rotational flux can be represented by a series of weighted non-linear Onsager fluxes using the Darboux theorem. The number of the terms of the representation is a nature of the rotational flux: the number increases as the flux removes from equilibrium.

The two levels of representation indicate that Ziegler fluxes can serve as the basic elements to construct any complex thermodynamic flux from near to far-from equilibrium. In other words, any complex phenomena can be described elementally by MEPP.

ACKNOWLEDGMENT

This work is supported by the National Natural Science Foundation of China under Projects 50925931 and 11172150 and subsidized by the special funds for major state basic research projects with Grant no. 2009CB724604.

REFERENCES

- [1] H. Ziegler, An Introduction to Thermomechanics, North-Holland, Amsterdam, 1977.
- [2] L.M. Martyushev, The Maximum Entropy Production Principle: Two Basic Questions, Phil. Trans. R. Soc. B, vol. 365, pp. 1333-1334, 2010.
- [3] A. Kleidon and R. Lorenz (eds), Non-equilibrium Thermodynamics and the Production of Entropy in Life, Earth, and Beyond, Springer, Heidelberg, 2004.

- [4] L.M. Martyushev and V.D. Seleznev, Maximum Entropy Production Principle in Physics, Chemistry and Biology, *Phys. Rep.*, vol. 426, pp. 1-45, 2006.
- [5] H. Ziegler, C. Wehrli, On a Principle of Maximal Rate of Entropy Production, *J. Non-Equil. Thermodyn.*, vol. 12, pp. 229-243, 1987.
- [6] H. Ozawa, A. Ohmura, R. Lorenz, and T. Pujol, The Second Law of Thermodynamics and the Global Climate Systems – A Review of the Maximum Entropy Production Principle, *Rev. Geophys.*, vol. 41, pp. 1018-1041, 2003.
- [7] K.R. Rajagopal, A.R. Srinivasa, On Thermomechanical Restrictions of Continua, *Proc. R. Soc. Lon. A.*, vol. 460, pp. 631-651, 2004.
- [8] H.W. Jr Haslach. Maximum Dissipation Non-equilibrium Thermodynamics and its Geometric Structure, Springer, Heidelberg, 2011.
- [9] L. Onsager, Reciprocal Relations in Irreversible Processes I., *Phys. Rev. II. Ser.*, vol. 37, pp. 405-426, 1931.
- [10] D. G. B. Edelen, A Nonlinear Onsager Theory of Irreversibility, *Int. J. Eng. Sci.*, vol. 10, pp. 481-490, 1972.
- [11] D. G. B. Edelen, Asymptotic Stability, Onsager Fluxes and Reaction Kinetics, *Int. J. Eng. Sci.*, vol. 11, pp. 819-839, 1973.
- [12] Q. Yang, L.G. Tham, G. Swoboda, Normality Structures With Homogeneous Kinetic Rate Laws, *J. Appl. Mech. Trans. ASME*, vol. 72, pp. 322-329, 2005.
- [13] Q. Yang, R.K. Wang, L.J. Xue, Normality Structures with Thermodynamic Equilibrium Points, *J. Appl. Mech. Trans. ASME*, vol. 74, pp. 965-971, 2007.
- [14] Q. Yang, L.J. Xue, Y.R. Liu, Thermodynamics of Infinitesimally Constrained Equilibrium States, *J. Appl. Mech. Trans. ASME*, vol. 76, pp. 014502.1-014502.5, 2009.
- [15] Q. Yang, J.Q. Bao, Y.R. Liu, Asymptotic Stability in Constrained Configuration Space for Solids, *J. Non-Equil. Thermodyn.*, vol. 34, pp. 155-170, 2009.
- [16] J.R. Rice, Inelastic Constitutive Relations for Solids: An Internal Variable Theory and Its Application to Metal Plasticity, *J. Mech. Phys. Solids*, vol. 19, pp. 433-455, 1971.
- [17] J.R. Rice, Continuum Mechanics and Thermodynamics of Plasticity in Relation to Microscale Deformation Mechanisms, *Constitutive Equations in Plasticity*, A.S. Argon ed., MIT Press, Cambridge, MA, pp. 23-79, 1975.
- [18] I. Prigogine, Introduction to Thermodynamics of Irreversible Processes, Springfield, Kalamazoo, 1955.
- [19] D. G. B. Edelen, The College Station Lectures on Thermodynamics. Texas A & M University, College Station Texas, 1993.
- [20] S. Whitaker, The Forchheimer Equation: a Theoretical Development, *Transp. Porous Media*, vol. 25, pp. 27-61, 1996.
- [21] M. Firdaouss, J.L. Guermond, P. Le Quere, Nonlinear Corrections to Darcy's Law at Low Reynolds Numbers, *J. Fluid Mech.*, vol. 343, pp. 331-350, 1997.

PANEL E

THERMODYNAMIC ENTROPY: THE VARIOUS DEFINITIONS AND THEIR REASONS

“DEFINING ENTROPY BEFORE HEAT, NOT VICEVERSA” IN INTRODUCTORY THERMODYNAMICS: TWENTYFIVE-YEAR TEACHING EXPERIENCE IN ENGINEERING PROGRAMS

A.M. Lezzi*, A. Niro**, M. Pilotelli*

*Department of Mechanical and Industrial Engineering, Università degli Studi di Brescia,
Via Branze 38, 25123, Brescia, Italy, E-mail: lezzi@ing.unibs.it

**Department of Energy, Politecnico di Milano,
Via Lambruschini 4, 20156 Milano, Italy, E-mail: alfonso.niro@polimi.it

ABSTRACT

As well as many other people, we have felt, both as students and as teachers, that some traditional approaches present ambiguities and logical inconsistencies in the exposition of the basics of thermodynamics. Since the late '80s we have adopted an approach developed over thirty years of course and research work at M.I.T.: rooted in the work of Hatsopoulos and Keenan [1], it has been presented in a systematic and detailed way by Gyftopoulos and Beretta [2]. On the basis of our teaching experience we believe that this approach is particularly suited for students attending engineering programs and our goal here is to underline the most important reasons of its success. In the paper we summarize and discuss how we have adapted the sequence of arguments proposed in [2, Chaps. 2-14] to meet the needs of undergraduate engineering students.

INTRODUCTION

A large variety of expositions of the foundations of thermodynamics are available in textbooks and scientific literature. Roughly, two groups of approaches can be identified. The concise exposition by Fermi [3] or the popular textbook by Zemansky [4] are among the best examples of the first group of approaches, that could be called traditional. Heat and empirical temperature are usually introduced at the outset of the logical development. Sometimes they are assumed as primitive concepts, sometimes the authors try to explain the difference between heat and work in terms of mechanical illustrations, mostly based on statistical arguments. As well as many other students or teachers, we have felt discomfort with some of these expositions because of ambiguities and logical inconsistencies. Moreover, we think that any confused reference to microscopic physics or statistical mechanics, which do not belong to the background of most engineering students, should be avoided when teaching thermodynamics in engineering programs.

The second group is based on an axiomatic approach. Examples can be traced back to the work of Carathéodory [5] and include textbooks as the one by Giles [6], or the popular one by Callen [7], or the recent work by Lieb and Yngvason [8]. These expositions are rigorous, but rather abstract, and do not seem a suitable choice for engineering students. As a matter of fact, Giles in the Preface of his book identifies his potential readers among “physicists who are not entirely satisfied with the logical basis of their subject, [...] mathematicians who may be interested to discover a novel application of pure mathematics, and [...] philosophers” [6, p. XII], without any mention of engineers.

As a result of long-time conversations and discussions with our friend and colleague G.P. Beretta, since the late '80s we have adopted an approach developed over thirty years of course and research work at M.I.T.: rooted in the work of Hatsopoulos

and Keenan [1], it has been presented in a systematic and detailed way by Gyftopoulos and Beretta [2]. The exposition follows an axiomatic approach which is characterized by a two-fold goal. On one hand the basic concepts are introduced and developed trying to avoid equivocal definitions and logical short-circuits. On the other hand, the operational approach typical of the best traditional expositions is preserved. Particular attention is paid to fundamental questions of important practical consequences, like the amount of energy of a system that can be used to perform a useful task. Here “to perform a useful task” means to produce mechanical effects such as rise weights, compress springs, moving electrical charges. Ideally most engineering applications can be reduced or described in terms of a set of useful tasks to be performed. Studying mechanics a student is led to think that all the energy of a system can be used to perform a useful task, whereas exposition to thermodynamics conveys the fundamental idea that, in general, only part of the energy can be exploited. In some case (systems in stable equilibrium states) energy is not available at all. Starting from the question: “how much energy can be extracted from a system to perform work?” two properties are introduced, the adiabatic availability and the available energy. They are defined for any system in any state. Then, entropy is defined as a linear combination of energy and available energy differences. The definition is operational and describe an ideal way to measure entropy. Moreover entropy results to be a property of systems in any state, just like energy, momentum, mass, etc. Another key feature of this approach, particularly important for engineering students, is that it naturally leads to the physical interpretation of entropy as a measure of the energy of a system that cannot be used to perform work and underlines the strong interrelation between entropy generation by irreversibility and loss of potential to perform work.

Following Gyftopoulos and Beretta [2; 9; 10], in our courses we introduce the basic concepts according to the following

order: system; properties; state; energy and energy balance; classification of states and existence of stable equilibrium states; available energy; entropy (both for equilibrium and non-equilibrium states) and entropy balance; properties of stable equilibrium states; temperature in terms of energy and entropy; pressure; work and heat. In this paper we discuss how we have adapted the sequence of arguments proposed in [2, Chaps. 2-14] to meet the needs of engineering students with different background (mechanical, industrial, civil, etc.), attending the course either during their 2nd or their 3rd year of program. On the basis of our teaching experience we believe that this approach is particularly suited for students attending engineering programs and our goal here is to underline the most important reason of its success.

UNIT 1: SYSTEMS, PROPERTIES, AND STATES

The first course hour is devoted to the introduction of the concepts of system, property and state.

A set or collection of constituents is called a *system* when it is clearly specified what follows.

1. Type of each constituent and allowed range of values of the corresponding amount.
2. Type and allowed range of values of the parameters that fully characterize any external forces exerted on the constituents by bodies other than the constituents. The external forces may depend on coordinates of the constituents of the system only.
3. The internal forces among constituents, such as intermolecular forces.

A force parameter can be a quantity that appears in the equation describing an external force field like g in the uniform gravitational field near the Earth ground, or like the charge q in the electrical field that it generates. In some cases the force field expression is not even necessary to describe its effects on the constituents: for many applications the effects of the walls of a container that confines a gas are fully described by the volume V of the enclosure, and we do not need to specify its actual geometry. Furthermore, point 2. expresses the fundamental request of *separability* of constituents of a system from other bodies. Constituents that are not separable cannot be considered a system: as an illustrative example from mechanics, consider a set A of material points subject to a force potential depending on coordinates of other material points external to A : in this case it is not possible to define the corresponding potential energy of A and, as a consequence, to determine the value of A 's energy.

Everything that is not included in the system is the *environment*, which is thought as a system itself.

For a system with r constituents, we denote their amounts by the vector $\mathbf{n} = (n_1, n_2, \dots, n_r)$. For a system with external forces described by s parameters we denote the parameters by the vector $\boldsymbol{\beta} = (\beta_1, \beta_2, \dots, \beta_s)$. For most systems studied in the course, volume is the only parameter, $s = 1$ and $\beta_1 = V$.

The notion of system can be suitably illustrated with examples from mechanics and electromagnetism: like a set of material points of different masses (type of constituents), in a uniform gravitational field characterized by the parameter g and subject to internal elastic forces.

At any instant of time, the amount of each constituent and the parameters of each external force have specific values, but these do not suffice to characterize completely the condition of the system: we need to know the values of a larger, specific set of

properties. For example, referring to systems of material points, we need to specify position and velocity of each particle.

A *property* is a system attribute that can be quantitatively evaluated at any given instant of time by means of a set of well-defined measurements and operations provided that the value is independent of the measuring devices, other systems in the environment and other instants of time. The difference of instantaneous velocity and average velocity can be used to illustrate the difference among properties and other physical observables.

Two properties are said to be *independent* if the value of one can be varied without affecting the value of the other. The characterization of the condition of a system at an instant of time is given by the values of a *complete* set of independent properties: this set of values is called the *state* of the system. The expression complete set denotes a set of properties which are sufficient to determine the values of all other properties: the existence of complete sets of independent properties is implicitly assumed here. As a final remark, we underline that the amounts of constituents and the force parameters are system properties.

As already mentioned, we try to follow a gradual approach from mechanics to thermodynamics. Definitions and results we are teaching must encompass as a special cases the ones known from introductory physics courses. This is the case, for example, with the definitions of system, property, and state which are valid without change in any physical theory.

UNIT 2: CHANGES OF STATE, PROCESSES

The second course unit takes into consideration the time evolution of systems and how it can be described. Roughly, it takes one hour.

It is self-evident that the state of a system may change in time. Two or more systems interact among them, when correlated changes of their properties can be observed. Through examples from mechanics (elastic collisions) or electromagnetism (contact between charged conductors) it is underlined that some property changes can be thought of as due to an exchange between interacting systems (momentum, electric charge), while other properties are not exchanged (velocity, electric potential). *Interactions* among systems are classified in terms of properties exchanged and modes of exchange.

In mechanics students learn that to describe the time evolution of a system, one has to solve an equation of motion to find a trajectory in a proper phase space. For more general systems such an equation is not available, thus we are content with a less strong description of motion. A collision experiment can be used to illustrate the concept. Even if we do not know exactly the internal forces acting during the collision, and therefore we are not able to reconstruct the particles motion, we do know that collision will result in an exchange of momentum and energy: both momentum and energy (kinetic plus internal potential energy) are conserved. In some cases one measures masses and velocities before and after the collision, to evaluate the amount of properties which have been exchanged. In other cases, one takes advantage of the conservation principles to determine properties of the initial or the final states that have not been measured.

As well as a collision among particles can be fully described in terms of values of properties before and after the collision, to describe system evolutions we introduce the concept of *process* that is the specification of the initial and the final states plus the interactions active during the change of state.

Different types of processes can be identified. A class of pro-

cesses of particular importance for the subsequent development of the exposure are the so-called *mechanical processes*. A process is denoted mechanical if the only net effect in the environment is a mechanical one. By mechanical effect we mean the change of elevation of a weight in a uniform gravitational field, the change of momentum of a material point, the change of distance of two masses or two electrical charges, the change of length of a spring etc. As taught in introductory physics courses all these examples are perfectly equivalent: it is always possible, for example, to modify the elevation of a weight without any other net effect but a change of the distance between two electrical charges. Without loss of generality, the change of elevation of a weight is taken as representative of all mechanical effects. The processes studied in mechanics and electromagnetism are all of this type.

A type of process which does not pertain to mechanics is the spontaneous process. Upon studying real systems one realizes that some changes of state are not induced by other systems nor produce a non-zero effect in the environment. Several examples from everyday life can be successfully used to exemplify this concept: some milk carefully poured into a cup of coffee will slowly change into white coffee even without any stirring or shaking from the environment; the battery of a cell phone left off for a few weeks will not supply enough charge to operate the phone. In some cases it is clear, in others it may require prolonged and careful observations, but one has to conclude that some changes of properties of a system are uncorrelated to any change of properties of any other system: these are called *spontaneous* changes of state. Systems which undergo only to spontaneous changes of state are said *isolated*. Consideration and analysis of spontaneous processes is a distinct feature of thermodynamics with respect to mechanics.

Finally, we introduce the concept of steady processes (when the state of the system does not vary in time, in spite of active interactions with other systems) and of reversible processes (when it is possible to perform a second process that restores the initial state of both the system and its environment).

UNIT 3: FIRST LAW, ENERGY, ENERGY BALANCE

This unit requires two hours at most to introduce the First Law of Thermodynamics and its main consequences, first of all the existence of a property, energy, which is defined for all states of any system. The First Law is stated as follows:

Any two states of a system may always be the end states of a mechanical process. Moreover, for a given weight m , the value of the product $mg\Delta z$ is fixed by the end states of the system, and independent of the details of the mechanical process.

Here m is the mass of the weight, g the gravitational acceleration and Δz the weight elevation change.

Commenting on this statement in class, it is important to underline that although any pair of states can be connected through a mechanical process, nothing can be said about the direction of the process. It is not guaranteed that each of the two states can be either the initial or the final state: in general, therefore, the mechanical process can be either reversible or irreversible.

The main consequence of the First Law is that every system A in any state A_1 has a property called *energy*, with a value denoted by E_1^A . If one chooses a reference state A_0 to which is assigned an arbitrary reference value E_0^A , then the energy E_1^A can be evaluated performing a mechanical process that connects A_0

and A_1 ,

$$E_1^A = E_0^A - mg(z_1 - z_0) \quad (1)$$

Next we introduce the concept of composite system, that is a set of two or more systems, which can be considered a system itself. On the other hand, a partition of a system does not guarantee that the single parts are systems themselves.

A series of important results for energy are proved. Conservation: energy is conserved in any spontaneous process (a spontaneous process is a zero-net-effect mechanical process, $mg\Delta z = 0$). Additivity: the energy of a composite system is the sum of the energies of its subsystems. Transferability: considering spontaneous processes of a composite system, it is shown that energy is a property that can be exchanged among systems when they interact. Energy balance: for any process of any system A it holds,

$$E_2^A - E_1^A = E^{A\leftarrow} \quad (2)$$

Here $E^{A\leftarrow}$ denotes the net energy transferred to A from all the other interacting systems during the process that changes the state of A from A_1 to A_2 . The energy gained by a system A must be accounted for by the energy transferred across the boundary of the system, because energy neither can be generated nor destroyed in A .

UNIT 4: EQUILIBRIUM STATES

This unit requires about one hour and is a necessary introduction to the Second Law statement. It should be illustrated to classes with examples from mechanics.

For most systems the number of possible states is infinite. Among these infinite states there are some that have important characteristics. We introduce a classification of states based on their time evolution in spontaneous processes.

A *non-equilibrium* state is one that changes spontaneously as a function of time. An *equilibrium* state is one that does not change as a function of time while the system cannot interact with other systems: it is a state that does not change spontaneously.

Equilibrium states can be divided further in non-stable equilibrium states and stable equilibrium states. Is it possible to perform a process that starts with the system in a non-stable equilibrium state and ends in a different state, with non-zero exchange of properties during the process, but without net final effects in the environment. A stable equilibrium state is an equilibrium state that can be altered to a different state only by interactions that leave net effects in the environment of the system. These definitions are equivalent to the ones presented in mechanics in introductory physics courses, but encompass a larger set of states than those encountered in mechanics. The motion of a material point in a force field with potential energy with relative minima (metastable states) and maxima (unstable states) and an absolute minimum (stable state) can be used to illustrate the concept.

UNIT 5: SECOND LAW, AVAILABLE ENERGY

This unit which takes about two hours, starts with the presentation of the Second Law of Thermodynamics, formulated as a statement about the existence of stable equilibrium states.

Among all the states of a system with given values of the energy, the amounts of constituents, and the parameters, there ex-

ists one and only one stable equilibrium state. Moreover, starting from any state of a system it is always possible to reach a stable equilibrium state with arbitrarily specified values of amount of constituents and parameters by means of a reversible mechanical process.

In this exposition the crucial difference between systems as studied in mechanics and electromagnetism, and systems as studied in thermodynamics, is the existence of a multitude of stable equilibrium states of a system, as experience and experimental evidence show. In mechanics and in electromagnetism a system has only one stable equilibrium state (ground state). At ground state the energy of the systems attains its minimum value: thus it is usually chosen as reference state and its energy is set equal to zero. In thermodynamics, it is stated that for fixed values of amounts of constituents and parameters, there exist one stable equilibrium state for each energy value and not for the ground energy value only. Moreover the stable equilibrium state corresponding to a value of E is unique.

Let's turn to what we could call a fundamental engineering problem: given a system with energy E , which fraction of it could we extract to perform useful tasks such as rise weights, compress springs, moving electrical charges?

In a mechanical process starting either from a non-equilibrium or a non-stable equilibrium state, a system can transfer energy out. In mechanics, the maximum transfer of energy to the environment occurs in a process ending in the ground state. If ground energy is set equal to zero, we convey the idea that all the energy of a system can be extracted in a mechanical process.

Therefore, in mechanics the answer to the previous question is "all", while, upon introduction of the Second Law, the answer is "only a fraction of it": furthermore, if the initial state is a stable equilibrium one the answer is "none". The latter conclusion is known as the *impossibility of the perpetual motion machine of the second kind*.

At this point a new property defined for any state of any system is introduced: the *adiabatic availability* Ψ . The adiabatic availability of system A in state A_1 represents the maximum energy that can be extracted from A by a mechanical process starting from state A_1 , without changing amounts of constituents and parameters. Let's consider all conceivable mechanical processes starting from state A_1 that do not change the amounts of constituents and the parameters, and compare the values of the energy extracted from A : the maximum value of the energy extracted satisfies all the independence requirements for a physical observable to be a property. The adiabatic availability is the maximum energy that can be extracted from a system in a given state to perform useful tasks (without vary amounts of constituents and parameters): it is equal to zero for any stable equilibrium state and it is positive for any other state. It allows to state a criterion for reversibility of a mechanical process: given two states A_1 and A_2 with the same amounts of the constituents and parameters, a mechanical process from A_1 to A_2 can be performed if and only if $\Psi_1^A - \Psi_2^A \geq E_1^A - E_2^A$. If the two differences are equal, the process is reversible. Unlike energy, adiabatic availability is not additive and does not satisfy a balance equation.

UNIT 6: THE ROUTE TO ENTROPY

This unit is the longest one and it may take up to three hours of lecturing. However it is possible to skip some minor points or proofs and save about an hour.

The fact that adiabatic availability is not additive represents a limitation to its extended use. In this unit we restrict to consider systems which are composed by a generic system and a special reference system, called *reservoir*. Upon studying the mechanical processes of the composite of a system and a reservoir, we are lead to introduce a new property which captures the important features of adiabatic availability and is additive: the *available energy*.

More than one property, available energies form a class of properties that differ by the reservoir taken as reference. So we speak of *available energy with respect to the reservoir R* and denote it as Ω^R . Each available energy is a property defined for any system in any state: $(\Omega^R)_1^A$ is the available energy with respect to R of system A in state A_1 .

In class we spend some time explaining with examples that in Nature many systems behave like a reservoir and, in particular, that the natural environment acts like a reservoir: the composite of a system and a reservoir is a realistic model of most engineering systems. As a consequence, it is of great practical importance to investigate how much energy can be extracted out of such a composite system in a mechanical process.

Let's consider all conceivable mechanical processes for AR – the composite of system A with reservoir R , that do not change the amounts of constituents and the parameters of both A and R and start with system A in state A_1 , and compare the values of the energy extracted from AR : the maximum value of the energy extracted satisfies all the independence requirements for a physical observable to be a property of A . We call it available energy of A in state A_1 (with respect to R).

As a matter of fact $(\Omega^R)^A$ is the energy extracted from AR in a reversible, mechanical process of AR that ends with A and R in mutual stable equilibrium without changes in amounts of constituents and parameters of A and R . It follows that the available energy $(\Omega^R)_1^A$ of system A coincides with the adiabatic availability Ψ_1^{AR} of composite system AR , whereas it is larger or equal to the adiabatic availability Ψ_1^A of system A .

The criterion for reversibility of a mechanical process of A can be stated in terms of $(\Omega^R)^A$ also: given two states A_1 and A_2 with the same amounts of the constituents and parameters, a mechanical process from A_1 to A_2 can be performed if and only if $(\Omega^R)_1^A - (\Omega^R)_2^A \geq E_1^A - E_2^A$. If the two differences are equal, the process is reversible. Unlike adiabatic availability, available energy is additive.

The energy E and the available energy with respect to a reference reservoir R , Ω^R determine a third property that is called entropy and denoted as S . In [2] is described the measurement procedure that allows to determine the value of S for any state A_1 of any system A . It is needed the auxiliary reservoir R , a reference state A_0 with energy E_0 and available energy $(\Omega^R)_0^A$, to which is assigned a reference value S_0 , then S_1 is evaluated by the expression

$$S_1^A = S_0^A + \frac{1}{c_R} \{ (E_1^A - E_0^A) - [(\Omega^R)_1^A - (\Omega^R)_0^A] \} \quad (3)$$

where c_R is a well-defined positive constant that depends on the auxiliary reservoir R only. Entropy S is shown to be independent of the reservoir, which is introduced only because it facilitates the definition of S . It is also shown that the reference value S_0^A can be chosen in such a way that S is always non-negative.

The proof of the independence of S from the particular reservoir chosen as reference is given in Par. 7.4 of [2], but in our experience is too abstract to be proposed in a ten-twenty hours introductory course to Engineering Thermodynamics.

UNIT 7: STABLE EQUILIBRIUM STATES

The points that we underline and stress in class are the following. Entropy is a property in the same sense that energy, momentum, electric charge are properties. Entropy is not restricted to equilibrium states: it is defined for both equilibrium and non-equilibrium states because energy and available energy are defined for all states. Being defined in terms of energy and available energy, its measure requires only energy difference measurements which, in principle, can be determined upon measurement of the changes of elevation of weights which occur in mechanical processes. Entropy definition does not involve the concepts of heat and temperature which have not yet been defined.

Entropy is an additive property being a linear combination of additive properties: energy and available energy¹.

Next, the reversibility criterion established for available energy, yields the following series of results.

Criterion for reversibility of a mechanical process: given two states A_1 and A_2 a mechanical process from A_1 to A_2 can be performed if and only if $S_2^A - S_1^A \geq 0$, moreover if $S_2^A = S_1^A$, the process is reversible.

Entropy increases in any irreversible spontaneous process (which is a zero-net-effect mechanical process): a phenomenon which is due to creation of entropy. Any process of any system may always be regarded as a process of a composite isolated system consisting of all the systems interacting with the first one. If the process of the composite system is irreversible, its entropy does increase. It is natural to think that it is the sum of the entropy created inside the single interacting systems. The entropy created in an irreversible process is called *entropy generated by irreversibility* and denoted by S_{irr} .

Analysis of a reversible process of a composite system shows that entropy is a property that can be exchanged among systems when they interact. Therefore, the entropy gained by a system A can be accounted for by the entropy transferred across the boundary of the system and by the entropy created inside the system. Entropy does satisfy a balance equation: for any process of any system A it holds,

$$S_2^A - S_1^A = S^{A\leftarrow} + S_{\text{irr}}, \quad S_{\text{irr}} \geq 0 \quad (4)$$

At this point, in class, we usually make two comments. First, the combined use of energy and entropy balance is the key to the solution of almost every thermodynamics problem. Second, the entropy of a system can even decrease in an irreversible process: it is sufficient that the entropy transferred out of the system be larger than the entropy created. Although this statement may seem obvious, many students tend to confuse the source term S_{irr} with the entropy system change $S_2^A - S_1^A$, perhaps they are confused by high-school reminiscences like “Entropy is always increasing”.

The dimensions of S depend on the dimensions of both energy and c_R . It turns out that the dimensions of c_R are independent of mechanical dimensions, and are the same as those of temperature (defined later).

¹Both adiabatic availability and available energy have been defined in terms of mechanical processes that do not change amounts of constituents and parameters of the system A . It is possible to consider also mechanical processes that end in states of A with assigned values of \mathbf{n}' and $\boldsymbol{\beta}'$ different from those of the initial state. That yields to the so-called *generalized* adiabatic availability and available energy. These properties share the same features of adiabatic availability and available energy, but can assume negative values also. Actually, entropy is defined in terms of energy and generalized available energy.

Also this unit is quite long, taking about three hours of lecturing.

One of the most important consequence of the Second Law statement is the existence of strong interrelations among the properties of the system when in stable equilibrium states.

For given values of E , \mathbf{n} , and $\boldsymbol{\beta}$ there exists one and only one stable equilibrium state, that implies the existence of a bijective relation between the set of E , \mathbf{n} , and $\boldsymbol{\beta}$ and the stable equilibrium states of A . Recalling that state is the set of values of all the system properties, the value of any property P at equilibrium can be expressed as

$$P = P(E, \mathbf{n}, \boldsymbol{\beta}) \quad (5)$$

this result will be referred to as the *state principle* and functions as Eq. 5 will be called *state equations*.

Borrowing the concept of basis from Vector Algebra, we say that $(E, \mathbf{n}, \boldsymbol{\beta})$ form a convenient basis to represent any other property of stable equilibrium states. As in Algebra the choice of a basis is not unique, in Thermodynamics any other set of $(1 + r + s)$ independent properties can be used to determine stable equilibrium states: $(S, \mathbf{n}, \boldsymbol{\beta})$ is another useful choice. Among the state equations a special role is played by the *fundamental relation*:

$$S = S(E, \mathbf{n}, \boldsymbol{\beta}), \quad \text{entropy form} \quad (6)$$

$$E = E(S, \mathbf{n}, \boldsymbol{\beta}), \quad \text{energy form} \quad (7)$$

Both $S(E, \mathbf{n}, \boldsymbol{\beta})$ and $E(S, \mathbf{n}, \boldsymbol{\beta})$ are almost everywhere analytic functions.

The first derivatives of the fundamental relations will play an important role in the subsequent developments of the subject presented in class. They are: the absolute temperature $T = \partial E / \partial S$; the i -th total potential $\mu_i = \partial E / \partial n_i$, $i = 1, 2, \dots, r$; the force conjugated to the j -th parameter $f_j = \partial E / \partial \beta_j$, $j = 1, 2, \dots, s$. In particular, the force conjugated to the parameter V , volume, is the opposite of pressure, $p = -(\partial E / \partial V)$.

By a simple argument we make the student understand that the abstract and somehow obscure quantity $-(\partial E / \partial V)$ does coincide with the idea of pressure introduced in mechanics, that is the ratio between normal force and the surface area on which it acts. After this proof it is easier for them to accept to call temperature the partial derivative of energy with respect to entropy!

At this point we introduce and prove the *highest-entropy principle* – among all the states with the same energy and given values of $(\mathbf{n}, \boldsymbol{\beta})$ the state of stable equilibrium has maximum entropy – and the *lowest-energy principle* – among all the states with the same entropy and given values of $(\mathbf{n}, \boldsymbol{\beta})$ the state of stable equilibrium has minimum energy. The highest-entropy principle is the basis to derive necessary conditions for mutual equilibrium between interacting systems. We usually prove explicitly that when two systems may exchange energy a necessary condition for mutual equilibrium is equality of temperature, then by analogy we simply state other conditions like equality of i -th total potential (for systems that may exchange i -th constituent) or equality of pressure (for systems that may exchange volume). Further developments of the last proof, allow to obtain the following results: temperature is a positive quantity; temperature is a non-decreasing function of energy (and entropy); entropy fundamental relation $S(E, \mathbf{n}, \boldsymbol{\beta})$ is concave with respect to energy, whereas energy fundamental relation $E(S, \mathbf{n}, \boldsymbol{\beta})$ is convex with respect to entropy; the constant c_R

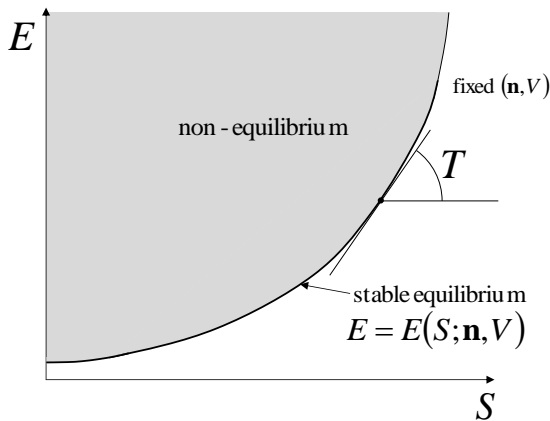


Figure 1. Energy vs. entropy graph for assigned values of \mathbf{n} and V .

of a reservoir coincides with its temperature; last, but not least, in a spontaneous interaction between systems (without changes of \mathbf{n} and β) initially at different temperatures energy and entropy are transferred from the hotter to the colder (which is the Second Law formulation due to Clausius).

To conclude this unit, relative temperature scales are introduced and illustrated. We point out that temperature measurement procedures require mutual equilibrium between two systems that can exchange energy, but neither constituents nor volume: the system whose temperature has to be measured and the thermometer. These remarks should remove any residual doubt about the identification of $\partial E/\partial S$ with temperature.

UNIT 8: WORK AND HEAT

This is a quite short unit which takes one hour at most.

Eventually the concepts of work and heat are introduced: both are modes of energy transfer. In UNIT 2 we said that it is possible to classify interactions on the basis of property exchanged and mode of exchange: the first criterion adopted is the transfer of entropy. Any interaction that results in a net exchange of energy, but no exchange of entropy is called a *work interaction*. The energy exchanged during a work interaction is called work.

Any interaction that results in entropy exchange is called *non-work interaction*. Any process that involves at least one non-work interaction is said *adiabatic*.

Consider a diabatic process for systems A and B that do not experience change of constituents or parameters. It can be reproduced as a sequence of a diabatic process that ends with one of the two system, say A , in the final state A_2 , followed by a mechanical process of the second system B that ends in final state B_2 . For this reason we say that the non-work interaction can be regarded as partly non-work and partly work. It is proved – but usually we do not do it in class – that if the initial states A_1 and B_1 are stable equilibrium states, in the limit $(T_1^A - T_1^B)$ tending to zero, the work transferred in the mechanical process vanishes: it can be said that in this limit the non-work interaction is totally distinguishable from work and it will be called heat interaction. Moreover, in the limit $(T_1^A - T_1^B)$ tending to zero the ratio between the energy and the entropy exchanged between A and B tends to the almost common value of the initial temperatures $T_1^A \cong T_1^B$.

Thus, we define heat interaction an interaction that results in a net exchange of energy and entropy but no constituents be-

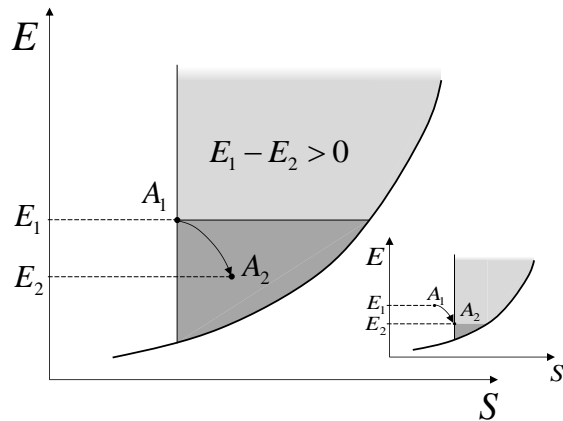


Figure 2. Allowed end states of a mechanical process starting from A_1 : energy is extracted out of the system in processes ending in the darker region. Small graph: the darker region collapses as the starting state approaches stable equilibrium.

tween two systems that are in stable equilibrium states at almost the same temperature T_Q , and such that the ratio of the amount of energy transferred to the amount of entropy transferred is equal to T_Q . The energy transferred is called heat.

The heat definition – we may called it, *strong* definition – just cited appears to many students rather puzzling. Why the interacting systems must be initially in stable equilibrium states with temperatures almost equal? Isn't it too a special case? After all when one thinks of heat, he thinks of systems whose temperatures are rather different. To answer to these objections a *weak* definition is introduced: in general, we talk of heat interaction between systems A and B which are not even in stable equilibrium states, if the interaction is localized into two subsystems A' and B' that satisfy the strong definition. We conclude quoting or anticipating that in conductive and convective heat transfer, the interaction between media always occurs through layers adjacent to the media interface that are almost at the same temperature.

We underline that the interacting systems must be almost at the same temperature because only in this case heat is entirely distinguishable from work. If it were not, one could not write

$$E_2^A - E_1^A = Q^{A\leftarrow} - W^{A\rightarrow} \quad (8)$$

$$S_2^A - S_1^A = S^{A\leftarrow} + S_{\text{irr}} \quad (9)$$

where $Q^{A\leftarrow}$ is the total energy transferred into A by heat interactions and $W^{A\rightarrow}$ is the total energy transferred out of A by work interactions. $S^{A\leftarrow}$ is the total entropy transferred into A : $S^{A\leftarrow} = Q_1^{A\leftarrow}/T_{Q_1}$ if there is only one heat interaction at temperature T_{Q_1} ; $S^{A\leftarrow} = Q_1^{A\leftarrow}/T_{Q_1} + Q_2^{A\leftarrow}/T_{Q_2}$ if there are two heat interactions at temperatures T_{Q_1} and T_{Q_2} , respectively; etc. Equations 8 and 9 hold for processes that do not involve changes of constituents. We conclude quoting [10, p. 215]: “Work and heat are ingenious concepts. For given end states of a system, they allow the quantitative distinction between entropy generated by irreversibility and entropy exchanged via interactions with other systems. As such, these two concepts provide practical means for identifying opportunities to reduce the entropy generation by irreversibility and, hence, improve the performance of the system. The identification of these opportunities would be missed if heat were defined as just any interaction that is not work, i.e., any non-work interaction.”

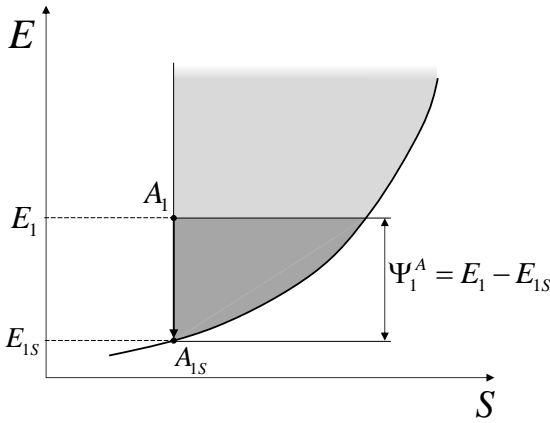


Figure 3. Graphical representation of adiabatic availability.

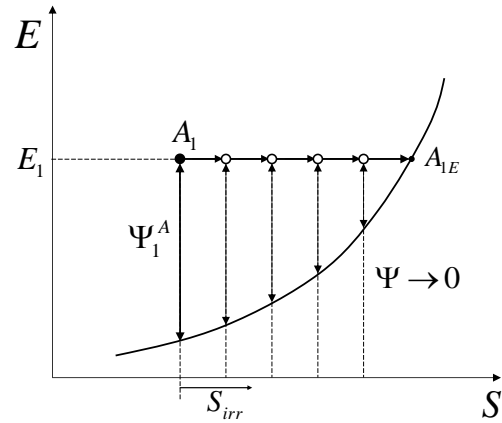


Figure 4. Graphical representation of a spontaneous process. As system state tends towards stable equilibrium, entropy increases by internal generation, whereas adiabatic availability is lost.

UNIT 9: ENERGY-ENTROPY GRAPHS

As a conclusion of this series of lessons we introduce the energy-entropy graphs. Although their use is not widespread, we consider them a very powerful educational tool. In particular, they are a simple mean to review and to put on firm basis the material presented in the preceding units. The graphs supply a clear and suggestive illustration of many concepts and make it easier for the student to grasp and retain the fundamental ideas. The material can be presented in about two hours.

For simplicity, but without loss of generality, we restrict ourselves to consider systems with one parameter only, the volume V . Then we represent on the plane S - E all the states of the system with prescribed values of \mathbf{n} and V (see Fig. 1). Only points in the gray region and on its boundary correspond to possible states of the system. The boundary of the gray region is called the *curve of the stable equilibrium states*. It is the graph of the fundamental relation $E(S, \mathbf{n}, V)$: each point of it corresponds to a single state of stable equilibrium and viceversa. Each point in the gray area represents several – usually infinite – non-equilibrium or non-stable equilibrium states. Points outside would have a combination of entropy and energy values that is not compatible with the assigned pair (\mathbf{n}, V) : it is a consequence of either the highest-entropy principle or lowest-energy principle.

The slope of the stable equilibrium state curve, $\partial E / \partial S = T$ is the geometric representation of the temperature. The curve is convex, since $\partial^2 E / \partial S^2 \geq 0$, therefore its slope T increases (better, non-decreases) with both S and E .

Mechanical process end states: the grey regions in Fig. 2 show which states can be end states of a mechanical process starting in state A_1 , without changes of \mathbf{n} and V . System entropy can not diminish in such a process. Furthermore, in processes ending in the light grey region energy is transferred into the system, in processes ending in the dark grey region energy is extracted out of the system. The latter processes are those “performing a useful task”. Considering a sequence of states approaching the stable equilibrium state curve, it is readily seen that the dark grey region quickly reduces, until collapsing in a state of stable equilibrium: that is the graphical representation of the impossibility of PMM2.

Adiabatic availability: it is the maximum energy that can be extracted from a system in a given state to perform useful tasks (without vary \mathbf{n} and V), a glance at Fig. 3 shows that is the energy extracted in the reversible, mechanical process from state

A_1 to the stable equilibrium state A_{1s} with the same values of S , \mathbf{n} and V .

Spontaneous process: Fig. 4 represents a spontaneous process starting from non-equilibrium state A_1 . As time proceeds the system state approaches the stable equilibrium state curve along a horizontal path (neither E , nor V , nor \mathbf{n} can vary) while its entropy increases due to production by irreversibility. At the end the system will reach the stable equilibrium state A_{1e} : it is possible to determine a relaxation time, τ_s , characteristic of the internal spontaneous mechanisms that drive the system towards equilibrium. In a spontaneous process like the one in Fig. 4, system energy does not change, but as system entropy increases by irreversibility, adiabatic availability decreases. The potential of extracting energy from the system to perform a useful task is progressively lost. It reduces to zero when stable equilibrium is attained: we do think that this graph is an important tool for students to understand the strict relation between entropy creation by irreversibility and destruction of capability of performing work.

Another remark that we consider enlightener, is the following. The internal spontaneous mechanisms towards stable equilibrium are always active causing entropy generation and destruction of adiabatic availability. If one wants to extract as much energy as possible from a non-equilibrium state by a mechanical process, it has to do it fast: in order to minimize entropy production the characteristic time scale of the mechanical process, τ_m , must be much shorter than the relaxation time, $\tau_m \ll \tau_s$. Some students have the wrong idea that a process close to be reversible can be performed only proceeding slowly, through a quasi-steady evolution. Here it is shown that quasi-reversible processes can be obtained operating fast, much faster than spontaneous mechanisms towards equilibrium.

Sound propagation is an interesting illustration of this concept. The time period of the sequence of reversible compression and rarefaction induced by a sound wave in gas through which it propagates, is much shorter than the time scale of dissipative heat exchange between hot, compressed layers of gas and the adjacent, colder, rarefied layers: thus sound attenuation is a secondary effect, which has to be taken into consideration only over long distance propagation.

Available energy: Fig. 5 illustrates the graphical representation of available energy of system A and shows in the small diagram the stable equilibrium state curve for a reservoir (a straight

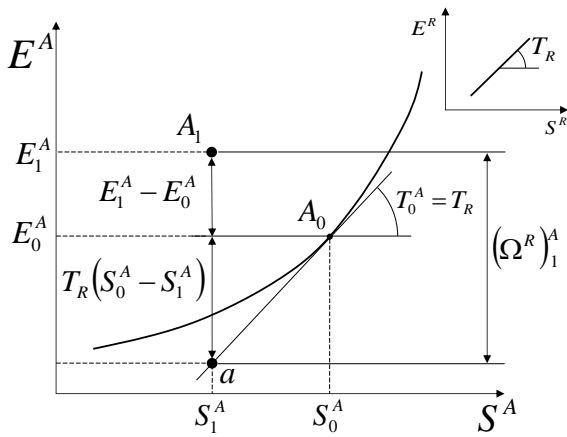


Figure 5. Graphical representation of available energy with respect to reservoir R . Small graph: the E vs. S graph for R .

line). In the energy-entropy graph of system A , state A_0 is the state of mutual equilibrium with reservoir R , that is the stable equilibrium state at $T_0^A = T_R$. Usually we show in class that available energy of state A_1 can be obtained as follows. Draw the tangent line at the stable equilibrium state curve through A_0 , draw the vertical line through A_1 , find the intersection a of the two lines: $(\Omega^R)_1^A$ is equal to the difference between the energy E_1^A and the energy level corresponding to point a .

CONCLUSIONS

After these lectures devoted to the foundations of thermodynamics, we proceed practicing the use of energy and entropy balances on heat engines and refrigeration units, introducing the concept of simple systems, i.e. systems whose behavior is somehow independent of the amounts of constituents, and deriving Gibbs, Maxwell, Euler and Gibbs-Duhem relations, presenting heterogeneous states and the phase-rule. Then, we address processes that result in exchanges of constituents and, upon introduction of the bulk-flow interaction, we extend balance equations of mass, energy, and entropy to these processes also. Eventually energy conversion devices and other standard applications are considered.

In our experience this exposition is particularly suited to undergraduate students of engineering programs. Its key points are the following.

It starts from concepts studied in mechanics and that are familiar to students, and try to use them to investigate a larger set of phenomena without resorting to empirical ideas of heat and temperature.

Spontaneous processes, easily recognizable in everyday life, and the existence of stable equilibrium states for any set of values of energy, amounts of constituents, and parameters are distinct features of thermodynamics with respect to mechanics: in any system in a non-equilibrium state are active internal mechanisms that spontaneously drive the system towards equilibrium.

Energy does not coincide with the possibility of performing work. Due to spontaneous evolution towards stable equilibrium, energy is conserved, but at the same time the possibility of extracting energy to perform work decreases reaching zero at stable equilibrium.

The maximum energy that can be extracted from a system

and from the composite of a system and a reservoir, to perform work, are identified as system properties: adiabatic availability and available energy. They are defined for any state of any system and they can be measured in terms of the change of elevation of a weight in a gravitational field. They are progressively destroyed in spontaneous evolution towards equilibrium. The engineering student faces here one of the challenges of his profession: devices, machines, and systems that perform work efficiently must be designed to operate on time scales much shorter than the relaxation time scales of spontaneous irreversible processes.

Entropy is defined in terms of energy and available energy, for both equilibrium and non-equilibrium states. The definition is operational, i.e. it is expressed in terms of a sequence of operations and measurements: this feature is usually missing in axiomatic exposition of thermodynamics.

Balance equations of energy and entropy are derived and extensively used as powerful tools to analyse processes and to improve their efficiency.

Last, but not least, the use of energy vs. entropy diagrams as an effective educational tool to illustrate in a graphical way most of the concepts presented in these lectures. In particular, they show in a clear way the close relation between the creation of entropy by irreversibility and the destruction of the possibility of performing useful task.

ACKNOWLEDGMENT

The authors thank Prof. Gian Paolo Beretta for the uncountable hours spent in fruitful discussion on thermodynamics.

REFERENCES

- [1] G.N. Hatsopoulos and J.H. Keenan, *Principles of General Thermodynamics*, Wiley, 1965.
- [2] E.P. Gyftopoulos and G.P. Beretta, *Thermodynamics. Foundations and Applications*, Macmillan, 1991, (Dover Edition, 2005).
- [3] E. Fermi, *Thermodynamics*, 1936, (Dover Edition, 1956).
- [4] M.W. Zemansky, *Heat and Thermodynamics*, McGraw-Hill, 1957.
- [5] C. Carathéodory, Untersuchungen über die Grundlagen der Thermodynamik, *Math. Ann.*, vol. 67, pp. 355-389, 1909.
- [6] R. Giles, *Mathematical Foundations of Thermodynamics*, Pergamon, 1964.
- [7] H.B. Callen, *Thermodynamics and an Introduction to Thermostatistics*, Wiley, 1985.
- [8] E.H. Lieb and J. Yngvason, The Physics and Mathematics of the Second Law of Thermodynamics, *Phys. Rep.*, vol. 310, pp. 1-96, 1999.
- [9] G.P. Beretta and E.P. Gyftopoulos, Teaching Energy and Entropy before Temperature and Heat Not Viceversa, *Atti Accademia Peloritana dei Pericolanti*, vol. LXX, pp. 331-340, 1992.
- [10] G.P. Beretta and E.P. Gyftopoulos, A Novel Sequence of Exposition of Engineering Thermodynamics, *Thermodynamics and the Design, Analysis, and Improvement of Energy Systems*, vol. AES 30/HDT 266, pp. 209-217, ASME 1993.

INTRODUCING THE LIEB-YNGVASON ENTROPY-DEFINITION INTO UNDERGRADUATE ENGINEERING THERMODYNAMICS EDUCATION: A CASE STUDY AT ILMENAU UNIVERSITY OF TECHNOLOGY

André Thess

Institute of Thermodynamics and Fluid Mechanics, Ilmenau University of Technology,
P.O. 100565, 98684 Ilmenau, Germany

ABSTRACT

Entropy is the most important and at the same time the most difficult-to-understand term of thermodynamics. Many students are discontent with its classical definition $dS = \delta Q/T$ since it is based on “temperature” and “heat” which both cannot be accurately defined without entropy. The physicists Elliott Lieb and Jakob Yngvason have recently developed a formulation of thermodynamics [1] which is free of these problems and defines entropy in a mathematically rigorous way in terms of adiabatic accessibility. Whereas the Lieb-Yngvason entropy-definition is readily accessible to scientists and engineers with previous knowledge and working experience in engineering thermodynamics, the question whether this accurate definition can be used in undergraduate engineering thermodynamics education for mechanical engineers was an open question until recently. This present communication describes a series of lectures and course material [2] aimed at introducing the Lieb-Yngvason entropy-definition into second-year engineering thermodynamics courses for mechanical engineers at Ilmenau University of Technology (Germany). The lecture will share the experience accumulated since 2007 with more than 2000 undergraduate students and indicate some ways in which the Lieb-Yngvason theory can help making undergraduate engineering thermodynamics education more mathematically rigorous.

REFERENCES

- [1] E. Lieb, J. Yngvason, The physics and mathematics of the second law of thermodynamics, *Phys. Rep.*, vol. 310 (1999) pp. 1-96
- [2] A. Thess, The entropy principle: thermodynamics for the unsatisfied, Springer Verlag Berlin Heidelberg (2011)

ENTROPY-LIKE FUNCTIONS IN MULTI-SCALE HIERARCHICAL ORGANIZATION

Daniel Tondeur

Laboratoire Réactions et Génie des Procédés CNRS
ENSIC, Université de Lorraine, Nancy, France

EXTENDED ABSTRACT

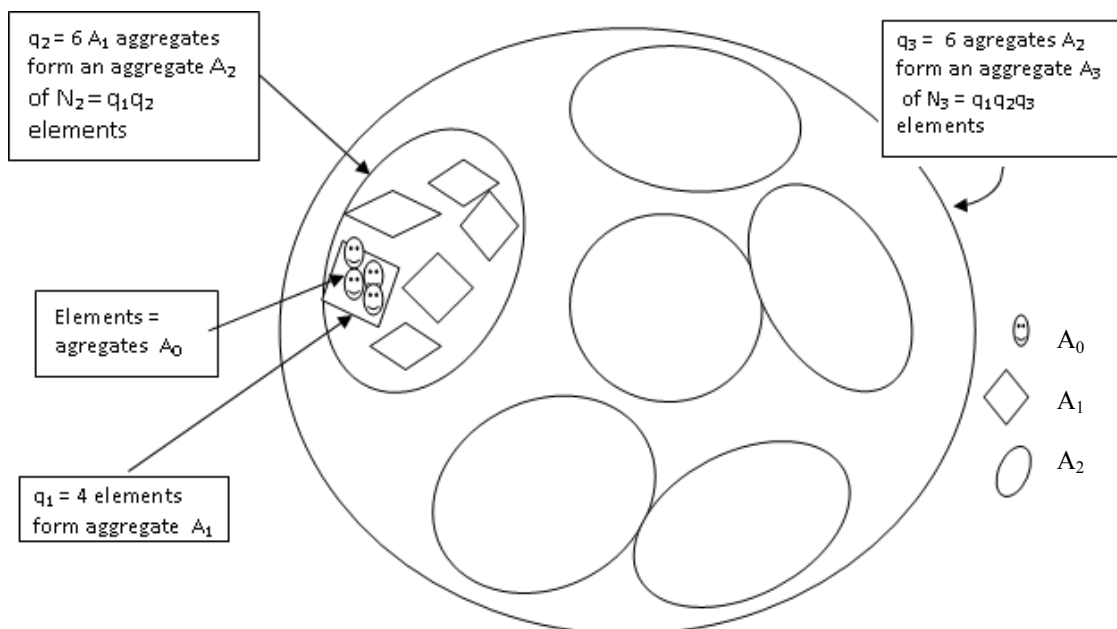
Multi-scale hierarchical organization of a population is understood here as the grouping of elements of this population into aggregates, these aggregates being grouped themselves into higher order aggregates, and so forth, to form a multi-scale organization. The characterization of such systems has been considered for various situations, going from particle clustering in fluidized beds, to collective behavior of micro-organisms in ecology, and including some attempts at modeling human organizations.

Entropy seems an appropriate concept to characterize order or organization. However, the classical statistical approach is not immediately transposable to this situation. The subject of the present communication is to illustrate the nature of the difficulty, which somehow connects to the non-extensivity issue addressed by the "new" entropies of Tsallis or Renyi.

The situation investigated differs from that of classical statistical thermodynamics in several respects. First, the multi-scale character requires a specific combinatorial analysis of particular ensembles, leading to a reformulation of the classical statistical entropy. Second, we are not dealing here with organization along dimensional physical quantities such as time, space or energy, but with organization in numbers. The corresponding entropy is therefore somehow analogous to probabilistic entropy or to informational entropy. Third, we are looking for the most ordered configurations, thus for distributions that minimize total entropy, rather than maximizing it. Fourth, we are considering systems with a small number of elements, in which the classical large number limits are not applicable or not useful.

Defining an entropy-like function that has suitable properties seems rather arbitrary. The approach explored here consists in defining entropies of the different scales in a nearly conventional way, and then weighting their contributions to account for their interdependence. Of course, this approach is not unique.

As an illustration, the value of trial functions having minimal properties is calculated with a very simple example, concerning the homogeneous organization of $N_{tot} = 144$ "elements" in $n = 3$ levels of aggregation such that $N_{tot} = N_3 = q_1 q_2 q_3$, where q_1 is the number of elements in the first level aggregates A_1 , q_2 is the number of aggregates A_1 in the second level aggregates A_2 and q_3 is the number of A_2 aggregates in the largest aggregate A_3 , as illustrated in the figure.



The choice of 144 is because this relatively small number has many integer divisors, leading to 90 triplet configurations of aggregates with integer numbers of elements or sub-aggregates. In the figure, we have the triplets $\mathbf{q} = (4,6,6)$, $N = (4, 24, 144)$

In this example, the entropy of an aggregation level is defined from the number of permutations of the elements within an aggregate of this level, multiplied by the number of aggregates. The total entropy is then assumed to be a weighted sum of the entropies of each aggregation level, so that we have for example:

$$S_{tot} = \sum_{k=1}^n S_k = \sum_{k=1}^n \lambda_k q_{k+1} \dots q_n \ln[q_k!] = \sum_{k=1}^n \lambda_k \frac{N}{N_k} \ln \left[\frac{N_k}{N_{k-1}}! \right]$$

with: $n=3$; $N_0=1$; $N_n = N_{tot}$, while λ_k is a weighting factor discussed below.

The total entropy S_{tot} can now be computed for the 90 configurations, assuming values of the weighting coefficients, and one may look for the configuration(s) that gives the smallest entropy. For example, taking first $\lambda_k = 1$, we find that the following triplets have total entropies distinctly smaller than all others, and in addition the different terms of the sum have similar orders of magnitude.

$\mathbf{q}_a = (2,4,18)$; $S_a = 143.5$ (18 A_2 aggregates, each containing 4 A_1 aggregates, each containing 2 elements)
 $\mathbf{q}_b = (3,4,12)$; $S_b = 144.1$

Note that taking $\lambda_i = 1$ amounts to adding up the entropies of the different levels as if they were independent, thus to ignore the embedding of these levels. Taking different values for the λ is a non-unique way to account for the hierarchical structure, and results in considerable changes in the "minimal" configuration. For example, taking the λ triplet as $\lambda = (1,4,8)$, one finds the following minimal distribution: $\mathbf{q} = (9,4,4)$ i.e. 4 A_2 aggregates, each containing 4 A_1 aggregates, of 9 elements each). This is a much more pyramidal configuration corresponding more to a human organization such as a research laboratory.

Other trial functions are explored: for example, a non-logarithmic function (possibly related to Tsallis' entropy) based on the number of **couples** of sub-aggregates in an aggregate $\frac{1}{2} q(q-1)$. It is found that with the same weighting factors, the minimal entropy configurations are almost the same as the above.

COMPARABILITY OF STATES AND THE DEFINITION OF ENTROPY

Jakob Yngvason

Faculty of Physics, University of Vienna, Boltzmannngasse 5, 1090 Vienna, Austria

EXTENDED ABSTRACT

In an axiomatic approach to equilibrium thermodynamics, developed more than a decade ago in collaboration with E.H. Lieb [1-4], the Second Law of Thermodynamics, understood as the increase of the entropy of equilibrium states in irreversible adiabatic processes, is derived from certain basic properties of the relation of adiabatic accessibility of states. This line of thought has its roots in the work of C. Carathéodory [5] that was taken up in subsequent work in the 1950's and 60's by P.T. Landsberg, H.A. Buchdahl, G. Falk, H. Jung and R. Giles [6-9], among others. In these earlier approaches it is usually taken for granted that two equilibrium states of the same chemical composition are always *comparable* with respect to the relation of adiabatic accessibility, i.e., that it is possible to transform at least one of the states into the other by means of a process whose only net effect on the surroundings is equivalent to the raising and lowering of a weight. By contrast, it is argued in [1-4] that this comparability is a highly nontrivial property and needs justification. In fact, the analytic backbone of the approach of [1-4] is its establishment starting from more plausible assumptions that include convex combinations of states, continuity properties of generalized pressure, and assumptions about thermal contact.

In the panel discussion it will be argued that adiabatic comparability is also of central importance for any attempt to extend the definition of entropy beyond thermodynamic equilibrium states. More specifically, we consider a situation where an (essentially unique) entropy function S is defined on a space Γ of equilibrium states that is contained in some larger space Γ^* of nonequilibrium states of the same system. We assume that any nonequilibrium state can be generated by an adiabatic process starting from some equilibrium state, and conversely, that any nonequilibrium state can be brought to equilibrium through such a process. Under these assumptions we show that any function S^* on the space Γ^* that extends the entropy S and is monotone under adiabatic state changes necessarily lies between two extremes, denoted S_- and S_+ . These two functions coincide, leading to a unique entropy function on Γ^* , if and only if all states in Γ^* are adiabatically comparable. We also argue that *assuming* that this property holds in general is highly implausible. A comparison with the definition of entropy (for equilibrium *and* nonequilibrium states) via the concept of generalized availability as in the monograph of Gyftopoulos and Beretta [10] will also be commented on. Some further details are given in ref. [11].

REFERENCES

- [1] Lieb, E. H. and Yngvason, J. 1998, A guide to entropy and the second law of thermodynamics, Notices of the Amer. Math. Soc. 45, 571-581
- [2] Lieb, E. H. and Yngvason, J. 1999, The physics and mathematics of the second law of thermodynamics, Phys. Rep. 310, 1-96; Erratum 314, 669
- [3] Lieb, E. H. and Yngvason, J. 2000a, A fresh look at entropy and the second law of thermodynamics, Phys. Today 53, 32-37
- [4] Lieb, E.H. and Yngvason, J. 2003, The Entropy of Classical Thermodynamics, in 'Entropy', pp. 147-193, A. Greven, G. Keller and G. Warnecke, Eds., Princeton University Press
- [5] Carathéodory, C. 1909, Untersuchung über die Grundlagen der Thermodynamik, Math. Annalen 67, 355-386
- [6] Landsberg, P.T. 1956, Foundations of thermodynamics, Rev. Mod. Phys. 28, 363-392
- [7] Buchdahl, H. A. 1958, A formal treatment of the consequences of the second law of thermodynamics in Carathéodory's formulation, Zeits.f. Phys. 152, 425-439
- [8] Falk G. and Jung H. 1959, Axiomatik der Thermodynamik, in Handbuch der Physik, III/2, pp. 199-175, S. Flügge Ed., Springer
- [9] Giles, R. 1964, Mathematical Foundations of Thermodynamics. Pergamon
- [10] Gyftopoulos, E.P. and Beretta, G. P. 1991, 2nd ed. 2005, Thermodynamics: foundations and applications, Dover
- [11] Lieb, E. H. and Yngvason, J. 2013, The entropy concept for non-equilibrium states, arXiv:1305.3912

RIGOROUS OPERATIONAL DEFINITION OF ENTROPY NOT BASED ON THE CONCEPTS OF HEAT AND OF EMPIRICAL TEMPERATURE

Enzo Zanchini*, Gian Paolo Beretta**

*University of Bologna – Department of Industrial Engineering

Viale Risorgimento 2, 40136 Bologna, Italy, E-mail: enzo.zanchini@unibo.it

**University of Brescia – Department of Mechanical and Industrial Engineering

Via Branze 38, 25123 Brescia, Italy, E-mail: beretta@ing.unibs.it

ABSTRACT

A rigorous and general logical scheme for the definition of entropy is presented, which is based on a complete set of operational basic definitions and is free of the unnecessary assumptions that restrict the definition of entropy to the stable equilibrium states of simple systems. The treatment applies also to systems with movable internal walls and/or semipermeable walls, and with chemical reactions and and/or external force fields. Preliminary and auxiliary to the definition of entropy are the definition of thermal reservoir and an important theorem which supports the operational definition of temperature of a thermal reservoir. Whereas the thermal reservoir must be a normal system, the definition of entropy applies, in principle, even to special systems, *i.e.*, system with both a lower and an upper bound in energy.

INTRODUCTION

From the origins of classical thermodynamics to the present time, several methods for the definitions of thermodynamic temperature and of entropy have been developed. If we exclude the treatments based on statistical mechanics and those which directly postulate the existence and additivity of entropy, as well as the structure of the fundamental relations [1], most of the methods can be divided in three main categories, which we will call as follows: classical methods, Carathéodory-derived methods, Keenan-school methods.

Classical methods start with the Zeroth-Law of thermodynamics (transitivity of mutual thermal equilibrium) and the definition of empirical temperature, then define energy by a suitable statement of the First Law, and finally define thermodynamic temperature and entropy through the Kelvin-Planck statement of the Second Law [2]: it is impossible to construct an engine which, working in a cycle, produces no effect except the raising of a weight and the cooling of a thermal reservoir.

In their original formulation, classical methods had a logical loop in the definition of energy. In fact, the First Law was stated as follows: in a cycle, the work done by a system is equal to the heat received by the system,

$$Q = W . \quad (1)$$

The energy difference between state A_2 and state A_1 of a system A was defined as the value of $Q - W$ for A in any process of A from A_1 to A_2 . Clearly, this definition is vitiated by a logical circularity, because it is impossible to define heat without a previous definition of energy.

The circularity of Eq. (1) was understood and resolved in 1909 by Carathéodory [3], who defined an adiabatic process without employing the concept of heat and stated the First Law as follows: the work performed by a system in any adiabatic process depends only on the end states of the system.

Among the best treatments of thermodynamics by the classical method we can quote, for instance, those by Fermi [4] and by Zemansky [5].

In his celebrated paper [3], Carathéodory proposed also a new statement of the Second Law and developed a completely new method for the definitions of thermodynamic temperature and entropy. The treatment refers to simple systems, stable equilibrium states, and quasistatic processes, *i.e.*, processes in which the system evolves along a sequence of stable equilibrium states. A simple system is defined as a system such that:

- its stable equilibrium states are determined uniquely by $n + 1$ coordinates, ξ_0, x_1, \dots, x_n , where x_1, \dots, x_n are deformation coordinates (*i.e.*, coordinates which determine the external shape of the system), while ξ_0 is not a deformation coordinate.
- in every quasistatic reversible process, the work performed by the system is given by

$$\delta W = p_1 dx_1 + \dots + p_n dx_n , \quad (2)$$

where p_1, \dots, p_n are functions of ξ_0, x_1, \dots, x_n ;

- the (internal) energy U of the system is additive, *i.e.*, equals the sum of the energies of its subsystems.

Carathéodory stated the Second Law (Axiom II) as follows: in every arbitrarily close neighborhood of a given initial state there exist states that cannot be reached by adiabatic processes. Then, by employing a mathematical theorem on Pfaffian equations, he proved that, on account of the Second Law, there exists a pair of properties, $M(\xi_0, x_1, \dots, x_n)$ and $x_0(\xi_0, x_1, \dots, x_n)$, such that for every quasistatic process

$$dU + \delta W = M dx_0 . \quad (3)$$

Through other assumptions on the conditions for mutual stable equilibrium, which include the Zeroth Law (transitivity of

mutual stable equilibrium), Carathéodory proved that there exists a function $\tau(x_0, x_1, \dots, x_n)$, called temperature, such that if two systems A and B are in mutual stable equilibrium they have the same temperature. Moreover, by applying the additivity of energy, he proved that there exists a function $f(\tau)$, identical for all systems, such that

$$M = f(\tau)\alpha(x_0) , \quad (4)$$

where $\alpha(\cdot)$ is another function that varies from system to system.

Finally, he defined thermodynamic temperature T and entropy S as

$$T = cf(\tau) , \quad S - S_{\text{ref}} = \int_{x_0|_{\text{ref}}}^{x_0} \frac{\alpha(x'_0)}{c} dx'_0 , \quad (5)$$

where c is an arbitrary constant and S_{ref} an arbitrary value assigned to the reference state with $x_0 = x_0|_{\text{ref}}$, and rewrote Eq. (3) in the form

$$dU + \delta W = T dS . \quad (6)$$

Although mathematically very elegant, Carathéodory's definition of entropy is rather abstract. For this reason, several authors proposed simplifications of Carathéodory's treatment [6; 7; 8].

On the opposite side, more recently, Lieb and Yngvason [9] developed a new treatment of the foundations of thermodynamics which can be classified among the Carathéodory-derived ones, because the key postulates concern adiabatic accessibility, but is more abstract and complex than the original presentation by Carathéodory. The treatment is based on 15 Axioms, which regard adiabatic accessibility, simple systems, thermal equilibrium, mixtures and reactions. The treatment by Lieb and Yngvason, like that by Carathéodory, refers exclusively to stable equilibrium states of simple systems.

An alternative method for the treatment of the foundations of thermodynamics was introduced by Keenan [10] and developed by Hatsopoulos and Keenan [11], by Gyftopoulos and Beretta [12], and, more recently, by Beretta and Zanchini [13; 14]. The treatments developed along this line of thought will be called Keenan-school methods.

Some advantages of the Keenan-school methods, with respect to the Carathéodory-derived ones, are the following:

- a) careful *operational* definitions of all the concepts employed in the theory are given; thus, the definition of entropy is completely free of ambiguities, and an operational procedure to measure entropy differences is clearly stated;
- b) the treatment does not employ the concepts of simple system and of quasistatic process, so that it is not necessarily restricted to the stable equilibrium states of simple systems.

A disadvantage is the use, in analogy with the classical methods, of the concept of thermal reservoir, which, however, is defined rigorously. This disadvantage will be removed in a research work under development.

In this paper, some improvements of the method developed in Refs. [13; 14] are introduced. In particular, the statements of the First Law and of the Second Law are split in parts, to form 5 independent Assumptions. This is done because the domain of validity could be different for different Assumptions.

Moreover, the restriction to normal systems is released. The treatment presented here refers exclusively to closed systems. A rigorous extension of the definitions of energy and entropy to open systems can be found, for instance, in Ref. [14].

SUMMARY OF BASIC DEFINITIONS

We briefly recall here some definitions of the basic concepts of thermodynamics employed in our treatment. A more complete and more detailed set of operational basic definitions can be found in Refs. [13; 14].

With the term *system* we mean a set of material particles, of one or more kinds, such that, at each instant of time, the particles of each kind are contained within a given region of space. If the boundary surfaces of the regions of space which contain the particles of the systems are all *walls*, *i.e.*, surfaces which cannot be crossed by material particles, the system is called *closed*.

Any system is endowed with a set of reproducible measurement procedures such that each procedure, if applied at an instant t , yields a result which is independent of the previous time evolution of the system; each procedure of this kind defines a *property* of the system. The set of all the values of the properties of a system, at a given instant of time, defines the *state* of the system at that instant.

A system can be in contact with other matter, or surrounded by empty space; moreover, force fields due to external matter can act in the region of space occupied by the system. If, at an instant of time, all the particles of the system are removed from the respective regions of space and brought far away, but a force field is still present in the region of space (previously) occupied by the system, then this force field is called an *external force field*. An external force field can be either gravitational, or electric or magnetic, or a superposition of the three.

Consider the union of all the regions of space spanned by a system during its entire time evolution. If no other material particles, except those of the system, are present in the region of space spanned by the system or touch the boundary of this region, and if the external force field in this region is either vanishing or stationary, then we say that the system is *isolated*. Suppose that an isolated system I can be divided into two subsystems, A and B . Then, we can say that B is the *environment* of A and viceversa.

If, at a given instant of time, two systems A and B are such that the force field produced by B is vanishing in the region of space occupied by A and viceversa, then we say that A and B are *separable* at that instant. The energy of a system A is defined only for the states of A such that A is separable from its environment. Consider, for instance, the following simple example from mechanics. Let A and B be rigid bodies in deep space, far away from any other object and subjected to a mutual gravitational force. Then, the potential energy of the composite system AB is defined, but that of A and of B is not.

If, at a given instant of time, two systems A and B are such that the outcomes of the measurements performed on B are statistically independent of those of the measurements performed on A , and viceversa, we say that A and B are *uncorrelated from each other* at that instant. The entropy of a system A is defined only for the states of A such that A is separable and uncorrelated from its environment.

We call *process* of a system A from state A_1 to state A_2 the time evolution $(AB)_1 \rightarrow (AB)_2$ of the isolated system AB from $(AB)_1$ (with A in state A_1) to $(AB)_2$ (with A in state A_2), where B is the environment of A . A process of A is *reversible* if the iso-

lated system AB can undergo a time evolution $(AB)_2 \rightarrow (AB)_1$, which restores it in its initial state $(AB)_1$ and is called *reverse* of $(AB)_1 \rightarrow (AB)_2$. A process of a system A is called a *cycle* for A if the final state A_2 coincides with the initial state A_1 . A cycle for A is not necessarily a cycle for AB .

An *elementary mechanical system* is a system such that the only admissible change of state for it is a space translation in a uniform external force field; an example is a particle which can only change its height in a uniform external gravitational field. A process of a system A from state A_1 to A_2 , such that both in A_1 and in A_2 system A is separable from its environment, is a *weight process* for A if the only net effect of the process in the environment of A is the change of state of an elementary mechanical system.

An *equilibrium state* of a system is a state such that the system is separable, the state does not vary with time, and it can be reproduced while the system is isolated. An equilibrium state of a closed system A in which A is uncorrelated from its environment B , is called a *stable equilibrium state* if it cannot be modified by any process between states in which A is separable and uncorrelated from its environment such that neither the geometrical configuration of the walls which bound the regions of space \mathbf{R}^A where the constituents of A are contained, nor the state of the environment B of A have net changes. Two systems, A and B , are in *mutual stable equilibrium* if the composite system AB (i.e., the union of both systems) is in a stable equilibrium state.

DEFINITION OF ENERGY FOR A CLOSED SYSTEM

Assumption 1. First Law Statement - Part 1. The works done by a system in any two weight processes between the same initial and final states are identical.

Assumption 2. First Law Statement - Part 2. Every pair of states (A_1, A_2) of a closed system A , such that A is separable from its environment in both states, can be interconnected by means of a weight process for A .

Definition of energy for a closed system. Proof that it is a property. Let (A_1, A_2) be any pair of states of a closed system A , such that A is separable from its environment in both states. We call *energy difference* between states A_2 and A_1 either the work $W_{12}^{A\leftarrow}$ received by A in any weight process from A_1 to A_2 or the work $W_{21}^{A\rightarrow}$ done by A in any weight process from A_2 to A_1 ; in symbols:

$$E_2^A - E_1^A = W_{12}^{A\leftarrow} \quad \text{or} \quad E_2^A - E_1^A = W_{21}^{A\rightarrow}. \quad (7)$$

The First Law yields the following consequences:

- (a) if both weight processes $A_1 \xrightarrow{w} A_2$ and $A_2 \xrightarrow{w} A_1$ exist, the two forms of Eq. (7) yield the same result ($W_{12}^{A\leftarrow} = W_{21}^{A\rightarrow}$);
- (b) the energy difference between two states A_2 and A_1 depends only on the states A_1 and A_2 ;
- (c) (*additivity of energy differences*) consider a pair of states $(AB)_1$ and $(AB)_2$ of a composite system AB , where both A and B are closed, and denote by A_1, B_1 and A_2, B_2 the corresponding states of A and B ; then, if A, B and AB are separable from their environment in the states considered,

$$E_2^{AB} - E_1^{AB} = E_2^A - E_1^A + E_2^B - E_1^B; \quad (8)$$

(d) (*energy is a property*) let A_0 be a reference state of a system A , in which A is separable from its environment, to which we assign an arbitrarily chosen value of energy E_0^A ; the value of the energy of A in any other state A_1 in which A is separable from its environment is determined uniquely by either

$$E_1^A = E_0^A + W_{01}^{A\leftarrow} \quad \text{or} \quad E_1^A = E_0^A + W_{10}^{A\rightarrow}, \quad (9)$$

where $W_{01}^{A\leftarrow}$ is the work received by A in any weight process for A from A_0 to A_1 , and $W_{10}^{A\rightarrow}$ is the work performed by A in any weight process for A from A_1 to A_0 .

Rigorous proofs of these consequences can be found in Refs. [12; 15], and will not be repeated here.

DEFINITION OF ENTROPY FOR A CLOSED SYSTEM

Lemma 1. Uniqueness of the stable equilibrium state for a given value of the energy. There can be no pair of different stable equilibrium states of a closed system A with identical regions of space \mathbf{R}^A and the same value of the energy E^A .

Proof. Since A is closed and in any stable equilibrium state it is separable from its environment, if two such states existed, by the First Law and the definition of energy they could be interconnected by means of a zero-work weight process. So, at least one of them could be changed to a different state with no change of the regions of space \mathbf{R}^A and no change of the state of the environment of A , and hence would not satisfy the definition of stable equilibrium state.

Normal System. Every closed system A whose energy is bounded from below and unbounded from above will be called a *normal system*.

Assumption 3. Second Law Statement - Part 1. Starting from any state, a normal system can be changed to a non-equilibrium state with higher energy by means of a weight process for A in which its regions of space have no net changes.

Comment. The additivity of energy implies that the union of two or more normal systems, each separable from its environment, is a normal system, and thus fulfils Assumption 3.

In traditional treatments of thermodynamics, Assumption 3 is *not stated explicitly*, but is used, for example when one states that any amount of work can be transferred to a thermal reservoir by a stirrer.

Theorem 1. Impossibility of a PMM2. If a normal system A is in a stable equilibrium state, it is impossible to lower its energy by means of a weight process for A in which the regions of space \mathbf{R}^A occupied by the constituents of A have no net change.

Proof. (See sketch in Fig 1). Suppose that, starting from a stable equilibrium state A_{se} of A , by means of a weight process Π_1 with positive work $W^{A\rightarrow} = W > 0$, the energy of A is lowered and the regions of space \mathbf{R}^A occupied by the constituents of A have no net change. On account of Assumption 3, it would be possible to perform a weight process Π_2 for A in which the regions of space \mathbf{R}^A occupied by the constituents of A have no net change, the weight M is restored to its initial state so that the positive amount of energy $W^{A\leftarrow} = W > 0$ is supplied back to A , and the final state of A is a nonequilibrium state, namely, a

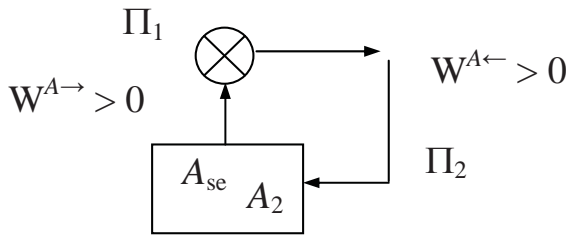


Figure 1. Illustration of the proof of Theorem 1.

state clearly different from A_{se} . Thus, the composite zero-work weight process (Π_1, Π_2) would violate the definition of stable equilibrium state.

Assumption 4. Second Law Statement - Part 2. Among all the states of a closed system A such that the constituents of A are contained in a given set of regions of space \mathbf{R}^A , there is a stable equilibrium state for every value of the energy E^A .

Lemma 2. Any stable equilibrium state A_{se} of a closed system A is accessible via an irreversible zero-work weight process from any other state A_1 in which A is separable from its environment, occupies the same regions of space \mathbf{R}^A and has the same value of the energy E^A .

Proof. By the First Law and the definition of energy, A_{se} and A_1 can be interconnected by a zero-work weight process for A . However, a zero-work weight process from A_{se} to A_1 would violate the definition of stable equilibrium state. Therefore, the process must be in the direction from A_1 to A_{se} . The absence of a zero-work weight process in the opposite direction implies that any zero-work weight process from A_1 to A_{se} is irreversible.

Corollary 1. Any state in which a closed system A is separable from its environment can be changed to a unique stable equilibrium state by means of a zero-work weight process for A in which the regions of space \mathbf{R}^A have no net change.

Proof. The thesis follows immediately from Assumption 4, Lemma 1 and Lemma 2.

Systems in mutual stable equilibrium. We say that two systems A and B , each in a stable equilibrium state, are in mutual stable equilibrium if the composite system AB is in a stable equilibrium state.

Thermal reservoir. We call *thermal reservoir* a normal and always separable system R with a single constituent, contained in a fixed region of space, with a vanishing external force field, with energy values restricted to a finite range in which any pair of identical copies of the reservoir, R and R^d , is in mutual stable equilibrium when R and R^d are in stable equilibrium states.

Comment. Every normal single-constituent system without internal boundaries and applied external fields, and with a number of particles of the order of one mole (so that the *simple system* approximation as defined in Ref. [12, p.263] applies), when restricted to a fixed region of space of appropriate volume and to the range of energy values corresponding to the so-called *triple-*

point stable equilibrium states, is an excellent approximation of a thermal reservoir.

Indeed, for a system of this kind, when three different phases (such as, solid, liquid and vapor) are present, two stable equilibrium states with different energy values have, with an extremely high approximation, the same temperature (here not yet defined), and thus fulfil the condition for the mutual stable equilibrium of the system and a copy thereof.

Reference thermal reservoir. A thermal reservoir chosen once and for all is called a *reference thermal reservoir*. To fix ideas, we choose water as the constituent of our reference thermal reservoir, *i.e.*, sufficient amounts of ice, liquid water, and water vapor at triple point conditions.

Standard weight process. Given a pair of states (A_1, A_2) of a closed system A and a thermal reservoir R , we call *standard weight process* for AR from A_1 to A_2 a weight process for the composite system AR in which the end states of R are stable equilibrium states. We denote by $(A_1R_1 \rightarrow A_2R_2)^{sw}$ a standard weight process for AR from A_1 to A_2 and by $(\Delta E^R)_{A_1A_2}^{sw}$ the corresponding energy change of the thermal reservoir R .

Assumption 5. Second Law Statement - Part 3. Every pair of states (A_1, A_2) of a closed system A , such that A is separable and uncorrelated from its environment in both states, can be interconnected by a reversible standard weight process for AR , where R is an arbitrarily chosen thermal reservoir.

Comment. The combination of Assumption 5, Assumption 4 and Lemma 1 forms our re-statement of the *Gyftopoulos-Beretta statement of the Second Law* [12, p. 62-63]. The motivation for the separation of the statement proposed in Ref. [12] into three parts is as follows: to extract from the postulate a part which can be proved (Lemma 1); to separate *logically independent* assumptions, *i.e.*, assumptions such that a violation of the first would not imply a violation of the second, and *vice-versa*.

Theorem 2. For a given closed system A and a given thermal reservoir R , among all the standard weight processes for AR between a given pair of states (A_1, A_2) of A in which A is separable and uncorrelated from its environment, the energy change $(\Delta E^R)_{A_1A_2}^{sw}$ of the thermal reservoir R has a lower bound which is reached if and only if the process is reversible.

Proof. Let Π_{AR} denote a standard weight process for AR from A_1 to A_2 , and Π_{ARrev} a reversible one; the energy changes of R in processes Π_{AR} and Π_{ARrev} are, respectively, $(\Delta E^R)_{A_1A_2}^{sw}$ and $(\Delta E^R)_{A_1A_2}^{swrev}$. With the help of Fig 2, we will prove that, regardless of the initial state of R :

- $(\Delta E^R)_{A_1A_2}^{swrev} \leq (\Delta E^R)_{A_1A_2}^{sw}$;
- if also Π_{AR} is reversible, then $(\Delta E^R)_{A_1A_2}^{swrev} = (\Delta E^R)_{A_1A_2}^{sw}$;
- if $(\Delta E^R)_{A_1A_2}^{swrev} = (\Delta E^R)_{A_1A_2}^{sw}$, then also Π_{AR} is reversible.

Proof of a). Let us denote by R_1 and R_2 the initial and the final states of R in process Π_{ARrev} . Let us denote by R^d the duplicate of R which is employed in process Π_{AR} , and by R_3^d and R_4^d the initial and the final states of R^d in this process. Let us suppose, *ab absurdo*, that $(\Delta E^R)_{A_1A_2}^{swrev} > (\Delta E^R)_{A_1A_2}^{sw}$, and consider the composite process $(-\Pi_{ARrev}, \Pi_{AR})$, where $-\Pi_{ARrev}$ is a reverse of Π_{ARrev} . This process would be a weight process for RR^d in which, starting from the stable equilibrium state $R_2R_3^d$,

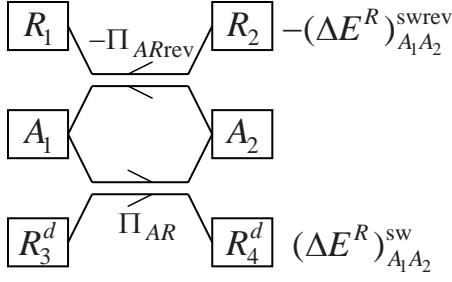


Figure 2. Illustration of the proof of Theorem 2: $-\Pi_{ARrev}$ is a reverse of the reversible standard weight processes Π_{ARrev} , and R^d is a duplicate of R ; see text.

the energy of RR^d is lowered and the regions of space occupied by the constituents of RR^d have no net changes, in contrast with Theorem 1. Therefore, $(\Delta E^R)_{A1A2}^{swrev} \leq (\Delta E^R)_{A1A2}^{sw}$.

Proof of b). If Π_{AR} is reversible too, then, in addition to $(\Delta E^R)_{A1A2}^{swrev} \leq (\Delta E^R)_{A1A2}^{sw}$, the relation $(\Delta E^R)_{A1A2}^{sw} \leq (\Delta E^R)_{A1A2}^{swrev}$ must hold too. Otherwise, the composite process $(\Pi_{ARrev}, -\Pi_{AR})$ would be a weight process for RR^d in which, starting from the stable equilibrium state $R_1R_4^d$, the energy of RR^d is lowered and the regions of space occupied by the constituents of RR^d have no net changes, in contrast with Theorem 1. Therefore, $(\Delta E^R)_{A1A2}^{swrev} = (\Delta E^R)_{A1A2}^{sw}$.

Proof of c). Let Π_{AR} be a standard weight process for AR , from A_1 to A_2 , such that $(\Delta E^R)_{A1A2}^{sw} = (\Delta E^R)_{A1A2}^{swrev}$, and let R_1 be the initial state of R in this process. Let Π_{ARrev} be a reversible standard weight process for AR , from A_1 to A_2 , with the same initial state R_1 of R . Thus, R_3^d coincides with R_1 and R_4^d coincides with R_2 . The composite process $(\Pi_{AR}, -\Pi_{ARrev})$ is a cycle for the isolated system ARB , where B is the environment of AR . As a consequence, Π_{AR} is reversible, because it is a part of a cycle of the isolated system ARB .

Theorem 3. Let R' and R'' be any two thermal reservoirs and consider the energy changes, $(\Delta E^{R'})_{A1A2}^{swrev}$ and $(\Delta E^{R''})_{A1A2}^{swrev}$ respectively, in the reversible standard weight processes $\Pi_{AR'} = (A_1R'_1 \rightarrow A_2R'_2)^{swrev}$ and $\Pi_{AR''} = (A_1R''_1 \rightarrow A_2R''_2)^{swrev}$, where (A_1, A_2) is an arbitrarily chosen pair of states of any closed system A , such that A is separable and uncorrelated from its environment in both states. Then the ratio $(\Delta E^{R'})_{A1A2}^{swrev} / (\Delta E^{R''})_{A1A2}^{swrev}$:

- a) is positive;
- b) depends only on R' and R'' , *i.e.*, it is independent of (i) the initial stable equilibrium states of R' and R'' , (ii) the choice of system A , and (iii) the choice of states A_1 and A_2 .

Proof of a). With the help of Fig 3, let us suppose that $(\Delta E^{R'})_{A1A2}^{swrev} < 0$. Then, $(\Delta E^{R''})_{A1A2}^{swrev}$ cannot be zero. In fact, in that case the composite process $(\Pi_{AR'}, -\Pi_{AR''})$, which is a cycle for A , would be a weight process for R' in which, starting from the stable equilibrium state R'_1 , the energy of R' is lowered and the regions of space occupied by the constituents of R' have no net changes, in contrast with Theorem 1. Moreover, $(\Delta E^{R''})_{A1A2}^{swrev}$ cannot be positive. In fact, if it were positive, the work performed by $R'R''$ as a result of the overall weight process $(\Pi_{AR'}, -\Pi_{AR''})$ for $R'R''$ would be

$$W^{R'R'' \rightarrow} = -(\Delta E^{R'})_{A1A2}^{swrev} + (\Delta E^{R''})_{A1A2}^{swrev}, \quad (10)$$

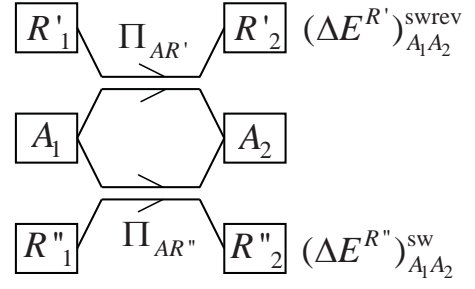


Figure 3. Illustration of the proof of Theorem 3, part a): reversible standard weight processes $\Pi_{AR'}$ and $\Pi_{AR''}$, see text.

where both terms are positive. On account of Assumption 3 and Corollary 1, after the process $(\Pi_{AR'}, -\Pi_{AR''})$, one could perform a weight process $\Pi_{R''}$ for R'' in which a positive amount of energy equal to $(\Delta E^{R''})_{A1A2}^{swrev}$ is given back to R'' and the latter is restored to its initial stable equilibrium state. As a result, the composite process $(\Pi_{AR'}, -\Pi_{AR''}, \Pi_{R''})$ would be a weight process for R' in which, starting from the stable equilibrium state R'_1 , the energy of R' is lowered and the regions of space occupied by the constituents of R' have no net changes, in contrast with Theorem 1. Therefore, the assumption $(\Delta E^{R'})_{A1A2}^{swrev} < 0$ implies $(\Delta E^{R''})_{A1A2}^{swrev} < 0$.

Let us suppose that $(\Delta E^{R'})_{A1A2}^{swrev} > 0$. Then, for process $-\Pi_{AR'}$ one has $(\Delta E^{R'})_{A2A1}^{swrev} < 0$. By repeating the previous argument, one proves that for process $-\Pi_{AR''}$ one has $(\Delta E^{R''})_{A2A1}^{swrev} < 0$. Therefore, for process $\Pi_{AR''}$ one has $(\Delta E^{R''})_{A1A2}^{swrev} > 0$.

Proof of b). Choose a pair of states (A_1, A_2) of a closed system A , such that A is separable and uncorrelated from its environment, and consider the reversible standard weight process $\Pi_{AR'} = (A_1R'_1 \rightarrow A_2R'_2)^{swrev}$ for AR' , with R' initially in state R'_1 , and the reversible standard weight process $\Pi_{AR''} = (A_1R''_1 \rightarrow A_2R''_2)^{swrev}$ for AR'' , with R'' initially in state R''_1 . Then, choose a pair of states (A'_1, A'_2) of another closed system A' , such that A' is separable and uncorrelated from its environment, and consider the reversible standard weight process $\Pi_{A'R'} = (A'_1R'_1 \rightarrow A'_2R'_3)^{swrev}$ for $A'R'$, with R' initially in state R'_1 , and the reversible standard weight process $\Pi_{A'R''} = (A'_1R''_1 \rightarrow A'_2R''_3)^{swrev}$ for $A'R''$, with R'' initially in state R''_1 .

With the help of Fig 4, we will prove that the changes in energy of the reservoirs in these processes obey the relation

$$\frac{(\Delta E^{R'})_{A1A2}^{swrev}}{(\Delta E^{R''})_{A1A2}^{swrev}} = \frac{(\Delta E^{R'})_{A'_1A'_2}^{swrev}}{(\Delta E^{R''})_{A'_1A'_2}^{swrev}}. \quad (11)$$

Let us assume: $(\Delta E^{R'})_{A1A2}^{swrev} > 0$ and $(\Delta E^{R''})_{A1A2}^{swrev} > 0$, which implies, on account of part a) of the proof, $(\Delta E^{R''})_{A1A2}^{swrev} > 0$ and $(\Delta E^{R'})_{A'_1A'_2}^{swrev} > 0$. This is not a restriction, because it is possible to reverse the processes under consideration.

Now, as is well known, any real number can be approximated with arbitrarily high accuracy by a rational number. Therefore, we will assume that the energy changes $(\Delta E^{R'})_{A1A2}^{swrev}$ and $(\Delta E^{R''})_{A1A2}^{swrev}$ are rational numbers, so that whatever is the value of their ratio, there exist two positive integers m and n such that

$$(\Delta E^{R'})_{A_1 A_2}^{\text{swrev}} / (\Delta E^{R'})_{A'_1 A'_2}^{\text{swrev}} = n/m, \text{ i.e.,}$$

$$m (\Delta E^{R'})_{A_1 A_2}^{\text{swrev}} = n (\Delta E^{R'})_{A'_1 A'_2}^{\text{swrev}}. \quad (12)$$

As sketched in Fig 4, let us consider the composite processes Π_A and Π'_A defined as follows. Π_A is the following composite weight process for the composite system $AR'R''$: starting from the initial state R'_1 of R' and R''_2 of R'' , system A is brought from A_1 to A_2 by a reversible standard weight process for AR' , then from A_2 to A_1 by a reversible standard weight process for AR'' ; whatever the new states of R' and R'' are, again system A is brought from A_1 to A_2 by a reversible standard weight process for AR' and back to A_1 by a reversible standard weight process for AR'' , until the cycle for A is repeated m times. Similarly, Π'_A is a composite weight process for the composite system $A'R'R''$ whereby starting from the end states of R' and R'' reached by process Π_A , system A' is brought from A'_1 to A'_2 by a reversible standard weight process for $A'R''$, then from A'_2 to A'_1 by a reversible standard weight process for $A'R'$; and so on until the cycle for A' is repeated n times.

Clearly, the whole composite process (Π_A, Π'_A) is a cycle for AA' . Moreover, it is a cycle also for R' . In fact, on account of Theorem 2, the energy change of R' in each process $\Pi_{AR'}$ is equal to $(\Delta E^{R'})_{A_1 A_2}^{\text{swrev}}$, regardless of its initial state, and in each process $-\Pi_{A'R'}$ is equal to $-(\Delta E^{R'})_{A'_1 A'_2}^{\text{swrev}}$. Therefore, the energy change of R' in the whole composite process (Π_A, Π'_A) is $m (\Delta E^{R'})_{A_1 A_2}^{\text{swrev}} - n (\Delta E^{R'})_{A'_1 A'_2}^{\text{swrev}}$ and equals zero on account of Eq. (12). As a result, after (Π_A, Π'_A) , reservoir R' has been restored to its initial state, so that (Π_A, Π'_A) is a reversible weight process for R'' .

Again on account of Theorem 2, the overall energy change of R'' in the whole composite process is $-m (\Delta E^{R''})_{A_1 A_2}^{\text{swrev}} + n (\Delta E^{R''})_{A'_1 A'_2}^{\text{swrev}}$. If this quantity were negative, Theorem 1 would be violated. If this quantity were positive, Theorem 1 would also be violated by the reverse of the process, $(-\Pi'_A, -\Pi_A)$. Therefore, the only possibility is that $-m (\Delta E^{R''})_{A_1 A_2}^{\text{swrev}} + n (\Delta E^{R''})_{A'_1 A'_2}^{\text{swrev}} = 0$, i.e.,

$$m (\Delta E^{R''})_{A_1 A_2}^{\text{swrev}} = n (\Delta E^{R''})_{A'_1 A'_2}^{\text{swrev}}. \quad (13)$$

Finally, taking the ratio of Eqs. (12) and (13), we obtain Eq. (11) which is our conclusion.

Temperature of a thermal reservoir. Let R be a given thermal reservoir and R^o a reference thermal reservoir. Select an arbitrary pair of states (A_1, A_2) of a closed system A , such that A is separable and uncorrelated from its environment in both states, and consider the energy changes $(\Delta E^R)_{A_1 A_2}^{\text{swrev}}$ and $(\Delta E^{R^o})_{A_1 A_2}^{\text{swrev}}$ in two reversible standard weight processes from A_1 to A_2 , one for AR and the other for AR^o , respectively. We call *temperature* of R the positive quantity

$$T_R = T_{R^o} \frac{(\Delta E^R)_{A_1 A_2}^{\text{swrev}}}{(\Delta E^{R^o})_{A_1 A_2}^{\text{swrev}}}, \quad (14)$$

where T_{R^o} is a positive constant associated arbitrarily with the reference thermal reservoir R^o .

Clearly, the temperature T_R of R is defined only up to the arbitrary multiplicative constant T_{R^o} . If for R^o we select a thermal reservoir consisting of ice, liquid water, and water vapor at triple-point conditions, and we set $T_{R^o} = 273.16$ K, we obtain the Kelvin temperature scale.

Corollary 2. The ratio of the temperatures of two thermal reservoirs, R' and R'' , is independent of the choice of the reference thermal reservoir and can be measured directly as

$$\frac{T_{R'}}{T_{R''}} = \frac{(\Delta E^{R'})_{A_1 A_2}^{\text{swrev}}}{(\Delta E^{R''})_{A_1 A_2}^{\text{swrev}}}, \quad (15)$$

where $(\Delta E^{R'})_{A_1 A_2}^{\text{swrev}}$ and $(\Delta E^{R''})_{A_1 A_2}^{\text{swrev}}$ are the energy changes of R' and R'' in two reversible standard weight processes, one for AR' and the other for AR'' , which interconnect the same pair of states (A_1, A_2) such that A is separable and uncorrelated from its environment in both states.

Proof. Let $(\Delta E^{R^o})_{A_1 A_2}^{\text{swrev}}$ be the energy change of the reference thermal reservoir R^o in any reversible standard weight process for AR^o which interconnects the same states (A_1, A_2) of A . From Eq. (14) we have

$$T_{R'} = T_{R^o} \frac{(\Delta E^{R'})_{A_1 A_2}^{\text{swrev}}}{(\Delta E^{R^o})_{A_1 A_2}^{\text{swrev}}}, \quad T_{R''} = T_{R^o} \frac{(\Delta E^{R''})_{A_1 A_2}^{\text{swrev}}}{(\Delta E^{R^o})_{A_1 A_2}^{\text{swrev}}}, \quad (16)$$

so that the ratio $T_{R'}/T_{R''}$ is given by Eq. (15).

Corollary 3. Let (A_1, A_2) be any pair of states of a closed system A , such that A is separable and uncorrelated from its environment in both states, and let $(\Delta E^R)_{A_1 A_2}^{\text{swrev}}$ be the energy change of a thermal reservoir R with temperature T_R , in any reversible standard weight process for AR from A_1 to A_2 . Then, for the given system A , the ratio $(\Delta E^R)_{A_1 A_2}^{\text{swrev}}/T_R$ depends only on the pair of states (A_1, A_2) , i.e., it is independent of the choice of reservoir R and of its initial stable equilibrium state R_1 .

Proof. Let us consider two reversible standard weight processes from A_1 to A_2 , one for AR' and the other for AR'' , where R' is a thermal reservoir with temperature $T_{R'}$ and R'' is a thermal reservoir with temperature $T_{R''}$. Then, equation (15) yields

$$\frac{(\Delta E^{R'})_{A_1 A_2}^{\text{swrev}}}{T_{R'}} = \frac{(\Delta E^{R''})_{A_1 A_2}^{\text{swrev}}}{T_{R''}}. \quad (17)$$

Definition of (thermodynamic) entropy, proof that it is a property. Let (A_1, A_2) be any pair of states of a closed system A , such that A is separable and uncorrelated from its environment in both states, and let R be an arbitrarily chosen thermal reservoir placed in the environment B of A . We call *entropy difference* between A_2 and A_1 the quantity

$$S_2^A - S_1^A = -\frac{(\Delta E^R)_{A_1 A_2}^{\text{swrev}}}{T_R}, \quad (18)$$

where $(\Delta E^R)_{A_1 A_2}^{\text{swrev}}$ is the energy change of R in any reversible standard weight process for AR from A_1 to A_2 , and T_R is the

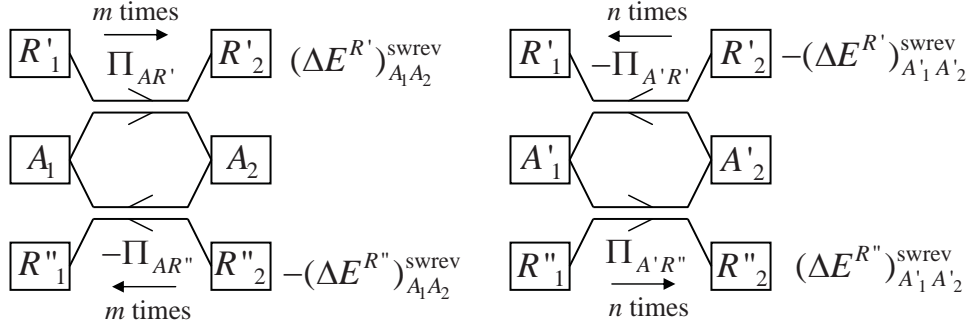


Figure 4. Illustration of the proof of Theorem 3, part b): composite process $(\Pi_A, \Pi_{A'})$, see text.

temperature of R . On account of Corollary 3, the right hand side of Eq. (18) is determined uniquely by states A_1 and A_2 ; therefore, entropy is a property of A .

Let A_0 be a reference state of A , in which A is separable and uncorrelated from its environment, and assign to A_0 an arbitrarily chosen value S_0^A of the entropy. Then, the value of the entropy of A in any other state A_1 of A in which A is separable and uncorrelated from its environment is determined uniquely by the equation

$$S_1^A = S_0^A - \frac{(\Delta E^R)_{A_0 A_1}^{\text{swrev}}}{T_R}, \quad (19)$$

where $(\Delta E^R)_{A_0 A_1}^{\text{swrev}}$ is the energy change of R in any reversible standard weight process for AR from A_0 to A_1 , and T_R is the temperature of R . Such a process exists for every state A_1 , on account of Assumption 5.

Theorem 4. Additivity of entropy differences. Consider the pair of states $(C_1 = A_1 B_1, C_2 = A_2 B_2)$ of the composite system $C = AB$, such that A and B are closed, A is separable and uncorrelated from its environment in both states A_1 and A_2 , and B is separable and uncorrelated from its environment in both states B_1 and B_2 . Then,

$$S_{A_2 B_2}^{AB} - S_{A_1 B_1}^{AB} = S_2^A - S_1^A + S_2^B - S_1^B. \quad (20)$$

Proof. Let us choose a thermal reservoir R , with temperature T_R , and consider the composite process (Π_{AR}, Π_{BR}) where Π_{AR} is a reversible standard weight process for AR from A_1 to A_2 , while Π_{BR} is a reversible standard weight process for BR from B_1 to B_2 . The composite process (Π_{AR}, Π_{BR}) is a reversible standard weight process for CR from C_1 to C_2 , in which the energy change of R is the sum of the energy changes in the constituent processes Π_{AR} and Π_{BR} , i.e., $(\Delta E^R)_{C_1 C_2}^{\text{swrev}} = (\Delta E^R)_{A_1 A_2}^{\text{swrev}} + (\Delta E^R)_{B_1 B_2}^{\text{swrev}}$. Therefore:

$$\frac{(\Delta E^R)_{C_1 C_2}^{\text{swrev}}}{T_R} = \frac{(\Delta E^R)_{A_1 A_2}^{\text{swrev}}}{T_R} + \frac{(\Delta E^R)_{B_1 B_2}^{\text{swrev}}}{T_R}. \quad (21)$$

Equation (21) and the definition of entropy (18) yield Eq. (20).

Comment. As a consequence of Theorem 4, if the values of entropy are chosen so that they are additive in the reference states, entropy results as an additive property.

Theorem 5. Let (A_1, A_2) be any pair of states of a closed system A , such that A is separable and uncorrelated from its environment in both states, and let R be a thermal reservoir with temperature T_R . Let $\Pi_{AR\text{irr}}$ be any irreversible standard weight process for AR from A_1 to A_2 and let $(\Delta E^R)_{A_1 A_2}^{\text{swirr}}$ be the energy change of R in this process. Then

$$-\frac{(\Delta E^R)_{A_1 A_2}^{\text{swirr}}}{T_R} < S_2^A - S_1^A. \quad (22)$$

Proof. Let $\Pi_{AR\text{rev}}$ be any reversible standard weight process for AR from A_1 to A_2 and let $(\Delta E^R)_{A_1 A_2}^{\text{swrev}}$ be the energy change of R in this process. On account of Theorem 2,

$$(\Delta E^R)_{A_1 A_2}^{\text{swrev}} < (\Delta E^R)_{A_1 A_2}^{\text{swirr}}. \quad (23)$$

Since T_R is positive, from Eqs. (23) and (18) one obtains

$$-\frac{(\Delta E^R)_{A_1 A_2}^{\text{swirr}}}{T_R} < -\frac{(\Delta E^R)_{A_1 A_2}^{\text{swrev}}}{T_R} = S_2^A - S_1^A. \quad (24)$$

Theorem 6. Principle of entropy nondecrease. Let (A_1, A_2) be a pair of states of a closed system A , such that A is separable and uncorrelated from its environment in both states, and let $(A_1 \rightarrow A_2)_W$ be any weight process for A from A_1 to A_2 . Then, the entropy difference $S_2^A - S_1^A$ is equal to zero if and only if the weight process is reversible; it is strictly positive if and only if the weight process is irreversible.

Proof. If $(A_1 \rightarrow A_2)_W$ is reversible, then it is a special case of a reversible standard weight process for AR in which the initial stable equilibrium state of R does not change. Therefore, $(\Delta E^R)_{A_1 A_2}^{\text{swrev}} = 0$ and by applying the definition of entropy, Eq. (18), one obtains

$$S_2^A - S_1^A = -\frac{(\Delta E^R)_{A_1 A_2}^{\text{swrev}}}{T_R} = 0. \quad (25)$$

If $(A_1 \rightarrow A_2)_W$ is irreversible, then it is a special case of an irreversible standard weight process for AR in which the initial stable equilibrium state of R does not change. Therefore, $(\Delta E^R)_{A_1 A_2}^{\text{swirr}} = 0$ and Equation (22) yields

$$S_2^A - S_1^A > -\frac{(\Delta E^R)_{A_1 A_2}^{\text{swirr}}}{T_R} = 0. \quad (26)$$

Moreover, if a weight process $(A_1 \rightarrow A_2)_W$ for A is such that $S_2^A - S_1^A = 0$, then the process must be reversible, because we just proved that for any irreversible weight process $S_2^A - S_1^A > 0$; if a weight process $(A_1 \rightarrow A_2)_W$ for A is such that $S_2^A - S_1^A > 0$, then the process must be irreversible, because we just proved that for any reversible weight process $S_2^A - S_1^A = 0$.

CONCLUSIONS

A rigorous and general logical scheme for the definition of entropy has been presented. The treatment is based on a complete set of operational definitions and does not employ the concepts of empirical temperature, of heat, of simple system and of quasistatic process. Therefore, in this scheme, the domain of validity of the definition of entropy is not constrained necessarily to the stable equilibrium states of simple systems. On the other hand, the important concepts of separability and non-correlation between system and environment have been introduced and the role of these concepts in the definitions of energy and of entropy has been pointed out.

With respect to previous presentations of this approach, some improvements have been introduced. The statements of the First Law and of the Second Law have been split in 5 separate Assumptions, each of which may have his own domain of validity. Moreover, the restriction to normal systems in the definition of entropy has been removed, so that the definition applies, in principle, also to special systems, such as spin systems.

REFERENCES

- [1] H.B. Callen, *Thermodynamics*, Wiley, New York, N.Y., 1960.
- [2] M. Planck, *Treatise on Thermodynamics*, translated by A. Ogg from the 7th German edition, Longmans, Green, and Co., London, U.K., 1927 (the first german edition appeared in 1897).
- [3] C. Carathéodory, Untersuchungen über die Grundlagen der Thermodynamik, *Math. Ann.*, vol. 67, pp. 355-389, 1909.
- [4] E. Fermi, *Thermodynamics*, Prentice-Hall, New Jersey, 1937.
- [5] M.W. Zemansky, *Heat and Thermodynamics*, Mc Graw-Hill, New York, N.Y., 1968.
- [6] L.A. Turner, Simplification of Carathéodory's treatment of thermodynamics, *Am. J. Phys.*, vol. 28, pp. 781-786, 1960.
- [7] P.T. Landsberg, On suggested simplifications of Carathéodory's thermodynamics, *Phys. Status Solidi (b)*, vol. 1, pp. 120-126, 1961.
- [8] F.W. Saers, A simplified simplification of Carathéodory's thermodynamics, *Am. J. Phys.*, vol. 31, pp. 747-752, 1963.
- [9] E.H. Lieb and J. Yngvason, The physics and mathematics of the second law of thermodynamics, *Phys. Rep.*, vol. 310, pp. 1-96, 1999.
- [10] J.H. Keenan, *Thermodynamics*, Wiley, New York, N.Y., 1941.
- [11] G.N. Hatsopoulos and J.H. Keenan, *Principles of General Thermodynamics*, Wiley, New York, N.Y., 1965.
- [12] E.P. Gyftopoulos and G.P. Beretta, *Thermodynamics. Foundations and Applications*, Dover, Mineola, N.Y., 2005 (first edition, Macmillan, 1991).
- [13] E. Zanchini and G.P. Beretta, Removing Heat and Conceptual Loops from the Definition of Entropy, *Int. J. Thermodynamics*, vol. 12, pp. 67-76, 2010.
- [14] G.P. Beretta and E. Zanchini, Rigorous and General Definition of Thermodynamic Entropy, in *Thermodynamics*, Edited by Mizutani Tadashi, Publisher: InTech, 2011, ISBN 978-953-307-544-0, 23-50 (2011), eprint: ArXiv-1010.0813v1.
- [15] E. Zanchini, On the Definition of Extensive Property Energy by the First Postulate of Thermodynamics, *Found. Phys.*, vol. 16, pp. 923-935, 1986.

PANEL F

**THERMODYNAMICS OF INTERFACIAL
PHENOMENA: SURFACE TENSION
AND NON-EQUILIBRIUM EFFECTS OF
KORTEWEG CAPILLARY FORCES**

HEAT AND MASS TRANSFER DURING NUCLEATION

Kirill Glavatskiy*, Dick Bedeaux**

*School of Applied Sciences, RMIT University,
GPO Box 2476, Melbourne, Victoria 3001, Australia,
E-mail: kirill.glavatskiy@rmit.edu.au

**Department of Chemistry, Norwegian University of Science and Technology,
7491 Trondheim, Norway,
E-mail: dick.bedeaux@chem.ntnu.no

ABSTRACT

In this paper we discuss a systematic procedure to assess the nucleation rate with the help of the non-equilibrium square gradient model, which is also known as H-model or diffuse-interface model. We first distinguish between the density (concentration) gradient caused by the phase coexistence in equilibrium and the density (concentration) gradient caused by the non-equilibrium conditions in bulk phases. The non-equilibrium description of the interfacial region requires a proper Gibbs relation, which is formulated in our theory. Non-equilibrium thermodynamics uses the constitutive relations between thermodynamic forces and thermodynamic fluxes. It does not provide the values of the transport coefficients. We use the transport coefficients in the interfacial region which follow from the square gradient model. Furthermore, the nonzero curvature of the surface modifies the expressions for thermodynamic quantities in the interfacial region. Next we combine all these pieces in a systematic picture, which gives a consistent description of heat and mass transport across curved interfaces.

INTRODUCTION

Nucleation is a dynamic process which involves formation and growth of small nuclei of one phase in another phase [1]. One could think of formation of bubbles in liquid or drops in a multicomponent fluid. This process requires formation of an interface between two phases, a region where the density or concentration gradient are large. Furthermore, during nucleation matter and heat are being transferred across the interface, which moves the system towards equilibrium. The interface poses an additional barrier to transport [2]. This barrier will affect the standard Fourier's or Fick's laws in the interfacial region, where the transport coefficients become dependent on the density gradients. For small nuclei of the new phase the curvature is rather high which will also modify the values of the integrated transport coefficients [3]. The knowledge of the integrated surface transfer coefficients, which determine the barrier of the interface to heat and mass transfer, is useful for a correct prediction of the nucleation rate.

In this paper we provide a systematic procedure to describe a non-equilibrium interface of a bubble or droplet, which combines non-equilibrium thermodynamics with the square gradient model for a curved interface. Following [4], we distinguish the following steps which are essential in any non-equilibrium thermodynamic theory: i) equilibrium thermodynamics; ii) Gibbs relation; iii) balance equations; iv) constitutive relations. It is the aim of this paper to emphasize the difference between these parts and at the same time to bring them together. We will go through these steps for spherical interface of one-component fluid, however, the established framework is not restricted to this particular case.

One of the interesting topics is the origin of so-called non-

equilibrium capillary forces, that are believed to cause the self-propelled motion of bubbles [5]. Analyzing the structure of the interface in equilibrium and non-equilibrium, we show that one should distinguish between the gradients of the density (concentration) in the interfacial region on the one hand and the gradients of the chemical potential or the pressure on the other hand [2]. The former ones are present even in equilibrium system and therefore cannot cause the motion of bubble interface nor the bubble as a whole. In contrast, the latter ones are the genuine measure of non-equilibrium and are not reduced to the interfacial density gradients.

The paper is organized as follows. First, we summarize the square gradient model for equilibrium interface. In particular, we discuss the different quantities all of which have a meaning of pressure. It is important to distinguish between them, especially when coming to non-equilibrium. We identify the meaning of these pressures. Next, we extend the equilibrium description to non-equilibrium. Care should be taken when extending these quantities in the interfacial region. In particular, we formulate the Gibbs relation for the interfacial region which differs from the one for a homogeneous phase. Furthermore, formulating the balance equations we identify the fluxes, which are a measure of non-equilibrium. Next, we formulate and discuss the constitutive relations between the fluxes and the thermodynamic forces in the context of linear irreversible thermodynamics. We discuss that on macro scale the surface can be viewed as a separate thermodynamic system, which, in particular, increases the number of dissipative fluxes by one. Now it is not only a diffusion flux, but also a component flux, which leads to dissipation. We also discuss a particular example of a simple system, where the above considerations are implemented. Finally, we give the concluding remarks.

SQUARE GRADIENT MODEL FOR EQUILIBRIUM SPHERICAL INTERFACE

In square gradient model one starts with the expression for the Helmholtz energy density $f^v(\mathbf{r})$ which can be represented as a sum of two terms [3]: the local contribution $f_0^v(\rho(\mathbf{r}), T)$, and the gradient contribution $f_{\nabla\rho}^v(\nabla\rho(\mathbf{r}))$,

$$f^v(\mathbf{r}) = f_0^v(\rho(\mathbf{r}), T) + f_{\nabla\rho}^v(\rho(\mathbf{r}), \nabla\rho(\mathbf{r})) \quad (1)$$

where T is the temperature, $\rho(\mathbf{r})$ is the local density, while $\nabla\rho(\mathbf{r})$ is the density gradient. For a spherical interface the density gradient has only nonzero component $\rho'(r)$, the derivative of the density with respect to the radial position r . For the sake of clarity we provide the description for a one-component system. The general analysis for multicomponent systems forming planar interface can be found in [6].

The local contribution $f_0^v(\rho(r), T)$ is determined by an equation of state. A particular choice of the equation of state is not important for the present analysis. In all further calculations we use van der Waals equation of state. Equation (1) can be considered as a Taylor expansion in the density derivatives, since in the interfacial region the density change abruptly. Therefore, the gradient contribution $f_{\nabla\rho}^v(\rho(r), \rho'(r))$ contains the first non-local terms in the Taylor expansion

$$f_{\nabla\rho}^v(\rho, \rho') = \frac{1}{2} \kappa \rho'(r)^2 \quad (2)$$

The coefficient $\kappa(\rho)$ is independent of the temperature but may depend on the density. Without restriction in generality we will consider it to be independent of the density as well.

For a closed system with fixed total volume and mass the density distribution is such that it minimizes the total grand potential $\Omega = \int dr 4\pi r^2 (f^v(r) - \mu_e \rho(r))$, where μ_e is the equilibrium chemical potential of the system. The density distribution satisfies therefore the equation

$$\mu_e = \frac{\partial f_0^v(\rho, T)}{\partial \rho} - \kappa \left(\rho'' + \frac{2}{r} \rho' \right) \quad (3)$$

We note, that the system considered is highly inhomogeneous, which contains the density gradients even in equilibrium. However, the condition of thermodynamic equilibrium requires that the chemical potential is constant through the system. Indeed, that is the case: the chemical potential μ_e , being the Lagrange multiplier of the variational minimization procedure, is a number which characterizes the whole system. Even though each term in Eq. (3) depends substantially on the position, the entire right hand side of Eq. (3) is independent of the position.

The pressure

In the interfacial region the pressure is no longer a scalar: it becomes a tensor. It is convenient therefore to consider its structure in general tensorial form. The tensorial pressure $\sigma_{\alpha\beta}$ can be represented as

$$\sigma_{\alpha\beta}(\mathbf{r}) = p(\mathbf{r}) \delta_{\alpha\beta} + \gamma_{\alpha\beta}(\mathbf{r}) \quad (4)$$

where

$$p(\mathbf{r}) = \mu_e \rho(\mathbf{r}) - f^v(\mathbf{r}) \quad (5)$$

is the thermodynamic pressure and

$$\gamma_{\alpha\beta}(\mathbf{r}) = \nabla_\alpha \rho(\mathbf{r}) \nabla_\beta \rho(\mathbf{r}) \quad (6)$$

is the tension tensor. Here $\delta_{\alpha\beta}$ is the Kronecker symbol and ∇_α represents the partial derivative with respect to the α coordinate. In equilibrium in the absence of external field it satisfies the relation

$$\nabla_\alpha \sigma_{\alpha\beta}(\mathbf{r}) = 0 \quad (7)$$

where the summation convention over double Greek symbol is used. In the presence of external field the right hand side of Eq. (7) contains the density of external field.

Identification of the scalar and tensorial terms in Eq. (4) is arbitrary. For instance, the thermodynamic pressure

$$p(\mathbf{r}) = p_0(\rho, T) - \kappa \rho \nabla^2 \rho - \frac{1}{2} \kappa |\nabla \rho|^2 \quad (8)$$

where $p_0(\rho, T)$ is the homogeneous pressure which is given by an equation of state. Equation (4) can therefore be written as

$$\sigma_{\alpha\beta} = p_0(\rho, T) \delta_{\alpha\beta} + \mathfrak{w}_{\alpha\beta} \quad (9)$$

where

$$\mathfrak{w}_{\alpha\beta}(\mathbf{r}) \equiv \gamma_{\alpha\beta}(\mathbf{r}) - \kappa \left(\rho \nabla^2 \rho + \frac{1}{2} \kappa |\nabla \rho|^2 \right) \delta_{\alpha\beta} \quad (10)$$

is the Korteweg tensor [7].

When using the pressure tensor in the interfacial region, it is common to speak of the scalar and tensorial parts separately. The particular identification may depend on the application one uses it for. In this paper we show that distinguishing the thermodynamic pressure and the tension tensor is natural in the context of non-equilibrium thermodynamics.

For instance, the expression for the thermodynamic pressure, Eq. (5), has the same functional form as in a homogeneous phase. This is important when one introduces the hypothesis of local equilibrium in non-equilibrium description. Furthermore, integral of the tension tensor over the interfacial region determines the surface tension. Finally, since Eq. (7) represents the condition of mechanical equilibrium, it is the gradient of the total pressure tensor $\sigma_{\alpha\beta}$, not the Korteweg tensor $\mathfrak{w}_{\alpha\beta}$, which changes the momentum of the system. We will see this when we discuss the balance equations.

For a spherical system the pressure tensor has a diagonal form with two independent components, the normal pressure $p_n(r) = p(r) + \kappa \rho'(r)^2$ and the tangential pressure $p_\tau(r) = p(r)$. The condition of mechanical equilibrium becomes

$$p'_n(r) + \frac{2}{r} \kappa \rho'(r)^2 = 0 \quad (11)$$

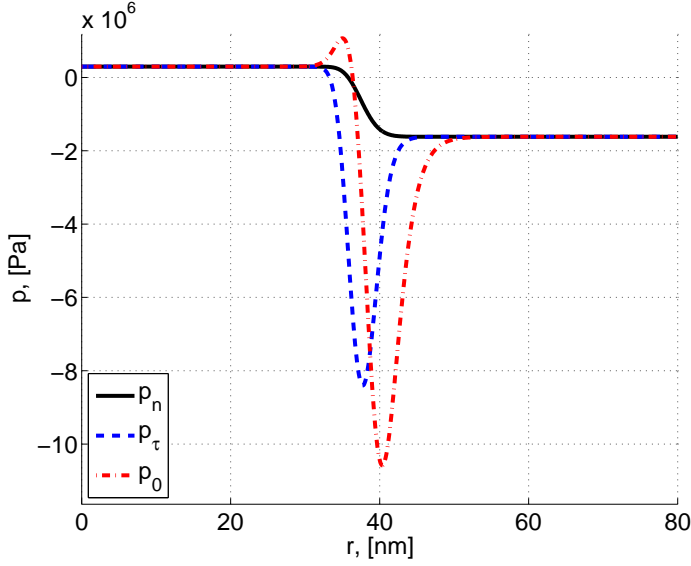


Figure 1. Profile of the normal, tangential and homogeneous pressure across the interfacial region for cyclohexane at 330 K

Variations in the pressure are of two kinds. First, due to nonzero curvature, the normal pressure is not constant across the interfacial region. The second term in Eq. (11) represents the local form of the Laplace pressure and is nonzero for a spherical interface. It is substantial for small bubbles and decreases when the bubble grows, becoming zero for a planar interface. Next, there exist variations in pressure which lead to the surface tension. They are present in the system even in the case of zero curvature. For a planar interface the normal pressure is constant through the interface, while the thermodynamic pressure has a large negative dip. The variation of the tension tensor is the opposite. Figure 1 represents typical profiles of the various pressures for a spherical bubble of cyclohexane in equilibrium at $T = 330$ K.

LOCAL EQUILIBRIUM AND BALANCE EQUATIONS

In order to use the above thermodynamic analysis in non-equilibrium, one has to assume that there exist so-called local equilibrium, i.e. that all the thermodynamic quantities and relations in non-equilibrium have the same functional form as in equilibrium. In formulating the local equilibrium hypothesis it is important to do the correct identification of the thermodynamic quantities. In homogeneous phase, where the spatial variations of all the quantities are small, this is straightforward. However, in the interfacial region, where the density changes a lot, care should be taken. For instance, as was discussed above, in the interfacial region one can identify at least three different quantities with the meaning of pressure: the normal pressure $p_n(r)$, the tangential pressure $p_\tau(r)$ and the homogeneous pressure p_0 .

We start with introducing the density $\rho(r,t)$ and the temperature $T(r,t)$ as independent thermodynamic variables. Next we define the non-equilibrium local Helmholtz energy $f^v(r,t)$ in the interfacial region in the same way as in equilibrium, see Eq. (1). In non-equilibrium the total grand potential does not have a minimum, so it is not possible to perform a variational minimization procedure. Thus, the pressure and the chemical potential have to be defined independently. We use Eq. (3) and Eq. (5) for this.

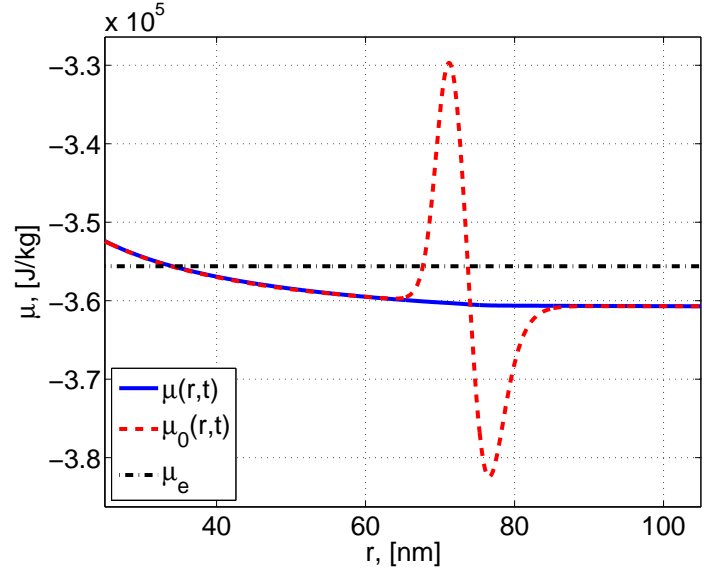


Figure 2. Profile of the non-equilibrium chemical potential, non-equilibrium homogeneous chemical potential and the equilibrium total chemical potential for cyclohexane. Equilibrium temperature is 330 K, while the non-equilibrium boundary temperature is 10 K higher than equilibrium value in the center.

Namely, the non-equilibrium chemical potential is

$$\mu(r,t) = \mu_0(\rho(r,t), T(r,t)) - \kappa \left(\rho''(r,t) + \frac{2}{r} \rho'(r,t) \right) \quad (12)$$

and the non-equilibrium thermodynamic pressure is

$$p(r,t) = \mu(r,t)\rho(r,t) - f^v(r,t) \quad (13)$$

We note, that unlike μ_e , the non-equilibrium chemical potential $\mu(r,t)$ is not constant through the system. However, the spatial variation of $\mu(r,t)$ is much less than the spatial variation of $\mu_0(\rho(r,t), T(r,t))$. The former one is determined by the rate of non-equilibrium perturbation, which is considered to be small, and vanishing in equilibrium. The latter one is determined by the rate of the density variation in the interfacial region, which is large and non-zero even in equilibrium. Typical variations of the chemical potential are represented in Figure 2.

The non-equilibrium normal pressure is defined with the help of Eq. (4) as

$$p_n(r,t) = p(r,t) + \kappa \rho'(r,t)^2 \quad (14)$$

Gibbs relation

An important part of specifying local equilibrium is to provide the rates of change of thermodynamic quantities, the Gibbs relation. A particular Gibbs relation can be justified only by the validity of the results, which follow from the analysis. We can, however, provide arguments which elucidate a particular form of the Gibbs relation.

In an inhomogeneous equilibrium system such as interfacial region the local thermodynamic properties can vary in two different dimensions. First, they can change when the whole system changes its thermodynamic state from, for instance, one

temperature to another. Since the temperature and the chemical potential are constant in equilibrium system, it means that every small element of the system follows the same change in thermodynamic state, but locally. For a one-component system this can be described by the ordinary Gibbs relation

$$T \delta s(r) = \delta u(r) + p(r) \delta v(r) \quad (15)$$

where symbol δ denotes a change in a thermodynamic state of the entire system. Furthermore, $u(r) = f^v(r)v(r) - Ts(r)$ is the specific internal energy, $s(r) = v(r)\partial f^v(r)/\partial T$ is the specific entropy, and $v(r) = 1/\rho(r)$ is the specific volume. Next, the thermodynamic properties in an inhomogeneous equilibrium system vary in space. This variation is not arbitrary and is constrained by the conditions of mechanical equilibrium, Eq. (4) and the conditions of the thermodynamic equilibrium, $T(r) = \text{const}$ and $\mu(r) = \text{const}$. Using Eq. (5), we obtain

$$T \nabla_{\alpha} s(r) = \nabla_{\alpha} u(r) + p(r) \nabla_{\alpha} v(r) - v(r) \nabla_{\beta} \gamma_{\alpha\beta}(r) \quad (16)$$

Equation (16) has the form of Eq. (15) except the last term. Since it accounts for spatial changes of thermodynamic properties, we will call it the spatial Gibbs relation. We note, that both Eq. (15) and Eq. (16) are exact in equilibrium.

The next step is to formulate the non-equilibrium Gibbs relation. One can observe that the change of a thermodynamic quantity in thermodynamic state at a given spatial position corresponds to the partial time derivative of this quantity, while its change in spatial position at a given thermodynamic state corresponds to the partial spatial derivative. Multiplying Eq. (16) with barycentric flow velocity \mathbf{v} and adding it to Eq. (15) we obtain

$$T \frac{ds}{dt} = \frac{du}{dt} + p \frac{dv}{dt} - J_{m,\alpha} v^2 \nabla_{\beta} \gamma_{\alpha\beta} \quad (17)$$

where $\mathbf{J}_m \equiv \rho \mathbf{v}$ is the mass flux across the interface and we have omitted the arguments (r,t) , as now all the quantities depend on position and time. Equation (17) is the Gibbs relation for a non-equilibrium interfacial region. The last term is nonzero only in the interfacial region and vanishes in the homogeneous phase, leading to the ordinary form of the Gibbs relation. The last term can be considered as a work required to transfer an element of specific volume v across the interface. We note that it is the tension tensor which comes to the non-equilibrium Gibbs relation, not the Korteweg tensor.

Balance equations

For a one-component system we can write four balance equations, for mass, energy, momentum and entropy respectively:

$$\frac{\partial \rho}{\partial t} = -\nabla \cdot \mathbf{J}_m \quad (18)$$

$$\frac{\partial e^v}{\partial t} = -\nabla \cdot \mathbf{J}_e \quad (19)$$

$$\frac{\partial \rho v_{\alpha}}{\partial t} = -\nabla_{\beta} J_{p,\alpha\beta} \quad (20)$$

$$\frac{\partial s^v}{\partial t} = -\nabla \cdot \mathbf{J}_s + \sigma_s \quad (21)$$

Here \mathbf{J}_m , \mathbf{J}_e , $J_{p,\alpha\beta}$, \mathbf{J}_s are the mass flux, the energy flux, the momentum flux and the entropy flux respectively. Furthermore, e^v is the total energy density, s^v is the entropy density and σ_s is the local entropy production. The form of the balance equations in an inhomogeneous region is the same as in an homogeneous region. In particular, the momentum flux $J_{p,\alpha\beta}$ consists of the kinetic term $\rho v_{\alpha} v_{\beta}$ and the mechanical pressure tensor $\sigma_{\alpha\beta}$. When there is no flux, the momentum balance equation, Eq. (20), reduces to the condition of mechanical equilibrium, Eq. (4). It is clear, therefore, that it is the total pressure tensor $\sigma_{\alpha\beta}$ which contributes to the momentum flux.

Using the Gibbs relation, Eq. (17), and the above balance equations we can derive the expression for the entropy production. In spherical coordinates it takes the following form

$$\sigma_s = J_q \left(\frac{1}{T} \right)' \quad (22)$$

where the heat flux $J_q \equiv J_e - J_m(u + v^2/2 + pv)$ is the measurable heat flux.

CONSTITUTIVE RELATIONS AND TRANSPORT COEFFICIENTS

We must provide constitutive relations between the thermodynamic driving forces and the fluxes. In case of one-component system the thermodynamic force is the radial temperature gradient, $(1/T)'$ while the flux is the heat flux J_q . In order for the entropy production to be positive, they must be related linearly, i.e.

$$\left(\frac{1}{T} \right)' = r_{qq}(r) J_q \quad (23)$$

where $r_{qq}(r)$ is the local resistivity to the heat transfer. A particular expression for the resistivity coefficient does not follow from the theory and must be given in addition. In the context of the square gradient theory we model the resistivity coefficient similarly to the local Helmholtz energy, Eq. (1), i.e.:

$$r_{qq}(r) = r_{qq,0}(\rho, T) + r_{qq,\nabla\rho}(\rho, \nabla\rho) \quad (24)$$

In this form the resistivity coefficient resembles the equilibrium profiles of the density and the density gradient. Even though it depends on the density gradient, it does not contribute to the driving force, as is expected in linear non-equilibrium thermodynamics. All the effects of non-equilibrium perturbation are therefore due to the nonzero heat flux J_q .

In equilibrium thermodynamics a smooth variation of local density profile across the interface leads to the surface excess properties, such as the interfacial tension or the Laplace pressure. For small bubbles or droplets these properties modify the state of the system such that the surface becomes its important part, together with the bulk phases. A similar situation is observed in non-equilibrium. Due to smooth variation of the local resistivity profile $r_{qq}(r)$ across the interface, the surface possesses excess resistance to the heat transfer. Additional resistance is particularly large for small bubbles or droplets as it may be comparable to the bulk resistance.

In a continuous description of a one-component non-equilibrium system there exist only one irreversible flux, the

heat flux, which is caused by the temperature gradient, as suggested, in particular, by Eq. (23). However, description in terms of the excess interfacial properties, in particular for bubble and droplets, reveals existence of the cross effects. Thus, the temperature gradient across the interface causes the mass flux, while the gradient in the chemical potential causes the heat flux. These phenomena are the essence of nucleation process, so the correct account for these phenomena is crucial for understanding the nucleation. The reason for the existence of the irreversible mass flux in the one-component system is the presence of surface. Its velocity does not necessarily coincide with the barycentric velocity of the fluid. This leads to the mass flux across the interface. This flux carries along additional heat due to the temperature gradient.

One can perform the analysis of non-equilibrium transport for a discrete system (see e.g. [8] or [2]) and in stationary states obtain the following constitutive relations

$$\begin{aligned} \Delta \frac{1}{T} &= R_{qq} J_q^s + R_{qm} J_m \\ -\Delta \frac{\mu}{T} + h^s \Delta \frac{1}{T} &= R_{mq} J_q^s + R_{mm} J_m \end{aligned} \quad (25)$$

where Δ indicates the difference between the extrapolated to the surface bulk values of the corresponding quantities. Furthermore, h^s is the specific enthalpy in the gas phase and J_q^s is the measurable heat flux in the same phase. Equation (25) suggests that there exist mass flux J_m across the interface, which depends both on the temperature difference and the chemical potential difference across the interface.

The coefficients R_{qq} , R_{qm} , R_{mq} , R_{mm} represent the excess interfacial resistances to the heat and mass transfer. Just like the local resistivity coefficient $r_{qq}(r)$, they can depend only on equilibrium properties of the system and do not depend on the non-equilibrium perturbation. They are related to the local resistivity profile in the following way:

$$\begin{aligned} R_{qq}(x) &= \mathfrak{E}[r_{qq}](x) \\ R_{mq}(x) &= R_{qm}(x) = \mathfrak{E}[r_{qq}(h^s - h)](x) \\ R_{mm}(x) &= \mathfrak{E}[r_{qq}(h^s - h)^2](x) \end{aligned} \quad (26)$$

where

$$\mathfrak{E}[q](x) \equiv \int_{r^s}^{r^\ell} dr \frac{x^2}{r^2} \left(q(r) - q^s \Theta(x - r) - q^\ell \Theta(r - x) \right) \quad (27)$$

In this expression Θ is the Heaviside step function, while r^s and r^ℓ are the positions in the homogeneous region of the gas and liquid phase. Furthermore, q^s and q^ℓ are the extrapolated to the position x homogeneous values of the quantity q . $\mathfrak{E}[q]$ represents therefore the excess of a quantity $q(r)$ across the interfacial region above the homogeneous values. Figure 3 illustrates the idea of excess: it is basically the difference between the shaded areas of different color. The value of the excess depends on the position of the dividing surface. Depending on the kind of profile it can be either positive or negative, such as in Figure 3(a), if the profile changes monotonically across the interface, or always positive, such as in Figure 3(b), if the profile has

a peak inside the interfacial region. Equations (26) show that interfacial resistances are the excesses of local profiles, which are the combinations of resistivity profile and the enthalpy profile.

A PARTICULAR SOLUTION FOR STATIONARY STATES

We consider here an example of solution for a bubble in stationary states. The balance equations 18-21 take the following form

$$\begin{aligned} (r^2 J_m)' &= 0 \\ (r^2 J_e)' &= 0 \\ (r^2 J_p)' &= 2r p(r) \\ (r^2 J_s)' &= \sigma_s \end{aligned} \quad (28)$$

where the momentum flux $J_p = p_n + \rho v^2$. Unlike the planar interface the mass, energy and momentum fluxes are not constant through the interfacial region. Due to spherical symmetry, it is $r^2 J_m$ and $r^2 J_e$ which are constant. In addition, $r^2 J_p$ is not even constant.

For a planar interface stationary states are typically realized by keeping different values of the temperature and pressure on the boundaries of the system. This leads to a flux of matter and energy into the system at one side of it and out of the system at the other side. An equivalent picture for a spherically symmetric system would be to control the temperature and pressure at the spherical boundary. This would lead to a flux of matter and energy through that boundary. In stationary states this flux should be compensated by the corresponding source or sink in the center of the bubble. Equation (28) suggests that this could be realized either if the flux of matter or energy is zero everywhere or if they are infinite in the center. In the first case we get equilibrium, while the second case is unphysical. In other words the stationary non-equilibrium state for a bubble or a droplet is not possible. It can either be in equilibrium, or grow (shrink).

The interfacial property of a bubble do not depend, however, on its motion. Besides, the most convenient condition to study these properties is stationary state. In order to circumvent the above problem in stationary state we need to allow matter and energy to be sinked not in the center of the bubble, but at some finite radius. Our system would be therefore have not only the outer boundary of the radius L^o , but also the inner boundary of radius L^i . The gas-liquid interfacial region lies entirely inside the layer between these boundaries. With this geometry we can control the temperature and pressure at the both boundaries.

To illustrate a particular solution we consider the case when there is no mass flux across the boundary. In this case Eq. (23) allows an analytic solution for the temperature:

$$\frac{1}{T(x)} = \frac{1}{T^i} + \left(\frac{1}{T^o} - \frac{1}{T^i} \right) \frac{\int_{L^i}^x dr \frac{r_{qq}(r)}{r^2}}{\int_{L^i}^{L^o} dr \frac{r_{qq}(r)}{r^2}} \quad (29)$$

The local resistivity profile depend only on equilibrium properties of the system. Equation (24) can take the following form

$$r_{qq}(r) = r_{qq}^i + (r_{qq}^o - r_{qq}^i) \frac{\rho_{eq}(r) - \rho_{eq}^i}{\rho_{eq}^o - \rho_{eq}^i} + \alpha (r_{qq}^o + r_{qq}^i) \frac{|\nabla \rho_{eq}|^2}{|\nabla \rho_{eq}|_{\max}^2} \quad (30)$$

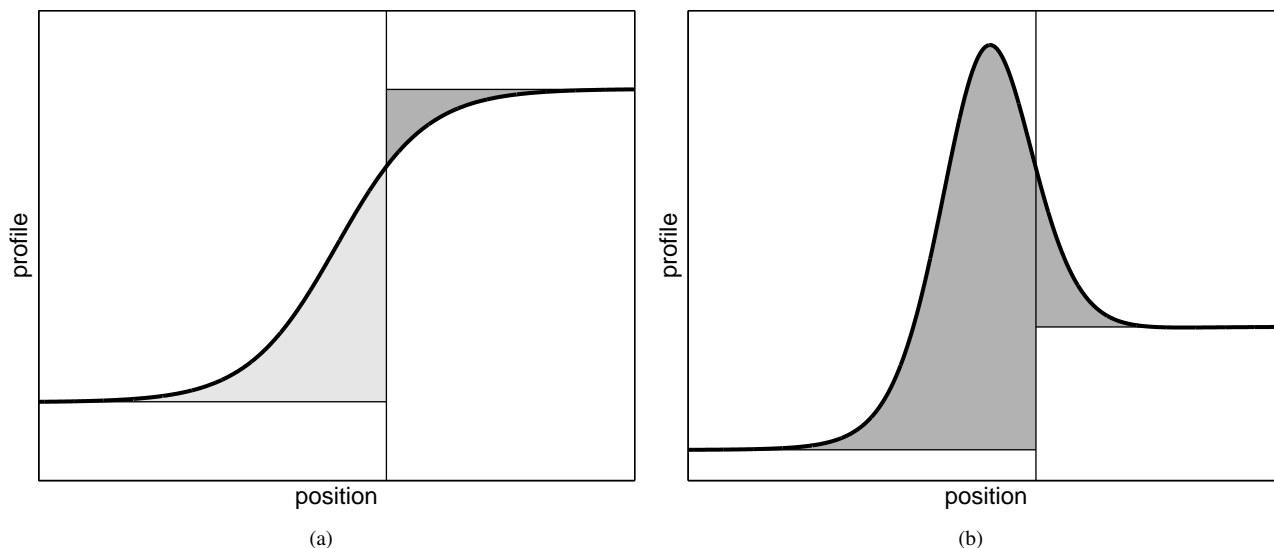


Figure 3. Illustration of the interfacial excess. The excess is the difference between the shaded areas of different color. (a) Depending on the position of the dividing surface the excess may be both positive and negative; (b) Irrespectively of the position of the dividing surface, the excess is always positive.

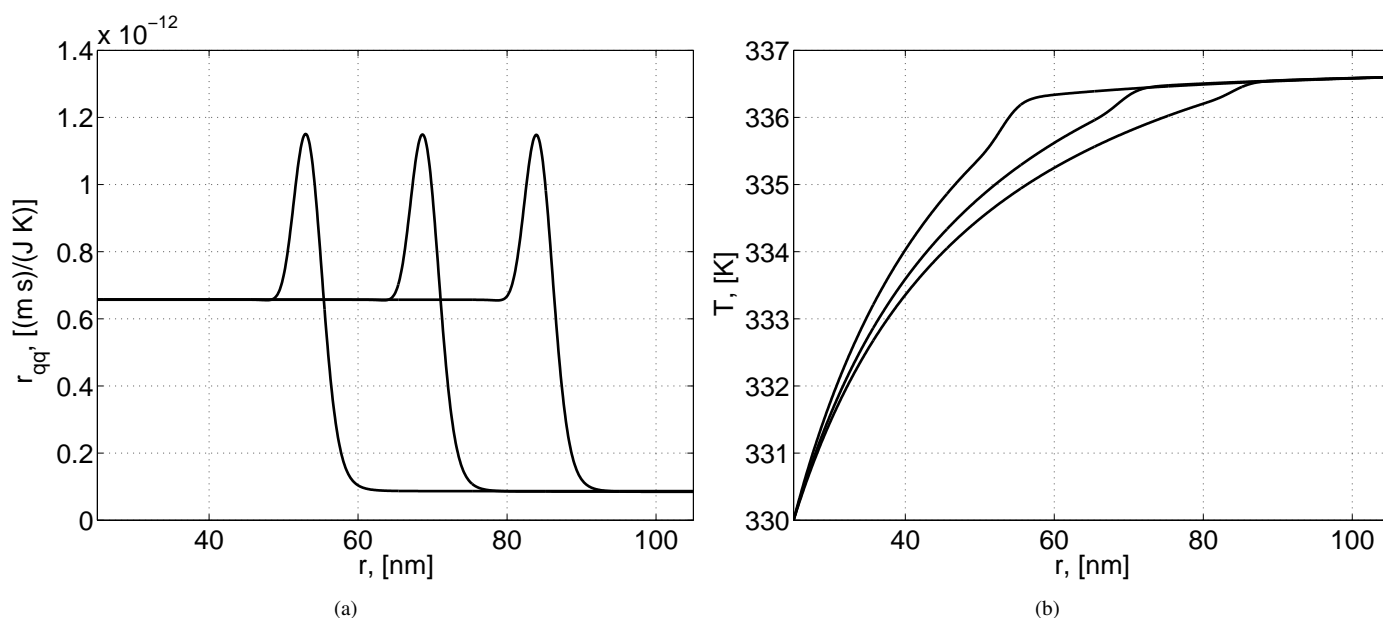


Figure 4. Local resistivity profiles (a) and temperature profiles (b) for spherical layer filled with various amounts of cyclohexane, boundaries of which are kept at 330 K and 336.6 K.

where superscripts i and o denote the values of the resistivity and the density at the boundaries. Typical resistivity profiles for different bubble sizes are given in Figure 4(a). Position of the peaks in the profiles correspond to the positions of the interfacial region. This lead to the temperature profiles illustrated in Figure 4(b). We see that the temperature profiles has different slopes in the gas and liquid phases. This is natural, since the gas and liquid resistivity are different. Higher gas resistivity leads to the more steep temperature profile in the gas phase. Another interesting thing is that the extrapolated temperature profiles in the gas and liquid phases are different at the interface.

CONCLUSIONS

In this article we have presented a systematic procedure for the description of a non-equilibrium spherical interface. We

considered separately the equilibrium square gradient model, non-equilibrium constitutive equations and the extension of the equilibrium thermodynamic quantities in an inhomogeneous region to non-equilibrium. We emphasized the importance of this extension as it allows one to identify correctly the forces which drive the system away from equilibrium.

In particular we have summarized the role of pressure. It was shown that one can identify several quantities with a meaning of the pressure, namely the thermodynamic pressure, the normal and tangential pressure, the tension tensor and the Korteweg tensor. In particular, the thermodynamic pressure is used in the definition of local thermodynamic potentials, such as local Helmholtz energy or local internal energy, and in the Gibbs relation. In addition, the tension tensor appears in the Gibbs relation for an inhomogeneous region, which illustrates an ad-

ditional work required to transfer a volume element across the interface. In contrast, the normal pressure is present in balance equation for momentum, i.e. equation of motion.

We have discussed that non-equilibrium fluxes are determined by the gradients of the chemical potentials rather than the gradients of the densities. While the variations of the thermodynamic quantities, such as p_0 or μ_0 , determined from the equation of state are large across the interfacial region, the non-equilibrium flux of matter is determined by the slow variation in the total chemical potential.

We have discussed the origin of an additional resistance met by a bubble to heat and mass transfer, which is caused by the interface. The excess resistance is essentially determined by the peak in the local resistivity profile caused by the large density gradients in the interfacial region. As the surface can be considered as a separate thermodynamic phase, its resistance is determined by the equilibrium properties, just like the resistance of the homogeneous phase.

Finally we considered a simple example of a bubble in non-equilibrium conditions. It illustrated the typical profiles of local properties which are developed in non-equilibrium bubble or droplet.

NOMENCLATURE

Vectors are indicated by the bold phase, tensors are indicated by two Greek subscripts.

o	Subscript indicating the homogeneous phase
f^v	Helmholtz energy density [J/m ³]
h	Specific enthalpy [J/kg]
J_m	Mass flux [kg/(m ² s)]
J_e	Energy flux [J/(m ² s)]
J_q	Measurable heat flux [J/(m ² s)]
J_p	Momentum flux [Pa]
J_s	Entropy flux [J/(m ² K)]
p	Thermodynamic pressure [Pa]
p_n	Normal pressure [Pa]
p_τ	Tangential pressure [Pa]
r	Position [m]
r_{qq}	Local heat resistivity coefficient [(m s)/(J K)]
R_{qq}	Excess heat resistance coefficient [(m ² s)/(J K)]
R_{qm}	Excess heat resistance coefficient [(m ² s)/(kg K)]
R_{mm}	Excess heat resistance coefficient [(m ² s)/(kg ² K)]

s	Specific entropy [J/kg]
T	Temperature [K]
t	Time [s]
u	Specific internal energy [J/kg]
v	Specific volume [m ³ /kg]
v	Velocity [m/s]
α, β	Spatial components of vectors and tensors []
\mathcal{E}	Excess operator []
$\gamma_{\alpha\beta}$	Tension tensor [Pa]
κ	Square gradient coefficient [J m ⁵ /kg ²]
μ	Chemical potential [J/kg]
ρ	Mass density [kg/m ³]
σ_s	Entropy production [J/(m ³ K)]
$\sigma_{\alpha\beta}$	Pressure tensor [Pa]
$\varpi_{\alpha\beta}$	Korteweg tensor [Pa]

REFERENCES

- [1] D. Kashchiev. *Nucleation*. Butterworth-Heinemann, 2000.
- [2] K.S. Glavatskiy. *Multi-component interfacial transport as described by the square gradient model; evaporation and condensation*. Springer Thesis Book Series. Springer, Berlin, 2011.
- [3] K. Glavatskiy and D. Bedeaux. Curvature dependent non-equilibrium square gradient model. *in preparation*, 2013.
- [4] S. R. de Groot and P. Mazur. *Non-Equilibrium Thermodynamics*. Dover, London, 1984.
- [5] P. Poesio, G. P. Beretta, and T. Thorsen. Dissolution of a liquid microdroplet in a nonideal liquid-liquid mixture far from thermodynamic equilibrium. *Phys. Rev. Lett.*, 103:064501, 2009.
- [6] K.S. Glavatskiy and D. Bedeaux. *Phys. Rev. E*, 77:061101, 2008.
- [7] D. J. Korteweg. Sur la forme que prennent les équations du mouvement des fluides si l'on tient compte des forces capillaires causés par les variations de densité. *Arch. Néerlandaises des Sci. Exact et Natur.*
- [8] S. Kjelstrup and D. Bedeaux. *Non-Equilibrium Thermodynamics of Heterogeneous Systems*. Series on Advances in Statistical Mechanics, vol. 16. World Scientific, Singapore, 2008.

INHOMOGENEOUS DENSITY THEORIES COUPLED INTO A MOLECULAR EQUATION OF STATE FOR THE DESCRIPTION OF THE FLUID-FLUID INTERFACE

Felix Llovell*, Oriol Vilaseca*, Lourdes F. Vega*

* MATGAS 2000 AIE, Campus de la UAB,
08193, Bellaterra, Barcelona, Spain

ABSTRACT

In this work, a short review of different approaches to estimate the surface tension, density profiles and other interfacial properties of pure fluids and mixtures is described. Particular attention is paid to two relevant methods usually coupled to molecular based equations of state from the SAFT family: the Density Functional Theory (DFT) and the Density Gradient Theory (DGT). The DFT approach is based on the construction of a free-energy functional by generally dividing the free-energy in two parts: a reference term that incorporates only the ideal and short-range interactions, and a perturbative term in which the long-range interactions are included. On the other hand, The DGT approach is based on the van der Waals theory for inhomogeneous fluids, as popularized by Cahn and Hilliard, where the Helmholtz free-energy density is expanded as a Taylor series in the density profile, which is truncated after the second term. Both treatments are physically well sounded and they are applicable to these type of EoSs, showing a very good performance to describe a wide variety of fluids, including hydrocarbons, amines, carbon dioxide, water and ionic liquids. Some examples will be shown here, highlighting the advantages and disadvantages of each methodology.

INTRODUCTION

The type and magnitude of the molecular interactions that occur at interfaces are responsible for many of the phenomena that are observed in nature. A detailed knowledge of the interfacial behaviour is required to deal with many industrial technological processes, especially those ones related to separation and extraction. However, the modelling of interfacial properties remains as a challenge due to its inhomogeneous nature. Only theories that explicitly consider property fluctuations are able to reproduce the physics behind the interface.

A quantitative evaluation of interfacial phenomena can be developed by starting from an accurate representation of the bulk homogeneous fluids. Among several possibilities, one of the most successful equations of state (EOSs) for fluid-phase equilibria is the statistical associating fluid theory (SAFT) [1], and its different versions. The general form of the SAFT expression for the Helmholtz free energy stems from the first-order perturbation theory for associating systems by Wertheim [2]-[4]. The total free energy comprises a sum of terms that contribute to the total energy of the systems, each with a rigorous statistical mechanical foundation.

A large body of literature has been devoted to the description and estimation of phase equilibrium properties of fluids following a variety of approaches. However, the application of theories of inhomogeneous systems is less common. One of the first successful approaches for the description of interfacial tensions in mixtures is the so-called parachor method, introduced by Macleod [5]. One can use this empirical approach to correlate the interfacial tension with the difference of the bulk coexisting densities. Despite its empirical basis, Fowler [6] showed that the relation can be derived as an explicit function of the intermolecular potential in the case of a stepwise density profile, which is a reasonable

assumption far away from the critical point. Other popular approaches are based on the corresponding-states principle of Guggenheim [7], where empirical relations can be developed in terms of a specific reference fluid to provide an accurate representation of the surface tension [8]. Though useful in correlating data for the interfacial tension of fluid mixtures, these empirical relations offer little in way of predictive capability. This is the advantage of approaches developed from a more rigorous theoretical foundation such as the squared gradient theory (also referred to as density gradient theory (DGT)) and density functional theory (DFT).

The DGT methodology is rooted in the original theory for inhomogeneous fluids of van der Waals [9], which was rediscovered and popularized by Cahn and Hilliard. [10] In DGT, the local free energy density is expanded as a Taylor series about the density profile to second order, i.e., to the second derivative of the profile with respect to the distance from the interface (which in this case also corresponds to the square of the density gradient). The first term of the DGT essentially corresponds to the Helmholtz free-energy density of the uniform fluid evaluated at the local density. The square-gradient term can be expressed in terms of $c(r)$, the direct correlation function [11] because the form of $c(r)$ is generally unknown, it is often treated phenomenologically with the help of an adjustable parameter, the so-called "influence" parameter, which is estimated from real surface tension data.

By contrast to DGT, the DFT formalism in principle offers an entirely predictive approach with no adjustable parameters. DFT methods are based on the construction of a free-energy functional from which the thermodynamic properties of the inhomogeneous system can be calculated. Several authors have discussed the general approaches for the construction of free-energy functionals and the different approximations that are commonly employed. Though the functional form of the free energy in typical DFTs is mathematically more complex

(involving iterative variational techniques for their solution) than for a DGT treatment, they have become quite popular because of the enhanced predictive capability.

As a consequence, intermolecular parameters which have been estimated by optimization of experimental data for the bulk phases are sufficient to provide a predictive platform for the interfacial properties of the system within a DFT formalism without the need for additional surface tension data. The fundamental details of the DFT approach can be found in the seminal reviews by Evans [12] and Davis [13], including the various options for going from a general DFT formalism to an approximated theory that can be used to compute accurate results when applied to real fluids.

The purpose of this contribution is to show the capability of combining a physically sounding SAFT-type equation of state with the DGT and DFT methods for the estimation of the surface tension, density profiles and other interfacial properties of pure fluids and mixtures.

THEORY

DGT

The Density Gradient Theory (DGT) was originally proposed by van der Waals,[9] and rediscovered many years later by Cahn and Hilliard [10]. In the DGT approach, the Helmholtz free energy density is expanded in a Taylor series around a_0 , the free energy density term of the homogeneous fluid at the local density, and truncated after the second order term.

$$A = \int \left[a_0(\rho) + \sum_i \sum_j \frac{1}{2} c_{ij} \nabla \rho_i \nabla \rho_j \right] d^3 r \quad (1)$$

where $a_0(\rho)$ is the Helmholtz free energy density of the homogeneous fluid at the local density ρ and ρ_i and ρ_j are the molar densities of components i and j ; c_{ij} is the influence parameter, which is treated as an adjustable temperature independent parameter regressed from experimental data.

Eq. (1) is usually simplified by assuming a planar interface and neglecting the density dependence of c_{ij} . Hence, the surface tension γ is related to the square gradient expression following

$$\gamma = \sum_i \sum_j \int_{-\infty}^{\infty} c_{ij} \frac{d\rho_i}{dz} \frac{d\rho_j}{dz} dz = 2 \int_{-\infty}^{\infty} \Delta\Omega(\rho_i, \rho_j) dz, \quad (2)$$

where $\Delta\Omega$ is, by definition, the grand thermodynamic potential: $\Delta\Omega(\rho_i, \rho_j) = a_0(\rho) - \sum_i \mu_{o,i} \rho_i + P_0$. $\mu_{o,i}$ and P_0

correspond to the equilibrium chemical potential and pressure, respectively, and z is the direction perpendicular to the interface. The right hand expression of Eq. (2) had infinite limits in the integration. Poser and Sanchez [14] applied a transformation from local space to density space, allowing a way to evaluate density profiles. For the particular case of a binary mixture, the equation reads:

$$z = z_0 + \int_{\rho_2(z_0)}^{\rho_2(z)} \sqrt{\frac{c'}{\Delta\Omega(\rho_1, \rho_2)}} d\rho_2 \quad (3)$$

where z_0 denotes an arbitrary chosen origin and c' is the result from the influence parameters of the pure components and the density profiles across the interface, and is described by,

$$c' = c_2 + 2c_{12} \left(\frac{d\rho_1}{d\rho_2} \right) + c_1 \left(\frac{d\rho_1}{d\rho_2} \right)^2 \quad (4)$$

The crossed parameter c_{12} is assumed to be given by the geometric mean combination rule, $c_{12} = \beta \sqrt{c_1 c_2}$. β is an adjustable parameter, either fitted to the mixture experimental surface tension data or kept equal to one for predictive purposes. For a fair comparison with DFT, β has been set to unity in all cases.

Using the above mentioned transformation, Poser and Sanchez [14] also derived an equation for the surface tension in binary mixtures that considers the change in the partial densities ρ_1 and ρ_2 within the interface,

$$\gamma = \sqrt{2} \int_{\rho_2(z_0)}^{\rho_2(z)} \sqrt{c' \Delta\Omega(\rho_1, \rho_2)} d\rho_2 \quad (5)$$

where the limits of integration are the bulk densities of component 2 in the coexisting phases. Further details concerning the computational performance of the grand thermodynamic potential for binary mixtures and how this can be coupled to a SAFT-type within framework can be found in literature [15].

DFT

The Density Functional Theory (DFT) formalism is based on a standard perturbative approach in which the Helmholtz free-energy functional is approximated as the sum of a reference functional and a perturbative contribution.

$$A[\{\rho_m(\mathbf{r})\}] = A^{\text{ref}}[\{\rho_m(\mathbf{r})\}] + A^{\text{att}}[\{\rho_m(\mathbf{r})\}] \quad (5)$$

The theory is based on the grand potential functional $\Omega[\rho_m(\mathbf{r})]$ of an inhomogeneous system. Assuming an open mixture at temperature T and chemical potential μ_i for each component in a volume V , and in the absence of external fields:

$$\Omega[\{\rho_m(\mathbf{r})\}] = A[\{\rho_m(\mathbf{r})\}] - \sum_{i=1}^n \mu_i \int d\mathbf{r} \rho_i(\mathbf{r}) \quad (6)$$

where $A[\{\rho_m(\mathbf{r})\}]$ is the intrinsic Helmholtz free energy functional. The minimum value of $\Omega[\{\rho_m(\mathbf{r})\}]$ is the equilibrium grand potential of the system and the corresponding equilibrium density profiles $\rho_{eq,i}(\mathbf{r})$ satisfy the condition

$$\left. \frac{\delta \Omega[\{\rho_m(\mathbf{r})\}]}{\delta \rho_i(\mathbf{r})} \right|_{\text{eq}} = \left. \frac{\delta A[\{\rho_m(\mathbf{r})\}]}{\delta \rho_i(\mathbf{r})} \right|_{\text{eq}} - \mu_i = 0 \quad (7)$$

The DFT approach tries to find an expression to relate the Helmholtz energy with the density of the system at the interface. From Eq. (5), the first term takes into account the short-range interactions between the segments that form the molecules. For a SAFT-type equation of state, they correspond to the ideal, hard-sphere, chain, and associative contributions, which are evaluated using the well-known local density approximation (LDA) [16].

$$A^\alpha[\{\rho_m(\mathbf{r})\}] = k_B T \int d\mathbf{r} f^\alpha(\{\rho_m(\mathbf{r})\}) \quad (8)$$

The second term accounts for the long-range attractive interactions among the molecules of the system (corresponding to the first-order perturbation terms of the free energy):

$$A^{\text{att}}[\{\rho_m(\mathbf{r})\}] = \frac{1}{2} \sum_{i=1}^n \sum_{j=1}^n \int d\mathbf{r} m_i \rho_i(\mathbf{r}) \int d\mathbf{r}' m_j \rho_j(\mathbf{r}') \times g_{ij}^{\text{hs}}[\mathbf{r}, \mathbf{r}'; \{\rho_m(\mathbf{r}), \rho_l(\mathbf{r}')\}] \phi_{ij}^{\text{att}}(|\mathbf{r} - \mathbf{r}'|). \quad (9)$$

At this point, two different approximations for the perturbative term can be applied: a full treatment in which the correlations between the chain segments are incorporated in an average manner through a set of approximations to estimate the pair distribution function of the inhomogeneous hard-sphere mixture fluid [17], and a mean-field approach where the effect of the pair distribution function is neglected.

The final expression using the full approach and applied to the case of the SAFT-VR equation of state reads:

$$A^{\text{att}}[\{\rho_m(\mathbf{r})\}] = \frac{1}{2} \sum_{i=1}^n \sum_{j=1}^n \int d\mathbf{r} m_i \rho_i(\mathbf{r}) \int d\mathbf{r}' m_j \rho_j(\mathbf{r}') \times g_0^{\text{hs}}[\sigma_x; \xi_x^{\text{eff}}(\lambda_{ij}; \{\rho_m(\mathbf{r}), \rho_l(\mathbf{r}')\})] \phi_{ij}^{\text{att}}(|\mathbf{r} - \mathbf{r}'|) \quad (10)$$

The simplified mean-field expression is:

$$A_{\text{mf}}^{\text{att}}[\{\rho_m(\mathbf{r})\}] = \frac{1}{2} \sum_{i=1}^n \sum_{j=1}^n \int d\mathbf{r} m_i \rho_i(\mathbf{r}) \int d\mathbf{r}' m_j \rho_j(\mathbf{r}') \phi_{ij}^{\text{att}}(|\mathbf{r} - \mathbf{r}'|) \quad (11)$$

The variation of the reference contribution with respect to densities $\rho_i(r)$ correspond to the local chemical potential which can be obtained from derivation of the Helmholtz free energy by the density. Once the equilibrium density profile is known, the surface tension is determined by using the thermodynamic relation

$$\gamma = \frac{\Omega + pV}{\mathcal{A}} \quad (12)$$

A final point to remark is the discussion about the effect of capillary waves on the surface tensions. The standard DFT approach washes out capillary fluctuations. These fluctuations, which can be viewed as a superposition of sinusoidal surface waves (or two-dimensional normal modes, provided their amplitudes are small), would become increasingly important close to the critical point. These capillary-wave fluctuations are not taken into account explicitly here, based on the fact that a significant contribution to the thermodynamic properties of the interface away from the critical region is not expected. In fact, Henderson [18] has shown that the interfacial tension described by a capillary wave theory is equivalent to the thermodynamic interfacial tension (accessible, e.g., through a DFT treatment) in the case of long wavelength fluctuations. However, this is a point for discussion among different authors who consider the effect of capillary waves to be important and necessary in order to have a proper estimation of the surface tension [19].

INTERESTING EXAMPLES

In this section, we want to show the surface tension of different compounds calculated with the DGT and DFT treatments. We start first with the Density Gradient Theory, which has been used in conjunction with the soft-SAFT

equation of state. Soft-SAFT is a variant of the original SAFT developed in 1997 by Vega and Blas [20] and it is mainly characterised by using a Lennard-Jones (LJ) interaction potential among the monomers that form each molecule.

In Fig. 1, the surface tension of three common refrigerants (hydrofluorocarbons R134, R143 and R152) are modelled with the soft-SAFT equation of state + the DGT treatment. As it can be observed, excellent agreement with the experimental data is obtained in the whole range of temperatures corresponding to the vapour-liquid equilibrium line.

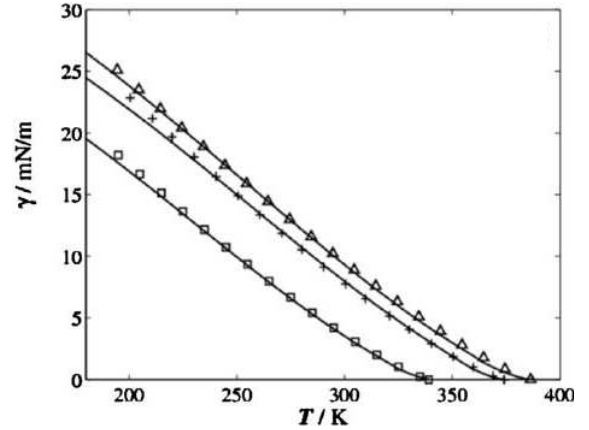


Fig. 1. Vapor-liquid interfacial tension for R125(Δ), R152a(+), R134a (\square). Lines are the theoretical calculations and the symbols represent the experimental data [21].

The density at each point of the interface is calculated using soft-SAFT, which establishes a reliable molecular model for each molecule. Hence, an accurate density estimation is also a key requirement for a good calculation of the surface tension. Additionally, it is important to remark that the influence parameter c_{ij} has been fitted to the surface tension data. This is the main disadvantage of the DGT approach, although in some cases, the influence parameter can be transferred from some compounds to others or related to the molecular weight within the same family of compounds [15]. An accurate estimation of the influence parameter is very important to have reliable predictions of mixtures. In Fig. 2, the surface tension of a mixture between two hydrofluorocarbons (R134 + R32) has been predicted from the information obtained for each pure compound [22]. No mixture data has been used. As it can be seen, the predicted results are in very good agreement with the experimental data.

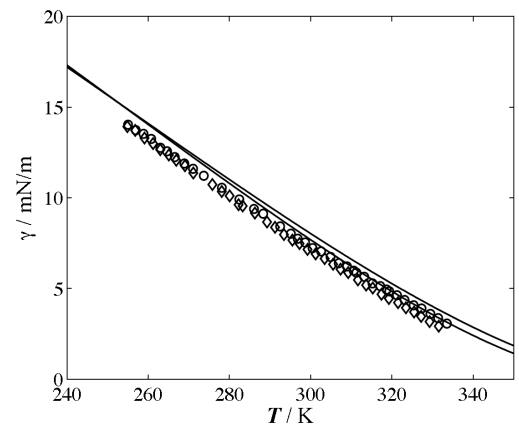


Fig. 2. Vapor-liquid interfacial tension of a R134 + R32 mixture at two different isopleths with a mass fraction of 0.4194 (Δ) and 0.6084 (\circ) of R32.

The DGT treatment is a very versatile treatment, not only limited to classical fluids but also applicable to novel fluids, such as ionic liquids. In Fig. 3, the surface tension of several ionic liquids from the $[C_n\text{mim}][\text{Tf}_2\text{N}]$ family have been calculated using the soft-SAFT + DGT treatment. The surface tension estimation of ionic liquids is particularly difficult, due to several reasons associated to their structure and thermophysical properties: Firstly, ionic liquids are characterized by a negligible vapour pressure. Secondly, as observed experimentally, the value of the interfacial tension decreases as the alkyl chain length of the cation increases, contrarily to the behaviour of other organic compounds. Finally, these compounds are exceptional in terms of interfacial phenomena, as they show an almost constant value when the alkyl chain length increases, as it happens for the $[C_n\text{mim}][\text{Tf}_2\text{N}]$ family beyond $[C_7\text{mim}][\text{Tf}_2\text{N}]$. All these particularities can be captured with DGT, and very good agreement is obtained between the experimental data and the theoretical calculations. Moreover, the fitted influence parameter can be correlated with the molecular weight (or number of carbons CN) following a parabolic function [23], allowing the prediction of other ionic liquids of the same family with a longer chain in the cation tail.

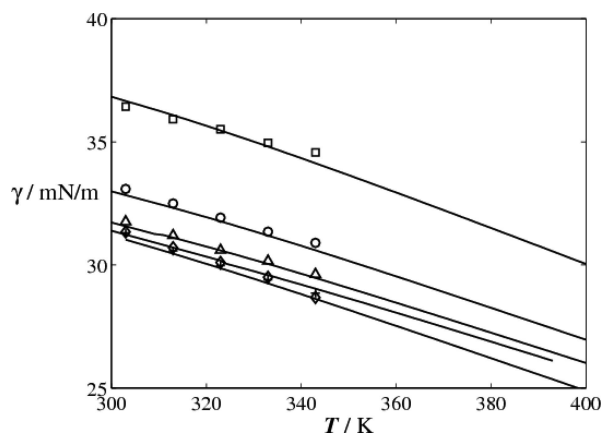


Fig. 3. Interfacial tensions for $[C_2\text{mim}][\text{Tf}_2\text{N}]$ (\square), $[C_4\text{mim}][\text{Tf}_2\text{N}]$ (\circ), $[C_6\text{mim}][\text{Tf}_2\text{N}]$ (Δ), $[C_8\text{mim}][\text{Tf}_2\text{N}]$ ($+$), and $[C_{10}\text{mim}][\text{Tf}_2\text{N}]$ (\diamond).

This is the expression obtained by fitting the ionic liquid members of the $[C_n\text{-mim}][\text{Tf}_2\text{N}]$ family with the alkyl chain length ranging from C_2 to C_8 .

$$10^{19} c_{\text{Tf}_2\text{N}} = 0.2233 CN^2 - 0.1872 CN + 15.275 [Jm^5 mol^{-2}] \quad (13)$$

This correlation allows obtaining the interfacial behaviour of heavier compounds of the series not included in the fitting procedure.

The surface tension is not the only property that can be evaluated through the use of DGT. Density profiles are a supporting tool that provide a lot of information on the mixture and cannot be obtained experimentally. For the case of mixtures, they allow explaining deviations from the ideal behaviour, due to the relative enrichment of one compound in the interface. In Fig. 4, an example of the density profile of a $[C_4\text{mim}][\text{NTf}_2] + [C_2\text{mim}][\text{NTf}_2]$ mixture. The dashed line corresponds to the $[C_4\text{mim}][\text{NTf}_2]$ density profile, who is adsorbed in the interface, reaching a maximum. However, this is not affecting the total density profile (solid line) of the mixture. As mentioned, this information can become crucial in order to understand the non-ideal behavior of some mixtures [24].

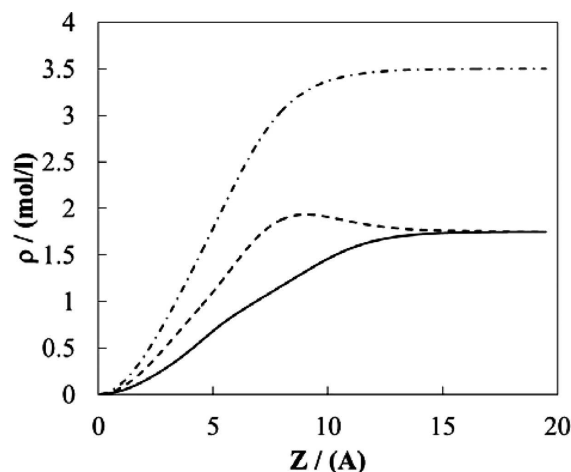


Fig. 4. Density profiles across the interface at 298.15 K for $[C_4\text{mim}][\text{NTf}_2] + [C_2\text{mim}][\text{NTf}_2]$.

Let us proceed to see some examples of the possibilities of the Density Functional Theory (DFT) methodology. As stated in the theory, this is a fully predictive approach, which can be particularly useful when experimental information is missing. The DFT theory has been coupled here with the SAFT-VR equation of state of Gil-Villegas and co-workers [25], another SAFT-type version that, in this case, uses a square-well potential to describe the interaction between the monomers of the system.

In Fig. 5 the interfacial tension of two amines is provided using SAFT-VR + DFT. The surface tension of monoethanolamine (MEA) is depicted in Fig. 4a and the one of 2-amino-1-propanol (AMP) is shown in Fig. 4b. In both cases, excellent agreement is achieved with the experimental data, although for the AMP case, only a limited range of data is available for comparison. As for the DGT case, the density at each point of the interface is taken from the SAFT-VR calculation, hence, a reliable estimation of this property is absolutely necessary for obtaining the right trends.

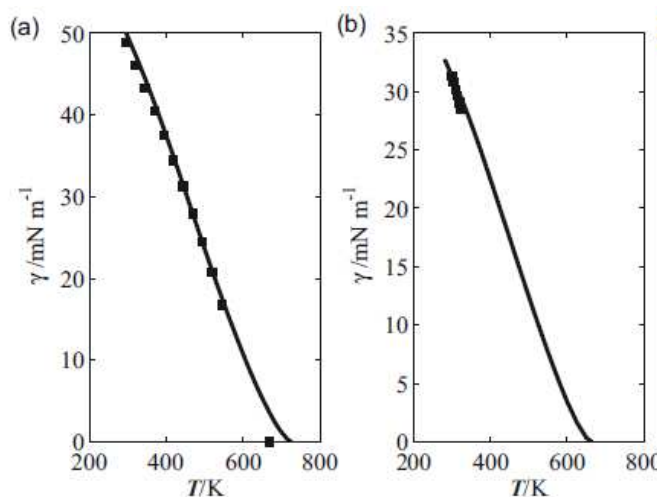


Fig. 5. Interfacial tensions for a) MEA b) AMP. More information is provided in reference [26].

The DFT treatment, as DGT, can also be applied to a wide variety of fluids and extended to mixtures. A very interesting field of application includes the carbon dioxide (CO_2) + hydrocarbon mixtures for enhanced oil recovery purposes. The $\text{CO}_2 + n$ -decane mixture is particularly relevant because it is seen as a reasonable first approximation of a crude oil

mixture. In Fig. 6 an example of the surface tension of this mixture is shown. The SAFT-VR DFT (solid lines) is found to provide good predictions of the surface tension of the mixture over the whole range of pressures [27]. As for the mixtures of *n*-alkanes, the use of the mean-field approximation (dashed lines) is seen to lead to lower values of the vapour–liquid interfacial tension (in comparison with those corresponding to the version of the functional incorporating the correlations), especially at low pressures.

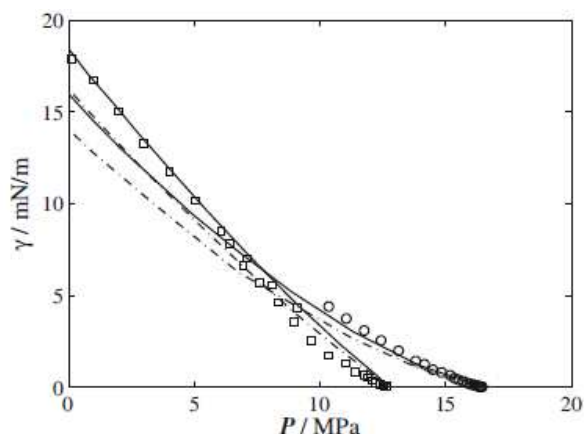


Fig. 6. Vapour-liquid interfacial tensions of a Carbon Dioxide + *n*-decane mixture at 344K (□) and 377K (○).

Another interesting ability of the DFT treatment is that it can be used to calculate either vapour-liquid (VL) or liquid-liquid (LL) interfacial tensions. In Fig. 7 the VL and LL interfacial tensions of a water + CO₂ mixture are modelled with SAFT-VR-DFT. Good agreement is found in a very wide range of temperatures and pressures, moving from one type of equilibrium to another. The methodology is able to capture the change from an equilibrium to another one using an only set of parameters and without mixture data [28].

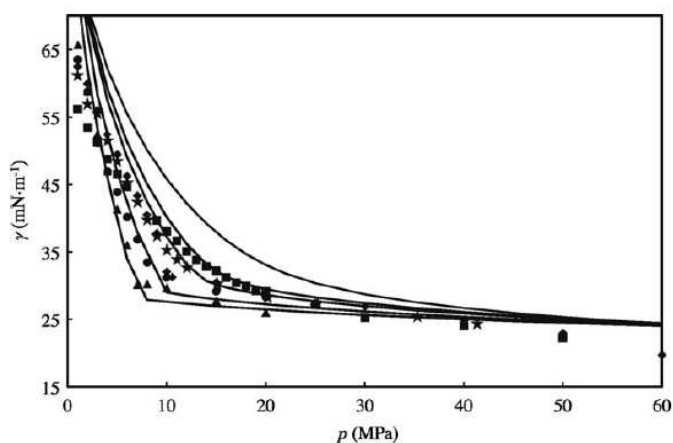


Fig. 7. Interfacial tension modelling and measurements of the (H₂O+CO₂) system as a function of pressure for different isotherms: (▲) at 297.9 K; (●) at 312.9 K; (◆) at 333.5 K; (x) at 343.3 K; (■) at 373.3 K.

CONCLUSIONS

A short review of different methodologies applied for the calculation of interfacial properties of fluid and fluid mixtures has been explored. In particular, the DGT and DFT treatments are highlighted based on their reliable physical background,

easiness of application and accuracy of results. These treatments have been coupled into SAFT-type equations of state to reproduce the surface tension of compounds of different molecular nature. Both approaches can accurately reproduce the surface tension of pure fluids and binary mixtures. The DGT approach requires the use of an additional parameter, the so-called influence parameter “*c*”, although it keeps an elevated degree of predictability for mixtures, with excellent agreement in the calculation of the surface tension of complex ionic liquid mixtures. On the other hand, the DFT approach is fully predictive and it is accurate enough to estimate aqueous and CO₂ mixtures in a semiquantitative way, although it is computationally more demanding and, as a consequence, more difficult to extend to multicomponent systems. Therefore, there are still some open questions for both approaches, like the use of the β binary parameter on DGT and the inclusion of the effect of capillary waves on DFT. In any case, they both offer a reliable path for an accurate estimation of the interface of a wide variety of compounds.

ACKNOWLEDGEMENTS

Some parts of these results were obtained during a postdoctoral stay at Imperial College London done by F. Llovel. He acknowledges G. Jackson, A. Galindo and F. J. Blas for allowing reproducing some of the results and conclusions about SAFT-VR + DFT approaches. Additionally, F. Llovel also acknowledges a TALENT fellowship (Catalan Government). Support from the Spanish Government (CENT SOST-CO₂, CEN-2008-1027), Carburis Metálicos and the Catalan Government (2009SGR-666) was also provided.

NOMENCLATURE

Symbol	Quantity	SI Unit
A	Helmholtz free energy	J/mol
a_0	Helmholtz free energy density	J/dm ³
γ	Surface tension	mN/m
c_{ij}	Influence parameter	J·m ⁵ /mol ²
ρ	Density	mol/dm ³
μ	Chemical Potential	J/mol
z	Distance from the interface	Å
β	Crossed influence parameter	Adim.
Ω	Grand Potential	J/mol
V	Volume	dm ³
T	Temperature	K
P	Pressure	MPa
g_{ij}	Pair radial distribution function	Adim.
k_B	Boltzmann constant	J / K
m	Chain length SAFT parameter	Adim.

REFERENCES

- [1] W. G. Chapman, K. E. Gubbins, G. Jackson, M. Radosz, New reference equation of state for associating liquids, *Ind. Eng. Chem. Res.*, vol. 29 pp.1709–1721, 1990.
- [2] M. S. Wertheim, Fluids with Highly Directional Attractive Forces. 1. Statistical Thermodynamics. *J. Stat. Phys.* vol. 35, pp.19-34, 1984.

- [3] M. S. Wertheim, Fluids with Highly Directional Attractive Forces. 2. Thermodynamic-Perturbation Theory and Integral-Equations. *J. Stat. Phys.* vol. 35, pp.35-47, 1984.
- [4] M. S. Wertheim, Fluids with Highly Directional Attractive Forces. 3. Multiple Attraction Sites. *J. Stat. Phys.* vol. 42, pp. 459-476, 1986.
- [5] D. B. Macleod, On a relation between surface tension and density. *Trans. Faraday Soc.*, vol. 19, pp. 38-41, 1923.
- [6] R. H. Fowler, A Tentative Statistical Theory of Macleod's Equation for Surface Tension, and the Parachor, *Proc. R. Soc. London, Ser. A*, vol. 159, pp. 229-246, 1937.
- [7] E. A. Guggenheim, The principle of corresponding states. *J. Chem. Phys.*, vol. 13, pp. 253-261, 1945.
- [8] Y. X. Zuo and E. H. Stendby, Corresponding-states and parachor models for the calculation of interfacial tensions, *Can. J. Chem. Eng.*, vol 75, 1130, 1997.
- [9] J.D. van der Waals, Thermodynamische Theorie der Kapillarität unter voraussetzung stetiger, Dichteänderung, *Zeitschrift für Physikalische Chemie-Leipzig*, vol. 13, pp. 657-725, 1894.
- [10] J.W. Cahn, J.E. Hilliard, Free energy of a non-uniform system. I: interfacial energy, *Journal of Chemical Physics*, vol. 28, pp. 258-266, 1958.
- [11] J. S. Rowlinson and B. Widom, *Molecular Theory of Capillarity*, Clarendon, Oxford, 1982.
- [12] R. Evans, "Density functionals in the theory of nonuniform fluids" *Fundamentals of Inhomogeneous Fluids*, Dekker, New York, 1992.
- [13] H. T. Davis, *Statistical Mechanics of Phases, Interfaces and Thin Films*, VCH, Weinheim, 1996.
- [14] C. I. Poser, I. C. Sanchez, Interfacial tension theory of low and high molecular weight liquid mixtures, *Macromolecules*, vol. 14, pp. 361-370, 1981.
- [15] O. Vilaseca, L.F. Vega, Direct calculation of interfacial properties of fluids close to the critical region by amolecular-based equation of state, *Fluid Phase Equilibria*, vol 306, pp. 4-14, 2011.
- [16] D.E. Sullivan, Statistical mechanics of a nonuniform fluid with long-range attractions, *Phys. Rev. A*, vol. 25 pp. 1669-1682, 1982.
- [17] F. Llovel, A. Galindo, F.J. Blas, G. Jackson, Classical density functional theory for the prediction of the surface tension and interfacial properties of fluids mixtures of chain molecules based on the statistical associating fluid theory for potentials of variable range, *J. Chem. Phys.* 133, 024704, 2010.
- [18] J. R. Henderson, *Statistical Mechanics of Spherical Interfaces in Fluid Interfacial Phenomena*, Wiley, New York, 1986.
- [19] J. Gross, A density functional theory for vapor-liquid interfaces using the PCP-SAFT equation of state, *J. Chem. Phys.* 131, 204705, 2009.
- [20] F.J. Blas, L.F. Vega, Thermodynamic behaviour of homonuclear and heteronuclear Lennard-Jones chains with association sites from simulation and theory, *Mol. Phys.* vol. 92, pp. 135-150, 1997.
- [21] NIST Chemistry Webbook; <http://webbook.nist.gov/chemistry>.
- [22] O. Vilaseca, F. Llovel, J. Yustos, R. M. Marcos, L. F. Vega. Phase equilibria, surface tensions and heat capacities of hydrofluorocarbons and their mixtures including the critical region. *J. Supercrit. Fluids*, 55 pp. 755-768, 2010.
- [23] F. Llovel, E. Valente, O. Vilaseca, L. F. Vega, Modeling Complex Associating Mixtures with [C_nmim][Tf₂N] Ionic Liquids: Predictions from the Soft-SAFT Equation. *J. Phys. Chem. B* vol. 115, pp. 4387-4398, 2011.
- [24] M. B. Oliveira, M. Domínguez-Pérez, M. G. Freire, F. Llovel, O. Cabeza, J. A. Lopes-da-Silva, L. F. Vega, J. A. P. Coutinho. Surface Tension of Binary Mixtures of 1-Alkyl-3-methylimidazolium Bis(trifluoromethylsulfonyl)-imide Ionic Liquids: Experimental Measurements and Soft-SAFT Modeling, *J. Phys. Chem. B*, 116, pp. 12133-12141, 2012.
- [25] A. Gil-Villegas, A. Galindo, P.J. Whitehead, S.J. Mills, G. Jackson, A.N. Burgess, Statistical associating fluid theory for chain molecules with attractive potentials of variable range, *J. Chem. Phys.*, vol. 106, pp. 4168-4186, 1998.
- [26] N. Mac Dowell, N. MacDowell, F. Llovel, C.S. Adjiman, G. Jackson, A. Galindo, Modelling the fluid phase behaviour of carbon dioxide in aqueous solutions of monoethanolamine using transferable parameters with the SAFT-VR approach, *Ind. Eng. Chem. Res.*, vol. 49, pp. 1883-1899, 2010.
- [27] F. Llovel, N. Mac Dowell, F. J. Blas, A. Galindo, G. Jackson, Application of the SAFT-VR density functional theory to the prediction of the interfacial properties of mixtures of relevance to reservoir engineering, *Fluid Phase Equilib.* vol 336, pp. 137-150, 2012.
- [28] A. Georgiadis, F. Llovel, A. Bismarck, F.J. Blas, A. Galindo, G. C. Maitland, J. P. M. Trusler, G. Jackson, Interfacial tension measurements and modelling of (carbon dioxide + n-alkane) and (carbon dioxide + water) binary mixtures at elevated pressures and temperatures, *J. Supercrit. Fluids* vol. 55, pp. 743-754, 2010.

PHASE FIELD MODELING OF MULTIPHASE SYSTEMS

Roberto Mauri

Department of Civil and Industrial Engineering,
Laboratory of Reactive Multiphase Flows,
Università di Pisa, 56126 Pisa, Italy.

EXTENDED ABSTRACT

Research on multiphase flows is very active, even if its beginning dates back in the 19th century, when Young, Laplace and Gauss developed the first theory of multiphase flow, assuming that different phases are separated by a sharp interface, that is a surface of zero thickness. At the end of the 19th century, though, another approach was proposed by Van der Waals [1], who assumed that interfaces have a non-zero thickness, i.e. they are "diffuse" over a region where the interfacial forces are smoothly distributed. Later, in 1901, Korteweg continued this work and proposed an expression for the capillary stresses, which are generally referred to as Korteweg stresses, showing that they reduce to surface tension when the region where density changes from one to the other equilibrium value shrinks on to a sharp interface (see review articles in [2]).

We can appreciate the importance of the phase field, or diffuse interface, method when we compare it to traditional multiphase flow modeling. In classical multiphase fluid mechanics, we assume that each phase is at chemical equilibrium (i.e. its density and composition correspond to their equilibrium value at the given pressure and temperature) and are separated from each other by a zero thickness interface, where appropriate boundary conditions are imposed. On the other hand, in the phase field method the interface consists of a transition zone between the phases, of finite thickness, where all the properties of the mixture vary continuously. Clearly, the classical model ceases to apply when the lengthscale of the phenomenon is comparable with the interface thickness, as it happens in the motion of contact lines along solid surfaces, in the breakup and coalescence of bubbles and droplets, and, of course, in multiphase flows in micro devices. Instead, the phase field approach remains valid in all these cases and therefore, in particular, can describe microfluidic phenomena, which the classical multiphase approach cannot model. In addition, because the composition of the mixture is a continuous function, no separate description of the time evolution of the sharp interface is required, thus avoiding mathematical complexities and numerical instabilities typical of interface tracking.

Perhaps the best-known example of phase field model is the Cahn-Hilliard equation [3], that is used for modeling the phase separation of binary alloys that are quenched into the unstable region of their phase diagram. Here, the relaxation of the order parameter (i.e. the mixture composition) is driven by local minimization of the free energy, subjected to phase field conservation and as a result, the interface layers do not deteriorate dynamically. Other applications for which phase field models are particularly well suited are structure formation and evolution in flow systems, an area of technological impact in soft materials processing. There, hydrodynamics can be introduced by coupling the convective Cahn-Hilliard equation of mass transport to a modified Navier-Stokes equation of momentum transport, that includes a phase field-dependent body force, which is generally referred to as Korteweg force. This latter is proportional to the chemical potential gradients and, accordingly, since at thermodynamic equilibrium the chemical potentials are uniform, it can be seen as a non-equilibrium body force that tends to restore chemical equilibrium. [4]

The main drawback of the phase field approach is that its characteristic length coincides, approximately, with the interface thickness. Accordingly, even introducing corrections (which however are rigorously correct only for regular mixtures) to increase the size of the computing domain, we can simulate volumes of, at most, one millimeter size. Therefore, we can simulate the whole domain only when we are dealing with microfluidic problems. Unfortunately, though, fully implicit numerical treatment of interfacial terms yields expensive schemes while explicit discretization quickly lead to numerical instability or impose impractical time-stepping constraints. Here, we would like to propose an efficient and robust numerical method for the coupled Cahn-Hilliard/Navier-Stokes system.

REFERENCES

- [1] J.D. Van der Waals, The Thermodynamic Theory of Capillarity under the Hypothesis of a Continuous Variation of Density, *Verhandel. Konink. Akad. Wetten. Amsterdam (Sect. 1)*, Vol. 1, No. 8, 1893; [English Translation: J.D. Rowlinson, *J. Stat. Phys.*, vol. 20, pp. 197-244, 1979.]
- [2] R. Mauri, Ed., *Multiphase Microfluidics: the Diffuse Interface Model*. CISM International Centre for Mechanical Sciences, vol. 538, Springer (2012).
- [3] J.W. Cahn and J.E. Hilliard, Free Energy of a Nonuniform System. I. Interfacial Free Energy, *J. Chem. Phys.*, vol. 28, pp. 258-266, 1958.
- [4] R. Mauri, *Non-Equilibrium Thermodynamics in Multiphase Flows*, Springer, 2013.

GRAND-CANONICAL FORMULATION OF PHASE-FIELD MODELS FOR ALLOY SOLIDIFICATION

Mathis Plapp*

*Physique de la Matière Condensée, École Polytechnique, CNRS, 91128 Palaiseau, France, E-mail: Mathis.Plapp@polytechnique.fr

EXTENDED ABSTRACT

The solidification of metallic alloys gives rise to the spontaneous formation of a large variety of different microstructures. This is a subject of fundamental interest as a well-controlled example of pattern formation, and of practical importance because of its applications in metallurgy [1]. These patterns arise from a subtle interplay between the destabilizing effects linked to the transport of heat and/or chemical constituents, and the stabilizing effect of interfacial properties such as capillarity and interface dissipation. In recent years, the phase-field technique has become the method of choice for the numerical modelling of solidification [2]. In its basic formulation, it can be obtained from Ginzburg-Landau free energy functionals through the standard phenomenological equations of out-of equilibrium thermodynamics that make use of variational principles. Its main advantage is that the explicit tracking of boundaries and interfaces is avoided by the introduction of scalar functions, the phase fields, which indicate the local state of matter and exhibit diffuse interfaces at phase boundaries. Moreover, this construction of the model implies that capillarity and interface dissipation are “automatically” contained in the equations.

For maximum computational efficiency, one would like to control independently the bulk and surface properties of the model. For alloy solidification, it can be shown that this is not the case in the formulations based on free-energy functionals [3; 4]. The basic underlying thermodynamic reason is that interface motion is controlled by the transport of an extensive quantity (chemical constituents), whereas interfacial equilibrium is controlled by the conjugate intensive quantities (the chemical potentials). Therefore, any model that describes the thermodynamics and transport phenomena in the bulk in terms of the extensive variables (compositions) makes the description of interface equilibrium (and the identification of the driving forces for interface motion) difficult. In contrast, a grand-canonical description in terms of the chemical potentials makes it easy to choose interpolation functions between the different phases that decouple bulk and interface properties [4]. In this formulation, the starting point is a grand-potential functional rather than a free-energy functional, and the dynamical variable is the local chemical potential. A complete analogy can be established between this formulation and the phase-field models for the solidification of a pure substance, which have traditionally used the temperature (the intensive quantity) as the dynamic variable. In this contribution, the formulation of the grand-canonical phase-field model for a binary alloy, its relation to the pure-substance model, and its extension to multi-component systems [5] will be discussed. Furthermore, a perspective for the construction of new phase-field models for other physical systems will be outlined.

REFERENCES

- [1] J. Dantzig and M. Rappaz, *Solidification*, EPFL Press, Lausanne, 2009.
- [2] W. J. Boettinger, J. A. Warren, C. Beckermann, and A. Karma, Phase-field simulation of solidification, *Annu. Rev. Mater. Res.*, vol. 32, pp. 163-194, 2002.
- [3] S. G. Kim, W. T. Kim, and T. Suzuki, Phase-field model for binary alloys, *Phys. Rev. E*, vol. 60, pp. 7186-7197, 1999.
- [4] M. Plapp, Unified derivation of phase-field models for alloy solidification from a grand-potential functional, *Phys. Rev. E*, vol. 84, art-no. 031601, 2011.
- [5] A. Choudhury and B. Nestler, Grand-potential formulation for multicomponent phase transformations combined with thin-interface asymptotics of the double-obstacle potential, *Phys. Rev. E*, vol. 85, art-no. 021602, 2012.

DYNAMICS OF COMPLEX FLUID-FLUID INTERFACES

Leonard M. C. Sagis*^o

*Food Physics Group, Wageningen University, Bomenweg 2, 6703 HD Wageningen, The Netherlands
^oPolymer Physics, Dept. of Materials, ETH Zurich, Wolfgang-Pauli-Str. 10, CH-8093 Zurich, Switzerland

EXTENDED ABSTRACT

Surface rheological properties like surface shear viscosities, or surface dilatational moduli often play an important role in the stability and dynamic behavior of emulsions, foam, biological fluids, liquid jets, coatings flows, or immiscible polymer blends [1]. This is particularly true when the interfaces in these systems have a complex microstructure, for example, when the surface active components stabilizing the interface form a 2d gel phase, a 2d glass phase, or 2d (liquid) crystalline phase. Such 2d mesophases are typically formed when interfaces are stabilized by colloidal particles, proteins, protein aggregates, protein-polymer complexes, or amphiphilic polymers [1]. Applied deformations induce changes in the microstructure of the interface, and the resulting changes in surface rheological properties (such as surface shear thinning, shear thickening, or thixotropic behavior) affect the behavior of the multiphase system on a macroscopic scale. Most currently available constitutive models for the surface extra stress tensor either do not account for the strain (rate) dependence of surface rheological properties, or are appropriate only for infinitesimally small rates, where departures from linear behavior are very small [1]. In this paper we will discuss recent advances in the development of nonlinear constitutive equations for the stress-deformation behavior of fluid-fluid interfaces in the framework of nonequilibrium thermodynamics. We will focus on two frameworks: the classical irreversible thermodynamics (CIT) framework, and the general-equation-for-the-nonequilibrium-reversible-irreversible-coupling (GENERIC) framework. We will illustrate the construction of surface rheological constitutive equations within these two frameworks for a specific example: interfaces stabilized by anisotropic colloidal particles, in the dilute particle concentration regime. In both frameworks we construct models describing the effect of microstructural changes on the nonlinear response of an interface to a deformation through a dependence of the surface stress tensor on a set of scalar and a tensorial structural variables. We present the time evolution equations for these structural variables, and evaluate the ability of these types of models to describe the shear thinning behavior typically observed experimentally for such interfaces. We compare the models in both simple and oscillatory shear. We find that both frameworks allow us to construct nonlinear expressions for the surface extra stress tensor capable of describing shear thinning behavior, but the CIT model gives realistic predictions only for small departures from equilibrium, whereas the GENERIC framework allows us to create models valid also far from equilibrium. Besides giving more accurate predictions for the shear thinning behavior the GENERIC model also predicts the existence of in-plane normal stresses (normal to the direction of flow), and effect of which its existence has been hypothesized, but that has so far not been observed experimentally. These results show that microstructural models developed using nonequilibrium thermodynamic frameworks provide a valuable tool for the analysis of the highly nonlinear dynamics of multiphase systems with complex liquid-liquid interfaces.

REFERENCES

- [1] L.M.C. Sagis, *Rev. Mod. Phys.* 83 (2011) 1367.

SURFACES AS NON-AUTONOMOUS THERMODYNAMIC SYSTEMS

Wilhelm Schneider

Institute of Fluid Mechanics and Heat Transfer
Vienna University of Technology
Resselgasse 3/2
1040 Vienna
Austria
wilhelm.schneider@tuwien.ac.at

ABSTRACT

To deal with negative surface heat capacities that are observed for many liquids, surfaces are treated as non-autonomous thermodynamic systems, i.e. together with the liquid that forms the surface. First, a few examples of lumped heat capacities are presented. Both quasistatic and non-static area changes of plane liquid films are considered. To provide a criterion for the applicability of the quasistatic limit, one-dimensional thermo-capillary waves in liquid films are investigated. Next, heat transfer at surfaces is considered. Various forms of the energy equation of surfaces are presented, non-dimensional parameters characterizing the relative importance of the surface heat capacity are defined, and a few applications are given. If the surface heat capacity is negative, a heat pulse supplied to the surface initially leads to a decrease of the surface temperature. Furthermore, negative surface heat capacities give rise to amplifications of small perturbations of the surface temperature. This physical instability may also cause numerical instabilities when solving heat conduction problems. Finally, the dependence of the surface tension on the radius of nano-droplets serves as a motivation for extending the relevant thermodynamic relations to systems with area-dependent surface tension. The implications for Kelvin's equation for the vapour pressure at small droplets are discussed.

INTRODUCTION

In classical thermodynamics, the surface of a chemically pure liquid is considered as a thermodynamic system, whose thermodynamic equilibrium state is uniquely given by the surface area, A , and the (absolute) temperature, T . The surface tension, σ , is then defined by the relation

$$d_e W = \sigma dA \quad (1)$$

for the work required to change the surface area by the infinitesimal amount dA in a quasistatic process. It is commonly assumed in classical thermodynamics that the surface tension is independent of A , i.e. a function of T only, with $\sigma = \sigma(T)$ representing the thermal equation of state of the surface. Furthermore, measurements as well as molecular models indicate that the value of the surface tension of common liquids is nearly independent of the surrounding gas, which may be a vapour or an inert gas.

The entropy, S_σ , of the surface is defined by Gibbs' fundamental equation

$$T dS_\sigma = dU_\sigma - \sigma dA \quad (2)$$

for a quasistatic process. Since the internal energy, U_σ , and the entropy, S_σ , are quantities of state, dU_σ and dS_σ have to satisfy the conditions for total differentials, leading to the following relation between the thermal and caloric quantities of state:

$$\left(\frac{\partial U_\sigma}{\partial A} \right)_T = u_\sigma = \sigma - T \frac{d\sigma}{dT}, \quad (3)$$

where u_σ is the internal energy of the unit surface area, while the heat capacity of the unit surface area, c_σ , is defined by the relation

$$\left(\frac{\partial U_\sigma}{\partial T} \right)_A = A c_\sigma. \quad (4)$$

Since σ is a function of T only, the same is true for u_σ and c_σ , i.e. $u_\sigma = u_\sigma(T)$ and $c_\sigma = c_\sigma(T)$, and from equations (3) and (4) one obtains

$$c_\sigma = \frac{du_\sigma}{dT} = -T \frac{d^2\sigma}{dT^2}. \quad (5)$$

Note that sometimes the temperature dependence of the surface tension is approximated by assuming $d\sigma/dT = \text{const}$. This, however, implies a vanishing surface heat capacity according to Eq.(5).

As u_σ is independent of A , Eq.(3) can easily be integrated. There appears an unknown function of T , which, however, must be a constant in order to be in accord with Eqs.(4) and (5). Thus $U_\sigma = A u_\sigma + \text{const}$, or

$$U_{\sigma 2} - U_{\sigma 1} = A_2 u_{\sigma 2} - A_1 u_{\sigma 1}. \quad (6)$$

Here, and in what follows, the subscripts 1 and 2 refer to an initial and a final state, respectively.

Making use of Eq.(3), Gibbs' fundamental equation, Eq.(2), gives

$$\left(\frac{\partial S_\sigma}{\partial A}\right)_T = -\frac{d\sigma}{dT}. \quad (7)$$

Introducing, finally, the entropy of the unit surface area, s_σ , according to $S_\sigma = As_\sigma$, gives

$$s_\sigma = -\frac{d\sigma}{dT} = \frac{u_\sigma - \sigma}{T}. \quad (8)$$

Note that the entropy of a surface can be responsible for the irreversibility of evaporation processes [1]. For instance, in order to completely evaporate a plane liquid film with surface area A under isothermal conditions, a supply of heat is required that is smaller than the evaporation enthalpy of the liquid by the amount Au_σ , cf. Eq.(3). The entropy change due to the disappearance of the surface, however, is not equal to $-Au_\sigma/T$, but only equal to $-As_\sigma = -A(u_\sigma - \sigma)/T$. The difference, which represents the work that is necessary to generate the surface in an isothermal process, indicates that the process of complete evaporation of a plane liquid film, being associated with the disappearance of the surface, is inherently irreversible. In most cases, however, it turns out that the entropy change due to the disappearance of the surface is very small in comparison with the entropy change due to the evaporation of the liquid. This justifies, in general, the idealization of a quasistatic isothermal evaporation process as a reversible process.

Since, according to the second law, the entropy is an extensive quantity of state, it follows from Eq.(7) that

$$\frac{d\sigma}{dT} < 0. \quad (9)$$

Note, however, that σ and u_σ vanish as the critical point is approached. From Eq.(3) it follows that $d\sigma/dT \rightarrow 0$ for $T \rightarrow T_c$, with T_c denoting the critical temperature.

While, according to Eq.(9), positive values of $d\sigma/dT$ are excluded as a consequence of the second law, the second law does not tell us anything about the sign of du_σ/dT or c_σ . A Carnot cycle, for instance, can be constructed for the surface as a thermodynamic system irrespective of the sign of c_σ . While the isothermal changes of state are characterized by $\sigma = \text{const}$, the isentropic changes of state satisfy the relation

$$dA = \frac{Ac_\sigma}{T} \left(\frac{d\sigma}{dT}\right)^{-1} dT, \quad (10)$$

which follows from Eqs. (2) to (4). Observing Eq.(9), one can see from Eq.(10) that the isentropic temperature increase in the Carnot cycle is associated with a decrease or increase of the surface area, depending on whether c_σ is positive or negative, and vice versa for the isentropic temperature decrease. But the thermal efficiency of the cycle is smaller than 1 in both cases, in accord with the second law.

In fact, positive as well as negative values of c_σ have been measured, and also calculated on the basis of molecular models, for various liquids in certain temperature regimes [1] [2] [3]. There is, however, a problem of stability. Let us assume that the thermodynamic equilibrium state (T, A) is perturbed by a small surface-area change, $\delta A > 0$. According to Eq.(10) together with Eq.(9), the system reacts with a temperature change $\delta T < 0$ and $\delta\sigma > 0$ if $c_\sigma > 0$. The increase of the surface tension will then lead to $dA < 0$, driving the surface back to the equilibrium state. The opposite is true in the case $c_\sigma < 0$, leading to the thermodynamic instability that is to be expected of any system with a negative heat capacity. Thus it is usually argued that the surface must not be considered as an "autonomous" system, but rather ought to be treated together with the liquid that forms the surface [4]. This, however, is sometimes easier said than done. The present contribution to the symposium is intended to provide a basis for the discussion of problems associated with considering the surface as a non-autonomous system. In accord with many applications, the discussion will be restricted to thermodynamic systems that consist of only one chemical substance, i.e. mixtures will not be considered, and phase transitions will not be taken into account in what follows.

LUMPED HEAT CAPACITIES

Isentropic film-area change

Consider a quasistatic, adiabatic, i.e. isentropic, change of the surface area, A , of a plane liquid film of constant mass, m . The liquid film is surrounded by an inert gas. The mass density of the liquid may be assumed constant, thereby allowing to neglect work due to volume changes. Accounting for the internal energy of the liquid with isochoric specific heat capacity c_v , one obtains in the same way as above the following relation [1]:

$$dA = \frac{mc_v + Ac_\sigma}{T} \left(\frac{d\sigma}{dT}\right)^{-1} dT. \quad (11)$$

Note that $mc_v + Ac_\sigma$ represents the "lumped" heat capacities of the two parts of the system, i.e. of the bulk liquid and the surface. As an approximation, lumped heat capacities are well known from the theory of heat transfer, but in the present case they result from the quasistatic limit, which implies thermal equilibrium between all parts of a system.

With $m = \rho\delta A/2$, where ρ is the mass density of the liquid and δ is the thickness of the film with two free surfaces, the condition for a positive lumped heat capacity, as required for stability reasons, becomes $\delta > -2c_\sigma/c_v\rho$. Estimates on the basis of known properties of various liquids, e.g. water (cf. [1], p. 94, and [5]) or argon (cf. [6], p. 12), show that a film thickness of the order of the size of molecules is sufficient to give a positive lumped heat capacity.

For film thicknesses that are much larger than the molecular size, Ac_σ may be neglected in comparison with mc_v , and upon integration one obtains from Eq.(11) the following relation between the area change $A_2 - A_1$ and the temperature change from T_1 to T_2 :

$$A_2 - A_1 = m \int_{T_1}^{T_2} \frac{c_v}{T} \left(\frac{d\sigma}{dT} \right)^{-1} dT, \quad (12)$$

or, using Eq.(3),

$$A_2 - A_1 = m \int_{T_1}^{T_2} c_v (\sigma - u_\sigma)^{-1} dT. \quad (13)$$

Equation (13) shows that the internal energy of the surface has to be taken into account, even if the heat capacity of the surface is negligible. This, perhaps surprising, result can be understood by considering the energy balance. As u_σ and σ are of the same order of magnitude, cf. Eq.(3), the contribution of the surface-energy change to the energy balance, i.e. $u_\sigma dA$, is of the same order of magnitude as the work performed by the surface tension, i.e. σdA .

Non-static film area change

Consider a plane liquid film that is stretched in a rectangular frame with a frictionless movable bar of length L forming one side of the frame. As before, the mass and the mass density of the film are assumed constant. In addition, the isochoric specific heat capacity, c_v , of the liquid is also assumed constant. In the initial state (surface area A_1 , temperature T_1) the film is in thermodynamic equilibrium. This implies that the force acting on the bar is $F_1 = 2L\sigma$. (The coefficient 2 is due to the fact that the film has two surfaces.) At a certain moment, the force acting on the bar suddenly changes to the value F_2 , which is then kept constant. Heat exchange with the surroundings may be neglected, i.e. the change of state is non-static, but adiabatic. The new state of thermodynamic equilibrium (surface area A_2 , temperature T_2) is to be determined [1].

Since thermodynamic equilibrium implies mechanical equilibrium, the surface tension in the final state is $\sigma_2 = F_2/2L$, and the temperature T_2 can be determined by inverting the thermal equation of state of the surface, i.e. $\sigma = \sigma(T)$. As the force acting on the system is constant, the work performed in the non-static process is

$$W_{12} = \sigma_2(A_2 - A_1), \quad (14)$$

and the energy balance, together with Eq.(6), gives

$$A_2 = [mc_v(T_1 - T_2) + A_1(u_{\sigma_1} - \sigma_2)] / (u_{\sigma_2} - \sigma_2). \quad (15)$$

Estimates for common liquids show that, with the exception of extremely thin films, the term with the coefficient A_1 in Eq.(15) is negligibly small, but the internal energy of the surface remains of importance via the term u_{σ_2} . As in the case of the isentropic process considered above, the negligible term is associated with the (positive or negative) surface heat capacity, as can be seen by making use of Eq.(3) and rewriting the term $(u_{\sigma_1} - \sigma_2)$ as

$$(u_{\sigma_1} - \sigma_2) = u_{\sigma_1} - u_{\sigma_2} - T_2(d\sigma/dT)_2, \quad (16)$$

with $u_{\sigma_1} - u_{\sigma_2} \approx c_{\sigma_1}(T_1 - T_2)$ for approximately constant surface heat capacity.

One-dimensional thermo-capillary waves

To justify the assumption of a quasistatic change of state, the rate of change of the surface area of the liquid film must be sufficiently small to allow the equalization of perturbations at any point in time. For the present treatment it suffices to consider a plane liquid film that is in thermodynamic equilibrium and at rest in the base state (subscript 0). Small perturbations of the film thickness, δ , and temperature, T , according to $\delta = \delta_0 + \varepsilon\delta_1$, $T = T_0 + \varepsilon T_1$, with $\varepsilon \ll 1$, are associated with small film velocities, εv_1 , in the direction of the longitudinal coordinate, x . Neglecting viscosity, the net force acting on a film element per length is $\partial\sigma/\partial x = \sigma'(T)\partial T/\partial x$, with $\sigma' = d\sigma/dT$. With regard to the energy balance, we assume local thermodynamic equilibrium and neglect heat transfer to the surroundings as well as heat conduction in the film in longitudinal direction. This allows us to apply Eq.(11), which describes quasistatic adiabatic changes of state. For unsteady one-dimensional flow of an incompressible liquid in a thin film, the linearized equations of continuity, momentum and energy can then be written as follows:

$$\frac{\partial\delta_1}{\partial t} + \delta_0 \frac{\partial v_1}{\partial x} = 0; \quad (17)$$

$$\rho\delta_0 \frac{\partial v_1}{\partial t} = \sigma'(T_0) \frac{\partial T_1}{\partial x}; \quad (18)$$

$$\frac{1}{T_0} \frac{\partial T_1}{\partial t} = - \frac{\sigma'(T_0)}{\rho\delta_0 c_v + c_\sigma} \frac{1}{\delta_0} \frac{\partial\delta_1}{\partial t}. \quad (19)$$

Eliminating δ_1 and v_1 from Eqs.(17)-(19), one obtains the linear wave equation

$$\frac{\partial^2 T_1}{\partial t^2} - C_0^2 \frac{\partial^2 T_1}{\partial x^2} = 0, \quad (20)$$

with

$$C_0^2 = \frac{T_0[\sigma'(T_0)]^2}{\rho\delta_0(\rho\delta_0 c_v + c_\sigma)}, \quad (21)$$

or

$$C_0 = -\sigma'(T_0) \sqrt{\frac{T_0}{\rho\delta_0(\rho\delta_0 c_v + c_\sigma)}}. \quad (22)$$

Since $\sigma'(T_0) < 0$ according to the second law, cf. above, the minus sign has been chosen for the square root in Eq. (22). C_0 can be identified as the wave speed, i.e. the propagation speed of small perturbations.

To justify the idealization of a quasistatic change of state of a film that is stretched in one direction, the wave speed must be much larger than the velocity of the film, i.e. $C_0 \gg v = \varepsilon v_1$. Note that the wave speed increases with

decreasing film thickness, δ_0 . The lumped heat capacity per surface area, $(\rho\delta_0c_v + c_\sigma)$, appears in the denominator on the right-hand side of Eq.(21). If the lumped heat capacity were negative, C_0^2 would be negative according to Eq.(21), and Eq.(20) would lose the character of a wave equation and become of elliptic type.

To give an idea about the orders of magnitude, a wave speed of about 1 m/s is obtained from Eq.(21) for a film of water at 300 K with a thickness of 50 nm.

HEAT TRANSFER AT SURFACES

Energy equation of a moving surface

If the energy balance of the surface is disregarded, as it is often done - though not always with sufficient justification - in problems of fluid mechanics and heat transfer, the temperature-dependent surface tension appears only in the momentum equation. Marangoni convection is a well-known example. In an attempt to clarify the effect of the internal energy, or the heat capacity, of the surface on the heat transfer at the surface, the energy balance of the surface is investigated in what follows. Local thermodynamic equilibrium will be assumed. It allows applying the relations given in the Introduction, locally and at any moment of time, as if any surface element or any volume element were in thermodynamic equilibrium. In particular, there is no temperature jump at the surface. In the interest of simplifying the presentation, the discussion will be restricted to one-dimensional motion of the surface, but the generalization to more dimensions will be obvious, cf. also the survey [7].

Consider a surface element of length dx , with x being the tangential coordinate at the surface, while the coordinate normal to the surface is denoted by z . The surface element is assumed to be fixed in space. The liquid is assumed to be surrounded by an inert gas, i.e. condensation and evaporation are disregarded. For a liquid that moves with the tangential velocity component v_x in x -direction, the energy balance of the surface may be written as

$$\frac{\partial u_\sigma}{\partial t} + \frac{\partial(v_x u_\sigma)}{\partial x} = \frac{\partial(v_x \sigma)}{\partial x} + [\dot{q}]_\pm - v_x [\tau]_\pm, \quad (23)$$

where \dot{q} is the heat flux in z -direction, τ is the shear stress at one side of the surface, and the symbol $[]_\pm$ stands for the difference across the surface ("jump" at the surface). The terms in Eq.(23) have the following physical meaning (in this order, from left to right): Rate of change of internal energy; net convective flux of internal energy; net work done by the surface tension due to moving the surface into, and out of, the surface element; net heat flux; net work done by the shear stresses at both sides of the surface.

Equation (23) may be re-written in various ways. A rather nice formulation is obtained by introducing the surface heat capacity according to Eq.(5), and, furthermore, the surface enthalpy (per surface area), h_σ , according to

$$h_\sigma = u_\sigma - \sigma = Ts_\sigma = -T d\sigma/dT. \quad (24)$$

Making then use of the force balance at the surface, i.e.

$$[\tau]_\pm = \frac{\partial \sigma}{\partial x}, \quad (25)$$

one finally obtains that at the surface the following boundary condition has to be satisfied:

$$\begin{aligned} c_\sigma \left(\frac{\partial T}{\partial t} + v_x \frac{\partial T}{\partial x} \right) &= -h_\sigma \frac{\partial v_x}{\partial x} + [\dot{q}]_\pm \\ &= -h_\sigma \frac{\partial v_x}{\partial x} - \left[k \frac{\partial T}{\partial z} \right]_\pm, \end{aligned} \quad (26)$$

where k is the thermal conductivity of the fluid on the respective side of the surface.

To check the analysis for self-consistency, Eq.(26) is applied to the quasistatic adiabatic, i.e. isentropic, change of the area of a plane surface in a rectangular frame with the bar on one side moving in x -direction. With $T = T(t)$ and $[\dot{q}]_\pm = 0$, Eq.(26) shows that the velocity is a linear function of x , which gives $v_x = (x/A) dA/dt$. With $h_\sigma = -T d\sigma/dT$ according to Eq.(24), one obtains from Eq.(26) the isentropic relation, Eq.(10).

Equation (26) shows that a material (substantial) time derivative of the surface temperature is, in general, associated with a jump in the normal component of the heat flux at the surface. For steady flow, the effects of the surface energy on the heat flux jump are characterized by the following two non-dimensional parameters:

$$N_1 = |c_\sigma^*| v_x^* / k^*; \quad (27)$$

$$N_2 = h_\sigma^* v_x^* / k^* T^*, \quad (28)$$

where $*$ denotes reference quantities. In the case of time-dependent processes, there is the additional non-dimensional parameter

$$N_3 = |c_\sigma^*| L^* / k^* t^*, \quad (29)$$

defined in terms of a characteristic length, L^* , and a characteristic time, t^* . If N_1 and N_2 are either irrelevant (liquid at rest) or much smaller than 1, and if, in addition, N_3 is either irrelevant (stationary state, steady flow) or much smaller than 1, the heat flux jump at the surface is negligible as far as the bulk of the liquid is concerned. In a very thin boundary layer at the surface, however, the solution may be substantially affected by the small heat flux jump. To give an example, the following problem is considered.

Heat pulse at surface

Consider the horizontal surface of a semi-infinite body of liquid. The liquid is at rest. In the initial state ($t=0$) the temperature of the liquid is independent of the downward-pointing vertical coordinate, z , i.e. $T = T_0 = \text{const}$. In the time interval $0 < t < t_e$ a constant heat flux \dot{q}_0 is supplied from the surroundings to the surface, e.g. by radiative heat transfer. Afterwards, the surface is adiabatic. Assuming constant thermal conductivity, k , it is convenient to formulate the

problem in terms of the heat flux, $\dot{q} = -k \partial T / \partial z$, as the dependent variable. The heat diffusion equation gives

$$\frac{\partial \dot{q}}{\partial t} = \alpha \frac{\partial^2 \dot{q}}{\partial z^2}, \quad (30)$$

where α is the thermal diffusivity, which is assumed to be constant, like all other material properties of the liquid. Equation (30) is to be solved subject to the initial condition

$$\dot{q} = 0 \quad \text{for } t = 0, z > 0, \quad (31)$$

and the boundary conditions

$$\dot{q} = 0 \quad \text{for } z \rightarrow \infty, \quad (32)$$

$$\dot{q} - l \frac{\partial \dot{q}}{\partial z} = \dot{q}_0 \quad \text{for } z = 0, 0 < t < t_e, \quad (33)$$

$$\dot{q} - l \frac{\partial \dot{q}}{\partial z} = 0 \quad \text{for } z = 0, t > t_e, \quad (34)$$

with the parameter l defined by

$$l = c_\sigma / \rho c_p, \quad (35)$$

where c_p is the isobaric specific heat capacity of the liquid. The parameter l has the physical dimension of a length, but, depending on the value of c_σ , it may be positive, zero or negative. Based on available data [1]-[3], [5],[6], $|l|$ is of the order of nanometers. Note that the second term on the left-hand sides of Eqs.(33) and (34), which follow from Eq.(26) with $v_x \equiv 0$ and the heat diffusion equation in terms of T , represents the heat-flux jump at the surface due to the surface heat capacity.

As it happens, the solution of the heat diffusion equation with initial and boundary conditions of the form of Eqs.(31)-(34) is given in [8], §2.8, case (i), though the problem is a different one. In the present notation the solution reads

$$\frac{\dot{q}}{\dot{q}_0} = G(z, t) \quad \text{for } 0 < t < t_e; \quad (36)$$

$$\frac{\dot{q}}{\dot{q}_0} = G(z, t) - G(z, t - t_e) \quad \text{for } t > t_e. \quad (37)$$

with

$$G(z, t) = \operatorname{erfc} \left(\frac{z}{2\sqrt{\alpha t}} \right) - \exp \left(\frac{z}{l} + \frac{\alpha t}{l^2} \right) \operatorname{erfc} \left(\frac{z}{2\sqrt{\alpha t}} + \frac{\sqrt{\alpha t}}{l} \right). \quad (38)$$

Of particular interest is, of course, the surface temperature, T_σ . With the solution according to Eqs.(36)-(38), one obtains from Eq.(26) the following differential equations for T_σ :

$$\frac{dT_\sigma}{dt} = (\dot{q}_0 / c_\sigma) G_0(t) \quad \text{for } 0 < t < t_e; \quad (39)$$

$$\frac{dT_\sigma}{dt} = (\dot{q}_0 / c_\sigma) [G_0(t) - G_0(t - t_e)] \quad \text{for } t > t_e, \quad (40)$$

with

$$G_0(t) = \exp \left(\frac{\alpha t}{l^2} \right) \operatorname{erfc} \left(\frac{\sqrt{\alpha t}}{l} \right). \quad (41)$$

A plot of the function G_0 can be found in [9], Fig. 7.1.

Equations (39)-(41) can easily be integrated numerically, but a qualitative discussion of the solution suffices for the present purpose. First of all, the influence of the surface heat transfer is remarkable. If $c_\sigma < 0$, the heat supply at the surface gives rise to a decrease of the surface temperature for times of the order of $t^* = l^2 / \alpha$. For $c_\sigma > 0$, $t/t^* \rightarrow \infty$, however, Eq.(39) gives

$$\frac{dT_\sigma}{dt} \sim \frac{\dot{q}_0}{\rho c_p \sqrt{\pi \alpha t}}, \quad (42)$$

i.e. the surface temperature changes in the classical manner as if there were no surface heat capacity. Since l is very small, cf. above, the time scale t^* is also very small, but well within the range of presently available pulsed lasers. Thus one could envision the application of picosecond lasers to reduce the surface temperature step by step. The analysis may be based on Duhamel's theorem, but cannot be given here.

Associated with the decrease of the surface temperature is, of course, a decrease of the temperature in the liquid near the surface. It follows from the solution for the heat flux, i.e. Eq.(36) together with Eq.(38), that the decrease is restricted to a boundary layer whose thickness is as small as $|l|$. For $z/|l| \rightarrow \infty$ the classical result, represented by the first term on the right-hand side of Eq.(38), is obtained even for times as small as t^* .

Instability due to negative surface heat capacity

When heat is supplied locally to a surface with negative heat capacity, the surface temperature will decrease, at least initially, in the region of heat supply. The temperature gradient in the liquid will then give rise to a heat flow from the bulk of the liquid to the surface, thereby enhancing the decrease of the surface temperature. Obviously, this effect may lead to an instability of the initial state. The following linear perturbation analysis is intended to provide a quantitative description of the instability. For non-linear phenomena far from thermodynamic equilibrium cf. [4].

As in preceding section, a semi-infinite body of liquid with horizontal surface is considered. However, it is now assumed that there is no heat transfer from the surroundings to the surface. Furthermore, it is assumed that the temperature in the liquid may depend not only on the vertical coordinate, z , but also on the horizontal coordinate, x . Thermo-convective motion of the liquid will be neglected in the energy balance, which, therefore, reduces to the heat diffusion equation

$$\frac{\partial T}{\partial t} = \alpha \left(\frac{\partial^2 T}{\partial x^2} + \frac{\partial^2 T}{\partial z^2} \right), \quad (43)$$

with the boundary conditions

$$c_\sigma \frac{\partial T}{\partial t} = k \frac{\partial T}{\partial z} \quad \text{for } z = 0; \quad (44)$$

$$T = T_\infty = \text{const} \quad \text{for } z \rightarrow \infty. \quad (45)$$

Of interest is now the evolution of spatially periodic perturbations of the thermodynamic equilibrium state, which is characterized by the uniform temperature $T = T_\infty$. Thus solutions of the form

$$(T - T_\infty)/T_\infty = f(z) \exp(\beta t + i\kappa x) \quad (46)$$

are sought, with the amplification rate, β , and the wave number, κ , being taken as real numbers. Of course, the wave number is always positive, whereas the amplification rate may be positive (amplified perturbations), zero (stationary perturbations), or negative (damped perturbations).

Eq.(46) satisfies the heat diffusion equation, Eq.(43), together with the boundary condition at infinity, Eq.(45), if

$$f = \exp\left(-\sqrt{\kappa^2 + \beta/\alpha} z\right), \quad (47)$$

while the boundary condition at the surface, Eq.(44), gives

$$\beta = \frac{\alpha}{2l^2} \left(1 \pm \sqrt{1 + 4K^2} \right), \quad \begin{array}{l} + \text{ for } K < 0, \\ - \text{ for } K > 0, \end{array} \quad (48)$$

with the non-dimensional wave number

$$K = l\kappa = c_\sigma \kappa / \rho c_p \quad (49)$$

and the parameter l according to Eq.(35). For $K = 0$, i.e. the surface heat capacity not taken into account, the classical result $\beta = -\alpha\kappa$ is obtained, of course. But note that Eq.(48) gives the classical result in the limit $K \rightarrow 0+$, whereas the solution diverges as $K \rightarrow 0-$ for a fixed value of l .

Equation (47) shows that the penetration depth of the perturbations is of the order of δ , with

$$\delta = (\kappa^2 + \beta/\alpha)^{-1/2}, \quad (50)$$

or

$$\delta = 2|l| \left(\pm 1 + \sqrt{1 + 4K^2} \right)^{-1}, \quad \begin{array}{l} + \text{ for } K < 0, \\ - \text{ for } K > 0. \end{array} \quad (51)$$

Equations (48) and (51) allow the following conclusions with regard to the stability of the state of thermodynamic equilibrium of the system consisting of the liquid and the surface. If the surface heat capacity is negative, K is also negative, while β is positive, i.e. the perturbations increase with time, and the state of thermodynamic equilibrium is unstable. However, the perturbations are confined to a

boundary layer, whose thickness is of the order of $|l|$, i.e. nanometers for common liquids, cf. above. In the case of amplified perturbations, the maximum value $\delta_{\max} = |l|$ of the penetration depth is obtained for $K \rightarrow 0-$, i.e. in the limit of long waves in the scale of $|l|$. For fixed values of c_σ , with $c_\sigma < 0$, the amplification rate attains the minimum value $\beta_{\min} = \alpha/l^2$ in this long-wave limit. In the limit of very short waves, on the other hand, $\delta/|l| \sim 1/(-K) \rightarrow 0$ and $\beta \sim |K| \alpha/l^2 = \kappa\alpha/|l|$ as $K \rightarrow -\infty$.

As the unstable perturbations are confined to a very thin layer near the surface, the physical relevance may be seen as rather limited. For numerical solutions of heat transfer problems, however, the instabilities may cause severe problems, in particular, when high resolution is desirable, or required, for small systems. It may be necessary to introduce a boundary layer at the surface in order to deal properly with the (numerical) stability problem.

NANO-DROPLETS: AREA-DEPENDENT SURFACE TENSION

It has been observed that the surface tension of very small droplets depends not only on the temperature, but also on the radius of the droplet, cf. [10], pp. 112 and 126-130, and [11], [12]. For constant temperature, the surface tension decreases, in general, with decreasing droplet radius. In view of recent discussions on the applicability of macroscopic thermodynamics to nano-droplets [13], it is investigated in what follows whether, and perhaps how, the dependence of the surface tension on the radius affects the classical thermodynamic relations given in the Introduction. As the surface tension is then no longer only a local quantity of the surface, but also depends on properties of the bulk of the liquid, this is another example of considering the surface as a non-autonomous system.

For the present purpose it is convenient to introduce the surface area instead of the droplet radius as an independent variable. Thus the thermal equation of state of the surface is formally written as

$$\sigma = \sigma(T, A). \quad (52)$$

Gibbs' fundamental equation, Eq.(2), remains valid, of course, but in Eq.(3) the ordinary derivative is to be replaced by the partial derivative to obtain

$$\left(\frac{\partial U_\sigma}{\partial A} \right)_T = u_\sigma = \sigma - T \left(\frac{\partial \sigma}{\partial T} \right)_A, \quad (53)$$

with $u_\sigma = u_\sigma(T, A)$. Similarly, Eq.(4) remains valid as the definition of the surface heat capacity, but Eq.(5) is to be replaced by

$$c_\sigma + A \frac{\partial c_\sigma}{\partial A} = \frac{\partial u_\sigma}{\partial T} = -T \frac{\partial^2 \sigma}{\partial T^2}, \quad (54)$$

with $c_\sigma = c_\sigma(T, A)$.

The entropy of the unit surface, s_σ , is defined as

$$s_\sigma = \left(\frac{\partial S_\sigma}{\partial A} \right)_T. \quad (55)$$

Based on this definition, the classical relation Eq.(8) is re-obtained, apart from the partial derivative instead of the ordinary one, i.e.

$$s_\sigma = - \left(\frac{\partial \sigma}{\partial T} \right)_A = \frac{u_\sigma - \sigma}{T}. \quad (56)$$

In addition, the classical relation

$$\left(\frac{\partial S_\sigma}{\partial T} \right)_A = \frac{1}{T} \left(\frac{\partial U_\sigma}{\partial T} \right)_A = \frac{Ac_\sigma}{T} \quad (57)$$

is also re-obtained from Eq.(3).

There are further thermodynamic relations that follow from Gibbs' fundamental equation together with the integrability conditions for the differentials of quantities of state. In particular, one re-obtains the classical "potential" relations for the surface internal energy, U_σ , and the surface free energy, $F_\sigma = U_\sigma - TS_\sigma$, i.e.

$$\left(\frac{\partial U_\sigma}{\partial S} \right)_A = T ; \quad \left(\frac{\partial U_\sigma}{\partial A} \right)_S = \sigma ; \quad (58)$$

and

$$\left(\frac{\partial F_\sigma}{\partial T} \right)_A = -S_\sigma ; \quad \left(\frac{\partial F_\sigma}{\partial A} \right)_T = \sigma , \quad (59)$$

as well as Maxwell's relations

$$\left(\frac{\partial S_\sigma}{\partial A} \right)_T = - \left(\frac{\partial \sigma}{\partial T} \right)_A ; \quad (60)$$

$$\left(\frac{\partial T}{\partial A} \right)_S = \left(\frac{\partial \sigma}{\partial S_\sigma} \right)_A. \quad (61)$$

$()_S$ indicates a partial derivative with S_σ kept constant.

Based on the thermodynamic relations given above, the problem of the vapour pressure, p_v , at a small droplet in thermodynamic equilibrium can be re-considered, e.g. following [14], §22. To be consistent, the surface area of the droplet, A , is related to the mole number, n , of the droplet according to the relation $dA/dn = 4\tilde{V}_l/d$, where \tilde{V}_l is the molar volume of the liquid, and d is the droplet diameter. It turns out that the classical result, i.e. the famous Kelvin equation

$$\ln \frac{p_v}{p_s} = \frac{4\sigma}{d} \frac{\tilde{V}_l}{\tilde{R}T}, \quad (62)$$

is re-obtained, with \tilde{R} as the universal (molar) gas constant, and p_s as the saturation pressure at a plane surface. This is not in accord, however, with the results of molecular

simulations for droplets with diameters of the order of a few nanometers, cf. [10], p. 127, although Laplace's equation

$$p_l - p_v = 4\sigma/d, \quad (63)$$

which follows from mechanical equilibrium, has been found to be in good agreement ([10], pp. 112 and 126). Preliminary investigations by the present author seem to indicate that the assumption of constant density of the liquid, which is – often implicitly – made in deriving Kelvin's equation, may be the reason for the discrepancies, but a further discussion of that question is beyond the scope of the present paper.

CONCLUSIONS

Treating surfaces as non-autonomous thermodynamic systems leads to interesting and sometimes strange results. The change of state of a liquid film that is sufficiently thin to allow neglecting the – possibly negative – surface heat capacity is, nevertheless, affected by the internal energy of the surface. Short pulses of heat supplied to a surface with negative surface heat capacity give rise to a decrease of the surface temperature and of the temperature in a boundary layer of liquid near the surface. For the case of no heat supply from the surroundings, thermal instabilities in the boundary layer are predicted for negative surface heat capacities. It is true that the boundary layers are of the order of nanometers, i.e. of the molecular size, for common liquids, but the macroscopic description of nano-systems has recently found much interest, cf. [15] for an example. Furthermore, numerical solutions of the macroscopic equations of fluid mechanics and heat transfer may face difficulties associated with those instabilities.

As far as the dependence of surface tension on the radius of nano-droplets is concerned, treating the surface as a non-autonomous system, but retaining the other assumptions, has not lead to a generalization of Kelvin's equation for the vapour pressure. Thus other generalizations, in particular accounting for the compressibility of the liquid, are desirable.

ACKNOWLEDGMENTS

The author is indebted to Mr C. Buchner and Dr R. Jurisits for providing valuable references to other authors' work on surface heat capacities. Furthermore, Dr R. Jurisits performed numerical evaluations that have been of much help for a better understanding of the analytical solutions. Financial support by Androsch International Consulting Ges.m.b.H, Vienna, is also gratefully acknowledged.

NOMENCLATURE

Symbol	Quantity	SI Unit
A	Surface area	m^2
c_p	Isobaric specific heat capacity	J/kgK
c_v	Isochoric specific heat capacity	J/kgK
c_σ	Surface heat capacity	J/m ² K
d	Droplet diameter	m
f	Auxiliary function	-
F	Force	N
F_σ	Free energy of surface	J
G	Auxiliary function	-

h_σ	Enthalpy of unit surface area	J/m ²
i	Imaginary unit	-
k	Thermal conductivity	W/mK
L	Length	m
l	Parameter, see Eq.(35)	m
m	Mass	kg
n	Mole number	mole/m ³
p	Pressure	N/m ²
\dot{q}	Heat flux	W/m ²
\tilde{R}	Universal gas constant	J/mole K
S_σ	Surface entropy	J/K
s_σ	Entropy of unit surface area	J/Km ²
T	Absolute temperature	K
T_c	Critical temperature	K
t	Time	s
U_σ	Internal energy of surface	J
u_σ	Internal energy of unit surface area	J/m ²
\tilde{V}	Molar volume	m ³ /mole
v	Velocity of liquid or surface	m/s
W	Work	J
x, z	Spatial coordinates	m

Greek symbols

α	Thermal diffusivity	m ² /s
β	Amplification rate	1/s
δ	Thickness of liquid film, or penetration depth	m
κ	Wave number	1/m
ρ	Mass density	kg/m ³
σ	Surface tension	N/m
τ	Shear stress	N/m ²

Subscripts

e	End of time interval
l	Liquid
v	Vapour
s	Saturation
x	Component in x -direction
0	Base state, or at surface
1	Initial state, or perturbation
2	Final state
σ	Surface
∞	At infinity

Superscript

* Reference quantity

Other symbol

[]_± Difference across surface

REFERENCES

- [1] W. Schneider, S. Haas und K. Ponweiser, Repetitorium Thermodynamik, 3. Aufl., Oldenbourg-Verlag, München, 2012.
- [2] J.D. Lewins, Plane Surface Tension, *Int. J. Mech. Eng. Edu.*, vol. 27, pp. 217-229, 1997.
- [3] D.E. Goldsack and L.J. Paquette, On the Correlation of the Excess Surface Heat Capacity and the Surface Molar Volume of Liquids, *Can. J. Chem.*, vol. 67, pp. 2201-2205, 1989.
- [4] R. Defay, I. Prigogine and A. Sanfeld, Surface Thermodynamics, *J. Coll. Interface Sci.*, vol. 58, pp. 498-510, 1977.
- [5] L. Haar et al., NBS/NRC Wasserdampfatafeln, Springer-Verlag, Berlin, 1988.
- [6] J.S. Rowlinson and B. Widom, *Molecular Theory of Capillarity*, Clarendon Press, Oxford, 1984.
- [7] L.G. Napolitano, Thermodynamics and Dynamics of Surface Phases, *Acta Astronautica*, vol. 6, pp. 1093-1112, 1979.
- [8] H.C. Carslaw and J.C. Jaeger, *Conduction of Heat in Solids*, 2nd Ed., Oxford University Press, Oxford, 1946. Reprinted, Clarendon Press, Oxford, 2011.
- [9] M. Abramowitz and I.A. Stegun, *Handbook of Mathematical Functions*, Dover Publications, New York, 1972.
- [10] S. Fujikawa, T. Yano and M. Watanabe, *Vapor-Liquid Interfaces, Bubbles and Droplets*, Springer-Verlag, Berlin Heidelberg, 2011.
- [11] J. Julin et al., A Thermodynamically Consistent Determination of Surface Tension of Small Lennard-Jones Clusters From Simulation and Theory, *J. Chem. Phys.*, vol. 133, pp.044704-1 – 044704-6, 2010.
- [12] Y.-Q. Xue et al., The Effect of Microdroplet Size on the Surface Tension and Tolman Length, *J. Phys. Chem. B*, vol. 115, pp. 109-112, 2011.
- [13] G.V. Kharlamov et al., About Applicability of Thermodynamic Parameters to Small Drops and Clusters, *J. Phys.: Conf. Series*, vol. 393, pp. 012006/1-4, 2012.
- [14] R. Becker, *Theorie der Wärme*, Springer-Verlag, Berlin Heidelberg New York, 1966.
- [15] A. Lervik, F. Bresme and S. Kjelstrup, Heat Transfer in Soft Nanoscale Interfaces: The Influence of Interface Curvature, *Soft Matter*, vol. 5, pp. 2407-2414, 2009.

PANEL G

**EQUILIBRIUM AND NON-EQUILIBRIUM
THERMODYNAMICS OF SMALL SYSTEMS,
MULTISCALE METHODS, AND ENERGY
HARVESTING FROM FLUCTUATIONS**

MOLECULAR DYNAMICS SIMULATION OF CARBON NANO-BINDERS INTO ZEOLITE THERMAL STORAGE

Matteo Fasano*^o, Masoud Bozorg Bigdeli*, Mohammad Rasool Vaziri Sereshk*, Eliodoro Chiavazzo*^{oo}, Pietro Asinari*

* Multi-Scale Modeling Laboratory (SMaLL - www.polito.it/small), Energy Department, Politecnico di Torino, Corso Duca degli Abruzzi, 10129 Torino, Italy

^{oo} Chemical and Biological Engineering Department, Princeton University, Princeton, NJ, USA

^o Department of Translational Imaging, The Methodist Hospital Research Institute, Houston, Texas, USA

EXTENDED ABSTRACT

In recent years, engineering nanostructures (nanowires, nanolayers and nanotubes) have attracted great attention in the development of new materials. Successful application of nanostructures requires better understanding of the emergence of normal as well as anomalous irreversible transport in such systems. Most of the times, some scales are not sufficiently well separated from the microscopic scales and, differently from the macroscopic scales, are reminiscent of the underlying reversible dynamics. Sorting out emergent continuum properties is extremely challenging. In this work, we will focus on carbon nano-binders into zeolite thermal storage as a remarkable example of such trend.

Scientists from the Fraunhofer Institute for Interfacial Engineering and Biotechnology, together with ZeoSys GmbH, have developed very recently a new type of thermal storage system [1]. This new system can store three to four times the amount of heat that water can. Moreover, it is able to store the heat loss-free over lengthy periods of time, almost indefinitely. The new system contains zeolite pellets and the key challenge is (a) to ensure optimal heat transfer (high conductivity) through the zeolite bunch during the thermal loading and (b) to ensure water percolation during the thermal release, in the same device. Recently, at Massachusetts Institute of Technology (USA), prof. Evelyn Wang is investigating carbon nano-binders (CNT, graphene and oxide graphene) surrounding the zeolite pellets, in order to meet such extreme requirements.

In the present work, we develop a simulation plan based on molecular dynamics (MD) [2] to find out the optimal functionalization of the carbon binders and the optimal density of the covalent bonds in order to build the binder matrix. The key idea is to minimize the Kapitza contact resistance between binder elements. Moreover, hybrid solutions consisting of different nano-structures (e.g. CNT and graphene) will be discussed. The most promising solutions are investigated with the aim to guide the further steps in the experimental activity.

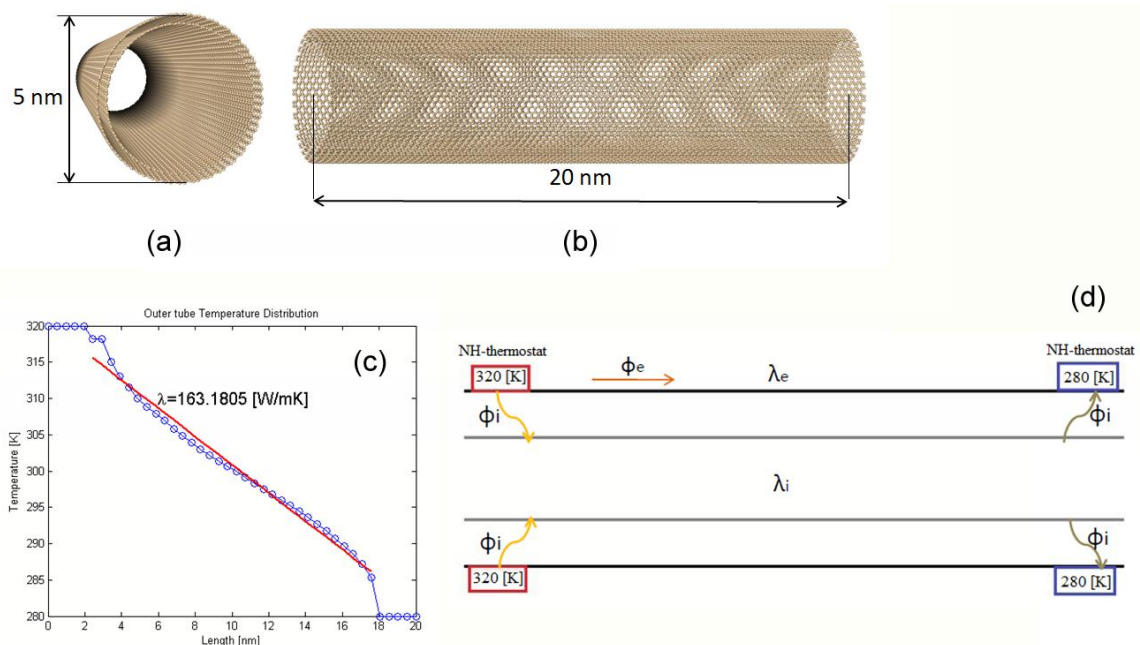


Figure 1: (a-b) Double-Walled Carbon Nano Tube (DWCNT) with chirality (33,33) and (37,37) respectively. (c) Measuring thermal conductivity by MD. (d) Schematic of the thermal power splitting between the concentric nanotubes.

REFERENCES

- [1] Fraunhofer, Research News, Issue 06, Topic 3, 2012.
- [2] D.C. Rapaport, The art of molecular dynamics simulation, Cambridge University Press, 2004.

NANOTHERMODYNAMICS: SMALL-SYSTEM THERMODYNAMICS APPLIED TO LARGE SYSTEMS*

Ralph V. Chamberlin

Department of Physics, Arizona State University, Tempe, AZ 85287-1504, USA

EXTENDED ABSTRACT

Standard thermodynamics was developed to describe homogeneous changes in large systems, but now it is known that the primary response of most materials comes from a heterogeneous distribution of independently-relaxing nanometer-sized regions. Nanothermodynamics provides a foundation for understanding finite-size thermal effects inside bulk materials [1,2]. A key feature is the subdivision potential, which is added to the fundamental equation of thermodynamics. The subdivision potential can be understood by comparison to the chemical potential. The chemical potential is the change in energy to take a single particle from a bath of particles into the system, whereas the subdivision potential is the change in energy to take a cluster of interacting particles from a bath of clusters into the system, and in general N interacting particles do not have the same energy as N isolated particles. Thus, the subdivision potential facilitates the treatment of non-extensive and nonlinear contributions to energy, thereby allowing a system to adjust its internal dynamics to find the true thermal equilibrium. We have applied the ideas of nanothermodynamics to standard theoretical models and found improved agreement with measured response, including: non-exponential relaxation, non-Arrhenius activation, and non-classical critical scaling in liquids, glasses, polymers and crystals [3-5].

Nanothermodynamics is based on the assumption that entropy is extensive and additive for independent subsystems of all sizes, whereas most computer simulations of small systems show non-extensive entropy. We study computer simulations of Ising-like models with binary spins that can be up, or down. (Similar statistics applies to binary alloys with sites that can be occupied by atom A, or B; a lattice gas of sites that can be occupied, or empty; or ideal-gas particles in a box that can be on the left side, or right.) Simulations of the standard Ising model using the usual Metropolis algorithm show that the change in entropy more than doubles when one identical subsystem is added to another, similar to the $M \ln(N)$ term that gives Gibbs' paradox when combining identical systems of distinguishable particles. Thus, for the heterogeneous primary response of most materials, either the Boltzmann definition of statistical entropy must be modified, or the Metropolis algorithm is incomplete. The Metropolis algorithm is based on the Boltzmann factor, which requires the usual assumptions of the canonical ensemble [6,7]: the system must be able to borrow an unlimited amount of energy from an effectively infinite heat bath, the system and its bath must be in weak thermal contact without direct interaction, the heat bath must contain a smooth distribution of closely-spaced energies, and units of energy in the system and bath must be uncorrelated. In other words, adding one unit of energy to the system must not change the likelihood of adding a second unit. We investigate nonlinear corrections to the Boltzmann factor that come from the local entropy [8], similar to the Gaussian-fluctuation term first used by Einstein in 1910 to describe critical opalescence.

We have found a nonlinear correction to the Boltzmann factor that makes computer simulations of the Ising model consistent with the concepts of nanothermodynamics. This nonlinear correction comes from the configurational entropy of a local bath, which can be understood by comparison to temperature that comes from the thermal entropy of a heat bath. Specifically, at low temperatures where the heat bath has low entropy, the heat bath is unlikely to allow large increases in energy of the system. Similarly, if the local bath is highly aligned so that it has low entropy, the local bath is unlikely to allow large changes in configuration of the system. Thus, the local bath acts as a reservoir of configurational entropy (e.g angular momentum), similar to how the heat bath acts as a reservoir of thermal entropy. Perhaps the local bath is one way to add conservation of momentum to the laws of thermodynamics. In any case, the nonlinear correction to Boltzmann's factor ensures conservation of energy and maximum entropy during normal thermal fluctuations. Furthermore, the nonlinear correction improves agreement between Monte-Carlo simulations of the Ising model and the measured critical scaling in ferromagnetic materials and fluids, the measured specific heat in imperfect crystals, and the structural correlations found near the Jahn-Teller distortion in LaMnO_3 [9]. Moreover, the nonlinear correction yields particles that are statistically indistinguishable, thereby avoiding Gibbs' paradox in computer simulations of classical particles.

*This research supported by the Army Research Office (W911NF-11-1-0419)

REFERENCES

- [1] T.L. Hill, Perspective: Nanothermodynamics, *Nano Lett.* **1**, pp. 111-112, 2001.
- [2] T.L. Hill, A different approach to nanothermodynamics, *Nano Lett.* **1**, pp. 273-275, 2001.
- [3] R.V. Chamberlin, Mesoscopic mean-field theory for supercooled liquids and the glass transition, *Phys. Rev. Lett.* **82**, pp. 2520-2523, 1999.
- [4] R.V. Chamberlin, Mean-field cluster model for the critical behaviour of ferromagnets, *Nature* **408**, pp. 337-339, 2000.
- [5] M.R.H. Javaheri and R.V. Chamberlin, A free-energy landscape picture and Landau theory for the dynamics of disordered materials, *J. Chem. Phys.* **125**, 154503 pp. 1-6, 2006.
- [6] R.P. Feynman, *Statistical Mechanics*, Perseus Books, Reading, MA, pp. 1-9, 1998.
- [7] R.V. Chamberlin, J.V. Vermaas, and G.H. Wolf, Beyond the Boltzmann factor for corrections to scaling in ferromagnetic materials and critical fluids, *Eur. Phys. J. B* **71**, pp. 1-6, 2009.
- [8] R.V. Chamberlin and G.H. Wolf, Fluctuation-theory constraint for extensive entropy in Monte Carlo simulations, *Eur. Phys. J. B* **67**, pp. 495-499, 2009.
- [9] R.V. Chamberlin, Monte Carlo simulations including energy from an entropic force, *Physica A* **391**, pp. 5384-5391, 2012.

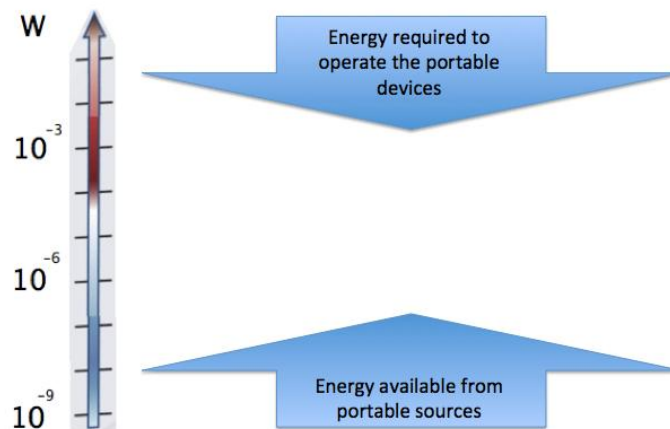
ENERGY HARVESTING AT MICRO AND NANOSCALE

Luca Gammaitoni

*NiPS Laboratory, Dipartimento di Fisica, Università di Perugia and INFN Perugia
I-06123 Perugia (IT)
Luca.gammaitoni@nipslab.org

EXTENDED ABSTRACT

It is a common understanding that ICT is the key engine of growth in modern society. Most importantly ICT is becoming strategic to improve energy efficiency by managing energy demand and use. The energy consumption and carbon dioxide emission from the expanding ICT use, however, is unsustainable. New methods are required to make ICT technology more energy efficient but also the development of new self-powered, energy-harvesting technologies that would enable micro- and nano-scale systems that consume ZEROPOWER through the harvesting of waste energy from the environment are required. Such technologies provide an opportunity for Europe to lead and generate significant economic benefit whilst simultaneously addressing climate change, healthcare and manufacturing efficiency benefits. Developing ZEROPOWER energy harvesting technology will be key for Europe to meet many of the Europe 2020 targets [1].



In this talk we will briefly address the two sides of the ICT-Energy problem: the decrease of energy dissipation in present ICT devices and the increase of energy efficiency in harvesting technologies [2]. We need to solve these two problems in order to bridge the gap between energy demand and energy request in mobile ICT devices. Both tasks require advances on the very same scientific topic: the management of energy transformation processes at nanoscale.

Ambient energy harvesting has been in recent years the recurring object of a number of research efforts aimed at providing an autonomous solution to the powering of small-scale electronic devices. Among the different solutions, micro scale vibration energy harvesting has played a major role due to the almost universal presence of mechanical vibrations mainly in the form of random fluctuations, i.e. noise. In this talk we specifically focus our attention to the possibility to harvest them by employing nonlinear dynamical systems[3, 4]. We will show that nonlinear vibration harvesters can beat linear vibration harvesters. The reason is twofold: on one side nonlinear harvesters can collect energy that is widely spread over the frequency spectrum (a typical condition of random vibrations available at micro and nano scales) with more efficiency compared to linear harvesters that can collect only in a narrow band around their resonance frequency. On the other side nonlinear harvesters can harvest energy in the low frequency part of the spectrum where usually most of the energy is, while linear harvesters can hardly be built with resonance frequency in the low frequency part due to mechanical constraints.

REFERENCES

- [1] ZEROPOWER Strategic Research Agenda, Nanoenergy Letters, 4, p.6, 2012
- [2] L. Gammaitoni, There's plenty of energy at the bottom (micro and nano scale nonlinear noise harvesting), Contemporary Physics, 53, 2, p. 119-135, 2012
- [3] F. Cottone, H. Vocca, and L. Gammaitoni, Nonlinear energy harvesting, Phys. Rev. Lett. 102 (2009), 080601
- [4] L. Gammaitoni, I. Neri, and H. Vocca, The benefits of noise and nonlinearity: extracting energy from random vibrations, Chem. Phys. 375 (2010), pp. 435-438.

THE FLUCTUATION THEOREM FOR CURRENTS AND NONEQUILIBRIUM THERMODYNAMICS

Pierre Gaspard

Center for Nonlinear Phenomena and Complex Systems,
Université Libre de Bruxelles,
Code Postal 231, Campus Plaine,
B-1050 Brussels, Belgium,
E-mail: gaspard@ulb.ac.be

ABSTRACT

Recently, remarkable results have been discovered for transport across small open systems in contact with reservoirs at different temperatures and chemical potentials. These results are deduced from the fluctuation theorem for the currents flowing across the system. A direct corollary of the fluctuation theorem is that the entropy production is non negative in agreement with the second law of thermodynamics. The fluctuation theorem has further corollaries, in particular, the Onsager reciprocity relations and the Green-Kubo formulas, as well as their extensions to the nonlinear response regime. These results find applications in physical, chemical, and biological systems at the microscale and the nanoscale. Their implications have been studied in transmembrane ion channels, molecular motors, effusion processes, chemical reactions, quantum electronic transport, among other systems.

1 INTRODUCTION

During the last decades, important advances have been carried out in our understanding of the thermodynamic properties of small nonequilibrium systems. Remarkable relationships, called fluctuation theorems [1; 2; 3; 4], have been established for the fluctuating currents flowing across open systems. These relationships find their origin in the microreversibility of the underlying Hamiltonian classical or quantum dynamics of the atoms and electrons composing matter. Yet, these relationships are associated with nonequilibrium conditions that break the time-reversal symmetry at the statistical level of description and they are in agreement with the second law of thermodynamics, according to which the entropy production is always non negative. These advances allow us to understand with unprecedented clarity the connections between the microscopic mechanical motion of atoms and electrons and the macroscopic thermodynamic properties of the global system. Moreover, the new relationships remain valid far from equilibrium. In this regard, the consequences of microreversibility can be investigated not only close to equilibrium, but also farther away from equilibrium in regimes where nonlinear response properties manifest themselves. In this way, generalizations of the Green-Kubo formulae and the Onsager reciprocity relations have been discovered among the nonlinear response coefficients.

These results apply to small nonequilibrium systems studied in nanosciences, such as transmembrane ion channels, molecular motors, chemical reactions, or mesoscopic electronic devices. The nanoscale starts just above the size of the atoms and smallest molecules that compose matter. Typically, the movement of atoms and molecules – although ruled by Hamiltonian dynamics – is at the origin of thermal and molecular fluctuations, which are inherent to the discrete atomic structure of matter. Therefore, the currents of electrons, atoms, or molecules flowing across nanosystems are fluctuating, which

requires a statistical description in terms of probability theory. Since nanosystems acquire their function if they are driven out of equilibrium, the new results play a central role to understand and characterize quantitatively the properties of their function and, in particular, the thermodynamic efficiency of energy transduction that they can perform.

The purpose of the present paper is to give an overview of these recent advances. Emphasis is given to the fluctuation theorem for currents, which is well founded because the currents are defined at the microscopic mechanical level of description. This fluctuation theorem is shown to imply the non-negativity of the thermodynamic entropy production in accordance with the second law. Further implications about nonlinear response are also presented. Nowadays, the current fluctuation theorem has been applied to several small systems and some of them have been investigated experimentally. Moreover, relations characterizing the nonequilibrium breaking of time-reversal symmetry in path statistics are also reviewed in the perspective they give to understand the thermodynamics of information processing at the molecular scale.

The plan of this paper is the following. The fluctuation theorem for currents and its consequences are presented in Section 2. Its applications are described in Section 3. In Section 4, further results are given about path statistics and the thermodynamics of information in copolymerization processes. Conclusions are drawn in Section 5.

2 THE FLUCTUATION THEOREM FOR CURRENTS AND ITS CONSEQUENCES

2.1 The multivariate fluctuation relation

Currents of particles or energy may flow across an open system in contact with several reservoirs at different temperatures and chemical potentials (see Fig. 1). The system is at equi-

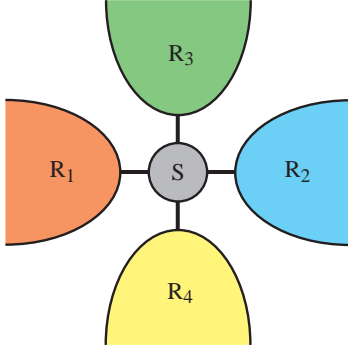


Figure 1. Schematic representation of an open system S in contact with the four reservoirs R_1 , R_2 , R_3 , and R_4 .

librium if the temperature and the chemical potentials are uniform in all the reservoirs. Otherwise, the global system is out of equilibrium and a nonequilibrium steady state may establish itself after some transient behavior. At the macroscale, the steady state is characterized by the average values of the currents across the open system. These currents depend on the thermodynamic forces or affinities \mathbf{A} including

$$\text{the thermal affinities: } A_{i0} = \frac{1}{k_B T_r} - \frac{1}{k_B T_i}, \quad (1)$$

$$\text{the chemical affinities: } A_{ip} = \frac{\mu_{ip}}{k_B T_i} - \frac{\mu_{rp}}{k_B T_r}, \quad (2)$$

between the reservoirs $i = 1, 2, \dots, r-1$ at the temperatures $\{T_i\}$ and the chemical potentials $\{\mu_{ip}\}$ for the different particle species $p = 1, 2, \dots, s$ and the reference reservoir $i = r$ [5; 6; 7]. k_B is Boltzmann's constant. The nonequilibrium conditions are thus fixed by $(r-1)(s+1)$ different affinities. All these affinities are vanishing at equilibrium.

At the mesoscale, the currents are fluctuating and their statistical properties are described by a stationary probability distribution if the system is in a steady state. The random variables of interest are the quantities of matter and energy $\Delta\mathbf{Q} = \{\Delta Q_\alpha\}$ that are transferred between the reservoirs during a time interval $[0, t]$. There are as many such quantities as there are affinities. The fluctuating currents are thus defined as $\mathbf{J} = \Delta\mathbf{Q}/t$. If $P_{\mathbf{A}}$ denotes the probability distribution describing the steady state corresponding to the affinities \mathbf{A} , the fluctuation relation for the currents reads

$$\frac{P_{\mathbf{A}}(\mathbf{J})}{P_{\mathbf{A}}(-\mathbf{J})} \simeq_{t \rightarrow \infty} \exp(\mathbf{A} \cdot \mathbf{J}t). \quad (3)$$

This theorem has been established for Markovian stochastic processes using graph theory [8]. Equation (3) compares the opposite fluctuations of the currents. At equilibrium where $\mathbf{A} = 0$, we recover the principle of detailed balancing, according to which opposite fluctuations are equiprobable. Out of equilibrium, the fluctuation relation (3) shows that opposite fluctuations no longer have equal probabilities. Since the ratio of probabilities is increasing or decreasing with time, one of both fluctuations dominates over the opposite and a directionality appears in the open system. Accordingly, the principle of detailed balance is no longer satisfied by the probability distribution $P_{\mathbf{A}}$, which breaks the time-reversal symmetry under nonequilibrium conditions $\mathbf{A} \neq 0$. Nevertheless, the fluctuation relation remains

compatible with the time-reversal symmetry because the ratio of the probabilities is inverted if the sign of the affinities or the currents is changed, which expresses the fact that the directionality is reversed together with the nonequilibrium conditions.

2.2 Consequences for the entropy production and the thermodynamic efficiencies

The fluctuation relation (3) implies that the entropy production, which is given by the sum of the affinities multiplied by the average values of the fluctuating currents, is always non negative:

$$\frac{1}{k_B} \frac{d_i S}{dt} = \mathbf{A} \cdot \langle \mathbf{J} \rangle_{\mathbf{A}} \geq 0. \quad (4)$$

This inequality can be proved by writing

$$\mathbf{A} \cdot \langle \mathbf{J} \rangle_{\mathbf{A}} = \lim_{t \rightarrow \infty} \frac{1}{t} \int d\mathbf{J} P_{\mathbf{A}}(\mathbf{J}) \ln \frac{P_{\mathbf{A}}(\mathbf{J})}{P_{\mathbf{A}}(-\mathbf{J})} \geq 0 \quad (5)$$

because the Kullback-Leibler divergence between the distributions $P_{\mathbf{A}}(\mathbf{J})$ and $P_{\mathbf{A}}(-\mathbf{J})$ is always non negative. Another way to obtain the non-negativity of the entropy production is by using Jensen's inequality $\langle e^X \rangle \geq e^{\langle X \rangle}$ with $X = -\mathbf{A} \cdot \mathbf{J}t$ and the statistical average $\langle \cdot \rangle_{\mathbf{A}}$ and by noting that $\langle e^X \rangle \simeq 1$ as the consequence of the fluctuation relation (3) in the long-time limit.

In order to drive a particular current $\langle J_\gamma \rangle_{\mathbf{A}}$ in the direction opposite to its associated affinity A_γ by using the other currents, energy should be supplied and the second law determines a limit to the efficiency of energy transduction. In this case, $A_\gamma \langle J_\gamma \rangle_{\mathbf{A}} < 0$ and a thermodynamic efficiency can be defined according to

$$0 \leq \eta \equiv -\frac{A_\gamma \langle J_\gamma \rangle_{\mathbf{A}}}{\sum_{\alpha \neq \gamma} A_\alpha \langle J_\alpha \rangle_{\mathbf{A}}} \leq 1. \quad (6)$$

Since the fluctuation relation (3) implies the non-negativity of the entropy production (4), it also implies that this efficiency cannot reach values larger than unity.

Since the currents are random, the question arises whether it is possible to guess the direction of the affinities \mathbf{A} imposed by the reservoirs from the observation of some current fluctuation \mathbf{J} . Bayesian inference gives the likelihood of the hypotheses that the observed current fluctuation \mathbf{J} goes either forward (+) or backward (-) with respect to the direction \mathbf{A} as [9; 10]

$$P(+|\mathbf{J}) = \frac{1}{1 + \frac{P(-)P(\mathbf{J}|-)}{P(+)P(\mathbf{J}|+)}}. \quad (7)$$

Tossing a fair coin on either hypothesis amounts to take $P(+) = P(-) = \frac{1}{2}$, while $P(\mathbf{J}|\pm) = P_{\mathbf{A}}(\pm\mathbf{J})$. According to the fluctuation relation (3), the likelihood that the observed current fluctuation \mathbf{J} indeed goes forward with respect to the direction of the affinities \mathbf{A} is thus given by

$$P(+|\mathbf{J}) \simeq \frac{1}{1 + \exp(-\mathbf{A} \cdot \mathbf{J}t)} \xrightarrow{t \rightarrow +\infty} \theta(\mathbf{A} \cdot \mathbf{J}) \quad (8)$$

where $\theta(x)$ is Heaviside's function. In the limit of a long positive time, the likelihood reaches the unit probability that

$\mathbf{A} \cdot \mathbf{J} \geq 0$, if the system is out of equilibrium with $\mathbf{A} \neq 0$. If the affinities vanish $\mathbf{A} = 0$, the likelihood remains at the value $P(+|\mathbf{J}) \simeq \frac{1}{2}$, which confirms the absence of directionality at equilibrium. The reasoning is compatible with the overall time-reversal symmetry because a similar result holds in the limit $t \rightarrow -\infty$ for $\mathbf{A} \cdot \mathbf{J}$ replaced by $-\mathbf{A} \cdot \mathbf{J}$. A further remark is that the characteristic time taken by the likelihood (8) to approach asymptotically the unit probability is estimated as the inverse of the entropy production in units of Boltzmann's constant: $\Delta t = (\mathbf{A} \cdot \langle \mathbf{J} \rangle_{\mathbf{A}})^{-1} = \left(\frac{1}{k_B} \frac{d_i S}{dt} \right)^{-1}$. This characteristic time becomes tiny if the system is macroscopic and driven far from equilibrium by increasing the affinities \mathbf{A} . We also notice that the observation of the current fluctuation \mathbf{J} in the frame defined by the reservoirs together with the knowledge of their affinities \mathbf{A} provides the answer to the question without having to guess it [11; 12].

2.3 Consequences for the response properties

An alternative expression of the fluctuation relation (3) can be obtained in terms of the generating function of the statistical cumulants defined as

$$Q_{\mathbf{A}}(\boldsymbol{\lambda}) \equiv \lim_{t \rightarrow \infty} -\frac{1}{t} \ln \int P_{\mathbf{A}}(\mathbf{J}) e^{-\boldsymbol{\lambda} \cdot \mathbf{J} t} d\mathbf{J} \quad (9)$$

where $\boldsymbol{\lambda}$ are the so-called counting parameters. The average values of the currents, their diffusivities, as well as their higher cumulants are given by taking the successive derivatives of this generating function with respect to the counting parameters:

$$\langle J_{\alpha} \rangle_{\mathbf{A}} = \left. \frac{\partial Q_{\mathbf{A}}}{\partial \lambda_{\alpha}} \right|_{\boldsymbol{\lambda}=0}, \quad (10)$$

$$D_{\alpha\beta}(\mathbf{A}) = -\left. \frac{1}{2} \frac{\partial^2 Q_{\mathbf{A}}}{\partial \lambda_{\alpha} \partial \lambda_{\beta}} \right|_{\boldsymbol{\lambda}=0}, \quad (11)$$

$$C_{\alpha\beta\gamma}(\mathbf{A}) = \left. \frac{\partial^3 Q_{\mathbf{A}}}{\partial \lambda_{\alpha} \partial \lambda_{\beta} \partial \lambda_{\gamma}} \right|_{\boldsymbol{\lambda}=0}, \quad (12)$$

$$B_{\alpha\beta\gamma\delta}(\mathbf{A}) = -\left. \frac{1}{2} \frac{\partial^4 Q}{\partial \lambda_{\alpha} \partial \lambda_{\beta} \partial \lambda_{\gamma} \partial \lambda_{\delta}} \right|_{\boldsymbol{\lambda}=0}, \quad (13)$$

⋮

On the other hand, the average value of a current can be expanded in powers of the affinities as

$$\langle J_{\alpha} \rangle_{\mathbf{A}} = \sum_{\beta} L_{\alpha,\beta} A_{\beta} + \frac{1}{2} \sum_{\beta,\gamma} M_{\alpha,\beta\gamma} A_{\beta} A_{\gamma} + \frac{1}{6} \sum_{\beta,\gamma,\delta} N_{\alpha,\beta\gamma\delta} A_{\beta} A_{\gamma} A_{\delta} + \dots \quad (14)$$

which defines the linear and nonlinear response coefficients:

$$L_{\alpha,\beta} = \left. \frac{\partial^2 Q_{\mathbf{A}}}{\partial \lambda_{\alpha} \partial A_{\beta}} \right|_{\boldsymbol{\lambda}=\mathbf{A}=0}, \quad (15)$$

$$M_{\alpha,\beta\gamma} = \left. \frac{\partial^3 Q_{\mathbf{A}}}{\partial \lambda_{\alpha} \partial A_{\beta} \partial A_{\gamma}} \right|_{\boldsymbol{\lambda}=\mathbf{A}=0}, \quad (16)$$

$$N_{\alpha,\beta\gamma\delta} = \left. \frac{\partial^4 Q_{\mathbf{A}}}{\partial \lambda_{\alpha} \partial A_{\beta} \partial A_{\gamma} \partial A_{\delta}} \right|_{\boldsymbol{\lambda}=\mathbf{A}=0}, \quad (17)$$

⋮

Remarkably, these properties are interrelated as the consequences of the fluctuation theorem (3), as the following reasoning shows. Inserting the fluctuation relation (3) in the definition (9) of the cumulant generating function yields the symmetry relation

$$Q_{\mathbf{A}}(\boldsymbol{\lambda}) = Q_{\mathbf{A}}(\mathbf{A} - \boldsymbol{\lambda}). \quad (18)$$

Taking successive derivatives of this relation with respect to the counting parameters and the affinities, the cumulants (11), (12), (13), ... and the response coefficients (15), (16), (17), ... are found to be interrelated.

Using second derivatives, the symmetry relation (18) implies the Green-Kubo formulas and the Onsager reciprocity relations for the linear response coefficients:

$$L_{\alpha,\beta} = D_{\alpha\beta}(0), \quad (19)$$

$$L_{\alpha,\beta} = L_{\beta,\alpha}. \quad (20)$$

With higher derivatives, generalizations of these relations to the higher cumulants and the nonlinear response coefficients can be deduced [13; 14; 15]. In particular, the nonlinear response coefficients (16) are related to the diffusivities (11) according to

$$M_{\alpha,\beta\gamma} = \left(\frac{\partial D_{\alpha\beta}}{\partial A_{\gamma}} + \frac{\partial D_{\alpha\gamma}}{\partial A_{\beta}} \right)_{\mathbf{A}=0}, \quad (21)$$

$$N_{\alpha,\beta\gamma\delta} = \left(\frac{\partial^2 D_{\alpha\beta}}{\partial A_{\gamma} \partial A_{\delta}} + \frac{\partial^2 D_{\alpha\gamma}}{\partial A_{\beta} \partial A_{\delta}} + \frac{\partial^2 D_{\alpha\delta}}{\partial A_{\beta} \partial A_{\gamma}} - \frac{1}{2} B_{\alpha\beta\gamma\delta} \right)_{\mathbf{A}=0}, \quad (22)$$

⋮

which are generalizations of the Green-Kubo formulas. A generalization of Onsager reciprocity relations is given by the total symmetry of the following fourth-order tensor:

$$N_{\alpha,\beta\gamma\delta} - \left(\frac{\partial^2 D_{\alpha\beta}}{\partial A_{\gamma} \partial A_{\delta}} + \frac{\partial^2 D_{\alpha\gamma}}{\partial A_{\beta} \partial A_{\delta}} + \frac{\partial^2 D_{\alpha\delta}}{\partial A_{\beta} \partial A_{\gamma}} \right)_{\mathbf{A}=0}, \quad (23)$$

which is the consequence of Eq. (22) and the total symmetry of the fourth-cumulant tensor (13) [13; 14; 15]. The derivative of the third-cumulant tensor (12) with respect to an affinity is also totally symmetric

$$\left(\frac{\partial C_{\alpha\beta\gamma}}{\partial A_{\delta}} \right)_{\mathbf{A}=0} = B_{\alpha\beta\gamma\delta}(0). \quad (24)$$

Similar relations exist at higher orders as well [15]. They are the consequences of the underlying microreversibility.

Similar results generalizing the Casimir-Onsager reciprocity relations have been obtained for open quantum systems in an external magnetic field [16].

2.4 From multivariate to univariate fluctuation relations

In general, the fluctuation relation (3) holds for all the currents flowing across an open system and it does not imply the

validity of similar relations for a subset of currents. Let us consider a system with two currents, in which case the fluctuation relation (3) is bivariate and reads

$$\frac{P_{A_1, A_2}(J_1, J_2)}{P_{A_1, A_2}(-J_1, -J_2)} \simeq_{t \rightarrow \infty} e^{(A_1 J_1 + A_2 J_2)t}. \quad (25)$$

We may wonder [17] if there exist specific conditions under which the univariate fluctuation relation

$$\frac{P_{A_1, A_2}(J_1)}{P_{A_1, A_2}(-J_1)} \simeq_{t \rightarrow \infty} e^{\tilde{A}_1 J_1 t} \quad (26)$$

is satisfied for the marginal distribution of the current J_1 defined as

$$P_{A_1, A_2}(J_1) \equiv \int dJ_2 P_{A_1, A_2}(J_1, J_2). \quad (27)$$

It turns out that the univariate fluctuation relation indeed holds under the following specific conditions.

Tight coupling between the currents. This condition is defined by requiring that both currents remain proportional to each other during their random time evolution:

$$J_2 = \sigma J_1, \quad (28)$$

which is only possible under special circumstances encountered for instance in molecular motors. Inserting the condition (28) in the bivariate fluctuation relation (25), we get the univariate fluctuation relation (26) with the affinity $\tilde{A}_1 \equiv A_1 + \sigma A_2$ associated with the coupled currents. In this case, the entropy production (4) reduces to

$$\frac{1}{k_B} \frac{d_i S}{dt} = \tilde{A}_1 \langle J_1 \rangle \geq 0 \quad (29)$$

so that the sole affinity \tilde{A}_1 drives the system out of equilibrium. Under the tight-coupling condition (28), the thermodynamic efficiency is directly determined by the affinities:

$$\eta \equiv -\frac{A_1 \langle J_1 \rangle}{A_2 \langle J_2 \rangle} = -\frac{A_1}{\sigma A_2} = \frac{1}{1 - \tilde{A}_1/A_1}. \quad (30)$$

Separation of time scales. In other circumstances, the transition rates for one current may be much higher than for the other current, e.g. $|\langle J_2 \rangle| \gg |\langle J_1 \rangle|$, and it is assumed that

$$\int dJ_2 e^{-A_2 J_2 t} P_{A_1, A_2}(J_1, J_2) \simeq P_{A_1, A_2}(J_1) e^{-\Delta A_1 J_1 t} \quad (31)$$

holds for some $\Delta A_1(A_1, A_2)$ in the long-time limit. Inserting the bivariate fluctuation relation (25) in the assumption (31), we get the univariate fluctuation relation (26) for the marginal (27) and the effective affinity $\tilde{A}_1 = A_1 + \Delta A_1 = \tilde{A}_1(A_1, A_2)$, which depends on both affinities A_1 and A_2 .

Using Jensen's inequality $\langle e^X \rangle \geq e^{\langle X \rangle}$ here with $X = \tilde{A}_1 J_1 t - (A_1 J_1 + A_2 J_2)t$ and noting that $\langle e^X \rangle \simeq 1$ as the consequence of

the assumption (31), we find that the entropy production has the following lower bound:

$$\frac{1}{k_B} \frac{d_i S}{dt} = A_1 \langle J_1 \rangle + A_2 \langle J_2 \rangle \geq \tilde{A}_1 \langle J_1 \rangle \geq 0 \quad (32)$$

in terms of the effective affinity \tilde{A}_1 of the univariate fluctuation relation (26). Accordingly, the thermodynamic efficiency is here limited to a value lower than unity:

$$\eta \equiv -\frac{A_1 \langle J_1 \rangle}{A_2 \langle J_2 \rangle} \leq \frac{1}{1 - \tilde{A}_1/A_1} < 1 \quad \text{if } \tilde{A}_1/A_1 < 0. \quad (33)$$

This situation is encountered in mesoscopic electronic devices where the current J_1 in quantum dots is driven by the Coulomb drag of a large current J_2 in a quantum point contact capacitively coupled to the quantum dots [18; 19]. We notice that the bound (33) is attained for the tight-coupling condition, which is thus stronger.

3 APPLICATIONS

3.1 Transmembrane ion channels

Biological cell membranes separate electrolyte solutions at different ionic concentrations maintained out of equilibrium by the metabolism. Membranes are known to host different kinds of proteins responsible for the active or passive transmembrane transport of ions. While transmembrane active transport is powered for instance by ATP hydrolysis, the passive but highly selective transport of small ions such as Na^+ , K^+ , or Cl^- proceeds in proteins forming a narrow ion channel [20]. In ion channels, the ionic current is driven by the combined effects of the different ionic concentrations and electric voltage across the membrane.

In the simplest models, the channel is supposed to contain a single ion moving along successive sites $i = 1, 2, \dots, L-1$ [21; 22]. Transport is described as a continuous-time Markovian jump process with L states including the empty state $i = L$. The master equation writes

$$\frac{d}{dt} P_t(i) = \sum_j [W(j|i) P_t(j) - W(i|j) P_t(i)] \quad (34)$$

where $P_t(i)$ denotes the probability to find the channel in the i^{th} state at the time t and $W(i|j)$ is the rate of the transition $i \rightarrow j$. They are given by

$$W(i|i+1) = k_i e^\phi \quad \text{for } i = 1, 2, 3, \dots, L-1, \quad (35)$$

$$W(i+1|i) = k_i e^{-\phi} \quad \text{for } i = L, 1, 2, \dots, L-2, \quad (36)$$

$$W(L|1) = c k_L e^\phi, \quad (37)$$

$$W(L|L-1) = c' k_L e^{-\phi}, \quad (38)$$

where c and c' are the ionic concentrations on both sides of the membrane and $\phi = zeF\Delta/(2Lk_B T)$ is a dimensionless parameter giving the strength of the applied electric field F in terms of the membrane thickness Δ , the ionic valency z , and the electronic charge e . The graph associated with this Markovian process is composed of a single cycle [21; 22]. The affinity is identified by considering the ratio of the products of transition rates

forward and backward along the cycle:

$$A = \ln \prod_{i=1}^L \frac{W(i|i+1)}{W(i+1|i)} = \ln \frac{c}{c'} + \frac{zeF\Delta}{k_B T} \quad (39)$$

with $L+1 \equiv 1$. We notice that the affinity vanishes at equilibrium where $c' = c \exp(2L\phi)$. The remarkable result is that the condition (39) implies the fluctuation theorem (3) for the ion current J in the direction $i = 1 \rightarrow L-1$ through the ion channel for any values of the rate constants $\{k_i\}_{i=1}^L$ [14].

The fluctuation theorem also holds for models based on the Nernst-Planck-Poisson equations [23] and for semi-Markovian models of ion channels [24].

3.2 Molecular motors

Energy transduction is possible in molecular motors where mechanical motion is powered by chemical energy from ATP hydrolysis [21]. In molecular motors, two currents – a mechanical and a chemical one – are thus coupled and driven by the chemical affinity

$$A_c = \frac{\Delta\mu}{k_B T} = \frac{\Delta\mu^0}{k_B T} + \ln \frac{[\text{ATP}]}{[\text{ADP}][\text{P}_i]} \quad (40)$$

of ATP hydrolysis into ADP and inorganic phosphate P_i , and the mechanical affinity

$$A_m = \frac{F}{k_B T} \quad \text{or} \quad \frac{\tau}{k_B T} \quad (41)$$

due to an external force F or torque τ . The chemical current J_c is the rate of ATP consumption, while the mechanical current J_m is the velocity in linear motors moving along filaments such as myosin-actin or kinesin-microtubule, or the angular velocity in rotary motors such as F_1 -ATPase.

In such systems, the bivariate fluctuation theorem (25) holds, which provides constraints on the chemomechanical coupling between both currents including the Onsager reciprocity relation and its generalization to the nonlinear response properties. Under physiological conditions, the nonlinear properties turn out to be essential because the Michaelis-Menten kinetics known for molecular motors has the consequence that the average currents have a highly nonlinear dependence on the affinities, as recent studies have pointed out [25; 26; 27].

In the case of the rotary motor F_1 -ATPase, experimental observations have revealed that the dynamics proceeds by steps and substeps [28]. A full revolution is performed with the hydrolysis of three ATP molecules. The random rotational motion of F_1 -ATPase can be described by different kinds of models [26; 27]. The simplest is by a Markovian master equation such as Eq. (34) with six internal states corresponding to the six observed steps and substeps. In such a model, the mechanical current is tightly coupled to the chemical one and the condition (28) is thus satisfied. Accordingly, the bivariate function relation (25) reduces to the univariate relation (26) [25] and the average currents are both proportional to the mean angular velocity

$$\langle V \rangle = V_{\max} \frac{[\text{ATP}] - K_{\text{eq}}[\text{ADP}][\text{P}_i]}{[\text{ATP}] + K_M + K_P[\text{ADP}][\text{P}_i]} \quad (42)$$

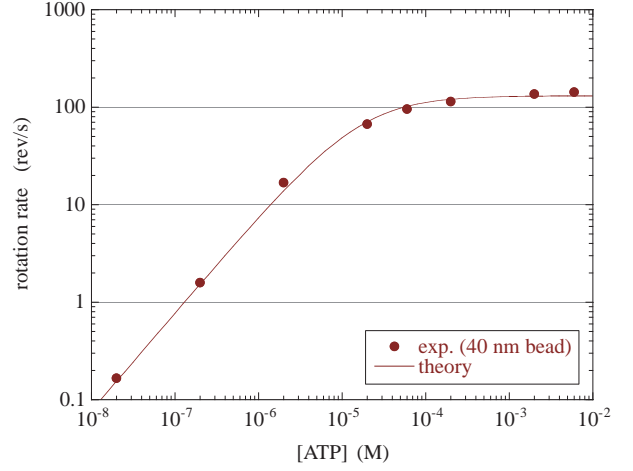


Figure 2. Mean angular velocity of the γ -shaft of F_1 -ATPase in revolutions per second, versus the ATP concentration $[\text{ATP}]$ in mole per liter for $[\text{ADP}][\text{P}_i] = 0$. The diameter of the bead attached to the axis of the motor is $d = 40$ nm, the temperature is of 23 degrees Celsius, and the external torque is zero. The circles are the experimental data of Ref. [28]. The solid line is the result of numerical simulation of the discrete-state model. Adapted from Ref. [27].

where V_{\max} is the maximum possible velocity of about 10^2 rev/s determined by the rate constant of ATP binding to a catalytic site, K_{eq} is the equilibrium constant of ATP hydrolysis, K_M is the Michaelis-Menten constant characterizing the release of ATP or hydrolytic products from a catalytic site, and K_P is the constant characterizing the reverse of the release of hydrolytic products [27]. Figure 2 shows the Michaelis-Menten dependence of the mean angular velocity as a function of ATP concentration with the crossover between the regime where rotation is limited by low concentration and the high-concentration regime with saturation at the maximum velocity V_{\max} . Now, Eq. (42) can be expressed in terms of the chemomechanical affinity resulting from the tight-coupling condition (28):

$$A = \underbrace{\frac{\Delta\mu}{k_B T}}_{\text{chemistry}} + \underbrace{\frac{2\pi}{3} \frac{\tau}{k_B T}}_{\text{mechanics}} \quad (43)$$

because one ATP molecule is consumed for a third of revolution. For given concentrations of ADP and P_i , the chemomechanical affinity determines the ATP concentration according to

$$[\text{ATP}] = K_{\text{eq}}[\text{ADP}][\text{P}_i] e^A. \quad (44)$$

Therefore, the mean velocity (42) has the alternative expression:

$$\langle V \rangle = V_{\max} \frac{e^A - 1}{e^A - 1 + \frac{3V_{\max}}{L}} \quad (45)$$

with some coefficient L depending on the given concentrations $[\text{ADP}]$ and $[\text{P}_i]$. This coefficient controls the linear response of the motor because $\langle V \rangle \simeq LA/3$ for $A \ll 1$. However, the mean velocity depends on the affinity A in a highly nonlinear way, as shown in Fig. 3. The linear regime extends around the thermodynamic equilibrium point at $A = 0$ where the velocity is essentially flat because the linear-response coefficient takes the very

small value $L \simeq 10^{-5} \text{ s}^{-1}$. Under physiological conditions, the affinity is about $A \simeq 21.4$ and the angular velocity would take the extremely low value $LA/3 \simeq 6.5 \text{ rev/day}$ if the motor was functioning in the linear regime. Thanks to the highly nonlinear dependence on the affinity A , the velocity can reach the maximum value $V_{\text{max}} \simeq 10^2 \text{ rev/s}$ under physiological conditions.

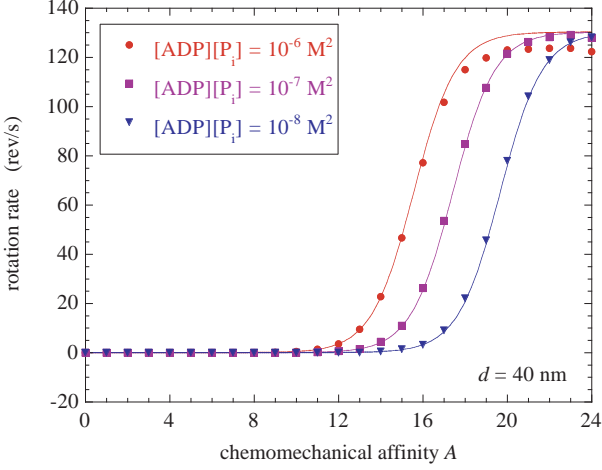


Figure 3. Mean angular velocity versus the affinity (43) for the F_1 -ATPase molecular motor. The results of the discrete-state model (solid lines) of Ref. [27] are compared with the continuous-angle model (dots) of Ref. [26] for three different values of $[ADP][P_i]$. The diameter of the bead is $d = 40 \text{ nm}$, the temperature 23 degrees Celsius, and the external torque zero. Adapted from Ref. [27].

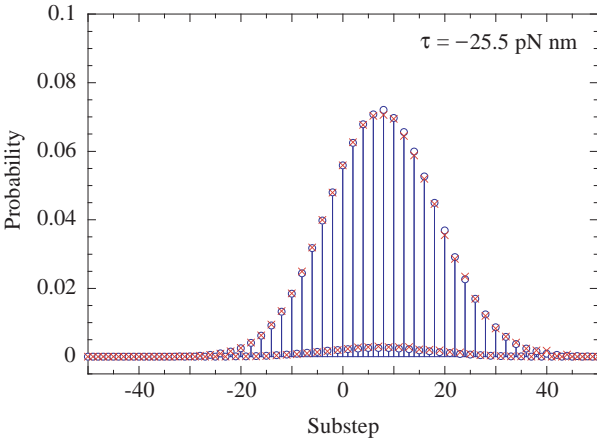


Figure 4. Probability $P(S_t = s)$ (open circles) versus the number $S_t = s$ of substeps of rotation of the F_1 -ATPase motor during the time interval $t = 10 \text{ s}$ compared with the prediction $P(S_t = -s)e^{sA/2}$ (crosses) of the univariate fluctuation relation (26), given that the consumption of one ATP molecule may drive two substeps. The concentrations are $[ATP] = 3 \times 10^{-6} \text{ M}$, $[ADP][P_i] = 10^{-6} \text{ M}^2$, and the torque $\tau = -25.5 \text{ pN nm}$. The diameter of the bead is $d = 80 \text{ nm}$ and the temperature of 23 degrees Celsius. For the given concentrations, the chemomechanical affinity (43) vanishes at the value $\tau_{\text{stall}} = -26.02 \text{ pN nm}$ of the torque. The counting statistics is obtained with 10^6 random trajectories simulated for the discrete-state model. Under the present conditions, the catalytic sites are more often empty than occupied, which explains that the probability of an even number of substeps is higher than for an odd number. Adapted from Ref. [27].

Because of thermal and molecular fluctuations, the rotation of such nanometric motors is random with forward and backward movements, which may become equiprobable if the chemomechanical affinity (43) is vanishing. In order to reach this condition, an external torque should be applied to stop the mean forward motion. Close to such a condition, the statistics of forward and backward random steps or substeps can be performed in order to test experimentally the validity of the fluctuation theorem. Figure 4 depicts an example of what would be the result of such a statistics, showing that the univariate fluctuation relation (26) is satisfied. Furthermore, the thermodynamic efficiency (30) has also been studied and it reaches the unit value in the tight-coupling regime if the chemomechanical affinity (43) is vanishing, because $A = A_1 + \sigma A_2 = 0$ if $A_1 = -\sigma A_2$, whereupon $\eta = 1$ [26; 27].

3.3 Mass separation by effusion

In the effusion of a binary gas mixture through a small pore across a thin wall, there are three possible currents: the two currents of particles of different species and the current of kinetic energy. The three corresponding affinities are determined by Eqs. (1)-(2) in terms of the temperatures and chemical potentials of the two reservoirs on both sides of the thin wall. The fluctuation relation (3) holds for the three currents [29; 30] and the formulae (21)-(24) generalizing the Green-Kubo and Onsager reciprocity relations beyond linear response have been verified in detail for this process [30]. A thermodynamic efficiency (6) can be introduced for the separation process, which may be larger in nonlinear regimes than expected with the linear approximation [30].

The fluctuation theorem has also been established for flows of dilute or rarefied gases ruled by the fluctuating Boltzmann equation [31].

3.4 Chemical reactions

At the mesoscopic scale, fluctuations manifest themselves in reacting systems of various kinds, which can be described in terms of stochastic processes ruled by the chemical master equation [32]. Such reactions can be maintained out of equilibrium by supplying the reactants at fixed concentrations and evacuating the products. For such processes, the current fluctuation theorem (3) has been proved as well [13; 33; 34].

3.5 Electron transport in mesoscopic semiconducting devices

The current fluctuation theorem (3) has been extended to electron transport and open quantum systems in the presence of an external magnetic field [3; 14; 16].

Single-electron transfers can be studied at low temperature in semiconducting devices with quantum dots capacitively coupled to quantum point contacts. The large current in the quantum point contact is modulated by the Coulomb repulsion of electrons transiently occupying the quantum dots. Such devices allow the experimental measurement of the full counting statistics for single-electron transfers in the quantum dots. The current fluctuations in the quantum point contact are not observable, but the time scale separation between both currents is such that the univariate fluctuation relation (26) indeed holds with an effective affinity [18; 19], as several experiments have shown [35; 36].

Moreover, the symmetry relations predicted by the fluctuation theorem for the nonlinear-response properties have also been investigated experimentally [37; 38].

4 THERMODYNAMICS OF INFORMATION PROCESSING AT THE MOLECULAR SCALE

4.1 Path statistics and entropy production

The random paths followed by a fluctuating system can be characterized for the temporal disorder they generate. The temporal disorder is defined as the exponential decay rate of the probability to observe a specific path by stroboscopic observation at equal time intervals Δt . If p_{ω} denotes the probability to observe the path $\omega = \omega_1 \omega_2 \cdots \omega_n$, during which the system has been observed in the coarse-grained states ω_j at the successive instants of time $t_j = j\Delta t$ with $j = 1, 2, \dots, n$, the temporal disorder of the process is defined as

$$h(\Delta t) = \lim_{n \rightarrow \infty} -\frac{1}{n\Delta t} \sum_{\omega} p_{\omega} \ln p_{\omega}. \quad (46)$$

To every path ω corresponds its time reversal $\omega^R = \omega_n \cdots \omega_2 \omega_1$ and we may wonder at which rate its probability decays. In this way, we introduce the average decay rate of the time reversals:

$$h^R(\Delta t) = \lim_{n \rightarrow \infty} -\frac{1}{n\Delta t} \sum_{\omega} p_{\omega} \ln p_{\omega^R}. \quad (47)$$

It turns out that the difference between the quantities (47) and (46) is equal to the thermodynamic entropy production in the limit $\Delta t \rightarrow 0$:

$$\frac{1}{k_B} \frac{d_i S}{dt} = \lim_{\Delta t \rightarrow 0} [h^R(\Delta t) - h(\Delta t)] \geq 0 \quad (48)$$

for the steady states of Markovian processes [39]. In agreement with the second law, this difference is always non negative because it forms a Kullback-Leibler divergence. In this regard, Eq. (48) shows that the thermodynamic entropy production characterizes the time asymmetry of the stochastic process and the breaking of the time-reversal symmetry by nonequilibrium steady states described by the path probability distribution p_{ω} .

To the extend that the decay rates of the path probabilities are the signatures of temporal disorder, the relation (48) shows that the temporal disorder among the typical paths is lower than among their time reversals, i.e., the time reversals are more rare among the typical paths than the typical paths among themselves. In this sense, the relation (48) brings a mathematical expression to the fact that dynamical order manifests itself in nonequilibrium systems [40]. The relation (48) has been tested experimentally in nonequilibrium Brownian motion and electric RC circuits [41; 42].

4.2 Entropy production in copolymerization

The previous result (48) suggests that, if the fluctuations – which evolves in time – can be recorded on a spatial support, they would generate a sequence carrying information on the history followed by the system. Copolymers are natural supports

of information coded in the sequence of covalent bonds in the different monomers composing the copolymer. The growth of a single copolymer is a stochastic process taking place at the molecular scale in a solution containing monomers. Their concentrations can be supposed to remain constant if the solution surrounding the copolymer is large enough. Accordingly, the monomer concentrations control the copolymerization and, in particular, its distance from equilibrium where the growth velocity should vanish.

The thermodynamic entropy production of a growing copolymer is given by

$$\frac{1}{k_B} \frac{d_i S}{dt} = v \left(-\frac{g}{k_B T} + D \right) \geq 0 \quad (49)$$

where v is its growth speed, i.e., the average number of monomers attached to the copolymer per unit time, g is the average free enthalpy per attached monomer, and D is the Shannon disorder per monomer in the copolymer sequence [43; 44]. This result shows that the growth of the copolymer may be powered either by the free enthalpy of attachment if $g < 0$, or by the disorder of the growing sequence if $D > g/(k_B T) > 0$.

The entropy production can also be obtained for copolymerizations on a template as in DNA replication [43; 44]. For such molecular processes, the entropy production depends on the mutual information between the template and the copy, which is a quantity characterizing the fidelity of information transmission from the template to the copy. It turns out that the mutual information takes a positive value under nonequilibrium conditions, but vanishes at equilibrium where information cannot be transmitted.

5 CONCLUSIONS

The present paper gives an overview of recent advances about the fluctuation theorem for currents and other time-reversal symmetry relations in the context of the nonequilibrium thermodynamics of small systems. The fluctuation theorem for currents is a large-deviation property of the currents flowing across a small system in contact with reservoirs at different temperatures and chemical potentials. It finds its origin in the microreversibility of the underlying classical or quantum Hamiltonian dynamics and it is valid far from equilibrium, as well as close to equilibrium. Consequently, the fluctuation theorem for currents leads to results generalizing the Green-Kubo formulae and the Onsager reciprocity relations from the linear to the nonlinear response properties.

Under nonequilibrium conditions, the fluctuation theorem characterizes the breaking of time-reversal symmetry at the statistical level of description and the directionality induced in the system by the affinities of the external reservoirs. At equilibrium, the principle of detailed balancing is recovered.

Interestingly, further symmetry breaking phenomena can also be characterized by relations analogous to the fluctuation relation but in equilibrium systems, such as a magnet in an external magnetic field. The analogy can be developed in detail between time-reversal symmetry breaking out of equilibrium and spin-reversal symmetry breaking at equilibrium [45; 46].

To conclude, the new relationships prove to be fundamental to understand the emergence of macroscopic thermodynamics from the underlying microscopic dynamics ruling the chaotic motion of atoms and the thermal or molecular fluctuations.

ACKNOWLEDGMENT

This research is financially supported by the Université Libre de Bruxelles and the Belgian Federal Government under the Interuniversity Attraction Pole project P7/18 “DYGEST”.

REFERENCES

- [1] G. Gallavotti, *Statistical Mechanics: A Short Treatise* (Springer, Berlin, 1999).
- [2] D. J. Evans and D. J. Searles, *The Fluctuation Theorem*, *Adv. Phys.* **51**, 1529 (2002).
- [3] M. Esposito, U. Harbola, and S. Mukamel, *Nonequilibrium fluctuations, fluctuation theorems, and counting statistics in quantum systems*, *Rev. Mod. Phys.* **81**, 1665 (2009).
- [4] U. Seifert, *Stochastic thermodynamics, fluctuation theorems and molecular machines*, *Rep. Prog. Phys.* **75**, 126001 (2012).
- [5] T. De Donder and P. Van Ryselberghe, *Affinity* (Stanford University Press, Menlo Park CA, 1936).
- [6] I. Prigogine, *Introduction to Thermodynamics of Irreversible Processes* (Wiley, New York, 1967).
- [7] H. B. Callen, *Thermodynamics and an Introduction to Thermostatistics* (Wiley, New-York, 1985).
- [8] D. Andrieux and P. Gaspard, *Fluctuation theorem for currents and Schnakenberg Network Theory*, *J. Stat. Phys.* **127**, 107 (2007).
- [9] P. Maragakis, F. Ritort, C. Bustamante, M. Karplus, and G. E. Crooks, *Bayesian estimates of free energies from nonequilibrium work data in the presence of instrument noise*, *J. Chem. Phys.* **129**, 024102 (2008).
- [10] C. Jarzynski, *Equalities and Inequalities: Irreversibility and the Second Law of Thermodynamics at the Nanoscale*, *Annu. Rev. Condens. Matter Phys.* **2**, 329 (2011).
- [11] P. Gaspard, *Time Asymmetry in Nonequilibrium Statistical Mechanics*, *Adv. Chem. Phys.* **135**, 83 (2007).
- [12] P. Gaspard, *Thermodynamic Time Asymmetry in Nonequilibrium Statistical Mechanics*, in: S. Ishiwata and Y. Matsunaga, Editors, *Physics of Self-Organization Systems* (World Scientific, Singapore, 2008) pp. 67-87.
- [13] D. Andrieux and P. Gaspard, *Fluctuation theorem and Onsager reciprocity relations*, *J. Chem. Phys.* **121**, 6167 (2004).
- [14] D. Andrieux and P. Gaspard, *Fluctuation theorem for transport in mesoscopic systems*, *J. Stat. Mech.* P01011 (2006).
- [15] D. Andrieux and P. Gaspard, *A fluctuation theorem for currents and non-linear response coefficients*, *J. Stat. Mech.* P02006 (2007).
- [16] D. Andrieux, P. Gaspard, T. Monnai, and S. Tasaki, *The fluctuation theorem for currents in open quantum systems*, *New J. Phys.* **11**, 043014 (2009).
- [17] D. Andrieux and P. Gaspard, *Network and thermodynamic conditions for a single macroscopic current fluctuation theorem*, *C. R. Physique* **8**, 579 (2007).
- [18] G. Bulnes Cuetara, M. Esposito, and P. Gaspard, *Fluctuation theorems for capacitively coupled electronic currents*, *Phys. Rev. B* **84**, 165114 (2011).
- [19] G. Bulnes Cuetara, M. Esposito, G. Schaller, and P. Gaspard, *Effective fluctuation theorems for electron transport in a double quantum dot coupled to a quantum point contact*, arXiv.1305.1830.
- [20] B. Alberts, D. Bray, A. Johnson, J. Lewis, M. Raff, K. Roberts, and P. Walter, *Essential Cell Biology* (Garland Publishing, New York, 1998).
- [21] T. L. Hill, *Free Energy Transduction and Biochemical Cycle Kinetics* (Dover, New York, 2005).
- [22] J. Schnakenberg, *Network theory of microscopic and macroscopic behavior of master equation systems*, *Rev. Mod. Phys.* **48**, 571 (1976).
- [23] D. Andrieux and P. Gaspard, *Stochastic approach and fluctuation theorem for ion transport*, *J. Stat. Mech.* P11007 (2008).
- [24] D. Andrieux and P. Gaspard, *The fluctuation theorem for currents in semi-Markovian processes*, *J. Stat. Mech.* P02057 (2009).
- [25] D. Andrieux and P. Gaspard, *Fluctuation theorems and the nonequilibrium thermodynamics of molecular motors*, *Phys. Rev. E* **74**, 011906 (2006).
- [26] P. Gaspard and E. Gerritsma, *The stochastic chemomechanics of the F_1 -ATPase molecular motor*, *J. Theor. Biol.* **247**, 672 (2007).
- [27] E. Gerritsma and P. Gaspard, *Chemomechanical coupling and stochastic thermodynamics of the F_1 -ATPase molecular motor with an applied external torque*, *Biophys. Rev. Lett.* **5**, 163 (2010).
- [28] R. Yasuda, H. Noji, M. Yoshida, K. Kinoshita Jr., and H. Itoh, *Resolution of distinct rotational substeps by submillisecond kinetic analysis of F_1 -ATPase*, *Nature* **410**, 898 (2001).
- [29] B. Cleuren, C. Van den Broeck, and R. Kawai, *Fluctuation theorem for the effusion of an ideal gas*, *Phys. Rev. E* **74**, 021117 (2006).
- [30] P. Gaspard and D. Andrieux, *Nonlinear transport effects in mass separation by effusion*, *J. Stat. Mech.* P03024 (2011).
- [31] P. Gaspard, *Time-reversal symmetry relation for nonequilibrium flows ruled by the fluctuating Boltzmann equation*, *Physica A* **392**, 639 (2013).
- [32] G. Nicolis, *Fluctuations Around Nonequilibrium States in Open Nonlinear Systems*, *J. Stat. Phys.* **6**, 195 (1972).
- [33] D. Andrieux and P. Gaspard, *Fluctuation theorem and mesoscopic chemical clocks*, *J. Chem. Phys.* **128**, 154506 (2008).
- [34] D. Andrieux and P. Gaspard, *Temporal disorder and fluctuation theorem in chemical reactions*, *Phys. Rev. E* **77**, 031137 (2008).
- [35] Y. Utsumi, D. S. Golubev, M. Marthaler, K. Saito, T. Fujisawa, and G. Schön, *Bidirectional single-electron counting and the fluctuation theorem*, *Phys. Rev. B* **81**, 125331 (2010).
- [36] B. Küng, C. Rössler, M. Beck, M. Marthaler, D. S. Golubev, Y. Utsumi, T. Ihn, and K. Ensslin, *Irreversibility on the Level of Single-Electron Tunneling*, *Phys. Rev. X* **2**, 011001 (2012).
- [37] S. Nakamura, Y. Yamauchi, M. Hashisaka, K. Chida, K. Kobayashi, T. Ono, R. Leturcq, K. Ensslin, K. Saito, Y. Utsumi, and A. C. Gossard, *Nonequilibrium Fluctuation Relations in a Quantum Coherent Conductor*, *Phys. Rev. Lett.* **104**, 080602 (2010).
- [38] S. Nakamura, Y. Yamauchi, M. Hashisaka, K. Chida, K. Kobayashi, T. Ono, R. Leturcq, K. Ensslin, K. Saito, Y. Utsumi, and A. C. Gossard, *Fluctuation theorem and microreversibility in a quantum coherent conductor*, *Phys.*

- Rev. B **83**, 155431 (2011).
- [39] P. Gaspard, *Time-reversed dynamical entropy and irreversibility in Markovian random processes*, J. Stat. Phys. **117**, 599 (2004).
- [40] P. Gaspard, *Temporal ordering of nonequilibrium fluctuations as a corollary of the second law of thermodynamics*, C. R. Physique **8**, 598 (2007).
- [41] D. Andrieux, P. Gaspard, S. Ciliberto, N. Garnier, S. Joubaud, and A. Petrosyan, *Entropy Production and Time Asymmetry in Nonequilibrium Fluctuations*, Phys. Rev. Lett. **98**, 150601 (2007).
- [42] D. Andrieux, P. Gaspard, S. Ciliberto, N. Garnier, S. Joubaud, and A. Petrosyan, *Thermodynamic time asymmetry in non-equilibrium fluctuations*, J. Stat. Mech. P01002 (2008).
- [43] D. Andrieux and P. Gaspard, *Nonequilibrium generation of information in copolymerization processes*, Proc. Natl. Acad. Sci. USA **105**, 9516 (2008).
- [44] D. Andrieux and P. Gaspard, *Molecular information processing in nonequilibrium copolymerizations*, J. Chem. Phys. **130**, 014901 (2009).
- [45] P. Gaspard, *Broken Z_2 symmetries and fluctuations in statistical mechanics*, Phys. Scr. **86**, 058504 (2012).
- [46] P. Gaspard, *Fluctuation relations for equilibrium states with broken discrete symmetries*, J. Stat. Mech. P08021 (2012).

THE IMPLICATIONS OF THE BREAKDOWN OF THERMODYNAMIC STABILITY IN ENERGY GENERATION AND CONVERSION NANODEVICES

A. Pérez-Madrid*, I. Santamaria-Holek°

*Departament de Física Fonamental, Universitat de Barcelona,
Martí Franqués 1, 08028 Barcelona, Spain

°UMDI-Facultad de Ciencias, Universidad Nacional Autónoma de México, Campus Juriquilla,
Querétaro 76230, México

EXTENDED ABSTRACT

The concept of stability is essential when describing the behaviour and properties of matter [1]. At the microscopic level, the stability of atoms becomes manifest through the existence of chemical elements. Macroscopic thermodynamic systems show stability through the existence of distinct phases which can coexist under the same physical conditions.

Unlike macroscopic systems, the existence of boundaries in small systems confers them peculiar characteristics. Finite size induces non-homogeneities of the interaction energy which may give rise to free-energy barriers separating two different configuration or aggregation (metastable) states. Passing from one of these configurations to the other is a matter of thermodynamic transformation theory, a well-understood problem in classical thermodynamics [2, 3].

When a macroscopic system is subjected to destabilizing conditions, it separates into two or more phases that may coexist in equilibrium [2, 3]. This partitioning involves the formation of new free-energy barriers associated to interfaces and finally, from the thermodynamic point of view, to the emergence of new systems with their own free energy which determines their physical properties: compressibilities, specific heats, etc. [3]

However, when the system is finite and small enough, the formation of an interface could become energetically unfavourable. This energetic restriction has been observed, for instance, in the formation of magnetic domains in ferromagnetic materials [4] or in atomic nanoclusters with magical numbers, and may be responsible for peculiar effects on the behaviour and properties of the system [5, 6].

A deeper analysis related to this last question must account for the implications of the finite size of the system on its thermodynamic behaviour. This analysis has shown that inflexions and barriers in the thermodynamic free energy are related to irreversible processes. This is revealed through the calculus of the entropy produced in a transformation implying the transition over a free energy barrier. This process is possible due to the existence of a thermodynamic affinity whose origin resides in the external constraints. Since these irreversible processes may be cyclical, they can be used to generate or convert energy at the nanoscale if the external constraints force the state of the system to reside in a region of the order parameter in correspondence with the unstable region of the free energy. Under these circumstances, we show that an oscillation between the two metastable states separated by the free energy barrier may be triggered. This cyclical motion persists while these external constraints maintain the system out of equilibrium. The results obtained are of great interest since they underlay the physics of energy generation and conversion nanodevices [7]. Potential applications have been recently reported for energy nanogenerators [8], systems based on the pyroelectric effect [9] and also for some storage systems [10]. Coupling of several small systems may lead to interesting effects that are in the thermodynamic origin of the electric hysteresis [11, 12]. Oscillating behaviours are also useful in energy-converting nanodevices whose operation depends on the pressure conditions imposed by the heat bath [13].

REFERENCES

- [1] Lieb, E. H. Stability of matter. *Rev. Mod. Phys.* 1976, 48, 553-569.
- [2] Stanley H. E. *Introduction to phase transitions and critical phenomena*; Clarendon Press: Oxford 1971.
- [3] Callen, H. L. *Thermodynamics and an introduction to thermostatistics*; John Wiley and Sons: New York, 1985.
- [4] Morrish, A. H. *The Physical Principles of Magnetism*; John Wiley and Sons: New York, 1965.
- [5] Reyes-Nava, J. A.; Garzón, I. L.; Michaelian, K. Negative heat capacity of sodium clusters. *Phys. Rev. B*, 2003, 67, 165401.
- [6] Labastie, P.; Whetten, R. L. Statistical Thermodynamics of the Cluster Solid-Liquid Transition *Phys. Rev. Lett.* 1990, 65, 1567-1570.
- [7] Kamat, P. V. Meeting the Clean Energy Demand: Nanostructure Architectures for Solar Energy Conversion. *J. Phys. Chem. C* 2007, 111, 2834-2860.
- [8] Hansen, B. J.; Liu, Y.; Yang, R.; Wang, Z. L. Hybrid Nanogenerator for Concurrently Harvesting Biomechanical and Biochemical Energy. *ACS Nano* 2010, 4, 3647-3652.
- [9] Yang, Y.; Guo, W.; Pradel, K. C.; Zhu, Guang; Zhou, Y.; Zhang, Y.; Hu, Y.; Lin, L.; Wang, Z. L.; Pyroelectric Nanogenerators for Harvesting Thermoelectric Energy, *Nano Lett.* 2012, 12, 2833-2838.
- [10] Wagemaker, M., Borghols, W.J.H., Mulder, F.M.: Large impact of particle size on insertion reaction. A Case for Anatase Lix TiO2. *J. Am. Chem. Soc.* 2007, 129, 4323-4327.
- [11] Dreyer, W.; Jammik, J.; Guhlke, C.; Huth, R.; Moskon, J.; Gaberscek, M. The thermodynamic origin of hysteresis in insertion batteries, *Nature Materials* 2010, 9, 448-453.
- [12] Dreyer, W.; Guhlke, C.; Herrmann, M.; Hysteresis and phase transition in many-particle storage systems. *Continuum Mech. Thermodyn.* 2011, 23, 211-231.
- [13] Chang, C.; Tran, V. H.; Wang, J.; Fuh, Y.-K.; Hilliard, J. E. Spinodal decomposition in Phase Transformations; American Society for Metals: Ohio, 1970.

HYBRID ATOMISTIC-CONTINUUM APPROACH TO DESCRIBE INTERFACIAL PROPERTIES BETWEEN IMMISCIBLE LIQUIDS

K. M. Issa^{*,1}, and P. Poesio^{*,2}

^{*}Università degli Studi di Brescia, via Branze 38, 25123, Brescia Italy
email:khaled.mo.issa@gmail.com¹, pietro.poesio@ing.unibs.it²

ABSTRACT

The study of immiscible liquid-liquid interfaces (LLIs) is of importance in many phenomena in engineering, chemical, and biological systems. At an immiscible LLI, a slip occurs as a result of poor mixing, and relatively weaker atomic interactions between the two liquids. One of the main difficulties in modeling immiscible (and partially miscible) LLIs is the assignment of boundary conditions at the interface. In continuum-based modeling of macroscale systems, a no-slip boundary condition is generally assumed at the LLI. The issue of interfacial slip, however, becomes especially relevant for micro-, and nanofluidics where interface dynamics play a key role, and the slip magnitude can strongly affect the flow behavior. In that respect, molecular dynamics (MD) is a vital tool for modeling LLIs at the atomic scale. In this paper, we present a hybrid atomistic-continuum (HAC) approach that utilizes MD at the LLI to directly extract boundary conditions needed by a continuum solver. Our focus is on the treatment of the atomistic subdomain (Ω_A), specifically when it comes to the proper termination of Ω_A , and the coupling to an external continuum field. The model is tested using a Couette flow under varying flow speeds. Finally, we demonstrate the ability of the model to accurately predict the slip coefficient at the LLI.

INTRODUCTION

Liquid-Liquid Interfaces (LLIs), formed by two immiscible liquids, occur in a wide range of systems. For instance, in biology, interfaces between two immiscible liquid electrolyte solutions are of great importance as they occur in tissues and cells of all living organisms. In oil and gas industry, the balance between break-up and coalescence (both interfacial phenomena) determine the occurrence of phase inversion, a process that can lead to the blockage of the entire pipeline with a huge economical impact. Furthermore, in recent lab-on-a-chip technology, liquid droplets, moving through an immiscible liquid, are used as chemical (and biological) reactors, where reactions are carried out while the droplet is transported along micro-channels. Hence, the proper understanding, and modeling of LLI dynamics is of great significance to many industries.

The slip behavior at immiscible LLIs is a nanoscale phenomenon, and requires atomic resolution to accurately capture the relevant physics. Continuum methods generally assume a no-slip boundary condition at the LLI, which could provide reasonable accuracy on a macroscale level. This approximation loses validity at the micro- and nanoscale, due to the relatively higher surface-to-volume ratio. Additionally, the amount of slip at such scales can be comparable to the characteristic length of the system and therefore should be carefully accounted for.

Continuum theory, in the form of the Navier-Stokes (NS) equations, can accurately predict flow dynamics in the regions far removed from LLI effects. On the other hand, molecular dynamics (MD) is capable of capturing important nanoscale physics at the LLI [1, 2, 3, 4]. The method is, however, computationally demanding and modeling is presently limited to systems within the nanoscale. Hybrid atomistic-continuum (HAC) modeling can alleviate these shortcomings by decomposing the domain into a continuum description (Ω_C) and an atomistic one

(Ω_A). By limiting Ω_A to the LLI, boundary conditions for the NS solution at the interface are naturally recovered through MD. With this domain-decomposition approach, the two descriptions partially overlap in a region ($\Omega_{C \rightarrow A} + \Omega_{A \rightarrow C}$) where information is exchanged [5]. The accuracy of the method relies on the proper application of continuum state variables onto Ω_A , and the consistency of transport coefficients between the two descriptions.

In this paper, we present a one-way coupling algorithm for the HAC modeling of one-dimensional LLIs. The focus is on the proper termination of Ω_A and on the imposition of boundary conditions of the form $\Omega_{C \rightarrow A}$. The boundaries of Ω_A are modeled as reflective walls supplemented with an adaptive boundary force, to prevent artificial density layering. The method is tested using a Couette flow with different velocities. The velocity profiles at the LLI are compared with the continuum NS solution. The predicted viscosity, and slip coefficients are shown to agree well with the literature.

METHODOLOGY

Particles in the atomistic subdomain (Ω_A) interact via the Lennard-Jones (LJ) potential:

$$U_{LJ}(r_{ij}) = 4\epsilon \left[\left(\frac{\sigma}{r_{ij}} \right)^{12} - \beta \left(\frac{\sigma}{r_{ij}} \right)^6 \right] \quad (1)$$

where r_{ij} is the separation distance between particles i , and j . The energy, and length scales are taken to be those of argon: $\epsilon = 0.996 \text{ kJmol}^{-1}$, and $\sigma = 3.4 \text{ \AA}$ ($1 \text{ \AA} = 10^{-10} \text{ m}$). The potential is force-shifted [6] and a cutoff radius of $r_c = 3\sigma = 10.2 \text{ \AA}$ is employed. The parameter β is used to tune the attractive part of the potential between the two liquids (L_1 , and L_2). To induce

complete immiscibility, we assign $\beta_{11} = \beta_{22} = 1.0$ and $\beta_{12} = 0.0$. The position (\mathbf{r}_i) and velocity (\mathbf{v}_i) vectors of each particle i are governed by Newton's equation of motion:

$$\frac{d\mathbf{r}_i}{dt} = \mathbf{v}_i \quad (2)$$

$$\frac{d\mathbf{v}_i}{dt} = \frac{\mathbf{F}_i}{m_i} \quad (3)$$

where $\mathbf{F}_i = -\sum_{j \neq i} \nabla_{\mathbf{r}_{ij}} U_{LJ}$ is the total force acting on particle i , with mass $m_i = 40 \text{ gmol}^{-1}$. Eqs. (2)-(3) are solved using the leap-frog algorithm:

$$\mathbf{v}_i^{n+1/2} = \mathbf{v}_i^{n-1/2} + \delta t \mathbf{F}_i^n / m_i \quad (4)$$

$$\mathbf{r}_i^{n+1} = \mathbf{r}_i^n + \delta t \mathbf{v}_i^{n+1/2} \quad (5)$$

where δt is the time step. Superscripts in Eqs. (4)-(5) denote the relative time level of each variable.

The atomistic subdomain Ω_A describing the LLI is shown in Fig. 1. The system dimensions are: $L_x \times L_y \times L_z = 14.2\sigma \times 13.6\sigma \times 6.8\sigma$. The size is chosen to give a bulk liquid density of $\rho = 1369 \text{ kgm}^{-3}$ ($\rho^* = \rho \sigma^3 N_{av} m^{-1} = 0.81$), with a total of $N = 1024$ particles. Periodic boundary conditions are used along the y - and z -axes. In the x -direction, the system is terminated using a reflective wall and an adaptive boundary force (details below). Velocity and temperature measurements are recorded in bins of size $\delta x = 0.79\sigma$ along the x -axis. To capture the LLI, a higher bin resolution of $\delta x_p = 0.1\delta x$ is used for the density profiles. The system is equilibrated at $T = 132 \text{ K}$ ($T^* = k_b T / \epsilon = 1.1$), using a Berendsen thermostat [7] with a time constant of 0.5 ps (1 ps = 10^{-12} s). A time step of $\delta t = 5 \text{ fs}$ (1 fs = 10^{-15} s , $\delta t^* = 0.0023\tilde{\tau}$, $\tilde{\tau} = \sigma m^{0.5} \epsilon^{-0.5}$) is used with total runs of 15 ns duration.

Particles that attempt to leave Ω_A along the non-periodic x -axis are specularly reflected back into Ω_A by reversing the velocity component normal to that plane (v_x). This guarantees a constant number of particles (N) in Ω_A , however, it does not account for the lack of periodicity along that direction. Thus, causing artificial density layering normal to the reflective boundary. One way to alleviate this issue is to supplement the reflections with a boundary force that 'mimics' on average the forces felt by a particle in a periodic system [8]. The boundary force in [8] was derived by measurement in a periodic system and applied as a function of distance to the reflective boundary. For supercritical conditions, this was found to significantly reduce the artificial layering. However, the performance of this technique was shown to deteriorate at higher densities, and/or lower temperatures, conditions which are relevant for LLI analysis. This drawback was overcome by extracting the boundary force using a control algorithm [9, 10], which we employ in our model. First, the density in each bin is averaged in time intervals of 5 ps. The noise in the density profile is then reduced by passing it twice through a Gaussian filter as follows (see appendix A for details):

$$\rho_1(x) = \phi^{-1} \int \rho(x) \exp\left[-(x-x_1)^2 / \phi^2\right] dx_1 \quad (6)$$

$$\rho_2(x) = \phi^{-1} \int \rho_1(x) \exp\left[-(x-x_2)^2 / \phi^2\right] dx_2 \quad (7)$$

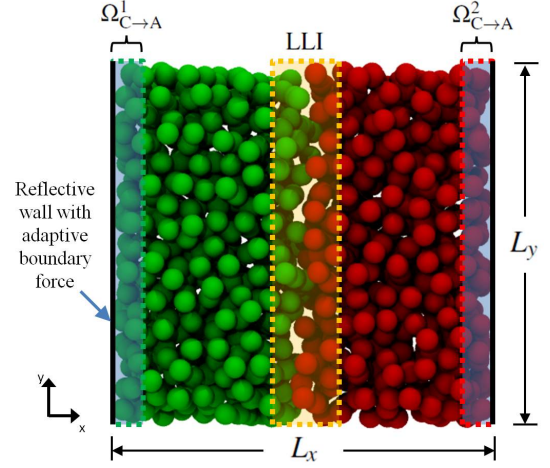


Figure 1. Atomistic liquid ($L_1 + L_2$) subdomain (Ω_A) at the LLI. External field quantities are applied within the shaded regions denoted by $\Omega_{C \rightarrow A}^j$ ($j = 1, 2$).

where: ρ_1 and ρ_2 are the density profiles subsequent to the first and second Gaussian smoothing, respectively. The integrals are evaluated discretely with a cutoff of $3\delta x_p$, and $\phi = 2\delta x_p$. The gradient of the density profile $\nabla \rho_2(x)$ is then used as a correction mechanism to adapt the boundary force F_b which is initially at zero:

$$F_b(x, t + t_{ad}) = F_b(x, t) - \nabla \rho_2 \sqrt{\lambda} \quad (8)$$

where t_{ad} is the 5 ps averaging period. The parameter λ is used to enact corrections faster away from the boundary which helps prevent the forces close to the boundary from over-shooting. In this study, we select $\lambda = 1.1 \times 10^{-4} q$, where q is the bin number counted from the boundary for each liquid, respectively.

The system is first thermostatted for 50 ps, with reflective boundaries only. The adaptation of F_b commences following the equilibration period. Additionally, the application of boundary conditions to the particles in $\Omega_{C \rightarrow A}^j$ ($j = 1, 2$) is carried out simultaneously. For the purpose of studying LLI dynamics in the presence of a Couette flow, we apply opposing velocities of $u_C^* = \pm 0.2, 0.4, 0.6$, and 0.8 , along the y -axis. The velocity u_C^* is ramped up to its target value over a period of 50 ps. For each liquid, u_C^* is enforced by applying an additional body force F_{u_C} in the y -direction to each atom within $\Omega_{C \rightarrow A}^j$ ($j = 1, 2$), as given by (see Appendix B):

$$F_{u_C} = \frac{m}{\delta t} (u_C - v_{\text{com}y}) - \frac{F_{\text{com}y}}{N_{\Omega_{C \rightarrow A}^j}} \quad (9)$$

$$v_{\text{com}y} = \frac{1}{N_{\Omega_{C \rightarrow A}^j}} \sum_{i=1}^{N_{\Omega_{C \rightarrow A}^j}} v_{y,i} \quad (10)$$

where $v_{\text{com}y}$ is the center-of-mass y -velocity of particles in $\Omega_{C \rightarrow A}^j$ ($j = 1, 2$), and $F_{\text{com}y}$ is the corresponding net force. Furthermore, the temperature is maintained at $T_C^* = 1.1$ via direct velocity scaling about the center-of-mass velocity:

$$\mathbf{v}_i = \left(\mathbf{v}_i - \mathbf{u}_{\Omega_{C \rightarrow A}^j} \right) \sqrt{\frac{T_C}{T_{\Omega_{C \rightarrow A}^j}}} + \mathbf{u}_{\Omega_{C \rightarrow A}^j} \quad (11)$$

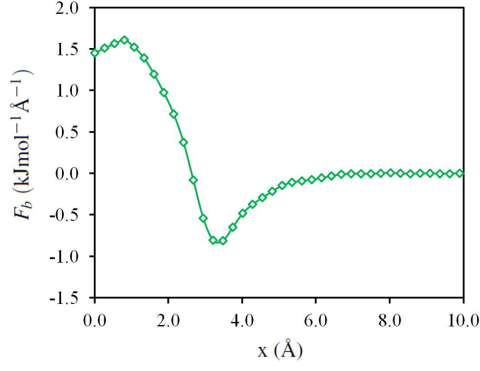


Figure 2. Adaptive boundary force (F_b) for L_1 with $u_C^* = 0.2$. Distance measured from the reflective boundary of $\Omega_{C \rightarrow A}^1$.

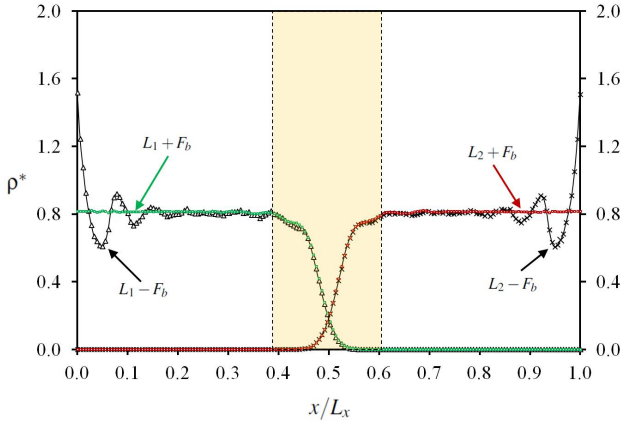


Figure 3. Density profiles for $u_C^* = 0.2$, with (+) and without (-) the action of F_b . The shaded region marks the depleted zone at the LLI.

where $\langle \mathbf{u}_{\Omega_{C \rightarrow A}^j} \rangle = [0, u_C, 0]$ for $j = 1$, and $[0, -u_C, 0]$ for $j = 2$.

The variable $T_{\Omega_{C \rightarrow A}^j}$ is the instantaneous temperature of particles in $\Omega_{C \rightarrow A}^j$ ($j = 1, 2$).

RESULTS & DISCUSSION

Data sampling was started after 5 ns, for which the boundary force, and velocity profiles exhibited steady-state behavior. The collection of data was carried out for an additional 10 ns. The adaptive boundary force (F_b) for $u_C^* = 0.2$ is shown in Fig. 2. Close to the boundary, F_b is repulsive in nature, with an attractive component further away. The effectiveness of F_b in eliminating the density layering at the boundary is shown in Fig 3. A uniform density of $\rho^* = 0.81$ can be seen away from the depleted region at the LLI between the two immiscible liquids.

The steady-state velocity profile for $u_C^* = \pm 0.4$ is shown in Fig. 4, along with the analytical solution for a Couette flow ($d^2u/dx^2 = 0$). Using the imposed velocities in $\Omega_{C \rightarrow A}^j$ ($j = 1, 2$) as boundary conditions, the resulting analytical velocity profile is given by:

$$u(x) = -\frac{2u_C}{L_x}x + u_C \quad (12)$$

When normalized by u_C , all other cases exhibited a similar trend. The deviation from the analytical solution increases closer to the LLI, as a result of the interfacial slip. To validate

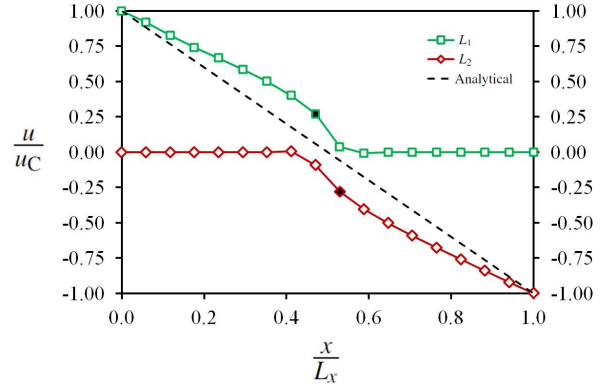


Figure 4. Velocity profile across the LLI for $u_C^* = \pm 0.4$, and the analytical solution given by Eq. (12). Shaded data points are used to measure apparent slip (δu).

Table 1. All values are in reduced units. Where appropriate, results are listed in the form $L_1(L_2)$.

u_C^*	$\frac{du}{dx} (\times 10^2)$	$\tau^* (\times 10^2)$	η^*	δu^*	α
0.2	2.10 (2.11)	4.47 (4.46)	2.13 (2.12)	0.115	2.56
0.4	4.23 (4.20)	9.20 (9.20)	2.17 (2.19)	0.220	2.39
0.6	6.33 (6.38)	13.9 (13.9)	2.20 (2.18)	0.326	2.36
0.8	8.69 (8.66)	18.2 (18.3)	2.13 (2.14)	0.522	2.83

the velocity profiles, we first compare the viscosity of the liquids to that measured using equilibrium MD [11], at a representative state point of $\rho^* = 0.81$, and $T^* = 1.1$. This is carried out by calculating the average amount of momentum (Δp) added every time step in $\Omega_{C \rightarrow A}^j$ ($j = 1, 2$) to maintain the flow. Using Δp , the shear stress (τ), or momentum flux, is estimated using:

$$\tau = \frac{\Delta p}{\delta t A} \quad (13)$$

where $A = L_y \times L_z$ is the cross-sectional area parallel to the flow. The viscosity is then computed from: $\eta = \tau (du/dx)^{-1}$. The calculation of the velocity gradient (du/dx) from the velocity profiles (similar to Fig. 4) is limited to the linear region ($x/L_x \approx 0.3$) away from the depleted zone. The viscosity values are given in Table 1, and are in good agreement with the value of $\eta_{\text{ref}}^* = 2.18$ obtained from [11]. Furthermore, we compare the slip coefficient (α) predicted using our model with that reported for immiscible LJ liquids $\alpha_{\text{ref,average}} = 2.53$ [1]. Using the velocity jump at the LLI, and the measured shear stress τ , the slip coefficient is estimated by:

$$\alpha = \frac{\delta u}{\tau} \quad (14)$$

where δu is the apparent slip, and is measured using the data points indicated in Fig. 4. As can be seen in Table 1, the slip coefficient is accurately predicted within Ω_A .

CONCLUSION

We have presented an HAC algorithm for imposing continuum field variables onto an atomistic subdomain (Ω_A) for the purpose of studying slip at immiscible LLIs. Density layering at the interface between the two descriptions was eliminated by the use of an adaptive boundary force. The momentum flux applied and the resulting velocity gradient in the linear zone produce a viscosity that is in close agreement with that reported in the literature. The method is also shown to accurately capture the slip coefficient (α) at the LLI. Our plans include the implementation of this algorithm with two-way coupling to the continuum description (Ω_C).

NOMENCLATURE

N_{av} Avogadro's number
 k_b Boltzmann constant [$m^2 kg s^{-2} K^{-1}$]

REFERENCES

- [1] J. Koplik, and J. R. Banavar, Slip, immiscibility, and boundary conditions at the liquid-liquid interface, *Phys. Rev. Lett.*, vol. 96, pp. 0445051-0445054, 2006.
- [2] Y. Hu, X. Zhang, and W. Wang, Boundary conditions at the liquid-liquid interface in the presence of surfactants, *Langmuir*, vol. 26, pp. 10693-10702, 2010.
- [3] G. Galliero, Lennard-Jones fluid-fluid interfaces under shear, *Phys. Rev. E*, vol. 81, pp. 0563061-0563067, 2010.
- [4] Q. Ehlinger, L. Joly, and O. Pierre-Louis, Giant slip at liquid-liquid interfaces using hydrophobic ball bearings, *Phys. Rev. Lett.*, vol. 110, pp. 1045041-1045045, 2013.
- [5] K. M. Mohamed, and A. A. Mohamad, A review of the development of hybrid atomistic-continuum methods for dense fluids, *Microfluid. Nanofluid.*, vol. 8, pp. 283-302, 2010.
- [6] M. P. Allen and D. J. Tildesley, *Computer simulation of liquids*, Oxford University Press, New York, 1987.
- [7] H. J. C. Berendsen, J. P. M. Postma, W. F. van Gunsteren, A. DiNola, and J. R. Haak, Molecular dynamics with coupling to an external bath, *J. Chem. Phys.*, vol. 81, pp. 3684-3690, 1984.
- [8] T. Werder, J. H. Walther, and P. Koumoutsakos, Hybrid atomistic-continuum method for the simulation of dense fluid flows, *J. Comput. Phys.*, vol. 205, pp. 373-390, 2005.
- [9] E. M. Kotsalis, J. H. Walther, and P. Koumoutsakos, Control of density fluctuations in atomistic-continuum simulations of dense liquids, *Phys. Rev. E*, vol. 76, pp. 0167091-0167097, 2007.
- [10] E. M. Kotsalis, J. H. Walther, E. Kaxiras, and P. Koumoutsakos, Control algorithm for multiscale flow simulations of water, *Phys. Rev. E*, vol. 79, pp. 0457011-0457014, 2009.
- [11] R. L. Rowley, and M. M. Painter, Diffusion and viscosity equations of state for a Lennard-Jones fluid obtained from molecular dynamics simulations, *Int. J. Thermophys.*, vol. 18, pp. 1109-1121, 1997.

Appendix A: Discrete Gaussian filter equations

For clarity, the density bin spacing is labeled δx instead of δx_p . In discrete form, the Gaussian filter of Eq. (6) with a cutoff

of $3\delta x$ is given by:

$$\rho_1(x) = \phi^{-1} \sum_{x_1=x-3\delta x}^{x+3\delta x} \rho(x_1) e^{-\frac{(x-x_1)^2}{\phi^2}} \delta x \quad (15)$$

which expands to:

$$\rho_1(x) = \phi^{-1} \left[\rho(x-3\delta x) e^{-\left(\frac{3\delta x}{\phi}\right)^2} + \rho(x-2\delta x) e^{-\left(\frac{2\delta x}{\phi}\right)^2} + \rho(x-\delta x) e^{-\left(\frac{\delta x}{\phi}\right)^2} + \rho(x) + \rho(x+\delta x) e^{-\left(\frac{\delta x}{\phi}\right)^2} + \rho(x+2\delta x) e^{-\left(\frac{2\delta x}{\phi}\right)^2} + \rho(x+3\delta x) e^{-\left(\frac{3\delta x}{\phi}\right)^2} \right] \delta x$$

using $\phi = 2 \delta x$:

$$\rho_1(x) = \frac{1}{2} \left[\rho(x-3\delta x) e^{-\left(\frac{3}{2}\right)^2} + \rho(x-2\delta x) e^{-\left(1\right)^2} + \rho(x-\delta x) e^{-\left(\frac{1}{2}\right)^2} + \rho(x) + \rho(x+\delta x) e^{-\left(\frac{1}{2}\right)^2} + \rho(x+2\delta x) e^{-\left(1\right)^2} + \rho(x+3\delta x) e^{-\left(\frac{3}{2}\right)^2} \right]$$

Normalizing by half the sum of the density coefficients: $\frac{1}{2} \left[2e^{-\left(\frac{3}{2}\right)^2} + 2e^{-\left(1\right)^2} + 2e^{-\left(\frac{1}{2}\right)^2} + 1 \right] = 1.75208$, produces the final discrete equation:

$$\rho_1^i = 0.0301\rho^{i\pm 3} + 0.1050\rho^{i\pm 2} + 0.2223\rho^{i\pm 1} + 0.2854\rho^i \quad (16)$$

where i refers to the bin number. Equation (16) is suitable for bins with at least three neighbors on either side. That is, for $i = 4$ to $N_{bin} - 3$. For the rest of the bins, the contribution to the smoothed value depends on the maximum number of neighboring bins on either side. The derivation is similar to the above, and can be shown to produce the following complete set:

$$\begin{aligned} \rho_1^i &= \rho^i & i = 1, \text{ or } N_{bin} \\ \rho_1^i &= 0.3045\rho^{i\pm 1} + 0.3910\rho^i & i = 2, \text{ or } N_{bin} - 1 \\ \rho_1^i &= 0.1117\rho^{i\pm 2} + 0.2365\rho^{i\pm 1} + 0.3036\rho^i & i = 3, \text{ or } N_{bin} - 2 \\ \rho_1^i &= 0.0301\rho^{i\pm 3} + 0.1050\rho^{i\pm 2} + 0.2223\rho^{i\pm 1} + 0.2854\rho^i & i = 4 \text{ to } N_{bin} - 3 \end{aligned}$$

where i denotes the bin number.

Appendix B: Derivation of flow driving body force (F_{uc})

The following derivation is based on the leap-frog algorithm Eqs. (4)-(5). For a system of N particles, the center of mass velocity along any one dimension is given by:

$$v_{com}^{n-\frac{1}{2}} = \frac{1}{N} \sum_{i=1}^N v_i^{n-\frac{1}{2}} \quad (17)$$

If the total force at step n is: $F_{com}^n = \sum_{i=1}^N F_i^n$, then we seek an additional body force F_{uc}^n to be applied uniformly to each

particle in order to drive the flow with a velocity u_C . By setting $v_{\text{com}}^{n+\frac{1}{2}} = u_C$:

$$u_C = v_{\text{com}}^{n-\frac{1}{2}} + \frac{\delta t}{Nm} F_{\text{com}}^n + \frac{\delta t}{Nm} \sum_{i=1}^N F_{u_C}^n \quad (18)$$

where Nm is the total mass of the system. Solving for the *total* body force gives:

$$\sum_{i=1}^N F_{u_C}^n = \frac{Nm}{\delta t} \left(u_C - v_{\text{com}}^{n-\frac{1}{2}} \right) - F_{\text{com}}^n \quad (19)$$

when applied uniformly to each particle, that translates to:

$$F_{u_C}^n = \frac{m}{\delta t} \left(u_C - v_{\text{com}}^{n-\frac{1}{2}} \right) - \frac{F_{\text{com}}^n}{N} \quad (20)$$

FLUCTUATION RELATIONS FOR THE DISSIPATION

Debra J. Searles*, James C. Reid*, Barbara M. Johnston^o, Denis J. Evans[^], Lamberto Rondoni[†], and Guillaume Michel^{††}

*Australian Institute of Bioengineering and Nanotechnology and School of Chemistry and Molecular Biosciences, The University of Queensland, Brisbane, Qld 4072, Australia

^oQueensland Micro-and Nanotechnology Centre and School of Biomolecular and Physical Sciences, Griffith University, Brisbane, Qld 4111, Australia

[^]Research School of Chemistry, Australian National University, Canberra, ACT 0200, Australia

[†]Dipartimento di Scienze Matematiche, Politecnico di Torino and INFN, Sezione di Torino, Via P. Giuria 1, Torino, Italy

^{††}Département de Physique, École Normale Supérieure, 24 Rue Lhomond, 75 005 Paris, France

EXTENDED ABSTRACT

The fluctuation theorems characterize the probability distribution of values of the dissipation in nonequilibrium systems and prove that the average dissipation will be positive. Transient Fluctuation relations are the best understood. They are known to be exact for systems of arbitrary size, arbitrarily near or far from equilibrium.[1] Previously very few exact results were known in nonequilibrium statistical mechanics. Their application to small systems coincided with an upsurge of interest in nanotechnology and nanobiology and the study of small bio-engines. The applicability of the transient fluctuation relations far from equilibrium also mean that they are an important for large deviation theory.

Here we will discuss variants of the fluctuation theorem that can be derived from the transient fluctuation theorem, and which are valid in various limits, or subject to particular conditions. We will focus on fluctuation theorems for steady states [2], in local regions within a larger system [3] and in systems subject to external noise [4].

The subject of the transient fluctuation theorems is the dissipation function, which is related to the entropy production from linear irreversible thermodynamics. We will show that in order for steady state fluctuation relations for the dissipation function to hold, time reversibility, ergodic consistency and a recently introduced form of correlation decay, called T-mixing, are sufficient conditions. Our results are not restricted to a particular model and show that the steady state fluctuation relation for the dissipation function holds near or far from equilibrium subject to these conditions. [2]

We will also consider how a fluctuation theorem can be obtained for a small open subsystem within the large system. If a fluctuation theorem for the dissipation in a subsystem is considered, we find that a correction term has to be added to the large system fluctuation theorem due to correlation of the subsystem with the surroundings. Its analytic expression can be derived provided some general assumptions are fulfilled, and its relevance has been checked using numerical simulations. [3]

Another system of interest is the systems that are subject to external noise. We provide a derivation of this fluctuation theorem for systems driven by both deterministic and stochastic forces. It turns out that it is still valid, provided the dissipation is carefully defined. The total dissipation is explicitly the sum of two dimensionless works for which fluctuation relations may fail. We numerically study their range of validity of fluctuation relations for the total dissipation, the contribution from the deterministic driving force and the stochastic force, and point out in which limit a noise can be neglected. [4]

REFERENCES

- [1] D. J. Evans, D. J. Searles, "The fluctuation theorem", *Ad. Phys.*, **52**, 1529, (2002).
- [2] D. J. Searles, B. M. Johnston, D. J. Evans and L. Rondoni, "Time reversibility, correlation decay and the steady state fluctuation relation for dissipation", **15**, 1503, (2013).
- [3] G. Michel and Debra J. Searles, "A local fluctuation theorem for large systems", accepted *Phys. Rev. Lett.*, arXiv:1208.3969 [cond-mat.stat-mech].
- [4] G. Michel and Debra J. Searles, "Contribution of the stochastic forces to the fluctuation theorem", *Phys. Rev. E* **85**, 042102 (2012).

PANEL H

CONCEPTUAL ANALYSIS OF THE ENTROPY PRINCIPLE IN CONTINUUM PHYSICS

CONCEPTUAL ANALYSIS OF THE ENTROPY PRINCIPLE IN CONTINUUM PHYSICS: AN OVERVIEW

V. A. Cimmelli

Department of Mathematics, Computer Science and Economics, University of Basilicata, Viale dell'Ateneo Lucano, 10, 85100, Potenza, Italy, e-mail: vito.cimmelli@unibas.it

EXTENDED ABSTRACT

In continuum physics the entropy constitutive principle offers a valuable help in modeling material properties. It has been proposed by Coleman and Noll [1] within the frame of Rational Thermodynamics (RT) [2], and asserts that:

The constitutive equations, which characterize the material properties of continuous media, must be assigned in such a way that second law of thermodynamics is satisfied along arbitrary thermodynamic processes.

These authors also provided a rigorous mathematical procedure (the Coleman-Noll procedure) to exploit the principle. Afterwards, Liu [3], developed an alternative and elegant method of exploitation, based on the Lagrange multipliers, known as Liu procedure. Hauser and Kirchner [4], recognized that the Liu procedure constitutes a special case of a more general result on linear programming [5]. In Thermodynamics of Irreversible Processes (TIP) [2], de Groot and Mazur [6] and Gyarmati [7] exploited it by a phenomenological method, which regards the entropy production as a bilinear function of thermodynamical forces and fluxes. A more rigorous formulation of this procedure has been achieved by Ván et al. [8; 9].

A new perspective has been open by Müller and Ruggeri [10], who applied the principle to determine the main field which renders the system of field equations of Rational Extended Thermodynamics (RET) [2], symmetric hyperbolic, and showed how the Lagrange multipliers provide this field [11; 12]. In Extended Irreversible Thermodynamics (EIT) [2], Jou, Lebon and Casas-Vazques applied the principle to obtain nonlocal extensions of classical transport equations [13; 14; 15].

In order to derive the entropy principle by general physical laws, Muschik and Ehentraut [16] proposed the following amendment to the classical second law:

The curves representing quasi-static processes in the state space are all contained in the equilibrium subspace.

As a consequence of this statement, they proved that second law of thermodynamics necessarily restricts the constitutive equations and not the thermodynamic processes. In this way, the classical Coleman-Noll approach follows by a more general assumption through a rigorous proof.

On the other hand, Ruggeri [12; 17], on the example of the Lax conditions for shock wave propagation in perfect fluids, observed that for weak solutions the entropy principle selects the thermodynamical processes instead of restricting the constitutive equations. Notwithstanding, in some recent articles [18; 19] it is proved that the result by Muschik and Ehentraut may be extended to non-regular processes and generalized exploitation procedures [20], so that this problem deserves a more deep analysis.

REFERENCES

- [1] B. D. Coleman, W. Noll, *The thermodynamics of elastic materials with heat conduction and viscosity*, Arch. Rational Mech. Anal., 13 (1963), 167-178.
- [2] V. A. Cimmelli, *Different thermodynamic theories and different heat conduction laws*, J. Non-Equilib. Thermodyn., 34 (2009), 299-333.
- [3] I-Shi Liu, *Method of Lagrange multipliers for exploitation of the entropy principle*, Arch. Rat. Mech. Anal., 46 (1972), 131-148.
- [4] N. P. Kirchner, R. A. Hauser, *A historical note on the entropy principle of Müller and Liu*, Continuum Mech. Thermodyn., 14 (2002), 223-226.
- [5] G. Farkas, *A Fourier-féle mechanikai elv alkalmazásai*, Matematikai és Természettudományi Értesítő, 12 (1894), 457472. (in Hungarian.)
- [6] S. R. de Groot, P. Mazur, *Non-equilibrium Thermodynamics*, North-Holland Publishing Company, Amsterdam, 1962.
- [7] I. Gyarmati, *On the wave approach of thermodynamics and some problems of non-linear theories*, J. Non-Equilib. Thermodyn., 2 (1977), 233-260.
- [8] P. Ván, *Weakly nonlocal irreversible thermodynamics*, Annalen der Physik, 12 (2003), 142-169.
- [9] V. A. Cimmelli, P. Ván, *The effects of nonlocality on the evolution of higher order fluxes in nonequilibrium thermodynamics*, J. Math. Phys. 46 (2005), 112901 (15 pages).
- [10] I. Müller and T. Ruggeri, *Rational Extended Thermodynamics. 2nd edition*, Springer Tracts in Natural Philosophy, 37, Springer Verlag, New York, 1998.
- [11] I. Müller, *Extended Thermodynamics: a Theory of Symmetric Hyperbolic Field Equations.*, Entropy, 10 (2008), 477-492.
- [12] T. Ruggeri, *Thermodynamics and Symmetric Hyperbolic Systems*, Rend. Sem. Mat. Univ. Pol. Torino, Special Issue: Hyperbolic Problems, (1988), 167-183.
- [13] D. Jou, J. Casas-Vázquez, G. Lebon, *Extended Irreversible Thermodynamics, 4th revised edition*, Springer Verlag, Berlin, 2010.
- [14] G. Lebon, D. Jou, J. Casas-Vázquez, *Understanding Non-equilibrium Thermodynamics*, Springer Verlag, Berlin, 2008.
- [15] G. Lebon, D. Jou, J. Casas-Vázquez, W. Muschik, *Weakly Nonlocal and Nonlinear Heat Transport in Rigid Solids*, J. Non-Equilib. Thermodyn., 23 (1998), 176-191.
- [16] Muschik W., Ehentraut H., *An Amendment to the Second Law*, J. Non-Equilib. Thermodyn. 21 (1996), 175-192.
- [17] T. Ruggeri, *The Entropy Principle from Continuum Mechanics to Hyperbolic Systems of Balance Laws: The Modern Theory of Extended Thermodynamics*, Entropy, 10 (2008), 319-333.
- [18] V. Triani, V. A. Cimmelli, *Interpretation of Second Law of Thermodynamics in the presence of interfaces*, Continuum Mech. Thermodyn., 24 (2012), 165-174.

- [19] V. Triani, V. A. Cimmelli, *Entropy principle, non-regular processes and generalized exploitation procedures*, J. Math. Phys., 53 (2012), 063509 (8 pages).
- [20] V. A. Cimmelli, F. Oliveri, V. Triani, *Exploitation of the entropy principle: proof of Liu Theorem if the gradients of the governing equations are considered as constraints*, J. Math. Phys., 52 (2011), 023511-1-15.

NON-NEGATIVE ENTROPY PRODUCTION BY QUASI-LINEAR OR POTENTIAL-BASED FORCE-FLUX RELATIONS¹

Markus Hütter*, Bob Svendsen**,***

*Department of Mechanical Engineering, Materials Technology (MaTe), Eindhoven University of Technology,
P. O. Box 513, 5600 MB Eindhoven, The Netherlands, E-mail: M.Huetter@tue.nl

**Material Mechanics, RWTH Aachen University, 52062 Aachen, Germany,

***Microstructure Physics and Alloy Design, Max-Planck Institute for Iron Research, 40237 Düsseldorf, Germany
E-mail: bob.svendsen@rwth-aachen.de

EXTENDED ABSTRACT

An essential part in modeling out-of-equilibrium dynamics is the formulation of the irreversible dynamics. In the latter, the main modeling task consists in specifying the relations between thermodynamic forces on the one hand and fluxes on the other hand. As a guardrail to ensure that these relations comply with macroscopic observations one uses, among other principles, the second law of thermodynamics. The latter is considered in this contribution as that the local production of entropy is non-negative. Mainly two major directions have been followed in the literature for the specification of force-flux relations. On the one hand, quasi-linear relations are employed, in which so-called transport coefficients occur, that may depend on the forces themselves in which case we call the relation quasi-linear rather than linear. If the (matrix of) transport coefficients is non-negative, the second law is respected. Such relations have a deeper foundation in the physics of fluctuation-dissipation theorems [1; 2]. On the other hand, force-flux relations are also often represented in potential form. In this case, the flux is given by the derivative of a so-called dissipation potential with respect to the force [3]. The second law of thermodynamics is respected by requiring certain properties of the potential, primarily its convexity. In this contribution, we address the question of how these two approaches, quasi-linear and potential-based, are related.

The main outcome of this presentation is that every potential-based force-flux relation can be cast into quasi-linear form, while the reverse statement does not hold true [4]. In other words, the potential-based relations are a subset of those that can be formulated in the quasi-linear setting. While this main result is derived in general terms, it is demonstrated also with the help of three examples: (i) heat conduction in rigid bodies, (ii) homogeneous chemical reactions, and (iii) slippage in complex fluids. In particular, whereas the irreversible processes (i) and (ii) are dissipative, (iii) is not dissipative although it is irreversible. For the models (i) and (ii), conditions for the existence of a dissipation potential are formulated. Conversely, the dissipation potential for model (iii) vanishes since this model is an example of a dissipation-free irreversible process.

It is also shown that the above conclusions about force-flux relations have ramifications for the General Equation for Non-Equilibrium Reversible-Irreversible Coupling (GENERIC: e.g., [5; 6; 7]), which has been formulated in a quasi-linear [6; 7] and a dissipation-potential based [8] form, respectively. Also for the GENERIC it is found that potential-based form is a special case of the quasi-linear approach, as is the case for force-flux relations [4]. It can even be shown that the potential-form of GENERIC exists if and only if one does for the underlying force-flux relations.

While the potential-based forms are subcases of the quasi-linear counterparts, one may still opt for the potential-based form. For example, the potential-based form is necessary to formulate initial-boundary-value problems in variational form. In addition, the differential-geometry perspective on irreversible processes suggests a potential-based formulation [8]. As well, it has recently been suggested [9] that the potential form of GENERIC emerges from an optimization principle. Despite all these arguments, there are convincing arguments in favor of the quasi-linear relations. Firstly, they are more general than the potential-based forms, as shown above. Secondly, the quasi-linear form is the result of systematic coarse-graining using projection-operator techniques [7; 10; 11]. And thirdly, the quasi-linear form is more amenable to experimental determination where one often determines the transport coefficients as the ratio of the flux to the force.

REFERENCES

- [1] S. R. de Groot and P. Mazur, *Non-equilibrium Thermodynamics*, North-Holland, Amsterdam, 1962.
- [2] E. M. Lifshitz and L. P. Pitaevskii, *Physical Kinetics. Volume 10, Landau and Lifshitz Series on Theoretical Physics*, Pergamon, Oxford, 1981.
- [3] M. Šilhavý, *The Mechanics and Thermodynamics of Continuous Media*, Springer, Berlin, 1997.
- [4] M. Hütter and B. Svendsen, Quasi-Linear versus Potential-Based Formulations of Force-Flux Relations and the GENERIC for Irreversible Processes: Comparisons and Examples, *Continuum Mech. Therm.*, in press, doi: 10.1007/s00161-012-0289-y, 2013.
- [5] M. Grmela and H. C. Öttinger, Dynamics and Thermodynamics of Complex Fluids, I. Development of a General Formalism, *Phys. Rev. E*, vol. 56, pp. 6620–6632, 1997.
- [6] H. C. Öttinger and M. Grmela, Dynamics and Thermodynamics of Complex Fluids. II. Illustrations of a General Formalism, *Phys. Rev. E*, vol. 56, pp. 6633–6655, 1997.
- [7] H. C. Öttinger, *Beyond Equilibrium Thermodynamics*, Wiley Interscience Publishers, Hoboken, 2005.
- [8] M. Grmela, Multiscale Equilibrium and Nonequilibrium Thermodynamics in Chemical Engineering, *Adv. Chem. Engin.*, vol. 39, pp. 75–129, 2010. *ibid.*, Why GENERIC?, *J. Non-Newtonian Fluid Mech.*, vol. 165, pp. 980–986, 2010.
- [9] B. Turkington, 6th Intl. Workshop on Nonequilibrium Thermodynamics (Røros, Norway, August 1924, 2012), arXiv:1207.2692.
- [10] H. Grabert, *Projection Operator Techniques in Nonequilibrium Statistical Mechanics*, Springer, Berlin, 1982.
- [11] H. C. Öttinger, General Projection Operator Formalism for the Dynamics and Thermodynamics of Complex Fluids, *Phys. Rev. E*, vol. 57, pp. 1416–1420, 1998.

¹For the full details of this presentation, the reader is referred to [4].

ENTROPY, ENTROPY FLUX, TEMPERATURE, AND SECOND LAW IN EXTENDED IRREVERSIBLE THERMODYNAMICS

David Jou

Grup de Física Estadística, Universitat Autònoma de Barcelona,
08193 Bellaterra, Catalonia, Spain
David.Jou@uab.cat

ABSTRACT

The formulation of the second law out of equilibrium implies several basic thermodynamic questions: a) the form of the entropy; b) the form of the entropy flux; c) the absolute temperature, and d) the concrete statement of the second law. Here, we illustrate these questions in the framework of extended irreversible thermodynamics, where fluxes are used as independent thermodynamic variables besides the classical variables. In this theory, the entropy and entropy flux depend on the several fluxes and are more general than their respective classical versions. This wider generality allows to explore for generalized transport equations including memory terms and non-local terms, which are not compatible with the local-equilibrium version of the second law, but whose consequences are experimentally observed.

INTRODUCTION

The second law was initially formulated by Clausius (1850) and Thomson (1851), in terms of impossibility of existence of some kind of engines or processes. Such reference to impossibility has been useful to extend the domain of applicability of thermodynamics to such surprising topics as black hole thermodynamics or quantum thermodynamics. The latter theories have been formulated by stating the impossibility of processes reducing the total area of black holes, in the first case, or increasing global quantum entanglement by means of local operations in the second one.

This way of formulating the second law is global in space and time: it refers to the globality of the system and to a whole process. Thus, it does not yield strong restrictions on specific parts of a process. For instance, it states that it is impossible to build a cyclic heat engine fully converting heat into work, but one may have full conversion of heat into work along an isothermal expansion of an ideal gas. Of course, in the total cyclic process this partial process is compensated by other parts, in such a way that, as a whole, only a part of heat may be converted into work.

In 1865, Clausius devised another way to formulate the second law, based on the definition of a new state quantity, called the entropy, defined in terms of the integral of heat reversibly exchanged over the absolute temperature. According to his formulation, in isolated systems processes increasing the total entropy are impossible (in other words, only those processes reducing or keeping constant the entropy are possible). Clausius entropy is defined only for equilibrium states, and his statement establishes whether it is possible in principle a process leading from an equilibrium state A to an equilibrium state B.

In 1872, Boltzmann related the entropy, a macroscopic quantity, to molecular disorder, a microscopic concept. In some occasions, attention to only a part of the system may be misleading. For instance, in a well-stirred solution of oil into water there are initially many oil droplets into water, but all these droplets aggregate in a single oil phase separated from the water phase. Apparently, this process goes from a more disordered state to a more ordered state. However, in fact this is not so, because the water molecules, not directly visible, have increased their global disorder, in such a way that the total disorder has indeed increased in the aggregation and separation process.

Thus, we see that the formulation of the second law in equilibrium has a global meaning, refers to equilibrium states, and must include all the relevant variables of the system. Going to non-equilibrium states leads to new challenges. One of the main aims of non-equilibrium thermodynamics is to analyze which transport equations are admissible according to the second law. This leads to restrictions on the sign of the transport coefficients, to relations between the several transport coefficients in coupled transport equations, and so on. Besides these restrictions coming from the second principle, one must add other restrictions arising from microscopic time reversibility, leading to the Onsager-Casimir reciprocity relations between linear coupled transport equations, established in 1931.

In general terms, going from equilibrium to non-equilibrium implies new problems: a) one is not dealing with equilibrium states, but with non-equilibrium states, which are not homogeneous and are, in general, time-dependent. This makes that a global description is not very illuminating, as we are precisely interested in the transfer of heat, mass, momentum and so on between different regions of the

system, in such a way that local features are needed, b) in non-equilibrium, many additional variables which do not play any role at equilibrium arise, and the choice of the variables necessary to describe the system is not clear a priori.

Thus, the formulation of the second principle in continuum non-equilibrium thermodynamics implies, at least, five basic questions [1-3]: a) the choice of variables; b) the form of the entropy; c) the form of the entropy flux; d) the meaning and form of absolute temperature [4,5]; and e) the concrete statement of the second law. Here we will discuss these topics.

LOCAL VERSUS GLOBAL, INSTANTANEOUS VERSUS HISTORICAL FORMULATIONS

In classical non-equilibrium thermodynamics, the first four questions are answered by taking for the mentioned quantities their corresponding usual form in equilibrium thermodynamics, but with a local –instead of a global– meaning, and the fifth question is stated as the positive definite character of the entropy production. Note, however, that this formulation of the second law is more restrictive than the classical formulation, which only refers to entropy in equilibrium states, and imposes that the entropy of the final equilibrium state is higher or equal than the entropy of the initial equilibrium state which, after a number of constraints acting on it have been removed, evolves to the final equilibrium state. In contrast, the idea that the local entropy production per unit time must be always positive or zero implies that between the initial and the final equilibrium states the entropy must increase at any time and in any region. This is a sufficient but not a necessary condition for the classical statement of the second law to be fulfilled. Some authors, as Meixner, tried thus to avoid the use of an entropy in the intermediate non-equilibrium states and tried to have less restrictive conditions for the second law.

In fact, there are several physical phenomena, as for instance thermal oscillations (in discrete systems) or thermal waves (in continuous systems) which are compatible with the classical form of the second law (as the total entropy of the final equilibrium state in a relaxation process towards equilibrium is higher than that of the initial state), but they are not compatible with the local-equilibrium version of the second law (as the total local-equilibrium entropy integrated over the whole system does not increase in a monotonic way, but it exhibits an undulatory approach, with alternating increasing and decreasing behaviours of the entropy).

Thus, several basic questions arise: 1) must these phenomena be forbidden, although they are allowed by the classical version of the second law? This is not so, of course, because they are observed. 2) If they are actually observed, must one abandon the idea of a local instantaneous statement of the second law? 3) Must one drop the idea of generalizing the concept of entropy to non-equilibrium states? 4) Does this imply that a thermodynamic theory of non-equilibrium steady states (where the concept of non-equilibrium state cannot be avoided) should be abandoned? Or, in contrast, should one abandon the local-equilibrium hypothesis, although it has been so useful and successful in so many physical situations? Probably, there is not a single set of reasonable answers to these several questions. Here, in particular, we propose to go beyond the local-equilibrium hypothesis by looking for more general versions of entropy for non-equilibrium states.

The local-equilibrium hypothesis is valid as far as the rate of change of the local variables is slow enough to reach local equilibrium. If the fluxes are too high, for instance, the energy arriving to the system will leave from it without having had time enough to distribute amongst the several degrees of freedom and the several particles according to the equilibrium distribution. Analogously, if the rate of change of variables of the system (for instance, the cooling rate, the reaction rate of the speed of a solidification front) is too high, the system has no time enough to reach internal thermal equilibrium. In this case, the local-equilibrium distribution will no longer be valid and some generalizations of it must be explored.

CHOICE OF STATE VARIABLES IN NON-EQUILIBRIUM STATES

Of course, many possibilities of additional variables arise when the system is in non-equilibrium. For instance, one can consider the rates of change of the classical variables, or the fluxes of the classical variables, or higher-order variables as for instance higher-order time derivatives or higher-order fluxes, or some internal variables related to the microstructure of the system, as for instance the configuration tensor or the polarization of polymeric molecules in polymer solutions. These variables vanish at equilibrium and therefore an entropy incorporating them should in principle reduce to the usual equilibrium entropy in equilibrium states. One of the possibilities of describing the system is to take into account the fluxes as additional variables, in such a way that higher values for the fluxes will imply a higher departure from local equilibrium.

The choice of variables is a relevant matter in non-equilibrium systems, and it depends on the relative values of the rates or frequencies of external perturbations and the reciprocal of the relaxation times of the several internal degrees of freedom of the system. The variables much faster than the external perturbation may be considered at equilibrium; the variables much slower will be frozen in values dependent on the initial conditions; and the interest of the researcher will be focused on the dynamics of those variables whose typical relaxation times are of the order of the rate of the external perturbations [6-8].

Another aspect of the choice of variables is between rates, fluxes, gradients, or internal variables. If one is interested in thermodynamics of non-equilibrium steady states, fluxes will be more useful than rates of change. Indeed, the latter vanish at steady states, whereas the fluxes indicate the rate of energy, matter, momentum and so on with the external world. Therefore, the fluxes provide essential information for non-equilibrium steady states. On the other side, if one is interested in a macroscopic description, where the fluxes are controlled parameters, the use of the fluxes will be more suitable than the use of internal variables which, instead, may be more useful if microscopic descriptions are sought for. The choice of variables will depend thus both on the time scales as on the particular interests and abilities of the observer.

In particular, the non-equilibrium thermodynamic theories taking the fluxes as independent variables are known as “extended thermodynamics” [9-14]. In extended thermodynamics, the questions mentioned in the introduction are given the following answers.

ENTROPY

The extended entropy is the local-equilibrium entropy plus a negative contribution proportional to the square of the fluxes; the corresponding coefficient is proportional to the relation time of the corresponding flux and inversely proportional to the respective transport coefficient; thus, the non-equilibrium contributions to the entropy are related to relaxational contributions to generalized transport equations. Two typical examples are: heat transport with non-vanishing relaxation time, in which the transport equation takes the form of the so-called Maxwell-Cattaneo equation

$$\tau \frac{dq}{dt} + q = -\lambda \nabla T \quad (1)$$

where λ is the thermal conductivity and τ the relaxation time of the heat flux. When the relaxation time is negligible, this equation reduces to the classical Fourier's equation. The corresponding extended entropy is

$$\mathfrak{S}(u, \mathbf{q}) = s_{\text{eq}}(u) - \frac{\tau}{2\lambda T^2} \mathbf{q} \cdot \mathbf{q} \quad (2)$$

with s_{eq} the local-equilibrium entropy.

Another typical situation is viscoelasticity, where a relaxational equation for the viscous pressure tensor is used, in the form

$$\tau \frac{d\mathbf{P}^v}{dt} + \mathbf{P}^v = -2\eta \mathbf{V} \quad (3)$$

or more general forms, taking more sophisticated kinds of time derivatives, as the corotational or the upper Maxwell convected ones. Here, η is the shear viscosity and \mathbf{V} is the symmetric part of the velocity gradient. When the perturbation of the flow is slow with respect to the time scale set by the relaxation time, the material behaves as a viscous fluid, and when they are fast it behaves as an elastic solid. The corresponding extended entropy has the form

$$\mathfrak{S}(u, c, \mathbf{P}^v) = s_{\text{eq}}(u, c) - \frac{\tau}{4\eta T} \mathbf{P}^v : \mathbf{P}^v \quad (4)$$

Note, in particular, that in both cases the transport equations as well as the entropy reduce to their classical forms when the relaxation times go to zero. Furthermore, as it will be commented below in more detail, the local production of the generalized entropy is always positive, whereas the production of the local-equilibrium entropy may be negative in some cases.

Eventually, note that when these expressions for the entropy are introduced into the Einstein equation for the probability of fluctuations, this extended entropy describes not only the second moments of the fluctuations of the classical variables but also the fluctuations of the corresponding fluxes [9-10]. This is a check of the physical interpretation of the non-equilibrium terms, and it shows that incorporating the fluxes in the description gives additional information on the system even in equilibrium situations, where the average value of the fluxes is zero but their fluctuations may be different from zero. In fact, the most

general versions of the fluctuation-dissipation theorem express the memory kernel of generalized transport equations in terms of the time-correlation function of the fluctuations of the corresponding dissipative fluxes (i.e the thermal conductivity in terms of the heat flux fluctuations; the shear viscosity in terms of the viscous pressure fluctuations, and so on). Thus, the interest on the dynamics of the fluxes is not something special of extended thermodynamics, but it is a general feature in modern non-equilibrium statistical physics.

ENTROPY FLUX

The entropy flux is the classical entropy flux plus a non-equilibrium contribution proportional to the product of the fluxes times their corresponding higher-order fluxes; thus, the non-equilibrium contribution is related to the non-local contributions appearing in generalized transport equations. A typical example is, for instance, the heat transport equation with relaxation terms and non-local terms, also known as Guyer-Krumhansl equation,

$$\tau \frac{dq}{dt} + q = -\lambda \nabla T + \ell^2 \nabla^2 q \quad (5)$$

with ℓ the mean free path. The entropy is still (2) but the entropy flux has the form

$$\mathbf{J}^s = \frac{\mathbf{q}}{T} - \frac{\ell^2}{\lambda T^2} (\nabla q) \cdot \mathbf{q} \quad (6)$$

Another typical example is the equation for dilute gases as obtained from Grad's approach in the second-order approximation

$$\tau \frac{dq}{dt} + q = -\lambda \nabla T + \beta \nabla \cdot \mathbf{P}^v \quad (7)$$

$$\tau \frac{d\mathbf{P}^v}{dt} + \mathbf{P}^v = -2\eta \mathbf{V} + \beta \nabla q \quad (8)$$

In general, the relaxation times will be different for the different variables. The corresponding entropy is a combination of (2) and (4), namely,

$$\mathfrak{S}(u, c, \mathbf{P}^v) = s_{\text{eq}}(u, c) - \frac{\tau_1}{2\lambda T^2} \mathbf{q} \cdot \mathbf{q} - \frac{\tau_2}{4\eta T} \mathbf{P}^v : \mathbf{P}^v \quad (9)$$

and the entropy flux is

$$\mathbf{J}^s = \frac{\mathbf{q}}{T} + \beta \mathbf{P}^v \cdot \mathbf{q} \quad (10)$$

It is seen in Eqs. (6) and (10) that non-local terms, related to the gradients or divergences of other fluxes, are related to extra contributions of the generalized entropy flux.

TEMPERATURE

Absolute temperature, was defined by the first time by

Thomson in 1848, and set the basis for a universal material-independent foundations for thermodynamics. Absolute temperature is given by the reciprocal of the derivative of the entropy with respect to the internal energy (at constant values of the other extensive variables). When the extended entropy (2) is used instead of the local-equilibrium entropy, the resulting absolute temperature θ

$$\frac{1}{\theta} = \left(\frac{\partial s}{\partial u} \right)_{\mathbf{v}, \mathbf{q}} = \frac{1}{T} - \frac{1}{2} \left(\frac{\partial \alpha}{\partial u} \right) \mathbf{q} \cdot \mathbf{q} \quad (11)$$

with $\alpha = \tau/\lambda T^2$. It differs from the local-equilibrium temperature T and depends on the fluxes;. Several comments about (11) are in order. A) Relation (11) is purely formal unless a process of measuring it is specified. In equilibrium, all the many possible operational definitions of temperature lead to the same value, and all the thermometers will indicate it. However, this is not so out of equilibrium, where different kinds of thermometers yield different values for the temperature. In particular, the temperature defined in (1) may be related to the average kinetic energy of the particles in the plane perpendicular to the fluxes, and it is in general different from the “temperatures” of the other degrees of freedom, which may have different values [4, 9]. B) The fact that θ depends on T and \mathbf{q} may be checked by considering a heat conducting bar introduced between two systems at the same T , but one of them at equilibrium and the other one submitted to a steady heat flux. According to the classical irreversible thermodynamics, where

$$\mathbf{q} = -\lambda \nabla T, \quad (12a)$$

heat should not flow; however, in extended irreversible thermodynamics, where

$$\mathbf{q} = -\lambda \nabla \theta, \quad (12b)$$

heat should flow between them. For ideal gases it may be shown that $\theta < T$ and heat would flow from the system at equilibrium to the system in non-equilibrium steady state. C) In the kinetic theory of ideal gases, the absolute temperature is defined through the caloric equation of state relating the average kinetic energy to the absolute temperature

$$\frac{3}{2} k_B T = \langle \frac{1}{2} m \mathbf{C}^2 \rangle \quad (13)$$

where m is the mass of the particles and \mathbf{C} their peculiar velocity with respect to the barycentric mass. However, in the presence of a heat flow along the z direction, and up to the second order in the heat flux, it may be seen, from maximum-entropy arguments, that

$$\langle \frac{1}{2} m \mathbf{C}_x^2 \rangle = \langle \frac{1}{2} m \mathbf{C}_y^2 \rangle = \frac{1}{2} k_B \theta < \frac{1}{2} k_B T \quad (14a)$$

and

$$\langle \frac{1}{2} m \mathbf{C}_z^2 \rangle = \frac{1}{2} k_B (3\theta - 2T) > \frac{1}{2} k_B T \quad (14b)$$

in such a way that the usual definition of T is satisfied, but there is also a place for a non-equilibrium temperature.

This simple example shows that beyond local equilibrium, energy equipartition should not be expected in general, so

that different degrees of freedom may have different values of the temperature. One of the aims of a non-equilibrium thermodynamics of steady states should be to relate the temperatures for the different degrees of freedom when the total energy and energy flux are specified. It is not sufficient to formally define a non-equilibrium temperature through a relation like (11), but one must also identify under which physical conditions this temperature may be measured, and which is its relation with other temperatures of other degrees of freedom. Furthermore, since different kinds of thermometers have different sensitivities to different degrees of freedom, it is also important to be able to relate the temperatures measured by different kinds of thermometers. Thus, thermodynamics beyond local equilibrium is indeed a demanding task.

STATEMENT OF THE SECOND LAW

The second law is usually stated as the positive definite character of the entropy production. Depending on the kind of entropy being considered, the entropy production will have different forms and will yield different restrictions on the transport equations. In particular, this statement expressed in terms of the extended entropy allows several surprising features which are forbidden by the classical form of the second law: at short time scales and short spatial scales, for instance, heat may flow from lower to higher temperature [5]. Some of these features have been checked through thermal waves, or could be checked in systems with relatively long mean-free paths. For instance, in a heat transport equation with a relaxation term, the heat exchange between two small subsystems in thermal contact take the form of a damped oscillation. During some time intervals, heat is flowing from lower to higher temperature. This is against the local-equilibrium version of the second law but not against the classical version of the second law, because during the total equilibration process the net heat exchange from higher to lower temperature is higher than in the opposite direction [9-14].

An analogous situation of heat flowing in the opposite direction as allowed by the second law is found in phonon backscattering in rough-walled silicon nanowires, in a thin layer (the so-called Knudsen layer) close to the walls. From a microscopic perspective this may be understood, as phonons collide against the roughness peaks and they recede backwards. This reduces very much the effective thermal conductivity of the nanowire. This feature violates the local-equilibrium version of the second law, but not the classical version, because the net heat flux is against the temperature gradient, as it should be. A similar situation may be found in radial heat transport at short scales [15].

In both cases, the local-entropy production of the EIT entropy is positive everywhere, in contrast with the production of the local-equilibrium entropy. Thus, at small lengths and short times the formulation of a local and instantaneous version of the second law need a generalization of the entropy. Note that these situations seem, in principle, out of the reach of thermodynamic descriptions, because the number of collisions is very small. However, in steady states one may make many different measurements and a statistical description is possible. Particular situations could violate the positive definite character of the extended entropy production but, on the average, they are expected not to violate it. However, the average value could violate the positive character of the local-equilibrium entropy production.

Furthermore, one may use information theoretical arguments to obtain the expression for the entropy, subject to constraints on the average values of the classical variables and the fluxes [6, 9]. Such arguments also imply a statistical meaning. However, one could explore the ideas of algorithmic information theory, where information does not require a statistical description, but the minimum amount of information to describe a given physical situation. In this case, one could use thermodynamic concepts in situations beyond the usual ones.

CONCLUDING REMARKS

In this final section we briefly comment on some questions arising in non-linear and in non-Markovian situations and concerning the relation between the entropy and the Boltzmann H-function in non-equilibrium situations.

Non-linear transport equations

A problem of the application of the second law is its use for non-linear transport laws. In principle, the admissible laws are those yielding a positive entropy production. However, when this restriction is applied not to the full laws but to second or fourth-order approximation in the forces, the restrictions may be unsuitable, in the sense that they may require some coefficient to be zero although they are not truly zero. Indeed, the negative contribution of some second or fourth-order terms may be compensated by the positive contributions of higher-order terms. In this case of approximations to fully nonlinear laws, the second law may indicate, rather than a strict restriction on the coefficients, a bound on the domain of applicability of such approximations; thus, instead of setting restrictions on material properties (as it is usual in the linear domain) they may set limits on the processes to which such equations may be applicable.

Non-Markovian systems

Another topic of interest is the formulation of the second law for non-Markovian systems. In this case, the value of the variables of the system at time $t + \tau$ are a function not only of the values at time t , but also at time $t - \tau$ (and maybe other precedent times). Then, a description of the evolution of the system requires knowing not only the values at t but also at $t - \tau$, namely

$$X_i(t + \tau) = F[X_j(t), X_k(t - \tau)] \quad (15)$$

where X_i are the variables of the system, and $F[\dots]$, a suitable functional or differential equation. Therefore, the entropy should be expressed in terms not only of the variables at t but also at $t - \tau$, namely

$$S = S(X_j(t), X_k(t - \tau)) \quad (16)$$

When the difference between the values at time t and time $t - \tau$ is expanded up to the first order in τ , the fluxes or the rates of change arise in a natural way in the entropy. Higher-order fluxes or time derivatives appear if the expansion goes to second or higher orders in τ . The formalism of EIT has been also applied to some situations of this kind at a microscopic level, when the usual H function is not sufficient to account for the second law restrictions [9]. Non-Markovian transport

equations may also be expressed in terms of memory functions; the second-law restrictions on memory functions are an interesting topic in the so-called rational thermodynamics.

H-function and non-equilibrium entropy

Another topic of interest for our discussion is the relation between the microscopic H-function and the extended entropy. In equilibrium states, the H-function reduces to the thermodynamic entropy. Then, it is logical to ask what is the relation between both functions out of equilibrium. The H-function, described in terms of the microscopic distribution function, may be a functional of many variables, as for instance, of many moments of the distribution function, may higher-order fluxes, or many higher-order gradients of the hydrodynamic variables. But a thermodynamic description is deemed to use only a relatively small number of independent variables, having a macroscopic (or mesoscopic) limit. Thus, the H-function does not directly provide a truly thermodynamic entropy.

To have a thermodynamic entropy, one should project the entropy onto a space of a relatively small but sufficiently efficient and realistic set of variables. This may be done, but it is not sure that such a projected (or reduced) version of the entropy must have a positive entropy production. As a consequence, the H-theorem does not yield a deep basis to the formulations of the second law based on reduced entropies.

To be more explicit, consider that the non-equilibrium distribution function may be written as

$$f(\mathbf{r}, \mathbf{C}, t) = f_{eq}(\mathbf{r}, \mathbf{C}, t)[1 + \Phi] \quad (17)$$

with f_{eq} the equilibrium distribution function characterized by the local values of the thermodynamic parameters, and Φ a non-equilibrium contribution. Up to the second order in Φ , the "entropy" s obtained from the H-function has the form

$$s = s_{eq} - \frac{1}{2} k_B \int f_{eq} \Phi^2 d\mathbf{C} \quad (18)$$

It is seen that, in principle, s will differ from the local-equilibrium entropy s_{eq} . However, in view of (17) and (18), the practical success of the local-equilibrium version of the second law may be easily understood. Indeed, from a microscopic basis, the local-equilibrium hypothesis does not imply a local-equilibrium form for the microscopic distribution function, but a suitable non-equilibrium contribution Φ is needed; otherwise, because of symmetry reasons, the values of the fluxes (which are usually odd functions of the molecular velocity) would be zero. But, up to the first order in Φ , the entropy reduces to the local-equilibrium entropy, because the first-order contribution in Φ may be shown to vanish. Then, the use of a non-vanishing Φ in the calculation of the fluxes is compatible with the use of the local-equilibrium entropy. This consistency is lost when the equations for the fluxes, i.e. the transport equations, incorporate second-order terms, because in this case second-order terms should also be considered in the entropy.

When Grad's approach to the solution of the Boltzmann equation is used, i.e. when Φ is expressed in terms of the second or the third moments of the velocity distribution function for ideal gases, which are directly related to the

viscous pressure tensor or the heat flux, respectively, the expressions (4) and (2) for the entropy are obtained, and expression (10) for the entropy flux is also obtained, consistent with linear transport equations (7) and (8). However, the microscopic transport equations are in fact more general than (7) and (8), as they contain non-linear contributions.

The extended entropy production is positive for equations (7) and (8), but it may become negative when non-linear terms are taken into consideration. However, these negative contributions could be balanced by positive contributions arising from higher-order non-linear terms, but this would require a knowledge of all such terms. Eu [12] made an interesting proposal to deal with non-linear terms, which leads to a positive entropy production for relatively complex and useful generalizations of the transport equations (7) and (8). Otherwise, in Grad's approach –and also in Chapman-Cowling approach–, the positive character of the truncated entropy cannot be shown, in contrast to the positive character of the production of the H function.

ACKNOWLEDGMENTS

I acknowledge the support of the Spanish Ministry for Economía y Competitividad (MINECO) under grant FIS 2012-32099 and of Direcció General de Recerca of the Government of Catalonia, under grant 2009 SGR 164. Discussions with Profs G. Lebon and J. Casas-Vázquez along more than thirty years are warmly acknowledged.

NOMENCLATURE

k_B Boltzmann constant
 s entropy per unit mass
 \mathcal{J}^s entropy flux
 \mathbf{q} heat flux
 u internal energy per unit mass
 ρ mass density
 ℓ mean free path
 τ relaxation time
 η shear viscosity
 λ thermal conductivity
 \mathbf{X} variables of a system
 \mathbf{C} velocity of molecules
 \mathbf{V} velocity gradient
 \mathbf{P}^v viscous pressure tensor

REFERENCES

- [1] G. Lebon, D. Jou, J. Casas-Vázquez, Understanding non-equilibrium thermodynamics, Springer, Berlin, 2008.
- [2] S. Kjelstrup and D. Bedeaux, Non-equilibrium Thermodynamics of Heterogeneous Systems, World Scientific, Singapore, 2008.
- [3] H.C. Oettinger, Beyond Equilibrium Thermodynamics, Wiley, New York, 2005.
- [4] J. Casas-Vázquez and D. Jou, Temperature in non-equilibrium states: a review of open problems and current proposals, *Rep. Prog. Phys.* Vol 66, pp. 1937-2023, 2003.
- [5] W. Muschik, Aspects of Non-equilibrium Thermodynamics, World Scientific, Singapore, 1990.
- [6] R. Luzzi, A R Vasconcellos and J G. Ramos, Statistical foundations of irreversible thermodynamics, Teubner, Leipzig, 2001
- [7] D. Jou and L. Restuccia, Mesoscopic transport equations and contemporary thermodynamics, *Contemp Phys* vol. 52, pp. 465-474, 2011.
- [8] G. Lebon, D. Jou and J. Casas-Vázquez, Questions and answers about a thermo dynamic theory of the third type, *Contemp Phys* vol. 33, pp. 41- 51, (1992).
- [9] D. Jou, J. Casas-Vázquez and G. Lebon, Extended irreversible thermodynamics, Springer, Berlin, 2010, fourth edition.
- [10] D. Jou, J. Casas-Vázquez and M. Criado Sancho, Thermodynamics of Fluids under Flow, Springer Verlag, Berlin 2000.
- [11] I. Müller and T. Ruggeri, Rational extended thermodynamics, Springer, New York, 1997.
- [12] B. C. Eu, Kinetic theory and irreversible thermodynamics, Wiley, New York, 1992.
- [13] D.Y. Tzou, Macro to Micro-scale Transfer. The Lagging Behaviour, Taylor and Francis, New York, 1997.
- [14] M. S. Mongiovi and D. Jou, “Evolution equations in superfluid turbulence”, in *Condensed matter: new research*, M. P. Das, editor, Nova Publishers, Hauppauge, New York, 2006
- [15] A. Sellitto, V A Cimmelli and D Jou, Entropy flux and anomalous axial heat transport at the nanoscale, *Phys. Rev. B* Vol 87, 054302, 2013.
- [16] P. Galenko and D. Jou, “Diffuse-interface model for rapid phase transformation in nonequilibrium system”, *Phys. Rev. E* Vol. 71, 046125, 2005.

ON THE FORMULATION OF ENTROPY FOR A PARTIALLY QUANTIZED ELECTRON SYSTEM IN SEMICONDUCTORS

V. Dario Camiola*, Giovanni Mascali**, Vittorio Romano*

*Dipartimento di Matematica e Informatica, Università di Catania, viale A. Doria 6, 95125 Catania, Italy,
E-mail: camiola@dmi.unict.it, romano@dmi.unict.it

**Dipartimento di Matematica, Università della Calabria and INFN-Gruppo c. Cosenza, 87036 Cosenza, Italy,
E-mail: g.mascali@unical.it

EXTENDED ABSTRACT

In the formulation of hydrodynamic subband models for charge carriers in semiconductors in presence of confinement effects in one or two directions, a crucial problem, in order to apply the maximum entropy principle (MEP), is an appropriate assumption on the entropy for a 2D or 1D electron gas which combines a semiclassical description in the transport direction and quantum effects in the transversal direction. The attempts already known in the literature are based on the quantum formulation of the maximum entropy principle, as proposed in the pioneering work of Jaynes [1] and its more recent revisitation in [2; 3; 4]. However the technical difficulties in solving the constraints in the quantum case are a very complex and daunting task because the algebraic relations are now operatorial ones. Even the expansion in powers of \hbar does not circumvent the problem since only low order terms can be retained otherwise the presence of too high order derivatives makes the resulting equations practically impossible to solve numerically.

When confined structures, like those arising in double-gate MOSFET's or standard MOSFET's are considered, one can take advantage from the symmetry of the problem which allows one to make a geometrical splitting in quantized direction and longitudinal direction. In [5; 6] we have proposed a hybrid expression for the entropy of the system under consideration where in each subband the semiclassical entropy, arising as the limit of the Fermi-Dicac one, is weighted by the square modulus of the envelope functions obtained by solving the Schroedinger-Poisson equations. Summing up the contribution of each subband, the resulting form of the entropy contains both semiclassical information, intended in the usual sense of statistical mechanics or information theory, and a quantum aspect which weights the importance of the single subband, giving more relevance to those associated with a lower energy.

Examples of applications of such an approach have been presented in [7; 8] where the simulations of nanoscale double gate MOSFET's show a good accuracy of the models.

REFERENCES

- [1] Jaynes, E. T.: Information Theory and Statistical Mechanics. Phys. Rev. B vol. 106, pp. 620–630, 1957.
- [2] Degond, P., Ringhofer, C., Quantum moment hydrodynamics and the entropy principle, J. Stat. Phys. vol.112, pp. 587-628, 2003.
- [3] Degond, P., Gallego, S., Méhats, F., Ringhofer, C. , Quantum hydrodynamic and diffusion models derived from the entropy principle, in *Quantum Transport: modelling, analysis and asymptotics - lectures given at the CIME summer school held in Cetraro (Italy), September 11-16, 2006* (N. Ben Abdallah & G. Frosali (eds.)), Lectures Notes in Mathematics vol. 1946, Springer, 2008, pp. 111-168.
- [4] Ben Abdallah, N., Méhats, F., Vauchelet, N.: Diffusive transport of partially quantized particles: existence, uniqueness and long-time behaviour. Proc. Edinb. Math. Soc. vol. 2, pp. 513–549, 2006.
- [5] Mascali, G., Romano, V.: Hydrodynamic subband model for semiconductors based on the maximum entropy principle. IL NUOVO CIMENTO C vol. 33, pp. 155–163, 2010.
- [6] Mascali, G., Romano, V.: A non parabolic hydrodynamical subband model for semiconductors based on the maximum entropy principle. Mathematical and Computer Modeling vol. 55, pp. 1003-1020, 2012.
- [7] Camiola V.D., Mascali G., Romano V. "Numerical simulation of a double-gate MOSFET with a subband model for semiconductors based on the maximum entropy principle. Continuum Mechanics and Thermodynamics" vol. 24, pp. 417–436, 2012.
- [8] Camiola V.D., Mascali G., Romano V. "Simulation of a double-gate MOSFET by a non-parabolic energy-transport model for semiconductors based on the maximum entropy principle ", to appear in MCM (2012)

RECENT RESULTS IN RATIONAL EXTENDED THERMODYNAMICS: MACROSCOPIC APPROACH AND MAXIMUM ENTROPY PRINCIPLE FOR DENSE AND RAREFIED POLYATOMIC GASES

Tommaso Ruggeri

University of Bologna

EXTENDED ABSTRACT

After a brief survey on the principles of Rational Extended Thermodynamics of monatomic gas (entropy principle, constitutive equations of local type, symmetric hyperbolic systems, main field, principal sub-system) we present in this talk a recent new approach to deduce hyperbolic system for dense gases not necessarily monatomic.

In the first part of the talk we study extended thermodynamics of dense gases by adopting the system of field equations with a different hierarchy structure to that adopted in the previous works. It is the theory of 14 fields of mass density, velocity, temperature, viscous stress, dynamic pressure and heat flux. As a result, all the constitutive equations can be determined explicitly by the caloric and thermal equations of state as in the case of monatomic gases. It is shown that the rarefied-gas limit of the theory is consistent with the kinetic theory of gases.

In the second part, we limit the result to the physically interesting case of rarefied polyatomic gases and we show a perfect coincidence between ET and the procedure of Maximum Entropy Principle. The main difference with respect to usual procedure is the existence of two hierarchies of macroscopic equations for moments of suitable distribution function, in which the internal energy of a molecule is taken into account.

REFERENCES

- [1] I. Müller and T. Ruggeri: Rational Extended Thermodynamics, 2nd ed., Springer Tracts in Natural Philosophy 37, (1998) Springer-Verlag (New York).
- [2] G. Boillat and T. Ruggeri: Moment equations in the kinetic theory of gases and wave velocities, *Continuum Mech. Thermodyn.* 9 (1997) 205-212.
- [3] T. Ruggeri: Can constitutive relations be represented by non-local equations? *Quart. of Appl. Math.*, 70, (3), (2012) 597–611.
- [4] T. Arima, S. Taniguchi, T. Ruggeri and M. Sugiyama: Extended thermodynamics of dense gases, *Continuum Mech. Thermodyn.* 24 (2012) 271-292.
- [5] T. Arima, S. Taniguchi, T. Ruggeri and M. Sugiyama: Extended thermodynamics of real gases with dynamic pressure: An extension of Meixner theory, *Phys. Lett. A* 376 (2012) 2799-2803.
- [6] T. Arima, S. Taniguchi, T. Ruggeri and M. Sugiyama: Dispersion relation for sound in rarefied polyatomic gases based on extended thermodynamics, *Continuum Mech. Thermodyn.* (2012) DOI 10.1007/s00161-012-0271-8.
- [7] M. Pavic, T. Ruggeri and S. Simic: Maximum entropy principle for rarefied polyatomic gases, *Physica A* (2012) 392 (2013) 1302–1317.

A PROPER NONLOCAL FORMULATION OF QUANTUM MAXIMUM ENTROPY PRINCIPLE FOR FERMI, BOSE AND FRACTIONAL EXCLUSION STATISTICS

M. Trovato*, L. Reggiani**

*Dipartimento di Matematica, Università di Catania,

Viale A. Doria, 95125 Catania, Italy, E-mail: trovato@dmf.unict.it

**Dipartimento di Matematica e Fisica "Ennio De Giorgi" and CNISM, Università del Salento,

Via Arnesano s/n 73100 Lecce, Italy, E-mail: lino.reggiani@unisalento.it.

ABSTRACT

By considering the Wigner formalism the quantum maximum entropy principle (QMEP) is here asserted as the fundamental principle of quantum statistical mechanics when it becomes necessary to treat systems in partially specified quantum mechanical states. From one hand, the main difficulty in QMEP is to define an appropriate quantum entropy that explicitly incorporates quantum statistics. From another hand, the availability of rigorous quantum hydrodynamic (QHD) models is a demanding issue for a variety of quantum systems like, interacting fermionic and bosonic gases, confined carrier transport in semiconductor heterostructures, anyonic systems, etc. We present a rigorous nonlocal formulation of QMEP by defining a quantum entropy that includes Fermi, Bose and, more generally, fractional exclusion statistics. In particular, by considering anyonic systems satisfying fractional exclusion statistic, all the results available in the literature are generalized in terms of both the kind of statistics and a nonlocal description for exclusion gases. Finally, gradient quantum corrections are explicitly given at different levels of degeneracy and classical results are recovered when \hbar tends to 0.

INTRODUCTION

In thermodynamics and statistical mechanics entropy is the fundamental physical quantity to describe the evolution of a statistical ensemble. Its microscopic definition was provided by Boltzmann through the celebrated expression $S = k_B \ln \Gamma$, where k_B is the Boltzmann constant and Γ is the number of microstates exploiting the given macroscopic properties. In this context, it is well known that in classical mechanics the entropy: i) allows the violation of the uncertainty principle [1]; ii) can be considered as a special case of the so-called *Boltzmann-Gibbs-Shannon* entropy that enables one to apply results of information theory to physics [1; 2]. In particular, maximum entropy principle (MEP) allows one to derive [2; 3; 4; 5] the nonequilibrium distribution function associated with particles, and to determine the microstate corresponding to the given macroscopic quantity.

We remark, that the MEP can be exploited in the completely nonlinear case, without any assumption on the nonequilibrium processes. Alternatively, an approximate distribution function is usually derived through a formal expansion around a local equilibrium configuration and so Extended Thermodynamics (ET) theories [3; 6] of \mathcal{N} moments and degree α ($ET_{\mathcal{N}}^{\alpha}$ models) were obtained. In this way, it was found possible to derive rigorous hydrodynamic (HD) models based on the *moments* of the distribution function to different orders of a power expansion and including appropriate closure conditions [3; 6; 7; 8]. Accordingly, making use of the Lagrange multipliers technique, it was found possible to construct the set of evolution equations for the macro-variables of interest.

Apart from some partial attempts [2; 9; 10], this is no longer the case in quantum mechanics. Here, the main difficulties concern with: i) the definition of a proper quantum entropy that includes particle indistinguishability; ii) the formulation

of a global quantum MEP (QMEP) that allows one to obtain a quantum distribution function both for thermodynamic equilibrium and nonequilibrium configurations. From one hand, in the framework of a nonlocal quantum theory, the generalization of the corresponding Lagrange multipliers is also an open problem. From another hand, a rigorous formulation of quantum HD (QHD) closed models is a demanding issue for many kinds of problems in quantum systems like, interacting fermionic and bosonic gases, anyonic systems, quantum turbulence, quantum fluids, quantized vortices, nuclear physics, confined carrier transport in semiconductor heterostructures, phonon and electron transport in nanostructures, nanowires and thin layers.

Recently, a comprehensive review on QMEP which summarizes the state-of-the-art on this subject was presented in Ref. [8]. Accordingly, all the results available from the literature for a three-dimensional (3D) Fermi and/or Bose gas, have been generalized in the framework of a nonlocal Wigner theory both in equilibrium and nonequilibrium conditions [11].

The aim of this work is to consider an extension of QMEP in the framework of fractional exclusion statistics (FES). In particular we consider anyonic systems satisfying FES [12], and to determine the thermodynamic evolution of an exclusion gas compatibly with the uncertainty principle. In this way, within the framework of a QMEP-Wigner formulation, we generalize all the results available from the literature in terms of both: the kind of statistics and a nonlocal description for the quantum gas.

FRACTIONAL STATISTICS

Whereas fermions and bosons can exist in all dimensions, certain low dimensional systems have elementary excitations that may obey quantum statistics interpolating between fermionic and bosonic behaviors. In particular, particles carrying these generalized statistics, are called generically *anyons*

[13]. For anyons, fractional statistics are related to the trajectory dependence in the particle exchange procedure in configuration space and are connected to the braid group structure of particle trajectories [13; 14; 15] in two spatial dimensions ($2D$). Mathematically, fractional statistics are parameterized by a phase factor that describes how the field operators of an anyonic system changes because of exchange procedure in $2D$ configuration space [13; 14; 15]. Thus, the concept of anyons is specific to two dimensions, and because of the trajectory dependence, the single particle state is inextricably connected with the complete state of the many-body configuration of the system. In $2D$ systems, the fractional statistics have been successfully applied to describe the charged excitations (Laughlin quasi-particles [16]) of a fractional quantum Hall (FQH) [17] where the electron gas shows a fractional electric charge [18] and, more recently, a direct evidence of fractional exchange phase factor was observed in experiments [19]. We remark, that fractional anyon statistics has been formalized, to some extent [20; 21], also in the one-dimensional ($1D$) case. In particular, for $1D$ systems the interactions and statistics are inextricably related, because the collision phenomena are the only way to interchange two particles. Accordingly, also in this case, anyons acquire a step-function-like phase when two identical particles exchange their positions in the scattering process. Anyons in $1D$ models are still unexplored to a wide extent, although many one-dimensional anyonic models have been introduced and investigated in literature [22; 23; 24; 25; 26; 27]. Thus, by defining the q -deformed bracket $[A, B]_q = AB - qBA$, we can introduce (for $D = 1, 2$) the anyon field operators $\Psi(\mathbf{r})$ and $\Psi^\dagger(\mathbf{r})$ with the general deformed relations [14; 28; 29]

$$[\Psi(\mathbf{r}), \Psi(\mathbf{r}')]_q = [\Psi^\dagger(\mathbf{r}), \Psi^\dagger(\mathbf{r}')]_q = 0, \quad (1)$$

$$[\Psi(\mathbf{r}), \Psi^\dagger(\mathbf{r}')]_{q^{-1}} = \delta^D(\mathbf{r} - \mathbf{r}'), \quad (2)$$

where $q(\mathbf{r}, \mathbf{r}')$ is a discontinuous function of its arguments [14; 29] corresponding to a phase factor that denotes the system statistics [30] and, for the sake of consistency

$$q(\mathbf{r}, \mathbf{r}') = q^{-1}(\mathbf{r}', \mathbf{r}), \quad \text{with} \quad q(\mathbf{r}, \mathbf{r}) = \pm 1, \quad (3)$$

A different notion of fractional statistics, in arbitrary dimension D , has been introduced by Haldane [31]. This approach is based on a generalized Pauli exclusion principle where it is necessary to count as changes the dimension of the single particle Hilbert space when extra particles are added, keeping constant both the boundary conditions and the size of the condensed-matter region. Particles that obey Haldane exclusion-statistics (HES) are called exclusions with (*in the case of single specie*) a statistics parameter $\kappa = -\delta G/\delta N$, where δG describes the change in size of the subset of available single-particle states corresponding to a variation of δN particles. It is known that HES is, in general, different from anyon statistics. Indeed, the exclusion statistics is assigned to elementary excitations of condensed matter systems, which are not necessarily connected with braiding considerations [21; 31]. However, there are some systems where a thermodynamics coincidence of the two statistics was shown [22; 25; 31; 32]. In this case, it is possible to think that the anyon model is a microscopic quantum realization of Haldane statistics.

In the next sections we consider anyonic systems satisfying the FES, to describe the thermodynamic evolution of an exclusion gas by using QMEP-Wigner formalism. In this way, compatibly with the uncertainty principle, we include both the statistical effects and a nonlocal description for the system.

THE WIGNER DYNAMICS

Following Ref. [8; 12] we consider a fixed number N of identical particles and introduce in Fock space the statistical density matrix ρ for the whole system, with $Tr(\rho) = 1$, (we suppress the symbol $\hat{\cdot}$ to refer to operators acting in Fock space) and the general Hamiltonian [33]

$$H = \int d^3r \Psi^\dagger(\mathbf{r}) \left[-\frac{\hbar^2}{2m} \nabla^2 + U(\mathbf{r}) \right] \Psi(\mathbf{r}) + \frac{1}{2} \int \int d^D r d^D r' \Psi^\dagger(\mathbf{r}) \Psi^\dagger(\mathbf{r}') V(\mathbf{r}, \mathbf{r}') \Psi(\mathbf{r}') \Psi(\mathbf{r}) \quad (4)$$

where m is the particle effective mass, $U(\mathbf{r})$ is the one-body potential, $V(\mathbf{r}, \mathbf{r}')$ is a two-body symmetric interaction potential, Ψ and Ψ^\dagger are wave field operators satisfying the anyon relations (1)-(3) with their properties [30; 33]. Analogously, in coordinate space representation, we define the reduced density matrix [8; 11] of single particle (here and henceforth we use the symbol $\hat{\cdot}$ for single particle operators) $\langle \mathbf{r} | \hat{\rho} | \mathbf{r}' \rangle = \langle \Psi^\dagger(\mathbf{r}') \Psi(\mathbf{r}) \rangle = Tr(\rho \Psi^\dagger(\mathbf{r}') \Psi(\mathbf{r}))$ that in an arbitrary representation takes the form $\langle \mathbf{v} | \hat{\rho} | \mathbf{v}' \rangle = \langle a_{\mathbf{v}'}^\dagger a_{\mathbf{v}} \rangle = Tr(\rho a_{\mathbf{v}'}^\dagger a_{\mathbf{v}})$ being \mathbf{v}, \mathbf{v}' single particle states, $a_{\mathbf{v}}, a_{\mathbf{v}'}^\dagger$ annihilation and creation operators for these states and $\langle \dots \rangle$ the statistical mean value. Thus, if we consider a one-particle observable $\hat{\mathcal{M}}$ then an ensemble average will lead to the expected value $Tr(\hat{\rho} \hat{\mathcal{M}}) = \int d^D r d^D r' \langle \Psi^\dagger(\mathbf{r}') \Psi(\mathbf{r}) \rangle \langle \mathbf{r}' | \hat{\mathcal{M}} | \mathbf{r} \rangle$. By using this formalism, we can define the *reduced* Wigner function

$$\mathcal{F}_W = \frac{1}{(2\pi\hbar)^D} \int d^D \tau e^{-\frac{i}{\hbar} \tau \cdot \mathbf{p}} \langle \Psi^\dagger(\mathbf{r} - \tau/2) \Psi(\mathbf{r} + \tau/2) \rangle \quad (5)$$

with $\int d^D p \mathcal{F}_W = \langle \mathbf{r} | \hat{\rho} | \mathbf{r} \rangle = \langle \Psi^\dagger(\mathbf{r}) \Psi(\mathbf{r}) \rangle = n(\mathbf{r})$, being $n(\mathbf{r})$ the quasi-particle numerical density, with $Tr(\hat{\rho}) = N$.

Accordingly, by considering an operator of single particle $\hat{\mathcal{M}}(\hat{\mathbf{r}}, \hat{\mathbf{p}})$, we look for a function $\tilde{\mathcal{M}}(\mathbf{r}, \mathbf{p})$ in phase space that *corresponds* unambiguously to operator $\hat{\mathcal{M}}$, introducing the Weyl-Wigner transform $\mathcal{W}(\hat{\mathcal{M}}) = \tilde{\mathcal{M}}(\mathbf{r}, \mathbf{p}) = \int d^D \tau \langle \mathbf{r} + \tau/2 | \hat{\mathcal{M}} | \mathbf{r} - \tau/2 \rangle e^{-\frac{i}{\hbar} \tau \cdot \mathbf{p}}$ and, analogously, we define the inverse Wigner transform $\mathcal{W}^{-1}(\tilde{\mathcal{M}}) = \langle \mathbf{r} | \hat{\mathcal{M}} | \mathbf{r}' \rangle = (2\pi\hbar)^{-D} \int d^D p \tilde{\mathcal{M}}((\mathbf{r} + \mathbf{r}')/2, \mathbf{p}) e^{i\mathbf{p} \cdot (\mathbf{r} - \mathbf{r}')}$ which maps the function $\tilde{\mathcal{M}}$ on phase space into the operator $\hat{\mathcal{M}}$.

Thus, by using the equation of motion in the Heisenberg picture $i\hbar \partial_t \Psi(\mathbf{r}) = [\Psi(\mathbf{r}), H]$, the relations (1)-(3) with their properties [30], and the symmetry of terms $V(\mathbf{r}, \mathbf{r}')$, we obtain the equations $i\hbar \partial_t \Psi(\mathbf{r}) = \mathcal{H}(\mathbf{r}) \Psi(\mathbf{r})$ and $-i\hbar \partial_t \Psi^\dagger(\mathbf{r}) = \Psi^\dagger(\mathbf{r}) \mathcal{H}(\mathbf{r})$ with

$$\mathcal{H}(\mathbf{r}) = -\frac{\hbar^2}{2m} \nabla^2 + U(\mathbf{r}) + \int d^D r' \Psi^\dagger(\mathbf{r}') V(\mathbf{r}, \mathbf{r}') \Psi(\mathbf{r}'). \quad (6)$$

Starting from these relations, we determine the equation of motion for the quantity $\Psi^\dagger(\mathbf{r}') \Psi(\mathbf{r})$ and by performing its statistical average we obtain, in the generalized Hartree approximation [34], the usual evolution-equation for the reduced density matrix of single particle

$$i\hbar \frac{\partial}{\partial t} \langle \mathbf{r} | \hat{\rho} | \mathbf{r}' \rangle = \int d^D r'' [\langle \mathbf{r} | \hat{\mathcal{H}} | \mathbf{r}'' \rangle \langle \mathbf{r}'' | \hat{\rho} | \mathbf{r}' \rangle - \langle \mathbf{r} | \hat{\rho} | \mathbf{r}'' \rangle \langle \mathbf{r}'' | \hat{\mathcal{H}} | \mathbf{r}' \rangle] \quad (7)$$

being $\widehat{\mathcal{H}} = \langle \mathcal{H} \rangle$ the single particle Hamilton operator. Accordingly, following a usual script [8; 11; 34], we can use all previous relations to obtain the formal full expansion, to all orders in \hbar , of the Wigner equation in the generalized Hartree approximation

$$\frac{\partial \mathcal{F}_{\mathcal{W}}}{\partial t} + \frac{p_k}{m} \frac{\partial \mathcal{F}_{\mathcal{W}}}{\partial x_k} = \sum_{l=0}^{\infty} \frac{(i\hbar/2)^{2l}}{(2l+1)!} \left[\frac{\partial^{2l+1} V_{eff}}{\partial x_{k_1} \cdots \partial x_{k_{2l+1}}} \right] \left[\frac{\partial^{2l+1} \mathcal{F}_{\mathcal{W}}}{\partial p_{k_1} \cdots \partial p_{k_{2l+1}}} \right] \quad (8)$$

where all effects of the interactions are entirely contained in the definition of the effective potential [35], $V_{eff}(\mathbf{r}) = U(\mathbf{r}) + \int d^D r' n(\mathbf{r}') V(\mathbf{r}, \mathbf{r}')$.

QUANTUM ENTROPY AND QMEP FORMALISM

The most used definition of quantum entropy is due to Von Neumann [36], and is expressed in the form

$$S = -k_B Tr(\rho \ln \rho) \quad (9)$$

where ρ is the statistical density matrix operator appropriate to the physical system under study.

Although the relation (9) does not refer to any special structure of the system, there are some particular features that must be satisfied for a system of identical particles. Indeed, a main drawback of the above definition stems in the fact that it does not include the statistical effects for a system of identical particles. To account for the effects of statistics in Eq. (9), it is mandatory to consider an additional information specifying whether the density operator ρ , defined in Fock space, is associated with an exclusion system, fermion or boson like. In order to take into account *ab initio* the statistics for a system of identical particles, we can follow the usual strategy of evaluating the quantum entropy as the logarithm of the *statistical weight* for the whole system.

Thus, to take into account *ab initio* the FES, we evaluate the entropy S for a noninteracting system under nonequilibrium conditions in terms of the occupation numbers [37]

$$S = -k_B \sum_{\mathbf{v}} y \left\{ \langle \overline{N}_{\mathbf{v}} \rangle \ln \langle \overline{N}_{\mathbf{v}} \rangle + (1 - \kappa \langle \overline{N}_{\mathbf{v}} \rangle) \ln (1 - \kappa \langle \overline{N}_{\mathbf{v}} \rangle) - [1 + (1 - \kappa) \langle \overline{N}_{\mathbf{v}} \rangle] \ln [1 + (1 - \kappa) \langle \overline{N}_{\mathbf{v}} \rangle] \right\} \quad (10)$$

with $\langle \overline{N}_{\mathbf{v}} \rangle = \langle a_{\mathbf{v}}^\dagger a_{\mathbf{v}} \rangle / y$, y the spin degeneration, and κ the statistical parameter of fractional statistics. If we consider the Schrödinger equation of single particle $[\widehat{\mathcal{H}}(\mathbf{r}) - E_{\mathbf{v}}] \phi_{\mathbf{v}}(\mathbf{r}) = 0$ then, the occupation numbers $\langle N_{\mathbf{v}} \rangle$, associated with the energies $E_{\mathbf{v}}$, will completely specify the macroscopic state of the gas. In particular, by using the relation (7) in stationary conditions, both the *reduced density matrix* and any operator $\widehat{\Phi}(\widehat{\rho})$ are diagonal in the base $\phi_{\mathbf{v}}$. Therefore, by introducing as function of $\widehat{\rho}$ the quantity

$$\widehat{\Phi}(\widehat{\rho}) = y \left\{ \frac{\widehat{\rho}}{y} \ln \left(\frac{\widehat{\rho}}{y} \right) + \left(\widehat{I} - \kappa \frac{\widehat{\rho}}{y} \right) \ln \left(\widehat{I} - \kappa \frac{\widehat{\rho}}{y} \right) - \left[\widehat{I} + (1 - \kappa) \frac{\widehat{\rho}}{y} \right] \ln \left[\widehat{I} + (1 - \kappa) \frac{\widehat{\rho}}{y} \right] \right\} \quad (11)$$

with \widehat{I} the identity, we obtain $\langle \mathbf{v} | \widehat{\rho} | \mathbf{v}' \rangle = \langle a_{\mathbf{v}}^\dagger a_{\mathbf{v}} \rangle \delta_{\mathbf{v}\mathbf{v}'}$ and

$$\langle \mathbf{v} | \widehat{\Phi}(\widehat{\rho}) | \mathbf{v}' \rangle = y \left\{ \langle \overline{N}_{\mathbf{v}} \rangle \ln \langle \overline{N}_{\mathbf{v}} \rangle + (1 - \kappa \langle \overline{N}_{\mathbf{v}} \rangle) \ln (1 - \kappa \langle \overline{N}_{\mathbf{v}} \rangle) - [1 + (1 - \kappa) \langle \overline{N}_{\mathbf{v}} \rangle] \ln [1 + (1 - \kappa) \langle \overline{N}_{\mathbf{v}} \rangle] \right\} \delta_{\mathbf{v}\mathbf{v}'} \quad (12)$$

We remark, that for $\kappa = 1$ or $\kappa = 0$ the entropy (10) recovers the usual expressions for fermions or bosons [38], and Eqs. (11)-(12) become

$$\widehat{\Phi}(\widehat{\rho}) = \widehat{\rho} \left\{ \ln \left(\frac{\widehat{\rho}}{y} \right) \pm y \widehat{\rho}^{-1} \left(\widehat{I} \mp \frac{\widehat{\rho}}{y} \right) \ln \left(\widehat{I} \mp \frac{\widehat{\rho}}{y} \right) \right\} \quad (13)$$

$$\langle \mathbf{v} | \widehat{\Phi}(\widehat{\rho}) | \mathbf{v}' \rangle = y \left[\langle \overline{N}_{\mathbf{v}} \rangle \ln \langle \overline{N}_{\mathbf{v}} \rangle \pm (1 \mp \langle \overline{N}_{\mathbf{v}} \rangle) \times \ln (1 \mp \langle \overline{N}_{\mathbf{v}} \rangle) \right] \delta_{\mathbf{v}\mathbf{v}'} \quad (14)$$

Analogously, under nondegenerate conditions Bose and Fermi statistics tend to Boltzmann statistics as limit case, and the general expressions (11)-(12) reduce to

$$\widehat{\Phi}(\widehat{\rho}) = \widehat{\rho} \left\{ \ln \left(\frac{\widehat{\rho}}{y} \right) - \widehat{I} \right\}, \quad (15)$$

$$\langle \mathbf{v} | \widehat{\Phi}(\widehat{\rho}) | \mathbf{v}' \rangle = y \langle \overline{N}_{\mathbf{v}} \rangle (\ln \langle \overline{N}_{\mathbf{v}} \rangle - 1) \delta_{\mathbf{v}\mathbf{v}'}. \quad (16)$$

Consequently, by generalizing existing definitions [1; 2; 9; 10; 36], the statistics can be implicitly taken into account by defining, for the whole system, the quantum entropy in terms of the functional of the reduced density matrix

$$S(\widehat{\rho}) = -k_B Tr[\widehat{\Phi}(\widehat{\rho})] \quad (17)$$

where $\widehat{\Phi}(\widehat{\rho})$ is given by Eq. (11) for the FES [12], by Eq. (13) for the Fermi or Bose gases [8; 11], and by Eq. (15) for the Boltzmann gas.

General formulation of QMEP in phase space

By considering an arbitrary set of single-particle observable $\{\widehat{\mathcal{M}}_A\}$ and the corresponding space-phase functions $\{\widetilde{\mathcal{M}}_A\}$, we define the macroscopic *local moments*

$$M_A(\mathbf{r}, t) = \int d^D p \widetilde{\mathcal{M}}_A(\mathbf{r}, \mathbf{p}) \mathcal{F}_{\mathcal{W}}(\mathbf{r}, \mathbf{p}, t) \quad (18)$$

and we use the functional (17) as an *informational entropy* for the system. To formulate the QMEP in phase space, we introduce the phase function $\widetilde{\Phi}(\mathbf{r}, \mathbf{p}) = \mathcal{W}(\widehat{\Phi}(\widehat{\rho}))$, we rewrite Eq. (17) in the form

$$S(\widehat{\rho}) = -\frac{k_B}{(2\pi\hbar)^D} \int \int d^D p d^D r \mathcal{W}(\widehat{\Phi}(\widehat{\rho})), \quad (19)$$

and we search the extremal value of the global entropy subject to the constraint that the information on the physical system is described by a set of local moments $\{M_A(\mathbf{r}, t)\}$ with $A = 1, \dots, \mathcal{N}$. To this purpose, we define the new *global* functional [8; 10; 11]

$$\widetilde{S} = S - \int d^D r \left\{ \sum_{A=1}^{\mathcal{N}} \widetilde{\lambda}_A \left[\int d^D p \widetilde{\mathcal{M}}_A \mathcal{F}_{\mathcal{W}} - M_A \right] \right\} \quad (20)$$

being $\tilde{\lambda}_A(\mathbf{r}, t)$ the nonlocal *Lagrange multipliers* to be determined.

By using the general relation (11) introduced for the FES, one can show that the solution of the constraint $\delta\tilde{S} = 0$ implies

$$\hat{\rho} = y \left\{ \hat{w}(\hat{\xi}) + \kappa \hat{I} \right\}^{-1} \quad (21)$$

where the operator \hat{w} satisfies the functional relation

$$[\hat{w}(\hat{\xi})]^\kappa [\hat{I} + \hat{w}(\hat{\xi})]^{1-\kappa} = \hat{\xi} \quad (22)$$

with the operator

$$\hat{\xi} = \exp \left[\mathcal{W}^{-1} \left(\sum_{A=1}^{\mathcal{N}} \lambda_A \tilde{\mathcal{M}}_A \right) \right] \quad \text{and} \quad \lambda_A = \frac{\tilde{\lambda}_A}{k_B} \quad (23)$$

The set of Eqs. (21)-(23) is a first major result. It generalizes existing results [37], in an operatorial sense, under both thermodynamic equilibrium and nonequilibrium conditions. Besides, the relations (21)-(23), together with Eqs. (11) and (17), provide a generalized definition of quantum entropy that includes nonlocal effects in FES. As a consequence, a nonlocal Wigner-theory for the system can be formulated by explicitly evaluating the corresponding reduced Wigner-function

$$\mathcal{F}_{\mathcal{W}} = (2\pi\hbar)^{-D} \mathcal{W}(\hat{\rho}[\lambda_A(\mathbf{r}, t), \tilde{\mathcal{M}}_A]). \quad (24)$$

We note, that by solving the general relation (22) for $\kappa = 1, 0$ we reobtain the Fermi and Bose statistics, being in this case [8; 11]

$$\hat{\rho} = y \left\{ \exp \left[\mathcal{W}^{-1} \left(\sum_{A=1}^{\mathcal{N}} \lambda_A(\mathbf{r}, t) \tilde{\mathcal{M}}_A \right) \right] \pm \hat{I} \right\}^{-1} \quad (25)$$

while for the Boltzmann statistics, we obtain the simplified expression

$$\hat{\rho} = y \exp \left\{ \mathcal{W}^{-1} \left(- \sum_{A=1}^{\mathcal{N}} \lambda_A(\mathbf{r}, t) \tilde{\mathcal{M}}_A \right) \right\} \quad (26)$$

We conclude by remarking that, by itself, the QMEP does not provide any information about the dynamical evolution of the system, but it offers only a definite procedure to construct a sequence of approximations for the nonequilibrium Wigner function. To obtain a dynamical description, it is necessary: (i) to know a set of evolution equations for the constraints that include the microscopic kinetic details, (ii) to determine the Lagrange multipliers in terms of these constraints. In this way, the QMEP approach implicitly includes all the kinetic details of the microscopic interactions among particles. Then, by knowing the functional form (21)-(24) of the reduced Wigner function, we use Eq. (8) to obtain a set of evolution equations for the constraints. This set completely represents the QHD model in which all the constitutive functions are determined starting from their kinetic expressions. Thus, for a given number of moments M_A , we consider a consistent expansion around \hbar of the Wigner function. In this way, we separate classical from quantum dynamics, and obtain order by order corrections terms.

Moyal expansion of the Wigner function

By using the Moyal formalism [39], one can prove that the phase function $\tilde{w} = \mathcal{W}(\hat{w})$, the Wigner function $\mathcal{F}_{\mathcal{W}}$ and, hence, the moments M_A can be expanded in even power of \hbar as

$$\tilde{w} = \sum_{k=0}^{\infty} \hbar^{2k} w^{(2k)}, \quad \mathcal{F}_{\mathcal{W}} = \sum_{k=0}^{\infty} \hbar^{2k} \mathcal{F}_{\mathcal{W}}^{(2k)}, \quad M_A = \sum_{k=0}^{\infty} \hbar^{2k} M_A^{(2k)}$$

To this end, the Lagrange multipliers λ_A must be determined by inverting, order by order, the constrains

$$M_A = \frac{1}{(2\pi\hbar)^D} \int d^D p \tilde{\mathcal{M}}_A \mathcal{W}(\hat{\rho}[\lambda_B(\mathbf{r}, t), \tilde{\mathcal{M}}_B]). \quad (27)$$

where the inversion problem can be solved [8; 11] only by assuming that also the Lagrange multipliers admit for an expansion in even powers of \hbar

$$\lambda_A = \lambda_A^{(0)} + \sum_{k=1}^{\infty} \hbar^{2k} \lambda_A^{(2k)}, \quad (28)$$

In this way, by using Eqs. (21)-(24) and (27)-(28), with the strategy reported in Ref. [8; 11], we succeed in determining the following expression for the reduced Wigner-function

$$\mathcal{F}_{\mathcal{W}} = \frac{\tilde{y}}{w^{(0)}(\xi) + \kappa} \left\{ 1 + \sum_{r=1}^{\infty} \hbar^{2r} \mathcal{P}_{2r} \right\}, \quad (29)$$

where $\tilde{y} = y/(2\pi\hbar)^D$, $\xi = \exp(\Pi)$ with $\Pi = \sum \lambda_A \tilde{\mathcal{M}}_A$, the nonlocal terms \mathcal{P}_{2r} expressed by recursive formulas and the function $w^{(0)}$ satisfying the usual functional equation

$$[w^{(0)}(\xi)]^\kappa [1 + w^{(0)}(\xi)]^{1-\kappa} = \xi. \quad (30)$$

Equation (29) is a second major result. Indeed, making use of $\xi_0 = e^{\Pi_0}$ with $\Pi_0 = \sum \lambda_A^{(0)} \tilde{\mathcal{M}}_A$, from (29) we obtain, explicitly, the following first order ($r = 1$) quantum correction

$$\begin{aligned} \mathcal{P}_2 = & \left\{ \frac{2}{[w^{(0)}(\xi_0) + \kappa]^2} \left(\xi_0 \frac{dw^{(0)}}{d\xi_0} \right)^2 - \frac{1}{w^{(0)}(\xi_0) + \kappa} \right. \\ & \times \left[\xi_0^2 \frac{d^2 w^{(0)}}{d\xi_0^2} + \xi_0 \frac{dw^{(0)}}{d\xi_0} \right] \left. \right\} \mathcal{H}_2^{(2)} - \left\{ \frac{6}{[w^{(0)}(\xi_0) + \kappa]^2} \right. \\ & \times \left[\frac{1}{w^{(0)}(\xi_0) + \kappa} \left(\xi_0 \frac{dw^{(0)}}{d\xi_0} \right)^3 - \left(\xi_0 \frac{dw^{(0)}}{d\xi_0} \right)^2 - \right. \\ & \left. \xi_0^3 \frac{d^2 w^{(0)}}{d\xi_0^2} \frac{dw^{(0)}}{d\xi_0} \right] + \frac{1}{w^{(0)}(\xi_0) + \kappa} \left[\xi_0^3 \frac{d^3 w^{(0)}}{d\xi_0^3} + \right. \\ & \left. \left. 3 \xi_0^2 \frac{d^2 w^{(0)}}{d\xi_0^2} + \xi_0 \frac{dw^{(0)}}{d\xi_0} \right] \right\} \mathcal{H}_3^{(2)} \quad (31) \end{aligned}$$

being the nonlocal functions $\mathcal{H}_2^{(2)}$ and $\mathcal{H}_3^{(2)}$ expressed by

$$\mathcal{H}_3^{(2)} = -\frac{1}{24} \left[\frac{\partial^2 \Pi_0}{\partial x_i \partial x_j} \frac{\partial \Pi_0}{\partial p_i} \frac{\partial \Pi_0}{\partial p_j} + \frac{\partial^2 \Pi_0}{\partial p_i \partial p_j} \frac{\partial \Pi_0}{\partial x_i} \frac{\partial \Pi_0}{\partial x_j} \right]$$

$$-2 \frac{\partial^2 \Pi_0}{\partial x_i \partial p_j} \frac{\partial \Pi_0}{\partial x_j} \frac{\partial \Pi_0}{\partial p_i} \Big], \quad (32)$$

$$\mathcal{H}_2^{(2)} = -\frac{1}{8} \left[\frac{\partial^2 \Pi_0}{\partial x_i \partial x_j} \frac{\partial^2 \Pi_0}{\partial p_i \partial p_j} - \frac{\partial^2 \Pi_0}{\partial x_i \partial p_j} \frac{\partial^2 \Pi_0}{\partial x_j \partial p_i} \right]. \quad (33)$$

We remark the following main points:

(i) For $\kappa = 1$ and $\kappa = 0$ we recover the gradient nonlocal results obtained for Fermi and Bose gases [8; 11], being in this case

$$\mathcal{F}_{\mathcal{W}} = \frac{\tilde{y}}{e^{\Pi \pm 1}} \left\{ 1 + \sum_{r=1}^{\infty} \hbar^{2r} \mathcal{P}_{2r}^{\pm} \right\}, \quad (34)$$

with the first quantum correction (31) that becomes

$$\begin{aligned} \mathcal{P}_2^{\pm} = & \left\{ 6 \left[\frac{e^{\Pi_0}}{e^{\Pi_0 \pm 1}} \right]^2 - 6 \left[\frac{e^{\Pi_0}}{e^{\Pi_0 \pm 1}} \right]^3 - \frac{e^{\Pi_0}}{e^{\Pi_0 \pm 1}} \right\} \mathcal{H}_3^{(2)} + \\ & \left\{ 2 \left[\frac{e^{\Pi_0}}{e^{\Pi_0 \pm 1}} \right]^2 - \frac{e^{\Pi_0}}{e^{\Pi_0 \pm 1}} \right\} \mathcal{H}_2^{(2)} \end{aligned} \quad (35)$$

Analogously, by considering a quantum Boltzmann gas [8; 11], we obtain the simplified relations

$$\mathcal{F}_{\mathcal{W}} = \tilde{y} e^{-\Pi} \left\{ 1 + \sum_{r=1}^{\infty} \hbar^{2r} \mathcal{P}_{2r} \right\} \quad \text{with} \quad \mathcal{P}_2 = \mathcal{H}_2^{(2)} - \mathcal{H}_3^{(2)} \quad (36)$$

(ii) The functions $\{\mathcal{H}_2^{(2)}, \mathcal{H}_3^{(2)}\}$ are in general, expressed in terms of the quantities $\{M_A, \frac{\partial M_A}{\partial x_k}, \frac{\partial^2 M_A}{\partial x_i \partial x_k}, \mathbf{p}\}$; in any case, these functions can be evaluated using different levels of approximation [40].

(iii) In thermodynamics equilibrium conditions we can write $\Pi|_E = \alpha + \beta \tilde{\varepsilon}$ where $\tilde{\varepsilon} = m \tilde{u}^2 / 2$, being $\tilde{u}_i = u_i - \lambda_i$ the peculiar velocity, $u_i = p_i / m$ the group velocity, and $\{\alpha, \beta, \lambda_i\}$ the equilibrium nonlocal Lagrange multipliers.

EXAMPLES AND APPLICATIONS

As relevant application of the above results, we consider an exclusion gas in isothermal equilibrium conditions. Accordingly, $\beta = (k_B T)^{-1}$, with T the constant temperature, and within a general approach all nonlocal effects can be described in terms of spatial derivatives of concentration $n(\mathbf{r}, t)$ and mean velocity $v_i(\mathbf{r}, t) = n^{-1} \int d^D p u_i \mathcal{F}_{\mathcal{W}}$. In this case it is necessary to determine a closed set of balance equations for the variables $\{n, v_i\}$ used as constraints in the QMEP procedure. Thus, by considering the kinetic fields $\tilde{\mathcal{M}}_A = \{1, u_i\}$ and using Eq. (8) we obtain the quantum drift-diffusion model [8; 11]

$$\dot{n} + n \frac{\partial v_k}{\partial x_k} = 0, \quad \dot{v}_i + \frac{1}{n} \frac{\partial M_{ik}}{\partial x_k} + \frac{1}{m} \frac{\partial V_{eff}}{\partial x_i} = 0, \quad (37)$$

where the unknown function M_{ik} can be decomposed as

$$M_{ik} = M_{(ik)} + \frac{P}{m} \delta_{ik} + O(\hbar^4) \quad (38)$$

being the traceless part of tensor

$$M_{(ik)} + O(\hbar^4) = \int d^D p \tilde{u}_{(i} \tilde{u}_{k)} \mathcal{F}_{\mathcal{W}}$$

and the generalized quantum pressure

$$P + O(\hbar^4) = \frac{2}{D} \int d^D p \tilde{\varepsilon} \mathcal{F}_{\mathcal{W}}|_E$$

independent constitutive quantities. Then, by making use of Eqs. (29)-(33), we calculate the variables of local equilibrium $\{n, P\}$ and the traceless tensor $M_{(ik)}$, determining the general relations

$$\begin{aligned} I_{D-1}(\alpha, \kappa) = & \gamma \frac{n}{T^{D/2}} \left\{ 1 - \frac{\hbar^2}{12m k_B T} \left[\sum_{p=1}^2 \eta_{1p}^{(0)} Q^{(1,p)} \right. \right. \\ & \left. \left. + \eta_{21}^{(0)} Q^{(2,1)} \right] \right\} + O(\hbar^4) \end{aligned} \quad (39)$$

$$\begin{aligned} P = & \frac{2}{D} n k_B T \frac{I_{D+1}}{I_{D-1}} \left\{ 1 + \frac{\hbar^2}{12m k_B T} \left[\sum_{p=1}^2 \left(\eta_{1p}^{(1)} - \eta_{1p}^{(0)} \right) \right. \right. \\ & \left. \left. \times Q^{(1,p)} + \left(\eta_{21}^{(1)} - \eta_{21}^{(0)} \right) Q^{(2,1)} \right] \right\} + O(\hbar^4) \end{aligned} \quad (40)$$

$$M_{(ik)} = -\frac{\hbar^2}{12 m^2} n (D-2) \frac{I_{D-3}}{I_{D-1}} Q_{(ik)} + O(\hbar^4) \quad (41)$$

where $\gamma = [\Gamma(D/2)/2y] (2\pi\hbar^2/mk_B)^{D/2}$, the integral functions $I_n(\alpha, \kappa)$, the quantities $\eta_{ij}^{(s)}$ and the nonlocal functions $\{Q^{(q,p)}, Q_{(ik)}\}$ are explicitly given in Eqs. (55) and (57)-(61) of Appendix.

By providing generalized differential constraints for the quantum system under interest, the relations (39)-(41) constitute a third major result. In particular, by solving Eq. (39) with respect to α , we determine the *generalized quantum chemical potential* $\mu = -\alpha k_B T$ and, by using Eq. (40), we obtain the *generalized quantum equation of state*. Thus, by introducing the usual Bohm quantum potential $Q_B = -(\hbar^2/2m\sqrt{n}) \Delta\sqrt{n}$, and the vorticity tensor $\mathcal{T}_{ij} = (\partial v_i/\partial x_j - \partial v_j/\partial x_i)$ the following simplified analytical cases are analyzed under isothermal equilibrium condition.

I) *High-temperature and/or low-density limits.*

First approximation: By using the first term of a suitable series expansion [41] for the functions $I_n(\alpha, \kappa)$, we obtain the completely nondegenerate case which is independent from κ (Boltzmann limit), being $I_n^{\pm}(\alpha) \approx (1/2)\Gamma[(n+1)/2] \exp(-\alpha)$. Thus, by defining the quantity $\chi^{(0)} = y^{-1} [(2\pi\hbar^2)/(mk_B)]^{D/2} (n/T^{D/2})$ and using Eqs. (39)-(41) we obtain the generalized quantum expressions

$$\mu = k_B T \ln \left[\chi^{(0)} \right] + \frac{Q_B^I}{3} + O(\hbar^4), \quad (42)$$

$$P = n k_B T + n Q_C^I + O(\hbar^4), \quad (43)$$

with the first quantum nonlocal gradient corrections

$$Q_B^I = Q_B - \frac{\hbar^2}{16 k_B T} \mathcal{T}_{ll}^2,$$

$$Q_C^I = -\frac{\hbar^2}{12D} \frac{1}{m} \left[\frac{\partial^2 \ln n}{\partial x_r \partial x_r} + \frac{m}{k_B T} \mathcal{T}_{II}^2 \right]$$

and the first approximation $M_{(ik)}^I$ for the tensor $M_{(ik)}$

$$M_{(ik)}^I = -\frac{\hbar^2}{12} \frac{n}{m^2} \left[\frac{\partial^2 \ln n}{\partial x_{(i} \partial x_{k)}} + \frac{m}{k_B T} \mathcal{T}_{(ik)}^2 \right] + O(\hbar^4). \quad (44)$$

By neglecting vorticity effects ($\mathcal{T}_{ik} = 0$) we recover relations well-known in literature [8; 11; 42], while, by including vorticity terms, we re-obtain some recent results for a quantum Boltzmann gas [43; 44].

Second approximation: By using the first two terms of the series expansion [41] we obtain $I_n^\pm(\alpha, \kappa) \approx (1/2)\Gamma[(n+1)/2] \exp(-\alpha) \{1 - (2\kappa - 1)/2^{(n+1)/2} \exp(-\alpha)\}$, and by considering Eqs. (39)-(41) and (57)-(61) with a standard iterative procedure [8; 11], we determine the correct quantum-statistical second approximation in terms of the quantity $\chi^{(0)} \ll 1$, being

$$\begin{aligned} \mu &= k_B T \ln \left[\left(1 + \frac{2\kappa - 1}{2^{D/2}} \chi^{(0)} \right) \chi^{(0)} \right] \\ &+ \frac{1}{3} \left(Q_B^I + \frac{2\kappa - 1}{2^{D/2}} \chi^{(0)} Q_B^{II} \right) + O(\hbar^4) \end{aligned} \quad (45)$$

$$\begin{aligned} P &= n k_B T \left(1 + \frac{2\kappa - 1}{2^{D/2+1}} \chi^{(0)} \right) \\ &+ n \left(Q_C^I + \frac{2\kappa - 1}{2^{D/2+1}} \chi^{(0)} Q_C^{II} \right) + O(\hbar^4) \end{aligned} \quad (46)$$

$$M_{(ik)} = M_{(ik)}^I + \frac{2\kappa - 1}{2^{D/2}} \chi^{(0)} M_{(ik)}^{II} + O(\hbar^4) \quad (47)$$

with the quantum nonlocal-gradient second corrections Q_B^{II} , Q_C^{II} and $M_{(ik)}^{II}$ explicitly given in Eqs. (62)-(64) of Appendix.

II) low-temperature limits.

Under strong degeneracy, we make use of an asymptotic expansion [41] for the functions $I_n(\alpha, \kappa)$ (with $\kappa \in (0, 1]$).

First approximation: When $T \rightarrow 0$ the degeneracy becomes complete and $I_n(\alpha, \kappa) \approx (-\alpha)^{(n+1)/2} / [\kappa(n+1)]$. Thus, by defining $\nu_E = [4\pi/(D+2)](\hbar^2/m)[(\kappa/y)\Gamma(D/2+1)]^{2/D}$ and $\mu^{(0)} = [(D+2)/2]\nu_E n^{2/D}$, for μ and P we obtain

$$\mu = \mu^{(0)} + \frac{D-2}{3D} Q_D^I + O(\hbar^4), \quad (48)$$

$$P = \nu_E n^{(D+2)/D} + n Q_E^I + O(\hbar^4), \quad (49)$$

with the quantum nonlocal-gradient first corrections

$$\begin{aligned} Q_D^I &= Q_B - \frac{\hbar^2}{32} \frac{D}{\mu^{(0)}} \mathcal{T}_{II}^2 \\ Q_E^I &= \frac{\hbar^2}{12D} \frac{1}{m} \left[\frac{\partial^2 \ln n}{\partial x_r \partial x_r} + \frac{2(D-1)}{D} \left(\frac{\partial \ln n}{\partial x_r} \right)^2 - \frac{m}{4} \frac{D}{\mu^{(0)}} \mathcal{T}_{II}^2 \right] \end{aligned}$$

and the first approximation $\mathcal{M}_{(ik)}^I$ for the tensor $M_{(ik)}$

$$\begin{aligned} \mathcal{M}_{(ik)}^I &= -\frac{\hbar^2}{12} \frac{n}{m^2} \left[\frac{\partial^2 \ln n}{\partial x_{(i} \partial x_{k)}} + \frac{2}{D} \frac{\partial \ln n}{\partial x_{(i}} \frac{\partial \ln n}{\partial x_{k)}} \right. \\ &\left. + \frac{m}{2} \frac{D}{\mu^{(0)}} \mathcal{T}_{(ik)}^2 \right] + O(\hbar^4). \end{aligned} \quad (50)$$

In particular, for $\kappa = 1$ (completely degenerate Fermi gas) and neglecting vorticity effects ($\mathcal{T}_{ik} = 0$), we recover the gradient corrections obtained in the context of Thomas-Fermi-Weizsacker theory [8; 11; 46]. For $\kappa \neq 1$ and, by including also the vorticity terms, we generalize these results to exclusion gases, in the low-temperature limit [12].

Second approximation: We consider the first two terms of the asymptotic expansion in series [41], $I_n(\alpha, \kappa) \approx (-\alpha)^{(n+1)/2} / [\kappa(n+1)] \{1 + (\pi^2/24) \kappa(n^2 - 1)(-\alpha)^{-2}\}$. Thus, by using Eqs. (39)-(41) and (57)-(61) with a suitable iterative procedure [8; 11], we obtain the second quantum-statistical correct approximation in terms of the quantities $(k_B T / \mu^{(0)})^2 \ll 1$, for μ , P and $M_{(ik)}$

$$\begin{aligned} \mu &= \mu^{(0)} \left[1 - \frac{\pi^2}{12} \kappa(D-2) \left(\frac{k_B T}{\mu^{(0)}} \right)^2 \right] \\ &+ \frac{D-2}{3D} \left[Q_D^I + \frac{\pi^2}{12} \kappa \left(\frac{k_B T}{\mu^{(0)}} \right)^2 Q_D^{II} \right] + O(\hbar^4), \end{aligned} \quad (51)$$

$$\begin{aligned} P &= \nu_E n^{(D+2)/D} \left[1 + \frac{\pi^2}{12} \kappa(D+2) \left(\frac{k_B T}{\mu^{(0)}} \right)^2 \right] \\ &+ n \left[Q_E^I + \frac{\pi^2}{18} \kappa(D-2) \left(\frac{k_B T}{\mu^{(0)}} \right)^2 Q_E^{II} \right] + O(\hbar^4), \end{aligned} \quad (52)$$

$$M_{(ik)} = \mathcal{M}_{(ik)}^I - \frac{\pi^2}{12} \kappa(D-2) \left(\frac{k_B T}{\mu^{(0)}} \right)^2 \mathcal{M}_{(ik)}^{II}, \quad (53)$$

with the quantum nonlocal-gradient second corrections Q_D^{II} , Q_E^{II} and $\mathcal{M}_{(ik)}^{II}$ explicitly given in Eqs. (65)-(67) of Appendix.

In conclusion, by knowing $M_{(ik)}$ and P and using Eq. (38), the system (37) is explicitly closed. However, by indicating with $\{\mu^{(c)}, P^{(c)}\}$ and $\{\mu^{(q)}, P^{(q)}\}$ the classic and the quantum part of the chemical potential and pressure, as reported respectively in Eqs. (42)-(43), (45)-(46), (48)-(49) and (51)-(52), the spatial derivative of M_{ik} can be expressed in the following general form

$$\begin{aligned} \frac{\partial M_{ik}}{\partial x_k} &= \frac{1}{m} \left\{ -\frac{\hbar^2}{12} \mathcal{T}_{ip} \frac{\partial}{\partial x_k} \left[\left(\frac{\partial \mu^{(c)}}{\partial n} \right)^{-1} \mathcal{T}_{pk} \right] \right. \\ &\left. + \frac{\partial P^{(c)}}{\partial x_i} + n \frac{\partial \mu^{(q)}}{\partial x_i} \right\} + O(\hbar^4). \end{aligned} \quad (54)$$

The relation above is a fourth major result. Indeed, in all cases (high and/or low temperature) and for any statistical approximation (i.e. different order of expansion), Eq. (54) represents a *general closure property* [45] for the quantum drift-diffusion system in Eq. (37).

We remark, that since many years the nonlocal gradient corrections have been extensively tested in real applications such as: atomic, surface, nuclear physics and electronic properties of clusters [46]. Analogously, density gradient expansions have been used to describe capture confinement and tunnelling processes for devices in the deca-nanometer regime, by showing a very good agreement both with available experiments and other microscopic methods [47]. The novelty of the present approach allows one to describe the Wigner gradient expansions in the framework of FES, by including also the vorticity. Consequently, the major results outlined above can have relevant applications in quantum turbulence, quantum fluids, quan-

tized vortices, nanostructures, nanowires, thin layers and, by including also gradient thermal corrections, in graphene quantum transport [48]. Finally, we stress that Monte Carlo (MC) simulations and measurements of the thermodynamic properties of quantum gases, including energy, chemical potential, sound velocity and entropy, have been explored and compared recently [49]. In some cases these results have been interpreted in the framework of FES behaviour [50]. Similar measurements and MC simulations may be thought also in the presence of strong spatial inhomogeneous conditions and tested within the present nonlocal FES strategy. Accordingly, the QMEP including fractional exclusion statistics is here asserted as the fundamental principle of quantum statistical mechanics.

ACKNOWLEDGMENT

The paper is supported by *Istituto Nazionale di Alta Matematica* (INDAM), and by Bioelectronic Olfactory Neuron Device (BOND) project within the grant agreement number 228685-2.

REFERENCES

- [1] A. Wehrl, General properties of entropy, *Review of Modern Physics* **50**, 221-260 (1978); G. Manfredi, M. R. Feix, Entropy and Wigner functions, *Physical Review E* **62**, 4665-4674, (2000);
- [2] E.T. Jaynes, Information Theory and Statistical Mechanics, *Physical Review* **106**, 620-630 (1957); E.T. Jaynes, Information Theory and Statistical Mechanics. II, *Physical Review* **108**, 171-190 (1957).
- [3] I. Müller, T. Ruggeri, *Rational Extended Thermodynamics* : Springer Tracts in Natural Philosophy, Vol. **37**, (Springer-Verlag New York) 1998.
- [4] D. Jou, J. Casas-Vazquez, G. Lebon, *Extended Irreversible Thermodynamics*, (Springer-Verlag New York) 2010.
- [5] *Maximum Entropy and Bayesian Methods*, edited by J. Skilling (Kluwer Academic Publishers) 2004.
- [6] T. Ruggeri, M. Trovato, Hyperbolicity in Extended Thermodynamics of Fermi and Bose gases, *Continuum Mech. Thermodyn.*, **16**, 551-576 (2004).
- [7] A.M. Anile, M. Trovato, Nonlinear closures for hydrodynamical semiconductor transport models, *Phys. Lett. A*, **230**, 387-395 (1997); M. Trovato, P. Falsaperla, Full nonlinear closure for a hydrodynamic model of transport in silicon, *Physical Review B*, **57**, 4456-4471 (1998) and Erratum: *Phys. Rev. B* **57**, 12617 (1998); M. Trovato, L. Reggiani, Maximum entropy principle for hydrodynamic transport in semiconductor devices, *J. Appl. Phys.*, **85** 4050-4065 (1999) ; M. Trovato, P. Falsaperla, L. Reggiani, Maximum entropy principle for nonparabolic hydrodynamic transport in semiconductor devices, *J. Appl. Phys.*, **86** 5906-5910 (1999); M. Trovato, L. Reggiani, Maximum entropy principle within a total energy scheme: Application to hot-carrier transport in semiconductors, *Physical Review B*, **61**, 16667-16681 (2000); G. Mascali, M. Trovato, Non-linear determination of the distribution function of degenerate gases with an application to semiconductors, *Physica A*, **310**, 121-138 (2002); M. Trovato, L. Reggiani, Maximum-entropy principle for static and dynamic high-field transport in semiconductors, *Physical Review B*, **73**, 245209-1-17 (2006).
- [8] M. Trovato, L. Reggiani, Maximum entropy principle and hydrodynamic models in statistical mechanics, *Rivista del Nuovo Cimento*, **35**, 99-266 (2012) and references therein.
- [9] Y. Alhassid, R. D. Levine, Connection between the maximal entropy and the scattering theoretic analyses of collision processes, *Physical Review A* **18**, 89-116 (1978).
- [10] P. Degond, C. Ringhofer, Quantum Moment Hydrodynamics and the Entropy Principle, *J. Stat. Phys.* **112**, 587-628 (2003); P. Degond, F. Mehats, C. Ringhofer, Quantum energy-transport and drift-diffusion models, *J. Stat. Phys.*, **118**, 625-667 (2005).
- [11] M. Trovato, L. Reggiani, Quantum hydrodynamic models from a maximum entropy principle, *J. Phys. A: Math. Theor.* **43**, 102001-1-11 (2010). M. Trovato, L. Reggiani, Quantum maximum entropy principle for a system of identical particles, *Physical Review E* **81** 021119-1-11 (2010); M. Trovato, L. Reggiani, Quantum maximum-entropy principle for closed quantum hydrodynamic transport within a Wigner function formalism, *Physical Review E* **84**, 061147-1-29 (2011);
- [12] M. Trovato, L. Reggiani, Quantum Maximum Entropy Principle for Fractional Exclusion Statistics, *Physical Review Letters* **110**, 020404-1-5 (2013).
- [13] J.M. Leinaas and J. Myrheim, On the theory of identical particles, *Nuovo Cimento*, **37B**, 1-23 (1977); F. Wilczek, in *Fractional Statistics and Anyon Superconductivity*, ed. by F. Wilczek (World Scientific, Singapore, 1993).
- [14] A. Lerda, *Anyons* (Springer, Berlin, 1992); A. Lerda and S. Sciuto, Anyons and quantum groups, *Nucl. Phys. B*, **401**, 613-643 (1993).
- [15] G. A. Goldin and D. H. Sharp, Diffeomorphism Groups, Anyon Fields, and q Commutators, *Phys. Rev. Lett.* **76**, 1183-1187 (1996); G. A. Goldin and S. Majid, On the Fock space for nonrelativistic anyon fields and braided tensor products, *J. Math. Phys.* **45**, 3770-3788 (2004).
- [16] R. B. Laughlin, Anomalous Quantum Hall Effect: An Incompressible Quantum Fluid with Fractionally Charged Excitations, *Phys. Rev. Lett.* **50**, 1395-1398 (1983).
- [17] B. I. Halperin, Statistics of Quasiparticles and the Hierarchy of Fractional Quantized Hall States, *Phys. Rev. Lett.* **52**, 1583-1586 (1984); D. Arovas, J.R. Schrieffer, and F. Wilczek, Fractional Statistics and the Quantum Hall Effect, *Phys. Rev. Lett.*, **53**, 722-723 (1984); R. E. Prange and S. M. Girvin, *The Quantum Hall Effect* (Springer, Berlin, 1990); E. Kim, M. Lawler, S. Vishveshwara, E. Fradkin, Signatures of Fractional Statistics in Noise Experiments in Quantum Hall Fluids, *Phys. Rev. Lett.*, **95**, 176402-1-4 (2005); P. Bonderson, A. Kitaev, K. Shtengel, Detecting Non-Abelian Statistics in the $\nu = 5/2$ Fractional Quantum Hall State, *Phys. Rev. Lett.*, **96**, 016803-1-4 (2006);
- [18] V. J. Goldman and B. Su, Resonant tunneling in the Quantum Hall regime: measurement of fractional charge, *Science* **267**, 1010-1012 (1995); J. Martin, S. Ilani, B. Verdenne, J. Smet, V. Umansky, D. Mahalu, D. Schuh, G. Abstreiter, A. Yacoby, Localization of Fractionally Charged Quasi-Particles, *Science* **305**, 980-983 (2004); V. Venkatachalam, A. Yacoby, L. Pfeiffer, K. West, Local charge of the $\nu = 5/2$ fractional quantum Hall state, *Nature* **469**, 185-188 (2011).
- [19] F. E. Camino, W. Zhou, V. J. Goldman, Realization of a Laughlin quasiparticle interferometer: Observation of fractional statistics, *Phys. Rev. B* **72**, 075342-1-8 (2005).
- [20] one-dimensional particles obey fractional statistics, but they are not *true anyons* since in $D \neq 2$ trajectories in the

- particle configuration space have no meaningful braiding property.
- [21] L. Amico, A. Osterloh and U. Eckern, One-dimensional XXZ model for particles obeying fractional statistics, *Phys. Rev. B*, **58**, R1703-R1705 (1998); A. Osterloh, L. Amico and U. Eckern, Fermionic long-range correlations realized by particles obeying deformed statistics, *J. Phys. A: Math. Gen.*, **33**, L487-L492 (2000); M. Greiter, Statistical phases and momentum spacings for one-dimensional anyons, *Phys. Rev. B*, **79**, 064409-1-5 (2009).
- [22] Z. N. C. Ha, Exact Dynamical Correlation Functions of Calogero-Sutherland Model and One-Dimensional Fractional Statistics, *Phys. Rev. Lett.* **73**, 1574-1577 (1994).
- [23] A. Kundu, Exact Solution of Double d Function Bose Gas through an Interacting Anyon Gas, *Phys. Rev. Lett.* **83**, 1275-1278 (1999);
- [24] M. D. Girardeau, Ground and Excited States of Spinor Fermi Gases in Tight Waveguides and the Lieb-Liniger-Heisenberg Model *Phys. Rev. Lett.* **97**, 210401-1-4 (2006).
- [25] M. T. Batchelor, X. W. Guan and N. Oelkers, One-Dimensional Interacting Anyon Gas: Low-Energy Properties and Haldane Exclusion Statistics, *Phys. Rev. Lett.* **96**, 210402-1-4 (2006); M. T. Batchelor, X. W. Guan, Generalized exclusion statistics and degenerate signature of strongly interacting anyons, *Phys. Rev. B* **74**, 195121-1-7 (2006); M. T. Batchelor, X. W. Guan, J. S. He, The Bethe ansatz for 1D interacting anyons, *J. Stat. Mech.*, P03007-1-20 (2007).
- [26] R. Santachiara, F. Stauffer and D. Cabra, Entanglement and moment distributions of a system of hard-core anyons, *J. Stat. Mech.: Theory and Exper.* L05003-1-9 (2007); P. Calabrese and M. Mintchev, Correlation functions of one-dimensional anyonic fluids, *Phys. Rev. B* **75** 233104-1-4, (2007). R. Santachiara and P. Calabrese, One-particle density matrix and momentum distribution function of one-dimensional anyon gases, *J. Stat. Mech.: Theory and Exper.*, P06005 (2008).
- [27] T. Keilmann, S. Lanzmich, I. McCulloch and M. Roncaglia, Statistically induced Phase Transitions and Anyons in 1D Optical Lattices, *Nature Comm.* (London) **2**, 361-369 (2011).
- [28] S. Forte, Quantum mechanics and field theory with fractional spin and statistics, *Rev. Mod. Phys.* **64**, 193-236 (1992)
- [29] P. Mitra, Structure of multi-anyon wavefunctions, *Phys. Lett. B*, **345**, 473-476 (1995)
- [30] The explicit relation with the statistics is expressed by $q(\mathbf{r}, \mathbf{r}') = \pm e^{i\nu\pi S(\mathbf{r}, \mathbf{r}')}$ where the signs + and - refer to the Bosonic and Fermionic representations [14; 23; 24; 29], ν denotes the statistics, $S(\mathbf{r}, \mathbf{r}')$ is the anyonic phase with $S(\mathbf{r}, \mathbf{r}') = \pm 1$ depending on whether the exchange is performed along a (counterclockwise) clockwise path [14; 28] for $D = 2$, while $S(\mathbf{r}, \mathbf{r}') = \text{sgn}(r - r')$ for $D = 1$ [23; 24; 25; 27]. We note that, in any case, the phases are some fixed constants, consequently the spatial derivatives ∂_{x_i} do not act on the phase factor, but only on the anyonic field operators [25].
- [31] F. D. M. Haldane, "Fractional statistics" in arbitrary dimensions: A generalization of the Pauli principle, *Phys. Rev. Lett.* **67**, 937-940 (1991).
- [32] D. Li, S. Ouvry, Haldane's fractional statistics and the Riemann-Roch theorem, *Nucl. Phys. B* **430**, 563-576 (1994).
- [33] For $D = 2$, by considering the Bose or Fermi field operator $\tilde{\Psi}$, we can use the relation [14] $\Psi(\mathbf{r}) = e^{-i\frac{e}{\hbar c}\Lambda(\mathbf{r})}\tilde{\Psi}(\mathbf{r})$ with the field gauge $\mathbf{A}(\mathbf{r}) = \nabla\Lambda(\mathbf{r})$, to rewrite the hamiltonian in the usual 2D anyonic form $H = 1/2m \int d^2r [(-i\hbar\partial_{x_j} - \frac{e}{c}A_j)\tilde{\Psi}(\mathbf{r})]^\dagger [(-i\hbar\partial_{x_j} - \frac{e}{c}A_j)\tilde{\Psi}(\mathbf{r})] + \int d^2r \tilde{\Psi}^\dagger(\mathbf{r})U(\mathbf{r})\tilde{\Psi}(\mathbf{r}) + \frac{1}{2} \int \int d^2r d^2r' \tilde{\Psi}^\dagger(\mathbf{r})\tilde{\Psi}^\dagger(\mathbf{r}')V(\mathbf{r}, \mathbf{r}')\tilde{\Psi}(\mathbf{r}')\tilde{\Psi}(\mathbf{r})$. For $D = 1$, by using the Bethe ansatz approach [25], the eigenvalue problem for H can be reduced to solving the quantum N-body problem $H_N\phi(r_1, \dots, r_N) = E\phi(r_1, \dots, r_N)$ where $H_N = \sum_{i=1}^N [-\frac{\hbar^2}{2m} \frac{\partial^2}{\partial r_i^2} + U(r_i)] + \sum_{1 \leq i < j \leq N} V(r_i, r_j)$ and ϕ is the wavefunction satisfying the usual anyonic symmetry [23; 24; 29].
- [34] Smith H., Jensen H. H., *Transport Phenomena*, (Clarendon Press Oxford) 1989.
- [35] A simple application is obtained by considering a δ -function interaction [14; 23; 25] with $V(\mathbf{r}, \mathbf{r}') = c\delta^D(\mathbf{r} - \mathbf{r}')$, and, consequently, $V_{eff}(\mathbf{r}) = U(\mathbf{r}) + cn(\mathbf{r})$. Other possible applications are given by considering a system with a Coulomb interaction potential $V(\mathbf{r}, \mathbf{r}') = e^2/|\mathbf{r} - \mathbf{r}'|$ or, for $D = 1$, a standard periodic potential $V(r, r') = g(L/\pi)^2 \sin^{-2}(\pi|r - r'|/L)$ on a ring of circumference L [24].
- [36] J. Von Neumann, *The Mathematical Foundations of Quantum Mechanics*. Princeton University Press, Princeton, (1955).
- [37] Y. S. Wu, Statistical Distribution for Generalized Ideal Gas of Fractional-Statistics Particles, *Phys. Rev. Lett.* **73**, 922-925 (1994).
- [38] L.D. Landau, E.M. Lifshitz, *Statistical Physics*, Vol. **5**, Chap. V §54, Pergamon Press, London-Paris (1959).
- [39] J.E. Moyal, Quantum mechanics as a statistical theory, *Proc. Cambridge Phil. Soc.* **45**, 99-124 (1949).
- [40] For example in Ref. [8; 11] $\mathcal{H}_2^{(2)}$ and $\mathcal{H}_3^{(2)}$ are expressed only in terms of variables $\{n, T\}$ and of their spatial variations.
- [41] K. Byczuk, J. Spalek, G.S. Joyce and S. Sarkar, Thermodynamic properties of particles with intermediate statistics, *Phys. Rev. B*, **53**, 990-993 (1996); R.T. Delves, G.S. Joyce and I.J. Zucker, Exact results in the theory of intermediate statistics, *Proc. R. Soc. Lond. A*, **453**, 1177-1194 (1997).
- [42] M. G. Ancona, G.J. Iafrate, Quantum correction to the equation of state of an electron gas in a semiconductor, *Phys. Rev. B* **39**, 9536-9540 (1989); C. Gardner, C. Ringhofer, Smooth quantum potential for the hydrodynamic model, *Phys. Rev. E* **53**, 157-167 (1996).
- [43] A. Jüngel, D. Matthes, J.P. Milišić, Derivation of new quantum hydrodynamic equations using entropy minimization, *SIAM J. Appl. Math.*, **67**, 46-68 (2006)
- [44] L. Barletti, C. Cintolesi, Derivation of Isothermal Quantum Fluid Equations with Fermi-Dirac and Bose-Einstein Statistics, *J. Stat. Phys.*, **148**, 353-386 (2012).
- [45] We note that for $D = 1$ the tensors $\mathcal{T}_{ik} = M_{(ik)} = 0$ and the closure relation (54) takes a very simplified form. Analogously, in the low temperature regime, for $D = 2$ it is $\mu^{(q)} = 0$, consequently all quantum nonlocal effects in Eq.(54) are imputable only to terms involving vorticity.
- [46] W. Yang, Gradient correction in Thomas-Fermi theory, *Phys. Rev A*, **34**, 4575-4585 (1986); W. Yang, R. G. Parr, C. Lee, Various functionals for the kinetic energy den-

sity of an atom or molecule, *Phys. Rev A*, **34**, 4586-4590 (1986); P. Tarazona, E. Chacon, Exact solution of approximate density functionals for the kinetic energy of the electron gas, *Phys. Rev. B*, **39**, 10366-10369 (1989); M. Brack, C Guet, H.B Hakansson, Selfconsistent semiclassical description of average nuclear properties a link between microscopic and macroscopic models, *Phys. Rep.* **123**, 275-364 (1985); E. Engel, P. I aRocca, R. M. Dreizler, Gradient expansion for $T_s[n]$: Convergence study for jellium spheres, *Phys. Rev B*, **49**, 16728-16732 (1994).

- [47] M.G. Ancona and A. Svizhenko, Density-gradient theory of tunneling: Physics and verification in one dimension, *J. Appl. Phys.*, **104**, 073726-1-13 (2008); A.R. Brown, J.R. Watling, G. Roy, C. Riddet, C.L. Alexander, U. Kovac, A. Martinez and A. Asenov, Use of density gradient quantum corrections in the simulation of statistical variability in MOSFETs, *J. Comput. Electron.*, **9**, 187-196 (2010); M.G. Ancona, Density-gradient theory: a macroscopic approach to quantum confinement and tunneling in semiconductor devices, *J. Comput. Electron.*, **10**, 65-97 (2011);
- [48] M. Chaichian, G. L. Klimchitskaya, V. M. Mostepanenko and A. Tureanu, *Phys. Rev A* **86**, 012515 (2012).
- [49] A. Bulgac, J. E. Drut, P. Magierski, Spin 1/2 Fermions in the Unitary Regime: A Superfluid of a New Type, *Phys. Rev. Lett.* **96**, 090404-1-4 (2006); E. Burovski, N. Prokofev, B. Svistunov, M. Troyer, Critical Temperature and Thermodynamics of Attractive Fermions at Unitarity, *Phys. Rev. Lett.* **96**, 160402-1-4 (2006); H. Hu, P. D. Drummond, Xia-Ji Liu, Universal thermodynamics of strongly interacting Fermi gases, *Nat. Phys.* **3**, 469-472 (2007); H. Hu, Xia-Ji Liu, P. D. Drummond, Comparative study of strong-coupling theories of a trapped Fermi gas at unitarity, *Phys. Rev. A* **77**, 061605(R)-1-4 (2008); L. Luo, B. Clancy, J. Joseph, J. Kinast, J. E. Thomas, Measurement of the Entropy and Critical Temperature of a Strongly Interacting Fermi Gas, *Phys. Rev. Lett.* **98**, 080402-1-4 (2007); L. Luo, J.E. Thomas, Thermodynamic Measurements in a Strongly Interacting Fermi Gas, *J. Low Temp. Phys.* **154**, 1-29 (2009).
- [50] F. Qin, J. Chen, Comparative study of the finite-temperature thermodynamics of a unitary Fermi gas, *Phys. Rev. A*, **79**, 043625-1-6 (2009); F. Qin, J. Chen, The finite-temperature thermodynamics of a trapped unitary Fermi gas within fractional exclusion statistics, *J. Phys. B: At. Mol. Opt. Phys.* **43**, 055302-1-5 (2010);

Appendix

Being $w^{(0)}(\xi)$ solution of (30) (with $\xi = e^{\alpha+x^2}$) we define the integrals

$$I_n(\alpha, \kappa) = \int_0^{+\infty} \frac{x^n}{w^{(0)}(e^{\alpha+x^2}) + \kappa} dx, \quad (55)$$

where, for $n < 0$, all the integral functions $I_n(\alpha, \kappa)$ can be obtained by means of the following general differentiation property

$$\frac{\partial^r I_n}{\partial \alpha^r} = (-1)^r \left[\frac{\Gamma\left(\frac{n+1}{2}\right)}{\Gamma\left(\frac{n+1}{2} - r\right)} \right] I_{n-2r}. \quad (56)$$

The functions $\eta_{ij}^{(s)}$, contained in (39)-(40), are given by

$$\eta_{ij}^{(s)} = (-1)^i 2^{j-1} \frac{\Gamma\left(\frac{D}{2} + s + j - 1\right)}{\Gamma\left(\frac{D}{2} + s + i + j - 5\right)} \frac{I_{D+2(s+i+j)-11}}{I_{D+2s-1}} \quad (57)$$

and all nonlocal terms $\{Q^{(q,p)}, Q_{(ik)}\}$ are expressed by

$$Q^{(1,1)} = -\frac{2}{(D-2)^2} \left(\frac{I_{D-1}}{I_{D-3}}\right)^2 \left(\frac{\partial \ln n}{\partial x_k}\right)^2 + O(\hbar^2), \quad (58)$$

$$Q^{(1,2)} = \frac{1}{D(D-2)} \frac{I_{D-1}}{I_{D-3}} \left\{ \left[1 - \frac{D-4}{D-2} \frac{I_{D-1}}{I_{D-3}} \frac{I_{D-5}}{I_{D-3}} \right] \times \left(\frac{\partial \ln n}{\partial x_k}\right)^2 + \frac{\partial^2 \ln n}{\partial x_k \partial x_k} \right\} + \frac{1}{2D} \frac{m}{k_B T} \mathcal{T}_{ll}^2 + O(\hbar^2), \quad (59)$$

$$Q^{(2,1)} = \frac{3}{D-2} \frac{I_{D-1}}{I_{D-3}} \left\{ \left[1 - \frac{D-4}{D-2} \frac{I_{D-1}}{I_{D-3}} \frac{I_{D-5}}{I_{D-3}} \right] \times \left(\frac{\partial \ln n}{\partial x_k}\right)^2 + \frac{\partial^2 \ln n}{\partial x_k \partial x_k} \right\} + \frac{3}{4} \frac{m}{k_B T} \mathcal{T}_{ll}^2 + O(\hbar^2), \quad (60)$$

$$Q_{(ij)} = \frac{1}{D-2} \frac{I_{D-1}}{I_{D-3}} \left\{ \left[1 - \frac{D-4}{D-2} \frac{I_{D-1}}{I_{D-3}} \frac{I_{D-5}}{I_{D-3}} \right] \times \frac{\partial \ln n}{\partial x_{(i)}} \frac{\partial \ln n}{\partial x_{(j)}} + \frac{\partial^2 \ln n}{\partial x_{(i)} \partial x_{(j)}} \right\} + \frac{1}{2} \frac{m}{k_B T} \mathcal{T}_{(ij)}^2 + O(\hbar^2). \quad (61)$$

The quantum gradient corrections terms in (45)-(47) are

$$Q_B^H = \frac{\hbar^2}{4m} \left[\frac{\partial^2 \ln n}{\partial x_r \partial x_r} + \left(\frac{\partial \ln n}{\partial x_r}\right)^2 + \frac{m}{2} \frac{\mathcal{T}_{ll}^2}{k_B T} \right], \quad (62)$$

$$Q_C^H = \frac{\hbar^2}{12D} \frac{1}{m} \left[2D \frac{\partial^2 \ln n}{\partial x_r \partial x_r} + (3D-2) \left(\frac{\partial \ln n}{\partial x_r}\right)^2 + (D+4) \frac{m}{2} \frac{\mathcal{T}_{ll}^2}{k_B T} \right], \quad (63)$$

$$M_{(ik)}^H = -\frac{\hbar^2}{12} \frac{n}{m^2} \left[\frac{\partial \ln n}{\partial x_{(i)}} \frac{\partial \ln n}{\partial x_{(j)}} - \frac{m}{k_B T} \mathcal{T}_{(ik)}^2 \right], \quad (64)$$

The quantum gradient corrections terms in (51)-(53) are

$$Q_D^H = -\frac{\hbar^2}{2D} \frac{1}{m} \left[2D \frac{\partial^2 \ln n}{\partial x_r \partial x_r} + (D-4) \left(\frac{\partial \ln n}{\partial x_r}\right)^2 \right] + \frac{\hbar^2}{32} D(D-6) \frac{\mathcal{T}_{ll}^2}{\mu^{(0)}}, \quad (65)$$

$$Q_E^H = -\frac{\hbar^2}{2D} \frac{1}{m} \left[\frac{\partial^2 \ln n}{\partial x_r \partial x_r} + \frac{(D-3)}{D} \left(\frac{\partial \ln n}{\partial x_r}\right)^2 \right] - \frac{\hbar^2}{32} \frac{\mathcal{T}_{ll}^2}{\mu^{(0)}}, \quad (66)$$

$$\mathcal{M}_{(ik)}^H = -\frac{\hbar^2}{12} \frac{n}{m^2} \left[\frac{4}{D} \frac{\partial \ln n}{\partial x_{(i)}} \frac{\partial \ln n}{\partial x_{(j)}} + \frac{m}{2} \frac{D}{\mu^{(0)}} \mathcal{T}_{(ik)}^2 \right], \quad (67)$$

THERMODYNAMICS OF CONTINUA: THE CHALLENGE OF UNIVERSALITY

Peter Ván^{1,2,3}

¹Dept. of Theoretical Physics, Wigner Research Centre for Physics, Institute for Particle and Nuclear Physics,
H-1525 Budapest, Konkoly Thege Miklós út 29-33, Hungary;

²Dept. of Energy Engineering, Budapest Univ. of Technology and Economics,
H-1111, Budapest, Műegyetem rkp. 3-9, Hungary;

³Montavid Thermodynamic Research Group
Email: van.peter@wigner.mta.hu

ABSTRACT

The explanation of the apparent universality of thermodynamics points toward the extension of the usual conceptual background of the second law. Arguments are collected that a basic guiding idea of stability of thermodynamic equilibrium combined with a proper interpretation of the entropy principle may provide the necessary solid foundation with verifiable consequences.

INTRODUCTION

When treating the conceptual background of the second law, it is reasonable to start from the foundations, analysing the principles behind the concepts.

The basic mystery in thermodynamics is the *universality*. The validity of thermodynamic equations and theories regularly exceed the expectations. There are three independent aspects here:

1. *Uniformity*. We expect uniform principles and clear transition methods between the modeling levels. The validity of the second law is accepted in
 - a) Thermostatistics, treating the relation of state variables,
 - b) Ordinary thermodynamics, when processes of homogeneous bodies are modeled by time dependent state variables,
 - c) Continuum thermodynamics, where the thermodynamic quantities are fields,
2. *Overdisciplinarity*. The concept of entropy and temperature appears from black holes to quark-gluon plasma, from general relativity to quantum chromodynamics.
3. *Mechanism independence*. The validity of the second law is independent of the particular mechanisms behind. Statistical mechanics, kinetic theory can provide particular demonstrations, but no proofs for a general principle.

One may wonder and discuss how extensive the validity of these aspects is. The question is whether and how one can understand the origin of the observed overdisciplinarity considering the expected uniformity. We consider as a key aspect the mentioned attitude to the mechanism independence – the generality.

In the following, we outline more exactly the challenge and a possible program of validation. Our working hypothesis is that the second law is a general principle and this is the reason of the universality of thermodynamics. Therefore, we need a guiding

general idea, a conceptual understanding and, at the same time, we need a working strategy to translate this understanding to proper mathematical formulation of physical theories.

THE SECOND LAW IS MATERIAL STABILITY

A guiding general idea cannot and must not postulate the existence of entropy, neither the increase of entropy: the aim is to introduce the physical origin of the entropy concept. The general idea cannot introduce statistical concepts because that violates the assumption of mechanism independence. Fluctuations or periodic machines are too specific. A general idea must be transparent. The general idea should produce a benchmark, a method of verification. A good idea should have a way of exact formulation in addition to flexibility. My suggestion is that

*Thermodynamic equilibrium of simple materials
is stable under neutral conditions.*

The idea that stability is connected to the second law, is ancient, it appears in the thermodynamic literature from different points of view and in different contexts (see, e.g. [1; 2; 3; 4; 5; 6]). Sometimes there are wrong connected claims. We do not state here the stability of steady-states (see, e.g. [7; 8] etc.). The validity of an idea can be discussed [9] and exact formulations of the statement are necessary. However, it is reasonable to believe that dissipation leads to stability of isolated simple materials. Without stability there is no observation, no reproduction of experiments. The above statement should be considered as a guiding idea, a challenge, a starting point of a program for the search of exact conditions [10]. This is not an exact statement yet, this is a principle.

On the other hand, the stability concept of the second law is fully compatible to the other formulations. The complete thermostatistics can be understood from this point of view. That entropy function is a potential in the thermodynamic phase space of classical homogeneous gases and fluids, that it is concave, and the requirement that entropy increases along several reasonable sets of differential equations, form the three conditions of a

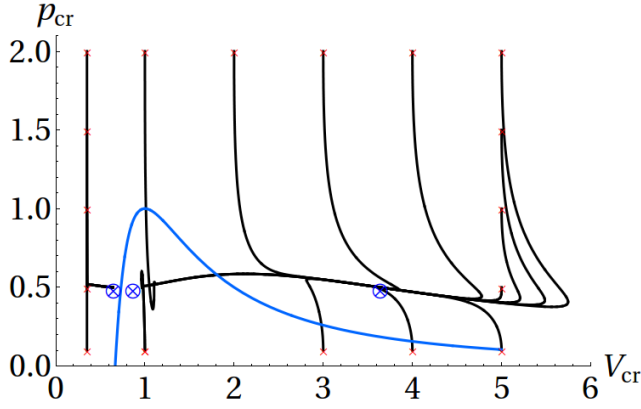


Figure 1. Irreversible processes in a homogeneous van der Waals gas in a cylinder closed by a piston are shown on the pressure-volume plane. The initial conditions form a rectangular area around the critical point. The three equilibrium points are denoted by crossed circles, the one under the spinodal is unstable. The tendency toward the equilibrium indicates a slow manifold.

Lyapunov theorem. The thermodynamic equilibrium of simple ordinary thermodynamic systems is asymptotically stable. This is a simple but rigorous result, developed thoroughly in the book of Matolcsi [11]. There are clear conditions when it is valid and this is the necessary step between thermostatics and continuum thermodynamics claimed e.g. in [12]. Instead of further details, I show here some integral curves of a van der Waals body in a constant environment at the pressure-volume plane with critical state normalization. These are processes, initial conditions are around the critical point indicated by crosses. The van der Waals gas body has a fold bifurcation at the critical point, and we can observe a slow manifold in Fig. 1 with the particular interaction parameters.

In case of continua, our basic expectation is similar. Dissipation has to ensure that a homogeneous equilibrium is asymptotically stable in the absence of excitations and in case of neutral boundary conditions. Otherwise the dissipative theory is not properly constructed, it is a wrong model for real materials. Construction and validation are not really separable when speaking about principles. One can build a theory by any methods, introducing the empirical experience and also exploiting the entropy inequality and then check the stability of the homogeneous equilibrium. Does the entropy principle ensures the stability? The Fourier-Navier-Stokes system is linearly stable [13], but generalized continua is not necessarily. Why? Is that a problem of the principle or of the formulation?

Now we have arrived at the subject of the next section. To formulate a reasonable attitude, we should clarify the relation between the expected universality and the entropy principle in continuum physics.

ENTROPY AND UNIVERSALITY

A possible and rather usual understanding of the relation of thermodynamics and statistical theories assumes parallel modeling levels according to the uniformity aspect of universality:

Thermodynamics	Statistical mechanics
Thermostatics	Equilibrium statistical mechanics
Ordinary thermodynamics	Stochastic theory
Continuum thermodynamics	Kinetic theory

Table 1. Conceptual relation of thermodynamics and statistical physics

There is also a relativistic version of these theories. There is a well-developed relativistic kinetic theory and also there are relativistic theories of fluids (some of them are unstable). A relativistic stochastic theory is a relatively new development [14]. However, our particular interest now is, that there is a *relativistic thermostatics*, too [15; 16]. It is the statics of fast motion. It is an interesting subject in itself, but for us only one aspect is remarkable. One of the basic relations, the most widely accepted one, that leads to relativistic equilibrium statistical mechanics, e.g. to Jüttner distribution, is the following:

$$dE = TdS - pdV + v dG.$$

This is a relation of energy E , temperature T , entropy S , pressure p and volume V of a thermodynamic body and its velocity v and momentum G . This relativistic generalization of the Gibbs relation expresses the fact that energy and momentum cannot be separated. The content of the above formula is that entropy is a function of the volume and also of the energy-momentum four-vector $S = S(E^a, V)$. Only for an observer can entropy be a function of energy *and* momentum separately. Relativistic thermostatics requires that entropy depends on momentum [17; 18].

Quantum versions of statistical theories at the second column of Table 1 are well known. We have been struggling with quantum thermostatics for a long time, mostly via statistical approaches, too. However, what is *quantum continuum thermodynamics*? It is originally not an outcome of a statistical theory. It is well-known for a long time that a special Korteweg fluid, where the pressure tensor is a function of the density gradient, the so-called Schrödinger-Madelung fluid, is equivalent to the one component Schrödinger equation [19]. The fluid equations are the following:

$$\begin{aligned} \dot{\rho} + \rho \partial_i v^i &= 0 \\ \rho v^j - \partial_j \left[\frac{\hbar^2}{8m^2} \left(\partial_k^k \rho \delta^{ij} + \partial^{ij} \rho - \frac{2\partial^i \rho \partial^j \rho}{\rho} \right) \right] &= 0, \end{aligned} \quad (1)$$

where ρ is the probability density, m is the mass of the particle, \hbar is the Planck constant and v^i is the velocity field. The connection with the wave function is given by the Madelung transformation $\psi = \sqrt{\rho} e^{iI}$, where I is related to the velocity potential in the simplest case $v_i = \frac{\hbar}{m} \partial_i I$. There are no complex fields, nor operators. Many researches extend the original analogy and put the Madelung idea into a wider context, and, at the same time, are speculating on the interpretational consequences. Some of the most interesting ones are [20; 21; 22; 23; 24; 25; 26; 27].

This is not just an inconvenient side effect that can be forgotten and put aside. Quantum field theories, let them be Abelian or not, can be reformulated as fluid theories in general [28; 29]. There are vortices there, too. There is a corresponding thermodynamic background that requires a density gradient dependent entropy density [30]. For quantum continuum thermodynamics, the entropy density depends on the gradient of velocity.

Finally, one of the most striking relativistic —not yet observed— phenomena is the Unruh effect. An accelerating observer may observe a thermal electromagnetic radiation of an oscillating charge. In a covariant framework a thermodynamic theory of Unruh effect may require an acceleration dependent entropy function. As acceleration is related to gravitation one may wonder the role of the second law here... [31].

Therefore, the manifest overdisciplinary aspects of thermodynamic concepts indicate a need of a profound generalization of our classical approaches. Velocity and acceleration dependent entropies are well justified by relativistic theories. The traditional nonrelativistic concept of objectivity, which forbids this dependence, is wrong [32]. Moreover, gradient dependent constitutive state spaces and entropies are required for the explanation of quantum-hydrodynamic relations...

There is a simple idea that unfolds the mystery of universal aspects of thermodynamics. A theory is as universal as general the built-in assumptions and the conditions are. In continuum physics, the entropy principle is interpreted as an inequality, constrained by all other relevant conditions of the corresponding theory. Objectivity, material symmetries, kinematic restrictions, and fundamental balances are among the constraints that should be considered by the exploitation. This is a general approach to the second law if we analyse and properly apply the constraints and the other fundamental aspects [33; 34; 35].

What are these fundamental aspects that should be scrutinized? It is already mentioned that the choice of the state space, both the basic and the constitutive one, is definitely one of them, where the known classical restrictions can be questioned. Moreover, entropy is a four-vector, entropy density and entropy current are frame dependent separations both in relativistic and in nonrelativistic spacetimes. Therefore, entropy current is a constitutive quantity, too.

These questions are connected. Assuming a classical entropy current, as the quotient of the heat flux and the temperature, $j_s^i = q^i/T$, one can prove that gradients are excluded from the state space [36; 37; 38]. One may wonder that the multiple methods and ideas in weakly nonlocal continuum theories appear to circumvent these restrictions. These are for example the square-gradient ideas [39; 40; 41], GENERIC [42; 43; 44], phase fields theories [45; 46; 47], different modifications of power [48; 49; 50; 51], and others [52; 53]. Which is the best idea? Some researches say that the triumph of Copenhagen interpretation is due to pure manpower and the beautiful mathematical framework of von Neumann [54]. What will happen in thermodynamics? Shall we able to discuss and reconcile the problematic aspects? Or, at least, shall we able to understand each other?

My opinion is that universality is the key for ordering the different approaches and understanding their relations. Our best tool toward universal thermodynamic theories is the formulation of the entropy inequality as generally as it is possible and applying proper formulation of the additional principles, first of all objectivity, that determine the choice of the basic and constitutive state spaces. Therefore, if our methods of the second law are general and correct then we will obtain a universal theory.

What is the role of stability then?

ENTROPY AND STABILITY

Thermodynamic equilibrium and thermodynamic state are delicate concepts. State variables should distinguish between the thermodynamic bodies, characterize the state and not the in-

teraction [55]. The stability concept of the second law alone does not clarify the state variables and it is not constructive without the entropy principle. On the other hand, the entropy principle without stability is a complicated formulation of the second law with an obscure physical content. Stability sometimes follows from the thermodynamic framework, but not always. Thermodynamic frameworks, the different entropy principles are not equivalent.

The relation between stability and entropy is not simple. This is a long-discussed, deeply investigated and frequently rejected relation in classical continuum mechanics. A non-negative entropy production with concave entropy density alone does not ensure the asymptotic stability of equilibrium. Higher grade fluids are unstable [56; 57]. At the local equilibrium level, a famous counterexample is the Eckart theory of relativistic fluids [58]. It is the simplest relativistic generalization of the Fourier-Navier-Stokes equations, constructed by thermodynamic principles. However, the homogeneous equilibrium of an Eckart fluid is violently unstable, in spite of the thermodynamic framework and nonnegative entropy production [59].

Technically, the Lyapunov method for partial differential equations is not easy. It is simpler and more straightforward to check the linear stability of the equilibrium. Linear stability should be the consequence of the expected more general stability requirement and therefore serves as a convenient necessary condition, a suitable benchmark in the theory development.

The universal extension of the entropy principle is a promising program. Recent examples of dissipative relativistic fluids indicate that an extension of the entropy principle may restore the expected stability [60; 61; 13; 62]. In this particular case, momentum also has to be among the state variables and, most importantly, the momentum balance is a constraint of the entropy inequality [61; 18].

The thermodynamic framework and the stability of homogeneous equilibrium in case of neutral conditions are two sides of the same coin. Stability is not only a general idea behind the second law, but also a verification tool of thermodynamic theories.

HOW UNIVERSAL?

The first book of the Landau-Lifshitz series of theoretical physics is about analytical mechanics [63]. It starts with a mind provoking derivation of the Lagrangian of a free point mass by spacetime symmetries and Hamiltonian variational principles. This is an attempt to understand the origin of evolution equations in physics. However, the variational principles as tools are not universal. Dissipation cannot be incorporated easily. Heat conduction and also dissipative mechanical systems in general cannot be understood with the help of variational principles, even the best attempts are artificial and their validity is restricted [64; 65; 66; 67; 68].

On the other hand, the previously outlined entropy principle provides a possibility to construct and derive evolution equations both for the nondissipative and the dissipative cases [69]. The clear examples in this respect are the evolution equations for internal variables, where restrictions from the second law provide the best way of construction, recovering and including results from dissipation potentials or variational assumptions, without these additional hypotheses [70]. Moreover, in some investigated cases, the nondissipative part of the resulted evolution equation has an Euler-Lagrange form, the thermodynamic potential is connected to a Lagrangian. This generality requires

the extension of the second law incorporating gradients of dual internal variables in the constitutive state space. This extension, the method of dual internal variables introduces a general framework of dissipative mechanical phenomena [71; 72; 73; 74].

Generalized mechanics provides an example where several independent methods were applied for generating evolution equations of internal variables of mechanical origin [75; 76; 77]. Here the thermodynamic method of dual internal variables—the previous extension of the entropy principle—can generate the evolution equations [78; 79]. The dissipative part of the evolution equations promisingly stabilizes the thermodynamic equilibrium according to linear stability analysis [80].

Then one may ask: how universal are the thermodynamic principles? As general laws of nature, their validity incorporates mechanics, electrodynamics and every discipline of physics [81; 82]. With a proper formulation and understanding, we can grasp the very origin and connection between these seemingly separated fields. This is the final dream of universality.

UNIVERSAL SUMMARY

There are some principles in physics that provide a driving force for the development. Those are sometimes subjective feelings, like the requirement of simplicity and harmony. Others express deeper and almost inevitable requirements of physical theories, like objectivity. In a sense it is convenient to say that some expected general principles are invalid [83; 84; 85; 86]. That way we may separate ourselves for some inconveniences and close a direction of investigations. This reductionism is frequently fruitful in focusing and deepening our understanding. On the other hand, general principles are pharoses in the scientific landscape, shining lights that keep ourselves on the right way. Focusing on the nearby stormy waves cannot prevent us from the greater dangers of reefs, which can be detected only from a right perspective. From this point of view an ostensible violation of a general principle is not only an indication that its validity is limited, but also a challenge that something is not properly formulated.

The experienced universality indicates the need for the following generalizations of the entropy principle in continuum theories:

- The entropy four-vector is a constitutive quantity, both in classical and relativistic theories. Therefore, the entropy current density is constitutive.
- Momentum should be incorporated in the basic state space when dealing with mechanics and thermodynamics.
- Space and time derivatives of the basic variables cannot be excluded from the constitutive state space.
- The momentum balance must be considered directly as a constraint in the entropy inequality, beyond the internal energy concept.

These generalizations, in particular the clarification of the role of energy and momentum, require the proper formulation and use of objectivity.

The tool of the validation of the mentioned generalizations—a benchmark—is provided by the stability concept of the second law. In particular, the linear stability of the evolution equations is a necessary condition.

Understanding the extent and the origin of the manifest universality of thermodynamic principles is one of the greatest challenges of thermodynamics.

ACKNOWLEDGEMENT

The work was supported by the grants OTKA K81161, K104260 and TÉT 10-1-2011-0061/ZA-15-2009.

REFERENCES

- [1] B. D. Coleman and V. J. Mizel. Existence of entropy as a consequence of asymptotic stability. *Archive for Rational Mechanics and Analysis*, 25:243–270, 1967.
- [2] P. Glansdorff and I. Prigogine. *Thermodynamic Theory of Structure, Stability and Fluctuations*. Wiley-Interscience, London-etc., 1971.
- [3] M. E. Gurtin. Thermodynamics and Stability. *Archive for Rational Mechanics and Analysis*, 59:63–96, 1975.
- [4] C. M. Dafermos. The Second Law of thermodynamics and stability. *Archive for Rational Mechanics and Analysis*, 70:167–179, 1979.
- [5] J. Casas-Vázquez and G. Lebon. Stability of thermodynamics systems. In *Proceedings of the Meeting Held at Bellaterra School of Thermodynamics Autonomous University of Barcelona Bellaterra (Barcelona) Spain, September 1981*, volume 164 of *Lecture Notes in Physics*. Springer Verlag, 1982.
- [6] G. P. Beretta. A theorem on Lyapunov stability for dynamical systems and a conjecture on a property of entropy. *Journal of Mathematical Physics*, 27(3):305–308, 1986.
- [7] P. Glansdorff, G. Nicolis, and I. Prigogine. The thermodynamic stability theory of nonequilibrium steady-states. *Proceedings of the National Academy of Sciences, USA*, 71(1):197–199, 1974.
- [8] J. Keizer and R. F. Fox. Qualms regarding the range of validity of the Glansdorff-Prigogine criterion for stability of non-equilibrium states. *Proceedings of the National Academy of Sciences, USA*, 71(1):192–196, 1974.
- [9] I. Müller and W. Weiss. Thermodynamics of irreversible processes - past and present. *Eur. Phys. J. H*, 37:139–236, 2012.
- [10] I. Prigogine and I. Stengers. *La nouvelle alliance*, Gallimard, Paris 1986. in French.
- [11] T. Matolcsi. *Ordinary thermodynamics*. Akadémiai Kiadó (Publishing House of the Hungarian Academy of Sciences), Budapest, 2005.
- [12] C. Truesdell and S. Bharatha. *Classical Thermodynamics as a Theory of Heat Engines*. Springer Verlag, Berlin-Heidelberg-etc., 1977.
- [13] P. Ván. Generic stability of dissipative non-relativistic and relativistic fluids. *Journal of Statistical Mechanics: Theory and Experiment*, page P02054, 2009.
- [14] J. Dunkel and P. Hänggi. Relativistic Brownian motion. *Physics Reports*, 471(1):1–73, 2009.
- [15] M. Planck. Zur Dynamik bewegter Systeme. *Annalen der Physik*, 331(6):1–34, 1908.
- [16] A. Einstein. Über das Relativitätssprinzip und die aus demselben gezogenen Folgerungen. *Jahrbuch der Radioaktivität und Elektronik*, 4:411–462, 1907.
- [17] T. S. Bíró and P. Ván. About the temperature of moving bodies. *EPL*, 89:30001, 2010.
- [18] P. Ván and Bíró T.S. Dissipation flow-frames: particle, energy, thermometer. 2012. in this volume, see also arXiv:...
- [19] E. Madelung. Quantentheorie in hydrodynamischer Form. *Zeitschrift für Physik*, 40:322–326, 1926. in German.
- [20] D. Bohm. *Quantum Theory*. Prentice-Hall, New York,

- 1951.
- [21] T. Takabayasi. Relativistic hydrodynamics of the Dirac matter Part I. General theory. *Supplement of the Progress of Theoretical Physics*, (4):1–80, 1957.
- [22] D. I. Blohincev. *Fundamental Questions of Quantum Mechanics*. Nauka, Moskva, 1966. in Russian.
- [23] Jánossy L. The physical interpretation of wave mechanics I. *Foundations of Physics*, 3(2):185–202, 1973.
- [24] S. Sonego. Interpretation of the hydrodynamic formulation of quantum mechanics. *Foundations of Physics*, 21(10):1135–1181, 1991.
- [25] P. R. Holland. *The Quantum Theory of Motion*. Cambridge University Press, Cambridge, 1993.
- [26] T. Fülöp and S. D. Katz. A frame and gauge free formulation of quantum mechanics. quant-ph/9806067, 1998.
- [27] R. Carroll. *On the quantum potential*. Anima Publishing, Suffolk, 2007.
- [28] B. Bistrovic, R. Jackiw, H. Li, V. P. Nair, and S.-Y. Pi. Non-Abelian fluid dynamics in Lagrangian formulation. (hep-th/0210143), 2002.
- [29] R. Jackiw, V. P. Nair, S.-Y. Pi, and A. P. Polychronakos. Perfect fluid theory and its extensions. *Journal of Physics A*, 37:R327–R432, 2004.
- [30] P. Ván and T. Fülöp. Weakly nonlocal fluid mechanics - the Schrödinger equation. *Proceedings of the Royal Society, London A*, 462(2066):541–557, 2006.
- [31] E. Verlinde On the origin of gravity and the laws of Newton *Journal of High Energy Physics*, (04):029, 2011.
- [32] T. Matolcsi and P. Ván. Can material time derivative be objective? *Physics Letters A*, 353:109–112, 2006.
- [33] B. D. Coleman and W. Noll. The thermodynamics of elastic materials with heat conduction and viscosity. *Archive for Rational Mechanics and Analysis*, 13:167–178, 1963.
- [34] I-Shih Liu. Method of Lagrange multipliers for exploitation of the entropy principle. *Archive of Rational Mechanics and Analysis*, 46:131–148, 1972.
- [35] V. A. Cimmelli. An extension of Liu procedure in weakly nonlocal thermodynamics. *Journal of Mathematical Physics*, 48:113510, 2007.
- [36] M. E. Gurtin. Thermodynamics and the possibility of spatial interaction in elastic materials. *Archive for Rational Mechanics and Analysis*, 19:339–352, 1965.
- [37] A. Acharya and T. G. Shawki. Thermodynamic restrictions on constitutive equations for second-deformation-gradient inelastic behaviour. *Journal of Mechanics and Physics of Solids*, 43:1751–1772, 1995.
- [38] P. Ván and C. Papenfuss. Thermodynamic consistency of third grade finite strain elasticity. *Proceedings of the Estonian Academy of Sciences*, 59(2):126–132, 2010.
- [39] D. Bedeaux, E. Johannessen, and A. Rojorde. A nonequilibrium van der Waals square gradient model. (I). the model and its numerical solution. *Physica A*, 330:329–353, 2003.
- [40] S. Kjelstrup and D. Bedeaux. *Non-equilibrium thermodynamics of heterogeneous systems*. World Scientific, Berlin, New Jersey, etc., 2008.
- [41] K. S. Glavatskiy and D. Bedeaux. Nonequilibrium properties of a two-dimensionally isotropic interface in a two-phase mixture as described by the square gradient model. *Physical Review E*, 77:061101, 2008.
- [42] M. Grmela and H. C. Öttinger. Dynamics and thermodynamics of complex fluids. I. Development of a general formalism. *Physical Review E*, 56(6):6620–6632, 1997.
- [43] H. C. Öttinger and M. Grmela. Dynamics and thermodynamics of complex fluids. II. Illustrations of a general formalism. *Physical Review E*, 56(6):6633–6655, 1997.
- [44] H. C. Öttinger. *Beyond equilibrium thermodynamics*. Wiley-Interscience, 2005.
- [45] P. C. Hohenberg and B. I. Halperin. Theory of dynamic critical phenomena. *Reviews of Modern Physics*, 49(3):435–479, 1977.
- [46] O. Penrose and P. C. Fife. Thermodynamically consistent models of phase-field type for the kinetics of phase transitions. *Physica D*, 43:44–62, 1990.
- [47] McFadden G. B. Anderson, D. M. and A. A. Wheeler. Diffuse-interface methods in fluid mechanics. *Annual Rev. in Fluid Mechanics*, 30:139–65, 1998.
- [48] G. A. Maugin. Nonlocal theories or gradient-type theories: a matter of convenience? *Archives of Mechanics (Stosowanej)*, 31(1):15–26, 1979.
- [49] J. E. Dunn and J. Serrin. On the thermomechanics of interstitial working. *Archive of Rational Mechanics and Analysis*, 88:95–133, 1985.
- [50] P. M. Mariano. Multifield theories in mechanics of solids. *Advances in Applied Mechanics*, 38:1–94, 2002.
- [51] M. Fabrizio, B. Lazzari, and R. Nibbi. Thermodynamics of non-local materials: extra fluxes and internal powers. *Continuum Mechanics and Thermodynamics*, 23:509–525, 2011.
- [52] G. Capriz. Continua with latent microstructure. *Archive for Rational Mechanics and Analysis*, 90(1):43–56, 1985.
- [53] M. G. Gurtin. Generalized Ginzburg-Landau and Cahn-Hilliard equations based on a microforce balance. *Physica D*, 92:178–192, 1996.
- [54] J. T. Cushing. The interpretation of quantum mechanics through 1935. *Annalen der Physik (Leipzig)*, 9(11-12):939–950, 2000.
- [55] T. S. Biró and P. Ván. Zeroth Law compatibility of non-additive thermodynamics. *Physical Review E*, 83:061147, 2011.
- [56] J. E. Dunn and R. L. Fosdick. Thermodynamics, stability, and boundedness of fluids of complexity 2 and fluids of second grade. *Archive of Rational Mechanics and Analysis*, 56(3):191–252, 1974.
- [57] D. D. Joseph. Instability of the rest state of fluids of arbitrary grade greater than one. *Archive of Rational Mechanics and Analysis*, 75(3):251–256, 1981.
- [58] Carl Eckart. The thermodynamics of irreversible processes, III. Relativistic theory of the simple fluid. *Physical Review*, 58:919–924, 1940.
- [59] W. A. Hiscock and L. Lindblom. Generic instabilities in first-order dissipative relativistic fluid theories. *Physical Review D*, 31(4):725–733, 1985.
- [60] P. Ván and T. S. Biró. Relativistic hydrodynamics - causality and stability. *The European Physical Journal - Special Topics*, 155:201–212, 2008.
- [61] P. Ván. Internal energy in dissipative relativistic fluids. *Journal of Mechanics of Materials and Structures*, 3(6):1161–1169, 2008.
- [62] P. Ván and T.S. Biró. First order and generic stable relativistic dissipative hydrodynamics. *Physics Letters B*, 709(1-2):106–110, 2012.
- [63] L. D. Landau and E. M. Lifshitz. *Mechanics (Course of Theoretical Physics, vol. 1)*. Pergamon Press, Oxford, 3th

- edition, 1976.
- [64] I. Gyarmati. *Non-equilibrium Thermodynamics /Field Theory and Variational Principles/*. Springer Verlag, Berlin, 1970.
- [65] B. Nyíri. On the construction of potentials and variational principles in thermodynamics and physics. *Journal of Non-Equilibrium Thermodynamics*, 16:39–55, 1991.
- [66] F. Márkus and K. Gambár. A variational principle in thermodynamics. *Journal of Non-Equilibrium Thermodynamics*, 16(1):27–31, 1991.
- [67] P. Ván and W. Muschik. Structure of variational principles in nonequilibrium thermodynamics. *Physical Review E*, 52(4):3584–3590, 1995.
- [68] P. Ván and B. Nyíri. Hamilton formalism and variational principle construction. *Annalen der Physik (Leipzig)*, 8:331–354, 1999.
- [69] P. Ván, A. Berezovski, and J. Engelbrecht. Internal variables and dynamic degrees of freedom. *Journal of Non-Equilibrium Thermodynamics*, 33(3):235–254, 2008.
- [70] Ván P. Weakly nonlocal non-equilibrium thermodynamics - variational principles and Second Law. In Ewald Quak and Tarmo Soomere, editors, *Applied Wave Mathematics (Selected Topics in Solids, Fluids, and Mathematical Methods)*, chapter III, pages 153–186. Springer-Verlag, Berlin-Heidelberg, 2009.
- [71] A. Berezovski, J. Engelbrecht, and T. Peets. Multiscale modeling of microstructured solids. *Mechanics Research Communications*, 37(6):531–534, 2010.
- [72] A. Berezovski, J. Engelbrecht, and G. A. Maugin. Thermoelasticity with dual internal variables. *Journal of Thermal Stresses*, 34(5-6, SI):413–430, 2011.
- [73] J. Engelbrecht and A. Berezovski. Internal structures and internal variables in solids. *Journal of Mechanics of Materials and Structures*, 7(10):983–996, 2012.
- [74] A. Berezovski and M. Berezovski. Influence of microstructure on thermoelastic wave propagation. *Acta Mechanica*, 2013. accepted.
- [75] E. Cosserat and Cosserat F. *Théorie des Corps Déformables*. Hermann and Fils, Paris, 1909.
- [76] R. D. Mindlin. Micro-structure in linear elasticity. *Archive for Rational Mechanics and Analysis*, 16:51–78, 1964.
- [77] A.C. Eringen and E.S. Suhubi. Nonlinear theory of simple micro-elastic solids I. *International Journal of Engineering Science*, 2:189–203, 1964.
- [78] A. Berezovski, J. Engelbrecht, and G. A. Maugin. Generalized thermomechanics with dual internal variables. *Archive of Applied Mechanics*, 81(2):229–240, 2011.
- [79] P. Ván, C. Papenfuss, and A. Berezovski. Thermodynamic foundations of generalized mechanics. 2013. arXiv:1304.4977.
- [80] P. Ván. Generic stability in dissipative generalized mechanics. 2013. ArXiv:1212.6892v1 (physics.class-ph).
- [81] J. Verhás. Non-equilibrium thermodynamics and the dynamics of particles. In O. Gues G. Iooss and A. Nouri, editors, *Trends in Applications of Mathematics to Mechanics*, pages 138–146, Boca Raton-London-New York-Washington, D. C., 2000. Chapman and Hall/CRC.
- [82] Verhás J. Onsager’s reciprocal relations and some basic laws. *Journal of Computational and Applied Mechanics*, 5(1):157163, 2004.
- [83] I. Müller. On the frame dependence of stress and heat flux. *Archive of Rational Mechanics and Analysis*, 45:241–250, 1972.
- [84] T. Ruggeri. Can constitutive equations be represented by non-local equations. *Quarterly of Applied Mathematics*, LXX(3):597–611, 2012.
- [85] D. M. Carberry, J. C. Reid, G.M. Wang, E. M. Sevick, D.J. Searles, and D.J. Evans. Fluctuations and irreversibility: An experimental demonstration of a second-law-like theorem using a colloidal particle held in an optical trap. *Physical Review Letters*, 92(14):14601, 2004.
- [86] See a collection of news reports about a violation (?) of the second law here: <http://rsc.anu.edu.au/evans/papers/selectnewsreportsFT.pdf>

PANEL I

**CONNECTING SECOND LAW ANALYSIS WITH
ECONOMICS, ECOLOGY, FLUID MECHANICS,
AND MORE**

RELEVANCE OF THE DEAD STATE TO ECOLOGICAL AND ECONOMIC ANALYSES

Richard A. Gaggioli

Department of Mechanical Engineering
Marquette University
Milwaukee, WI 53201-1881 USA
Richard.Gaggioli@mu.edu

ABSTRACT

Traditionally, an exergy analysis has from the outset inherently *assumed* a ‘reference state’ and exergies of subsystems have been evaluated relative thereto. Moreover, the evaluations *assume* a limited class of processes (for example, thermal, mechanical and chemical) for bringing the subsystems to equilibrium with the ‘reference’. These habitual practices have limitations, especially important in applications to ecology and thermoeconomics. The limitations, which may be misleading, can by and large be avoided by referring back to the more fundamental concept underlying exergy, namely Gibbs’ *available energy of a body*, and the consequent *dead state* of the body. At any instant, given any *body* – any overall system – the overall dead state and the dead states of all subsystems and their materials is unique. The dead state may change with time, while the overall available energy decreases. At every instant the exergy of each subsystem can be defined and represents its contribution to the overall available energy. The preceding paragraph began with “. . . *given* any overall system . . . the overall dead state . . . is unique.” That statement is subject to several, related stipulations:

- The class of processes within each subsystem must be specified (i.e. *assumed*).
- The modes of interaction between subsystems must be specified.
- The constraints upon subsystems must be specified.

That is, defining the dead state of an overall system (making it ‘given’) requires not only identification of its parts, but also how they will be allowed to interact and what constraints are imposed upon the parts and the interactions.

The purpose of this presentation is

- to provide guidance for the selection of the dead state for exergy analysis, and to elucidate
 - the relevance of *assumptions* made at the outset of the analysis, and
 - their implications upon conclusions drawn from the analysis.

Every exergy and thermoeconomic analysis that has been (or will be) done makes assumptions, implicitly if not explicitly, that can make the conclusions misleading. It is of critical importance for the reader of any exergy analysis to realize the significance of the inherent assumptions upon the conclusions, especially when the analysis has implications upon ecology and sustainability.

INTRODUCTION

This paper has two principal parts: Fundamentals, and Practical Applications.

Fundamentals. Following Gibbs [1,2] the ‘available energy of a body’ is defined for any ‘body’ – i.e., for any overall system, no matter how *complex* the system’s structure. The structure generally includes several subsystems or processes *and* how they interact. While a subsystem *may* be an ‘environment’, an environment is not necessary. Given the structure, the ‘dead state’ of the system follows directly from this general definition of available energy. Moreover, the dead state of the overall system dictates the dead state of each subsystem. The overall dead state and hence the dead states of the subsystems can change with time.

In practice, the overall dead state and hence the subsystem dead states depend upon underlying *choices*. Above all, the practitioner must delineate the makeup of the overall system. That is, given the purpose of the analysis, choose the parts of the ‘universe’ to be included in the overall system (as subsystems). Moreover, it is essential to choose ‘constraints’ placed upon (i) spontaneous processes allowed within each subsystem, (ii) modes of interaction¹ between subsystems,

(iii) modes whereby products are delivered from the overall system (to its ‘market’).

It is apparent that the available energy of a body – of an overall system – is a consequence of disequilibrium within the body. Conversely, were a body subjected to specified ‘constraints’ it would be at equilibrium if the available energy were zero. So, when a body is subjected to particular constraints, available energy can be used to define equilibrium, relative to those constraints.

Applications. Exergy is an additive property. The exergy of a subsystem represents its contribution to the available energy of the overall system. Exergy is definable whether or not any subsystem is an ‘environment.’

Yet, in many if not most engineering applications of ‘exergy analysis’ to a conversion plant – for efficiency analysis and/or costing – an important subsystem is a local environment with which it interacts.¹ The dead state of each plant subsystem and its contents depends upon the assumed constraints applied to it and to the environment. The delineation (‘choice’) of constraints can have a significant effect upon the conclusions drawn from the analysis.

Among the factors that are relevant to the delineation of constraints (and hence to the outcome of an analysis) are:

- The projected time-period for which the analysis will be relevant

¹ Interaction is synonymous with ‘exchange of additive property.’

- The scope of the environment
 - Its breadth
 - The accessibility of materials therein
 - The stability of the materials
 - Relevance of variations with time
- The scope of technology – i.e., its ‘state of the art’ for the projected time period
- The scope of science – i.e., its ‘state of development’ for the period

These delineations (relevant to engineering applications) are all the more important when exergy and ‘dead state’ considerations are applied to ecology and sustainability.

Closure. The fundamentals will be presented and illustrated in the context of simple examples. Nevertheless, these examples will be used to draw broad, general principles relevant to complex practical applications.

GIBBS AVAILABLE ENERGY

In [1] Gibbs defines the *available energy*, for two cases.

(a) **Case 1**, the more general case, is for that of a ‘body’ – any closed system which, *overall*, may have parts (subsystems). Shown in Figure 1 is a very simple example of an overall system. In this special case the overall system, the *subject*, consists of two subsystems, 1 and 2. The subsystems are separated by an impermeable movable piston. At any instant t the system has values of energy, entropy and of volume. Using different symbols than Gibbs, here they are denoted by $E(t), S(t), V(t)$.²

- Subject to the ‘constraints’ that (a) energy transfers from the overall system are restricted to transfers via volume or entropy exchange, but (b) that there be no *net* transfers of volume or entropy, then
- The available energy $A(t)$ of the overall system at t , a characteristic of this system only, is the maximum amount of energy attainable from this system. That is,
 - attainable from the *subject*, and deliverable to any other system – to any *object*,
 - with no *net* transfer of either entropy or volume to external systems.
 - During the hypothetical delivery, entropy and volume can be exchanged between the subject’s parts.
 - Furthermore, except for the object, external devices may be employed to deliver the energy from the subject to the object, while transferring entropy and/or volume between subsystems of the subject.
 - Moreover, in order to assure that no external devices makes a net contribution to the energy delivered from subject to object, their net change of energy must be zero.

Reference [3] presents some elaboration on processes for delivering the available energy, $A(t)$. It is shown that

- The energy delivered is a maximum, $A(t)$, when there is no entropy generation within the subject.
- $A(t) = E(t) - E_{min}(S, V)$ when $S = S(t)$ and $V = V(t)$
 - The function $E_{min}(S, V)$ represents the energy at ‘thermodynamic equilibrium’, when $\{S, V\}$ are the constrained variables.

- It represents what Gibbs called ‘the surface of dissipated energy’.
- The ‘thermodynamic property relations’ follow from it.

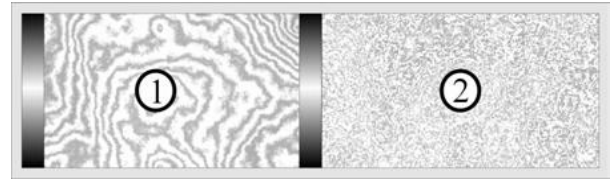


Figure 1. Example of an overall system or ‘subject’

On Figure 2, from Gibbs [1], the curve through MBCN represents a hypothetical $E_{min}(S, V)$, at a fixed V . The location A represents an arbitrary nonequilibrium state of the system, and the distance AB is the available energy A of that state. Figure 3 (from Gaggioli et al, [5]) shows a complete $E_{min}(S, V)$ surface and the points A and B. It is notable that Point A with its unique values of E, S and V – does not represent a unique state of the overall system. For example, consider Figure 1 again; at any fixed (S, V) there are many conceivable states of the ‘subject’ with the same energy E .³

The Dead State. When the overall system is at Point B, it is at a ‘dead state’ – a state of zero available energy. Whenever the overall system is at a condition vertically above B, Point B is the corresponding dead state.

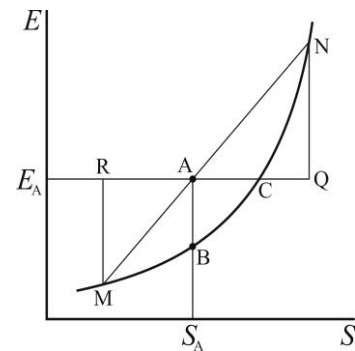


Figure 2. Depiction of E_{min} vs. S at fixed V , of available energy (AB), and capacity for entropy (AC).

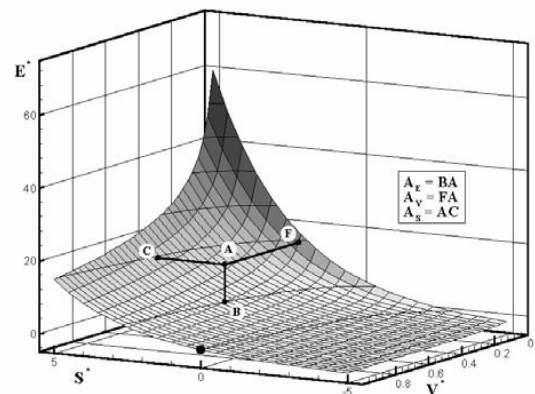


Figure 3. Depiction of $E_{min}(S, V)$, of available energy (AB), of ‘available vacuum’ (AF), and ‘capacity for entropy’ (AC).

³ States with the same E could differ as a result, for example, from disparities in the pressure and temperature differences between the subsystems. (Notably, Gibbs also defined ‘capacity for entropy’ and ‘available vacuum’ as alternative measures of disequilibrium.)

² The existence of entropy is taken for granted here. See Appendix I of Reference [3] for an elaboration, as well as [4].

Gibbs called $E_{min}(S, V)$ “the surface of dissipated energy”. If an overall system like that in Fig. 1 were allowed to reach equilibrium without delivering energy (say by letting entropy flow through the piston and letting it oscillate, uncontrolled), entropy would be produced. The system would end up at Point C, another dead state.

Additional Measures of Potential Influence. The available energy represents the system’s intrinsic potential to influence any other system. Gibbs defined other equivalent measures of disequilibrium and potential to influence. The distance AC on either figure represents the system’s ‘capacity for entropy’ – at least that amount of entropy could be extracted from any system (at $T > 0$), no matter how cold. The distance AF on Figure 3 is Gibbs ‘available vacuum’ which is the volume increase impossible upon any system no matter how low its pressure.

These three characteristics (represented by AB, AC and AF) are measures of a system’s disequilibrium and potential to influence *any* object; they are attributes of the system alone. Gibbs also described the potential influence upon specific objects. For example consider a large object, at any temperature T represented by the slope of the straight line MAN on Figure 2. The distance QA on the figure is the amount of entropy that could be extracted from the object; starting at A the system would end up at N. The distance AR is the amount of entropy that could be imposed upon the object.

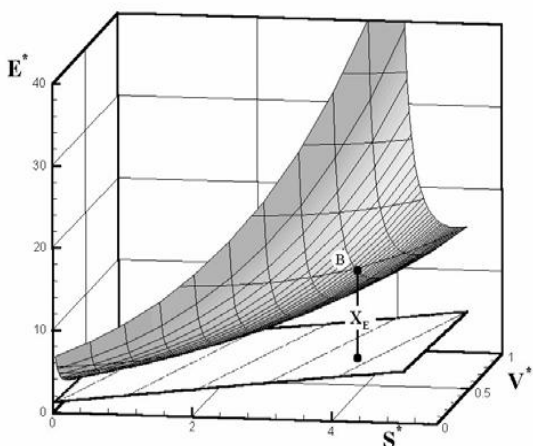


Figure 4. Depiction of the available energy of a body-and-medium (exergy of a body).

(b) Case 2. This is the *special case* presented by Gibbs, for a circumstance where one part of the *overall system* is a ‘medium’ – a large subsystem which has a constant temperature and a constant pressure and, by itself, is at equilibrium. In Gibbs’ terminology the *overall system* consists of a ‘body’ (*any body*) and the ‘medium’ (made up of the same components as the body). In both cases, 1 and 2, his development is for circumstances where the *overall system* – the *subject* – reaches equilibrium without *net* transports of entropy or volume between the *overall system* and *its* surroundings. In Case 2, net transports between the body and the medium (subsystems) are allowed; the body and medium together represent the *subject*. Its available energy – energy transmittable to any *object* – is what we call, today, the exergy of the ‘body’. Figure 4 (from Gaggioli et al, [5]) shows two surfaces, the curved surface of Figure 2 for the ‘body’ *alone*, and a planar surface. The plane is tangent to the curved surface at the location where the body and the medium have the same temperature and pressure – namely the constant T and p of the medium. If the body is at internal equilibrium at B (of Figures 3 and 4), the vertical distance from B to the planar surface represents the available energy of the composite subject of body and medium together. If the body is at A, the available energy from the composite subject equals that vertical distance plus AB.

At the dead state of the overall, subject system (body and medium) the body will be at the location where its T and p are equal to that of the medium – where the body’s surface is tangent to that of the medium.

Gibbs Available Energy with Variable Composition. Subsequently, in “On the Equilibrium of Heterogeneous Substances,” [2], Gibbs presented – implicitly – the available energy of a body and medium for the case of open systems, where exchanges with a ‘medium’ include not only entropy and volume but also chemical *components*.⁴

GENERALIZED AVAILABLE ENERGY

In the foregoing review of Gibbs 1873 development of available energy, leading to $A = E - E_{min}(S, V)$, the entropy and volume were ‘constrained’. That is, the hypothetical process that delivers available energy is carried out with limitations: no *net* transport of volume or entropy to or from the surroundings of the overall system. Such limitations will, herein, be called *constraints*. This word will be used not only for limitations upon *transports* but also for restrictions on *spontaneous changes* (such as changes of composition by chemical reactions).

Constraints. To illustrate the concept of constraints, consider Figure 1 again. Suppose the piston to be fixed in place (or replaced by an immovable wall). This additional constraint upon the overall system could be represented by the symbol V_1 (for the volume of I). When V_1 is constrained, interchanges of volume between the two subsystems would be precluded, and full advantage of pressure difference between the two could not be taken. In general the available energy from the composite of I and 2 would be less. Because, the minimum energy reachable would in general be greater than that reachable if the constraint on V_1 were removed: $E_{min}(S, V, V_1) > E_{min}(S, V)$, and so $A(E, S, V, V_1) = E - E_{min}(S, V, V_1) < A(E, S, V) = E - E_{min}(S, V)$.⁵

This example illustrates that the imposition of additional constraints changes the amount of available energy, and it changes the dead state. While adding constraints may *seem* to be ‘strictly theoretical’ and even questionable, later in this paper it will be illustrated that it has important consequences in practice. There are relevant effects on delivery of available energy, on subsystem dead states, on calculated exergy values, and on costing.

Moreover, it is important to recognize that available energy is *defined*:

- For an overall system, consisting of specific relevant subsystems (and one *may be* a large ‘medium’),
- Subject to constraints, which may restrict
 - how subsystems can interact, and
 - spontaneous changes within a subsystem, and
 - modes of interaction between the subject system and external devices.

⁴ The word ‘component’ is to be understood as distinct from ‘constituent’. Constituents are species actually present; components are species from which the constituents could be composed (e.g., see Hatsopoulos and Keenan [11]). In the case at hand, components are constituents of the ‘medium’ from which the constituents of the ‘body’ could be composed.

⁵ In theory, the $>$ and the $<$ shown should be \geq and \leq because there are special, though rare circumstances when, upon taking advantage of temperature difference between I and 2, upon reducing that difference to zero, the pressure difference would also happen to become zero. The $E_{min}(S, V, V_1)$ surface would be tangent to $E_{min}(S, V)$. Otherwise $E_{min}(S, V, V_1)$ will be above $E_{min}(S, V)$.

See Gaggioli and Paulus [5] for further elaboration on generalization of Gibbs available energy, including the relevance of constraints to equilibrium.

Exergy. Available energy is not an additive property, which is readily illustrated by considering Figure 1. Suppose that Subsystem 1, alone is at equilibrium; likewise for Subsystem 2. Then each, alone, has zero available energy. Whereas, when the two are not in equilibrium with each other, the composite of the two (the overall system) has available energy.⁶

For *any* overall system the author [7] has derived ‘subsystem exergy’ such that (i) exergy is additive, (ii) the sum of the subsystem exergies is equal to the available energy of the overall system, (iii) hence each subsystem’s exergy can be viewed as its contribution to the overall available energy, and (iv) because it is additive, an ‘exergy balance’ can be written for any subsystem, so that ‘exergy analysis’ can be carried out.

Unlike the usual, ‘textbook’ derivations for exergy equations, which depend upon having a ‘reference environment’, the derivation in [7] is for any overall system. No reference environment is required. In the derivation, the dead state of the overall system becomes relevant, in lieu of a reference environment. The dead state of each subsystem is dictated by the dead state of the overall system. Incidentally, these dead states can change with time, when E_{min} increases because of dissipations.

For the case when subsystems are free to exchange entropy S , volume V , and chemical components N_i , the expression for exergy *content* of a subsystem is:

$$X = E + p_f V - T_f S - \sum \mu_{if} N_i \quad (1)$$

The subscript f denotes the pressure, temperature and component chemical potential at the dead state. The expressions for exergy *transports* and *destruction* follow directly from this expression for *content*.

When one of the subsystems is a ‘medium’, large and at equilibrium (or constrained equilibrium), it has zero exergy. And the medium dictates the dead state of all the subsystems.

In the foregoing expression for exergy, the f ’s become the usual 0’s. However, as argued later, there are many practical instances where it is erroneous (if not presumptuous) to assume an *equilibrium* environment (or a finite, non-equilibrium environment with a quasi-stable equilibrium ‘dead state’).

Understanding (a) the meaning of ‘dead state’ in general (including in the absence of an ‘environment’), and (b) the relevance of constraints upon the dead state is important. Otherwise, in practice, the choices made to determine the overall dead state can be questionable if not erroneous (even when one subsystem is an ‘environment’).

(The author’s 1999 derivation of exergy [7] is a simplification of one made by Wepfer [6], where there is an error in line 2 of Eq. (14); the subscripts shown as B should be A.)

PRACTICAL EXAMPLES

Subsystem Dead States for Engineering Exergy Analysis of Conversion Systems and Plants.

What is meant here by *Engineering Exergy Analysis* is this: analysis of an existing, operating plant (or system), or analysis of a plant that is being designed. The intent is that all of the subsystems should consist of technologies that are

⁶ Figure 4 illustrates another example: B represents an equilibrium state of the ‘body’ and all points on the planar surface are equilibrium states of the ‘medium’; X_B represents the available energy of the overall system – the exergy attributed to the ‘body’.

currently available. (Comments relevant to R&D and resource assessment are presented later in this paper.)

Before a plant (or system) is analyzed it is important to ascertain (or make reasonable assumptions) regarding the dead state of the materials in every subsystem.

Given a plant and its surroundings, (a) the *first step* in determining appropriate subsystem dead states is to *establish* the *relevant* “composite system” (overall system, consisting of subsystems). That is, what parts of the ‘universe’ have *significant effect* on the performance of the plant or system.

- *Relevant*: considering the purpose of the analysis.
- *Significant effect*: having an effect that influences the outcome of the analysis within the desired *significant* figures.

The *2nd step*: (b) the practical, technological constraints on (i) the interactions between subsystems and on (ii) the spontaneous processes within each subsystem need to be specified.

These principles – (a) and (b) – are illustrated with several cases, by Wepfer and Gaggioli [6]. That article includes a section on “The selection of reference datums [dead states] for subsystem [exergy].” Rather than duplicate that section, see [6] and also [3].

Relevance to Analyses for R&D and for Resource and Sustainability Assessment.

This section will be devoted to the importance of the constraint concept, and to the significance of choosing a relevant dead state.

Significance of Constraints. Again, consider a simple example, referred to earlier. Suppose that the system in Figure 1 is at a condition like A in Figure 2, and consider a *real* process that is striving to deliver the available energy represented by AB. Invariably there would be entropy production, due to ‘mechanical friction’ and to heat transfer through temperature differences. As a result the system would end up at a condition to the right of B on the curve, toward C; the more the entropy production the closer to C (but never above C, which is the condition reached if the system is allowed, uncontrolled, to equilibrate internally, so no energy is delivered). Let us suppose that, with more or less well-controlled, but real equilibration the final condition reached was at α , on Figure 5 (For convenience of the artwork the ordinate (for E) is not linear; α appears closer to C than if it were linear; i.e. the energy delivered ($E_A - E_\alpha$) is supposed to be significantly greater than the dissipation of available energy ($E_\alpha - E_B$)). Moreover suppose that the entropy production was predominantly caused by mechanical, viscous friction.

Now, consider the following alternative scheme, starting at A, for delivering available energy: If the piston were fixed in place (constraining V_1), and available energy was delivered with very little entropy production due to heat transfer, that delivery process would end up at a place like β , below and slightly to the right of A. Next, deliver more available energy by letting V_1 change by a modest amount (to V_1'), with some but less viscous friction (because of the controlling of V_1 ’s change). By repeating, once more, this procedure of fixing and then changing V_1 , the path to equilibrium would be like that from A to γ on Figure 5.

able energy. (Relatedly, there may exist available energy that is more or less ‘hidden’, within the context of today’s science – like nuclear disequilibrium was hidden 100 years ago).

- If a medium is accessible with a lower temperature and/or with a lower pressure, and/or lower chemical potentials (or lower potentials associated with any new controlling constraint), the delivery can be increased.

CLOSURE

Traditionally, the development of exergy has assumed the existence of a ‘surrounding environment’. Necessarily then, in practice exergies are evaluated relative to a reference environment, which must be selected by the evaluator. Several alternative ‘standard’ reference environments have been proposed by various authors, and commonly the evaluator will choose one of them. In any case, the ‘dead state’ of zero exergy is dictated by the selected ‘standard’ environment. That is, by equilibrium with that environment. And it is commonly held that, in theory at least, the dead state should be the same for all of the contents of, and the flow streams between, the subsystems of the facility being analyzed.

These habitual practices have shortcomings. By and large the shortcomings can be circumvented by referring back to the more fundamental concept underlying exergy, namely available energy.

As described above, *if* an overall system is *given*, then (at any moment) the overall dead state and the dead states of all subsystem and their materials is unique. No reference environment is necessary. If, as usual, one of the subsystems is a large surrounding medium, in a sense it is ‘just one more subsystem’. Nevertheless, it may have a dominant (if not total) effect upon the dead state of the other subsystems. However, those subsystem dead states will not necessarily all be in *complete* equilibrium with the surrounding medium. Generally, subsystems will be in constrained equilibrium with the surroundings (For example, the dead state the refrigerant in a vapor-compression system will be in thermal equilibrium with the system’s surroundings, but not in pressure or chemical equilibrium; [6,3])¹⁰

The preceding paragraph began with “. . . *if* an overall system is *given* . . . the overall dead state . . . is unique.” That statement is subject to several, related stipulations:

- The modes of interaction between subsystems must be specified.
- The constraints on subsystems must be specified.

That is, defining an overall system (making it ‘given’) requires not only identification of its parts, but also how they will be allowed to interact and what constraints are imposed upon the parts and the interactions.

Defining an Overall System. It is imperative that whenever the results of an exergy analysis or exergy evaluation of resources is presented, it should be clear to the reader what the underlying “overall system” is – its make-up and the assumed interactions and constraints. Ideally, this requirement

should be fulfilled by the author(s). If they have not been fulfilled explicitly, a careful reader will seek to determine what overall system has been *assumed*. If an answer cannot be found or assumed judiciously, the reader should question (if not be skeptical, or even dismiss) the conclusions that have been drawn.

Engineering Systems. In the case of exergy analyses of engineering systems, it is generally straightforward for the reader to ascertain the overall system, as long as a reference environment has been clearly stated. The reader will naturally assume that the subsystems shown on the flowsheet, are ‘standard’ – current technology. If some are not standard the authors hopefully will have made that known.

Resource and Ecologic Assessment. Many laudable applications of exergy to ecology and sustainability have been carried out. These studies refer to the future and often project into the future – and make predictions (often dire) about the future, and then make recommendations. Care needs to be exercised when considering some of the conclusions drawn (especially when the conclusions and recommendations are presented ardently).

It seems that there generally are assumptions that go unrecognized or are taken for granted by both authors and readers. So the following kinds of questions arise:

- What is the overall system? Generally, it is evident that the overall system has been limited to the earth (or earth-sun) and its resources. Is that a reasonable limitation when predicting the future?
 - Are there resources outside our ‘sphere’ that will become accessible? Literal ‘energy resources’? Or subsystems that could be invoked?
 - E.g., in some remote places, the night sky is used as a source of exergy today. The background temperature of the universe is about 3K; could it be used as a ‘medium’? Consider the two straight lines on Figure 5.
 - ‘What’s the point of all this’? Only that the reader of the assessments should realize that the *assumed* scope of the overall system has a very big effect on the results and conclusions.
- Again, ‘What is the overall system?’ For available energy and exergy to be meaningful, there must be a *complete* overall system; that is, besides the resources there must be means for harvesting and converting them that are assumed.
 - What technologies have been assumed for the harvesting and converting? Presumably today’s technologies, with their ‘control constraints’? (Or improved equipment but with the same constraints.)
 - If so, that dismisses prospective, relevant developments in science and technology.
 - Scientific advances can lead not only to new technologies but also to new resources (like fission and fusion have ‘made’ new resources).
- What *are* the ‘controlling constraints’?
 - Is it implicit that the control variables are classical? Electrical, mechanical, chemical and perhaps nuclear? – such that the perceived resource conversion is subject to the laws of ‘classical’ science (e.g. today’s chemical thermodynamics, with its assumed variables – its thermostatic properties).
 - Again, the reader of assessments should realize that there is an implicit science and technology being assumed. (Future developments likely will introduce

¹⁰ Some might think that it doesn’t matter what the dead state is, because when one calculates exergy differences between points in a cycle, the dead state values cancel. That thinking is flawed; it is important to know the correct, total values at every point. Otherwise significant mistakes can occur in evaluating subsystem efficiencies and especially unit costs [6].

unforeseen variables, which could be employed to control/constrain phenomena relevant to resource conversion.)

Viewpoints. All ‘energy resources’ (for *example* hydrocarbons) have usefulness because there exists an associated disequi-librium with our environment. It is typical of resources (like the hydrocarbons) that the disequilibrium is ‘constrained’ such that there is a metastable equilibrium. Their usefulness depends upon ‘breaking’ – overcoming – the metastable equilibrium. The better the control of the ensuing equilibration, using constraints, the more efficient the use of the resource.

Particularly regarding resources, history is filled with dreadful forecasts which have arisen in the face of *challenging* circumstances. Invariably, the forecasts have been made under the (inherently pessimistic) assumption that the then-current science and technology was definitive.

However, humankind has not only overcome the *challenges* but in dealing with them has *advanced* – has discovered ‘new’ resources, unlocked them with new science and new technologies, improved the efficiency of usage, . . . and as a consequence has *improved* our subsistence.

One could say that the advances resulted, at least in part, as consequences of the challenges. So assessments of the type referred to above should be appreciated – as challenges and as opportunities, for improvement.

There is a great amount of disequilibrium, particularly metastable equilibrium in our *universe*. Our future technology is not earthbound. Moreover, it can be hoped (and from a historical perspective, *expected*) that – spurred on by challenges – future science and technology will unlock not only remote resources but ‘hidden’ or currently ‘unreachable’ earthly resources as well. Some would say, “That’s overly optimistic.” “Careless.” “We should ‘play it safe!’” The readers will have a variety of viewpoints (worth discussing!).¹¹

In any case, let the readers of ‘assessment’ papers that refer to the future understand that there are implicit assumptions that are very important, and will prove to have been very significant – rightly or wrongly.

The Appendix outlines what I believe are reasons for optimism.

ACKNOWLEDGEMENTS

I would like to acknowledge the following ‘schools of thermo’ that I have learned from: Goodenough-Obert, Hirschfelder-Curtiss-Bird, Tribus-Evans-ElSayed, Keenan-Hatsopoulos-Gyftopoulos-Beretta. Also, study of the early history of the 2nd Law, of available energy and of entropy – particularly the contributions of Thomson (Lord Kelvin), Rankine, Gibbs and Maxwell – has been enlightening [10]. Finally, I appreciate and thank all of the students, colleagues, and contemporaries that I have learned with.

REFERENCES

- [1] Gibbs, J.W., 1873, “A Method of Geometrical Reperesentation of the Thermodynamic Properties of Substances by Means of Surfaces,” in The Scientific

Papers of J.W. Gibbs, vol. 1, Dover Publications, 1961.

- [2] Gibbs, J.W., 1875, “On the Equilibrium of Heterogeneous Substances,” in The Scientific Papers of J.W. Gibbs, vol. 1, Dover Publications, 1961.
- [3] Gaggioli, R.A., 2012, “The Dead State,” *Int. J. of Thermodynamics*, vol. 15 (No. 4), pp. 191-199.
- [4] Gaggioli, R.A., 2010, “Teaching Elementary Thermodynamics and Energy Conversion: Opinions,” *Energy*, Vol. 35, pp. 1047–1056.
- [5] Gaggioli, R.A., Richardson, D.H., Bowman, A.J., Paulus, D.M. Jr., 2002, “Available Energy: a. Gibbs Revisited, b. Gibbs Extended”, *Trans. ASME*, vol. 124, pp. 105-115).
- [6] Wepfer, W.J. and Gaggioli, R.A., 1980, “Reference Datums for Available Energy [Exergy]”, Ch. 5, pp. 78-92, *Thermodynamics: Second Law Analysis*, American Chemical Society, Symposium Series Vol. 122.
- [7] Gaggioli, R.A., 1999, “Available Energy and Exergy”, *International Journal of Thermodynamics*, Vol. 1, pp. 1-8.
- [8] Keenan, J.H., 1941, *Thermodynamics*, Wiley.
- [9] Obert, E.F., 1973, *Internal Combustion Engines*, Harper and Row.
- [10] Gaggioli, R.A., 1999, “Reflections on the History of Exergy,” pp. 5-13, *Proc. ECOS’99*, M. Ishida, ed., Tokyo Institute of Technology, Japan.
- [11] Hatsopoulos, G.N. and Keenan, J.H., 1965, *Principles of General Thermodynamics*, Wiley.

Appendix. Regarding the future

Predicting it requires *assumptions*:

- The Subject (overall system) – its ‘extent’
 - The Subsystems; i.e., Resources from the universe.
- Exergy content of subsystems
 - Depends upon the available science.
- Constraints/Controls – depend upon:
 - Available Science
 - Available Technology

Assessing predictions requires knowing:

- The assumed subject – its ‘extent’
 - The Subsystems
- The assumed future Constraints/Controls
 - The assumed future available science

Future Prospects:

The subject – determined by exploration, prospecting, discovering, and ‘mining’ of *disequilibrium*:

- Unexplored land and sea, and depths of earth
- Space – e.g., asteroids
- Solar system, . . . Universe – e.g., night sky at 2.5 K
- Reducing E_{\min} – Recuperation of generated entropy
- New ‘elements’ (subjects) – exergetic; functional
- Unexpected discoveries of resources, resulting from exploration.

Constraints/controls – exploration, prospecting, discovering, ‘mining’ of *knowledge* about:

¹¹There is an old saying, “Don’t let a crisis go by without taking advantage of the opportunity.” Pessimists miss the opportunity. It should not be assumed that to ‘play it safe’ is without ‘cost’. Entrepreneurs – including many scientists – are optimists.

- Science: Universe, megaverse, . . . Nanoverse, microverse, . . .
 - Technology, from Science, for: Controlling constraints; Unlocking and controlling metastable constraints
- Again, . . . and again, . . . because:
- There is a tremendous amount of disequilibrium
 - There is a tremendous amount of unknown science, I believe – I am sure!
-

- The resourcefulness of the ‘young at heart’ – of today and the future (near and distant) – find them: Discover, develop, . . . with exploration: physical, mental. Optimism, versus stultifying pessimism.

FUEL AND PRODUCT DEFINITIONS IN COST ACCOUNTING EVALUATIONS: IS IT A SOLVED PROBLEM?

Andrea Lazzaretto

Department of Industrial Engineering
University of Padova
Via Venezia, 1 35131 Padova – Italy
Email: andrea.lazzaretto@unipd.it

ABSTRACT

Exergoeconomic cost evaluations are based on the principle that costs are apportioned among mass and energy streams in proportion to the exergy that is carried by the Fuel and Product streams of the energy system components. The Specific Exergy Costing (SPECO) method was developed to find a general and unambiguous “process based” criterion to define the Fuel and Product of each component based on the record of all additions and removals of exergy to and from the mass and energy streams of the real energy system. This criterion in conjunction with the so called Fuel and Product Rules allows one to directly extract the exact number of auxiliary equations that are needed to evaluate costs.

Several examples have been already shown in the last years to demonstrate the reduction of ambiguities in the Fuel and Product definitions and in turn in cost calculations deriving by the use of the SPECO approach. Other more specific examples of application to components having a “double purpose” are considered in this paper to compare the SPECO approach with other approaches, and to demonstrate the more reliable costs obtained by the former also in these cases.

INTRODUCTION

Exergoeconomics is aimed at evaluating the exergy and monetary costs associated with all mass and energy streams in the energy system. The basic principle of all exergoeconomic methodologies proposed in the literature consists in apportioning the costs of the input streams according to the exergy carried by the Fuel and Product of the system components. Thus, in addition to the exergy values associated with mass and energy streams calculated by the exergy analysis, this criterion of cost allocation requires a correct formulation of Fuel and Product of each system component. On the other hand, there is an intrinsic degree of subjectivity in the Fuel and Product definitions, i.e. there is more than one definition that fulfills the component exergy balance. And additional ambiguities may derive from the definition of the component boundaries which may include more than a single device.

Some of the basic exergoeconomic papers written in the literature ([1], [2], [3], [4]) focused on the direct relationship between Fuel and Product and associated costs but did not put specific emphasis on the need of unambiguous Fuel and Product definitions, implicitly assuming that these definitions are “given” by the exergy analysis and accepting a certain degree of flexibility in their formulation depending on the role of the component in the overall system structure. Exergoeconomic functional approaches ([5], [6], [7]) gave instead a basic importance to the formulation of Fuel and Product of the system components, which were called component “functions” and specifically defined according to the role and location of the component in the system structure. These approaches require a preliminary analysis of the overall systems and its components to decide all the “productive” interactions between each component and the other system components. In [8] it was named “a logical approach” to underline that the functional interactions among system

components depend on how each component “serves” the other system components.

The Specific Exergy Costing Method (SPECO) [9] started from a basically different idea for the formulation of the components Fuel and Product, consisting in taking a record of all exergy additions and removals that are performed by each component on the mass and energy streams of the system. Exergy additions and removals were considered as parts of the Product and the Fuel, respectively. Specific exergies give the name to the method because they are to be calculated when different mass streams join within the component. The SPECO idea simply derives from observing that the productive “function” of the component is independent of the presence of the other components in the system, depending on its behavior only. Thus, the component interacts with exergy additions to and removals from the rest of the system only through the mass and energy streams crossing its boundaries. Accordingly, the formulation of each component Fuel and Product involves only exergy streams associated with these mass and energy streams. This concept implies that the exergy links of the component with the rest of the system remain the same as those of the system flowsheet (often named “physical structure”) because all the “productive” interactions between each component and the rest of the system are defined within the component boundaries. So, the “productive structure” does not alter the physical structure of the system, and it is built by analyzing each component separately without the need of a specific analysis of the total system configuration. In this first “SPECO” paper exergy and monetary costs were calculated using the Last In First Out (LIFO) criterion. In [10] the SPECO approach was extended to the calculation of average costs, and a computer code was developed to take an automatic record of all exergy and cost additions to and removals from mass and energy streams in order to avoid the need of defining in advance Fuel and Product of each component. This approach was further extended and developed and finally lead to a general criterion to formulate

Fuel and Product and the associated costs ([11], [12], [13]). In particular in [13] it was shown how to apply the general addition/removal criterion in the formulation of Fuel and Product, and general F and P rules were formulated to obtain the necessary and sufficient number of cost equations in agreement to the Fuel and Product definitions. Several examples of applications were presented to underline the general applicability of the SPECO criterion, which basically consists in

- i) calculating of the exergy differences between outlet and inlet of the component along each mass and energy stream crossing the component boundaries,
- ii) checking the sign of these differences (positive and negative differences correspond to exergy additions and removals, respectively);
- iii) including in the Product only the desired exergy additions, and leaving exergy removals and undesired exergy additions on the Fuel side.

Only in some cases in which chemical transformations are involved (e.g., in a gasification reactor in which a solid fuel is transformed into a gas) it may be meaningful to consider input exergies on the Fuel side and output exergies on the Product side.

This paper focuses on some specific components in which there might be uncertainties in the definition of Fuel and Product and in the consequent auxiliary cost equations, and tries to remove this uncertainties by comparing the results of the application of the SPECO method with a possible alternative approach under changes of the component behavior.

EXAMPLES OF APPLICATION

Heat exchangers in which both cooling and heating are desired and useful

The SPECO criterion involving exergy differences in the Fuel and Product definitions is compared to a different approach according to which the exergy at the outlet and inlet of the component are to be considered on the Product and Fuel side, respectively. The comparison is performed using two kinds of heat exchangers having separated or mixed streams, respectively. In both kinds of heat exchangers the cooling on the hot side and heating on the cold side are useful and desired to improve the exergy efficiency of the overall system in which the heat exchangers are included.

The criterion to used here to "evaluate" the F and P definitions and associated costs consists in checking the variation of the exergy efficiency and the cost of product of the component under a change of its behavior.

Separate streams

This first example refers to a heat exchanger in which the hot stream to be cooled and the cold stream to be heated are separate. Both cooling of the hot stream and heating of the cold stream are desired and useful to improve the exergy efficiency of the total system. A practical application is the intercooler in a multi-stage compressor (see Fig.1 [1]) in which the decrease of the exergy at hot side reduces the compression work whereas the increase of the exergy on the cold side is used to increase the temperature of the hot reservoirs, the heat of which is then supplied to a reheated

expansion (not appearing in the figure). The heat exchanger flowsheet is shown in Fig.2.

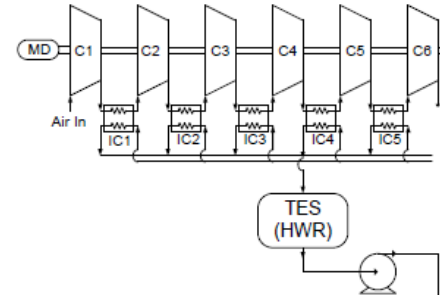


Figure 1: Multi-stage compression with heat recovery from intercooling (see, [14])

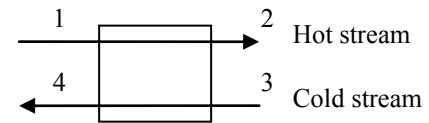


Fig.2. Heat exchanger with separate streams

According to the SPECO method the addition of exergy to the cold stream is desired and therefore it makes up the product, whereas the Fuel is equal to the exergy needed to generate the Product, i.e to the removal of exergy from the hot stream

$$\dot{E}_P = \dot{E}_4 - \dot{E}_3 \quad \dot{E}_F = \dot{E}_1 - \dot{E}_2 \quad (\text{SPECO}) \quad (1)$$

Instead, considering the heat exchanger as having the "double purpose" (named in the following DP) of heating the output stream 4 and cooling the output stream 2 leads to the following definition of Product and to the consequent (according to exergy balance) definition of Fuel (see, e.g., [14])

$$\dot{E}_P = \dot{E}_2 + \dot{E}_4 \quad \dot{E}_F = \dot{E}_1 + \dot{E}_3 \quad (\text{DP}) \quad (2)$$

Thus, using the SPECO approach (Equations (1)), the exergy efficiency of the heat exchanger is

$$\varepsilon = \frac{\dot{E}_P}{\dot{E}_F} = \frac{\dot{m}_{cold}(e_4 - e_3)}{\dot{m}_{hot}(e_1 - e_2)} \quad (\text{SPECO}) \quad (3)$$

where e indicates a specific exergy (kJ/kg) and \dot{m} a mass flow rate, whereas using the DP approach (Equations (2))

$$\varepsilon = \frac{\dot{E}_P}{\dot{E}_F} = \frac{\dot{E}_2 + \dot{E}_4}{\dot{E}_1 + \dot{E}_3} \quad (\text{DP}) \quad (4)$$

The cost balance of the component indicates that the sum of all cost flow rates at the inlet is equal to the sum of all cost flow rates at the outlet

$$c_1 \dot{E}_1 + c_3 \dot{E}_3 = c_2 \dot{E}_2 + c_4 \dot{E}_4 + \dot{Z} \quad (5)$$

where c represent specific costs (\$/kJ), \dot{E} are exergy flow rates (kJ/s) and \dot{Z} (\$/s) amortization cost flow rates. The latter are neglected here for simplicity. Specific costs c_1 and c_3 are assumed to be known and equal to 1 (kJ/kJ). The cost balance is not sufficient to calculate the two unknown costs c_2 and c_4 of the outlet streams. The F rule of the SPECO method states that the average specific cost at which the exergy is removed in the component is equal to the average specific cost at which the same exergy was supplied in the upstream components. This rule applied to the Fuel defined according to the SPECO criterion (Eq. 1) supplies the auxiliary equation

$$c_1 = c_2 \quad (\text{SPECO}) \quad (6)$$

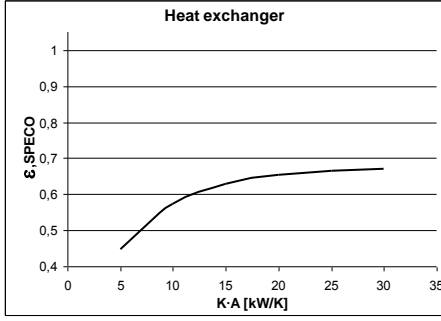


Figure 3: SPECO exergetic efficiency of the heat exchanger in Fig.2.

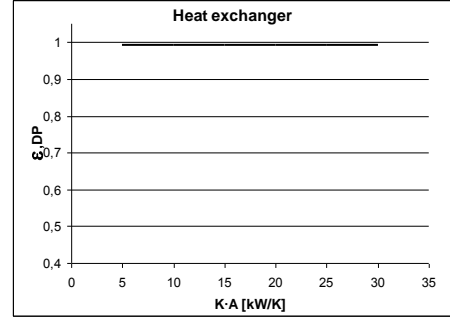


Figure 4: DP exergetic efficiency of the heat exchanger in Fig.2.

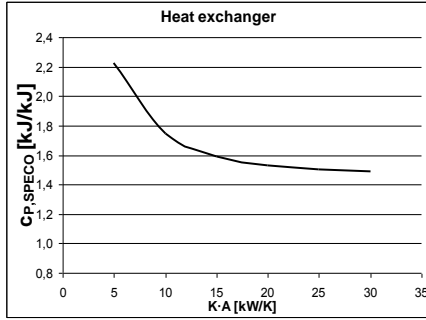


Figure 5: SPECO cost of product of the heat exchanger in Fig.2.

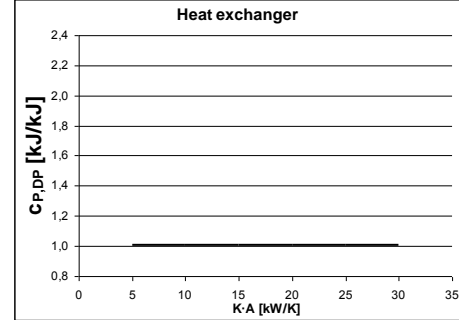


Figure 6: DP cost of product of the heat exchanger in Fig.2.

Instead, the DP exergy efficiency imposes the P rule to be used, which states that the component products (\dot{E}_2 and \dot{E}_4) are generated at the same unit costs, i.e.

$$c_2 = c_4 \quad (\text{DP}) \quad (7)$$

According to the Product definitions given in Eqs. (1) and (2) the costs per unit of exergy of the products (c_P) are

$$c_P = \frac{c_4 \dot{E}_4 - c_3 \dot{E}_3}{\dot{E}_4 - \dot{E}_3} \quad (\text{SPECO}) \quad (8)$$

$$c_P = c_2 \quad (\text{DP})$$

The heat exchanger behavior was simulated by considering air on the hot side and water on the cold side. Mass flow rates, temperatures and pressures at the inlet were assumed to be fixed input data ($\dot{m}_1=10$ kg/s, $\dot{m}_2=1$ kg/s, $T_1 = T_3 = 298.15$ K, $p_1 = 10$ bar, $p_2 = 1$ bar). To consider a wide spectrum of operating conditions, the heat transfer coefficient KA (kW/K) was varied from 0.1 to 40 kW/K. The variation of ε and c_P versus KA are shown in Figs. 3-4, and Figs. 5-6, respectively.

As expected, if the SPECO approach is used, the exergetic efficiency increases and the cost of Product decreases when improving the behavior of the heat exchanger (i.e., for higher KA values). This is because the increase of exergy is assigned to the Product side, whereas the decrease of exergy to the Fuel side (Eq.7), and the latter occurs at constant cost per unit of exergy (see Eq. 8). Instead, using the DP approach the component behavior does not affect neither the exergetic efficiency nor the cost per unit of exergy of the Product, which remain constant. Thus, the DP definitions of Fuel and Product and the resulting exergetic efficiency and unit cost of product do not “detect” the improved behavior of the component deriving from higher KA values, although they are consistent with the exergetic balance of the component. This is because the “desired products” (\dot{E}_2 and \dot{E}_4) formulated by the DP approach are independent of the actual behavior of the component, which shows an exergy consumption on the hot

side ($\dot{E}_1 - \dot{E}_2$) that is used to increase the exergy on the cold side ($\dot{E}_4 - \dot{E}_3$), as the SPECO approach simply records. In fact, when KA increases, T_2 decreases and T_4 increases and \dot{E}_2 and \dot{E}_4 show a similar trend, being \dot{E}_1 and \dot{E}_3 fixed at constant values by hypothesis. The two effects compensate so that the DP exergetic efficiency and cost per exergy unit of the product remain approximately constant.

Mixed streams

This second example consider the mixer of the two stage vapor-compression system in Fig. 7. Working fluid is ammonia (NH_3), cooling fluid in the condenser is water, heating fluid in the evaporator is a water-ethylene glycole mixture (50/50 %weight).

In the mixer the energy rejected during de-superheating and condensation of the refrigerant in the low temperature cycle is used to evaporate the refrigerant of the higher temperature cycle. Thus, as in the heat exchanger of the previous example, both cooling of the hot stream and heating of the cold stream are desired and useful (the mixer operates both as condenser and evaporator). The stream 6-3 gains exergy due to the condensation below the reference temperature, whereas the stream 2-7 loses exergy due to the evaporation below the reference temperature.

Accordingly, using the SPECO approach the exergy difference ($\dot{m}_3(e_3 - e_6)$) is positive (addition) and desired, and becomes part of the Product, whereas the exergy difference ($\dot{m}_2(e_2 - e_7)$) is negative (removal) and becomes part of the Fuel, i.e

$$\dot{E}_P = \dot{E}_3 - \dot{E}_6 \quad \dot{E}_F = \dot{E}_2 - \dot{E}_7 \quad (\text{SPECO}) \quad (9)$$

Instead, using the DP approach, the output and input exergy streams are on the Product and Fuel sides, respectively

$$\dot{E}_P = \dot{E}_7 + \dot{E}_3 \quad \dot{E}_F = \dot{E}_6 + \dot{E}_2 \quad (\text{DP}) \quad (10)$$

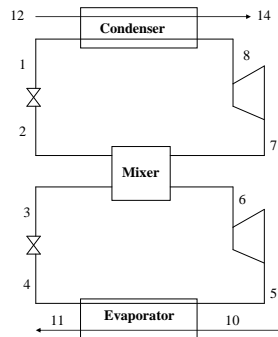


Figure 7: Two stage vapor-compression system

Thus, the exergy efficiencies of the mixer are

$$\varepsilon = \frac{\dot{E}_P}{\dot{E}_F} = \frac{\dot{m}_6(e_3 - e_6)}{\dot{m}_2(e_2 - e_7)} \quad (\text{SPECO}) \quad (11)$$

$$\varepsilon = \frac{\dot{E}_P}{\dot{E}_F} = \frac{\dot{E}_7 + \dot{E}_3}{\dot{E}_6 + \dot{E}_2} \quad (\text{DP}) \quad (12)$$

The cost balance of the mixer is

$$c_2\dot{E}_2 + c_6\dot{E}_6 = c_7\dot{E}_7 + c_3\dot{E}_3 + \dot{Z} \quad (12)$$

Amortization cost flow rates (\dot{Z}) are neglected here for simplicity as in the previous example. Specific costs c_2 and c_6 are known as they are calculated in the upstream components by the overall system model.

The F rule of the SPECO method applied to the exergy removal $\dot{m}_2(e_2 - e_7)$ (i.e to \dot{E}_F , see Eq.(9)) supplies the auxiliary equation

$$c_2 = c_7 \quad (\text{SPECO}) \quad (13)$$

Using the DP approach the auxiliary equation is obtained by the P rule applied to the two terms of the component Product (\dot{E}_7 and \dot{E}_3)

$$c_3 = c_7 \quad (\text{DP}) \quad (14)$$

According to the Product definitions in Eqs. (9) and (10) the costs per unit of exergy of the Products are

$$c_P = \frac{c_3\dot{E}_3 - c_6\dot{E}_6}{\dot{E}_3 - \dot{E}_6} \quad (\text{SPECO}) \quad (15)$$

$$c_P = \frac{c_3\dot{E}_3 + c_7\dot{E}_7}{\dot{E}_3 + \dot{E}_7} = c_3 \quad (\text{DP})$$

The behavior of the mixer was simulated considering different values of the mixer pressure for two different temperatures of the water-ethylene glycole mixture at the inlet of the evaporator ($T_{10} = -15^\circ\text{C}$, -30°C) and a fixed value of the heat transfer rate at the evaporator (10 kW). The water temperature at the inlet of the condenser was fixed at 25°C .

Results of the simulation are shown in Figures 9 to 12. The increase in the SPECO exergetic efficiency at increasing values of the mixer pressure (Fig. 9) is substantially due to the increasing value of T_6 which reduces the desired cooling of stream 6.

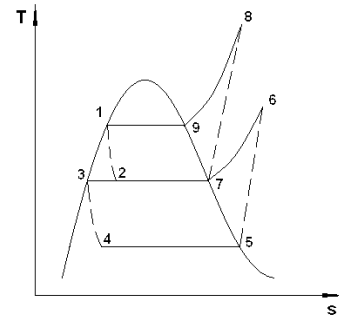


Figure 8: T-s diagram of the system in Fig.7

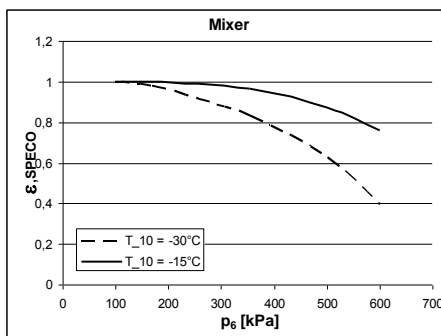


Figure 9: SPECO exergetic efficiency of the mixer in Fig.7.

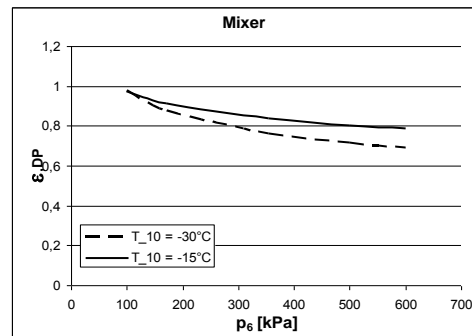


Figure 10: DP exergetic efficiency of the mixer in Fig.7.

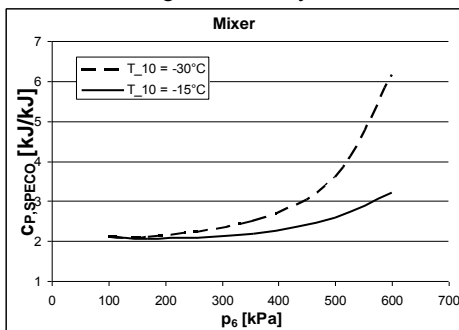


Figure 11: SPECO cost of product of the mixer in Fig.7.

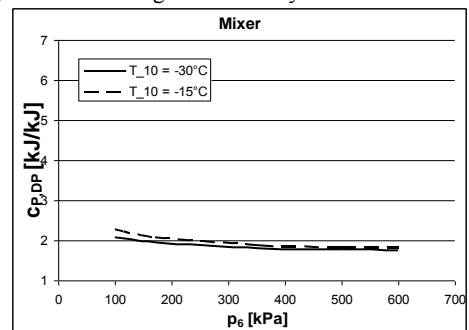


Figure 12: DP cost of product of the mixer in Fig.7.

The effect is more remarkable at $T_{10}=-30^{\circ}\text{C}$. This worsening of the component behavior leads to the expected progressive increase in c_P (Fig. 10), which is more remarkable at $T_{10}=-30^{\circ}\text{C}$ as well. Instead, the DP exergetic efficiency decreases at increasing values of the mixer pressure (Fig. 11), and it is apparently not consistent with the worse component behavior. On the other hand, also c_P shows a decreasing (although smoother) trend (see Fig. 12), which does not appear to be consistent with the exergetic efficiency growth. So, also in this case the information deriving from ε and c_P does not seem useful in a design improvement procedure of the component in which improvements of the component behavior are expected to result in a higher exergetic efficiency and a lower c_P cost.

Cogeneration steam turbine

The last example considers the back-pressure steam turbine in Fig. 13 in which the steam at the exit is used for heating purposes.

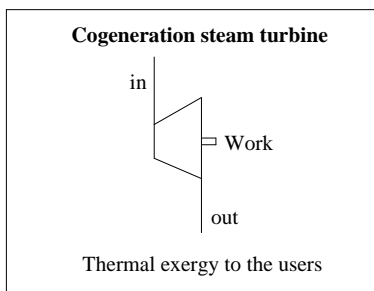


Figure 13: Cogeneration steam turbine.

According to the SPECO method the desired Product of the turbine is the shaft mechanical work, whereas the Fuel is equal to the exergy needed to generate the Product, i.e the removal of exergy from the steam crossing the turbine

$$\dot{E}_P = \dot{W} \quad \dot{E}_F = \dot{E}_{in} - \dot{E}_{out} \quad (\text{SPECO}) \quad (16)$$

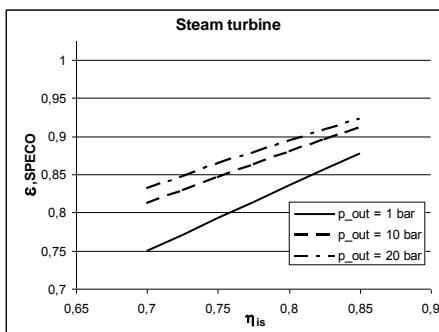


Figure 14: SPECO exergetic efficiency of the steam turbine in Fig. 13.

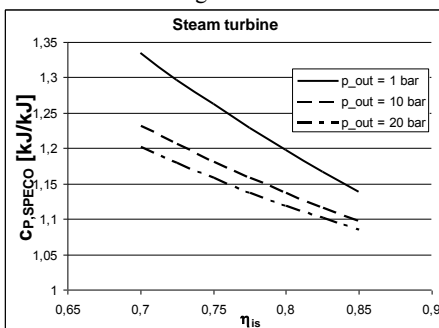


Figure 16: SPECO cost of product of the steam turbine in Fig. 13.

Instead, using to the DP criterion both the thermal exergy and mechanical work at the outlet are considered as useful Products

$$\dot{E}_P = \dot{W} + \dot{E}_{out} \quad \dot{E}_F = \dot{E}_{in} \quad (\text{DP}) \quad (17)$$

Thus, the SPECO and DP exergetic efficiencies are

$$\varepsilon = \frac{\dot{E}_P}{\dot{E}_F} = \frac{\dot{W}}{\dot{E}_{in} + \dot{E}_{out}} \quad (\text{SPECO}) \quad (18)$$

$$\varepsilon = \frac{\dot{E}_P}{\dot{E}_F} = \frac{\dot{W} + \dot{E}_{out}}{\dot{E}_{in}} \quad (\text{DP})$$

The cost balance of the component is

$$c_{in}\dot{E}_{in} = c_{out}\dot{E}_{out} + \dot{Z} \quad (19)$$

Amortization cost flow rates (\dot{Z}) are neglected for simplicity as in the previous cases.

The F rule of the SPECO method applied to the exergy removal (Eq. 12) supplies the auxiliary equation

$$c_{in} = c_{out} \quad (\text{SPECO}) \quad (20)$$

Using the DP approach the auxiliary equation is obtained by the P rule applied to the two terms of the component Product (\dot{E}_7 and \dot{E}_3)

$$c_W = c_{out} \quad (\text{DP}) \quad (21)$$

The costs per exergy unit of the Products are

$$c_P = c_W \quad (\text{SPECO}) \quad (22)$$

$$c_P = \frac{c_{in}\dot{E}_{in}}{\dot{W} + \dot{E}_{out}} \quad (\text{DP})$$

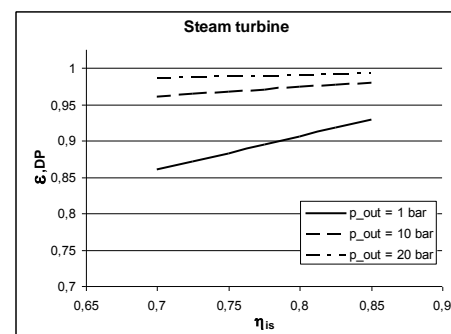


Figure 15: DP exergetic efficiency of the steam turbine in Fig. 13.

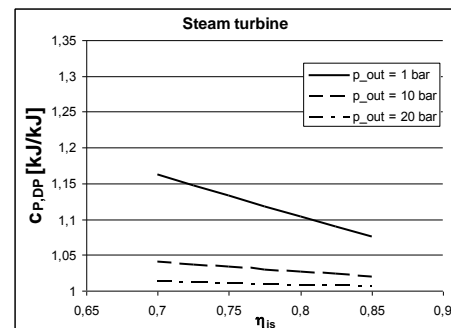


Figure 17: DP cost of product of the steam turbine in Fig. 13.

The turbine behavior was modified by varying the isentropic efficiency in the range 0.7-0.85 at fixed inlet thermodynamic conditions ($T_{in}=400^{\circ}\text{C}$, $p_{in}=40\text{bar}$) and for three values of the outlet pressure ($p_{out}=1\text{bar}$, 10bar , 20bar). Results of the simulation are shown in Figures 9 to 12.

In this example both the SPECO and DP exergetic efficiencies increase as the isentropic efficiency increases. However, the rate of increase is higher for the SPECO formulation, and becomes very small for the DP one when p_{out} is closer to p_{in} (at $=20\text{bar}$ ε_{DP} is almost constant, see Fig.17). The cost per exergy unit of the Product shows a similar trend, which is almost flat for p_{out} 20 bar. In this latter case, as in all previous examples, the improvements of the component behavior are not detected by ε_{DP} and $c_{P,DP}$. This is because the definitions of these parameters places the “desired performance” of the users (that are stated according to the requirement of the users) before the real thermodynamic behavior of the component itself. So, the exergy stream at the output of the cogeneration turbine, which the turbine is not able to use, is considered as being generated in the same way of the mechanical work, and having the same exergetic (and monetary) value (per exergy unit) of the mechanical work at the turbine shaft. None of these two hypotheses corresponds to the real behavior of the turbine. The turbine “extracts” mechanical work from the steam flowing through it and leaves at the outlet some exergy which cannot be practically converted into mechanical work with 100% efficiency. So, its value cannot be the same as the value of the mechanical work.

CONCLUSIONS

The three examples presented in the paper show that components having a “double purpose” in the system in which they are included may suggest different Fuel and Product formulations, and consequently a different cost of Product. Two criteria were considered to formulate the Fuel and Product of these components:

- The SPECO one, which takes a record of all the exergy differences between inlet and outlet of the component and includes on the Product side the desired additions and on the Fuel side the exergy removals (consumption) needed to obtain the Product according to the actual component behavior;
- The so called Double Purpose approach, which states that input and output exergy streams belong to the Fuel and Product, respectively.

Both criteria are consistent with the exergy balance, but they supply very different values of the exergetic efficiency, and in turn of the cost of Product. The amplitude of these differences varies depending on the design features of the component. In particular, it is observed that the Double Purpose approach may lead to constant exergetic efficiency and constant exergetic cost of Product when the design behavior of the component is modified. This implies that improvements in the component design might not be “detected” by the exergetic efficiency and cost of Product, which may therefore become useless performance parameters in a design improvement procedure. This is because the definitions of these parameters given by the Double Purpose approach places the “desired performance” of the component (that are stated according to the requirement of the users) before the real thermodynamic behavior of the component itself. So, different forms of exergy that undergo different processes within the component may be considered as being

generated in the same way and having the same value. Although this approach is “allowed” by exergoeconomics, it should in general be avoided when not dictated by the aggregation level of the system components. In this case (e.g., complex cogeneration plants that are considered as black-boxes having two or more products carrying different forms of exergy) it is necessary to consider the same cost for all the exergy units belonging to the different products. However, it is opinion of the author that the results of the analysis are strongly improved if the need of this approach is eliminated by considering a lower aggregation level of the component combined with the SPECO method.

ACKNOWLEDGMENT

Dr. Sergio Rech is gratefully acknowledged for helpful discussions and suggestions.

NOMENCLATURE

Symbol	Quantity	SI Unit
c	Specific monetary cost or Specific exergetic cost	\$/J J/J
e	Specific exergy	J/kg
\dot{E}	Exergy flow rate	J/s
KA	Heat transfer coefficient	W/K
\dot{m}	Mass flow rate	Kg/s
\dot{z}	Amortization cost flo rate	\$/s

Subscripts

P	Associated with the Product of the component
F	Associated with the Fuel of the component

REFERENCES

- [1] R.A. Gaggioli, W.J. Wepfer, Exergy economics. Energy;5:823–38, 1980.
- [2] G. Tsatsaronis, M.Winhold, Exergoeconomic analysis and evaluation of energy conversion plants. Energy Int. J.;10:69–94, 1985.
- [3] A. Valero, M.A. Lozano, M. Munoz, A general theory of exergy savings, Part I: on the exergetic cost, part II: on the thermoeconomic cost. In: Gaggioli R, Ed. Computer-Aided Engineering of Energy Systems, vol. 2–3. New York: ASME; p. 1–21, 1986.
- [4] M.A. Lozano, Metodologia para el analisis exergetico de calderas de vapor en centrales termicas. PhD Thesis. Univ. of Zaragoza, 1987.
- [5] C.A. Frangopoulos, Thermoeconomic functional analysis: a method for optimal design or improvement of complex thermal systems. PhD Thesis. Georgia Institute of Technology, 1983.
- [6] C.A. Frangopoulos, Thermo-economic functional analysis and optimization. Energy;12(7):563–71, 1987.
- [7] M.R. Von Spakovsky, A practical generalized analysis approach to the optimal thermoeconomic design and improvement of real-world thermal systems. PhD Thesis. Georgia Institute of Technology, 1986.

- [8] A. Lazzaretto, A. Macor, Direct Calculation of Average and Marginal Costs from the Productive Structure of an Energy System. *Journal of Energy Resources Technology*, Transactions of the ASME, vol.117, n.3, pp. 171-178, September 1995.
- [9] G. Tsatsaronis, L. Lin, On exergy costing in exergoeconomics. In: Tsatsaronis G., Bajura R.A., Kenney W.F., Reistad G.M., Eds. *Computer-aided energy systems analysis*, vol. 21. New York: ASME; p. 1–11, 1990.
- [10] A. Lazzaretto, R. Andreatta, Algebraic Formulation of a Process-Based Exergy Costing Method. *Proc. of ASME Advanced Energy Systems Division*, Ed. R.J. Krane, AES-Vol. 35, pp. 395-403. San Francisco California (USA), November 12-17, 1995.
- [11] A. Lazzaretto, G. Tsatsaronis, A General Process-Based Methodology for Exergy Costing, *Proc. of ASME Advanced Energy Systems Division*, Ed. A.B. Duncan, J.Fiszdon, D. O'Neal, K.Den Braven. AES-vol. 36 pp. 413- 428. Atlanta (USA), November 17-22, 1996.
- [12] A. Lazzaretto, G. Tsatsaronis, On the Quest of Objective Equations in Exergy Costing. *Proc. of ASME Advanced Energy Systems Division*, Ed. M.L. Ramalingam, J.L.Lage, V.C. Mei, J.N.Chapman. AES-vol.37. Dallas (USA), pp. 197-210, November 16-21, 1997.
- [13] A. Lazzaretto, G. Tsatsaronis, SPECO: A systematic and general methodology for calculating efficiencies and costs in thermal systems, *Energy*, Volume 31, Issues 8-9, Luglio, pp. 1257-1289, 2006.
- [14] S. Kemble, G. Manfrida, A. Milazzo, F. Buffa, Thermoeconomics of a ground-based CAES plant for peak-load energy production system, *Proc. of ECOS2012*, Perugia, Italy, June 26-29, 2012.

ENERGY/EXERGY BASED COST ACCOUNTING IN LARGE ECOLOGICAL-TECHNOLOGICAL ENERGY SYSTEMS

Mauro Reini*, Silvia Daniotti^o

*Dept. of Engineering and Architecture, University of Trieste, Italy

^oDept. of Electrical, Management and Mechanical Engineering, University of Udine, Italy

ABSTRACT

If a sufficiently extensive network of energy connections is considered, it is evident how all production and technological systems are directly or indirectly supported by relationships with the ecological systems of the biosphere that surrounds them. As a consequence, some of the energy flows, consumed inside production processes and technological devices, cross the limits of the control-volume and finally, in order to take into account the effects on the whole macro-system of the optimal design choices that we are looking for, the following question has to be answered:

“How much primary energy has been used by the macro-system to maintain each one of those flows at a defined value?”

In spite of some similarities, the two widely used methodologies show important differences, too, so that the answers to the previous question are often not-consistent, even if very simple systems are considered. Nevertheless, an almost complete integration among the two methodologies appears to be at hand, while all major differences can be explained, if we think about the possible behavior of the different components inside the system, instead of the axioms of previous formulations. The integrated approach is expected to enlarge the options the analyst can use to define and optimize the system and to allow the correct use of the results of both methodologies.

INTRODUCTION

An energy system can be synthetically described as a network of energy flows, connecting some nodes (named components, or sub-systems) where different kinds of irreversible, energy conversion processes may occur. This point of view is widely adopted for analyzing either natural, biological and ecological systems, or human-made, technological production systems. In Fig.1 a combined heat and power (CHP) system is shown, while in Fig.2 a simple energy diagram is reported for a forest with natural wood production.

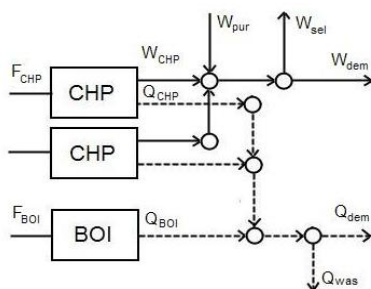


Fig.1 CHP system [1]

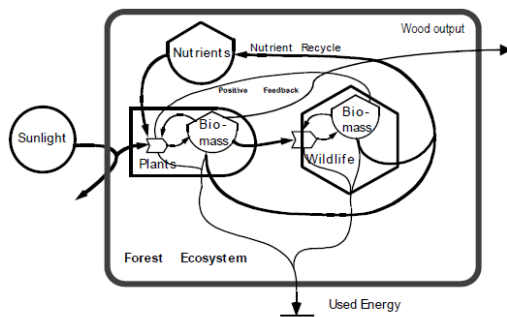


Fig.2 Emergy diagram for the wood production [2]

Indeed, ecological and technological energy systems are not disjoint sets of things, but they are strongly interconnected and interact each other, as it is especially evident when biomass-to-energy conversion systems, or bio-fuel production plants are taken into account.

Not only that, if we consider a sufficiently extensive network of energy connections, it is evident how all technological systems are directly or indirectly supported by relationships with the ecological systems of the biosphere that surrounds them. Therefore, when we focus on the design and optimization of an energy conversion system, or of a component inside a production plant, we actually define a control-volume, isolating a sub-system from a much bigger and much more complicated macro-system. As a consequence, some of the energy flows, consumed inside the sub-system, cross the limits of the control-volume and finally, in order to take into account the effects on the whole macro-system of the optimal design choices that we are looking for, the following question has to be answered:

“How much primary energy has been used by the macro-system to maintain each one of those flows at a defined value?”

Various methodologies can be found in literature to address this problem. Two of them, in particular, are widely used and defined in details. They are:

- The EMerger Analysis (EMA), defined in the ambit of the ecological modeling and ecological economics,
- The Exergy Cost Theory (ECT), defined in the ambit of energy conversion engineering.

In spite of some similarities, these two methodologies show more than a few important differences, so that the answers to the previous question are often not-consistent, even if very simple systems are considered.

The paper highlights first the similarities, avoiding confusion between exergy and exergy cost analysis, in the comparison with the EMA, and introducing the parallel concepts of transformity (x) and unit exergy cost (k^*), by using the derivative approach, typical of the Structural Theory of Termoeconomics. The possible interpretation of x and k^* as shadow (marginal) or average cost is also briefly discussed.

The differences arising when bifurcating flows, or recycles, are considered inside the system, are then introduced by showing some very simple cases, and an effort is done to bring the different approach about bifurcating flows to some (implicit or explicit) hypothesis on the physical behavior of the multi-product component, where the bifurcation occurs. Finally, by extending a recent result of the EMA (the Dynamic EMergy Accounting), a general formulation of cost allocation problem in case of recycling flows is obtained: in this way, the unit exergy cost (k^*) of the ECT can be re-obtained as a particular case, with a well-defined physical meaning.

THE SYSTEM AS A NETWORK OF ENERGY FLOWS

Let's consider a steady state operation of a multi-component energy system (notice that its Total Fuel (F_T) could be regarded as the whole consumed energetic and/or economical resources). If the energy/exergy flows inside the network are defined in order to properly describe the productive relations among components and with the outside of the system, each component (or process) can be regarded, at local level, as an autonomous production unit, having one, or more, output flow named *Products* or *Functions* and one or more input flows, named *Fuels* or *internal resources*. As a result, a sort of *local model* of each component is isolated from the whole system thermodynamic model, while the network can be regarded as the so called Productive Structure (PS) of the system.

Each flow E_i describing a *productive relation* among components has to be defined on the basis of heat, work and mass flow rates and of thermodynamic conditions of working fluids inside the plant. From a mathematical point of view, the choice of the analytic formulation is free and is left to the Analyst. If exergy flows were used to describe the productive relations inside the system, additional information could be obtained about losses inside each control volume and about distance from reversibility of each energy conversion process [3, 4, 5, 6]. Nevertheless, the definition of a simple (e.g. linear) model can be sometimes simplified by using energy based descriptions for the productive relations (E_i). In any case, exergy based productive relations have to be regarded as the general option [7, 8, 6].

Let's go back to the basic question: "How much primary energy has been used by the macro-system to maintain each flows of the PS at a defined value?" If the system is similar to a linear chain (like the one in Fig.3) and it is operating in stationary condition, the answer can be easily inferred. In fact, flows E_1 and E_2 do correspond to the primary energy F_1 and F_2 , respectively; flow E_3 is maintained by F_1 , so that its *unit energy/exergy cost* is defined as $k^*_3 = F_1 / E_3$, and a similar situations happens for flows E_4 and E_5 , too. Let's

think at the bifurcation of flow E_3 as a split, without any thermodynamic transformation or process, therefore flow E_7 results maintained by a fraction E_7 / E_3 of flow F_1 and its unit cost is defined as $k^*_7 = (E_7 / E_3) (F_1 / E_7) = k^*_3$. Flow E_8 is maintained by the remaining part of flow F_1 and by the entire flow F_2 . Its unit cost is $k^*_8 = k^*_3 (E_6 / E_8) + k^*_5 (E_5 / E_8)$.

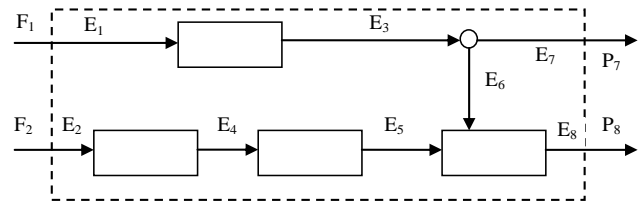


Fig. 3 A simple linear system with a split.

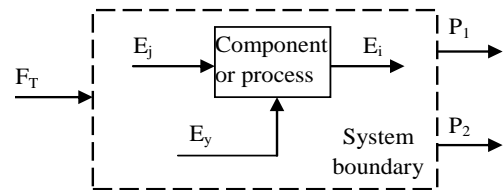


Fig. 4 A generic single product component.

The ratios like F_1 / E_3 (or E_6 / E_8) can be defined as the specific consumptions (or the partial specific consumptions) for obtaining a certain energy/exergy flow inside the system. This approach is formalized in deep detail in [4], where specific exergy consumptions are named κ_{ij} and a very elegant matrix formulation is introduced. In matrix form, the input/output relations for all components or processes inside the PS, as well as all unit energy/exergy costs, can be expressed as follows:

$$\mathbf{E} = {}^t\mathbf{K}\mathbf{E} + \boldsymbol{\omega} \quad (1)$$

$$\mathbf{k}^* = [\mathbf{U}_D - \mathbf{K}]^{-1} \cdot \mathbf{c}_e \quad (2)$$

where \mathbf{K} is a square matrix containing the specific energy/exergy consumptions κ_{ij} , while $\boldsymbol{\omega}$ and \mathbf{c}_e are vectors containing the out coming products (required by external users) and the unit energy/exergy cost of the incoming primary energy resources, respectively. Eq.(1) is named the *Characteristic Equation* of the PS.

Notice that costs inside vector \mathbf{k}^* have to be regarded as *average costs*, because they are obtained at constant specific energy/exergy consumption (or at constant energy/exergy efficiency) of all components and processes inside the PS. Therefore, all energy/exergy units, making up a certain flow, are regarded as obtained with the same efficiency of the production chain that starts with the incoming energy resources and reaches the considered flow.

For optimization purposes, *marginal costs* may be regarded as more appropriate, but two remarks have to be taken into account:

- Dealing with large ecological-technological energy systems, the *state* of a production chain is generally supposed to be not affected by the additional production of a unit of a certain commodity (so that we can speak about the unit energy cost of electricity, natural gas, paper or corn without the need of specifying the exact production level at which that unit has been produced);

- Marginal cost cannot be simply obtained from the values of all flows in the steady state operation of the system, even if it is similar to a linear chain, but variable load operation of each component or process has to be taken into account. In addition, marginal cost can be directly calculated from the system model for those flows only corresponding to *independent* variables of the model. For dependent flows (or state variables) shadow costs only can be calculated, by introducing some additional fictitious variables into the system model.

To introduce marginal and shadow costs, let's suppose that the global model of the whole system is available. In this model each exergy / energy or cost flows in the PS can be expressed as a function of an independent variables set (τ_T), made with all necessary variables for describing the behavior of the specific component or process obtaining that flow as a Product.

The *local model* of a general single-product component (Fig.4) can be first formulated as shown in the left hand side below, by operating a simple variable change, i.e. by identify the Product as one of the local independent variables:

$$\begin{aligned} E_i &= f_i(\tau_i) = f_i(\tau_1, \tau_{T-1}) \Rightarrow f_i^{-1}(E_i, \tau_{T-1}) & (3) \\ E_j &= f_j(\tau_T) = f_j(f_i^{-1}(E_i, \tau_{T-1}), \tau_{T-1}) \Rightarrow E_j = f_j^+(E_i, \tau_{T-1}) \\ E_y &= f_y(\tau_T) = f_y(f_i^{-1}(E_i, \tau_{T-1}), \tau_{T-1}) \Rightarrow E_y = f_y^+(E_i, \tau_{T-1}) \end{aligned}$$

The hypothesis that a component has to have one and only one Product is widely applied in Literature. The choice of a single outgoing flow, representing the purpose, or the *Product* of the component, makes easier the economic interpretation of the PS, as seen before.

The problem of multi-product components is the key point where differences arise between ECT and EMA and will be discussed in the following. In this paragraph it has to be stressed that in a lot of cases the apparent second product is an outgoing flow from a control volume having its main product, but the second product may be regarded as a sub-product or a residue, depending on whether its production implies a reduction, or an increase of total fuel consumption, respectively, at global level. The cost formation process of by-products and residues in the ambit of the ECT is discussed in [9, 10]. The heat cogenerated by an internal combustion engine can be regarded as an example of sub-product (when it is supplied to thermal users), or of residue (when it is not).

In other cases, inside the multi-product component an internal PS could be defined, where each sub-component obtains only one product [3].

The previous local model formulation, expressing local resources as well as eventual sub-product and residue vs. the local product, can be linearized, with the aim of obtaining the Local Linear Model (LLM).

$$\begin{aligned} E_j &= \mu_{ij}(\tau_{T-1}, E_i)E_i + \theta_j(\tau_{T-1}, E_i) \\ E_y &= \mu_{iy}(\tau_{T-1}, E_i)E_i + \theta_y(\tau_{T-1}, E_i) \end{aligned} \quad (4)$$

In these relations the coefficients of the linearizations are regarded as functions of the product too. This is the general case. But, if the production level variations are restricted inside an interval where a specific linear relation is acceptable, the linearization coefficients can be regarded as

independent from the production level of the component. This property of the LLM is expected to be an important advantage in further optimization procedures. In fact, recollecting the LLMs of all components and nodes (junctions and branches), the minimum resource consumption for the system described by the PS, can be obtained as the solution of the following MILP problem:

$$\min. F_T = {}^t\mathbf{c}_e \cdot \mathbf{E} \quad (5)$$

$$\mathbf{E} = {}^t\mathbf{M}\mathbf{E} + \mathbf{Q} + \boldsymbol{\omega} \quad (6)$$

$$\mu_{ij} = f_{ij}(\tau_{T-1}) \quad (7)$$

$$\theta_i = g_i(\tau_{T-1}) \quad (8)$$

where \mathbf{M} is a square matrix and \mathbf{Q} is a vector containing the linearization coefficients μ and θ , respectively.

Let's suppose that a feasible solution were available; a general variation in the objective function F_T can be expressed rearranging the total derivative of Eq.(5), taking into account linearization coefficients behavior (Eq.(7), (8)). The procedure is very similar to that presented in [16], where additional details can be found. In this way the so called *Fuel impact formula* is obtained:

$$dF_T = \sum [{}^t\mathbf{E} \cdot d\mathbf{M}(\tau_T) \cdot \boldsymbol{\lambda} + {}^t\boldsymbol{\lambda} \cdot d\mathbf{Q}(\tau_T) + \sum \lambda_u \cdot d\omega_u] \quad (9)$$

$$\boldsymbol{\lambda} = [\mathbf{U}_D - \mathbf{M}(\tau_T)]^{-1} \cdot \mathbf{c}_e \quad (10)$$

Eq.(10) corresponds to the structural cost formulation, obtained by Valero - Lozano - Serra [11] through a lagrangian procedure, when vector \mathbf{Q} is equal to zero. It can be demonstrated [12] that costs $\boldsymbol{\lambda}$ in Eq.(10) are the dual costs of the restrictions expressed by Eq.(6), therefore they have to be regarded as the marginal and shadow costs of flows \mathbf{E} .

Notice that costs $\boldsymbol{\lambda}$ and average costs (\mathbf{k}^*) do coincide [13, 5, 14, 15] if the LLM is replaced with the characteristic equation, i.e. if the input/output relations of each component or process are replaced by the definitions of specific energy/exergy consumptions k_{ij} :

$$\begin{aligned} E_j &= k_{ij}(\tau_{T-1}, E_i)E_i \\ E_y &= k_{iy}(\tau_{T-1}, E_i)E_i \end{aligned} \quad (11)$$

It is important to notice that this means that average costs (\mathbf{k}^*) also can be ideally obtained through a derivative procedure; in addition they can be calculated from a single *picture* (state) of the system, while the costs $\boldsymbol{\lambda}$ have to be obtained through an actual linearization of the energy system model.

THE EXERGY COST THEORY AND THE EMERGY ANALYSIS

Even if the ECT terminology has been used in the previous paragraph, it can be stated that the outlined procedure for obtaining the average costs is consistent also with EMA, at least from a methodological point of view.

To recall the complete formulation of the two methodologies is behind the object of this work. Various papers about this topic may be find in the literature (see only few of them in the References: Frangopoulos [16], Odum et al. [17], Reini et al. [18], Lozano and Valero [4], von Spakovsky and Evans [20]). Nevertheless, the main point of

ECT and EMA will be re-obtained in the following, from the PS of an energy system.

Let's first focus only on the similarities between the two approaches:

- They both describe an energy system as a network of energy/exergy flows, connecting sub-systems (or components), where energy conversion (or production) processes occur.
- They both introduce junction and splitter as nodes of the network, to obtain a meaningful picture of interactions among components.
- They deal with systems in stationary state (ECT), or evaluate flows through their annual average values (EMA).
- In the network, primary energy is continuously consumed, converted and dissipated to obtain one or more product flows for the outside the system.
- They both face the fundamental question: How much of primary energy flows is directly or indirectly required for obtaining a power unit of a certain flow inside the network making up the system? The answer is the transformity (x_i) and the unit exergy cost (k^*_i) of the generic flow E_i for EMA and ECT, respectively.

It can be inferred that transformity and unit exergy cost have to be analogous magnitudes and the same happens for the Energy flow (Empower: $Em_i \equiv x_i E_i$) and the exergy cost ($E^*_i \equiv k^*_i E_i$). Energy flow and exergy cost have, in some cases, the same value too, as can be easily demonstrated for the case in Fig.3, if solar energy is regarded as the only input.

These results make evident that a strong analogy may be identified between ECT and EMA, whereas it does not make sense comparing EMA with Exergy Analysis, because the latter does not incorporate any concept of *indirect* resources consumption.

Some differences arise between the two methodologies because they suggest different solutions to the fundamental problem of multi-product component or process. In fact they both pretend to obtain the answer only on the basis of the steady state values of all flows, without the need of introducing a more detailed model of component behavior.

EMA consider two options for multi-product components:

- There are only one true product and it is then spitted in two flows, without any transformation or losses, so that the true product and the spitted flows have to be qualitatively homogeneous; this is the case of flow 3 in Fig.3.
- There are two (or more) simultaneous, heterogeneous products; in this case the whole energy (exergy cost) of the inputs is allocated on each one of the so-called co-products, without any apportionment.

The second case introduces a complication, because the co-products are the origins of different production chains that can be (partially) reunited, so that double counting of primary resources consumption has to be carefully avoided in the evaluation of the unit costs, or transformities, for the final products. This kind of double counting has naturally to be avoided also when a co-product is reunited upstream the multi-product component, i.e. when a co-product is recycled backward in its own production chain. It is surprising to notice that the same *not-double-counting* rule is applied to all recycling flows, even if they come from a split, where the

energy accounting methodology has not introduced any duplication of the primary energy resources!

The EMA methodology is often presented as a set of axiomatic rules, that can be summarized in four points (Brown and Herendeen, [21]):

- 1) All source energy to a process is assigned to the processes' output (or outputs).
- 2) By-products (multi-products) from a process have the total energy assigned to each pathway.
- 3) When a pathway splits, the two "legs" have the same transformity.
- 4) Energy cannot be counted twice: (a) Energy in feedbacks cannot be double counted; (b) by-products, when reunited, cannot be added to equal a sum greater than the source of energy from which they were derived.

If a sub-system has two product flows, the original ECT postulates one of the following three cases:

- the exergy cost of the two products is the same; this case corresponds to the first option of EMA.
- the exergy cost of one of the two products is externally fixed; this case has been afterwards developed into the residue and sub-product concepts [22].
- inside the multi-product component an internal PS could be defined, where each sub-component obtains only one product [18].

It has to be pointed out that the last hypothesis brings to a generalization of the average cost definition. In fact, the matrix formulation (Eq.(2)) allows average costs to be calculated also in cases where they cannot be inferred from the conservative cost balance of each component.

The characteristic equations for the last case and for a residue and a sub-product accompanying the main product are shown in Fig.5.

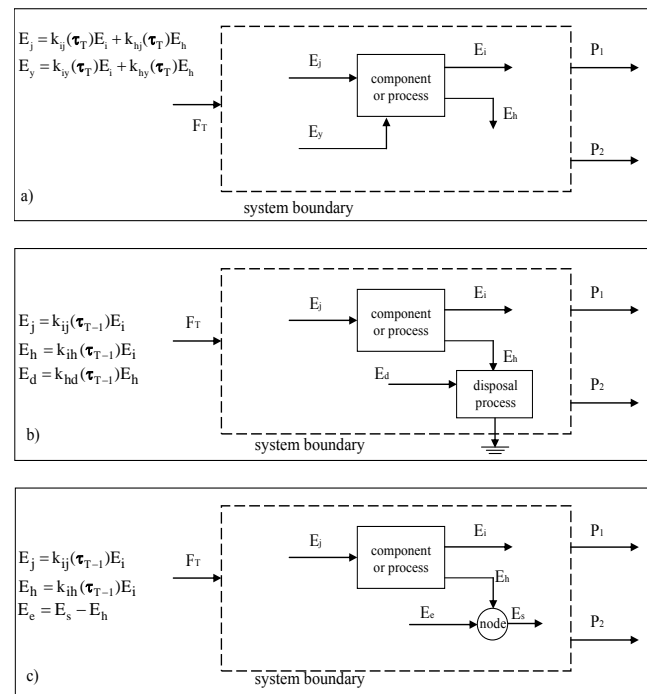


Fig.5 Characteristic Equations and PS for a multi-product component (a), a component with a residue (b) or a sub-product (c), agreeing with the ECT.

The additional main differences between the two methodologies are summarized and in the following:

- The limit of the system is not the same. In fact ECT is typically applied to power plants (or other energy conversion systems), having a fossil fuel as the main input and electric and/or thermal power as output. EMA include inside the analyzed system also the ecological sub-system of the biosphere and goods and services from the market, directly or indirectly required for operating the system.
- EMA measures energy flows through their energy content, while ECT measures energy flows through their exergy content, evaluated with respect of a proper set of ambient conditions.

The first point is not a real problem. In fact, the system limits usually defined by the ECT could be extended, up to coincide with those of EMA. In any case, the exergy input consumed by the ecological sub-system of the biosphere, as well as the exergy required to make available goods and services in the market, could be introduced into the analysis through a proper set of additional exergy costs for the system. The problem lies in the practical evaluation of these additional exergy costs, rather than in some mathematical limitation of the methodology. In this matter, the large experience of EMA could be of help to extend the application of the energy/exergy based cost accounting methodology.

The difference in the second point is vanishing in the recent years. In fact the idea of measuring energy flows through their exergy content is now widely accepted and practiced in the field of EMA (Odum, [23], Ulgiati and Brown, [24]). In addition, it could be noted that energy and exergy based cost accounting actually provide different results only if some flow splits (like flow 3 in Fig.3). Otherwise, in spite of being the unit costs different, the cost flows (E^* , or E_m) are the same.

Thus, the different hypotheses, formulated to deal with bifurcation and recycling of flows, have to be regarded as the main impediment towards a unified formulation of the two methodologies. Notice that analogous differences can be found when comparing EMA with Embodied energy Analysis (Brown and Herendeen, [21]).

RECENT DEVELOPMENTS

In recent years, the effort to re-think the fundamental background of EMA and the aim to enlarge its application field, are bringing inside the EMA some new contributions that could bring the two methodologies closer [25, 26, 27].

Yang et al. [25] proposed a new EMA method for waste treatment, reuse and recycle that is very similar to the sub-product and residue concepts defined in the ambit of ECT and briefly summarized in previous Fig. 5.

Reini and Valero [22, 10] have suggested how a cost allocation criteria, very similar to the case of co-product in the EMA, can be obtained in the ambit of ECT. In fact this is the result when there are two (or more) products, but only one degree of freedom is available for the multi-product component.

In this case, only one of the two products may be identified as the component degree of freedom in the LM, so that a LM similar to that shown inside Fig.5.a cannot represent the *actual behavior* of the multi-product

component, because in that case at least two, independent degrees of freedom are *implicitly* required to allow that one product could be modified independently by the other.

In other words, one product only may be put in relation with the single degree of freedom, while the second one has to be regarded as a dependent flow of the LM.

If the PS does not allow the second product to be identified as a sub-product, or a residue, the result obtained by applying Eq.(2) show a unit cost equal to zero for the second product, like it was a not required output, or a residue without any cost for disposal. To obtain the not-null value of its transformity, a complication has to be accepted: The roles of the dependent/independent flow have to be exchanged and Eq.(2) has to be applied a second time. This two-step procedure allows obtaining a couple of cost (k^*), consistent with the co-product concept of EMA. Notice that the simultaneous production of two flows of different nature, where each one cannot be obtained without the other, has always been used in the emergy Literature to support its co-product concept and its peculiar, not-conservative, cost allocation rule. Moreover, it has to be pointed out that co-products are quite common inside living energy systems, whereas sub-product and residue cannot be easily identified in this kind of systems; the opposite happens dealing with the technological energy conversion systems, where the ECT has been generally applied.

To come to the problem of recycling flows, Tilley and Brown [26, 27] have developed an approach to deal with those process in which the recycle of material is present inside the process itself. This kind of approach (named Dynamic Emergy Accounting, DEA) provides for explicitly taking into account the dynamic characteristic of the components inside the system, not only the stationary conditions, which are supposed to be reached at the end of a transient period.

At a generic instant, the recycled flow is separated from the main product and is sent to a buffer, where it is cumulated and lies in wait to be reused within the productive process. At the equilibrium, the material quantity inside the buffer remains constant, therefore the situation is the same of the steady state operation of the system without buffer.

In reality the transient period has an impact on the transformities at the equilibrium, in fact, the recycled flow has its own emergy value which is regarded as a productive factor in the upstream production chain. This is different from what traditionally happens in the EMA, in which the not-double-counting rule applies to all recycling flows, without regarding if they come from splits or co-products.

It follows that the transformity of the material recycled flow do coincide with that of the material inside the buffer: therefore, the transformity value of the material recycled flow becomes an input datum, that must be known prior by the analyst.

Moreover, in the DEA approach, a sort of *emergy ring* results made up by the recycled flow, together with a fraction of its production chain, so that the emergy of some flows in that chain may be greater than the total emergy input of the system.

TOWARD A UNIFIED APPROACH

By extending the result of the DEA, a general formulation of cost allocation problem in case of recycling flows can be

obtained. In fact, if the idea of an externally defined transformity, or unit cost, were accepted for every recycled flow (of both material and energy, homogeneous or heterogeneous with the not-recycled part of the product) the following three cases could be considered:

- The transformity is equal to zero: this case allows the transformities of all other flows (different from the recycling one) to be obtained, in agreement with *classical* EMA,
- The transformity is equal to that of the not-recycled part of the product: This is a split for the EMA, but its energy, or energy/exergy cost, is taken into account as productive factor in the upstream production chain, as the ECT requires.
- The transformity is equal to a value inferred by the analyst (e.g. from the market): this is the original DEA approach.

It is important to point out that the same results can be derived also from the cost allocation criteria of co-product, split and sub-product, once it has been observed that *every* recycled flow has to come from a multi-product component, or, in other words, that the presence of a recycle inside the PS implies the presence of a bifurcation, too [4].

This observation is the key to combine the generalized results of the DEA with those obtained by ECT, where the co-product, split and sub-product concepts have been introduced, as recently suggested in [22, 10]. In this way, a new general cost accounting method could be outlined, in which the cost allocation rules of EMA and ECT apply to a set of particular cases, but it has to be recognized that neither EMA nor ECT can be properly applied to all components or processes inside the ecological-technological energy systems.

To fix the ideas, let's consider the system illustrated in Fig.6 which has two process units (represented by the components A and B) and 6 exergy flows, where the component B is supposed to have only one degree of freedom.

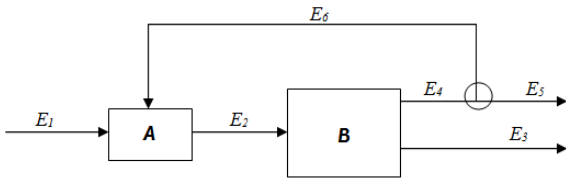


Fig.6 Scheme of a system with 6 flows, 2 black boxes (A, B), a co-product and feedback

To find the unit exergy cost of every flow, it is necessary to fix the independent flow outgoing from the process unit B, either E_4 or E_3 . Choosing the latter as the independent flow, the characteristic equations of the PS in Fig.6 are listed below:

$$\begin{cases} E_1 = k_{21} \cdot E_2 \\ E_2 = k_{32} \cdot E_3 \\ E_3 = P_3 \\ E_4 = k_{34} \cdot E_3 \\ E_5 = E_4 - E_6 \\ E_6 = k_{26} \cdot E_2 \end{cases} \quad (12)$$

where P_3 is the only one independent product, even though there are two outgoing flows from the system. The previous equations can be written in the matrix form, Eq.(2), and therefore the unit exergy costs can be calculated (remembering that c_e is a vector containing the unit exergy cost of the input flow, it follows that for Fig.6 the vector c_e turns out to be equal to $[k_1^* \ 0 \ 0 \ 0 \ 0 \ 0]^T$). To obtain the unit exergy cost of the flows E_4 , E_5 and E_6 the roles of the dependent/independent flow have to be exchanged and Eq.(2) has to be applied a second time. The resulting costs are shown in Table 1, together with those obtained by means of *classical* ECT and the rules of Emergy Algebra.

Adopting the exergy cost theory (ECT), at least two degrees of freedom are *implicitly* required to allow independent variations of each one of the two products, P_3 and P_5 . therefore, the characteristic equations of the PS in Fig.6 become different, as it can be seen below:

$$\begin{cases} E_1 = k_{21} \cdot E_2 \\ E_2 = k_{42} \cdot E_4 + k_{32} \cdot E_3 \\ E_3 = P_3 \\ E_4 = E_5 + E_6 \\ E_5 = P_5 \\ E_6 = k_{26} \cdot E_2 \end{cases} \quad (13)$$

The unit exergy costs are obtained in a similar way as before, thus applying the same matrix form, Eq.(2).

To compare these results with those obtained by the emergy analysis, it is necessary to apply the emergy algebra rules to the system illustrated in Fig.6, involving a quite different set of equations:

$$\begin{cases} Em_1 = Em_2 \\ Em_2 = Em_4 \\ Em_4 = Em_5 + Em_6 \\ Em_2 = Em_3 \end{cases} \quad (14)$$

It can be noticed that the rules concerning the co-product, split and feedback were properly taken into account. The resulting values of transformities (x_i) are shown in Tab.1. The same table contains: unit costs calculated by Eq.(2), emergies and transformities obtained from the emergy algebra rules and exergy costs as a function of the steady-state values of the exergy flows in the PS.

Notice that the exergy cost column of ECT has been left empty; this is because, if the two simultaneous product of component B are supposed to be *independent*, the ECT does not allow the specific unit consumptions (k_{ij}) to be obtained on the basis of exergy flow only, but additional information is required in order to made completely defined all terms in Eq. (13), e.g. the *internal* PS of component B.

The table shows that the unit costs and the transformities of the splitting flows (E_4 , E_5 and E_6) are equal each other, in all cases considered, but the value of transformity is lower than that of the unit exergy cost. This is because an *exergy cost ring* arises in consequence of the recycling flow E_6 ; this ring is completely the same of the *emergy ring* highlighted in the DEA approach [26], when a bifurcating flow is recycled upstream in the production chain. In fact, taking into account the value of the total cost for the flow E_4 (in the second column of Table 1), it can be re-written in such a manner:

$$E_1^* \cdot \frac{E_4}{E_5} = E_1^* \cdot \left(1 + \frac{E_6}{E_5}\right) = E_1^* + E_1^* \cdot \frac{E_6}{E_5} \quad (15)$$

Tab.1 Summary of the results (unit costs and total cost) obtained for every theory considered above

Flow n°	E ₃ independent		E ₄ independent		ECT (E ₃ and E ₄ independent)		Energy Algebra	
	Unit Cost	Exergy cost	Unit Cost	Exergy cost	Unit Cost	Exergy cost	Transformity	Emergy
1	k_1^*	E_1^*	k_1^*	E_1^*	k_1^*	E_1^*	k_1^*	E_1^*
2	$k_{21} \cdot k_1^*$	E_1^*	$\frac{k_{21}}{1 - k_{26} \cdot k_{42}} \cdot k_1^*$	$E_1^* \cdot \frac{E_4}{E_5}$	$\frac{k_{21}}{1 - k_{26} \cdot k_{42}} \cdot k_1^*$		$\frac{E_1^*}{E_2}$	E_1^*
3	$k_{21} \cdot k_{31} \cdot k_1^*$	E_1^*	0	0	$\frac{k_{21} \cdot k_{32}}{1 - k_{26} \cdot k_{42}} \cdot k_1^*$		$\frac{E_1^*}{E_3}$	E_1^*
4	0	0	$\frac{k_{21} \cdot k_{42}}{1 - k_{26} \cdot k_{42}} \cdot k_1^*$	$E_1^* \cdot \frac{E_4}{E_5}$	$\frac{k_{21} \cdot k_{42}}{1 - k_{26} \cdot k_{42}} \cdot k_1^*$		$\frac{E_1^*}{E_4}$	E_1^*
5	0	0	$\frac{k_{21} \cdot k_{42}}{1 - k_{26} \cdot k_{42}} \cdot k_1^*$	E_1^*	$\frac{k_{21} \cdot k_{42}}{1 - k_{26} \cdot k_{42}} \cdot k_1^*$		$\frac{E_1^*}{E_4}$	$E_1^* \cdot \frac{E_5}{E_4}$
6	0	0	$\frac{k_{21} \cdot k_{42}}{1 - k_{26} \cdot k_{42}} \cdot k_1^*$	$E_1^* \cdot \frac{E_6}{E_5}$	$\frac{k_{21} \cdot k_{42}}{1 - k_{26} \cdot k_{42}} \cdot k_1^*$		$\frac{E_1^*}{E_4}$	$E_1^* \cdot \frac{E_6}{E_4}$

It turns out that the total cost (i.e. the emergy) of the flow E₄ is given by the exergy cost of the input flow, plus a term exactly equal to the exergy cost of the recycling flow (E₆).

As previously highlighted, the presence of such a ring makes the exergy cost of some internal flows (in this case E₂ and E₄) greater than the total input; but the overall cost balance is kept conservative, in fact the total cost input equals the output.

Moreover, if the flows E₃ and E₄ are two co-products of component B, the two-step procedure outlined previously supplies an exergy cost value of E₃ consistent with the emergy algebra rules;

CONCLUSIONS

In conclusion, an almost complete integration among the EMA and ECT methodologies appears to be at hand, while all major differences can be explained, if we think about the possible behavior of the different components inside the system, instead of the axioms of previous *classical* formulations. In particular, the actual degree of freedom of component and process and the constraints that act on each of them, in consequence of the remaining part of the PS, should be carefully considered. In this way, the co-product, split and sub-product concepts can be introduced in the ECT, as recently suggested.

By combining such an extended formulation of the ECT with a quite natural generalization of the results of the DEA, a new general cost accounting method could be outlined.

It has to be recognized that, in the integrated approach, the cost allocation rules of *classical* EMA and ECT apply to a set of particular cases, but it has to be recognized also that neither EMA nor ECT can be properly applied to *all* components or processes inside both the natural, biological and ecological systems and human-made, technological production systems. The integrated approach is expected to enlarge the options the analyst can use to define and to opti-

mize the system and to allow the correct use of the results of both methodologies.

NOMENCLATURE

- μ, θ = linear coefficients
- \mathbf{b}, \mathbf{b} = additional extraction and additional extractions vector
- \mathbf{c}_e = vector of unit energy/exergy cost of the incoming primary energy resources
- E^*, \mathbf{E}^* = exergy cost and exergy cost vector
- \mathbf{E}, \mathbf{E} = generic flow and flows vector of the energy system
- Em_i = emergy of flow E_i
- f = generic function
- F, P = fuel and product of a component / a system
- \mathbf{K} = unit exergy consumption matrix
- $\mathbf{k}^*, \mathbf{k}^*$ = unit exergy cost and unit exergy cost vector
- \mathbf{k}_e = unit exergy costs vector of the primary energy input
- k_{ij} = unit exergy consumption of flow E_j to obtain flow E_i
- \mathbf{M} = matrix of coefficients μ
- \mathbf{Q} = matrix of coefficients θ
- \mathbf{U}_D = unit diagonal matrix
- x_i = transformity of flow E_i
- λ = vector of ratios λ_i
- λ_i = $(\Delta F_T/b_i)$
- $\boldsymbol{\tau}$ = independent variables vector
- $\boldsymbol{\omega}, \boldsymbol{\omega}$ = final product and final products vector
- indices:*
- e, s = input and output of a node without exergy dissipation
- h, i, j, y = generic indices
- t = transposed
- T = total system

REFERENCES

- [1] Reini M., Buoro D., 2010. "Mixed Integer Linearized Exergoeconomic (MILE) method for energy system synthesis and optimization". In Proc. of the 23th International Conference ECOS 2010; Jun. 14-17; EPFL, Lausanne, Switzerland.
- [2] <http://www.cep.ees.ufl.edu/emergy/resources/presentations.shtml>
- [3] Reini M., Lazzaretto A., Macor A., 1995. "Average Structural and Marginal Costs as Result of a Unified Formulation of the Thermoeconomic Problem". In Proc. of Int. Conf. Second Law Analysis of Energy System Towards the 21st Century, E. Sciubba, M. J. Moran Eds, Esagrafica Roma. Roma, July 5-7.
- [4] Lozano M.A., Valero A., 1993. "Theory of the exergetic cost". Energy vol. 18, pp. 939-960.
- [5] Serra L., Lozano M. A., Valero A., Torres C., 1995. "On average and marginal costs in thermoeconomics". In Proc. ECOS'95. Efficiency, Costs, Optimization, Simulation and Environmental Impact of Energy Systems. Eds. A. Gogus, A. Ozturk and G. Tsatsaronis, pp. 428-435, Istanbul, Turkey
- [6] Tsatsaronis G, Winhold M., 1985. "Exergoeconomic analysis and evaluation of energy conversion plants". Energy vol. 10, pp. 69-80.
- [7] Gaggioli R.A., 1983. "Second law analysis for process and energy engineering". In efficiency and costing. ACS Symposium Series 235, pp. 3-50.
- [8] El-Sayed Y.M., Gaggioli R.A., 1989. "A critical review of second law costing methods: Parts I and II". ASME Journal of Energy Research Technology vol. 111, pp. 1-15.
- [9] Reini, M., Taccani, R., 2004. "On the Thermoeconomic Approach to the Diagnosis of Energy System Malfunctions The Role of the Fuel Impact Formula". Int. J. Thermodynamics vol. 7, n° 2, pp. 61-72.
- [10] Torres C., Valero A., Rangel V., Zaleta A., 2008. "On the cost formation process of the residues". Energy vol. 33, pp. 144-152.
- [11] Valero A., Lozano M.A. Serra L, 1993. "Structural Theory of Thermoeconomics". Proc. of ASME AES v.30, Book N° H00874.
- [12] Wikipedia, The Karush-Kun-tucker conditions, consulted Feb. 26, 2010: http://en.wikipedia.org/wiki/Karush-Kuhn-Tucker_conditions
- [13] El-Sayed Y.M., 2003. "The thermoeconomics of energy conversions". Pergamon.
- [14] Lazzaretto A., Macor A., 1994. "Marginal and Average Costs in Engineering Functional Analysis". In Proc. of the 3rd Florence World Energy Research Symposium, July, Florence.
- [15] Von Spakovsky M.R., Evans R.B., 1990. "The foundations of engineering functional analysis". In Proc. of FLOWERS' 90, June 28, pp. 445-72, Florence, Italy.
- [16] Frangopoulos C. A., 1987. "Thermoeconomic Functional Analysis and Optimization". Energy - The Int. J. vol. 7, pp. 563-571.
- [17] Odum T. H. et al., 2000. "Handbook of Emergy Evaluation - Folio #1: Introduction and Global Budget, Centre for Environmental Policy". Environmental Engineering Science University of Florida, Gainesville.
- [18] Reini M., Lazzaretto A. and Macor A., 1995. "Average Structural and Marginal Costs as Result of a Unified Formulation of the Thermoeconomic Problem". In Proc. of Second Law Analysis of Energy System: Towards the 21st Century, Rome, July 5 - 7, 1995.
- [19] Lozano M. A. and Valero A., 1993. "Thermoeconomic Analysis of a Gas Turbine Cogeneration System". A.S.M.E. W.A.M..
- [20] Von Spakovsky M. R. and Evans R. B., 1990. "The Foundations of Engineering Functional Analysis (Part I and II)". A Future for Energy, FLOWERS 1990, Stecco and Moran Eds., Florence.
- [21] Brown M. T. and Herendeen R. A., 1996. "Embodied energy analysis and EMERGY analysis: a comparative view". Ecological Economics vol. 19, pp. 219-235.
- [22] Reini M., Valero A., 2002. "Towards a Unified Formulation of Exergy Cost Theory and Emergy Algebra for Ecological and Technological Energy System Evaluation". 2nd Int. Workshop on Advances in Energy Studies, Porto Venere, Sept. 24-28 2002.
- [23] Odum T. H., 2000. "Emergy Accounting". Centre for Environmental Policy Environmental Engineering Science University of Florida, Gainesville.
- [24] Ulgiati, S. and Brown, M. T., 2001. "Emergy Accounting of Human-Dominated, Large-Scale Ecosystems". In Thermodynamics and Ecological Modelling, Jorgensen Ed., Lewis Publisher, London.
- [25] Yang H., Li Y., Shen J., Hu S., 2003. "Evaluating waste treatment, recycle and reuse in industrial system: an application of the eMergy approach". Ecological Modelling vol. 160, pp. 13-21.
- [26] Tilley D. R., 2011. "Dynamic accounting of emergy cycling". Ecological Modelling, vol. 222, pp. 3734-3742.
- [27] Tilley, D.R. and M.T. Brown, 2006. "Dynamic emergy accounting for assessing the environmental benefits of a subtropical wetland storm water management system". Ecological Modelling vol. 192, pp. 327-361.

CORRELATING THERMODYNAMICS AND ECONOMIC INVESTMENTS TO IMPROVE THE RATIONALE FOR ENERGY RESEARCH

Marc A. Rosen

Faculty of Engineering and Applied Science, University of Ontario Institute of Technology, 2000 Simcoe Street
North, Oshawa, Ontario, L1H 7K4, Canada
(Email: Marc.Rosen@uoit.ca)

ABSTRACT

The use of exergy to correlate energy-utilization efficiencies and energy research investments is described. Specifically, energy and exergy losses are compared with to energy research and development spending, demonstrating that the latter correlates with energy losses, even though it would be more sensible to allocate energy research and development funding in line with exergy losses, as they represent the actual deviation of efficiency from the ideal. The methodology is outlined and illustrated with two case studies (the province of Ontario, Canada and the United States). The results are expected to be of use to government and public authorities that administer research and development funding and resources and should help improve the effectiveness of such investments.

INTRODUCTION

The energy utilization of a country or region is conventionally analyzed by examining the flows of energy through various sectors of the economy. But energy analysis can be misleading when used to analyze how effectively energy is utilized, and such analyses sometimes indicate the main inefficiencies to be in the wrong sectors and tend to state a technological efficiency higher than actually exists. Many feel that in order to properly assess how well a country or region utilizes its energy resources, an examination of the flows of exergy, rather than energy, through the sectors is required. The author has used exergy analysis to assess energy utilization in various countries, including Canada, Turkey and Saudi Arabia. Many other investigations have also focused on evaluating the energy utilization efficiency of regions and countries (Ertesvag, 2001; Rosen, 1992, 1993; Reistad, 1975; Ayres et al., 2003; Wall, 1990, 1991; Chen and Qi, 2007; Chen and Chen, 2006; Chen et al., 2006; Hammond and Stapleton, 2001; Gasparatos et al., 2008; Warr et al., 2008; Wall, 1987, 1991, 1997; Ertesvag and Mielnik, 2000; Ertesvag, 2005; Ptasinski et al., 2006; Wall et al., 1994; Stepanov, 1995; Ozdogan and Arikol, 1995; Dincer and Rosen, 2013; Ileri and Gurer, 1998; Dincer and Rosen, 2013; Schaeffer and Wirtshafter, 1992; Nakicenovic et al., 1996; Hermann, 2006).

Given that exergy is often viewed as a measure of value of energy resources, research has been carried out on the relation of exergy to economics and several related tools have been developed. Bryant (2007) and others suggest that the first and second laws of thermodynamics have significant implications for economic theory. Further, many researchers observe that exergy, but not energy, is often a consistent measure of economic value, and that accounting and pricing are better performed when based on exergy rather than energy. Several exergy-based economic-analysis techniques have been developed, usually to help determine appropriate allocations

of economic resources for optimal or improved systems and operations, aid design efforts, and enhance economic feasibility and profitability. Exergy-based economic techniques include exergoeconomics, thermoeconomics, exergy-based pricing, EXCEM analysis and analysis based on the ratio of thermodynamic loss to capital cost (Gogus, 2005; Tsatsaronis, 1987; Kotas, 1995; Rosen and Dincer, 2013; Yantovskii, 1994; El-Sayed, 2004; Sciubba, 2005; Valero, 2006; Valero et al., 2006a, 2006b; Lazzaretto and Tsatsaronis, 2006). One outcome of this research is the suggestion that financial investments in energy R&D should be related to or guided by exergy rather than energy measures. This work extends that research.

Several researchers have suggested linkages between energy R&D investments and exergy factors (Dincer and Rosen, 2013). However, little research relating exergy efficiencies or inefficiencies to energy R&D for countries or regions appears to have been undertaken. The principal objective of the work reported here is to analyze the R&D allocations in the energy sectors and compare these allocations to sector energy and exergy losses. This investigation is intended to yield insights on how R&D funding and effort can best be allocated. The research utilizes assessments of energy resource use in countries and regions, aimed at determining the efficiency with which energy resources are utilized and based on energy and exergy analyses. Only two preliminary studies have been reported, to the best of the author's knowledge, from over 20 years ago (Gaggioli, 2005, 2003; Lemieux and Rosen, 1989), and these form the basis of the case studies considered here.

APPROACH AND METHODOLOGY

One recommendation by the author a study of Canadian energy utilization (Rosen, 1992) was to analyze R&D funding in Canada or a subset thereof and to compare it to the corresponding energy and exergy efficiencies. The intention

of that recommendation was to determine if R&D funding is being allocated as beneficially as possible, by assessing whether R&D allocations were being made based primarily on an energy analysis of a sector or on the more rational exergy analysis. This idea is reinforced by Gaggioli (1985), who wrote, “exergy methods for analyzing ‘energy’ systems are the key ... for the purposes of decision-making for allocation of resources capital [and] research and development efforts. The exergy methods ... are a valuable first step for ascertaining likely prospects (opportunities) for cost effective capital expenditures for ‘energy’ conservation.” Some preliminary research in this area was performed by Gaggioli (1985, 1983).

The methodology used in this investigation to compare R&D spending in a system with the energy and exergy losses of that system is based on that utilized by Gaggioli (1985, 1983). The methodology involves four main steps:

1. The country or region is modeled. One model is shown in Fig. 1, where four main economic sectors are considered: residential-commercial (including institutional), industrial, transportation and utility (electrical and other). In analyzing such a system, the energy and exergy flows through the overall system and its sectors are evaluated, and efficiencies and losses are determined. To model and assess the individual sectors, each is broken down into its main categories and the categories are divided into specific types. For instance, transportation can be broken down into land, air and water categories, and several types of transportation can be considered for each category (e.g., road and rail for land transportation). Energy and exergy efficiencies can be determined for each of the processes occurring in the system, the main ones of which are heating (electric, fossil fuel, other), cooling (electric, thermal, other), work production (electric, fossil-fuel), electricity generation and kinetic energy production. The industrial sector is particularly complex due to the range of processes occurring in it (Brown et al., 1985). A reference environment must be specified to evaluate exergy commodities and, in this analysis, a reference environment which simulates the natural environment is utilized.

2. Energy and exergy efficiencies and inefficiencies are evaluated for a region or country, and for its sectors. For energy or exergy, the inefficiency is the difference between one (or 100% on a percentage basis) and the corresponding efficiency. The fraction of the total energy loss for a sector is considered the *perceived inefficiency*. This quantity is believed by many not to represent a true picture of inefficiency, despite public perception (Gaggioli, 1985, 1983, Dincer and Rosen, 2013). The fraction of total exergy loss (internal destructions plus waste emissions) for a sector is considered the *actual inefficiency* or *real inefficiency*. This label is justified, since the value measures how far the efficiency deviates from the ideal efficiency and is therefore meaningful. The perceived and actual inefficiencies for a sector can be determined. For a sector j , for instance,

$$\text{Sector } j \text{ perceived inefficiency} = 1 - \eta_j = \frac{(\text{Sector } j \text{ energy loss})}{(\text{Sector } j \text{ energy input})} \quad (1)$$

$$\text{Sector } j \text{ actual inefficiencies} = 1 - \psi_j = \frac{(\text{Sector } j \text{ exergy loss})}{(\text{Sector } j \text{ exergy input})} \quad (2)$$

where η_j denotes the energy efficiency and ψ_j the energy efficiency of sector j . It is sometimes more informative to

consider the breakdown of the total inefficiencies by sector. Then, we can write

$$\text{Fraction of perceived inefficiency for sector } j = \frac{(\text{Sector } j \text{ energy loss})}{(\text{Total energy loss})} \quad (3)$$

$$\text{Fraction of actual inefficiency for sector } j = \frac{(\text{Sector } j \text{ exergy loss})}{(\text{Total exergy loss})} \quad (4)$$

3. Funding allocations by the relevant entities (government, private sector, etc.) to R&D in the sectors are acquired and assessed to ensure they are properly interpreted.
4. The R&D funding allocations to the different sectors are compared with the energy and exergy inefficiencies to help assess how the justified the allocations are and to help recommend future allocations.

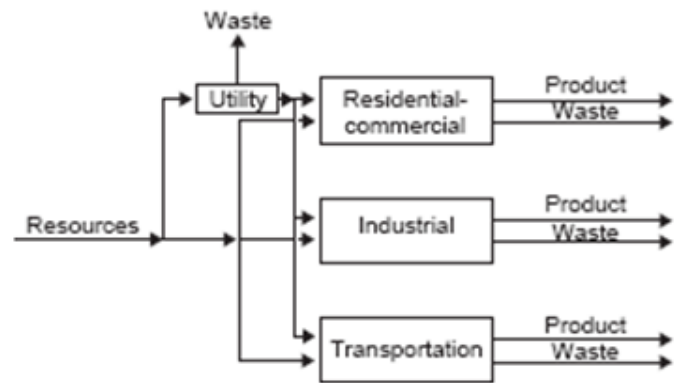


Fig. 1. Model of a region, country or the world, showing flows of resources like energy.

In the next two sections, the author utilizes the methodology described here to compare R&D spending with energy and exergy losses in the United States and in Ontario, Canada. Only two case studies are considered here because only a few analyses like this have been carried out. The case studies are based on previous analyses, and permit the relation between R&D spending and energy and exergy losses in the U.S. and Ontario to be analyzed and contrasted. Although the results presented are based on past data, implications can be inferred from them for the present and future.

CASE STUDY: ONTARIO, CANADA

In this case study, the author uses the methodology described earlier to assess and compare R&D spending with energy and exergy losses, for the province of Ontario, Canada and for its sectors. Ontario is Canada’s most populous province and consumes over 30% of all the energy resources used nationally.

Data and analysis

R&D funding data. Energy R&D in Ontario occurs primarily in the private sector and universities. There are three main sources of funding for these projects: the federal and provincial governments and the private sector. A variety of programs within the federal and provincial governments exists from which universities and companies obtain energy research funding, e.g., a major federal funding body is the Natural Sciences and Engineering Research Council (NSERC). Two Ontario funding programs at the time the data for this study were acquired were the University Research Incentive Fund

(URIF) of the Ministry of Colleges and Universities and the Enersearch program of the Ministry of Energy.

Accessing data for all R&D projects in Ontario's energy sector as well as their sources of funding was deemed impractical for the case study due to the variety of R&D sources. For this study, therefore, the authors chose to assess spending only in the Enersearch program. It is expected that research spending trends in this program are somewhat representative of all energy R&D efforts in Ontario, justifying this simplification. This simplification was made for the following reasons (MOE, 1989):

- The requirements for Enersearch funding for a project are broad enough to encompass energy-related projects in all sectors. Enersearch projects are required to address such goals as reducing energy demand through the application of innovative technology to achieve efficient utilization of existing energy sources, developing innovative technology to gain additional supplies from alternative and renewable sources, developing the equipment and capabilities required to utilize these new energy forms, and encouraging replication and use of new energy processes and innovative technologies among potential users.
- The range of activities to which Enersearch applies is broad, and include research and laboratory testing, equipment development and testing, pilot plant equipment, full-scale field trials and technical demonstrations of innovative technologies to determine system performance and economics, initial demonstrations of existing technologies used outside Canada to determine their suitability for application in Ontario, and technology and information transfer of results.
- The program applies to a range of energy technologies, including fuel research and evaluation, transportation, bio-energy conversion, electro-technologies, energy production from waste, residential, industrial and commercial building technologies, energy-efficient industrial processes, heat recovery and recuperation, hydrogen technology, and renewable energy systems.
- A wide variety of organizations can apply for funding under this program, including energy equipment manufacturers and suppliers, industrial and commercial energy users and producer, consulting firms, industrial and research organizations (but excluding electric utilities and publicly funded institutions except when they are in support of private sector proponents).
- Enersearch participated in over sixty projects totalling \$27 million between 1986 and 1989, making it the largest government energy R&D program for Ontario.
- The projects undertaken in this program by the participants received an average total government contribution of 33% of their projected eligible net cost. With this substantial yet limited government contribution to the project, the participants incur a large portion of the R&D costs thus projects are typically well planned and thought out. Further, the projects thus directly account for private-sector R&D expenditures as well as those by government.

The funding data were processed to render them suitable for the investigation. In order to analyze the research initiatives under the Enersearch program, a summary of the approved Enersearch projects was obtained (Appendix C of Lemieux and Rosen, 1989; MOE, 1989). These projects are divided into two categories by the Ministry of Energy: projects related to improved energy efficiency and projects

related to new energy supply. In order to assess R&D funding for individual sectors, the sector (or sectors) are determined to which each project is most applicable. However, some projects are applicable to more than one sector. Therefore, the sum of the individual sector funding is greater than the actual total funding. The total project cost (Appendix C of Lemieux and Rosen, 1989), which includes both private sector and government funding, is used to determine the total funding for each sector. Sector allocation totals are determined by summing the total project costs of each project in a sector.

Energy and exergy data. Actual inefficiencies and perceived inefficiencies evaluated elsewhere (Section 6.1 of Lemieux and Rosen, 1989, Rosen, 1993) are used. These inefficiencies are determined from the sector and total waste quantities given for Ontario in Fig. 2 for energy and Fig. 3 for exergy. It is observed that 43% of the total energy consumed in Ontario is converted to useful energy. The most efficient sector on an energy basis is the residential sector with an efficiency of 74%, followed closely by the commercial and industrial sectors with efficiencies of 66% and 65% respectively. The least efficient sector on an energy basis is the transportation sector with an efficiency of 18%. The exergy analysis indicates that 24% of Ontario's exergy consumption is converted into useful exergy for end uses. The most efficient sector based on exergy is the industrial sector (45%), followed by the utility sector (39%), the commercial sector (27%), the transportation sector (18%) and finally the residential sector (16%).

The reason for the low exergy efficiencies in the residential and commercial sectors is due to the poor utilization of the quality (or work potential) of the energy entering these sectors. In each of these sectors, the primary use of energy is to produce heat. With the production of heat from a fossil fuel or electrical energy source, there is a loss in the quality of energy that can be reflected only with an exergy analysis. The lower the temperature of the heat produced, the lower is the exergy efficiency. The residential, commercial and industrial sectors exhibit a wide variation between energy and exergy efficiencies. This is attributable to the extent to which heating and cooling processes occur in these sectors.

Results and discussion

Energy R&D budget allocations. The allocations for energy R&D funding in Ontario and each of its five sectors via Enersearch projects for the period May 1986 to April 1989 are listed in Table 3, in absolute terms and as a percentage of the overall budget allocation.

Table 3. R&D Funding Data for All Sectors in Ontario*

Sector	Total project costs (\$)	Breakdown of budget allocation (%)
Residential	3,278,524	7
Commercial	1,133,101	2
Industrial	24,793,117	54
Transportation	6,806,834	15
Utility	10,008,471	22
Overall	46,020,047	100

* Data are obtained from MOE (1989).

Based on these data, the sector that receives the most funding is the industrial sector, with approximately 54% of the spending in the Enersearch program. The funding allocations range from 2% (\$1,133,101) in the commercial sector to 54%

(\$24,793,117) in the industrial sector. It is noted that the actual total R&D allocations made through the Enersearch program are approximately \$26.8 million and not \$46.0 million shown in Table 3. This inflated overall amount is due to the manner in which projects are treated that are applicable to more than one sector, as discussed earlier.

Sector inefficiencies. Inefficiencies for Ontario and each of its sectors are broken down in Table 4, based on data in Figs. 2 and 3.

Table 4. Breakdowns of Sectoral Inefficiencies with Sectoral Energy R&D Budget Allocations for Ontario

Sector	Breakdown of overall inefficiencies		Breakdown of total energy R&D budget allocations (%)
	Portion of perceived inefficiency attributable to sector (%)	Portion of actual inefficiency attributable to sector (%)	
Residential-commercial	12	24	9
Industrial	21	25	54
Transportation	27	20	15
Utility	40	31	22
Overall	100	100	100

A sample calculation for the industrial sector is presented of the breakdown of energy (perceived) and exergy (actual) inefficiencies listed in Table 4. From Fig. 3, it can be seen that the industrial sector contributes 613.5 PJ of waste exergy to the overall waste exergy (2454.3 PJ). Therefore, the actual inefficiency contribution of the industrial sector is as follows:

$$\text{Industrial sector contribution to overall actual inefficiency} = 613.5/2454.3 = 0.25 \text{ (or 25\%)}$$

The perceived inefficiency breakdown is calculated similarly but using the waste energy values of Fig. 2, which show that the industrial sector contributes 398.4 PJ of waste energy to the overall waste energy (1875.8 PJ). Therefore,

$$\text{Industrial sector contrib. to overall perceived inefficiency} = 398.4/1875.8 = 0.21 \text{ (or 21\%)}$$

Relation between energy sector R&D funding and inefficiencies. The breakdowns of actual and perceived inefficiency values for Ontario and its sectors are compared with the breakdown of values for energy sector R&D funding in Table 4. The breakdown in total energy R&D allocations there is based on data in Table 3. Several trends are evident in Table 4, two of the most prominent of which are as follows:

- Actual inefficiencies exceed perceived inefficiencies in the residential-commercial sector and the industrial sector. For the transportation and utility sectors, the actual inefficiencies are lower than the perceived inefficiencies.
- A relationship is observed between perceived inefficiency and R&D allocations, in that energy R&D budget allocation increases as sector perceived inefficiency increases in Ontario for all sectors (except industrial).

These two trends in the Ontario analysis support the existence of a relationship between R&D allocations and perceived inefficiency levels. It appears that, of all factors

affecting energy R&D budget allocations to the sectors, the perceived inefficiency is significant and the actual inefficiency is of less importance or is overlooked. If actual inefficiencies were considered in R&D budget allocations, one would expect to observe more funding for the residential-commercial and utility sectors, because these are the sectors with the largest margins for improvement.

CASE STUDY: UNITED STATES

Data and analysis

Gaggioli applies exergy analysis to the energy utilization in the United States in order to calculate energy sector inefficiencies and then compare them to energy sector R&D funding in the U.S (Gaggioli, 1985, 1983). The main data used in this work are presented in Table 5, which shows the breakdown of actual inefficiencies, as a percentage of total exergy loss in the sector, and the perceived inefficiency, as a percentage of the total energy loss in the sector. These inefficiency breakdowns are calculated using Equations 3 and 4. The budget allocation breakdown in that table lists the amount of funding that was allocated by the United States Department of Energy to sector energy R&D.

Results and discussion

Table 5 shows a clear relationship between the perceived inefficiency and the budget allocations. Although R&D allocations are not based on inefficiency levels alone, the results indicate that budget allocations increase as perceived inefficiencies increase. This leads one to believe that the actual (exergy) inefficiencies are being overlooked when the decision-making for allocating R&D spending is being made.

For example, the two following observations in Table 5 support the statement that R&D funding in the U.S. is based on an energy analysis:

- The utility sector receives the second largest budget allocation of any sector and yet has the least losses on an exergy basis while, on an energy basis, it is second only to the transportation sector as having the most losses.
- The industrial sector which consumes the most energy of any end use sector (Gaggioli, 1985, 1983) and has the most room for improvement on an exergy basis is funded the least mainly because it is perceived as being the most efficient sector on an energy basis.

Table 5. Breakdown of Sectoral Inefficiencies with of Sectoral Energy R&D Budget Allocations for the U.S.*

Sector	Breakdown of overall inefficiencies		Breakdown of total energy R&D budget allocations (%)
	Portion of perceived inefficiency attributable to sector (%)	Portion of actual inefficiency attributable to sector (%)	
Residential-commercial	30	20	20
Industrial	32	15	18
Transportation	24	40	34
Utility	14	25	28
Overall	100	100	100

* Adapted from Gaggioli (1985, 1983).

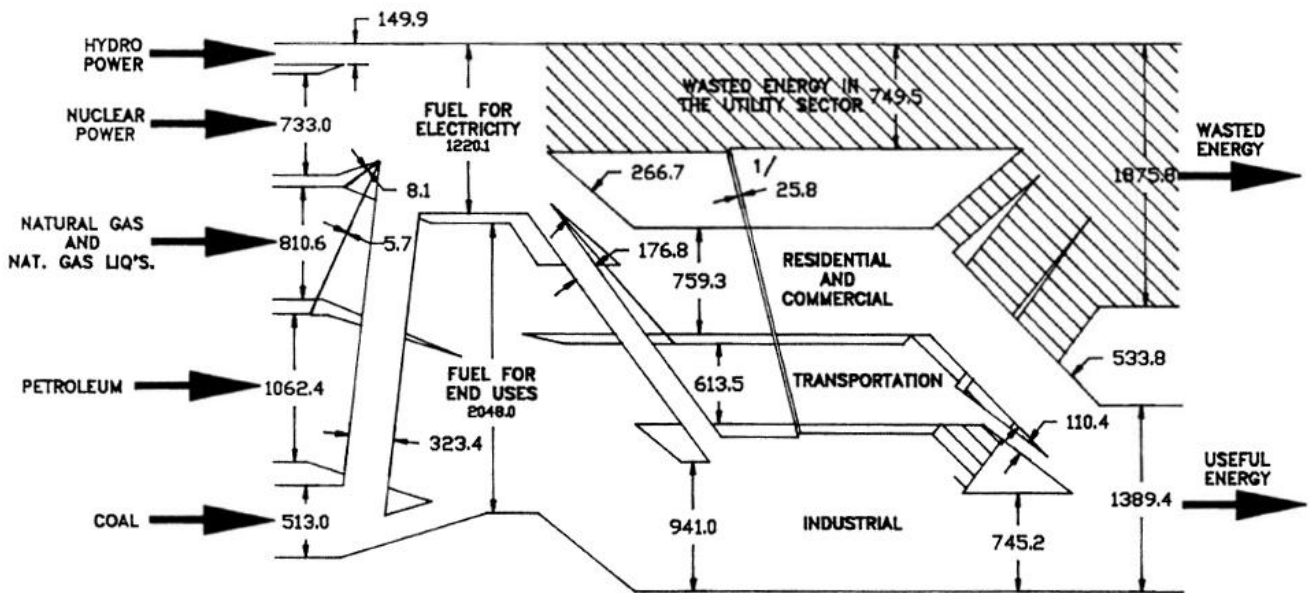


Fig. 2. Energy flow diagram for Ontario (in PJ or 10^{15} J) for 1987. The hatched region denotes losses and the note “1/” indicates steam extracted from the utility sector. Hydraulic energy is shown in kinetic energy equivalent.

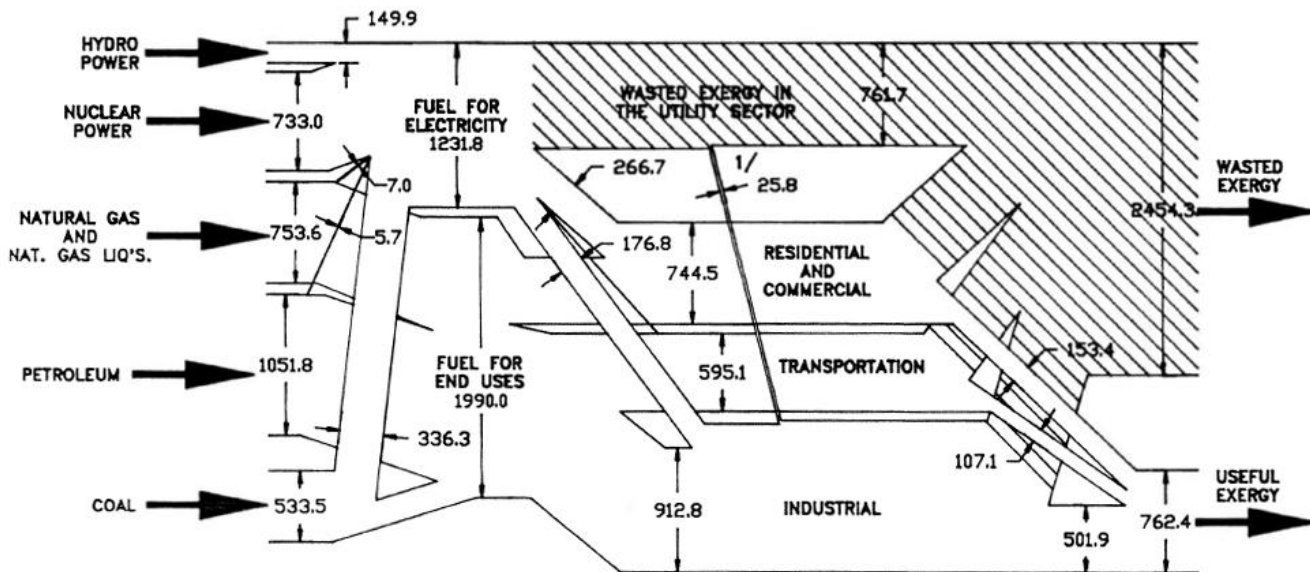


Fig. 3. Exergy flow diagram for Ontario (in PJ or 10^{15} J) for 1987. The hatched region denotes losses (external exergy emissions and internal exergy destructions) and the note “1/” indicates steam extracted from the utility sector. Hydraulic exergy is shown in kinetic exergy equivalent.

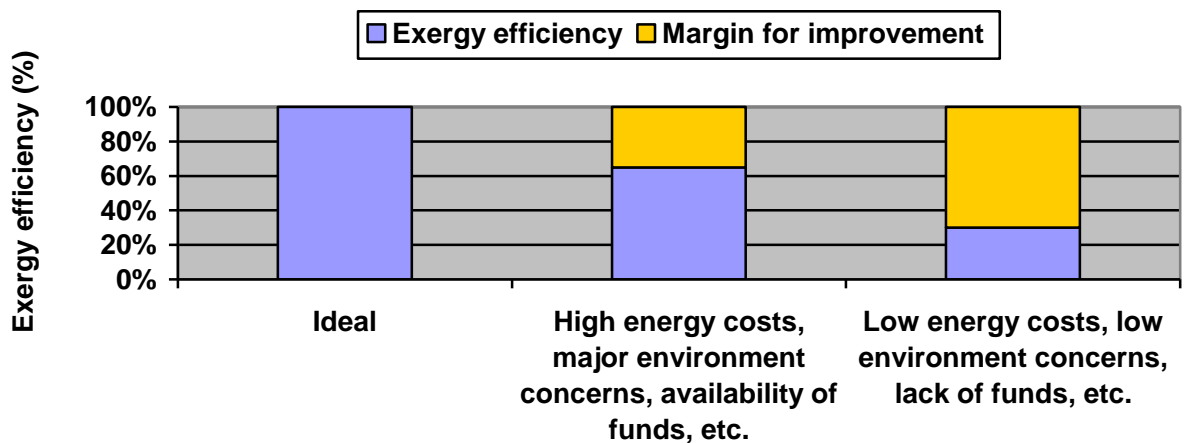


Fig. 4. Comparison of exergy efficiencies and margin for improvement (or actual inefficiency) for regions and countries having various attributes.

DISCUSSION

Comparison of case studies

Several similar trends are exhibited in Table 4 for Ontario and in Table 5 for the U.S. First, in both jurisdictions actual inefficiencies in the residential, commercial and industrial sectors are higher than the perceived inefficiencies, while actual inefficiencies are lower than the perceived inefficiencies for the transportation and utility sectors.

Second, as sector perceived inefficiency increases, energy R&D budget allocation increases in both jurisdictions (except for the Ontario industrial sector). These trends support the general contention that R&D allocations are related to perceived inefficiency levels, while the actual inefficiency is of less importance or neglected. Following actual inefficiencies would direct larger R&D budgets to the residential, commercial and utility sectors to exploit their relatively larger margins for efficiency improvement.

Different behaviour is observed for the industrial sector in Ontario compared to that in the U.S. The industrial sector in Ontario has a perceived inefficiency level of 21% which is higher than anticipated based on perceived efficiencies. The U.S. industrial sector has a perceived inefficiency level of 32% (Table 5) whereas, on the basis of the methodology, one would expect the energy R&D budget allocations for this sector to be between 15% and 9% for Ontario instead of 54% (Table 4). There are several reasons why the industrial sector funding in Ontario is not similar to that for the U.S. Size difference is important, as one jurisdiction is a province with a population exceeding 12 million while the second is a country with a population over 300 million. The U.S. study included all energy R&D funded by the United States Department of Energy which greatly exceeds that of the Enersearch program for Ontario. Not only did the Ontario analysis assess a province instead of a country, it assessed only one of many R&D funding programs in that province. If, for instance, the Ontario report is based R&D budget allocations on all provincial government R&D spending, the trend between perceived inefficiencies and R&D allocations may closer resemble that of the U.S. study. If we go one step further and include all R&D spending allocations in the province by government and private sector sources, the results may be closer still. Some other reasons why the industrial sector funding in Ontario in Table 4 differs from that for the U.S. in Table 5, and is higher than expected, are discussed below:

- The fact that the Enersearch program operates on a two-thirds, one-third funding policy (i.e., 2/3 of the cost of a project is incurred by the participant and 1/3 by the Ministry of Energy) results in participants primarily from industry, and thus may skew energy R&D budget allocations. Approximately 46 of the 55 projects are directly related to specific industrial processes, 19 of which are completely disassociated with any other sector (see Appendix C of Lemieux and Rosen (1989)).
- Electric utilities and publicly funded institutions (e.g., universities, electrical utilities) are not eligible for funding, except in support of private sector proponents. This restriction significantly reduces the number of publicly funded organizations in the program. For instance, only 2 of the 55 projects involve universities. If universities participated more, one would likely see different energy R&D budget allocations to the sectors, and, in particular,

less funding to the industrial sector.

- The documentation on the Enersearch program provided by the Ontario Ministry of Energy does not indicate funding amounts on a sector basis. Thus, since the authors had to subjectively estimate the separation of projects into sectors, inaccuracies may have been introduced.
- The large variation in project costs in comparison to the overall budget may also skew the results. For example, it can be seen in Appendix C of Lemieux and Rosen (1989) that the actual total project costs in the Enersearch program for the period considered are \$28,678,131 and the individual project costs range from \$23,300 to \$6,085,100. This large variation in individual project costs in relation to the total budget results in large variations between energy sector funding and may suppress the trend between perceived inefficiencies and R&D budget allocations.
- The fact that other Ontario government ministries also allocate funding to energy R&D for specific sectors (e.g., the Ministry of Transportation likely allocates money for R&D to the transportation sector) may also skew the results. This skewing may be amplified because the Enersearch program may tend not to fund R&D in a sector if a particular ministry is funding it significantly. Therefore, a sector may in reality be receiving considerably more funding than indicated in Table 3.
- The subset or sample group used in this report to assess R&D funding trends is relatively small. To realize more meaningful statistics, it is important to include as many sources of R&D funding as possible when analysing a system. In particular, confidence in the results would increase if a larger sample size were used, preferably by attaining data on the entire R&D spending in the province.

Implications for the present and future

The results of the case studies, although based on past data, have implications for the present and future. The author has begun an investigation of several countries using present and predicted future data and, based on the initial stages of this examination of research funding and energy and exergy efficiencies, many approximate similarities exist between the situation today for many countries and that at the time of the study for Ontario and the U.S., regarding the relation between sectoral energy R&D funding and sectoral inefficiencies. It is thus anticipated that several aspects of the trends indicated by the results of the case studies considered here are likely still valid today. In particular, energy R&D funding appears to be allocated more based on perceived rather than actual efficiencies, thereby potentially missing opportunities for large efficiency gains by focusing on the sectors with the largest margins for efficiency improvement.

It is possible that this trend will continue into the future, unless understanding and appreciation of exergy methods increases and reaches the levels of policy makers and industry leaders. Thus, the need to improve knowledge of exergy in society appears to be of great importance, so that strategic steps can be taken to allocate energy R&D funding where it can be most beneficially utilized.

This discussion can be extended so as to illustrate the variations of exergy efficiencies for regions and countries, characterized by their circumstances and settings, with margin for efficiency improvement, i.e., actual inefficiency. Factors and attributes that characterize the region for purposes of this discussion include energy resource availability and costs,

environmental constraints, and availability of funds. Other related factors are also considered implicitly.

Exergy efficiencies and the corresponding margin for efficiency improvement for regions and countries with two sets of realistic characteristics are presented in Fig. 4. Countries and regions with high energy costs and major environment concerns and availability of funds are likely represented by the second bar, while those with low energy costs, low environment concerns and lack of funds are likely represented by the rightmost. These cases likely bracket other regions and countries, i.e., those having some but not all of high energy costs, major environment concerns, availability of funds, etc. The hypothetical case of ideal efficiency is also shown in the figure, both for comparison and because an exergy efficiency of 100% always specifies ideal but unattainable thermodynamic behaviour. Several other important points can be observed in Fig. 4:

- Countries and regions with lower rather than higher exergy efficiencies have greater margins for efficiency improvement, as characterized by actual inefficiencies.
- Low exergy efficiencies often are observed in countries and regions with low energy costs, lax environmental constraints and a lack of funding for efficient technologies, awareness of efficient technologies and processes, and a sufficiently educated and skilled workforce. High exergy efficiencies are usually observed in countries/regions where circumstances foster high efficiency, e.g., high energy costs, funding availability for efficient technologies, available energy export markets, strict environmental constraints or emissions limitations, etc.
- The ultimate margin for efficiency improvement is seen to be the difference between the ideal exergy efficiency of 100%, which applies to ideal processes or devices, and the actual exergy efficiency. An awareness of this limit helps in establishing realistic targets for efficiency improvement.
- When energy-related factors change, countries and regions tend to respond (or should respond as it is usually in their best interests to do so). For instance, countries and regions tend to introduce measures that lead to increased exergy efficiency when energy costs increase or environmental regulations become stricter.
- An important observation for any region or country related to the above point is that exergy efficiency increases when circumstances warrant improved efficiency, but energy efficiencies do not necessarily increase. Appropriate efficiency targets and energy research efforts and support should be established based on exergy, as confusion and waste can result if efforts to determine appropriate efficiency research and targets are based on energy.

Specific regions or countries are not easily identified in Fig. 4 because their characteristics are usually much more complicated than the two simple cases shown. Nonetheless some generalities and trends, which likely apply in some cases, can be pointed out:

- Although the characteristics of countries with developing economies vary greatly, many less developed countries fall into rightmost category in Fig. 4 because for them energy resources are often less affordable (i.e., energy costs are high as a proportion of gross domestic product or average income per capita), obtaining funding for efficient technologies is difficult, and environmental laws are less strict. This behaviour is partly related to the focus of such

countries on developing economically and in other ways and/or meeting basic needs.

- Developed or industrialized countries tend to fall into the middle category in Fig. 4, since they usually have high energy costs and readily available mechanisms for exporting energy resources, strict environmental restrictions and laws, and funding for efficient energy conversion and utilization technologies. The wealth of such countries often makes them require or expect energy resources to be used efficiently and cleanly.
- In our globalized economy, it is unlikely that a country would have an extremely low exergy efficiency based on market forces, which exist in a similar form for developed or developing regions, because globalization makes it relatively easy to buy and sell energy commodities.

The ideas discussed here are somewhat confirmed in many countries and regions, where significant disparities exists in factors like energy costs and environmental regulations. In much of Europe and Asia, for example, energy prices are roughly double those in North America, and higher exergy efficiencies are observed. In the future, the ideas discussed in this section suggest that countries and regions are generally likely to move towards higher exergy efficiencies due to factors like energy price increases (long-term), resource scarcities, environmental limitations, and growth in developing economies (which can have very significant impacts for large countries like China and India). An important strategy would be to make investments in energy R&D guided in part by actual rather than perceived inefficiencies, i.e., by exergy factors.

CONCLUSIONS

In comparing energy R&D budget allocations with energy and exergy losses, it appears that of all factors affecting energy R&D budget allocations to the sectors, the perceived inefficiency is significant and the actual inefficiency is of less importance or is overlooked completely. If actual inefficiencies are considered in energy R&D budget allocations, one would probably see more funding for the residential, commercial, and utility sectors, because these are the sectors with a large room for improvement. The results are expected to assist government and public authorities that deal with research and development funding and should help improve the effectiveness of such investments of funds and resources. The comparison made in the case studies between energy R&D spending for the sectors of a region (Ontario) and a country (United States) with energy and exergy inefficiencies in those sectors reinforces these conclusions.

ACKNOWLEDGMENTS

Financial support provided by the Natural Sciences and Engineering Research Council of Canada is gratefully acknowledged. In addition, the author acknowledges the significant contributions to this work of Mark A. Lemieux, who carried out research under the supervision of the author at what is now Ryerson University in Toronto.

NOMENCLATURE

Symbol	Quantity	SI Unit
η	energy efficiency	
ψ	exergy efficiency	

REFERENCES

- Al-Ghandoor A, Al-Hinti I, Akash B, Abu-Nada E. 2008. Analysis of energy and exergy use in the Jordanian urban residential sector. *International Journal of Exergy* 5:413-428.
- Ayres RU, Ayres LW, Warr B. 2003. Exergy, power and work in the US economy, 1900-1998. *Energy-The International Journal* 28:219-273.
- Brodyanski VM, Sorin MV, Le Goff P. 1994. *The efficiency of industrial processes. Exergy Analysis and Optimization*. Elsevier: London.
- Brown, H.L. Hamel, B.B., Hedman, B.A., Koluch, M., Gajanana, B.C., Troy, P. 1985. *Analysis of 108 Industrial Processes*. Fairmount Press, Liburn, GA.
- Bryant, J. 2007. A thermodynamic theory of economics. *International Journal of Exergy*, 4, 302-337.
- Chen B., Chen GQ. 2006. Exergy analysis for resource conversion of the Chinese Society 1993 under the material product system. *Energy* 31:1115-1150.
- Chen GQ. 2005. Exergy consumption of the earth. *Ecological Modelling* 184:363-380.
- Chen B., Chen GQ, Yang ZF. 2006. Exergy-based resource accounting for China. *Ecological Modelling* 196:313-328.
- Chen GQ, Qi ZH. 2007. Systems account of societal exergy utilization: China 2003. *Ecological Modelling* 208:102-118.
- De Jong ED, Keuken H, Van Der Pol E, Den Dekker E., Kerckhoffs EJH. 1996. Exergy analysis of industrial processes using AI techniques. *Computers Chem. Engng* 20:S1631-S1636 (Suppl.).
- Dincer I, Hussain MM, Al-Zaharnah I. 2004a. Energy and exergy use in the utility sector of Saudi Arabia. *Desalination* 169:245-255.
- Dincer I, Hussain MM, Al-Zaharnah I. 2004b. Energy and exergy use in public and private sector of Saudi Arabia. *Energy Policy* 32:1615-1624.
- Dincer I, Hussain MM, Al-Zaharnah I. 2005. Energy and exergy utilization in agricultural sector of Saudi Arabia. *Energy Policy* 33:1461-1467.
- Dincer, I., Rosen, M.A. 2013. *Exergy: Energy, Environment and Sustainable Development*. 2d ed. Oxford, UK: Elsevier.
- Ediger, VS, Camdali, UO, 2007. Energy and exergy efficiencies in Turkish transportation sector, 1988–2004. *Energy Policy* 35, 1238-1244.
- El-Sayed, Y. 2004. *The Thermoconomics of Energy Conversion*. Elsevier: Amsterdam.
- Engineering Interface Limited and Marbek Resource Consultants Limited. 1988. *Commercial/Institutional Buildings, Electrical Energy Technology Study*. Ontario Ministry of Energy.
- Ertesvag IS. 2001. Society exergy analysis: A comparison of different societies. *Energy* 26:253-270.
- Ertesvag IS. 2005. Energy, exergy, and extended-exergy analysis of the Norwegian society 2000. *Energy* 30:649-675.
- Ertesvag IS, Mielnik M. 2000. Exergy analysis of the Norwegian society. *Energy* 25:957-973.
- Federici M, Ulgiati S, Basosi R. 2008. A thermodynamic, environmental and material flow analysis of the Italian highway and railway transport systems. *Energy* 33:760-775.
- Gaggioli RA, Petit PJ. 1977. Use the second law first. *Chemtech* 7:496-506.
- Gaggioli, R.A. 1983. *Second law analysis for process and energy engineering. Efficiency and Costing. Second Law Analysis of Processes*. ACS Symposium Series 235, pp. 7-50. American Chemical Society, Washington, D.C.
- Gaggioli, R.A. 1985. Personal communication. Presentation to Technical Staff at Institute for Hydrogen Systems. Mississauga, Ontario, Canada.
- Gasparatos A, El-Haram M, Horner M. 2008. Assessing the sustainability of the UK society using thermodynamic concepts: Part 2. *Renewable and Sustainable Energy Reviews*. In Press, Corrected Proof, Available online 22 April 2008.
- Gogus, Y. A. 2005. Thermo-economic optimization. *International Journal of Energy Research*, 29, 559-580.
- Hammond GP, Stapleton AJ. 2001. Exergy analysis of the United Kingdom energy system. *Proc. Instn Mech. Engrs* 215(2):141-62.
- Hepbasli A, Ozalp N. 2003. Development of energy efficiency and management implementation in the Turkish industrial sector. *Energy Conversion and Management* 44:231-249.
- Hermann WA. 2006. Pages Quantifying global exergy resources. *Energy* 31:1685-1702.
- Ileri A, Gurer T, 1998. Energy and exergy utilization in Turkey during 1995. *Energy* 23:1099-1106.
- International Energy Agency (IEA). 2007a. *Energy Balances of Non-OECD Countries, 2004-2005, 2007 Edition*, Paris, France.
- International Energy Agency (IEA). 2007b. *Energy Balances of OECD Countries, 2004-2005, 2007 Edition*, Paris, France.
- Jaber JO, Al-Ghandoor A, Sawalha SA. 2008. Energy analysis and exergy utilization in the transportation sector of Jordan. *Energy Policy* 36:2995-3000.
- Ji X, Chen GQ. 2006. Exergy analysis of energy utilization in the transportation sector in China. *Energy Policy* 34:1709-1719.
- Koroneos CJ, Nanaki EA. 2008. Energy and exergy utilization assessment of the Greek transport sector. *Resources, Conservation and Recycling* 52:700-706.
- Kotas, T. J. 1995. *The Exergy Method of Thermal Plant Analysis* (reprint ed.). Malabar, Florida: Krieger.
- Lazzaretto, A., Tsatsaronis, G. 2006. SPECO: A systematic and general methodology for calculating efficiencies and costs in thermal systems. *Energy*, 31, 1257-1289.
- Lemieux, M.A., Rosen, M.A. 1989. *Energy and Exergy Analyses of Energy Utilization in Ontario*. Report for Imperial Oil Ltd., by Ryerson Polytechnical Inst., Toronto.
- Marbek Resource Consultants. 1987a. *Electricity Conservation Supply Curves for Ontario*. Ontario Ministry of Energy, Toronto.
- Marbek Resource Consultants Ltd. 1987b. *Appliance Efficiency Information Base*. Ontario Ministry of Energy.
- Ministry of Supply and Services Canada. 1988. *Quarterly Report on Energy Supply and Demand, 1987-IV*. Vol. 12, No.4. Ottawa, Ontario.
- Moran, M. J., Shapiro, H. N., Boettner, D. D., Bailey, M. B. (2011). *Fundamentals of Engineering Thermodynamics* (7th ed.). New York: Wiley.
- Nakicenovic N, Gilli PV, Kurz R. 1996. Regional and global exergy and energy efficiencies. *Energy* 21:223-237.
- Oladiran MT, Meyer JP. 2007. Energy and exergy analyses of energy consumptions in the industrial sector in South Africa. *Applied Energy* 84:1056-1067.
- Ontario Ministry of Energy (MOE). 1986. *An Energy Efficient Ontario Toward the Year 2000*. Energy Policy Paper. Ontario Ministry of Energy, Toronto.

- Ontario Ministry of Energy (MOE). 1987. Ontario's Future Electricity Demand. Ontario Ministry of Energy, Toronto.
- Ontario Ministry of Energy (MOE). 1989. Enersearch Program Proposal criteria and application form. Energy Programs and Technology Division.
- Ozdogan O, Arikol M. 1995. Energy and exergy analyses of selected Turkish industries, *Energy-The International Journal* 20:73-80.
- Ozturk HK, Canyurt OE, Hepbasli A, Utlu Z. 2004. Three different genetic algorithm approaches to the estimation of residential exergy input/output values. *Building and Environment* 39:807-816.
- Ptasinski KJ, Koymans MN, Verspagen HHG. 2006. Performance of the Dutch energy sector based on energy, exergy and extended exergy accounting. *Energy* 31:3135-3144.
- Reistad GM. 1975. Available energy conversion and utilization in the United States. *J.Eng. Power* 97:429-434.
- Reistad, G.M. 1980. Available energy utilization in the United States. *Thermodynamics: Second Law Analysis*. ACS Symposium Series 122, pp. 93-110, American Chemical Society, Washington, D.C.
- Robinson, J.B. 1987a. An embarrassment of riches: Canada's energy supply resources. *Energy*. 12:379-402.
- Robinson, J.B. 1987b. Insurmountable opportunities? Canada's energy efficiency resources. *Energy*. 12:403-417.
- Rosen MA. 1992. Evaluation of energy utilization efficiency in Canada using energy and exergy analyses. *Energy-The International Journal* 17:339-350.
- Rosen MA. 1993. Energy utilization efficiency in a macrosystem (Ontario): evaluation and improvement through cogeneration. *Proceedings of the International Symposium on CO2 Fixation and Efficient Utilization of Energy*, Tokyo, pp. 17-26.
- Rosen MA, Le MN, Dincer I. 2005. Efficiency analysis of a cogeneration and district energy system. *Applied Thermal Engineering* 25(1):147-159.
- Rosen MA, Scott DS. 2003. Entropy production and exergy destruction—Part I: Hierarchy of Earth's major constituencies. *Int. J. Hydrogen Energy* 28:1307-1313.
- Saidur R, Masjuki HH, Jamaluddin MY. 2007a. An application of energy and exergy analysis in residential sector of Malaysia. *Energy Policy* 35:1050-1063.
- Saidur R, Sattar MA, Masjuki HH, Abdessalam H, Shahrwan BS. 2007b. Energy and exergy analysis at the utility and commercial sectors of Malaysia. *Energy Policy* 35:1956-1966.
- Saidur R, Sattar MA, Masjuki HH, Ahmed S, Hashim U. 2007c. An estimation of the energy and exergy efficiencies for the energy resources consumption in the transportation sector in Malaysia. *Energy Policy* 35:4018-4026.
- Schaeffer R, Wirtshafter RM. 1992. An exergy analysis of the Brazilian economy: From energy production to final energy use. *Energy* 17:841-855.
- Sciubba, E. 2005. Exergo-economics: Thermodynamic foundation for a more rational resource use. *International Journal of Energy Research*, 29, 613-636.
- Stepanov VS. 1995. A method for estimating the energy efficiency of the economy. *Energy* 20:577-583.
- Tsatsaronis, G. 1987. A review of exergoeconomic methodologies. In *Second Law Analysis of Thermal Systems* (pp. 81-87). New York: American Society of Mechanical Engineers.
- Utlu Z, Hepbasli A. 2003. A study on the evaluation of energy utilization efficiency in the Turkish residential-commercial sector using energy and exergy analyses. *Energy and Buildings* 35:1145-1153.
- Utlu Z, Hepbasli A. 2005. Analysis of energy and exergy use of the Turkish residential-commercial sector. *Building and Environment* 40:641-655.
- Utlu Z, Hepbasli A. 2006a. Assessment of the energy utilization efficiency in the Turkish transportation sector between 2000 and 2020 using energy and exergy analysis method. *Energy Policy* 34:1611-1618.
- Utlu Z, Hepbasli A. 2006b. Estimating the energy and exergy utilization efficiencies for the residential-commercial sector: An application. *Energy Policy* 34:1097-1105.
- Utlu Z, Hepbasli A. 2007a. Parametrical investigation of the effect of dead (reference) state on energy and exergy utilization efficiencies of residential-commercial sectors: A review and an application. *Renewable and Sustainable Energy Reviews* 11:603-634.
- Utlu Z, Hepbasli A. 2007b. A review on analyzing and evaluating the energy utilization efficiency of countries. *Renewable and Sustainable Energy Reviews* 11:1-29.
- Utlu Z, Hepbasli A. 2007c. A review and assessment of the energy utilization efficiency in the Turkish industrial sector using energy and exergy analysis method. *Renewable and Sustainable Energy Reviews* 11:1438-1459.
- Utlu Z, Hepbasli A. 2007d. Assessment of the Turkish utility sector through energy and exergy analyses. *Energy Policy* 35:5012-5020.
- Utlu Z, Hepbasli A. 2008a. Energetic and exergetic assessment of the industrial sector at varying dead (reference) state temperatures: A review with an illustrative example. *Renewable and Sustainable Energy Reviews* 12:1277-1301.
- Utlu Z, Hepbasli A. 2008b. Thermoeconomic analysis of energy utilization in the residential-commercial sector: An application. *Building and Environment* 43:896-904.
- Valero, A. 2006. Exergy accounting: Capabilities and drawbacks. *Energy*, 31, 164-180.
- Valero, A., Serra, L., Uche, J. 2006a. Fundamentals of exergy cost accounting and thermoeconomics. Part I: Theory. *Transactions of the ASME: Journal of Energy Resources Technology*, 128, 1-8.
- Valero, A., Serra, L., Uche, J. 2006b. Fundamentals of exergy cost accounting and thermoeconomics. Part II: Applications. *Transactions of the ASME: Journal of Energy Resources Technology*, 128, 9-15.
- Wall G. 1987. Exergy conversion in the Swedish society. *Resources and Energy* 9:55-73.
- Wall, G. 1988. Exergy Flows through industrial processes. *Energy*. 13:197-208.
- Wall G. 1990. Exergy conversion in the Japanese Society. *Energy-The International Journal* 15:435-444.
- Wall G. 1991. Exergy conversions in the Finnish, Japanese and Swedish societies. *OPUSCULA Exergy Papers*: 1-11.
- Wall G. 1997. Exergy use in the Swedish society 1994. *Proceedings of the International Conference on Thermodynamic Analysis and Improvement of Energy Systems (TAIES'97)*, June 10-13, Beijing, China, pp. 403-413.
- Wall G, Sciubba E, Naso V. 1994. Exergy use in the Italian society. *Energy-The International Journal* 19:1267-1274.
- Warr B, Schandl H, Ayres RU, 2008. Long term trends in resource exergy consumption and useful work supplies in the UK, 1900 to 2000. *Ecological Economics* 68:126-140.
- Yantovskii, E. I. 1994. *Energy and Exergy Currents: An Introduction to Exergonomics*. New York: Nova Science Publishers.

USE OF EXERGY ANALYSIS TO COMPUTE THE RESOURCE INTENSITY OF BIOLOGICAL SYSTEMS AND HUMAN SOCIETIES

Enrico Sciubba

Dept. of Mechanical & Aerospace Engineering
University of Roma Sapienza
enrico.sciubba@uniroma1.it

ABSTRACT

Exergy analysis (ExA) has a quite extensive history of successful applications in Engineering, and especially in the original niche in which it saw the light, Energy Conversion Systems. A vast body of literature confirms that a correctly formulated exergy approach leads to a better design, in that it helps identify and refine the configuration of systems that generate the desired outputs (conventionally called “products”, P) by the minimum feasible use of primary resources (conventionally called “fuels”, F). A similarly vast body of literature deals with the more fundamental aspects of the theory: where and how ExA improves a conventional energy analysis, how large is the attainable marginal improvement in the efficiency (P/F), what are the implications of these improvements, what is their theoretical significance (especially with regard to the so-called “sustainability issue”). When combined with the concept of “cost”, ExA has originated a novel and industrially relevant method, Thermo-Economics (TE), which expresses the monetary cost of P not in terms of €/kg or €/unit but in terms of €/(exergy content). TE led to interesting reassessments of “optimal” energy conversion chains, and did itself undergo a quantum leap when the innovative Ecological Cost (EC) theory was introduced to include one of the “costs of externalities” of P. EC expresses the production cost not on the basis of a monetary proxy, but of the amount of exergy in F needed to generate P. Obviously, both TE and EC are amenable to a genuine life-cycle analysis. Still, all of the above applications are limited to the study of engineered systems, which are usually designed on the basis of process diagrams that apply the concepts of Classical Equilibrium Thermo-dynamics and introduce proper corrections to model irreversible and non-equilibrium effects. But, unlike entropy, exergy does not require an extension of Classical Thermodynamics to be applied to non-equilibrium processes: if a system proceeds from whatever initial state S1 (equilibrium or non-equilibrium) to a final state S2 in which it is no longer capable of producing useful external work, the exergy is a well defined quantity, regardless of S1 being homogeneous or not, in local equilibrium or not. This peculiarity suggests that the current methods of exergy analysis may be extended to assess the “conversion efficiency” (P/F) of systems that are not amenable to a classical treatment: the extension discussed in this lecture deals with societal and biological systems. Societal systems are treated as complex non-homogeneous thermodynamic systems interacting with a conventional environment. On the basis of a sufficiently detailed exergy flow diagram, it is possible to relate a set of properly defined “products” (commodities, including money, labour, etc.), “wastes” (discharges) and “environmental impact” with the amount of primary exergy required to maintain the system at a certain pre-assigned state. The theory leads to the definition of an “embodied primary exergy content” called the *extended exergy cost* of P. Biological systems are treated in much the same way, with the *caveat* that the description is global (group, species, herd), and therefore is only valid for ensembles rather than for individuals. Here, too, it is possible to define a “species efficiency” as the ratio of the useful accumulated exergy to the total incoming exergy flow.

INTRODUCTION

When addressing issues related to “environmental interactions”, the difference between “anthropic” and “natural” systems fades: whenever a system A of either type interacts with an environment O, it can do so only by exchanging mass and/or energy through its boundaries, and such exchanges are ruled by the applicable laws of Thermodynamics and constrained by the applicable (internal and external, and possibly time-dependent) boundary conditions. Therefore we shall drop the distinction here. Another important consideration is that real systems are open: they either have permeable or/and perforated or/and diabatic or/and displaceable boundaries that allow exchanges of mass, heat and work with the “outside” against an externally imposed potential (concentration, temperature or pressure respectively). A common feature all systems of relevance display is their being -for a finite period of time- not in equilibrium: the study of “systems that have reached stable equilibrium” is actually of no interest to engineering sciences, because in such a state there can be no meaningful energy exchange; and arouses even

less interest in biological sciences, where “stable equilibrium” is synonym of “dead organism”. Thus, to understand the dynamics of systems behaviour, we must use non-equilibrium paradigms, in particular non-equilibrium Thermodynamics. We capitalize naturally on the large, well-established and very useful body of knowledge that “classical” or “equilibrium” Thermodynamics has contributed to create: only, the features of complex systems require some additional principles and tools to be described with sufficient (and operative) approximation. Non-equilibrium Thermodynamics is a relatively new field (a clear and rigorous review is offered in [19], and a discussion is provided in Panel B), and its topics are not as crisp as those of its equilibrium counterpart: we shall use here the following assumptions, which we posit without further justification:

- The systems of interest are not so far from equilibrium that catastrophic changes happen in their structure (in other words, they remain sufficiently far from any bifurcation point may exist in their phase space evolution);

- However complex the system, it is always possible to subdivide it in sufficiently small portions (subsystems) such that each one of them is in equilibrium (assumption of local equilibrium);
- Under the above stipulations, a property “temperature” can be defined for the system;
- Under the above stipulations, entropy is a state function for the entire system and for each of its sub-systems;
- The boundary conditions are not a variable in this study: they are specified once and for all by the problem position and can vary both in space- and in time¹;
- All properties of the system and of its environment can be described in terms of legitimate thermodynamic quantities.

In such a perspective, the representation of any system of interest for the present discussion is relatively simple (figure 1): a system A is in a certain configuration A_0 at an arbitrary initial time t_{init} , then exchanges a certain amount of mass and energy with its surroundings, “growing” and/or “shrinking” in space state, possibly in a pseudo-periodic fashion, until it reaches the end of our observation window at time t_{fin} , having reached a state A_{fin} not necessarily equal to A_0 . The equations ruling the evolution from t_{init} to t_{fin} are: mass conservation

$$\frac{dM}{dt} = \sum m_{in} - \sum m_{out} \quad (1)$$

energy conservation

$$\frac{dE}{dt} = \sum E_{in} - \sum E_{out} \quad (2)$$

entropy balance

$$\frac{dS}{dt} = \sum \dot{S}_{in} - \sum \dot{S}_{out} + \dot{S}_{irr} \quad (3)$$

exergy equation

$$\frac{dEx}{dt} = \sum \dot{Ex}_{in} - \sum \dot{Ex}_{out} - \dot{Ex}_{\delta} \quad (4)$$

We are seeking a general expression for the evolution of the state of the system in time. The independent variables are the extensive quantities M, E, S and Ex, and since their respective initial values are known (A_0 must be well-defined for the analysis to be meaningful), the system of four equations in four unknowns appears well posed. The system of equations (1-4) must be closed by explicitly calculating the right-hand sides of either equation: let us examine in detail these input/output/generation/destruction terms.

a) Mass in- and outflows

Mass cannot be created in any of the sub-portions of A, and thus the variation in the total mass of A can only be given by the net material convection and diffusion flows through the boundary:

$$\begin{aligned} m_{in,conv,j} &= \int_b \rho_j v_{in,j} dA_b \\ m_{out,conv,k} &= \int_b \rho_k v_{out,k} dA_b \end{aligned} \quad (5)$$

Where $j=1\dots J$ and $k=1\dots K$ (J not necessarily equal to K) are the inlet and outlet “ports” on the boundary b where convection is allowed.

¹ This implies that the “surroundings” do not change appreciably their thermodynamic state as a direct consequence of their interaction with the system: any change in the state of the environment O is specified in advance for each case under consideration.

$$\begin{aligned} m_{in,diff,i} &= \int_b D_i \Delta c_{b,i} dA_b \\ m_{out,diff,l} &= \int_b D_l \Delta c_{l,b} dA_b \end{aligned} \quad (6)$$

Where $i=1\dots I$ and $l=1\dots L$ are the permeable portions of the boundary b , D are the diffusion coefficients and Δc are the concentration gradients across these portions. Substituting (5) and (6) into (1) closes the balance: however, it must be noted that the coefficients D in general depend on the diffusion dynamics across all other internal “layers” that contribute to mass diffusion inside of the system [10] (figure 2). Even in the oversimplifying assumption of the absence of chemical reaction inside of A, we need to solve a set of N “internal” diffusion equations for each chemical species, where N is the number of “diffusion exchanges” among sub-systems: this is though feasible numerically, with a degree of accuracy satisfactory for most practical cases, and therefore equation (1) can be considered “solvable”.

b) Energy in- and outflows

Energy is also globally conserved, and the variation in the total energy of A can only be produced by material and immaterial convection, and work done at the boundary:

$$e_{in,conv,j} = \int_b m_{in,j} h_{in,j} dA_b \quad (7)$$

$$e_{out,conv,k} = \int_b m_{out,k} h_{out,k} dA_b$$

$$e_{in,heat,j} = \int_b q_{in,j} dA_b = \int_b \Lambda_j \Delta T_{b,j} dA_b \quad (8)$$

$$e_{out,heat,k} = \int_b q_{out,k} dA_b = \int_b \Lambda_k \Delta T_{k,b} dA_b$$

$$e_{in,work,j} = \int_b \Delta p_{b,j} \square dx_{b,j} dA_b \quad (9)$$

$$e_{out,work,k} = \int_b \Delta p_{k,b} \square dx_{b,k} dA_b$$

The physical meaning of the above equations is simple: every elementary portion of incoming or outgoing mass carries an energy content equal to its enthalpy²; heat in- and outfluxes can be expressed as product of an equivalent transmittance of the system/environment interface times an appropriate temperature difference across each diabatic portion of the boundary³; work can be expressed as an “equivalent force” due to a local pressure difference at the boundary times the local displacement of the boundary in the direction of the (local) normal versor.

c) Entropy in- and outflows, irreversible entropy generation

The entropy balance can be derived along the same line of reasoning: neglecting here again the contribution of chemical reactions, the variation of the total entropy of A is the result of material and immaterial convection, heat exchange at the boundary, and entropy generation inside of A:

$$\begin{aligned} s_{in,conv,j} &= \int_b m_{in,j} s_{in,j} dA_b \\ s_{out,conv,k} &= \int_b m_{out,k} s_{out,k} dA_b \end{aligned} \quad (10)$$

² Total enthalpy, if we include kinetic energy (often negligible in practical cases)

³ By selecting proper expressions for \square and $\square T$, this simple formalism can be used to include heat exchanges due to convection and radiation.

$$s_{in,heat,j} = \int_b \frac{q_{in,j}}{T_{in,j}} dA_b = \int_b \frac{A_j \Delta T_{b,j}}{T_{in,j}} dA_b \quad (11)$$

$$s_{out,heat,k} = \int_b \frac{q_{out,k}}{T_{out,k}} dA_b = \int_b \frac{A_k \Delta T_{b,k}}{T_{out,k}} dA_b$$

$$\dot{S}_{irr} = \dot{S}_{ext} + \int_{V_A} \sigma dV \quad (12)$$

The physical meaning of the above equations is also clear: every elementary portion of incoming or outgoing mass carries an entropy content; heat in- and outfluxes contribute to the global entropy balance each according to an appropriate temperature difference across the respective diabatic portions of the boundary; and the irreversible entropy generation consists of two terms: the first is purely internal and takes place over the entire volume of A, while the second accounts for possible effects of A on the surroundings.

d) Exergy in- and outflows, exergy destruction

Exergy is not a conserved quantity, but its equation can be written in a “conservative form” by introducing a fictitious term, the *exergy destruction*, which is not a physical flux but rather a convenient mathematical artefact. However, this exergy destruction does have a physical meaning, in that it measures the energy degradation (dispersion) in the process. Neglecting again the contribution due to chemical reactions, we have:

$$ex_{in,conv,j} = \int_b m_{in,j} ex_{in,j} dA_b \quad (13)$$

$$ex_{out,conv,k} = \int_b m_{out,k} ex_{out,k} dA_b$$

$$ex_{in,heat,j} = \int_b f(T_{in,j}, T_0) q_{in,j} dA_b = \int_b f(T_{in,j}, T_0) A_j \Delta T_{b,j} dA_b$$

$$ex_{out,heat,k} = \int_b f(T_{out,k}, T_0) q_{out,k} dA_b = \int_b f(T_{out,k}, T_0) A_k \Delta T_{k,b} dA_b \quad (14)$$

$$ex_{in,work,j} = \int_b \Delta p_{b,j} dx_{b,j} dA_b \quad (15)$$

$$ex_{out,work,k} = \int_b \Delta p_{k,b} dx_{b,k} dA_b$$

The factor f is the so-called exergetic factor, and takes a different form for conduction/convection (for which it is equal to the Carnot factor $1 - T_0/T_j$) and radiation (for which it is equal

$$\text{to } 1 + \frac{\left(\frac{T_0}{T_j}\right)^4}{3} - \frac{4T_0}{3T_j} \quad [22]).$$

Equations (5-15) reveal by inspection the difficulty in closing the system of equations (1-4): even in the assumption of perfectly specified boundary conditions, the general balance equations depend on the *internal behaviour* of the system, because the rates of mass and energy exchange are dictated not only by the “layer” of the system that is in immediate contact with the environment through its boundary, but from the interactions among the internal “cells” in which we imagine to subdivide A. This suggests that a “lumped” treatment may be more appropriate for a useful description of the system’s behaviour.

THE EXERGY COST OF A PROCESS

Let us consider the exergy flow diagram of the system under study (figure 3): we shall follow Tsatsaronis’ notation [34], and

denote by “F” the exergy inputs, by “P” the “products” of the system, and by “W” its byproducts (unused discharges into the environment): from the exergy equation we derive a measure of the exergy destruction (overdots omitted from now on):

$$Ex_{\delta}(t) = F(t) - P(t) - W(t) \quad (16)$$

With the additional stipulation that P(t) includes the “products” internally incorporated by A at time t , i.e., those that contribute to its growth: conversely, a positive difference between W(t) and P(t), for a fixed F(t) denotes a “shrinking” system. At any instant t , the conversion efficiency of A is given by:

$$\eta_A(t) = \frac{P(t)}{F(t)} \quad (17)$$

And the exergetic cost of the products is the reciprocal of the efficiency:

$$c_A(t) = \frac{F(t)}{P(t)} \quad (18)$$

Thus, provided we have a complete knowledge of the input flows F and of the instantaneous mode of operation of A, equation (18) provides a measure of how many exergy “units” of fuel are embodied in every exergy unit of product.

Since it is unlikely that all “fuels” reach the boundary of A directly from the environment, without any previous treatment, it is necessary to backtrack the production process of each one of them, to compute its own exergy cost: this backtracking comes to a halt when all inputs have been assigned a valid equivalent primary exergy value (content). This procedure was proposed by Szargut [32] and results in the calculation of the Cumulative Exergy Content (CEC) of a product: provided a sufficiently disaggregated database is available, equation (18) can be computed at any instant of time. The “cost” thus calculated represents *the amount of primary exergy “embodied” in the product*, and is a rational measure of the load placed by A on the environment at any instant of its (technical or real) life.

But the picture is not yet complete: some of the effluents (cumulatively represented by the flux W) may be discharged in a physical state different than their respective “environmental conditions” (for example, they may consist of a material discharge at $T \neq T_0$ and $c \neq c_0$). This poses an additional “load” on the environment, which must use a portion of the primary exergy it can avail itself of (chemical, kinetic, radiative...) to exert some buffering action and reduce each discharge to its environmental state. The amount of exergy necessary for the buffering can be calculated if we know the processes involved: if a chemical reaction is required, its activation exergy is the additional cost; if a heat exchange is needed, the exergy of the corresponding amount of thermal exergy is the cost, and so on. If the system under consideration is artificial (of anthropic origin), a substantial portion of the effluent treatment is enforced by means of technical “pollution abatement” devices located downstream of the main process: here, the calculation of the extra exergy cost (called *environmental remediation cost*) requires an additional process analysis of the effluent treatment system: since technical pollution abatement is never complete, but inevitably relies on some amount of environmental buffering, the “technical” cost c must usually be augmented by the cost c' of the residual treatment performed by the biosphere. In principle, it is always possible to calculate this additional exergy requirement F'^4 that must be considered as an added cost of the product P:

⁴ In real cases, the calculation of F' is not so simple as represented here, because the “remedial action” takes place not at time t , but with an obvious delay: we shall neglect this effect here, and consider that F' can be “allocated” properly over the relevant time windows.

$$c_{tot,A}(t) = c_A(t) + c'_A(t) + c''_A(t) = \frac{F(t)+F'(t)+F''(t)}{P(t)} = \frac{F_{tot}(t)}{P(t)} \quad (19)$$

THE CONCEPT OF EXTENDED EXERGY

The cost defined by equation (19) is expressed in units of $\text{kJ}_{\text{fuel}}/\text{kJ}_{\text{product}}$, and constitutes a significant indicator of environmental load: if a product P is generated by two different production chains A_1 and A_2 , the one with the lower value of the $\int c_{tot}(t)dt$ over its entire lifetime is the more environmentally benign (less unsustainable) process. Notice that the rather simple considerations developed so far result in a proper internalization of the so-called *environmental externalities*, whose exergy cost is reallocated to the products of A.

In technical systems, the economic side must also be taken into account: several methods exist, and the most rigorous from a thermodynamic point of view is the Thermo-Economic costing, in which a monetary cost is assigned to the unit of exergy of fuels, products and discharges. [2,13,18,35,36,37 and in other papers in this Panel] present a complete and rigorous treatment of the underlying theory and demonstrate several engineering applications. The approach we propose here is though somewhat different: since the cost expressed by equation (19) represents the primary equivalent exergy embodied in the product and already includes the environmental externality, is it possible to devise a similar treatment for the remaining externalities, namely Labour and Capital? The answer is affirmative, and the method, called Extended Exergy Accounting (EEA), has been presented and discussed in several papers [25,26,31]. EEA computes the primary exergy equivalents of Labour (ee_L , in $\text{kJ}/\text{workhour}$) and Capital (ee_K , in $\text{kJ}/\text{€}$) on the basis of two econometric coefficients: the first (α) is derived from the *pro-capite* exergy consumption in the society within which the technical process A is operating and the second (β) from the society capital intensity, measured by a monetary circulation indicator, usually M2 (also called “money plus quasi-money). Though the procedure adopted in EEA to calculate the primary equivalents of Labour and Capital has been subjected to some criticism, we shall not address this point in the present discussion, and not delve into the numerical values of these equivalents, but assume that they can be calculated in an accurate and reproducible way [25]. Once $c_L=f(ee_L)$ and $c_K=f(ee_K)$ are known, both labour and capital expenses can be expressed in primary exergy units and included in the exergy flow diagrams as “fuels”: the final result is that an extended exergy cost can be assigned to any product P:

$$c_{ee,A}(t) = c_A(t) + c'_A(t) + c''_A(t) + c_L(t) + c_K(t) = \frac{F_{tot}(t)+F_L(t)+F_K(t)}{P(t)} \quad (20)$$

The extended exergy cost defined by equation (20) is based solely on thermodynamic concepts, and is the most comprehensive indicator of environmental load: it includes the total amount of primary exergy embodied in the product, including the production chain “from mine to dump”, and considering also the equivalent primary exergy required by the workers’ consumptions standards. It can therefore be regarded as the *exergy footprint* of product P, a rigorous EI measured in

kJ/kJ and rooted both in system analysis and thermodynamic principles.

Obviously, the approach just described identifies c_{ee} as a *global* EI, because the environmental effects it considers concern the entire production chain and thus a large portion of the biosphere (the mine can be located very far away from the conversion plant, and the latter very far away from the final user, so that the environmental impact that must be remedied affect areas only remotely connected with the location where the product is used). But in a broader vision of a globally interconnected biosphere [4,17] it is clear that c_{ee} can be correctly applied to the analysis of systems also at a local scale. In the EEA method, it suffices to have access to a properly disaggregated database that allows for the calculation of the CEC of all the “fuels” entering the system under consideration. If such a database is not available, the non-negligible effort necessary to compute these CEC anew brings a substantial payback, in that it leads to a consistent and rigorous calculation of the total environmental load placed by the system on the environment. For anthropic systems, yet an additional complication is posed by the calculation of the primary exergy equivalents of Labour and Capital (ee_L and ee_K), but again the benefit in terms of the reproducibility and of the coherence of the approach is more than worth the effort. EEA analyses of several individual processes and industrial/societal sectors have been performed in the last few years, and they consistently lead to a deeper insight of the exergy dynamics sustaining the system operation. Most of the published studies of the more complex systems were performed at steady state, due to the difficulty of obtaining reliable time series for the large amount of data needed for the analysis, but as the database is incrementally augmented, it becomes possible to attempt comparative studies about non-steady situations.

METHODOLOGY

The calculation of the follows the same lines as any exergy analysis, with a couple of additional steps:

- Obtain a detailed exergy flow diagram of the system (mass and energy balances are a required input);
- Compute the CExC of all the fuels. For imports (e.g., electricity imported from another country) the respective production chain must be analyzed;
- Derive the econometric coefficients necessary for the calculation of ee_L and ee_K . For imports (e.g., materials imported from another country), the econometric coefficients must refer to the country of origin;
- Add the costs of externalities. For fuels, simply add the terms $L*ee_L$ and $K*ee_K$ to the CExC, where L are the total workhours and K the capital involved in the production of the fuel. For the environmental cost, add for each effluent the product of its respective c' and c'' by the effluent exergy.

EXAMPLES OF APPLICATION

As previously mentioned, several applications of the EEA method have been published in the archival literature. Processes assessed or re-assessed by means of an EEA analysis include the analysis of an academic institution [3]; the analysis of a transient in a gas turbine plant [5]; the production process of a commercial truck [7]; an innovative CO_2 capture process [8]; gas-flaring in oil extraction [12]; a comparison of different desalination technologies [15]; the nuclear fuel extraction and

processing [21]; a comparative study of six different methods of hydrogen production [24]; biodiesel recovery from spent oils [33]. Additionally, EEA analysis of societal systems were published for China [6]; the Chinese transportation and agricultural sectors [9]; Norway [14]; England [16]; Italy [20]; the Netherlands [23]; the Turkish transportation and wastewater sector [30]; Turkey [31]. More recently, EEA analyses of living systems have been performed [28,29].

All applications demonstrate that the EEA results provide additional insight in the thermodynamic intensity of the internal flows in a process (or in a society) and result in useful information about possible improvements that may be obtained by reducing the primary exergy consumption for a prescribed output. The exergy cost indicator c_{ee} defined above represents therefore a proper Environmental Indicator (the use of C_{ee} as an *exergy footprint* was proposed for it [27]) and its use ought to be encouraged in the assessment of alternative scenarios towards a lower degree of unsustainability.

CONCLUSIONS

An elementary lumped analysis of a generic energy conversion system, intended in its broadest sense of “any system that operates by converting energy forms into one other”, performed by means of an exergy analysis paradigm, leads to the conclusion that from a technical point of view it is always possible to calculate the primary equivalent exergy embodied in a product or products: an exergy cost is defined as the ratio of the total embodied exergy to the cumulative production, in a life-cycle sense (i.e., integrated over time and space). Then, on the basis of the assumption that the equivalent primary exergy content of the remaining externalities (Labour and Capital) can also be computed, a novel indicator, the extended specific exergy cost c_{ee} , is defined. This indicator possesses all the requisites requested of an Environmental Indicator, and -while including *global effects*- it can be applied at a *local level*, to assess and compare individual processes, industrial sectors or entire societies. This indicator represents a useful and thermodynamically correct measure of the absolute (primary) consumption of exergy in a process, and may therefore be used as a measure of the degree of unsustainability of the process itself.

REFERENCES

- [1] S.Bastianoni et al., 2008: *Exergy and extended exergy accounting of very large complex systems with an application to the province of Siena, Italy*, J.Env. Management, v.86, n.2
- [2] A.Bejan, G.Tsatsaronis, M.J.Moran, 1996: *Thermal Design and Optimisation*, J.Wiley.
- [3] M.Belli, E.Sciubba, 2007: *Extended Exergy Accounting as a general method for assessing the primary resource consumption of Social and Industrial systems*. IJEX, v.4, n.4
- [4] K.Boulding, 1966: *The Economics of the Coming Spaceship Earth*, Proc. VI “Resources for the Future” Forum on Environmental Quality in a Growing Economy, Washington, D.C., March 8, 1966
- [5] S.Cennerilli et al., 2009: *Extended Exergy Analysis of the Response of a Gas Turbine Process to Variations in the Turbine Inlet Temperature*, Proc. ECOS’09, Foz de Iguazu, Brasil
- [6] B.Chen, G.Q.Chen, 2007: *Ecological footprint accounting and analysis of the Chinese Society 1981-2001 based on embodied exergy*, Ecological Economics, 61 (2-3)
- [7] E.Cheremnykh, F.Gori, 2010: *Exergy and Extended Exergy cost assessment of a commercial truck*, Proc. ASME-IMECE 2010, Vancouver, Canada
- [8] A.Corrado et al., 2004: *Environmental assessment and extended exergy analysis of a “zero CO₂ emission”, high-efficiency steam power plant*, Proc. ECOS’04, Guanajuato, Mexico
- [9] J.Dai, B.Chen, 2010: *Extended exergy-based ecological accounting of China during 2000-2007*, Int. Congr. Environmental Modelling and Software, Fifth Biennial Meeting, Ottawa, Canada, July 5-8
- [10] Y.Demirel
- [11] J.Dewulf et al., 2008: *Exergy: its potential and limitations in Environmental Science and Technology*. Env. Sci. & Technology 42 (7)
- [12] S.E.Diaz-Mendez et al., 2012: *Extended exergy accounting applied to the flaring practice in oil fields*, IJEX v.10,n.4
- [13] Y.M.El-Sayed, 2003: *The Thermo-Economics of energy conversion*, Elsevier,
- [14] I.Estervåg, 2003: *Energy, exergy, and extended-exergy analysis of the Norwegian society*. Energy 25
- [15] P.Fiorini et al., 2006: *Economic Comparison of Small Solar-Powered Desalination Plants*, Proc. ECOS’06, Gliwice, Poland
- [16] A.Gasparatos et al., 2008: *Assessing the sustainability of the UK society using thermodynamic concepts: Part 2*, Renewable & Sustainable Energy Reviews
- [17] J.J. Kay, 2002: *On complexity theory, exergy, and industrial ecology*, in Kibert, Sendzimir & Guy Eds, Construction Ecology: Nature as a Basis for Green Buildings, Spon Press
- [18] T.Kotas, 1985: *The exergy method of thermal plant analysis*, Butterworths, Academic Press, London
- [19] G.Lebon, D.Jou, J.Casas-Vázquez, 2008: *Understanding Nonequilibrium Thermodynamics*, Springer Berlin
- [20] D.Milia, E.Sciubba, 2006: *Exergy-based lumped simulation of complex systems: An interactive analysis tool*, Energy, v.31, n.1
- [21] G.Orsini, E.Sciubba, *Exergy Life-Cycle Analysis of the Uranium Cycle. Part 1: From Uranium Ore to Nuclear Fuel*. Proc. ECOS’2010, Lausanne, Switzerland
- [22] R.Petela, 1964: *The exergy of heat radiation*, J. Heat Transfer v.86, n.2
- [23] K.Ptasinski et al., 2006: *Performance of the Dutch Energy Sector based on energy, exergy and Extended Exergy Accounting*. Energy 31
- [24] R.Ridolfi et al., 2008: *A multi-criteria assessment of six energy conversion processes for H₂ production*, Int. J. Hydr. Energy, v.34, n.12.
- [25] E.Sciubba, 2001: *Beyond thermoeconomics? The concept of Extended Exergy Accounting and its application to the analysis and design of thermal systems*. Exergy, The International Journal 1 (2):68-84. 2001.
- [26] E.Sciubba, 2004: *From Engineering Economics to Extended Exergy Accounting: A Possible Path from “Monetary” to “Resource-Based” Costing*, J. Ind. Ecology, v.8, n.4

- [27] E.Sciubba, 2012: *An exergy-based Ecological Indicator as a measure of our resource use footprint*, IJEx v.10, n.3
- [28] E.Sciubba, F.Zullo, 2011: *Exergy-based population dynamics: A thermodynamic view of the "sustainability" concept*. J. Ind. Ecol., 15, 172–184
- [29] E.Sciubba, F.Zullo, 2012: *An Exergy-Based Model For Population Dynamics: Adaptation, Mutualism, Commensalism And Selective Extinction*, Sustainability, 4, 2611-2629
- [30] C.Seçkin et al., 2012: *Resource Use Evaluation of Turkish transportation Sector via the Extended Exergy Accounting Method*, Proc. ECOS 2012, U.Desideri, G.Manfrida, E.Sciubba Eds., Perugia, July 2012
- [31] C.Seçkin et al., 2012: *An application of the Extended Exergy Accounting method to the Turkish Society, year 2006*, Energy v.40, n.1, 151–163
- [32] J.Szargut, 2005: *The Exergy Method: Technical and Ecological Applications*, WIT press, Southampton, England
- [33] L.Talens-Peiro et al., 2010: *Extended Exergy Accounting applied to Biodiesel production*, Energy 35
- [34] G.Tsatsaronis, M.Winhold, 1985: *Exergoeconomic Analysis and Evaluation of Energy Conversion Plants. Part I-A New General Methodology*, Energy-The International J. v.10 n. 1
- [35] A.Valero et al., 1986: *A general theory of exergy saving. I. On the exergetic cost*, Proc. ASME-WAM, Anaheim, California, v.3 - Second law analysis and modelling
- [36] A.Valero et al., 1986: *A general theory of exergy saving. II. On the thermoeconomic cost*, Proc. ASME-WAM, Anaheim, California, v.3 - Second law analysis and modelling
- [37] A.Valero et al., 1986: *A general theory of exergy saving. III. Energy saving and thermo-economics*, Proc. ASME-WAM, Anaheim, California, v.3 - Second law analysis and modelling

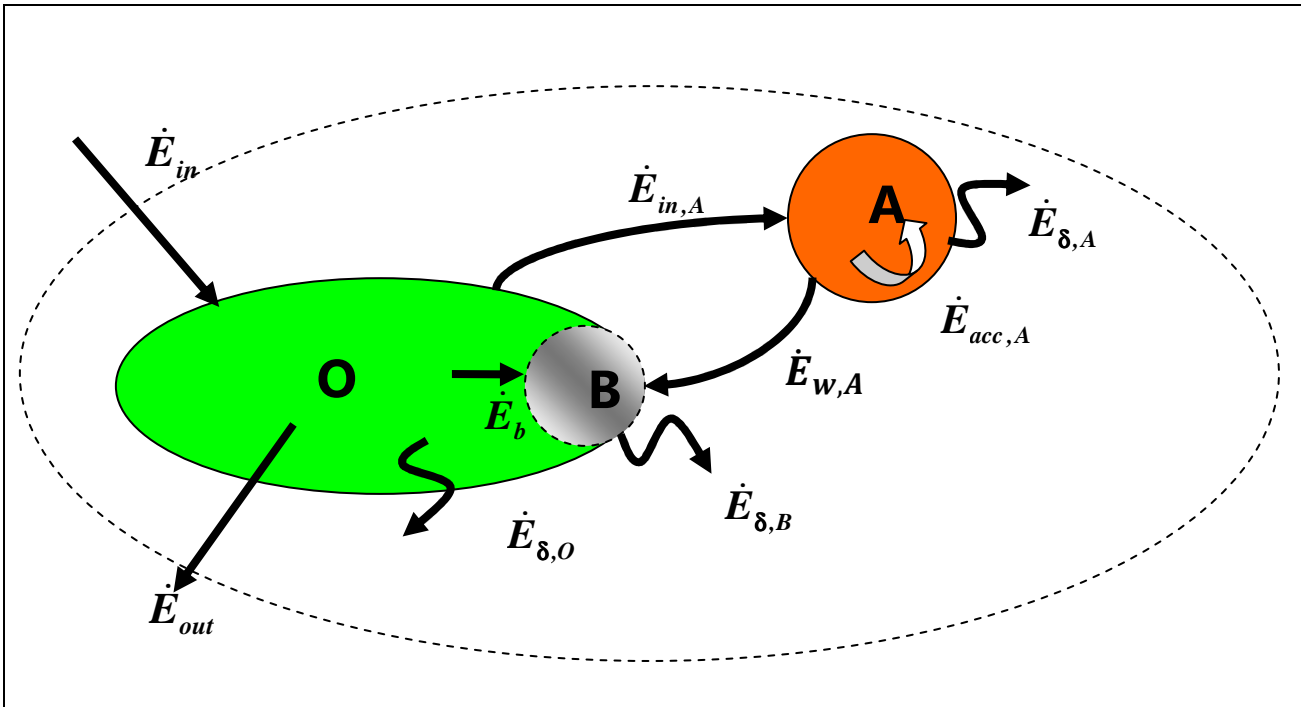


Figure 1 – Possible evolution of a system **A** interacting with a reference environment **O**

Legenda: **O**=reference environment; **B**=buffering portion of **O**; \dot{E}_{in} , \dot{E}_{out} =net exergy input and output in **O**; \dot{E}_b =buffering exergy (see text); $\dot{E}_{in,A}$ =exergy flux from **O** to **A**; $\dot{E}_{acc,A}$ =exergy accumulation rate in **A**; $\dot{E}_{w,A}$ =exergy discharge from **A**; \dot{E}_{δ} =exergy destruction rate

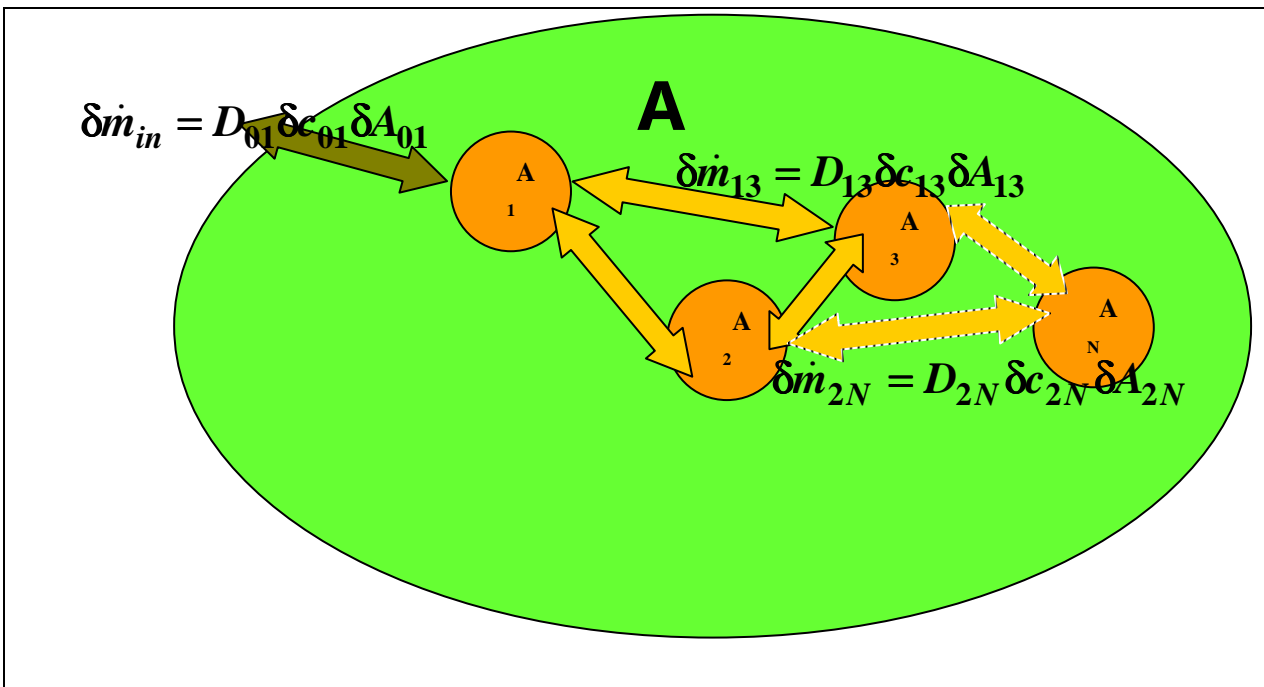


Figure 2 – Schematic representation of internal complex diffusion chains

Legenda: $\cdot A_{ij}$ = permeable contact area; $\cdot c_{ij}$ = concentration gradient; D_{ij} = Diffusion coefficient

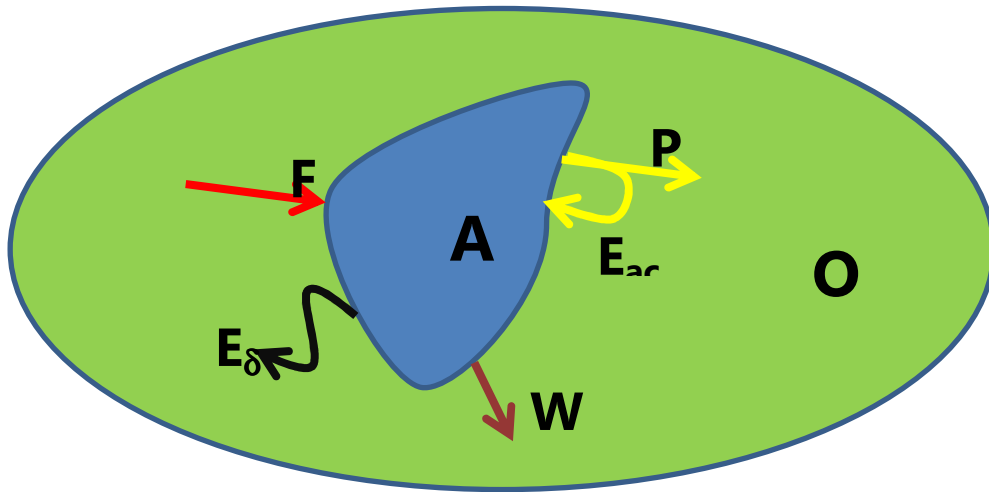


Figure 3 – Exergy flow diagram for a generic system

ADVANCED EXERGY-BASED METHODS

George Tsatsaronis

Institute for Energy Engineering, Technische Universität Berlin
Marchstrasse. 18, 10587 Berlin, Germany, email: tsatsaronis@iet.tu-berlin.de

EXTENDED ABSTRACT

An exergetic analysis identifies the location, magnitude, and sources of thermodynamic inefficiencies in an energy conversion system. This information is used for improving the thermodynamic performance and for comparing various systems [1]. In addition, an exergetic analysis forms the basis for the exergoeconomic [1] and exergoenvironmental [2] analyses. These two analyses (including an exergetic analysis) are called exergy-based methods.

A so-called *conventional* exergetic analysis does not consider the interactions among the components of a system and the real potential for improving the system. These effects can be estimated and the quality of the conclusions obtained from an exergetic evaluation is improved, when for each important system component the value of the exergy destruction is split into endogenous/exogenous [3] and avoidable/unavoidable [4] parts. We call the analyses employing such a splitting *advanced exergetic analysis*.

Endogenous exergy destruction is the part of exergy destruction within a component obtained when all other components operate ideally and only the component being considered operates with the same efficiency as in the real system. The *exogenous* part of the exergy destruction is the difference between the value of total exergy destruction within the component in the real system and the endogenous part.

The *unavoidable* exergy destruction cannot be further reduced in the foreseeable future due to technological limitations such as availability and cost of materials and manufacturing methods. The difference between total and unavoidable exergy destruction for a component is the *avoidable* exergy destruction. Improvement efforts should be focus only on *avoidable* exergy destructions, costs, and environmental impacts.

In analogy to the advanced exergetic analysis, an exergoeconomic and an exergoenvironmental analysis can be conducted by considering separately the endogenous / exogenous and the avoidable / unavoidable costs and environmental impacts. In this way we obtain a consistent evaluation of a system from the viewpoints of thermodynamics, economics, and environmental protection. All evaluations are conducted using consistent definitions for *exergy of fuel* [5], *cost of fuel*, *environmental impact associated with the fuel*, *exergy of product* [5], *cost of product*, and *environmental impact associated with the product*.

The presentation will demonstrate how advanced analyses, including exergetic, exergoeconomic, and exergoenvironmental analyses, provide the user with information on the formation processes and the sources of thermodynamic inefficiencies, costs, and environmental impacts [6], and how they can enhance the creativity of engineers to develop ways for their minimization.

REFERENCES

- [1] A. Bejan, G. Tsatsaronis and M. Moran. Thermal Design and Optimization (New York: John Wiley & Sons, 1996).
- [2] Meyer L., Tsatsaronis G., Buchgeister J., Schebek L. (2009) Exergoenvironmental Analysis for Evaluation of the Environmental Impact of Energy Conversion Systems. Energy – The International Journal, Vol. 34, pp. 75-89.
- [3] Kelly S, Tsatsaronis G, Morosuk T. Advanced exergetic analysis: Approaches for splitting the exergy destruction into endogenous and exogenous parts. Energy – The International Journal, 2009, Vol. 34, pp. 384-391.
- [4] G. Tsatsaronis and M.-H. Park. On avoidable and unavoidable exergy destructions and investment costs in thermal systems. Energy Conversion and Management, 43 (2002), 1259-70.
- [5] Lazzaretto A., Tsatsaronis G. (2006) SPECO: A systematic and general methodology for calculating efficiencies and costs in thermal systems. Energy – The International Journal, Vol.31, No.8-9, pp.1257-1289.
- [6] Tsatsaronis, G., 2011. Exergoeconomics and Exergoenvironmental Analysis, Bakshi, B.R., Gutowski, T.G., Sekulic, D.P. (Eds.) Thermodynamics and the Destruction of Resources, Cambridge University Press, New York, Chapter 15, pp. 377–401.

THERMODYNAMIC ACCOUNTING OF THE GLOBAL DEPLETION OF THE MINERAL CAPITAL ON EARTH. A PROPOSAL TO THE U.N.

Antonio Valero* and Alicia Valero*

* CIRCE – Research Centre for Energy Resources and Consumption, Universidad de Zaragoza, Mariano Esquillor 15, 50018 Zaragoza, 4 Spain

ABSTRACT

Thermodynamics can be used as tool for accounting scarcity, unavailability and dispersion of minerals. If a mine is a very improbable occurrence in the Earth's Crust, exergy and its parent concept of replacement exergy cost, could be used and accounted for to make a systematic inventory of the loss of Mineral Capital on Earth. For calculating exergy resources the authors proposed a model of the Planet Earth, namely Thanatia. It hypothetically would consist of a planet totally exhausted of minerals in the crust and completely decimated by climate change in its atmosphere and hydrosphere. Mineral exergy resources are calculated as a function of quantity, composition and ore grade. In this way exergy constitutes a universal, objective and useful tool for assessing resources depletion. Presented over time, it could provide the velocity at which extraction of each and every mineral resource is occurring. The methodology and a case study are briefly presented. The authors propose that the United Nations System of Environmental-Economic Accounting (SEEA) and its global framework would be the best world infrastructure to convert the replacement cost accounts into a Global System of Environmental-Thermo-Economic Accounts (SETEA). In such a way, "Thermodynamic accounting of mineral resources" may play an important role in the global management of the natural resources of the Planet.

INTRODUCTION

The message of Thermodynamics is universal in the sense of it permeates any physical phenomena, but also in the sense of space and time. It covers and explains the whole Planet at any moment in history when time intervals are sufficiently large to reach stabilizations, patterns of change or equilibriums. That is in contrast to transport phenomena sciences like fluid mechanics, or in another realm, finances that describe short time-dependent behaviours.

Economics is a science to live with in the short term. Money is always depreciating and historically no money survived more than the power of the country supporting it. We cannot rely on Economics to have a historical perspective of Man in this planet. Degradation, dissipation, deterioration, entropy, time's arrow and Second Law are thermodynamic concepts, not economic ones. Notwithstanding, economists, social scientists and policy makers use these terms quite freely and metaphorically, not as an accounting instrument. The global and temporal perspective of our troubled planet can only be understood with the help of Thermodynamics. Thermodynamics is the Economy of Physics.

Two global problems concern responsible men about this planet: Destruction and degradation of ecosystems (biotic resources), and the problem of depletion of mineral resources and materials dissipation in the Planet (abiotic resources).

Our hypothesis is that Thermodynamics can be used as tool for accounting scarcity, unavailability and dispersion of minerals. This approach has not sufficiently considered as an important problem to be studied from a thermodynamic point of view. However, a mine is a very improbable occurrence in the Earth's crust and exergy can be used and accounted for to make a systematic inventory of the loss of Mineral Capital on Earth.

This paper deals with it. It proposes a thermodynamic theory for calculating the annual loss of Mineral Capital on the Earth by using as numeraire, the exergy and replacement exergy cost of mines and minerals.

THE STARTING POINT: THANATIA

The exergy value of any system depends on its intensive properties and the chosen reference environment (RE). Mines, rivers, glaciers, or clouds are natural resources which have exergy. However if we do not care about the reference state, the exergy number one obtains may have nonsense. It is important to distinguish between "exergy" and "exergy resource". In other words, it is critical to choose an appropriate RE to give full sense to the exergy and exergy cost values associated to natural resources.

In 2011, the authors proposed a model of the Planet Earth, namely Thanatia. It hypothetically would consist of a Planet totally exhausted of minerals in the crust and completely decimated by climate change in its atmosphere and hydrosphere. See refs [1] and [2].

Thanatia is a guess thermodynamic model for a terrestrial "grave", where all fossil fuels have been burned and converted into CO₂ and with the absence of concentrated mineral deposits. The resulting degraded atmosphere has a carbon dioxide content of 683 ppm and a mean surface temperature of 17°C. The degraded hydrosphere is assumed to have the current chemical composition of seawater at 17°C. For the upper continental crust, the authors proposed a model which includes composition and concentration of the 294 most abundant minerals currently found on Earth as bare rocks.

In this sense, Thanatia constitutes a coherent baseline for the assessment of mineral resources in exergy terms. Any

substance like mineral deposits or the poles are exergy resources with respect to Thanatia.

Note that Thanatia itself has exergy to some other reference environment like that of the conventional Szargut's RE [3]. Therefore it is not in itself another alternative RE as others profusely published. Thanatia is in fact an imaginary degraded planet that our civilization could smoothly but surely approach, but in the authors hope it will be never reached. (Thanatos means death in Greek). On the other hand, it is a consistent tool sufficient for providing coherent calculations.

EXERGY AND EXERGY COSTS

Once defined the baseline, exergy may be assessed depending on the properties that the resource is considered valuable, such as quantity, composition and ore grade. In this way exergy constitutes a universal, objective and useful tool for assessing resources depletion. Presented over time, it could provide the velocity at which extraction of each and every mineral resource is occurring. The exergy of a mineral resource has at least three components: chemical composition, concentration and cohesion. The chemical exergy of a mineral is equivalent to the minimum energy required to form the minerals from the substances in Thanatia and is given in Eq. 1:

$$b_{ch} = \sum \nu_k b_{chel,k}^0 + \Delta G_{\text{mineral}} \quad (1)$$

where $b_{chel,k}^0$ is the standard chemical exergy of the elements that compose the mineral, ν_k is the number of moles of element k in the mineral and ΔG is the Gibbs free energy of the mineral.

Since Thanatia contains virtually every mineral found in the crust, the chemical exergy of the minerals from that reference is zero (as they do not need to be constructed).

As opposed to chemical exergy, concentration exergy expresses the minimum energy required to concentrate the given mineral from the depleted state in Thanatia to the conditions found in the mine (with the specific ore grade). The concentration exergy is calculated with Eq. 2:

$$b_c = -\overline{R}T_0 \left[\ln(x_i) + \frac{(1-x_i)}{x_i} \ln(1-x_i) \right] \quad (2)$$

where R is the universal gas constant (8.314 kJ/kmolK), T_0 is the temperature of the reference environment (298.15 K) and x_i is the concentration of the substance i . The exergy accounting of mineral resources implies to know the ore grade which is the average mineral concentration in a mine x_m as well as the average concentration in the Earth's crust (in Thanatia) x_c . The value of x in Eq. 2 is replaced by x_c or x_m to obtain their respective exergies, whilst the difference between them represents the minimum energy (exergy) required to form the mineral from the concentration in the Earth's crust to the concentration in the mineral deposits.

However, Eq.2 is only strictly valid for ideal mixtures such as solids where there is no chemical cohesion among the substances. But cohesion energy is always present in any mineral. Thus Eq.2 would only strictly remain valid for the exergy of a mixture, and not for the exergy needed to break the binding forces among solids such as hydrogen, hydration, ionic and/or covalent bonds. Such forces are sufficiently strong enough to require physical comminution processes like crushing, grinding, or milling. Therefore, there is an important

factor missing in the characterisation, namely the comminution exergy, i.e. the minimum energy required to bind the solids from the dispersed state conditions of Thanatia to those in the mineral deposits. Nevertheless, in [4], the authors demonstrated that comminution is a very energy intensive process when it comes to fine grinding and milling operations but is not so relevant in crushing operations and becomes negligible when evaluating the Mineral loss of Capital on Earth. This is why only the concentration exergy term is taken into account when assessing the Mineral Capital on Earth.

It should be stated though that since exergy is assessed only supposing reversible processes, the numbers obtained are paradoxically far from expected. Hence, we need to complement it with actual exergy costs (kJ), which represent the sum of all *actual* exergy resources that would be required if we were to replace a mineral from Thanatia (or grave) to the conditions actually found in nature (or cradle). This calculation assumes that the same "backup" technologies are applied in the imaginary process from Thanatia to the mine (grave to cradle stage) than in the mine to industry (cradle to gate stage). Therefore Life Cycle Assessments of mining to industry processes become essential for assessing costs, which are calculated with Eq. 3:

$$b_{ci}^* = k_c \cdot b_{ci} \quad (3)$$

where k_c is a constant called unit exergy cost and is the ratio between the real energy required for the real process to concentrate the mineral from the ore grade x_m to the refining grade x_r and the minimum thermodynamic exergy required to accomplish the same process (Eq. 4).

$$k_c = \frac{E_{\text{realprocess}}}{\Delta b_{\text{mineral } x_m \rightarrow x_r}} \quad (4)$$

Since the energy required for mining is a function of the ore grade of the mine and the technology used, so it is the unit exergy cost.

Then, the exergy cost of concentrating a mineral from the Earth's crust is named exergy replacement cost. Table 1 shows typical values for x_c , x_m , k_c and exergy replacement costs for key minerals.

All proposed concepts, Thanatia, exergy resource and exergy replacement cost are solidly based on the Second Law.

The exergy and exergy replacement costs provide a measure for quantifying this degradation, which is systematically being ignored in conventional accounting systems.

CASE STUDY

As the method provides values in energy units, the annual exergy decrease in the mineral endowment of the planet can now take into account the fossil fuel's exergy plus the losses in nonfuel exergy replacement costs.

As a case study, the exergy replacement costs due to the extraction of minerals in 2008 are explored. The figures reported by the US Geological Survey concerning annual commodity production are considered [5], together with the

exergy replacement costs values calculated and shown in Table 1.

According to the authors' calculations, the exergy replacement costs associated to the 2008 production of the studied minerals is equal to 5.3 Gtoe. It is worth to note that conventional economics only accounts for the energy required in the extraction and refining processes. In the case of the materials studied, these account for around 9% of the total world fossil fuel produced in year 2008 (see Fig. 1).

Nevertheless a fair accountability of resources should also take into account the use and the decrease of the non-fuel mineral capital endowment. This means that the true yearly balance of the exergy decrease in the mineral endowment of the planet should account for at least, the exergy of fossil fuels world production plus the loss of the mineral exergy replacement costs of the non-fuel minerals. As can be seen in Fig. 2, this accounts for 32% of the whole energy stages, if the cradle to grave stage is taken into account. This is a considerable and unexpected percentage since it has the same order of magnitude as the yearly loss of coal, oil or natural gas.

But these minerals are not lost at all. Only those that are not recycled and are not in use (in-use-stock) become really lost. Considering the same recycling ratios for the whole world as in the US [5], means that from the total exergy replacement costs of the minerals extracted, only 72% is either lost or yet in use, i.e. around 3.8 Gtoe. Unfortunately only mass consumable metals like steel, aluminium, copper and few others are recycled in rates no greater than 50-60% worldwide. The same happens with precious metals[6]. Adding the exergy of the fossil fuels used in the extraction and processing of the minerals, we obtain that the total exergy expenditure due to mineral production in 2008 was equal to 5.3 Gtoe. It should be stated that only 37 minerals have been considered.

Hence, the previous reported value would increase, if all mineral commodities were to be included in the analysis.

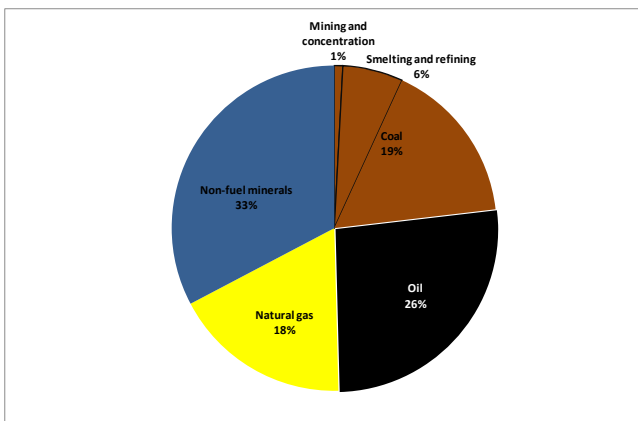


Fig 2: Distribution of the exergy costs associated to the 2008 world production of the main mineral commodities

FROM SEEA TO A GLOBAL SYSTEM OF ENVIRONMENTAL-THERMO-ECONOMIC ACCOUNTS.

The depletion of a mineral should not be more the difference between its world price and its economic cost of production as economists propose. On the contrary, it should be assessed as the loss of reserves quantified through its replacement cost with current best available technologies,

from the bare rock to the ore grade conditions of the mine. This depletion indicator can be used for all fossil fuels and minerals no matter their chemical composition and concentration. Fossil fuels must be replaced with renewable energy sources and this replacement need to be accounted for such progress. In the same way, stopping depletion of metals will largely come from greater resource-efficient techniques such as designing for recyclability, reducing the number of alloys used, avoiding the design of monstrous hybrids, [7] designing for disassembly, symbiosis of industrial complexes, increasing the efficiency of smelters to avoid metal losses in slags, increasing the throughput of scrap, etc.[8].

Conservation means, in fact, avoided replacement. Actually, the cost of replacement is a mind barrier for hampering deliberate destructions. Indeed, one can associate a cost of replacement to each and every conservation act, not only to mineral resources but, more in general, to any natural resource. The more irreplaceable an object is the stronger will be the need for its conservation. Irrecoverability would need eternal conservation. Accounting replacement costs is accounting our debt with future generations.

On the other hand, valuing technological improvements is as important as conservation of resources. An essential fact is that replacement costs using the "best available or back-up technologies" decrease as much as knowledge improves. The evolution of replacement costs of natural resources is a straightforward and quantitative indicator of technological achievements. Therefore, if the evolution of best available technologies is a reflex of increased embodied knowledge, one should see to what extent it decreases the debt owed to future generations. Nevertheless, it is not clear that any new technology, both directly or indirectly, improves efficiency in production processes, and thus diminishes the negative balance of the current generation. This is because of the rebound effect, in which better resource efficiencies may lead to increased resource usage. Anyhow, the concept of replacement cost apprehends both ideas: conservation and technological improvements.

Yet conservation goes beyond repair, restoration, or replacement. It is a value that requires a change in lifestyle brought about through education. Education is an indispensable tool not just in terms of conservation but also in the learning of technological innovation. Education systems must cope with both. In fact, an intense tech oriented society should need to be counterbalanced with a deep sense of conservation. Consequently, as Snow (1959) proposed, the Second Law of Thermodynamics ought to be placed at the core of literacy classes[9].

If replacement can be calculated and registered for almost any action of Man on the planet, an international framework to provide concepts, definitions, classifications, accounting rules and standard tables for all countries could be built. The System of Environmental-Economic Accounts (SEEA) of the United Nations may well provide such statistical framework [10]. The System of National Accounts (SNA) is an established system for producing internationally comparable economic statistics which imposes the organization and standardization of domestic accounts. It is widely accepted and established worldwide. Bureaus of statistical office (BSO) for data recovering and economic accounting exist in almost any country. Companies and countries report economic and physical data following the established accounting procedure and BSOs integrate them. It is a huge infrastructure. From households to companies and to countries, these accounts are

presented in monetary values with the SEEA following the accounting structure of the SNA and thus facilitating the integration of environmental statistics with economic accounts. Each national BSO needs to take responsibility for the environmental data recovery and environmental-economic accounting practice. Unfortunately the information recovered by the physical tables needed for SEEA is rather poor since simply registering material tonnage is not sensitive enough for qualifying most of the physical phenomena.

The aggregation level of accounting determines the numeraire to be used in the accounts. Monetization runs well from households to companies. At the countries level the money yardstick is proved insufficient for economic-environmental accounts whilst at the aggregated global level accounts, money losses weight in favour of physical accounts. Furthermore, for the proper viewing of the planet's evolution, monetary accounting is not only insufficient but inappropriate.

Replacement is the keyword for accounting the remaining planetary global resources. What is the cost of replacing those natural resources our society destroys? We lack costing accounts even though technology and enjoyment of life are the benefits. Technology increases knowledge at the cost of natural resources, but technology may be used either for improving its productivity or for destroying them quicker. There is a need to raise the awareness that it is now possible to put numbers to this debate. This can be done just using the Second Law of Thermodynamics through the exergy and exergy cost measured in S.I. units as a numéraire. The cost of replacement of non-renewable resources and the cost of restoring deteriorated renewable resources may be used to account how much effort our society should need to close the natural and man-made cycles. Having this accounting knowledge, the doors are open for a global managing of natural resources. This knowledge could induce efforts to pay some of the debt, even though many others will remain as a debt to future generations. These generations will thank these accounts. As the former Deputy Secretary-General of OECD, B. Ásgeirsdóttir [11] said "*the luxuries of one generation are often the needs of the next*" and, "*We need to achieve more sustainable consumption and production patterns, to increasingly decouple environmental pressure from economic growth, to ensure sustainable management of natural resources, and to work together in partnership to reduce poverty*".

The United Nations System of Environmental-Economic Accounting and its global framework would be the best starting point for achieving these accounts. To do this the SEEA would need another step forward to convert them into a Global System of Environmental-Thermo-Economic Accounts (SETEA). In the same way that the System for National Accounts has smoothly evolved into the SEEA, someday it would be possible to have complementary accounts for natural resources replacement costs into the framework of SEEA. A major intellectual effort needs to be done from the concepts stated here. At the end, the real overall accounting unit will be the residence time of the human species on the planet.

For making a solid proposal, we have already developed the thermodynamic tools for minerals, water, natural resources. But the way to go is too long for only one research group. JETC could be a good platform for discussing such project and launch a truly European/international proposal to UN in this way."

CONCLUSIONS

The power of thermodynamics is simply fascinating to give answers to ecological problems when thinking in a very broad perspective: temporal, (i.e. historic), and spatial, (i.e. planetary level).

In our view, Thermodynamics may still play an important role in managing our planet's resources. We think "Thermodynamic Accounting" may count in a global management of the natural resources of the Planet. Ecology could receive an important intellectual support, and economists could better understand the need for planning and caring today what could happen in the near long term, beyond several generations. Just converting ideas into numbers one can go beyond the debate between techno-optimists and techno-pessimists and provide real tools for a rational management of the Mineral Capital on Earth.

ACKNOWLEDGMENT

This paper has been financed by the IDERE II project from the Spanish Ministry of Industry and Science.

REFERENCES

- [1] Valero A, Agudelo A, and Valero AI: The crepuscular planet. A model for the exhausted atmosphere and hydrosphere. *Energy* 36(6):3745-3753 (2011).
- [2] Valero AI, Valero A, and Gómez J: The crepuscular planet. A model for the exhausted continental crust. *Energy* 36(6), 694-707 (2011).
- [3] Szargut, J., Morris, D. and Steward, F. (1988). *Exergy analysis of thermal, chemical, and metallurgical processes* (Hemisphere Publishing Corporation).
- [4] Valero, A., Valero, AI., (2012) Exergy of Comminution and the Thanatia Earth's model *Energy* 44, Issue 1(August 2012) Pages 1085-1093
- [5] USGS. Mineral commodity summaries. Technical report, US Geological Survey, 2010.
- [6] UNEP (2010) Metal Stocks in Society-Scientific Synthesis, A Report of the Working Group on the Global Metal Flows. Graedel, T.E., Dubreuil, A., Gerst, M., Hashimoto, S., Moriguchi, Y., Muller, D., Pena, C., Rauch, J., Sinkala, T., Sonnemann, G.; <http://www.unep.org/resourcepanel/Portals/24102/PDFs/Metalstocksinsociety.pdf>, Accessed Jan 2013.
- [7] McDonough, W. and Braungart, M.(2002). "Cradle to Cradle: Remaking the Way We Make Things". North Point Press, ISBN 0-86547-587-3.
- [8] Wernick, I. and Themelis, N.J. (1998) "Recycling Metals for the Environment". *Annual Reviews Energy and Environment*, Vol. 23, p.465-97]
- [9] Snow, C.P. (1959). *The Two Cultures and the Scientific Revolution*. London: Cambridge University Press. ISBN 0-521-45730-0.

[10]UN System of Environmental-Economic Accounting (SEEA).
<https://unstats.un.org/unsd/envaccounting/seea.asp>

Development, Integrated Economic, Environmental and Social Frameworks (2004) pp.15-20. Ed. by OECD

[11]Ásgeirsdóttir,B. (2004) Opening Remarks “The Role of the OECD” in Measuring Sustainable

	x_c [g/g]	x_m [g/g]	$k(x-x_c)$	Exergy replacement costs	Mining and conc.	Smelting and refining
Al-Bauxite (Gibbsite)	1.38E-03	7.03E-01	2088	627	11	24
Antimony (Stibnite)	2.75E-07	5.27E-02	3929	474	1	12
Arsenic (Arsenopyrite)	4.71E-06	2.17E-02	1470	400	9	19
Beryllium (Beryl)	3.22E-05	7.80E-02	362	253	7	450
Bismuth (Bismuthinite)	5.10E-08	2.46E-03	7859	489	4	53
Cadmium (Greenockite)	1.16E-07	1.28E-04	39230	5898	264	279
Chromium (Chromite)	1.98E-04	6.37E-01	48	5	0	36
Cobalt (Linnaeite)	5.15E-09	1.90E-03	-	10872	9	129
Copper (Chalcopyrite)	6.64E-05	1.67E-02	525	110	29	21
Fluorite	1.12E-05	2.50E-01	582	183	1	-
Gold	1.28E-09	2.24E-06	6380357	583668	107752	-
Gypsum	1.26E-04	8.00E-01	118	15	0	-
Iron ore (Hematite)	9.66E-04	7.30E-01	165	18	1	13
Lead (Galena)	6.67E-06	2.37E-02	384	37	1	3
Lime	8.00E-03	6.00E-01	13	3	0	6
Lithium (Spodumene)	3.83E-04	8.04E-01	190	546	13	420
Manganese (Pyrolusite)	4.90E-05	5.00E-01	37	16	0	57
Mercury (Cinnabar)	5.73E-08	4.41E-03	209116	28298	157	252
Molybdenum (Molybdenite)	1.83E-06	5.01E-04	6505	908	136	12
Nickel (sulphides) Pentlandit	5.75E-05	3.36E-02	13039	761	15	100
Nickel (laterites) Garnierite	4.10E-06	4.42E-02	876	167	2	412
Phosphate rock (Apatite)	4.03E-04	5.97E-03	77	0	0	5
Potassium (Sylvite)	2.05E-06	3.99E-01	1926	1224	3	N.A.
REE (Bastnaesite)	2.54E-03	8.11E-02	588	31	10	374
Silicon (Quartz)	2.29E-01	6.50E-01	6	1	1	76
Silver (Argentite)	1.24E-08	4.27E-06	112846	7371	1281	285
Sodium (Halite)	5.89E-04	2.00E-01	71	44	3	40
Tantalum (Tantalite)	1.58E-07	7.44E-03	6729367	482828	3083	8
Tin (Cassiterite)	2.61E-06	6.09E-03	2704	426	15	11
Ti-ilmenite	4.71E-03	2.42E-02	172	5	7	128
Ti-rutile	2.73E-04	2.10E-03	143	9	14	244
Uranium (Uraninite)	1.51E-06	3.18E-03	13843	901	189	N.A.
Vanadium	9.70E-05	2.00E-02	4174	1055	136	381
Wolfram (Scheelite)	2.67E-06	8.94E-03	69721	7429	213	381
Zinc (Sphalerite)	9.96E-05	6.05E-02	104	25	1	40
Zirconium (Zircon)	3.88E-04	4.02E-03	10580	654	739	633

Table 1: Exergy replacement costs of key minerals compared to conventional costs of mining and concentrating and smelting and refining. Values are in GJ/ton if not specified.

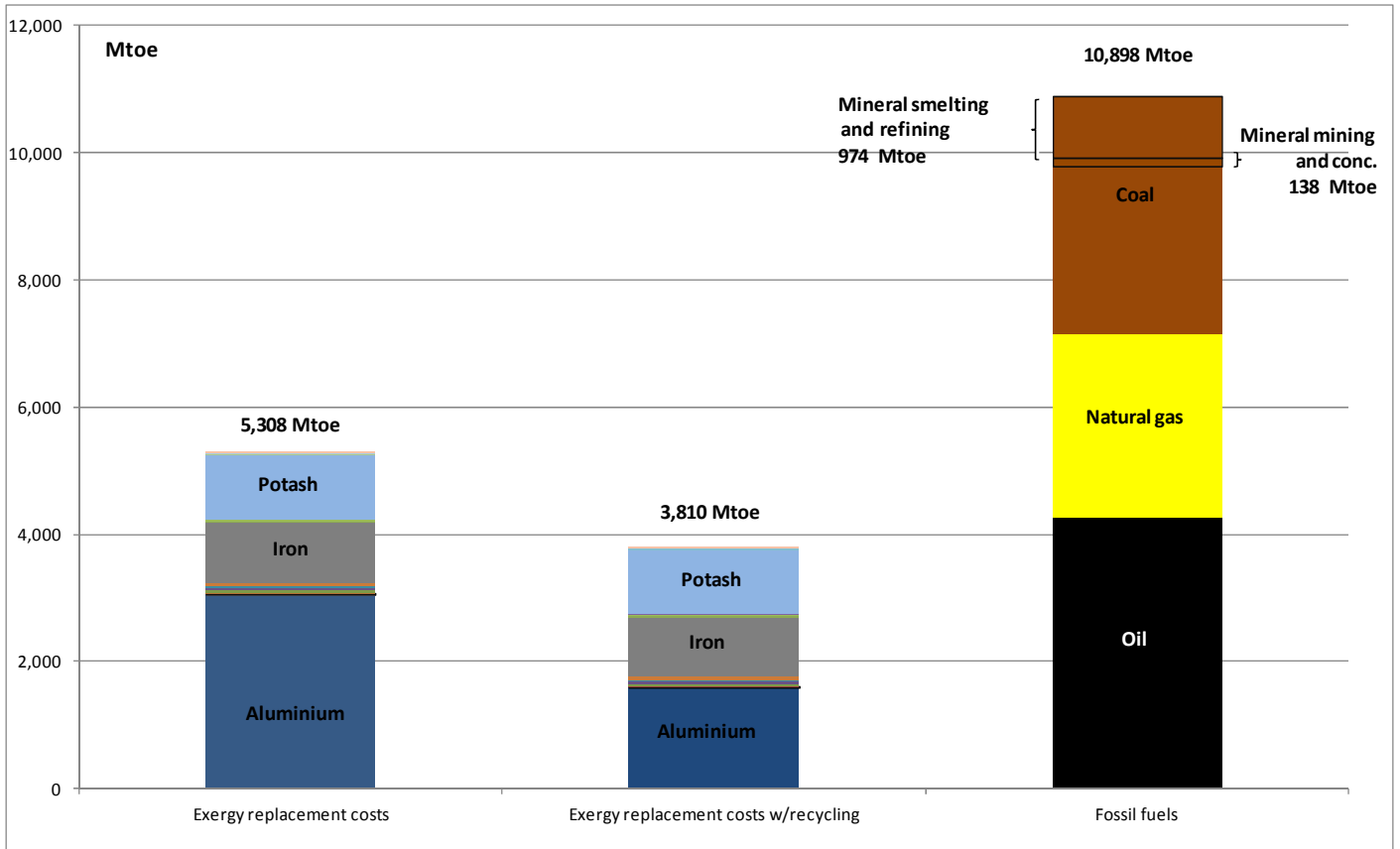


Fig. 1: Exergy replacement costs associated with the extraction of mineral commodities in 2008.

THERMOECONOMICS AS A REGULATION TOOL IN FUTURE DISTRICT HEATING NETWORKS

Vittorio Verda*, Marco Caccin°, Albana Kona*

*Politecnico di Torino Dipartimento Energia, c.so Duca degli Abruzzi 24, 10129 Torino, Italy
Phone: +390110904449, Fax: +390110904499, email: vittorio.verda@polito.it
°Centro Ricerche Fiat, Strada Torino 50, 10043 Orbassano, Italy

ABSTRACT

District heating networks have significantly evolved in the last years thanks to the role that are expected to play in the future energy scenarios. New problems should be considered in district heating operation, such as the third party access and low temperature heating systems. These problems involve common concepts: the competition between various energy forms (particularly heat and power), the quality of energy and the production cost of heat in the thermal plants. All these concepts can be considered through thermoeconomic analysis, which costing approach is based on the concept of exergy. In this paper, the use of thermoeconomics in district heating operation is examined. A parametric analysis is applied to two simple examples in order to show how the various aspects involved in the operation affect the unit cost of heat supplied to the users.

INTRODUCTION

The concept of district heating was quite standardized but has evolved in the last few years, mainly because of new opportunities that the development of renewable energy plants and energy saving techniques have created. Using low-temperature heat from industrial waste heat in district heating has proven to be attractive from energy and economic viewpoints [1]. Furthermore an important aspect of new building development is their increasingly high standards of efficiency. In order for district heating networks to remain an effective option for such developments, reductions in temperature supply should be achieved. This allows one to use different sources of locally available waste and renewable heat [2] and to reduce the heat losses.

The role of district heating in future renewable energy systems has been evaluated in Lund et.al [3]. More specifically, district heating is expected to supply heat to the buildings located in more densely populated areas, primarily taking advantage of thermal energy sources that are recovered from industries or produced by WTE plants, cogeneration systems and renewable energy plants. Areas with lower population density are more suitable for heating through alternative technologies such as geothermal heat pumps.

District heating networks involve the use of at least two forms of energy: mechanical and thermal energies. In fact, the network distributes heat, that is produced in one or more plants, to the users, while power is required for the fluid flow. These energy forms are somehow competing, since a reduction in the quality of heat generally allows one to increase the performance of the thermal plant, but may involve larger amount of power for pumping. Moreover there are links between the design/operation conditions of the network and the performance of the thermal plant and thus the production cost of heat.

Thermoeconomic approaches have proven to be suitable for the design of this kind of systems since they allow one to account for the effects that the characteristics of the various users (mainly their position and their thermal needs) have on the cost of heat supplied and on the total primary energy requirements. Thermoeconomics is a branch of engineering combining exergy and economic principles (Reference [4] provides an introduction to the subject, and references to earlier works.) The thermoeconomic analysis of an energy system allows one to calculate on a thermodynamic and economic base the cost rate of all the fluxes flowing in, out and through the system, and in particular its products. The cost calculation gives as much information as the representation of the system is detailed. This is more important as the number of products is high, because in those cases the number of components and fluxes, both with physical and productive meaning, are high. Thermoeconomics can be used for costing purpose, design improvement, optimization and the analysis of operating conditions, as illustrated in [5].

For these reasons, thermoeconomics has been used for the design of optimal district heating networks, for the optimization of the supply temperature during operation and the analysis of possible network expansions.

The first application of exergy costing to a district heating system was proposed by Keenan in 1932 [6], who suggested that the production costs of a cogeneration plant should be distributed among the products according to their exergy. Various applications of thermoeconomic analysis to DHS have been proposed successively.

Adamo et al. [7] have used a thermoeconomic approach for the optimal choice of diameters in a district heating network. Verda et al. [8] have proposed the design optimization of a district heating system using a thermoeconomic approach. The relation between exergy based parameters of the network

and the unit cost of heat supplied to the users is also investigated. A procedure for the search of the optimal configuration of district heating networks is proposed in [9]. The optimization was performed using a probabilistic approach based on the calculation of thermoeconomic cost of heat associated to each single user connected with the network. It was shown that the minimum cost for the entire community is obtained by disconnecting from the network some small buildings, which are located far from the thermal plant, and providing them heat with local boilers. Oktay and Dincer [10] presented an application of an exergoeconomic model, which included both exergy and cost accounting analyses for a geothermal district heating system.

In [11], a thermoeconomic approach for the analysis of other possible improvements of existing district heating networks is proposed. These are related to changes in the operating strategies, connection of new users and application of energy savings initiatives in buildings connected to the network.

Other problems are still open in district heating that can be solved through a thermoeconomic approach. In particular, the link between quality of heat and its price should be considered in the analysis of both the producers and the users. In the near future it is expected that multiple producers are allowed to supply heat to the same district heating network, similarly to what happens in the case of the electric grid. Not only the amount of heat they may produce should be properly accounted, but also its quality. Exergy is an effective way to evaluate both quantity and quality of energy flows. Moreover, users characterized by a heating system able to operate at lower temperatures should be considered in a different way than users requiring the same amount of heat, but at higher temperature. As an example, in buildings where radiant panels are installed, the temperature difference between supply and return piping can be increased significantly. As an alternative, these buildings may be theoretically connected directly with the return piping network (i.e. water supplied to the buildings comes from the main return piping instead of the supply piping network), thus using low grade heating. In both cases there is generally a big benefit for the overall energy system, since the returning temperature decreases and a more effective heat recovery is obtained in the thermal plant. In all cases, low temperature heating systems use less exergy than conventional heating systems.

In the present work, the use of thermoeconomics for the analysis of these aspects is proposed. Some scenarios are also analyzed in order to provide a quantitative evaluation of the various cost terms as the function of the operating conditions, topology and characteristics of the users/producers.

THERMOECONOMIC ANALYSIS OF DISTRICT HEATING NETWORKS

Thermoeconomic analysis is based on cost balance equations that are written for all components. This balance can be written for the i th component as

$$\sum_j \Pi_{ji} + \dot{Z}_i = 0 \quad (1)$$

where Π_{ji} is its thermoeconomic cost and \dot{Z}_i the monetary cost rate of owning the i th component. Physical flows can be composed in order to define resources (F) and products (P) of the components. Equation (1) can be thus rewritten as

$$\Pi_{Fi} + \dot{Z}_i = \Pi_{Pi} \quad (2)$$

Unit costs can be also introduced. The thermoeconomic unit cost c_{ji} is the ratio between the thermoeconomic cost of a flow Π_{ji} and its exergy Ψ_{ji} . Using these concepts, equations (1) and (2) become:

$$\sum_j \Psi_{ji} \cdot c_{ji} + \dot{Z}_i = 0 \quad (3)$$

$$\Psi_{Fi} \cdot c_{Fi} + \dot{Z}_i = \Psi_{Pi} \cdot c_{Pi} \quad (4)$$

Equation (4) can be rearranged introducing the relation between resources and products, when these quantities are expressed in terms of exergy flows

$$\Psi_{Fi} = \Psi_{Pi} + I \quad (5)$$

where I is the irreversibility. The unit cost of the product is expressed as:

$$c_{Pi} = c_{Fi} + c_{Fi} \cdot \frac{I}{\Psi_{Pi}} + \frac{\dot{Z}_i}{\Psi_{Pi}} \quad (6)$$

In a network, each single pipe can be considered as a component, which goal consists in transporting the inlet exergy flow to the outlet section. The inlet flow can be considered as the resource while the outlet flow as the product. This concept can be applied to the entire system. In this case the unit cost of exergy supplied to the users depends on the unit cost of resource (i.e. the heat flux supplied by the thermal plants to the network), the irreversibilities occurring in the network (heat losses, pressure drops, mixing of streams at different temperature) and the investment cost. In addition, it should be considered that “users need energy not exergy”. This means that the final product that is supplied to the users is a heat flux at the indoor temperature, no matter the operating temperature of the system, therefore the comparison between district heating and alternative systems or between different district heating configuration or operating conditions should be performed on the basis of a product evaluated in energy basis:

$$c_{\Phi} = c_P \cdot \frac{\Psi_P}{\Phi} \quad (7)$$

where c_{Φ} is the unit cost of heat (calculated using exergy accounting) and Φ is the heat flux supplied to the users.

The same type of analysis can be performed at component level, which brings to a different unit cost for the various users. This cost depends on the characteristics of the user, particularly its heat request and the position of the user with respect to the other users and the thermal plants. Its position affects the irreversibilities and the investment cost of the portion of network required to reach it. This concept is the basis for using thermoeconomics in optimal planning of district heating networks (see for example [9]).

Among the available techniques that have been proposed in the literature for thermoeconomic analysis, a useful approach that can be adopted for the analysis of district heating network is that proposed by Valero and co-workers in the eighties [12, 13]. One of its main characteristics is the matrix based approach, in particular the use of incidence matrix for expressing the equation of cost conservation. The incidence matrix (see for example [14]) was formulated in the ambit of the graph theory [15], which is widely adopted for the topology definition as well as the fluid dynamic and thermal calculation of distribution networks [16]. The incidence matrix, \mathbf{A} , is characterised by as many rows as the

branches (m) and as many columns as the nodes (n). The general element A_{ij} is equal to 1 or -1 , respectively if the branch j is entering or exiting the node i and 0 in the other cases. The use of the incidence matrix allows one to express the balance equation of the flow of the general extensive quantity G_x as:

$$\mathbf{A} \cdot \mathbf{G}_x + \mathbf{G}_{x_d} = \mathbf{0} \quad (8)$$

where \mathbf{G}_x is the vector containing the values assumed by the quantity G_x in the nodes and \mathbf{G}_{x_d} is the vector that allows to account for the amount destructed in the branches, if non null. In thermoeconomics, equation (9) allows one writing the cost balance:

$$\mathbf{A} \cdot \mathbf{\Pi} + \mathbf{Z} = \mathbf{0} \quad (9)$$

where $\mathbf{\Pi}$ is the vector containing the cost of all the flows, while \mathbf{Z} contains the cost rate of the components. The calculation of all the costs require the formulation of n - m auxiliary equations, which are obtained through definition of resources and products of each component, expressed in terms of exergy flows [17]. The auxiliary equations were formulated as four propositions, whose first (P1) is the conservation of cost, expressed by equation (14) [12]. The others are: (P2) in absence of a different evaluation the economic unit cost of an exergy flow entering the system from the environment can be assumed equal to its price; (P3) in absence of a different evaluation, the unit cost of a lost exergy flow is the same; (P4a) if the fuel of a component is defined as the difference between two exergy flows, the unit cost of these flows is equal; (P4b) if the product of a component is defined as the summation of two or more flows, the unit cost of these flows is the same.

In the case of a DHN the only auxiliary equations to be applied is the assignment of the same unit cost to the flow exiting each bifurcation and the assignment of unit costs to the flows entering the system from outside, i.e. the unit cost of thermal exergy supplied in the plants and the unit cost of electricity required for pumping [18].

THIRD PARTY ACCESS TO DISTRICT HEATING NETWORKS

In 1996, when the European electricity market opened up for competition, the earlier regulated district heating market was de-regulated in the sense that the companies now could set their own prices. The earlier directive that the district heating companies should not make any profit was removed, and any firm (not only municipal) could enter the market [19].

However, the lack of attention and targeted policies, the absence of a European directive that takes care of the particular case of district energy led to a situation in which district heating sector becomes substantially an example of market failure, because, in the absence of regulation authorities and measures, economic operators in free market have not been able to solve the main problem related to district heating systems: natural monopoly, third party access and effective competition, increasing prices due to unbalances in the market concentration.

This situation entails costs and inefficiencies for consumers and communities, for this reason in the current years many voices were raised in favour of a new regulation of the sector according to its new free market configuration, both on the academic side [19-21], both on the consumers side [22]. Also

National Competition Authorities have several time - in Sweden for instance - urged the need for adjustment in district energy system free market, or are starting to do it, as in the case of Italian Competition Authority, which in January 16, 2012, launch a survey on the level of prices, constraints on choice for consumers of whether or not connect to the network of district heating and procedures for service management.

According to Becchis et al. [21], absence of regulation in the district energy markets exposes consumers to possible exploitations by a monopolist willing to maximise his profit. Considering the strong pressure against DHC projects coming from conflicting market interest and the relevant transaction and regulatory costs, a bit of regulation of the costs and tariffs might improve the penetration capacity of the technology and should be welcomed by DHC true supporters.

The main causes of market inefficiencies that require regulation are:

- situations leading to highly prices, such situations of economies of scale or scope, anticompetitive behaviour, network externalities, government limits to competition (patents, for instance);
- externalities leading to inappropriate prices;
- information problems, that might lead to market breakdown, for example quality;

Regulation deals with the considered situation, explicitly controlling prices, profits and quality. Regulation specifies precise details of what companies can and cannot do (ex-ante intervention).

The aim of regulation is fundamentally to reach economic efficiency, that is, prices equal to marginal costs, taking into account the externalities, assuring entry of most efficient companies (productive efficiency), dynamic efficiency. Moreover it has also re-distributional concerns between consumers and shareholders and between poor and rich consumers.

Third Party Access (TPA), i.e., separation between generation and retailing of district heating in order to open up the network for more competitors, is one suggestion that has been addressed in order to increase the competition in the market. Generally TPA implies that a third party can access the district heating network in a non-discriminatory way, in order to supply its heat, but there exist different forms of TPA that all are compatible with the above definition:

1) Regulated TPA refers to a situation of full access to the district heating networks, where the network owner has a legal obligation to allow access to the network. The network operations are regulated ex ante, i.e., the conditions for access to the network (e.g., fees, etc.) are determined in advance.

2) Negotiated TPA implies that the district heating network owners are required to negotiate about access to the network with the producers of heat. The main difference between regulated and negotiated TPA is thus that the latter form implies that the network operations are determined ex post. The specific conditions for network access are negotiated between the network owner and the third party.

3) Finally, a so-called single-buyer solution means that all potential consumers in the network have the right to negotiate contracts with all eligible suppliers to the network. The single-buyer is obliged to purchase the contracted volume

from this supplier and resell it to the customer at a price equal to the contract price plus distribution or system costs.

In this paper the third party access is analyzed from technical and economic viewpoints. This analysis aims at showing that these aspects can be correctly captured using a thermo-economic approach for costing purpose. A simple example, shown in Figure 1, is considered. This consists of a district heating network with two thermal plants that can supply heat to the users. The two plants are characterized by a different position, which involves a different contribution due to pumping. The quality of heat that is supplied to the network by the two plants is considered as different, which means that water is heated by the two plants at different temperature.

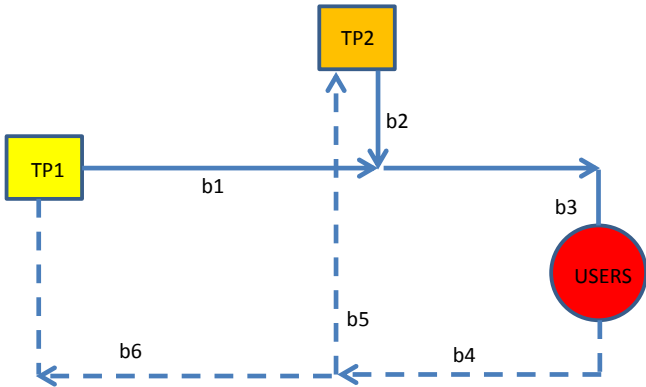


Figure 1. Schematic of a district heating network with two heating plants

For sake of simplicity some assumptions are considered. Pressure drops in the pipes are assumed as proportional to the square of the mass flow rate:

$$\Delta p_i = \beta_i \cdot G_i^2 \quad (10)$$

Pipes in the present analysis are considered as perfectly insulated. The following quantities are assumed:

- 1) thermal request of the users in design conditions, $\Phi=20$ MW;
- 2) pressure loss coefficient in pipe b1, $\beta_1=10$;
- 3) supply temperature from the thermal plant TP1, $T_{b1}=100$ °C;
- 4) supply and return temperatures on the secondary circuit of the users, $T_s=80$ °C and $T_r=60$ °C;
- 5) return temperature on the main temperature of the district heating network, $T_{b4}=65$ °C;
- 6) cost of thermal exergy produced by the thermal plant TP1, $c_{TP1}=0.16$ €/kWh.

The latter has been considered as constant in all operating conditions. This is a good approximation of the behavior of combined cycles operating in cogeneration mode, if the effect of ambient temperature is not considered. In fact these kind of plants are characterized by an almost constant exergetic efficiency when steam extraction is varied from zero to the maximum value.

Only operating costs have been considered in the analysis, since the district heating network has been considered as existing, therefore the contribution of the investment cost is the same in all the examined scenarios.

A first case that can be considered in the analysis corresponds to the thermal plant TP2 producing heat at lower temperature than TP1. TP2 is considered as located closer to the users with respect to TP1. The pressure loss coefficient in the pipe b2 is assumed as 10% of that in b1, the supply temperature from thermal plant TP2 is assumed as 90 °C. The analysis has been conducted by varying the percentage of heat supplied by TP2, the unit cost of thermal exergy supplied by the thermal plant TP2 and the heat requested by the users.

Figure 2 shows the unit cost of heat supplied to the users as the function of the percent heat load supplied by the thermal plant TP1, for three different values of the unit cost of thermal exergy. If this cost is considered equal to that for TP1, the unit cost of heat supplied to the users decreases with increasing contribution of the thermal plant TP2. This means that, despite the reduced temperature of the water flow exiting TP2, the smaller friction losses associated with b2 allow one to reduce the cost of heat supplied to the users. Similar results are obtained by increasing the unit cost of thermal exergy produced by TP2 up to 4%. If this unit cost is increase to 8% (i.e. about 0.173 €/kWh) the minimum cost is obtained by using the plant TP1 only. This means that the beneficial effects of a reduced pumping cost is always lower than the effects due to the smaller unit cost of thermal exergy produced by TP1 and the larger specific exergy.

In the case of costs of thermal exergy produced by TP2 between 4% and 8% larger than the cost of TP1, the optimal cost of heat is obtained by supplying heat from the two plants.

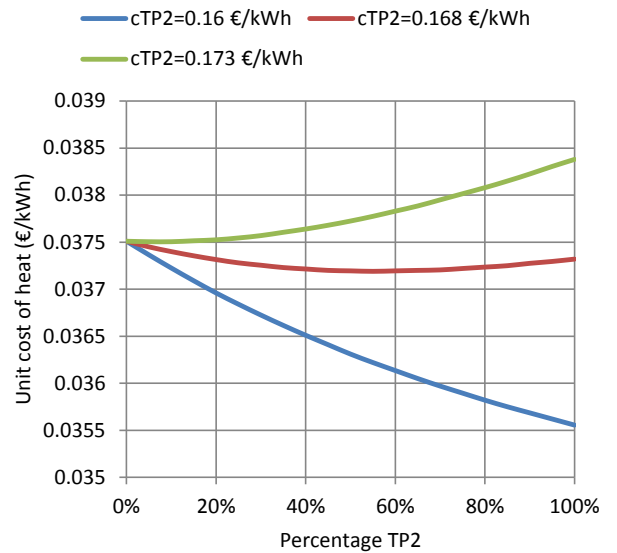


Figure 2. Unit cost of heat as the function of the percent thermal supply from TP2 at design load.

At partial load, the unit cost of heat reduces, because of the reduction in pumping costs as well as the reduction in the temperatures on the secondary circuit. The latter causes a reduction in the returning temperature of the district heating network, which means that the exergy content associated to the enthalpy flux supplied by the thermal plant to the network reduces and so the corresponding unit cost of heat. Figure 3 shows the unit cost of heat supplied to the users as the function of the percentage of heat supplied by the thermal plant TP2. The curves refer to three different percentage of the total heat request and are obtained considering a cost for

the thermal exergy produced by TP2 6% higher than that produced by TP1. In the case of design load, there is a minimum when 45% of heat is produced by TP2. When a smaller heat load is considered, the curves is flattened and the minimum shifts towards lower percentage of contribution by TP2. In the case of heat load reduced to 75% of the design value, the minimum is obtained when about 40% of heat is produced by TP2. In this case, the minimum cost is 5% lower than the minimum cost at design load. When the heat load is reduced to 50%, the minimum is obtained when heat is entirely produced by TP1, but the cost is almost constant. The unit cost of heat is about 11% lower than at design load.

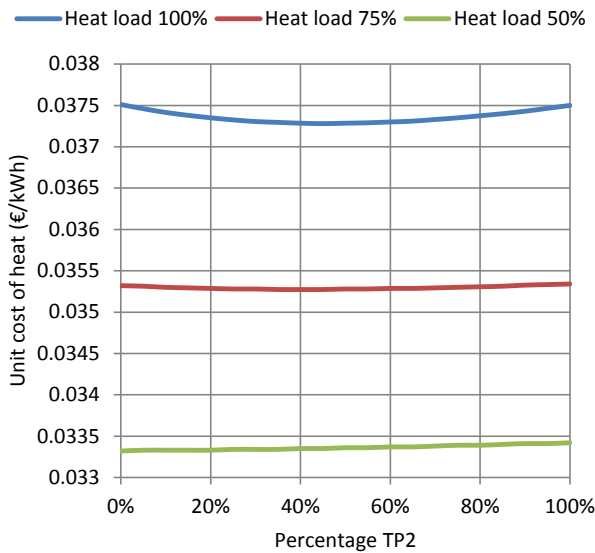


Figure 3. Unit cost of heat as the function of the percent thermal supply from TP2 per various thermal loads, at fixed cost of thermal exergy.

Similarly, when lower costs of thermal exergy supplied by TP2 are considered, the unit cost of heat is reduced as the heat load reduces. The curves are flattened and keep a similar slope as the one shown in figure 2. Analogous behavior is observed when the unit cost of thermal exergy produced by TP2 is increased.

The present analysis highlights that cost analysis applied to district heating operation in the case of multiple heat producers requires the evaluation of various aspects: unit cost of heat supplied to the network, quality of heat (i.e. supply temperature) and pressure required for correct operation. An additional aspect that should be considered refers to the use of thermal storage devices, which operation (charge and discharge) may be decided on the basis of the cost of heat, total heat request, supply temperature of the network.

All these aspects are included in the costing analysis when a method based on the exergy evaluation of energy flows is considered, therefore thermoeconomics is a suitable tool to manage third-party access to the district heating network.

USERS WITH REDUCED OPERATING TEMPERATURES

A further aspect that deserves to be considered refers to users using low temperature heating systems, such as radiant floor. This kind of systems have positive impact on the efficiency of district heating systems, since network can be

reduced. Similar effect is achieved in existing buildings, where energy savings initiatives (e.g. wall, roof or window insulation) are introduced. In this case, the existing heating system becomes oversized and its operating temperatures can be reduced.

Buildings with these characteristics can be connected on the supply network as the other buildings. In this case the temperature difference between supply and return values can be significantly increased. In fact the return temperature has a lower bound imposed by the return temperature on the secondary circuit. If the latter is lowered, the return temperature can be lowered as well. The positive effect is particularly important in the case of small networks, which are designed with small difference between the supply and return temperature. An alternative configuration is also possible. Buildings with low temperature heating system can be theoretically connected to the return pipeline. The inlet temperature on the hot side of the heat exchanger is therefore equal to the return temperature of the district heating network. Water is then rejected, at lower temperature, on the same pipe.

Figure 4 shows the unit cost of heat supplied to a user connected with the supply network as the function of the operating temperature on the secondary circuit. The analysis is performed considering two values of the supply temperature on the main circuit.

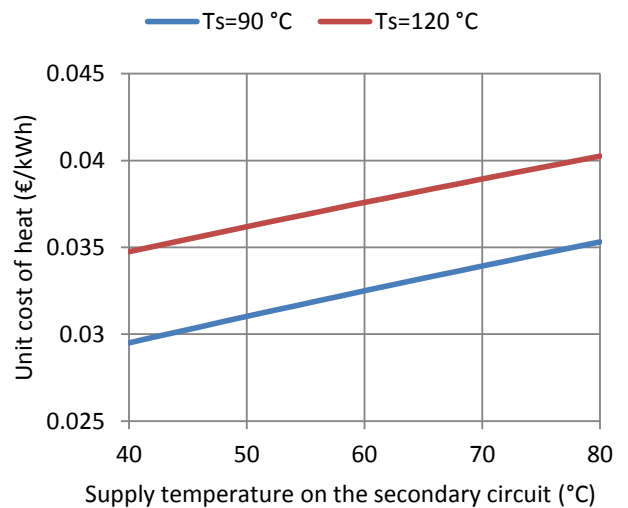


Figure 4. Unit cost of heat as the function of the supply temperature on the secondary circuit.

The figure shows that, for fixed value of the supply temperature of the district heating network, unit cost of heat decreases with decreasing operating temperature on the secondary circuit. A reduction in the network temperature also allows on to reduce the unit cost of heat.

As already mentioned the main advantage in the reduction of the operating temperatures consists in the larger plant efficiency. An additional advantage that is obtained by lowering the return temperature consists in the reduction of the mass flow rate flowing in the district heating network, which allows one to reduce the pumping cost. The effect of secondary temperature on the specific mass flow rate (i.e. the mass flow rate per unit heat flux) flowing in the network is shown in figure 5. The curves show that there is a significant

reduction, especially in the case of network operating with smaller supply temperature. An additional potential advantage in lowering the mass flow rate is registered in the case of existing network in areas where there are possible urban expansions. In this case, new users may be connected to the network even in the case of a “saturated” network, i.e. when the thermal request of the user causes water velocity in portions of the system close to the upper limit. A reduction in the mass flow rate that is requested to supply the connected users with their thermal request allows one to connect new users.

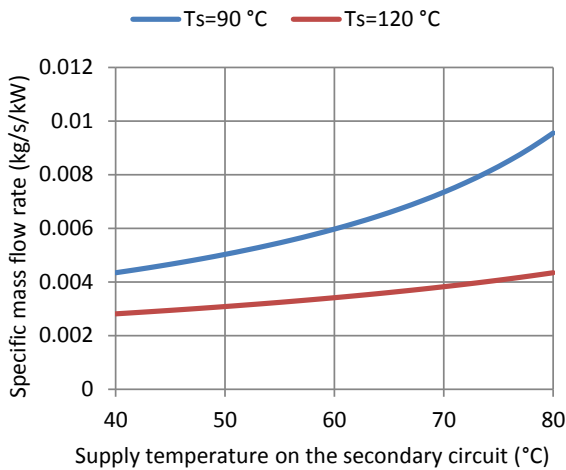


Figure 5. Specific mass flow rate in the district heating network as the function of the supply temperature on the secondary circuit.

It is finally worth considering the analysis of unit cost of heat as the function of the temperature on the district heating network, for fixed operating temperatures on the secondary circuit. These have been fixed equal to 40 °C (supply) and 30 °C (return).

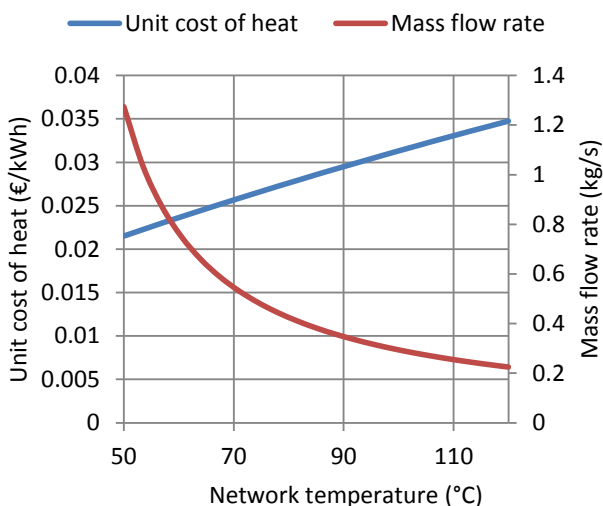


Figure 6. Unit cost of heat as the function of the network temperature.

The figure shows that unit cost decreases with decreasing temperature, which means that a configuration with the building connected on the returning pipe would allow a cost reduction, therefore the price of heat for this user should be

lower than a user connected on the supply network. In addition, the figure shows that a reduction in the source temperature causes a significant increase in the mass flow rate, about 4 to 6 times larger than usual connection, depending on the supply temperature. Therefore this kind of configurations is possible only in portion of the network where the number of users is large enough, so that the mass flow rate flowing in the pipes is sufficient.

CONCLUSIONS

Future district heating systems are expected to be flexible in the operation, based on renewable energy sources and open to various producers. In principle, the users can also become producers, thus implementing a sort of “peer-to-peer” energy exchange system. Additional aspects related to this new vision of district heating networks are related with the possibility of also supply cooling to the users through thermally driven chillers, or the possibility to distribute heat produced by heat pumps that are fed with excess productions of electricity (e.g. from wind farms).

The present paper represents a first attempt to tackle particular aspects that can occur in the operation of advanced district heating systems, such as the third party access and the low temperature heating systems. The analysis is conducted by examining simple examples, that show how the use of different energy forms, their quality and cost can affect the cost of the product supplied to the users. Thermoeconomics, which is based on exergy based costing, allows one to account for the various thermodynamic and economic aspects that are involved, thus it represent a useful tool not only in the design process but also in the operation.

REFERENCES

- [1] Woods P., Gunning R., Snoek C., Onno T., Yang L., Ahonen M., Wiltshire R. Optimization of operating temperatures and an appraisal of the benefits of low temperature district heating. Report IEA district heating 1999. www.iea-dhc.org
- [2] Wiltshire R, Low temperature district energy systems. 16th Building Services, Mechanical and Building Industry Days. International conference, 14-15 october 2011, Debrecen, Hungary
- [3] Lund H., Möller B., Mathiesen B.V., Dyrrelund A., The role of district heating in future renewable energy systems. Energy, Vol 35, Issue 3, March 2010, Pages 1381-1390
- [4] R. A. Gaggioli, W. J. Wepfer, Exergy Economics, Energy, Vol. 5, pp. 823-837 (1980).
- [5] Y.M. El Sayed (2003). The Thermoeconomics of Energy Conversions. Elsevier.
- [6] J.H. Keenan (1932) A Steam Chart for Second Law Analysis. Mechanical Engineering 54: 195-204.
- [7] L. Adamo, G. Cammarata, A. Fichera, L. Marletta (1997). Improvement of a district heating network through thermoeconomic approach. Renewable Energy 10: 213-216.
- [8] V. Verda, R. Borchiellini, M. Cali (2001). A Thermoeconomic Approach for the Analysis of District Heating Systems. International Journal of Thermodynamics 4: 183-190.
- [9] V. Verda, C. Ciano (2005). Procedures for the Search of the Optimal Configuration of District Heating Networks. International Journal of Thermodynamics 8: 143-153.

- [10] Z. Oktay, I. Dincer (2009). Exergoeconomic analysis of the Gonen geothermal district heating system for buildings, *Energy and Buildings* 41: 154–163.
- [11] V. Verda, A. Kona (2012). Thermoeconomics as a tool for the design and analysis of energy savings initiatives in buildings connected to district heating networks. *International Journal of Thermodynamics*, 15: 221-229.
- [12] M. A. Lozano and A. Valero (1993). Theory of the Exergetic Cost. *Energy*, Vol.18 No.9, pp.939-960.
- [13] A. Valero, M. A. Lozano, M. Muñoz (1986). A general Theory of exergy saving I, II, III. *AES Vol. 2-3. ASME Book H0341C*, pp. 1,9,17.
- [14] M. Chandrashekar, F. C. Wong (1982). Thermodynamic System Analysis – A graph-theoretic Approach. *Energy*, Vol.7 No.6, pp.539-566.
- [15] F. Harary (1995). *Graph Theory*, Narosa Publishing House, New Delhi.
- [16] M. Cali, R. Borchiellini, (2002). District Heating Network Calculation and Optimization. *Encyclopedia of Life Support Systems*, UNESCO (paper 3.19.3.8).
- [17] G. Tsatsaronis, M. Winhold (1985). Exergoeconomic Analysis and Evaluation of energy-conversion Plants – I. A new general Theory. *Energy*, Vol.10 N.1, pp. 69-80.
- [18] Verda V., Borchiellini R., Cali M., 2001. A thermoeconomic approach for the analysis of district heating systems. *The International Journal of Applied Thermodynamics*. Vol.4, No. 4. pp 183-190.
- [19] Westin, P., Lagergren F., Re-regulating District Heating in Sweden, *Energy Policy*, 2002.
- [20] Soderholm P, Warell L., Market opening and third party access in district heating networks, *Energy Policy*, 2010.
- [21] Becchis F., Genon G., Russolillo D., Tariff regulation and competition as means to improve the market penetration of district heating and cooling system, *Mimeo Fondazione per l’Ambiente*, 2011.
- [22] Magnusson D., Swedish district heating - A system in stagnation: current and future trends in the district heating sector, *Energy Policy*, 2012.

PANEL J

MODEL ORDER REDUCTION OF COMPLEX COMBUSTION THERMODYNAMICS AND KINETICS

DOMINANT PATHS AND SYSTEMS IN MULTISCALE REACTION NETWORKS

A.N. Gorban*, A. Zinovyev,** O. Radulescu ***

*University of Leicester, LE1 7RH, UK E-mail: ag153@le.ac.uk

**Institut Curie, INSERM/Curie/Mines ParisTech, Paris, France

***DIMNP UMR CNRS, University of Montpellier 2, Montpellier, France

EXTENDED ABSTRACT

We develop the classical idea of limiting step to the asymptotology of multiscale reaction networks. The concept of limit simplification is proposed. For multiscale reaction networks the dynamical behavior is to be approximated by the system of simple dominant networks. The dominant systems can be used for direct computation of steady states and relaxation dynamics, especially when kinetic information is incomplete, for design of experiments and mining of experimental data, and could serve as a robust first approximation in perturbation theory or for preconditioning. They give an answer to an important question: given a network model, which are its critical parameters? Many of the parameters of the initial model are no longer present in the dominant system: these parameters are non-critical. Parameters of dominant systems indicate putative targets to change the behavior of the large network.

Following Kruskal [1], asymptotology is “the art of describing the behavior of a specified solution (or family of solutions) of a system in a limiting case.” We analyze dynamics and steady states of multiscale reaction networks. We focused mostly on the case when the elementary processes have significantly different time scales. In this case, we obtain “limit simplification” of the model: all stationary states and relaxation processes could be analyzed “to the very end”, by straightforward computations, mostly analytically. For any ordering of reaction rate constants we look for the dominant kinetic system. The dominant system is, by definition, the system that gives us the main asymptotic terms of the stationary state and relaxation in the limit for well separated rate constants.

The theory of dominant systems for linear reaction networks and Markov chains is well developed [2; 3]. Complete theory for linear networks with well separated reaction rate constants allows us to elaborate algorithms for explicit approximations of eigenvalues and eigenvectors of kinetic matrix. We found the explicit asymptotics of eigenvectors and eigenvalues. All algorithms are represented topologically by transformation of the graph of reaction (labeled by reaction rate constants). The reaction rate constants for dominant systems may not coincide with constant of original network. In general, they are monomials of the original constants. In the simplest cases, the dominant system can be represented as dominant path in the reaction network. In the general case, the hierarchy of dominant paths in the hierarchy of lumped networks is needed.

Accuracy of estimates is proven. Performance of the algorithms is demonstrated on simple benchmarks and on multiscale biochemical networks [4]. These methods are applied, in particular, to the analysis of microRNA-mediated mechanisms of translation repression [5; 6; 7]. Although remarkable progress has been made in deciphering the mechanisms used by miRNAs to regulate translation, many contradictory findings have been published that stimulate active debate in this field. There is a hot debate in the current literature about which mechanism and in which situations has a dominant role in living cells. The same experimental systems dealing with the same pairs of mRNA and miRNA can provide ambiguous evidences about which is the actual mechanism of translation repression observed in the experiment. We analyse dominant systems for the reaction kinetic network that includes all known mechanisms of miRNA action and demonstrate that among several coexisting miRNA mechanisms, the one that will effectively be measurable is that which acts on or changes the sensitive parameters of the translation process. This analysis of dominant systems explains the majority of existing controversies reported.

For general nonlinear systems, the problem of dominant systems is still open. It is discussed in the framework of the modern theories of tropical asymptotic [8; 9]. For nonlinear reaction networks, we present a new heuristic algorithm for calculation of hierarchy of dominant paths. Our approach is based on the asymptotic analysis of fluxes on the Volpert graph [10; 11].

The results of the analysis of the dominant systems often support the observation by Kruskal [1]: “And the answer quite generally has the form of a new system (well posed problem) for the solution to satisfy, although this is sometimes obscured because the new system is so easily solved that one is led directly to the solution without noticing the intermediate step.”

REFERENCES

- [1] M.D. Kruskal, Asymptotology, In: *Mathematical Models in Physical Sciences*, ed. by S. Dobrot, Prentice-Hall, New Jersey, Englewood Cliffs, pp. 17–48, 1963.
- [2] A.N. Gorban, O. Radulescu, A.Y. Zinovyev, Asymptotology of chemical reaction networks, *Chemical Engineering Science*, vol. 65, pp. 2310–2324, 2010.
- [3] A.N. Gorban and O. Radulescu, Dynamic and Static Limitation in Multiscale Reaction Networks, Revisited, *Advances in Chemical Engineering*, vol. 34, pp. 103–173, 2008.
- [4] O. Radulescu, A.N. Gorban, A. Zinovyev, and A. Lilienbaum, Robust simplifications of multiscale biochemical networks, *BMC Systems Biology*, 2:86, 14 October 2008.
- [5] N. Morozova, A. Zinovyev, N. Nonne, L.-L. Pritchard, A.N. Gorban, and Annick Harel-Bellan, Kinetic signatures of microRNA modes of action, *RNA*, vol. 18 (9), pp. 1635–1655, 2012.
- [6] A. Zinovyev, N. Morozova, A.N. Gorban, and A. Harel-Bellan, Mathematical Modeling of microRNA-Mediated Mechanisms of Translation Repression, in U. Schmitz et al. (eds.), *MicroRNA Cancer Regulation: Advanced Concepts, Bioinformatics and Systems Biology Tools* (Series Advances in Experimental Medicine and Biology, vol. 774), Springer, pp. 189–224, 2013.

- [7] A. Zinovyev, N. Morozova, N. Nonne, E. Barillot, A. Harel-Bellan, and A.N. Gorban Dynamical modeling of microRNA action on the protein translation process, *BMC Systems Biology* 4:13, 24 February 2010.
- [8] O. Radulescu, A.N. Gorban, A. Zinovyev, V. Noel, Reduction of dynamical biochemical reaction networks in computational biology, *Frontiers in Genetics (Bioinformatics and Computational Biology)*, vol. 3, Article 131, July 2012.
- [9] V. Noel, D. Grigoriev, S. Vakulenko, O. Radulescu, Tropicalization and tropical equilibration of chemical reactions, arXiv:1303.3963 [q-bio.MN].
- [10] A.I. Vol'pert, Differential equations on graphs, *Mathematics of the USSR–Sbornik*, vol. 17 (4), pp. 571–582, 1972.
- [11] G.S. Yablonskii, V.I. Bykov, A.N. Gorban, and V.I. Elokhin, *Kinetic models of catalytic reactions*. (Series Comprehensive Chemical Kinetics, vol. 32), Elsevier, Amsterdam, 1991.

CPT INVARIANCE AND ITS IMPLICATIONS FOR THERMODYNAMICS AND KINETICS

A. Y. Klimenko*, U. Maas**

*The University of Queensland, SoMME, QLD 4072, Australia, E-mail: klimenko@mech.uq.edu.au

**Karlsruher Institut für Technologie, ITT, 76131, Germany, E-mail:Ulrich.Maas@kit.edu

ABSTRACT

This work reviews the modern understanding of thermodynamics and kinetics while taking into account CPT (charge-parity-time) invariance. The CPT invariance is one of the key principles of modern physics and is linked to Lorentz invariance of special relativity. While CPT invariance has been proven in quantum mechanics as a theorem, we consider this principle as a general law applicable to the universe and not restricted to quantum mechanics. Consistency between two perspectives on the real world – that of thermodynamics and that of CPT invariance is the focus of our consideration. While extending thermodynamics from matter to antimatter and postulating that there is a fundamental similarity in physical laws controlling matter and antimatter, we show that there are two different extensions possible: CP-invariant thermodynamics, which is commonly implied in various applications, and CPT-invariant thermodynamics, which has not been explored yet. Since both thermodynamics are different only by their treatment of antimatter but are the same in describing our world dominated by matter, making a clear experimentally justified choice between CP invariance and CPT invariance in context of thermodynamics is not possible at this stage. This work investigates the comparative properties of CP- and CPT-invariant thermodynamics and their implications for kinetic processes.

INTRODUCTION

Boltzmann's time hypothesis

In the 1890s, the kinetic theory of Ludwig Boltzmann, which represents an important link between thermodynamics and classical mechanics, attracted both interest and criticism. The criticism was to some extent motivated by doubts about the atomic (molecular) structure of matter, which were quite persistent at that time, but also involved a series of very interesting questions about consistency of the reversibility of classical mechanics with the irreversible nature of thermodynamics. Some of these questions (e.g. the exact physical mechanism determining the direction of time) are not fully answered even today. In response to his critics, Boltzmann put forward a number of hypotheses of remarkable originality and depth [1]. One of these hypotheses identifies our perceived direction of time with the second law of thermodynamics. Another hypothesis links the second law to the temporal boundary conditions imposed on the Universe (or the observed part of it). The consequence of these hypotheses is the astonishing possibility (which was explicitly discussed by Boltzmann [1]) that, given different temporal boundary conditions, the perceived time may run in opposite directions in different parts of the Universe.

More than 100 years after, we still do not have a full explanation for the physical mechanism of the direction of time, and the second law of thermodynamics remains our key indicator for the time arrow. It seems, however, that while the low entropy conditions in the past of the Universe are important, there should be a more specific and more local mechanism that enacts asymmetry of time. Indeed, consider the following gedanken experiment. Figure 1 depicts a piston-cylinder device, which is placed in a very remote part of the Universe, surrounded by a perfect reflective mirror and, hence, is completely insulated from the rest

of the Universe for a very long time. This removes any direct external influence of the Universe on the system with exception of the position of the piston. The piston is moved by an external force in a manner that is symmetric with respect to the past and the future. As we can guess, if the piston motion is sufficiently fast, the response of the system to this motion is not time symmetric: a compression shock wave appears when the piston is moving in, and a rarefaction wave is formed when the piston is moving out. Note that rarefaction shock waves do not violate the first law of thermodynamics but are prohibited by the second law, since entropy would decrease in these waves. The time asymmetry in this experiment is enforced not by the direct influence of the Universe but through the property of matter placed into the cylinder. The low-entropy initial conditions imposed on the Universe result in the formation of matter, which can exist for a very long time and, as it seems from the example of Figure 1, is not fully time-symmetric.

The time primer.

From the perspective of the ergodic theory, increase of entropy in dynamic systems of large dimensions is associated with ergodic mixing [2; 3]. This perspective is based on classical mechanics, which is time-reversible and preserves volume measures in the extended phase space (whose dimension is very large and determined by the overall number of microscopic degrees of freedom in the system). Note that quantum mechanics possesses similar properties linked to the unitarity of quantum evolutions. Ergodic mixing can be understood through analogy between evolution of volumes in the extended phase space with mixing of fluids. This analogy was first introduced by Gibbs in his fundamental work [4], which laid the foundations of statistical physics. Ergodic mixing can be illustrated by Figure 2, which depicts the extended phase space of a dynamic system.

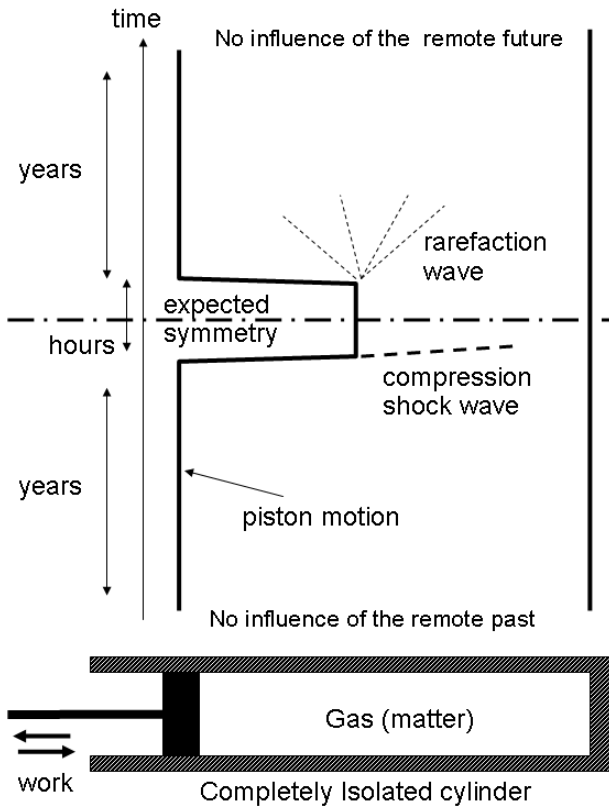


Figure 1. Direction of time in a system, which is completely isolated and affected only by piston movement.

The ensemble of states is initially (at $t = 0$) confined to the black region in Figure 2(IIa). The evolution of the system changes the shape of the region but does not alter its volume measure so that after a sufficiently long period of time t_1 , the trajectories become densely distributed in a larger and larger segment of the domain; Refer to Figure 2 : the black areas have exactly the same measure (i.e. the same number of black pixels) in IIa and IIIa but the segment effectively occupied by the black spot is larger in IIIa. The increasing volume measure of this segment is conventionally associated with an increasing entropy, as required by the second law. This logic, however, encounters severe problems when states of the system are considered back in time [5]. Since the evolution of a dynamic systems is time-reversible, it can be extended back to negative times and a state of the system similar to the state shown in IIIa should also be expected at $t = -t_1$ (see Figure 2, Ia). How can time-symmetric evolution (compare Ia and IIIa in Figure 2) be consistent with the second law?

The resolution of this apparent paradox in the process, which can be called the *time primer*. This process causes a diffusion-like increase of the black volume into the white region so that the state of the system at $t = t_1$ looks as shown in Figure 2(IIIb). The time primer is a violation of both classical mechanics and quantum mechanics, but its magnitude is so small that it is very difficult to detect the time primer directly. The influence of the time primer on the Universe is nevertheless profound. Due to ergodic mixing, the area of the black/white interface in Figure 2(IIIa) becomes so large that even very small coarsening of the distribution results in a large increase of the black volume. Hence entropy increases forward in time. The time primer is not time-symmetric and when we move back in time to $t = -t_1$,

it acts to decrease the black volume as depicted in Figure 2(Ib). Hence entropy reduces back in time.

In spite of the overwhelming evidence for directional asymmetry of time around us, the physical nature of the time primer still remains a mystery. In quantum mechanics, the time primer is linked with the process of decoherence, which is expected to violate unitarity of quantum evolutions. Although time symmetry is broken in quantum mechanics by weak interactions, there is no evidence that the known T-violating processes are the ones enacting the direction of time. Penrose [5] believes that decoherence is linked to interactions of quantum mechanics and gravity (although gravity, classical or relativistic, is conventionally seen as time-symmetric). A few theories (see, for example, [6; 7]) are related to the process of quantum decoherence. We, however, do not link the time primer to any specific theory or mechanism. In principle, the time primer may be a) a spontaneously generated property of matter and antimatter or b) can be induced by interactions with a special time-generating field. It is likely that generation of the time primer combines *spontaneous* (a) and *induced* (b) mechanisms. This means that the temporal irreversibility can be initially generated within matter (and also antimatter) and then propagate through interactions (for example, interactions by radiation). Even very small interactions, which have magnitudes below the detection limits, can be sufficient to tip entropy increase towards the common time direction.

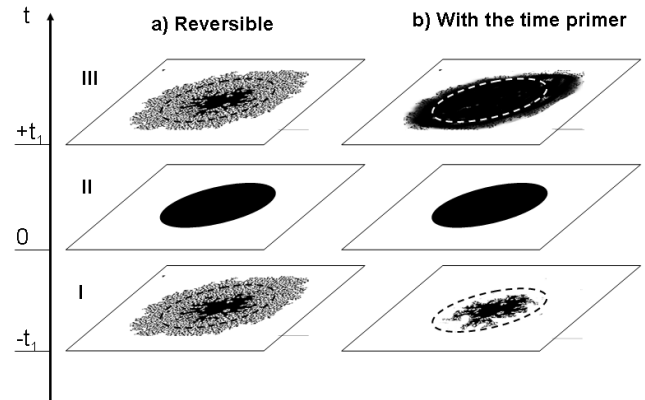


Figure 2. Evolution of a selected volume in the phase space.

Causality

The asymmetric nature of the time primer enacts causality: we see that future is determined by the past but not vice versa. Indeed, consider evolution of the phase volume schematically shown in Figure 3. If the initial state of the system is known as, say, area A at $t = t_0$, the state of the system at any following moment can be predicted: for example, it is area B at $t = t_1$. The converse statement is, however, incorrect: knowing that the system is in state B at $t = t_1$ does not allow us to conclude that it was in state A at $t = t_0$, since the system state at $t = t_0$ could well be A', or many other states determined by various possible contractions of the phase volume measure. While moving backwards in time, the choice between A and A' is seen as a random event. We interpret this by saying that A causes B but B is not a cause for A. The causality principle allows to treat mechan-

ical evolutions (classical or quantum) as time-reversible, while replacing the temporal irreversibility by requirement of setting the initial conditions before and not after the process under consideration. This principle provides a great simplification and works really well in many respects. The philosophical aspects of causality are discussed by Price [8].

The causality principle has another important implication: a non-equilibrium state must have its cause in the past but not in the future. For example, footsteps on a beach will eventually reach equilibrium with the sand and disappear (no special effort is needed for this) but the footsteps could not appear without a reason (i.e. someone walking across the beach) as this would contradict to the second law. A system that evolves very slowly towards its equilibrium (a photograph, for example) is a testimony of a distant past when its initial state was created by an external disturbance. The main implication of causality is that we can remember the past and can forecast the future but we cannot remember the future and cannot forecast the past.

The time primer does not have to be a fully deterministic process and the phase volume may fluctuate slightly from point to point, provided the overall trend for the phase volume to increase forward in time is dominant. We may observe some randomness forward in time (which, as the reader may notice, should be seen as causality backward in time). The forward-time randomness can be seen as a minor fluctuation of the time primer process, which results in a small local reduction of the phase volume. For example a rolling coin will finish on one of its sides, but it is impossible to predict if this is going to be "heads" or "tails". When the outcome becomes known, the reduction of uncertainty in this single bit (i.e. heads or tails) does not cause a global entropy decrease since the falling coin dissipates energy and this is accompanied by a large increase in molecular entropy.

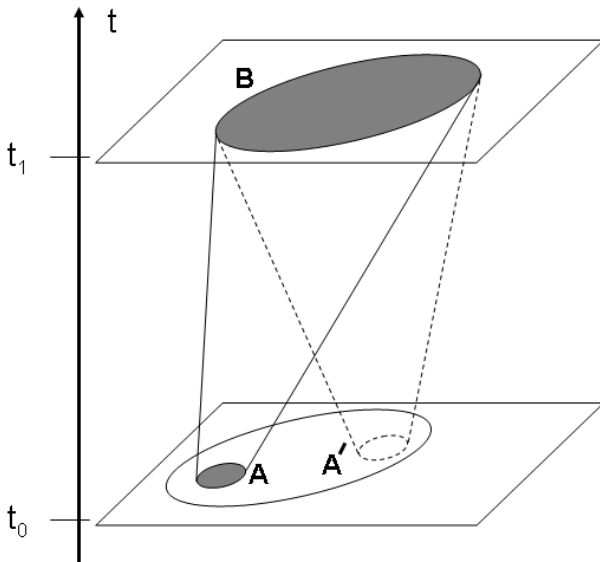


Figure 3. Causality induced by the time primer.

SYMMETRY OF MATTER AND ANTIMATTER

The Universe is populated mostly by radiation, has significant quantities of matter and, as far as we know, very small

quantities of antimatter in the form of scattered elementary particles. Antimatter is not identical to matter but there is a strong similarity between them [9]. We give this similarity a very broad interpretation: if our Universe were mostly composed from antimatter, we (also made of antimatter) would not be able to tell the difference as the physical laws of the antimatter universe would be the same.

If we change matter to corresponding antimatter by so called charge conjugation or (C-conjugation), the heat fluxes \mathbf{q} can change according to the following linear operation $\mathbb{C}(\mathbf{q}) = \alpha\mathbf{q}$, where \mathbf{q} is a conventional vector and α is a real constant. This operation takes us to antiuniverse with the same physical laws as ours but the constant α is not necessarily 1 since we do not know the correspondence of space and time between the two universes, composed of matter and antimatter. Applying the charge conjugation again results in converting antimatter back to matter, i.e. to going back to the original state. This means

$$\mathbf{q} = \mathbb{C}(\mathbb{C}(\mathbf{q})) = \mathbb{C}(\alpha\mathbf{q}) = \alpha^2\mathbf{q} \implies \alpha = \pm 1 \quad (1)$$

We will show that these two values of α correspond to different thermodynamics: CP-invariant ($\alpha = +1$) and CPT-invariant ($\alpha = -1$). Here, we refer to parity, which represents change of directions of spatial coordinates ($\mathbb{P}(\mathbf{x}) = -\mathbf{x}$), as P and to time reversal, which represents change of directions of time ($\mathbb{T}(t) = -t$), as T. These operations are known in quantum mechanics but here we follow Sakharov [10] and interpret them as general physical principles not confined to the field of quantum mechanics. Sakharov's principles that are necessary for explanation of the matter/antimatter bias are often quoted as:

- ◆ existence of reactions violating baryon numbers
- ◆ violation of the C and CP symmetry
- ◆ deviation from thermodynamic equilibrium

This list, however, does not include the fourth important assumption made by Sakharov in the same work [10]: CPT invariance is a global property of the Universe. While CPT invariance is commonly known as a theorem in quantum mechanics, its more general interpretation is a hypothesis, not a theorem. Penrose [5] believes that CPT invariance will not hold if applied to the whole of the Universe due to action of the second law. In the terms used here, this view corresponds to CP-invariant thermodynamics. The current status of the experimental confirmation of quantum symmetry principles is that C, P, T and CP symmetries are broken by weak interactions but the CPT symmetry, which is linked to the fundamental Lorentz invariance, is believed to be upheld. The CP and T violations have been found in meson decays but are much less common than CP-preserving C and P violations. Note that CP violation combined with CPT invariance implies T violation [9].

Since thermodynamics mainly deals with macroscopic scalar quantities, parity transformations are not important for a thermodynamic analysis.¹ In the following consideration we preserve conventional notations adopted in quantum mechanics and retain P in transformations. The implications of having positive and negative α in (1) are shown in Figure 4, which illustrates an experiment conducted by placing matter and antimatter in the focuses of a perfectly reflective ellipsoid (Figure 4(A)). Heat is transferred by radiation between matter and antimatter. The direction of the heat transfer changes as the transformations are

¹Although particles with opposite chiralities may need to be treated as different species in thermodynamics and kinetics.

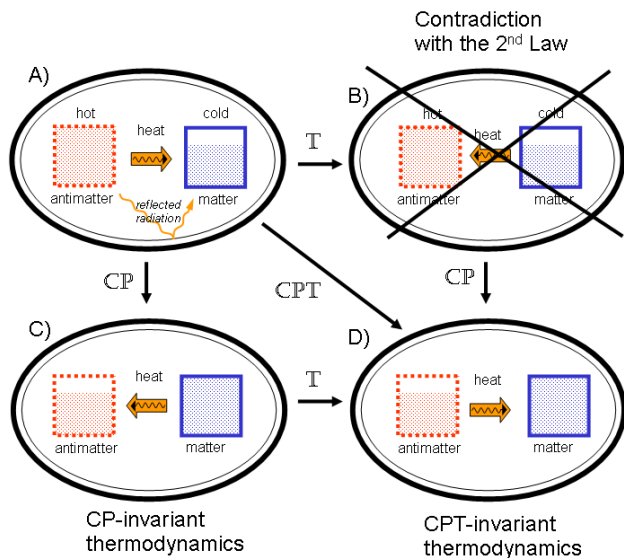


Figure 4. CP and T transformations of thermodynamics systems; "cold" and "hot" refer to intrinsic temperatures

applied. In simple terms, T reverses the direction of the heat transfer, C converts matter into antimatter and vice versa, while P swaps the systems located in the focuses and reverses the heat flux accordingly. Since thermodynamic laws are not time-invariant, the T-transformation of case (A) results in case (B) prohibited by the second law. The other cases, (C) and (D), are possible and correspond to CP-invariant and CPT-invariant thermodynamics. Note that, since thermodynamics is not T-symmetric, it must also violate at least one of the symmetries, CP or CPT.

In general, it is difficult to determine how thermodynamics should be extended from matter to antimatter due to the paucity of antimatter in the Universe. Both CP- and CPT- invariant thermodynamics give the same description for our current world populated by matter. CP-invariant thermodynamics is conventional and thus does not need extensive analysis here. CPT-invariant thermodynamics, it seems, has not been considered in the past but it is linked to the status of the CPT invariance, which is commonly seen as fundamental, and to our existing knowledge that CP symmetry is not a universal property of the Universe.

CPT-INVARIANT THERMODYNAMICS

Our previous discussion results in postulating the following key principles:

- ◆ **Reversible equivalence.** There is no distinction between matter and antimatter with respect to the first law of thermodynamics.
- ◆ **Inverted irreversibility.** Thermodynamically isolated antimatter can increase its entropy only backward in time (unlike any isolated matter, whose entropy increases forward in time).
- ◆ **Observational symmetry.** Antimatter and its interactions with matter are seen (i.e. observed, experimented with or measured) by antiobservers in exactly the same way as matter and its interactions with antimatter are seen by observers.

These principles correspond to CPT-invariant thermodynamics. In the case of CP-invariant thermodynamics (not considered in this section), the second principle is to be replaced by entropy increase forward in time for both matter and antimatter. Hypothetical observers made of antimatter, are called *antiobservers*, while the term *observers* refers only to us — observers made of matter. Properties of matter measured by us (the observers) and properties of antimatter measured by antiobservers are referred to as *intrinsic*. The properties of matter and antimatter measured by observers are referred to as *apparent*, while the properties of matter and antimatter measured by antiobservers are referred to as *antiapparent*.

The competing physical intuitions of CPT invariance and of conventional thermodynamics has been recently discussed by Downes et al [11]. The present approach should not be confused with the thermodynamic analysis conducted by Dunning-Davies [12] on the basis of Santilli isodualities and having physical outcomes and interpretations very different from ours. The reversible equivalence principle treats matter and antimatter as being the same with respect to mechanical laws, does not change the signs of energy and mass, and does not imply existence of antigravity and anti-photons that are associated with Santilli isodualities. A popular presentation of CPT-invariant thermodynamics is given in Ref.[13] from the perspective of a space traveller visiting world made of antimatter.

Interactions of thermodynamic systems and antisystems

In this subsection, we consider thermodynamic interactions of two systems comprised of matter and antimatter (i.e. a system and an antisystem). The interactions are limited, while the systems remain autonomous and isolated from the rest of the Universe. Due to autonomy, we can still apply causality in its modified form: the initial conditions for the matter system are set before and for the antimatter system are set after the interaction. Here, "before" and "after" refer to the observer's time.

Thermodynamics is based on determining the direction of processes where states (i.e. macrostates) can be realised by the largest possible number of microstates (given the constraints imposed on the system) and thus are overwhelmingly more likely than states encompassing fewer microstates. The logic of thermodynamics considers what is likely and neglects what is unlikely. The most likely state is called equilibrium. In conventional thermodynamics, unlikely states may be set as initial states while the system tends to move towards its equilibrium as time passes. This is reflected by the well-known Boltzmann-Planck entropy equation

$$S_i = k_B \ln(\Gamma_i) \quad (2)$$

linking the entropy S_i in the state i to the number of microstates Γ_i in this state. The number of microstates Γ_i is further referred to as the statistical weight of the thermodynamic state i . The constant k_B is the Boltzmann constant that rescales very large changes in Γ_i to more manageable thermodynamic quantities. Here, we do not discriminate the past and the future a priori — thermodynamic principles are applied by maximising the number of microstates associated with macroscopic evolutions, given spatial and temporal boundary conditions as well as other physical constraints imposed on the overall system. The term "overall" stresses inclusion of both the system and the antisystem.

Apparent temperatures. The temporal boundary conditions for the example shown in Figure 5 are: energy U_m and entropy S_m are specified for the system at $t = -t_1$ and $\bar{t} = t_1$, while \bar{U}_a \bar{S}_a are specified for the antisystem at $\bar{t} = -t_1$ and $t = t_1$. The overbar symbol indicates that the value is antiapparent, i.e. evaluated from the perspective of an antiobserver, whose time $\bar{t} = -t$ goes in the opposite direction as compared to our time t . The system and antisystem are isolated from each other for most of the time but a limited thermodynamic contact of matter and antimatter, allowing for transition of a small quantity of heat δQ through exchange of radiation, occurs at $t = 0$ (and $\bar{t} = 0$). The time window is selected so that $|\delta Q|$ cannot exceed δQ_{\max} where δQ_{\max} is sufficiently small. According to the observer the thermal energy δQ is transferred from the antisystem to the system as shown by the black solid arrow. According to the antiobserver, who interpret the same event in the opposite direction of time, the same thermal energy δQ is transferred from the system to antisystem as shown by the red dashed arrow. Heat δQ is assumed to be positive when transferred in the direction shown in Figure 5: from the antisystem to the system according to the observer and from the system to the antisystem according to the antiobserver. The total energy

$$U_{tot} = U_m + (\bar{U}_a + \delta Q) = (U_m + \delta Q) + \bar{U}_a \quad (3)$$

(evaluated at any constant time $t = -\bar{t}$) is preserved in this example, as it should since the formulation of the first law of thermodynamics does not depend on the differences between matter and antimatter due to the postulated reversible equivalence.² Note that $\bar{U}_a = U_a$ due to reversible equivalence. The entropy change of the system as observed by us and the entropy change of the antisystem as seen by the antiobserver (these are the entropies linked to Γ) can be easily evaluated and these changes of intrinsic entropy are shown in Figure 5 for the states m' and a' .

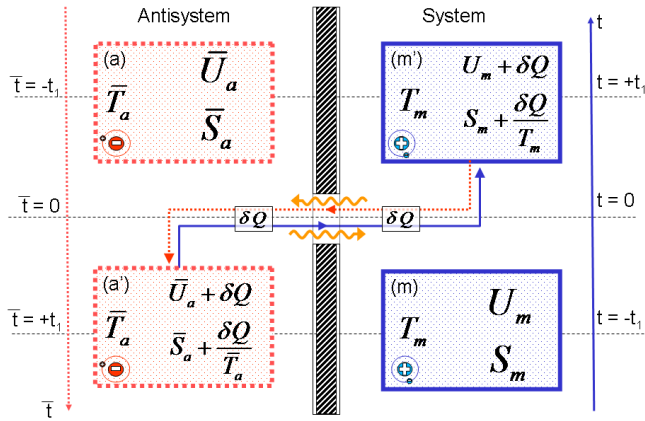


Figure 5. Thermodynamic interactions of a system and antisystem.

We now evaluate the overall statistical weight Γ_{tot} that corresponds to different trajectories that are allowed by the first

law of thermodynamics. The overall state is related to the four sub-states: m , a , m' and a' . The overall statistical weight Γ_{tot} is linked to the product of the statistical weights of the sub-states $\Gamma_m \Gamma_{m'} \Gamma_a \Gamma_{a'}$ and, according to equation (2), becomes

$$\Gamma_{tot}(\delta Q) \sim \Gamma_m \Gamma_{m'} \Gamma_a \Gamma_{a'} = \exp\left(\frac{S_m + S_{m'} + \bar{S}_a + \bar{S}_{a'}}{k_B}\right) \quad (4)$$

The value Γ_{tot} depends on δQ . Note that S_m and \bar{S}_a are fixed by the boundary conditions and only $S_{m'}$ and $\bar{S}_{a'}$ depend on δQ . In this example, we should place the time moments $t = -t_1$ and $t = +t_1$ as far apart as needed to ensure establishment of equilibria within the system and the antisystem before and after the interaction, which is used in (4) in form of stochastic independence of microstates that correspond to the macrostates m and m' , a' and a . Two of the states, m and a , are fixed by the boundary conditions.

Equation (4) can be simplified through normalising Γ_{tot} by the value of Γ_{tot} at $\delta Q = 0$

$$\frac{\Gamma_{tot}(\delta Q)}{\Gamma_{tot}(0)} = \exp\left(\frac{\delta Q}{k_B} \left(\frac{1}{T_m} + \frac{1}{\bar{T}_a}\right)\right) \quad (5)$$

where conventional definitions of the temperature

$$\frac{1}{T_m} = \frac{\partial S_m}{\partial U_m}, \quad \frac{1}{\bar{T}_a} = \frac{\partial \bar{S}_a}{\partial \bar{U}_a} \quad (6)$$

are used. (The quantity δQ is assumed to be too small to affect the intrinsic temperatures of matter and antimatter, which remain T_m and \bar{T}_a correspondingly.). From observer's perspective, the conventional equilibrium condition is given by equivalence of apparent temperatures $T_m = T_a$. If the system and the antisystem are in thermodynamic equilibrium, both directions of heat transfer $\delta Q > 0$ and $\delta Q < 0$ must be equally likely and have the same statistical weight Γ_{tot} . This occurs only when $T_m = -\bar{T}_a$ indicating that the apparent temperature of antimatter is $T_a = -\bar{T}_a$. In the same way, the antiapparent (i.e. perceived by the antiobserver) temperature of matter is $\bar{T}_m = -T_m$. It is easy to see that thermodynamic quantities \bar{S}_a , \bar{T}_a , and \bar{U}_a that characterise the intrinsic properties of antimatter are apparent as

$$T_a = -\bar{T}_a, \quad S_a = -\bar{S}_a, \quad U_a = \bar{U}_a \quad (7)$$

from our perspective. The sign of U_a is selected to be consistent with the first law of thermodynamics (3), while the sign of S_a is chosen to be consistent with the definition of temperature $T_a^{-1} = \partial S_a / \partial U_a$ and with equations (6). The change of sign does not affect our interpretation of reversible transformations of antimatter since S_a is constant whenever \bar{S}_a is constant, which is consistent with our assumption that matter and antimatter behave in the same way in reversible processes. The state of having the same positive (and finite) intrinsic temperatures $T_m = \bar{T}_a$ does not correspond to equilibrium and, according to (5), transfer of heat from antisystem to system in observer's time is strongly favoured by thermodynamics.

It appears that a system created in our world with negative temperatures can, at least in principle, be placed into thermal

²Interactions of matter and antimatter may include the third key component — coherent radiation. In thermodynamics, this would correspond to considering work reservoirs in addition to heat reservoirs (see, for example, the "weight process" of Ref.[14]). The energy balance at the moment of contact is $U_{tot} = U_{m0} + U_{a0} + U_r$ where U_r is the radiation energy and the subscript "0" indicates states taken at $t = 0$.

equilibrium with an antisystem or, analogously, an antisystem at negative intrinsic temperatures can be in thermodynamic equilibrium with a system having a positive intrinsic temperature. This equilibrium state, however, would be predominantly unstable, since in most cases the antimatter system according to (7) is likely to have negative apparent heat capacities

$$C_a = \frac{-1}{T_a^2} \left(\frac{\partial^2 S_a}{\partial U_a^2} \right)^{-1} = \frac{1}{\bar{T}_a^2} \left(\frac{\partial^2 \bar{S}_a}{\partial \bar{U}_a^2} \right)^{-1} = -\bar{C}_a \quad (8)$$

This equation indicates that changing the sign of the entropy S changes the sign of the heat capacity C irrespective of the sign of the temperature T . Hence, a thermodynamic contact of an antisystem and a system predominantly results not in reaching the corresponding thermal equilibrium state but in the antisystem losing energy (to the system) and further increasing its apparent temperature until the temperature of the antisystem reaches its intrinsic ground state $-T_a = \bar{T}_a \rightarrow +0$. Note that stable thermodynamic equilibrium between a system and an antisystem is possible at $T_m = T_a = \bar{T}_a = \infty$.

Mass exchange between matter and antimatter. An antimatter system with a variable number of particles is characterised by the equation

$$d\bar{U}_a = \bar{T}_a d\bar{S}_a + \bar{\mu}_a d\bar{N}_a \quad (9)$$

which remains the same as conventional as long as it is presented from the perspective of the antiobserver. From our perspective, this equation changes according to (7). The reversible equivalence requires preservation of mass, which demands that the apparent and intrinsic numbers of particles composing antimatter are the same. Hence, the apparent and intrinsic values of the number of particles (or moles) N and of the chemical potentials μ coincide:

$$N_a = \bar{N}_a, \quad \mu_a = \bar{\mu}_a \quad (10)$$

Similar relations can be drawn for other thermodynamic quantities such as volume and pressure. Due to the observational symmetry, $\mu_a = \bar{\mu}_a(\bar{T}_a, \bar{N}_a, \dots)$ is the same function as $\mu_m = \mu_m(T_m, N_m, \dots)$.

We note first the at infinite temperatures $T_m = T_a = \bar{T}_a = \infty$, the same quantities of matter and antimatter $N_a = \bar{N}_a = N$, which are kept under the same conditions, are in both thermal and chemical equilibrium since $\mu_a = \bar{\mu}_a(\infty, N, \dots) = \mu_m(\infty, N, \dots)$. If, however, $T_m < \infty$, then thermal equilibrium $T_m = T_a = -\bar{T}_a$ does not imply that matter and antimatter under similar conditions are in chemical equilibrium since $\mu_a = \bar{\mu}_a(-T, \dots)$ is generally different from $\mu_m = \mu_m(T, \dots)$ for the same T . Hence, even if it might be possible to put an antisystem in thermal equilibrium with a system by using negative temperatures, this equilibrium does not extend to chemical stability between matter and antimatter.

If a system and an antisystem are kept at the same intrinsic temperatures $T_m = \bar{T}_a = T < \infty$ (and the same other conditions), then $\mu_a = \bar{\mu}_a(T, N, \dots) = \mu_m(T, N, \dots)$. In this case, however, equality of chemical potentials does not ensure chemical equilibrium since there is no thermal equilibrium $T_m \neq T_a = -\bar{T}_a$. Consider the following example: matter and antimatter are confined to the system and antisystem correspondingly and can not

mix (mixtures are considered in the following subsection). Matter and antimatter can react with each other $n \rightleftharpoons \bar{n}$ and can annihilate to produce radiation $n + \bar{n} \rightleftharpoons 2\gamma$.³ These two reactions can be combined to result in conversion $2\bar{n} \rightleftharpoons 2\gamma \rightleftharpoons 2n$; that is antimatter is moved from antisystem to system by radiation and converted to matter possessing the same energy. Assuming that pressures are kept the same and constant in the system and antisystem, this transition does not affect intrinsic temperatures $T_m = \bar{T}_a$ and intrinsic entropy per particle (or per mole) $s_m = \bar{s}_a$, where $s = S/N$. The total apparent entropy $S_{tot} = N_m s_m - N_a \bar{s}_a$ clearly increases. We see that CPT-invariant thermodynamics strongly favours conversion of antimatter into matter (from observer's perspective), even if the intrinsic properties of matter and antimatter are exactly the same. For an antiobserver, this process seems as conversion of matter into antimatter.

Mixed matter and antimatter

When matter and antimatter are mixed, they do not form semi-autonomous thermodynamic systems with effectively independent directions of time. We shall distinguish two cases: when matter dominates antimatter in the mixture and when a 50:50 mixture is formed.

Mixtures dominated by matter. Consider a mixture of many particles n_m with very few antiparticles n_a . The translational degrees of freedom are entangled to produce a dominant direction of thermodynamic time for the whole mixture. Since particles have the numbers, this direction must be forward in time. Presence of antiparticles may slightly increase the fluctuating components of the time primer without any noticeable effect on thermodynamic properties. If particles and antiparticles are considered as mechanical or quantum systems and the direct effect of the spontaneous time primer on the particles is below detection limits, the presence of antiparticles does not affect the thermodynamic properties of the mixture (we do not consider annihilations, of course).

A different situation appears when each particle (and each antiparticle) represents an autonomous thermodynamic subsystem (i.e. having a large number of comparable internal degrees of freedom). In this case, the thermodynamic time runs in opposite directions within particles and antiparticles (and in the normal direction for the whole mixture). While the thermodynamic subsystems can, in principle, be placed in thermal equilibrium when intrinsic temperature of the antiparticles is negative (this is possible when internal energy levels of antiparticles are bounded — see [15]) but this equilibrium is typically unstable as discussed previously. Hence, antiparticle subsystems should fall into their ground state (which is nevertheless subject to fluctuations, significant for microscopic subsystems), while particle subsystems remain in conventional thermal equilibrium with the mixture. While techniques based on evaluating statistical sums can not be used for systems with negative heat capacity (see [15]), there is no contradiction in using these techniques when antiparticle systems are in their ground state. Let us see

³We use hypothetical reactions with neutrons n and antineutrons \bar{n} to illustrate our point. The reaction $n \rightleftharpoons \bar{n}$ (or similar) is predicted by the 1st Sakharov condition but has not been observed so far under current conditions prevailing in the Universe.

how the partition function Z should be evaluated in this case

$$Z = (Z_0)^{N_m+N_a} \frac{(Z_m)^{N_m}}{N_m!} \frac{(Z_a)^{N_a}}{N_a!}, \quad (11)$$

$$Z_m = \sum_i \exp\left(-\frac{E_i}{k_B T}\right), \quad Z_a = \exp\left(-\frac{E_0}{k_B T}\right), \quad (12)$$

where Z_0 is the partition function without considering internal degrees of freedom, Z_m is partition function for particle internal energy levels and Z_a is the partition function for antiparticles in their ground state. Note that Z_a can be made unity ($Z_a = 1$) without loss of generality by selecting E_0 as the reference energy level (i.e. $E_0 = 0$). The difference in chemical potentials of particle and antiparticles can be evaluated by using standard techniques [16]

$$\begin{aligned} \Delta\mu &= \mu_a - \mu_m = \left(\frac{\partial A}{\partial N_a} - \frac{\partial A}{\partial N_m} \right)_T \\ &= k_B T \left(\ln\left(\frac{N_a}{N_m}\right) + f_m(T) \right) \end{aligned} \quad (13)$$

where $A = -k_B T \ln(Z)$ is the Helmholtz potential and $f_m(T) = \ln(Z_m(T)) \geq 0$. The asymmetry of the chemical potentials $\Delta\mu$ tends to be higher at higher temperatures. Note that particles and antiparticles may have not only different chemical potentials but also slightly different masses as they have different average energies.

The 50:50 mixture. The case of having 50% particles and 50% corresponding antiparticles in the mixture is the most difficult case to analyse. The thermodynamic time can not run in any direction due to matter/antimatter symmetry. This generally means that only reversible processes can occur in this mixture and there is no relaxation towards equilibrium state in any direction of time. Any process that is irreversible (formation of a black hole, for example) is impossible in this mixture.

Although there is no direction of thermodynamic time on average in this mixture, there are fluctuations in the system. The thermodynamic time might also fluctuate, moving slightly forward or backward due to a minor local prevalence of one of the mixture components over the other. At this point things get more complicated. The areas with a small excess of matter can be seen as forming systems, while the areas with a small excess of antimatter form antisystems. If all temperatures are infinite $T_m = T_a = \bar{T}_a = \infty$, then systems and antisystems are in equilibrium according to the analysis of the previous subsection. If, however, the intrinsic temperatures are high but finite, then (as also discussed in the previous subsection) thermodynamics favours transfer of energy, volume and matter/antimatter from antisystems to systems. This process can be seen as thermodynamic instability resulting in systems (with the forward-directed thermodynamic time) taking over and antisystems (with the backward-directed thermodynamic time) disappearing. In anti-system regions matter and antimatter can unmix forward in time reducing further the volume occupied by antisystems. Matter needs to retain its leading role over antimatter within the system regions, if the forward-time evolution is to continue in these regions. The asymmetry of chemical potentials (13) stimulates conversion of antimatter into matter within the systems. Note that the same mechanism converts matter into antimatter within the antisystems but this happens in the forward direction of an-

tiobserver's time; hence antimatter is converted into matter in our time.

DISCUSSION AND CONCLUSIONS

Thermodynamics can be extended to include antimatter in two different ways: CP-invariant and CPT-invariant. Due to the time-directional nature of thermodynamics, its CP-invariant and CPT-invariant versions can not be valid at the same time. Philosophically, CPT-invariant thermodynamics connects two major asymmetries in nature — the observed direction of time and abundance of matter combined with absence of antimatter, while CP-invariant thermodynamics sees these issues as separate. In the absence of appreciable quantities of antimatter in our world, it is very difficult to determine, which one of these thermodynamics is not only logically possible but also real: both versions give the same predictions for the matter and similar predictions for autonomous particles and antiparticles. If, however, baryons (neutrons and protons) can be treated as stochastic systems, then CP-invariant thermodynamics requires the similarity of particles and antiparticles, while CPT-invariant thermodynamics predicts differences in chemical potentials (and, possibly, other properties) between particles and their antiparticles. Is there experimental evidence to make a choice between the two versions of thermodynamics on this basis?

Recent experiments in high-energy accelerators, indicate that thermodynamics might be relevant to very small scales (within a hadron) and high energies [17]. Protons and neutrons seem to contain myriads of appearing and annihilating gluons and quarks. Collisions involving protons and nuclei produce various particles and antiparticles with distributions strongly resembling a thermodynamic equilibrium. This equilibrium is characterised by a number of parameters, including μ_B — the chemical potential associated with the baryon number B , so that baryons ($B = +1$) and antibaryons ($B = -1$) have different chemical potentials [17]. This seems to confirm the CPT-invariant version of thermodynamics but, in our opinion, this is probably not the case. In the absence of reactions violating B , true chemical potential associated with the baryon number is not revealed⁴. Hence, μ_B is likely to be an effective quantity reflecting initial conditions, although it does seem that thermodynamic equilibrium is achieved in these experiments with respect to the other parameters.

We assume that spontaneous time-priming processes are of very small magnitude and, thus, are not directly detectable in conventional experiments. This is plausible since, in spite of the clear presence of an arrow of time (presumably everywhere, including in remote and isolated systems), we still do not know its exact mechanism. Induced time priming, whose magnitude is amplified by thermodynamic surroundings, may be possible to detect in quantum systems. Interactions of a quantum system with time-priming process do not cause any detectable anomalous behaviour when the system is CP-symmetric. If, however, a quantum system displays a CP violation, its interactions with time priming induced by the environment are likely to produce an impression of a CPT violation. Two versions of thermodynamics differ in its interpretation. CP-invariant thermodynamics admits that CPT is violated. CPT-invariant thermodynamics insists that the world is CPT-invariant so that the CPT violation is only an apparent phenomenon created by asymmetrically dominant presence of matter in the Universe.

⁴One can compare this with assigning elements arbitrary chemical potentials in chemical reactions conserving the elements

The difference between CP- and CPT-invariant thermodynamics is not limited to philosophical interpretations. CPT-invariant thermodynamics indicates that nature has difficulties in assembling substantial quantities of antimatter due to its thermodynamic antagonism with matter (thermodynamics favours the latter over the former when observed forward in our time). Collecting statistically significant quantities of antimatter at a sufficient density and insulating it from the dominant time priming influence of the environment should result, according to CPT-invariant thermodynamics, in changing the thermodynamic arrow of time and a very unstable state associated with negative apparent temperatures. The chaotic energy of random motions can then be converted to coherent light of high intensity in complete agreement with the laws of thermodynamics. CP-invariant thermodynamics, on the contrary, does not expect any dangerous thermodynamic instabilities in these experiments.

While CPT-invariant thermodynamics seems to be conceptually consistent with the invariance principles adopted in other branches of physics, making an experimentally justified choice between two versions of thermodynamics is not possible at present, since both of the versions give the same predictions for our world populated by matter. However, this may change as more and more substantial quantities of antimatter are produced in experiments by high-energy accelerators [18].

ACKNOWLEDGMENT

The authors acknowledge funding by the Australian Research Council and the Deutsche Forschungsgemeinschaft.

NOMENCLATURE

k_B	Boltzmann constant
t	time
C	heat capacity
N	number of particles
Q	heat energy
S	entropy
T	temperature
U	energy
Γ	number of microstates
μ	chemical potential
\mathbf{q}	heat flux
\mathbb{C}	charge conjugation
\mathbb{H}	Hamiltonian
\mathbb{P}	parity transformation
\mathbb{T}	time reversal

REFERENCES

- [1] L. Boltzmann. *Lectures on gas theory*. English translation by S.G. Brush. University of California Press, Berkeley and L.A., 1964 (1895,1897).
- [2] J. L. Lebowitz and O. Penrose. Modern ergodic theory. *Physics today*, (Feb.):23–28, 1973.
- [3] A. Y. Klimentko. What is mixing and can it be complex? *Physica Scripta*, 2012.
- [4] J. W. Gibbs. *Elementary principles in statistical mechanics*. University Press, Cambridge, USA, 1902.
- [5] R. Penrose. *Road to Reality: A Complete Guide to the Laws of the Universe*. A. Knopf Inc., 2005.
- [6] G.P. Beretta. On the general equation of motion of quantum thermodynamics and the distinction between quantal and nonquantal uncertainties (MIT, 1981). arXiv: quant-ph/0509116, 2005.
- [7] A. Bassia and G. Ghirardi. Dynamical reduction models. *Physics Reports*, 379:257–426, 2003.
- [8] H. Price. *Time's Arrow and Archimedes' Point: New Directions for the Physics of Time*. Oxford Univ. Press, Oxford, UK, 1996.
- [9] W. M. Gibson and B. R. Pollard. *Symmetry principles in elementary particle physics*. Cambridge Univ. Press, UK, 1976.
- [10] A. D. Sakharov. Violation of CP invariance, C asymmetry, and baryon asymmetry of the universe. *J. Exp. Theor. Phys.*, 5:24–27, 1967.
- [11] S. Downes, B. Dutta, and K. Sinha. Attractors, universality and inflation. arXiv: 1203.6892 [hep-th], 2012.
- [12] J. Dunning-Davies. Thermodynamics of antimatter vis Santilli's isodualities. *Foundations of Physics Letters*, 12(6):593–599, 1999.
- [13] A. Y. Klimentko and U. Maas. Thermodynamics and time-directional invariance. arXiv: 1209.1982 [gen-ph], 2012.
- [14] E.P. Gyftopoulos and G.P. Beretta. *Thermodynamics. Foundations and Applications*. Macmillan, N.Y., USA, 1991.
- [15] A.Y.Klimentko. Teaching the third law of thermodynamics. *Open Thermodynamic Journal*, 6:1–14, 2012, (arXiv:1208.4189 [physics.class-ph]).
- [16] L. D. Landau and E. M. Lifshits. *Statistical physics*, volume 5. Pergamon Press, Oxford ; Sydney, N.S.W, 1980.
- [17] A. Andronic, P. Braun-Munzinger, J. Stachel, and H. Stcker. Production of light nuclei, hypernuclei and their antiparticles in relativistic nuclear collisions. *Physics Letters B*, 697:203–207, 2011.
- [18] Niels Madsen. Cold antihydrogen: a new frontier in fundamental physics. *Phil.Trans. Roy. Soc. A*, 368(1924):3671–3682, 2010.
- [19] V. Weisskopf and E. Wigner. Berechnung der natürlichen linienbreite auf grund der diracschen lichttheorie. *Z. Phys.*, 63:54–73, 1930.

Appendix A: Quantum Example

Consider a quantum system, which involves particles and antiparticles and is placed into environment filled by radiation (see Figure 6). The radiation is equilibrated by surroundings, which, of course, is made of matter prevalently present in the Universe. The system is quantum and not thermodynamic; hence its time priming is induced and not spontaneous. Note that we do not consider emission or adsorption but only very weak interactions of the system and radiation. We conduct our analysis within the limits of quantum mechanics and take into account time priming through causality and choice of the interaction parameters⁵.

The state of the environment (i.e. radiation bath) is characterised by its set of energy eigenstates $\mathbb{H}_B |\beta\rangle = E_\beta |\beta\rangle$. The

⁵In principle, the time primer can violate unitarity of quantum mechanics equations by increasing the phase volume available to the system, although the magnitude of this direct violation is expected to be very small. Here, we are interested not in intrinsic spontaneous increase of the phase volume within the system but in transferring the phase volume increases from environment to the system (i.e. induced time priming). This can be modelled within the framework of conventional quantum mechanics but the time-asymmetric nature of this process should be noted and taken into account as a selection rule. Radiation is understood as any field or interaction that can induce time priming, whose effect is related but not necessarily limited to quantum decoherence.

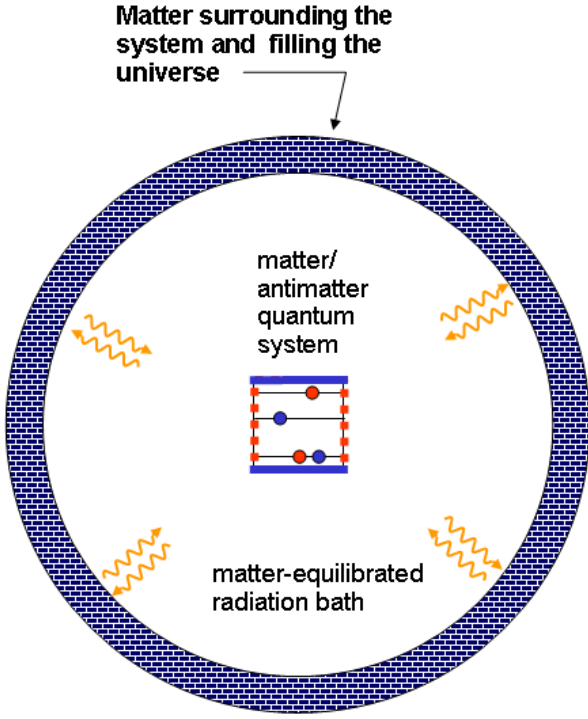


Figure 6. Quantum system placed into a radiation bath.

wave function of the environment is deemed to be in thermal equilibrium

$$\Psi_B = \sum_{\beta} c_{\beta} |\beta\rangle |\beta\rangle, \quad p_{\beta} = c_{\beta}^* c_{\beta} \sim \exp\left(\frac{-E_{\beta}}{k_B T}\right) \quad (14)$$

Here, we specify the maximally mixed state of the environment by using the random phase notation detailed in Appendix B. The environment is large and not significantly affected by interactions with the system and remains in its maximally mixed state.

The state of the system can be characterised by a set of system ket states $|s\rangle$ while the state of the supersystem, which involves the system and the radiation bath, are specified by the tensor product $|s\rangle \otimes |\beta\rangle = |s\rangle |\beta\rangle = |s\beta\rangle$. The overall wave function Ψ and the reduced wave function of the system Ψ_S can be represented in form of the expansions:

$$\Psi = \sum_{s,\beta} c_{s\beta} |s\beta\rangle |\beta\rangle, \quad \Psi_S = \sum_{s,\beta} c_{s\beta} |s\rangle |\beta\rangle \quad (15)$$

where Ψ_S is obtained by multiplying Ψ by the environmental bra state $\langle\alpha|$, noting orthonormality $\langle\alpha|\beta\rangle = I_{\alpha\beta}$ and summing over all α . Here, $I_{\alpha\beta}$ is the identity matrix $I_{\alpha\beta} = 0$, $\alpha \neq \beta$ and $I_{\alpha\beta} = 1$, $\alpha = \beta$. The random phase $|\beta\rangle$ in Ψ_S indicates a mixture of states that correspond to different β . This is similar to writing the overall state as $|s\rangle |\beta\rangle$ and then assuming that states $|\beta\rangle$ are not measurable and replacing $|\beta\rangle$ by $|\beta\rangle$. Since $|\beta\rangle$ do not evolve in conventional quantum mechanics, the system wave functions $\Psi_S^{(\beta)}$ that correspond to different β can be considered independently

$$\Psi_S^{(\beta)} = \sum_s c_s^{(\beta)} |s\rangle, \quad c_s^{(\beta)} = \frac{c_{s\beta}}{(p_{\beta})^{1/2}}, \quad p_{\beta} = \sum_s c_{s\beta}^* c_{s\beta} \quad (16)$$

The overall Hamiltonian that corresponds to our assumptions is written in the form

$$\mathbb{H} = \mathbb{H}_S \otimes \mathbb{I}_B + \mathbb{I}_S \otimes \mathbb{H}_B + \mathbb{H}_{SB} \quad (17)$$

where \mathbb{H}_S is Hamiltonian of the system, \mathbb{H}_{SB} is the system/bath interaction Hamiltonian and \mathbb{I} is the identity operator. Assume that

$$\langle\alpha q| \mathbb{H}_{SB} |s\beta\rangle = h_{qs}^{(\beta)} I_{\alpha\beta} \quad (18)$$

The system/radiation bath interaction term can be approximated by $h_{qs}^{(\beta)} = \phi(\beta) h_{qs}^{(0)}$, where $\phi(\beta)$ is the β -dependent intensity of coupling and $h_{qs}^{(0)}$ is the associated Hamiltonian.

The interactions with radiation-induced time priming should be CP-invariant and T-asymmetric so that the corresponding properties of the Hamiltonian are

$$\langle\alpha q| \mathbb{H}_{SB} |s\beta\rangle = \langle\overline{\alpha q}| \mathbb{H}_{SB} |\overline{s\beta}\rangle \Rightarrow h_{qs}^{(\beta)} = h_{\overline{q}\overline{s}}^{(\beta)} \quad (19)$$

$$\Delta h_{qs}^{(\beta)} = \langle\beta q| \mathbb{H}_{SB} |s\beta\rangle - \langle\beta s| \mathbb{H}_{SB} |q\beta\rangle \neq 0 \quad (20)$$

where the overbars denote anti-states. The property $\beta = \overline{\beta}$ is taken into account for radiation (i.e. matter and antimatter interact with radiation in the same way). Note that $\Delta h_{qs}^{(\beta)}$ is imaginary when \mathbb{H} is Hermitian. Equations (19) and (20) imply a CPT violation:

$$\langle\beta q| \mathbb{H}_{SB} |s\beta\rangle \neq \langle\overline{\beta s}| \mathbb{H}_{SB} |\overline{q\beta}\rangle \quad (21)$$

The different versions of thermodynamics, however, give different interpretations for this violation:

- ◆ **CP-invariant thermodynamics** admits (21) as CPT violation;
- ◆ **CPT-invariant thermodynamics** sees (21) as apparent and induced by the fact that matter, which surrounds the experiment and is implicitly present in the interactions by equilibrating the radiation, is not replaced by antimatter.

Decay kinetics

Among the system states $|s\rangle$, we distinguish two groups: the initial states $|k\rangle$ (or $|j\rangle$ when an alternative symbol is needed for the bra-space), and the final states, which are indexed by $|f\rangle$. The system is initially placed into a pure state that spans over the k -states but then decays into one or several of the f -states. Both, the k -states and the f -states, are eigenstates $\mathbb{H}_0 |f\rangle = E_f |f\rangle$, $\mathbb{H}_0 |k\rangle = E_k |k\rangle$ of the undisturbed Hamiltonian \mathbb{H}_0 ; the initial states are degenerate: $E_k = E_0$ for all k . The system Hamiltonian is given by $\mathbb{H}_S = \mathbb{H}_0 + \mathbb{H}_1$, where smaller component \mathbb{H}_1 is responsible for interactions of the initial and final states. After tracing out the state of the environment and denoting $\mathbb{H}^{(\beta)} = \langle\beta| \mathbb{H} |\beta\rangle - E_{\beta} \mathbb{I}_S$ and $\mathbb{h}^{(\beta)} = h_{kf}^{(\beta)} |k\rangle \langle f|$, we can write

$$\mathbb{H}^{(\beta)} = \mathbb{H}_0 + \mathbb{H}_2^{(\beta)}, \quad \mathbb{H}_2^{(\beta)} \equiv \mathbb{H}_1 + \mathbb{h}^{(\beta)} \quad (22)$$

The effective Hamiltonian $\Lambda_{jk}^{(\beta)}$ of the decaying k -states is obtained by using the Weisskopf-Wigner approximation [19], which plays in quantum decays the same role as kinetic equations in chemistry,

$$\Lambda_{jk}^{(\beta)} = \langle j | \mathbb{H}^{(\beta)} | k \rangle + \lambda_{jk}^{(\beta)} \quad (23)$$

$$\lambda_{jk}^{(\beta)} \equiv \sum_f \frac{\langle j | \mathbb{H}_2^{(\beta)} | f \rangle \langle f | \mathbb{H}_2^{(\beta)} | k \rangle}{E_0 - E_f + i\varepsilon}$$

where $\varepsilon \rightarrow 0$ and the sign of ε is selected to produce decaying exponents required by causality. Approximation (23) is conventionally used to analyse decay of neutral kaons, K^0 and \bar{K}^0 [9]. We investigate the CPT-compliance of the decay, which requires that $\Theta^{(\beta)} \equiv \Lambda_{kk}^{(\beta)} - \Lambda_{\bar{k}\bar{k}}^{(\beta)} = 0$ [9].

The case of CP symmetry. Most quantum systems possess CP symmetry and relatively few CP violations are known in quantum mechanics. When the system Hamiltonian \mathbb{H}_S is CP-invariant, we obtain

$$H_{kf} = \langle k | \mathbb{H}_S | f \rangle = \langle \bar{k} | \mathbb{H}_S | \bar{f} \rangle = H_{\bar{k}\bar{f}} \quad (24)$$

$$\Theta^{(\beta)} \equiv \Lambda_{kk}^{(\beta)} - \Lambda_{\bar{k}\bar{k}}^{(\beta)} = 0 \quad (25)$$

Here we use equations (19), (23), (24) to obtain (25) and conclude that the system appears to be CPT-compliant.

The case of CPT symmetry and CP violation. The system Hamiltonian \mathbb{H}_S is CPT-invariant provided

$$H_{kf} = \langle k | \mathbb{H}_S | f \rangle = \langle \bar{f} | \mathbb{H}_S | \bar{k} \rangle = H_{\bar{f}\bar{k}} \quad (26)$$

We use equations (19), (23) and (26) and note that the first term in (23) does not contribute to $\Theta^{(\beta)}$ so that

$$\Theta^{(\beta)} = \lambda_{kk}^{(\beta)} - \lambda_{\bar{k}\bar{k}}^{(\beta)}$$

$$= \sum_f \frac{\left(H'_{kf} + h_{kf}^{(\beta)} \right) \left(H'_{fk} + h_{fk}^{(\beta)} \right) - \left(H'_{\bar{k}\bar{f}} + h_{\bar{k}\bar{f}}^{(\beta)} \right) \left(H'_{\bar{f}\bar{k}} + h_{\bar{f}\bar{k}}^{(\beta)} \right)}{E_0 - E_f + i\varepsilon}$$

$$= \sum_f \frac{\left(H'_{kf} + h_{kf}^{(\beta)} \right) \left(H'_{fk} + h_{fk}^{(\beta)} \right) - \left(H'_{fk} + h_{fk}^{(\beta)} \right) \left(H'_{kf} + h_{kf}^{(\beta)} \right)}{E_0 - E_f + i\varepsilon}$$

$$= - \sum_f \frac{\Delta H'_{kf}}{E_0 - E_f + i\varepsilon} \Delta h_{kf}^{(\beta)} \quad (27)$$

where $H'_{kf} \equiv \langle k | \mathbb{H}_1 | f \rangle$, $\Delta H'_{kf} = H'_{kf} - H'_{fk}$. Hence, interactions with time priming can appear in CP-violating (but CPT preserving) systems as an apparent CPT violation. Absence of the time symmetry $\Delta H'_{kf} \neq 0$ and $\Delta h_{kf}^{(\beta)} \neq 0$ is essential for this effect.

Appendix B: Random Phase Notation

This appendix explains the notations, which are used to distinguish pure and mixed states of quantum mechanics and are based on random phases. Let

$$|\beta\rangle = \exp(i\theta_\beta) \quad (28)$$

where θ_β is a random angle uniformly distributed between 0 and 2π . The inner product is defined as averaging

$$\langle \alpha | \beta \rangle = \langle \exp(i(\theta_\beta - \theta_\alpha)) \rangle = I_{\alpha\beta} \quad (29)$$

and different random phases are presumed to be stochastically independent so that the system of vectors $|\alpha\rangle, |\beta\rangle, \dots$ is orthonormal. These vectors can be seen as special quantum states that cannot be measured since only one operator — the identity operator \mathbb{I} — can be applied to these states: $\langle \alpha | \mathbb{I} | \beta \rangle = \langle \alpha | \beta \rangle = I_{\alpha\beta}$.

Let ψ be a wave function represented by the expansion

$$\psi = \sum_{j,\beta} c_{j\beta} |j\rangle |\beta\rangle \quad (30)$$

then the density matrix is evaluated by tracing out the random phases, that is

$$\rho = \sum_{i,j,\alpha,\beta} c_{i\alpha}^* c_{j\beta} |j\rangle \langle i| \langle \alpha | \beta \rangle = \sum_{\beta} \sum_{i,j} c_{i\beta}^* c_{j\beta} |j\rangle \langle i| \quad (31)$$

As an example of using this notation, consider the following expressions

$$\psi_{+1} = \frac{|\uparrow\rangle + |\downarrow\rangle}{\sqrt{2}} |\alpha\rangle, \quad \psi_{-1} = \frac{|\uparrow\rangle - |\downarrow\rangle}{\sqrt{2}} |\beta\rangle$$

$$\psi_2 = \frac{|\uparrow\rangle |\alpha\rangle + |\downarrow\rangle |\beta\rangle}{\sqrt{2}}, \quad \psi_3 = \frac{\psi_{+1} + \psi_{-1}}{\sqrt{2}}$$

The first two expressions specify ψ_{+1} and ψ_{-1} as pure states (with arbitrary phases nominally given as $|\alpha\rangle$ and $|\beta\rangle$). The last two expressions indicate that ψ_2 is a mixture of two pure states $|\uparrow\rangle$ and $|\downarrow\rangle$ with equal probability and that ψ_3 is a mixture of another two pure states ψ_{+1} and ψ_{-1} (since ψ_{+1} and ψ_{-1} have different random phases $|\alpha\rangle$ and $|\beta\rangle$). Note that ψ_3 is different from ψ_2 and this difference is reflected by the random phase notation. The density matrices corresponding to these cases are evaluated according to (31):

$$\rho_{+1} = \frac{1}{2} \begin{bmatrix} 1 & 1 \\ 1 & 1 \end{bmatrix}, \quad \rho_{-1} = \frac{1}{2} \begin{bmatrix} 1 & -1 \\ -1 & 1 \end{bmatrix}$$

$$\rho_2 = \frac{1}{2} \begin{bmatrix} 1 & 0 \\ 0 & 1 \end{bmatrix}, \quad \rho_3 = \frac{1}{2} \begin{bmatrix} 1 & 0 \\ 0 & 1 \end{bmatrix}$$

In conventional quantum mechanics, the random phase multipliers $|\alpha\rangle, |\beta\rangle$ are orthonormal and do not evolve in time. Spontaneous decoherence, however, corresponds to $|\alpha\rangle$ being the same as $|\beta\rangle$ initially but then evolving into stochastically independent quantities.

HIERARCHICAL CONCEPTS FOR MODEL REDUCTION FOR REACTING FLOWS BASED ON LOW-DIMENSIONAL MANIFOLDS

U. Maas*, A. Y. Klimenko**

*Karlsruhe Institute of Technology, 76131 Karlsruhe, Germany E-mail: Ulrich.Maas@kit.edu

**The University of Queensland, QLD 4072, Australia, E-mail: a.klimenko@uq.edu.au

ABSTRACT

The description of chemically reacting systems leads very often to reaction mechanisms with far above hundred chemical species (and, therefore, to more than a hundred partial differential equations), which possibly react within more than a thousand of elementary reactions. These kinetic processes cover time scales from nanoseconds to seconds. An analogous scaling problem arises for the length scales. Due to these scaling problems the detailed simulation of three-dimensional turbulent flows in practical systems is beyond the capacity of even today's super-computers. Using simplified sub-models is a way out of this problem. The question arising in mathematical modeling of reactive flows is then: How detailed, or down to which scale has each process to be resolved (chemical reaction, chemistry-turbulence-interaction, molecular transport processes) in order to allow a reliable description of the entire process. Both the chemical source term and the transport term have one important property, namely that they cause the existence of low-dimensional attractors in composition space. These manifolds can be parameterized by a small number of variables. In this work we discussed several model reduction aspects based on the concept of low-dimensional manifolds, namely the efficient identification of the low-dimensional manifolds, the efficient implementation to simplify the chemical kinetics, the hierarchical nature of the low-dimensional manifolds the use of the hierarchical nature to devise hierarchical modeling concepts for turbulent reacting flows.

INTRODUCTION

Reacting flows are governed by a complex interplay of chemical reaction, flow and molecular transport. They can be described mathematically based on conservation equations for mass, momentum, energy and species masses. These conservation equations form a large system of stiff partial differential equations and, therefore, their solution is a great challenge [1; 2]. In the past many attempts have been made to simplify the description of chemically reacting flows while still capturing the essential features of the dynamics of the system. The developed methods focus both on a simplified description of the chemical kinetics and on a simplified description of the turbulent flow and the chemistry-turbulence interaction (see e.g. [3; 4; 5]). Different methods for dimension reduction have been proposed for the chemical kinetics. Many of them are based on a detailed analysis of the chemical source term (see e.g. [6; 7; 8; 9; 10; 11; 12; 13; 14]). Methods that account for the interaction of chemical reactions and physical processes are e.g. [15; 16; 17; 18; 19; 20]. An overview of several methods can be found in [21]. Furthermore many methods for the description of the chemistry-turbulence interaction make use of the existence of low-dimensional manifolds in composition space. Examples are the flamelet concept [22], conditional moment closure [23] and multiple mapping conditioning [24].

The dynamics of reacting flows is governed by the system of conservation equations for mass, momentum, energy, and species masses [25]. For the following analysis it is useful to separate the equations for the thermokinetic state variables from the equations for the flow field and to assume (for sake of simplicity) a low Mach number flow with constant thermodynamic pressure (a generalization to general flows is straight forward

and shall not be considered here). The governing equation system for the scalar field can be written as:

$$\frac{\partial \psi}{\partial t} = F - \vec{v} \text{grad} \psi - \frac{1}{\rho} \text{div} (D \text{grad} \psi), \quad (1)$$

where t denotes the time, ψ the $(n = n_s + 2)$ -dimensional thermokinetic state vector (which is, e.g. given as $\psi = (h, p, y_1, \dots, y_{n_s})^T$, where n_s is the number of species, h is the specific enthalpy, p the pressure, and y_i the mass fraction of species i), and ρ is the density, \vec{v} the velocity, D the $(n$ by $n)$ -dimensional matrix of transport coefficients (see, e.g., [26] for details), and F the (n) -dimensional vector of source terms. The source terms F as well as the transport matrix D are complicated nonlinear functions of the thermokinetic state vector ψ [27; 26; 28]. Because (1) does not invoke any modeling procedure, it is valid for laminar as well as for turbulent flows.

Both the chemical source term and the transport term have one important property, namely that they cause the existence of low-dimensional attractors in composition space. They result from fast chemical processes leading to species in steady states or reactions in partial equilibria. These manifolds can be parameterized by a small number m of variables, represented by the vector θ of reduced coordinates ($\theta = (\theta_1, \theta_2, \dots, \theta_m)^T$).

$$\mathcal{M} = \{\psi = \psi(\theta), \theta \in R^m, \psi \in R^n\}, \quad m \ll n \quad (2)$$

At each point ψ of a manifold \mathcal{M}^m perturbations off the manifold are relaxed according to a relaxation rate $|\omega|$ that is larger than a given $|\omega^m(\psi)|$. Note that this relaxation rate ω is for example for intrinsic low-dimensional manifolds given by the

value of the smallest (in magnitude) decoupled eigenvalue [8; 9]. Many model reduction techniques make use of the existence of such low-dimensional attractors (see e.g. [21]). Furthermore, methods like conditional moment closure [23] and multiple mapping conditioning [24] rely on the existence of such attractors in composition space. However, there exists also a hierarchy of the attractors, i. e. in the state space relaxation to equilibrium can be represented as a cascade through a nested hierarchy of smooth hypersurfaces [29]. While it is now well accepted that such a hierarchy exists, it is still necessary and useful to show, whether mathematical constructions of low-dimensional manifolds (i.e. model reduction concepts) can represent this behavior. It can be shown for several manifold based reduction concepts (see below) that attractors \mathcal{M}^m of dimension $m < m + p$ are under certain conditions embedded in attractors \mathcal{M}^{m+p} of dimension $m + p$, i.e. $\mathcal{M}^m \subset \mathcal{M}^{m+p}$. This hierarchical nature can be used in many applications, e.g.

for an efficient construction of low-dimensional manifolds
for a hierarchical improvement of the model accuracy in
reacting flow calculations
for devising hierarchical methods for turbulence/chemistry
interaction closure.

These issues will be addressed below.

In the following we shall focus only on some examples of manifold concepts, namely those based on quasi steady state assumptions (QSSA) and partial equilibrium assumptions (PEA) [30], intrinsic low-dimensional manifolds (ILDM) [8] and global quasi-linearization (GQL) [11], which are based on an analysis of the chemical source term only, and the concept of reaction diffusion manifolds (REDIM) [19], which is based on a coupled analysis of reaction and molecular transport.

THE HIERARCHICAL NATURE OF QSSA, PEA, ILDM AND GQL

For a pure homogeneous reaction system (1) reduces to

$$\frac{\partial \psi}{\partial t} = F(\psi). \quad (3)$$

In principle the assumption of species i being in steady state simply implies $F_{i+2} \approx 0$ (note that the first two entries in ψ are the enthalpy and the pressure, and the first species evolution equation has index 3). For $n_f = n - m$ species being in steady state the steady state conditions can be written as

$$\tilde{C}^m F(\psi) = 0, \quad (4)$$

with

$$\tilde{C} = \begin{pmatrix} 0 & 0 & \delta_{1k_1} & \delta_{2k_1} & \cdots & \delta_{n_s k_1} \\ 0 & 0 & \delta_{1k_2} & \delta_{2k_2} & \cdots & \delta_{n_s k_2} \\ \vdots & \vdots & \vdots & \vdots & \ddots & \vdots \\ 0 & 0 & \delta_{1k_{n_f}} & \delta_{2k_{n_f}} & \cdots & \delta_{n_s k_{n_f}} \end{pmatrix}, \quad (5)$$

where δ denotes the Kronecker- δ , and k_j is the index of the species in the j^{th} steady state assumption. This yields a definition of the $(m = n - n_f)$ -dimensional QSSA manifold:

$$\mathcal{M}^m = \{\psi | \tilde{C}^m F(\psi) = 0\} \quad (6)$$

It is easy to see that if we have a set of $(n - (m + p))$ species assumed to be in steady state, which is a subset of $(n - m)$ species assumed to be in steady state

$$\{k_1, k_2, \dots, k_{n-(m+p)}\} \subset \{\hat{k}_1, \hat{k}_2, \dots, \hat{k}_{n-m}\}, \quad (7)$$

(where $\hat{\cdot}$ is only used to indicate a possible different ordering of the species in the two subsets), then the matrix C^{m+p} is in the span of the matrix C^m , and it follows directly from (6) that

$$\mathcal{M}^m \subset \mathcal{M}^{m+p} \quad (8)$$

In partial equilibrium approximations (in the simplest formulation, see [21]) each partial equilibrium assumption defines a nonlinear equation via equating the rates of the forward and backward reaction. It is easy to show that if we define two low-dimensional manifolds via $(n - (m + p))$ and $(n - m)$ partial equilibrium conditions, respectively, where the $(n - (m + p))$ vectors of the stoichiometric coefficients of the partial equilibrium reactions for \mathcal{M}^{m+p} are in the span of the $(n - m)$ vectors of stoichiometric coefficients of the partial equilibrium reactions for \mathcal{M}^m , then again the m -dimensional manifold is a subset of the $m + p$ -dimensional manifold.

This means that QSSA and PEA manifolds can be constructed in such a way, that a hierarchy of the manifolds exists, although it shall be noted that very often different sets of assumptions for different dimensions are used, i.e.

$$\{k_1, k_2, \dots, k_{n_f}\} \not\subset \{\hat{k}_1, \hat{k}_2, \dots, \hat{k}_{n_f}\}, \quad (9)$$

In this case a hierarchical nature of the manifolds is not guaranteed.

Let us now discuss the hierarchy in the context of ILDM and GQL. The mathematical model of these methods is described in detail in previous works (see e.g. [8; 31; 9; 32; 33; 34; 11; 35]). Here, only a short repetition to clarify the presentation shall be given. ILDM and GQL differ in principle how the fast and slow processes are identified. For ILDM [8] the $(n \text{ by } n)$ -dimensional Jacobian matrix $V^{ILDM} = F_\psi$ (with $\{F_\psi\}_{ij} = \partial F_i / \partial \psi_j$) of the chemical source terms is used to identify the fast/slow decomposition of chemical processes. For GQL [11] the analysis is based on the so-called global quasi-linearization matrix. This matrix is obtained by picking n random states in the composition space and looking for a linear representation of $F(\psi)$.

$$V^{GQL} = \begin{pmatrix} | & & | \\ F(\psi_1) & \cdots & F(\psi_n) \\ | & & | \end{pmatrix} \begin{pmatrix} | & & | \\ \psi_1 & \cdots & \psi_n \\ | & & | \end{pmatrix}^{-1} \quad (10)$$

Issues like the choice of the reference points cannot be discussed here, and we simply refer to [11; 35]. The equation for the low-dimensional manifolds is then obtained by an invariant subspace decomposition of the matrices V^{ILDM} or V^{GQL}

$$V = \begin{pmatrix} Z_s & Z_f \end{pmatrix} \cdot \begin{pmatrix} N_s & 0 \\ 0 & N_f \end{pmatrix} \cdot \begin{pmatrix} \tilde{Z}_s \\ \tilde{Z}_f \end{pmatrix}. \quad (11)$$

The matrices Z and \tilde{Z} span up the right invariant subspace and

the left invariant subspace, respectively:

$$\tilde{Z} = Z^{-1} = (Z_s \ Z_f)^{-1} = \begin{pmatrix} \tilde{Z}_s \\ \tilde{Z}_f \end{pmatrix}. \quad (12)$$

Here Z_s is the (n by n_s)-dimensional invariant subspace belonging to the n_s eigenvalues $\lambda(N_s)$ having the largest real parts and Z_f is the (n by n_f)-dimensional invariant subspace belonging to the n_f eigenvalues $\lambda(N_f)$ having the smallest real parts, respectively, where n_s and n_f denote the number of eigenvalues according to slow and fast processes. This means that the eigenvalues of the matrix V are divided into two groups

$$i = 1, \dots, n_s \quad k = n_s + 1, \dots, n_s + n_f \quad n_s + n_f = n \quad (13)$$

$$|\operatorname{Re}(\lambda_i(V))| \leq a \ll b \leq |\operatorname{Re}(\lambda_k(V))| \quad \operatorname{Re}(\lambda_k(V)) < 0 \quad (14)$$

and fulfill a spectral gap condition (for more details see [36; 11]).

The general assumption that the fast processes have already relaxed defines an $m = n_s = n - n_f$ -dimensional manifold in the state space (note that additional constraints for the conserved variables can be used to further reduce the dimension m of the manifold[8; 36]). This subspace is composed of points where the reaction rates in direction of the n_f fast processes vanish

$$\tilde{Z}_f(\psi)F(\psi) = 0, \quad (15)$$

This under-determined equation system can be solved using path following algorithms [36] to yield an ($m = n - n_f$)-dimensional manifold. In this case the manifolds are parameterized by a set of m reduced coordinates (e.g. mixture fraction, reaction progress variables) $\theta = (\theta_1, \theta_2, \dots, \theta_m)^T$:

$$\mathcal{M} = \{\psi = \psi(\theta), \theta \in R^m, \psi \in R^n\} \quad (16)$$

The investigation of the hierarchical nature of ILDM and GQL is now quite straight forward, due to the algebraic definition of the manifolds. Let us assume that we decompose the matrix V into invariant subspaces according to two different splitting conditions with $n_s = m$ and $n_s = m + p$, respectively ($p > 0$).

$$V = \begin{pmatrix} Z_s^m & Z_f^m \\ 0 & N_f^m \end{pmatrix} \cdot \begin{pmatrix} N_s^m & 0 \\ 0 & N_f^m \end{pmatrix} \cdot \begin{pmatrix} \tilde{Z}_s^m \\ \tilde{Z}_f^m \end{pmatrix}. \quad (17)$$

$$V = \begin{pmatrix} Z_s^{m+p} & Z_f^{m+p} \\ 0 & N_f^{m+p} \end{pmatrix} \cdot \begin{pmatrix} N_s^{m+p} & 0 \\ 0 & N_f^{m+p} \end{pmatrix} \cdot \begin{pmatrix} \tilde{Z}_s^{m+p} \\ \tilde{Z}_f^{m+p} \end{pmatrix}. \quad (18)$$

In this case it follows directly from the definition of the invariant subspaces that the $(n - (m + p))$ by n -dimensional matrix \tilde{Z}_f^{m+p} is in the span of the $(n - m)$ by n -dimensional matrix \tilde{Z}_f^m , and together with the manifold equation (16) we obtain

$$\{\psi | \tilde{Z}_f^m F(\psi) = 0\} \subset \{\psi | \tilde{Z}_f^{m+p} F(\psi) = 0\} \quad (19)$$

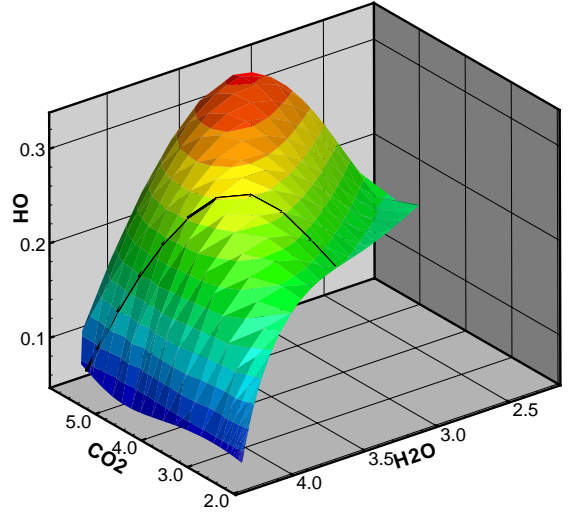


Figure 1. Example of a 1-dimensional ILDM (thick curve) embedded in a 2D-ILDM (mesh) plotted into the space of specific mole numbers (mass fractions divided by the molar mass in mol/kg) for the syngas/air system (composition and conditions are the same as in [8])

yielding

$$\mathcal{M}^m \subset \mathcal{M}^{m+p} \quad (20)$$

An example of a one-dimensional manifold embedded in a two-dimensional manifold for a syngas-air system is shown in Figure 1. Note that there exists also a hierarchy caused by the chemistry of higher hydrocarbon oxidation in the case of combustion processes. A discussion on this subject can be found in [33].

THE HIERARCHICAL NATURE OF REDIM

In contrast to ILDM and GQL the REDIM concepts takes into account the molecular transport processes in the identification of the low-dimensional manifolds. Based on equation (1) the REDIM method uses estimates for the spatial gradients and solves an evolution equation for an m -dimensional manifold parameterized by the reduced coordinates $\theta = (\theta_1, \theta_2, \dots, \theta_m)^T$ for a pseudo-time $\tau \rightarrow \infty$

$$\rho \frac{\partial \psi}{\partial \tau} = (I - \psi_\theta \psi_\theta^+) \{ \rho F + (D \psi_\theta \chi)_\theta \chi \} \quad (21)$$

where $F = F(\psi(\theta))$, $D = D(\psi(\theta))$, $\rho = \rho(\psi(\theta))$, $\chi = \chi(\psi(\theta))$, $\psi_\theta = \psi_\theta(\theta)$, $\psi_\theta^+ = \psi_\theta^+(\theta)$. In these equations I is the identity matrix, ψ_θ is the matrix of partial derivatives of ψ with respect to θ ($\{\psi_\theta\}_{ij} = \partial \psi_i / \partial \theta_j$, and ψ_θ spans the tangent space to the manifold), and ψ_θ^+ is a pseudo-inverse (e.g. the Moore Penrose pseudo-inverse) of ψ_θ , see [11]. Note that this is a partial differential equation system with the thermokinetic state vector ψ as dependent and the time t and the reduced coordinates θ as independent variables.

The m -dimensional vector χ of gradient estimates used in this equation relies on a gradient guess $\zeta(\psi)$ for the thermokinetic

state vector $\zeta(\psi) = \text{grad } \psi$, which is assumed to be a function of the local thermodynamic state (see [19; 37; 38]) The gradient estimates χ are calculated via

$$\chi = \psi_{\theta}^{+} \zeta(\psi) \quad (22)$$

The solution

$$\mathcal{M}^m = \{\psi = \psi(\theta), \theta \in R^m\} \quad (23)$$

for $\tau \rightarrow \infty$ fulfills the invariance condition

$$(I - \psi_{\theta} \psi_{\theta}^{+}) \{\rho F + (D\psi_{\theta} \chi)_{\theta} \chi\} = 0 \quad (24)$$

For the following analysis it is useful to investigate the dependence of the REDIM evolution equation with respect to a change of the parametrization. Let a change of the parametrization of the manifold from θ to $\hat{\theta}$ be given by the $(m \times m)$ -dimensional regular transformation matrix $X = \hat{\theta}_{\theta}$. It can be shown (see Appendix A) that the projection matrix is invariant with respect to a change of the parameterization (equation 35), and it can also be shown (see Appendix A) that the diffusion term $\Delta = (D\psi_{\theta} \chi)_{\theta} \chi$ is invariant with respect to a change of the parameterization (equation 36). This means that the governing equation system does not depend on the choice of the parameterizing coordinates, a result which allows a simple analysis of the hierarchy of manifolds of different dimensions.

Let \mathcal{M}^m denote an m -dimensional Manifold with a tangent space defined by the matrix ψ_{θ} of tangent vectors, and \mathcal{M}^{m+p} denote an $m+p$ -dimensional Manifold with a tangent space defined by the matrix ψ_{η} of tangent vectors, where $\theta = (\theta_1, \dots, \theta_m)^T$, and $\eta = (\eta_1, \dots, \eta_{m+p})^T$. From the invariance of the equation system with respect to a change of the parameterization, it follows that we can represent the manifold \mathcal{M}^{m+p} by new coordinates $\theta = (\theta_1, \dots, \theta_m, \xi_1, \dots, \xi_p)^T$ with

$$\psi_{\xi} \in \text{span}(\psi_{\eta}) \quad \wedge \quad \psi_{\xi} \perp \psi_{\theta}. \quad (25)$$

This has several consequences for the evolution equation (21) for the REDIM. The projection operators P^m and P^{m+p} are related via (see Appendix B).

$$(I - \psi_{\eta} \psi_{\eta}^{+}) = (I - \psi_{\theta} \psi_{\theta}^{+} - \psi_{\xi} \psi_{\xi}^{+}), \quad (26)$$

In Appendix C it is shown that if the vector of gradient estimates for $\psi \in \mathcal{M}^m$ is tangent to the m -dimensional manifold ($\zeta \parallel \psi_{\theta}$), then it follows that the m -dimensional manifold is invariant with respect to the evolution equation of the $(m+p)$ -dimensional manifold, and therefore the m -dimensional manifold is embedded in the $(m+p)$ -dimensional manifold.

Examples of one-dimensional manifolds embedded in a two-dimensional manifold for a syngas-air system are shown in Fig. 2 for a premixed reaction system (conditions were taken from [19]) and in Fig. 3 for a non-premixed system (conditions were taken from [20]).

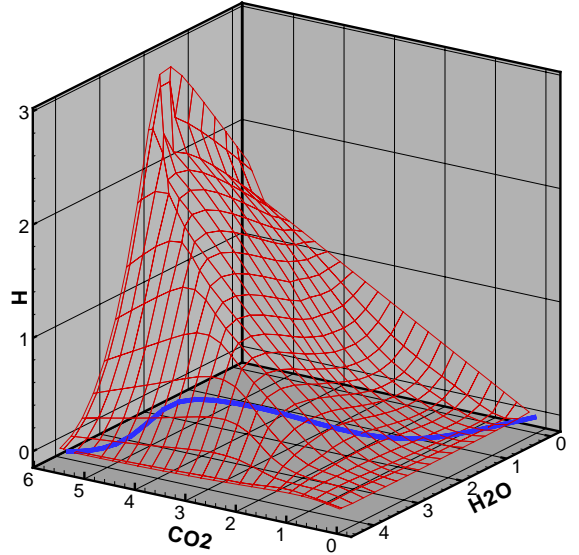


Figure 2. Example of a 1-dimensional REDIM (thick curve) embedded in a 2D-REDIM (mesh) plotted into the space of specific mole numbers (mass fractions divided by the molar mass in mol/kg) for the syngas/air system.

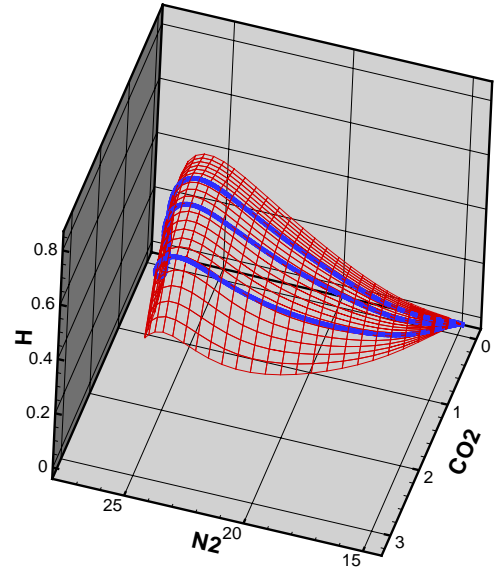


Figure 3. Example of 1-dimensional REDIMs (thick curves) for different gradient estimates embedded in a 2D-REDIM (mesh) plotted into the space of specific mole numbers (mass fractions divided by the molar mass in mol/kg) for the syngas/air system.

CONSEQUENCES OF THE HIERARCHICAL NATURE OF LOW-DIMENSIONAL MANIFOLDS

Having shown that REDIMs exhibit a similar hierarchical nature as QSSA, PEA, ILDM and QGL, we can state that in all these concepts lower dimensional manifolds \mathcal{M}^m are embedded in higher dimensional manifolds \mathcal{M}^{m+p} . This has several consequences for the identification and the use of these low-dimensional manifolds.

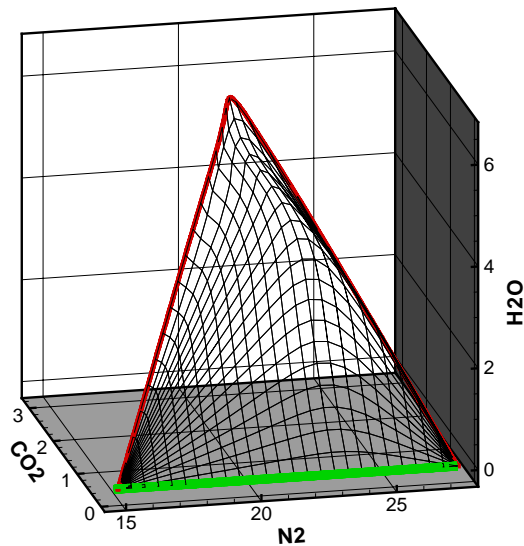


Figure 4. Example of two 1-dimensional REDIMs (thick curves) defining the boundary of a 2D-REDIM (mesh) plotted into the space of specific mole numbers (mass fractions divided by the molar mass in mol/kg) for the syngas/air system.

Efficient hierarchical construction of higher dimensional manifolds

One aspect where the hierarchy of the low-dimensional manifolds can be used efficiently is the hierarchical generation of higher dimensional manifolds starting from lower-dimensional manifolds. In the case of ILDM this concept has already been applied successfully [39], and due to the similarity of GQL and REDIM in the identification of the manifolds [11], an extension to GQL is straight forward. Therefore we shall focus here on discussing a possible implementation in the REDIM concept. One possibility to calculate higher dimensional REDIMs starting from lower-dimensional ones is based on two ingredients. The first is to construct boundaries for $m + 1$ -dimensional manifolds starting from m -dimensional ones. This can be illustrated by Fig. 4. It shows a two-dimensional REDIM for a non-premixed syngas system (same system as above, but Lewis number assumed to be 1). The green curve corresponds to a one-dimensional REDIM with a very high estimated gradient (corresponding to a dissipation rate much above the quenching limit). The red curve corresponds to a REDIM with gradient estimates taken from a counterflow flame with a small strain rate. An initial guess for the construction of the 2D REDIM has been obtained by a simple interpolation method (see [38]). Then the evolution equation for the REDIM has been solved to yield the 2D REDIM (mesh in the figure). This strategy can be further improved if lower-dimensional manifolds are not only used as boundaries, but also within the domain to improve convergence of the REDIM equation (cf. Fig 3).

Efficient adaptive use of REDIMs and control of the model error

In typical computational fluid dynamics (CFD) applications the overall computational domain exists of many different domains, which are governed, e.g., by mixing and diffusion, convection and chemical reaction. The hierarchical nature of the

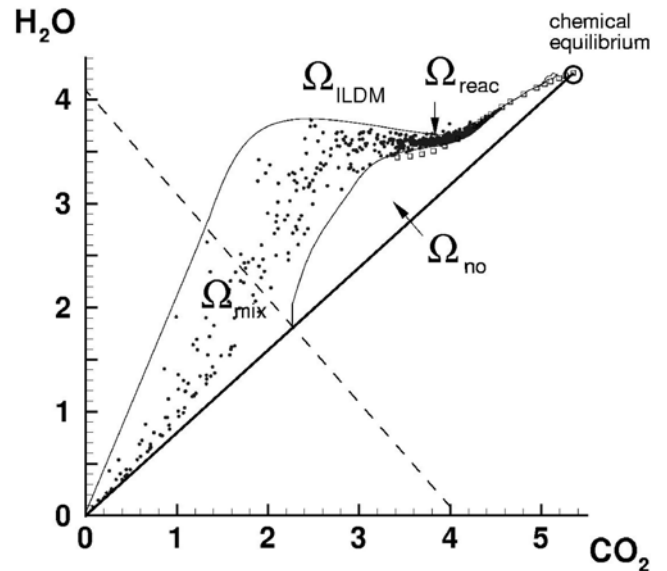


Figure 5. Effects of mixing and chemistry. Scatter plots of specific mole numbers of CO_2 and H_2O (mass fractions divided by the molar mass in mol/kg) for the syngas/air system in a partially stirred reactor, reprinted with permission from [41]

manifolds allows to use different degrees of approximation in different domains. In domains far from equilibrium (e.g. in the transient fuel conversion zone in combustion processes) high dimensional manifolds can be used, whereas close to equilibrium a representation by one or two-dimensional REDIMs is sufficient. Recently methods have become popular, which can estimate the modelling error [40]. Such methods could in future be used to estimate the error resulting from an approximation of the state space by low-dimensional manifolds of different dimensions.

Hierarchical concepts for the chemistry/turbulence coupling

Due to the enormous computational effort, reduced mechanisms based on low-dimensional manifolds are frequently used for modeling of turbulent reacting flows [5; 4; 3]. In many cases reduced models are only used to describe the kinetics. On the other hand the coupling of the chemical kinetics with the turbulent micro-mixing is governed by the hierarchy of the kinetics, too. This can be seen from a scatter plot of a PDF-calculation of a partially stirred reactor with a syngas/air mixture [41]. Calculations were performed until a statistically stationary solution was obtained. The scatter plots in the state space using detailed chemistry are shown in Fig. 5. Obviously only a small domain is actually accessed, a behavior which is also well known from direct numerical simulations [42]. The domain Ω_{mix} shows considerable scatter, and Ω_{reac} shows considerably less scatter, which is caused by a one-dimensional attracting manifold (note that in this representation it cannot be identified whether in the domain Ω_{mix} higher dimensional attractors exist. The lower boundaries of the accessed domain is the mixing line between the unburnt mixture (origin) and the completely burnt mixture (chemical equilibrium state). Due to fast chemical reaction the domain Ω_{no} is never accessed, because even if mixing brought particles into this domain, fast chemistry would relax the states towards the accessed domain (note that the re-

sults of the calculation were plotted after the chemistry step in the PDF method [41]. From these observations we can state that the chemical kinetics does not only give rise to low-dimensional manifolds in composition space, but that it also influences the chemistry/turbulence coupling. In methods like the conditional moment closure (CMC) [43; 23] or multiple mapping conditioning (MMC) [24] exactly this effect is used in the statistical treatment of turbulent flows. Whereas in CMC the correlations are used explicitly to describe the thermokinetic state, in MMC the correlations introduced by the low-dimensional attractors in composition space are used only for conditioning mixing operation, which is not necessarily confined to a low-dimensional manifold associated with the attractor.

The Manifold's Hierarchy in the context of MMC

Based on the observations made above, we suggest to use the hierarchical structure of the manifolds in the context of MMC. The basic idea is to use the results from a low-dimensional manifold \mathcal{M}^m to represent the evolution of the reference variables. Let $\psi(\theta(\mathbf{x}, t))$ represent a solution of a transport problem obtained with a high spatial resolution and the use of low-dimensional manifolds parametrized by $\theta = (\theta_1, \dots, \theta_m)^T$. The function $\theta^\circ = \theta(\mathbf{x}^\circ(t), t)$ denotes the values of θ evaluated at Lagrangian trajectories — these values are deployed as MMC reference variables. The scalars are modelled by quantities $\psi^*(t)$ that represent unrestricted kinetics (or kinetics confined to a manifold of a larger dimension \mathcal{M}^{m+p} in a hierarchical treatment of the problem) evaluated on a system of Pope particles; only relatively few particles are to be used in calculations (the reader is referred to sparse-Lagrangian methods [44]). Mixing operation is performed in MMC with localization in the combined space of the reference variables and physical coordinates. This enforces transport properties, which are accurately evaluated for θ° , on scalars ψ^* that have only sparse representations in physical space. Unrestricted treatment of chemical kinetics gives indication whether solution deviates from the m -dimensional manifold. Let us consider this point by introducing $\psi^\circ = \psi(\theta^\circ(t))$. These values do not coincide with $\psi^*(t)$ but, if the chemical kinetics of the fast subspace is indeed fast, ψ^* can be represented by $\psi^* = \psi(\theta^*(t))$. Note that values θ^* do not coincide with θ° , and can experience so called minor fluctuations with respect to θ° . The main difference between ψ^* and ψ° is that ψ^* is not forced to be confined to the m -dimensional manifold and may deviate from the manifold when the absolute values of the eigenvalues of the fast subspace are not sufficiently large. The use of the manifold-constructed reference variables θ° plays an important role in the method, as these variables allow to perform economical evaluations of ψ^* on a very sparse system of particles. The suggested method combines advantages of the manifold-based reduction techniques and MMC. In principle, a hierarchical system of manifolds of increasing dimensions can be deployed to form a hierarchical system of MMC reference variables.

ACKNOWLEDGMENT

The authors acknowledge funding by the Australian Research Council and the Deutsche Forschungsgemeinschaft.

A INVARIANCE OF THE REDIM WITH RESPECT TO THE PARAMETERIZATION

Let a change of the parametrization of the manifold from θ to $\hat{\theta}$ be given by the $(m \times m)$ -dimensional regular transformation matrix

$$X = \hat{\theta}_\theta \quad (27)$$

where ψ_θ transforms according to

$$\psi_{\hat{\theta}} = \psi_\theta \theta_{\hat{\theta}} \quad (28)$$

and $\chi(\theta)$ transforms according to

$$\hat{\chi}(\hat{\theta}) = \psi_{\hat{\theta}}^+ \zeta(\psi) = (\psi_\theta \theta_{\hat{\theta}})^+ \zeta(\psi) = \theta_{\hat{\theta}}^{-1} \psi_\theta^+ \zeta(\psi) = \theta_{\hat{\theta}}^{-1} \chi(\theta) \quad (29)$$

and

$$\hat{\theta}_\theta \theta_{\hat{\theta}} = I, \quad \theta_{\hat{\theta}} = \hat{\theta}_\theta^{-1} \quad (30)$$

The projection matrix is given as

$$P = (I - \psi_\theta \psi_\theta^+), \quad (31)$$

and in the new parameterization the projection matrix \hat{P} is given as

$$\hat{P} = (I - \psi_{\hat{\theta}} \psi_{\hat{\theta}}^+) \quad (32)$$

Using $\psi_{\hat{\theta}} = \psi_\theta \theta_{\hat{\theta}}$ we obtain

$$\psi_{\hat{\theta}}^+ = (\psi_\theta \theta_{\hat{\theta}})^+ \quad (33)$$

which yields

$$\psi_{\hat{\theta}}^+ = \theta_{\hat{\theta}}^{-1} \psi_\theta^+ \quad (34)$$

yielding

$$\hat{P} = (I - \psi_{\hat{\theta}} \psi_{\hat{\theta}}^+) = (I - \psi_\theta \theta_{\hat{\theta}} \theta_{\hat{\theta}}^{-1} \psi_\theta^+) = (I - \psi_\theta \psi_\theta^+) = P \quad (35)$$

This means that the projection matrix is invariant with respect to a change of the parameterization. The diffusion term $\Delta = (D\psi_\theta \chi)_\theta \chi$ with the changed parametrization is:

$$\begin{aligned} \hat{\Delta} &= (D\psi_{\hat{\theta}} \hat{\chi})_{\hat{\theta}} \hat{\chi} = (D\psi_\theta \theta_{\hat{\theta}} \hat{\theta}_\theta \chi)_{\hat{\theta}} \hat{\chi} \\ &= (D\psi_\theta \theta_{\hat{\theta}} \hat{\theta}_\theta \chi)_\theta \hat{\theta}_\theta \hat{\theta}_\theta \chi = (D\psi_\theta \chi)_\theta \chi = \Delta \end{aligned} \quad (36)$$

This means that the diffusion term is invariant with respect of a change of the parameterization, too.

B EMBEDDING REACTION/DIFFUSION MANIFOLDS

At each $\psi \in \mathcal{M}^m$ the tangent space of \mathcal{M}^{m+p} can be represented by an alternative set of basis vectors given by

$$\psi_\eta = \begin{pmatrix} | & | & & | \\ \psi_{\eta_1} & \psi_{\eta_2} & \cdots & \psi_{\eta_{m+p}} \\ | & | & & | \end{pmatrix} = \begin{pmatrix} | & | & | & | \\ \psi_{\theta_1} & \cdots & \psi_{\theta_m} & \psi_{\xi_1} & \cdots & \psi_{\xi_p} \\ | & | & | & | \end{pmatrix} \cdot Z \quad (37)$$

or in simplified notation

$$\psi_\eta = (\psi_\theta \quad \psi_\xi) \cdot Z, \quad (38)$$

where Z denotes an $(m+p)$ by $(m+p)$ -dimensional regular transformation matrix, and where ψ_ξ is constructed such that it is in the span of ψ_η and orthogonal to ψ_θ :

$$\psi_\xi \in \text{span}(\psi_\eta) \quad \wedge \quad \psi_\xi \perp \psi_\theta. \quad (39)$$

Noting that the projection operator P is invariant with respect to a change of the parameterization (see 35), we obtain

$$(I - \psi_\eta \psi_\eta^+) = (I - (\psi_\theta \quad \psi_\xi)(\psi_\theta \quad \psi_\xi)^+), \quad (40)$$

and because ψ_ξ is orthogonal to ψ_θ it follows that

$$\begin{aligned} (I - \psi_\eta \psi_\eta^+) &= \left(I - (\psi_\theta \quad \psi_\xi) \begin{pmatrix} \psi_\theta^+ \\ \psi_\xi^+ \end{pmatrix} \right) \\ &= \left(I - \psi_\theta \psi_\theta^+ - \psi_\xi \psi_\xi^+ \right). \end{aligned} \quad (41)$$

From this several useful properties can be derived:

$$\begin{aligned} (I - \psi_\eta \psi_\eta^+) \psi_\xi &= \left(I - \psi_\theta \psi_\theta^+ - \psi_\xi \psi_\xi^+ \right) \psi_\xi \\ &= \left(I - \psi_\xi \psi_\xi^+ \right) \psi_\xi = 0, \end{aligned} \quad (42)$$

$$\begin{aligned} (I - \psi_\eta \psi_\eta^+) \psi_\theta &= \left(I - \psi_\theta \psi_\theta^+ - \psi_\xi \psi_\xi^+ \right) \psi_\theta \\ &= \left(I - \psi_\theta \psi_\theta^+ \right) \psi_\theta = 0, \end{aligned} \quad (43)$$

$$\begin{aligned} P^{n+p} P^n &= (I - \psi_\eta \psi_\eta^+) (I - \psi_\theta \psi_\theta^+) \\ &= \left(I - \psi_\theta \psi_\theta^+ - \psi_\xi \psi_\xi^+ \right) (I - \psi_\theta \psi_\theta^+) \\ &= (I - \psi_\theta \psi_\theta^+) (I - \psi_\theta \psi_\theta^+) - (\psi_\xi \psi_\xi^+) (I - \psi_\theta \psi_\theta^+) \\ &= (I - \psi_\theta \psi_\theta^+) - (\psi_\xi \psi_\xi^+) (I - \psi_\theta \psi_\theta^+) \\ &= \left(I - \psi_\theta \psi_\theta^+ - \psi_\xi \psi_\xi^+ \right) = P^{n+p} \end{aligned} \quad (44)$$

$$\begin{aligned} P^n P^{n+p} &= (I - \psi_\theta \psi_\theta^+) (I - \psi_\eta \psi_\eta^+) \\ &= (I - \psi_\theta \psi_\theta^+) \left(I - \psi_\theta \psi_\theta^+ - \psi_\xi \psi_\xi^+ \right) \\ &= (I - \psi_\theta \psi_\theta^+) (I - \psi_\theta \psi_\theta^+) - (I - \psi_\theta \psi_\theta^+) (\psi_\xi \psi_\xi^+) \\ &= (I - \psi_\theta \psi_\theta^+) - (I - \psi_\theta \psi_\theta^+) (\psi_\xi \psi_\xi^+) \\ &= \left(I - \psi_\theta \psi_\theta^+ - \psi_\xi \psi_\xi^+ \right) = P^{n+p} \end{aligned} \quad (45)$$

C ANALYSIS OF THE HIERARCHY OF THE REDIM INVARIANCE CONDITION

Let $\psi \in \mathcal{M}^m$ fulfill the invariance equation

$$0 = \psi_\theta^{\perp T} \{ \rho F + (D\psi_\theta \chi)_\theta \chi \} \quad (46)$$

which is in this case equivalent to

$$\{ \rho F + (D\psi_\theta \chi)_\theta \chi \} = \psi_\theta X, \quad (47)$$

where X denotes the coordinates in the local coordinate system of the ψ_θ . The evolution of the \mathcal{M}^{m+p} -dimensional manifold is given by

$$\rho \frac{\partial \psi}{\partial t} = (I - \psi_\eta \psi_\eta^+) \{ \rho F + (D\psi_\eta \vartheta)_\eta \vartheta \} \quad (48)$$

with

$$\vartheta = \psi_\eta^+ \zeta(\psi) \quad (49)$$

Using the transformation equations for the projection term we obtain.

$$\rho \frac{\partial \psi}{\partial t} = \left(I - \psi_\theta \psi_\theta^+ - \psi_\xi \psi_\xi^+ \right) \{ \rho F + (D\psi_\eta \vartheta)_\eta \vartheta \} \quad (50)$$

In the local coordinate system the gradient estimate vector is given by

$$\hat{\vartheta} = \begin{pmatrix} \chi \\ \sigma \end{pmatrix} = \begin{pmatrix} \psi_\theta^+ \\ \psi_\xi^+ \end{pmatrix} \zeta \quad (51)$$

Because of the invariance of the diffusion term we have

$$\begin{aligned} (D\psi_\eta \vartheta)_\eta \vartheta &= \left\{ D\psi_{(\theta\xi)} \begin{pmatrix} \chi \\ \sigma \end{pmatrix} \right\}_{(\theta\xi)} \begin{pmatrix} \chi \\ \sigma \end{pmatrix} \\ &= (D\psi_\theta \chi)_\theta \chi + (D\psi_\theta \chi)_\xi \sigma + (D\psi_\xi \sigma)_\theta \chi + (D\psi_\xi \sigma)_\xi \sigma \end{aligned} \quad (52)$$

If $\zeta \parallel \psi_\theta$ it follows with $\psi_\xi \perp \psi_\theta$ that $\sigma = 0$, and we obtain

$$(D\psi_\eta \vartheta)_\eta \vartheta = (D\psi_\theta \chi)_\theta \chi \quad (53)$$

This results in an evolution equation for the subset \mathcal{M}^m according to

$$\rho \frac{\partial \psi}{\partial t} = \left(I - \psi_\theta \psi_\theta^+ - \psi_\xi \psi_\xi^+ \right) \{ \rho F + (D\psi_\theta \chi)_\theta \chi \} \quad (54)$$

and using $\{ \rho F + (D\psi_\theta \chi)_\theta \chi \} = \psi_\theta X$

$$\begin{aligned} \rho \frac{\partial \psi}{\partial t} &= \left(I - \psi_\theta \psi_\theta^+ - \psi_\xi \psi_\xi^+ \right) \psi_\theta X \\ &= \left(\psi_\theta - \psi_\theta \psi_\theta^+ \psi_\theta - \psi_\xi \psi_\xi^+ \psi_\theta \right) X = 0 \end{aligned} \quad (55)$$

This means that an m -dimensional manifold is (for the given conditions) invariant with respect to the evolution equation of the $(m+p)$ -dimensional manifold.

REFERENCES

- [1] J. O. Hirschfelder and C. F. Curtiss. *Theory of Propagation of Flames. Part I: General Equations*, page 121. Williams and Wilkins, Baltimore, 1949.
- [2] C.K. Westbrook, Y. Mizobuchi, T.J. Poinso, P.J. Smith, and J. Warnatz. Computational combustion. *Proc. Comb. Inst.*, 30(1):125 – 157, 2005.
- [3] N. Peters. Multiscale combustion and turbulence. *Proceedings of the Combustion Institute*, 32(1):1 – 25, 2009.
- [4] Stephen B. Pope. Small scales, many species and the manifold challenges of turbulent combustion. *Proceedings of the Combustion Institute*, 34(1):1 – 31, 2013.
- [5] T. Echekki and E. Mastorakos. *Turbulent Combustion Modeling: Advances, New Trends and Perspectives*. Fluid mechanics and its applications. Springer Netherlands, 2011.
- [6] S. H. Lam and D. A. Goussis. Understanding complex chemical kinetics with computational singular perturbation. In *22nd Symposium (International) on Combustion*, page 931. The Combustion Institute, Pittsburgh, PA, 1988.
- [7] S.H. Lam and D.A. Goussis. The csp method for simplifying kinetics. *Intl. J. of Chem. Kinetics*, 26:461–486, 1994.
- [8] U. Maas and S.B. Pope. Simplifying chemical kinetics: Intrinsic low-dimensional manifolds in composition space. *Combustion and Flame*, 88:239–264, 1992.
- [9] U. Maas and S.B. Pope. Laminar flame calculations using simplified chemical kinetics based on intrinsic low-dimensional manifolds. In *25th Symposium (International) on Combustion*, pages 1349–1356. The Combustion Institute, Pittsburgh, PA, 1994.
- [10] Z. Ren, S.B. Pope, A. Vladimirov, and J.M. Guckenheimer. The invariant constrained equilibrium edge preimage curve method for the dimension reduction of chemical kinetics. *The Journal of Chemical Physics*, 124(11):114111, 2006.
- [11] V. Bykov, V. Gol'dshteyn, and U. Maas. Simple global reduction technique based on decomposition approach. *Combustion Theory and Modelling*, 12(2):389–405, 2008.
- [12] A.N. Gorban and I.V. Karlin. Method of invariant manifold for chemical kinetics. *Chemical Engineering Science*, 58(21):4751 – 4768, 2003.
- [13] M. Valorani, H.N. Najm, and D.A. Goussis. Csp analysis of a transient flame-vortex interaction: Time scales and manifolds. *Comb. Flame*, 134:35–53, 2003.
- [14] D. Lebiecz. Computing minimal entropy production trajectories: An approach to model reduction in chemical kinetics. *The Journal of Chemical Physics*, 120(15):6890–6897, 2004.
- [15] J.A Van Oijen and L.P.H. De Goeij. Modelling of premixed laminar flames using flamelet-generated manifolds. *Combustion, Science and Technology*, 161:113, 2000.
- [16] P.D. Nguyen, L. Vervisch, V. Subramanian, and P. Domingo. Multidimensional flamelet-generated manifolds for partially premixed combustion. *Combustion and Flame*, 157(1):43 – 61, 2010.
- [17] S.H. Lam. Reduced chemistry-diffusion coupling. *Comb. Sci. Tech.*, 179:767–786, 2007.
- [18] D.A. Goussis, M. Valorani, F. Creta, and H.N. Najm. Reactive and reactive-diffusive time scales in stiff reaction-diffusion systems. *Prog. Comp. Fluid Dyn.*, 5:316–326, 2005.
- [19] V. Bykov and U. Maas. The extension of the ildm concept to reaction-diffusion manifolds. *Combustion Theory and Modelling*, 11(6):839–862, 2007.
- [20] U. Maas and V. Bykov. The extension of the reaction/diffusion manifold concept to systems with detailed transport models. *Proceedings of the Combustion Institute*, 33(1):1253 – 1259, 2011.
- [21] Dimitris A. Goussis and Ulrich Maas. Model reduction for combustion chemistry. In Tarek Echekki and Epaminondas Mastorakos, editors, *Turbulent Combustion Modeling*, volume 95 of *Fluid Mechanics and Its Applications*, pages 193–220. Springer Netherlands, 2011.
- [22] N. Peters. Laminar diffusion flamelet models in non-premixed turbulent combustion. *Prog. Energy Combust. Sci.*, 10:319–339, 1984.
- [23] A.Y. Klimenko and R.W. Bilger. Conditional moment closure for turbulent combustion. *Progress in Energy and Combustion Science*, 25(6):595–687, 1999. cited By (since 1996)333.
- [24] A.Y. Klimenko and S.B. Pope. The modeling of turbulent reactive flows based on multiple mapping conditioning. *Physics of Fluids*, 15(7):1907–1925, 2003. cited By (since 1996)51.
- [25] J. O. Hirschfelder and C. F. Curtiss. *Molecular Theory of Gases and Liquids*. John Wiley & Sons, Inc., New York, 1964.
- [26] A. Ern and V. Giovangigli. *Multicomponent Transport Algorithms*. Lecture Notes in Physics. Springer, Berlin, Heidelberg, New York, 1994.
- [27] J.O. Hirschfelder, C.F. Curtiss, and R.B. Bird. *Molecular Theory of Gases and Liquids*. Wiley, New York, 1954.
- [28] R.B. Bird, W.E. Stewart, and E.N. Lightfoot. *Transport Phenomena*. Wiley Interscience, New York, 1960.
- [29] M.R. Roussel and S.J. Fraser. On the geometry of transient relaxation. *The Journal of Chemical Physics*, 94(11):7106–7113, 1991.
- [30] M. Bodenstein. Zur kinetik des chlorknallgases. *Z. Phys. Chem.*, 85:329, 1913.
- [31] U. Maas and S.B. Pope. Implementation of simplified chemical kinetics based on intrinsic low-dimensional manifolds. In *24th Symposium (International) on Combustion*, page 103. The Combustion Institute, Pittsburgh, PA, 1992.
- [32] T. Blasenbrey, D. Schmidt, and U. Maas. Automatically simplified chemical kinetics and molecular transport and its application in premixed and non-premixed laminar flame calculations. In *27th Symposium (International) on Combustion*. The Combustion Institute, Pittsburgh, PA, 1998.
- [33] T. Blasenbrey and U. Maas. ILDMs of higher hydrocarbons and the hierarchy of chemical kinetics. *Proc. Comb. Inst.*, 28:1623–1630, 2000.
- [34] J. Nafe and U. Maas. A general algorithm for improving ILDMs. *Combustion Theory and Modeling*, 6(4):697–709, 2002.
- [35] V. Bykov and U. Maas. Investigation of the hierarchical structure of kinetic models in ignition problems. *Zeitschrift für Physikalische Chemie*, 233(4-5):461–479, 2009.
- [36] U. Maas. Efficient calculation of intrinsic low-dimensional manifolds for the simplification of chemical kinetics. *Computing and Visualization in Science*, 1:69–

- 82, 1998.
- [37] V. Bykov and U. Maas. Problem adapted reduced models based on reaction-diffusion manifolds (redims). In *Proc. Comb. Inst.*, volume 32, pages 561–568. Elsevier, 2009.
- [38] Gerd Steinhilber and Ulrich Maas. Reaction-diffusion manifolds for unconfined, lean premixed, piloted, turbulent methane/air systems. *Proceedings of the Combustion Institute*, 34(1):217 – 224, 2013.
- [39] J. Nafe and U. Maas. Hierarchical generation of {ILDMS} of higher hydrocarbons. *Combustion and Flame*, 135(12):17 – 26, 2003.
- [40] M. Braack and A. Ern. A posteriori control of modeling errors and discretization errors. *Multiscale Modeling and Simulation*, 1(2):221–238, 2003.
- [41] R. Bender, T. Blasenbrey, and U. Maas. Coupling of detailed and ildm-reduced chemistry with turbulent mixing. *Proc. Comb. Inst.*, 28:101–106, 2000. Figure reprinted with permission from Elsevier.
- [42] U. Maas and D. Thevenin. Correlation analysis of direct numerical simulation data of turbulent non-premixed flames. In *27th Symposium (International) on Combustion*. The Combustion Institute, Pittsburgh, PA, 1998.
- [43] R. W. Bilger. Conditional moment closure for the turbulent reacting flow. *Phys. Fluids A*, 5:436, 1993.
- [44] Yipeng Ge, M.J. Cleary, and A.Y. Klimenko. Sparse-lagrangian {FDF} simulations of sandia flame e with density coupling. *Proceedings of the Combustion Institute*, 33(1):1401 – 1409, 2011.

THE RATE-CONTROLLED CONSTRAINED-EQUILIBRIUM (RCCE) METHOD: A REDUCTION TECHNIQUE FOR COMPLEX KINETIC MODELS

Ghassan Nicolas*, Mohammad Janbozorgi^o, Hameed Metghalchi*

*Department of Mechanical and Industrial Engineering, Northeastern University, Boston MA 02115

^oDepartment of Aerospace and Mechanical Engineering, University of Southern California, Los Angeles, CA 90089

ABSTRACT

The method of Rate-Controlled Constrained-Equilibrium (RCCE) offers great potentials for modelling kinetic systems involving unknown kinetic pathways and parameters. It is a logical extension of classical thermodynamics and involves local maximization of entropy or minimization of a relevant free energy at any time during the non-equilibrium evolution of the system subject to a set of transient kinetic constraints. Constraints are imposed by slow rate-limiting kinetics. Consistent with classical thermodynamics, it is conjectured that the number of required constraints to describe the observed macroscopic kinetic behaviour is far smaller than the number of species in the system. We present a review of application of the method to chemical kinetic modelling of combustion of H₂, C₁ and C₂ hydrocarbon fuels. The rate equations have been cast in terms of constraint potentials, once the values of which are known, the concentration of all species can be calculated immediately. Three kinetic systems have been studied: H₂/O₂, CH₄/air and C₂H₅OH/air mixtures. The detailed kinetic models include 9, 60 and 68 species along with 19, 352 and 383 chemical reactions, while their corresponding RCCE models involve 6, 16 and 16 constraints, respectively.

INTRODUCTION

The development of kinetic models for describing the time evolution of chemically reacting systems is a fundamental objective of chemical kinetics. Such models can easily include several hundred of species and several thousands of reactions for heavy hydrocarbon fuels. The fact that the equations governing the dynamics under such models are highly stiff necessitates the development of tools to reduce the complexity of the model while maintaining the degree of detail of predictions. Many approaches for this problem have been proposed over the last two decades among which are the Quasi-Steady State Approximation QSSA [1], Partial Equilibrium Approximation PEA [2], Intrinsic Low Dimensional Manifolds (ILDM) [3], Computational Singular Perturbation (CSP) [4], Adaptive Chemistry [5], Directed Relation Graph (DRG) [6], ICE-PIC method [7], and Rate-Controlled Constrained-Equilibrium (RCCE) [8].

Perhaps the most appealing feature of RCCE, as has also been explained in [9] is that, contrary to all dimension reduction models in which the constrained equilibrium assumption is not used, it is not necessary to start with a detailed kinetic model (DKM) which must then be simplified by various mathematical approximations. Instead, one starts with a small number of constraints, to which more constraints can be added, if necessary, to improve the accuracy of the calculations. The number of constraints needed to describe the dynamic state of the system within experimental accuracy can be very much smaller than the number of species in the system.

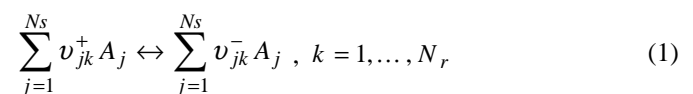
Therefore fewer reactions are needed to describe the system's evolution. Given the fact that in the entire body of thousands of chemical reactions perhaps less than hundred have rate constants known better than a factor of two, this feature of RCCE could help remove a great deal of uncertainty from the system by properly invoking the constrained-equilibrium assumption. Reactions which do not change any

constraint are in constrained-equilibrium and need not to be specified. Nonetheless, the successful implementation of the RCCE method depends critically on the choice of constraints and knowledge of the rates of the constraints-changing reactions is required.

In this paper we use the method of RCCE to study the kinetics of H₂/O₂, CH₄/Air and C₂H₅OH/Air under constant volume, constant energy constraints. The aim of this paper is to present a set of constraints, for each kinetic model, based on a careful study of the kinetics of the system, which yields good agreements with the corresponding DKM over a wide range of initial temperatures and pressures.

GOVERNING EQUATIONS

The changes in the species composition of a system are the result of chemical reactions of the form



where A_j is the symbol of species j , N_r is the number of reactions, N_s is the number of species, ν_{jk}^+ and ν_{jk}^- are the forward and reverse stoichiometric coefficients of species j for reaction k .

For a given mechanism, the rate equation for an individual species j is given by

$$\frac{dN_j}{dt} = V \sum_{k=1}^{N_r} \nu_{jk} (r_k^+ - r_k^-), \quad j = 1, \dots, N_s \quad (2)$$

where N_r is the number of reactions, $\nu_{jk} = \nu_{jk}^+ - \nu_{jk}^-$ is the net stoichiometric coefficient of species j in reaction k and r_k^+

and r_k^- are the forward and the reverse rates of reaction k defined as:

$$r_k^+ = k_k^+ \prod_{j=1}^{N_s} [N_j]^{V_{jk}^+}, \quad r_k^- = k_k^- \prod_{j=1}^{N_s} [N_j]^{V_{jk}^-}$$

The principle of detailed balance is also used to relate the forward and reverse reaction rate constants, k_k^+ and k_k^- through the reaction equilibrium constant.

Constrained Equilibrium

Constraints are assumed to be a linear combination of species composition present in the system, namely

$$C_i = \sum_{j=1}^{N_s} a_{ij} N_j, \quad i = 1, \dots, N_c \quad (3)$$

where a_{ij} is the value of the i^{th} constraint for the j^{th} species and N_c is the number of constraints. The constrained equilibrium composition found by minimizing the Gibbs free energy subject to a set of constraints using the method of Lagrange multipliers is

$$N_j = V Q_j(T) \exp\left(-\sum_{i=1}^{N_c} a_{ij} \gamma_i\right) \quad (4)$$

where

$$Q_j(T) = \frac{p_0}{R_u T} \exp(-\mu_j^0(T))$$

is the partition function of species j . Also $\mu_j^0 = (h_j^0 - T s_j^0)/R_u T$ and γ_i are, respectively, the non-dimensional standard Gibbs free energy of species j and the constraint potential (Lagrange multiplier) conjugate to constraint i . It is important to notice that once the value of constraint potentials are obtained, the mole number of all species can be obtained through equation (4). This equation also established the reduced dimensional space as

$$N_j = N_j(T, V, \gamma_i)$$

which in conjunction with equation (4) yields

$$\frac{1}{N_j} \frac{dN_j}{dt} = \frac{1}{V} \frac{dV}{dt} + \left(\frac{E_j}{R_u T}\right) \frac{1}{T} \frac{dT}{dt} - \sum_{n=1}^{N_c} a_{nj} \frac{d\gamma_n}{dt} \quad (5)$$

Rate Equations for the Constraints

The rate equations of constraints can be determined by differentiating equation (3):

$$\frac{dC_i}{dt} = \sum_{j=1}^{N_c} a_{ij} \frac{dN_j}{dt}, \quad i = 1, \dots, N_c \quad (6)$$

and then using equation (2) to obtain

$$\frac{dC_i}{dt} = V \sum_{k=1}^{N_r} b_{ik} r_k, \quad i = 1, \dots, N_c \quad (7)$$

where

$$b_{ik} = \sum_{j=1}^{N_c} a_{ij} V_{jk}$$

is the change of constraint i due to reaction k . Since elements are conserved $b_{ik} = 0$ for $i=1, \dots, N_e$ where N_e is the number of elements in the system. Upon integration of N_c rate equations (6), the N_c algebraic equations (3) and (4) must be solved to obtain the constrained-equilibrium mixture composition.

Constraint Potential Rate Equations

To avoid solving the algebraic equations involved in integration of constraints, the RCCE equations can be directly cast into the constraint potential forms, γ . Following similar steps detailed in [11], the equations governing the constraint potentials can be obtained by combining equations (5), (6) and (7) as follows

$$\sum_{n=1}^{N_c} C_{in} \frac{d\gamma_n}{dt} - \frac{C_{iV}}{V} \frac{dV}{dt} - \frac{C_{iT}}{T} \frac{dT}{dt} + \sum b_{ik} (r_k^+ - r_k^-) = 0 \quad (8)$$

where

$$C_{in} = \sum_{j=1}^{N_s} a_{ij} a_{nj} [N_j],$$

$$C_{iV} = \sum_{j=1}^{N_s} a_{ij} [N_j],$$

$$C_{iT} = \sum_{j=1}^{N_s} a_{ij} \frac{E_j}{RT} [N_j],$$

Integration of equations, either (2), (7) or (8) need to be coupled with the equation of state and an appropriate energy equation.

Equation of state

For an ideal gas mixture the equation of state can be written:

$$pV = \sum_{j=1}^{N_{sp}} N_j RT \quad (9)$$

Energy Equation

For an ideal gas mixture, the energy can be written:

$$E = \sum_{j=1}^{N_s} N_j e_j(T) \quad (10)$$

where $e_j(T)$ is the energy per unit mole of species j . Also, the energy equation for an adiabatic, closed homogeneous system is:

$$\frac{dE}{dt} = -p \frac{dV}{dt} \quad (11)$$

Obviously, energy remains constant during an adiabatic constant volume process, while for an adiabatic constant pressure process enthalpy, i.e. $H=E+pV$, is conserved. Substituting relation (10) into equation (11), one obtains

$$\frac{dE}{dt} = \sum_{j=1}^{N_s} E_j \frac{dN_j}{dt} + \left(\sum_{j=1}^{N_s} N_j C_{vj}\right) \frac{dT}{dt} \quad (12)$$

Also, replacing equation (5) into equation (12), the energy equation will have the following form:

$$\sum_{n=1}^{N_c} C_{en} \frac{d\gamma_n}{dt} + \frac{C_{eV}}{V} \frac{dV}{dt} + \frac{C_{eT}}{T} \frac{dT}{dt} - \frac{1}{V} \frac{dE}{dt} = 0 \quad (13)$$

where

$$C_{en} = -\sum_{j=1}^{N_s} E_j a_{nj} [N_j], \quad C_{eV} = \sum_{j=1}^{N_s} E_j [N_j],$$

$$C_{eT} = \sum_{j=1}^{N_s} \left(C_{vj} T + \frac{E_j^2}{RT} \right) [N_j], \quad \dot{E} = -\frac{p}{V} \frac{dV}{dt}$$

C_{vj} is the frozen molar heat capacity of species j at constant volume and p is pressure.

Equations (8), (9) and (13) form a set of N_c+2 equations for N_c+2 unknowns (T, V, γ).

SELECTION OF CONSTRAINTS

The major area of research in RCCE is selection of kinetic constraints. Constraints could be either linear combinations of species or single species.

The main aim of our studies in RCCE is directed toward identifying the pattern of conversion of heavy hydrocarbons to smaller intermediates and ultimately to combustion products. In this paper we will discuss three chemical kinetic models, H_2/O_2 [13], CH_4/air and C_2H_5OH/air . The mechanism used for CH_4/air studies is the GRI-mech3.0 [14] plus an additional nine C_1 alkylperoxides and organic acids, with rates obtained from [15]. These species enable the model to be used at high pressures and low temperatures. Also, the C_2H_5OH mechanism is taken from [16].

Since the set of constraints required to model the chemistry of each kinetic model is different, we will only present one set of constraints, that for CH_4/air model. For more information about the other two kinetic models, please review [12-13]. Over the range of temperature and time scales of interest to combustion applications, the rates of ionization reactions are negligible compared to those of chemical reactions and the fixed constraints are the neutral elements of hydrogen, carbon, oxygen, nitrogen, designated by EH, EC, EO, EN.

Moreover, the slowest reactions controlling the chemical composition are three-body dissociation/recombination reactions and reactions which make and break valence bonds. Such reactions are slow in the endothermic direction because of the high activation energies required, and in the exothermic direction because of small three-body collision rates and small radical concentrations. They impose slowly varying time-dependent constraints on the number of moles, M , and the free valence, FV , of the system, respectively. A finite value of FV is a necessary condition for chain branching chemical reactions to proceed.

A third important time-dependent constraint is free oxygen, FO which is defined as any oxygen atom not directly bound to another oxygen atom. Free oxygen is imposed by slow OO bond-breaking reactions. An increase in FO is a necessary condition for the formation of the major reaction products of hydrocarbon oxidation, H_2O , CO_2 and CO .

Two additional time-dependent constraints which slightly improve the agreement between RCCE and DKM calculations under some conditions are: Moles of water radicals $OHO \equiv OH+O$ and moles of $HCO+CO \equiv DCO$. The OHO

constraint is a consequence of the relatively slow constraint-changing reaction $RH+OH = R+H_2O$ coupled with the fast reaction $RH + O = OH+R$ which equilibrate OH and O . The DCO constraint is a consequence of the slow reaction $CO + HO_2 = CO_2+OH$ coupled with the fast reaction $HCO+O_2 = CO+HO_2$ which equilibrate HCO and CO .

For systems involving the elements C, H, O and N , the nine constraints $EC, EH, EO, EN, M, FV, FO, OHO$, and DCO are independent of the initial reactants and may, therefore, be considered "universal" constraints.

In the present investigation of C_1 hydrocarbon oxidation, additional fuel-dependent constraints have been used. The first is a constraint on the fuel, FU , imposed by slow hydrogen – abstraction reactions of the type $FU+O_2=FR+HO_2$ and even slower dissociation/recombination of the type $AB+M = A+B+M$. This constraint is necessary to hold the system in its initial state. The second is a constraint on fuel radicals, FR , which is necessary to prevent the equilibration of forbidden exothermic global reactions such as $CH_3+2O_2+2H_2O \Rightarrow CO_2+2H_2O_2+H_2+H$, which will otherwise convert fuel radical directly to products.

The third is a constraint on alkyl peroxides, $APO \equiv CH_3OOH+CH_3OO+CH_2OOH$, imposed by slow reactions which convert APO to hydro peroxides coupled with fast reactions which equilibrate the species comprising APO . The fourth is a constraint on alcohol plus formaldehyde, $ALCD \equiv CH_3OH+CH_3O+CH_2OH+CH_2O$ imposed by relatively slow reactions which generate/remove $ALCD$ coupled with fast reactions which equilibrate the species comprising $ALCD$.

In the case of close to stoichiometric or rich conditions the path from C_1 to C_2 becomes important, which introduces an important structural constraint on the number of $C-C$ bonds. A change in the value of this constraint is a necessary condition for formation or consumption of heavier hydrocarbons. This constraint controls the paths from C_2 to C_1 and vice versa. It takes the value of zero for C_1 species and the values of one and two for non-ether C_2 and C_3 molecules, respectively.

The next constraint identified is C_2H_6 , which in a species map is directly connected to C_2H_5 . The calculations of the rate of formation and consumption of C_2H_6 compared to the rate of consumption of C_2H_5 show that C_2H_6 is an important rate-controlling constraint over a wide range of thermodynamic conditions. Such calculations further show that the path from C_2H_5 to C_2H_4 can be assumed equilibrated subject to formation of C_2H_5 and consumption of C_2H_4 . In other words, the slow reactions: $C_2H_6+M = CH_3+CH_3+M$, $C_2H_6+O_2=C_2H_5+HO_2$ and $C_2H_4+O_2=C_2H_3+HO_2$ coupled with fast reaction $C_2H_5+O_2=C_2H_4+HO_2$ impose C_2H_6 and $C_2H_5 + C_2H_4$ as extra C_2 -specific constraints.

The set of constraints mentioned above, enables agreements too within 5% accuracy with DKM calculations over a wide range of initial temperatures, pressures and equivalence ratios

RESULTS

H_2/O_2 Model

Ignitions of H_2/O_2 , CH_4/air and C_2H_5OH/air have been studied using RCCE over a wide range of initial temperatures and pressures. Comparisons have also been made with DKM results. In all Figures, solid lines represent the DKM predictions while the dashed lines represent the RCCE predictions.

The H_2/O_2 chemical kinetic model includes 9 species and 19 chemical reactions. Ignition has been studied for initial temperatures varying from 900 K to 1500 K and initial pressures varying from 30 atm to 100 atm under stoichiometric conditions. The RCCE calculations were carried out under 6 constraints, namely EH, EO, EN, M, FV and FO. Results are shown in figures 1 and 2 respectively.

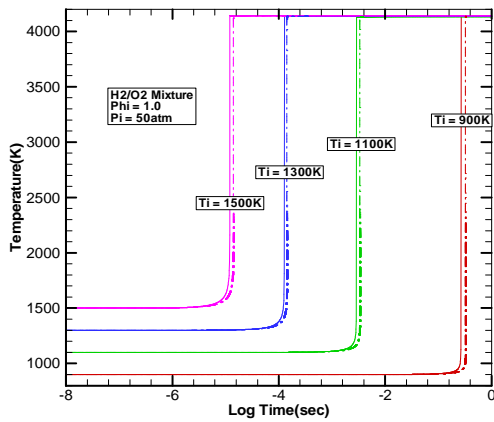


Fig.1: Temperature profiles for stoichiometric H_2/O_2 mixtures at $p_i=50$ atm and for varying initial temperatures.

For this range of initial conditions, the set results in predictions to within 5% accuracy against DKM calculations.

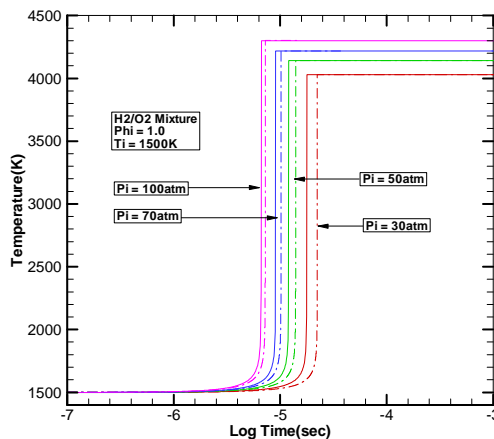


Fig.2: Temperature profiles for a stoichiometric mixture of H_2/O_2 at $T_i=1500$ K and different initial pressures.

CH₄/Air Model

The CH_4 /air kinetic model includes 60 species and 352 chemical reactions. Ignition has been studied for an initial temperature ranging from 900 K to 1200 K and an initial pressure changing from 1 atm to 50 atm. The RCCE calculations were carried out using the 16 constraints in Table I. Comparison between DKM and RCCE has been performed and results are shown in figures 3 and 4 respectively. Although 16 equations (constraints) were used in the RCCE calculations versus 60 equations in the DKM calculations, RCCE predictions were within 5-10% of DKM's over the entire range of initial conditions. The same level of agreements was found for the species profiles. Reference [13] can be consulted for more details.

C₂H₅OH/Air Model

The C_2H_5OH /air kinetic model includes 68 species and 383 chemical reactions. The RCCE calculations required only 16

constraints to model the ignition. These constraints are discussed in details in [13]. Ignition was studied over an initial temperature ranging from 1000 K to 1300 K and an initial pressure varying from 1 atm to 20 atm. Results are shown in figures 5 and 6 respectively. The RCCE predictions agree favourably well with those of DKM.

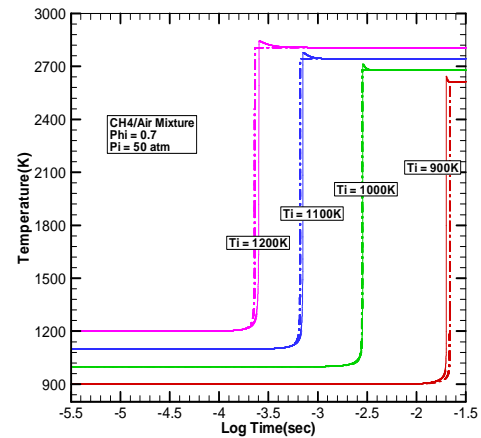


Fig.3: Temperature profiles for lean CH_4 /air mixtures at $p_i=50$ atm and varying initial temperatures.

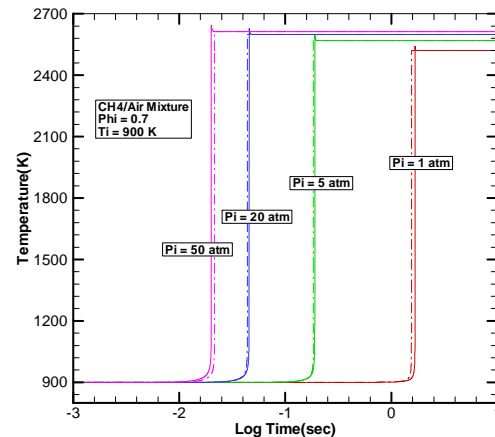


Fig.4: Temperature profiles for CH_4 /air mixtures at $T_i=900$ K and varying initial pressures.

CONCLUSIONS

RCCE calculations of H_2/O_2 , CH_4 /air and C_2H_5OH /air have been conducted over a wide range of initial temperatures and initial pressures. Sets composed of 6, 16 and 16 constraints were used, respectively for each case and the results showed good agreements with detailed kinetic model predictions using 9, 60 and 68 species respectively. The RCCE models demonstrate consistent accuracies, within 5-10%, with respect to the corresponding detailed kinetic models.

The RCCE method offers several advantages among which are:

1. It is based on the Maximum Entropy or minimum free energy Principle of Thermodynamics rather than mathematical approximations.
2. The total number of constraints required to determine the non-equilibrium state of a system can be much smaller than the number of species in the system.
3. Every species for which the thermodynamic data is available can evolve dynamically based on the constrained-equilibrium requirement. This feature could be used to investigate whether a species, which is not explicitly included in the kinetic model, may be kinetically important or not.

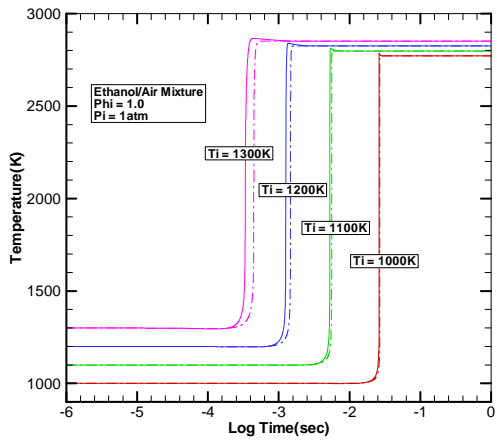


Fig.5: Temperature profiles for C_2H_5OH/air mixture at $p_i=1atm$ and varying initial temperatures.

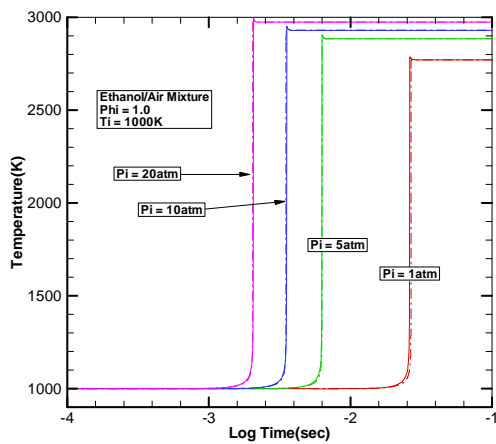


Fig.6: Temperature profiles for C_2H_5OH/air mixtures at $T_i=1000 K$ and varying initial pressures.

NOMENCLATURE

Symbol	Quantity	SI Unit
C_i	Constraint i	Unitless
a_{ij}	Value of constraint i for species j	Unitless
ν_{jk}^+	Forward stoichiometric coefficient of species j for reaction k	Unitless
ν_{jk}^-	Reverse stoichiometric coefficient of species j for reaction k	Unitless
r_k	Net rate of reaction k	$Mol.m^{-3}.s^{-1}$
N_r	Number of reaction	Unitless
N_c	Number of constraints	Unitless
N_{sp}	Number of species	Unitless
b_{ik}	The value of the i^{th} constraint in k^{th} reaction	Unitless
γ_i	Constraint potential of constraint i	Unitless
μ_j^0	Non dimensional Gibbs free energy of species j	Unitless
R_u	Gas constant	$J.mol^{-1}.K^{-1}$
N_j	Number of Moles of species j	Mol
V	Volume	m^3
r_k^+	Forward rate of reaction k	$Mol.m^{-3}.s^{-1}$
r_k^-	Reverse rate of reaction k	$Mol.m^{-3}.s^{-1}$
$[N_j]$	Concentration of species j	$Mol.m^{-3}$
Q_j	Partition function of species j	Mole
T	Temperature	K

p_0	Atmospheric pressure	Pa
p	Pressure	Pa
E_j	Specific internal energy of species j	J
E	Total energy of the system	J
C_{vj}	Specific heat at constant volume for species j	$J.Kg^{-1}.K^{-1}$
t	time	s

REFERENCES

- [1] S.W. Benson, the Induction Period in Chain Reactions, *J. Chem. Phys.* 20 (1952), pp. 1605-1612.
- [2] M. Rein, The Partial Equilibrium Approximation in Reacting Flows, *Phys.Fluids A* 4 (1992), pp. 873-886.
- [3] U. Maas, S.B. Pope, Simplifying Chemical Kinetics: Intrinsic Low-Dimensional Manifolds in Composition Space, *Combust. Flame* 88 (1992), pp. 239-264
- [4] S.H. Lam, D.A. Goussis, Understanding Complex Chemical Kinetics with Computational Singular Perturbation, *Proc. Combust. Inst.* 22 (1988), pp.931- 941.
- [5] O. Oluwole, B. Bhattacharjee, J.E. Tolsma, W.H. Green, Rigorous Valid Ranges for Optimally Reduced Kinetic Models, *Combust. Flame* 146 (2006), pp. 348-365.
- [6] T. Lu, C.K. Law, Linear time reduction of large kinetic mechanisms with directed relation graph: n-Heptane and iso-octane, *Combust. Flame* 144 (2006), pp. 24-36.
- [7] Z. Ren, S.B. Pope, A. Vladimirov, J.M. Guckenheimer, The ICE-PIC method for the dimension reduction of chemical kinetics Coupled with Transport, *Chem. Phys.* 124, 114111 (2006), pp. 1-15.
- [8] J.C. Keck and D. Gillespie, Rate-controlled partial-equilibrium method for treating reacting gas mixtures, *Combust. Flame* 17 (1971), pp. 237-241.
- [9] J.C. Keck, Rate-Controlled Constrained-Equilibrium Theory of Chemical Reactions in Complex Systems, *Prog. Energy Combust. Sci.* 16 (1990), pp. 125-154.
- [10] L. Petzold, Differential/Algebraic Eq. are not ODEs, *SIAM J. Sci. Stat. Comput.* 3 (1982), pp. 367-384.
- [11] M. Janbozorgi, S. Ugarte, M. Metghalchi, J.C. Keck, Combustion Modeling of Mono-Hydrocarbon Fuels using the Rate-Controlled Constrained-Equilibrium Method, *Combust. Flame* 156 (2009) 1871-1885.
- [12] G. Nicolas, The Rate-Controlled Constrained-Equilibrium Modeling of $C_1-C_2/O_2/Diluent$ Mixtures, Ph.D. thesis, Northeastern University, Boston, Mass., 2012.
- [13] D. Hamiroune, P. Bishnu, M. Metghalchi, J.C. Keck, Rate-controlled constrained-equilibrium method using constraint potentials, *Combust. Theory Modelling* 2 (1998), pp. 81-94
- [14] Gregory P. Smith, David M. Golden, Michael Frenklach, Nigel W. Moriarty, Boris Eiteneer, Mikhail Goldenberg, C. Thomas Bowman, Ronald K. Hanson, Soonho Song, William C. Gardiner, Jr., Vitali V. Lissianski, and Zhiwei Qin, Available at: http://www.me.berkeley.edu/gri_mech/
- [15] W. Tsang, R.F. Hampson, *Chemical Kinetic Data Base for Combustion Chemistry. Part I. Methane and Related Compounds*, *J. Phys. Chem. Ref. Data*, 15 (1986), pp. 1087-1193.
- [16] Personal communication: Li, J., Chaos, M., Kazakov, A., Dryer, F.L., and Haas, F.M., "Ethanol Model v1.0", Princeton University, December 2009.

Table 1: List of constraints used

Constraints		Definition	H ₂	CH ₄	C ₂ H ₅ OH
1	EH	Total moles of Hydrogen element	✓	✓	✓
2	EO	Total moles of Oxygen element	✓	✓	✓
3	EC	Total moles of Carbon element	-	✓	✓
4	EN	Total moles of Nitrogen element	✓	✓	✓
5	M	Total number of moles	✓	✓	✓
6	FV	Moles of Free valance	✓	✓	✓
7	FO	Moles of Free Oxygen	✓	✓	✓
8	OHO	Moles of O+OH	-	✓	✓
9	DCO	Moles of HCO+CO	-	✓	✓
10	FU	Moles of fuel molecules (CH ₄ or C ₂ H ₅ OH)	-	✓	✓
11	FR	Moles of fuel radicals (CH ₃ or CH ₃ CHOH+CH ₂ CH ₂ OH+CH ₃ CH ₂ O)	-	✓	✓
12	APO	Moles of alkyl peroxides (CH ₃ OO+CH ₃ OOH+CH ₂ OOH)	-	✓	-
13	ALCD	Moles of alcohols + aldehydes (CH ₃ O+CH ₃ OH+CH ₂ OH+CH ₂ O)	-	✓	✓
14	C ₂ H ₆	Moles of C ₂ H ₆	-	✓	✓
15	C-C	Moles of C-C bond	-	✓	✓
16	C ₂ H ₅ +C ₂ H ₄	Moles of C ₂ H ₅ +C ₂ H ₄	-	✓	✓

MODEL REDUCTION IN REACTING FLOW

Habib N. Najm

Sandia National Laboratories
Livermore, CA 94551, USA
hnnajm@sandia.gov

ABSTRACT

In this abstract, I present a brief overview of model analysis and reduction methods as applied to chemically reacting flows. I highlight specifically the computational singular perturbation method for analysis of chemical systems, and associated model reduction strategies. I outline our use of this method for analysis and model reduction in a range of chemically reacting flow systems. I also touch on challenges and opportunities associated with the use of CSP for analysis and model reduction in both macroscale and stochastic chemical systems, as well in uncertain chemical systems in general.

INTRODUCTION

Chemically reacting flows exhibit a range of computational challenges associated with their large range of length and time scales, as well as underlying chemical model complexity. In particular, chemical model complexity leads to range of complications. The large number of chemical species involved in detailed elementary reaction-step mechanisms, for even the simplest hydrocarbon fuels, leads to an associated large number of partial differential equations that need to be handled in a reacting flow computation. Further, the large number of reactions results in complex chemical source terms with a significant associated computational cost. Moreover, strong nonlinearity and fast time scales, in chemical rate expressions, lead to the formation of sharp reaction fronts and high spatial gradients of species concentration profiles. The resulting range of length scales necessitates fine mesh discretizations with associated computational loads. Similarly, the resulting range of time scales leads to extreme levels of temporal stiffness, and the need for specialized stable and accurate time integration strategies.

Given this set of difficulties, it is clear that chemical model reduction, to say nothing of efficient turbulence modeling requirements, is a necessary step towards enabling the utilization of chemically reacting flow computations in studies of practical combustion systems. In the following I will present brief highlights of existing work in chemical model reduction, with a more focused discussion of our work, followed by an outline of interesting challenges and opportunities in the field.

BACKGROUND

There has been extensive development of chemical model reduction methods targeting detailed hydrocarbon kinetics over a number of decades [1, 2]. Available techniques include lumping methods [2], sensitivity and principal component analysis [3], and elementary reaction flux based methods [4–6]. Given the strong stiffness and nonlinearity of typical chemical mechanisms for oxidation of hydrocarbon fuels, however, it is important that comparisons of sensitivity and reaction fluxes be done with care. In particular, brief dominance of reaction processes

with fast time scales can obscure the importance of slower reactions that can ultimately be of much higher relevance. Therefore, ideally, chemical model analysis ought to be done with proper attention to the dynamical landscape of the associated equation system. Time-scale analysis has been accordingly used from an early time, starting with the quasi-steady state approximation (QSSA) [2, 7–10]. The partial equilibrium approximation (PEA) [10–13] has also been used to identify effective algebraic constraints relevant in model reduction. A detailed analysis of the conditions under which QSSA and PEA are valid has been recently presented [14].

The computational singular perturbation (CSP) method [10, 15–17] has also been used successfully for analysis and reduction of a range of chemical systems [18–25]. The underlying stiffness and separation of time scales in chemical systems results in dynamics that are characterized by distinct fast and slow subspaces. These systems exhibit slow invariant manifolds defined by the equilibration of fast processes. Given an arbitrary initial state, the system evolves quickly towards a nearby slow manifold according to the fast time scales, and then evolves along the manifold according to the slow processes. CSP relies on eigenanalysis of the Jacobian of the equation system to allow analysis of the dynamics separately in the fast or slow subspaces, identifying important processes [26–30]. This analysis has provided means for development of a chemical model reduction strategy that retains important slow *and* fast reactions, and associated species. Further, the identification of the fast and slow directions enabled the development of time integration strategies that eliminate the fast time scales and enable time integration along the slow manifold with large explicit time steps [31, 32]. Identification of slow invariant manifolds, and their use for efficient time integration of chemical systems, is also at the core of the intrinsic low dimensional manifold (ILDM) method [33]. Similarly, the rate-controlled constrained-equilibrium (RCCE) technique [34, 35], based on the Second Law of thermodynamics, describes the evolution of a chemical system along rate-controlled constrained equilibrium paths. The invariant constrained equilibrium edge preimage curve method (ICE-PIC) [36] is based on RCCE, and makes use of trajectory-generated low-dimensional manifolds.

CHALLENGES AND OPPORTUNITIES

We have used dynamical analysis methods, specifically CSP, for the analysis of laminar flame computational databases and chemical model reduction for a number of hydrocarbon fuels including methane, propane, n-heptane, and jet fuel. This included both 1D flames as well as edge and jet flames. We identified and studied the dynamical structure of these flames under different operating conditions, providing information on the relative importance of specific reaction pathways and transport processes in the dynamical response of species concentrations and temperature in specific flame layers. We have used these results to arrive at an understanding of flame structure and dynamics, identifying dominant processes that contribute to either the time-dynamics or the underlying partial-equilibria. We have also used them to identify simplified chemical mechanisms under a range of operating conditions, and in different flame locations. Looking forward, there are a number of challenges in the utilization of CSP for model reduction in chemical systems, along with opportunities for further investigation.

To begin with, it is worth noting that the existing CSP-based model simplification strategy [19,20] is global over the database of states, and therefore not necessarily optimal at any given state. Typical means of generation of such data bases have included computations of ignition using the detailed mechanism over a range of initial conditions. Thus, the database covers a range of behaviors from slow preheat-phase reactions, through fast ignition, and decay to equilibrium, over a range of initial states. In principle, tabulation of simplified mechanisms for ranges of state values would provide a more optimal construction, however one then has to deal with the change in the size of the state vector in time/space [5]. Similarly, CSP-based model reduction *on the fly*, based on the projection of the governing equations onto the slow manifold, is local and has some optimality properties, but is computationally prohibitive unless suitable solution tabulation techniques are employed [25]. Another point to note is that CSP-based model reduction does not *explicitly* enforce a specific *error* measure on the state space trajectories. Rather, it attains control on the state error employing an error threshold on the importance index set, *i.e.* essentially on the projected chemical source terms. However, there is no guarantee that any specific resulting simplified N -species mechanism has the smallest state-error, relative to the detailed model, among all N -species mechanisms. Further, given nonlinearity, there are no explicit guarantees on the accuracy of computations using the simplified model *outside* the range of database of states, with this or other reduction schemes. Finally, note that since, by design, the simplified mechanism has both fast *and* slow species, this mechanism does retain some stiffness, albeit typically to a smaller degree than the original detailed mechanism. Clearly, there is significant room for improvement of the present CSP-based model reduction methodology.

From another perspective, there is a significant need for extension of dynamical analysis methods, such as CSP, to the realm of stochastic chemical systems [37]. Stochastic effects are non-negligible in chemical processes at the microscale, *e.g.* in a biological cell or at a catalytic surface nano-scale feature, where molecular counts are small. Accordingly, depending on the range of molecule counts, these systems are modeled using jump Markov processes or stochastic differential equations [38–42]. In this broad context, there is a need for well-founded practical definitions of stochastic “slow” manifolds and

fast/slow subspaces. With proper setup of the requisite stochastic dynamical analysis framework, one can then address analysis of stiff stochastic chemical system dynamics and associated model reduction strategies. While there has been work in this area [43–51], much more remains to be done.

Finally, the area of model reduction under uncertainty is of particular interest. Allowing for model error and/or noise in empirical measurements, it is clear that models generally involve some degree of uncertainty in their parameters. Accordingly, there is a need to account for this uncertainty in the model reduction context. In particular, user-specified error thresholds on reduced models ought to be informed by the degree of uncertainty in the starting detailed model predictions. Thus, for example, it does not seem justifiable to insist on reduced model errors that are orders of magnitude smaller than the uncertainty in the detailed model predictions. Rather, it is natural to consider all relevant sources of error and uncertainty in the model-reduction error budget. On the other hand, there are many challenges in this area related to the reformulation of dynamical analysis and model reduction techniques to account for uncertainty. Here again, the underlying dynamical objects, manifolds and fast/slow subspaces, need to be properly defined and represented before adequate model reduction strategies can be arrived at. Further, the very notion of *error* in a reduced model has to be revised, when both reduced and detailed predictions are uncertain. There has been some work with relevance in this context [52–54], but there is need for significant more development.

CLOSURE

I have tried in the above to give a brief overview of methods for analysis and model reduction in reacting flow. I covered with some detail our experience with the use of CSP in this context. I also presented brief highlights of challenges and opportunities going forward in the context of both continuum and atomistic chemical systems, and the need for addressing uncertainties in both analysis and reduction of chemical systems. These challenges are of relevance in a number of applications, providing opportunities for advancing the state of the art and impacting scientific and technical progress.

ACKNOWLEDGMENT

This work was supported by the US Department of Energy (DOE), Office of Basic Energy Sciences (BES) Division of Chemical Sciences, Geosciences, and Biosciences. Sandia National Laboratories is a multi-program laboratory managed and operated by Sandia Corporation, a wholly owned subsidiary of Lockheed Martin Corporation, for the U.S. Department of Energy’s National Nuclear Security Administration under contract DE-AC04-94AL85000.

REFERENCES

- [1] Griffiths, J. F., Reduced Kinetic Models and Their Application to Practical Combustion Systems, *Prog. Energy Combust. Sci.*, 21:25–107 (1995).
- [2] Okino, M.S., and Mavrouniotis, M.L., Simplification of Mathematical Models of Chemical Kinetics, *Chemical Reviews*, 98:391–408 (1998).
- [3] Turanyi, T., Berces, T., and Vajda, S., Reaction Rate Anal-

- ysis of Complex Kinetic Systems, *Int. J. Chem. Kin.*, 21:83–99 (1989).
- [4] Frenklach, M., Kailasanath, K., and Oran, E.S., Systematic Development of Reduced Reaction Mechanisms for Dynamic Modeling, *Progress in Astronautics and Aeronautics*, 105(2):365–376 (1986).
- [5] Schwer, D.A., Lu, P., and Jr., W.H. Green, An Adaptive Chemistry Approach to Modeling Complex Kinetics in Reacting Flows, *Combustion and Flame*, 133:451–465 (2003).
- [6] Lu, T., and Law, C.K., A directed relation graph method for mechanism reduction, *Proc. Comb. Inst.*, 30:1333–1341 (2005).
- [7] Bodenstein, M., and Lutkemeyer, H., Die photochemische Bildung von Bromwasserstoff und die Bildungsgeschwindigkeit der Brommolekul aus den Atomen., *Z. Phys. Chem.*, 114:208–236 (1924).
- [8] E.Hesstvedt O.Hov and I.S.A.Isaksen Quasi-Steady-State Approximations in Air Pollution Modeling: Comparison of Two Numerical Schemes for Oxidant Prediction, *Int. J. Chem. Kinetics*, 10:971–994 (1978).
- [9] Løvås, T., Amnéus, P., Mauss, F., and Mastorakos, E., Comparison of Automatic Reduction Procedures for Ignition Chemistry, *Proc. Comb. Inst.*, 29:1387–1393 (2002).
- [10] Lam, S.H., Using CSP to Understand Complex Chemical Kinetics, *Combustion Science and Technology*, 89:375–404 (1993).
- [11] Bulewicz, E.M., James, C.G., and Sugden, T.M., Photometric Investigations of Alkali Metals in Hydrogen Flame Gases, II, *Proc. Roy. Soc. (London), Series A*, 235:89–106 (1956).
- [12] Williams, F.A., *Combustion Theory*, Addison-Wesley, New York, 2nd edition, 1985.
- [13] Goussis, D.A., On the Construction and Use of Reduced Chemical Kinetics Mechanisms Produced on the Basis of Given Algebraic Relations, *J. Comput. Physics*, 128:261–273 (1996).
- [14] Goussis, D.A., Quasi steady state and partial equilibrium approximations: Their relation and their validity, *Combustion Theory and Modelling*, 16(5):869–926 (2012).
- [15] Lam, S.H., and Goussis, D.A., Understanding Complex Chemical Kinetics with Computational Singular Perturbation, *Proc. Comb. Inst.*, 22:931–941 (1988).
- [16] Goussis, D.A., and Lam, S.H., On the Homogeneous Methane-Air Reaction System, Report 1892-MAE, Princeton Univ., (1990).
- [17] Goussis, D.A., and Lam, S.H., A Study of Homogeneous Methanol Oxidation Kinetic Using CSP, *Proc. Comb. Inst.*, 24:113–120 (1992).
- [18] Valorani, M., Goussis, D.A., Creta, F., and Najm, H.N., Higher Order Corrections in the Approximation of Low Dimensional Manifolds and the Construction of Simplified Problems with the CSP Method, *J. Comput. Phys.*, 209:754–786 (2005).
- [19] Valorani, M., Creta, F., Goussis, D.A., Lee, J.C., and Najm, H.N., Chemical Kinetics Simplification via CSP, *Combustion and Flame*, 146:29–51 (2006).
- [20] Valorani, M., Creta, F., Donato, F., Najm, H.N., and Goussis, D.A., Skeletal Mechanism Generation and Analysis for *n*-heptane with CSP, *Proc. Comb. Inst.*, 31:483–490 (2007).
- [21] Goussis, D.A., and Valorani, M., An Efficient Iterative Algorithm for the Approximation of the Fast and Slow Dynamics of Stiff Systems, *J. Comp. Phys.*, 214:316–346 (2006).
- [22] Goussis, D.A., and Najm, H.N., Model Reduction and Physical Understanding of Slowly Oscillating Processes: The Circadian Cycle, *Multiscale Modeling and Simulation*, 5(4):1297–1332 (2006).
- [23] Lee, J.C., Najm, H.N., Lefantzi, S., Ray, J., Frenklach, M., Valorani, M., and Goussis, D., A CSP and Tabulation Based Adaptive Chemistry Model, *Combustion Theory and Modeling*, 11(1):73–102 (2007).
- [24] Najm, H.N., Valorani, M., Goussis, D.A., and Prager, J., Analysis of Methane-Air Edge Flame Structure, *Combustion Theory and Modelling*, 14(2):257–294 (2010).
- [25] Debusschere, B.J., Marzouk, Y.M., Najm, H.N., Rhoads, B., Goussis, D.A., and Valorani, M., Computational Singular Perturbation with Non-Parametric Tabulation of Slow Manifolds for Time Integration of Stiff Chemical Kinetics, *Combustion Theory and Modelling*, 16(1):173–198 (2012).
- [26] Valorani, M., Najm, H.N., and Goussis, D., CSP Analysis of a Transient Flame-Vortex Interaction: Time Scales and Manifolds, *Combustion and Flame*, 134(1-2):35–53 (2003).
- [27] Najm, H.N., Ponganis, D., and Prager, J., Analysis of NO Structure in a Methane-Air Edge Flame, *Proc. Comb. Inst.*, 32(1):1117–1124 (2008).
- [28] Prager, J., Najm, H., Valorani, M., and Goussis, D., Skeletal Mechanism Generation with CSP and Validation for Premixed *n*-Heptane Flames, *Proc. Comb. Inst.*, 32(1):509–517 (2008).
- [29] Prager, J., Najm, H.N., Valorani, M., and Goussis, D., Structure of *n*-Heptane/Air Triple Flames in Partially-Premixed Mixing Layers, *Combustion and Flame*, 158:2128–2144 (2011).
- [30] Kazakov, A., Chaos, M., Zhao, Z., and Dryer, F.L., Computational Singular Perturbation Analysis of Two-Stage Ignition of Large Hydrocarbons, *J. Phys. Chem. A*, 110:7003–7009 (2006).
- [31] Valorani, M., and Goussis, D.A., Explicit Time-Scale Splitting Algorithm For Stiff Problems: Auto-Ignition Of Gaseous-Mixtures Behind A Steady Shock, *J. Comput. Phys.*, 169:44–79 (2001).
- [32] Valorani, M., and Paolucci, S., The *G-Scheme*: A framework for multi-scale adaptive model reduction, *Journal of Computational Physics*, 228:4665–4701 (2009).
- [33] Maas, U., and Pope, S.B., Simplifying Chemical Kinetics: Intrinsic Low Dimensional Manifolds in Composition Space, *Combustion and Flame*, 88:239–264 (1992).
- [34] Keck, J.C., Rate-Controlled Constrained-Equilibrium Theory of Chemical Reactions in Complex Systems, *Prog. Energy Combust. Sci.*, 16:125–154 (1990).
- [35] Law, R., Metgalchi, M., and Keck, J.C., Rate-Controlled Constrained Equilibrium Calculation of Ignition Delay Times in Hydrogen-Oxygen Mixtures, *Twenty-Second Symposium (International) on Combustion*, The Combustion Institute, 1988, , pp. 1705–1713.
- [36] Ren, Z., Pope, S.B., Vladimirov, A., and Guckenheimer, J.M., The invariant constrained equilibrium edge preimage curve method for the dimension reduction of chemical kinetics, *J. Chem. Phys.*, 124:114111 (2006).
- [37] Gillespie, D. T., The chemical Langevin equation., *Jour-*

- nal of Chemical Physics*, 113(1):297 – 306 (2000).
- [38] Gillespie, D.T., A General Method for Numerically Simulating the Stochastic Time Evolution of Coupled Chemical Reactions, *J. Comput. Phys.*, 22:403–434 (1976).
- [39] Gillespie, D.T., Exact Stochastic Simulation of Coupled Chemical Reactions, *Journal of Physical Chemistry*, 81(25):2340–2361 (1977).
- [40] Gillespie, D.T., A Rigorous Derivation of the Chemical Master Equation, *Phys. A*, 188:404–425 (1992).
- [41] Gillespie, D.T., *Markov Processes: An Introduction for Physical Scientists*, Academic Press, San Diego, CA, 1992.
- [42] Gillespie, D. T., Approximate accelerated stochastic simulation of chemically reacting systems., *Journal of Chemical Physics*, 115(4):1716 – 33 (2001).
- [43] Haseltine, E. L., and Rawlings, J. B., Approximate simulation of coupled fast and slow reactions for stochastic chemical kinetics., *Journal of Chemical Physics*, 117(15):6959 – 6969 (2002).
- [44] Rathinam, M., Petzold, L. R., Cao, Y., and Gillespie, D. T., Stiffness in stochastic chemically reacting systems: the implicit tau-leaping method., *Journal of Chemical Physics*, 119(24):12784 – 94 (2003).
- [45] Cao, Y., Petzold, L. R., Rathinam, M., and Gillespie, D. T., The numerical stability of leaping methods for stochastic simulation of chemically reacting systems, *Journal of Chemical Physics*, 121(24):12169 – 12178 (2004).
- [46] Haseltine, E.L., and Rawlings, J.B., On the origins of approximations for stochastic chemical kinetics, *Journal of Chemical Physics*, 123(16):164115–1–16 (2005).
- [47] Goutsias, J, Quasiequilibrium approximation of fast reaction kinetics in stochastic biochemical systems, *Journal of Chemical Physics*, 122(18):184102 (2005).
- [48] Cao, Yang, Gillespie, Daniel T., and Petzold, Linda R., The slow-scale stochastic simulation algorithm, *The Journal of Chemical Physics*, 122(1):014116 (2005).
- [49] Cao, Yang, Gillespie, Dan, and Petzold, Linda, Multi-scale stochastic simulation algorithm with stochastic partial equilibrium assumption for chemically reacting systems, *Journal of Computational Physics*, 206:395–411 (2005).
- [50] Mastny, E.A., Haseltine, E.L., and Rawlings, J.B., Stochastic simulation of catalytic surface reactions in the fast diffusion limit, *Journal of Chemical Physics*, 125(19):194715–1–10 (2006).
- [51] Mastny, E.A., Haseltine, E.L., and Rawlings, J.B., Two classes of quasi-steady-state model reductions for stochastic kinetics, *Journal of Chemical Physics*, 127(9):094106–1–16 (2007).
- [52] Homescu, Chris, Petzold, Linda R., and Serban, Radu, Error Estimation for Reduced-Order Models of Dynamical Systems, *SIAM Review*, 49(2):277–299 (2007).
- [53] Salloum, M., Alexanderian, A., Maître, O.P. Le, Najm, H.N., and Knio, O.M., Simplified CSP Analysis of a Stiff Stochastic ODE System, *Computer Methods in Applied Mechanics and Engineering*, 217-220:121–138 (2012).
- [54] Sonday, B.E., Berry, R.D., Najm, H.N., and Debusschere, B.J., Eigenvalues of the Jacobian of a Galerkin-Projected Uncertain ODE System, *SIAM J. Sci. Comp.*, 33:1212–1233 (2011).

ENTROPY PRODUCTION AND THE G-SCHEME

Mauro Valorani*, Samuel Paolucci**

*Mechanical and Aerospace Engineering, Sapienza University of Rome, Rome, Italy

**Aerospace and Mechanical Engineering, University of Notre Dame, Notre Dame, IN, USA

ABSTRACT

Spatially homogeneous batch reactor systems are characterized by the simultaneous presence of a wide range of time scales. When the dynamics of such reactive systems develop very-slow and very-fast time scales separated by a range of active time scales, with large gaps in the fast/active and slow/active time scales, then it is possible to achieve multi-scale adaptive model reduction along-with the integration of the governing ordinary differential equations using the G-Scheme framework. The G-Scheme assumes that the dynamics is decomposed into active, slow, fast, and when applicable, invariant subspaces. We computed the contribution to entropy production by the four subspaces, with reference to a constant volume, adiabatic reactor. The numerical experiments indicate that the contributions of the fast and slow subspaces are much smaller than that of the active subspace.

INTRODUCTION

The numerical solution of mathematical models for reaction systems in general, and reacting flows in particular, is a challenging task because of the simultaneous contribution of a wide range of time scales to the systems' dynamics. However, it is typical that the dynamics can develop very-slow and very-fast time scales separated by a range of active time scales.

An opportunity to reduce the complexity of the problem arises when the gaps in the fast/active and slow/active time scales become large. In [1], we provided an asymptotic analysis and proposed a numerical technique consisting of an algorithmic framework, named the G-Scheme, to achieve multi-scale adaptive model reduction along-with the integration of ordinary differential equations (ODEs) using objective criteria. In the G-Scheme, it is assumed that the dynamics is (locally) decomposed into active, slow, fast, and when applicable, invariant subspaces. The method is directly applicable to initial-value ODEs and (by using the method of lines) to partial differential equations (PDEs).

For irreversible (non-equilibrium) multi-scale processes, such as a detailed kinetic model (DKM), one question not addressed in [1] is how does the entropy production relate to the decomposition into fast, active, slow, and invariant subspaces. A quick qualitative answer could be obtained by establishing a correspondence among fast, active, slow, and invariant subspaces with near-equilibrium, non-equilibrium, near-frozen, and isentropic processes. Indeed, near-equilibrium and near-frozen processes are expected to be nearly isentropic (and quasi-linear), the algebraic invariants (linear and nonlinear) correspond to isentropic processes, and non-equilibrium processes are expected to be non-isentropic (and nonlinear). As a consequence, the entropic contributions of the fast and slow subspaces are expected to be small with respect to that of the active subspace. In this paper, we will analyze this aspect of the G-Scheme with the help of illustrative examples in the context of auto-ignition in a spatially homogeneous batch reactor.

Einstein's treatment [2] of the propagation of small-

disturbances in a monochromatic reacting gas showed that the limiting values of frozen and equilibrium sound speeds arise as the limits for the high and low frequencies of the acoustic velocity of the linearized (about the state of thermodynamic equilibrium) wave equation with a single relaxation process.

To this regard, our discussion can be considered as an attempt at generalizing this classic finding to the case of an unlimited number of nonlinear relaxation processes, where the concepts of high and low frequencies in oscillatory phenomena are replaced by those of fast and slow subspaces of dissipative/explosive phenomena.

Theory

We would like to verify empirically the contributions of the slow, active, and fast subspaces to the overall rate of entropy production in a system featuring chemical non-equilibrium. To this end, we resort to the standard model of a constant volume, adiabatic, batch reactor, where the mixture's temperature is initially set above the auto-ignition temperature.

Batch Reactor

The set of ODEs describing the time evolution of the state of the system is:

$$\begin{aligned} \frac{dT}{dt} &= -\frac{1}{\rho C_p} \sum_{j=1}^N h_j(T) W_j \dot{\omega}_j(T, Y_j), \\ \frac{dY_j}{dt} &= \frac{W_j \dot{\omega}_j(T, Y_j)}{\rho}, \quad j = 1, \dots, N \end{aligned} \quad (1)$$

where T and Y_j are the temperature and composition (expressed in terms of mass fractions) of the mixture, t is time, ρ is the constant mixture density, C_p is the mixture constant pressure specific heat, N is the number of species, h_j is the species enthalpy, W_j is the species molecular weight, and $\dot{\omega}_j$ is the molar rate of formation/destruction of the j -th species. The set of ODEs is closed by the thermal equation of state for a mixture of ideal

*Corresponding author: mauro.valorani@uniroma1.it

gases

$$p = \rho R(Y_j) T, \quad (2)$$

where p is the pressure, R is the mixture's gas constant, and the caloric equation of state

$$C_p(T, Y_j) = \sum_{j=1}^N C_{p,j}(T) Y_j, \quad (3)$$

where $C_{p,j}$ is the constant pressure specific heat of the j -th species.

The customary relations between mass fractions Y_j , molar fractions X_j , and molar concentrations c_j read:

$$c_j = \rho \frac{X_j}{\bar{W}} = \rho \frac{Y_j}{W_j} Y_j, \quad (4)$$

where \bar{W} is the mean molecular weight of the mixture. The molar rate of formation/destruction of the j -th species reads:

$$\dot{\omega}_j(T, Y_j) = \sum_{k=1}^K \Delta v_{j,k} r^k(T, Y_j) \quad (5)$$

where $\mathbf{v}'_k = \mathbf{v}'_{j,k}$ and $\mathbf{v}''_k = \mathbf{v}''_{j,k}$ are the forward and reverse stoichiometric coefficients of the j -th species in the k -th reaction out of K total reactions, and $\Delta \mathbf{v}_k = \Delta v_{j,k} = \mathbf{v}''_k - \mathbf{v}'_k$ is the net stoichiometric coefficient. The net rate of the k -th reaction reads:

$$r^k(T, Y_j) = r^k_f - r^k_b = K_f^k \prod_{j=1}^N c_j^{\mathbf{v}'_k} - K_b^k \prod_{j=1}^N c_j^{\mathbf{v}''_k}, \quad (6)$$

where r^k_f and r^k_b are the forward and backward reaction rates, and K_f^k and K_b^k are the forward and backward reaction constants, which depend exponentially on temperature according to the standard Arrhenius form.

The definition of entropy of a mixture of N ideal gases used in this paper is:

$$s(T, X_j) = \sum_{j=1}^N \Delta s_{f,j}^0(T) X_j - R \log \left(\frac{p}{p_{\text{ref}}} \right) - R \sum_{j=1}^N X_j \log(X_j). \quad (7)$$

Entropy production

If the system is spatially homogeneous, the following ODE describes the time evolution of entropy (per unit mass):

$$\frac{ds}{dt} = -\frac{1}{\rho T} \sum_{j=1}^N \mu_j(T, Y_j) W_j \dot{\omega}_j(T, Y_j) \quad (8)$$

where $\mu_j = h_j - T s_j$ is the chemical potential (per mole unit) of the j -th species.

The net rate of the k -th reaction is usually re-written by taking advantage of the relation between the equilibrium coefficient, and the forward and backward reaction coefficients

$$K_c^k = \frac{K_f^k}{K_b^k} \quad (9)$$

to obtain

$$r^k = K_f^k \left(\prod_{j=1}^N c_j^{\mathbf{v}'_k} - \frac{1}{K_c^k} \prod_{j=1}^N c_j^{\mathbf{v}''_k} \right). \quad (10)$$

Finally, introducing the affinity (per unit mass) of the k -th reaction,

$$A_k = -\sum_{j=1}^N \mu_j W_j \Delta v_{j,k}, \quad (11)$$

allows us to cast the time evolution of entropy in the final form:

$$\frac{ds}{dt} = \frac{1}{\rho T} \sum_{k=1}^K A_k K_f^k \left(\prod_{j=1}^N c_j^{\mathbf{v}'_k} - \frac{1}{K_c^k} \prod_{j=1}^N c_j^{\mathbf{v}''_k} \right). \quad (12)$$

Canonical form

The set of ODEs for the batch reactor is simply a dynamical system defined by

$$\frac{d\mathbf{x}}{dt} = \mathbf{f}(\mathbf{x}), \quad \mathbf{x}(0) = \mathbf{x}_0, \quad \text{with} \quad (13)$$

$$\mathbf{x} \in \mathbb{R}^{N+2}, \quad t \in (0, T) \subset \mathbb{R}, \quad \text{and } \mathbf{f}: E \subset \mathbb{R}^{N+2} \rightarrow \mathbb{R}^{N+2}.$$

where the state of the system is defined as $\mathbf{x} = \{Y_j, T, s\}$ and the vector field is defined by

$$\mathbf{f}(Y_j, T, s) = \left\{ \begin{aligned} & \frac{W_j \dot{\omega}_j(T, Y_j)}{\rho}, -\frac{1}{\rho C_p} \sum_{j=1}^N h_j W_j \dot{\omega}_j(T, Y_j), \\ & -\frac{1}{\rho T} \sum_{j=1}^N \mu_j(T, Y_j) W_j \dot{\omega}_j(T, Y_j) \end{aligned} \right\}. \quad (14)$$

Note that for a constant volume system, the entropy equation is slaved to the other ODEs.

Basic Concepts for the G-Scheme

We have assumed that the dynamics is decomposed into active, slow, fast, and when applicable, invariant subspaces. The G-Scheme introduces a local curvilinear frame of reference, defined by a set of orthonormal basis vectors with corresponding coordinates, attached to this decomposition. The evolution of the curvilinear coordinates associated with the active subspace, $\Delta \xi^a$, is described by non-stiff ODEs, whereas those associated with the slow, $\Delta \xi^h$, and fast, $\Delta \xi^f$, subspaces are accounted for

by applying asymptotic approximations of the original problem to provide $\Delta\xi_{FF}^h$, and $\Delta\xi_{SIM}^t$, respectively. Adjusting the active ODEs dynamically during the time integration is the most significant feature of the G-Scheme, since the numerical integration is accomplished by solving a number of ODEs, typically much smaller than the dimension of the original problem, with corresponding savings in computational work.

The Adaptive Reduced Model

The G-Scheme involves two main stages:

1. Evolution of the active modes described by $N_{\mathbb{A}}$ non-stiff ODEs;
2. Corrections associated with the slow/fast dynamics.

The active ODEs evolve in subspace \mathbb{A} which is freed from fast scales, i.e., they are non-stiff. They can be solved by resorting to any explicit scheme of integration (e.g., explicit Runge-Kutta). When compared to a standard BDF implicit scheme for stiff problems, the G - Scheme requires the solution of $N_{\mathbb{A}}$ explicit ODEs instead of $N + 2$ implicit ODEs. However, the scheme requires the identification of the tangent space decomposition.

Adjusting the active ODEs dynamically is the most significant feature of the G-Scheme, because the numerical integration of a state vector $\mathbf{x} \in N + 2$ is obtained by solving a number ($\ll N$) non-stiff ODEs with the corresponding saving in CPU work.

Tangent Space Decomposition

Ideal decomposition of the tangent space $\mathcal{T}_{\mathbf{x}}$ at any point $\mathbf{x} \in \mathbb{C} \subset \mathbb{R}^{N+2}$ involves the identification of $N + 2$ invariant subspaces, a difficult task. The G-Scheme decomposes the tangent space in four subspaces having time scales of comparable magnitude, $\mathcal{T}_{\mathbf{x}} = \mathbb{E} \oplus \mathbb{H} \oplus \mathbb{A} \oplus \mathbb{T}$, where \mathbb{E} is the linear subspace spanned by directions associated with invariants, if any exists (conservation laws). All scales slower than the active ones are confined to the slow subspace \mathbb{H} (ead) (dormant/near-frozen processes). The active subspace \mathbb{A} contains all the current intermediate dynamic time scales (active/non-equilibrium). All scales faster than the active ones are confined in the fast subspace \mathbb{T} (ail) (exhausted/near-equilibrium). Thus, the basic concept in the G-Scheme is to ‘distill’ the Heart, and ‘cut’ the Head and Tail in a generic multi-scale dynamical system.¹

Basis Vectors and Time Scales

The most important decision to be taken in the implementation of the G-Scheme framework is the choice of a curvilinear frame of reference, i.e., a basis matrix yielding a maximal degree of slow/fast decoupling. In fact, the basis vectors used to define the matrix might be found, in principle, by different means, if they can provide the ideal block-diagonalization of the eigenvalue matrix in a cost efficient way. The Computational Singular Perturbation [3] method offers a computational algorithm to achieve this goal. The CSP refinements converge to the right/left eigenvectors of $J(\mathbf{x}(t_n))$ if nonlinearities are neglected. In this case, we can rank the basis vectors according to

the magnitude of the corresponding eigenvalues, to obtain

$$0 = \lambda_1 = \dots = \lambda_E < |\lambda_{E+1}| \leq \dots \leq |\lambda_{H-1}| \ll |\lambda_H| \leq \dots \leq |\lambda_T| \ll |\lambda_{T+1}| \leq \dots \leq |\lambda_{N+2}|, \quad (15)$$

where

$$\begin{aligned} 0 = \lambda_1 = \dots = \lambda_E & \text{ identify the scales in } \mathbb{E}, \\ |\lambda_{E+1}| \leq \dots \leq |\lambda_{H-1}| & \text{ identify the scales in } \mathbb{H}, \\ |\lambda_H| \leq \dots \leq |\lambda_T| & \text{ identify the scales in } \mathbb{A}, \\ |\lambda_{T+1}| \leq \dots \leq |\lambda_{N+2}| & \text{ identify the scales in } \mathbb{T}. \end{aligned} \quad (16)$$

As estimate of the time scale associated to an eigendirection, we take the inverse of the magnitude of the corresponding eigenvalue.

Asymptotics of Fast and Slow Time Scales

The G-Scheme exploits the two archetypes for reduction, slow-invariant-manifold (SIM) and fast-fibers (FF), to define the adaptive reduction: SIM and FF concepts are invoked to define the T(ail) and H(ead) subspaces, respectively. The concepts of SIM and FF are invoked on a local basis. Differently from other approaches, for the G-Scheme to be applicable it is not required that a global SIM exist, nor that the SIM dimension be constant or prescribed in advance. Similar comments apply for the exploitation of the FF. The contributions of fast and slow scales are accounted for with SIM and FF algebraic corrections obtained through asymptotic analysis.

The G-Scheme Step-by-Step

The following section is illustrated in full detail in [1], and is reported here for the reader convenience. For time interval t_0 , and for the state vector $x(t_0)$, initialize the integration as:

1. Compute:

$$T(x(t_0)) = N, J(x(t_0)), \lambda_i(x(t_0)), A(x(t_0)), B(x(t_0))$$
 where J is the Jacobian matrix of the vector field of Eq. (13), λ_i is the eigenvalue of the i -th eigenmode of J , and the matrix A/B collect all the right (row)/left(column) eigenvectors of J ; T is a scalar value denoting the fastest of the active modes..

For each time interval t_n ($\tau = 0$), and for the state vector $x(t_n)$, with $n = 0, 1, 2, \dots$, proceed as follows:
2. Define Time Step as : $\Delta t = \gamma / |\lambda_T(x(t_n))|$ $\gamma \approx O(1)$;
3. Update Time : $t_{n+1} = t_n + \Delta t$;
4. Identify the Head Subspace dimension, $H(x(t_n))$ on the basis of a user specified accuracy vector defined as $\epsilon_{acc} = rtol|y_j| + atol$;
5. Solve the set of non-stiff Active ODE’ s:

$$\frac{d\Delta\xi^a(\tau)}{d\tau} = B^a(t_n) f[x(t_n) + A_a(t_n) \Delta\xi^a(\tau)] \quad (17)$$

with $\Delta\xi^a(0) \equiv 0^a$ $a = H, T$.

6. Update state vector: $x^a(t_{n+1}) = x(t_n) + A_a(t_n) \Delta\xi^a(\Delta t)$
7. Apply Head Correction:

$$x^h(t_{n+1}) = x^a(t_{n+1}) + A_h(t_n) \Delta\xi_{FF}^h(\Delta t)$$

¹G stands for Grappa, an Italian liquor produced by distillation.

that is the contribution to the rate of entropy production of the k -th reaction on the fast subspace is negligible because of Eq. (23) even if $K_f^k \gg 1$, as is the case for fast reactions, and therefore:

$$\begin{aligned} s^t(t_{n+1}) &= s^h(t_{n+1}) + \Delta s_{\text{SIM}(t_n)}^t \sim s^h(t_{n+1}) \\ s(t_{n+1}) &= s^t(t_{n+1}) + \Delta s_{\text{SIM}(t_{n+1})}^t \sim s^t(t_{n+1}). \end{aligned} \quad (26)$$

RESULTS

The specific test case considered refers to a methane/air system, using GRI 3.0 kinetics (53 species). The batch reactor model is adiabatic and at constant volume. The initial conditions for the test case are defined by prescribing the initial temperature $T_0 = 1000 \text{ K}$ and pressure $p_0 = 1 \text{ atm}$ of a stoichiometric mixture of reactants. The constant density in Eq. (1) is set on the basis of the thermal equation of state.

Figure 2 shows the evolution of temperature (solid, black line) as a function of the number of iteration steps (to avoid the compression of the plot about the reaction time). On the same figure, we plot the evolution of the dimension A of the active subspace (green solid line) obtained by subtracting H (blue line) from T (red line), where H and T are the mode numbers corresponding to $|\lambda_H|$ and $|\lambda_T|$, respectively. The dimension of the active subspace also corresponds to the number of non-stiff ODEs solved by the G-Scheme. The modes comprised between 5 and $H-1$ span the slow subspace, those between H and T the active subspace, and those between $T+1$ and $N+2$ the fast subspace.

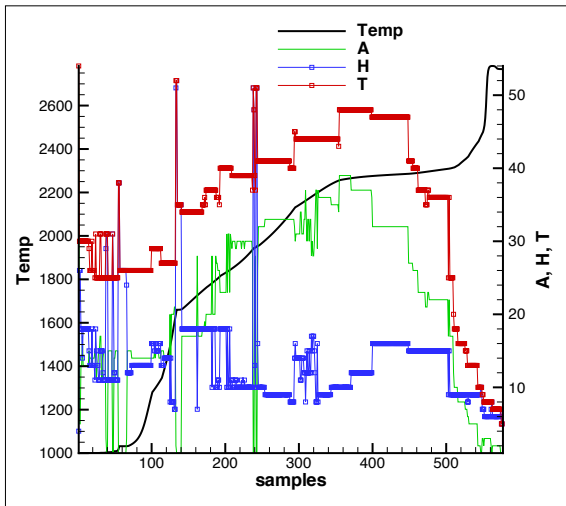


Figure 2. Time evolution of the dimension of the active (green), slow (blue), and fast (red) subspaces; temperature (solid black line); $rtol = 10^{-3}$.

Figure 3 shows the time evolution of the reciprocal of the modulus of the (complex) eigenvalues of the 55 modes as a function of the number of iteration steps. On the same figure, we plot the evolution of the characteristic scales of the G-Scheme, namely, the reciprocal of $|\lambda_{H-1}|$ (green), $|\lambda_H|$ (red), $|\lambda_T|$ (cyan), $|\lambda_{T+1}|$ (blue), and $|\lambda_{N+2}|$ (black). The blue solid line reports the entropy evolution. The slow/active scale gap is visually comprised between the green and red lines, while the active/fast gap

is between the cyan and blue lines. The black line marks the fastest time scale at all times. The spectral width of the fast subspace is between the black and blue lines. The width of the active subspace is between the cyan and red lines. The width of the slow subspace is above the red line. The invariant subspace is associated with the randomly scattered markers visible at very large time scales.

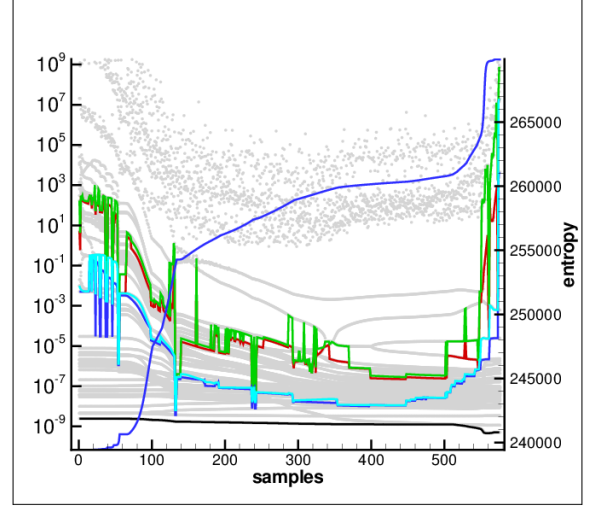


Figure 3. Reciprocal of the modulus of the (complex) eigenvalues (light grey markers); reciprocal of $|\lambda_{H-1}|$ (green), $|\lambda_H|$ (red), $|\lambda_T|$ (cyan), $|\lambda_{T+1}|$ (blue), and $|\lambda_{N+2}|$ (black); the red solid line reports the entropy evolution; $rtol = 10^{-3}$.

The quantitative assessment of the relative contribution to the rate of entropy production from the slow, active, and fast subspaces is carried out by considering that the entropy of the mixture is a state function of temperature and composition. Therefore, during the numerical integration of the batch reactor model, we evaluated the entropy of the mixture before and after each of the changes of the system state due to the slow (Δs_h), active (Δs_a), and fast (Δs_t) subspaces. With these definitions, we introduced the following:

$$\begin{aligned} s_a(t_n) &= s_a(t_{n-1}) + \Delta s_a(t_n) \\ s_h(t_n) &= s_h(t_{n-1}) + \Delta s_h(t_n) \\ s_t(t_n) &= s_t(t_{n-1}) + \Delta s_t(t_n) \\ s(t_n) &= s_a(t_n) + s_h(t_n) + s_t(t_n) \end{aligned} \quad (27)$$

where $s_\alpha(t_0) = s(T_0, p_0, Y_{j,0})$, $\alpha = a, h, t$. Figure 4 shows the time evolution of the contribution to the entropy of the mixture from the slow, active, and fast subspaces as obtained using three different accuracy levels ($rtol = 10^{-3}, 10^{-4}, 10^{-5}$), while Fig. 5 shows the entropy contribution of each subspace scaled with respect to the overall contribution ($s_\alpha(t_n)/s(t_n)$ with $\alpha = a, h, t$). It is apparent that the active subspace contribution is always very close to 100%, while the slow contribution is generally larger than the fast contribution.

The sensitivity to the accuracy level of the contribution to the entropy of the mixture can be appreciated with the help of Fig 6, which indicates that the magnitude of the overall entropy contribution, that is, evaluated at large times, of the fast subspace

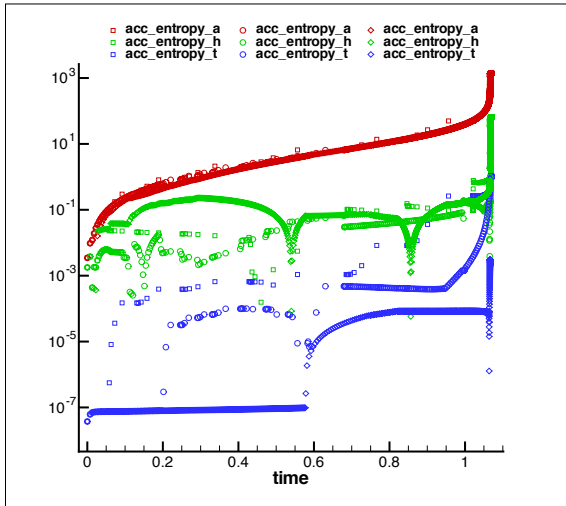


Figure 4. Contribution to the entropy of the mixture from the slow ($s_h(t_n)$, green), active ($s_a(t_n)$, red), and fast ($s_f(t_n)$, blue) subspaces, as obtained using three different accuracy levels ($rtol = 10^{-3}$ (square markers), 10^{-4} (circles), 10^{-5} (diamonds)).

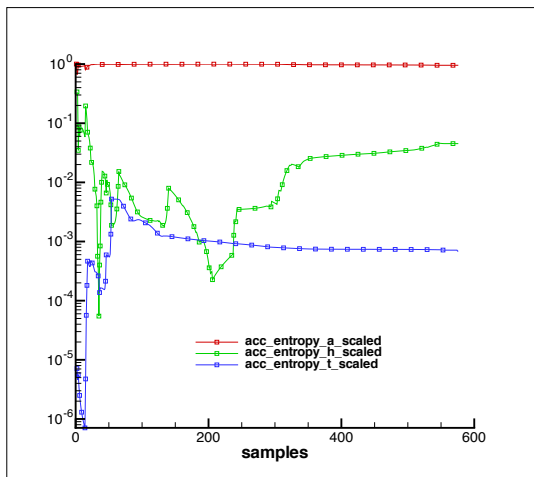


Figure 5. Contribution to the entropy of the mixture from the slow ($s_h(t_n)/s(t_n)$, green), active ($s_a(t_n)/s(t_n)$, red), and fast ($s_f(t_n)/s(t_n)$, blue) subspaces scaled with respect to the overall contribution ($rtol = 10^{-3}$).

is of the same order of the accuracy level specified by the user. Instead the overall entropy contribution of the slow subspace is always smaller than the active contribution, but it does not seem to depend much on the accuracy level specified by the user.

Figure 7 shows that the relative contribution to the rate of entropy production ($\Delta s_\alpha(t_n)/\Delta s(t_n)$) of the slow and fast subspaces are approximately 10^{-3} and 10^{-4} , respectively, whereas that of the active subspace is always of order one. This indicates that the contribution to the rate of entropy production of the fast subspace is always negligible with respect to that of the active subspace, whereas that of the slow subspace can occasionally become comparable to that of the active subspace within the reaction period of the auto-ignition process.

CONCLUSIONS

Reaction systems are characterized by the simultaneous presence of a wide range of time scales. When the dynamics of reactive systems develop very-slow and very-fast time scales

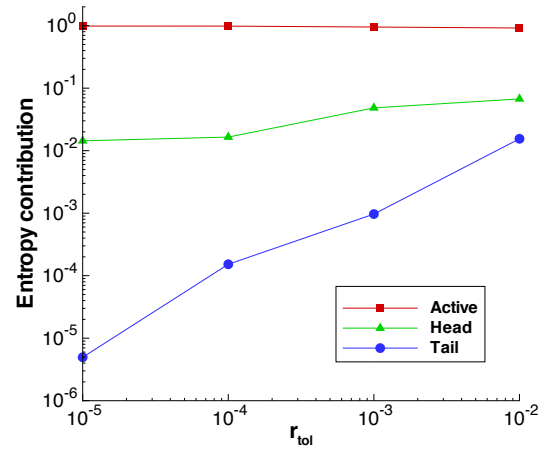


Figure 6. Overall entropy production per each subspace; slow ($s_h(t_\infty)$, green), active ($s_a(t_\infty)$, red), and fast ($s_f(t_\infty)$, blue) subspaces.

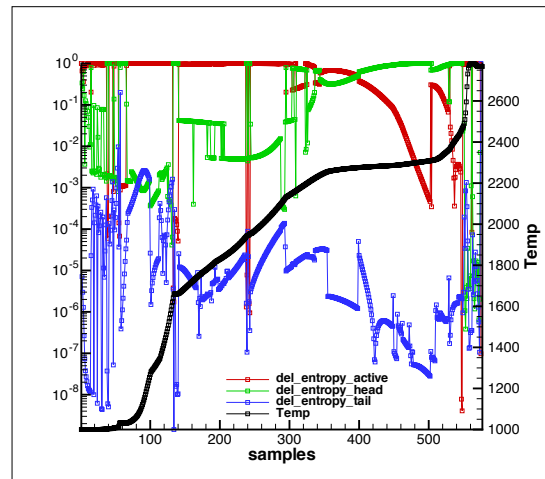


Figure 7. Contribution to the rate of change of entropy of the mixture from the slow ($\Delta s_h(t_n)/\Delta s(t_n)$, green), active ($\Delta s_a(t_n)/\Delta s(t_n)$, red), and fast ($\Delta s_f(t_n)/\Delta s(t_n)$, blue) subspaces ($rtol = 10^{-3}$).

separated by a range of active time scales, with large gaps in the fast/active and slow/active time scales, then it is possible to achieve multi-scale adaptive model reduction along-with the integration of the ODEs using the G-Scheme framework. The G-Scheme assumes that the dynamics is decomposed into active, slow, fast, and invariant subspaces. To calculate the contribution to entropy production related to the four subspaces, we resorted to a standard model of a constant volume, adiabatic, batch reactor, where the mixture temperature of the reactants is initially set above auto-ignition temperature. The specific test case considered refers to a methane/air system, using GRI 3.0 kinetics. The numerical experiments indicate that the contributions of the fast and slow subspaces are typically much smaller (of the order of the user defined accuracy of the numerical integration) both locally and globally than the contribution of the active subspace. A preliminary analysis of the relevant theory is offered to indicate why this conclusion might be of general validity.

ACKNOWLEDGMENT

MV acknowledges the support of the Italian Ministry of University and Research (MIUR).

References

- [1] M Valorani and S Paolucci. “The G-Scheme: A framework for multi-scale adaptive model reduction”. In: *Journal of Computational Physics* 228.13 (2009), pp. 4665–4701.
- [2] A. Einstein. “Schallgeschwindigkeit in teilweise dissoziierten Gasen”. In: *Sitzungsberichte d. preussischen Adak. d. Wiss. Wien* 18.1 (1920), p. 380.
- [3] S. H. Lam and D. a. Goussis. “The CSP method for simplifying kinetics”. In: *International Journal of Chemical Kinetics* 26.4 (Apr. 1994), pp. 461–486. ISSN: 0538-8066. DOI: 10 . 1002 / kin . 550260408. URL: [http : //doi.wiley.com/10.1002/kin.550260408](http://doi.wiley.com/10.1002/kin.550260408).

GRASPING COMPLEXITY IN CHEMICAL KINETICS: TOP-DOWN, BOTTOM-UP AND SOME MORE

Gregory S. Yablonsky*, Denis Constaes^o, Guy B. Marin**

*Parks College of Engineering, Aviation, and Technology, Department of Chemistry, Saint Louis University, St. Louis MO, 63103, USA

^oDepartment of Mathematical Analysis, Ghent University, Galglaan 2, B-9000, Ghent (Belgium)

**Laboratory for Chemical Technology, Ghent University, Krijgslaan, S5, B-9000, Ghent (Belgium)

EXTENDED ABSTRACT

The analysis of complex reaction networks can be performed in two complementary ways:

- (a) Insight in the chemistry of the investigated process can be translated into so-called chemical rules. This can be implemented as algorithms in computer code, allowing the automatic generation of reaction networks consisting of several thousands of elementary steps. Databases, which are based either on experiments or on the quantum chemical calculation of model reactions, then provide the corresponding thermodynamic and kinetic parameters.

Numerical integration techniques and kinetic Monte-Carlo simulations finally allow, e.g. via a sensitivity analysis, to assess the significance of each elementary reaction family considered, and the effects of the reaction conditions on them.

Recent results by Gorban et al. [1-2] provide the means for a rigorous asymptotic analysis of complex kinetic models for both reversible and irreversible mechanisms. This first way can be interpreted as a *top-down* approach.

- (b) Alternatively, under the *bottom-up* approach, the so-called minimal reaction networks and mechanisms are the starting point. For the steady-state kinetics of catalytic reactions a general, a thermodynamically consistent rate equation can be constructed using algebraic methods and/or graph theory [3]. For linear reaction mechanisms this rate equation consists of a driving force, which ensures thermodynamic consistency, and a resistance, which is the inverse of the total weight of the node-spanning trees of the graph corresponding to the reaction mechanism. This resistance can actually be measured as the ratio of the driving force to the reaction rate.

The analysis of the concentration and temperature dependence of the resistance then provides direct information on the nature of the elementary steps involved in the reaction mechanism. For nonlinear reaction mechanisms an implicit equation for the reaction rate can conveniently be used to obtain insights. This so-called *kinetic polynomial* is a generalization of the well-known Langmuir-Hinshelwood-Hougen-Watson (LHHW) rate equation for linear reactions mechanisms.

In the non-steady-state kinetic description, data from pulse-response experiments with insignificant perturbation (data obtained from Temporal Analysis of Products) can be used to construct the model in the bottom-up style. In such cases, the model is built using decision tree procedures.

A new, additional form of pattern analysis exists that lies beyond the alternative between the top-down and bottom-up approaches:

- (c) It is based on the following new kinetic phenomena that were discovered theoretically [4-8] and experimentally confirmed [8].
- (1) Intersections of concentration dependencies, coincidences of such intersections, and the structure of possible orderings of concentration and time values defined by intersections.

The intersections under consideration are defined by the concentration dependencies of the system when started from special, extreme initial conditions. For instance, the two-step reversible-irreversible mechanism $A \rightleftharpoons B \rightarrow C$ can be studied for an initial state where all substance is A and no B or C occur (the A-trajectory) and from the initial state where all substance is B and no A or C occur (the C-trajectory). We then denote by $C_{AA}(t)$ the time evolution of the concentration of A in the A trajectory, by $C_{AB}(t)$ that of A in the B trajectory, etc.

As examples of intersections, we can investigate whether $C_{AA}(t)$ and $C_{BA}(t)$ intersect, and whether $C_{BA}(t)$ intersects with $C_{CB}(t)$. Given two such intersections, we consider their ordering, either in time or in concentration value: for some choices of the parameters the first will come before the second, or vice versa. At the boundary between both parameter domains there occurs a coincidence: the two intersections coincide in their time or concentration value.

The various cases are best presented in graphical form, as in Fig. 1, where the black means neither intersection occurs, the dark yellow only the first, the dark blue only the second, the blue that the first intersection occurs before the second, and the yellow that the first occurs after the second. See [6] for the detailed study of this two-step mechanism.

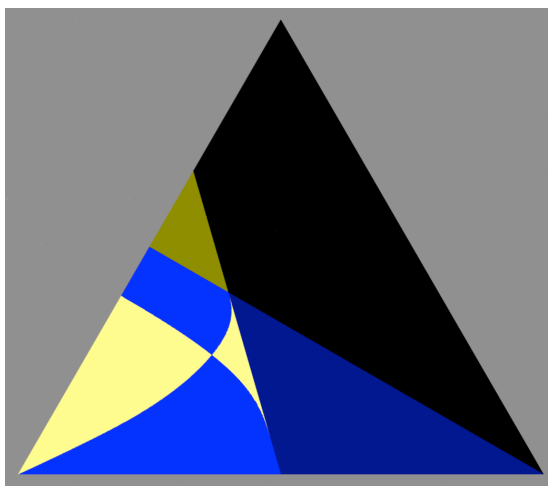


Figure 1: Example parameter domain for intersections.

- (2) Invariances of a special type observed in so-called dual experiments.

When studying these intersections, a remarkable property arises: some of the concentration dependencies are always proportional to each other, so that their intersection is either empty (in positive time) or they coincide at all points in time. In our simple example $A \rightleftharpoons B \rightarrow C$ this is the case for $C_{AB}(t)$ and $C_{BA}(t)$: at all $t > 0$, $C_{BA}(t)/C_{AB}(t) = k^+ / k^-$, the equilibrium constant of the first reaction step. Closer analysis reveals that this property holds in all linear reaction schemes for each pair of substances A and B between which a reversible reaction occurs, and that it is a consequence of Onsager reciprocity (see [7]).

ACKNOWLEDGMENT

Financial support from the Long Term Structural Methusalem Funding by the Flemish Government is gratefully acknowledged.

REFERENCES

- [1] A.N. Gorban, and G.S. Yablonsky, Extended Detailed Balance for Systems with Irreversible Reactions, *Chem. Eng. Sci.*, vol. 66, pp. 5388-5399, 2011.
- [2] A.N. Gorban, E.M. Mirkes, and G.S. Yablonsky, Thermodynamics in the Limit of Irreversible Reactions, *Physica A*, vol. 392, pp. 1318-1335, 2013.
- [3] G.B. Marin and G.S. Yablonsky, *Kinetics of Chemical Reactions: Decoding Complexity*, Wiley-VCH, 2011.
- [4] G.S. Yablonsky, D. Constaes, G.B. Marin, Equilibrium relationships for non-equilibrium chemical dependencies. *Chem. Eng. Sci.*, vol. 66, pp. 111-114, 2011.
- [5] D. Constaes, G.S. Yablonsky, G.B. Marin, Thermodynamic time invariances for dual kinetic experiments: nonlinear single reactions and more, *Chem. Eng. Sci.*, vol. 73, pp. 20-29, 2012.
- [6] D. Constaes, G.S. Yablonsky, and G.B. Marin, Intersections and coincidences in chemical kinetics: linear two-step reversible-irreversible reaction mechanism, accepted by *Computers and Mathematics with their Applications*, 2013.
- [7] G.S. Yablonsky, A.N. Gorban, D. Constaes, V.V. Galvita, G.B. Marin, Reciprocal relations between kinetic curves. *EPL - Europhysics Letters*, vol. 93, 20004, 2011.
- [8] D. Constaes, G.S. Yablonsky, V.V. Galvita, G.B. Marin, Thermodynamic time-invariances: theory of TAP pulse-response experiments. *Chem. Eng. Sci.*, vol. 66, 4683-4689, 2011.

PANEL K

**QUANTUM THERMODYNAMICS:
WHAT IS IT AND WHAT CAN BE DONE WITH IT**

QUANTUM-MECHANICAL ANALOG OF THE CARNOT CYCLE: GENERAL FORMULA FOR EFFICIENCY AND MAXIMUM-POWER OUTPUT

Sumiyoshi Abe

Department of Physical Engineering, Mie University, Mie 514-8507, Japan

ABSTRACT

The quantum-mechanical Carnot cycle is an analog of the thermodynamic one and is constructed without heat baths. The cycle is realized by controlling quantum states of particles as well as a confining potential. Here, recent developments about such a cycle are reported. The general formula for the efficiency is presented for an arbitrary potential. A finite-time process is also discussed, and the value of the efficiency under the maximum power condition is derived in the case of a one-dimensional infinite square-well potential.

INTRODUCTION

Small systems are of interest from various viewpoint in contemporary science. In particular, the problems of constructing microscopic machines/engines and understanding their operating mechanisms are relevant to biology (e.g., biomolecular motors), information theory (e.g., Maxwell's demon), nanoscience and so on.

The subject of the present article is concerned with a reversible engine made of a single quantum-mechanical particle confined in an variable potential. This system does not contain heat baths, and the volume change (i.e., expansion and compression) is realized by external control of the potential. Accordingly, quantum coherence remains intact. In Ref. [1], it has been shown, by considering a cycle of a system consisting of a particle in an infinite square-well potential with the movable walls, that it is in fact possible to construct a reversible cycle and to extract work from it. The cycle constructed there is analogous to Carnot's, and is therefore referred to as *quantum-mechanical Carnot cycle*. However, because of the absence of hot and cold heat baths, it should not be confused with cycles of genuine quantum heat engines discussed in the literature (see, for example, Refs. [2-7]).

QUANTUM-MECHANICAL ANALOG OF THE CARNOT CYCLE

The cycle is described in Fig. 1. We discuss a case, which is much more general than that in Ref. [1].

Initially, the system is in a state, $|u_1(V_A)\rangle$, at A. After the volume expansion, the system reaches B in a higher state, say $|u_2(V_B)\rangle$. During the expansion process $A \rightarrow B$, the system is in a superposed state, $a_1(V)|u_1(V)\rangle + a_2(V)|u_2(V)\rangle$

$(|a_1(V)|^2 + |a_2(V)|^2 = 1)$, but the average energy (i.e., an analog of the internal energy) $E_H \equiv \langle H \rangle_H = \sum_{n=1,2} E_n(V) |a_n(V)|^2$ is kept unchanged. Here, $H = H(V)$

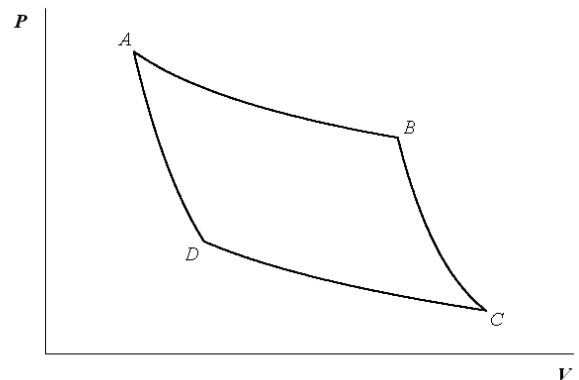


Figure 1. The cycle depicted in the plane of volume V and pressure P .

is the system Hamiltonian for the stationary Schrödinger equation, $H(V)|u_n(V)\rangle = E_n(V)|u_n(V)\rangle$, which is valid under the adiabaticity condition, that is, slow change of V . The time scale of change of V is much larger than that of the dynamical one, $\sim \hbar / E$, with E being a typical value of the energy. Note that $E_H = E_1(V_A) = E_2(V_B)$ and $a_1(V_B) = a_2(V_A) = 0$. Similar is the process $C \rightarrow D$, in which the state changes from $|u_2(V_C)\rangle$ to $|u_1(V_D)\rangle$, and in-between it is a superposed one,

$b_1(V)|u_1(V)\rangle + b_2(V)|u_2(V)\rangle$ ($|b_1(V)|^2 + |b_2(V)|^2 = 1$), but the average energy $E_L \equiv \langle H \rangle_L = \sum_{n=1,2} E_n(V) |b_n(V)|^2$ is kept unchanged. We have $E_L = E_2(V_C) = E_1(V_D)$ and $b_1(V_C) = b_2(V_D) = 0$. These two processes are analogs of the isothermal processes in the thermodynamic Carnot cycle. On the other hand, $B \rightarrow C$ and $D \rightarrow A$ are analogs of the adiabatic processes. During $B \rightarrow C$ ($D \rightarrow A$), the state remains as $|u_2(V)\rangle$ ($|u_1(V)\rangle$). These analogies have been clarified in Ref. [8] from the viewpoint of a formal similarity between quantum mechanics and thermodynamics. An explicit example using a one-dimensional infinite square-well potential with movable walls shows [1] that it is in fact possible to construct a cycle of this kind.

Work is defined by $d'W = \langle \partial H(V) / \partial V \rangle dV \equiv -P dV$, where P is pressure. The work during each process is given as follows: $W_{AB} = \int_{V_A}^{V_B} dV \sum_{n=1,2} [\partial E_n(V) / \partial V] |a_n(V)|^2$, $W_{BC} = \int_{V_B}^{V_C} dV \partial E_2(V) / \partial V$, $\int_{V_C}^{V_D} dV \sum_{n=1,2} [\partial E_n(V) / \partial V] |b_n(V)|^2$ and $W_{DA} = \int_{V_D}^{V_A} dV \partial E_1(V) / \partial V$. It can be shown [9] that $W_{BC} = -W_{DA}$ holds, in general. Therefore, the work extracted after a single cycle is $W = W_{AB} + W_{BC} + W_{CD} + W_{DA} = W_{AB} + W_{CD}$. The efficiency of the cycle is then given by $\eta = W / W_{AB}$. In Ref. [9], the following general formula for the efficiency has been presented:

$$\eta = 1 - \frac{\int_{V_D}^{V_C} dV \Delta E(V) \frac{\partial}{\partial V} \left[\frac{E_L - \bar{E}(V)}{\Delta E(V)} \right]}{\int_{V_A}^{V_B} dV \Delta E(V) \frac{\partial}{\partial V} \left[\frac{E_H - \bar{E}(V)}{\Delta E(V)} \right]} \quad (1)$$

where

$$\bar{E}(V) = \frac{1}{2} [E_1(V) + E_2(V)], \quad (2)$$

$$\Delta E(V) = E_2(V) - E_1(V). \quad (3)$$

Eq. (1) shows how the efficiency depends on the structure of the energy spectrum. Since a potential is the analog of a working material in thermodynamics, this formula exhibits how the quantum-mechanical Carnot cycle is nonuniversal. This is due to the fact that, in pure-state quantum mechanics, the von Neumann entropy identically vanishes and, therefore, there does not exist an analog of the second law of thermodynamics.

Closing this section, we would like to mention an intriguing point regarding the efficiency in Eq. (1) for a certain class of spectra. Suppose the energy eigenvalues to have the form

$$E_n(V) = \frac{\varepsilon_n}{V^\alpha} \quad (n = 1, 2, 3, \dots) \quad (4)$$

where α and ε_n 's are independent of V , $\alpha > 0$ and $\varepsilon_1 < \varepsilon_2 < \varepsilon_3 < \dots$. The spectra of this form are referred to here as *homogeneous type*. In this case, Eq. (1) is calculated to have the following simple form:

$$\eta = 1 - \frac{E_L}{E_H}. \quad (5)$$

A homogeneous-type spectrum will be discussed in the next section.

FINITE-TIME PROCESSES AND MAXIMUM POWER OUTPUT

So far, we have seen the nonuniversal nature of the quantum-mechanical Carnot cycle. Here, we wish to examine this point from a different aspect. Specifically, we consider finite-time processes and the condition for the maximum power output [10]. For this purpose, we employ a simple system of a particle confined in a one-dimensional infinite square-well potential as in Ref. [1]. The energy eigenvalues are given by $E_n(L) = n^2 \pi^2 \hbar^2 / (2mL^2)$ ($n = 1, 2, 3, \dots$), where L is the width of the potential well and slowly changes in time. (Since the system is one-dimensional, L corresponds to the volume V in the preceding section.) We note that this spectrum is of the homogeneous type. Taking the ground ($n = 1$) and first excited ($n = 2$) states and applying Eq. (5), we obtain

$$\eta = 1 - 4 \left(\frac{L_A}{L_C} \right)^2, \quad (6)$$

where L_A and L_C are the values of the potential width at A and C , respectively.

Now, let $v(t)$ be the speed of the change of the width. The total amount of movement of L during a single cycle is given by

$$L_{\text{total}} = 2(L_C - L_A) = \int_0^\tau dt v(t) \equiv \bar{v} \tau, \quad (7)$$

where τ is the cycle time and \bar{v} is the average speed. Eq. (7) allows one to express the cycle time as follows:

$$\tau = \frac{2}{\bar{v}} (L_C - L_A). \quad (8)$$

On the other hand, the work extracted after a single cycle is $W = (\pi^2 \hbar^2 / m) (1/L_A^2 - 4/L_C^2) \ln 2$. The condition

$$r \equiv \frac{L_C}{L_A} > 2 \quad (9)$$

has to be fulfilled in order for the work extracted to be positive. The power output is then expressed as follows [10]:

$$\Pi \equiv \frac{W}{\tau} = \frac{\pi^2 \hbar^2 \bar{v} \ln 2}{2mL_A^3} \cdot \frac{r^2 - 4}{r^3 - r^2}. \quad (10)$$

Our interest is in maximization of Π . This problem turns out to be given by the solution of the equation, $r^3 - 12r + 8 = 0$. This cubic equation has three real solutions, but $r = 4 \cos(2\pi/9)$ is the one and only solution consistent with the condition in Eq. (9). Then, the corresponding value of the efficiency is

$$\eta^* = 1 - \frac{1}{4 \cos^2(2\pi/9)} = 0.573977952\dots \quad (11)$$

This result is *universal* in the sense that it does not contain any of the parameters characterizing the system under consideration.

CONCLUSION

We have reported recent developments made about the quantum-mechanical Carnot cycle. We have discussed the general formula derived for the efficiency for an arbitrary potential confining a particle. Also, we have mentioned the result on the efficiency under the maximum power condition by employing a one-dimensional infinite square-well potential.

As stressed in the very beginning of this article, the systems' quantum coherence remains intact, since no heat baths are present. This fact leads to the following question: Can the principle of superposition plays some role here? The answer to this question seems to be affirmative. It is in fact shown in Ref. [11] that the efficiency can be enhanced by superposition of relevant states. It is also of extreme interest to examine roles and effects of quantum entanglement in systems consisting of more than one particle.

ACKNOWLEDGMENT

This work has been supported in part by a Grant-in-Aid for Scientific Research from the Japan Society for the Promotion of Science (JSPS).

REFERENCES

- [1] C. M. Bender, D. C. Brody and B. K. Meister, Quantum Mechanical Carnot Engine, *J. Phys. A: Math. Gen.*, vol. 33, pp. 4427-4436, 2000.
- [2] J. E. Geusic, E. O. Schulz-DuBois and H. E. D. Scovil, Quantum Equivalent of the Carnot Cycle, *Phys. Rev.*, vol. 156, pp. 343-351, 1967.
- [3] T. D. Kieu, The Second Law, Maxwell's Demon, and Work Derivable from Quantum Heat Engines, *Phys. Rev. Lett.*, vol. 93, pp. 140403:1-4, 2004.
- [4] H. T. Quan, P. Zhang and C. P. Sun, Quantum Heat Engine with Multilevel Quantum Systems, *Phys. Rev. E*, vol. 72, pp. 056110:1-10, 2005.
- [5] R. S. Johal, Quantum Heat Engines and Nonequilibrium Temperature, *Phys. Rev. E*, vol. 80, 041119:1-5, 2009.
- [6] G. P. Beretta, Quantum Thermodynamic Carnot and Otto-Like Cycles for a Two-Level System, *EPL*, vol. 99, pp. 20005:1-5, 2012.
- [7] K. Nakamura, Z. A. Sobirov, D. U. Matrasulov and S. K. Avazbaev, Bernoulli's Formula and Poisson's Equations for a Confined Quantum Gas: Effects due to a Moving Piston, *Phys. Rev. E*, vol. 86, pp. 061128:1-10, 2012.
- [8] S. Abe and S. Okuyama, Similarity between Quantum Mechanics and Thermodynamics: Entropy, Temperature, and Carnot Cycle, *Phys. Rev. E*, vol. 83, pp. 021121:1-3, 2011.
- [9] S. Abe, General Formula for the Efficiency of Quantum-Mechanical Analog of the Carnot Engine, *Entropy*, vol. 15, pp. 1408-1415, 2013.
- [10] S. Abe, Maximum-Power Quantum-Mechanical Carnot Engine, *Phys. Rev. E*, vol. 83, pp. 041117:1-3, 2011.
- [11] S. Abe and S. Okuyama, Role of the Superposition Principle for Enhancing the Efficiency of the Quantum-Mechanical Carnot Engine, *Phys. Rev. E*, vol. 85, pp. 011104:1-4, 2012.

MICROSCOPIC BROWNIAN HEAT ENGINES: A QUANTUM DYNAMICAL FRAMEWORK

S. Chaturvedi

School of Physics, University of Hyderabad, Hyderabad 500046, India, E-mail: scsp@uohyd.ernet.in

EXTENDED ABSTRACT

Inspired by a recent experimental work of Blicke and Bechinger [Nature, **8**, 143 (2011)] on a microscopic realization of the Stirling cycle through a colloidal particle in an optical trap, we develop a self contained formalism for describing the performance of microscopic Brownian heat engines like Carnot, Stirling and Otto engines modelled after a quantum harmonic oscillator in contact with a heat bath [quant-ph arXiv:1303.1233]. The appropriate combinations of isobaric, isochoric and isentropic steps involved in the three cycles considered here are achieved by controlling the 'spring constant' of the harmonic potential and the temperature of the heat bath. Our starting point is the master equation for describing the Brownian motion of a quantum harmonic oscillator obtained by Agarwal [Phys. Rev. A **4**, 739 (1971)]. This master equation can be cast into Langevin equations through the use of Wigner phase space description which in turn permit a convenient thermodynamic interpretation in a manner similar to that developed by Sekimoto [J. Phys. Soc. Jpn, **66**, 123 (1997)] in the classical context. The formalism developed here, besides reproducing the standard thermodynamics results in the steady state enables us to study the role dissipation plays in determining the efficiency of Brownian heat engines under actual laboratory conditions. In particular, we analyse in detail the dynamics associated with decoupling a system in equilibrium with one bath and recoupling it to another bath and obtain exact analytical results which are shown to have significant ramifications on the efficiencies of engines involving such a step. We also develop a simple yet powerful technique for computing corrections to the steady state results arising from finite operation time and use it to arrive at the thermodynamic complementarity relations for various operating conditions and also to compute the efficiencies at maximum power for the three engines cited above. Our principal results include (i) development of a self contained formalism for computing efficiencies of Brownian engines both in the classical as well as quantum contexts (ii) an exact analysis of the role of damping in the process of coupling the system to a bath at a higher temperature and its influence on the performance of the Stirling engine (iii) computation of the irreversible heat in isothermal processes and the derivation of complementarity relations (iv) a detailed analysis of the role of damping as well as finite time corrections on the efficiency of the Stirling engine at maximum power.

TYPICALITY APPROACH TO QUANTUM THERMODYNAMICS

J. Gemmer

University of Osnabrueck, Barbarastr.7, 49069 Osnabrueck, jgemmer@uos.de

ABSTRACT

Why do thermodynamical systems reach (more or less universal) final states that no longer exhibit any macroscopically visible evolution while the underlying microscopic equations of motion do not feature any attractive fixed points? The quantum typicality approach to thermodynamics is at present intensely debated. If Hilbert space is considered as the quantum analogue of phase space, any pure state is represented by a point which ventures eternally through this Hilbert space without coming to a halt. The apparent non-evolving equilibrium state of the macroscopic system is now explained by the following concept: Almost all states from some accessible region in Hilbert space may exhibit very similar properties such as expectation values of pertinent observables, probabilities to measure certain values, reduced density matrices corresponding to smaller parts of a larger system, etc. Thus as long as some concrete pure state ventures through regions in Hilbert space that are entirely filled with such typical states this motion will never be visible from considering only the above properties. Of course it is inherent to such a theory of thermalization that it cannot directly predict thermalizing dynamics of specific initial states as generated by specific Hamiltonians, it primarily addresses relative frequencies.

INTRODUCTION

Despite the fact that some call it a “tired old question” [1] the search for the origin and the true nature of the second law of thermodynamics has recently regained considerable impact. Although all researches are utterly used to the second law, the idea of almost any system always approaching a state (equilibrium) which is in accord with the concept of the system occupying an immense multitude of micro states at the same time (ensemble) is still quite puzzling. How can the system end up in a multitude of states given that there is conservation of phase space volume? And, even worse, always in the same well defined multitude? How can this be explained on the basis of an underlying theory? The traditional answers are of course well known: Some are based on the the microstate of the system wandering rapidly through all accessible phase space (ergodicity), others are based on the idea of the system occupying an initial multitude of states due to inevitable imperfections of measurements, that then effectively, in a coarse grained consideration, grows in time (mixing).

Although not really being new, lately the concept of “typicality” has also attracted some attention . The idea is that there are different, individual microstates each of which which leads for a set of observables to the same outcomes as if the system was in a multitude of states which form the ensemble. Furthermore these micro states are supposed to fill almost the entire accessible phase space such that, drawing states at random, they appear as being “typical”. Or, from a more dynamical point of view, a generic evolution will likely eventually lead to and proceed inside a region in phase space which is filled with the above mentioned typical states if this region is overwhelmingly large. This concept immediately raises some questions: For what class of observables can this concept hold at all? How can the overwhelming relative frequency of the above mentioned states be proven?

A number of publications [2; 3; 4; 5; 6; 7] aim at show-

ing that the typicality-principle applies to quantum physics in a quite general sense. Some of these papers consider a quantum system in contact with some quantum environment. Instead of considering one or a few observables the authors consider the reduced density matrix for the system which is tantamount to considering the set of all observables that may be locally defined for the system. These papers convincingly show that for a large majority of pure states drawn from an energy interval $E, E - \Delta E$ (of the full system) the reduced local density matrix assumes the same form as the one resulting from a microcanonical ensemble corresponding to the same interval. In the case of standard environment spectra and weak couplings this accounts for the typicality of the canonical equilibrium state. Other papers intend to avoid the system-environment partition as well as the restriction of the states onto energy intervals. They essentially analyze the (Hilbert space-) variance of a distribution of expectation values $\langle \psi | \hat{A} | \psi \rangle$ corresponding to a more general distribution of states ψ in Hilbert space. This way an upper bound to this variance based on the difference between the highest and the lowest eigenvalue of \hat{A} and the purity of the averaged density matrix is established.

In the paper at hand we consider both, the typicality of observables and of reduced states. The fashion according to which we “draw” our states from Hilbert space is neither just given by a restriction onto a projective subspace as in [2; 4; 3] nor is it defined by a rather general probability distribution as in [5]. Instead we consider a region in Hilbert space which is in accord with the system, occupying different projective (invariant) subspaces with different probabilities. We define these subspaces (labeled by α) by projectors

$$\hat{\Pi}_\alpha = \sum_i |\alpha, i\rangle \langle \alpha, i|, \quad W_\alpha = \langle \psi | \hat{\Pi}_\alpha | \psi \rangle \quad (1)$$

i.e. the probability to find the system in state ψ in some subspace α is W_α . The accessible region (AR) we are going to con-

sider may now be defined by a set of probabilities W_α . If and only if ψ is in accord with Eq. (1) it belongs to the AR. This choice of AR has primarily dynamical reasons: If the $\hat{\Pi}_\alpha$ correspond to natural invariants of the system (e.g. particle number, magnetization, etc.) the (pure) state of the system $\psi(t)$ can never leave the AR it started in. Of course subspaces that correspond to energy eigenstates are invariants of motion. However, if there is a small perturbation of strength ϵ , one can nevertheless expect subspaces spanned by the eigenstates of the unperturbed system corresponding to an energy interval $\Delta E > \epsilon$ to be approximately invariant. I.e. even the perturbed system will not substantially leave the AR defined on the basis of such subspaces.

TYPICALITY OF OBSERVABLES

In the following we are interested in the Hilbert Space Average (HA) of an expectation value of an arbitrary Hermitian operator \hat{A} (an observable) restricted to the above defined AR. The average is defined as a mean of the expectation value over all states of AR with respect to the unitary invariant measure (Haar measure), $[\langle \psi | \hat{A} | \psi \rangle]_{\text{AR}} = [\langle \hat{A} \rangle]_{\text{AR}}$. For details how to concretely compute such integrals see [6].

According to the partitioning in subspaces α the general operator \hat{A} can be decomposed in subspaces defined by the projection operators Eq. (1) finding

$$\hat{A} = \sum_{\alpha\beta} \hat{\Pi}_\alpha \hat{A} \hat{\Pi}_\beta =: \sum_{\alpha\beta} \hat{A}_{\alpha\beta}. \quad (2)$$

Using this decomposition the HA yields

$$\begin{aligned} [\langle \hat{A} \rangle]_{\text{AR}} &= \text{Tr}\{\hat{A} [\hat{\rho}_\psi]_{\text{AR}}\}, \quad \hat{\rho}_\psi \equiv |\psi\rangle\langle\psi| \\ [\hat{\rho}_\psi]_{\text{AR}} &\equiv \hat{\omega} = \sum_{\alpha} \frac{W_\alpha}{N_\alpha} \hat{\Pi}_\alpha \end{aligned} \quad (3)$$

where $N_\alpha := \text{Tr}\{\hat{\Pi}_\alpha\}$ is the dimension of the corresponding subspace. We have skipped some calculations and used some averages which can be found in [6]. Here $\hat{\omega}$ is simply the state that corresponds to the Boltzmann ‘‘a priori principle of equal weights’’, a state for which probability in each subspace W_α is uniformly distributed onto all states that span the subspace $\hat{\Pi}_\alpha$.

So far, however, this does not classify an $\langle \hat{A} \rangle$ in accord with the Boltzmann ensemble as being typical. To quantify this typicality, i.e., whether or not a concrete the expectation value of \hat{A} is most frequently close to the average, we furthermore introduce the Hilbert space variance (HV)

$$\Delta_{\text{H}}^2(\langle \hat{A} \rangle) := [(\langle \hat{A} \rangle)^2]_{\text{AR}} - [\langle \hat{A} \rangle]_{\text{AR}}^2. \quad (4)$$

Using again the decomposition given in Eq. (2), carefully calculating these HV’s using techniques described in [6] yields

$$\begin{aligned} \Delta_{\text{H}}^2(\langle \hat{A} \rangle) &= \sum_{\alpha\beta} \frac{W_\alpha W_\beta}{N_\alpha (N_\beta + \delta_{\alpha\beta})} \left(\text{Tr}\{\hat{A}_{\alpha\beta} \hat{A}_{\alpha\beta}^\dagger\} - \frac{\delta_{\alpha\beta}}{N_\alpha} \text{Tr}\{\hat{A}_{\alpha\alpha}\}^2 \right). \end{aligned} \quad (5)$$

This is a rigid result and may in principle be evaluated for any given AR, \hat{A} . Whenever it is small, the average result (3) can

be considered as being typical. For what scenarios can such typicality be expected? Specializing without substantial loss of generality to observables with $\text{Tr}\{\hat{A}\} = 0$ the variance of the spectrum of \hat{A} reads:

$$\Delta_{\text{S}}^2(\hat{A}) = \frac{1}{N} \sum_{\alpha\beta} \text{Tr}\{\hat{A}_{\alpha\beta} \hat{A}_{\alpha\beta}^\dagger\} \quad N \equiv \sum_{\alpha} N_\alpha \quad (6)$$

where N is simply the total dimension of the system. A HV is by construction positive, so are both terms that appear in the difference in (5) thus omitting the second of those will only make the outcome larger. Hence an upper bound to the HV written in a suggestive way reads:

$$\Delta_{\text{H}}^2(\langle \hat{A} \rangle) \leq \frac{1}{N^2} \sum_{\alpha\beta} \left(\frac{W_\alpha W_\beta}{n_{\alpha n\beta}} \right) \text{Tr}\{\hat{A}_{\alpha\beta} \hat{A}_{\alpha\beta}^\dagger\} \quad (7)$$

with $n_{\alpha(\beta)} \equiv N_{\alpha(\beta)}/N$. Thus, whenever the system occupies with significant probability only subspaces that are large enough to represent a substantial fraction of the full dimension of the system the HV is roughly by a factor N smaller than the variance of the spectrum. Thus, a result for $\langle \hat{A} \rangle$ as calculated from $\hat{\omega}$ classifies as typical for a wide range of accessible regions if \hat{A} has a bounded spectrum and is defined on a large-dimensional Hilbert space. This essentially reflects results by Reimann [5]

In which cases can this be expected? Consider as an instructive example the case of no restriction, i.e., the AR being all Hilbert space. One may be interested in a ‘‘local’’ variable \hat{A} which should really be written as $\hat{A} \otimes \hat{1}_E$, where $\hat{1}_E$ denotes the unit operator acting on the (for this inquiry irrelevant) rest of the system. If this rest of the system is enlarged N increases drastically while $\Delta_{\text{S}}^2(\hat{A})$ remains constant. Thus the corresponding HV will decrease according to Eq. (7). This means whenever a bounded local variable of interest is embedded in a large surrounding featuring a high dimensionality, typicality can be expected. Such a scenario is naturally implemented if a considered system is coupled to a large environmental system. One may then even observe a set of local variables which determine the reduced (local) state of the considered system completely, finding that they all relax to equilibrium due to all their HV’s being small. Such a scenario will be considered in more detail below. However, since the above reasoning does not require weak coupling, it also applies in principle to scenarios in which the system-environment partition in the traditional sense is absent. If one, e.g., considers a many particle system of some solid state type, one may be interested in the number of particles that can be expected in some spatial region of the system. The variance of the corresponding number operator surely remains unchanged if the whole system is increased (at constant particle density) but the dimension on which the number operator is defined increases exponentially. Thus a strongly typical occupation number will result from this scenario.

The same overall picture can be considered more or less appropriate even if there are restrictions to different subspaces $\hat{\Pi}_\alpha$. Thus, in very many scenarios and for many observables one finds small HV’s and in all those cases the typicality argument applies.

TYPICALITY OF STATES

Thus, measuring only one (or a few) observable(s) \hat{A} one is most likely not able to distinguish some ψ from the AR from $\hat{\omega}$.

However, measuring more and more observables on will eventually be able to determine the full, true quantum state of the system (ψ). Thus one may ask the question whether a true quantum state from the AR is typically close to the state that represents the ensemble, i.e., $\hat{\omega}$? To quantify this question we use as a measure for the “size” of an operator $D^2(\hat{O}) \equiv \text{Tr}\{\hat{O}\hat{O}^\dagger\}$ thus the distance between, two operators \hat{A}, \hat{B} is simply $D^2(\hat{A} - \hat{B})$. As the HV of $\langle \hat{A} \rangle$ is simply the HA over the squared distance between $\langle \hat{A} \rangle$ and $\text{Tr}\{\hat{A}\hat{\omega}\}$, we define

$$\Delta_H^2(\hat{\rho}_\psi) \equiv \llbracket D^2(\hat{\rho}_\psi - \hat{\omega}) \rrbracket_{\text{AR}} = \llbracket D^2(\hat{\rho}_\psi) \rrbracket_{\text{AR}} - D^2(\hat{\omega}) \quad (8)$$

For the situation discussed above this HV is easy to calculate since $D^2(\hat{\rho}_\psi)$ is simply the purity of $\hat{\rho}_\psi$. Since in this example the purity of $\hat{\rho}_\psi$ is always one, regardless of the actual ψ , we find: $\Delta_H^2(\hat{\rho}_\psi) = 1 - D^2(\hat{\omega})$. If the purity of $\hat{\omega}$ is low, which will be the case for most realistic scenarios, the HV will be close to one and thus not small at all. This means that regardless of $\text{Tr}\{\hat{A}\hat{\rho}_\psi\} \approx \text{Tr}\{\hat{A}\hat{\omega}\}$ for very many \hat{A} the states $\hat{\rho}_\psi$ from the HA are not close to $\hat{\omega}$, i.e., there is no typical state in the HA. This also obviously includes the purities or entropies (e.g. Von Neumann entropy) of states $\hat{\rho}_\psi$ from the HA being very different from the purity or entropy of $\hat{\omega}$.

In the following we analyze whether or not there is a typical state for a considered system which is in contact with some environment E . Here we require the pure state of the full system to be confined to some HA which is also defined in the full system. The considered state however is now a reduced state, i.e., $\hat{\rho}_\psi \equiv \text{Tr}_E\{|\psi\rangle\langle\psi|\}$. Its possibly typical outcome, i.e., its HA is

$$\llbracket \hat{\rho}_\psi \rrbracket = \text{Tr}_E\{\llbracket |\psi\rangle\langle\psi| \rrbracket\} = \text{Tr}_E\{\hat{\omega}\} \quad (9)$$

To analyze typicality in this case it is more convenient to write $\Delta_H^2(\hat{\rho}_\psi)$ in terms of matrix elements of $\hat{\rho}_\psi$, i.e., $\rho_\psi^{lm} := \langle l|\hat{\rho}_\psi|n\rangle$, where $|l\rangle, |n\rangle$ are energy eigenstates of the local system. Defining $X_{lm} \equiv \text{Re}(\rho_\psi^{lm})$ and $Y_{lm} \equiv \text{Im}(\rho_\psi^{lm})$, we straightforwardly find

$$\Delta_H^2(\hat{\rho}_\psi) = \sum_{lm} \Delta_H^2(X_{lm}) + \Delta_H^2(Y_{lm}) \quad (10)$$

The quantities X_{lm}, Y_{lm} may be expressed as expectation values of the corresponding (local) operators $\hat{X}_{lm}, \hat{Y}_{lm}$ with

$$\hat{X}_{lm} := \frac{1}{2}(|l\rangle\langle m| + |m\rangle\langle l|) \otimes \hat{1}, \quad (11)$$

$$\hat{Y}_{lm} := \frac{i}{2}(|l\rangle\langle m| - |m\rangle\langle l|) \otimes \hat{1} \quad (12)$$

Writing it this way we can use Eq. (7) to compute an upper bound to the HV as given by Eq. (10). Concentrating for simplicity on the case of the HA consisting of a restriction onto just one projective subspace, we may write, $\Delta_H^2(X_{lm}) \leq \Delta_S^2(\hat{X}_{lm})/N_\alpha$ and the corresponding for Y_{lm} . Since $\Delta_S^2(\hat{X}_{lm}), \Delta_S^2(\hat{Y}_{lm}) \leq 1/N_S$ (N_S being the dimension of the considered system) for all l, m we find plugging all this into Eq. (10)

$$\Delta_H^2(\hat{\rho}_\psi) \leq \frac{2N_S}{N_\alpha} \quad (13)$$

for this situation. Hence, whenever the dimension of the subspace onto which the full system is confined is much larger than

the dimension of the Hilbert space of the considered system, $\hat{\omega}$ will be the most likely, typical reduced state of the considered system for almost all pure states from the AR. In this case also the local entropies and purities of the $\hat{\rho}_\psi$'s are close to those of $\hat{\omega}$. In short: in this case there is a typical state. This essentially reflects the results by Popescu et. al. [7]

EIGENSTATE THERMALIZATION HYPOTHESIS AND TYPICALITY

So far everything stated above referred to the relative frequency of states featuring certain typical properties in Hilbert space. However, this does not imply directly anything rigorous on the dynamics, especially not on whether they may be classified as equilibrating, thermalizing, etc. Even though almost all of Hilbert space may be filled with typical states, concrete evolutions may never reach this giant region of typical states. Or depending on the initial state, some evolutions may do so while others may not. It is thus instructive to consider the link between typicality and concrete quantum dynamics. Let us start by considering a generic evolution of a quantum expectation value (QEV):

$$\langle \psi(t)|\hat{A}|\psi(t) \rangle = \sum_{mn} \psi_m^* \psi_n \langle m|\hat{A}|n \rangle \exp(-i(E_n - E_m)t) \quad (14)$$

with $|m\rangle, |n\rangle$ being energy eigenstates of the system corresponding to eigenvalues E_m, E_n and ψ_m, ψ_n being amplitudes of the initial wave function $|\psi(0)\rangle$ with respect to the energy eigenbasis. If the QEV reaches a more or less constant value at all after a (possibly very long) time, this value can only be the time average over an even longer time. Denoting this average (somewhat vaguely) as $\overline{\langle \psi(t)|\hat{A}|\psi(t) \rangle}$ and specializing to cases without degeneracy yields:

$$\overline{\langle \psi(t)|\hat{A}|\psi(t) \rangle} = \sum_n |\psi_n|^2 \langle n|\hat{A}|n \rangle \quad (15)$$

For a thermodynamical system one would expect the expectation value of a relevant variable to reach an equilibrium value that is independent of the details of the initial state, even though it may depend e.g., on the overall energy, etc. This equilibrium value would be given by the r.h.s. of Eq. (15) This, however, can only be independent of the initial state if $\langle n|\hat{A}|n \rangle$ does not (strongly) depend on n , at least not for energy eigenstates within a given energy region of a pertinent width. Such an independence has become popular under the name of “eigenstate thermalization hypothesis” [8; 9; 10]. But it may also be rephrased from the perspective of typicality: This approximate independence results if the energy eigenstates belong to the typical set. This in turn is to be expected in an unbiased guess. Simply because if the energy region is high-dimensional and the spectrum of \hat{A} is bounded, there are much more typical states than there are non-typical ones. This, however is only an unbiased guess. Whether or not it holds for a concrete Hamiltonian and a concrete observable within a concrete energy regime cannot be answered on the basis of typicality arguments.

DYNAMICAL TYPICALITY

So far we have been concerned with the question whether or not certain QEV's (or reduced states) will reach constant values

that are independent of the details of the initial states, possibly after a very long time. The experiences with non-equilibrium thermodynamics are, however, even more far reaching. Thermodynamical observables do not only reach final equilibrium values that are independent of the details of the initial states, but starting from the same non-equilibrium values, all evolutions, at any point in time, will be more or less the same irrespective of the details of the initial state. In the following we turn towards the question how this can be understood on the basis of typicality. More specifically we demonstrate that pure states from a set $\{|\phi\rangle\}$ featuring a common QEV of some observable \hat{A} at some time t , i.e. $\langle\phi|\hat{A}(t)|\phi\rangle = a$, most likely yield very similar QEV's at any later time, i.e. $\langle\phi|\hat{A}(t+\tau)|\phi\rangle \approx \langle\phi'|\hat{A}(t+\tau)|\phi'\rangle$ (with $|\phi\rangle, |\phi'\rangle$ both being states from the above set). We present some analytical derivations based on the above considerations, in particular on Eqs. (3 and 7) and we additionally support the results with numerical calculations. Finally, we discuss what consequences arise for the validity of projection operator methods (Nakajima-Zwanzig (NZ), etc. [12; 13; 14]) w.r.t. initial states and the corresponding inhomogeneities. Furthermore, we comment on the irreversibility of QEV's corresponding to individual pure states.

We specify our considered observable \hat{A} only by the moments, c_i of its spectrum ($c_i := \text{Tr}\{\hat{A}^i\}/n$, with n being the dimension of the relevant Hilbert space), and specialize without substantial loss of generality to observables which are trace-free, $c_1 = 0$, and normalized to $c_2 = 1$. Furthermore we require the c_i with $i = 2, \dots, 8$ to be of the order 1. Next, we introduce an ensemble of pure states $|\phi\rangle$ which is characterized as follows: All its states must feature the same QEV of the observable \hat{A} , $\langle\phi|\hat{A}|\phi\rangle = a$, must be normalized ($\langle\phi|\phi\rangle = 1$), and uniformly distributed otherwise. That means the ensemble has to stay invariant under all unitary transformations in Hilbert space that leave the expectation value of \hat{A} unchanged, i.e. those transformations that commute with \hat{A} , or, concretely, transformations of the form $e^{i\hat{B}}$, with $[\hat{B}, \hat{A}] = 0$. This specifies the most general ensemble consistent with the restriction that all its state should yield a given a .

For the following calculations we further introduce some kind of ‘‘substitute’’ ensemble $\{|\omega\rangle\}$, which is much easier to handle. As will be shown below, this ensemble approximates the exact ensemble $\{|\phi\rangle\}$ described above very well for large Hilbert spaces.

The ensemble $\{|\omega\rangle\}$ is generated by

$$|\omega\rangle = (1/\sqrt{1+d^2})(1+d\hat{A})|\psi\rangle, \quad (16)$$

where $|\psi\rangle$ are pure states drawn from a uniform distribution of normalized states without further restriction as described above Eq. (3). d is some small parameter which describes the deviation from the ‘‘equilibrium’’ ensemble $\{|\psi\rangle\}$. Since it is essentially the operator \hat{A} itself that generates $\{|\omega\rangle\}$ from the entirely uniform distribution, $\{|\omega\rangle\}$ is invariant under the above uniform transformations that leave a invariant.

The construction (16) allows for an evaluation of moments of the distribution of $\langle\omega|\hat{C}|\omega\rangle$ based on results on moments of the distribution of $\langle\psi|\hat{D}|\psi\rangle$, or concretely (for simplicity of notation we denote in the remainder of this paper Hilbert space averages

as $\text{HA}[\dots]$ and Hilbert space variances as $\text{HV}[\dots]$):

$$\begin{aligned} \text{HA}[\langle\omega|\hat{C}|\omega\rangle^i] &= \text{HA}[\langle\psi|\hat{D}|\psi\rangle^i] \\ \text{with } \hat{D} &= \frac{1}{1+d^2}(1+d\hat{A})\hat{C}(1+d\hat{A}). \end{aligned} \quad (17)$$

(Of course the average on the l.h.s. corresponds to the substitute ensemble $\{|\omega\rangle\}$ while the average on the r.h.s is based on the completely uniform ensemble $\{|\psi\rangle\}$). Exploiting this, average and variance of $\langle\omega|\hat{C}|\omega\rangle$ may be evaluated with the help of Eqs. (3,7).

To assure that the ensemble $\{|\omega\rangle\}$ indeed approximates the ensemble $\{|\phi\rangle\}$, in the limit of large n , we evaluate the following four quantities

$$\begin{aligned} \text{HA}[\langle\omega|\omega\rangle], & \quad \text{HA}[\langle\omega|\hat{A}|\omega\rangle], \\ \text{HV}[\langle\omega|\omega\rangle], & \quad \text{HV}[\langle\omega|\hat{A}(t)|\omega\rangle], \end{aligned} \quad (18)$$

where $\hat{A}(t)$ denotes the time dependence according to the Heisenberg picture. (For clarity: the results are given in Eqs. (19), (20), (21) and (23).)

The states $|\omega\rangle$ are not exactly normalized which would render them unphysical, of course. However, one finds from Eqs. (3) and (17) (by implementing $\hat{C} = \hat{1}$) that

$$\text{HA}[\langle\omega|\omega\rangle] = 1. \quad (19)$$

By exploiting Eq. (7) and Eq. (17) one finds analogously for the variance

$$\text{HV}[\langle\omega|\omega\rangle] = \frac{1}{n+1} \cdot \frac{4d^2 + 4d^3c_3 + d^4(c_4 - 1)}{(1+d^2)^2}. \quad (20)$$

As defined above, the c_i are of the order 1, i.e. the HV of the norms scales with $1/n$ and becomes small for large Hilbert spaces. Therefore, the vast majority of the states $|\omega\rangle$ are approximately normalized for large n .

The average of the QEV's of \hat{A} w.r.t. the ensemble $\{|\omega\rangle\}$ (which is meant to correspond to the above a) is calculated by exploiting Eq. (3) and Eq. (17) (by implementing $\hat{C} = \hat{A}$)

$$\text{HA}[\langle\omega|\hat{A}|\omega\rangle] = \frac{2d + d^2c_3}{1+d^2}. \quad (21)$$

That is, the mean QEV can be adjusted through the choice of the parameter d . However, the replacement ensemble is restricted on expectation values not too far away from zero (i.e. the average expectation value of the ‘‘equilibrium’’ ensemble $\{|\psi\rangle\}$) because by sweeping through all possible d not all possible expectation values up to the maximum eigenvalue of \hat{A} are reachable.

The evaluation of $\text{HV}[\langle\omega|\hat{A}(t)|\omega\rangle]$ turns out to be somewhat more complicated, since we, in general, cannot fully diagonalize the Hamiltonian and thus do not know $\hat{A}(t)$ in detail. However, we are able to perform an estimation for an upper bound. For this purpose we make use of the Hilbert Schmidt scalar product for complex matrices defined as $(\hat{X}, \hat{Y}) := \text{Tr}\{\hat{X}^\dagger \hat{Y}\}$.

Thus, one can formulate a Cauchy-Schwarz inequality of the form

$$\text{Tr}\{\hat{X}^\dagger \hat{Y}\} \leq \sqrt{\text{Tr}\{\hat{X}^\dagger \hat{X}\} \text{Tr}\{\hat{Y}^\dagger \hat{Y}\}}. \quad (22)$$

Particularly, one obtains $\text{Tr}\{\hat{A}(t)\hat{A}\} \leq \text{Tr}\{\hat{A}^2\}$. Evaluating $\text{HV}[\langle \omega | \hat{A}(t) | \omega \rangle]$ based on Eq. (7) and Eq. (17) (by implementing $\hat{C} = \hat{A}(t)$), realizing that $\text{Tr}\{\hat{D}\}^2$ is always positive and repeatedly applying the Cauchy-Schwarz inequality Eq. (22) yields the inequality

$$\text{HV}[\langle \omega | \hat{A}(t) | \omega \rangle] \leq \frac{1}{n+1} \cdot \frac{1 + 4d\sqrt{c_4} + 6d^2c_4 + 4d^3\sqrt{c_4}\sqrt[4]{c_4c_8} + d^4\sqrt{c_4c_8}}{(1+d^2)^2}. \quad (23)$$

Again, since the c_i are of the order 1, the upper bound decreases as $1/n$. Thus, the variance Eq. (23) becomes small for large Hilbert spaces, just like the variance of the norms Eq. (20). This result yields two major direct implications.

First, if one evaluates (23) at $t = 0$, one finds that the majority of the states $|\omega\rangle$ feature approximately the same QEV of the observable \hat{A} for large n . From this property together with the result that the states $|\omega\rangle$ are nearly normalized one concludes that the replacement ensemble $\{|\omega\rangle\}$ indeed approximates the exact ensemble $\{|\phi\rangle\}$ very well for large Hilbert spaces (with $a = \text{HA}[\langle \omega | \hat{A} | \omega \rangle]$ as given in Eq. (21)).

Second, the upper bound from Eq. (23) is valid for any time t . Thus, for large enough systems, the dynamical curves for $a_\omega(t) := \langle \omega | \hat{A}(t) | \omega \rangle$ of the vast majority of pure states from the initial ensemble $\{|\omega\rangle\}$ are very close to each other and thus to the evolving ensemble average at any time t . Due to the similarity of $\{|\omega\rangle\}$ and $\{|\phi\rangle\}$ this should also hold true for the “exact” ensemble $\{|\phi\rangle\}$. Thus, there is a typical evolution for the expectation values $\langle \phi | \hat{A}(t) | \phi \rangle$ or, to rephrase, there is “dynamical typicality”. This statement represents the main result of this paper. Particularly, this typicality is independent of the concrete form of the dynamics, which may be a standard exponential decay into equilibrium or something completely different. For more details on and a numerical demonstration of dynamical typicality see [11]

The mean QEV, i.e., essentially a , can alternatively be reformulated using the notion of a density matrix as usually done in the framework of projection operator formalisms

$$a = \text{HA}[\langle \omega | \hat{A} | \omega \rangle] = \text{HA}[\text{Tr}\{\hat{A}|\omega\rangle\langle\omega|\}] = \text{Tr}\{\hat{A} \text{HA}[|\omega\rangle\langle\omega|]\}. \quad (24)$$

The $\text{HA}[|\omega\rangle\langle\omega|]$ takes the role of the density matrix. Further evaluation gives (using the “substitute” ensemble $\{|\omega\rangle\}$) (see [6])

$$\text{HA}[|\omega\rangle\langle\omega|] = \frac{1 + 2d\hat{A} + d^2\hat{A}^2}{n(1+d^2)}. \quad (25)$$

For ensembles close to equilibrium, i.e., small d , which is fulfilled in the examples presented here, one can neglect the terms which grow quadratically in d . In this case, the density matrix takes approximately the same form as the initial state which is often used in projection operator calculations which aim at determining the dynamics of expectation values like $a(t)$ ([15]).

There, for reasons given below, the (mixed) initial state is simply taken to be $\rho(0) = 1/n + c\hat{A}$ such that $c = a(0)$. That means, correct dynamical results from the projection operator methods based on the above initial state describe the dynamics of the ensemble average of $\{|\omega\rangle\}$.

From this point of view some consequences on the applicability of projection operator theories (NZ, time-convolutionless, Mori formalism etc.), which are standard tools for the description of reduced dynamics, arise. These methods have in common the occurrence of an inhomogeneity in the central equations of motion that typically has to be neglected in order to solve them. Generally, the inhomogeneity depends on the true initial state, it, however, vanishes if the true initial state indeed is of some specific form determined by the pertinent projector [13; 16; 14]. For the above mentioned case the above $\hat{\rho}(0)$ is exactly of that form, which means the dynamics of the ensemble are equal to the dynamics generated by the pertinent projected equation of motion without the inhomogeneity. However, the evolution of the ensemble is typical, this implies that the inhomogeneity, as generated by most of the true initial states, should be negligible.

On the other hand, there are investigations in the field of open quantum systems, e.g., [17] and [18], suggesting that the true initial states may have an utterly crucial influence on the dynamics, such that, e.g., some correlated initial states may yield projected dynamics which are entirely different from the ones obtained by corresponding product states.

Nevertheless, to rephrase, the results of this paper indicate that in the limit of large (high dimensional) systems the inhomogeneity should become more and more irrelevant in the sense that the statistical weight of initial states, which yield an inhomogeneity that substantially changes the solution of the projected equation of motion, should decrease to zero. Note that this does not contradict the concrete results of [17] and [18].

The above results also shed some light on the relation of the apparently irreversible dynamics of QEV’s to the, in some sense, reversible dynamics of the underlying Schrödinger equation. If a mean QEV as generated by some initial non-equilibrium ensemble (pertinent density matrix) relaxes to equilibrium (which can often be reliably shown [13]), then for the majority of the individual states that form the ensemble, the corresponding individual QEV’s will relax to equilibrium in the same way. Thus, for the relaxation of the QEV’s, the question whether or not the initial ensemble truly exists is largely irrelevant. Of course, there may be individual initial states giving rise to QEV evolutions that do not (directly) relax to equilibrium, but, to repeat, for high dimensional systems, their statistical weight is low.

ACKNOWLEDGMENT

J. Gemmer thanks C. Bartsch, M. Michel, S. Goldstein, R. Tumulka, and J. Lebowitz for fruitful discussions and collaborations on this subject

REFERENCES

- [1] C. H. Bennett, stament at the symposium “Meeting the Entropy Challenge” held at the MIT, 2007.
- [2] S. Goldstein, J. L. Lebowitz, R. Tumulka and N. Zanghi, *Eur. Phys. J. H* vol. 35, pp. 173, 2010
- [3] E. Lubkin, *J. Math. Phys.* vol. 19, pp. 1028-1031, 1978
- [4] S. Goldstein, J. L. Lebowitz, R. Tumulka and N. Zanghi,

- Phys. Rev. Lett* vol. 96, pp. 050403, 2006
- [5] P. Reimann, *J. Math. Phys.* vol. 19, pp. 1028-1031, 1978
- [6] J. Gemmer, M. Michel and G. Mahler, *Quantum Thermodynamics* LNP 784, Springer, Berlin, 2009
- [7] S. Popescu, A. J. Short and A. Winter, *Nature Physics* vol. 2, 758, 2006
- [8] J. M. Deutsch, *Phys. Rev. A* vol. 43, pp. 2046, 1991
- [9] M. Srednicki, *Phys. Rev. E* vol. 50, pp. 888, 1994
- [10] M. Rigol, V. Dunjiko and M. Olshanii, *Nature* vol. 452, pp. 854, 2008
- [11] C. Bartsch and J. Gemmer, *Phys. Rev. Lett* vol. 102, pp. 110403, 2009
- [12] H. P. Breuer, J. Gemmer and M. Michel, *Phys. Rev. E* vol. 73, pp. 016139, 2006
- [13] H. P. Breuer and F. Petruccione, *Theory of Open Quantum Systems* Oxford University Press, Oxford, 2007
- [14] E. Fick and G. Sauermaun, *The Quantum Statistics of Dynamic Processes* Springer, Berlin, 1990
- [15] C. Bartsch, R. Steinigeweg and J. Gemmer, *Phys. Rev. E* vol. 77, pp. 011119, 2008
- [16] U. Weiss, *Dissipative Quantum Systems* World Scientific, Singapore, 1999
- [17] P. Pechukas, *Phys. Rev. Lett* vol. 73, pp. 1060, 1994
- [18] K. M. F. Romero, P. Talkner and P. Haenggi, *Phys. Rev. A* vol. 69, pp. 052109, 2004

QUANTUM REFRIGERATORS AND THE III-LAW OF THERMODYNAMICS

Ronnie Kosloff* and Amikam Levi

*Institute of Chemistry, The Hebrew University, Jerusalem 91904 Israel, E-mail: ronnie@afh.huji.ac.il

ABSTRACT

Quantum thermodynamics addresses the emergence of thermodynamical laws from quantum mechanics. The III-law of thermodynamics has been mostly ignored. There are seemingly two independent formulations of the third law of thermodynamics, both originally stated by Nernst. The first is known as Nernst heat theorem, which is purely static, and implies that the entropy flow from any substance at the absolute zero is zero. And the second formulation known as the unattainability principle practically states that no refrigerator can cool a system to absolute zero at finite time. We explore the dynamic version which is the vanishing of rate of temperature decrease of a cooled quantum bath when $T \rightarrow 0$. The III-law is then quantified dynamically by evaluating the characteristic exponent ξ of the cooling process:

$$\frac{dT(t)}{dt} \propto -T^\xi$$

when approaching absolute zero, $T \rightarrow 0$. A generic continuous model of a quantum refrigerator is presented. The refrigerator is a nonlinear device merging three currents from three heat baths: a cold bath to be cooled, a hot bath as an entropy sink, and a driving bath which is the source of cooling power. A heat-driven refrigerator (absorption refrigerator) is compared to a power-driven refrigerator. Similar results are obtained from reciprocating Otto refrigerators. When optimized, all cases lead to the same exponent ξ , showing a lack of dependence on the form of the working medium and the characteristics of the drivers. The characteristic exponent is therefore determined by the properties of the cold reservoir and its interaction with the system. Two generic heat bath models are considered: a bath composed of harmonic oscillators and a bath composed of ideal Bose/Fermi gas. The restrictions on the interaction Hamiltonian imposed by the third law which are discussed.

INTRODUCTION

Quantum thermodynamics is the study of thermodynamical processes within the context of quantum dynamics. Thermodynamics preceded quantum mechanics, consistency with thermodynamics led to Planck's law, the dawn of quantum theory. Incorporating the ideas of Planck on black body radiation, Einstein (1905), quantised the electromagnetic field [1]. *Quantum thermodynamics* is devoted to unraveling the intimate connection between the laws of thermodynamics and their quantum origin requiring consistency. For many decades the two theories developed separately. Scovil [2; 3; 4] pioneered the study of quantum engines and quantum refrigerators showing the equivalence of the Carnot engine [5] with the three level Maser.

With the establishment of quantum theory the emergence of thermodynamics from quantum mechanics becomes a key issue. The two theories address the same subject from different viewpoints. This requires a consistent view of the state and dynamics of matter. Despite its name, dynamics is absent from most thermodynamic descriptions. The standard theory concentrates on systems close to equilibrium. We advocate a dynamical perspective on quantum thermodynamics [6] and in particular its implication on the III-law of thermodynamics. I will emphasize *learning by example* analyzing quantum refrigerators to unravel the III-law.

Quantum mechanics has been used to reintroduce dynamical processes into thermodynamics. In particular, the theory of quantum open systems supplies the framework to separate the system from its environment. The Markovian master equation pioneered by Lindblad and Gorini-Kossakowski-Sudarshan

(LGKS generator) [7; 8] is one of the key elements of the theory of quantum thermodynamics [9; 10]. The dynamical framework allows to reinterpret and justify the theory of finite time thermodynamics [11; 12; 13] which addresses thermodynamical processes taking place in finite time.

Two major classes of refrigerators will serve to illustrate the III-law, continuous and reciprocating. These classes can be examined up to the level of a single quantum device. The prime example of a continuous quantum refrigerator is laser cooling. In this case light is used to power the refrigerator. The device can be understood as reversing the operation of a 3-level laser [4; 14; 15; 16; 17; 18; 19; 20; 21; 22; 23; 24; 25; 26; 27]. An important addition is a quantum absorption refrigerator which is a refrigerator with heat as its power source [28; 29; 19; 30]. An example could be a refrigerator driven by sunlight [31]. Amazingly, in all these examples a thermodynamical description is appropriate up to the level of a single open quantum system [10; 32; 33; 34].

The minimum requirement for constructing a continuous refrigerator is a system connected simultaneously to three reservoirs [12]. These baths are termed hot, cold and work reservoir as described in Fig. 1.

This framework has to be translated to a quantum description of its components which include the Hamiltonian of the system \hat{H}_s and the implicit description of the reservoirs. Different designs of refrigerators are reflected in the Hamiltonian of the working medium.

Reciprocating refrigerators operate by a working medium shuttling heat from the cold to the hot reservoir. The task is carried out by a controlled dynamical system. A change in the

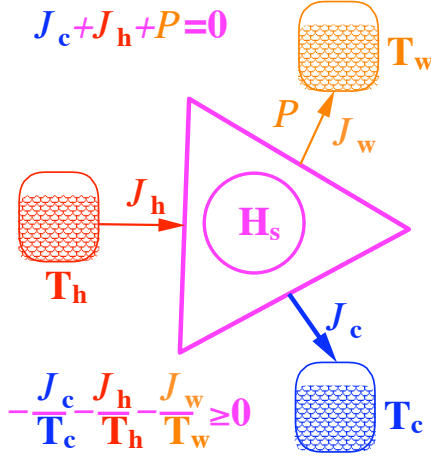


Figure 1. A quantum heat pump designated by the Hamiltonian \hat{H}_s coupled to a work reservoir with temperature T_w , a hot reservoir with temperature T_h and a cold reservoir with temperature T_c . The heat and work currents are indicated. In steady state $J_h + J_c + P = 0$ and the entropy production $\frac{J_h}{T_h} + \frac{J_c}{T_c} + \frac{J_w}{T_w} \geq 0$.

Hamiltonian of the system is accompanied by a change in the internal temperature. Upon contact with the cold side the temperature of the working medium is forced to be lower than T_c -the cold bath temperature. In a quantum reciprocating refrigerator the control of temperature is governed by manipulating the energy levels of the system through external perturbation [35; 36; 37].

The adiabatic condition is an important idealisation in thermodynamics. In quantum thermodynamics there is a close connection to the quantum adiabatic condition. When the adiabatic conditions are not fulfilled, additional work is required to reach the final control value. For an isolated system this work is recoverable since the dynamics are unitary and can be reversed. The coherences stored in the off-diagonal elements of the density operator carry the required information to recover the extra energy cost and reverse the dynamics. Typically, this energy is not recoverable due to interaction with a bath that causes energy dephasing. This lost energy is the quantum version of friction [38; 39; 40].

There are several strategies to minimise the effect of quantum friction. One possibility, termed *quantum lubrication*, is to force the state of the system to commute with the instantaneous Hamiltonian $[\hat{\rho}(t), \hat{H}(t)] = 0$. This can be achieved by adding an external source of phase noise [41]. In the case of quantum refrigerators this noise was always harmful leading to a minimum temperature the refrigerator can reach [37; 42].

Is it possible to find non-adiabatic control solutions with an initial and final state diagonal in the energy representation $[\hat{\rho}_i, \hat{H}(0)] = 0$, $[\hat{\rho}_f, \hat{H}(t_f)] = 0$? This possibility, which relies on special dynamical symmetries, has been termed *shortcut to adiabaticity* [43; 44; 45; 46; 36; 47; 48]. The idea is to optimise the scheduling function $f(t)$ of the control $\hat{H}_C(t) = \hat{V}_C f(t)$ in such a way that in the shortest time the frictionless transformation from an initial value of the control function to a final value is achieved. Refrigerators which are able to approach $T_c \rightarrow 0$ are frictionless.

Eventually all refrigerators converge to a universal behaviour where the heat conductivity with the cold bath and the heat capacity of the cold bath determine the III-law characteristics.

THE QUANTUM TRICYCLE

A quantum description enables to incorporate dynamics into thermodynamics. The tricycle model is the template for almost all continuous engines and refrigerators. The tricycle engine has a generic structure displayed in Fig. 1.

The basic model consists of three thermal baths: a hot bath with temperature T_h , a cold bath with temperature T_c and a work bath with temperature T_w .

Each bath is connected to the engine via a frequency filter which we will model by three oscillators:

$$\hat{H}_F = \hbar\omega_h \hat{a}^\dagger \hat{a} + \hbar\omega_c \hat{b}^\dagger \hat{b} + \hbar\omega_w \hat{c}^\dagger \hat{c}, \quad (1)$$

where ω_h , ω_c and ω_w are the filter frequencies on resonance $\omega_w = \omega_h - \omega_c$.

The device operates as an engine by removing an excitation from the hot bath and generating excitations on the cold and work reservoirs. In second quantization the hamiltonian describing such an interaction becomes:

$$\hat{H}_I = \epsilon \left(\hat{a}^\dagger \hat{c}^\dagger + \hat{a} \hat{b} \hat{c} \right), \quad (2)$$

where ϵ is the coupling strength.

The device operates as a refrigerator by removing an excitation from the cold bath and from the work bath and generating an excitation in the hot bath. The r.h.s of the Hamiltonian of Eq. (2) describes this action.

The frequency filters select from the continuous spectrum of the bath the working component to be employed in the tricycle. These frequency filters can be constructed also from two-level-systems (TLS) or formulated as qubits [32]. Finally, the interaction term is strictly non-linear incorporating three heat currents simultaneously. This crucial fact has important consequences. A linear device cannot operate as a heat engine or refrigerator [49].

The I-law of thermodynamics is the energy balance of heat currents originating from the three baths and collimating on the system [50; 9]:

$$\frac{dE_s}{dt} = J_h + J_c + J_w. \quad (3)$$

At steady state no heat is accumulated in the tricycle thus $\frac{dE_s}{dt} = 0$. In addition entropy is only generated in the baths leading to the II-law of thermodynamics:

$$\frac{d}{dt} \Delta S_u = \frac{J_h}{T_h} + \frac{J_c}{T_c} + \frac{J_w}{T_w} \geq 0. \quad (4)$$

When the temperature $T_w \rightarrow \infty$ no entropy is generated in the power bath. An energy current with no accompanying entropy production is equivalent to producing pure power: $P = J_w$ where P is the output power.

A reduced description for the dynamical equations of motion of tricycle are set within the formalism of quantum open system:

$$\frac{d}{dt} \hat{\rho}_s = \mathcal{L} \hat{\rho}_s \quad (5)$$

where $\hat{\rho}_s$ is the density operator of the tricycle \mathcal{L} is the Liouville superoperator. Under Markovian conditions \mathcal{L} takes the form of the Gorini-Kossakowski-Sudarshan-Lindblad (GKS-L) generator [7; 8]. We chose to present the generator in Heisenberg form for the system operator \hat{O}

$$\frac{d}{dt}\hat{O} = \mathcal{L}^*(\hat{O}) = \frac{i}{\hbar}[\hat{H}_s, \hat{O}] + \sum_k \hat{V}_k \hat{O} \hat{V}_k^\dagger - \frac{1}{2} \{ \hat{V}_k \hat{V}_k^\dagger, \hat{O} \} \quad (6)$$

Where the operators \hat{V}_k are system operators still to be determined. The task of evaluating the modified system Hamiltonian \hat{H}_s and the operators \hat{V}_k is made extremely difficult due to the nonlinear interaction in Eq. (2). Any progress from this point requires a specific description of the heat baths and approximations to deal with the nonlinear terms.

The noise driven absorption refrigerator

The absorption refrigerator is the most simple example of a device able to cool up to the absolute zero. Other devices such as power driven refrigerators lead to very similar results. In the absorption refrigerator the noise is the source of power driving the refrigerator replacing Eq. (2) with:

$$\hat{H}_I = f(t) (\hat{a}^\dagger \hat{b} + \hat{a} \hat{b}^\dagger) = f(t) \hat{X}, \quad (7)$$

where $f(t)$ is the noise field. $\hat{X} = (\hat{a}^\dagger \hat{b} + \hat{a} \hat{b}^\dagger)$ is the generator of a swap operation between the two oscillators. In addition \hat{X} is part of a closed set of $SU(2)$ operators, $\hat{Y} = i(\hat{a}^\dagger \hat{b} - \hat{a} \hat{b}^\dagger)$, $\hat{Z} = (\hat{a}^\dagger \hat{a} - \hat{b}^\dagger \hat{b})$ and the Casimir $\hat{N} = (\hat{a}^\dagger \hat{a} + \hat{b}^\dagger \hat{b})$.

The Heisenberg equation for tricycle operators \hat{O} reduced to:

$$\frac{d}{dt}\hat{O} = i[\hat{H}_s, \hat{O}] + \mathcal{L}_n(\hat{O}) + \mathcal{L}_h(\hat{O}) + \mathcal{L}_c(\hat{O}), \quad (8)$$

where $\hat{H}_s = \hbar\omega_h \hat{a}^\dagger \hat{a} + \hbar\omega_c \hat{b}^\dagger \hat{b}$. For a Gaussian source of white noise characterised by zero mean $\langle f(t) \rangle = 0$ and delta time correlation $\langle f(t)f(t') \rangle = 2\eta\delta(t-t')$. The noise dissipator becomes $\mathcal{L}_n(\hat{O}) = -\eta[\hat{X}, [\hat{X}, \hat{O}]]$ [51].

The generators \mathcal{L}_h and \mathcal{L}_c become the standard energy relaxation terms driving oscillator $\omega_h \hat{a}^\dagger \hat{a}$ to thermal equilibrium with temperature T_h and \mathcal{L}_c drives oscillator $\hbar\omega_c \hat{b}^\dagger \hat{b}$ to equilibrium T_c [52].

$$\begin{aligned} \mathcal{L}_h(\hat{O}) &= \Gamma_h(N_h + 1) \left(\hat{a}^\dagger \hat{O} \hat{a} - \frac{1}{2} \{ \hat{a}^\dagger \hat{a}, \hat{O} \} \right) \\ &\quad + \Gamma_h N_h \left(\hat{a} \hat{O} \hat{a}^\dagger - \frac{1}{2} \{ \hat{a} \hat{a}^\dagger, \hat{O} \} \right) \\ \mathcal{L}_c(\hat{O}) &= \Gamma_c(N_c + 1) \left(\hat{b}^\dagger \hat{O} \hat{b} - \frac{1}{2} \{ \hat{b}^\dagger \hat{b}, \hat{O} \} \right) \\ &\quad + \Gamma_c N_c \left(\hat{b} \hat{O} \hat{b}^\dagger - \frac{1}{2} \{ \hat{b} \hat{b}^\dagger, \hat{O} \} \right) \end{aligned} \quad (9)$$

In the absence of the stochastic driving field these equations drive oscillator a and b separately to thermal equilibrium provided that $N_h = (\exp(\frac{\hbar\omega_h}{kT_h}) - 1)^{-1}$ and $N_c = (\exp(\frac{\hbar\omega_c}{kT_c}) - 1)^{-1}$. The kinetic coefficients $\Gamma_{h/c}$ are determined from the system bath coupling and the spectral function [14].

The absorption refrigerator can also be powered by a high temperature source. At the high temperature limit of the work

bath $T_w \rightarrow \infty$ the nonlinearity of Eq. (2) can be simplified. The generator of dissipation of the work bath becomes:

$$\begin{aligned} \mathcal{L}_w(\hat{O}) &= \Gamma_w(N_w + 1) \left(\hat{a}^\dagger \hat{b} \hat{O} \hat{b}^\dagger \hat{a} - \frac{1}{2} \{ \hat{a}^\dagger \hat{a} \hat{b} \hat{b}^\dagger, \hat{O} \} \right) \\ &\quad + \Gamma_w N_w \left(\hat{a} \hat{b}^\dagger \hat{O} \hat{a}^\dagger \hat{b} - \frac{1}{2} \{ \hat{a} \hat{a}^\dagger \hat{b}^\dagger \hat{b}, \hat{O} \} \right) \end{aligned} \quad (10)$$

where $N_w = (\exp(\frac{\hbar\omega_w}{kT_h}) - 1)^{-1}$. At finite temperature $\mathcal{L}_w(\hat{O})$ does not lead to a close set of equations. But in the limit of $T_w \rightarrow \infty$ it becomes equivalent to the Gaussian noise generator: $\mathcal{L}_w(\hat{O}) = -\eta/2 ([\hat{X}, [\hat{X}, \hat{O}]] + [\hat{Y}, [\hat{Y}, \hat{O}]])$, where $\eta = \Gamma_w N_w$.

The equations of motion in both case are closed to the $SU(2)$ set of operators. The cooling current $\mathcal{J}_c = \langle \mathcal{L}_c(\hbar\omega_c \hat{b}^\dagger \hat{b}) \rangle$, is solved for stationary conditions for \hat{N} and \hat{Z} .

Optimal cooling power is obtained for balanced heat conductivity $\Gamma_h = \Gamma_c \equiv \Gamma$, then:

$$\mathcal{J}_c = \hbar\omega_c \frac{2\eta\Gamma(N_c - N_h)}{\Gamma + 4\eta}. \quad (11)$$

Cooling occurs for $N_c > N_h \Rightarrow \frac{\omega_h}{T_h} > \frac{\omega_c}{T_c}$ which is the Carnot condition. The coefficient of performance (COP) for the absorption chiller is defined by the relation $COP = \frac{\mathcal{J}_c}{\mathcal{J}_n}$, with the help of Eq. (11) we obtain the Otto cycle COP [53]:

$$COP = \frac{\omega_c}{\omega_h - \omega_c} \leq \frac{T_c}{T_h - T_c}. \quad (12)$$

Optimizing the cooling current \mathcal{J}_c Eq. (11) first with respect to the gain $G = N_h - N_c$ leads to $\omega_c \propto T_c$. Then optimizing the power input leads to $\mathcal{J}_c \propto \hbar\omega_c \Gamma$. This means that the cooling rate as $T_c \rightarrow 0$ depends on the characteristics of the heat conductivity as the filter frequency $\omega_c \rightarrow 0$. Other continuous driven refrigerators show the same phenomena [20].

RECIPROCATING REFRIGERATORS

The quantum reciprocating refrigerator employs a working medium to shuttle heat from the cold to the hot reservoir. This requires a Hamiltonian that can be controlled externally changing the energy level structure. Typically the external control influences only part of the Hamiltonian operator::

$$\hat{H} = \hat{H}_{int} + \hat{H}_{ext}(\omega) \quad (13)$$

where $\omega = \omega(t)$ is the time dependent external control field. Generically, the internal and external parts do not commute $[\hat{H}_{int}, \hat{H}_{ext}] \neq 0$. This has a profound effect on the adiabatic segments of the refrigerator since then $[\hat{H}(t), \hat{H}(t')] \neq 0$. A state which was initially prepared to be diagonal in the temporary energy eigenstates, cannot follow adiabatically the changes in energy levels induced by the control. The result is an additional power required to execute the adiabatic segment termed quantum friction [38]. This friction has been found to limit the performance of the heat engines [39; 54; 41; 40]. In quantum refrigerators the frictional heating in the expansion-demagnetization segment limits the minimal temperature of the working medium. This in turn puts a restriction on the minimum temperature that can be achieved. This means that a refrigerator that can reach the absolute zero has to be frictionless.

One obvious solution to a frictionless operation is perfect adiabatic following i.e. at each time the system is diagonal in the temporary energy eigenstates. The drawback of such an approach is that it requires ever increasing time to execute this move when the temperature approaches $T_c = 0$. The question then arises what is the minimum time required to execute an adiabatic move.

Demanding that only at the initial and final time the system is diagonal in the energy representation leads to additional opportunities for frictionless solutions. For a working medium consisting of harmonic oscillators such solutions have been found [46; 36; 48] which are characterized by a fast finite expansion time. If negative frequencies are permissible this time can be reduced further [43]. For these models where the energy gap can be controlled to follow the cold bath temperature T_c , the absolute zero seems attainable.

THE QUANTUM OTTO HEAT PUMP

The Otto model is a solvable example of a reciprocating refrigerator. The objective is to optimize the cooling rate in the limit when the temperature T_c of the cold bath approaches absolute zero. A necessary condition for operation is that upon contact with the cold bath the temperature of the working medium be lower than the bath temperature $T_{int} \leq T_c$ [55]. The opposite condition exists on the hot bath. To fulfil these requirements the external controls modify the internal temperature by changing the energy level spacings of the working fluid. The control field varies between two extreme values ω_c and ω_h , where ω is a working medium frequency induced by the external field. The working medium consists of an ensemble of non interacting particles in a harmonic potential. The Hamiltonian of this system, $\hat{H} = \frac{1}{2m}\hat{P}^2 + \frac{K(t)}{2}\hat{Q}^2$, is controlled by changing the curvature $K = m\omega^2$ of the confining potential.

The cooling cycle consists of two heat exchange branches alternating with two adiabatic branches. The heat exchange branches (the *isochores*) take place with $\omega = \text{constant}$, while the adiabatic branches take place with the working medium decoupled from the baths. This is reminiscent of the Otto cycle in which heat is transferred to the working medium from the hot and cold baths under constant volume conditions.

The heat carrying capacity of the working medium limits the amount of heat Q_c which can be extracted from the cold bath. Under the quantum adiabatic condition. This means also $n_D \geq n_h^{eq}$, leading to $Q_c \leq \hbar\omega_c (n_c^{eq} - n_h^{eq})$. Maximum Q_c is obtained for high frequency $\hbar\omega_h \gg k_B T_h$, leading to $n_h^{eq} = 0$ and $E_A = \frac{1}{2}\hbar\omega_h$ being the ground state energy. Then for $T_c \rightarrow 0$:

$$Q_c^* = \hbar\omega_c n_c^{eq} = \hbar\omega_c e^{-\frac{\hbar\omega_c}{k_B T_c}} \leq k_B T_c \quad (14)$$

where we have substituted the value of n_c^{eq} obtained from the partition function and the last inequality is obtained by optimizing with respect to ω_c leading to $\hbar\omega_c^* = k_B T_c$. The general result is that as $T_c \rightarrow 0$, Q_c^* and ω_c^* become linear in T_c .

Only a finite cycle period τ leads to a non vanishing cooling power $\mathcal{R}_c = Q_c/\tau$. This cycle time $\tau = \tau_{hc} + \tau_c + \tau_{ch} + \tau_h$ is the sum of the times allocated to each branch. An upper bound on the cooling rate \mathcal{R}_c is required to limit the exponent as $T_c \rightarrow 0$. The optimal cooling rate \mathcal{R}_c^{opt} depends on the time allocation on the different branches.

Optimization of the cooling rate

For sufficiently low T_c , the rate limiting branch of the cycle is cooling the working medium to a temperature below T_c along the expansion *adiabat*. As $T_c \rightarrow 0$, the total cycle time τ is of the order of the time of this cooling adiabat, τ_{hc} , which tends to infinity.

Quantum friction is completely eliminated if the *adiabat* proceeds quasistatically with $\mu \ll 1$. This leads to a scaling law $\mathcal{R}_c \propto T_c^\delta$ with $\delta \geq 3$. It turns out however that it is not the only frictionless way to reach the final state at energy $E_D = (\omega_c/\omega_h)E_A$. Other possibilities which require less time and result in improved scaling, $\delta = 2$ and $\delta = 3/2$ $\delta \sim 1$ have been worked out.

All frictionless solutions lead to an upper bound on the optimal cooling rate of the form:

$$\mathcal{R}_c \leq A\omega^\nu n_c^{eq} \quad (15)$$

where A is a constant and the exponent ν is either $\nu = 2$ for the $\mu = \text{const}$ solution or $\nu = \frac{3}{2}$ for the three-jump solution of attractive potentials [36] and $\nu \sim 1$ for repulsive potentials [47]. Optimizing \mathcal{R}_c with respect to ω_c leads to a linear relation between ω_c and T_c ,

At high compression ratio $\omega_h \gg \omega_c$ and if in addition $\omega_c \ll \Gamma$ we obtain:

$$\mathcal{R}_c^* \approx \hbar\omega_c^2 n_c^{eq} \quad (16)$$

for the $\mu = \text{const}$ frictionless solution. For the three-jump frictionless solution if one restricts to attractive traps:

$$\mathcal{R}_c^* \approx \frac{1}{2}\hbar\omega_c^{\frac{3}{2}}\sqrt{\omega_h}n_c^{eq}, \quad (17)$$

and for repulsive traps [47]:

$$\mathcal{R}_c^* \approx \frac{1}{2}\hbar\omega_c \log \omega_c \sqrt{\omega_h}n_c^{eq}, \quad (18)$$

Due to the linear relation between ω_c and T_c , Eq. (16) and (17) the exponent δ where $\delta = 3$ for the quasistatic scheduling, $\delta = 2$ for the constant μ frictionless scheduling and $\delta = \frac{3}{2}$, $\delta \sim 1$ for the three-jump frictionless scheduling.

Once optimising the time allocated for the adiabatic expansion it becomes clear that the heat transport branch will become eventually the time limiting step. This means that as $T_c \rightarrow 0$ the reciprocating and the continuous refrigerator will both be limited by the heat transport rate Γ_c .

THE III-LAW

The third law of thermodynamics was initiated by Nernst [56; 57; 58]. Nernst formulated two independent statements. The first is a purely static (equilibrium) one, also known as the "Nernst heat theorem": phrased:

The entropy of any pure substance in thermodynamic equilibrium approaches zero as the temperature approaches zero.

The second formulation is dynamical, known as the unattainability principle:

It is impossible by any procedure, no matter how idealised, to reduce any assembly to absolute zero temperature in a finite number of operations [59; 58].

There is an ongoing debate on the relations between the two formulations and their relation to the II-law regarding which and if at all, one of these formulations implies the other [60; 61; 62; 63]. Quantum considerations can illuminate these issues.

At steady state the second law implies that the total entropy production is non-negative, cf. Eq. (4). When the cold bath approaches the absolute zero temperature, it is necessary to eliminate the entropy production divergence at the cold side. When $T_c \rightarrow 0$ the entropy production scales as

$$\dot{S}_c \sim -T_c^\alpha, \quad \alpha \geq 0. \quad (19)$$

For the case when $\alpha = 0$ the fulfilment of the second law depends on the entropy production of the other baths, which should compensate for the negative entropy production of the cold bath. The first formulation of the III-law modifies this restriction. Instead of $\alpha \geq 0$ the III-law imposes $\alpha > 0$ guaranteeing that at absolute zero the entropy production at the cold bath is zero: $\dot{S}_c = 0$. This requirement leads to the scaling condition of the heat current $J_c \sim T_c^{\alpha+1}$.

The second formulation is a dynamical one, known as the unattainability principle; *No refrigerator can cool a system to absolute zero temperature at finite time*. This formulation is more restrictive, imposing limitations on the system bath interaction and the cold bath properties when $T_c \rightarrow 0$ [20]. The rate of temperature decrease of the cooling process should vanish according to the characteristic exponent ζ :

$$\frac{dT_c(t)}{dt} \sim -T_c^\zeta, \quad T_c \rightarrow 0. \quad (20)$$

Solving Eq. (20), leads to;

$$T_c(t)^{1-\zeta} = T_c(0)^{1-\zeta} - ct, \quad \text{for } \zeta < 1, \quad (21)$$

where c is a positive constant. From Eq. (21) the cold bath is cooled to zero temperature at finite time for $\zeta < 1$. The III-law requires therefore $\zeta \geq 1$. In order to evaluate Eq.(20) the heat current can be related to the temperature change:

$$J_c(T_c(t)) = -c_V(T_c(t)) \frac{dT_c(t)}{dt}. \quad (22)$$

This formulation takes into account the heat capacity $c_V(T_c)$ of the cold bath. $c_V(T_c)$ is determined by the behaviour of the degrees of freedom of the cold bath at low temperature. Therefore the scaling exponents can be related $\zeta = 1 + \alpha - \eta$ where $c_V \sim T_c^\eta$ when $T_c \rightarrow 0$.

To get additional insight specific cases are examined. The quantum refrigerator models differ in their operational mode being either continuous or reciprocating. When $T_c \rightarrow 0$ the refrigerators have to be optimised adjusting to the decreasing temperature. The receiving mode of the refrigerator has to become

occupied to transfer energy. The rate of this process is proportional to a Boltzmann term $\omega_c^\gamma \exp[-\frac{\hbar\omega_c}{k_B T_c}]$. When optimised for maximum cooling rate the energy difference of the receiving mode should scale linearly with temperature $\omega_c \sim T_c$ [15; 28; 36; 19; 20]. Once optimised the cooling power of all refrigerators studied have the same dependence on the coupling to the cold bath. This means that the III-law depends on the scaling properties of the heat conductivity $\gamma_c(T_c)$ and the heat capacity $c_V(T_c)$ as $T_c \rightarrow 0$.

Harmonic oscillator cold heat bath

The harmonic heat bath is a generic type of a quantum bath. It includes the electromagnetic field: A photon bath, or a macroscopic piece of solid; a phonon bath, or Bogliuyubov excitations in a Bose-Einstein condensate. The model assumes linear coupling of the refrigerator to the bath. The standard form of the bath's Hamiltonian is:

$$\hat{H}_{int} = (\hat{\mathbf{b}} + \hat{\mathbf{b}}^\dagger) \left(\sum_k (g(k)\hat{\mathbf{a}}(k) + \bar{g}(k)\hat{\mathbf{a}}^\dagger(k)) \right),$$

$$\hat{H}_B = \sum_k \omega(k)\hat{\mathbf{a}}^\dagger(k)\hat{\mathbf{a}}(k), \quad (23)$$

where $\hat{\mathbf{a}}(k), \hat{\mathbf{a}}^\dagger(k)$ are annihilation and creation operators for a mode k . For this model the weak coupling limit procedure leads to the LGKS generator with the cold bath relaxation rate given by [20]

$$\gamma_c \equiv \gamma_c(\omega_c) = \pi \left(\sum_k |g(k)|^2 \delta(\omega(k) - \omega_c) \left[1 - e^{-\frac{\hbar\omega(k)}{k_B T_c}} \right]^{-1} \right). \quad (24)$$

For the Bosonic field in d -dimensional space, and with the linear low-frequency dispersion law ($\omega(k) \sim |k|$) the following scaling properties for the cooling rate at low frequencies are obtained

$$\gamma_c \sim \omega_c^\kappa \omega_c^{d-1} \left[1 - e^{-\hbar\omega_c/k_B T_c} \right]^{-1} \quad (25)$$

where ω_c^κ represents the scaling of the coupling strength $|g(\omega)|^2$ and ω_c^{d-1} the scaling of the density of modes. It implies the following scaling relation for the cold current

$$J_c \sim T_c^{d+\kappa} \left[\frac{\omega_c}{T_c} \right]^{d+\kappa} \frac{1}{e^{\hbar\omega_c/k_B T_c} - 1} \quad (26)$$

Optimization of Eq. (26) with respect to ω_c leads to the frequency tuning $\omega_c \sim T_c$ and the final current scaling

$$J_c^{opt} \sim T_c^{d+\kappa}. \quad (27)$$

Taking into account that for low temperatures the heat capacity of the bosonic systems scales like

$$c_V(T_c) \sim T_c^d \quad (28)$$

which produces the scaling of the dynamical equation, Eq. (20):

$$\frac{dT_c(t)}{dt} \sim -(T_c)^\kappa. \quad (29)$$

Similarly, the same scaling Eq. (29) is achieved for the periodically driven refrigerator, with the optimization tuning $\omega_c, \lambda \propto T_c$.

The III-law implies a constraint on the form of interaction with a bosonic bath

$$\kappa \geq 1. \quad (30)$$

For standard systems like electromagnetic fields or acoustic phonons with linear dispersion law $\omega(k) = v|k|$ and the form-factor $g(k) \sim |k|/\sqrt{\omega(k)}$ the parameter $\kappa = 1$ as for low ω , $|g(\omega)|^2 \sim |k|$. However, the condition (30) excludes exotic dispersion laws $\omega(k) \sim |k|^\alpha$ with $\alpha < 1$ which anyway produce the infinite group velocity forbidden by the relativity theory. Moreover, the popular choice of Ohmic coupling is excluded for systems in dimension $d > 1$. The condition (30) can be also compared with the condition

$$\kappa > 2 - d, \quad (31)$$

which is necessary to assure the existence of the ground state for the bosonic field interacting by means of the Hamiltonian (23). The third law loses its validity if the cold bath does not have a ground state. For a harmonic bath this could happen if even one of the effective oscillators has an inverted potential.

The existence of a ground state

A natural physical stability condition which should be satisfied by any model of an open quantum system is that its total Hamiltonian should be bounded from below and should possess a ground state. In the quantum degenerate regime even a mixture of isotopes will segregate and lead to a unique ground state. In the case of systems coupled linearly to bosonic heat baths it implies the existence of the ground state for the following bosonic Hamiltonian (compare with (23)):

$$H_{bos} = \sum_k \{ \omega(k) a^\dagger(k) a(k) + (g(k) a(k) + \bar{g}(k) a^\dagger(k)) \}. \quad (32)$$

Introducing a formal transformation to a new set of bosonic operators

$$a(k) \mapsto b(k) = a(k) + \frac{\bar{g}(k)}{\omega(k)}. \quad (33)$$

we can write

$$H_{bos} = \sum_k \omega(k) b^\dagger(k) b(k) - E_0, \quad E_0 = \sum_k \frac{|g(k)|^2}{\omega(k)} \quad (34)$$

with the formal ground state $|0\rangle$ satisfying

$$b(k)|0\rangle = 0, \quad \text{for all } k. \quad (35)$$

For the interesting case of an infinite set of modes $\{k\}$, labeled by the d -dimensional wave vectors, two problems can appear:

1) The ground state energy E_0 can be infinite, i.e. does not satisfy

$$\sum_k \frac{|g(k)|^2}{\omega(k)} < \infty. \quad (36)$$

2) The transformation (33) can be implemented by a unitary one, i.e. $b(k) = U a(k) U^\dagger$ if and only if

$$\sum_k \frac{|g(k)|^2}{\omega(k)^2} < \infty. \quad (37)$$

Non-existence of such a unitary implies non-existence of the ground state (35) (in the Fock space of the bosonic field) and is called *van Hove phenomenon* [64].

While the divergence of the sums (36), (37) (or integrals for infinite volume case) for large $|k|$ can be avoided by putting an *ultra-violet cutoff*, the stronger condition (37) imposes restrictions on the form of $g(k)$ at low frequencies. Assuming, that $\omega(k) = v|k|$ and $g(k) \equiv g(\omega)$ the condition Eq. (37) is satisfied for the following low-frequency scaling in the d -dimensional case

$$|g(\omega)|^2 \sim \omega^\kappa, \quad \kappa > 2 - d. \quad (38)$$

These conditions on the dispersion relation of the cold bath required for a ground state are identical to the conditions for the III-law Eq. (31). The consistency with the III-law ensures the existence of the ground state.

Ideal Bose/Fermi gas cold heat bath

An important generic cold bath consists of a degenerate quantum gas composed of ideal Bose or Fermi gas. The model refrigerator consists of the working medium of (infinitely) heavy particles with the internal structure approximated (at least at low temperatures) by a two-level-system (TLS) immersed in the low density gas at the temperature T_c . Insight into the III-law comes from realising that the degenerate gas is in equilibrium with a normal part. The external refrigerator only couples to the normal part. Once the temperature approaches zero the fraction of the normal part decreases, eventually nulling the cooling current. Another source of excitations are collective excitations of Bogoliubov type [65]. The low energy tail can be described as a phonon bath with linear dispersion thus the previous section covered the III-law for these excitations.

The Markovian dynamics of such systems was derived by Dumcke [66] in the low density limit and N -level internal structure. For the case of the TLS there is one receiving Bohr frequency ω_c . Cooling occurs due to the non-elastic scattering leading to energy exchange with this frequency [20]:

$$\gamma_c = 2\pi\mathbf{n} \int d^3\vec{p} \int d^3\vec{p}' \delta(E(\vec{p}') - E(\vec{p}) - \hbar\omega_c) f_{T_c}(\vec{p}_g) |T(\vec{p}', \vec{p})|^2 \quad (39)$$

with \mathbf{n} the particles density, $f_{T_c}(\vec{p}_g)$ the probability distribution of the gas momentum strictly given by Maxwell's distribution, \vec{p} and \vec{p}' are the incoming and outgoing gas particle momentum.

$E(\vec{p}) = p^2/2m$ denotes the kinetic energy of gas particle. At low-energies (low-temperature), scattering of neutral gas at 3-d can be characterized by s-wave scattering length a_s , having a constant transition matrix, $|T|^2 = (\frac{4\pi a_s}{m})^2$. For this model the integral (39) is calculated

$$\gamma_c = (4\pi)^4 (2\pi m T_c)^{-\frac{1}{2}} a_s^2 \mathbf{n} \omega_c \mathcal{K}_1\left(\frac{\hbar \omega_c}{2k_B T_c}\right) e^{\frac{\hbar \omega_c}{2k_B T_c}}, \quad (40)$$

where $\mathcal{K}_p(x)$ is the modified Bessel function of the second kind. Notice that formula (40) is also valid for an harmonic oscillator instead of TLS, assuming only linear terms in the interaction and using the Born approximation for the scattering matrix.

Optimizing formula (22) with respect to ω_c leads to $\omega_c \sim T_c$. Then the scaling of the heat current becomes:

$$j_c^{opt} \sim \mathbf{n}(T_c)^{\frac{3}{2}}. \quad (41)$$

When the Bose gas is above the critical temperature for the Bose-Einstein condensation the heat capacity c_V and the density \mathbf{n} are constants. Below the critical temperature the density \mathbf{n} in formula (39) should be replaced with the density \mathbf{n}_{ex} of the excited states, having both c_V, \mathbf{n}_{ex} scale as $\sim (T_c)^{\frac{3}{2}}$ which finally implies

$$\frac{dT_c(t)}{dt} \sim -(T_c)^{\frac{3}{2}}. \quad (42)$$

In the case of Fermi gas at low temperatures only the small fraction $\mathbf{n} \sim T_c$ of fermions participate in the scattering process and contribute to the heat capacity, the rest is "frozen" in the "Dirac sea" below the Fermi surface. Again, this effect modifies in the same way both sides of (20) and therefore (42) is consistent with the III-law. Similarly, a possible formation of Cooper pairs below the critical temperature does not influence the scaling (42).

Figure 2 demonstrates the III-law showing the vanishing of the cooling current j_c and the temperature decrease rate $\frac{dT_c}{dt}$ as a function of T_c for the cases of the harmonic bath and Bose gas bath.

The dynamical version of the III-law is up for critical analysis [20]. The examples of quantum refrigerators show that the cooling exponents are independent of the type of refrigerator model used. The III-law exponents depend on the cold bath characteristics, the ratio between the heat conductivity and the heat capacity for a specific bath. This ratio should scale as $\sim T_c^\zeta$, $\zeta > 1$ for the III-law to hold cf, Eq. (20). There has been a recent challenge to the III-law claiming that zero temperature can be reached [30; 67]. In our view this discrepancy is caused by an uncontrolled approximation leading to the particular dispersion used.

CONCLUSIONS

Quantum thermodynamics is applicable up to the level of a single particle [6]. Very simple models have the same thermodynamical characteristics of macroscopic devices. For example efficiency at maximum power related to finite-time-thermodynamics. Also the quantum and thermodynamical adiabatic behaviour are closely linked. Deviations lead to friction resulting in reduced efficiency.

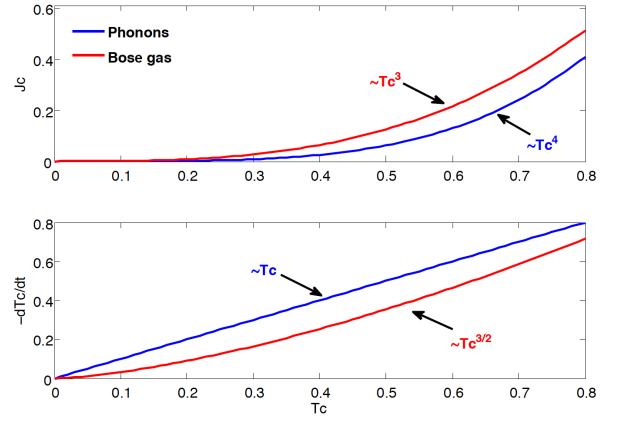


Figure 2. A demonstration of the III-law. The vanishing of the cooling current and the rate of temperature decrease as $T_c \rightarrow 0$. The harmonic bath in 3-d indicated in blue and Bose gas in three dimensions indicated in red. The Bose gas cools faster when $T_c \rightarrow 0$ but its rate of temperature decrease is slower than the harmonic bath.

After analysing many types of continuous and reciprocating refrigerators universal conclusions can be drawn. When $T_c \rightarrow 0$ the cooling current is the product of three terms:

$$j_c \sim -\hbar \omega_c \Gamma_c G$$

where $\hbar \omega_c$ is the energy quantum to be extracted from the cold bath. Γ_c is the rate of extraction or the heat conductivity. $G = N_h - N_c$ is the gain, the population difference between the hot and cold side. Optimizing the gain leads to $\omega_c \sim T_c$. This means that fulfilment of the III-law requires the ratio Γ_c/c_V to vanish as $T_c \rightarrow 0$, otherwise the cold bath can be cooled to its ground state in finite time.

The III-law can be thought of as an attempt to isolate completely a subsystem. Once a system is cooled to the absolute zero temperature it reaches a pure ground state and therefore becomes disentangled from the rest of the universe. The III-law is a statement that obtaining an isolated pure state is an idealisation impossible at finite time.

ACKNOWLEDGMENT

Thanks to Tova Feldmann and Robert Alicki for their insights. Work supported by the Israel Science Foundation.

REFERENCES

- [1] A. Einstein. "über einen die erzeugung und verwandlung des liches betreffenden heuristischen gesichtspunkt (on a heuristic viewpoint concerning the production and transformation of light)". *Annalen der Physik*, 17:132, 1905.
- [2] H. E. Scovil and E. O. Schulz du Bois. Three-level masers as heat engines. *Phys. Rev. Lett.*, 2:262, 1959.
- [3] J. Geusic, E. O. Schulz du Bois, R. D. Grasse, and H. E. Scovil. Quantum equivalence of the carnot cycle. *Phys. Rev.*, 156:343, 1967.
- [4] J. Geusic, R. D. Grasse E. O. Schulz-du Bois, and H. E. Scovil. Sympathetic crystallization of trapped ions. *J. App. Phys.*, 30:1113, 1959.
- [5] S. Carnot. *Réflexions sur la Puissance Motrice du Feu et*

- sur les Machines propres à Développer cette Puissance.* Bachelier, Paris, 1824.
- [6] Ronnie Kosloff. Quantum Thermodynamics: A Dynamical Viewpoint. *Entropy*, 15:2100–2128, 2013.
- [7] G. Lindblad. On the generators of quantum dynamical semigroups. *Comm. Math. Phys.*, 48:119, 1976.
- [8] Vittorio Gorini Andrzej Kossakowski and E. C. G. Sudarshan. Completely positive dynamical semigroups of n -level systems. *J. Math. Phys.*, 17:821, 1976.
- [9] R. Alicki. Quantum open systems as a model of a heat engine. *J. Phys A: Math. Gen.*, 12:L103, 1979.
- [10] R. Kosloff. A Quantum Mechanical Open System as a Model of a Heat Engine. *J. Chem. Phys.*, 80:1625–1631, 1984.
- [11] F.L. Curzon and B. Ahlborn. Efficiency of a carnot engine at maximum power output. *Am. J. Phys.*, 43:22, 1975.
- [12] Peter Salamon Bjarne Andresen and R. S. Berry. "thermodynamics in finite time". *"Physics Today"*, 37:9:62, 1984.
- [13] P. Salamon, J.D. Nulton, G. Siragusa, T.R. Andersen and A. Limon. Principles of control thermodynamics. *Energy*, 26:307, 2001.
- [14] Eitan Geva and Ronnie Kosloff. The Quantum Heat Engine and Heat Pump: An Irreversible Thermodynamic Analysis of The Three-Level Amplifier. *J. Chem. Phys.*, 104:7681–7698, 1996.
- [15] Ronnie Kosloff, Eitan Geva and Jeffrey M. Gordon. The quantum refrigerator in quest of the absolute zero. *J. Appl. Phys.*, 87:8093–8097, 2000.
- [16] Ikuji Tsujikawa and Tsuyoshi Murao. Possibility of Optical Cooling of Ruby. *J. Phys. Soc. Jpn.*, 18:503, 1962.
- [17] T. W. HŁnsch and A. L. Schawlow. Cooling of Gases by Laser Radiation. *Opt. Commun.*, 13:68, 1975.
- [18] D. J. Wineland and H. Dehmelt. . *Bull. Am. Phys. Soc.*, 20:637, 1975.
- [19] Amikam Levy and Ronnie Kosloff. Quantum absorption refrigerator. *Phys. Rev. Lett.*, 108:070604, 2012.
- [20] Amikam Levy, Robert Alicki, and Ronnie Kosloff. Quantum refrigerators and the third law of thermodynamics. *Phys. Rev. E*, 85:061126, 2012.
- [21] K. Sandner and H. Ritsch. Temperature gradient driven lasing and stimulated cooling. *Phys. Rev. Lett.*, 109:93601, 2012.
- [22] Romain Quidant Jan Gieseler, Bradley Deutsch and Lukas Novotny. Subkelvin parametric feedback cooling of a laser-trapped nanoparticle. *Phys. Rev. Lett.*, 109:103603, 2012.
- [23] Juncheng Guo, Guozhen Su and Jincan Chen. The performance evaluation of a micro/nano-scaled cooler working with an ideal bose gas. *Physics Letters A*, 376:270, 2012.
- [24] Zhen Yi, Wen-ju Gu and Gao-xiang Li. Sideband cooling of atoms with the help of an auxiliary transition. *Phys. Rev. Lett.*, 109:055401, 2012.
- [25] J. D. Teufel, T. Donner, Dale Li, J. W. Harlow, M. S. Allman, K. Cicak, A. J. Sirois, J. D. Whittaker, K. W. Lehnert and R. W. Simmonds. Sideband cooling of micromechanical motion to the quantum ground state. *Nature*, 475:359, 2011.
- [26] E. Verhagen, S. Delłglise, S. Weis, A. Schliesser and T. J. Kippenberg. Quantum-coherent coupling of a mechanical oscillator to an optical cavity mode. *Nature*, 482:63, 2012.
- [27] Eugene Demler Armin Rahmani, Takuya Kitagawa and Claudio Chamon³. Cooling through optimal control of quantum evolution . *Phys. Rev. A*, 87:043607, 2013.
- [28] José P. Palao, Ronnie Kosloff, and Jeffrey M. Gordon. Quantum thermodynamic cooling cycle. *Phys. Rev. E*, 64:056130–8, 2001.
- [29] J. P. Pekola and F. W. J. Hekking. Normal-Metal-Superconductor Tunnel Junction as a Brownian Refrigerator. *Phys. Rev. Lett.*, 98:210604, 2007.
- [30] Amikam Levy, Robert Alicki, and Ronnie Kosloff. Comment on Cooling by Heating: Refrigeration Powered by Photons". *Phys. Rev. Lett.*, 109:248901, 2012.
- [31] B. Rutten B. Cleuren and C. Van den Broeck. Cooling by Heating: Refrigeration Powered by Photons. *Phys. Rev. Lett.*, 108:120603, 2012.
- [32] P. Skrzypczyk N. Linden, S. Popescu. "how small can thermal machines be? towards the smallest possible refrigerator". *Phys. Rev. Lett.*, 105:130401, 2010.
- [33] B. J. Lester A. M. Kaufman and C. A. Regal. Cooling a Single Atom in an Optical Tweezer to Its Quantum Ground State. *Phys. Rev. X*, 2:041014, 2012.
- [34] R. Alicki D. Gelbwaser-Klimovsky and G. Kurizki. Minimal universal quantum heat machine. *Phys. Rev. E*, 87:012140, 2013.
- [35] Tova Feldmann and Ronnie Kosloff. Performance of Discrete Heat Engines and Heat Pumps in Finite Time. *Phys. Rev. E*, 61:4774–4790, 2000.
- [36] Yair Rezek, Peter Salamon, Karl Heinz Hoffmann and Ronnie Kosloff. The quantum refrigerator: The quest for the absolute zero. *Euro. Phys. Lett.*, 85:30008, 2009.
- [37] Tova Feldmann and Ronnie Kosloff. Minimal temperature of quantum refrigerators. *Euro. Phys. Lett.*, 89:20004, 2010.
- [38] Ronnie Kosloff and Tova Feldmann. A Discrete Four Stroke Quantum Heat Engine Exploring the Origin of Friction. *Phys. Rev. E*, 65:055102 1–4, 2002.
- [39] Tova Feldmann and Ronnie Kosloff. The Quantum Four Stroke Heat Engine: Thermodynamic Observables in a Model with Intrinsic Friction. *Phys. Rev. E*, 68:016101, 2003.
- [40] Yair Rezek, Ronnie Kosloff. Irreversible performance of a quantum harmonic heat engine. *New J. Phys.*, 8:83, 2006.
- [41] Tova Feldmann and Ronnie Kosloff. Quantum lubrication: Suppression of friction in a first-principles four-stroke heat engine. *Phys. Rev. E*, 73:025107(R), 2006.
- [42] Ronnie Kosloff and Tova Feldmann. Optimal performance of reciprocating demagnetization quantum refrigerators. *Phys. Rev. E*, 82:011134, 2010.
- [43] Xi Chen, A. Ruschhaupt, S. Schmidt, A. del Campo, D. Guery-Odelin, J. G. Muga. Fast optimal frictionless atom cooling in harmonic traps. *Phys. Rev. Lett.*, 104:063002, 2010.
- [44] Xi Chen, I. Lizuain, A. Ruschhaupt, D. Gury-Odelin, and J. G. Muga. Shortcut to adiabatic passage in two- and three-level atoms. *Phys. Rev. Lett.*, 105:123003, 2010.
- [45] S. Ibez, Xi Chen, E. Torrontegui, J. G. Muga, and A. Ruschhaupt. Multiple schrödinger pictures and dynamics in shortcuts to adiabaticity. *Phys. Rev. Lett.*, 109:100403, 2012.
- [46] Peter Salamon, Karl Heinz Hoffmann, Yair Rezek and Ronnie Kosloff. Maximum work in minimum time from a conservative quantum system. *PCCP*, 11:1027, 2009.
- [47] K. H. Hoffmann, P. Salamon, Y. Rezek and R. Kosloff.

- Time-optimal controls for frictionless cooling in harmonic traps. *Euro. Phys. Lett.*, 96:60015, 2011.
- [48] F. Boldt, K. H. Hoffmann, P. Salamon and R. Kosloff. Time-optimal processes for interacting spin systems. *Euro. Phys. Lett.*, 99:40002, 2012.
- [49] E. A. Martinez and J. P. Paz. Dynamics and thermodynamics of linear quantum open systems. *Phys. Rev. Lett.*, 110:130406, 2013.
- [50] H. Spohn and J. Lebowitz. Irreversible thermodynamics for quantum systems weakly coupled to thermal reservoirs. *Adv. Chem. Phys.*, 109:38, 1978.
- [51] Vittorio Gorini and Andrzej Kossakowski. N-level system in contact with a singular reservoir. *J. Math. Phys.*, 17:1298, 1976.
- [52] H.-P. Breuer and F. Petruccione. *Open quantum systems*. Oxford university press, 2002.
- [53] J. Birjukov T. Jahnke and G. Mahler. On the nature of thermodynamic extremum principles: The case of maximum efficiency and maximum work. *Ann.Phys.*, 17:88, 2008.
- [54] Tova Feldmann and Ronnie Kosloff. Characteristics of the Limit Cycle of a Reciprocating Quantum Heat Engine. *Phys. Rev. E*, 70:046110, 2004.
- [55] G. Mahler J. Birjukov, T. Jahnke. Quantum thermodynamic processes: a control theory for machine cycles. *Eur. Phys. J. B*, 64:105, 2008.
- [56] W. Nernst. Ueber die Berechnung chemischer Gleichgewichte aus thermischen Messungen. *Nachr. Kgl. Ges. Wiss. Gött.*, 1:40, 1906.
- [57] W. Nernst. Über die Beziehung zwischen Wärmeentwicklung und maximaler Arbeit bei kondensierten Systemen. *er. Kgl. Pr. Akad. Wiss.*, 52:933, 1906.
- [58] W. Nernst. *The theoretical and experimental bases of the New Heat Theorem Ger., Die theoretischen und experimentellen Grundlagen des neuen Wärmesatzes*. W. Knapp, Halle, 1918.
- [59] R. H. Fowler and E. A. Guggenheim. *Statistical Thermodynamics*. Cambridge university press, 1939.
- [60] P. T. Landsberg. Foundations of thermodynamics. *Rev. Mod. Phys.*, 28:363, 1956.
- [61] P. T. Landsberg. A comment on nernst's theorem. *J. Phys A: Math.Gen.*, 22:139, 1989.
- [62] F. Belgiorno. Notes on the third law of thermodynamics i. *J. Phys A: Math.Gen.*, 36:8165, 2003.
- [63] F. Belgiorno. Notes on the third law of thermodynamics ii. *J. Phys A: Math.Gen.*, 36:8195, 2003.
- [64] G. G. Emch. *Algebraic Methods in Statistical Mechanics and Quantum Field Theory*. Wiley Interscience, New York, 1972.
- [65] N. N. Bogoliubov. On the theory of superfluidity. *J. Phys. (USSR)*, 11:23, 1947.
- [66] R. Dumcke. The low density limit for an N-level system interacting with a free Bose or Fermi gas. *Comm. Math. Phys.*, 97:331, 1985.
- [67] Robert Alicki Michal Kolar, David Gelbwaser-Klimovsky and Gershon Kurizki. Quantum bath refrigeration towards absolute zero: unattainability principle challenged. *Phys. Rev. Lett.*, 108:090601, 2012.

THERMODYNAMICS UNDER QUANTUM SIZE EFFECTS

Altug Sisman*, Fatih Ozturk, Coskun Firat and Gulru Babac

Istanbul Technical University, Energy Institute, 34469 Maslak, Istanbul, Turkey.

*Corresponding author, e-mail: sismanal@itu.edu.tr

ABSTRACT

Thermodynamics of nanoscale systems is considerably different than that of macro ones. Wave nature of particles cause quantum size effects (QSE) which change the thermodynamic behaviors of nano systems considerably. QSE become important when thermal de Broglie wavelength of particles is not negligible in comparison with the characteristic size of the system. In such a case, QSE make thermodynamic state functions depend on size and shape of the system and cause some new and interesting behaviors which cannot be observed at macro scale. The subject of QSE on thermodynamics of nano systems is a relatively new research subject and it has many potential applications for nano technology. New effects caused by the wave nature of particles can be used to design and produce completely new nano devices and even new thermodynamic cycles. In this study; after the brief introduction of QSE and the methodology used for the calculation of thermodynamic properties under QSE, corollaries of QSE on thermodynamics are summarized and discussed by considering some novel results.

INTRODUCTION

Wave nature of particles modifies the probability density at thermodynamic equilibrium from a constant quantity to a space and momentum dependent quantity and also particle's momentum spectrum from continuous quantity to a discrete one. These modifications cause quantum size effects (QSE) which change the thermodynamic behaviors of nano systems. Therefore the following questions emerge: how thermodynamic behaviors change at nanoscale, how it can be modeled, how one can make use of these different behaviors, how new devices and technologies can be developed based on the effects appearing at this scale. The subject of QSE on thermodynamics of nano systems is a relatively new research topic [1-13] and it has many potential applications for nano technology. New effects caused by the wave nature of particles can be used to design and produce completely new nano devices and even new thermodynamic cycles [14-19].

QSE become important when thermal de Broglie wavelength of particles is not negligible in comparison with the system's characteristic size ($L_g = V/A$, V is volume and A is surface area of the domain). Therefore, they are mainly the nanoscale effects. Due to QSE, thermodynamic state functions become dependent on size and shape of the system and some new and interesting behaviors appear at nano scale [1-13]. It has been shown that due to wave character of particles, density distribution of a gas in a finite domain is not homogenous even at thermodynamic equilibrium. There is a layer near to the boundaries of the domain and gas density goes to zero within this layer, which has been called as quantum boundary layer (QBL) since it disappears when the Planck's constant goes to zero [8, 9, 11]. Another unusual behavior appearing at nano scale is the anisotropic pressure of a gas confined in an anisometric domain.

The aim of this study is to give a brief review of some recent published results besides some very recent and

unpublished ones yet. After the brief introduction of QSE and the methodology used for the calculation of thermodynamic properties under QSE, some novel results are summarized and discussed. These are quantum surface energy, loss of additivity rule for extensive quantities, anisotropic gas pressure, diffusion driven by size and shape differences, thermosize effects (similar to thermoelectric effects), quantum boundary layer, quantum forces as a macroscopic manifestation of quantum boundary layer, discrete nature of thermodynamic properties of a Fermi gas and multi-step Bose-Einstein condensation.

QUANTUM SIZE EFFECTS ON THERMODYNAMIC QUANTITIES

In general, size effects are the changes in material behaviors due to change in material sizes. They appear when the characteristic size of a material is not sufficiently larger than the characteristic lengths of physical processes. Characteristic size of a material (a domain) can simply be represented by $L_g = V/A$. On the other hand, there are many characteristic lengths for physical processes and they are classified into two groups, namely classical and quantum. Classical ones are mean free path, mean distance between particles, characteristic length for a driving force, like $L_T = T/|\vec{\nabla}T|$, etc. Quantum characteristic lengths are thermal de Broglie wave length λ_{th} , quantum coherence length, etc. Quantum size effects appear if λ_{th} is not negligible in comparison with L_g , ($L_g \gg \lambda_{th}$). In that case, wave nature of particles become important and causes some fundamental assumptions and approximations to change: Momentum values of a particle become a discrete set although it is assumed to be a continuous quantity during the classical

treatments of macro systems. Besides the discrete nature of momentum, its minimum value is not zero in a finite-size system and this value is inversely proportional with the system size. Another quantity which has to be modified is the probability density. When the wave nature of particles is negligible, it is a homogenous quantity and equal to the classical probability density given by I/V for a system of volume V . On the other hand, when the wave nature of particles becomes important, it is equal to the quantum probability density $|\Psi(\mathbf{x},\mathbf{p})|^2$ where Ψ is the wave function obtained by the solution of the Schrödinger equation. The classical probability density predicts a homogenous density distribution at thermodynamic equilibrium whereas quantum one predicts a non-homogenous density distribution [8].

An ideal Maxwell gas confined in a rectangular finite domain: the simplest case

To understand the appearance of QSE on thermodynamic quantities, the simplest way is to consider an ideal Maxwell gas of mono particles (like monatomic gas, free electron gas etc.) confined in a non-penetrable rectangular domain with sizes of L_1, L_2 and L_3 . Free energy expression of gas is

$$F = N(\mu - k_b T) \quad (1)$$

where k_b is the Boltzmann's constant, T is temperature, N is number of particles in the domain and μ is chemical potential determined by

$$\mu = -k_b T \ln\left(\frac{\zeta}{N}\right) \quad (2)$$

where ζ is the single particle partition function defined by

$$\zeta = \sum_r \exp(-\varepsilon_r/k_b T). \quad (3)$$

Here the summation is over the quantum states r , ε_r is the energy eigenvalue of particles corresponding to quantum state r . Energy eigenvalues of a single particle confined in a rectangular box are well known and they are given as follows,

$$\varepsilon_r = \varepsilon_{ijk} = \frac{h^2}{8m} \left[\left(\frac{i_1}{L_1}\right)^2 + \left(\frac{i_2}{L_2}\right)^2 + \left(\frac{i_3}{L_3}\right)^2 \right] \quad \left\{ \begin{matrix} i_1 \\ i_2 \\ i_3 \end{matrix} \right\} = 1, 2, 3, \dots \quad (4)$$

where m is the particle mass, h is the Planck's constant, i_1, i_2 and i_3 are quantum state variables which are integer numbers running from one to infinity. By using Eq.(4), Eq.(3) can be expressed as

$$\zeta = \sum_{i_1, i_2, i_3=1}^{\infty} \exp\left[-\left[(\alpha_1 i_1)^2 + (\alpha_2 i_2)^2 + (\alpha_3 i_3)^2\right]\right] \quad (5)$$

where $\alpha_1 = L_c/L_1$, $\alpha_2 = L_c/L_2$, $\alpha_3 = L_c/L_3$ and the length $L_c = h/\sqrt{8mk_b T} = \sqrt{\pi}\lambda_{th}/2$ is one half of the most probable de Broglie wavelength of the particles.

In macro system; $\{L_1, L_2, L_3\} \gg L_c$ and $\{\alpha_1, \alpha_2, \alpha_3\} \ll 1$. In that case; discrete nature of momentum values of particles (and so the energy values) is negligible and they are assumed to be continuous quantities. Therefore, infinite summations can be replaced by infinite integrals and the trivial

thermodynamic expressions, which are independent of the system size and shape, are obtained. In nano systems, however, at least one of the domain sizes is near to the order of L_c . Therefore wave nature of particles becomes important.

In this case, discrete nature of momentum values is noticeable and their discrete values are running from a non-zero value to infinity. Therefore, integral representations of summations give the incorrect results and more precise methods, like Poisson, Abel-Plana or Euler-Mac Lauren summation formula, should be used for the calculations of summations. Poisson summation formula is given for an even function $f(i)$ as

$$\sum_{i=1}^{\infty} f(i) = \int_0^{\infty} f(i) di - \frac{f(0)}{2} + 2 \sum_{s=10}^{\infty} \int_0^{\infty} f(i) \cos(2\pi s i) di \quad (6)$$

The first term on the right hand side is the dominant and conventional integral term. The second one is the zero correction term, which excludes the false contribution of the zero value of i to the integral term. The third one is the discreteness correction due to discrete values of i instead of continuous ones. It is possible to show numerically that the contribution of discreteness correction is much smaller than that of the zero correction as long as the system size is bigger than L_c ($\alpha < 1$). As an example, the ratio of the discreteness correction to the zero correction for the summation in Eq.(5) is less than 10^{-4} even for $\alpha=1$. Therefore, the main correction to the integral approximation comes from the second term in Eq.(6) for $\alpha \leq 1$.

By using the first two terms of Eq.(6), partition function in Eq.(5) is determined as

$$\zeta = \frac{\pi^{3/2}}{8\alpha_1\alpha_2\alpha_3} \left(1 - \frac{\alpha_1}{\sqrt{\pi}}\right) \left(1 - \frac{\alpha_2}{\sqrt{\pi}}\right) \left(1 - \frac{\alpha_3}{\sqrt{\pi}}\right) \quad (7)$$

If the values of alphas are smaller than unity but greater enough than zero, then the second and third order terms in alphas can be neglected. In that case, Eq.(7) is simplified as [5]

$$\zeta = n_q V \left[1 - \frac{1}{\sqrt{\pi}}(\alpha_1 + \alpha_2 + \alpha_3)\right] \quad (8)$$

where $n_q = 1/\lambda_{th}^3$ is the quantum density and $V = L_1 L_2 L_3$ is the domain volume. Thus free energy expression is obtained by using Eq.(8) in Eqs.(2) and (1) as follows

$$F = -nk_b T \left[\ln\left(\frac{n_q}{n}\right) + 1 \right] V + nk_b T \frac{\lambda_{th}}{4} A \quad (9)$$

The first term in Eq.(9) is the classical bulk free energy while the second term is the quantum surface energy [5, 6, 8, 9, 11]. It is seen that free energy is proportional to both volume and surface area of the domain. This means that free energy of a simple system does not depend on only two variables like temperature and density but also depend on surface over volume ratio which is the quantity sensitive to size and shape of the domain. In other words, thermodynamic state functions of nano systems are size and shape dependent. It should be noted that quantum surface energy disappears when the system size becomes macroscopic since $\lambda_{th} A/V$ goes to zero.

Furthermore, it also disappears when the Planck's constant goes to zero. Therefore, the second term is a pure quantum term which is noticeable only in nano systems.

Instead of using the summations over quantum states, it is also possible to use summations over energy states by considering the density of states. In that case, the same free energy expression can be obtained by using the Weyl's conjecture, which gives a precise formula for density of states depending on not only the domain volume but also the surface area, periphery and even the corners or end points of the domain [2-4, 7]. The advantage of using the Weyl's conjecture is that there is no need to solve the Schrödinger equation for each different domain shape. It is the general expression for any domain shape. In other words, in addition to the rectangular domain, Eq.(9) is valid also for cylindrical, spherical or other shapes of domain [6, 11].

COROLLARIES OF QSE ON THERMODYNAMICS

By using Eq.(9), internal energy, pressures in each direction, entropy and chemical potential are obtained as follows respectively,

$$U = \frac{3}{2} Nk_b T + Nk_b T \frac{\lambda_{th}}{8} \frac{A}{V} \quad (10)$$

$$p_1 = nk_b T \left(1 + \frac{\lambda_{th}}{2L_1} \right) \quad (11a)$$

$$p_2 = nk_b T \left(1 + \frac{\lambda_{th}}{2L_2} \right) \quad (11b)$$

$$p_3 = nk_b T \left(1 + \frac{\lambda_{th}}{2L_3} \right) \quad (11c)$$

$$S = Nk_b \left[\ln \left(\frac{n_q}{n} \right) + \frac{5}{2} \right] - Nk_b \frac{\lambda_{th}}{8} \frac{A}{V} \quad (12)$$

$$\mu = -k_b T \ln \left(\frac{n_q}{n} \right) + k_b T \frac{\lambda_{th}}{4} \frac{A}{V} \quad (13)$$

Non-extensivity: Due to the second terms of Eqs.(9), (10), (12) and (13), additivity rule of extensive quantities is not valid in nano systems [5].

Pressure anisotropy: Eqs.(11a-11c) shows that pressure becomes an anisotropic quantity in an anisometric nano domain since it is different in each directions. In other words, pressure of even an ideal gas is not a scalar quantity and it becomes a tensorial quantity generally in nano systems [5, 6].

Size and shape difference driven diffusion: As a result of the second term in Eq.(13), a chemical potential difference can be created by size or shape differences even if density and temperature are kept constant. This causes a diffusion driven by size and shape differences [5].

Thermosize effects: Another interesting behaviour appearing due to QSE is thermosize effects. They are very similar to thermoelectric effects which arise when two different conductors or semi-conductors are under the same temperature gradient. The temperature gradient induces an electrochemical potential gradient in each conductor and it is known as Seebeck effect. As long as the conductors are made by the different materials, the same temperature gradient causes different electrochemical potential gradients in each conductor. Therefore, a net electrochemical potential difference is obtained at hot or cold side when the conductors

are connected to each other at the other side. This potential difference can drive an electrical current on an external load. During the isothermal flow of electrical current from one material to the other, a heat exchange between the charge carriers and their environment at interface is observed which is known as Peltier effect. Therefore, two different types of conductors having different electrical properties should be used to observe the thermoelectric effects. Consequently, differences in both temperature and electrical properties are necessary to get the thermoelectric effects. If the conductors are made by the same material, then the thermoelectric effects disappear. On the other hand, since the size itself becomes a control variable on thermodynamic state functions at nano scale, instead of using two different materials, it becomes possible to get a net potential difference by using the two different sized (macro and nano) structures made by the same material under the same temperature gradient. In that case, differences in both temperature and size cause some new effects so called "thermosize effects" [5, 13]. After the proposition of thermosize effects, some recent works have been done to analyze the thermodynamic cycles based on thermosize effects [14-19].

Quantum boundary layer: For an ideal Maxwellian gas confined in a domain with finite size, the local density is given by [8]

$$n(\mathbf{x}) = n_{cl} \frac{\sum_r \exp(-\varepsilon_r/k_b T) |\psi_r(\mathbf{x})|^2}{\frac{1}{V} \sum_r \exp(-\varepsilon_r/k_b T)} \quad (14)$$

where n_{cl} is the classical density defined by $n_{cl} = N/V$, N is the total number of particles in the whole confinement volume V and $\psi_r(\mathbf{x})$ is the eigenfunction corresponding to quantum state r . For an ideal Maxwell gas confined in a rectangular box, dimensionless density distribution in one direction is

$$\tilde{n}(\tilde{x}) = \frac{2 \sum_{i=1}^{\infty} \exp[-(\alpha i)^2] \sin^2 \left(\frac{\pi i}{L_*} x \right)}{\sum_{i=1}^{\infty} \exp[-(\alpha i)^2]} \quad (15)$$

where $\tilde{n} = n(\tilde{x})/n_{cl}$, $\tilde{x} = x/L_*$ and L_* is the size of the domain in chosen direction [8]. Figure 1 shows the density distribution for $\alpha = 0.2$. It is seen that density distribution is not homogenous and there is a boundary layer where the density goes to zero. As a result of the wave character of particles, particles tend to accumulate in the inner parts of the domain and this tendency causes higher local gas density than the classical one, $\tilde{n} > 1$, for the interior region. Thickness of quantum boundary layer is given as [8]

$$\delta = \frac{L_c}{2\sqrt{\pi}} = \frac{\lambda_{th}}{4} \quad (16)$$

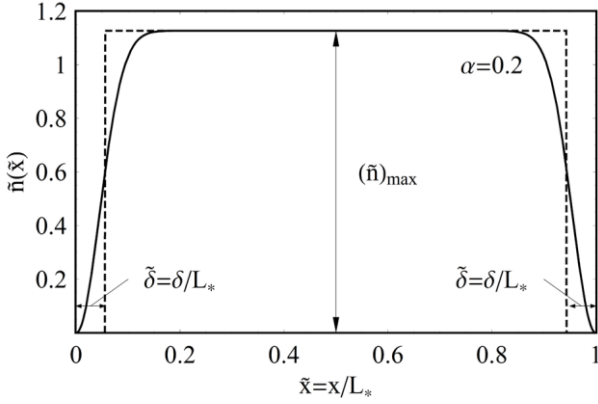


Figure 1: Dimensionless density distribution in a box.

Since the thickness of boundary layer depends on thermal de Broglie wavelength of particles, it has been called as quantum boundary layer, QBL.

Effective volume and effective density: By using the concept of QBL, it is possible to define an effective volume and effective density respectively as

$$V_{eff} = V - A\delta \quad (17)$$

$$n_{eff} = \frac{N}{V_{eff}} = \frac{N}{V - A\delta} = \frac{n_{cl}}{\left(1 - \frac{A\delta}{V}\right)} \quad (18)$$

Therefore, if the effective density is used instead of classical density in trivial free energy expression of an ideal Maxwell gas, Eq.(9) is directly obtained without following its relatively complicated calculation procedure. Application of effective density in trivial free energy expression gives

$$\begin{aligned} F &= -Nk_bT \left[\ln \left(\frac{n_q}{n_{eff}} \right) + 1 \right] \\ &= -Nk_bT \left[\ln \left(\frac{n_q}{n_{cl}} \right) + 1 \right] - Nk_bT \ln \left(1 - \frac{A\delta}{V} \right) \end{aligned} \quad (19)$$

In case of $A\delta \ll V$, by use of the approximation $\ln(1-x) \approx -x$ for $x \ll 1$ and considering $\delta = \lambda_{th}/4$, Eq.(19) is expressed as

$$F = -nk_bT \left[\ln \left(\frac{n_q}{n} \right) + 1 \right] V + nk_bT \frac{\lambda_{th}}{4} A \quad (20)$$

Eq.(20) is exactly equal to Eq.(9). Thus the concepts of effective volume and density give an opportunity to derive the thermodynamic quantities under QSE in a simple way. Furthermore, the second term can physically be explained as a compression work against the normal gas pressure to push the gas particles into the inner parts of the domain from the boundaries for a distance of $\delta = \lambda_{th}/4$, [8]. This work simply results from the wave nature of particles. Collisions between particles and the boundary are switched on when the distance is less than $2\delta = \lambda_{th}/2$ as it can be seen from Figure 1.

Density distributions in quantum gases: For ideal Fermi and Bose gases, dimensionless density distribution is expressed as [10]

$$\tilde{n}(\tilde{x}) = \frac{\sum_w \frac{|\psi_w(\tilde{x})|^2}{\exp[-\Lambda + \varepsilon_w/k_bT] \pm 1}}{\frac{1}{V} \sum_w \frac{1}{\exp[-\Lambda + \varepsilon_w/k_bT] \pm 1}} \quad (21)$$

where Λ is dimensionless chemical potential defined as $\Lambda = \mu/k_bT$. Density distributions are shown in comparison with that of a Maxwell gas in Figure 2. α is chosen as $\alpha = 0.2$ while the values of Λ are $\Lambda = 10$ and $\Lambda = -0.05$ for Fermi and Bose gases respectively.

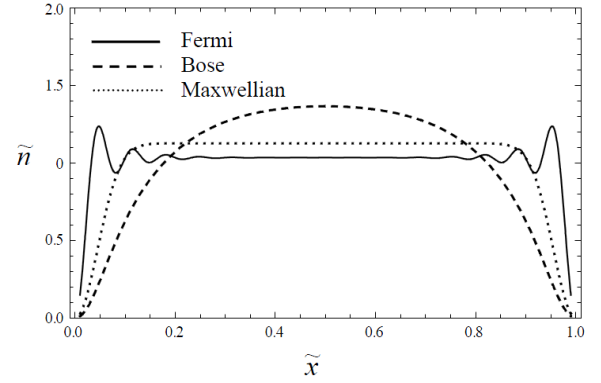


Figure 2: Dimensionless density distributions of ideal monatomic Maxwell, Fermi and Bose gases in one direction.

It is seen that in a degenerate Fermi gas, there is also density oscillation, which is called Friedel oscillation in literature for the electron gas. In a degenerate Bose gas, inhomogeneous region expands and covers the whole domain.

Quantum surface tension and quantum forces: A hypothetical experimental setup is shown in figure 1. A rectangular box is filled by a Maxwellian gas and separated into two parts by a movable and infinitesimally thin wall.

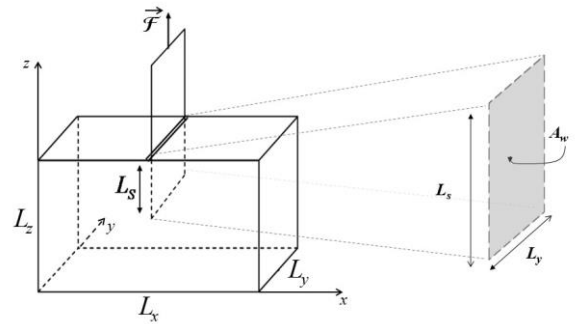


Figure 3: A schematic view of a quantum force, \vec{F} , acting on a moving wall.

The change in total surface area of the domain is only due to the change in lateral area of the interior part of the moving wall ($A_w = 2L_yL_s$). By making use of Eq.(20), quantum surface tension of a Maxwellian gas can be determined as [12],

$$\sigma = \left(\frac{\partial F}{\partial A} \right)_{N,V,T} = \frac{1}{2L_y} \left(\frac{\partial F}{\partial L_s} \right)_{N,V,T} = n_{cl} k_b T \frac{\lambda_{th}}{4} = P_{cl} \delta \quad (22)$$

Surface tension is an unexpected behavior for an ideal gas in a classical manner. On the other hand, even an ideal gas has surface tension due to the existence of QBL. Since the thickness of QBL goes to zero in classical limit ($\hbar \rightarrow 0$), it has been called as quantum surface tension (QST) [12]. QST is approximately 10^{-6} Nm^{-1} for He-4 gas under the standard conditions (300 K and 10^5 Pa). As shown in Figure 3, surface tension of a gas causes an outward quantum force on the moving wall to minimize the quantum surface energy. Derivative of free energy with respect to L_s gives the quantum force as,

$$\vec{F} = \left(\frac{\partial F}{\partial L_s} \right)_{N,V,T} \vec{e}_z = P_{cl} 2\delta L_y \vec{e}_z = \sigma 2L_y \vec{e}_z \quad (23)$$

The effective thickness of the wall is 2δ because of the QBL around infinitesimally thin moving wall. Thus, quantum force \vec{F} acting on the wall in outward direction can easily be expressed by means of the normal component of stress tensor (pressure) or surface tension as in equation (23). In other words, quantum force can be explained by a normal force due to gas pressure acting on the effective area of the movable wall ($2\delta L_y$). If quantum forces of gases are experimentally verified, this can be one of the macroscopic manifestations of quantum boundary layer and quantum surface energy.

Discrete nature of thermodynamic quantities: If the confinement is strong enough, then alpha values are greater than unity. In that case, the discrete nature of momentum states becomes very dominant and makes the thermodynamic quantities of an ideal Fermi gas discrete. In figure 4, the relation between number of particles and dimensionless chemical potential is shown just to give an idea. It is clearly seen that only some certain values of chemical potential are available since the number of particles has an integer value. The similar behavior can be observed in internal energy. The most interesting results is obtained for the specific heat at constant volume. There are lots of peaks in the relation between specific heat and number of particles, see Figure 5.

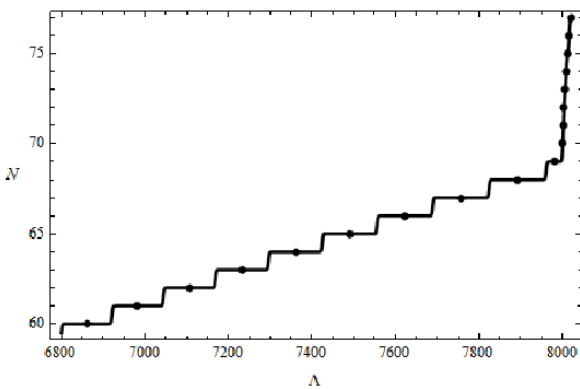


Figure 4: Number of Fermi particles strongly confined in an anisometric rectangular domain versus dimensionless chemical potential, $\Lambda = \mu/k_b T$.

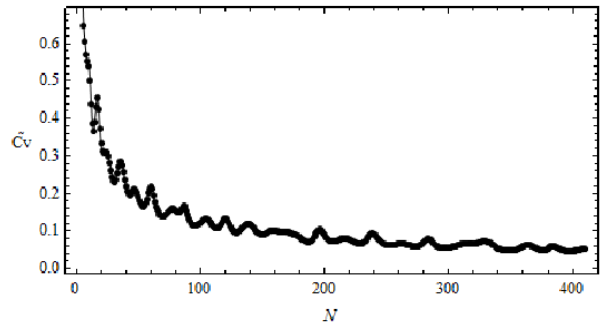


Figure 5: Dimensionless specific heat at constant volume, $\tilde{c}_v = c_v/k$, of a Fermi gas strongly confined in a cubic domain versus to number of Fermi particles.

Multiple Bose-Einstein Condensation: Bose-Einstein condensation phenomenon is the accumulation of particles in ground state. It is a well-known effect observed in Bose gases. This phenomenon causes very interesting and known behaviors like superconductivity and super fluidity. It appears if the temperature is below the Bose-Einstein condensation (BEC) temperature. In the problems considered in literature, there is only one BEC temperature. Due to QSE, however, it is possible to show that there are seven different BEC temperatures in a Bose gas confined in an anisometric rectangular domain. In an ongoing study, it is shown that BEC does not occurs directly on ground state but instead, gas particles condense first on surface modes of momentum space. In each surface mode, one momentum component takes its ground state value. Therefore there are three different surface modes for an anisometric rectangular confinement domain. After the condensations on surface modes are completed, particles start to condense on line modes. Similarly, there are three different line modes where two momentum components take their ground state values. After condensations on the line modes are also completed, particles finally condense on ground state in which three momentum components take their ground state values. This subject is an ongoing research project and some new results will be published very soon.

All the results summarized above show that thermodynamics in nano scale is completely different than that in macro scale. QSE on thermodynamics cause entirely new behaviors and effects that can be experimentally verified for the exploration of nano world as well as used to design some new nano devices.

REFERENCES

- [1] M. I. Molina, Ideal gas in a finite container, *Am. J. Phys.* vol. 64, pp. 503-505, 1996.
- [2] R. K. Pathria, An ideal quantum gas in a finite-sized container, *Am. J. Phys.* vol. 66, pp.1080-1085, 1998.
- [3] W. S. Dai and M. Xie, Quantum statistics of ideal gases in confined space, *Phys. Lett. A* vol. 311, pp. 340-346, 2003.
- [4] W. S. Dai and M. Xie, Geometry effects in confined space, *Phys. Rev. E* vol. 70, 016103, 2004.
- [5] A. Sisman and I. Müller, The Casimir-like size effects in ideal gases, *Phys. Lett. A* vol. 320, pp. 360-366, 2004.
- [6] A. Sisman, Surface dependency in thermodynamics of ideal gases, *J. Phys. A- Math. Gen.* vol. 37, pp. 11353-11361, 2004.
- [7] H. Pang, W. S. Dai and M. Xie, The difference of boundary effects between Bose and Fermi systems, *J. Phys. A-Math. Gen.* vol. 39, pp. 2563-2571, 2006.

- [8] A. Sisman, Z. F. Ozturk and C. Firat, Quantum boundary layer: a non-uniform density distribution of an ideal gas in thermodynamic equilibrium, *Phys. Lett. A* vol. 362, pp.16-20, 2007.
- [9] C. Firat and A. Sisman, Universality of quantum boundary layer for a Maxwellian gas, *Phys. Scripta* vol. 79, 065002, 2009.
- [10] Z. F. Ozturk and A. Sisman, Quantum Size Effects on the Thermal and Potential Conductivities of Ideal Gases, *Phys. Scripta* vol. 80, 065402, 2009.
- [11] C. Firat, A. Sisman and Z. F. Ozturk, Thermodynamics of gases in nano cavities, *Energy* vol. 35, Sp.Iss.SI: pp. 814-819, 2010.
- [12] C. Firat and A. Sisman, Quantum forces of a gas confined in nano structures, *Phys. Scr.* vol. 87, 045008, 2013.
- [13] A. Sisman and G. Babac, Quantum Size Effects on Classical Thermosize Effects, *J. Continuum Mechanics & Thermodynamics* vol. 24, pp.339-346, 2012.
- [14] W. J. Nie, J. Z. He and X. J. He, A micro-/nano thermosize refrigerator and its performance analysis, *J. App. Phys.* vol. 103, 114909, 2008.
- [15] W. J. Nie and J. Z. He, Performance analysis of a thermosize micro/nano heat engine, *Phys. Lett. A* vol. 372, pp. 1168-1173, 2008.
- [16] W. J. Nie, J. Z. He and J. Du, Performance characteristic of a Stirling refrigeration cycle in micro/nano scale, *Physica A* vol. 388, pp. 318-324, 2009.
- [17] W. Nie and J. He, Quantum boundary effect on the work output of a micro-/nanoscaled Carnot cycle, *J. App. Phys.* vol. 105, 054903, 2009.
- [18] W. J. Nie, Q. Liao, C. Zhang, and J. He Micro-/nanoscaled irreversible Otto engine cycle with friction loss and boundary effects and its performance characteristics, *Energy* vol.35, pp. 4658-4662, 2010.
- [19] G. Su, L. Chen, T. Lin, and J. Chen, Thermosize Effects of Ideal Fermi Gases Confined in Micro/Nano-Scale Tubes, *J. Low Temp. Phys.* vol. 163, pp.275-283, 2011.

INTRINSIC QUANTUM THERMODYNAMICS: WHAT IT IS AND WHAT CAN BE DONE WITH IT

Michael R. von Spakovsky

Mechanical Engineering Department
Virginia Tech, Blacksburg, Virginia, 24061, USA

ABSTRACT

Experimental evidence over the last three decades has seen the emergence at atomistic scales of the phenomenon of “spontaneous decoherence”, which in turn has led to a revival of interest in matters related to the unitary foundations of quantum mechanics (QM) and what, if anything, non-equilibrium thermodynamics may have to say about this. Decoherence at these scales suggests the presence of non-linearities not envisioned by the unitary dynamics of QM, non-linearities that, in contrast, are foreseen by the dynamics of intrinsic quantum thermodynamics (IQT). IQT provides a reasonable, coherent, and comprehensive explanation for these non-linearities, unifying QM and thermodynamics into a single kinematics and dynamics applicable to all systems and all states and doing so in part by supplementing the postulates of QM by the 2nd law from which a physically meaningful nonlinear dynamics emerges. This paper provides a brief summary of a number of applications of this theory to non-reactive and reactive systems by the author and his co-workers along with comparisons of predicted results to experimental and numerical data found in the literature.

INTRODUCTION

New experimental evidence (e.g., [1-8]) over the last three decades has seen the emergence at atomistic scales of the phenomenon of “spontaneous decoherence”, which in turn has led to a revival of interest in matters related to the unitary foundations of quantum mechanics (QM) and what if anything non-equilibrium thermodynamics (NET) may have to say about this. This renewed interest is fuelled to a large extent by the impact that this phenomenon has on a large number of applications. Thus, understanding and predicting modern physics phenomena such as decoherence, entanglement and coherence structure, and dynamics in applications involving nanometric devices, fast switching times, clock synchronization, super-dense coding, quantum computation, teleportation, quantum cryptography, etc. [9-27] is of great importance. Since “spontaneous decoherence” at these scales suggests the presence of non-linearities not envisioned by the unitary dynamics of QM, a number of recent publications [28-33] have proposed possible fundamental tests of standard unitary QM, emphasizing on the basis of the fairly general ansatz developed in [28-32] “that if the pure states happen to be attractors of a nonlinear evolution, then testing the unitary propagation of pure states alone cannot rule out a nonlinear propagation of mixtures” [33].

This last statement is illustrated in the context of recent work on nonlinear Lie-Poisson dynamics [29-32]. However, testing these particular dynamics experimentally is necessarily a matter of guesswork since the physicality of these theories is quite obscure. In contrast, a physically meaningful nonlinear dynamics emerges when the postulates of QM are supplemented by both the 1st and 2nd laws of thermodynamics. In such an approach, the evolution of state of a quantum system is no longer unitarily constrained but can, in fact, occur non-unitarily in time. Thus, at the expense of only violating the unitary constraint, an approach such as intrinsic quantum thermodynamics (IQT) [34-56] (not to be confused with

quantum thermodynamics (QT), i.e., dissipative quantum dynamics [27,57]) provides an overall physical framework for such non-unitary evolutions. Central to IQT is the fact that the dynamics of any change in state is at all times consistent with the laws of physics and thermodynamics [34-40]. To satisfy both the requirements of thermodynamics, particularly that of the 2nd law, as well as those of QM, IQT relies on two fundamental insights. The first is that the ontological entity representing any state of a quantum system¹ is not the density operator (i.e., wave function projector) of QM, i.e., a projector onto a wave function,² but instead a density or “state” operator based on an ensemble consisting of an infinite number of identical systems identically prepared [34]. The second is that the Schrödinger equation of motion of QM, though correct, is incomplete since it is unable to describe the dynamics of a system with entropies greater than zero [34,37-40]. IQT completes this equation on the basis of the steepest-entropy-ascent (SEA) principle or today better known as the locally-maximal entropy generation (LMEG) dynamical law, which encompasses the Hatsopoulos-Keenan statement of the 2nd law via the Hatsopoulos-Gyftopoulos ansatz [34] as a theorem about the dynamical (Lyapunov) stability of equilibrium states [53]. This equation is able to describe the irreversible (i.e., non-linear and non-unitary) relaxation of system state to one of stable equilibrium based solely on changes occurring intrinsic to the system.

In contrast, QT, which presents an alternative framework, is based on the so-called “open-system model” in which the dynamics of relaxation to stable equilibrium result from assumed “weak-interactions”, i.e., statistical perturbations (the so-called Born-Markov approximation), with an environment or heat bath. However, the “dissipative” state evolutions,

¹ All systems are in the end quantum systems; but as the size of a system increases, the importance of quantum effects decreases, since the dispersions representing observables approach delta functions.

² The density operator of QM only represents a limited class of states and is, thus, a special case of the density operator of IQT.

which this approach predicts, are still linear in nature and, thus, can at best only mimic the non-linear dynamics that may be in play. Despite this weakness, QT has engendered a great deal of work over the last few decades [27,57-71]. Even so, whatever the reality of the assumed “weak interactions”, Nakatani and Ogawa [60] have shown that the Born-Markov approximation for obtaining evolution equations, i.e., quantum master equations (QMEs), cannot be used for composite systems in the strong-coupling regime, no matter how short the reservoir correlation time. Indeed, the assumption of very short correlation times is problematic even in the weak-coupling regime, since it comes at the expense of introducing the so-called Loschmidt paradox [72]. In other words, because the overall linear dynamics of the closed and isolated system-plus-environment composite is reversible and unitary, the assumption of weak coupling is equivalent to assuming that system and environment are effectively maintained decorrelated, which in turn gives rise to an irreversible and non-unitary linear dynamics of the system alone. This paradox as well as the inherent weaknesses outlined in [52] limit the applicability of these QMEs.

Other more traditional approaches to the modelling at the atomistic level of phenomena typically viewed as irreversible (e.g., heat transfer) are the so-called “closed quantum systems” (CQS) approach [73] and the two heat reservoirs mediated by a quantum system (HRQS) approach [74-95]. Results shown to date with the former [73] indicate that as long as a “persistent coherence” is maintained between the amplitudes of the different energy eigenlevels, the heat flux remains constant. This observation may indeed have important implications for other “irreversible” phenomena such as the decoherence of qubits, which is a major obstacle to the construction of quantum computers [18]. Thus, if a qubit were placed, for example, in contact with a non-equilibrium environment so that a persistent energy flux through the qubit could be induced, would it protect the qubit from complete decoherence? This question requires an answer, which needs further investigation to see if it can be answered generally in the affirmative and if so, how such a system and interaction could be set up. Note that an early candidate for the role of qubit, i.e., a trapped ion, can be described to *some* extent by the model of a particle confined to a harmonic potential well exposed to statistical perturbations due to electromagnetic noise [96–99]. It is also interesting to note that it can be described quite well by IQT [56], which is able to describe its behaviour in terms of a relaxation from a state of non-equilibrium to that of stable equilibrium.

As to the HRQS approach, results to date (e.g., [74]) show that certain quantities (i.e., a non-equilibrium temperature T_p equal to the kinetic energy of the quantum system (mediator) and another, T_x , to its potential energy) have proven useful in quantifying the strengths of the couplings between the mediator (quantum particle or system) and the heat reservoirs [91]. When the so-called friction kernel, which is a measure of the interaction between mediator and reservoirs, is non-zero, the difference between these two temperatures as well as between T_x and the average of the two reservoir temperatures is also non-zero; and, therefore, these temperatures and differences can be used as a measure of the quantum entanglement, i.e., the degree of coherence, between the mediator and reservoirs [91]. As a criterion for quantifying the coupling strength, these quantities are equally applicable to steady as well as unsteady state. Nonetheless, it is doubtful that the HRQS model even if modified could be used to determine

the rate of decoherence, which takes place as the composite system relaxes to stable equilibrium. In contrast, IQT is not limited in this way.

THE IQT APPROACH

At the heart of IQT is the concept that irreversible relaxations of state occur due to the intrinsic characteristics, i.e., endogenous (as opposed to exogenous) statistics, of the system itself. Thus, the framework of IQT suggests that “spontaneous decoherence” is a consequence of intrinsic system irreversibilities and that thermodynamics and in particular NET do indeed have a great deal to say about it. Beyond the theoretical work, which has laid the foundations for IQT, this assertion has found a number of verifications via experimental comparisons found in [41,44,56,100,101] and is reasonable in the context of a quantum system (even a one-particle system) in a non-equilibrium state spontaneously³ relaxing to stable equilibrium.

The foundations of IQT were developed by Hatsopoulos and Gyftopoulos [34] with important preliminary work by Park [35]. In 1981, Beretta contributed a fundamental dynamical postulate embodied in a non-linear equation of motion [37] consistent with the proof by Simmons and Park [36] that the evolution in state of a closed thermodynamic system to stable equilibrium is necessarily non-linear. Important subsequent work includes [38-56,100,101,106,107]. IQT asserts that the 2nd law of thermodynamics, with its implications of intrinsic irreversibility, applies at all physical levels of description from the macroscopic and classical to the atomistic and quantum [34]. Central to the foundations of IQT is the recovery of the concept of “state of a system”, a bedrock of physical thought and a concept lost in quantum statistical mechanics (QSM) where the state necessarily refers only to the state of an ensemble, which consists of an infinite number of identical systems not identically prepared [34,35]. Also central to IQT is the fact that the dynamics of any change in state is at all times consistent with the laws of physics and thermodynamics [34-40].

The rationale behind the concept that the density operator is synonymous with the state of a system is based on the idea that in QM the density operator contains all the information necessary to characterize the state (i.e., the so-called pure state) of a quantum system at any given instant of time. Thus, for example, the expectation value $\langle S \rangle$ for the entropy, as defined by von Neumann, can be written in terms of the density or “state” operator ρ via

$$\langle S \rangle = -k_B \text{Tr}(\rho \ln \rho) \quad (1)$$

Here k_B is Boltzmann’s constant. In QM, the value of $\langle S \rangle$ is necessarily zero for all pure states. For states whose entropy is greater than zero, the density operator of QM can be replaced with the von Neumann statistical operator of QSM. However, the problem which arises with using QSM to describe non-zero entropy states is that not only does this introduce the difficulty mentioned above about the loss of the concept of “state of the system” but as well leads to an entropy, which is not the entropy of thermodynamics [45]. In fact, QSM leads to the so-called ‘irreversibility paradox’, the resolution of which requires a simultaneous consideration of questions that specifically go to the heart of issues surrounding the 2nd law of thermodynamics, namely, i) what the physical roots of

³ A physical mechanism for such relaxations may, for example, be spontaneous emissions resulting from vacuum fluctuations and/or self-radiation reactions [102-105].

“entropy” and “irreversibility” are, ii) whether or not “entropy generation” due to irreversibility is merely a *statistical illusion*⁴, and iii) what a general description of *non-equilibrium* is [54]. Such a general description is not possible with QSM without the addition of a non-thermodynamic principle (microscopic reversibility), assumption (e.g., small perturbations to ensure linear behaviour), or approximation (e.g., sufficiently small deviations from stable equilibrium) [54]. In contrast, IQT and its density operator exhibit none of these drawbacks and instead lead to an entropy that is *physical* and exists for all zero-entropy and non-zero entropy states and all systems regardless of size. Moreover, the entropy at a fundamental level of description is seen as a measure of how the system energy $\langle E \rangle$ is distributed amongst the system’s available degrees of freedom, i.e., its energy eigenlevels, while the entropy generation is a measure of how the energy $\langle E \rangle$ is redistributed in a change of state [54].

The second insight mentioned above that the Schrödinger equation of motion is incomplete has prompted the search for an equation able to describe irreversible processes. In QT, this has led to master equations of various types [27,57]. These equations have been developed to model the “open quantum systems” introduced by Lindblad and Kossakowski and others [62-65] where the increase in the entropy of a system is brought about through interactions with an external reservoir. In IQT, the generalization to irreversible or “dissipative” processes is provided by an equation of motion originally developed by Beretta [37,39,40], which assumes a priori a tendency for an intrinsic increase in system entropy, i.e., the entropy of thermodynamics, along the direction of steepest entropy ascent compatible with the system’s constraints. Unlike the master equations of QT, which are often second order approximations [108], the Beretta equation represents the full nonlinear dynamics, which describes the irreversible evolutions in state of systems that are arbitrarily far from stable equilibrium.

Thus, the outlook provided by IQT avoids the inconsistencies pointed out by Loschmidt [72], which arise when trying to force the emergence of irreversible, non-unitary behaviour from dynamics that is intrinsically reversible and unitary. Avoided as well is the need for the exogenous statistics found in QSM that destroy the concept of state of a system by requiring that a system possessing entropy be described with heterogeneous ensembles of identical systems in “pure” states. Statistical mixtures of pure states have the additional inconsistency which arises when work can be extracted from subsets of the ensemble even though none can be extracted from the ensemble as a whole. Clearly, this violates the 2nd law [54].

IQT also avoids the violations of the 2nd law that are inherent with the QT approach. In contrast to QSM, QT is not based on statistical mixtures of pure states and, thus, the definition of “state of the system” is preserved. However, because the entropy for the “overall closed system” (i.e., open system plus reservoir) cannot increase, the potential for extracting energy to do work remains unchanged (i.e., is not degraded) regardless of whether gradients of thermodynamic potentials between the open system and reservoir exist and change over time. This cannot be since it suggests that regardless at what point in time energy is extracted that the

potential to do work remains unchanged even when all thermodynamic potentials have ceased to exist. This is inconsistent with what is observed in nature and, thus, violates the 2nd law. IQT obviates such difficulties because the increase in entropy is a process that is intrinsic to the closed (isolated) system, leading to a degradation in the potential to do work.

THE IQT EQUATION OF MOTION

The equation of motion of IQT governs how the diagonal and off-diagonal elements of the thermodynamic state or density operator (or matrix) ρ ⁵ evolve in time. The formulation is based on the hypothesis that physical systems naturally seek the path of local steepest entropy increase on their way to stable equilibrium [4,46,53,109]. For an isolated or non-isolated, single elementary constituent (i.e., a single particle, a single assembly of indistinguishable particles, or a single field) closed (i.e., not experiencing a non-work interaction) system, this equation is given by

$$\frac{d\rho}{dt} = -\frac{i}{\hbar}[H, \rho] + \frac{1}{2k_B\tau} \{ \Delta M, \rho \} \quad (2)$$

where H is the Hamiltonian operator and τ a scalar time constant or functional⁶. Both the 1st and 2nd laws of thermodynamics are implied by this equation and its other forms given below⁷. The first term on the right of this equation is the Schrödinger term, which governs the reversible (linear) dynamics for the system, and it along with the time-derivative term on the left are equivalent to the temporal part of the Schrödinger equation. This term governs the relative phases between system energy eigenlevels and quantum interference effects. The second term on the right, $\{ \Delta M, \rho \} / 2k_B\tau$, the so-called dissipation term, depends on ρ , $\ln\rho$, and H and pulls the state operator in the direction of the projection of the gradient of the entropy functional $\langle S \rangle$ onto the hyper-plane of constant system energy $\langle E \rangle$. This term governs the dissipation of a system’s adiabatic availability [111] as its state relaxes to one of maximal entropy and is written as

$$\{ \Delta M, \rho \} = \Delta M \rho + \rho \Delta M \quad (3)$$

where $M = S - H / \theta_H(\rho)$ (4)

$$\theta_H(\rho) = \langle \Delta H \Delta H \rangle / \langle \Delta S \Delta H \rangle \quad (5)$$

Here M is a non-equilibrium Massieu function and ΔH and ΔS are the deviation operators of H and S defined as

$$\Delta H = H - I \langle H \rangle \quad (6)$$

$$\Delta S = S - I \langle S \rangle \quad (7)$$

The S operator is expressed as

$$S = -k_B \ln(\rho + P_o) = -k_B B \ln \rho \quad (8)$$

with P_o and B , respectively, the projection operators onto the range and the kernel of ρ .

For a closed composite system composed of two distinguishable particles, assemblies of particles, fields, or a

⁵ The state operator is a linear, self-adjoint, non-negative definite, unit-trace operator (i.e., an operator whose diagonal elements sum to one) on Hilbert space \mathcal{H} .

⁶ Note, that a lower bound for τ and, thus, an upper bound on $\{ \Delta M, \rho \} / 2k_B$ may be suggested by the time-energy Heisenberg uncertainty relation [53].

⁷ This equation implies the 1st law because as is proven in Beretta et al. [39], each of the generators (e.g., the identity and Hamiltonian operators) of the motion (i.e., the evolution or change in state of the system) is also a constant of the motion of the system. Thus, $\langle E \rangle = \text{Tr}(\rho H)$ is conserved and the ΔE in any adiabatic process is uniquely related to the amount of work involved in the process. This equation also implies the 2nd law since as proven in Beretta et al. [39], a system admits of one and only one stable equilibrium state for given finite mean values of the generators of the motion. This, of course, is simply a generalization of the Hatsopoulos-Keenan statement of the second law [34,110].

⁴ In fact, this is the conclusion drawn from statistical mechanics that entropy generation due to irreversibility does not result from the endogenous dynamics but instead from temporal changes of some exogenous statistical description.

combination of these, Eq. (2) is replaced by the following equation [40,52,53]:

$$\frac{d\rho}{dt} = -\frac{i}{\hbar}[H, \rho] + \frac{1}{2k_B\tau_A} \left\{ (\Delta M)^A, \rho_A \right\} \otimes \rho_B + \frac{1}{2k_B\tau_B} \rho_A \otimes \left\{ (\Delta M)^B, \rho_B \right\} \quad (9)$$

where $(\Delta M)^J = (\Delta S)^J - (\Delta H)^J / \theta_H(\rho)$ (10)

$$(\Delta H)^J \equiv Tr_{\bar{J}} \left[(I_J \otimes \rho_{\bar{J}}) \Delta H \right] \quad (11)$$

$$(\Delta S)^J \equiv Tr_{\bar{J}} \left[(I_J \otimes \rho_{\bar{J}}) \Delta S \right] \quad (12)$$

and $J = A, B$, while $\bar{J} = B, A$. Equation (9) is easily generalized to three or more distinguishable constituents.

Finally, for a system experiencing a non-work interaction (i.e., a heat or mass interaction), the IQT equation of motion in the form of Eq. (2) may be extended to the following [56,112]:

$$\frac{d\rho}{dt} = -\frac{i}{\hbar}[H, \rho] + \frac{1}{2k_B\tau} \{ \Delta M, \rho \} + \frac{1}{2k_B\tau_G} \{ \Delta \tilde{G}, \rho \} \quad (13)$$

where the last term on the right accounts for either a heat or mass interaction. If the latter, \tilde{G} is a non-equilibrium, Massieu-like, mass-interaction operator as described in detail in [112]. If the former, \tilde{G} is a non-equilibrium Massieu heat interaction operator expressed as

$$\tilde{G} = \tilde{G}_Q(\tilde{H}, \tilde{S}) = \tilde{S} - \frac{\tilde{H}}{\tilde{\theta}_H} \quad (14)$$

where $\tilde{\theta}_H$ is a non-equilibrium temperature defined as

$$\tilde{\theta}_H = \frac{\langle \Delta \tilde{H} \Delta \tilde{H} \rangle}{\langle \Delta \tilde{H} \Delta \tilde{S} \rangle} \quad (15)$$

and the \tilde{S} and \tilde{H} operators result from a rotation of the original S and H operators, i.e.,

$$\begin{bmatrix} \tilde{S} \\ \tilde{H} \end{bmatrix} = \begin{bmatrix} 1 & 0 \\ 0 & T^* \end{bmatrix} \begin{bmatrix} \cos \varphi & -\sin \varphi \\ \sin \varphi & \cos \varphi \end{bmatrix} \begin{bmatrix} 1 & 0 \\ 0 & 1/T^* \end{bmatrix} \begin{bmatrix} S \\ H \end{bmatrix}. \quad (16)$$

The angle of rotation φ is a function of the slope of the heat interaction trajectory and is expressed as

$$\varphi = \tan^{-1}(T_Q/T^*). \quad (17)$$

The quantity T^* is a constant with units of temperature and a value of one, while T_Q is yet another non-equilibrium temperature that corresponds to the slope of the line in the energy versus entropy operator plane, which connects the current state of the system and a state in mutual stable equilibrium with the heat reservoir.

We now turn to a brief discussion of the application of each one of these equations of motion and a comparison of the results generated with experimental data found in the literature. The results presented and discussed are taken from [56,100,101]. Equation (2) is used to predict the reaction rate constant of the chemically reactive systems in [101] based on the IQT framework laid out by Beretta and von Spakovsky in [107], while Eq. (9) is employed to predict the rate of decoherence of a composite atom-field system [100]. Finally, Eq. (13) is utilized to predict the relaxation to stable equilibrium of a single ion in a cat state contained in a Paul trap as it interacts with a heat reservoir [56].

CHEMICALLY REACTIVE SYSTEM RESULTS

Since the IQT equation of motion implements the principle of SEA, its application to chemical kinetics is

consistent with the idea put forward by Ziegler [113] concerning the thermodynamic consistency of the standard model of chemical kinetics. In [107], Beretta and von Spakovsky develop a general modeling framework for applying IQT to chemically reactive systems at very small scales, i.e., to an isolated, chemically reactive mixture with one or more active reaction mechanisms. In modeling the non-equilibrium time evolution of state of these systems, both the system energy and particle number eigenvalue problems as well as the non-linear IQT equation of motion must be solved, i.e., in this case Eq. (2). The former establish the so-called energy and particle number eigenstructure of the system, i.e., the landscape of quantum eigenstates available for the system, while the latter determines the unique non-equilibrium thermodynamic path, i.e., unique cloud of trajectories, taken by the system, showing how the density operator, which represents the thermodynamic state of the system at every instant of time, evolves from a given initial non-equilibrium state to the corresponding stable chemical equilibrium state. Once this path is established, the time dependences of all the non-equilibrium thermodynamic properties (e.g., composition, chemical potentials, chemical affinities, reaction coordinates, reaction rates), including, of course, the entropy, are known. In fact, the reaction rate in the literature is typically reported at a given temperature in terms of the so-called reaction rate constant (i.e., the forward reaction rate constant), which is determined both experimentally as well as numerically via a plethora of classical (e.g., [114]), quasi-classical (e.g., [115-121]), and time-independent (e.g., [122,123]) and time-dependent quantum methods (e.g., [123,124]). The IQT results presented here and the more extensive ones in [101] are reported in terms of this parameter. It should be noted that no a priori limiting assumption of stable equilibrium via a specific choice of temperature nor of pseudo-equilibrium between reactant and activated complex, both of which are common to the other methods in the literature, is made. In addition, the reaction rate constants found via the IQT formulation are in reality not constants but instead instantaneous values found at each instant of time along the non-equilibrium path determined by the IQT equation of motion.

The IQT kinematic model for the chemically reactive system, which establishes the energy and particle number eigenstructure of the system, is not repeated here due to its complexity and, thus, the reader is referred to [101,107] for details. This model includes vibrational, rotational, and translational degrees of freedom consistent with the number and types of degrees of freedom used by other models found in the literature. The dynamic model is that of Eq. (2).

For purposes of the comparisons given below, the system considered here initially consists of 1 particle of F and 1 of H_2 and is governed by the following reaction mechanism:



An initial non-equilibrium state is established by finding a metastable equilibrium state far from equilibrium, which is then perturbed into the initial non-equilibrium state used by the equation of motion, Eq. (2). This equation evolves the system density or state operator ρ for the reacting mixture in time at constant system energy until a state of stable equilibrium is reached. The temperature at this final state is found to be 298 K. The degrees of freedom for each of the molecules and atoms in the IQT model are given in Table 1. Results for the non-equilibrium compositional changes of the reacting mixture are shown in Figure 1, while Figure 2 provides the instantaneous values of the forward and backward reaction rate

constants $k_f(T,t)$ and $k_b(T,t)$, respectively, at every instant of time t . Included as well is the equilibrium constant $K(T)$, which is the ratio between k_f and k_b . The time evolutions of the net, forward and backward reaction rates (i.e., r , r_f , and r_b) corresponding to these rate constants are shown in Figure 3. Similar time-evolutions for other non-equilibrium thermody-

Table 1. Degrees of freedom for each of the molecules and atoms in the IQT model [101].

Species	Translational quantum #'s ^a	Vibrational quantum #'s	Rotational quantum #'s
F	1,...,400		
H_2	1,...,400	0	0,1
FH	1,...,400	0,1,2,3	0,1,...,7
H	1,...,400		

^a Although the translational principal quantum number k varies here from 1 to 400 for each species, only a sampling (30) of these quantum numbers across this range is used for each species in the IQT model.

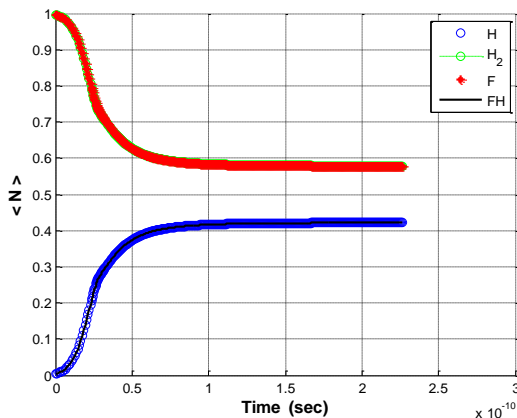


Figure 1. IQT time evolution of the non-equilibrium compositions of the reacting mixture reported as the number of particles for each species for a system expectation energy, which at stable equilibrium corresponds to a temperature of 298 K [101].

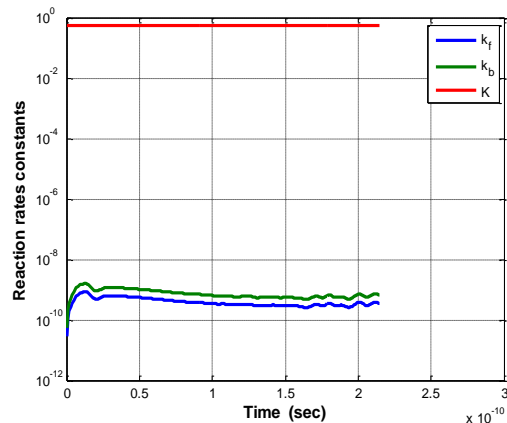


Figure 2. IQT time evolution of the forward and backward reaction rate constants and the equilibrium constant for a system expectation energy, which at stable equilibrium corresponds to a temperature of 298 K [101].

dynamic properties such as the reaction coordinate, reaction coordinate rate, entropy, entropy generation, species energies, non-equilibrium temperature, etc. can be generated. The relaxation time τ for the time evolutions presented in the previous figures is 3.8×10^{-15} sec and is based on a fit of the IQT results to the value of k_f at 298 K reported in the fourth column of Table 2 [101, 124]. This table also includes the values of k_f from a number of other researchers. Note that the computational time to complete a single evolution, which

provides a complete picture of the non-equilibrium quantum and thermodynamic evolution in time of the system is on the order of seconds for this size system on a conventional PC with a dual-core processor. Much larger systems have already been simulated.

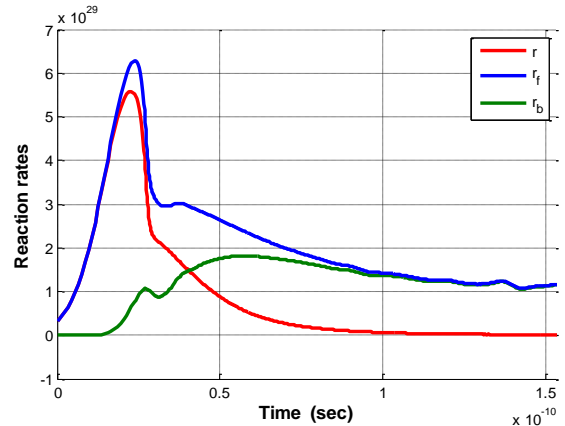


Figure 3. The forward, reverse and net reaction rates for a system expectation energy, which at stable equilibrium corresponds to a temperature of 298 K [101].

Table 2. Values of the forward reaction rate constant reported in the literature for the reaction mechanism of Eq. (18) [101,124].

T (K)	$k_f(T)/10^{-11}$ (cm ³ /molecule-sec)				
	WH ^a	SBA ^b	HBGM ^c	RHPB ^d	WTM ^e
298	2.33	2.48	2.93	2.81	2.26

^a Wurzberg and Houston; ^b Stevens, Brune, and Anderson; ^c Heidner, Bott, Gardner, and Melzer; ^d Rosenman, Hochman-Kowal, Persky, and Baer; ^e Wang, Thompson and Miller.

Finally, additional validation of the IQT predictions is needed via a comparison of the forward reaction rate constants predicted with IQT to those given in Table 2 based on a τ , which is a functional of the density operator ρ and which reflects the physics of the problem. This validation has not yet been done. The present author and his co-authors in [101] are currently working on identifying a unique functional $\tau(\rho)$ capable of capturing the dynamics of the reaction without the use of adjustable parameters.

COMPOSITE ATOM-FIELD SYSTEM RESULTS

In [100], the modeling of the non-linear dynamic change in state of a composite system formed by an atom and an electromagnetic field mode is accomplished using IQT (Eq. (9)). The state of the composite (closed and adiabatic) microscopic system evolves in time towards stable equilibrium, resulting in the loss of correlations between its constituents. The IQT description assumes the composite system to be isolated and the time evolution of its state to be intrinsically both Hamiltonian and non-Hamiltonian. In so doing, a loss of quantum entanglement or coherence is fully predicted.

The IQT model of the composite system considered here is that given in [100] and for sake of brevity is not repeated here. A description of the Cavity Quantum Electrodynamics (CQED) experimental system upon which the IQT theoretical model is based is given in [125-131,100]. A very brief description is provided here beginning with the experimental configuration depicted in Figure 4. Rb atoms are contained in oven B from which one atom in an excited state $|\psi_B\rangle = |e\rangle$ is selected and subsequently subjected to a classical resonant microwave

$\pi/2$ pulse in R_1 supplied by source S' . This creates a state in a superposition of circular Rydberg levels $|e\rangle$ and $|g\rangle$ (ground level) for the atom, corresponding to principal quantum numbers 51 and 50, respectively. The atom is then allowed to enter the high-Q quantum cavity C that contains an electromagnetic field mode in a Fock state $|\alpha\rangle$ previously injected into the cavity by an external source S . The atom-field interaction lasts for a time t_i and since the atom and cavity are off-resonant, absorption of photons is not exhibited during the interaction; and the atom only shifts the phase of the field mode by an amount ϕ . This dephasing provokes the coupling of the excited level of the atom to the field mode state with phase $|\alpha e^{i\phi}\rangle$ and the coupling of the ground state of the atom to the field mode state with phase $|\alpha e^{-i\phi}\rangle$. In this manner, an entanglement between the states of the constituents is created. After leaving the cavity, the atom is

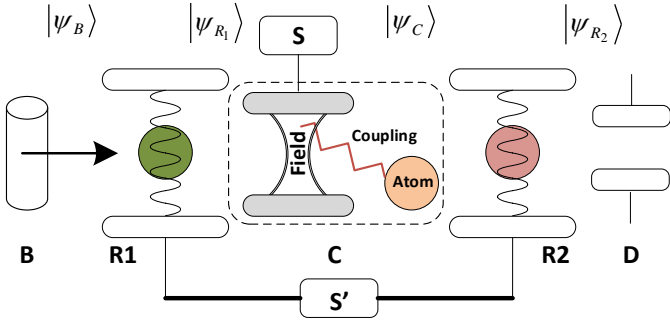


Figure 4. Schematic representation of an atom-field Cavity QED experiment [126,100].

subjected again to a resonant microwave pulse in R_2 equal to that at R_1 , mixing the atom energy levels and creating a “blurred” state for the composite, $|\psi_{R_2}\rangle$, which preserves the quantum ambiguity of the field phase. The excited level state of the Rb atom is then observed and recorder at D.

To measure the decay of coherence left on the field mode state by the Rb atom, a second atom of identical characteristics to the first is sent along the same path after a delay time of t_d . The state of the second atom recorded at D reveals the effects left by the first atom on the state of the field mode. A theoretical description of the experimental observations in [127] provides a functional for the correlation signal which is plotted in Figure 5 relative to the measured data found in [128]. The red triangles with error bars correspond to the experimental values, while the blue line corresponds to the theoretical prediction made using the correlation functional of [127]. The initial point of the correlation has been moved consistent with [128] from a value of 0.5 to 0.18 on the vertical axis to account for experimental imperfections. As can be seen the fit is good for the initial points but deviates at the end and even becomes negative, which is inconsistent with what is observed.

The IQT prediction is given by the green line, which is the norm $\|C\|$ of the commutator operator ($C = i[H, \rho]$). It is used as a direct indicator of how the coherence of the electromagnetic field mode is dissipated in time since the detection of the atom in the excited level state projects the state of the field in a maximally coherent local state. The green line corresponds to a value for the internal relaxation times of $\tau_A = \tau_B = 0.26$ for the atom and field in Eq. (9). This value is comparable to that reported in [132]. As in the case of the correlation functional, the maximum value for $\|C\|$ is moved to

0.18 on the vertical axis. As seen in this figure, IQT predicts the experimental data well. A very slight deviation from the

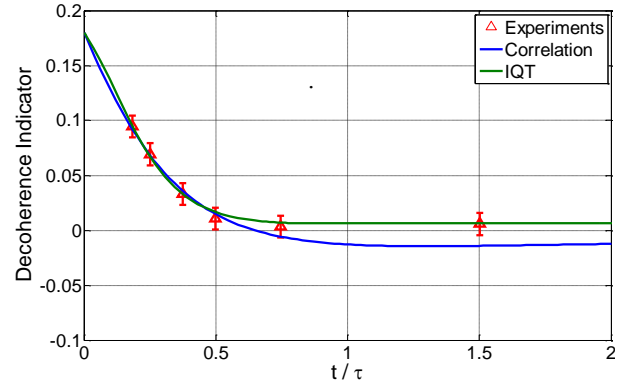


Figure 5. Comparison of the loss of coherence predicted by IQT and by the correlation function of [127] with the CQED experimental results of the group at Paris [128].

experimental values is observed with the fourth and fifth points but is well within the experimental error bars. The deviation may correspond to normal imperfections in the experimental equipment (e.g., the quality of mirror reflections which allows a leak of photons from the cavity [130, 133]); or it may be that the value chosen for τ_A and τ_B do not completely take into account the physical characteristics of the constituents. For example, it may be that slightly differing values for each relaxation time are needed or that these times are instead functionals of the state operator as described in [37, 134].

SINGLE TRAPPED ION SYSTEM RESULTS

In [56], the modeling of the non-linear dynamic change in state of a single ion system in an excited cat state interacting with a heat reservoir is accomplished using IQT and Eq. (13). In this case, the system is not isolated and experiences a heat interaction. The time evolution of its state is intrinsically governed by the dissipation term and extrinsically by the heat interaction term in Eq. (13).

The IQT model for this system is that given in [56] and for sake of brevity is not repeated here. A description of the experimental system upon which the theoretical model is based is given in [96,97,56] and involves a single trapped ion contained in a Paul trap put into various quantum superposition states. A very brief description is provided here beginning with the experimental configuration depicted in Figure 6. The decay of the initial state is observed and measured after the ion trap is

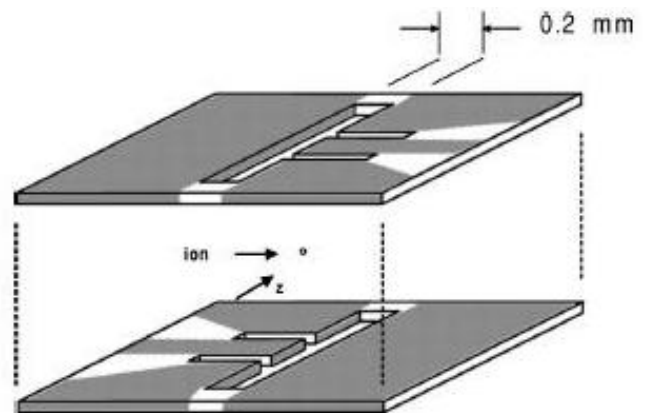


Figure 6. Schematic of the Paul trap used in the experiment of Turchette et al. [97].

put into contact with a range of engineered external electromagnetic sources. Radio frequency fields are produced to trap an ion, while noise signals serve as an external electromagnetic source. The strength of the fields is quadratic so the particle behaves as a quantum harmonic oscillator within the trap. The harmonic superposition or “cat” or “motional” states that are produced in the experiments are also known as Fock states, and density matrices describing these states contain only diagonal elements [96]. The amount of decoherence over time is measured using interferometry techniques. Nuclear spin states in the ion are excited and combined by means of optical pumping and laser cooling methods with the superpositions of the motional eigenstates of interest. The spins constitute a “carrier” signal that enables the degree of decoherence of the cat states to be readily measured. Because the spin states are correlated with the energy eigenstates of the harmonic oscillator, any changes or degradation of the cat state result in proportional changes between the phases of the spin eigenstates. During the experimental procedure, a state is created and immediately coupled to the electromagnetic source. After a given delay, a measurement is made. The phase shift between the spin components is seen as a loss of signal contrast from which the magnitude of decoherence of the cat state is calculated. The electromagnetic source consists of a noise spectrum of a given mean frequency and power that is applied to the fields containing the ion in the Paul trap. Numerous measurements are conducted to produce ensemble average values that make up each experimental data point.

Both Turchette et al. [96] using QT and Smith and von Spakovsky using IQT [56] have successfully modelled the decay (i.e. decoherence) observed in this first experiment. Levin et al. have studied this problem minus the external source using CQS [73]. The IQT simulations use 100 equally spaced energy eigenlevels to represent the lowest eigenlevels of the trap. Results are presented here for one of the superposition eigenstates experimentally studied in [97], i.e., cat state $|3\rangle$ which is the state associated with the energy eigenlevel three levels above the ground energy level. In the experiments, the power applied to the heat source $\langle V^2 \rangle$ is used to represent the relaxation time.

Results for the IQT simulations are compared with the experimental probability distribution versus time data in Figure 7 as well as with experimental data plotted on the energy-entropy diagram in Figure 8 [56]. The temperatures of the heat reservoirs of the experiment are estimated by noting the tightness of the probability distribution for the data as stable equilibrium is approached. In Figure 7, comparisons between the IQT results and the experimental data for the lowest 5 energy eigenlevels of the cat state are shown. The experimental data is indicated by the symbols. The solid lines are the probabilities predicted by IQT using Eq. (13). The time constants used for the IQT simulation are $\tau = 20.0$ and $\tau_G = 25.0$ for the dissipation term and heat interaction term, respectively. The scaled reservoir temperature in each figure for a Boltzmann constant set to 1.0 is estimated to be 0.15. As can be seen, the IQT simulation matches the data quite well.

Comparisons with the experimental data shown in Figure 8 include predictions from the QT quantum master equation used in [97] and from the IQT equation of motion, Eq. (13). Comparisons are made for the 5 lowest eigenlevels with the experimental data given in dark blue, those for QT in light blue

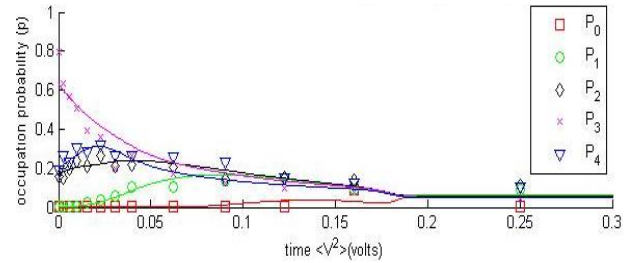


Figure 7. Comparison of the experimentally measured dissipative decay of cat state $|3\rangle$ with IQT predictions [56].

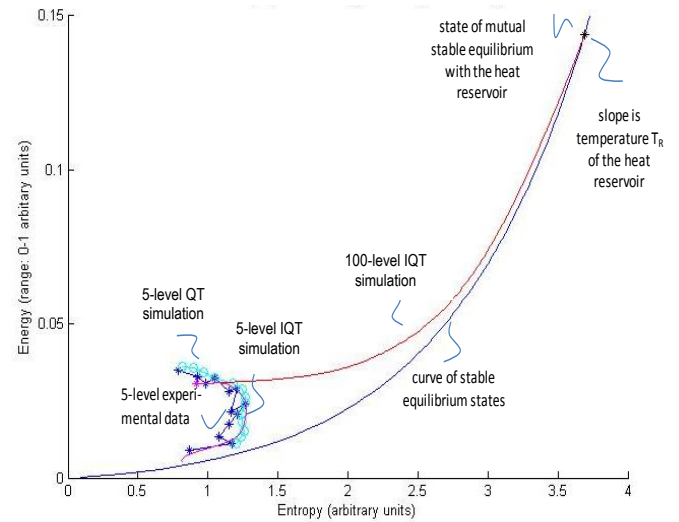


Figure 8. Non-equilibrium evolutions in thermodynamic state for the lowest 5 energy eigenlevels as well as for the lowest 100 [56].

and those for IQT in magenta. Note that the fact that the experimental data as well as the QT and IQT trajectories curve back on themselves is, of course, physically impossible, i.e., violates the 2nd law. However, this occurs here solely due to the fact that these trajectories are only based on the lowest 5 energy eigenlevels. When 100 eigenlevels are considered, the result for the IQT equation of motion is the magenta curve, which shows the evolution in state predicted by IQT from the initial state designated by the cross in magenta to a state of mutual stable equilibrium with the heat reservoir. Clearly, the IQT simulations do a good job of matching the experimental data, providing an alternative, comprehensive, and reasonable explanation to that provided by QT.

CONCLUSIONS

This paper has provided a brief summary of what IQT is and what can be done with it. The power of this rather unique approach has been illustrated via a number of applications of the IQT framework to non-reactive and reactive systems. Validations of this theory via comparisons of predicted results to experimental and numerical data found in the literature demonstrate the power of this approach and support the claim that IQT provides an alternative, comprehensive, and reasonable explanation of irreversible phenomena at an atomistic level.

REFERENCES

- [1] Bollinger, J. J., et al., 1989, *Phys. Rev. Lett.* **63**, 1031.
- [2] Walsworth, R. L., Silvera, F., Mattison, E. M., Vessot, R. F. C., 1990, *Phys. Rev. Lett.* **64**, 2599.
- [3] Chupp T. E., Hoare, R. J., 1990, *Phys. Rev. Lett.* **64**, 2261.

- [4] P. K. Majumder, P. K., et al., 1990, *Phys. Rev. Lett.* **65**, 2931.
- [5] Benatti, F., Floreanini, R., 1996, *Phys. Lett. B* **389**, 100 and 1999, *Phys. Lett. B* **451**, 422.
- [6] Lisi, E., Marrone, A., Montanino, D., 2000, *Phys. Rev. Lett.* **85**, 1166.
- [7] Klapdor-Kleingrothaus, H. V., Päs, H., Sarkar, U., 2000, *Eur. Phys. J. A* **8**, 577.
- [8] D. Hooper, D., Morgan, D., E. Winstanley, E., 2005, *Phys. Lett. B* **609**, 206.
- [9] Weinberg, S., 1989, *Phys. Rev. Lett.* **62**, 485.
- [10] Stern, A., Aharonov, Y., Imry, Y., 1990, *Phys. Rev. A* **41**, 3436.
- [11] Ekert, A. K., 1991, *Phys. Rev. Lett.* **67**, 661.
- [12] Holyst, J. A., Turski, L. A., 1992, *Phys. Rev. A* **45**, 6180.
- [13] Vidal, G., Werner, R. F., 1993, *Phys. Rev. A* **65**, 032314.
- [14] Unruh, W. G., Wald, R. M., 1995, *Phys. Rev. D* **52**, 2176.
- [15] Bennett, C. H., Brassard, G., Popescu, S., Schumacher, B., Smolin, J. A., Wootters, W. K., 1996, *Phys. Rev. Lett.* **76**, 722.
- [16] Grigorescu, M., 1998, *Physica A* **256**, 149.
- [17] Miranowicz, A., Matsueda, H., Wahiddin, M. R. B., 2000, *J. Phys. A: Math. Gen.* **33**, 5159.
- [18] Nielsen, M. A., Chung, I. L., 2002, *Quantum Computation and Quantum Information*. Cambridge Univ. Pres., Cambridge.
- [19] Bergmann, G., 1984, *Phys. Rep.* **107**, 1.
- [20] Pierre, F., Gougam, A. B., Anthore, A., Pothier, H., Estève, D., Birge, N., 2003, *Phys. Rev. B* **68**, 085413.
- [21] Washburn, S., Webb, R., 1986, *Adv. Phys.* **35**, 375.
- [22] Pierre, F., Birge, N., 2002, *Phys. Rev. Lett.* **89**, 206804.
- [23] Sigwarth, O., Labeyrie, G., Jonckheere T., Delande, D., Kaiser, R., Miniatura, C., 2004, *Phys. Rev. Lett.* **93**, 143906.
- [24] Buchleitner, A., Viviescas, C., Tiersch, M. (eds.), 2009, *Entanglement and Decoherence: Foundations and Modern Trends*, Lect. Notes in Phys. 768, Springer.
- [25] Kleinekathöfer, U., 2009, *Time-local quantum master equations and their applications to dissipative dynamics and molecular wires, energy transfer dynamics in biomaterial systems*, Springer Series in Chemical Physics **93**, 339, DOI 10.1007/978-3-642-02306-4_10.
- [26] Rand, S. C., 2010, *Lectures on Light: Nonlinear and Quantum Optics using the Density Matrix*. Oxford Univ. Press, Oxford, UK
- [27] Weiss, U., 2008, *Quantum Dissipative Systems*. World Scientific, series in Modern Condensed Matter Physics – vol. 13, Singapore-London
- [28] Domokos, G., Kovési-Domokos, S., 1999, *J. Phys. A: Math. Gen.* **32**, 4105.
- [29] Czachor, M., 1998, *Phys. Rev. A* **57**, 4122
- [30] Czachor, M., Kuna, M., 1998, *Phys. Rev. A* **58**, 128
- [31] Czachor, M., Naudts, J., 1999, *Phys. Rev. E* **59**, R2497
- [32] Jordan, T. F., 1993, *Ann. Phys. (N.Y.)*, **225**, 83 .
- [33] S. Gheorghiu-Svirschevski, S., 2001, *Phys. Rev. A* **63**, 022105 and the Addendum, *Phys. Rev. A* **63**, 054102.
- [34] Hatsopoulos, G. N., Gyftopoulos, E. P., 1976, *Found. Phys.* **6**, 15-31, 127-141, 439-455, 561-570.
- [35] Park, J. L., 1968, *Am. J. Phys.* **36**, 211.
- [36] Simmons Jr., R. F., Park, J. L., 1981, *Found. Phys.* **11**, 297.
- [37] Beretta, G. P., 1981, *On the general equation of motion of Quantum Thermodynamics and the distinction between quantal and nonquantal uncertainties*, Sc.D. dissertation, (advisor: E. P. Gyftopoulos, MIT, Cambridge, MA). arXiv:quant-ph/0509116
- [38] Park, J. L., Simmons Jr., R. F., 1983, “The knots of thermodynamics: Old and New Questions in Physics,” *Cosmology, Philosophy, and Theoretical Biology*, ed. A. van der Merwe (New York: Plenum).
- [39] Beretta, G. P., Gyftopoulos, E. P., Park, J. L., Hatsopoulos, G. N., 1984, *Il Nuovo Cimento B*, **82**, 169.
- [40] Beretta, G. P., Gyftopoulos, E. P., Park, J. L., 1985, *Nuovo Cimento B*, **87**, 77.
- [41] Beretta, G. P., 1985, *Int. J. Theor. Phys.* **24**(12), 1233.
- [42] Beretta, G. P., 1986, *Frontiers of Nonequilibrium Statistical Physics: Proc. of the NATO Advanced Study Institute (Santa Fe, 1984) Series B: Physics* **135**, ed. G. T. Moore, M.O. Scully (N.Y.: Plenum) p.193 and p.205.
- [43] Beretta, G. P., 1987, *Found. Phys.* **17**, 365.
- [44] Çubukçu, E., 1993, *Thermodynamics as a nonstatistical theory*, Sc.D. dissertation, M.I.T.
- [45] Gyftopoulos, E. P., Çubukçu, E., 1997, *Phys. Rev. E* **55**, 3851-3858.
- [46] Beretta, G. P., 1986, *Lecture Notes in Physics*, **278**, 441.
- [47] Gyftopoulos, E. P., von Spakovsky, M. R., 2003, *J. of En. Res. Tech.* ASME transactions, **125**, 1, 1-8.
- [48] Beretta, G. P., Gyftopoulos, E. P., 2004, *J. Chem. Phys.* **121**, 2718.
- [49] Beretta, G. P., 2005, *Mod. Phys. Letters A*, **20**, 977.
- [50] Beretta, G. P., 2006, *Phys. Rev. E* **73**, 026113.
- [51] Beretta, G. P., 2008, *Entropy*, **10**, 160.
- [52] Beretta, G. P., 2009, *Reports on Math. Phys.* **64**, 139.
- [53] Beretta, G. P., 2010, *J. Phys.: Conf. Ser.* **237**, 012004.
- [54] von Spakovsky, M. R., 2008, *Am. Inst. Phys. CP Series* **1033**, 1, 302.
- [55] Smith, C. E., Sciacovelli, A., von Spakovsky, M. R., Verda, V., 2010, *J. of Phys.: Conf. Series*, **237**, 012022.
- [56] Smith, C. E., von Spakovsky, M. R., 2012, *J. of Phys.: Conf. Series*, **380**, 012015.
- [57] Blum, K., 1996, *Density Matrix Theory and Applications*, 2nd ed., Physics of Atoms and Molecules Series, Plenum Press, NY.
- [58] Coffey, W. T., Kalmykov, Y. P., Titov, S. V., Mulligan, B. P., 2007, *A Lett. J. Explor. Front. Phys.*, EPL, **77**, 20011.
- [59] Yu, T., Diosi, L., Gisin, N., Strunz, W. T., 2000, *Phys. Lett. A* **265**, 331–336.
- [60] Nakatani, M., Ogawa, T., 2010, *J. Phys. Soc. Jpn.* **79**, 084401.
- [61] Pomyalov, A., Tannor, D. J., 2005, *J. of Chem. Phys.* **123**, 20, 204111.
- [62] Kossakowski, A., 1972, *Bull. Acad. Sci. and Math.* **20**, 1021.
- [63] Kossakowski, A., 1972, *Rep. on Math. Phys.* **3**, 247.
- [64] Ingarden, R. S., Kossakowski, A., 1975, *Annals of Phys.* **89**, 451.
- [65] Lindblad, G., 1976, *Comm. in Math. Phys.* **48**, 2, 119.
- [66] Giddings, S. B., Strominger, A., 1988, *Nucl. Phys. B* **307**, 854.
- [67] Ellis, J., Mavromatos, N. E., Nanopoulos, D., 1992, *Phys. Lett. B* **293**, 142.
- [68] Huet, P., Peskin, M. E., 1995, *Nucl. Phys. B* **434**, 3.
- [69] Ellis, J., Lopez, J. L., Mavromatos, N. E., Nanopoulos, D., 1996, *Phys. Rev. D* **53**, 3846.
- [70] Chang, C.-H., Dong, H.-S., Feng, X.-C., Li, X.-Q., Ma, F.-C., Tao, Z.-J., 1997, arxiv.org:hep-ph/9711310.
- [71] Benatti, F., Floreanini, R., 2000, *J. High Energy Phys.* **2**,

- 32.
- [72] Loschmidt, J., 1876, *Sitzungsber. Kais. Akad. Wiss. Wien, Math. Naturwiss. Classe* **73**, 128–142.
- [73] Levin, G. A., Jones, W. A., Walczak, K., Yerkes, K. L., 2012, *Phys. Rev. E* **85**, 031109
- [74] Panysyuk G. Y., Levin, G. A., Yerkes, K. L., 2012, *Phys. Rev. E.*, **86**, 021116.
- [75] Landauer, R., 1970, *Philos. Mag.* **21**, 83.
- [76] Anderson, P. W., Thouless, D. J., Abrahams, E., Fisher, D. S., 1980, *Phys. Rev. B* **22**, 3519.
- [77] Imry, Y., Landauer, R., 1999, *Rev. Mod. Phys.* **71**, S306.
- [78] Lepri, S., Livi, R., Politi, A., 2003, *Phys. Rep.* **377**, 1.
- [79] Dhar, A., 2008, *Advances in Phys.* **57**, 457.
- [80] Dubi, Y., Di Ventra, M., 2011, *Rev. of Modern Phys.* **83**, 131.
- [81] Jortner, J., Ratner, M. (eds.), 1997, *Molecular Electronics*, Blackwell Science, Oxford.
- [82] Hanggi, P., Ratner, M., Yalíkari, S., 2002, *Chem. Phys.* **281**, 111.
- [83] Boneto, F., Lebowitz, J. L., Rey-Bellet, L., 2000, *Fourier law: A challenge to theorists*, in *Mathematical Physics 2000*, Imperial College Press, London.
- [84] Senitzky, I. R., 1960, *Phys. Rev.* **119**, 670.
- [85] Mori, H., 1965, *Prog. Theor. Phys.* **33**, 423.
- [86] Ford, G.W., Cac, M., Mazur, P., 1965, *J. Math. Phys.* **6**, 504.
- [87] Haken, H., 1975, *Rev. Mod. Phys.* **47**, 67.
- [88] Klimontovich, Y. L., 1997, *Statistical Theory of Open Systems*, Kluwer, Amsterdam.
- [89] Caldeira, A. O., Leggett, A. J., 1983, *Physica A* **121**, 587.
- [90] Allahverdyan, A. E., Nieuwenhuizen, Th. M., 2000, *Phys. Rev. Lett.* **85**, 1799.
- [91] Nieuwenhuizen, Th. M., Allahverdyan, A. E., 2002, *Phys. Rev. E* **66**, 036102.
- [92] Zürcher, U., Talkner, P., 1990, *Phys. Rev. A* **42**, 3278.
- [93] Saito, K., Takesue, S., Miyashita, S., 2000, *Phys. Rev. E* **61**, 2397.
- [94] Dhar, A., Shastry, B. S., 2003, *Phys. Rev. B* **67**, 195405.
- [95] Segal, D., Nitzan, A., Hanggi, P., 2003, *J. Chem. Phys.* **119**, 6840
- [96] Turchette, Q. A., Kielinski, D., King, B. E., Leibfreid, D., Meekhof, D. M., Myatt, Rowe, M. A., C. J., Sackett, C. A., Wood, C. S., Itano, W. M., Monroe, C., Wineland, D. J., 2000, *Phys. Rev. A* **61**, 063418.
- [97] Turchette, Q. A., Myatt, C. J., King, B. E., Sackett, C. A., Kielinski, D., Itano, W. M., Monroe, C., Wineland, D. J., 2000, *Phys. Rev. A* **62**, 053807.
- [98] Myatt, C. J., King, B. E., Turchette, Q. A., Sackett, C. A., Kielinski, D., Itano, W. M., Monroe, C., Wineland, D. J., 2000, *Nature (London)* **403**, 269.
- [99] Leibfreid, D., Blatt, R., Monroe, C., Wineland, D., 2003, *Rev. Mod. Phys.* **75**, 281.
- [100] Cano-Andrade, S., Beretta, G. P., von Spakovsky, M. R., 2013, *12th Joint European Thermodynamics Conference*, Brescia, Italy, July 1-5.
- [101] Al-Abbasi, O., von Spakovsky, M. R., Beretta, G. P., 2013, *12th Joint European Thermodynamics Conference*, Brescia, Italy, July 1-5.
- [102] Milonni, P. W., 1984, *Am. J. of Phys.* **52**(4), 340.
- [103] Milonni, P. W., 1982, *Phys. Rev. A* **25**(3), 1315.
- [104] Armijo, J., 2012, *Phys. Rev. Lett.* **108**, 225306
- [105] Monroe, D., 2012, *Phys.* **5**, 62.
- [106] Cano-Andrade, S., Beretta, G. P., von Spakovsky, M. R., 2013, *ASME IMECE*, paper no. IMECE2013–63596, Nov. 15-21, San Diego, CA.
- [107] Beretta, G. P., von Spakovsky, M. R., 2013, in preparation.
- [108] Zhu, W., Rabitz, H., 2005, *J. of Math. Phys.* **46**, 022105.
- [109] Beretta, G. P., 2008, *Am. Inst. of Phys. CP Series*, **1033**, 180.
- [110] Hatsopoulos, G. N., Keenan, J. H., 1965, *Principles of General Thermodynamics* (New York: Wiley).
- [111] Gyftopoulos, E. P., Beretta, G. P., 2005, *Thermodynamics: Foundations and Applications* (2nd ed., New York: Dover).
- [112] Smith, C. E., 2012, *Intrinsic Quantum Thermodynamics: Application to hydrogen storage on a carbon nanotube and theoretical consideration of non-work interactions*, Ph.D. dissertation (advisor: M. R. von Spakovsky, Virginia Tech, Blacksburg).
- [113] Ziegler H., 1983 *J of Applied Math. and Phys. (ZAMP)* **34** 832-844.
- [114] Wilkins, R. L., 1972, *J. of Chem. Phys.*, **57**(2), pp. 912-917.
- [115] Karplus, M., Porter, R. N., Sharma, R. D., 1965, *Journal of Chemical Physics*, **43**(9), pp. 3259-3287.
- [116] Fernandez-Ramos, A., Ellingson, B. A., Garrett, B. C. *et al.*, 2007, *Rev. in Compu.l Chem.*, pp. 125-232: Wiley.
- [117] Simons, J. *An introduction to theoretical chemistry*, Cambridge; N. Y.: Cambridge University Press, 2003.
- [118] Manthe, U., Miller, W. H., *Journal of chemical physics*, **99**, pp. 3411, 1993.
- [119] Garrett, B. C., Truhlar, D. G., Grev, R. S. *et al.*, 1980, *J. of Phys. Chem.*, **84**(13), 1730-1748, 1980/06/01.
- [120] Marcus, R. A., Coltrin, M. E., 1977, *Journal of Chemical Physics*, **67**(6), pp. 2609-2613.
- [121] Yang, X. and Liu, K., 2004, *Modern Trends in Chemical Reaction Dynamics: Experiment and Theory*: World Scientific Publishing Company Incorporated.
- [122] Schatz, G. C., 1996, *Journal of Physical Chemistry*, **100**(31), pp. 12839-12847, 1996/01/01.
- [123] Neuhauser, D., Baer, M., Judson, R. S. *et al.*, 1991, *Computer Physics Communications*, **63**(1), pp. 460-481.
- [124] Wang, H., Thompson, W. H., and Miller, W. H., 1998, *J. of Physical Chemistry A*, 102(47), pp. 9372-9379.
- [125] Zhou, X., Dotsenko, I., Peaudecerf, B., Rybarczyk, T., Sayrin, C., Gleyzes, S., Raimond, J. M., Brune, M. and Haroche, S., 2012, *Phys. Rev. Lett.*, **108**, p. 243602.
- [126] Haroche, S., Brune, M., Raimond, J. M., 2013, *Physics Today*, **66**, 1, 27..
- [127] Raimond, J. M., Brune, M., Haroche, S., 1997, *Phys. Rev. Lett.*, **79**.
- [128] Brune, M., Hagley, E., Dreyer, J., Maitre, X., Maali, A., Wunderlich, C., Raimond, J. M., Haroche, S., 1996, *Phys. Rev. Lett.*, **77**, 4887–4890.
- [129] Deleglise, S., Dotsenko, I., Sayrin, C., Bernu, J., Brune, M., Raimond, J. M. and Haroche, S., 2008, *Nature Letters*, **455**, 510-514.
- [130] Haroche, S., Raimond, J. M., *Exploring the quantum*. Oxford, UK: Oxford University Press, 2006.
- [131] Raimond J. M., Haroche, S., 2007, *Quantum Decoherence*. **48**, ed: Birkhäuser Verlag Basel, p. 33-83.
- [132] Brune, M., Schmidt-Kaler, F., Maali, A., Dreyer, J., Hagley, E., Raimond, J. M., Haroche, S., 1996, *Phys. Rev. Lett.*, **76**, 1800–1803.
- [133] Raimond, J. M., Brune, M., Haroche, S., 2001, *Reviews of Modern Physics*, **73**, 565-582.
- [134] Beretta, G. P., 2006, *Int. J. of Thermodynamics*, **9**, 117.

PANEL L

**COMPUTATION OF THERMODYNAMIC
PROPERTIES, PHASE EQUILIBRIA, AND MIXING
AND SEPARATION DYNAMICS OF INDUSTRIAL
BLENDS AND NANOSTRUCTURED FLUIDS**

COMBINING CONSTANT PROPERTY PREDICTION TECHNIQUES FOR WIDER APPLICABILITY AND IMPROVED ACCURACY

Neima Brauner*, Mordechai Shacham^o

* School of Engineering, Tel-Aviv University, Tel-Aviv, Israel

^o Chem. Eng. Dept., Ben-Gurion University, Beer-Sheva, Israel

ABSTRACT

The property prediction field is a continuously evolving field where the objective is to extend the capabilities to additional groups of compounds and to additional properties, and to reach the ultimate goal of prediction accuracy within the uncertainty level of the experimental data. We have shown that these goals cannot be reached by using one type of technique (like group contribution, QSPR or QPPR). A broader algorithm should be developed which can fit the most adequate prediction technique/s to a wide range of compound-property combinations.

A general procedure for development a constant property prediction system is proposed. The procedure includes continuous update and maintenance of the physical property database, mapping the range of applicability of the descriptors in the descriptor database and checking the self-consistency of both the descriptor and property values. Included are also general guidelines and recommendations for the selection of the prediction method, the most appropriate training set and the regression technique to be used for a particular target compound-property combination.

INTRODUCTION

Current state of the art property prediction techniques rely on the use of databases which contain molecular structure related information and the corresponding physical property data for deriving property prediction models. These models are consequently used for predicting properties of "target" compounds for which only molecular structure related information is available. For example, the QSPR (Quantitative Structure Property Relationship) methods use molecular descriptors for representation of the molecular structure. Prediction models, in terms of molecular descriptors, are derived using stepwise linear or nonlinear regressions, artificial neural networks, particle swarm algorithms etc. The accuracy of the QSPR predictions is often limited because the "training set" used for deriving the QSPR may not adequately represent the structure and properties of some of the target compounds.

In contrast to the QSPRs, the "Group Contribution"(GC) methods use training sets "similar" to the target compound in order to derive models which represent the property variation in terms of the functional groups of the target compound. The compounds included in the training set (i.e., "predictive compounds") are supposed to represent the functional groups of the target compound. State of the art GC methods also discriminate between properties that change linearly with the molecular mass (M_w), such as liquid molar volume, enthalpy and entropy of formation, and properties that change nonlinearly with M_w (e.g., critical temperature and pressure and normal boiling point). Nonlinear change of some properties requires derivation of nonlinear prediction models, which are less reliable in extrapolation and involve the use of less rigorous nonlinear regression techniques. Independent studies (Poling et. al., [1]) have shown that the presently used GC methods yield predictions of satisfactory accuracy for

several properties and various groups of compounds. However, there are groups of compounds (e.g. low M_w or very high M_w) and certain properties (such as solid properties) for which the prediction accuracies are unsatisfactory. By satisfactory accuracy we mean that the prediction error is within the experimental uncertainty level of the pertaining property data of the training set members.

Brauner et. al.,[2] have developed the so called Targeted QSPR (TQSPR) method. Using this method a unique linear QSPR is derived for a particular property of a selected target compound. The training set that is used for the derivation of the TQSPR is automatically selected by the TQSPR algorithm, and essentially includes compounds that contain the functional groups present in the target compound. The selection of descriptors to the QSPR model is performed by applying a step wise regression algorithm, which considers also the noise in the data. Since the functional groups are included in the descriptor database, the TQSPR method actually represents a generalization of the GC method. The availability of additional large number of descriptors that are related to the chemical structures of the compounds included in the training set enables the representation of the property variation within the selected training set by a linear model (rather than a nonlinear model which is often required in the GC method). The larger the training set size is, larger number of descriptors required to adequately represent the property variation. The number of descriptors that can be selected to the TQSPR model is limited only by the noise level in the data due to experimntal errors in the property values of the training set members [2]. However, larger training sets and more descriptors in the TQSPR model cause difficulties in estimating the prediction errors for the target compound and for the other (structurally similar) compounds which are not

members the training set.

To reach the goal of minimizing the error associated with the predicted property value of the target compound (to the data uncertainly level) Shacham et al.,[3,4] suggested to tailor a tight training set to the target compound, which includes a limited number of compounds with high structural similarity to the target compound. Such a tight training set enables derivation of a linear TQSPR model in terms of a single descriptor (TQSPR1 model). The use of a single descriptor TQSPR1 model enabled development of several statistical indicators associated with the information pertaining only to the training set that enable reliable estimation of the prediction error for the desired property value of the target compound.

We have employed the TQSPR1 method (Shacham et al., [3]) for predicting 15 constant properties for 80 groups of compounds in order to discriminate between the property-compound combinations for which predictions of satisfactory accuracy are obtained and those associated with excessive prediction errors. Causes of excessive prediction errors that were identified, which are common to all QSPR methods, will be discussed below. These types of errors can be easily prevented by a careful selection of the training-set compounds and/or the descriptor for the TQSPR1 model.

There are however certain compound/property combinations for which neither the TQSPR/TQSPR1 methods (nor the GC methods) can provide predictions of satisfactory accuracy. One such combination involves the prediction of properties that change nonlinearly with M_w for long chain substances by extrapolation. Another combination involves prediction of solid properties (normal melting point and heat of fusion) in the region where differentiation between odd and even n_c compounds is required. In the following the three methods that we have developed: TQSPR1 (Shacham and Brauner[4]), long chain extrapolation (Paster et al.[5]) and reference series (Shacham et al.[6], Brauner and Shacham[7]) will be briefly reviewed and their combination for extending the range of a satisfactory prediction accuracy will be described.

RECENTLY DEVELOPED PROPERTY PREDICTION TECHNIQUES

The Dominant Descriptor Targeted QSPR Method (TQSPR1)

The Dominant Descriptor Targeted QSPR (TQSPR1) method was introduced by Shacham and Brauner [4]. The first stage of the method involves identification of the similarity group and a training set that is structurally related to the target compound. The similarity between the target compound (the compound for which the property needs to be predicted) and a potential predictive compound is measured by the partial correlation coefficient between their molecular-descriptor vectors. The training set is established by selecting from the similarity group the p predictive compounds (usually $p = 10$) with the highest correlation with the target compound for which experimental property values y_i are available.

The selected training set is used for the development of a TQSPR1 model for a particular property of the target compound. A linear structure-property relation is assumed of the form:

$$\mathbf{y} = \beta_0 + \beta_1 \zeta_D + \boldsymbol{\varepsilon} \quad (1)$$

In this equation \mathbf{y} is a p -dimensional vector of the respective property values, ζ_D is a p -dimensional vector of the (dominant) molecular descriptor (to be selected via a stepwise regression algorithm), β_0 and β_1 are the corresponding model parameters to be estimated, and $\boldsymbol{\varepsilon}$ is a p -dimensional vector of random errors.

To identify the dominant descriptor (DD), we examine the partial correlation coefficient between the vector of the particular property values of the compounds included in the training set (i.e., \mathbf{y}) and the vector of descriptor values for these compounds, for all descriptors available in the database. These correlation coefficients will be referred to as the *descriptor-property (D-P) correlation* for the particular property. The DD, ζ_D , is the descriptor that is associated with the highest value of the D-P correlation.

The so-obtained TQSPR1 can be subsequently employed for estimating the property value for the target compound, \tilde{y} , in terms of the (known) dominant-descriptor value, ζ_{D_i} :

$$\tilde{y}_i = \beta_0 + \beta_1 \zeta_{D_i} \quad (2)$$

Equation (2) is applicable, also, to additional compounds in the similarity group for which no property data are available.

There may be circumstances where there is a need to replace one or more members of the training set in order to improve the accuracy of the prediction. In such cases the next predictive compound to enter the training set is the one with the highest correlation with the target compound that also fulfills some additional requirements (like being in the same phase condition as the target compound at standard state). Similarly, the DD need to be occasionally replaced. In such cases the new DD is the one with the highest D-P correlation coefficient which also fulfills some additional requirements (e.g., preferring a non- 3D descriptor).

Considering the property value at $n_c \rightarrow \infty$ in derivation of the TQSPR1 model

Experimental property data are available, most often, for low n_c compounds as many of the properties of high n_c compounds cannot be measured due to thermal instability. Thus, property prediction of high n_c compounds often involves extrapolation (to higher n_c). Since the selection of the DD is carried out using only the available experimental data, extrapolation to higher n_c may yield inaccurate predictions. Recently, Paster et al. [5] presented a technique where the property value at $n_c \rightarrow \infty$ (y^∞) is also considered when selecting the DD, whereby the asymptotic behaviour of the DD should match the asymptotic behaviour of the property considered. For example, for properties that converge to a constant y^∞ value (such as normal boiling and melting temperatures), a DD is sought which also converges to a constant value for $n_c \rightarrow \infty$ (ζ_D^∞). If the use of this descriptor in Eq.(1) enables accurate representation of the training set property data (\mathbf{y}), as well as convergence to a generally accepted y^∞ value, the linear structure-property relationship is used. Otherwise, if Eq.(1) converges to a different y^∞ value, Eq. (1) is modified by including an additional non-linear correction term (with an additional regression parameter, β_2):

$$y = \beta_0 + \beta_1 \zeta_D - (\beta_0 + \beta_1 \zeta_D - y^\infty) [1 - \exp(-\beta_2 n_C)] + \varepsilon$$

and

$$y_i = \beta_0 + \beta_1 \zeta_{D_i} - (\beta_0 + \beta_1 \zeta_{D_i} - y^\infty) [1 - \exp(-\beta_2 n_C)] \quad (3)$$

For properties which are additive in nature (like molar volume, enthalpy and entropy), in the limit of large n_C , each additional carbon unit contributes a fixed increment to the property value. For representation of such properties it is preferable to use n_C as a DD for extrapolation to high n_C compounds.

The reference series method

Shacham et al. [6] and Brauner and Shacham [7] introduced the "reference series" method for improving the prediction accuracy in homologous series of properties for which insufficient data are available. A two-stage procedure is used, whereby a linear (or nonlinear) Quantitative Structure-Property Relationship (QSPR) is fitted to a "reference" series, for which an adequate amount of precise data is available. This QSPR should represent correctly both the available data and the asymptotic behavior of the property. In the second stage a Quantitative Property-Property Relationship (QPPR) is derived to represent the predicted property values of a "target" series in terms of the property values of the reference series.

It has been shown that properties of compounds in two homologous series can be represented (at least locally) by a linear QPPR:

$$y_t = B_0 + B_1 y_r \quad n_C \geq n_{C,min} \quad (4)$$

where y_r is the property value of a compound in the reference series, y_t is the property of a compound (related to the reference compounds in terms of n_C) in the target series, and B_0 and B_1 are parameters obtained by regression of the experimental data. The n -alkane series, for which the largest amount and highest precision property data are available, is most often used as the reference series. This method does not require computation of molecular descriptors, which can be considered as an advantage if no molecular structure files and/or descriptor computational programs are available. For predicting properties for long chain substances, a nonlinear version of Eq. (4) (similar to Eq. 3) can be used.

METHODOLOGY

The TQSPR1 method was evaluated by predicting 15 constant properties for a set of 471 compounds (Shacham et al.[3]). The database used in that study contains physical property data for 1798 compounds. Included in this data base are numerical values and data uncertainties (U_i) for 34 properties (e.g., critical properties, normal melting and boiling temperatures, heat of formation, flammability limits etc.). All the property data is from the DIPPR database (Rowley et al., [8]). The DIPPR database often contains a large number of experimental, predicted or smoothed values for a particular compound-property combination, while one particular value is designated as the "recommended" value. For the evaluation of the TQSPR1 method usually the recommended values were used.

Our database contains also 3224 molecular descriptors generated by the Dragon, version 5.5 software (DRAGON is copyrighted by TALETE srl, <http://www.taletе.mi.it>) from minimized 3D molecular structures that were obtained from Rowley[9].

A Visual Basic program that uses the TQSPR1 method was developed. The program can operate in batch mode and attempts to predict all the properties for all the compounds in the data base. Most of the computations reported were carried out using this program. For the examples presented here, some additional details were computed with a special version of the SROV (MATLAB) program of Shacham and Brauner [10], which was revised in order to fit the needs of the TQSPR1 algorithm.

The identification of the similarity group and the training set is performed by using a subset of 294 selected descriptors, mostly 1-D descriptors from the "atom centred fragment" and "functional group count" categories. This subset was selected based on its ability to identify compounds belonging to the target compound's homologous series (if available), and to discriminate between compounds according to the number and location of branches and double bonds (Paster [11]). Some of the results were compared with predictions obtained by various GC methods. To this aim, the implementation of the GC methods in the Dortmund Data Bank (DDBST, 2011 release, <http://www.ddbst.de>) was used for the predictions.

The selected 15 constant properties included in the study from the DIPPR database are listed in Table 1. Included in the Table are the symbols of the properties (as defined by DIPPR) and short descriptions of the properties. Out of the 34 properties (included in DIPPR), 19 were excluded for several reasons. Some were excluded because they are categorized as "defined", namely, they are calculated from other properties and/or from the molecular structure (i.e., the molecular weight, or critical compressibility factor that is calculated based on the critical properties). Excluded are also properties for which most of the values in the database are predicted and/or are associated with very high uncertainties. The 471 compounds included in the study could be associated with 84 groups (mostly homologous series).

Table 1. Constant properties included in the study from the DIPPR database

No.	Symbol	Property description
1	ENT	Absolute Entropy of Ideal Gas at 298.15 K and 100000 Pa
2	FP	Flash Point
3	HCOM	Net Enthalpy of Combustion Standard State (298.15 K)
4	HFOR	Enthalpy of Formation of Ideal gas at 298.15 K and 100000 Pa
5	HFUS	Enthalpy of Fusion at Melting Point
6	HSTD	Enthalpy of Formation in Standard State at 298.15 K and 100000 Pa
7	HSUB	Heat of Sublimation at the triple point
8	LVOL	Liquid Molar Volume at 298.15 K
9	MP	Melting Point (1 atm)
10	NBP	Normal Boiling Point (1 atm)
11	PC	Critical Pressure
12	RI	Refractive Index at 298.15 K
13	SSTD	Absolute Entropy in Standard State at 298.15 K and 100000 Pa
14	TC	Critical Temperature
15	VC	Critical Volume

SOURCES OF EXCESSIVE PREDICTION ERRORS AND RECOMMENDATIONS FOR IMPROVEMENTS

The results of the evaluation of the TQSPR1 method are reported in detail by Shacham et al., [3]. For the great majority of the compound/property combinations, predictions of acceptable accuracy (meaning that the prediction error is

lower than the highest data uncertainty) were obtained. For many of the compound/property combinations the TQSPR1 predictions were compared with predictions obtained with state of the art GC methods (Constantinou and Gani, [12], Wen and Qiang, [13]) and the TQSPR1 predictions were of comparable or higher accuracy than the GC methods. There were, however, cases where the prediction error exceeded the data uncertainty. In the following the causes of excessive prediction errors are discussed. These are common to the QSPR methods that we are familiar with. Our recommendations for improving the prediction accuracy are also outlined

"Recommended" property value of a compound is inconsistent with values for similar compounds.

For many compound-property combinations several experimental values are reported in the literature, often with a considerable difference between them. It is not an easy task to categorize some of the values as "unacceptable" and to recommend the value which is most probably the correct one. For example, Shacham et al. [6] discuss a case where excessive prediction error the heat of formation of 1-octene is caused by use of the recommended value in the DIPPR database, which is however found to be inconsistent with the recommended values of the rest of the members of the 1-alkene series. Shacham et al. [6] show that selection of a different value as "recommended" from the available experimental data reduces the error below the data uncertainty.

To prevent errors that may be caused by miss-selection of the "recommended" property value, an iterative prediction-replacement process can be carried out in the database. For a group of similar compounds (like members of a homologous series), the prediction method is applied by targeting each of the members in turn, while using the others as a training set. If the prediction error exceeds the data uncertainty, another "recommended" value closer to the predicted value for the target compound is selected. This prediction-replacement process is carried out for all the members of the group until no more replacements need to (or can) be made.

Use of 2D descriptors whose range of definition does not cover the entire compound space

There are many 2D descriptors whose range of definition is limited in terms of the number of non-Hydrogen molecule atoms. Shacham et al. [3] mentioned for example the descriptor *EEig13d*, which is defined only for molecules that contain more than 12 non-Hydrogen atoms. Usually a (pseudo) zero value is assigned by Dragon to the descriptors when their calculation is attempted outside their range of definition. Obviously if the descriptor used in the QSPR model is associated with pseudo zero for the target compound and/or for some members of the training set, excessive prediction errors can be expected.

To prevent prediction errors of this source, the descriptors with limited range of definition should be clearly marked in the database (in order not to confuse real zeros with pseudo zeros). Compounds associated with a pseudo-zero value of the DD, should be removed from the training set (and replaced by other compounds from the similarity group, if necessary). When the DD value for the target compound is a pseudo zero, another DD must be selected according to the principles

outlined in the description of the TQSPR1 method.

Inconsistency in the 3D molecular structure files and or 3D descriptors

We have studied extensively the potential sources of excessive prediction errors when 3D descriptors are used in QSPRs or TQSPRs ([3], [14], [15]). Paster et al. [14] demonstrated that the 3D descriptors are very sensitive to the method, parameters and the initial configuration used to generate the 3D optimized molecular structure. 3D structure (MOL) files available from different sources may be non-optimized, or partially optimized configurations, with no documentation on how these were obtained. Many computational algorithms may converge to a local minimum and finding a global optimum structure will depend upon the starting configuration. For flexible molecules (e.g., long chain hydrocarbons) the 2D to 3D conversion by different software can render different conformers, resulting in variation of the calculated value for the same 3D descriptor. Thus, if QSPR or TQSPR that contains 3D descriptors are used for prediction, it is very important to get the 3D structures of all the compounds involved (predictive and target) from the same reliable source.

Shacham et al., [3] presented an example where the critical volume of 1-decanol is predicted using a 3D (*D_s*) descriptor as DD. The prediction error in that case was very high. Examination of the 3D molecular structure (MOL) files of 1-decanol and its two immediate neighbours in the homologous series (1-nonanol and 1-undecanol) revealed inconsistency of the 1-decanol's MOL file, and consequently, also in the value of the *D_s* descriptor. The inconsistency in that case was rotation of the -CH₂OH group in the 1-decanol structure file compared to its position in the structure files of the other members of the 1-alkanol series. Such a difference is hardly noticeable, but it can affect a considerable variation in the value of the DD of the target compound, causing excessive prediction errors.

Methods for debugging of the descriptor data base have been developed [14, 15]. These should reveal inconsistent representation of some of the molecular structures and the associated 3D descriptors which are included in the database, and identify noisy 3D descriptors that exhibit extremely high sensitivity to insignificant variations in the 3D representation of the molecular structure. The use of the latter in QSPR models should be avoided. These methods should be applied also whenever new compounds are added to the database.

Phase change at standard state within the training set

There are several properties listed in Table 1 for which the reported values are for the "standard state", which is defined as the stable phase at 298.15 K and 1 bar. These properties include standard state enthalpy of formation (*HSTD*), entropy of formation (*SSTD*) and enthalpy (heat) of combustion (*HCOM*). Refractive indexes (*RI*) are reported usually for the liquid phase, which may not be the valid phase at the "standard state" (i.e., the compound is in gas phase at the standard state). Liquid molar volume (*LVOL*) is usually reported at standard state temperature, unless $T_c < 298.15$, in which case *LVOL* is reported at the normal boiling point (T_b), or at the triple point temperature if $T_{tp} > 298.15$. Obviously, phase and/or temperature variations maybe reflected also in

the property variation within the group of similar compounds (i.e., homologous series).

Shacham et al.[3] showed an example of prediction of *SSTD* of *n*-tridecane using *n*-alkanes in the $12 \leq n_C \leq 22$ region as a training set. The target compound and the members of the training set are in liquid phase at standard state, while for $n_C \geq 18$ the compounds are in solid phase. The TQSPR1 model obtained when using the full training set yields prediction error of 15 %. Removing the five compounds with $n_C \geq 18$ from the training set yields prediction with negligible error of 0.022 %.

Thus, for prediction of properties whose value is determined at the standard state, the phase condition of the target compound at standard state must be first determined. Only compounds which are in the same phase condition as the target (at the standard state) should be included in the training set.

Change of property values by orders of magnitude within the training set

Shacham et al., [3] demonstrated excessive prediction errors caused by order of magnitude change in the property values within the training set. For example, predicting the ideal gas enthalpy of formation (*HFOR*) for the first 11 members of the 1-alkene series: the DIPPR recommended values of *HFOR* are 2.023e7 for propylene, -5.0e5 for 1-butene and -2.162e7 for 1-pentene. Thus, there are at least two orders of magnitude difference between the *HFOR* value of 1-butene and the rest of the members of the 1-alkene series. Consequently the TQSPR1 prediction of the *HFOR* of 1-butene is very poor (86 % prediction error). However, if the coefficients of the TQSPR1 model are determined by minimization of the relative error (rather than the absolute error least squares) the prediction errors are reduced to acceptable levels for all the compounds.

Thus, in cases where there are order of magnitudes differences between the property values of the training set members (or a change of sign in the property value), it is recommended to use relative error least squares for determining the QSPR/TQSPR1 model parameters.

Long range extrapolation to higher n_C compounds

The DD descriptor selected based on property values of relatively low n_C compounds does not necessarily comply with the asymptotic behaviour of the property at large n_C . In such cases, applying the TQSPR for prediction the property value of a high n_C compound may result in excessive prediction errors. For example, the highest n_C compound for which property data are available for the 1-alkene series in the DIPPR database is 1-triacontene (with $n_C=30$). Shacham et al., [16] reported *LVOL* prediction results for 1-triacontene using 10 1-alkenes in the range of $11 \leq n_C \leq 20$ as the training set. Relying on the training set *LVOL* data for identification of the DD, yields *LVOL* prediction which differ by 21% from the value reported by DIPPR. Selecting the DD while matching its asymptotic behaviour at $n_C \rightarrow \infty$ with the asymptotic behaviour of *LVOL* (as explained in the "Considering the property value at $n_C \rightarrow \infty$..." section) leads to a TQSPR1 model which gives *LVOL* value with 1.7 % difference from the value reported by DIPPR. This difference is considerably lower than the DIPPR data uncertainty (10%).

Thus, in cases of extrapolation to higher n_C compounds it is

always advisable to match the asymptotic behaviour of the DD with the asymptotic behaviour of the target property.

Irregularities in the solid properties related to the crystalline structure

The irregularities with regard to solid properties (e.g., normal melting temperature, T_m and heat of fusion, *HFUS*) are demonstrated in reference to the T_m of members of the *n*-alkane and the *n*-alkanoic acid homologous series (Fig. 1). Three distinct regions can be identified in the T_m curves. In the "low n_C " region there is a decreasing trend of the T_m values with increasing n_C . This region includes the first 3 members of the *n*-alkane series and the first 4 members of the alkanolic acid series. At medium range n_C , a general trend of increasing T_m values with n_C is observed in both curves. However, there are "local" oscillations in the T_m values between consecutive members with odd and even n_C values. The oscillations are the highest for lower n_C compounds and diminish for $n_C > 20$ (*n*-alkanes) or $n_C > 25$ (alkanoic acids). These oscillations in the T_m values are attributed to the melting from different crystalline phases (Marano and Holder, [17]). In the high n_C region, there is a smooth increase of T_m with a diminishing slope converging to the asymptotic $T_m = 415$ K value for $n_C \rightarrow \infty$ (Paster et al., [5]).

Brauner and Shacham, [7] reported very good results for predicting T_m in the medium and high n_C regions using the "reference series" method. In the medium n_C region two versions of Eq. 4 are used: one for odd n_C target compounds and one for even n_C target compounds. In this case we use in Eq. 4 the definition of $y_i = (T_m)_{i,n_C}$, where n_C is the number of carbon atoms in the respective member of the target series, and $y_r = (T_m)_{r,i}$ where i is the number of carbon atoms in the matching member of the reference series, it can obtain the values $i = n_C$ or $i = n_C + 1$ or $i = n_C - 1$ (see details in Brauner and Shacham, [7]).

For predicting T_m in the high n_C region, Brauner and Shacham, [7] provided a QSPR (of the form of Eq. 3) for predicting T_m of the members of the *n*-alkane (reference) series, and recommended the use of a nonlinear version of the QPPR (Eq. 4) for members of other target series.

Further development of the "reference series" method is underway to enable reliable prediction of other solid properties of compounds belonging to of homogenous series, (such as *HFUS*) and to extend its applicability for property prediction of other groups of compounds.

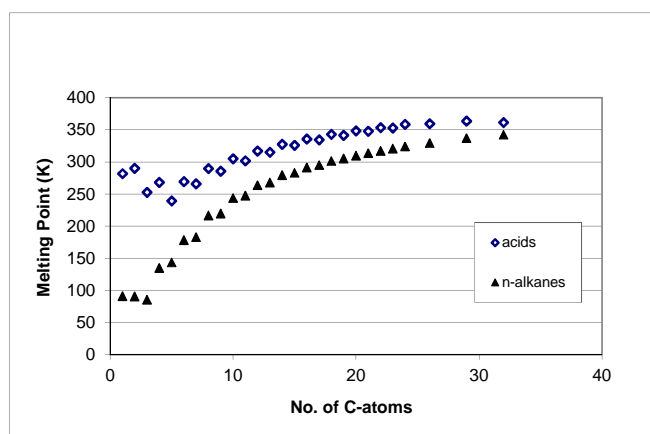


Fig. 1. Plot of normal melting point data of *n*-alkanes and *n*-alkanoic acids vs. n_C up to $n_C = 32$.

Prediction errors for low carbon number compounds and first members of homologous series

Shacham et al. [3] list extrapolation to a low n_C target compound as the most common cause for excessive prediction error. In Fig. 1, for example, the T_m values of n -alkanes with $n_C > 3$ have very little relevance when predicting T_m for methane, as the trend of change of T_m in the low n_C region differs from the trend in the medium n_C region. This change in trend is caused by the influence of the functional groups that is attached to the methyl group (the dominant group in higher n_C compounds) on the property value. For low n_C compounds the effect of the functional group is dominant, but it diminishes with the addition of methyl groups. Because of that experimental information on the property values of low n_C compounds (or first members of homologous series) is essential for correctly assessing the functional groups contribution to the property values.

Phase change at standard state for the members of the training set can be another reason for excessive prediction errors for low n_C compounds. Shacham et al. [3] used the first 11 members of the 1-alkene series to demonstrate this difficulty. For this series the first three members: ethylene, propylene and 1-butene, are in the gaseous phase at standard state, while the rest of the compounds are in the liquid phase. The liquid phase compounds cannot provide reliable information regarding the standard state properties of the gas phase compounds.

The absolute value of some properties of low n_C compounds is often much smaller than the absolute values of the same properties of the high n_C compounds. This may inflate the relative errors in prediction of the property for a low n_C compound. Shacham et al. [3] provided an example where similar absolute prediction error for T_b of ethylene ($T_b = 169.41$ K) yields much higher relative error than for T_b of 1-dodecene ($T_b = 486.15$). As discussed above, minimization of the sum of squares of the relative error should be considered in such cases.

CONCLUSIONS

The property prediction field is a constantly evolving field where the objective is to extend its applicability to additional groups of compounds and additional properties, and to reach the ultimate goal of prediction accuracy within the experimental data uncertainty level. We have shown that these goals cannot be reached by using one type of technique (like group contribution, QSPR or QPPR), but a broader algorithm should be developed, which can fit the most adequate prediction technique/s to a wide range of compound-property combinations.

Based on our experience in developing several new prediction techniques and applying them to a wide variety of compound-property combinations, we propose the following procedure and principles in developing a general property prediction system.

1. Continuous update of the property data base with new experimental property data that becomes available. Continuous maintenance of this database by verifying the consistency of the "recommended" property values with such values of similar compounds.
2. Continuous maintenance of the descriptor database by mapping the range of applicability of certain 2D

descriptors and checking the consistency of 3D structure (MOL) files and 3D descriptors with MOL files and descriptors of similar compounds.

3. When predicting properties for a new target compound, the prediction technique needs to be adjusted to the specific compound/property combination and the available training set. For fluid properties the use of the TQSPR1 method is recommended provided that enough similar predictive compounds are available. The selection of the DD should consider both the training set property data and the asymptotic property behaviour (in case of extrapolation to larger n_C). For properties defined at standard state, first the phase condition of the target at standard state should be predicted. Only predictive compounds of the target's phase condition can be included in the training set for predicting the desired property. If the property values change by orders of magnitude within the training set, the minimization of the relative (instead of absolute) errors is recommended. For solid properties (and fluid properties with insufficient amount of predictive compounds) the use of the reference series method should be preferred.

Prediction of properties by extrapolation to low n_C compounds (or first members of homologous series) so as to keep the prediction error below experimental uncertainty level requires further research.

The extension of TQSPR1 method to predict temperature – dependent properties (e.g., vapor pressure) and other phase equilibrium related properties (e.g., interaction parameters for phase equilibrium calculations, when applying EoS) was demonstrated in Shacham et al., [18] and Paster et al., [19]). Preliminary results show that our methods can be used also for predicting other important parameters (e. g., activity coefficients for non-ideal binary systems).

REFERENCES

- [1] B.E. Poling, J.M. Prausnitz and J.P. O'Connell, Properties of Gases and Liquids, fifth ed. McGraw-Hill, New York, 2001.
- [2] N. Brauner, R. P. Stateva, G. St. Cholakov and M. Shacham, A structurally "targeted" QSPR method for property prediction, Ind. Eng. Chem. Res., vol. 45, pp. 8430–8437, 2006.
- [3] M. Shacham, M. Elly, I. Paster and N. Brauner, Evaluation and refinement of the property prediction stage of the targeted QSPR method for 15 constant properties and 80 groups of compounds, *Chem.Eng.Sci.*, In Press, Accepted Manuscript, Available online 18 April 2013.
- [4] M. Shacham and N. Brauner, Analysis and Refinement of the Training set in Predicting a Variety of Constant Pure Compound Properties by the Targeted QSPR Method, *Chem. Eng. Sci.*, vol. 66, pp. 2606–2615, 2011
- [5] I. Paster, M. Shacham and N. Brauner, Adjustable QSPRs for prediction of properties of long-chain substances, *AIChE J.*, vol 57, pp. 423–433, 2011.
- [6] M. Shacham, I. Paster and N. Brauner, Property Prediction and Consistency Analysis by a Reference Series Method,

- AIChE J.*, vol. 59, pp. 420–428, 2013.
- [7] N. Brauner and M. Shacham, Prediction of Normal Melting Point of Pure Substances by a Reference Series Method, *AIChE J.*, DOI 10.1002/aic.14128, Accepted manuscript, online: 28 APR 2013.
- [8] R. L. Rowley, W. V. Wilding, J. L. Oscarson, Y. Yang and, N. A. Zundel, DIPPR Data Compilation of Pure Chemical Properties Design Institute for Physical Properties. Brigham Young University Provo Utah, 2010. <<http://dippr.byu.edu>>.
- [9] R. L. Rowley, Personal Communication, 2010.
- [10] M. Shacham, and N. Brauner, The SROV Program for Data Analysis and Regression Model Identification, *Comp. Chem. Eng.*, vol. 27, pp. 701-714, 2003.
- [11] I. Paster, Prediction of Properties Using Molecular Descriptors, PhD Thesis, Ben-Gurion University of the Negev, Beer-Sheva, 2013.
- [12] L. Constantinou, and R. Gani, New Group-Contribution Method for Estimating Properties of Pure Compounds. *AIChE J.*, vol. 10, pp. 1697-1710, 1994.
- [13] X. Wen and Y. Qiang, Group vector space (GVS) method for estimating boiling and melting points of hydrocarbons. *Chem. Eng. Data*, vol. 47, pp. 286-288, 2002.
- [14] I. Paster, M. Shacham and N. Brauner, Investigation of the Relationships between Molecular Structure, Molecular Descriptors and Physical Properties, *Ind. Eng. Chem. Res.*, vol. 48, pp. 9723–9734, 2009.
- [15] I. Paster, G. Tovarovski, M. Shacham and N. Brauner, Combining Statistical and Physical Considerations in Deriving Targeted QSPRs Using Very Large Molecular Descriptor Databases, pp. 61 - 66 in S. Pierucci and G. Buzzi Ferraris (Eds), 20th European Symposium on Computer Aided Process Engineering – ESCAPE 20, June 6- 9, 2010, Ischia, Naples, Italy.
- [16] M. Shacham, M. Elly, I. Paster, and N. Brauner, Self-Consistency Analysis of Physical Property and Molecular Descriptor Databases Using a Variety of Prediction Techniques, paper 181b, Presented at the 2012 AIChE Annual Meeting, Pittsburgh, PA, Oct. 28 – Nov. 2, 2012.
- [17] J. J. Marano and G. D. Holder, General equations for correlating the thermophysical properties of n-paraffins, n-olefins and other homologous series. 2. Asymptotic behavior correlations for PVT properties. , *Ind. Eng. Chem. Res.*, vol. 36, pp. 1895-1907, 1997.
- [18] M. Shacham, G. St. Cholakov, R. P. Stateva and N. Brauner, Quantitative structure-property relationships for prediction of phase equilibrium related properties. *Ind. Eng. Chem. Res.*, vol. 49, pp. 900–912, 2010.
- [19] I. Paster, N. Brauner and M. Shacham, Analysis and refinement of the TRC-QSPR method for vapor pressure prediction. *The open Thermodynamic Journal*, vol. 5, pp. 29-39, 2011

ASPHALTENE OR HOW AND WHY I BECAME A FAN OF THE REGULAR SOLUTIONS THEORY

Sebastiano Correra*

*eni e&p division - ISDEW, via Emilia, 1 - 20097 San Donato Milanese

ABSTRACT

Petroleum is a mixture of tens of thousands of organic compounds, with molecular weights spanning in a very large range. It was generated underground from the degradation of organic material accumulated over millions of years, and it stays at great depths within porous rocks, at high temperature and pressure. The crude oil is produced by means of long pipes, which allow the extraction of the oil to the surface, where it is then subject to processes of separation into different fractions.

Along the extraction process and the pipeline transport, the operating conditions change; this fact can induce phase separations. A first separation may occur when, due to the depressurization along the production string, the boiling pressure of the mixture is reached: a liquid-vapor separation happens, and the overall system becomes biphasic. In some oilfields and in some wells, however, the separation of a third phase is also observed. This solid or gel-like phase is mainly constituted by a specific class of compounds: the asphaltenes. The asphaltenes are "the bottom of the bottom of the barrel". Asphaltene is a fraction of the oil that contains the heavier and aromatic compounds.

At the beginning, the nature of this separation seemed mysterious, due to the fact that the oil industry has not observed such a phenomenon before. Different physical models and empirical studies have been proposed to explain the phenomenon, and each author has defended his own model. For this reason, at first, a thorough analysis of the various models has been carried out in our company, looking for a particular behavior and a possible "experimentum crucis" to evaluate the physical consistency of the models. We ended up focusing on a particular behavior observed by different researchers and linked to the beginning of phase separation. It is possible, in fact, to induce the asphaltene separation by adding a n-paraffin to the crude. For this reason the titration of the oil has been and is very employed to study the phenomenon; in this way a lot of data has been accumulated in the literature. In particular, there was a general agreement in the literature on an empirical observation that concerns the onset of phase separation. After checking that the oils of our interest had this behavior, we focused on finding a physical model consistent with the observations. We were able to reconcile the observations with the Flory-Huggins theory. In particular, an experimental linear trend is attributable to the regular solutions theory, in the limit of infinite dilution.

This presentation outlines a history of this logical path.

INTRODUCTION

One of the distinguishing characteristics of the mankind is the conscious use of energy sources for its own purposes. For a very long time the only available energy was that of animals (or even that of other human beings); occasionally the energy of the wind and rivers was employed. But it was only with the extensive use of the fossil fuels that the industrial revolution became possible. The widespread availability of energy (ability to work) created the world in which we live.

The first industrial revolution was based on coal, and started in coal countries (Germany, France, England). The main energy source thus became then the oil, and we still live in the world of oil and gas. Our current way of life is based on the exploitation of fossil energy sources.

Fossil fuels (oil and gas) are formed due to the accumulation, in millions of years of organic material. This material over the millennia has been covered by the ground and has been subject to a burial process. In this way, in anaerobic conditions and at high temperatures and pressures, hydrocarbons were generated and accumulated in the underground porous rocks.

The first step to be able to produce hydrocarbons is to locate possible deposits; for this purpose seismic technologies have been developed. After the identification of a target reservoir, an oil field development plan is prepared and implemented. Hydrocarbons are produced through wells that are drilled from the ground surface to the reservoir. If the reader believes this

whole process is too simple, we can add that, due to the increasing energy request, oil production has increasingly shifted to offshore fields. This greatly increases the difficulty of exploration, development and production: the overall production system can easily be something as complex as shown in Figure 1.

THE OIL

What is commonly called petroleum (from latin "petrae oleum", meaning "oil from rock") turns out to be a mixture of many hydrocarbon components, twenty thousand compounds approximately. The composition is strongly dependent on the origin and the formation conditions of the oil reservoir: the overall properties may span from very dark, almost solid, bitumen-like materials to light, clear yellow liquid, to end up with light gas such as methane. The properties and the physical status of aggregation result to depend on the operating conditions, and separation of different physical phases is possible.

Along the producing pipe (tubing), from reservoir to the surface, the mixture is subject to variations in operating conditions. In particular, along the tube production, there is a pressure draw-down. If the pressure drops below the so-called bubble pressure of the mixture, a second phase separate: the overall system becomes a liquid-vapor biphasic one.



Figure 1: Overall oil production system

Due to this vapour-liquid separation, in the higher part of the tubing a bi-phase flux is realized.

completely dissolved in the liquid: in the reservoir hydrocarbons constitute in a single phase liquid



Figure 2: Asphaltene deposits

In the surface facilities, the fluid stream reaches ambient conditions. Due to this change in conditions, various streams are separated. The main ones are: associated gas (gaseous mixture of hydrocarbon compounds), stock tank oil and produced water. Often the stock-tank oil is also referred to as "dead oil", as opposed to "live oil", that is the reservoir oil. Indeed, in the reservoir the gas, due to the high pressure, is

THE ASPHALTENE PROBLEM

A production problem was noticed from the beginning of the twentieth century in some fields: it was observed a gradual decrease in the production, linked to the formation of deposits into the tubing. The deposition occurred especially in the area around the bubble point condition, and deposits were called "asphaltene", i.e. "asphalt-like" compounds. Properties and structure of asphaltene are still being studied, as it is a difficult and tricky topic [1,2]. The asphaltene deposition problem is in often encountered in field characterized by relatively "light" oil, with very low asphaltene content.

eni encountered this problem for the first time in the eighties, in relation to the production of one oil field located in the Po Valley. Various research projects were addressed at better understand and afford this problem.

MODELING OF THE PHASE SEPARATION

Various possible physical models of asphaltene phase separation were proposed in literature, spanning from liquid-liquid equilibrium (LLE), solid-liquid equilibrium (SLE), colloidal and empirical models [3]. This variety of models was linked to the various physical picture proposed by researchers.

On the other hand, in order to have a strong physical basis, we looked for an unambiguous and reproducible behaviour,

that could allow an insight into the physics of the phenomenon. After a careful analysis of the literature, we identified the “onset of precipitation” test as a distinctive behaviour [4]. Our effort were the focused on these data.

The onset of asphaltene precipitation is detected by gradually adding to the oil (eventually pre-diluted with a solvent) a n-paraffin (often n-heptane or n-cetane). After some additions of paraffin, an asphaltene-rich phase precipitate out of the mixture. The onset is identified as the point at which this second phase start nucleating. If the following definitions are adopted:

$$X = \frac{(\text{solvent amount})}{(\text{oil amount})} \quad (1)$$

$$Y = \frac{(\text{anti - solvent amount})}{(\text{oil amount})} \quad (2)$$

then straight lines are obtained by plotting Y vs. X. These straight lines constituted the empirical set-up against which we tested our models.

On the basis of our knowledge of the physical system and of the analysis of the previous literature, we choose to try to describe our system by employing a pseudo-binary Flory-Huggins approach [5]. Indeed, the Flory-Huggins theory was developed to thermodynamically describe polymer-solvent solutions, i.e. mixtures in which there is a big amount of relatively small molecules “solvent” and a little amount of relatively big “solute” molecules. From what we knew about asphaltene, this description seemed to be right one. In order not to have a very complex model, with a lot of tunable parameters, we adopted a pseudo-binary approach: in the mathematical description, the overall mixture is constituted by two components, component (2) being the asphaltene and component (1) being the overall mixture constituted by others chemical species. The following equations are then to be considered:

$$\frac{\Delta\mu_1}{RT} = \ln \varphi_1 + \left(1 - \frac{1}{r}\right)\varphi_2 + \chi\varphi_2^2 \quad (3)$$

$$\frac{\Delta\mu_2}{RT} = \ln \varphi_2 - (r-1)(1-\varphi_2) + r\chi(1-\varphi_2)^2 \quad (4)$$

$$\chi = \frac{V_1}{RT} (\delta_2 - \delta_1)^2 \quad (5)$$

$$r = \frac{V_2}{V_1} \quad (6)$$

Symbols are defined as follows:

r ratio of molar volumes
 V_i molar volume of component i

R gas constant
 T temperature

$\Delta\mu_i$ chemical potential of component i

δ_i solubility parameter of component i

φ_i volume fraction of component i

χ interaction parameter

A phase equilibrium between two phases (I and II) is considered, by imposing that the chemical potential of each component in both phases must be the same:

$$\Delta\mu_1^I = \Delta\mu_1^{II} \quad (7)$$

$$\Delta\mu_2^I = \Delta\mu_2^{II} \quad (8)$$

The properties of the pseudo-component 1 are to be evaluated -of course- by means of opportune mixing rules. In particular the molar volume can be evaluated as molar average of molar volumes:

$$V_1 = \sum_{\text{mixture}} x_i V_i \quad (9)$$

Here x_i is the molar fraction.

The solubility parameter has to be evaluated instead as a volumetric average:

$$\delta_1 = \sum_{\text{mixture}} \varphi_i \delta_i \quad (10)$$

The overall model (i.e. Eq.s (3) ÷ (10)), when applied, give rise to a miscibility gap as reported in Figure 3.

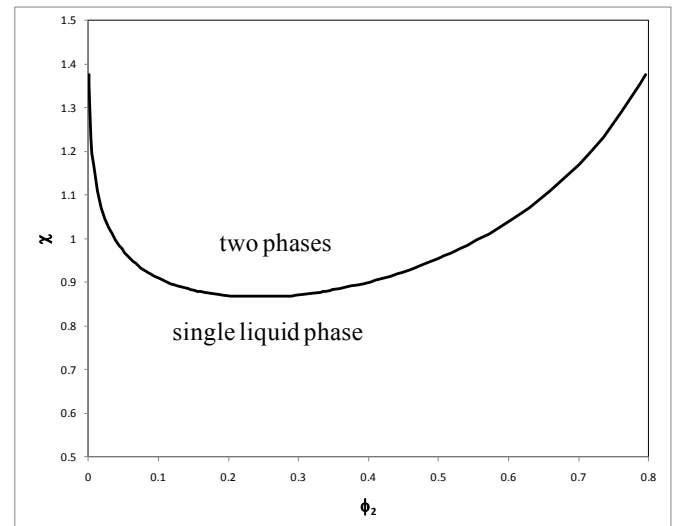


Figure 3: Miscibility gap for r = 10

The curve, of course, depends on the ratio of molar volumes r. In the plane (asphaltene volume fraction) vs. (interaction parameter) there is a two-phase zone, corresponding to the equilibrium between two solutions at different compositions.

THE APORIA IN WHICH WE FOUND OURSELVES

At this point, we found ourselves in an aporia.

On one hand, we had a lot of experimental confirm (from worldwide labs) of the “straight lines” behaviour. Besides, this behaviour seemed to be physically reasonable: the more the good solvent is present (higher X) the more the precipitant is needed (higher Y).

On the other hand, we must consider the description of the experiments in terms of the model: when a precipitant is added to the solution, there is an increase in the interaction parameter (χ) and a decrease of the concentration (a decrease of the volume fraction ϕ_2). The first effect tends to de-stabilize the mixture, while the second one tends to keep asphaltene in solution. However, is predicted an effect of concentration that is not observed.

What had gone wrong?

IT'S A LONG WAY...

A first possible explanation could be that the chosen physical model was not the right one. But we discharged this possibility for two main reasons:

- (1) the physical system (i.e. the oil) is a liquid mixture, and asphaltene are similar, from a chemical-physic point of view, to the other oil components. This justifies the proposed approach, in which to the ideal entropy of mixing is added a regular solution's mixing enthalpy term;
- (2) the other proposed models are more complex, with even more parameters. It seems that the physical behaviour is even simpler than the very simple model we adopted: other models would be unnecessarily complicated.

We started a long re-elaboration work, in order to reconnect the model and the experimental behaviour. A first observation was that the observed behaviour means that the onset of asphaltene precipitation happens at a fixed overall "solvent quality" (expressed in the model by the solubility parameter of the mixture), and that this condition does not depends on the asphaltene concentration [6]. This consideration led to the following onset condition:

$$\chi = \chi_{Cr} \quad (11)$$

i.e., the onset of asphaltene separation corresponds to a critical value of the interaction parameter. When a n-paraffin is added to the mixture, both δ_1 and v_1 change, according to Eq.s (9) and (10); in this way χ (Equation 5) increases. When χ is greater than a critical value, the asphaltene precipitation happens.

As critical value, on the basis of the polymer solutions theories, 0.5 was adopted. But, when we tried to fit experimental data with this model, a greater value was obtained: estimated values span in the range $0.8 \div 1.1$ [7]. By trying to explain this observation, we found that the instability condition $\chi \geq 1$ is equivalent to the condition:

$$\left[\lim_{x_2 \rightarrow 0} \Delta \tilde{G}_{mix} \right] > 0 \quad (12)$$

Equation (12) means that it is possible to obtain the observed instability condition by considering the Flory-Huggins expression of the enthalpy of mixing. If the solute is significantly bigger than the solvent ($r > 10$) and if the limit of

infinite dilution is considered, $\chi = 1$ is the condition at which the molar free energy of mixing is zero.

The physical consequences of this reasoning are remarkable. The onset of precipitation is reached by gradually adding a precipitant to the (stable) initial mixture. In doing this, the concentration of asphaltene (ϕ_2) decreases, and this is a stabilizing effect. The other effect that counteracts this one is the change of the "quality" of the solvent, expressed by the solubility parameter of the mixture (δ_1). The onset happens when the overall solvent power of the mixture is such that asphaltene results to be perfectly immiscible (insoluble in the mixture). A strong implication of this is that at the onset a "pure asphaltene" phase precipitates out of the solution.

Currently we know that this is the physical behavior that is realized in the onset tests on stock-tank oils. In reservoir the destabilization of asphaltene happens in a slightly different way, and there could be another type of phase separation. Deposits formed under these conditions could contain significant amounts of non-asphaltenic constituents. This topic is still under investigation.

WHAT ABOUT THE STRAIGHT LINES?

The model for the onset results to be:

$$@ \text{onset: } \frac{v_1}{RT} (\delta_2 - \delta_1)^2 = 1 \quad (13)$$

When trying to calculate the precipitant amount through Equation (13), a quadratic equation is obtained. However it is possible to show that, if the molar volumes of the pseudocomponents are similar, straight lines are recovered [6]. Besides, when the values of the properties are substituted into the equations, the straight lines are always found.

BACK DOWN TO EARTH

The logical path described so far has a concrete motive. Working in the oil industry implies facing extremely complex and variable systems with very limited available information. Often it is not easy or possible to have samples to be directly analyzed, or it is impossible to directly make test at the desired conditions. For this reason is of paramount importance to have physically founded models. In this way it is possible to perform a limited number of tests in the laboratory, and then extrapolating the results to different conditions.

On the basis of this physical model of the onset, the following procedure was proposed to determine the region of instability in a (P,T) diagram, to forecast well bore asphaltene precipitation from stock tank oil measurements:

- (1) Characterization of stock tank oil by means of lab measurements and previously developed empirical relationship. In this way it is possible to evaluate molar volume and solubility parameter of the stock-tank oil [8].
- (2) Experimental determination of stock-tank oil precipitation onset. At the onset, the $\chi = 1$ has to be fulfilled. By imposing this condition, it is possible to calculate the asphaltene solubility parameter.
- (3) Calibration of an equation of state (usually the Soave-Redlich-Kwong EOS [9]) by using the onset data. The oil is represented by means of components and

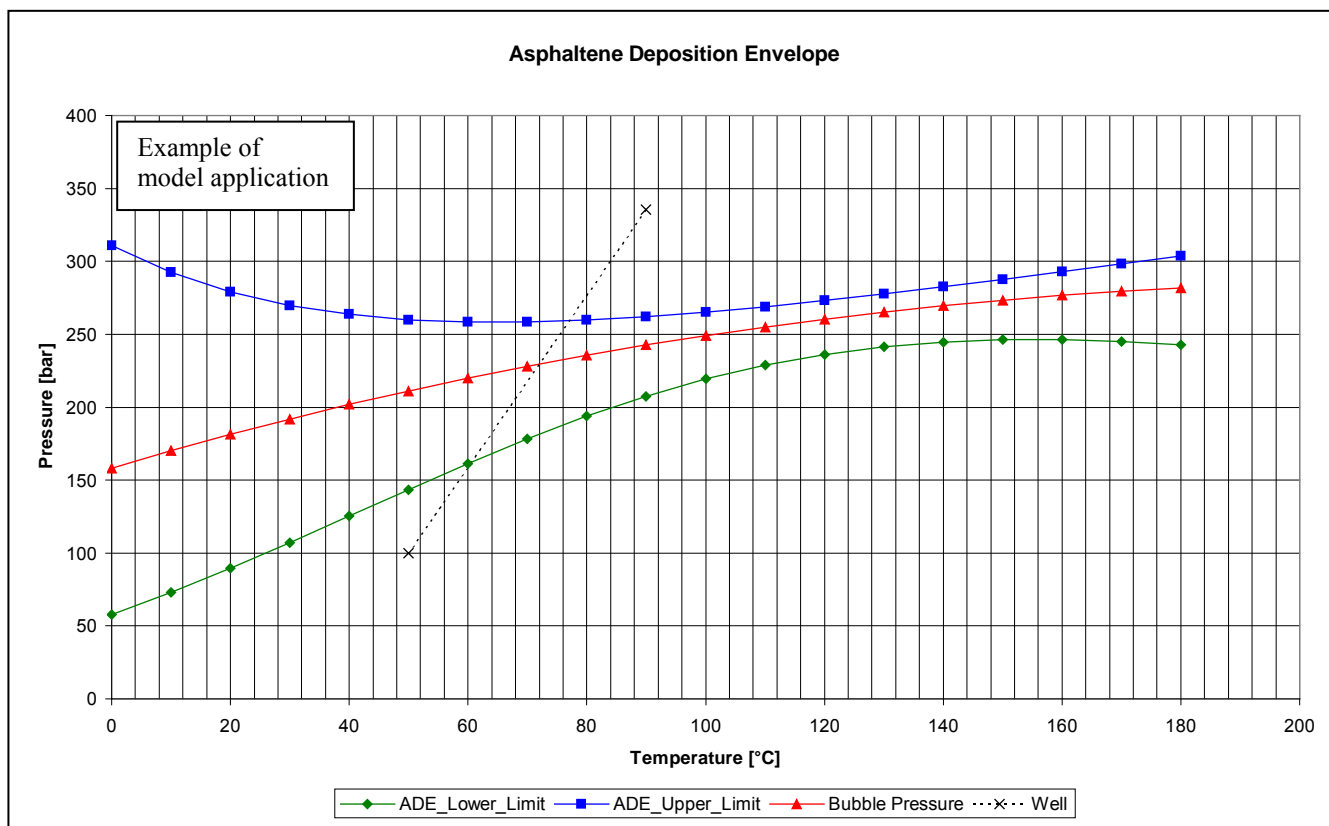


Figure 3: Asphaltene Deposition Envelope

pseudo-components, each one characterized by critical temperature (T_c), critical pressure (P_c) and acentric factor (ω). The parameters of the pseudocomponents can be evaluated from their boiling point and specific gravity by means of empirical relationships.

- (5) Calculation of live oil molar volume and solubility parameter at different T and p conditions (up to reservoir conditions) by means of the calibrated equation of state.
- (6) Calculation of asphaltene solubility parameter at the same conditions, by means of an empirical relationship.
- (7) Determination of the asphaltene deposition envelope (ADE): at each pair (T, P), χ is calculated with Eq. [5]; if the oil conditions are inside the envelope ($\chi > 1$), then at these conditions the asphaltenes are not stable.

An example of ADE determined with this procedure is reported in Figure 3. Therefore, with a relatively simple measurement of stock tank oil, it is possible to calculate an Asphaltene Deposition Envelope that identifies the pressure and temperature conditions in which there is a risk of asphaltene separation. If there is an area in the reservoir, the pipeline etc. where asphaltene enter the region of instability, asphaltene may deposit in that area.

This model has been employed in eni to assess the asphaltene deposition risk in many cases, with good results.

CONCLUSIONS

The history of the eni's asphaltene deposition model has been here synthetically described. It is a model characterized by

a very limited number of parameters and by the strong adherence to experimental observations. The model, gradually built over the years, has been and is used to assess the risk of asphaltene deposition in well.

The work of these years allowed me to appreciate the elegance and ingenuity of the theory of regular solutions and Flory-Huggins theory for polymer solutions.

ACKNOWLEDGMENT

I gratefully acknowledge all the colleagues in eni for their contributions. A special thanks is due to dr. Carlo Carniani, whose suggestions have always been lighting.

REFERENCES

- [1] E.Y. Sheu and O.C. Mullins (eds.), *Asphaltenes: Fundamentals and Applications*, Plenum Press, New York, 1995
- [2] O.C. Mullins, E.Y. Sheu, A. Hammami, A.G. Marshall (eds.), *Asphaltenes, Heavy Oils, and Petroleomics*, Springer Science, New York, 2007
- [3] F. Donaggio, S. Corraera and T.P. Lockhart, Precipitation Onset and Physical Models of Asphaltene Solution Behavior, *Petroleum Science and Technology*, vol. 19(1-2), pp. 129-142, 2001.
- [4] R.Cimino, S.Corraera, P.A.Sacomani, C.Carniani, Thermodynamic modelling for prediction of asphaltene deposition in live oils, *SPE Int. Symp. on Oilfield*

Chemistry, San Antonio, TX, U.S.A., 14-17 February 1995.

- [5] H. Tompa, *Polymer Solutions*, Butterworths Scientific Publications, London, 1956.
- [6] S. Correra and F. Donaggio, OCCAM: Onset-Constrained Colloidal Asphaltene Model, SPE paper 58724, *2000 SPE International Symposium on Formation Damage*, Lafayette, Louisiana, 23-24 February 2000.
- [7] S. Correra and D. Merino-Garcia, Simplifying the Thermodynamic Modeling of Asphaltenes in Upstream Operations, *Energy & Fuels*, vol. 21 (3), pp. 1243-1247, 2007.
- [8] S. Correra, D. Merino-Garcia, A. Di Lullo, M. Merlini, Estimation of the solvent power of crude oils, *Ind. Eng. Chem. Res.*, vol. 44 (24), pp. 9307-9315, 2005.
- [9] G. Soave, Application of equation of state and the theory of group solutions to phase equilibrium prediction, *Fluid Phase Equilibria*, vol. 87, pp. 23-25, 1993.

THERMODYNAMICS—OLD SCIENCE AND NEW CHALLENGES

Ulrich K. Deiters

University of Cologne, Institute of Physical Chemistry,
Luxemburger Str. 116, 50939 Köln, Germany, E-mail: ulrich.deiters@uni-koeln.de

ABSTRACT

Thermodynamics is one of the oldest branches of physical chemistry; its foundations were laid in the late 19th Century. This leads to some peculiar problems. The first is that some good ideas and good data from “thermodynamic antiquity” became forgotten. This could happen if there was no practical application, but also if—before the advent of electronic computers—the mathematical treatment was too difficult or time-consuming. The second peculiarity is that some old concepts, developed solely as means of survival in the age of the logarithmic tables and slide rules, are still in use today. Now, in the 21st Century, there are new classes of chemical compounds to consider (e.g., ionic liquids) as well as old classes under unusual conditions (e.g., hydrocarbons at pressures exceeding 1 kbar), and there are new models based on statistical thermodynamics and quantum mechanics.

In this contribution we shall give examples for these peculiarities. In particular, it will be demonstrated that a “clean and lean” axiomatic approach can simplify and speed up computations. Furthermore, the problem of recognizing weaknesses of equations of state will be discussed, as well as molecular theory-based ways to improve them.

INTRODUCTION

In a recent textbook on physical chemistry¹, the chapter on freezing-point depression contains a derivation of the famous equation

$$\frac{1}{T} = \frac{1}{T_{\text{fus},1}} - \frac{R \ln x_1}{\Delta_{\text{fus}} H_{\text{m},1}}, \quad (1)$$

(component 1 being the solvent) which then leads to the final result

$$\Delta T = - \frac{R M_1 T_{\text{fus},1}^2}{\Delta_{\text{fus}} H_{\text{m},1}} c_2 \quad (2)$$

after making the simplifications

$$\ln x_1 = \ln(1 - x_2) \approx -x_2 \approx c_2 M_1 \quad (3)$$

and

$$\frac{1}{T} - \frac{1}{T_{\text{fus},1}} \approx - \frac{\Delta T}{T_{\text{fus},1}^2}, \quad (4)$$

which are allowed in the case of diluted solutions.

All this correct—but why do we have to make these simplifications? They were certainly useful 50 years ago, before the advent of pocket calculators, when calculations had to be made with a slide rule or logarithmic tables. But do we really have to burden our students with such equations anymore in the 21st Century?

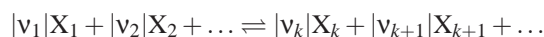
The beginning of thermodynamics as an exact science can be placed in the first half of the 19th Century. We can therefore look back on a success story of about 200 years. But these 200 years were not merely a period of data accumulation; they were a period of quantitative and qualitative development, and of the evolution of concepts. It has happened—and may then happen again—that some concepts reach limits of applicability and then are superseded by new developments. So it may be necessary to replace an equation of state, that was good and sufficient in 1950, by a more powerful one in 2013. One can certainly chop wood with a stone axe, and one can make it really sharp—but in the long run, one should switch to steel!

This article will discuss some cases where models or procedures have arguably been kept too long.

OLD LAWS

Chemical reaction equilibria

One of the cornerstones of chemical thermodynamics is the mass action law, which states that for a chemical reaction



between chemical species X_i (stoichiometric factors v_i assumed to be negative for educts $i < k$ and positive for products ($i \geq k$)) the partial pressures p_i of the species must obey the equation

$$\prod_{i=1}^N \left(\frac{p_i}{p^\ominus} \right)^{v_i} = K, \quad (5)$$

where the equilibrium constant K is related to the Gibbs energy of the reaction,

$$K = \exp \left(- \frac{\Delta_r G_m^\ominus}{RT} \right). \quad (6)$$

¹reference purposely omitted

p^\ominus denotes the thermodynamic reference pressure (usually 0.1 MPa). Eq. (5) is correct for ideal gas mixtures only; for real systems, we have to use fugacities,

$$\prod_{i=1}^N \left(\frac{f_i}{p^\ominus} \right)^{\nu_i} = K, \quad (7)$$

with

$$f_i \equiv \exp \left(\frac{\mu_i - \mu_i^\ominus}{RT} \right); \quad (8)$$

here the μ_i and μ_i^\ominus denote the chemical potentials of the reacting species, which evidently are functions of temperature, pressure, and composition; the μ_i^\ominus are reference values. Moreover, there is an impressive number of variants of the mass action law expressed in terms of mole fractions, concentrations, or activities, most of these involving equilibrium constants that are no longer dimensionless.

Solving Eq. (5), together with the material balance equations, for the equilibrium compositions *analytically* is usually not feasible, except for very simple chemical reactions involving few components under ideal conditions. But if we have to resort to determine the equilibrium *numerically*, there is no need to invoke the mass action law at all. It is more straightforward to use the exact equation from which the mass action law is derived,

$$\sum_{i=1}^N \nu_i \mu_i = \vec{\nu} \cdot \vec{\mu} = 0, \quad (9)$$

where $\vec{\nu}$ and $\vec{\mu}$ are vectors of stoichiometric coefficients and chemical potentials, respectively. This equation is applicable to all chemical reactions and to all states of aggregation. Furthermore, it can be easily extended to multiphase/multireaction systems by applying Eq. (9) to each phase and each chemical reaction, and observing the phase equilibrium condition of having the same μ_i in all phases, e.g., for a system consisting of two phases and having one chemical reaction,

$$\begin{aligned} \sum_{i=1}^N \nu_i \mu_i' &= \vec{\nu} \cdot \vec{\mu}' = 0 \\ \sum_{i=1}^N \nu_i \mu_i'' &= \vec{\nu} \cdot \vec{\mu}'' = 0 \\ \vec{\mu}' &= \vec{\mu}'' \end{aligned} \quad (10)$$

This formulation is easy to teach and easy to program; it does not need activities or fugacities. This does not mean that, after formulating thermodynamic problems in terms of chemical potentials, all computational problems evaporate, but we have at least achieved a clean separation of the modeling (i.e., the way how we compute the $\mu_i(x_i, p, T)$ from the numerical problem of solving the above equations.

Phase equilibria

The phase equilibrium condition in Eq. (9) is applicable to all kinds of phase equilibria and not restricted to subcritical vapour–liquid equilibria like Raoult’s law, another left-over from the past.

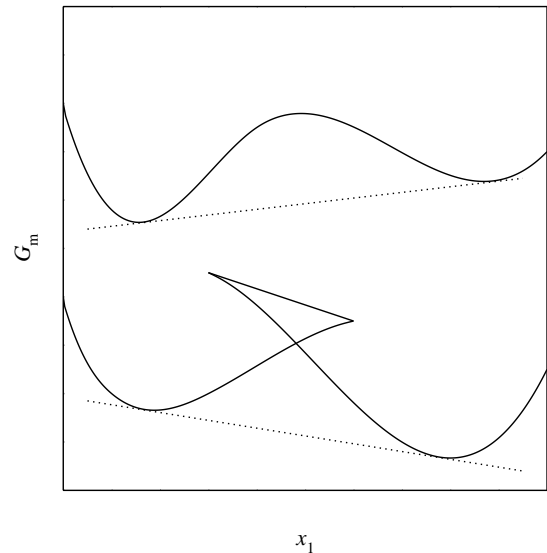


Figure 1. Schematic representation of the Gibbs energy “function” for a 2-phase equilibrium of a binary fluid mixture (continuous and discontinuous case). —: molar Gibbs energy,: double tangent indicating the equilibrium compositions.

It is possible, of course, to pull tricks that make Raoult’s law applicable at supercritical conditions, and the use other equations for liquid–liquid equilibria, and still others for solid–fluid equilibria. But why should me make thermodynamics more complicated than it is?

Principal energy functions

Another time-hallowed concept is the formulation of equilibrium and stability criteria with the help of the Gibbs energy. The Gibbs energy, $G_m(p, T, \vec{x})$ can be obtained from the internal energy, $U_m(V_m, S_m, \vec{x})$, by a series of Legendre transformations. These transformations replace “density variables” (i.e., variable that may have different values in coexisting phases) by “field variables” (i.e., variables that have the same value in coexisting phases). At a first glance, using the Gibbs energy function for phase equilibrium problems simplifies matters. But this simplification comes at a price: As there can be more than one density at a given pressure, the Gibbs energy is, in the strict sense, not a function. A diagram of the Gibbs energy vs. mole fraction for a two-phase equilibrium may exhibit the usual S-shape, but it may alternatively consist of three separate branches—a fact that is not mentioned in many textbooks (Fig. 1). Of course, the physically significant (= stable) value at each composition is always the one with lowest Gibbs energy. But the existence of three branches has consequences for the computation of phase equilibria: Algorithms relying on the local curvature may fail to find the phase equilibrium, as there is no locally concave region along the stable portion of the graph; algorithms not making use of the local curvature are less efficient.

It is advantageous to use the Helmholtz energy instead, $A_m(V_m, T, \vec{x})$, and for many years this has been the customary approach for work based on equations of state. It is better, however, to the Helmholtz energy density, $\Psi(\vec{\rho}, T)$, where $\vec{\rho}$ is the vector of molar densities, $\rho_i = x_i/V_m$. Both functions do not have discontinuities for fluid phase equilibria. The local curva-

ture of the Helmholtz energy surface is described by its Hessian matrix,

$$\hat{A} = \begin{pmatrix} \frac{\partial^2 A_m}{\partial x_1^2} & \frac{\partial^2 A_m}{\partial x_1 \partial x_2} & \cdots & \frac{\partial^2 A_m}{\partial x_1 \partial x_{N-1}} & \frac{\partial^2 A_m}{\partial x_1 \partial V_m} \\ \frac{\partial^2 A_m}{\partial x_2 \partial x_1} & \frac{\partial^2 A_m}{\partial x_2^2} & \cdots & \frac{\partial^2 A_m}{\partial x_2 \partial x_{N-1}} & \frac{\partial^2 A_m}{\partial x_2 \partial V_m} \\ \vdots & \vdots & \ddots & \vdots & \vdots \\ \frac{\partial^2 A_m}{\partial x_{N-1} \partial x_1} & \frac{\partial^2 A_m}{\partial x_{N-1} \partial x_2} & \cdots & \frac{\partial^2 A_m}{\partial x_{N-1}^2} & \frac{\partial^2 A_m}{\partial x_{N-1} \partial V_m} \\ \frac{\partial^2 A_m}{\partial V_m \partial x_1} & \frac{\partial^2 A_m}{\partial V_m \partial x_2} & \cdots & \frac{\partial^2 A_m}{\partial V_m \partial x_{N-1}} & \frac{\partial^2 A_m}{\partial V_m^2} \end{pmatrix}, \quad (11)$$

and that of the Helmholtz energy density by

$$\hat{\Psi} = \begin{pmatrix} \frac{\partial^2 \Psi}{\partial \rho_1^2} & \frac{\partial^2 \Psi}{\partial \rho_1 \partial \rho_2} & \cdots & \frac{\partial^2 \Psi}{\partial \rho_1 \partial \rho_N} \\ \frac{\partial^2 \Psi}{\partial \rho_2 \partial \rho_1} & \frac{\partial^2 \Psi}{\partial \rho_2^2} & \cdots & \frac{\partial^2 \Psi}{\partial \rho_2 \partial \rho_N} \\ \vdots & \vdots & \ddots & \vdots \\ \frac{\partial^2 \Psi}{\partial \rho_N \partial \rho_1} & \frac{\partial^2 \Psi}{\partial \rho_N \partial \rho_2} & \cdots & \frac{\partial^2 \Psi}{\partial \rho_N^2} \end{pmatrix}. \quad (12)$$

In principle, the two Hessians are equivalent. But the elements of \hat{A} have different dimensions, and this makes it impossible to calculate the trace or eigenvalues, which are very useful for stability analysis². It has been shown that initial values for phase equilibrium calculations can be found reliably and the calculation of the equilibrium performed more efficiently with algorithms based on an eigenvalue search on a $\Psi(\vec{\rho}, T)$ surface [1,2].

In particular, the well-known phase equilibrium conditions

$$\begin{aligned} p' &= p'' \\ \mu'_i &= \mu''_i, \quad i = 1 \dots N \end{aligned} \quad (13)$$

become vector equations,

$$\begin{aligned} \nabla \Psi' \cdot (\vec{\rho}'' - \vec{\rho}') &= \Psi'' - \Psi' \\ \nabla \Psi' &= \nabla \Psi'' \end{aligned} \quad (14)$$

Formulating thermodynamic equations this way is not merely an estheticism: modern computer languages and symbolic-algebra packages have built-in vector and matrix operations, and using these features makes programming easier the the program code better readable and maintainable.

The customary way to check for local (diffusion) stability is by calculating the determinant of \hat{A} ; $\det \hat{A} = 0$ is a necessary condition for spinodal and critical states. It can be shown, however, that the computation of eigenvalues λ_i of $\hat{\Psi}$ and setting $\lambda_{\min} = 0$ is a far more efficient method.

Another advantage is that, in a $\vec{\rho}$ -based system, azeotropy does not play a role and thus cannot disturb the convergence of the algorithms.

OLD CONCEPTS FOR EQUATIONS OF STATE

Many recently used equations of state are based on the concept of the hard-sphere fluid, and they are known to perform

²The situation can be remedied by using scaling factors with appropriate dimensions. An axiomatic derivation of Eq. (11) shows that these must exist. But they are usually omitted in the literature.

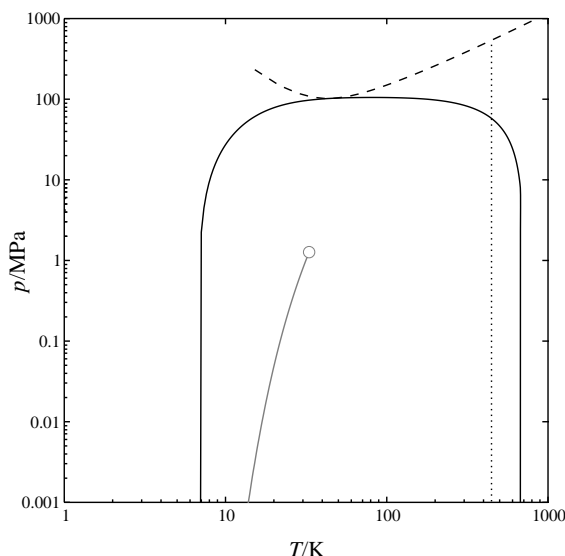


Figure 2. Amagat (Joule inversion) curve of hydrogen, calculated with several equations of state. —: “soft SPHCT equation” (temperature dependence of the size parameter based on perturbation theory) [5], - - : PC-SAFT equation [6], - · - · : Peng–Robinson equation (its Joule inversion curve is an artifact of the temperature function of its attraction term.) [7]; grey line: vapour pressure curve with critical point.

satisfactorily. But is it safe to conclude that an equation that performs well up to 20 MPa will also perform well at 200 MPa? An easy-to-use test is the calculations of Brown’s characteristic curves [3,4]. Along these curves, one of the thermodynamic properties of a real fluid is the same as that on an ideal gas. Here we restrict ourselves to the discussion of the Amagat curve, also known as Joule inversion curve. Its mathematical conditions are either one of

$$\left(\frac{\partial Z}{\partial T} \right)_V = 0 \quad \left(\frac{\partial Z}{\partial p} \right)_V = 0 \quad \left(\frac{\partial p}{\partial T} \right)_V = \frac{p}{T} \quad \left(\frac{\partial U}{\partial V} \right)_T = 0. \quad (15)$$

In a pT diagram, the Amagat curve should have a single maximum and no inflection points, as indicated in Fig. 2. The pressure at the maximum is extremely high, usually 50–100 times the critical pressure. For some compounds, however, this is still in the technically relevant range, e.g., for hydrogen.

But even users not interested in such high pressures are advised to check the Amagat curve, for if there is anything amiss, deviations or odd behaviour of thermodynamic functions can already make themselves felt at lower pressures.

1. As a rule, equations of state containing a hard-sphere term with a temperature-independent size parameter (this applies to most cubic equations of state) do not show a correct Amagat curve, or they do not have an Amagat curve at all. Such equations should be used with caution at high pressures, for some of their derivative properties behave wrongly. The commonly used remedy, namely devising a more complicated temperature dependence of the attraction term, invariably fails when the pressure are high enough.
2. Equations of state containing a hard-sphere term with a simplistic temperature dependence of the size parameter

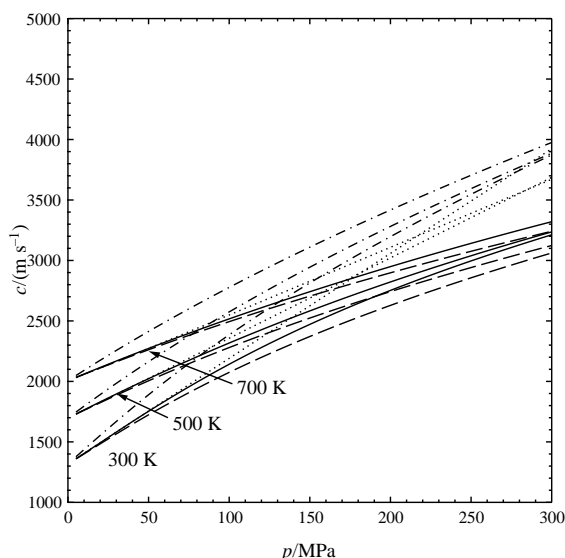


Figure 3. The speed of sound of hydrogen computed with several equations of state. —: reference equation [11], - - : “soft SPHCT” [5], — · — : PC-SAFT [6], ····· : Peng–Robinson equation [7] (using an acentric factor of 0.0). The parameters of the soft SPHCT, PC-SAFT, and PR equations were determined from the critical temperature and pressure.

(usually a T^{-1} dependence or a Boltzmann factor, e.g., BACK [8] or PC-SAFT [6]) usually give distorted Amagat curves. They are not safe at high pressures, too. Moreover, it is known that a temperature dependence of the size parameter may lead to isotherm crossing [9, 10].

- Using a temperature dependence of the size parameter derived from perturbation theory can lead to equations of state with correctly shaped Amagat curves and a very wide pressure range. With modern computers, the numerical overhead for the calculation of the temperature functions is affordable.

The effect on an important thermodynamic property, the speed of sound, is shown in Fig. 3: The curve of the Peng–Robinson equation starts at low pressures with the correct slope, but departs from the reference equation [11] as soon as softness effects make themselves felt. The PC-SAFT equation deviates even more. Only the “soft SPHCT” equation [5], which has a temperature dependence based on Weeks–Chandler–Andersen perturbation theory, can match the behaviour of the reference equation reasonably well³.

Admittedly, the underlying SPHCT equation is too simple for really accurate work. But the principle of the softness correction used for the “soft SPHCT” equation can easily be applied to other equations of state. This adds a numerical complication, but it is desirable to not let real or perceived difficulties of the computational implementation let the design of thermodynamic models too much. In the long run, it is better to use advanced numerical techniques and to keep the better model.

CONCLUSION

Solving scientific or engineering problems can often be regarded as a three-step process, namely

³The reference equation is probably beyond its range of validity at 700 K and 300 MPa.

- devising a mathematical model,
- solving it,
- and interpreting the results.

Ideally, solving and model making should be distinct steps: It is not wise to let our (sometimes insufficient) capabilities to solve equations influence the way how we devise models. Of course, sometimes we cannot avoid it. But if we have to make compromises, we must remember so and look for ways to remedy the situation. Overcoming limitations of models by merely adding one more adjustable parameter usually helps for a while, but not in the long run.

We should not introduce simplifications and approximation at a too early stage of the model making. We should especially avoid making obsolete simplifications and retain exact thermodynamic relations as long as possible.

Over the previous decades, our computing power has become enormous. We can afford to use theories beyond cubic equations of state. But our higher computing power is not only caused by higher processor clock frequencies. Much of it is owed to the availability of high-level programming languages and program libraries. If we formulate our thermodynamic problems in a modern and clear way, using tools of differential geometry, we can efficiently make use of the available numerical tools.

Let us cease honing our stone axes and try to get chainsaws instead!

NOMENCLATURE

A	Helmholtz energy; \hat{A} : its Hessian matrix
f	fugacity
G	Gibbs energy
K	chemical equilibrium constant
N	number of components of a mixture
p	pressure
R	gas constant
S	entropy
T	temperature
U	internal energy
V	volume
x	mole fraction; \vec{x} : vector of all mole fractions of a phase
Z	compression factor, $Z = pV_m/(RT)$
μ	chemical potential; $\vec{\mu}$: vector of all μ_i of a phase
ν	stoichiometric coefficient; $\vec{\nu}$: vector of ν_i for a chemical reaction
ρ	molar density; $\vec{\rho}$: vector of all densities
Ψ	Helmholtz energy density, $\Psi = A/V$; $\hat{\Psi}$: its Hessian matrix

Subscripts

i	component i of a mixture
m	molar property
r	chemical reaction

Superscripts

\ominus	reference value
' , ''	phase indicators

References

- [1] U. K. Deiters and T. Kraska, *High-Pressure Fluid Phase Equilibria—Phenomenology and Computation*, vol. 2 of

- Supercritical Fluid Science and Technology (E. Kiran, ed.), Elsevier, Amsterdam, 2012.
- [2] S. E. Quiñones-Cisneros and U. K. Deiters, An Efficient Algorithm for the Calculation of Phase Envelopes of Fluid Mixtures, *Fluid Phase Equilib.*, vol. 329, pp. 22–31, 2012. doi:10.1016/j.fluid.2012.05.023.
- [3] E. H. Brown, On the Thermodynamic Properties of Fluids, *Bull. Intl. Inst. Refrig., Paris*, Annexe 1960–1961, pp. 169–178, 1960.
- [4] U. K. Deiters and K. M. de Reuck, Guidelines for Publication of Equations of State. I. Pure Fluids, *Pure Appl. Chem.*, vol. 69, pp. 1237–1249, 1997. doi:10.1351/pac199769061237.
- [5] O. L. Boshkova and U. K. Deiters, Soft Repulsion and the Behavior of Equations of State at High Pressures, *Int. J. Thermophys.*, vol. 31, pp. 227–252, 2010. doi:10.1007/s10765-010-0727-7.
- [6] J. Gross and G. Sadowski, Perturbed-Chain SAFT: an Equation of State Based on a Perturbation Theory for Chain Molecules, *Ind. Eng. Chem. Res.*, vol. 40, pp. 1244–1260, 2001.
- [7] D. Y. Peng and D. B. Robinson, A New Two-Constant Equation of State, *Ind. Eng. Chem. Fundam.*, vol. 15, pp. 59–64, 1976.
- [8] S. S. Chen and A. Kreglewski, Applications of the Augmented van der Waals Theory for Fluids. I. Pure Fluids, *Ber. Bunsenges. Phys. Chem.*, vol. 81 pp. 1048–1052, 1977.
- [9] M. A. Trebble and P. R. Bishnoi, Accuracy and Consistency Comparisons of Ten Cubic Equations of State for Polar and Non-polar Compounds, *Fluid Phase Equilib.*, vol 29, pp. 465–474, 1986.
- [10] P. H. Salim and M. A. Trebble, A Modified Trebble–Bishnoi Equation of State: Thermodynamic Consistency Revisited, *Fluid Phase Equilib.*, vol. 65, pp. 59–71, 1991.
- [11] J. W. Leachman, R. T. Jacobsen, S. G. Penoncello, and E. W. Lemmon, Fundamental Equations of State for Parahydrogen, Normal Hydrogen, and Orthohydrogen, *J. Phys. Chem. Ref. Data*, vol. 38, pp. 721–748, 2009.

USE OF A UNIQUE SET OF TEMPERATURE-DEPENDENT BINARY INTERACTION PARAMETERS TO SIMULTANEOUSLY DESCRIBE EXCESS PROPERTIES AND FLUID-PHASE EQUILIBRIUM WITH A CUBIC EQUATION OF STATE

JAUBERT Jean-Noël, PRIVAT Romain

Université de Lorraine, École Nationale Supérieure des Industries Chimiques, Laboratoire Réactions et Génie des Procédés (UMR 7274), 1 rue Grandville, BP 20451, Nancy cedex 9, France.

ABSTRACT

PPR78 is a predictive thermodynamic model that combines the Peng–Robinson equation of state in its 1978 version and the Van Laar activity coefficient model under infinite pressure. A group contribution method is used to accurately quantify the interactions between each pair of molecules. During the last decade, the group–interaction parameters were determined in order to minimize the deviations between experimental and calculated fluid–phase equilibria on hundreds of binary systems. It is indeed acknowledged that accurate phase equilibria is the key point to design and optimize chemical processes. Excess enthalpies and excess heat capacities are however very important quantities because they are involved in the energy and exergy balances of any process. The prediction of such properties with parameters obtained from fluid–phase equilibrium data however does not give satisfactory results. It was thus decided to refit all the group–interaction parameters of the original PPR78 model taking simultaneously into account phase equilibria and excess property data. The resulting model, called *E*–PPR78 (*E* for *Enhanced*) has the same accuracy as the original PPR78 to predict phase equilibria but is able to much better describe excess enthalpies and excess heat capacities.

INTRODUCTION

Today, the synthesis design and optimization steps of chemical processes require more and more to access quasi immediately to PVT properties of a nearly infinite set of molecules in order to select the most efficient ones without having to perform costly and fastidious experiments. In that purpose, group–contribution methods can be of great interest since they allow guesstimating thermodynamic properties of a given mixture from the mere knowledge of chemical structures of molecules constituting it. Starting from these observations, the so–called PPR78 model (for Predictive Peng–Robinson 1978) is developed since 2004 [1–12]. This predictive equation of state (EoS) combines the Peng–Robinson equation in its 1978 version and the Van Laar activity coefficient model under infinite pressure. In addition a group contribution method is used to accurately quantify the interactions between each pair of molecules. Nowadays, the PPR78 model can manage complex mixtures containing alkanes, cycloalkanes, aromatic compounds, alkenes, carbon dioxide, nitrogen, hydrogen sulfide, mercaptans and hydrogen. The group–interaction parameters were determined in order to minimize the deviations between experimental and calculated fluid–phase equilibria on hundreds of binary systems. It is indeed acknowledged that accurate phase equilibria is the key point to design and optimize chemical processes. However, excess enthalpies (h^E) and excess heat capacities (c_P^E) are also very important quantities because they are involved in the energy and exergy balances of any process. Our first task was thus to check whether the PPR78 model could accurately predict such data. The obtained results were however not fully satisfactory. It was realized that while the Peng–Robinson EoS can accurately correlate vapor–liquid equilibrium (VLE) and h^E data separately, attempting to predict the values of one

property with parameters obtained from the other does not give satisfactory results. We thus decided to refit all the group–interaction parameters of the original PPR78 model taking simultaneously into account phase equilibria and excess properties data. Our goal was obviously to obtain an enhanced model having the same accuracy as the original PPR78 to predict phase equilibria but also able to accurately describe excess enthalpies and excess heat capacities.

THE PPR78 MODEL

The PPR78 model relies on the Peng–Robinson EoS [13] which for a given pure component i , can be written as:

$$\begin{aligned}
 P &= \frac{RT}{v-b_i} - \frac{a_i(T)}{v(v+b_i)+b_i(v-b_i)} \\
 \left\{ \begin{aligned}
 R &= 8.314472 \text{ J} \cdot \text{mol}^{-1} \cdot \text{K}^{-1} \\
 X &= \frac{-1 + \sqrt[3]{6\sqrt{2} + 8} - \sqrt[3]{6\sqrt{2} - 8}}{3} \approx 0.253076587 \\
 b_i &= \Omega_b \frac{RT_{c,i}}{P_{c,i}} \\
 \Omega_b &= \frac{X}{X+3} \approx 0.0777961 \\
 a_i &= \Omega_a \frac{R^2 T_{c,i}^2}{P_{c,i}} \left[1 + m_i \left(1 - \sqrt{\frac{T}{T_{c,i}}} \right) \right]^2 \\
 \Omega_a &= \frac{8(5X+1)}{49-37X} \approx 0.4572355 \\
 &\text{if } \omega_i \leq 0.491 \\
 m_i &= 0.37464 + 1.54226\omega_i - 0.26992\omega_i^2 \\
 &\text{if } \omega_i > 0.491 \\
 m_i &= 0.379642 + 1.48503\omega_i - 0.164423\omega_i^2 + 0.016666\omega_i^3
 \end{aligned} \right. \quad (1)
 \end{aligned}$$

where P is the pressure, R is the gas constant, T is the temperature, a and b are respectively the energy parameter and the covolume, v is the molar volume. $T_{c,i}$ is the critical temperature, $P_{c,i}$ is the critical pressure, and ω_i is the acentric factor of a pure component i . Extension to mixtures requires mixing rules for the energy parameter and the covolume.

- A widely employed way to extend the cubic EoS to a mixture containing p components, the mole fractions of which are x_i , is via the so-called Van der Waals one-fluid mixing rules [quadratic composition dependency for both parameters – see Eqs. (2) and (3)] and the classical combining rules, i.e. the geometric mean rule for the cross-energy [Eq. (4)] and the arithmetic mean rule for the cross covolume parameter [Eq. (5)]:

$$a = \sum_{i=1}^p \sum_{j=1}^p x_i x_j a_{ij} \quad (2)$$

$$b = \sum_{i=1}^p \sum_{j=1}^p x_i x_j b_{ij} \quad (3)$$

$$a_{ij} = \sqrt{a_i a_j} (1 - k_{ij}) \quad (4)$$

$$b_{ij} = \frac{1}{2}(b_i + b_j)(1 - l_{ij}) \quad (5)$$

Doing so, two new parameters, the so-called binary interaction parameters (k_{ij} and l_{ij}) appear in the combining rules. One of them, namely k_{ij} is by far the most important one. Indeed, a non null l_{ij} is only necessary for complex polar systems and special cases. This is the reason why, phase equilibrium calculations are generally performed with $l_{ij}=0$ and the mixing rule for the covolume parameter simplifies to:

$$b = \sum_{i=1}^p x_i b_i \quad (6)$$

When used with temperature-independent k_{ij} , cubic EoS with Van der Waals one-fluid mixing rules (VdW1f) lead to very accurate results at low and high pressures for *simple* mixtures (few polar, hydrocarbons, gases). They can however not be applied with success to polar mixtures.

- In order to avoid the limitations of the VdW1f mixing rules, extension of cubic EoS to mixtures can be performed via the so-called EoS/ g^E models. Indeed, g^E models (activity-coefficient models) are applicable to low pressures and are able to correlate polar mixtures. It thus seems a good idea to combine the strengths of both approaches, i.e. the cubic EoS and the activity coefficient models and thus to have a single model suitable for phase equilibria of polar and non-polar mixtures and at both low and high pressures.

The starting point for deriving EoS/ g^E models is the equality of the excess Gibbs energies from an EoS and from an explicit activity coefficient model at a suitable reference pressure. The activity coefficient model may be chosen among the classical forms of molar excess Gibbs energy functions (Redlich-Kister, Margules, Wilson, Van Laar, NRTL, UNIQUAC, UNIFAC...). Such models are

pressure-independent (they only depend on temperature and composition) but the same quantity from an EoS depends on pressure, temperature and composition explaining why a reference pressure needs to be selected before equating the two quantities. In order to avoid confusion, we will write with a special font (G^E) the selected activity coefficient model and with a classical font (g^E) the excess Gibbs energy calculated from an EoS. The starting equation to derive EoS/ g^E models is thus:

$$\left[\frac{g^E}{RT} \right]_P = \frac{G^E}{RT} \quad (7)$$

where subscript P indicates that a reference pressure has to be chosen. The first systematic successful effort in developing such models is that of Huron and Vidal [14], who used the infinite pressure as the reference pressure. Starting from Eq. (7), Huron and Vidal (HV) obtained:

$$\begin{cases} \frac{a(T, \mathbf{x})}{b(\mathbf{x})} = \sum_{i=1}^p x_i \frac{a_i(T)}{b_i} - \frac{G^E}{C_{EoS}} \\ b(\mathbf{x}) = \sum_{i=1}^p x_i b_i \end{cases} \quad (8)$$

where $C_{EoS} = \frac{\sqrt{2}}{2} \ln(1 + \sqrt{2}) \approx 0.62$ for the Peng-Robinson EoS.

Jaubert and Privat [15–16] demonstrated that the introduction of a Van Laar-type excess Gibbs energy model:

$$\frac{G_{Van\ Laar}^E}{C_{EoS}} = \frac{1}{2} \cdot \frac{\sum_{i=1}^p \sum_{j=1}^p x_i x_j b_i b_j E_{ij}(T)}{\sum_{j=1}^p b_j x_j} \quad (9)$$

in Eq. (8) was rigorously equivalent to using VdW1f mixing rules with temperature-dependent k_{ij} . The mathematical relation between $k_{ij}(T)$ [Eq. (4)] and the interaction parameter of the Van-Laar g^E model [$E_{ij}(T)$ in Eq. (9)] is:

$$k_{ij}(T) = \frac{E_{ij}(T) - (\delta_i - \delta_j)^2}{2\delta_i \delta_j} \quad \text{with} \quad \delta_i = \frac{\sqrt{a_i}}{b_i} \quad (10)$$

The works by Jaubert and Privat thus demonstrate that the use of temperature-dependent k_{ij} in the VdW1f mixing rules can overcome the limitations encountered with a constant k_{ij} .

The previous considerations were the starting point for the development of the PPR78 model. We indeed wanted a model which could be used with commercial process simulators in which the PR EoS is systematically available but we also wanted to overcome the limitations of the constant k_{ij} VdW1f mixing rules (which, as previously explained, only apply to simple fluids). This is why, following the previous works of Abdoul et al. [17] a group contribution method (GCM) to estimate indifferently the interaction parameters $E_{ij}(T)$ in Eq. (9) or the $k_{ij}(T)$ in Eq. (4) was developed.

The following equations were considered:

$$E_{ij}(T) = -\frac{1}{2} \sum_{k=1}^{N_g} \sum_{l=1}^{N_g} (\alpha_{ik} - \alpha_{jk}) (\alpha_{il} - \alpha_{jl}) A_{kl} \cdot \left(\frac{298.15}{T/K} \right)^{\left(\frac{B_{kl} - 1}{A_{kl}} \right)} \quad (11)$$

$$k_{ij}(T) = \frac{E_{ij}(T) \left(\text{given by Eq. 11} \right) - \left(\frac{\sqrt{a_i(T)}}{b_i} - \frac{\sqrt{a_j(T)}}{b_j} \right)^2}{2 \sqrt{a_i(T) \cdot a_j(T)} \cdot b_i \cdot b_j} \quad (12)$$

Eq. (11) will be employed with the HV mixing rules and Eq. (12) with the VdW1f mixing rules. In both cases, the same results will be obtained. In Eqs. (11) and (12), T is the temperature. a_i and b_i are the attractive parameter and the covolume of pure i . N_g is the number of different groups defined by the method (for the time being, twenty-one groups are defined and $N_g = 21$). α_{ik} is the fraction of molecule i occupied by group k (occurrence of group k in molecule i divided by the total number of groups present in molecule i). $A_{kl} = A_{lk}$ and $B_{kl} = B_{lk}$ (where k and l are two different groups) are constant parameters determined during the development of the model ($A_{kk} = B_{kk} = 0$). As can be seen, to calculate the k_{ij} (or E_{ij}) parameter between two molecules i and j at a selected temperature, it is only necessary to know: the critical temperatures of both components ($T_{c,i}$, $T_{c,j}$), the critical pressures of both components ($P_{c,i}$, $P_{c,j}$), the acentric factors of each component (ω_i , ω_j) and the decomposition of each molecule into elementary groups (α_{ik} , α_{jk}). It means that no additional input data besides those required by the EoS itself is necessary. Such a model relies on the Peng–Robinson EoS as published by Peng and Robinson in 1978 [Eq. (1)]. The addition of GC method to estimate the temperature-dependent k_{ij} (or E_{ij}) makes it predictive; it was thus decided to call it PPR78 (predictive 1978, Peng Robinson EoS).

For the 21 groups, we had to estimate 420 parameters ($210A_{kl}$ and $210B_{kl}$) the values of which were determined in order to minimize the deviations between calculated and experimental vapor–liquid equilibrium data from an extended data base containing roughly 100,000 experimental data points (56,000 bubble points + 42,000 dew points + 2,000 mixture critical points).

The following objective function was minimized:

$$F = \frac{F_{obj,bubble} + F_{obj,dew} + F_{obj,crit.comp} + F_{obj,crit.pressure}}{n_{bubble} + n_{dew} + n_{crit} + n_{crit}} \quad (13)$$

with:

$$\left\{ \begin{aligned} F_{obj,bubble} &= 100 \sum_{i=1}^{n_{bubble}} 0.5 \left(\frac{|\Delta x|}{x_{1,exp}} + \frac{|\Delta x|}{x_{2,exp}} \right)_i ; |\Delta x| = |x_{1,exp} - x_{1,cal}| \\ F_{obj,dew} &= 100 \sum_{i=1}^{n_{dew}} 0.5 \left(\frac{|\Delta y|}{y_{1,exp}} + \frac{|\Delta y|}{y_{2,exp}} \right)_i ; |\Delta y| = |y_{1,exp} - y_{1,cal}| \\ F_{obj,crit.comp} &= 100 \sum_{i=1}^{n_{crit}} 0.5 \left(\frac{|\Delta x_c|}{x_{c1,exp}} + \frac{|\Delta x_c|}{x_{c2,exp}} \right)_i ; |\Delta x_c| = |x_{c1,exp} - x_{c1,cal}| \\ F_{obj,crit.pressure} &= 100 \sum_{i=1}^{n_{crit}} \left(\frac{P_{cm,exp} - P_{cm,cal}}{P_{cm,exp}} \right)_i \end{aligned} \right.$$

n_{bubble} , n_{dew} and n_{crit} are the number of bubble points, dew points and mixture critical points respectively. x_1 is the mole fraction in the liquid phase of the most volatile component and x_2 the mole fraction of the heaviest component (it is obvious that $x_2 = 1 - x_1$). Similarly, y_1 is the mole fraction in the gas phase of the most volatile component and y_2 the mole fraction of the heaviest component (it is obvious that $y_2 = 1 - y_1$). x_{c1} is the critical mole fraction of the most volatile component and x_{c2} the critical mole fraction of the heaviest component. P_{cm} is the binary critical pressure.

For all the data points included in our database, the objective function defined by Eq. (13) is only:

$$F_{obj} = 7.6 \% \quad (14)$$

The average overall deviation on the liquid phase composition is:

$$\overline{\Delta x \%} = \frac{\overline{\Delta x_1 \%} + \overline{\Delta x_2 \%}}{2} = \frac{F_{obj,bubble}}{n_{bubble}} = 7.4 \% \quad (15)$$

The average overall deviation on the gas phase composition is:

$$\overline{\Delta y \%} = \frac{\overline{\Delta y_1 \%} + \overline{\Delta y_2 \%}}{2} = \frac{F_{obj,dew}}{n_{dew}} = 8.0 \% \quad (16)$$

The average overall deviation on the critical composition is:

$$\overline{\Delta x_c \%} = \frac{\overline{\Delta x_{c1} \%} + \overline{\Delta x_{c2} \%}}{2} = \frac{F_{obj,crit.comp}}{n_{crit}} = 7.1 \% \quad (17)$$

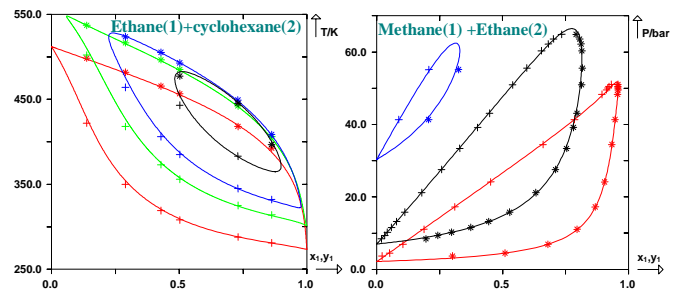
The average overall deviation on the binary critical pressure is:

$$\overline{\Delta P_c \%} = \frac{F_{obj,crit.pressure}}{n_{crit}} = 4.9 \% \quad (18)$$

We can thus assert that the PPR78 model is an accurate thermodynamic model which it is able to predict fluid–phase equilibria in any mixture containing alkanes, aromatics, naphthenes, CO₂, N₂, H₂S, H₂, mercaptans, water and alkenes.

It is today integrated in many process simulators like ProSimPlus, PRO/II, ChemSep, GEM–Selektor, EQ–COMP (and probably soon in UniSim).

Figure 1 graphically illustrates the accuracy of the PPR78 model.



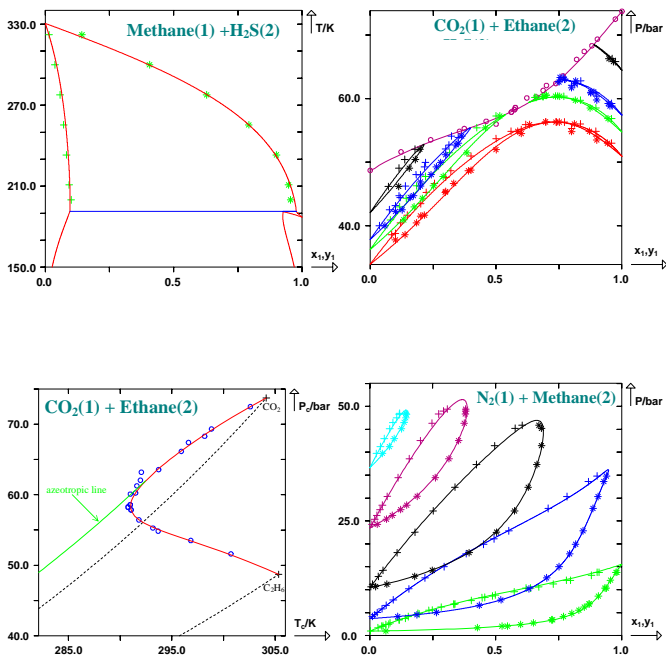


Figure 1. Illustration of the accuracy of the PPR78 model. The symbols are the experimental data points. The full lines are the predictions with the PPR78 model.

FROM THE PPR78 MODEL TO THE E -PPR78 MODEL

The PPR78 model being able to predict with accuracy fluid–phase equilibria, it was decided to test its ability to predict excess enthalpies (h^E) and excess heat capacities (c_P^E). A literature review made it possible to collect 30,000 h^E data points over 500 binary systems and 2,000 c_P^E data points over 100 binary systems.

By definition, the molar excess enthalpy h^E [see Eq. (19)] is the difference between the molar enthalpy of a solution and the sum of the molar enthalpies of the components which make it up, all at the same temperature and pressure as the solution, in their actual state weighted by their mole fractions z_i :

$$h^E(T, P, z) = h(T, P, z) - \sum_{i=1}^P z_i \cdot h_{\text{pure } i}(T, P) \quad (19)$$

For nearly ideal solutions i.e. when the molecules of a mixture are similar, h^E tends to zero and its influence on an energy balance is negligible. For such systems (e.g. mixture of n–hexane and n–heptane), high relative deviations – even higher than 200 % – are totally acceptable. In return, for highly non–ideal systems, h^E values can reach several kJ/mol and important absolute deviations can have a detrimental impact on the energy balance even if the corresponding relative deviations remain low (20 % deviation on a h^E value of 5 kJ/mol leads to a non–acceptable absolute deviation of 1 kJ/mol). For these reasons, the deviations on the excess enthalpies were neither expressed as relative nor absolute deviations but instead as a temperature difference defined by:

$$\Delta T = \left| \frac{h_{\text{cal}}^E - h_{\text{exp}}^E}{c_P} \right| \quad (20)$$

where h_{cal}^E and h_{exp}^E are respectively the calculated and the experimental h^E values. c_P is the heat capacity of the mixture.

From an engineering point of view, a deviation of 1 K is considered as acceptable. For the 30,000 experimental h^E data point collected, the PPR78 model lead to an average deviation of: $\overline{\Delta T}_{\text{PPR78}} = 2.1 \text{ K}$ which is at least twice too high.

Regarding the accuracy on the c_P^E prediction, an average deviation (on the 2,000 experimental data points) of: $\overline{\Delta c_P^E}_{\text{PPR78}} = 14.5 \text{ J} \cdot \text{mol}^{-1} \cdot \text{K}^{-1}$ was obtained. Such a

deviation is huge and totally unacceptable. c_P^E values are indeed generally small and only a deviation smaller than $0.5 \text{ J} \cdot \text{mol}^{-1} \cdot \text{K}^{-1}$ can be considered as acceptable. In front of such disappointing results, the group–interaction parameters [A_{kl} and B_{kl} in Eq. (11)] were fitted in order to minimize an objective function which took into account only the deviations on h^E and c_P^E . In that case, very accurate predictions could be obtained on such quantities but the deviations on VLE data were really too large. Moreover, we found unacceptable to have two sets of parameters: one for phase–equilibrium calculations and another one to perform energy balances. Indeed phase equilibrium and enthalpy calculations are frequently made together and it is thus useful to consider the applicability of a single set of parameters to both these properties. This statement was the basis to develop the E -PPR78 model in which the group–interaction parameters were determined in order to minimize an objective function which included both the deviations on the fluid–phase compositions [see Eq. (13)] and the deviations on the excess properties. The corresponding A_{kl} and B_{kl} group–interaction parameters are not yet published but can be found in the thesis by Qian [18]. The deviations obtained with such an enhanced model can be summarized as follows:

- the deviation on fluid–phase equilibria is:

$$\overline{F_{\text{obj } E\text{-PPR78}}} = 7.8 \% \quad [\text{see Eq. (13)}]$$

- the deviation on h^E is:

$$\overline{\Delta T}_{E\text{-PPR78}} = 0.6 \text{ K}$$

- the deviation on c_P^E is:

$$\overline{\Delta c_P^E}_{E\text{-PPR78}} = 0.5 \text{ J} \cdot \text{mol}^{-1} \cdot \text{K}^{-1}$$

Such deviations highlight that the accuracy of the E -PPR78 model to predict fluid–phase equilibria, is the same as the one obtained with the original PPR78 model (the two objective functions: 7.6 % and 7.8 % are very close). On the other hand, the E -PPR78 model allows a much better prediction of the h^E (ΔT has been divided by a factor 3.5) and a spectacular improvement on the c_P^E prediction can be noticed.

Figure 2 graphically illustrates the accuracy of the E -PPR78 model to predict excess properties.

the simultaneous correlation of phase equilibrium and excess properties data.

ACKNOWLEDGEMENT

The French Petroleum Company TOTAL and more particularly Dr. Pierre Duchet–Suchaux (expert in thermodynamics) is gratefully acknowledged for sponsoring this research.

REFERENCES

- [1] Jaubert, J.N. & Mutelet, F. (2004). VLE predictions with the Peng–Robinson equation of state and temperature dependent k_{ij} calculated through a group contribution method. *Fluid Phase Equilib.*, Vol.224, No.2, pp. 285–304
- [2] Jaubert, J.N.; Vitu, S.; Mutelet, F. & Corriou, J.P. (2005). Extension of the PPR78 model to systems containing aromatic compounds. *Fluid Phase Equilib.*, Vol.237, No.1–2, pp 193–211
- [3] Vitu, S.; Jaubert, J.N. & Mutelet, F. (2006). Extension of the PPR78 model (Predictive 1978, Peng Robinson EoS with temperature dependent k_{ij} calculated through a group contribution method) to systems containing naphthenic compounds. *Fluid Phase Equilib.*, Vol.243, pp. 9–28
- [4] Vitu, S.; Privat, R.; Jaubert, J.N. & Mutelet, F. (2008). Predicting the phase equilibria of CO₂ + hydrocarbon systems with the PPR78 model (PR EoS and k_{ij} calculated through a group contribution method). *J. Supercrit. Fluids.*, Vol.45, No.1, pp. 1–26
- [5] Privat, R.; Jaubert, J.N. & Mutelet, F. (2008). Addition of the Nitrogen group to the PPR78 model (Predictive 1978, Peng Robinson EoS with temperature dependent k_{ij} calculated through a group contribution method). *Ind. Eng. Chem. Res.*, Vol.47, No.6, pp. 2033–2048
- [6] Privat, R.; Jaubert, J.N. & Mutelet, F. (2008). Addition of the sulfhydryl group (–SH) to the PPR78 model (Predictive 1978, Peng–Robinson EoS with temperature dependent k_{ij} calculated through a group contribution method). *J. Chem. Thermodyn.*, Vol. 40, No.9, pp. 1331–1341
- [7] Privat, R.; Jaubert, J.N. & Mutelet, F. (2008). Use of the PPR78 model to predict new equilibrium data of binary systems involving hydrocarbons and nitrogen. Comparison with other GCEOS. *Ind. Eng. Chem. Res.*, Vol.47, No.19, pp. 7483–7489
- [8] Privat, R.; Mutelet, F. & Jaubert, J.N. (2008). Addition of the Hydrogen Sulfide group to the PPR78 model (Predictive 1978, Peng Robinson EoS with temperature dependent k_{ij} calculated through a group contribution method). *Ind. Eng. Chem. Res.*, Vol.47, No.24, pp. 10041–10052
- [9] Jaubert, J.N.; Privat, R. & Mutelet, F. (2010). Predicting the phase equilibria of synthetic petroleum fluids with the PPR78 approach. *AIChE J.*, Vol.56, No.12, pp. 3225–3235
- [10] Privat, S. & Jaubert, J.N. (2012). Addition of the sulfhydryl group (SH) to the PPR78 model: Estimation of missing group–interaction parameters for systems containing mercaptans and carbon dioxide or nitrogen or methane, from newly published data. *Fluid Phase Equilib.*, Vol.334, pp. 197–203
- [11] Qian, J.W.; Jaubert J.N. & Privat R. (2013). Phase equilibria in hydrogen–containing binary systems modeled with the Peng–Robinson equation of state and

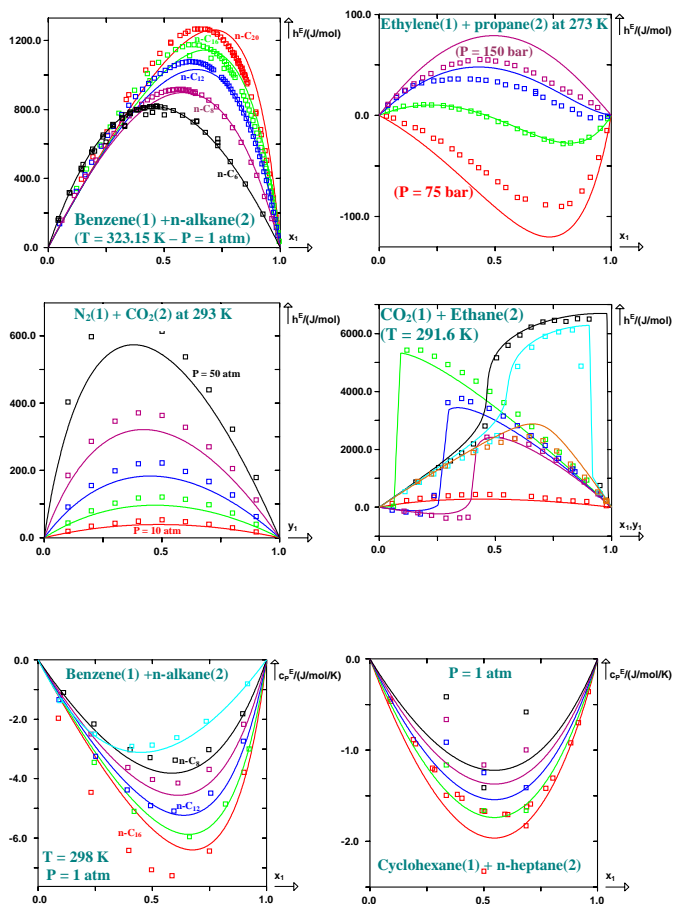


Figure 2. Illustration of the accuracy of the E–PPR78 model. The symbols are the experimental data points. The full lines are the predictions with the E–PPR78 model.

CONCLUSION

In this study, the parameters of the PPR78 model have been readjusted by considering phase equilibrium (vapor–liquid equilibrium, liquid–liquid equilibrium, mixture critical points), excess enthalpy and excess heat capacity data, in order to have a simultaneous correlation of VLE, LLE, h^E and c_p^E . The resulting model has been called E–PPR78 where E means enhanced.

Several conclusions can be made from this work:

- (1) In comparison with the original PPR78 model, by using this enhanced version, the prediction quality of VLE and LLE is retained, as well as that of mixture critical points. On the other hand, the accuracy of the predicted h^E (and c_p^E) data has been remarkably improved.
- (2) It is possible to use a cubic EoS with a unique set of temperature–dependent binary interaction parameters to represent both phase equilibrium and excess properties.
- (3) Fitting parameters only to excess properties data or only to phase–equilibrium data deteriorates the prediction of VLE data and of excess properties, respectively. Consequently, parameters must be fitted by considering

- temperature-dependent binary interaction parameters calculated through a group-contribution method. *J. Supercrit. Fluids.*, Vol.75, pp. 58–71
- [12] Qian, J.W.; Jaubert J.N. & Privat R. (2013). Prediction of the phase behavior in alkene-containing binary systems with the PPR78 model. *Fluid Phase Equilib.*, (submitted for publication).
- [13] Peng, D.Y. & Robinson, D.B. (1978). The characterization of the heptanes and heavier fractions for the GPA Peng–Robinson programs. Gas Processors Association Research Report 28 pp. 1–36
- [14] Huron, M.J. & Vidal, J. (1979). New mixing rules in simple equations of state for strongly non-ideal mixtures. *Fluid Phase Equilib.*, Vol.3, pp. 255–271
- [15] Jaubert, J.N. & Privat, R. (2010). Relationship between the binary interaction parameters (k_{ij}) of the Peng–Robinson and those of the Soave–Redlich–Kwong equations of state. Application to the definition of the PR2SRK model. *Fluid Phase Equilib.*, Vol.295, pp. 26–37
- [16] Jaubert, J.N.; Qian, J.W.; Privat, R. & Leibovici C.F. (2013). Reliability of the correlation allowing the k_{ij} to switch from an alpha function to another one in hydrogen-containing systems. *Fluid Phase Equilib.*, Vol.338, pp. 23–29
- [17] Abdoul, W.; Rauzy, E. & Péneloux, A. (1991). Group-contribution equation of state for correlating and predicting thermodynamic properties of weakly polar and non-associating mixtures. Binary and multicomponent systems. *Fluid Phase Equilib.*, Vol.68, pp. 47–102
- [18] Qian, J.W. (2011). Développement du modèle E–PPR78 pour prédire les équilibres de phases et les grandeurs de mélange de systèmes complexes d'intérêt pétrolier sur de larges gammes de températures et de pressions. Ph.D thesis, Université de Lorraine, pp. 1–266.

COARSE-GRAINED SIMULATIONS OF OIL-WATER-SURFACTANT MIXTURES

Bernard Rousseau*

*Laboratoire de Chimie Physique, CNRS & Université Paris-Sud, Bâtiment 349, 91405 Orsay Cedex, France, E-mail: bernard.rousseau@u-psud.fr

EXTENDED ABSTRACT

Mixtures of oil and water are naturally unstable but they can be stabilized by addition of surfactant molecules to form microemulsions. Microemulsions are macroscopically homogeneous mixtures but present, at the microscopic scale, large heterogeneities with water-rich and oil-rich domains separated by a surfactant film. The properties of this film are essential for microemulsions as a whole; amongst them, interfacial tension plays a crucial role as it is strongly related with the microemulsion structure [1].

Intensive research in this area have shown that interfacial tension at the oil-water interface can be modified by several factors including the chemistry of the surfactant hydrophilic part (ionic or non-ionic), the number and length of the hydrophobic parts, surfactant concentration, addition of a co-surfactant, addition of salts [2,3,4]. . . In order to understand the interplay between the different species in presence and eventually to tailor new surfactants or even surfactant mixtures, several attempts have been made to compute interfacial tension from molecular dynamics, Monte Carlo or coarse-grained simulation tools. As usual, the prediction of thermodynamical properties using approaches based on statistical mechanics, requires both an efficient tool to sample the phase space of the system and an empirical forcefield that describes intermolecular interactions as accurately as possible.

Monte Carlo and Molecular Dynamics simulations make an intensive use of empirical forcefields that can accurately predict surface tension in simple liquids or liquid mixtures. By using a system description at the atomistic level, a good understanding of processes can be gained. However, the time and length scales involved in the simulation of oil-water-surfactant usually go beyond what is commonly attainable today with these tools. Therefore, coarse-grained simulations, where particles represent several molecules, or groups of atoms inside a given molecule, are nowadays used as an alternative tool to study such complex systems. One of the most commonly used tool is dissipative particle dynamics proposed by Hoogerbrugge and Koelman [5].

In this paper, we will try to review the difficulties that arise from studying such systems using coarse-grained models [6], in particular when direct comparison with experimental data is wished (see Fig. 1 and Fig. 2).

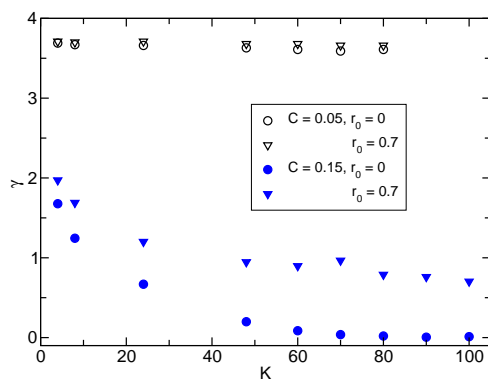


Figure 1. Interfacial tension γ in a model oil-water-surfactant mixture, versus the intramolecular bonding force constant K for different equilibrium bond lengths r_0 and different surfactant concentrations. At large surfactant concentration, surface tension strongly depends on surfactant intramolecular parameters.

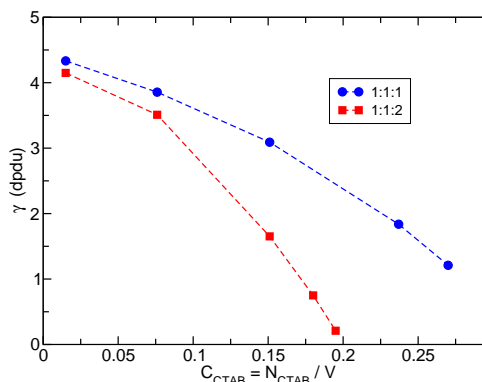


Figure 2. Interfacial tension γ in a model oil-water-surfactant mixture, versus total surfactant concentration in boxes with different shapes (cubic and parallelepipedic). It is shown that interfacial tension depends on box shape if plotted versus total surfactant concentration. Rather, "bulk concentration" or "interfacial concentration" must be used in order to get meaningful results.

We will present the conditions under which chemical (and thermodynamical...) equilibrium is reached and show that spurious effects can arise such as *box shape* effects. We will discuss the possible solutions that have been proposed to handle electrostatic interactions in coarse-grained models, and how consistent forcefield can be derived to describe accurately such systems. Last but not least, we will wonder how dynamical informations can be obtained from dissipative particle dynamics simulations.

REFERENCES

- [1] H. Kellay, B. P. Binks, Y. Hendriks, L.T. Lee and J. Meunier, Properties of surfactant monolayers in relation to microemulsion phase behaviour, *Advances in Colloid and Interface Science* vol. 49, pp. 85-112, 1994.

- [2] R. Aveyard, B.P. Binks and J. Mead, Interfacial tension in Oil+Water+Surfactant systems; Effect of Salt and Temperature in Systems containing Non-ionic Surfactants, *J. Chem. Soc., Faraday Trans 1* vol. 81, pp. 2155-2168, 1985
- [3] R. Aveyard, B.P. Binks and J. Mead, Interfacial tension in Oil+Water+Surfactant systems; Effects of Salt, Temperature and Alkane in systems containing Ionic Surfactants, *J. Chem. Soc., Faraday Trans 1* vol. 81, pp. 2169-2177, 1985
- [4] R. Aveyard, B.P. Binks and J. Mead, Interfacial tension in Oil-Water-Surfactant systems; Effect of Cosurfactant in Systems containing SDS, *J. Chem. Soc., Faraday Trans 1* vol. 83, pp. 2347-2357, 1987
- [5] P.J. Hoogerbrugge and J.M.V.A. Koelman, Simulating Microscopic Hydrodynamic Phenomena with Dissipative Particle Dynamics, *Europhysics Letters* vol. 19, pp.155160, 1992.
- [6] E. Deguillard, N. Pannacci, B. Creton and B. Rousseau, Interfacial tension in oil–water–surfactant systems: On the role of intra-molecular forces on interfacial tension values using DPD simulations, *J. Chem. Phys.* vol. 138, pp. 144102, 2013.

STATISTICAL THERMODYNAMICS-BASED SIMULATION METHODS FOR THE PREDICTION OF POLYMER PROPERTIES

Doros N. Theodorou

School of Chemical Engineering, Department of Materials Science and Engineering, National Technical
University of Athens, Zografou Campus, 157 80 Athens, Greece

ABSTRACT

Molecular simulations can quantitatively relate thermodynamic properties and phase equilibria to atomic-level structure and therefore serve as a basis for “molecular engineering design” of materials. For polymeric materials, however, the broad spectra of length scales and relaxation times governing structure and molecular motion pose severe challenges for conventional simulation techniques. Many of these challenges have been met by designing simulation methods based on the principles of statistical thermodynamics, which can sample complex configuration spaces efficiently. Examples of such methods include connectivity-altering Monte Carlo simulations, which enable the reliable prediction of equation of state properties, molecular packing, and entanglements in polymer melts; particle deletion (inverse Widom) methods for the calculation of solubilities of large molecules in polymers; and Gibbs-Duhem integration methods, based on the imposition of an artificial potential, to capture polymer melting points. Many problems are still not completely resolved, however, such as (a) how to coarse-grain the molecular representation into one involving fewer degrees of freedom; (b) how to address systems which do not achieve equilibrium over ordinary time scales, such as glasses; (c) how to deal with crack propagation and fracture.

INTRODUCTION

Molecular simulations are gaining ground as tools for the prediction of properties of a wide variety of physicochemical, materials, and biomolecular systems [1]. In materials science simulations are starting to be used within high-throughput screening strategies to optimize atomic-level structure for best performance in specific applications. This is exemplified by recent work on the design of nanoporous materials for methane storage [2].

One challenge faced by molecular simulations of materials is that accurate potentials for interatomic interactions are often unavailable. A second, perhaps more important challenge, is that structure and molecular motion in most materials of engineering interest are governed by very broad spectra of length and time scales, which are impossible to address with a single simulation technique. In response to these challenges, multiscale strategies are being developed, which extend from electronic structure calculations to atomistic molecular mechanics, molecular dynamics (MD), and Monte Carlo (MC) simulations, to mesoscopic methods, to formulations based on the continuum engineering sciences [3].

The challenge of long time scales is painfully clear in the case of polymeric materials. The longest relaxation times of polymer melts encountered in processing operations are typically on the order of ms to s. It is these broad spectra of relaxation times that are responsible for the complex viscoelastic behavior exhibited by polymer melts. On the other hand, the longest times that have been simulated with MD using classical force fields for interatomic interactions on specialized computational equipment are on the order of ms [4], with hundreds of ns being more typical of Beowulf clusters in university laboratories. Clearly, there are still several orders of magnitude on the time scale to be bridged in order to connect atomic-level structure with macroscopic

performance.

Fortunately, one can devise simulation methods that can sample rugged potential energy hypersurfaces very efficiently and equilibrate atomistic or coarse-grained polymer models many orders of magnitude faster than “brute force” MD. These methods are based directly on the principles of statistical and macroscopic thermodynamics and take advantage of some geometric characteristics of macromolecular systems.

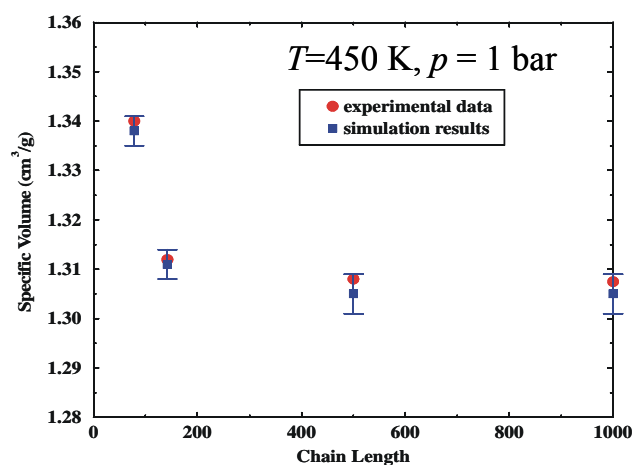
In this paper we will briefly present some examples of efficient equilibration strategies for polymers and estimates of thermodynamic properties and phase equilibria that are obtained from their application, mainly at the atomistic level. We will then outline remaining challenges to the development of reliable multiscale simulation strategies for polymers.

EFFICIENT EQUILIBRATION STRATEGIES FOR POLYMERS

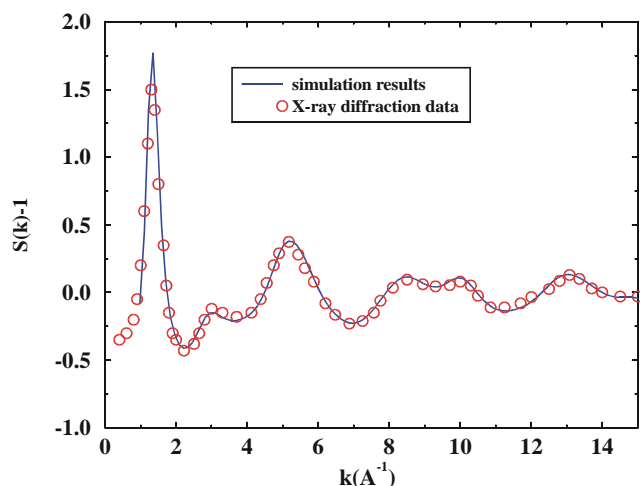
Connectivity-altering MC

MC algorithms that employ moves which rearrange the connectivity among polymer segments can dramatically enhance the equilibration of long-range conformational characteristics, such as the end-to-end distance and the radius of gyration. While the longest relaxation time of a real, or MD-simulated, long-chain melt scales with molar mass as $M^{3.4}$, the CPU time required by End-Bridging MC for the displacement of chain centers of mass to reach the root mean square end-to-end distance of chains, $\langle R^2 \rangle^{1/2}$, scales as M^{-1} [5]. Thus, the equilibration of long-chain polymer systems, well within the entangled regime, comes within reach. Predictions for the density as a function of M , for X-ray diffraction patterns and SANS single-chain structure factors are in excellent agreement with experiment, using force fields validated for small-molecule analogues [5] (see Figure 1).

Moreover, topological analysis of well-equilibrated long-chain configurations leads to estimates of the molar mass between entanglements, M_e , which are validated by plateau modulus measurements [6]. Recently, connectivity-altering MC has been used to elucidate how the melt density, entanglement properties, and cohesive energy density depend on short-chain branching in polyethylenes [7].



(a)



(b)

Figure 1: (a) Specific volume as a function of chain length, in carbon atoms, for linear polyethylene melts at 450 K and 1 atm, as predicted by connectivity-altering Monte Carlo simulations and as measured experimentally; (b) Static structure factor as predicted from the simulations and as measured by X-ray diffraction.

Particle Deletion for Chemical Potentials

The calculation of chemical potentials is central to the prediction of phase equilibria. Widom's test particle insertion [8] is an ingenious method for computing chemical potentials from simulation. Unfortunately, when the size of inserted molecules is large in comparison to clusters of accessible volume present in the matrix material, overlaps occur with overwhelming probability and a reliable estimation of the chemical potential becomes impossible.

A number of methods have been proposed to alleviate the insertion problem. One that has worked well for polymers is the particle deletion, or inverse Widom, method [9]. Here one estimates the chemical potential not by inserting a molecule, but rather by deleting an already existing molecule from the system. One has to realize that deleting a molecule does not lead to a typical configuration of the remaining system, but rather to a configuration that contains a hole. The bias associated with the hole can be rigorously removed through computationally efficient analytical calculations of the accessible volume. Application of the particle deletion method has led to excellent estimates of the solubility of large solvent molecules, such as benzene, in equilibrated polyethylene melts [10] (see Figure 2). Using the same method, it has been possible to capture sorption equilibria of compressed CO₂ in glassy atactic polystyrene, as well as swelling and plasticization effects caused by the sorption [11].

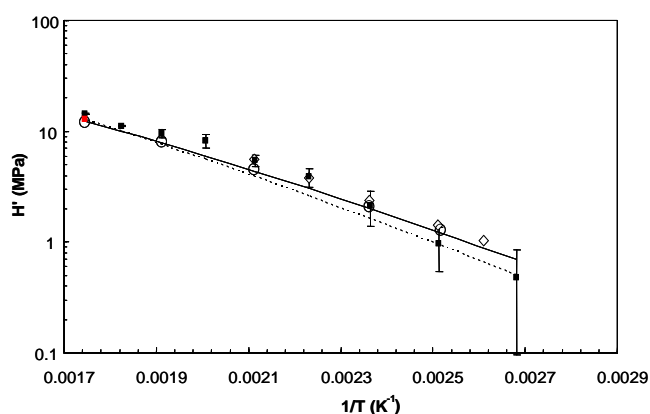


Figure 2: Solubility of benzene in molten polyethylene as a function of temperature, as predicted by isothermal-isobaric MC simulations with the direct particle deletion method (filled points) [10] and as measured experimentally (open points). The solid and broken lines display estimates from the PC SAFT and the Lattice Fluid equations of state, respectively. The red point is a simulation estimate obtained from a simulation box of octuple volume, in order to establish that there are no system size effects. The solubility is expressed in terms of a weight fraction-based Henry's law constant, H' . H' is the ratio of the fugacity of benzene to the weight fraction of benzene in the polyethylene, in the limit where the latter weight fraction goes to zero.

Melting Points Through Gibbs-Duhem Integration

Predicting the complex morphology and properties of semicrystalline polymers is a grand challenge for molecular simulation. Even the prediction of T_m , the equilibrium melting point of a polymer crystal, presents difficulties. By analogy to what is done for small-molecule materials, one can build a composite (sandwich) structure consisting of alternating crystalline and melt domains and try to determine T_m by MD as that temperature where none of the two types of domains increases at the expense of the other. Unfortunately, however, polymer crystal growth rates are too low to be observed reliably with MD. For example, the crystal growth

rate for high molar mass isotactic polypropylene (iPP) has been reported as $2.2 \times 10^{-7} \text{ m s}^{-1}$. This means that, in order to observe growth of a facet by an average distance of 1 \AA , one would need to simulate for 450 \mu s , a prohibitively long time.

One way to get around this problem is to introduce an artificial potential along polymer chains which encourages the adoption of helical conformations. The resulting system of stiffened chains has a much higher T_m which can be predicted reliably by MD, as the molecular dynamics there is fast. The objective then is to compute how the predicted T_m will change upon removal of the artificial potential. Starting from the condition of equality of chemical potentials between solid and liquid phases, one can derive, through straightforward thermodynamics, an expression for the derivative of T_m with respect to a parameter, λ , controlling the stiffness of the artificial potential. This expression involves only ensemble averaged energies and volumes of the individual solid and liquid phases at given λ , which can be extracted from single-phase simulations at fixed λ . Gibbs-Duhem integration of the derivative down to $\lambda=0$ gives T_m for the “real”, unconstrained polymer [12]. Application of this strategy has yielded very good estimates of T_m for oligomers of iPP of various molar masses (Figure 3).

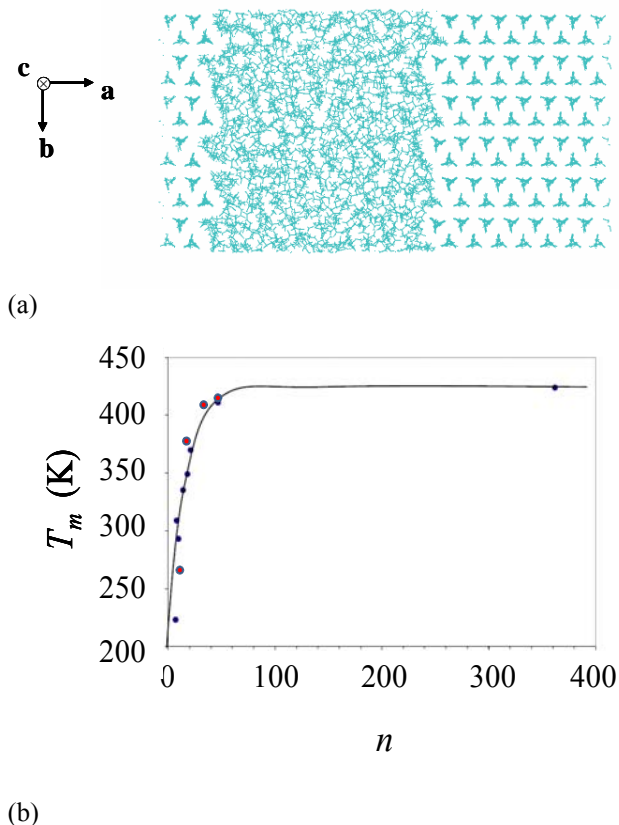


Figure 3: (a) “Sandwich” configuration of molten and crystalline isotactic polypropylene considered for the calculation of the melting point T_m . **a**, **b**, and **c** are the crystallographic axes of the monoclinic $\alpha 1$ form of isotactic polypropylene. At equilibrium, none of the two coexisting phases will grow against the other. (b) Equilibrium melting point of isotactic polypropylene at 1 atm as a function of chain length (number of repeat units n), as predicted by MD simulations of the melt and crystal phases through a Gibbs-Duhem integration scheme (red points) [12] and as measured experimentally (blue points and line).

POLYMERS UNDER STRESS: CAVITATION OF RUBBERS

Statistical thermodynamics-based simulation methods are often called to provide insight into the stress-strain and terminal mechanical behaviour of polymeric materials. We briefly outline here a recently developed approach for exploring cavitation in rubbery polymers [13].

Cavitation, i.e. the development of cavities in a rubbery polymer subjected to hydrostatic tension, is a very important problem. The development of cavities in the rubbery primary coating between the inner core and the hard secondary coating of an optical fibre upon temperature cycling, due to thermal expansion mismatch, compromises light transmission through the fibre. Cavitation is also the first step in debonding two solid surfaces across a layer of pressure-sensitive adhesive.

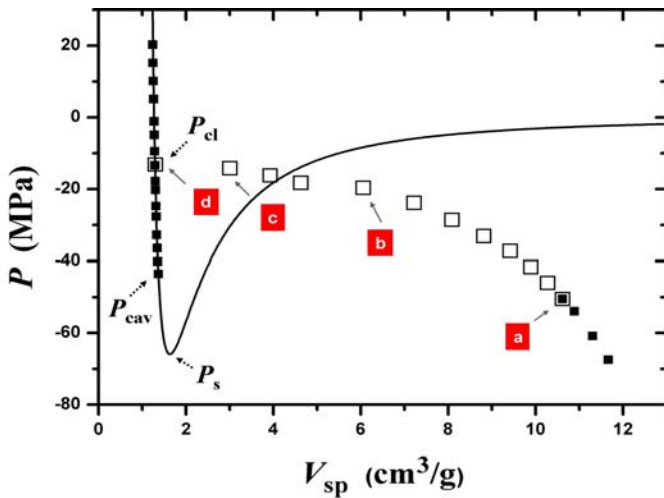
Perfect polymer network “specimens” with the chemical constitution of polyethylene, consisting of monodisperse subchains terminally linked at tetrafunctional crosslink points with no dangling ends, have been prepared and fully characterized mechanically under tension/compression via MD simulations. The specimens have been subjected to hydrostatic tension computer experiments at various levels of stress (negative pressure) [13]. They have been found to cavitate at a stress level, $-P_{cav}$, which is somewhat lower than the limit of mechanical stability, $-P_s$, of the rubbery polymer and of the corresponding linear melt. Analysis of the time to cavitation reveals a nucleation process involving the formation of a critical cavity in unstable mechanical equilibrium, through density fluctuations in the material.

Upon unloading a cavitated specimen, hysteresis is observed on the pressure-specific volume diagram. The volume of the cavitated specimen decreases as the hydrostatic stress is reduced, cavities coalescing into a single spherical cavity which snaps closed at a characteristic stress level $-P_{cl}$, considerably lower than $-P_{cav}$ (see Figure 4). Repeating the loading and unloading experiment in a cyclic fashion causes the material to retrace the loading path of its homogeneous state on the pressure-volume diagram, cavitate at P_{cav} , then trace the unloading path of its cavitated state, and snap back closed at P_{cl} . The isothermal behaviour is thus entirely analogous to a van der Waals loop associated with a first-order phase transition between a homogeneous and a cavitated phase.

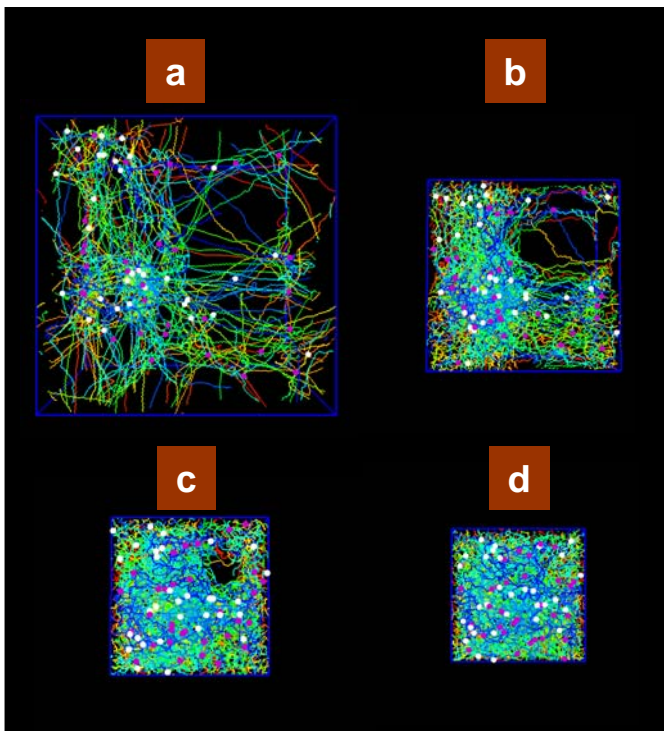
The closure stress, $-P_{cl}$, i.e., the stress below which a pre-existing cavity cannot survive within the material, is commensurate with the Young's modulus of the rubber, E . It is entirely comparable to the critical stress anticipated by A.N. Gent and collaborators [14] on the basis of continuum mechanical arguments. Gent et al. considered a pre-existing spherical cavity within a material exhibiting nonlinear large-deformation elasticity following the neo-Hookean equation of state and showed that the cavity will start growing without limit at a critical stress of $5E/6$. The actual values of $-P_{cl}$ in the perfect networks subjected to MD simulation are very close to this critical stress. Furthermore, upon increasing the subchain length in the material, $-P_{cl}$ decreases, remaining commensurate with E , which decreases due to the smaller crosslink density.

Performing the loading and unloading computer experiments at different temperatures T reveals opposite temperature dependences for the cavitation stress $-P_{cav}$ and for the closure stress $-P_{cl}$. The cavitation stress $-P_{cav}$ decreases upon increasing T and depends mainly on the cohesive energy

density of the material. On the contrary, the closure stress $-P_{cl}$ increases upon increasing T , reflecting the entropy elasticity associated with stretching the subchain conformations, and paralleling the behaviour exhibited by the Young's modulus E .



(a)



(b)

Figure 4: (a) Pressure as a function of specific volume for a computer specimen of a perfect tetrafunctional polyethylene network consisting of end-linked 201 carbon-long subchains subjected to hydrostatic tension experiments at 450 K. Bonds are not allowed to break in the model. Simulation points for loading and unloading are shown with filled and open symbols, respectively. The solid line is a fit of the homogeneous (uncavitated) data with the Sanchez-Lacombe equation of state. The (negative) pressure levels P_{cav} , P_{cl} , P_s are indicated. Hysteresis and a van der Waals loop consisting of a homogeneous (left) and a cavitated (right) branch are evident. (b) Snapshots of the specimen at characteristic points marked in (a).

THE CHALLENGES AHEAD

Thermodynamics-based strategies, such as the ones outlined above, can be invoked within multiscale simulation schemes to predict equilibrium structure and properties of polymeric materials. Moreover, they can be used to relate generator functions and parameters appearing in nonequilibrium thermodynamic formulations for the temporal evolution of material systems, such as GENERIC [15]. Typically, one chooses a set of slowly evolving variables and invokes a time scale separation, assuming that all remaining variables distribute themselves according to the requirements of equilibrium, subject to the constraints imposed by the slow variables. Molecular simulations can then provide the “potential of mean force” (pomf) as a Gibbs or Helmholtz energy that is a function of the slow variables and will dictate their evolution.

Often dynamics is slow because the system has to overcome high (relative to $k_B T$) barriers in the pomf in order to move from one basin of the pomf (“state”) to another in the space of slow variables. The dynamics then acquires the character of a sequence of infrequent jumps between states, successive jumps being practically uncorrelated. Rate constants, i.e., probabilities per unit time, for the jumps to occur can be computed from atomic-level information via the theory of infrequent events. The evolution of the system can then be tracked via solution of a master equation in the occupancy probabilities of the states [16].

Coarse-graining is necessary and basic tools for its implementation are in place. There is still a lot to do, however, to make coarse-graining a generally applicable strategy, subject to minimal loss of information as one passes between different levels of description. For one thing, the choice of slow variables requires a lot of good judgement, which can often be developed by analysis of atomistic simulation trajectories.

In polymers a popular mode of coarse-graining is to group multi-atom moieties into single quasi-atomic entities (“superatoms”). As the pomf with respect to the superatoms is highly multidimensional, approximate expressions are postulated for it, which typically break it up into bonded and nonbonded effective potentials analogous to the ones invoked by atomistic force fields. These contributions can be accumulated in numerical form by iteratively matching intra- and intermolecular correlation functions between atomistic and coarse-grained simulations. This strategy, Iterative Boltzmann Inversion (IBI) [17], has worked well for polymer melts. IBI effective potentials, however, are thermodynamic state-dependent and cannot be used for temperatures, densities, and compositions far from the ones for which they have been accumulated. Using them across phase boundaries is especially unreliable.

Many systems do not reach equilibrium over ordinary time scales. The description of their properties must necessarily be time-dependent. On the other hand, in some of these systems it is not at all obvious how one should define slow variables. A typical example is glasses, which are ubiquitous in the polymer field. Their structure and properties depend on the history of their formation and change with time in the course of physical ageing. Their mechanical response is complex and rate-dependent. “Energy landscape-based” descriptions

are promising for the prediction of glassy dynamics. The molecular configuration is viewed as undergoing infrequent transitions between basins constructed around local minima of the potential energy, the paths and rate constants of each transition being computed by atomistic transition-state theory and the overall evolution of the system being tracked by a master equation. At long times, lumping basins into “metabasins” is necessary, in order to keep the description tractable [16].

Predicting the ultimate mechanical behaviour of polymeric materials is another major challenge for multiscale simulation. Crack propagation typically involves bond breaking, i.e., chemical phenomena, and calls for electronic structure calculations, or refined “reactive force fields”. On the other hand, damage zones are large in extent, due to the relative softness of polymeric materials, and the constitutive behaviour around crack tips may be highly viscoelastic. The state of the art in simulating fracture of primarily nonpolymeric materials has been summarized [18].

NOMENCLATURE

Symbol	Quantity	SI Unit
E	Young's modulus	Pa
H'	Weight fraction-based Henry's law constant	Pa
\mathbf{k}	Wave vector	m^{-1}
k_B	Boltzmann's constant	J K^{-1}
M	Number average molar mass of chains	kg mol^{-1}
M_e	Molar mass between entanglements	kg mol^{-1}
n	Degree of polymerization, measured in repeat units	-
P	Pressure	Pa
P_{cav}	Cavitation pressure of rubbery polymer	Pa
P_{cl}	Closure pressure of rubbery polymer	Pa
P_s	Limit of mechanical stability, i.e. pressure at which the isothermal slope of pressure with respect to specific volume becomes zero.	Pa
$\langle R^2 \rangle$	Mean squared end-to-end distance of a chain	m^2
S	Static structure factor for X-ray diffraction	-
T	Absolute temperature	K
T_m	Equilibrium melting point	K

V_{sp}	Specific volume	$\text{m}^3 \text{kg}^{-1}$
λ	Parameter inducing helical conformation of chains	-

REFERENCES

- [1] see, for example, P. Nielaba, M. Mareschal, and G. Ciccotti (eds.) *Bridging Time Scales: Molecular Simulations for the Next Decade*, Springer, Heidelberg, 2002.
- [2] C.E. Wilmer, M. Leaf, C.Y. Lee, O.K. Farha, B.G. Hauser, J.T. Hupp, and R.Q. Snurr, Large-scale Screening of Hypothetical Metal-organic Frameworks for Methane Storage, *Nature Chemistry*, vol. 4, pp. 83-89, 2012.
- [3] see, for example, M. Wilson, M. Allen, G. Jackson, S. Marrink, M. Sansom, and D. Theodorou (eds.) *Multiscale Modelling of Soft Matter, Faraday Discussion, Vol. 144*, RSC Publishing, 2010.
- [4] R.O. Dror, R. M. Dirks, J.P. Grossman, H.Xu, and D.E. Shaw, Biomolecular Simulation: A Computational Microscope for Molecular Biology, *Annual Review of Biophysics*, vol. 41, pp. 429-452, 2012.
- [5] D.N. Theodorou, Variable Connectivity Monte Carlo Algorithms for the Atomistic Simulation of Long-Chain Polymer Systems, in P. Nielaba, M. Mareschal, and G. Ciccotti (eds.) *Bridging Time Scales: Molecular Simulations for the Next Decade*, chap. 3, Springer, Heidelberg, 2002.
- [6] C. Tzoumanekas and D.N. Theodorou, Topological Analysis of Linear Polymer Melts: A Statistical Approach, *Macromolecules*, vol. 39, pp. 4592-4603, 2006.
- [7] K. Moorthi, K. Kamio, J. Ramos, and D.N. Theodorou, Monte Carlo Simulation of Short-chain Branched Polyolefins: Structure and Properties” *Macromolecules*, vol. 45, pp. 8453-8466, 2012.
- [8] B. Widom, Some Topics in the Theory of Fluids, *J. Chem. Phys.*, vol 39, pp. 2808-2812, 1963.
- [9] G.C. Boulougouris, I.G. Economou, D.N.Theodorou, On the Calculation of the Chemical Potential Using the Particle Deletion Scheme, *Molec. Phys.*, vol. 96, pp. 905-913, 1999.
- [10] M.G. De Angelis, G.C. Boulougouris, and D.N. Theodorou, Prediction of Infinite Dilution Benzene Solubility in Linear Polyethylene Melts via the Direct Particle Deletion Method, *J. Phys. Chem. B*, vol. 114, pp. 6233-6246, 2010.
- [11] T. Spyriouni, G.C. Boulougouris, and D.N. Theodorou, Prediction of Sorption of CO₂ in Glassy Atactic Polystyrene at Elevated Pressures Through a New Computational Scheme, *Macromolecules*, vol. 42, pp 1759-1769, 2009.
- [12] A. Romanos and D.N. Theodorou, Crystallization and Melting Simulations of Oligomeric $\alpha 1$ Isotactic Polypropylene, *Macromolecules*, vol. 43, pp. 5455-5469, 2010.
- [13] A. K. Morozinis, C. Tzoumanekas, S.D. Anogiannakis, and D. N. Theodorou, Atomistic Simulations of Cavitation in a Model Polyethylene Network, *Polymer Science, Ser. C*, vol. 55, 2013, in press.

- [14] A.N. Gent and P.B. Lindley, Internal Rupture of Bonded Rubber Cylinders in Tension, Proc. Roy. Soc. (Lond.), vol. A249, pp. 195-205, 1958.
- [15] H.C. Öttinger, *Beyond Equilibrium Thermodynamics*, Wiley, 2005.
- [16] D.N. Theodorou, Tracking the Dynamics of Systems Evolving through Infrequent Transitions in a Network of Discrete States, in J. Grotendorst, G. Sutmann, G. Gompper, and D. Marx (eds.) *Hierarchical Methods for Dynamics in Complex Molecular Systems*, Schriften des Forschungszentrums Jülich, IAS Series volume 10, pp 347-389, Jülich, 2012.
- [17] D. Reith, M. Pütz, F. Müller-Plathe, Driving Effective Mesoscale Potentials from Atomistic Simulations, *J. Comp. Chem.*, vol. 24, pp. 1624-1636, 2003.
- [18] M.J. Buehler, *Atomistic Modeling of Materials Failure*, Springer, New York, 2008.

BLOCK COPOLYMERS IN CONFINEMENTS AND UNDER EXTERNAL FIELDS

Andrei V Zvelindovsky*, Marco Pinna*

*University of Central Lancashire, Preston, UK

EXTENDED ABSTRACT

Block copolymers (BCPs) are long chain molecules consisting of several chemically different blocks. Due to the chemical nature of the bond between blocks they do not macrophase, but form various structures on the nano-scale. BCP systems can be used as templates for the energy materials, advances separation templates, catalysts and for nano-electronics devices. Modern materials science uses block copolymers in solutions and mixtures of several BCPs and homopolymers. Due to the intrinsic complexity of the systems, which have a very large physical parameter space, their experimental study is a much elaborated task. With the advances of computers, computational methods become a crucial component in the BCP research and the advances materials design. In our contribution we discuss computer simulation results for BCP systems and their relation to experimental data. Computer simulation results presented are based on two models: a Ginzburg-Landau type description and on self-consistent field theory (SCFT) for polymers. The Ginzburg-Landau model used is a basis for Cell Dynamics simulation (CDS) [1]. It is an extension of the square gradient model, which has proven to be very useful for polymer blends, while CDS is a powerful tool for BCP systems. In this talk we focus on two topics – confinements and external fields (electric, shear). In real practice BCP are often found in thin films (of the thickness of several structural domains), and most recently - in nano-pores. Confined structures are found to be very different from the bulk ones. We investigate various BCP systems: lamellae, cylindrical, spherical, and gyroid. Confinement has a profound influence on the BCP structure. In thin films non-bulk structures are formed in the layers next to the confining surfaces. In this way some such structures as perforated lamellae can be formed. In cylindrical pores helical and toroid structures are formed in various combinations. In spherical confinement the observed structures are reminiscent of knitting ball, onion, perforated spherical layer, virus-like morphology and others. Manipulation by the external electric or flow fields is a way of the nanostructure alignment. Kinetics of this process can be different depending on the field strength. We observe various phase transformations in these two types of fields. Examples include: spheres-to-cylinders and gyroid-to-cylinders, as well as orientation transitions, such as changing lamellae orientation. In the case of the electric field lamellae orientation is found to depend on the strength of the electric field and the temperature. Using CDS can serve as a first part of the simulation tandem together with SCFT in a computer-aided design of novel nanostructured materials [1].

REFERENCES

- [1] M. Pinna and A.V. Zvelindovsky, Large scale simulation of block copolymers with Cell Dynamics, *Eur. Phys. J. B*, vol. 85, 210, 18 pp., 2012.

**ORAL PRESENTATIONS BY A PHD
STUDENT OR POSTDOC AUTHOR OR
COAUTHOR**

OF DICE AND MEN. SUBJECTIVE PRIORS, GAUGE INVARIANCE, AND NONEQUILIBRIUM THERMODYNAMICS

Matteo Poletti*, Francesco Vedovato†

* Complex Systems and Statistical Mechanics, University of Luxembourg,
162a avenue de la Faïencerie, L-1511 Luxembourg, G. D. Luxembourg,
E-mail: matteo.poletti@uni.lu

† Zeeburgerdijk 11b, 1093SJ Amsterdam, The Netherlands
Website: <http://aspectacularmachine.net>

ABSTRACT

“Ceci n’est pas une pipe” wrote René Magritte on what was only the *representation* of a pipe. Phenomena and their physical descriptions differ, and in particular the laws ruling the former might enjoy symmetries that have to be spent to attain the latter. So, inertial frames are necessary to draw numbers out of Newtonian mechanics and confront with experiment, but ultimately the laws of mechanics are independent of reference frames. Generalizing work done in Ref. [M. Poletti, EPL **97** (2012) 30003] to continuous systems, we discuss from a foundational point of view how subjectivity in the choice of reference prior probability is a (gauge) symmetry of thermodynamics. In particular, a change of priors corresponds to a change of coordinates. Employing an approach based on the stochastic thermodynamics of continuous state-space diffusion processes, we discuss the difference between thermostatic and thermodynamic observables and show that, while the quantification of entropy depends on priors, the second law of thermodynamics is formulated in terms of invariant quantities, in particular the curvature of the thermodynamic force (gauge potential), which we calculate in a few examples of processes led by different nonequilibrium mechanisms.

INTRODUCTION

We can say nothing about the thing in itself, for we have eliminated the standpoint of knowing. A quality exists for us, i.e. it is measured by us. If we take away the measure, what remains of the quality?

F. Nietzsche [1]

At a first sight the varied terms appearing in the title pair as fish with bicycles. Indeed, it is our final purpose to convey that these concepts, bundled together, solve a controversy about the role of the observer in statistical mechanics, and partake to a fundamental symmetry of thermodynamics. On a less ambitious tone, objectives of this contribution are: To discuss a simple but compelling foundational aspect of nonequilibrium statistical mechanics, to extend the theory developed in Ref. [2] to systems with a continuous state space and, with the aid of some examples, to further back up the role of a thermodynamic curvature for the determination of the equilibrium/nonequilibrium character of steady states of diffusive systems.

It is renowned that statistical mechanics has been enormously successful in describing systems at thermodynamic equilibrium, bestowing a probabilistic nature on physical concepts such as that of entropy, which notoriously has two facets. The head is a state function coined in the 19th-century to put limits on the efficiency of machines. After the intuitions of Boltzmann, the tail was coined by Gibbs, and later Shannon in applications to information theory, to yield a much known but poorly understood measure of “disorder” or, more precisely, of “missing information” [3]. A baffling feature of the latter acceptance is that it

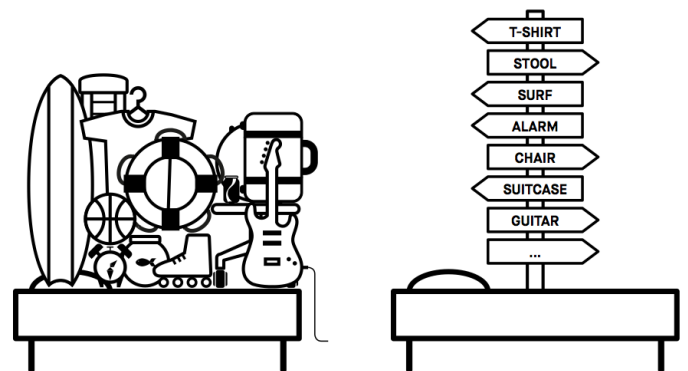


Figure 1. A room as perceived by two observers with different prior knowledge of its state. Is there an objective criterion to quantify its disorder, given that entropy is “missing information”?

is prone to a certain degree of subjectivity, that only apparently does not affect its thermodynamic counterpart. We are all acquainted with the following fact (see Fig.1): As children, when mum scolded us for being messy, we would whine claiming to know exactly where our toys were. Wryly, when she tidied up we would not be able to retrieve them again. If entropy is missing information, then what is the entropy of a room? Is it the mom’s barren neatness, or the child’s playing strategy?

Making a huge leap upward: The Universe today presents a high degree of structure and information (from galaxies to planets down to ourselves) due to the ordering effect of gravity, but in the far past it was a fluctuating quark-gluon plasma that cosmologists describe solely in terms of its temperature and few

*Corresponding author.

† Artwork author.

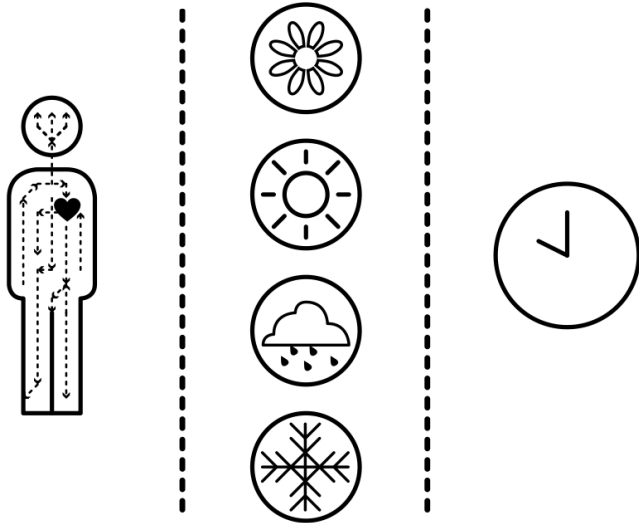


Figure 2. Currents circulate in nonequilibrium steady states.

other parameters. Then, did entropy decrease ever since, contrary to the second law of thermodynamics?

The latter question introduces the theme of nonequilibrium processes. Today, statistical methods encompass the response of equilibrium states to small perturbations, to embrace the sophisticated phenomenology of systems subject to nonequilibrium conditions. A special mention goes to the framework of stochastic thermodynamics [4], a prominent theory that describes the thermodynamics of open systems evolving under Markovian dynamics. Nonequilibrium systems produce entropy as they evolve under the influence of thermodynamic forces towards steady states that maintain a constant heat flux towards the environment. A crucial feature of nonequilibrium steady states is the circulation of currents around loops (see Fig.2). If on the one hand the *thermostatistics* of equilibrium states is based on state functions, such as the entropy, the *thermodynamics* of nonequilibrium processes deals with dynamical quantities like the entropy production. The second law of thermodynamics, by many (including Einstein and Ehrenfest) considered to be the most universal law of physics, states that entropy production along a time interval dt is non-negative

$$\sigma dt = dS - \frac{dQ}{T} \geq 0 \quad (1)$$

and that it only vanishes at equilibrium states. Here σ is the entropy production rate and d denotes an inexact differential. This law eventually provides an “arrow of time”. But then, if entropy is a subjective quantity, will the validity of the second law and the direction of time depend on the observer?

Similar dreaded outlooks led to criticisms about the actual relevance of the information-theoretic approach to thermodynamics, as pioneered by Jaynes [5]. For example Ref. [6] is a funny skeptical fable about an obtuse physicist questioning an omniscient angel about who is the “right” observer. At the 11th Granada Seminar [7] Lebowitz prodded the scarce informationist supporters that an observer who’s no Ph.D. might threaten the fate of physical laws.

Our apology of the informationist approach supports the following point of view. A change of observer is analogous to a change of reference frame in mechanics, or of coordinate system in general relativity: It does not alter the process, but it does alter the representation of the process. While it is always

necessary to choose an observer to actually do physics (and this choice can be done in a more or less awkward way¹), it is necessary that the fundamental laws remain invariant. For this reason, while thermostatic quantities like the entropy can change, it is necessary that the entropy production rate involved in the second law does not. In other words, changes of subjective observer must be a symmetry of nonequilibrium thermodynamics. In particular, as we will see, it can be implemented as a so-called *gauge* symmetry, that is, a symmetry that acts locally, from point to point, rather than globally (like a change of units does).

PLAYING DICE AND SITTING ON STOVES

Dice are a common tool for intuitive probabilistic thinking, so much that Einstein declared that “God doesn’t play dice”, objecting the probabilistic nature of quantum mechanics (but he would also say that “physical concepts are free creations of the human mind, and are not uniquely determined by the external world”). Sticking to classical statistical mechanics, we don’t dare challenge the divine intentions, and rather consider different human observers rolling dice.

Given the common-sense symmetry of a die with respect to its bouncing on a table, one is compelled to assign prior $1/6$ to all faces. This seems such an obvious choice, that it is hard to admit that it is just as subjective as any other. This prior is related to a measure of a die’s properties, made by an observer who has a sufficiently complete perspective on the die with respect to the process being performed and to uncountable previous experiences of seeing and hearing of similar dice rolling. It is nevertheless legit to color a die’s faces one red, one green, one blue and all others yellow, and have an heavily myopic person examine it from a distance, so that he can only resolve spots of color. He will have sufficient reason to believe that the system is a tetrahedron. According to his most plausible probability assignment, the die’s faces would have probability $(1/4, 1/4, 1/4, 1/12, 1/12, 1/12)$ to show up. From his perspective, this makes perfectly sense.

Suppose that ourselves and the myopic person play dice, correcting our prior according to the output. If, by the law of large numbers, the die’s faces come out approximately $1/6$ of the times, we the seeing will gather no further information, since we had a fully satisfactory estimation of the die’s entropy in the beginning. The myopic, who had a worse estimation, will gain further information. By the paradigm that information is physical, we can say that our measure of the initial entropy and of the forthcoming heat fluxes differed from his. Nevertheless, the process occurred in the same way. This *gedankenexperiment* can provoke an objection: The half-blind person is in a chronicle state of ignorance and he doesn’t see the “truth”. But so are we with respect to a loaded die, in which case we either know technical details about how it was loaded and then formulate a reasonable prior, or else we can just make an hypothesis and then correct it according to the output, as in Fig. 3.

Let’s now move to physical quantities, in particular temperature. Consider a hot stove, and let’s ask:

What is the stove’s temperature?

Taking a naïve materialistic approach, one could say a stove is a stove and it has the temperature it has. We can sit on it and

¹For example, it doesn’t make much sense to describe the ballistics of a rocket on the Earth using the rest frame of a merry-go-round on the Moon, although in principle it is possible.

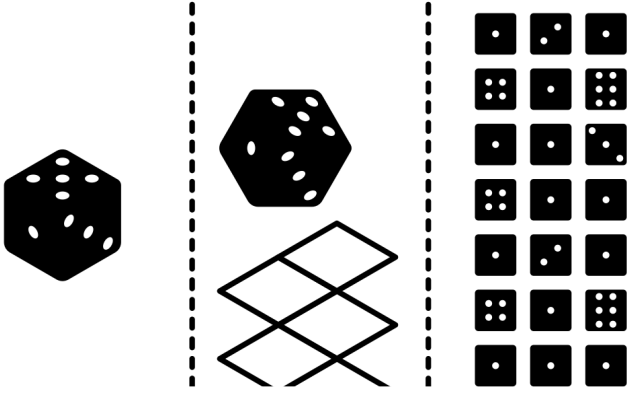


Figure 3. A die and the process of throwing a die suspect of being loaded, given the biased set of outputs on the right-hand side.

perceive it. But things are more sophisticated. We ourselves are thermometers. Every-day thermometers interact with certain degrees of freedom of the system, say, the electromagnetic forces of the outer non-shielded electrons of a solid's molecules, but essentially do not interact strongly with the nuclei, electroweakly with neutrinos, they do not exchange gluons, massive vector bosons, gravitons, strings, quanta of space-time and whatever is beyond our present state of knowledge. But one can in principle put the stove in an accelerator and get a much more accurate estimate of the temperature. So, the answer to the above question depends on the coarse graining of "reality" that physical apparatuses always entail. We leave aside the question whether there exists an ultimate temperature (see Fig.4).

A different question that we can pose is:

What *happens* when a thermometer is put on the stove?

Italics was used to emphasize their different natures: The first questions an essential property of the system, while the second concerns a process which occurs when two physical systems are put in relation. Much like in the Zen koan "What is the sound of one hand?", we claim that the first question is unphysical (but, rather, metaphysical), while the second is physical, and giving an answer necessarily calls into play observers. If we sit on the stove, we will get burnt in a few seconds, again according to an Einstein's estimate, independently of what we think of it.

The punchline is: We should not worry about subjectivity of physical quantities, just as much as we don't deem it necessary to wear another coat when we express 75.2° Fahrenheit as 24° Celsius. We should rather make sure that fundamental physical laws are independent of this choice of reference frame. This is the main objective of this paper.

SWITCHING PRIORS AND COORDINATE FRAMES

Let $\mathbf{x} \in X$ be a generic state of a system, labeling some microscopic degrees of freedom (for example, positions and momenta of the molecules of a gas, spin states of a ferromagnet etc.). For simplicity we suppose that the state space has finite volume normalized to unity, $\int_X d\mathbf{x} = 1$. Statistical descriptions of the system assign a probability density $p(\mathbf{x})$ to microstates. For example when the mechanisms involved in a physical process involve exchange of a form of energy with a single heat bath at temperature T the most plausible distribution compatible with an observed average value of the energy $\langle E \rangle$, assuming that the underlying microstates are equiprobable, is Gibbs's

canonical distribution $p_{\text{Gibbs}}(\mathbf{x}) = \exp[-(E(\mathbf{x}) - F)/(k_B T)]$, with F Helmholtz's free energy and k_B Boltzmann's constant, that we set to unity in the following. Notice that our prudent wording emphasized that the choice of probability density is congenial to a particular process, and that there is a choice of prior involved.

The Gibbs-Shannon (differential) entropy

$$S = - \int_X d\mathbf{x} p(\mathbf{x}) \ln p(\mathbf{x}) \quad (2)$$

is a measure of the missing information of the probability distribution with respect to a state of perfect knowledge. It vanishes when $p(\mathbf{x}) = \delta(\mathbf{x} - \bar{\mathbf{x}})$, and it is maximum when the distribution is uniform. As announced, there is a correspondence between statistical and physical entropies, as one can appreciate by plugging the canonical distribution to recover the well-known expression between equilibrium thermodynamic potentials $TS = \langle E \rangle - A$.

In regard to probability densities, an important mathematical detail that we need to point out is that they are obtained by taking the so-called Radon-Nikodym derivative of a probability measure P with respect to another² that we call the prior P_{pr} ,

$$p = \frac{dP}{dP_{pr}}. \quad (3)$$

In Eq. (2) the prior is implied to be the uniform normalized distribution over microstates, $dP_{pr} = d\mathbf{x}$. Hence the definition of entropy always pivots on a prior. Also, the canonical distribution can be obtained as the maximum entropy distribution compatible with a measured value of the average energy $\langle E \rangle$, assuming the uniform prior over microstates, viz. starting with the microcanonical ensemble.

Let us rewrite entropy in terms of probability measures:

$$S = - \int_X dP \ln \frac{dP}{d\mathbf{x}}. \quad (4)$$

Our point of view in this paper is that the choice of uniform prior is just as subjective as any other choice, and that changes of priors

$$d\mathbf{x} \rightarrow dP'_{pr}, \quad (5)$$

at fixed probability measure P (that is, at fixed macrostate) are legitimate and need to be coped with in a consistent manner. Under such a transformation we obtain

$$S' = - \int_X dP \ln \frac{dP}{dP'_{pr}} = S + \left\langle \ln \frac{dP'_{pr}}{d\mathbf{x}} \right\rangle, \quad (6)$$

where the average is taken with respect to P . Entropy is not an invariant object, as it gains an additional term. It is also well known that entropy is not invariant under orientation-preserving coordinate transformations $\mathbf{x} \mapsto \mathbf{x}'(\mathbf{x})$, with Jacobian

$$\Lambda = \det \left(\frac{\partial \mathbf{x}'}{\partial \mathbf{x}} \right) > 0. \quad (7)$$

²We assume that all probability measures are absolutely continuous with respect to the uniform distribution.

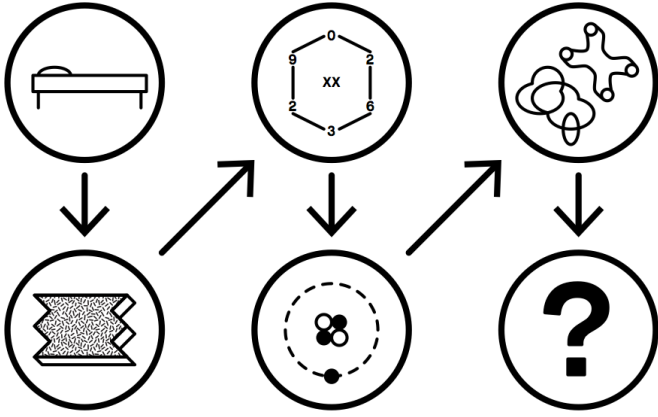


Figure 4. Is there an ultimate temperature of a bed?

Being the probability measure a volume form, viz. $dP = dP'$ so as to preserve probabilities of events, and since the volume element transforms according to $d\mathbf{x}' = \Lambda d\mathbf{x}$, one finds the transformation law for the probability density $p' = \Lambda^{-1} p$. Plugging into Eq. (2), under a change of coordinates the entropy gains an inhomogeneous term

$$S' = - \int_{\mathbf{x}'(x)} dP' \ln \frac{dP'}{d\mathbf{x}'} = S + \langle \ln \Lambda \rangle. \quad (8)$$

Notice that a volume-preserving transformation with $\Lambda = 1$ preserves the entropy. This is the case for canonical transformations in Hamiltonian mechanics and for the Hamiltonian flux (indeed it is inappropriate to say that “entropy of an isolated system cannot decrease”, since it is a constant of motion). However, volume-preserving transformations are too restrictive. For example, in the approach to nonequilibrium thermodynamics based on dynamical systems and Gaussian thermostats, evolution does not preserve the phase space volume [8].

The analogy of Eq. (8) with Eq. (6) suggests that every change of prior can be achieved by a change of coordinates with $dP'_{pr} = d\mathbf{x}'$. In fact, inspecting Eq. (4) we realize that a coordinate transformation maintains dP but replaces $d\mathbf{x}$ with a new prior. In the new coordinates $d\mathbf{x}'$ is the uniform measure while $d\mathbf{x}$ is not anymore. A coordinate transformation realizes a change of the relevant degrees of freedom that are supposed to be equiprobable. This is well illustrated by this riddle: Picking a number \mathbf{x} between 1 and 10 at random, the probability that it is smaller than 5 is $1/2$, while picking \mathbf{x}' at random between 1 and 100, the probability that it is smaller than 25 is $1/4$. How is it possible that picking either a number or its square aren't equally likely? The solution is to recognize that different choices of prior were made in the two cases, and that the uniform prior (“at random”) in one set of coordinates is not the uniform prior in the other set of squared coordinates.

To some authors, non-invariance of the entropy sounds as a dazzling puzzle that discredits its utility. The Italian-speaking readers will also find a discussion on this tone in Ref. [9], which comes to the conclusion that Jaynes's MAXENT reasoning is circular. Our point of view is that there is not a preferred set of coordinates, and while the determination of thermostatic quantities does depend on coordinates, thermodynamics should not. Hence the entropy must be complemented with another quantity that grants the overall invariance of thermodynamics.

ENTROPY PRODUCTION RATE

We now suppose that the system is in contact with an environment that determines a Markovian evolution of its probability density, dictated by the Fokker-Planck equation

$$\dot{p} = -\nabla \cdot (p\mathbf{A} - T\nabla p) = -\nabla \cdot \mathbf{J}, \quad (9)$$

with \mathbf{A} a thermodynamic force and T an environmental temperature. The dot derivative is with respect to time. On the right-hand side we put it in the form of a continuity equation in terms of a probability density current \mathbf{J} . Under mild assumptions the Fokker-Planck equation evolves towards a unique steady state p^* , at which the current has no sinks and sources, $\nabla \cdot \mathbf{J}^* = 0$ (the asterisk will mark the steady value of any observable). A steady state is in equilibrium when the steady state currents vanish, while nonequilibrium steady states are characterized by nonvanishing currents that circulate in the system's state space.

Since this equation regulates the dynamics of the process, we assume it to be invariant under change of priors/coordinates. Unfortunately, a fully satisfactory treatment would require more advanced tools from the theory of differential forms, including the introduction of a metric. Ref. [10] contains further details. The current transforms like a vector density. A suitable transformation law for the divergence grants that $\nabla \cdot \mathbf{J}$ is a scalar density. Within the current, under a change of coordinates the gradient of the probability density develops an inhomogeneous term that must be reabsorbed by the thermodynamic force. Hence overall invariance enforces the transformation laws

$$p' = \Lambda^{-1} p, \quad \mathbf{A}' = \frac{\partial \mathbf{x}}{\partial \mathbf{x}'} (\mathbf{A} - T\nabla \log \Lambda). \quad (10)$$

This pair of equations is reminiscent of gauge transformations as encountered in (quantum) field theory, with p playing the role of the wave function, \mathbf{A} that of gauge potential, and T that of coupling constant. As a technical note, the gauge group in this case is the noncompact group of real positive numbers under multiplication, whose elements are the Jacobians of orientation-preserving diffeomorphisms.

One can now use the transformation law for the gauge potential to counterbalance the inhomogeneous term developed by the entropy. To this purpose we prefer to consider the rate of entropy production \dot{S} . Its transformation law is

$$\dot{S}' = \dot{S} + \int \mathbf{J} \cdot \nabla \log \Lambda d\mathbf{x}. \quad (11)$$

It can then be seen³ that the following *heat flux rate*

$$\frac{dQ}{dt} = - \int \mathbf{J} \cdot \mathbf{A} d\mathbf{x} \quad (12)$$

has exactly the same transformation law as \dot{S} but for a factor $1/T$, so that the *entropy production rate*

$$\sigma = \dot{S} - \frac{1}{T} \frac{dQ}{dt} \quad [dS_i = dS - dS_e] \quad (13)$$

³Notice that the scalar product in this expression denotes the presence of a metric, which also has to transform properly altogether.

is indeed an invariant quantity (between square parenthesis we reported the analogous decomposition of the entropy production as found in older thermodynamics textbooks [11]). This expression for the entropy production rate is well-known in the stochastic thermodynamics literature [4]. It can easily be proven to be positive, which is a statement of the second law, Eq. (1). By construction σ is invariant under gauge transformations, hence the second law holds in all coordinates/with respect to all choices of prior.

CURVATURE AND STEADY STATES

In general, \mathbf{A} is not a conservative force, that is, it is not a gradient. Then σ is not the total time derivative of a state function, from which it follows that $dQ^*/dt \neq 0$ and the steady state value of the entropy production does not vanish: Nonequilibrium steady states maintain a constant entropy production as currents circulate. Instead when $\mathbf{A} = -\nabla\Phi$, which we refer to as the condition of *detailed balance*, then σdt is an exact differential and it vanishes at the steady state.

The characterization of nonequilibrium can be elegantly made in terms of the curvature of the gauge potential. Curvature is a crucially important quantity in gauge theories. For example, in the field-theoretic formulation of electromagnetism, the curvature tensor contains the components of the electric and magnetic fields and entails the peculiar differential form of Maxwell's equations. In this section we discuss thermodynamic curvature and express the steady state entropy production in terms of it. The main messages are that one should consider several different contributions to the curvature, and that a vanishing curvature is intimately related to the occurrence of equilibrium steady states.

Nonconservative force

The curvature associated to the non-conservative force \mathbf{A} in Eq. (9) is defined as

$$F_{ab} = \frac{\partial A_b}{\partial x^a} - \frac{\partial A_a}{\partial x^b}, \quad (14)$$

Here a, b denote vector and tensor components. Notice that it transforms like a 2-tensor under coordinate transformations and it does not gain inhomogeneous terms, hence it is gauge invariant. When the force is a gradient, then the curvature vanishes. The converse is not generally true, as there might be topological contributions to the entropy production, such as isotropic flows around the fundamental cycles of a torus. Such topological contributions have been studied by several authors in Ref. [12]. Here we discard them.

A theorem by Hodge implies that the current can always be decomposed as (letting δ^{ab} be the Kroenecker's delta)

$$J^a = \sum_b \frac{\partial}{\partial x^b} \left(\Theta^{ab} - \Psi \delta^{ab} \right) + \Omega^a, \quad (15)$$

where Ψ is a scalar potential, Θ is a skew-symmetric tensor, and Ω is an harmonic vector, such that $\Delta\Omega = 0$. The latter term is the one that provides topological contributions, and we discard it. Taking the gradient, since Θ is skew-symmetric, we find that

$$-\nabla \cdot \mathbf{J} = \Delta\Psi = p. \quad (16)$$

In particular at a steady state one has $\Delta\Psi^* = 0$. It is known that on a compact manifold without boundary the only harmonic scalar is a constant function $\Psi^* = const.$, hence we find that only the term in Θ^* survives in the expression for the steady current. Plugging into the entropy production rate and integrating by parts we obtain the steady state value

$$\sigma^* = \frac{1}{2T} \sum_{a,b} \int F_{ab} \Theta^{*ab} dx. \quad (17)$$

This result can be seen as a continuous version of a decomposition by Schnakenberg of the steady entropy production rate in terms of fundamental cycles of a graph [13].

Competition between heat reservoirs

We now consider a Brownian particle interacting with two baths at different temperature. Its stochastic motion is described by the differential equation

$$\dot{\mathbf{x}} = -\nabla\Phi_1 + \sqrt{2T_1} \boldsymbol{\zeta}_1 - \nabla\Phi_2 + \sqrt{2T_2} \boldsymbol{\zeta}_2, \quad (18)$$

where, as usual, $\boldsymbol{\zeta}_1$ and $\boldsymbol{\zeta}_2$ are uncorrelated sources of white noise, $\langle \zeta_i^a(t) \zeta_j^b(t') \rangle = \delta^{ab} \delta_{ij} \delta(t-t')$, $i, j \in (1, 2)$. The key aspect regarding this system is that, although the two forces are gradients (condition of *local detailed balance* [14]), meaning that detaching either bath returns equilibrium, competition between the two baths to impose their own equilibrium gives rise to nonequilibrium character, and further curvature terms.

The Fokker-Planck equation for this system reads

$$\dot{p} = -\nabla \cdot \mathbf{J}_1 - \nabla \cdot \mathbf{J}_2 = \nabla \cdot (p \nabla\Phi_1 + T_1 \nabla p + p \nabla\Phi_2 + T_2 \nabla p). \quad (19)$$

It is known that a proper description of the thermodynamics of the system requires to resolve the two mechanisms, otherwise one would systematically underestimate the entropy production [14]. For this reason we distinguished two currents that flow in parallel and we resolve two driving forces $\mathbf{A}_i = -\nabla\Phi_i$. The steady state can be easily computed giving $p^* \propto \exp -(\Phi_1 + \Phi_2)/(T_1 + T_2)$, and while the total steady current $\mathbf{J}_1^* + \mathbf{J}_2^*$ vanishes, one finds that the individual currents do not:

$$\mathbf{J}_1^* = -\mathbf{J}_2^* = \frac{p^*}{T_1 + T_2} (T_2 \nabla\Phi_1 - T_1 \nabla\Phi_2). \quad (20)$$

Again, we can perform the Hodge decomposition of \mathbf{J}_1^* as in Eq. (15) to obtain

$$\sigma^* = \int \left(\frac{\mathbf{A}_1 \cdot \mathbf{J}_1^*}{T_1} + \frac{\mathbf{A}_2 \cdot \mathbf{J}_2^*}{T_2} \right) dx = \int \left(\frac{\Delta\Phi_2}{T_2} - \frac{\Delta\Phi_1}{T_1} \right) \Psi_1^* dx. \quad (21)$$

Notice that Ψ_1^* in this case does not vanish, since $\nabla\mathbf{J}_1^* \neq 0$. The above formula shows that when several baths compete one shall also consider contributions from the cross scalar curvature $\Delta\Phi_2/T_2 - \Delta\Phi_1/T_1$ even if local detailed balance holds.

Blowtorch

Systems subject to a temperature gradient undergo the so-called blowtorch effect, first described by Landauer [15]: Even

if the thermodynamic force is conservative, the varying temperature profile $T = T(\mathbf{x})$ might turn it into a nonequilibrium driving force. The steady entropy production now reads

$$\sigma^* = - \int \frac{\nabla\Phi \cdot \mathbf{J}^*}{T} d\mathbf{x} = \frac{1}{2} \sum_{a,b} \int F_{ab}^{(T)} \Theta^{*ab} d\mathbf{x}, \quad (22)$$

where again we employed Hodge's decomposition and introduced an additional curvature term given by

$$F_{ab}^{(T)} = \frac{\partial}{\partial x^a} \Phi \frac{\partial}{\partial x^b} \frac{1}{T} - \frac{\partial}{\partial x^b} \Phi \frac{\partial}{\partial x^a} \frac{1}{T}. \quad (23)$$

The thermodynamics force $\nabla(1/T)$ appears. The blowtorch effect vanishes when $\Phi(\mathbf{x}) = \Phi(T(\mathbf{x}))$. It can be shown that this curvature term is the infinitesimal version of a cycle $\oint d\Phi/T$ when the integral is performed along a small square cycle with sides in the a -th and b -th directions. The latter expression is reminiscent of Clausius's expression for the entropy along a closed individual realization of a process (rather than of an ensemble). In a recent paper one of the authors [16] interpreted temperature gradients as a deformation of the metric of space.

CONCLUSIONS

You never oughta drink water when it ain't runnin'.
J. Steinbeck, *Of Mice and Men*

In this paper we faced the problem of subjectivity of information-theoretic entropy under a change of reference prior probability, and turned it into an opportunity for a symmetry principle of nonequilibrium thermodynamics. We argued that the physical counterpart of a reference prior choice is the inherent coarse-graining that any description of a physical system entails. We observed that while thermostatic quantities pertaining to fixed states such as the entropy need not be invariant, fundamental laws pertaining to processes like the second law of thermodynamics must be independent of the observer. We then formulated transformation properties as so-called gauge transformations and built an appropriate gauge-invariant entropy production, returning a well known expression in the framework of the stochastic thermodynamics of diffusion processes. At a nonequilibrium steady state, the entropy production can be expressed in terms of the curvature of the nonequilibrium force (gauge potential). Several contributions coming from different nonequilibrium mechanisms have been described.

From a slightly more philosophical perspective, we supported the informationist approach to statistical mechanics, rejecting imputations of solipsism ("reality doesn't exist") or cognitive-relativism ("reality depends on the observer"), but rather arguing that it is a very laic and prudent point of view that purports that the only physically meaningful concepts are those that can be measured, and measures require observers. In other words, there are no omniscient angels in physics. Nevertheless, we showed that physical laws such as the second law of thermodynamics are ultimately be independent of the observer.

ACKNOWLEDGMENT

Artwork by designer Francesco Vedovato. Discussion with A. Vulpiani and A. Montakhab is at the origin of this work. The research was in part supported by the National Research Fund Luxembourg in the frame of project FNR/A11/02.

NOMENCLATURE

All quantities can be considered to be dimensionless.

A	Thermodynamic force / gauge potential
$F_{ab}, F_{ab}^{(T)}$	Curvature, blowtorch curvature
J	Probability density current
p	Probability density
P, P_{pr}	Probability measure, prior probability measure
$Q, \dot{Q}/dt$	Heat, heat flux rate
S	Gibbs-Shannon entropy
t	Time
T	Temperature
\mathbf{x}, X	Microstate, state space
Λ	Jacobian of a coordinate transformation
σ	Entropy production rate
ζ	White noise
Φ	Scalar potential for the force
Ψ, Θ, Ω	Scalar, tensor and vector current terms

REFERENCES

- [1] F. W. Nietzsche, in P. Poellner, *Nietzsche and Metaphysics*, Oxford University Press, Oxford, 2000.
- [2] M. Poletti, Nonequilibrium Thermodynamics as a Gauge Theory, *Eur. Phys. Lett.*, vol. 97, p. 30003, 2012.
- [3] A. Ben-Naim, *A Farewell to Entropy: Statistical Thermodynamics Based on Information*, World Scientific, Singapore, 2008.
- [4] U. Seifert, Stochastic Thermodynamics, Fluctuation Theorems and Molecular Machines, *Rep. Progr. Phys.*, vol. 75, p. 126001, 2012.
- [5] E. T. Jaynes, Information Theory and Statistical Mechanics, *Phys. Rev.* vol. 106, p. 620, 1957.
- [6] J. L. Lebowitz and C. Maes, Entropy – A Fable, <http://itf.fys.kuleuven.be/~christ/pub/fablejoel.ps>
- [7] VV. AA., Nonequilibrium Statistical Physics Today. Where Shall We go from here?, *AIP Conf. Proc.*, vol. 1332, 2011.
- [8] D. Ruelle, Smooth Dynamics and New Theoretical Ideas in Nonequilibrium Statistical Mechanics, *Jour. Stat. Phys.*, vol. 95, pp. 393-468, 1999.
- [9] G. Boffetta and A. Vulpiani, *Probabilità in Fisica*, Springer, Milan, 2012, pp. 173-185.
- [10] M. Poletti, Generally Covariant State-Dependent Diffusion, arXiv:1206.2798, 2012.
- [11] P. Glansdorff and I. Prigogine, *Thermodynamic Theory of Structure, Stability and Fluctuations*, Wiley, London, 1971.
- [12] D.-J. Jiang, M. Qian and M. Qian, *Mathematical Theory of Nonequilibrium Steady States*, Springer, Berlin, 2004.
- [13] J. Schnakenberg, Network Theory of Microscopic and Macroscopic Behavior of Master Equation Systems, *Rev. Mod. Phys.*, vol. 48, p. 571, 1976.
- [14] M. Esposito and C. Van Den Broeck, The Three Faces of the Second Law: I. Master Equation Formulation, *Phys. Rev. E*, vol. 82, p. 11143, 2010.
- [15] R. Landauer, Inadequacy of Entropy and Entropy Derivatives in Characterizing the Steady State, *Phys. Rev. A*, vol. 12, p. 636, 1975.
- [16] M. Poletti, Diffusion in Nonuniform Temperature and its Geometric Analog, *Phys. Rev. E* vol. 87, p. 032126, 2013.

THE INFEASIBILITY OF REVERSIBILITY AND ITS CONSEQUENCES FOR ENGINEERING DESIGN

R. Gielen*, M. Baelmans

Division of Applied Mechanics and Energy Conversion,
Department of Mechanical Engineering, Katholieke Universiteit Leuven,
Celestijnenlaan 300A bus 2421, B-3001 Heverlee, Belgium,
E-mail: ruben.gielen@mech.kuleuven.be

ABSTRACT

Applications like exergy and entropy generation minimization (EGM) are widely used in engineering research and industry. Exergy attributes work potential to heat and therefore it allows to conduct meaningful analyses on systems where the First Law seems to fail. Entropy generation minimization, the design methodology used to seize the opportunities identified by exergy analyses, enables the engineer to optimize thermodynamic efficiency of systems under consideration. However, it seems that popularity of the Second Law in engineering has pushed its application beyond the limits. Does the result of an exergy analysis allow to allocate engineering efforts? Can we consider and isolate components or local phenomena in an EGM procedure without fully taking into account their interdependencies? Although those questions appear to be answered affirmative in a significant amount of recent publications, we question the accuracy of that answer in this paper by presenting a number of illustrative examples.

INTRODUCTION

The pursuit of solutions to a problem drives the engineer to apply analysis and design techniques on a system aiming at technical and economic opportunities. One analysis technique which acquired major scientific attention in recent decades is the exergy analysis together with its design counterpart entropy generation minimization (EGM) [1–5]. This paper endeavors to elaborate an assessment on these Second Law based techniques and their use in engineering methodologies.

Exergy analyses pinpoint and quantify thermodynamic imperfections as irreversibilities which either are not identified or misevaluated by energy analyses [6, 7]. These irreversibilities are the differences between the actual work performed and the maximum theoretical useful work obtained if a system is brought into thermodynamic equilibrium [4]. Entropy generation minimization on the other hand seizes the possibilities exergy analyses identify as entropy generation is directly proportional to irreversibility. Minimization of the total entropy generation is therefore equal to system efficiency optimization [8].

In this paper we present the limits of exergy analyses and entropy generation minimization indicated by the infeasibility of reversibility. Illustrative cases are discussed to demonstrate how the inevitability of irreversibility on macro-level crops the applicability of both Second Law based techniques. Although the authors are convinced of the benefits of exergy analyses to visualize losses and of entropy generation minimization as a cost function to optimize an entire system, it seems appropriate to sound a note of caution considering their application on subsystems which are thermodynamically connected.

The relevance of this work can be founded by following non-exhaustive list of articles dealing with Second Law analysis and design on a local scale without considering the system in

which these parts, components or subsystems (eventually) operate [9–17]. Moreover the content of this paper will provide an argument to regard the Second Law of thermodynamics as an alternative for rather than an addition to the First Law in engineering analysis and design.

The remainder of this contribution is structured as follows. We start with a comparison between First and Second Law efficiency and discuss the implications of the differences. Subsequently we offer three perspectives on the Second Law in engineering: a modeling, analysis and design perspective. These perspectives enable us to demarcate the field of application of the Second Law in engineering. Finally conclusions are summarized.

SECOND LAW EFFICIENCY

Efficiency is a ratio of actual performance and ideal performance. The essential difference between First Law efficiency and Second Law efficiency is the definition of that ideal performance which serves as a benchmark. The First Law of thermodynamics puts every form of energy on the same level

$$\frac{\partial E}{\partial t} = \left[\sum \dot{m} \left(h + \frac{1}{2} V^2 + gz \right) \right]_{\text{out}}^{\text{in}} + \sum_{i=0}^n \dot{Q}_i - \dot{W}. \quad (1)$$

From a First Law perspective heat and power are therefore interchangeable modes of energy transfer. The Second Law of thermodynamics associates heat transfer with entropy

$$\frac{\partial S}{\partial t} \geq \sum_{\text{in}} \dot{m} s - \sum_{\text{out}} \dot{m} s + \sum_{i=0}^n \frac{\dot{Q}_i}{T_i}, \quad (2)$$

$$\dot{S}_{\text{gen}} = \frac{\partial S}{\partial t} - \sum_{i=0}^n \frac{\dot{Q}_i}{T_i} - \sum_{\text{in}} \dot{m} s + \sum_{\text{out}} \dot{m} s. \quad (3)$$

*Corresponding author

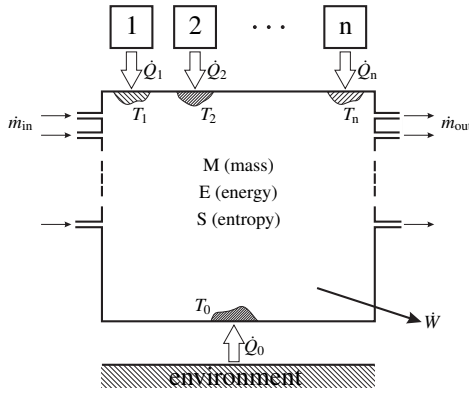


Figure 1. General representation of an open thermodynamic system.

Elimination of \dot{Q}_0 in Eq. (1) and (3) gives the Gouy-Stodola theorem [18]

$$\dot{W} = \left[\sum \dot{m} \left(h - T_0 s + \frac{1}{2} V^2 + gz \right) \right]_{\text{out}}^{\text{in}} - \frac{\partial}{\partial t} (E - T_0 S) \quad (4)$$

$$+ \sum_{i=1}^n \dot{Q}_i \underbrace{\left(1 - \frac{T_0}{T_i} \right)}_{\eta_c} - \underbrace{T_0 \dot{S}_{\text{gen}}}_i$$

which indicates that the Second Law introduces a scaling factor, known as the Carnot efficiency η_c , to devalue heat transfer. Due to this devaluation, the Second Law benchmark will always be lower than the First Law benchmark.

Although the ideal performance associated with the First Law and Second Law are different, optimization of First and Second Law efficiency both lead to the design with maximum thermodynamic efficiency. The benchmark put forward by both thermodynamic laws are in reality unattainable. Whether one minimizes the gap between reality and the First Law ideal or the Second Law ideal, the absolute gap reduction will be equal. Therefore we can state that Second Law efficiency optimization is an alternative for First Law efficiency optimization.

The First Law holds energy conservation and falls short in defining an efficiency metric for components which only transfer (and not use or transform) energy. The Second Law pinpoints all losses \dot{I} including those associated with energy transfer. As such there exists a Second Law efficiency for components like heat sinks and heat exchangers. Therefore Second Law efficiency is a popular objective function to design those type of components (e.g. [9, 14, 16]).

PERSPECTIVES ON THE SECOND LAW

The birth of the Second Law of thermodynamics is associated with the work “Réflexions sur la puissance motrice du feu et sur les machines propre à développer cette puissance” (1824) by Sadi Carnot, a French military engineer and physicist [19]. A few decades later, Lord Kelvin and Clausius formalized the Second Law of thermodynamics. Ever since the Second Law has been of major interest in exact and applied sciences [20].

Today the Second Law has several appearances in engineering. In this section we provide and illustrate three perspectives on the application of the Second Law in engineering, i.e. a modeling perspective, an analysis perspective and a design perspective.

Modeling

A thermodynamic model is a mathematical representation of a physical situation, defined by a system, the system boundary and the environment [21]. A system is a quantity of matter or a region in space upon which attention is concentrated in the analysis of a problem [22]. As such the definition of a system is an artificial concept to isolate scientific focus justifying a model to describe reality. The correspondence of a model to reality however is heavily dependent on the choice of the system boundary which separates the system from the environment and on the mathematical description of the interaction between system and environment.

The exergy method can be regarded as a modeling technique with a peculiar definition of the environment and its interaction with the system. The environment is a very large body or medium in the state of perfect thermodynamic equilibrium. It has no gradients or differences involving pressure, temperature, chemical potential, kinetic or potential energy [23]. The interaction between the system and the environment is represented by a Carnot engine. The work output of this reversible machine is the exergy of the system. It is the maximum theoretical useful work obtained if the system is brought into thermodynamic equilibrium with the environment by means of processes in which the system interacts only with this environment (Gibbs) [4].

Exergy represents a reversible limit which reveals what is impossible rather than what is feasible. The mathematical derivation of exergy only incorporates the equality sign of the Second Law of thermodynamics and with this it omits constraints reality imposes (e.g. time, material properties). Exergy therefore is an inaccurate model to describe reality. The question that arises is: “Can you draw conclusions based on an exergy model?”

Analysis

Second Law analysis comprises a comparison of reality (or an accurate model) with the corresponding exergy model. It uses exergy as a benchmark to pinpoint and quantify thermodynamic imperfection as irreversibility which is the difference between the actual work performed and the maximum theoretical useful work determined by the reversible model (Carnot).

As an example consider a thermal power plant. A power plant generates electricity from mechanical power which is obtained through a conversion of thermal power (\dot{Q} on T_{cc}). Figure 2 shows two possible thermodynamic models for this installation. On the left hand side there is the exergy model which represents the ideal power plant. According to this model the power plant output power is

$$\dot{W}_c = \dot{Q} \left(1 - \frac{T_0}{T_{cc}} \right). \quad (5)$$

On the right hand side we have a more realistic model presented by A. Bejan [3]. This endoreversible power plant model isolates the irreversibility due to heat transfer across finite temperature differences by inserting two heat exchangers (HE1 and HE2) with a limited heat transfer surface inventory ($C \leq C_1 + C_2$). Based on this model the maximum power plant output is

$$\dot{W}_B = \dot{Q} \left(1 - \frac{T_0}{T_{cc} - \dot{Q}/C} \right), \quad (6)$$

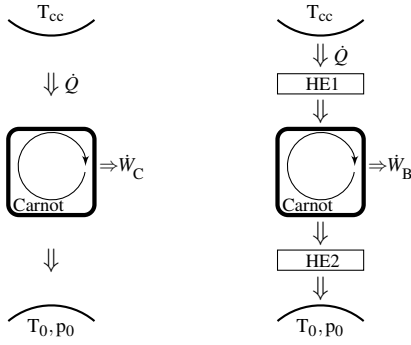


Figure 2. Power plant: exergy model (l), model by Bejan (r) [3].

which is smaller than \dot{W}_C .

An exergy analysis reveals irreversibility as a result of heat transfer across finite temperature differences. Unfortunately this irreversibility can not be eliminated since finite time and space, construction material properties, system topology and economic considerations constrain the heat transfer surface inventory (cf. constraint on C in the endoreversible model). In reality some irreversibilities are intrinsic and consequently unavoidable [18, 23–29]. A quantification of losses based on a comparison with the reversible limit (exergy model) is deceptive because large irreversibilities can be imposed and are therefore inevitable [29]. The value of irreversibility as a result of an exergy analysis does not indicate the potential to reduce it.

An exergy analysis implicitly performs a system decomposition as it aspires to compare reality with the reversible ideal on a local scale to allocate engineering efforts [3]. However, although an exergy analysis pinpoints and quantifies losses which might or might not be reducible, it does not necessarily reveal the source of these losses. Some irreversibilities are caused by the component in which they occur (endogenous exergy destruction) others are caused by other components (exogenous exergy destruction) [27, 28, 30, 31] which implies that a reduction of irreversibility in one component can induce a larger increase of irreversibility in another component [30]. This can be understood by considering the discrepancy between reality and the exergy model since the latter one inherently does not take into account any interaction between interconnected components. A local reduction of irreversibility can therefore have a pernicious effect on the overall efficiency.

As an illustration, consider a heat sink cooled chip (see Fig. 3). The chip provides a heat load \dot{Q} at a junction temperature T_j with a corresponding exergy

$$\dot{E}_{\text{chip}} = \iint_A \dot{q}'' \left(1 - \frac{T_0}{T_j} \right) dA \quad (7)$$

and hands it over to the heat sink.

Subsequently this exergy is (partly) transferred to the passing fluid

$$\Delta \dot{E}_f = \dot{m} (e_{f,\text{out}} - e_{f,\text{in}}). \quad (8)$$

The endogenous irreversibility of the heat sink is then naturally defined as

$$\dot{I}_{\text{hs}} \equiv \dot{E}_{\text{chip}} - \Delta \dot{E}_f. \quad (9)$$

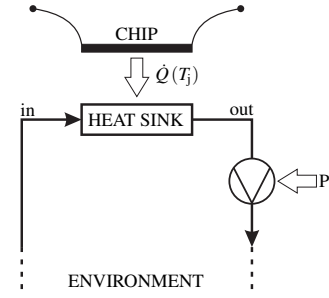


Figure 3. Schematic representation of a heat sink cooled chip.

The chip itself receives electric power and converts it to the heat load \dot{Q} . The conversion of electricity to heat generates an irreversibility \dot{I}_{chip} which can be decomposed in an intrinsic part \dot{I}_i and an avoidable part \dot{I}_a

$$\dot{I}_{\text{chip}} \equiv \dot{Q} - \dot{E}_{\text{chip}}, \quad (10)$$

$$\equiv \dot{I}_i + \dot{I}_a. \quad (11)$$

The intrinsic irreversibility \dot{I}_i is the loss of exergy due to the conversion from electricity to heat at a temperature $T_{j,\text{max}}$. This loss is fixed by electrical integrity of the chip and in particular by the maximum allowable junction temperature $T_{j,\text{max}}$ which is a technical constraint.

$$\dot{I}_i = \iint_A \dot{q}'' \left(\frac{T_0}{T_{j,\text{max}}} \right) dA \quad (12)$$

The avoidable irreversibility \dot{I}_a on the other hand is the loss of exergy due to the fact that the junction temperature T_j remains below the maximum allowable junction temperature $T_{j,\text{max}}$.

$$\dot{I}_a = \iint_A \dot{q}'' \left(\frac{T_0}{T_j} - \frac{T_0}{T_{j,\text{max}}} \right) dA \quad (13)$$

This avoidable loss is actually an exogenous irreversibility since it is not constrained by the chip but determined by heat sink design. Indeed, it is the heat sink which governs the junction temperature T_j . Therefore minimization of \dot{I}_a should be regarded as a challenge in heat sink design.

Figure 4 shows the Grassmann diagram of the heat sink cooled chip. The intrinsic irreversibility \dot{I}_i together with the maximum amount of exergy which can be passed on to the heat sink are hatched. Notice that although the intrinsic irreversibility \dot{I}_i often is the largest irreversibility in a heat sink cooled chip system, it is unavoidable. This illustrates that it is not always possible to allocate engineering efforts solely based on the absolute value of irreversibility. Furthermore one can deduce from the diagram and corresponding equations (Eq. (7) and (13)) that a reduction in junction temperature T_j reduces the irreversibility in the heat sink \dot{I}_{hs} but on the other hand increases the avoidable irreversibility in the chip \dot{I}_a . Since chip and heat sink are thermodynamically dependent one can not lower the irreversibility in one component while assuming the other won't be affected.

Design

Second Law based design endeavors to minimize the difference between reality and the corresponding exergy model. Al-

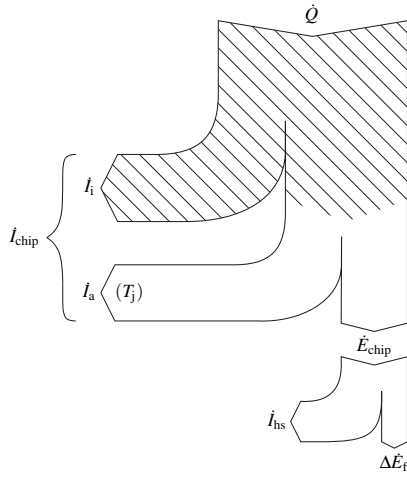


Figure 4. Grassmann diagram for a chip heat sink combination with $T_{in} = T_0$.

ternatively formulated it strives to minimize the irreversibility. Since irreversibility is proportional to entropy generation, engineering literature conveniently baptized Second Law based design as entropy generation minimization or EGM [18].

Entropy generation minimization allows to compare different interactions on a common basis [3]. This is one of the benefits associated with a Second Law based design methodology often found in literature. The Second Law reduces the number of objectives as it eliminates an ad hoc trade-off between heat transfer and fluid flow losses since a trade-off is embedded in the concept of irreversibility or entropy generation [32–34]. Yet this trade-off is based on the exergy model. How meaningful is this trade-off if applied to real applications which are irreversible?

To answer this question we examine a Brayton cycle as depicted in Fig. 5. This Brayton cycle takes a mechanical exergy input (P_C) and a thermal exergy input (\dot{Q}_{cc} at temperature T_{cc}) to generate a mechanical exergy output (P_T) while producing an exhaust flow exergy (e_6). A Brayton cycle with a topology as is presented will not use this flow exergy e_6 . Therefore the exergy of e_6 is lost. Since this flow exergy is mainly composed of thermal exergy we can conclude that due to the cycle topology the actual work potential of heat transfer irreversibility is lower than the theoretical work potential indicated by the exergy model.

The cycle turbine uses a pressure and temperature difference to generate the turbine power P_T . Divergence of the isobaric lines, the compressor pressure ratio, the heat transfer and fluid flow efficiency of the recuperator together with the isentropic efficiency of the turbine determine how P_C on one hand and \dot{Q}_{cc} on the other will be used to produce power. Since all components are irreversible, exergy as such and work potential attributed to thermal or mechanical energy specifically do not reflect the true potential of the energy streams to produce turbine power.

Previous reflections illustrate that entropy generation minimization of a heat exchanger as a component cannot provide the most optimal recuperator for a Brayton cycle. Although heat exchanger design is a trade-off between momentum losses and heat transfer enhancement it is not necessarily entropy generation that provides the optimal trade-off. Indeed, the actual work potential of energy streams is determined by irreversible components. Therefore it is different from the theoretical work potential as derived from an exergy model.

Entropy generation minimization has been applied to design

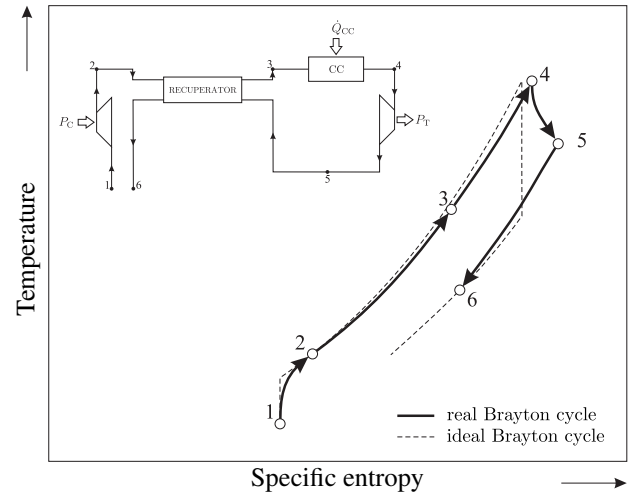


Figure 5. T-s diagram of a Brayton cycle with recuperation.

a large variety of components. Especially in the field of heat exchangers and heat sinks EGM has acquired some renown as optimization criterion since energy falls short in quantifying the performance of these components (e.g. [14, 16, 33, 35–37]). However, component optimization is not necessarily in correspondence with system optimization.

Thermodynamic optimization of a system is equivalent to a minimization of the total entropy generation \dot{S}_{gen}^{tot} which is an addition of the entropy generation in all components (n)

$$\dot{S}_{gen}^{tot} = \sum_{i=1}^n \dot{S}_{gen}^i \quad (14)$$

Minimizing \dot{S}_{gen}^{tot} is

$$\min \dot{S}_{gen}^{tot} = \min \sum_{i=1}^n \dot{S}_{gen}^i \quad (15)$$

$$\neq \sum_{i=1}^n \min \dot{S}_{gen}^i \quad (16)$$

meaning that optimized components do not necessarily result in an optimized system unless these components are thermodynamically isolated [18]. This simple mathematical reflection urges to raise a note of caution considering the application of EGM on component or on smaller scales without considering the overall system.

Entropy generation minimization assumes an invariable environment. Applying entropy generation minimization on a component or subsystem is therefore identical to casting the remaining part of the system as an invariable environment model. Such a model does not represent reality as it does not incorporate the effects of a local entropy generation minimization on another location or in another time frame.

Beyer addressed this issue already in the 70s [23, 30, 38] and also in subsequent decades similar remarks have been formulated mainly in the field of thermo-economics [25, 31, 39–42]. Entropy generation minimization has to be applied on the overall system or on independent components or subsystems. If not, the objective is different from system efficiency and therefore meaningless if thermodynamic efficiency is targeted. A system is in general more than the sum of its parts. It is a complex network of components and elements which influence each other.

CONCLUSION

If reversibility would be feasible then exergy can be conserved and the exergy model could be an accurate model. Unfortunately reversibility is unattainable and therefore the equality sign in the formulation of the Second Law is deceptive. The inequality sign of the Second Law is what reality defines. It is this inequality that represents the arrow of time and indicates direction. A direction which is incorporated in transfer and transport functions (e.g. Fourier's Law, Fick's Law).

The Second Law only enables us to pinpoint and quantify losses relative to the reversible ideal. Since reversibility is infeasible every entity under consideration creates losses. However the causes of these losses remain unknown and consequently engineering or economic efforts can not be allocated based on these losses. Minimization of all losses is equivalent to thermodynamic efficiency optimization. Entropy generation minimization is therefore an alternative cost function for First Law optimization. Anyhow it does not allow to decouple a system and design interacting components in thermodynamic isolation.

ACKNOWLEDGMENT

The work of Ruben Gielen is sponsored by the Institute for the Promotion of Innovation through Science and Technology in Flanders (IWT Vlaanderen).

Nomenclature

A	heat source base area [m ²]
C	heat transfer surface inventory [W/K]
\dot{E}	exergy [W]
E	energy [J]
e	flow exergy [J/kg]
g	gravitational acceleration [m/s ²]
h	specific enthalpy [J/kg]
\dot{I}	irreversibility [W/K]
\dot{m}	mass flow rate [kg/s]
P	power [W]
\dot{Q}	heat [W]
q''	chip heat load per source base area [W/m ²]
S	entropy [J/K]
s	specific entropy [J/kg K]
\dot{S}_{gen}	entropy generation [W/K]
T	temperature [K]
V	velocity [m/s]
\dot{W}	work [W]
z	height [m]

sub/superscripts

0	dead state
cc	combustion chamber
f	fluid
in	inlet
j	junction
max	maximum
out	outlet
tot	total

REFERENCES

[1] A. Bejan, Entropy Generation Minimization: The New Thermodynamics of Finite-Size Devices and Finite-Time

- Processes, *Journal of Applied Physics*, vol. 79, pp. 1191–1218, Feb. 1996.
- [2] L. Chen, C. Wu and F. Sun, Finite Time Thermodynamic Optimization or Entropy Generation Minimization of Energy Systems, *Journal of Non-Equilibrium Thermodynamics*, vol. 24, pp. 327–359, Oct. 1999.
- [3] A. Bejan, Fundamentals of Exergy Analysis, Entropy Generation Minimization, and the Generation of Flow Architecture, *International Journal of Energy Research*, vol. 26, pp. 1–43, 2002.
- [4] E. Sciubba and G. Wall, A Brief Commented History of Exergy From the Beginnings to 2004, *International Journal of Thermodynamics*, vol. 10, pp. 1–26, March 2007.
- [5] A. Hepbasli, A Key Review on Exergetic Analysis and Assessment of Renewable Energy Resources for a Sustainable Future, *Renewable and Sustainable Energy Reviews*, vol. 12, pp. 593–661, Apr. 2008.
- [6] M. J. Moran and E. Sciubba, Exergy Analysis: Principles and Practice, *Journal of Engineering for Gas Turbines and Power*, vol. 116, pp. 285–290, 1994.
- [7] I. Dincer and M. A. Rosen, Exergy: energy, environment and sustainable development, Elsevier, 2007.
- [8] A. Bejan, Entropy Generation Minimization The Method of Thermodynamic Optimization of Finite-Size Systems and Finite-Time Processes, CRC Press LLC, 1996.
- [9] J. E. Hesselgreaves, Rationalisation of Second Law Analysis of Heat Exchangers, *International Journal of Heat and Mass Transfer*, vol. 43, pp. 4189–4204, Nov. 2000.
- [10] F. Kock and H. Herwig, Local Entropy Production in Turbulent Shear Flows: a High-Reynolds Number Model with Wall Functions, *International Journal of Heat and Mass Transfer*, vol. 47, pp. 2205–2215, May 2004.
- [11] E. B. Ratts and A. G. Raut, Entropy Generation Minimization of Fully Developed Internal Flow with Constant Heat Flux, *J. Heat Transfer*, vol. 126, pp. 656–659, Aug. 2004.
- [12] T. Ko, Analysis of Optimal Reynolds Number for Developing Laminar Forced Convection in Double Sine Ducts Based on Entropy Generation Minimization Principle, *Energy Conversion and Management*, vol. 47, pp. 655–670, Apr. 2006.
- [13] A. J. Shah, V. P. Carey, C. E. Bash and C. D. Patel, An Exergy-Based Figure-of-Merit for Electronic Packages, *J. Electron. Packag.*, vol. 128, pp. 360–369, Dec. 2006.
- [14] H. Abbassi, Entropy Generation Analysis in a Uniformly Heated Microchannel Heat Sink, *Energy*, vol. 32, pp. 1932–1947, Oct. 2007.
- [15] B. Taufiq, H. Masjuki, T. Mahlia, R. Saidur, M. Faizul and E. Niza Mohamad, Second Law Analysis for Optimal Thermal Design of Radial Fin Geometry by Convection, *Applied Thermal Engineering*, vol. 27, pp. 1363–1370, Jun. 2007.
- [16] N. Sahiti, F. Krasniqi, X. Fejzullahu, J. Bunjaku and A. Muriqi, Entropy Generation Minimization of a Double-Pipe Pin Fin Heat Exchanger, *Applied Thermal Engineering*, vol. 28, pp. 2337–2344, Dec. 2008.
- [17] G. F. Naterer and J. A. Camberos, Entropy Based Design and Analysis of Fluids Engineering Systems, CRC Press LLC, Taylor & Francis Group, 2008.
- [18] A. Bejan, G. Tsatsaronis and M. Moran, Thermal design & optimization, John Wiley & sons, Inc., 1996.
- [19] S. Carnot, Réflexions sur la Puissance Motrice du Feu et sur les Machines Propre à Développer cette Puissance,

- Bachelier, Paris, 1824.
- [20] C. S. Helrich, *Modern Thermodynamics with Statistical Mechanics*, Springer, 2009.
- [21] E. G. Cravalho and J. L. Smith, *Engineering Thermodynamics*, Pitman, 1981.
- [22] P. K. Nag, *Basic And Applied Thermodynamics*, McGraw-Hill Education, 2nd edn., 2010.
- [23] T. J. Kotas, *The Exergy Method of Thermal Plant Analysis*, Exergon Publishing Company, UK, 2012.
- [24] J. Beyer, Einige Probleme der Praktischen Anwendung der Exergetischen Methode in Wärmewirtschaftlichen Untersuchungen Industrieller Produktionsprozesse – Teil II, *Energieanwendung*, vol. 28, pp. 66–70, April 1979.
- [25] M. A. Lozano and A. Valero, Theory of the Exergetic Cost, *Energy*, vol. 18, pp. 939–960, 1993.
- [26] V. A. Mironova, A. M. Tsirlin, V. A. Kazakov and R. S. Berry, Finite-Time Thermodynamics: Exergy and Optimization of Time-Constrained Processes, *Journal of Applied Physics*, vol. 76, pp. 629–636, Jul. 1994.
- [27] A. Valero, Exergy Accounting: Capabilities and Drawbacks, *Energy*, vol. 31, pp. 164–180, 2004.
- [28] S. Kelly, G. Tsatsaronis and T. Morosuk, Advanced Exergetic Analysis: Approaches for Splitting the Exergy Destruction into Endogenous and Exogenous Parts, *Energy*, vol. 34, pp. 384–391, March 2009.
- [29] R. Gielen, F. Rogiers, Y. Joshi and M. Baelmans, On the Use of Second Law Based Cost Functions in Plate Fin Heat Sink Design, in *Semiconductor Thermal Measurement and Management Symposium (SEMI-THERM)*, pp. 81–88, 2011.
- [30] J. Beyer, Strukturuntersuchungen-Notwendiger Bestandteil der Effektivitätsanalyse von Wärmeverbrauchersystemen, *Energieanwendung*, vol. 19, pp. 358–361, December 1970.
- [31] G. Tsatsaronis, Thermodynamic Optimization of Complex Energy Systems, vol. 69 of *NATO Science Series*, chap. Strengths and Limitations of Exergy Analysis, pp. 93–100, Kluwer Academic Publishers, 1st edn., 1999.
- [32] A. Bejan, *Advanced Engineering Thermodynamics*, John Wiley & sons, Inc., 2nd edn., 1997.
- [33] Z. Jian-hui, Y. Chun-xin and Z. Li-na, Minimizing the Entropy Generation Rate of the Plate-Finned Heat Sinks Using Computational Fluid Dynamics and Combined Optimization, *Applied Thermal Engineering*, vol. 29, pp. 1872–1879, Jun. 2009.
- [34] H. Herwig, The Role of Entropy Generation in Momentum and Heat Transfer, in *14th International Heat Transfer Conference*, vol. 8, pp. 363–377, Jan. 2010.
- [35] S. Aceves-Saborio, J. Ranasinghe and G. Reistad, An Extension to the Irreversibility Minimization Analysis Applied to Heat Exchangers, *Journal of Heat Transfer*, vol. 111, pp. 29–36, 1989.
- [36] J. R. Culham, W. A. Khan, M. M. Yovanovich and Y. S. Muzychka, The Influence of Material Properties and Spreading Resistance in the Thermal Design of Plate Fin Heat Sinks, *Journal of Electronic Packaging*, vol. 129, pp. 76–81, Mar. 2007.
- [37] W. Khan, J. Culham and M. Yovanovich, Optimization of Microchannel Heat Sinks Using Entropy Generation Minimization Method, *IEEE Transactions on Components and Packaging Technologies*, vol. 32, pp. 243–251, 2009.
- [38] J. Beyer, Strukturuntersuchung des Wärmeverbrauchs in Zuckerfabriken, *Energieanwendung*, vol. 21, pp. 79–82, March 1972.
- [39] C. A. Frangopoulos and R. B. Evans, Second Law Aspects of Thermal Design, vol. 33, chap. Thermoeconomic Isolation and Optimization of Thermal System Components, pp. 86–98, ASME, New York, 1984.
- [40] Y. M. El-Sayed, A Decomposition Strategy for Thermoeconomic Optimization, *Journal of energy resources technology*, vol. 111, pp. 111–120, September 1989.
- [41] Y. M. El-Sayed, Application of Exergy to Design, *Energy Conversion and Management*, vol. 43, pp. 1165–1185, Jun. 2002.
- [42] D. F. Rancruel and M. R. von Spakovsky, Decomposition with Thermoeconomic Isolation Applied to the Optimal Synthesis/Design and Operation of an Advanced Tactical Aircraft System, *Energy*, vol. 31, pp. 3327–3341, December 2006.

DIMENSIONAL TRANSITIONS IN THERMODYNAMIC PROPERTIES

Sevan Karabetoglu and Altug Sisman*

Istanbul Technical University, Energy Institute, 34469 Maslak, Istanbul, Turkey.

*Corresponding author, sismanal@itu.edu.tr

ABSTRACT

In this work, dimensional transitions in thermodynamic properties of an ideal Maxwell gas confined in a finite domain are studied. When one of the sizes of confinement domain becomes shorter than the thermal de Broglie wavelength of particles, momentum space is subject to a dimensional transition. Dimension of momentum space is defined based on mean probability change per quantum state step. Variation of the dimension with domain sizes is examined. Dependencies of internal energy, specific heat at constant volume and entropy on domain sizes as well as dimension of momentum space are analyzed. Dimensional transitions in momentum space from 3D to 2D and similarly from 2D to 1D and 1D to 0D are considered. It is shown that there is an increment in specific heat at constant volume during the dimensional transitions. Furthermore, all quantities considered here decreases when the confinement increases.

INTRODUCTION

Recent developments in nano science and technology reveal the difference between nano and macro scale material properties. Quantum wells, quantum wires and quantum dots are the remarkable examples for the diversity in transport and optical properties of the same material. Similarly, thermodynamic properties of gases confined in nano domains become size and shape dependent due to wave nature of particles [1-12].

Here, dimensional transitions in thermodynamic properties of an ideal monatomic Maxwell gas confined in a rectangular box are considered. Partition function is used to determine free energy. From expression of free energy; entropy, internal energy and specific heat at constant volume are then derived in exact forms based on expressions of infinite summations. Therefore the expressions are valid even for strongly confined domains although the trivial macroscopic expressions based on integral approximation are valid only for unbounded domains.

To examine the dimensional transitions in thermodynamic properties, dimension of momentum space is defined based on mean probability change per step in quantum state space. Internal energy of excited states is taken into account by eliminating ground state energy from internal energy to consider only thermal contributions instead of size dependent contribution of ground state energy. Similarly instead of considering entropy itself, only the entropy of momentum space is considered by subtracting entropy of the ground state, which is the pure configurational entropy, from the entropy itself. Dimensionless inverse scale factors $\alpha_1, \alpha_2, \alpha_3$ are defined as the ratio of the sizes of rectangular box in each direction (L_1, L_2 and L_3) to L_c . Thermodynamic quantities and their dimensional transitions are examined in terms of these dimensionless scale factors.

THERMODYNAMIC PROPERTIES OF AN IDEAL MAXWELL GAS IN A RECTANGULAR BOX

Free energy expression of an ideal Maxwell gas is given as

$$F = -Nk_b T \left[1 + \ln \left(\frac{\zeta}{N} \right) \right] \quad (1)$$

where, N is number of particles, T is temperature, k_b is the Boltzmann's constant and ζ is the partition function. For particles confined in a rectangular box, ζ is defined below [5]

$$\zeta = \zeta(\alpha_1, \alpha_2, \alpha_3) = \sum_{\{i,j,k\}=1}^{\infty} e^{-(\alpha_1 i)^2 - (\alpha_2 j)^2 - (\alpha_3 k)^2} \quad (2)$$

Here $\{i, j, k\}$ are the quantum state numbers running from unity to infinity, α_n is the dimensionless inverse scale factor defined as $\alpha_n = L_n / L_c$ where L_n is the size of the box in direction n and $L_c = h / (2\sqrt{2mk_b T})$.

Entropy is determined by the derivation of free energy with respect to temperature as follows,

$$S = - \left(\frac{\partial F}{\partial T} \right)_V = Nk_b \left[1 + \ln \left(\frac{\zeta}{N} \right) + \frac{\eta}{\zeta} \right] \quad (3)$$

where $\eta = \eta(\alpha_1, \alpha_2, \alpha_3)$ is given by

$$\eta = \sum_{\{i,j,k\}=1}^{\infty} \left[(\alpha_1 i)^2 + (\alpha_2 j)^2 + (\alpha_3 k)^2 \right] e^{-(\alpha_1 i)^2 - (\alpha_2 j)^2 - (\alpha_3 k)^2} \quad (4)$$

Free energy and entropy relations are used to obtain internal energy expression as

$$U = F + TS = Nk_b T \left(\frac{\eta}{\zeta} \right) \quad (5)$$

On the other hand, by differentiating the internal energy with respect to temperature, specific heat at constant volume is determined as

$$C_v = \left(\frac{\partial U}{\partial T} \right)_V = Nk_b \left(\frac{\gamma}{\zeta} \right) - Nk_b \left(\frac{\eta}{\zeta} \right)^2 \quad (6)$$

where $\gamma = \gamma(\alpha_1, \alpha_2, \alpha_3)$ is defined as

$$\gamma = \sum_{(i,j,k)=1}^{\infty} \left[(\alpha_1 i)^2 + (\alpha_2 j)^2 + (\alpha_3 k)^2 \right]^2 e^{-(\alpha_1 i)^2 - (\alpha_2 j)^2 - (\alpha_3 k)^2} \quad (7)$$

To examine the dimensional transition in thermodynamic properties above, dimensionless entropy, internal energy and specific heat at constant volume are introduced as,

$$\tilde{s} = \frac{S}{Nk_b} = 1 + \ln \left(\frac{\zeta}{N} \right) + \frac{\eta}{\zeta} \quad (8)$$

$$\tilde{u} = \frac{U}{Nk_b T} = \frac{\eta}{\zeta} \quad (9)$$

$$\tilde{c}_v = \frac{C_v}{Nk_b} = \frac{\gamma}{\zeta} - \left(\frac{\eta}{\zeta} \right)^2 \quad (10)$$

It should be noted that conditions of $N \gg 1$ and $N \ll \zeta$ should be satisfied to use both statistical approach and MB statistics respectively. In case of confinement in two directions (directions 2 and 3), these conditions are expressed as

$$1 \ll N \ll \frac{\sqrt{\pi}}{2\alpha_1} e^{-(\alpha_2^2 + \alpha_3^2)}. \quad (11)$$

Therefore, MB statistical approach can still be used if the value of α_1 is sufficiently small in spite of large values of α_2 and α_3 , $\{\alpha_2, \alpha_3\} > 1$.

DIMENSION DEFINITION AND TRANSITION IN MOMENTUM SPACE

Before examining dimensional transition in thermodynamic properties, dimension in momentum space should be defined with probabilistic approach. Excitation probability of particles in momentum space drastically decreases for the confinement direction and particles lose their excitation chance in that direction. In other words, only the ground state of momentum in confined direction can be occupied by the particles and all the excited states of momentum in that direction become empty. Occupation probability of quantum state r is

$$p_r = \frac{e^{-(\alpha_r, r)^2}}{\sum_{r=1}^{\infty} e^{-(\alpha_r, r)^2}}. \quad (12)$$

Change of probability per change of quantum state number is

$$\Delta p_r = p_r(\alpha_r, r+1) - p_r(\alpha_r, r) \quad (13)$$

The ensemble average of absolute value of Δp_r is

$$\langle |\Delta p_r| \rangle = -\sum_r p_r \Delta p_r \quad (14)$$

When α_r is greater than unity, the probability of ground state goes to unity which means that the whole particles accumulate in ground state. In that case, $\langle |\Delta p_r| \rangle$ also goes to unity since the probabilities of the excited states are zero and probability distribution becomes a single point in probability space. Therefore, this situation corresponds to a zero dimensional probability space. On the contrary, as α_r goes to zero each state becomes equally probable which corresponds one dimensional space. Consequently the dimension of momentum space can be determined by

$$D = 3 - \langle |\Delta p_i| \rangle - \langle |\Delta p_j| \rangle - \langle |\Delta p_k| \rangle \quad (15)$$

Thereby, dimensional transition from 3D to 0D can be examined by Eq.(15) as a function of $\alpha_1, \alpha_2, \alpha_3$. The dimensional transition due to change of domain sizes in directions of 1 and 2 is shown in Fig.1.

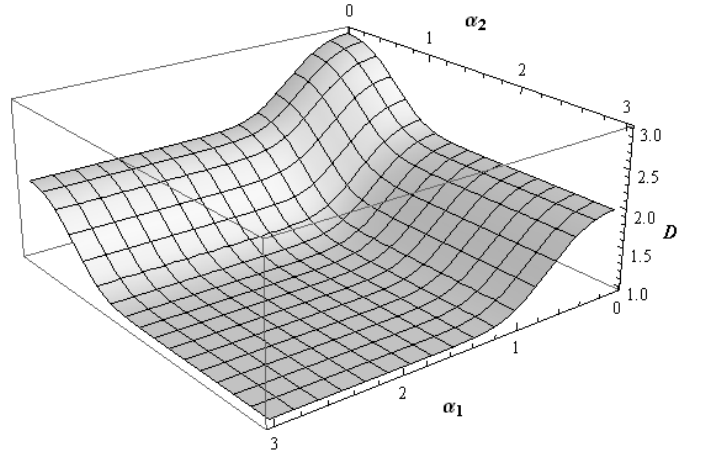


Figure 1: Dimensional transition from 3D to 2D and 1D.

Similarly dimensional transition from 1D to 0D is given in Fig.2.

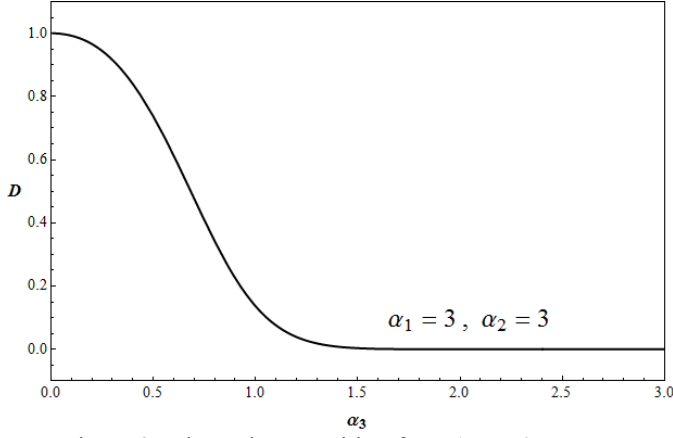


Figure 2: Dimension transition from 1D to 0D.

As seen in Fig.(1) and Fig.(2), even the value of 3 for α_n is enough for a strong confinement and dimensional transition in direction n .

DIMENSIONAL TRANSITION IN THERMODYNAMIC PROPERTIES

Internal energy of particles in excited states is calculated as

$$\tilde{u}_{ex} = \tilde{u} - u_o = \frac{\eta}{\zeta} - \alpha_1^2 - \alpha_2^2 - \alpha_3^2 \quad (16)$$

where u_o is the ground state energy. The reason of subtracting u_o is that the ground state energy considerably increases when the domain sizes decreases. Thus thermal energy can stimulate only the particles in excited states instead of particles in ground state. Therefore confinement energy represented by the ground state energy is eliminated if \tilde{u}_{ex} is considered. Similarly dimensionless entropy of particles in excited states is determined by

$$\tilde{s}_{ex} = \tilde{s} - s_o = \ln \zeta + \frac{\eta}{\zeta} \quad (17)$$

By subtracting entropy of the ground state, which is the pure configurational entropy, from the entropy itself, only the entropy of momentum space is considered. In other words, \tilde{s}_{ex} is the measure of disorder in momentum space only. Due to the first term of the right hand side of Eq.(17), however, the value of \tilde{s}_{ex} goes to infinity when α_n goes to zero as expected. Therefore, \tilde{s}_{ex} is normalized by dividing to its value for unconfined domain (3D domain) as follows

$$\hat{s}_{ex} = \frac{\tilde{s} - \tilde{s}_o}{(\tilde{s} - \tilde{s}_o)_{3D}} \quad (18)$$

Variation of \tilde{u}_{ex} , \tilde{s}_{ex} and \tilde{c}_v with domain sizes can be examined by changing α_3 for different set of $\{\alpha_1, \alpha_2\}$ values. Since the variation of dimension with domain sizes is also known, it is possible to examine the variation of thermodynamic quantities also with dimension by matching the values of dimension and thermodynamic properties for the same $(\alpha_1, \alpha_2, \alpha_3)$ values.

RESULTS AND DISCUSSIONS

3D unbounded domain is represented by $\{\alpha_1 = 0, \alpha_2 = 0, \alpha_3 = 0\}$. Confinement of the domain in one direction needs an increment of α value in that direction from zero to the values higher than unity. By following the same procedures for other directions, it is possible to confine the systems into smaller dimension in momentum space. Therefore the dimension of momentum space can be decreased from 3D to 2D, 1D and 0D.

The change of dimensionless internal energy and specific heat at constant volume of particles in excited states with respect to α_3 are given in Fig.3. and Fig.4 respectively.

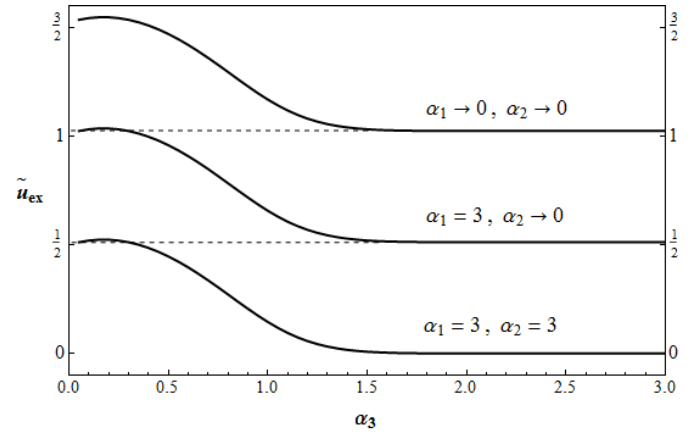


Figure 3: Variation of internal energy of particles in excited states with α_3 .

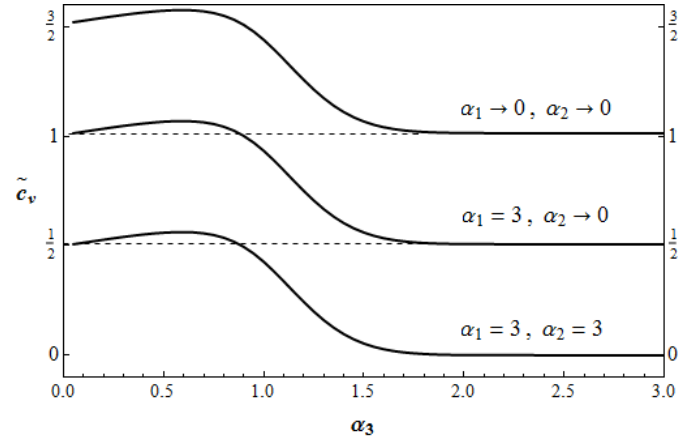


Figure 4: Variation of specific heat at constant volume of particles in excited states with α_3 .

In Figure 4., it seems that there is an increment in specific heat at constant volume as an interesting behavior during the dimensional transitions. Functional analysis of Eq.(10) shows that the first term represents the ensemble average of the square of dimensionless energy $\langle (\varepsilon/k_b T)^2 \rangle$ while the second one represents the square of ensemble average of dimensionless energy $\langle \varepsilon/k_b T \rangle^2$. Therefore Eq.(10) can be rewritten as

$$\tilde{c}_v = \left\langle \left(\frac{\varepsilon}{k_b T} \right)^2 \right\rangle - \left\langle \frac{\varepsilon}{k_b T} \right\rangle^2 \quad (19)$$

The first term in Eq.(19) increases faster than the second one up to a critical value of $\alpha = 0.56$ and then the first one approaches to the second one. Therefore the contribution of momentum component to the heat capacity becomes negligible for each direction when the related alpha value gets higher and higher values. In this case, also the dimension of momentum space decreases a unit value. This increment in specific heat is a pure quantum size effect which may be experimentally verified.

In Fig.5, variation of normalized dimensionless entropy of the particles in excited states with α_3 is given for different set of $\{\alpha_1, \alpha_2\}$ values.

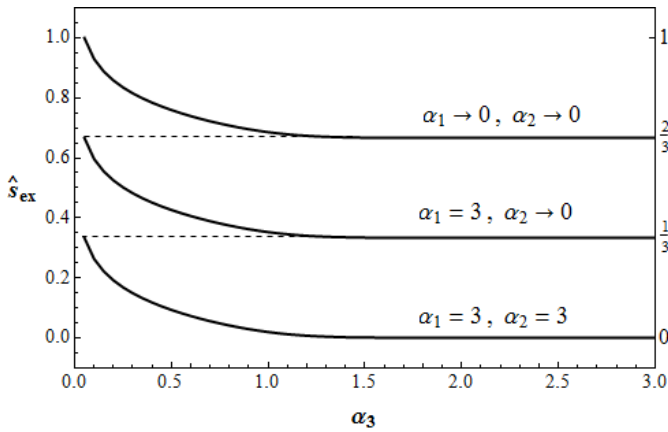


Figure 5: Variation of normalized entropy of gas in excited states with α_3

Normalized entropy of the particles in excited states decreases with increase of α_3 . For each confinement process, change in \tilde{s}_{ex} is $1/3$. For the case of $\{\alpha_1 = 3, \alpha_2 = 3\}$, \tilde{s}_{ex} goes to zero when α_3 goes to higher values than unity. Because all particles occupy ground state which has zero entropy. On the other hand, it should be noted that in case of $\{\alpha_1 = 3, \alpha_2 = 3, \alpha_3 = 3\}$, Eq.(11) becomes

$$N \ll e^{-(\alpha_1^2 + \alpha_2^2 + \alpha_3^2)} \ll 1 \quad (20)$$

Therefore, number of particles should be much less than unity to use Maxwell statistics which is physically meaningless. Consequently, although the expressions mathematically give the consistent results for $\{\alpha_1 = 3, \alpha_2 = 3, \alpha_3 = 3\}$ they represent a physically impossible condition.

As a result of increasing values of α_1, α_2 and α_3 , dimensional transitions occur from 3D to 2D, 2D to 1D and 1D to 0D. Dimensionless internal energy and specific heat of particles in excited states versus to dimension is given in Fig. 6 and Fig. 7 respectively. Both \tilde{u}_{ex} and \tilde{c}_v decrease $1/2$ for each unit dimensional transition.

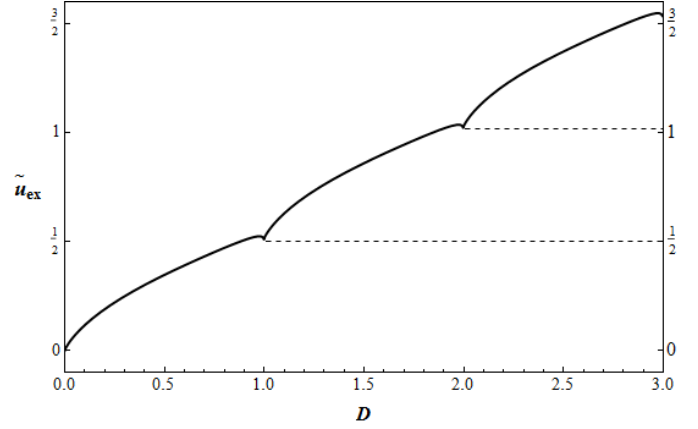


Figure 6: Variation of internal energy of gas in excited states with confined domain dimension

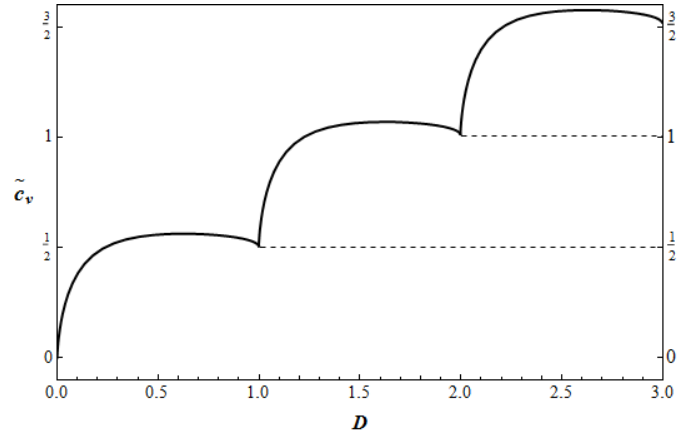


Figure 7: Variation of specific heat at constant volume of gas in excited states with confined domain dimension

In Fig.8 dimensional transition of normalized entropy of particles in excited states is shown. As expected, entropy value decreases with decreasing dimension.

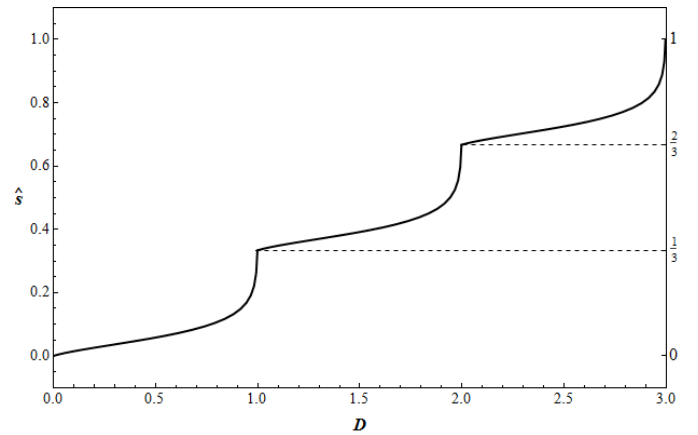


Figure 8: Variation of normalized entropy of gas in excited states with confined domain dimension

NOMENCLATURE

Symbol	Quantity	SI Unit
C_v	Heat capacity at constant volume	J K^{-1}
\tilde{c}_v	Dimensionless Specific heat at constant volume	
F	Free energy	J
h	Planck's constant	J s
k_B	Boltzmann's constant	J K^{-1}
L	Domain length	m
L_c	Half of the most probable wave length	m
m	Particle mass	kg
S	Entropy	J K^{-1}
\tilde{s}	Dimensionless entropy	
\tilde{s}_{ex}	Dimensionless entropy of particles in excited states	
\tilde{s}_o	Dimensionless entropy of ground state	
T	Temperature	K
U	Internal energy	J
\tilde{u}	Dimensionless internal energy	
\tilde{u}_{ex}	Dimensionless internal energy of particles in excited states	
\tilde{u}_o	Dimensionless energy of ground state	
α_n	Dimensionless inverse scale factor	
ζ	Partition function	

REFERENCES

- [1] M. I. Molina, Ideal gas in a finite container, *Am. J. Phys.* 64 pp. 503-505, 1996.
- [2] R. K. Pathria, An ideal quantum gas in a finite-sized container, *Am. J. Phys.* 66 pp.1080-1085, 1998.
- [3] W. S. Dai and M. Xie, Quantum statistics of ideal gases in confined space, *Phys. Lett. A* 311 pp. 340-346, 2003.
- [4] W. S. Dai and M. Xie, Geometry effects in confined space, *Phys. Rev. E* 70 016103, 2004.
- [5] A. Sisman and I. Müller, The Casimir-like size effects in ideal gases, *Phys. Lett. A* 320 pp. 360-366, 2004.
- [6] A. Sisman, Surface dependency in thermodynamics of ideal gases, *J. Phys. A- Math. Gen.* 37 pp. 11353-11361, 2004.
- [7] H. Pang, W. S. Dai and M. Xie, The difference of boundary effects between Bose and Fermi systems, *J. Phys. A-Math. Gen.* 39 pp. 2563-2571, 2006.
- [8] A. Sisman, Z. F. Ozturk and C. Firat, Quantum boundary layer: a non-uniform density distribution of an ideal gas in thermodynamic equilibrium, *Phys. Lett. A* 362 pp.16-20, 2007.
- [9] C. Firat and A. Sisman, Universality of quantum boundary layer for a Maxwellian gas, *Phys. Scripta* 79 065002, 2009.
- [10] Z. F. Ozturk and A. Sisman, Quantum Size Effects on the Thermal and Potential Conductivities of Ideal Gases, *Phys. Scripta* 80 065402, 2009.
- [11] C. Firat, A. Sisman and Z. F. Ozturk, Thermodynamics of gases in nano cavities, *Energy* 35 Sp.Iss.SI: pp. 814-819, 2010.
- [12] A. Sisman and G. Babac, Quantum Size Effects on Classical Thermosize Effects, *J. Continuum Mechanics & Thermodynamics* 24, pp.339-346, 2012.

QUANTUM SIZE AND DEGENERACY EFFECTS ON THERMAL SELF-DIFFUSION UNDER FREE MOLECULAR TRANSPORT REGIME

Gulru Babac, Altug Sisman* and Z. Fatih Ozturk

Istanbul Technical University, Energy Institute, 34469 Maslak, Istanbul, Turkey.

*Corresponding author, sismanal@itu.edu.tr

ABSTRACT

Thermal self-diffusion coefficients of monatomic ideal Fermi and Bose gases (like He3 and He4) are analytically determined by considering quantum size effects (QSE) for free molecular flow regime. The variations of thermal diffusion coefficients for Fermi and Bose gases with chemical potential are analyzed by neglecting QSE to understand the pure effect of quantum degeneracy. The results show that quantum degeneracy causes a substantial difference especially in degeneracy limit. It is seen that quantum degeneracy reduces thermal diffusion rate for both Fermi and Bose gases. There is a limit value for diffusion rate in a completely degenerate Bose gas. Furthermore, diffusion rates for Fermi and Bose gases are different from each other for the same degeneracy level. This difference in diffusion rates can be used for isotopic separation. QSE on thermal diffusion coefficients are also investigated. QSE cause tiny deviations from macroscopic behavior of thermal self-diffusion. QSE have negative contribution on thermal self-diffusion at low degeneracy while an opposite contribution appears at high degeneracy limit. Dimensionless diffusion coefficient goes to unity for a completely degenerate Fermi gas while it goes to infinity for a Bose gas.

INTRODUCTION

Nano Scale transport has a great deal of attention in recent years because of the increasing trend of manufacturing on these scales. Many transport phenomena in macro scale have to be revised or modified since many negligible effects in macro scale can be dominant in nano scale [1-3]. Quantum size effects (QSE) are one of these effects and they arise when thermal de Broglie wavelength of particles is not negligible in comparison with the characteristic size of the system. In such a case, wave character of particles becomes important and make thermodynamic and transport properties depend on shape and size of the domain [4-16].

Quantum degeneracy is another effect, which can be important in case high density or low temperature conditions. Under those conditions, thermal de Broglie wave length of particles is large enough in comparison with the mean distance between particles. Therefore quantum degeneracy becomes important and cause considerable changes in transport behaviours. In this case, quantum statistics (Fermi or Bose) should be used in calculations.

Transport processes in nano domains are generally considered within the scope of free molecular transport regime in which particle wall collisions are dominate instead of particle-particle ones. Therefore, size and surface effects can be more important in free molecular flow regime.

In this paper, thermal self-diffusion in free molecular transport regime is considered and both quantum degeneracy and QSE are taken into account in the calculations. Thermal self-diffusion fluxes of monatomic ideal Fermi and Bose gases (like He3 and He4) are determined. The influences of quantum degeneracy and QSE on thermal self-diffusion rates are examined.

THERMAL-SELF DIFFUSION IN QUANTUM DEGENERACY LIMIT

Thermal self-diffusion coefficient built up a relation between the diffusive flux and the temperature gradient and it is written in the following form

$$\vec{J} = -D_{th} \vec{\nabla} T \quad (1)$$

Here, D_{th} is the thermal self-diffusion coefficient, J is the particle flux due to temperature gradient, $\vec{\nabla} T$. To examine quantum size effects on thermal self-diffusion, nano scale transport domain is considered. Therefore free molecular transport regime is dominant since the mean free path of particles is usually larger than the characteristic size of the domain at nano scale. For ideal Maxwellian and quantum gases (Fermi and Bose) thermal self-diffusion coefficient can be given for free molecular transport regime as [17];

$$D_{th} = -\frac{\vec{J}}{\vec{\nabla} T} = nL_g \sqrt{\frac{2k_B}{mT}} \frac{g_2}{\eta} \left(1 - \Lambda \frac{g_0}{g_2} \right) \quad (2)$$

In Eq. (2), n is particle density, L_g is the characteristic size of the domain which can be given by $V/2A$ where V and A are domain volume and surface area respectively, k_B is the Boltzmann's constant, T is temperature, m is the particle mass and Λ is the dimensionless chemical potential defined as $\Lambda = \mu/k_B T$ in terms of chemical potential, μ . Definitions of η , g_0 and g_2 functions are given in Refs. [13, 17] and their ratios in Eq.(2) can be obtained for an ideal quantum gases (namely Fermi Dirac-FD and Bose Einstein-BE gases) as follows

$$\frac{g_2}{\eta} = \frac{4}{3\sqrt{\pi}} \frac{Li_2[\mp e^\Lambda]}{Li_{3/2}[\mp e^\Lambda]} \quad (3)$$

$$\frac{g_0}{g_2} = \frac{1}{2} \frac{Li_1[\mp e^\Lambda]}{Li_2[\mp e^\Lambda]} \quad (4)$$

where Li represents the Polylogarithm functions while negative and positive signs stand for Fermi and Bose gases, respectively. The strength of degeneracy increases with increasing value of Λ . Completely degenerate Fermi and Bose gases are obtained for the corresponding limits of $\Lambda \rightarrow \infty$ and $\Lambda \rightarrow -\infty$. In classical limit, $\Lambda \rightarrow 0$, degeneracy disappears and Polylogarithm functions reduces to $Li[\mp e^\Lambda] \rightarrow \mp e^\Lambda$. Thus, Eqs. (3) and (4) reduce to the equations given below for an ideal Maxwell gas

$$\frac{g_2}{\eta} = \frac{4}{3\sqrt{\pi}} \quad (5)$$

$$\frac{g_0}{g_2} = \frac{1}{2} \quad (6)$$

To examine the pure quantum degeneracy effects on thermal self-diffusion, dimensionless diffusion coefficient is defined and determined by using Eqs. (3) and (4) in Eq.(2) as

$$\tilde{D}_{th} = \frac{D_{th}}{nL_g \sqrt{\frac{2k_B}{mT}}} = \frac{4}{3\sqrt{\pi}} \frac{Li_2[\mp e^\Lambda]}{Li_{3/2}[\mp e^\Lambda]} \left(1 - \frac{1}{2} \Lambda \frac{Li_1[\mp e^\Lambda]}{Li_2[\mp e^\Lambda]} \right) \quad (7)$$

Degeneracy effects can be analysed for Fermi and Bose gases separately by using the proper value intervals of Λ in Eq.(7). The results are given in Fig. 1.

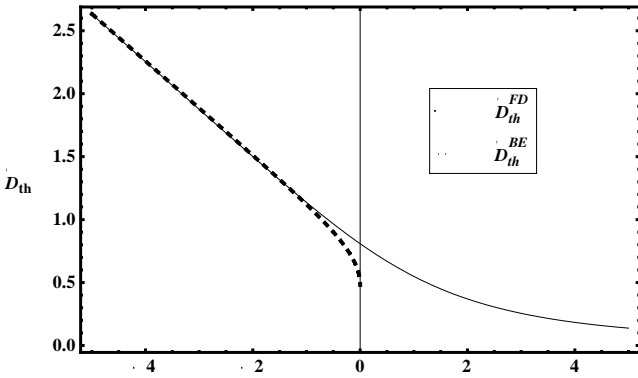


Figure 1: Variation of dimensionless diffusion coefficient with dimensionless chemical potential for Bose (dashed curve) and Fermi (solid curve) gases.

It is seen that quantum degeneracy reduces thermal diffusion rate for both Fermi and Bose gases. Furthermore, diffusion rates for Fermi and Bose gases are different from each other for the same degeneracy level (the same value of Λ). This difference in diffusion rates can be used for isotopic separation if one isotope obeys Fermi statistics while the other one obeys Bose, like He3 and He4 gases. For a

completely degenerate Bose gas ($\Lambda \rightarrow -\infty$), by using the asymptotic forms of Polylogarithm functions, it is possible to show that Eq.(7) goes to $4\zeta(2)/3\sqrt{\pi}\zeta(3/2) \cong 0.474$. On the other hand, for a completely degenerate Fermi gas, it goes to zero.

SELF-THERMAL DIFFUSION UNDER QUANTUM SIZE EFFECTS

In order to consider quantum size effects, which result from the wave character of particles and may cause considerable changes in transport phenomena at nano scale, it is necessary to calculate the functions of η , g_0 and g_2 more precisely. These calculations have been done in Ref. [17] and the following ratios can be given

$$\frac{g_2}{\eta} = \frac{4}{3\sqrt{\pi}} \frac{Li_2[\mp e^\Lambda]}{Li_{3/2}[\mp e^\Lambda]} \frac{\left[1 - \frac{\alpha}{\sqrt{\pi}} \frac{9\pi}{32} \frac{Li_{3/2}[\mp e^\Lambda]}{Li_2[\mp e^\Lambda]} \right]}{\left[1 - \frac{\alpha}{\sqrt{\pi}} \frac{Li_1[\mp e^\Lambda]}{Li_{3/2}[\mp e^\Lambda]} \right]} \quad (8)$$

$$\frac{g_0}{g_2} = \frac{1}{2} \frac{Li_1[\mp e^\Lambda]}{Li_2[\mp e^\Lambda]} \frac{\left[1 - \frac{\alpha}{\sqrt{\pi}} \frac{3\pi}{8} \frac{Li_{1/2}[\mp e^\Lambda]}{Li_1[\mp e^\Lambda]} \right]}{\left[1 - \frac{\alpha}{\sqrt{\pi}} \frac{9\pi}{32} \frac{Li_{3/2}[\mp e^\Lambda]}{Li_2[\mp e^\Lambda]} \right]} \quad (9)$$

where $\alpha = \alpha_2 + \alpha_3$, α_j is inverse scale factor defined as $\alpha_j = L_c/L_j$, L_c is the half of the most probable de Broglie wave length given by $L_c = h/\sqrt{2mk_bT}$ and L_j is the domain size in j direction. Since the direction 1 is chosen as a transport direction here, $\alpha_1 = 0$ (there is no confinement in direction 1). It is clear that Eqs.(3) and (4) can easily be recovered from Eqs. (8) and (9) when domain sizes in directions 2 and 3 are larger enough in comparison with L_c , $\{\alpha_2, \alpha_3\} \rightarrow 0$.

To examine the pure quantum size effects on thermal self-diffusion rate, a dimensionless diffusion coefficient for quantum gases is defined as the ratio of diffusion coefficient with and without QSE. By using Eqs.(8) and (9) as well as Eqs.(3) and (4) in Eq.(2), dimensionless diffusion coefficient is obtained as

$$\tilde{D}_{th}^{QSE} = \frac{D_{th}^{FD/BE}}{D_{th}^{FD/BE}} = \frac{\left[1 - \frac{\alpha}{\sqrt{\pi}} \frac{9\pi}{32} \frac{Li_{3/2}[\mp e^\Lambda]}{Li_2[\mp e^\Lambda]} \right]}{\left[1 - \frac{\alpha}{\sqrt{\pi}} \frac{Li_1[\mp e^\Lambda]}{Li_{3/2}[\mp e^\Lambda]} \right]} \frac{\left[1 - \frac{1}{2} \Lambda \frac{Li_1[\mp e^\Lambda]}{Li_2[\mp e^\Lambda]} \right] \frac{\left[1 - \frac{\alpha}{\sqrt{\pi}} \frac{3\pi}{8} \frac{Li_{1/2}[\mp e^\Lambda]}{Li_1[\mp e^\Lambda]} \right]}{\left[1 - \frac{\alpha}{\sqrt{\pi}} \frac{9\pi}{32} \frac{Li_{3/2}[\mp e^\Lambda]}{Li_2[\mp e^\Lambda]} \right]}}{\left[1 - \frac{1}{2} \Lambda \frac{Li_1[\mp e^\Lambda]}{Li_2[\mp e^\Lambda]} \right]} \quad (10)$$

Equation (10) can be used to analyse QSE on thermal self-diffusion rate for Fermi and Bose gases as well as Maxwell gas by using the proper Λ values. The variation of dimensionless diffusion coefficient with dimensionless chemical potential is seen in Fig.2 for $\alpha = \alpha_2 + \alpha_3 = 0.1$.

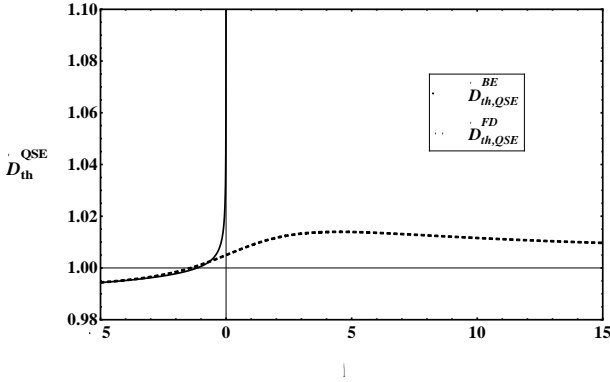


Figure 2: The variation of dimensionless diffusion coefficient with dimensionless chemical potential for $\alpha = 0.1$.

Fig. 2 shows that QSE cause tiny deviations from macroscopic behavior of thermal self-diffusion. QSE have negative contribution on thermal self-diffusion at low degeneracy or classical limit ($\Lambda \rightarrow -\infty$), while an opposite contribution appears at high degeneracy limit. Dimensionless diffusion coefficient goes to unity for a completely degenerate Fermi gas while it goes to infinity for Bose gas. In Maxwellian limit ($\Lambda \rightarrow -\infty$), Eq.(10) can be simplified by using the asymptotic forms of Polylogarithm functions, $Li\left[\mp e^\Lambda\right] \rightarrow \mp e^\Lambda$, as

$$\tilde{D}_{th,QSE}^{MB} = \frac{D_{th,QSE}^{MB}}{D_{th}^{MB}} = \left[\frac{1 - \frac{\alpha}{\sqrt{\pi}} \frac{9\pi}{32}}{1 - \frac{\alpha}{\sqrt{\pi}}} \right] \left[\frac{1 - \frac{1}{2}\Lambda - \frac{\alpha}{\sqrt{\pi}} \frac{3\pi}{8}}{1 - \frac{1}{2}\Lambda} \right] \quad (11)$$

CONCLUSION

The results show that quantum degeneracy decreases thermal self-diffusion rate. There is a limit value for diffusion rate in a completely degenerate Bose gas. On the other hand, diffusion rate goes to zero in degeneracy limit for a Fermi gas. Different diffusion rates of Fermi and Bose gases for the same degeneracy level may allow to design an isotopic enrichment process if one isotope obeys Fermi statistics while the other one obeys Bose one, like He3 and He4 gases.

Although quantum degeneracy causes a considerable difference in diffusion rate, only tiny deviations from macroscopic behavior of thermal self-diffusion arises due to QSE. On the other hand, opposite contributions of QSE on diffusion rates of Fermi and Bose gases are also obtained for strongly degenerate limit. Therefore, QSE may also be used for isotopic enrichments.

A possible experimental verification of QSE on thermal self-diffusion rate can be a macroscopic manifestation of wave nature of particles in diffusion process. The results may be used to design some new devices and processes.

NOMENCLATURE

Symbol	Quantity	SI Unit
D_{th}	Thermal self-diffusion coefficient	$m^{-1} \cdot s^{-1} \cdot K^{-1}$
J	Particle flux	$(\# \text{ of particle}) \cdot m^{-2} \cdot s^{-1}$
k_B	Boltzmann's constant	$J K^{-1}$
L_c	Half of the most probable wave length	m
L_g	Characteristic size of the domain	m
L_j	Size of the domain in direction j	m
n	Particle density	$\# / m^3$
m	Particle mass	kg
T	Temperature	K
α	Dimensionless inverse scale factor	
A	Dimensionless chemical potential	
μ	Chemical potential	Joule
BE	Bose-Einstein statistics	
FD	Fermi-Dirac statistics	
MB	Maxwell-Boltzmann statistics	
QSE	Quantum size effect	

REFERENCES

- [1] G.E. Karniadikis, N. Aluru and A. Beskok, *Micro and Nano Flows: Fundamentals and Simulation*, Springer, New York, 2005.
- [2] G. Babac and A. Sisman, Thermodynamic cycles based on classical thermosize effects, *Int. J. Computational and Theoretical Nano Science*, vol. 8, pp. 1-7, 2011.
- [3] G. Babac and A. Sisman, Classical thermosize effects in degenerate quantum gases, *Int. J. Computational and Theoretical Nano Science*, vol. 8(11), pp. 1-4, 2011.
- [4] M.I. Molina, Ideal gas in a finite container, *Am. J. Phys.*, vol. 64, pp. 503-505, 1996.
- [5] R.K. Pathria, An ideal quantum gas in a finite-sized container, *Am. J. Phys.*, vol. 66, pp.1080-1085, 1998.
- [6] W.S. Dai and M. Xie, Quantum statistics of ideal gases in confined space, *Phys. Lett. A*, vol. 311, pp. 340-346, 2003.
- [7] W.S. Dai and M. Xie, Geometry effects in confined space, *Phys. Rev. E* **70** 016103, 2004.
- [8] A. Sisman and I. Müller, The Casimir-like size effects in ideal gases, *Phys. Lett. A*, vol. 320, pp. 360-366, 2004.
- [9] A. Sisman, Surface dependency in thermodynamics of ideal gases, *J. Phys. A- Math. Gen.*, vol. 37, pp. 11353-11361, 2004.
- [10] H. Pang, W.S. Dai and M. Xie, The difference of boundary effects between Bose and Fermi systems, *J. Phys. A-Math. Gen.*, vol. 39, pp. 2563-2571, 2006.
- [11] A. Sisman, Z.F. Ozturk and C. Firat, Quantum boundary layer: a non-uniform density distribution of an ideal gas in thermodynamic equilibrium, *Phys. Lett. A*, vol. 362, pp.16-20, 2007.
- [12] C. Firat and A. Sisman, Universality of quantum boundary layer for a Maxwellian gas, *Phys. Scripta*, vol. 79, pp. 065002, 2009.

- [13] Z.F. Ozturk and A. Sisman, Quantum Size Effects on the Thermal and Potential Conductivities of Ideal Gases, *Phys. Scripta*, vol. 80, pp. 065402, 2009.
- [14] Z.F. Ozturk, A. Sisman and C. Firat, Quantum Effects on Gas Diffusion at the Nano Scale, *Int. J. Thermodynamics*, vol. 14(4), pp. 163-166, 2011.
- [15] C. Firat, A. Sisman and Z.F. Ozturk, Thermodynamics of gases in nano cavities, *Energy*, vol. 35, pp. 814-819, 2010.
- [16] A. Sisman and G. Babac, Quantum Size Effects on Classical Thermosize Effects, *J. Continuum Mechanics & Thermodynamics*, vol. 24, pp.339-346, 2012.
- [17] Z.F. Ozturk, Quantum Size Effects on Nano Gas Transport (in Turkish), Ph.D. thesis, Istanbul Technical University, Istanbul, 2007.

DISCRETE NATURE OF THERMODYNAMIC PROPERTIES

Alhun Aydın* and Altuğ Şişman**

Istanbul Technical University, Energy Institute, 34469 Maslak, Istanbul, Turkey

*e-mail: alhunaydin@gmail.com

**e-mail: sismanal@itu.edu.tr

ABSTRACT

In this paper, we examined 0D and 1D Fermi gases (for example an electron gas in semiconductors or even atom gases like He₃) confined in certain dimensions. It has been shown that thermodynamic properties have a discrete nature in nanoscale. Also, they have certain physically meaningful values, which mean thermodynamic properties cannot take any continuous value, unlike classical thermodynamics in which they are considered as continuous quantities. We conclude that, as long as the confinement is strong enough, discrete nature of thermodynamic properties can be observed. Since quantum confinement in semiconductors is a well-established experimental research area, it is also possible to experimentally verify the results obtained here. Furthermore, the possibility of introducing new effects and developing new thermodynamic devices that depend on the discrete nature of thermodynamics in nanoscale will be discussed.

INTRODUCTION

Leap forwards in nanotechnologies in recent years, make it necessary to study thermodynamic behaviors of matter in nanoscale, which leads to a relatively new research area called as nano thermodynamics.[1-12] Numerous researches are going on in these areas recently. There are considerable deviations from classical thermodynamics and there have been proposed new effects based on the quantum nature of the systems. One of these new effects is examined under the name of Quantum Size Effects (QSE) in literature recently.

Thermodynamic properties such as number of particles, free energy, entropy, internal energy, chemical potential and heat capacity are represented with summations over quantum states, in their fundamental and exact forms. In macro scale, these summations in thermodynamic expressions may be replaced by integrals to make algebraic operations easy. However, when the sizes of the domain are comparable to the thermal de Broglie wavelength of particles, for instance in nanoscale; wave nature of particles become dominant, so we cannot use integrals instead of summations, since continuum approximation is no longer valid. Exact forms of thermodynamic properties must be considered in nanoscale thermodynamics. There are several ways to calculate exact sums in thermodynamics; one way is using Poisson summation formula. Evaluating partition function by Poisson summation formula expands the sum to three terms. Integral term is the conventional term that has been used in classical thermodynamics under continuum approximation. Zero correction term is a consequence of the fact that there are no zero-momentum states for particles in a system. Eventually, discrete term represents the discrete nature of momentum states and becomes dominant in nanoscale. Effects of zero correction term have been studied in literature as QSE. When the domain size is comparable to the thermal de Broglie wavelength of particles, contribution of zero correction term becomes recognizable. In addition to zero correction, in Fermi-Dirac statistics, discrete nature of thermodynamic properties, which depend

on Pauli Exclusion Principle, starts to reveal itself. Intrinsic discrete nature has not seen in Maxwell-Boltzmann and Bose-Einstein statistics, since discretization is a consequence of Pauli Exclusion Principle, which is used fundamentally in the derivation of Fermi-Dirac statistics.

EXACT EXPRESSIONS OF THERMODYNAMIC PROPERTIES FOR A FERMI GAS CONFINED IN A RECTANGULAR DOMAIN

For a rectangular domain with dimensions L_1, L_2 and L_3 , energy eigenvalues from Schrödinger equation are

$$\epsilon = \frac{h^2}{8m} \left[\left(\frac{i_1}{L_1} \right)^2 + \left(\frac{i_2}{L_2} \right)^2 + \left(\frac{i_3}{L_3} \right)^2 \right], \quad (1)$$

with $(i_1, i_2, i_3) = 1, 2, 3, \dots$,

where h is the Planck's constant and m is the mass of the fermion. Fermi-Dirac distribution function is

$$f = \frac{1}{e^{-\Lambda + (\alpha_1 i_1)^2 + (\alpha_2 i_2)^2 + (\alpha_3 i_3)^2} + 1} \quad (2)$$

where $\Lambda = \mu/k_b T$ and α_n 's are dimensionless scale factors defined as $\alpha_n = L_c(T)/L_n$ with $n = 1, 2, 3$ and $L_c(T) = h/\sqrt{8mk_b T} = \frac{\sqrt{\pi}}{2} \lambda_{th}$, where λ_{th} is the thermal de Broglie wavelength, k_b is the Boltzmann's constant and T is the temperature of the gas. Summations over all states of the distribution function will give the number of particles of a Fermi gas

$$N = \sum_{(i_1, i_2, i_3)=1}^{\infty} \frac{1}{e^{-\Lambda + (\alpha_1 i_1)^2 + (\alpha_2 i_2)^2 + (\alpha_3 i_3)^2} + 1} \quad (3)$$

Now we can write the exact forms of thermodynamic properties such as internal energy U and heat capacity at constant volume C_V respectively as follows

$$U = k_b T \sum_{(i_1, i_2, i_3)=1}^{\infty} [(\alpha_1 i_1)^2 + (\alpha_2 i_2)^2 + (\alpha_3 i_3)^2] f \quad (4)$$

$$C_V = k_b \frac{\sum_{(i_1, i_2, i_3)=1}^{\infty} [(\alpha_1 i_1)^2 + (\alpha_2 i_2)^2 + (\alpha_3 i_3)^2]^2 f(1-f)}{\sum_{(i_1, i_2, i_3)=1}^{\infty} [(\alpha_1 i_1)^2 + (\alpha_2 i_2)^2 + (\alpha_3 i_3)^2] f(1-f)} \quad (5)$$

DISCRETE NATURE IN STRONGLY ANISOMETRIC QUANTUM DOTS

For 0D, we examined two cases; strongly anisometric domain and isometric domain. In strongly anisometric domain, dimensionless scale factors are chosen as $\alpha_1 = 1$, $\alpha_2 = 40$ and $\alpha_3 = 40$, so that domain is confined in all three directions to make it a quantum dot, only 2 directions are confined much strongly than the other direction. Note that, $\alpha = 40$ is not a physically meaningless confinement, since it can be reached by using today's techniques in laboratories. For strongly anisometric domain, dimensionless chemical potential Λ against particle number N has been shown in Figure 1:

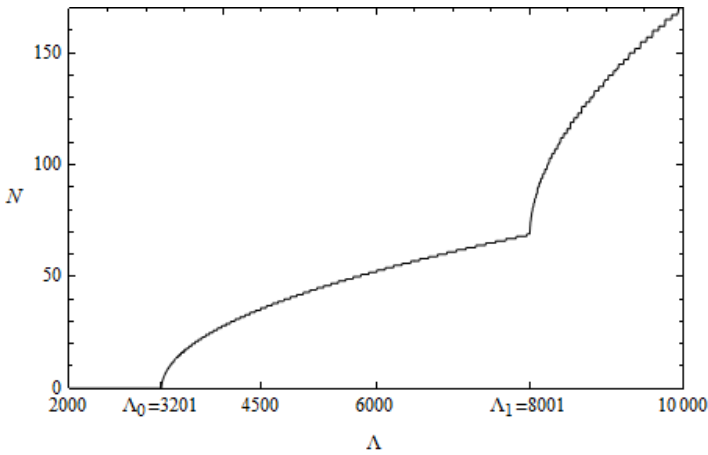


Figure 1. Strongly anisometric 0D domain (Quantum Dot), N vs Λ

Dimensionless chemical potential values between 0 and Λ_0 corresponds to zero particle. In other words, physically meaningful Λ values start from Λ_0 . In Figure 1, critical Λ values are $\Lambda_0 = (\alpha_1)^2 + (\alpha_2)^2 + (\alpha_3)^2$ and $\Lambda_1 = (\alpha_1)^2 + (\alpha_2)^2 + (2\alpha_3)^2$. Beginning from $\Lambda_0 = (1)^2 + (40)^2 + (40)^2 = 3201$, states of the momentum component in direction-1, start to be occupied by particles since the discreteness of momentum in direction-1 is not as strong as in directions-2 and 3. That means, occupation of momentum states in direction-1 is possible, although the others are not. Hence, we can convert triple sum into a single sum, in a limited range of Λ .

$$N = \sum_{i_1=1}^{\infty} \frac{1}{e^{-\Lambda + (\alpha_1 i_1)^2 + (\alpha_2)^2 + (\alpha_3)^2} + 1} \quad (6)$$

Thereby, Eq. 6 gives exactly the same results of Eq. 3, for $\Lambda < \Lambda_1$. After $\Lambda_1 = (1)^2 + (40)^2 + (2 \times 40)^2 = 8001$ value, we have to consider excitations also in other directions. As it is shown in Figure 1, Λ changes with N in a stepwise manner. These steps can be seen in close-up more easily in Figure 2

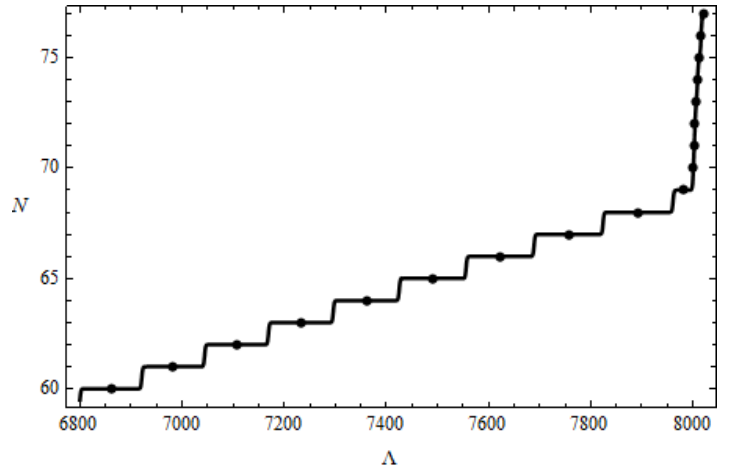


Figure 2. Strongly anisometric 0D domain (Quantum Dot) close-up, N vs Λ

Points on the middle of stepwise plateaus indicate Λ values corresponding to the integer particle numbers. As long as number of particles has integer values, continuous parts which do not contain points, are the forbidden region for Λ values. In other words, chemical potential can take only some certain discrete values which correspond to the integer number of particles. That is a very crucial deviation from classical thermodynamics. After Λ_1 , the second modes of momentum components in direction-2 and 3 start to be occupied and the relation between N and Λ has a new character. Pay attention to that, horizontal steps are not completely flat, so the derivative of the function in any point is never zero. Similar stepwise behavior of particle number vs Λ , can be seen also in internal energy of Fermi gas. In Figure 3 and 4, dimensionless internal energy and specific heat at constant volume; $\tilde{U} = \frac{U}{Nk_b T}$ and $\tilde{C}_V = \frac{C_V}{Nk_b}$, versus Λ are shown respectively.

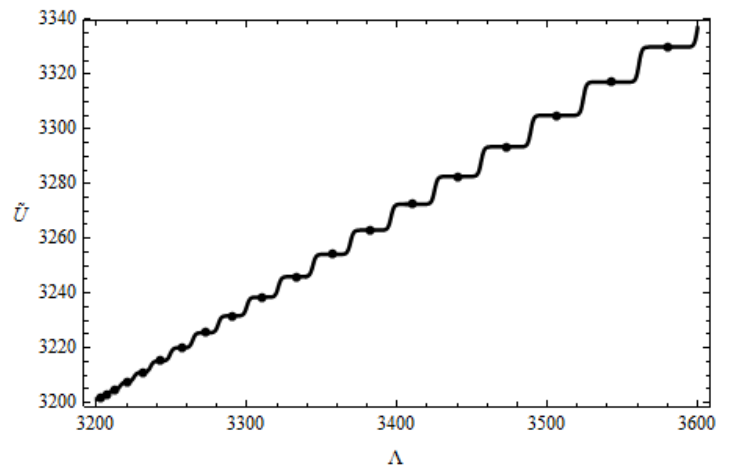


Figure 3. Strongly anisometric 0D domain (Quantum Dot), \tilde{U} vs Λ

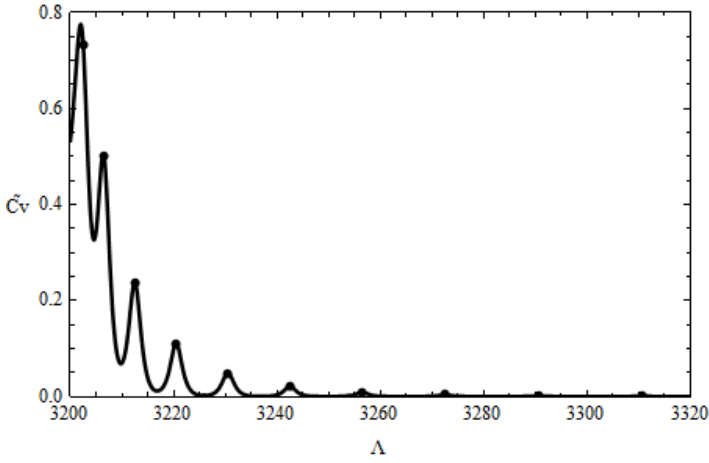


Figure 4. Strongly anisotropic 0D domain (Quantum Dot), \widetilde{C}_V vs Λ

Behavior of specific heat is as shown in Figure 4. Definite Λ values, marked with points, are determined from N vs Λ relationship and they are same in all figures. Besides, effects of particle addition to the system which is moderately confined in direction-1 and strongly confined in direction-2 and 3, can be shown in Figure 5.

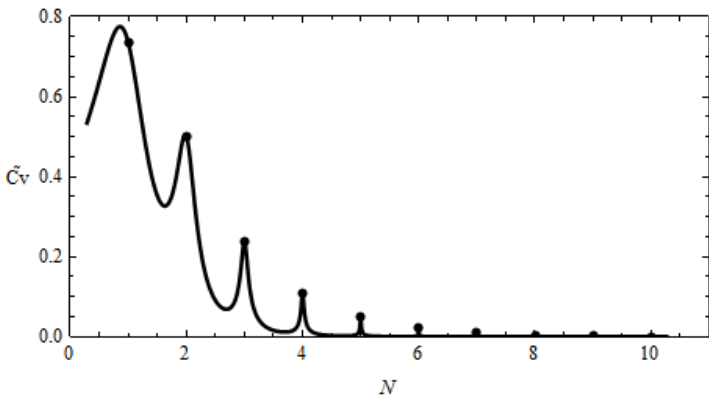


Figure 5. Strongly anisotropic 0D domain (Quantum Dot), \widetilde{C}_V vs N

DISCRETE NATURE IN ISOMETRIC QUANTUM DOTS

Now, let's consider isometric quantum dot. In isometric domain, dimensionless scale factors are chosen as $\alpha_1 = 3$, $\alpha_2 = 3$ and $\alpha_3 = 3$. So, confinement is not extremely strong, however it is strong enough to make the structure a quantum dot. Because of the contribution of the excited modes of momentum components, we have to do triple sum in order to express state functions and particle number, in all range.

For this case, N , U and C_V versus Λ are shown respectively in Figures 6, 7 and 8. Unlike the first case, for this case there are allowed values also in the steepnesses of the function, since excited modes in each direction start to be occupied from the very early $\Lambda = (3)^2 + (3)^2 + (3)^2 = 9$ value.

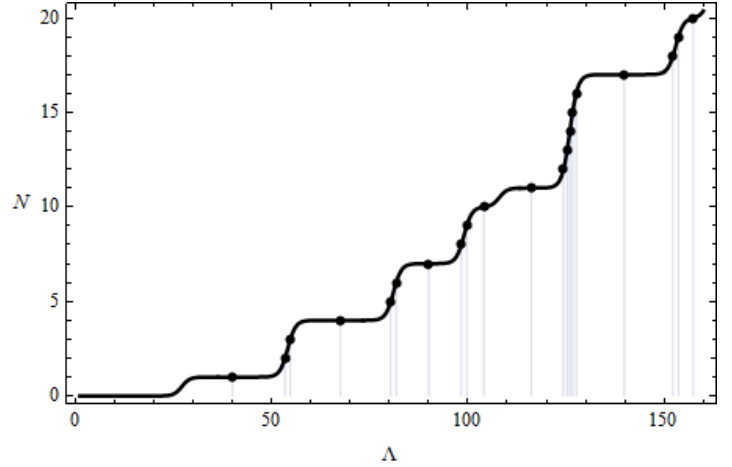


Figure 6. Isometric 0D domain (Quantum Dot), N vs Λ

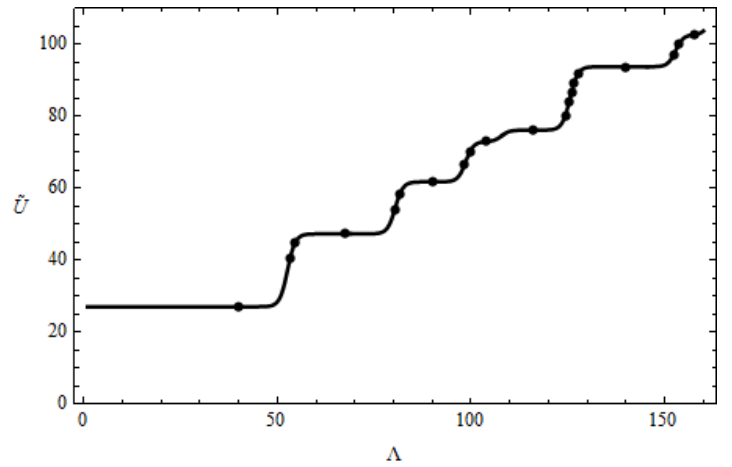


Figure 7. Isometric 0D domain (Quantum Dot), \widetilde{U} vs Λ

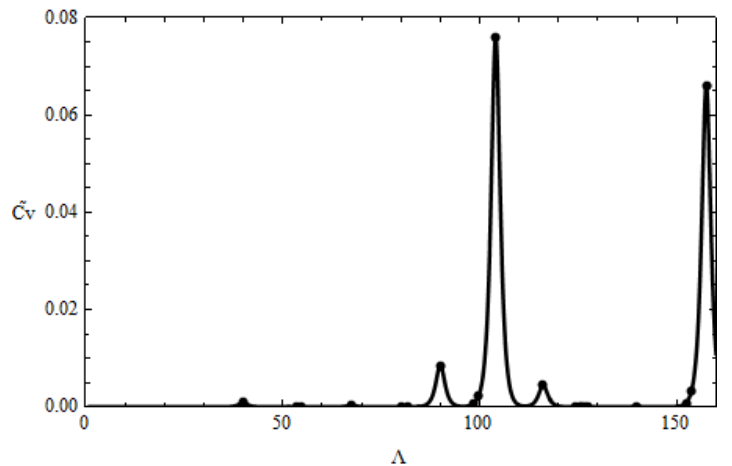


Figure 8. Isometric 0D domain (Quantum Dot), \widetilde{C}_V vs Λ

Another interesting inference is that, unlike the first case we considered, adding particles does not affect thermodynamic properties equally in this case. Since occupation of momentum states in all directions are possible, particle addition causes sometimes to an increase, and sometimes to a decrease in specific heat C_V as in Figure 9. Particle number dependency of heat capacity is so severe that in some cases (high magnitude peaks on the Figure 9), changing number of particles in the domain causes to eight or more times radical changes in heat capacity

of the system. Also, for a quantum dot with α values $\alpha_1 = 1$, $\alpha_2 = 1$ and $\alpha_3 = 1$, we can see oscillations in heat capacity, in Figure 10. Even for the large number of particles, oscillations are still observable.

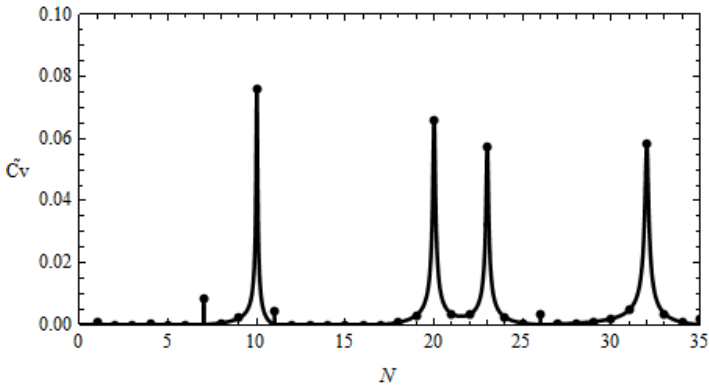


Figure 9. Isometric 0D domain (Quantum Dot), \widetilde{C}_V vs N

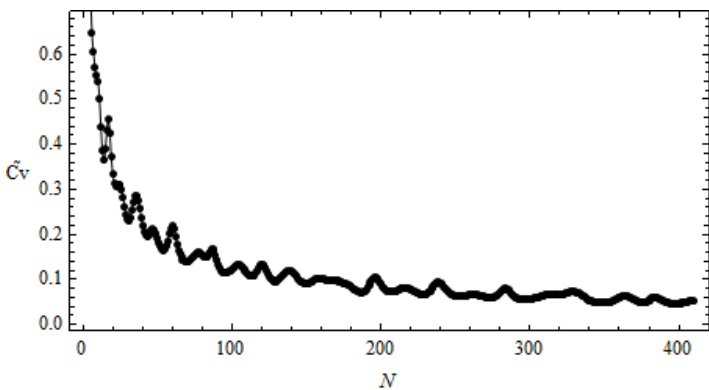


Figure 10. Isometric moderately ($\alpha_1 = \alpha_2 = \alpha_3 = 1$) confined 0D domain (Quantum Dot), \widetilde{C}_V vs N

THE CASE OF QUANTUM WIRES

For 1D structures, it is shown in Figures 11 and 12, that step-wise behavior turns into kind of a quasi-continuous behavior. In spite of that, noticeable peaks can still be observed in heat capacity, in Figure 13. Again changing number of particles in the system has different effects on the heat capacity, as it is shown in Figure 14. Change of particle number affects system drastically, so that C_V doubles and halves even for small changes in large number of particles. Such strong dependencies can be verified experimentally.

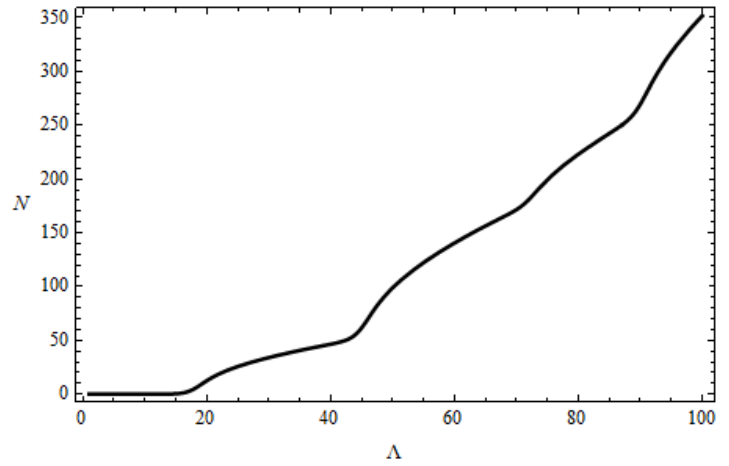


Figure 11. 1D domain (Quantum Wire), N vs Λ

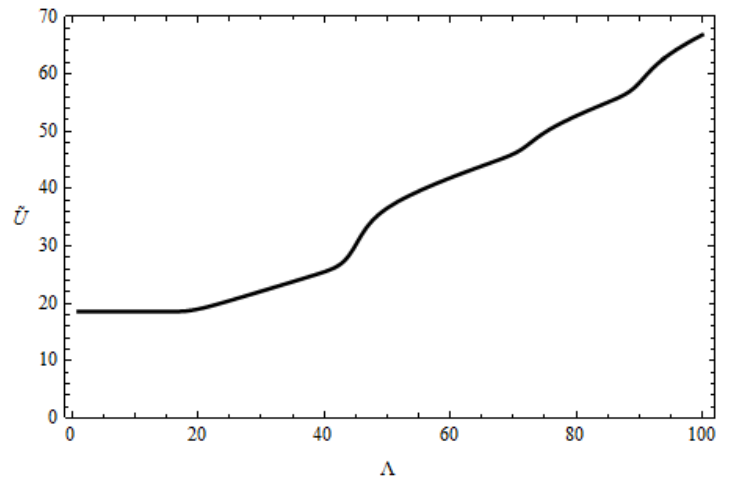


Figure 12. 1D domain (Quantum Wire), \widetilde{U} vs Λ

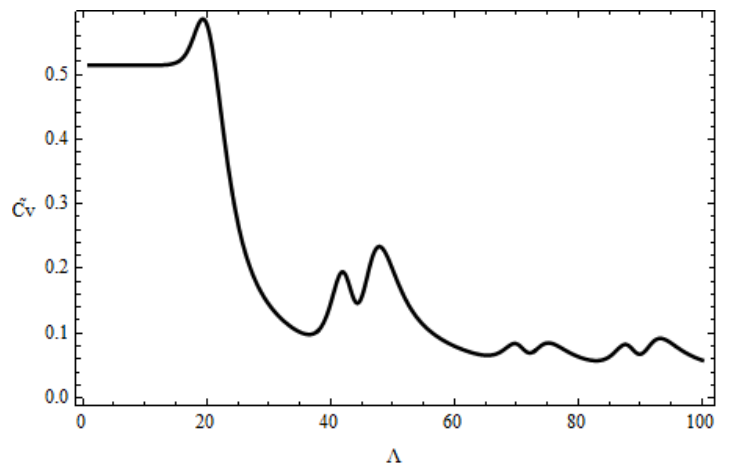


Figure 13. 1D domain (Quantum Wire), \widetilde{C}_V vs Λ

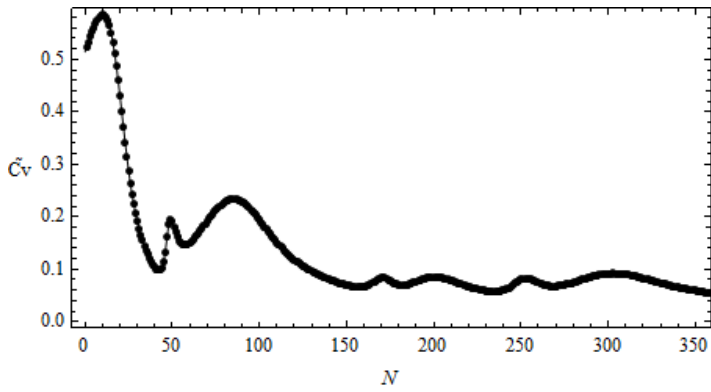


Figure 14. 1D domain (Quantum Wire), \tilde{C}_V vs N

As we expected, discrete nature of thermodynamics becomes slighter and slighter as we decrease the number of confined directions. For quantum wire (1D) and well (2D), discrete nature and peaks in heat capacity are still partially observable. Conversely, for the bulk (3D), discrete nature disappears almost completely.

DISCUSSION

In this study, we made numerical calculations on several thermodynamic quantities (N , U , C_V) by using exact summations. We showed that in nano scale, there is an intrinsic discrete nature in 0D and 1D Fermi gases (quantum dots and nanowires) and thermodynamic quantities can take only some certain values, if there is no applied external potential field to the system.

In case of the existence of electrical field, chemical potential becomes electrochemical potential. Therefore, it is possible to change Λ value by changing the strength of the field. In that case, intermediate values between certain Λ values, which correspond to the integer number of particles, correspond now to the non-integer number of particles. This means that, by applying and changing an electrical field, it is possible to create quasi-particles which have non-integer numbers. This also leads to a possibility of making quantum dot energy conversion and storage units. If the external electrical field is increased, quantum dot will store the energy and when the external field is disabled, system will turn back into its initial state, by releasing energy.

Considering the development rate of nanotechnology, it is very likely not only to verify the discrete nature of thermodynamic properties, but also to make efficient quantum energy storage devices which can easily be used later in new energy technologies. In addition to numerical results, evaluation of exact sums into analytical expressions is under consideration.

REFERENCES

- [1] M. I. Molina, Ideal gas in a finite container, *Am. J. Phys.* **64** pp. 503-505, 1996.
- [2] R. K. Pathria, An ideal quantum gas in a finite-sized container, *Am. J. Phys.* **66** pp.1080-1085, 1998.
- [3] W. S. Dai and M. Xie, Quantum statistics of ideal gases in confined space, *Phys. Lett. A* **311** pp. 340-346, 2003.
- [4] W. S. Dai and M. Xie, Geometry effects in confined space, *Phys. Rev. E* **70** 016103, 2004.
- [5] A. Sisman and I. Müller, The Casimir-like size effects in ideal gases, *Phys. Lett. A* **320** pp. 360-366, 2004.
- [6] A. Sisman, Surface dependency in thermodynamics of ideal gases, *J. Phys. A- Math. Gen.* **37** pp. 11353-11361, 2004.
- [7] H. Pang, W. S. Dai and M. Xie, The difference of boundary effects between Bose and Fermi systems, *J. Phys. A-Math. Gen.* **39** pp. 2563-2571, 2006.
- [8] A. Sisman, Z. F. Ozturk and C. Firat, Quantum boundary layer: a non-uniform density distribution of an ideal gas in thermodynamic equilibrium, *Phys. Lett. A* **362** pp.16-20, 2007.
- [9] C. Firat and A. Sisman, Universality of quantum boundary layer for a Maxwellian gas, *Phys. Scripta* **79** 065002, 2009.
- [10] Z. F. Ozturk and A. Sisman, Quantum Size Effects on the Thermal and Potential Conductivities of Ideal Gases, *Phys. Scripta* **80** 065402, 2009.
- [11] C. Firat, A. Sisman and Z. F. Ozturk, Thermodynamics of gases in nano cavities, *Energy* **35** Sp.Iss.SI: pp. 814-819, 2010.
- [12] A. Sisman and G. Babac, Quantum Size Effects on Classical Thermosize Effects, *J. Continuum Mechanics Thermodynamics* **24**, pp.339-346, 2012.

NON-EQUILIBRIUM THERMODYNAMIC MODELING OF AN ATOM-FIELD STATE EVOLUTION WITH COMPARISONS TO PUBLISHED EXPERIMENTAL DATA

Sergio Cano-Andrade*, Gian Paolo Beretta°, Michael R. von Spakovsky*

* Mechanical Engineering Department, Virginia Tech, Blacksburg, Virginia, 24061, USA

° Department of Mechanical and Industrial Engineering, Università di Brescia, Brescia, 25123, Italy

ABSTRACT

The analysis of the decoherence phenomenon between the local states of an electromagnetic field mode and an atom, such as that experimentally studied in Cavity Quantum Electrodynamics (CQED), is presented in this paper. The equation of motion of Intrinsic Quantum Thermodynamics (IQT) is used to model the dynamics of the state of the general microscopic system constituted by the two distinguishable and indivisible elementary subsystems. The evolution of state of the composite, as well as the reduced states of its constituents, is traced from a state of non-equilibrium to a state of stable equilibrium. Results show how the entanglement and coherence initially present between the locally-perceived states of each subsystem are erased when the state of the composite system evolves towards a state of stable equilibrium. The results presented provide an alternative and comprehensive explanation to that obtained with the “open system” approach of Dissipative Quantum Dynamics (DQD) and its associated quantum master equations of the Kossakowski-Lindblad-Gorini-Sudarshan type. Results of the relaxation modeling are compared with those of decoherence obtained experimentally by the CQED group at Paris.

INTRODUCTION

Efforts of the scientific community to understand the fundamental behaviour of nature and as a consequence effectively develop new technologies has placed quantum entanglement and coherence in the spotlight. Understanding the loss of quantum entanglement and coherence is at the core of explaining the transition between the microscopic and macroscopic worlds [1, 2]. Furthermore, manipulation of these type of communication phenomena is of great importance for the development of nanometric devices such as, for example, quantum computers [3-5] and quantum cryptographic systems [6, 7].

Entanglement among zero-entropy states or coherence among non-zero-entropy states is produced when two initially independent systems interact with each other. During this interaction, their states become correlated and can no longer be described independently of each other, that is, a single nonseparable system behavior is observed for the states of the two constituents. According to unitary dynamics, the state of the newly born composite should evolve in a superposition of outcomes. Nevertheless, daily observations of Nature and experiments on microscopic systems [8, 9] indicate that a loss of coherence among the local states of the constituents is always present. For example, during the physical measurement of a nonseparable microscopic system (e.g., a particle), the macroscopic measuring device (meter) gets entangled with the state of the particle and there after behaves as a macroscopic system in a superposition of states. The particle-meter composite system is then created, and an understanding of the loss of correlations between its constituents is at the core of quantum mechanics. Different theories are proposed to describe this phenomenon. One of them, that of dissipative quantum dynamic (DQD), considers that after its first entanglement with the particle, the meter gets involved into a second entanglement, this time with its surrounding environment, which provokes a fast dissipation of its quantum coherence originating from its initial entanglement with the

atom [1, 2]. Spontaneous relaxation is then modeled under the concept of the so-called “open-system model”, which assumes that the system interacts with a thermal bath of harmonic oscillators (reservoir). The loss of coherence, disentanglement, or spontaneous relaxation is attributed to an irreversible reduction process resulting from weak interactions between the system and reservoir. Under this assumption, the dissipation phenomenon results from a loss of information only. The dynamic equation of DQD is a linear Markovian quantum master equations (i.e., those of the Kossakowski-Lindblad-Gorini-Sudarshan type [10-12]). These type of equations mimic well the non-linear dissipative behavior of simple systems. However, a proper description of the non-linear dynamics of the state of composite systems is not achieved [13, 14].

In this paper, the modeling of the non-linear dynamic behavior of the state of a composite system formed by an atom and an electromagnetic field mode is developed using IQT and its dynamical law of time evolution along the direction of steepest entropy ascent (SEA), which is an effective implementation of the locally maximal entropy production (LMEP) principle [15-17]. The state of the composite (closed and adiabatic) microscopic system evolves in time towards stable equilibrium, resulting in the loss of correlations between its constituents. The non-linear IQT equation of motion consists of two terms, the first of which captures the unitary, Hamiltonian dynamics of the Schrödinger-von Neumann equation, and the second the non-linear dynamics of a dissipative evolution in state based on the principle of SEA [16-19], which allows each constituent to follow the path of locally-perceived SEA [20]. Within the IQT framework, the dissipative aspects of the time evolution emerge from the non-Hamiltonian terms in the IQT equation of motion. Thus, instead of focusing on the non-Hamiltonian effects of the interactions between a microscopic system and its surroundings, the IQT description assumes the composite system to be isolated and its time evolution to be intrinsically non-Hamiltonian. In so doing, a loss of quantum entanglement or coherence is fully predicted.

are the reduced state operators, and τ_A and τ_F are time functionals or scalars that are a particular characteristic of each subsystem. For the case presented, they are assumed to be constants.

A correlation functional or entropy of entanglement function is [20]

$$\sigma_{AF}(\rho) = \text{Tr}(\rho \ln \rho) - \text{Tr}_A(\rho_A \ln \rho_A) - \text{Tr}_F(\rho_F \ln \rho_F) \quad (8)$$

It measures the coherence between the constituents of the system. The norm of the commutator operator ($C = i[H, \rho]$) is

$$\|C\| = \text{Tr}(CC^\dagger) \quad (9)$$

and is used as an indicator of how the off-diagonal elements of the matrix representing the state operator evolve towards zero. It can, thus, also be thought of as a measure of the evolution of the coherence of the constituents.

The rate of change of the correlation functional given by Eq. (8) is expressed as

$$\frac{d(\sigma_{AF}(\rho))}{dt} = \dot{\sigma}_{AF}|_H - \dot{\sigma}_{AF}|_D \quad (10)$$

where the first term on the right-hand side represents the contribution, which the Hamiltonian term of Eq. (7) makes to the rate of change of the correlation functional. The second term on the right-hand side represents the contribution of the dissipative term of Eq. (7). Based on the characteristics of Eq. (7), it has been conjectured [20] that $\dot{\sigma}_{AF}|_D$ only destroys correlations between the constituents, namely, it should be nonnegative at all times.

Important ingredients of the IQT model are the local observables given by the linear local operators

$$(H)^A \equiv \text{Tr}_F[(I_A \otimes \rho_F)H] \quad (11a)$$

$$(H)^F \equiv \text{Tr}_A[(\rho_A \otimes I_F)H] \quad (11b)$$

which represent the local effective reduced Hamiltonians and can be interpreted as the “locally perceived energy” of the overall system by each constituent [16, 20], and the local observables given by the nonlinear local operators

$$(S)^A \equiv -k_B \text{Tr}_F[(I_A \otimes \rho_F)B \ln \rho] \quad (12a)$$

$$(S)^F \equiv -k_B \text{Tr}_A[(\rho_A \otimes I_F)B \ln \rho] \quad (12b)$$

which represent the local effective reduced entropy operators and can be interpreted as the “locally perceived entropy” of the overall system by each constituent [16, 20].

The entropy of the overall isolated, composite, microscopic system is given by the von Neumann entropy relation [33]

$$S = -k_B \text{Tr}(\rho \ln \rho) \quad (13)$$

where k_B is Boltzmann’s constant.

For the IQT modeling, it is considered that $t = 0$ when the state of the atom is detected in its excited level state at D. The initial state operator

$$\rho_0 = |\psi_{R_2}\rangle\langle\psi_{R_2}| \quad (14)$$

for the composite represents a pure (zero entropy) state. In order for the state operator to evolve in time according to Eq. (7), a slight perturbation in agreement with [34] is induced. A value of $\lambda = 0.95$ is used in the perturbation in order to start the evolution in a very close state to the original zero-entropy initial state ($\lambda = 1$) given by Eq. (14). Values for $2\phi = 100^\circ$ [9] and the probability of the atom to be on its excited level state $P_e \approx 1$ are used.

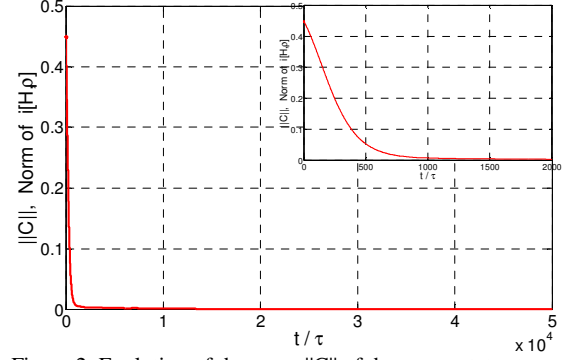


Figure 2. Evolution of the norm $\|C\|$ of the commutator term.

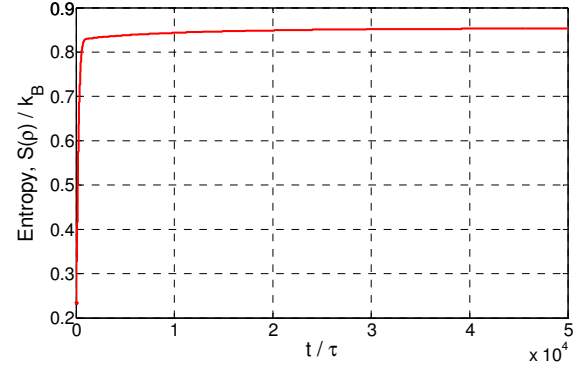


Figure 3. Entropy evolution corresponding to the composite system.

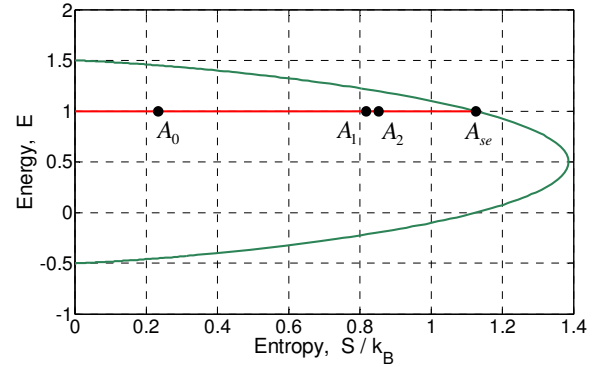


Figure 4. Energy-entropy diagram depicting the evolution in state of the composite system.

In the next section, the internal-relaxation time in the IQT equation of motion for each constituent is considered to be a real positive constant with values of $\tau_A = \tau_F = 300$ ms. This value is chosen because it is long enough to show well the various features of the state evolution in time of the composite system and its constituents. As seen below in the comparison with the experimental results of [9], a value of 0.26 ms is also used.

RESULTS

Figure 2 shows the norm of the commutator operator formed by the Hamiltonian and density operators, as given by Eq. (9). This shows how the off-diagonal elements in the overall density or state matrix are decaying with time as the system evolves towards a state of stable equilibrium. Thus, it is also an indicator on the degree to which the coherence between the constituents is being dissipated in time. As seen in the figure,

the steepest descent occurs at the beginning of the time evolution. This steep descent is in accord with the steepest-entropy-ascent principle pictorially described in Figure 3 for the entropy evolution. Note that only the first part of the complete evolution in state of the composite system is depicted in Figures 2 and 3, i.e., that part from the initial perturbed state A_0 in Figure 4 to state A_1 which occurs at $t/\tau = 5 \times 10^4$. Both states are non-equilibrium states quite far from that of stable equilibrium, i.e., state A_{se} . The latter is estimated to occur at or after $t/\tau = 5.2 \times 10^6$ based on the simulation actually completed, which was stopped at state A_2 after an elapsed time of $t/\tau = 6 \times 10^5$ (also a non-equilibrium state), since the state of the system at this point was evolving very slowly, i.e., asymptotically in a non-linear manner, towards A_{se} and the primary coherence and decoherence features of interest had already been captured.

Figure 5a depicts the evolution of the local density operator for the electromagnetic field mode. When the atom is detected in its excited level state, the state of the electromagnetic field is projected into a state of maximum local coherence. Subsequently, this local coherence decays in a steep fashion according with the evolution of Eq. (7). Figure 5b shows the evolution of the local density operator for the Rb atom where revival and death of its local coherence is observed during the evolution but with ever smaller amplitudes until the local coherence dies out at stable equilibrium.

Figure 6 shows the evolution of the rate of change of the contribution of the dissipation term of the equation of motion to the rate of change of the entropy correlation functional. Its value is non-negative always, showing that the dissipative term of the equation of motion does not create correlations between the constituents, but instead always destroys the correlations formed during the initial interaction between the constituents.

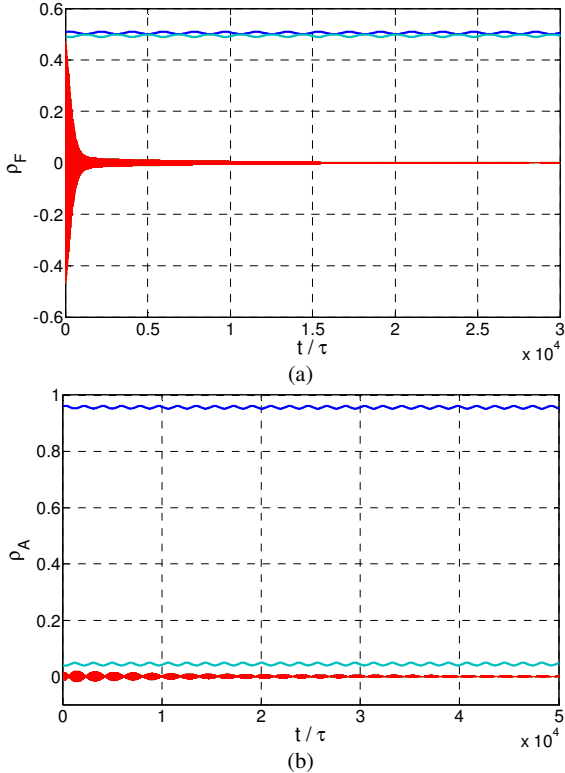


Figure 5. Evolution of the reduced density operators for (a) the electromagnetic field mode and (b) the Rb atom.

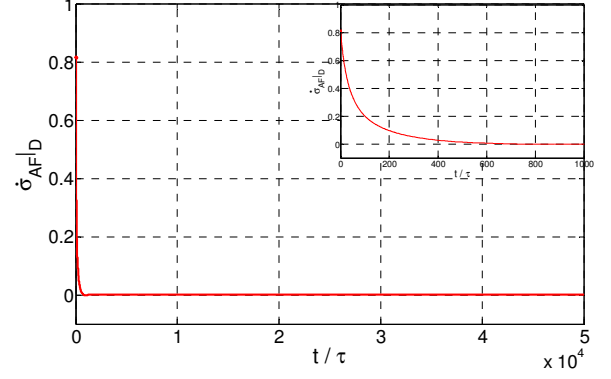


Figure 6. Rate of change $\dot{\sigma}_{AF|D}$ corresponding to the contribution of the dissipative term of Eq. (7) to the rate of change of the correlation functional or entropy of entanglement in Eq. (10).

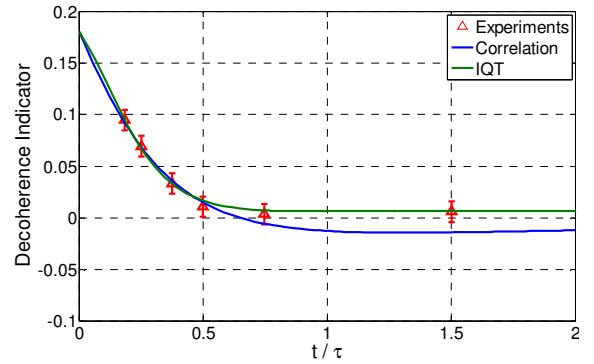


Figure 7. Comparison of the loss of coherence predicted by IQT (green) and by the correlation function of [23] (blue) with the CQED experimental results of the group at Paris [9] (red triangles).

In Figure 7, the results of the present model are compared to experimental data reported in the literature by Haroche and co-workers [9]. The red triangles correspond to average values of experimental measurements obtained from [9]. The blue line corresponds to the theoretical prediction made using the correlation functional given by Eq. (3) [23]. The initial point of the correlation has been moved in accord with [9] from a value of 0.5 to 0.18 on the vertical axis to take into account experimental imperfections. The detection of the atom in the excited level state projects the state of the field in a maximally coherent local state. Thus, $\|C\|$ can be used as a direct indicator of how the coherence of the electromagnetic field mode is being dissipated in time. The green line corresponds to $\|C\|$ using a value of $\tau_A = \tau_F = 0.26$ ms for the internal-relaxation times of the constituents in the equation of motion. This is comparable to the characteristic time reported for the CQED experiment in [35]. As in the case of the correlation functional, the maximum value for $\|C\|$ is moved to 0.18 in the vertical axis.

As can be seen in the figure, this decoherence indicator of IQT predicts the experimental data well, especially at the beginning and at the end of the decoherence evolution. A very slight deviation from the experimental values is observed with the fourth and fifth values but this is well within the error bars for the experiment indicated in the figure. Thus, this deviation may well correspond to normal imperfections in the experimental equipment such as the quality of reflexion of the mirrors, which allows a leak of photons from the cavity [25,

36]. Another factor may be that the value chosen for the internal-relaxation times τ_A and τ_F do not completely take into account the physical characteristics of the constituents. For example, it may be that slightly differing values for each relaxation time are needed or that these times are instead functionals of the state operator as described in [15, 34]. Of course, this is still an open area of research.

CONCLUSIONS

In this paper, an approach based on the principle of steepest entropy ascent, which provides the basis for the non-linear IQT equation of motion, is applied to the case of a composite microscopic system consisting of an atom and an electromagnetic field mode, the simplest model in which matter and light can be examined. Results show how the coherence of the composite system is dissipated when the system evolves towards a state of stable equilibrium and how this affects the local coherence of each constituent. For the electromagnetic field mode, the local coherence decays from some maximum to zero. The loss of coherence of the electromagnetic field follows the same trend as for the composite system. For the atom, the coherence is zero at the beginning of the evolution. Subsequently, however, several revivals and deaths of the coherence for the atom are observed. Nevertheless, even the amplitudes of these revivals and deaths decay with time.

Finally, the decoherence phenomenon predicted with the IQT model is compared to the experimental data of Haroche and co-workers [9]. The comparison shows that IQT prediction is in good agreement with the experiments and is, in fact, in much better agreement than that for the correlation function developed for this experiment in [23].

ACKNOWLEDGMENTS

The first and third authors would like to thank the National Council of Science and Technology (CONACyT), México, under assistantship ID 213158 for their financial support. The second author gratefully acknowledges the Cariplo-UniBS-MIT-MechE faculty exchange program co-sponsored by UniBS and the CARIPLO Foundation, Italy, under grant 2008-2290.

REFERENCES

- [1] W. H. Zurek, "Decoherence, einselection, and the quantum origins of the classical," *Reviews of Modern Physics*, vol. 75, (2003).
- [2] W. H. Zurek, "Decoherence and transition from quantum to classical-revisited," *Los Alamos Science*, vol. 27, (2002).
- [3] C. Bennett and D. P. DiVincenzo, "Quantum information and computation," *Nature* 404, pp. 247-255, (2000).
- [4] B. P. Lanyon, M. Barbieri, M. P. Almeida, and A. G. White, "Experimental quantum computing without entanglement," *Physical Review Letters*, vol. 101, p. 200501, (2008).
- [5] A. Ardavan, O. Rival, J. J. L. Morton, and S. J. Blundell, "Will spin-relaxation times in molecular magnets permit quantum information processing?," *Physical Review Letters*, vol. 98, p. 057201, (2007).
- [6] W. Tittel, H. Zbinden, and N. Gisin, "Experimental demonstration of quantum secret sharing," *Physical Review A*, vol. 63, p. 042301, (2001).
- [7] D. S. Naik, C. G. Peterson, A. G. White, A. J. Berglund, and P. G. Kwiat, "Entangled state quantum cryptography: eavesdropping on the Ekert protocol," *Physical Review Letters*, vol. 84, (2000).
- [8] Q. A. Turchete, C. J. Myatt, B. E. King, C. A. Sackett, D. Kielpinski, W. M. Itano, C. Monroe, and D. J. Wineland, "Decoherence and Decay of Motional Quantum States of a trapped Atom Coupled to Engineered Reservoirs," *Physical Review A*, vol. 62, pp. 053807(1-22), (2000).
- [9] M. Brune, E. Hagley, J. Dreyer, X. Maitre, A. Maali, C. Wunderlich, J. M. Raimond, and S. Haroche, "Observing the progressive decoherence of the "meter" in a quantum measurement," *Physical Review Letters*, vol. 77, (1996).
- [10] M. Nakatani and T. Ogawa, "Quantum master equations for composite systems: is Born-Markov approximation really valid?," *Journal of the Physical Society of Japan*, vol. 79, p. 084401, (2010).
- [11] X. Z. Yuan, H. S. Goan, and K. D. Zhu, "Non-Markovian reduced dynamics and entanglement evolution of two coupled spins in a quantum spin environment," *Physical Review B*, vol. 75, (2007).
- [12] G. Lindblad, "On the generators of quantum dynamics semigroups," *Communications in Mathematical Physics*, vol. 48, pp. 119-130, (1976).
- [13] D. F. Walls, "Higher order effects in the master equation for coupled systems," *Z. Physik*, vol. 234, (1970).
- [14] H. J. Carmichael and D. F. Walls, "Master equation for strongly interacting systems," *J. Phys. A: Math. and Gen.*, vol. 6, (1973).
- [15] G. P. Beretta, "On the general equation of motion of quantum thermodynamics and the distinction between quantal and nonquantal uncertainties," Ph.D. Thesis Mechanical Engineering Dept., Massachusetts Institute of Technology, Boston, MA, (1981). arXiv:quant-ph/0509116.
- [16] G. P. Beretta, E. P. Gyftopoulos, J. L. Park, and G. N. Hatsopoulos, "Quantum thermodynamics. A new equation of motion for a single constituent of matter," *Il Nuovo Cimento*, vol. 82, pp. 169-191, (1984).
- [17] G. P. Beretta, "Steepest entropy ascent in quantum thermodynamics," *Lecture Notes in Physics*, vol. 278, (1986).
- [18] G. P. Beretta, "Nonlinear model dynamics for closed-system, constrained, maximal-entropy-generation relaxation by energy redistribution," *Physical Review E*, vol. 73, p. 026113, (2006).
- [19] G. P. Beretta, "Nonlinear quantum evolution equations to model irreversible adiabatic relaxation with maximal entropy production and other nonunitary processes," *Reports on Mathematical Physics*, vol. 64, pp. 139-168, (2009).
- [20] G. P. Beretta, E. P. Gyftopoulos, and J. L. Park, "Quantum thermodynamics. A new equation of motion for a general quantum system," *Il Nuovo Cimento*, vol. 87, pp. 77-97, (1985).
- [21] S. Haroche, M. Brune, and J. M. Raimond, "Atomic clocks for controlling light fields," *Physics Today*, vol. 66, (2013).
- [22] X. Zhou, I. Dotsenko, B. Peaudecerf, T. Rybarczyk, C. Sayrin, S. Gleyzes, J. M. Raimond, M. Brune, and S. Haroche, "Field locked to a fock state by quantum

- feedback with single photon corrections," *Physical Review Letters*, vol. 108, p. 243602, (2012).
- [23] J. M. Raimond, M. Brune, and S. Haroche, "Reversible decoherence of a mesoscopic superposition of field states," *Physical Review Letters*, vol. 79, (1997).
- [24] S. Deleglise, I. Dotsenko, C. Sayrin, J. Bernu, M. Brune, J. M. Raimond, and S. Haroche, "Reconstruction of non-classical cavity field states with snapshots of their decoherence," *Nature Letters*, vol. 455, (2008).
- [25] S. Haroche and J. M. Raimond, *Exploring the quantum*. Oxford, UK: Oxford University Press, 2006.
- [26] J. M. Raimond and S. Haroche, "Monitoring the decoherence of mesoscopic quantum superpositions in a cavity," in *Quantum Decoherence*. vol. 48, ed: Birkhäuser Verlag Basel, p. 33-83, 2007.
- [27] J. M. Fink, M. Göppl, M. Baur, R. Bianchetti, P. J. Leek, A. Blais, and A. Wallraff, "Climbing the Jaynes–Cummings ladder and observing its nonlinearity in a cavity QED system," *Nature*, vol. 454, pp. 315-318, (2008).
- [28] K. Fujii and T. Suzuki, "An approximate solution of the Jaynes–Cummings model with dissipation II : another approach," *International Journal of Geometric Methods in Modern Physics*, vol. 9, (2012).
- [29] M. A. Marchioli, "Quantitative aspects of entanglement in the driven Jaynes–Cummings model," *Journal of Modern Optics*, vol. 53, pp. 2733-2751, (2006).
- [30] E. T. Jaynes and F. W. Cummings, "Comparison of quantum and semiclassical radiation theories with application to the beam maser," *Proceedings of IEEE*, vol. 51, (1963).
- [31] F. W. Cummings, "Stimulated emission of radiation in a single mode," *Physical Review*, vol. 140, (1965).
- [32] E. T. Jaynes, "Some aspects of maser theory," Microwave Laboratory Report No. 502 (unpublished), Stanford University, Stanford, CA (1958).
- [33] E. P. Gyftopoulos and E. Cubukcu, "Entropy: thermodynamic definition and quantum expression," *Physical Review E*, vol. 55, pp. 3851-3858, (1997).
- [34] G. P. Beretta, "Steepest-entropy-ascent irreversible relaxation towards thermodynamic equilibrium: the dynamical ansatz that completes the Gyftopoulos-Hatsopoulos unified theory with a general quantal law of causal evolution," *Int. J. of Thermodynamics*, vol. 9, pp. 117-128, (2006).
- [35] M. Brune, F. Schmidt-Kaler, A. Maali, J. Dreyer, E. Hagley, J. M. Raimond, and S. Haroche, "Quantum Rabi oscillation: a direct test of field quantization in a cavity," *Physical Review Letters*, vol. 76, (1996).
- [36] J. M. Raimond, M. Brune, and S. Haroche, "Colloquium: manipulating quantum entanglement with atoms and photons in a cavity," *Reviews of Modern Physics*, vol. 73, pp. 565-582, (2001).

THERMODYNAMIC DESCRIPTION OF BRANCHED MOLECULES

K. Langenbach*, D. Browarzik^o, C. Browarzik*, S. Enders*

*Technische Universität Berlin, Chair of Thermodynamics BH 7-1, Ernst-Reuter-Platz 1, 10587 Berlin, Germany.

^oMartin-Luther University Halle-Wittenberg, Chemistry / Physical Chemistry, Mühlpforte 1, 06108 Halle (Saale), Germany.

EXTENDED ABSTRACT

In equilibrium thermodynamics physically based equations of state, like the perturbed-chain statistical associating fluid theory [1] of state, have undergone great advancement during the past two decades. These theories based on Wertheim's perturbation theory [2–5] focus on the different functional groups present in the molecule, but assume the molecules to be linear chains. It is often possible to describe branched molecule despite that assumption, but this description demands the adjustment of new pure component parameters. Moreover, for strongly branched molecules like hyper-branched polymers, these kinds of models are not able to describe vapour-liquid equilibria and liquid-liquid equilibria simultaneously [6], even though using a second order perturbation theory. The introduction of molecular architecture, however, does involve higher order perturbation theories. Local correlations between different segments have to be introduced and in this process unknown radial distribution functions occur that have to be approximated somehow [7].

This difficulty can be overcome by assuming the molecules to live on a lattice, where local correlations can be introduced through a Mayer like [8] series expansion in the inverse coordination number z^{-1} and the reduced segmental nearest neighbour interaction energy $\epsilon/k_B T$. Freed and co-workers [e.g. 9] derived the Lattice Cluster Theory (LCT) in such a manner, with local correlations of up to four consecutive segments. This lattice free energy was made compressible by Dudowicz and Freed [10] by introducing holes into the lattice. However, the LCT in the multi-component formulation is quite unwieldy due to its large equations. Also it is prone to numerical error due to heavy summations. This issue is usually addressed by breaking down the multi-component approach to a lower and specified number of compounds [e.g. 11–14]. However, in this contribution a way is shown to lower the complexity of the multi-component version without losing any algebraic information, effectively reducing the number of contributions to the free energy from 102 in the original papers [10] to 26 in the new version. Moreover the theory is shown to depend only on the numbers of singly connected self avoiding walks of specific lengths on the graph representation of the respective molecule and no longer on some unconnected or crossing paths, which are usually employed in the equations.

Using the new equations for the free energy of multi-component lattice trees, the mixing behaviour of some hypothetical compounds is calculated in order to assess the influence of architecture on the phase equilibrium of upper critical solution liquid-liquid behaviour. Moreover the vapour-liquid equilibrium of branched alkanes is predicted from the knowledge of the phase behaviour, their linear counterparts show. Mixtures of linear and branched alkanes are investigated and the prediction on the basis of simple mixing rules is compared to experimental data. Furthermore the phase behaviour of Boltorn H3200 in propane correlated with LCT shows the ability of the theory to simultaneously describe vapour-liquid, liquid-liquid and vapour-liquid-liquid behaviour of this hyper-branched polyester with alkane end-groups in propane. Together the theoretical investigations show that LCT in this new version is a highly versatile tool for the description and prediction of the thermodynamics involving branched and highly branched molecules.

REFERENCES

- [1] J. Gross, G. Sadowski, *Ind. Eng. Chem. Res.* 40 (2001) 1244–1260.
- [2] M.S. Wertheim, *J. Stat. Phys.* 35 (1984) 19–34.
- [3] M.S. Wertheim, *J. Stat. Phys.* 35 (1984) 35–47.
- [4] M.S. Wertheim, *J. Stat. Phys.* 42 (1986) 459–476.
- [5] M.S. Wertheim, *J. Stat. Phys.* 42 (1986) 477–492.
- [6] M.K. Kozłowska, B.F. Jürgens, C.S. Schacht, J. Gross, T.W. de Loos, *J. Phys. Chem. B* 113 (2009) 1022–1029.
- [7] B.D. Marshall, W.G. Chapman, *J. Phys. Chem. B* 115 (2011) 15036–15047.
- [8] J.E. Mayer, M.G. Mayer, *Statistical Mechanics*, Third Printing, John Wiley & Sons Inc, 1940.
- [9] K.W. Foreman, K.F. Freed, in: I. Prigogine, S.A. Rice (Eds.), *Advances in Chemical Physics*, John Wiley & Sons, Inc., Hoboken, 2007, pp. 335–390.
- [10] J. Dudowicz, K.F. Freed, *Macromolecules* 24 (1991) 5076–5095.
- [11] J. Dudowicz, M.S. Freed, K.F. Freed, *Macromolecules* 24 (1991) 5096–5111.
- [12] T. Zeiner, D. Browarzik, S. Enders, *Fluid Phase Equilib.* 286 (2009) 127–133.
- [13] S. Enders, K. Langenbach, P. Schrader, T. Zeiner, *Polymers* 4 (2012) 72–115.
- [14] K. Langenbach, S. Enders, C. Browarzik, D. Browarzik, *The Journal of Chemical Thermodynamics* 59 (2013) 107–113.

LONG-RANGE INTERACTING SYSTEMS AND THE GIBBS-DUHEM EQUATION

Ivan Latella and Agustín Pérez-Madrid

Departament de Física Fonamental, Facultat de Física, Universitat de Barcelona
Martí i Franquès 1, 08028 Barcelona, Spain
E-mail: ilatella@ffn.ub.edu

ABSTRACT

The generalized Gibbs-Duhem equation is obtained for systems with long-range interactions in d spatial dimensions. We consider that particles in the system interact through a slowly decaying pair potential of the form $1/r^\nu$ with $0 \leq \nu \leq d$. The local equation of state is obtained by computing the local entropy per particle and using the condition of local thermodynamic equilibrium. This local equation of state turns out to be that of an ideal gas. Integrating the relation satisfied by local thermodynamic variables over the volume, the equation involving global magnitudes is derived. Thus, the Euler relation is found and we show that it is modified by the addition of a term proportional to the total potential energy. This term is responsible for the modification of the Gibbs-Duhem equation. We also point out a close relationship between the thermodynamics of long-range interacting systems and the thermodynamics of small systems introduced by Hill.

INTRODUCTION

Long-range interacting systems have received considerable attention in recent years due to their remarkable dynamical and statistical behavior [1, 2]. Self-gravitating systems [3–7], two-dimensional vortices [8], nuclear physics [9] and also toy models such as the Hamiltonian mean field model [10] are examples of systems presenting such a behavior. These systems are intrinsically non-additive and may have negative heat capacity in the microcanonical ensemble leading to ensemble inequivalence [1, 11, 12].

Systems with long-range interactions are characterized by slowly-decaying pair potentials through which the constituent parts of the system interact at large distances. When particles interact all with the same coupling, the absence of screening causes inhomogeneous configurations (except for the limiting case of non-decaying interactions), in equilibrium or meta-equilibrium, where the formalism of thermodynamics can be applied. Unlike the case of short-range interacting systems, where many features are well understood, there is a lack of complete knowledge about the dynamical and statistical properties of systems with long-range interactions.

To be more specific, a definition of what we mean by long-range potentials can be formulated as follows: a potential that at large distances decays as $1/r^\nu$ is formally said to be long-range if $\nu \leq d$, where d is the dimension of the embedding space [1, 2]. Below we will give an argument that justifies why this particular range for the power of the decaying potential deserves special attention. Thus, here we are concerned with the study of the thermodynamics of d -dimensional systems with these power-law interaction potentials ($0 \leq \nu \leq d$) by using the mean field approximation.

In the mean field approach it is implicitly assumed that the number of particles is large enough so that the system can be treated as a continuous medium and the description of the relevant physical quantities is assumed to depend on the density (or distribution function) in the one-particle phase space. Despite

the fact that correlations are ignored in the mean field approach, this model offers a mathematical tool for a suitable treatment of self-interactions in the system. It turns out to be very accurate in the thermodynamic limit, except near the critical points where the system undergoes a phase transition or collapses [9, 13–16]. Although the validity of the mean field solutions strongly depends on the control parameters used to specify the thermodynamic state of the system, the functional form of any thermodynamic potential in the mean field limit is the same in each ensemble representation.

Quite remarkably, de Vega and Sánchez obtained the local equation of state of the self-gravitating gas assuming local hydrostatic equilibrium [14]. This equation coincides with that of an ideal gas. Additionally, the same local equation of state is found using the condition of local hydrostatic equilibrium for a system with arbitrary long-range interactions in the mean field limit [17].

We will see that the local ideal gas equation of state of the system can be obtained by computing the local entropy per particle and using the condition of local thermodynamic equilibrium [18]. Although the result is the same, this procedure is conceptually different. The local entropy per particle (and also other thermodynamic potentials) can be obtained from the volume of the phase space using the saddle point approximation or, equivalently, using the one-particle distribution function approach. After volume integration of the relation satisfied by local quantities, an equation involving global thermodynamic quantities can be found. This is the Euler relation, which for systems with the interaction potentials considered here, is modified by the addition of an extra term containing the total potential energy. This reflects the fact that an extra degree of freedom, proportional to the potential energy, has to be considered to formulate a thermodynamic description of systems with long-range interactions. The formal structure of thermodynamic relations for systems with long-range interactions is thus the same as the corresponding one for small systems. It can be seen that the total potential energy plays the role of the subdivision po-

tential introduced by Hill [19] to treat small systems. Because systems with long-range interactions may also be considered as small, this connection can be seen as more than a formal mapping between mathematical relations.

LOCAL EQUATION OF STATE

Consider a d -dimensional system of N point-like particles of mass m enclosed in a spherical container of volume V (and radius R), which interact through a pair interaction potential that at large distances behaves as

$$\phi_{ij} = \kappa |\mathbf{q}_i - \mathbf{q}_j|^{-\nu}, \quad (1)$$

where κ is a coupling constant, \mathbf{q}_i is the coordinate of particle i , $i = 1, 2, \dots, N$, and $0 \leq \nu \leq d$. In $d = 1$ the container is a 0-sphere which is the pair of end-points of the line segment of length $2R$, in $d = 2$ the 1-sphere is formed by the points at the boundary of a circumference of radius R , and so on. The Hamiltonian is given by $H_N = E_0 + W$, where E_0 is the kinetic energy and $W = \sum_{i>j}^N \phi_{ij}$ is the total potential energy.

In the microcanonical description, the state of the system is characterized by a fixed value of the total energy E and the number of microstates in full $2d$ -dimensional phase space is given by $\Sigma(E) = (2\pi\hbar)^{-dN} (N!)^{-1} \int_{E>H_N} d\tau$, where \hbar is the reduced Planck's constant and $d\tau$ is the volume element in phase space. Thus, the microcanonical entropy reads $S(E) = k_B \ln \Sigma(E)$, where k_B is Boltzmann's constant. To compute the entropy in the mean field limit, the volume of the system is divided in cells and, after integrating over momentum, the configurational integrals in $\Sigma(E)$ become summations over all possible occupation number distributions. In the limit $N \rightarrow \infty$, the discrete occupation number distributions become continuous fields and summations become a functional integration over the number density $n(\mathbf{x})$, where now \mathbf{x} represents the spatial components of a single point in the one-particle configuration space. This functional integration is solved with the saddle-point approximation in such a way that the number density that maximizes the entropy (hence defining the equilibrium configurations) is given by [18]

$$n(\mathbf{x}) = \lambda_T^{-d} \exp \left[\frac{\mu - \Phi(\mathbf{x})}{k_B T} \right], \quad (2)$$

where $\lambda_T = [2\pi\hbar^2/(mk_B T)]^{1/2}$ is the thermal wavelength, μ is the chemical potential and T is the temperature. Here we have introduced the self-consistent potential $\Phi(\mathbf{x})$ which takes the form

$$\Phi(\mathbf{x}) = \int n(\mathbf{x}') \phi(\mathbf{x}, \mathbf{x}') d^d \mathbf{x}', \quad (3)$$

where now $\phi(\mathbf{x}, \mathbf{x}') = \kappa |\mathbf{x} - \mathbf{x}'|^{-\nu}$ describes the interaction between particles in the one-particle configuration space. Notice that $\Phi(\mathbf{x})$ depends explicitly on ν and, therefore, so does the density. As a result, the microcanonical mean field entropy becomes [18]

$$S = k_B \int n(\mathbf{x}) \left[-\ln \left(n(\mathbf{x}) \lambda_T^d \right) + \frac{2+d}{2} \right] d^d \mathbf{x}. \quad (4)$$

In addition, in terms of $\Phi(\mathbf{x})$ the total potential energy takes the usual form

$$W = \frac{1}{2} \int n(\mathbf{x}) \Phi(\mathbf{x}) d^d \mathbf{x}, \quad (5)$$

and the total energy reads

$$E = \frac{dk_B T}{2} \int n(\mathbf{x}) d^d \mathbf{x} + \frac{1}{2} \int n(\mathbf{x}) \Phi(\mathbf{x}) d^d \mathbf{x}. \quad (6)$$

The details of the above calculations can be found in [18], where the used method is based on a previous work [13, 14] concerning self-gravitating systems ($\nu = 1$). This method and the validity of the expressions for the thermodynamic quantities that are obtained in the mean field approach rest on the assumption that the interactions are long-ranged. In other words, it is assumed that the main contribution to the interaction energy of a particle is due to distant particles rather than to its immediate neighbors. To see that this is fulfilled with $0 \leq \nu \leq d$, we now come back to the argument that justifies the formal definition of long-range potentials. We will follow [1]. Let us consider a particle placed at the origin of the $(d-1)$ -dimensional sphere of radius R . In order to estimate the energy ε of the particle due to the interaction with the rest of particles in the bulk, let us assume that particles are homogeneously distributed so that $n(\mathbf{x}) = \text{constant}$. We also assume that there is a short-distance cutoff $\delta \ll R$ describing the scale where short-range interactions have to be considered. Writing $r = |\mathbf{x} - \mathbf{x}'|$ we have

$$\varepsilon = \int_{\delta}^R d^d r n \frac{\kappa}{r^{\nu}} = \begin{cases} n \kappa \Omega_{(d)} \frac{R^{d-\nu} - \delta^{d-\nu}}{d-\nu}, & \nu \neq d \\ n \kappa \Omega_{(d)} \ln(R/\delta), & \nu = d \end{cases}, \quad (7)$$

where $\Omega_{(d)} = 2\pi^{d/2}/\Gamma(d/2)$ is the solid angle factor, $\Gamma(x)$ being the Gamma function. On the one hand, we see that if $0 \leq \nu \leq d$, the integral is dominated by the contribution coming from its upper limit and then by long-range interactions. The energy ε grows as $\varepsilon \propto V^{\sigma}$ if $0 \leq \nu < d$ (logarithmically in the marginal case $\nu = d$), where $\sigma \equiv 1 - \nu/d$ is the long-range parameter, and hence the total energy scales as $E \propto V^{\sigma+1}$. On the other hand, if $\nu > d$ the energy ε remains finite for $\delta/R \ll 1$ and consequently $E \propto V$. This is the usual scaling of extensive systems where interactions are short-ranged ($\nu > d$). Therefore, the mean field approach can suitably describe interactions in the system only if they are long-ranged and the formulation considered here is not valid for short-range potentials. It is worth noting that, in general, the equilibrium or metaequilibrium configurations have to be obtained by using numerical calculations due to the non-trivial functional relation between the potential and the density. For the case of self-gravity, the potential satisfies the Poisson-Boltzmann equation. Therefore, thermodynamic quantities can be expressed in closed form in terms of its solution. However, this equation has to be solved numerically as well.

Local thermodynamic quantities can be defined taking into account our ability to write the entropy and the energy as integrals over the volume. In view of (4), the local entropy per particle is given by $s(\mathbf{x}) = k_B [-\ln(n(\mathbf{x})\lambda_T^d) + \frac{2+d}{2}]$. This is a Sackur-Tetrode-type entropy per particle written in terms of local variables. In the same way, the local kinetic energy

and local energy per particle take the form $e_0 = \frac{d}{2}k_B T$ and $e(\mathbf{x}) = e_0 + \frac{1}{2}\Phi(\mathbf{x})$, respectively. Thus we have

$$S = \int n(\mathbf{x})s(\mathbf{x})d^d\mathbf{x}, \quad (8)$$

$$E = \int n(\mathbf{x})e(\mathbf{x})d^d\mathbf{x}, \quad (9)$$

$$E_0 = \int n(\mathbf{x})e_0d^d\mathbf{x}. \quad (10)$$

We also introduce the local volume per particle defined by $v(\mathbf{x}) = 1/n(\mathbf{x})$, so that the local entropy can be written as a function of the local kinetic energy and this local volume, $s = s(e_0, v)$. From the condition of local thermodynamic equilibrium we have [20, 21],

$$\frac{1}{T} = \left(\frac{\partial s}{\partial e_0} \right)_v \quad \text{and} \quad \frac{p}{T} = \left(\frac{\partial s}{\partial v} \right)_{e_0}, \quad (11)$$

which leads to the local equation of state [18]

$$p(\mathbf{x}) = n(\mathbf{x})k_B T. \quad (12)$$

This implies that particles at a certain point \mathbf{x} behave as an ideal gas, but the pressure and density vary from point to point (except in the limiting case of non-decaying interaction potential, i.e. $\sigma = 1$). Since local interactions (short-ranged) are neglected in comparison to the interaction with distant particles, this result is physically consistent. Therefore, the system behaves locally as a free gas under the action of an external field created by the particles in the bulk. The same result can be found by considering local hydrostatic equilibrium [13, 14, 17]. This is achieved by equating the gradient of pressure to the force density:

$$\nabla p(\mathbf{x}) = n(\mathbf{x})\nabla\Phi(\mathbf{x}). \quad (13)$$

In addition to the functional form of the local variables, we can also write down an explicit relation among them. Taking into account the expression for the local entropy and introducing the ideal gas chemical potential $\mu_0(\mathbf{x}) = k_B T \ln [n(\mathbf{x})\lambda_T^d]$, one deduces

$$Ts(\mathbf{x}) = e_0 + p(\mathbf{x})v(\mathbf{x}) - \mu_0(\mathbf{x}). \quad (14)$$

The same equation could have been deduced if as a starting point one assumes that the system locally behaves as an ideal gas. Since $\mu = \mu_0(\mathbf{x}) + \Phi(\mathbf{x})$, equation (14) can also be rewritten in the form

$$Ts(\mathbf{x}) = e(\mathbf{x}) + p(\mathbf{x})v(\mathbf{x}) - \mu + \frac{1}{2}\Phi(\mathbf{x}). \quad (15)$$

Notice the presence of the last term on the r.h.s. in the above expression; it is due to the definition of the local energy $e(\mathbf{x})$. As we will see in the next section, such a term will give rise to an extra term in the Euler relation and therefore, in the Gibbs-Duhem equation.

An alternative way to address the local description of the system is by considering the distribution function $f(\mathbf{x}, \mathbf{p})$ defined in one-particle phase space, where \mathbf{p} is the momentum of a particle. The distribution function is normalized so that $N = \int f(\mathbf{x}, \mathbf{p})d^d\mathbf{x}d^d\mathbf{p}$. In order to obtain equilibrium or meta-equilibrium configurations, using variational calculus one looks for the distribution function which maximizes the Boltzmann entropy $S = -k_B \int f(\mathbf{x}, \mathbf{p}) \ln(f(\mathbf{x}, \mathbf{p})/f_c) d^d\mathbf{x}d^d\mathbf{p}$, where f_c is a constant fixing the origin of the entropy. Consequently, the distribution function that maximizes the entropy (at least locally) turns out to be the Maxwell-Boltzmann distribution with the self-consistent potential (3), and the number density is given by (2). Besides, the constant f_c is chosen so that the entropy coincides with the one in the microcanonical description: $f_c = e/(2\pi\hbar)^d$.

Thus, any local magnitude per particle $q(\mathbf{x})$ associated with the global quantity Q can be defined according to

$$n(\mathbf{x})q(\mathbf{x}) \equiv \int f(\mathbf{x}, \mathbf{p})Q(\mathbf{x}, \mathbf{p})d^d\mathbf{p} \quad (16)$$

provided $Q = \int f(\mathbf{x}, \mathbf{p})Q(\mathbf{x}, \mathbf{p})d^d\mathbf{x}d^d\mathbf{p}$. For instance, in the case of the Boltzmann entropy one takes $Q(\mathbf{x}, \mathbf{p}) = -k_B \ln(f(\mathbf{x}, \mathbf{p})/f_c)$. After integrating over momentum using the Maxwell-Boltzmann distribution, the resulting local entropy per particle $s(\mathbf{x})$ is the same as the one found in the microcanonical ensemble using the mean field approximation. Therefore, the condition of local thermodynamic equilibrium leads to the same local equation of state [18], equation (12).

GLOBAL THERMODYNAMIC RELATIONS

Once the relation between thermodynamic variables is established at a local level, the corresponding relation between global variables is obtained by integrating over the volume. Concretely, we want to obtain the corresponding Euler relation from which a generalization of the Gibbs-Duhem equation can be deduced. In this way, multiplying both sides of (15) by $n(\mathbf{x})$ and integrating over the volume yields

$$TS = E + \frac{2}{d}E_0 - \mu N + W, \quad (17)$$

where we have used that $\int p(\mathbf{x})d^d\mathbf{x} = k_B T \int n(\mathbf{x})d^d\mathbf{x} = \frac{2}{d}E_0$. We now introduce the pressure evaluated at the boundary of the d -dimensional system, $P \equiv p(\mathbf{x})|_{\mathbf{x} \in \text{boundary}}$. To proceed further, the pressure P has to be related to (17). This can be done if the global equation of state is taken into account, which can be computed by rescaling the energy in the microcanonical density of states and using the usual thermodynamic relations for the total entropy [13, 14, 18]. The rescaled energy reads $\Lambda \equiv ER^v / (|\kappa|N^2)$ [13, 16]. As a result, the global equation of state takes the form

$$\frac{PV}{Nk_B T} = 1 + v \frac{W}{dNk_B T}. \quad (18)$$

Therefore, with the help of (18), equation (17) can be rewritten in such a way that

$$TS = E + PV - \mu N + \sigma W, \quad (19)$$

which is the Euler relation for the systems discussed here. Moreover, by differentiating (19) one gets

$$TdS = dE + PdV - \mu dN + \sigma dW - Nd\mu - SdT + VdP \quad (20)$$

and since $TdS = dE + PdV - \mu dN$ one obtains [18]

$$\sigma dW = SdT - VdP + Nd\mu, \quad (21)$$

which is the generalized Gibbs-Duhem equation for long-range interacting systems.

The marginal case $\nu = d$ corresponds to systems with long-range parameter $\sigma = 0$. In such a case, the Euler relation and the generalized Gibbs-Duhem equation reduce to the usual one in the thermodynamics of short-range interactions. For $\sigma \neq 0$, the temperature, chemical potential and pressure are independent variables, so that $W = W(T, P, \mu)$. The thermodynamic relations in terms of partial derivatives of W have been considered in [18] and verified for the case of a self-gravitating gas ($\sigma = 2/3$) and for a system with spatially uniform interactions ($\sigma = 1$).

In what follows we will see that the thermodynamic relations satisfied by systems with long-range interactions can be mapped to the corresponding relations satisfied by small systems introduced by Hill [19]. Hill's small systems bear this name because they are composed by a small (non-macroscopic) number of particles. The systems we have considered above are macroscopic in the sense that the number of particles is assumed to be infinite. However, the latter are small in the sense that the range of the interactions is large compared to the size of the system. Due to this finiteness, an extra degree of freedom has to be considered to account for a complete thermodynamic description. This extra degree of freedom in long-range systems is σW while for systems with small number of particles it is incorporated through the subdivision potential \mathcal{E} .

In the formalism introduced by Hill [19], an ensemble of non-interacting small systems is considered. Thus, the subdivision potential accounts for the energy gained by the system when the number of members of the ensemble varies. For any single small system one has

$$TS = E + PV - \mu N - \mathcal{E}, \quad (22)$$

$$TdS = dE + PdV - \mu dN, \quad (23)$$

$$d\mathcal{E} = -SdT + VdP - Nd\mu. \quad (24)$$

As it can be seen, these relations are exactly the same as those we have obtained for systems with long-range interactions if the identification $\mathcal{E} = -\sigma W$ is made.

To conclude, it is important to stress here, as was mentioned by Hill, that the use of different environmental variables, i.e. control parameters, would lead to different descriptions of the thermodynamic phenomena when small systems are considered [19]. The same occurs in long-range interacting systems when different ensemble representations are not equivalent. We have considered only the microcanonical ensemble, but the results apply also for the canonical and grand canonical ensembles. This is because in the mean field approximation the thermodynamic potentials all have the same functional form in the different ensembles [18]. However, the critical points where the mean field approximation ceases to be valid are characteristic of each ensemble.

DISCUSSION

By integration of the relation among the different local thermodynamic variables over the volume of the system, we find the corresponding equation satisfied by the global variables. It is shown that the potential energy enters as a thermodynamic variable which modifies the global thermodynamic equations. That is, the Euler relation is modified if the system possesses long-range interactions and takes the form $TS = E + PV - \mu N + \sigma W$. As a result, we find a generalized Gibbs-Duhem equation which relates the potential energy to the intensive variables: $\sigma dW = SdT - VdP + Nd\mu$. For the marginal case where the power of the decaying interaction potential is equal to the dimension of the embedding space, the usual Gibbs-Duhem equation is recovered. Therefore, when long-range interactions are present in the system, the intensive variables become independent due to the freedom introduced by the potential energy. The potential energy naturally depends on the intensive variables. We also emphasize that this deviation from standard thermodynamics is similar to what happens with Hill's thermodynamics of small systems.

ACKNOWLEDGMENT

This work was supported by the Spanish Government under grant FIS2011-22603. I L acknowledges financial support through an FPI scholarship (BES-2012-054782) from the Spanish Government.

NOMENCLATURE

d	Dimension of the embedding space
$d\tau$	Volume element in full phase space
$e(\mathbf{x})$	Local energy per particle at point \mathbf{x}
E	Total energy
\mathcal{E}	Subdivision potential
e_0	Local kinetic energy per particle
E_0	Total kinetic energy
$f(\mathbf{x}, \mathbf{p})$	Distribution function in one-particle phase space
f_c	Constant in Boltzmann entropy = $e/(2\pi\hbar)^d$
\hbar	Reduced Planck's constant = $1.054571726(47) \times 10^{-34}$ Js
H_N	N -particle Hamiltonian
k_B	Boltzmann's constant = $1.3806488(13) \times 10^{-23}$ JK $^{-1}$
m	Mass of a particle
$n(\mathbf{x})$	Number density at point \mathbf{x}
N	Number of particles
\mathbf{p}	Momentum in one-particle phase space
$p(\mathbf{x})$	Local pressure at point \mathbf{x}
P	Pressure at the boundary of the system
$q(\mathbf{x})$	Generic local magnitude per particle
Q	Generic global magnitude
$Q(\mathbf{x}, \mathbf{p})$	Generic magnitude in one-particle phase space
\mathbf{q}_i	Coordinate of particle i
r	Interparticle distance
R	Radius of the spherical container
$s(\mathbf{x})$	Local entropy per particle at point \mathbf{x}
S	Total entropy
T	Temperature
$\nu(\mathbf{x})$	Local volume per particle at point \mathbf{x}
V	Volume of the system
W	Total potential energy
\mathbf{x}	Position in one-particle configuration space

δ	Short-distance cutoff
$\Gamma(x)$	Gamma function of x
ε	Energy of a particle at the center of the system
κ	Generic coupling constant
Λ	Rescaled energy
λ_T	Thermal wavelength
μ	Chemical potential
$\mu_0(\mathbf{x})$	Ideal gas chemical potential at point \mathbf{x}
ν	Power of the decaying pair interaction potential
σ	Long-range parameter = $1 - \nu/d$
$\Sigma(E)$	Number of microstates
$\phi(\mathbf{x}, \mathbf{x}')$	Pair interaction potential between particles in one-particle phase space
$\Phi(\mathbf{x})$	Potential at point \mathbf{x}
ϕ_{ij}	Pair interaction potential in full phase space
$\Omega_{(d)}$	Solid angle factor for the $(d - 1)$ -sphere

REFERENCES

- [1] Alessandro Campa, Thierry Dauxois, and Stefano Ruffo. Statistical mechanics and dynamics of solvable models with long-range interactions. *Physics Reports*, 480(3–6):57–159, 2009.
- [2] F. Gupta S. Bouchet and D. Mukamel. Thermodynamics and dynamics of systems with long-range interactions. *Physica A: Statistical Mechanics and its Applications*, 389(20):4389–4405, 2010. Proceedings of the 12th International Summer School on Fundamental Problems in Statistical Physics.
- [3] V. A. Antonov. Most Probable Phase Distribution in Spherical Star Systems and Conditions for Its Existence. *Vest. Leningrad Univ.*, 7:135, 1962.
- [4] D. Lynden-Bell and R. Wood. The gravo-thermal catastrophe in isothermal spheres and the onset of red-giant structure for stellar systems. *Monthly Notices of the Royal Astronomical Society*, 138:495, 1968.
- [5] W. Thirring. Systems with negative specific heat. *Zeitschrift fur Physik*, 235:339–352, August 1970.
- [6] T. Padmanabhan. Statistical mechanics of gravitating systems. *Physics Reports*, 188:285–362, April 1990.
- [7] P. H. Chavanis. Gravitational instability of finite isothermal spheres. *A&A*, 381(1):340–356, 2002.
- [8] Pierre-Henri Chavanis. Statistical Mechanics of Two-Dimensional Vortices and Stellar Systems. In Thierry Dauxois, Stefano Ruffo, Ennio Arimondo, and Martin Wilkens, editors, *Dynamics and Thermodynamics of Systems with Long-Range Interactions*, volume 602 of *Lecture Notes in Physics*, pages 208–289. Springer Berlin Heidelberg, 2002.
- [9] Philippe Chomaz and Francesca Gulminelli. Phase Transitions in Finite Systems. In Thierry Dauxois, Stefano Ruffo, Ennio Arimondo, and Martin Wilkens, editors, *Dynamics and Thermodynamics of Systems with Long-Range Interactions*, volume 602 of *Lecture Notes in Physics*, pages 68–129. Springer Berlin Heidelberg, 2002.
- [10] T. Dauxois, V. Latora, A. Rapisarda, S. Ruffo, and A. Torcini. The Hamiltonian Mean Field Model: From Dynamics to Statistical Mechanics and Back. In T. Dauxois, S. Ruffo, E. Arimondo, and M. Wilkens, editors, *Dynamics and Thermodynamics of Systems with Long-Range Interactions*, volume 602 of *Lecture Notes in Physics*, Berlin Springer Verlag, pages 458–487, 2002.
- [11] Francois Leyvraz and Stefano Ruffo. Ensemble inequivalence in systems with long-range interactions. *Journal of Physics A: Mathematical and General*, 35(2):285, 2002.
- [12] F. Bouchet and J. Barré. Classification of Phase Transitions and Ensemble Inequivalence, in Systems with Long Range Interactions. *Journal of Statistical Physics*, 118:1073–1105, 2005.
- [13] H.J. de Vega and N. Sánchez. Statistical mechanics of the self-gravitating gas: I. Thermodynamic limit and phase diagrams. *Nuclear Physics B*, 625(3):409–459, 2002.
- [14] H.J. de Vega and N. Sánchez. Statistical mechanics of the self-gravitating gas: II. Local physical magnitudes and fractal structures. *Nuclear Physics B*, 625(3):460–494, 2002.
- [15] I. Ispolatov and E. G. D. Cohen. Collapse in Systems with Attractive Nonintegrable Potentials. *Phys. Rev. Lett.*, 87:210601, Nov 2001.
- [16] I. Ispolatov and E. G. D. Cohen. Collapse in $1/r^\alpha$ interacting systems. *eprint arXiv:cond-mat/0106381*, June 2001.
- [17] Pierre-Henri Chavanis. Brownian particles with long- and short-range interactions. *Physica A: Statistical Mechanics and its Applications*, 390(9):1546–1574, 2011.
- [18] I. Latella and A. Pérez-Madrid. Local thermodynamics and the generalized Gibbs-Duhem equation in systems with long-range interactions. *arXiv:1302.4923 [cond-mat.stat-mech]*, 2013.
- [19] T.L. Hill. *Thermodynamics of Small Systems*. Parts I and II. W. A. Benjamin, INC., 1963.
- [20] S. de Groot and P. Mazur. *Non-Equilibrium Thermodynamics*. North-Holland Publishing Co, 1962.
- [21] P Glansdorff and Ilya Prigogine. *Thermodynamic theory of structure, stability and fluctuations*. Wiley-Interscience, London, 1977.

DEBYE LENGTH MATCHES CHANNEL BOTTLENECK: CORRUGATION-GOVERNED REGIME IN TRACER DIFFUSION THROUGH A VARYING-SECTION CHANNEL

Paolo Malgaretti*, Ignacio Pagonabarraga*, J. Miguel Rubi*

*Universitat de Barcelona, Departament de Física Fonamental, C. Martí i Franques 1, 08028 Barcelona, Spain
E-mail: paolomalgaretti@ffn.ub.es

ABSTRACT

We study the motion of charged and neutral tracers, in an electrolyte embedded in a varying section channel. Making use of systematic approximations, we map the convection diffusion equation governing the motion of tracers density in an effective 1D equation describing the dynamic along the channel where its varying-section is encoded as an effective entropic potential. This simplified approach allows us to characterize tracer diffusion in semi-confined environment by measuring its mean first passage time (MFPT). We disentangle the MFPT dependence upon channel geometry, electrolyte properties and tracers charge even at equilibrium. Such behavior can be exploited in different biological as well as synthetic situation whenever relevant phenomena can be triggered by the presence of few particles.

INTRODUCTION

The motion of charged tracers in an electrolyte has become a matter of interest due to its implication in both biological situations as well in the development of micro- nano- fluidic devices. In many cases tracers move in an electrolyte that is embedded in a channel or in a porous media. Due to the interaction with the electrolyte, the walls of the channel or the porous media accumulate net charge. Hence a net, screened, electrostatic field develops inside the channel. This feature is at the basis of phenomena such as electro-osmosis and it has been exploited for micro- nano-pumping. The currents in these devices generally relies on the control of some external force as hydrostatic or electrostatic fields. Tuning the external forcing leads to the control of particle currents as it happens, e.g. in sodium-potassium pumping in neurons.

An alternative route to current control relies on the geometrical confinement provided by the channel itself. It has been shown [1],[2] that the rectification provided by local variation in channel section can strongly affect particle transport. Moreover, the geometrically-induced current control is affected by the inhomogeneous distribution of particles along the radial direction [1]. This is the case of neutral tracers under an external field as gravity, or of charged tracers embedded in an electrolyte confined in charged-wall channel. Recently different groups [3], [4] have characterized the flow in varying-section channels when the electrostatic field generated by the charge channel walls is characterized by a screening (Debye) length, k^{-1} , that is vanishing small compared to the channel half-amplitude, $h(x)$.

However, the regime where k^{-1} is comparable to the channel bottleneck leads to a competition between electrostatic driving and geometric confinement and can lead to new dynamic scenarios where channel modulation plays a relevant role in charged tracer transport. Such regime has already shown interesting features as current inversion and negative mobility for forced electrolytes [5].

In this piece of work we show that, even at equilibrium, a sig-

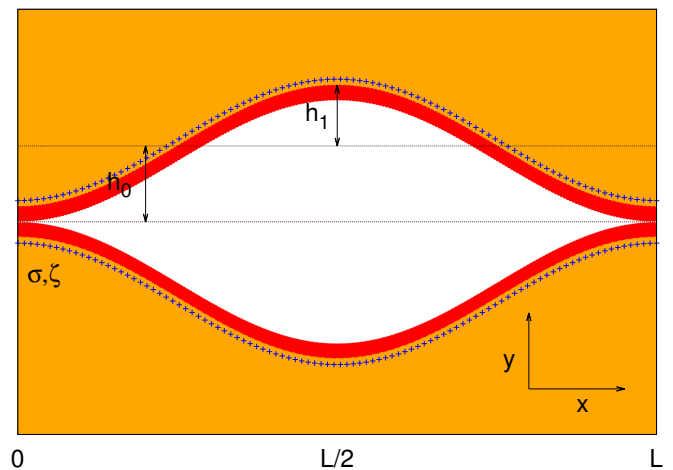


Figure 1. Electrostatic field inside a varying-section channel whose bottleneck amplitude $h_0 - h_1$ is comparable with the Debye double layer thickness k^{-1} .

nature of the interplay between the local rectification provided by the varying-section channel and the inhomogeneous distribution of charged tracers, provided by the transverse electrostatic field, can be read out from the tracers mean first passage time (MFPT) along the channel. Our results show a remarkable dependence of the MFPT on particle charge as well as on channel corrugation. For positively charged channel walls, positive (negative) tracers are depleted (attracted) towards the channel walls and their MFPT is enlarged (reduced) respectively. We expect such features to be relevant for several biological situations where channel walls are made by bilipidic membrane while the cytoplasm or physiologic solution particles are transported is rich in salt. In the latter situation the MFPT is a key quantity since cell fate might be determined by the recognition of, low concentrated, receptors. On the other hand in synthetic

situations such as nuclear waste containers or pattern forming system, a charge-dependence of the MFPT can lead to enlargement of the half-life of the former as well to, transitory, pattern formation/deformation for the latter.

To capture the main features of such an interplay between the geometrically induced local rectification provided by the varying-section channel and the electrostatic field we study a $z-z$ electrolyte embedded in a conducting channel (similar results have been obtained for an insulating channel). To keep an analytical insight we assume a highly diluted ion concentration and a small ζ potential on the channel walls, i.e. $\beta e \zeta \ll 1$ where $\beta^{-1} = k_B T$ is the inverse temperature (being k_B the Boltzmann constant) and e the elementary charge. This choice keeps the electrostatic field inside the channel in the linear regime hence allowing for a Debye-Huckel approximation to the electrostatics inside the channel. In order to gain insight in the properties of the MFPT of charged tracers and the which are the most relevant parameters determining their dynamic, we will assume that the channel amplitude, $h(x)$, varies slowly, i.e. $\partial_x h(x) \ll 1$. Such assumption allows for a projection of the $2D-3D$ convection diffusion equation to an effective $1D$ equation, where the varying-section of the channel will enter as an entropic effective potential. This approximation, called Fick-Jacobs, has been used and validated in many different scenarios [6], [1], [7].

The structure of the text is the following: in section II we will derive the Fick-Jacobs equation for charged tracers moving in a varying-section channel, in section III we will present our results while in section IV we will summarize our conclusions.

THEORETICAL FRAMEWORK: EQUILIBRIUM

The motion of suspension of charged particles is characterized by a convection-diffusion equation, that in the overdamped regime, reads:

$$\partial_t P(x, y, t) = D \beta \nabla \cdot (P(x, y, t) \nabla U(x, y)) + D \nabla^2 P(x, y, t) \quad (1)$$

where D is the diffusion coefficient and $U(x, y)$ is the total conservative potential acting on the particles. When particles are embedded in a confined region as is the case for tracers moving across a channel, the boundary condition of eq. 1 along the channel longitudinal axis will vary according to its channel amplitude. If the channel section varies only along the x -direction and it is constant in z , the free space accessible to the center of mass of a point-like particle is $2h(x)L_z$, being $h(x)$ the half-width of the channel along the y -direction and L_z the width along the z -direction. For such a situation, we encode the presence of the channel and the electrostatic potential in the overall potential $U(x, y, z)$ defined as:

$$\begin{aligned} U(x, y, z) &= U(x + L, y, z) \\ U(x, y, z) &= \psi(x, y), |y| \leq h(x) \ \& \ |z| \leq L_z/2 \\ U(x, y, z) &= \infty, |y| > h(x) \ \text{or} \ |z| > L_z/2 \end{aligned} \quad (2)$$

that is periodic along the longitudinal direction, x , and confines the particles inside the channel.

In order to find the electrostatic potential, $\psi(x, y)$, inside the channel, we should solve the, $2D$, Poisson equation:

$$\partial_x^2 \psi(x, y) + \partial_y^2 \psi(x, y) = -\frac{\rho_q(x, y)}{\epsilon} \quad (3)$$

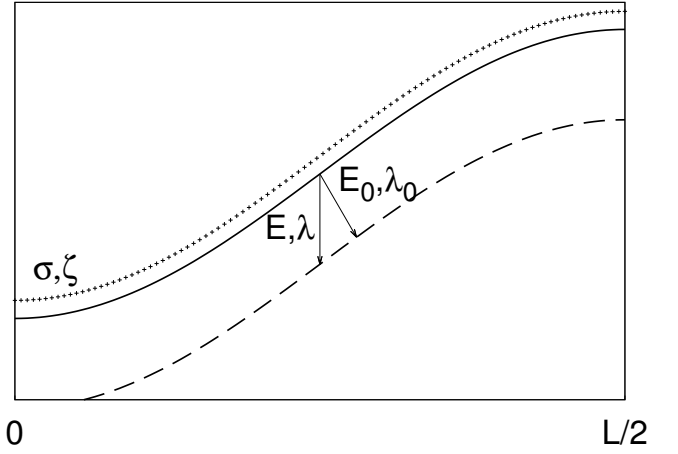


Figure 2. Debye double layer inside a varying-section channel. The Debye length $k_0^{-1} = \lambda_0$ is shown as well as the approximated Debye length $k^{-1} = \lambda$.

with the boundary condition given by eq. 3, being $\rho_q = \rho_0 \exp(-\beta z e \psi(x, y))$ the, equilibrium, charge density inside the channel in the absence of tracers. Assuming smoothly-varying channel walls, $\partial_x h \ll 1$, we can take advantage of the lubrication approximation, $\partial_x^2 \psi(x, y) \ll \partial_y^2 \psi(x, y)$. In this way we can reduce eq. 3 to a $1D$ equation for the potential $\psi(x, y)$. Such an approximation introduces an error in the electrostatic field that can be estimated. In fact we know that, prior to our lubrication approximation, the electrostatic field is perpendicular to the channel wall. Hence, for varying-section channel, we should count for the projection of the electrostatic field along the radial direction as shown in fig. 2 when solving the Poisson equation. For a smoothly-varying channel amplitude, the projected electrostatic field reads:

$$E = E_0 \cos(\alpha) \quad (4)$$

with $\alpha = \arctan[\partial_x h(x)]$. Due to the smoothness of the variation of channel amplitude, we have $\partial_x h(x) \ll 1$ hence leading to a second order correction in $\partial_x h(x)$ for the electrostatic field

$$E = E_0 \left[1 - \frac{1}{2} (\partial_x h(x))^2 \right]. \quad (5)$$

In the following we will neglect such correction assuming, $E = E_0$ along the channel. For low salt concentration in the electrolyte and small ζ potential on channel walls, we can further simplify eq. 3 by linearizing the charge density $\rho_q(x, y) \simeq \rho_0 (1 - \beta z e \psi(x, y))$, hence getting:

$$\psi(x, y) = \zeta \frac{\cosh(ky)}{\cosh(kh(x))} \quad (6)$$

for a channel made by conducting walls or

$$\psi(x, y) = \frac{\sigma}{2\epsilon} \frac{\cosh(ky)}{\sinh(kh(x))} \quad (7)$$

for an insulating-walls channel characterized by a constant surface-density of electric charge σ , being ϵ the dielectric con-

stant of the electrolyte. Such assumption, known as Debye-Huckel approximation, allows to identify the screening length, k_0^{-1} , of the electrostatic potential as $k_0^2 = \beta z e \rho_0 / \epsilon$. The approximation made for the electrostatic field reflects in the Debye length. Fig. 2 shows the common origin of the corrections for both the Debye length and the electrostatic field, provided by the change in the channel section. Consistently with the choice for the electrostatic field, we can assume constant Debye length, $k^{-1} = k_0^{-1}$, along the channel by safely ignoring the second order correction given by eq. 5.

Under the assumption of smoothly varying-section channels, $\partial_x h \ll 1$, we can approximate the radial profile of the probability distribution function (pdf), $P(x, y, t)$, of a tracer of charge q by its profile at equilibrium, i.e we can factorize the pdf by assuming:

$$P(x, y, z, t) = p(x, t) \frac{e^{-\beta q \Psi(x, y)}}{e^{-\beta A(x)}} \quad (8)$$

$$e^{-\beta A(x)} = \int_{-L_z/2}^{L_z/2} \int_{-h(x)}^{h(x)} e^{-\beta q \Psi(x, y)} dy dz.$$

By integration over dy, dz we obtain:

$$\dot{p}(x, t) = \partial_x D [\beta p(x, t) \partial_x A(x) + \partial_x p(x, t)] \quad (9)$$

where we have assumed vanishing small tracers concentration so not to perturb the equilibrium electrostatic potential $\Psi(x, y)$. Eq. 9 encodes both the confining as well as the electrostatic potential given by eq. 3 in the free energy $A(x)$. Since all the quantities of interest are independent of z , without loss of generality we can assume $\int_{-L_z/2}^{L_z/2} dz = 1$. Defining the average, x -dependent, electrostatic energy as:

$$\langle V(x) \rangle = e^{\beta A(x)} \int_{-h(x)}^{h(x)} q \Psi(x, y) e^{-\beta q \Psi(x, y)} dy \quad (10)$$

from eq. 8 we can define the entropy along the channel as $TS(x) = \langle V(x) \rangle - A(x)$ hence getting:

$$S(x) = \ln \left[\int_{-h(x)}^{h(x)} e^{-\beta q \Psi(x, y)} dy \right] + \beta \langle V(x) \rangle. \quad (11)$$

In the linear regime $\beta q \Psi(x, y) \ll 1$; we can linearize eq. 11 getting:

$$S(x) \simeq \ln(2h(x))$$

where the entropy has a clear geometric interpretation, being the logarithm of the space, $2h(x)$, accessible to the center of mass of the tracer. Accordingly, we introduce the entropy barrier, ΔS , defined as:

$$\Delta S = \ln \left(\frac{h_{max}}{h_{min}} \right) \quad (12)$$

that represent the difference, in the entropic potential, evaluated at the maximum, h_{max} , and minimum, h_{min} of channel aperture.

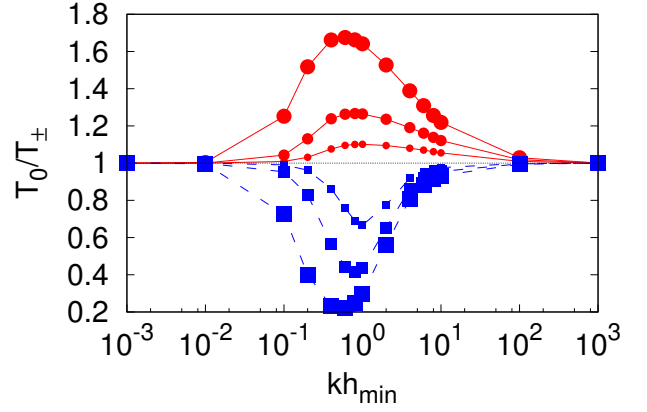


Figure 3. Filled points: inverse of the MFPT, $1/T_{\pm}$, normalized by the MFPT of neutral tracers T_0 , as a function of the inverse Debye length, k^{-1} , normalized by the minimum channel amplitude h_{min} for positive, $\beta q \zeta = 3$, (blue squares) or negative, $\beta q \zeta = -3$, (red dots) tracers in a conducting channel characterized by $\Delta S = 2.2$.

RESULTS

In the present work we analyze the motion of charged tracers in a channel characterized by conducting walls (similar results have been obtained for the case of insulating channel walls) whose half section along the y -direction is characterized by

$$h(x) = h_0 + h_1 \sin \frac{2\pi}{L}(x + \phi) \quad (13)$$

where h_0 is the, average channel section, and h_1 is the, possible, modulation, while we assume the channel to be flat along the z -direction. ϕ controls the channel shape with respect to its boundaries fixed at $x = 0$ and $x = L$. According to eq. 13 we have $h_{max} = h_0 + h_1$ and $h_{min} = h_0 - h_1$.

In order to characterize the geometrically induced contribution to the diffusion of charged tracers at equilibrium, we choose to analyze the first passage time distribution. In particular we focus on the mean of such distribution, i.e. the mean first passage time (MFPT) tracers take to pass through the channel. Such quantity has a twofold interest. On one hand, the MFPT captures, even at equilibrium where electrostatic current vanishes, the role played by the geometrically-induced potential. On the other hand, it is an interesting quantity for situations like ion trapping or chemical segregation as happens in nuclear waste containers. In the following we assume that one of the ends of the channel, namely the one at $x = 0$, is in contact with a reservoir of tracers and we are interested in the MFPT of positive negative or neutral tracers, $t_{\pm,0}(x)$, tracers take to diffuse from x to the other end of channel situated at $x = L$. Such situation leads to a reflecting boundary condition on the end of the channel in contact with the reservoir, i.e at $x = 0$, and to an absorbing condition on the other end, at $x = L$. Taking advantage of the 1D projection, eq. 9, we can calculate the x -dependent MFPT, $t(x)$, which reads [8]:

$$\beta D \partial_x A(x) \partial_x t_{\pm,0}(x) + D \partial_x^2 t_{\pm,0}(x) = -1 \quad (14)$$

By numerically solving eq. 14 the MFPT of tracers crossing the channel is given by $T_{\pm,0} = t_{\pm,0}(0)$. Fig. 3 shows the MFPTs

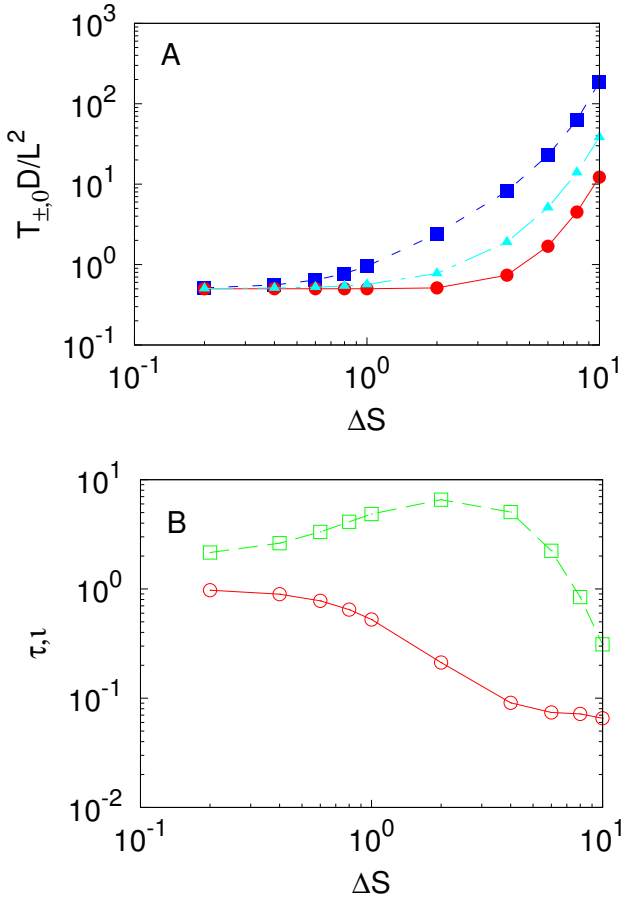


Figure 4. A: MFPT, T , normalized by L^2/D , as a function of the entropic barrier ΔS for positive (blue squares), $\beta q \zeta = 3$, or negative (red dots), $\beta q \zeta = -3$, tracers in a channel with $kh_{min} = 1$. B: ratio of the MFPTs (red circles), $\tau = T_-/T_+$, and “current” (green squares), $i = \frac{2L^3}{\sigma D} \frac{|\rho_+ T_- - \rho_- T_+|}{T_- T_+}$, with T_{\pm} the MFPT of positive (negative) tracers and σ the charge density on the channel walls as a function of the entropic barrier ΔS for the same parameters as panel A.

for positive (blue squares) as well negative tracers (red dots) across a varying-section channel normalized by the MFPT of neutral tracers, T_0 , whose MFPT does not depend on k^{-1} . When the Debye length k^{-1} is comparable with the channel minimum amplitude, h_{min} , negative tracers, attracted towards the positive charged walls, benefit from the modulation induced by the corrugation of the channel and their MFPT is smaller than the one corresponding to neutral tracers. Positive tracers, depleted from the channel walls, experience an enhanced electrostatic barrier at the channel bottleneck that increases their MFPT. Interestingly such a modulation in the MFPT for charged tracers vanishes for $kh_{min} \ll 1$ as well as for $kh_{min} \gg 1$, underlying the relevance of the regime, $kh_{min} \sim 1$, under study.

The dependence of the MFPTs on the entropy barrier is shown in fig. 4.A. While for vanishing values of ΔS all tracers show the same MFPT, a monotonous increase in the MFPT for all tracers is registered upon increasing ΔS . The increase in the MFPT even for neutral tracers is of solely entropic origin. Hence fig. 4.A confirms the enhanced sensitivity of positive tracers with respect to negative ones upon variation of the geometry of the channel. The relative behavior of positive with respect to negative tracers can be useful for application as chemical segregation or particle separation. The ratio of the MFPTs for positive and negative tracers, $\tau = \frac{T_-}{T_+}$ is shown in fig. 4.B.

For vanishing values of ΔS , positive and negative tracers experience the same MFPT while for increasing ΔS negative tracers can be as faster as an order of magnitude leading to a ratio of the order of $\tau \sim 10^{-1}$. The asymmetry in the MFPT for positive and negative tracers suggest the onset of net currents as a response to fluctuations in tracers density. In the spirit of linear response theory, we can define the adimensional current $i = \frac{2L^3}{\sigma D} \frac{|\rho_+ T_- - \rho_- T_+|}{T_- T_+}$. Fig. 4.B shows that the asymmetry in tracer motion leads to an effective current, suggesting that entropic rectification can give rise to non-negligible electrostatic currents with a non-monotonous dependence on channel corrugation. This indicates that one can exploit geometrical modulation to tune electrostatic currents. This requires a more detailed analysis.

CONCLUSIONS

The motion of charge tracers suspended in an electrolyte embedded in a channel with charged walls is strongly affected by the geometry of the channel. The geometrical confinement introduces an effective potential due to the local bias induced by the varying section of the channel. Such feature is captured by neutral tracers whose MFPT is modulated by the channel shape through the amplitude of the entropy barrier, ΔS . The dependence of the MFPT of charged tracers upon different parameters, such as the Debye length k^{-1} and the entropy barrier ΔS , allows for a particle-diffusion control mechanism relying on the geometrical properties of the channel as well as on the electrolyte properties encoded in the Debye length k^{-1} . The MFPT of charged tracers is very sensitive to tracers charge q . According to it, tracers are depleted or attracted to the channel walls hence experiencing different energetic barriers. Such a dependence leads to an additional control parameter that can be exploited to promote/reduce the crossing of the channel by charged tracers as registered in extensive numerical simulations [9].

The phenomenology we have just described has a twofold interest. It shows that interesting behavior, such as particle current inversion or negative mobility, observed when the system is drive out of equilibrium [5] can be captured even studying the properties of the system at equilibrium. By analyzing the MFPT we have been able to show that when the Debye length matches the channel bottleneck, i.e. $kh_{min} \sim 1$ novel effects can rise to due the overlap between the geometrically induced local bias in the diffusion and the geometrically modulated electrostatic field inside the channel. Such an interplay leads to a non-trivial behavior of the MFPT upon different parameters. On the other hand in situations such as cellular signaling, gene regulation or chemical segregation where many phenomena are triggered by the capture of few molecules rather than on the steady state concentration, one is interested in the time a few tracers reach the target rather than on the steady values. For such situations our study shows that in the case in which particles have to diffuse across an inhomogeneous (porous) media, such inhomogeneity can lead to significant advances or delays of the typical triggering time.

ACKNOWLEDGMENTS

We acknowledge the Direcció General de Investigaci6n (Spain) and DURSI project for financial support under projects FIS 2011-22603 and 2009SGR-634, respectively. J.M. Rubi acknowledges financial support from *Generalitat de Catalunya*

under program *Icrea Academia*

REFERENCES

- [1] D. Reguera and J.M. Rubi, Kinetic equations for diffusion in the presence of entropic barriers, *Phys. Rev. E*, vol. 64, pp. 061106, 2001
- [2] P. Malgaretti, I.Pagonabarraga and J. M. Rubi, Confined Brownian ratchets, in press *J. Chem. Phys.*
- [3] I.D. Kosinska, I. Goychuk, M. Kostur, G. Schmidt, G. and P. Hänggi, Rectification in synthetic conical nanopores: A one-dimensional Poisson-Nernst-Planck model, *Phys. Rev. E*, vol. 77, pp. 031131, 2008
- [4] S. Ghosal, Lubrication theory for electro-osmotic flow in a microfluidic channel of slowly varying cross-section and wall charge, *J. Fluid. Mech.*, vol. 459, pp. 103, 2002
- [5] P. Malgaretti, I. Pagonabarraga and J.M. Rubi, submitted
- [6] R. Zwanzig, Diffusion Past an Entropy Barrier, *J. Phys. Chem.*, vol. 96, pp. 3926, 1992
- [7] P. Kalinay and J. K. Percus, Approximation of the generalized Fick-Jacobs equation, *Phys. Rev. E.*, vol. 78, pp. 021103, 2008
- [8] H. Risken, *The Fokker-Planck Equation*, Springer-Verlag, Berlin, 1988. *Proc. Symp. Interaction between Fluids and Particles*, vol. 1, pp. 50-63, 1962.
- [9] B. Rotenberg, I. Pagonabarraga and D. Frenkel, Dispersion of charged tracers in charged porous media, *EPL*, vol. 83, pp. 34004, 2008; B. Rotenberg, I. Pagonabarraga and D. Frenkel, Coarse-grained simulations of charge, current and flow in heterogeneous media, *Faraday Discuss.*, vol. 144, pp.223, 2010

PUMPING OF WATER WITH ROTATING ELECTRIC FIELDS AT THE NANOSCALE

Sergio De Luca¹, B.D.Todd¹, Jesper S. Hansen², Peter J. Daivis³

¹Mathematics, Swinburne University of Technology, Melbourne Victoria 3122, Australia

²Department of Science, Systems and Models, Roskilde University, DK-4000, Roskilde, Denmark

³Department of Applied Physics, RMIT University, Melbourne, Victoria 3001, Australia

ABSTRACT

We present the first non-equilibrium molecular dynamics results for pumping of water at the nanoscale, utilizing a new, completely non intrusive approach. The flow production is sustained by means of a body force acting on the polar molecules in the form of an external, spatially uniform rotating electric field. The theoretical background relies upon the coupling of the spin angular momentum to linear streaming momentum, enhanced when the interaction of the permanent dipole moment of the molecules with the external field is significant. By further embedding the small fluid volume between two different planar surfaces, one hydrophobic and one hydrophilic, it is possible to generate unidirectional fluid flow. Concomitantly, by properly tuning the frequency and strength of the external field, moderate fluid operational temperatures can be maintained, thereby revealing some exciting and potentially useful applications in the field of nanotechnology.

INTRODUCTION

Manipulation and generation of fluid flow at the micro-nanoscale is usually achieved by micropumps exerting pressure on the fluid by means of moving solid boundaries, or by exerting forces directly onto the fluid, for instance by means of an external electric fields. Among the techniques belonging to the second category, electroosmotic micropumps constitutes a widespread and efficient methodology to drive flow, based on the draining effect of dissolved ions in liquids, subjected to an external dc field. We use a completely new method to pump fluid flow of polar molecules, that requires neither any form of intrusive mechanical device into the fluid, or any addition of solute carrier charges. The mechanism rests on the coupling of the spin angular momentum to linear translational motion of a highly confined polar fluid (water as one of the most important examples). We have shown that ignoring the coupling of spin angular momentum to linear translational motion of a highly confined fluid can lead to significant overestimation of the predicted flow rates using conventional Navier-Stokes treatments. By including spin-coupling into the extended Navier-Stokes equations, hydrodynamic prediction is seen to be very accurate down to length scales of a few atomic diameters [1]. We also demonstrate how this knowledge, coupled with our knowledge of the different behaviour of dipolar liquids when confined between hydrophobic and hydrophilic solid surfaces, can be used to pump molecular fluids such as water via non-intrusive application of a rotating electric field [2,3]. By both theoretical modelling and nonequilibrium molecular dynamics (NEMD) simulations of such a system we show that a steady uni-directional flow can be generated at microwave frequency ranges using external rotating electric fields[4].

METHODS

We performed NEMD simulations of $N = 270$ water molecules confined between two planar surfaces, distinguishable for the different crystal structure and surface charge characteristics. A schematic of the system is reported in Fig (1), which represents an asymmetric channel. From a mathematical point of view, the asymmetric channel reproduce the different velocity boundary conditions near the interfaces. The hydrophilic wall implements a BCC (body-centered-cubic) crystal structure, with the addition of small dipole charges (not visible) to enforce the no-slip velocity boundary condition at this interface. The hydrophobic wall particles are distributed in conformity with the FCC (face-centered-structure) crystal structure, such that the density is larger than the hydrophilic wall. Further details on the construction of the channel surfaces are given in [4]. We emphasize at this point that the use of the asymmetric channel is a necessary condition for having a net flow production along the channel. Fluid volumes confined between two equal hydrophobic or two equal hydrophilic walls result in a zero net flow, as we will see in the next section.

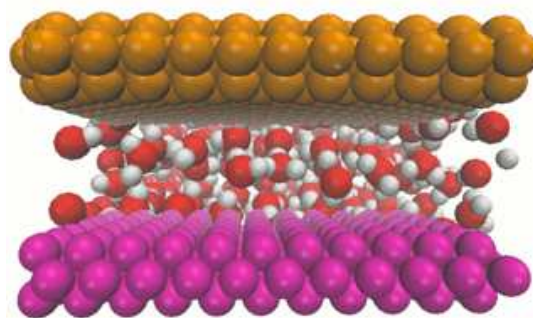


Fig. 1. System composed of two planar walls confining water molecules. The yellow wall represents a hydrophobic surface while the purple wall models the hydrophilic side.

Liquid water is modeled with the SPC/E pair potential [5], with partial charges $q_H = 0.4238 e$ and $q_O = -0.8476 e$ for hydrogen and oxygen, respectively ($e = 1.6 \times 10^{-19} C$ is the fundamental unit of charge). Bonds and angles are constrained with the SHAKE algorithm [6]. Molecule interactions are modeled by means of the Lennard-Jones (LJ) pair potential, with the addition of the Coulomb term for the charged particles, which reads

$$\Phi = \sum_i \sum_{j>i} 4\epsilon \left[\left(\frac{\sigma}{r_{ij}} \right)^{12} - \left(\frac{\sigma}{r_{ij}} \right)^6 \right] + \sum_i \sum_{j>i} \frac{q_i q_j}{r_{ij}} \quad (1)$$

with the energy scale parameter $\epsilon = 0.65 \text{ KJ mol}^{-1}$ and the length scale parameter $\sigma = 0.32 \text{ nm}$. The sum extends over the total number of the molecules, noting that the indices i and j do not belong to the same molecule. The r_{ij} term represents the distance between the particles, i.e. the sites of different water molecules and between water and wall particles. The Coulomb term, representative of the long range electrostatic interactions, is incorporated in the Wolf algorithm [7]. The simulation box sides are $L_x = 1.9 \text{ nm}$, $L_y = 4.5 \text{ nm}$ and $L_z = 1.9 \text{ nm}$, and the vertical separation between the two plates is 2.25 nm (y -direction in Fig. (1)). This configuration yields the density of water $\rho = 998 \text{ Kg/m}^3$. The x axis corresponds to the flow direction, i.e. from the right to the left side of Fig. (1) and the z -axis is perpendicular to the other two. Both the x and z axes are treated as periodic. To avoid expensive and unnecessary force computations, the LJ interaction potential is truncated at the distance $r = 1 \text{ nm}$.

The external rotating electric field, which acts on the sites of the water molecule, is spatially uniform and time dependent, and can be represented with the vector $E = [\cos(\omega t), \sin(\omega t), 0]$, where ω is the angular frequency and t is the time. The resulting electric field is polarized along the plane generated from the direction perpendicular to the two surfaces (x -axis, see Fig (1)) and parallel to the two plates, from the left to the right of the same figure (x -direction). The action of the electric field results in the torque exerted on the water permanent dipoles

$$\vec{\tau} = \sum_i (\vec{r}_i - \vec{r}_{CM}) \times q_i \vec{E}_i \quad (2)$$

with the sum ranging over the three sites of the SPC/E water, \vec{r}_i and \vec{r}_{CM} vector positions of the site i and the center of mass of the water molecule, q_i and \vec{E}_i represent the charge attached to the site i and the electric field acting on the particle positions. The torque injected into fluid constrains the dipole moments to align with the field. This alignment tendency competes with the disordering effect of the thermal energy but, with a proper choice of the amplitude and frequency of the field, generates an average rotation of the dipoles along the z -direction, which in turn gives rise to a net flow rate production (in the asymmetric channel).

The leap-frog scheme was used to integrate the Newtonian equations of motion for the fluid and wall particles [8], with the time step $\Delta t = 1.6 \text{ fs}$ which yields a good stability of the integrator. Full details on the integrator implementation, in conjunction with the insertion of the external body force term in the algorithm are given in [4]. The work supplied by the external field on the fluid results in a thermal energy increase,

due to the enhanced friction between molecules. The heating produced is removed with the Nosé-Hoover thermostat applied only to the wall particles [9-11]. To implement this technique, the wall atoms are forced to oscillate around their equilibrium positions, subjected to an elastic force whose strength is tuned to optimize the thermostat efficiency, maintaining at the same time the proper stability of the crystal wall structure. This approach has the merit to leave the rotational degree of freedom of the water molecules unaltered [12-15].

At the beginning of the simulation, the system is allowed to equilibrate and typically relaxes in a configuration of minimum potential energy approximately after 500 ps. Then the field is turned on and after 5-6 ns achieves steady state, which means that all the physical properties of interest, like velocity and temperature, attain approximately constant values. Averages are accumulated in the next 7 ns implementing standard binning techniques [16], with 200 bins of width 0.02 nm . The aforementioned properties are plotted against the distance between the two surfaces (y -direction) and are evaluated from their microscopic definition. The streaming velocity profile has been computed by means of

$$v_x(y) = \frac{\left\langle \sum_i m_i v_{x,i} \delta(y_i - y) \right\rangle}{\left\langle \sum_i m_i \delta(y_i - y) \right\rangle} \quad (3)$$

i.e. the momentum flux density

$$J_x(\vec{r}, t) = \sum_i m_i v_{x,i} \delta(\vec{r} - \vec{r}_i) \quad (4)$$

is divided by the mass density

$$\rho = \sum_i m_i \delta(\vec{r} - \vec{r}_i) \quad (5)$$

where i ranges over the molecule i , m_i is the mass of a water molecule, $v_{x,i}$ represents the velocity component of the i -th molecule in the direction parallel to the surfaces and \vec{r}_i is the center of mass location of molecule i . The angle brackets in (3) stand for time averages, to be taken at the end of the simulation run. The response of the fluid system to the external field is further investigated averaging the molecular temperature profile (computed with the aforementioned binning technique)

$$T_{mol} = \frac{1}{3K_B N} \sum_i m_i \bar{c}_{i,cm}^2 \quad (6)$$

with N the total number of water molecules, k_B the Boltzmann constant and $\bar{c}_{i,cm}^2$ the square of the thermal velocity of the i -th water molecule center of mass.

RESULTS

We plot in Fig. 2 the streaming velocity profile, computed from Eq. (3), for the asymmetric channel depicted in Fig (1). The picture overlaps ten independent simulations, with the electric field amplitude kept fixed at 1.8 V/nm whereas the frequency ranges from 10 to 100 GHz, in steps of 10 GHz. The profile with the smallest slope, indicated in the picture with the x symbol, corresponds to the frequency of 10 GHz. Increasing the frequency from 20 GHz to 90 GHz, (see profiles drawn with solid lines in Fig. (2)), coincides with a monotonically increasing absolute value of the slope, which in turn means a larger value of the absolute streaming velocity next to the hydrophobic side. The case with the highest frequency, 100 GHz, depicted in Fig (2) with the asterisk symbol, gives an absolute streaming velocity adjacent to the hydrophobic side (right side of the picture) of approximately 100 m/s. Note that for frequencies larger than 120 GHz, a value which corresponds to the inverse of the dipolar relaxation time of water, the trend reverses and the absolute velocities decrease as the frequency increases (not shown)

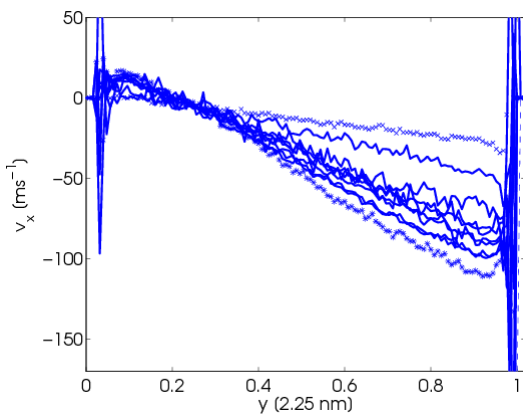


Fig. 2. Streaming velocity profile of water for the asymmetric channel. The hydrophilic wall is located on the left side and the hydrophobic wall on the right side.

To clarify the dependence of the streaming velocity on the frequency of the external field, we plot in Fig. (3) the maximum (absolute) values of the velocities adjacent to the hydrophobic side, as plotted in Fig. (2). For the field frequency 10 GHz up to the final value 100 GHz, the absolute value of the streaming velocity increases. Moreover, we see that the trend is nonlinear and that at the highest frequencies the velocity begins to saturate at values close to $v_x = 100$ m/s. This saturation point also depends on the amplitude of the electric field. In Fig. (4) we report the maximum (absolute) streaming velocity values, next to the hydrophobic wall, for the case of fixed field frequency and varying amplitude. We investigate the amplitude range from 1 V/nm up to 10 V/nm, at the same time keeping the frequency fixed at 20 GHz. Again, we see an increase of the absolute streaming velocity as the amplitude intensifies from the strength value 0.8 V/nm. For amplitude values of the order of 3-4 V/nm the streaming velocities saturate again

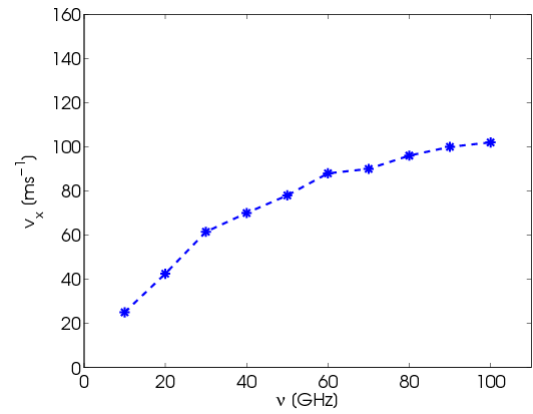


Fig. (3). Maximum (absolute) streaming velocity of water for the asymmetric channel. The amplitude is fixed at 1.8 V/nm.

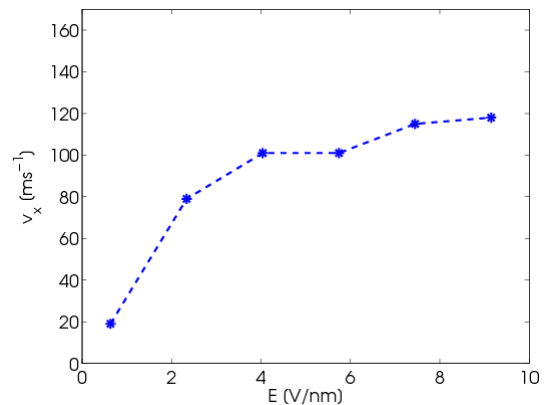


Fig. 4. Maximum (absolute) streaming velocity of water for the asymmetric channel. The field frequency is fixed at 20 GHz.

towards the approximate value 110 m/s. The explanation of this tendency relies on Eq. (2), in which a larger amplitude of the electric field results in an increase of the torque injected into the fluid. Again, the velocities begin to saturate around 3 V/nm, stabilizing approximately at 100 m/s.

The work performed by the external electric field on the fluid volume is partly converted in translational kinetic energy (due to the coupling between the spin angular momentum to linear streaming momentum) and partly is dissipated in internal energy. In Fig. (5) we show the temperature profiles for the same fluid system and external field parameters employed for the results of Fig. (2). The lowest temperature, depicted with the cross symbol, relates to the lowest frequency used, 10 GHz. Gradually increasing the frequency from 10 GHz to 90 GHz, yields a corresponding monotonic increase of the temperature. As the frequency of the field increases, the friction between dipoles is enhanced, due to the faster alignment of the dipole moments. The frequency of 100 GHz, the largest used in this work, corresponds the maximum heating of the fluid system (the top profile).

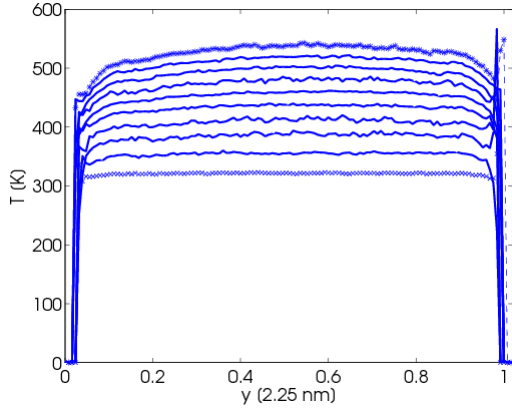


Fig. 5. Temperature profile of water for the asymmetric channel, corresponding to results reported in Fig. 2.

In Fig. (6) we plot the velocity profile with the field 1.8 V/nm and frequency 20 GHz for the symmetric channel. In this case, both surfaces are modelled with equal hydrophilic surfaces. The net flow rate production, i.e. the integrated area under the curve with respect the y -coordinate, is zero, since the two portion of area situated in the two halves of the channel are equal in magnitude but opposite in sign.

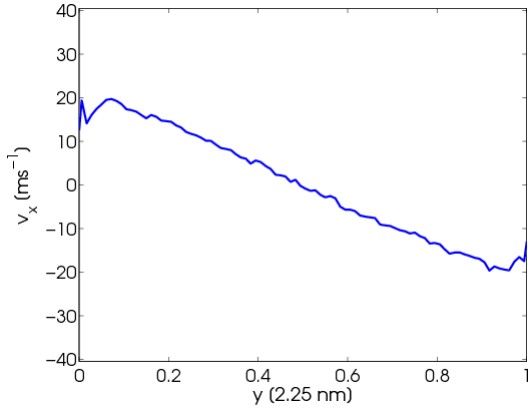


Fig. 6. Streaming velocity profile of water for the symmetric system. Amplitude and frequency are 1.8 V/nm and 20 GHz.

Finally, we compare our molecular dynamics results with the extended Navier-Stokes equations (ENS), which take into consideration the coupling of the spin angular momentum to the linear momentum [17-19]. The equations read:

$$\rho \frac{\partial v_x}{\partial t} = \rho F_e + (\eta_0 + \eta_r) \frac{\partial^2 v_x}{\partial y^2} - 2\eta_r \frac{\partial \Omega_z}{\partial y} \quad (7)$$

$$\rho I \frac{\partial \Omega_z}{\partial t} = \rho \Gamma_z + 2\eta_r \left(\frac{\partial v_x}{\partial y} - 2\Omega_z \right) + \zeta \frac{\partial^2 \Omega_z}{\partial y^2} \quad (8)$$

We consider the asymmetric channel, with the amplitude set at 1.8 V/nm and the frequency at 20 GHz and we solve only Eq. (7), with respect to the streaming velocity v_x . Details on the streaming angular velocity solution Ω_z are given in [4]. The

velocity boundary conditions, i.e. the streaming velocity v_x next to the two surfaces necessary to solve the second order partial differential equations, are 2.7 m/s for the hydrophilic wall and -45 m/s for the hydrophobic surface. F_e is the external force, set to zero as the electric field is the only external force acting on the system. The quantities Γ_z , η_0

η_r and ζ represent the torque per unit mass injected into the system, the shear, vortex and spin viscosity, respectively. Note that the electric field enters the ENS by means of the torque term, as can be seen in Eq. (2). Specific considerations and technicalities are required for the selection of proper values for the torque term and for the fluid transport properties listed, detailed in [4] and references therein. As can be seen in Fig. (7) the agreement between the ENS numerical solutions and the NEMD profile result is excellent.

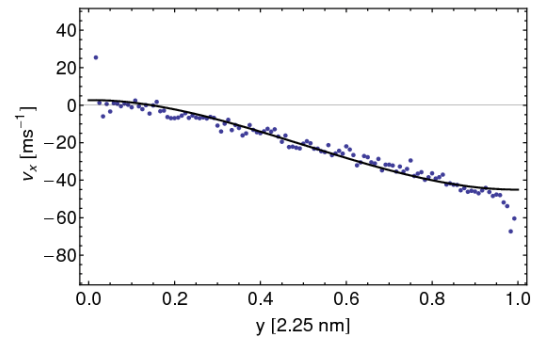


Fig. 7. NEMD streaming velocity profile of water (points) and numerical solution of the ENS (solid line) for the asymmetric channel.

CONCLUSIONS

We have demonstrated via nonequilibrium molecular dynamics simulations that a significant water flow production is attainable at the nanoscale, only exploiting the coupling between the spin angular momentum and the linear translational momentum. Furthermore, we showed that if the external field frequencies and amplitudes are properly tuned, then the temperature of the fluid can be maintained at reasonable low values. Finally, a good agreement between the extended Navier-Stokes equations and the NEMD results has been found. The non-intrusive characteristic of this water pumping method renders it attractive to the experimentalist, and may open the road for useful applications in the field of nanofluidics.

ACKNOWLEDGMENT

Computation utilized the Swinburne Supercomputer Centre, the Victorian Partnership for Advanced Computing HPC Facility and Support Services and an award under the Merit Allocation Scheme on the NCI National Facility at the Australian National University.

REFERENCES

- [1] J. S. Hansen, J. C. Dyre, P. J. Daivis, B. D. Todd, H. Bruus, Nanoflow hydrodynamics, *Phys. Rev. E*, 84, 036311, 2011.
- [2] J. D. Bonthuis, D. Horinek, L. Bocquet, R. R. Netz, Electrohydraulic power conversion in planar nanochannels, *Phys. Rev. Lett.*, 103, 144503, 2009.
- [3] J. S. Hansen, H. Bruus, B. D. Todd, P. J. Daivis, Rotational and spin viscosities of water: Application to nanofluidic, *J. Chem. Phys.*, 133, 144906, 2010.
- [4] S. De Luca, B. D. Todd, J. S. Hansen, P. J. Daivis, Electropumping of water with rotating electric fields, *J. Chem. Phys.*, 138, 154712, 2013.
- [5] H. J. C. Berendsen, J. R. Grigera, T. P. Straatsma, The missing term in effective pair potentials, *J. Phys. Chem.*, 91, 6269, 1987.
- [6] G. Ciccotti, M. Ferrario, J. P. Ryckaert, Molecular dynamics of rigid systems in cartesian coordinates: a general formulation, *Mol. Phys.*, 47, 1253, 1982.
- [7] D. Wolf, P. Keblinski, S. R. Phillpot, J. Eggebrecht, Exact method for the simulation of the Coulombic systems by spherically truncated, pairwise r^{-1} summation, *J. Chem. Phys.*, 110, 8254, 1999.
- [8] D. Rapaport, *The Art of Molecular Dynamics Simulation*, 2nd ed., Cambridge University Press, New York, 2004.
- [9] S. Nosé, A unified formulation of the constant temperature molecular dynamics methods, *J. Chem. Phys.*, 81, 511, 1984.
- [10] S. Nosé, A molecular dynamics method for simulations in the canonical ensemble, *Mol. Phys.*, 52, 255, 1984.
- [11] W. G. Hoover, G. Canonical dynamics: Equilibrium phase-space distributions, *Phys. Rev. A*, 31, 1695, 1985.
- [12] S. Bernardi, B. D. Todd, D. J. Searles, Thermostating highly confined fluids, *J. Chem. Phys.*, 132, 244706, 2010.
- [13] K. P. Travis, P. J. Daivis, D. J. Evans, Computer-simulation algorithms for molecules undergoing planar couette-flow - A nonequilibrium molecular-dynamics study, *J. Chem. Phys.*, 103, 1109, 1995.
- [14] K. P. Travis, P. J. Daivis, D. J. Evans, Thermostats for molecular fluids undergoing shear flow: Application to liquid chlorine, *J. Chem. Phys.*, 103, 10638, 1995.
- [15] K. P. Travis, P. J. Daivis, D. J. Evans, Erratum: Thermostats for molecular fluids undergoing shear flow: Application to liquid chlorine, *J. Chem. Phys.*, 105, 3893, 1996.
- [16] M. P. Allen, D. J. Tildesley, *Computer Simulation of Liquids*, Clarendon Press, Oxford., 1987.
- [17] D. J. Evans, W. B. Streett, Transport properties of homonuclear diatomics II. Dense fluids, *Mol. Phys.*, 36, 161, 1978.
- [18] S. R. de Groot, P. Mazur, *Non-Equilibrium Thermodynamics*, Dover, Mineola, 1984.
- [19] D. W. Condiff, J. S. Dahler, Fluid mechanical aspects of antisymmetric stress, *Phys. Fluids*, 7, 842, 1964.

COMPUTING THE EXERGY OF SOLAR RADIATION FROM REAL RADIATION DATA ON THE ITALIAN AREA

Manuela Neri*, Davide Luscietti, Mariagrazia Pilotelli

Department of Mechanical and Industrial Engineering, University of Brescia, via Branze, Brescia, Italy

*E-mail: m.neri001@studenti.unibs.it

ABSTRACT

The decrease of fossil fuels availability and the consequent increase of their price, has led to a rapidly evolution of renewable market and policy frameworks in recent years. Renewable resources include solar radiation which is of considerable interest as it is inexhaustible, free and clean. In order to calculate how much work can be obtained from solar radiation, several methods have been proposed in the literature. The aim of this work has been to calculate the exergy content of solar radiation in Italy. To do this, we have analyzed real radiation data and we have treated direct and diffuse radiation separately. We have proposed a single exergy factor valid on the Italian area, which is to be applied to the total radiation measured on horizontal surface.

INTRODUCTION

Renewable resources include solar radiation which is of considerable interest as it is inexhaustible, free and clean. Since it is intermittent, diluted and not evenly distributed on the Earth surface, systems that exploit solar energy are almost always coupled with ones that use fossil fuels. This coupling set up the so called hybrid systems which ensure consistent performance over time. Solar radiation exploitation is divided into capture, conversion into another kind of energy (for example electricity or work) and storage. In this article only the passage through the atmosphere is analyzed, with the aim to determine the exergy content of solar radiation. Governments encourage the development of hybrid systems through incentives: their payment is based on the fraction of the produced power that is allocated to renewable resources, as explained in [1]. One aspect that still causes uncertainty is the allocation of solar radiation energy, more precisely the computing of solar radiation exergy content. Exergy represents the maximum work obtainable from a system or a process in a given environment. Unlike energy, exergy is not conservative, and it gives information about the room for improvement of a process. In the literature, various models have been proposed for computing solar radiation exergy: the studies began considering black-body radiation, then considering the radiation spectral distribution, up to consider the radiation components - direct and diffuse - separately. Also the assumption of thermodynamic models representative of the phenomena in the atmosphere to which solar radiation undergoes changed in the course of scientific research. The aim of this article is to determine a reference value for computing solar radiation exergy in Italy.

SOLAR RADIATION

Solar radiation is electromagnetic energy which propagates in the space at light speed. It is concentrated in the range of lower wavelengths ($0.2\mu\text{m} \leq \lambda \leq 3\mu\text{m}$) with the maximum irradiance at $0.5\mu\text{m}$. The annual average radiation outside the ter-

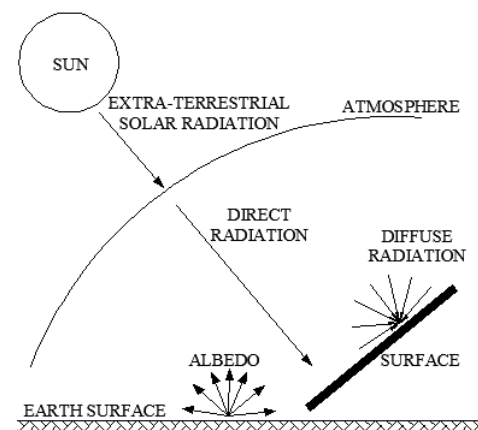


Figure 1. Solar radiation scheme.

restrial atmosphere is estimated about 1376 W/m^2 . The annual average radiation that reaches the Earth surface is considered equal about to 1000 W/m^2 : this value refers to a collecting surface perpendicular to the sun, in clear sky conditions and the sun at the zenith. However the exact amount in a given place is sensitive to atmospheric composition and to solar rays path: these factors affect diffusion and absorption phenomena that occurs in the atmosphere. Analyzing solar radiation that reaches the Earth surface, it is necessary to distinguish its components, which are sketched in Fig. 1. Let us consider a surface placed on the Earth which receives solar radiation. The radiation received directly from the sun is called direct radiation. The amount of scattered radiation coming from all the directions is called diffuse radiation. The ratio of radiation which reaches the surface after being reflected from the ground is called albedo. The sum of all the components incident on the surface is called total radiation.

THE SOLAR EXERGY ON THE EARTH

According to the first and second laws of thermodynamics, energy can not be created or destroyed. However, a process can

diminish the capacity of energy to perform work due to the generation of entropy by irreversibility. In order to take into account this latter feature, exergy has been defined. Exergy represents the maximum work that can be extracted from a system in a given environment, that is carrying the system to its dead state. The dead state is the condition in which the system is in mutual equilibrium with the environment and so no more work can be extracted from it.

In order to determine the solar radiation exergy on the Earth, let us consider a cyclic machine placed on the terrestrial surface, as represented in Fig. 2. The machine extracts the maximum work W_{\max} obtainable from the energy source E_s (solar energy) and it delivers heat Q_0 to the environment at temperature T_0 . The machine also emits the energy by radiation E_e . The maximum work $W_{\max} = Ex_s$ is the exergy of the solar energy E_s . This scheme is quite general and it permits to obtain all the three most famous expressions for the solar exergy. In the scheme energies and entropies are per unit of time (indicated by a dot over the respective symbol) and per unit of area of the device represented by the cyclic machine: then the equations of balance involve specific fluxes of energy and of entropy.

Without emission by radiation from the cyclic machine

In this case the energy balance $\dot{E}_s - \dot{E}x_s - \dot{Q}_0 = 0$ and the entropy balance $\dot{S}_s - (\dot{Q}_0/T_0) = 0$ lead to the expression for the specific exergy flux

$$\dot{E}x_s = \dot{E}_s - T_0\dot{S}_s \quad (1)$$

Solar energy is transferred by heat interaction If it is considered that the solar energy is transferred by a heat interaction at sun temperature T_s , $\dot{S}_s = \dot{E}_s/T_s$ and it is obtained the specific exergy flux

$$\dot{E}x_s = \dot{E}_s \left(1 - \frac{T_0}{T_s}\right) \quad (2)$$

and the efficiency

$$\eta_J = \frac{\dot{E}x_s}{\dot{E}_s} = 1 - \frac{T_0}{T_s} \quad (3)$$

This efficiency is always positive and lesser than the unity as long as $T_0 < T_s$. This formula was proposed by Jeter [2]. Zamfirescu [3] adopted Eq. (3) but he introduced a lower temperature of the radiation on the terrestrial surface, in order to take into account the atmospheric filter.

Solar energy is a radiation flux If the source is radiation, some particularities should be taken into account: these regard the difference between black-body radiation and diluted black body radiation, more precisely the entropy transported by the two kinds of radiation.

It is known that a black-body radiation flux transports the specific energy flux

$$\dot{E} = \sigma T_s^4 \quad (4)$$

and the specific entropy flux

$$\dot{S} = \frac{4}{3} \sigma T_s^3 \quad (5)$$

where σ represents the Stefan-Boltzman constant, as reported for example in [4, 5].

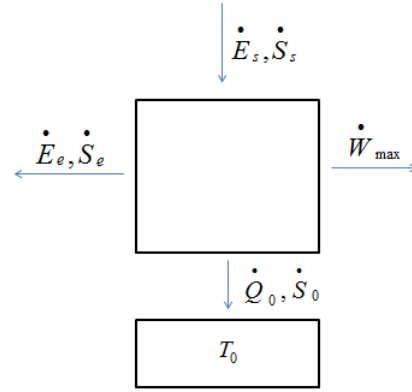


Figure 2. The cyclic machine.

Therefore, if the source is black-body radiation, specific energy and exergy fluxes are represented by Eq. (4) and Eq. (5) and the specific exergy flux of Eq. (1) become

$$\dot{E}x_s = \dot{E}_s \left(1 - \frac{4 T_0}{3 T_s}\right) = \sigma T_s^4 \left(1 - \frac{4 T_0}{3 T_s}\right) \quad (6)$$

whereas the efficiency obtained is

$$\eta_S = \frac{\dot{E}x_s}{\dot{E}_s} = 1 - \frac{4 T_0}{3 T_s} \quad (7)$$

This formula was determined by Spanner [6].

Pons [7] used the expression Eq. (1) for computing the specific exergy flux of the solar radiation, but he used for \dot{E}_s and \dot{S}_s the values measured on the Earth in some locations.

With emission by radiation from the cyclic machine

In this case the energy balance $\dot{E}_s - \dot{E}x_s - \dot{Q}_0 - \dot{E}_e = 0$ and the entropy balance $\dot{S}_s - (\dot{Q}_0/T_0) - \dot{S}_e = 0$ lead to the expression for the specific exergy flux

$$\dot{E}x_s = (\dot{E}_s - T_0\dot{S}_s) - (\dot{E}_e - T_0\dot{S}_e) \quad (8)$$

If the machine is considered a black-body at the same temperature of the environment T_0 , the second term in Eq. (8) becomes

$$(\dot{E}_e - T_0\dot{S}_e) = -\frac{1}{3} \sigma T_0^4 \quad (9)$$

Solar energy is a radiation flux If the solar energy is a black-body radiation flux at temperature T_s , the specific energy and entropy fluxes are represented by Eq. (4) and Eq. (5) and the specific exergy flux of Eq. (8) become

$$\dot{E}x_s = \sigma T_s^4 \left(1 - \frac{4 T_0}{3 T_s} + \frac{1 T_0^4}{3 T_s^4}\right) \quad (10)$$

whereas the efficiency obtained is

$$\eta_P = \frac{\dot{E}x_s}{\dot{E}_s} = 1 - \frac{4 T_0}{3 T_s} + \frac{1 T_0^4}{3 T_s^4} \quad (11)$$

This formula was proposed by Petela [8].

Eq. (3), Eq. (7) and Eq. (11) were far discussed by various authors over the years, included Bejan [9] and Petela [5].

THE SOLAR ENERGY: FROM THE SUN TO THE EARTH SURFACE

Solar radiation undergoes to dissipation phenomena passing through the atmosphere: terrestrial solar radiation has lower irradiance than the extraterrestrial one.

The DBR model

Landsberg and Tonge [10, 11] took into account the losses suffered by radiation in the atmosphere by means of the DBR (diluted black-body radiation) model: they introduced a dilution factor ϵ , ranging between 0 and 1, independent of both the direction and the wavelength. If the sun is considered a diluted black-body, the specific energy and entropy fluxes are

$$\dot{E}_s = \epsilon \sigma (T_s)^4 \quad (12)$$

$$\dot{S}_s = \chi \frac{4}{3} \epsilon \sigma (T_s)^3 \quad (13)$$

where the χ function is

$$\chi = \frac{45}{4\pi^4} \frac{1}{\xi} \int_0^\infty y^2 [(1+n_v)\ln(1+n_v) - n_v \ln(n_v)] dy \quad (14)$$

where $y = (vh)/(kT_s)$ represents a dimensionless frequency and n_v is the mean occupation number of frequency v .

For a more detailed analysis, it would be necessary to take into account the radiation spectral distribution of the radiation on the Earth surface, because the atmospheric absorption is not equal on all frequencies. Chu and Liu [12] investigated on the difference between extraterrestrial and terrestrial solar radiation and on the difference between direct and diffuse solar radiation: they do not use measured data, but a model for the spectrum of the solar energy on the Earth surface.

Exergy of diffuse and direct beam according to Pons

As already mentioned in the introduction, the passage of solar radiation through the atmosphere involves the splitting of solar radiation into direct and diffuse beams. Since these two components are subjected to different processes, in a deeper analysis it is not possible to unify them into a single entity.

Pons [7] treated the two components separately using representation illustrated by Eq. (6) and applying the correction factor χ proposed by Landsberg and Tongue [10, 11] to the direct and to the diffuse component separately. He analyzed real data of direct \dot{E}_{dr} and diffuse \dot{E}_{df} specific fluxes of solar radiation relative to Saint-Pierre de la Reunion, Odeillo and Ouagadougou. In Odeillo data was measured with a time step of 1 second and averaged over 5 minutes, in Saint Pierre de la Reunion data was measured with a time step of 6 seconds and averaged over 5 minutes, while data for Ouagadougou was calculated every hour by means of a software. The data was measured on a horizontal surface, and thus only the vertical component of direct radiation was determined. For computing the ϵ factor, it is necessary to divide the overall direct radiation on the Earth surface (not only the vertical component) by the extraterrestrial radiation. To calculate the direct radiation from its vertical component, the measured value E_{dr} was divided by the $\cos\theta$. θ is the angle between direct radiation and vertical direction and it depends on the latitude of the considered location and on the

time. The atmospheric attenuation factor for direct and diffuse radiation was determined as follows

$$\epsilon_{dr} = \frac{\dot{E}_{dr}/[\cos\theta\omega_s]}{\sigma T_s^4/\pi} \quad (15)$$

$$\epsilon_{df} = \frac{\dot{E}_{df}/\pi}{\sigma T_s^4/\pi} \quad (16)$$

where ω_s is the Sun solid angle, that is the solid angle occupied by the direct radiation, while diffuse radiation occupies a solid angle equal to 2π . Regarding the χ functions for the diffuse and the direct radiation, Pons proposed the following functions

$$\chi_{dr}(\epsilon_{dr}) = (0.973 - 0.275 \ln \epsilon_{dr} + 0.0273 \epsilon_{dr}) \quad (17)$$

$$\chi_{df}(\epsilon_{df}) = (0.9659 - 0.2776 \ln \epsilon_{df}) \quad (18)$$

Then, the specific entropy fluxes \dot{S}_{dr} and \dot{S}_{df} were determined as follows

$$\dot{S}_{dr} = \chi_{dr} \frac{4}{3} \frac{\dot{E}_{dr}}{T_s} \quad (19)$$

$$\dot{S}_{df} = \chi_{df} \frac{4}{3} \frac{\dot{E}_{df}}{T_s} \quad (20)$$

The specific exergy flux was determined applying Eq. (1) for the two components

$$\dot{E}x_{dr} = \dot{E}_{dr} - T_0 \dot{S}_{dr} \quad (21)$$

$$\dot{E}x_{df} = \dot{E}_{df} - T_0 \dot{S}_{df} \quad (22)$$

where T_0 is the yearly air temperature average. The author [13] stated that for exergy computing T_0 has to be taken constant, in order to guarantee that exergy can be conserved in a reversible process. These formulas were integrated over a periodic time equal to the day (from sunrise to sunset). As the solid angles of direct and diffuse radiation are complementary, the total specific exergy flux was calculated as $E_{xs} = E_{xdr} + E_{xdf}$

SOLAR EXERGY FROM REAL SOLAR DATA ON THE ITALIAN AREA

Referring to the cyclic machine in Fig. (2), it could represent any sort of device that performs some useful effect by means of solar radiation. The aim of this work is the evaluation of the exergy of the solar radiation on the Italian area: this value should represent the maximum obtainable work and it should not be dependent on the device.

The device surface can absorb only a fraction of the short wave-length radiation coming from the sun, depending on its emissivity. Moreover, it can emit long wave-length radiation, because its temperature is rather close to the environmental one. The surface temperature and its emissivity are unknown and some authors supposed that it behaves like a black-body at environmental temperature T_0 . For example, this hypothesis permits to obtain Eq. (10) and Eq. (11).

Since emissivity could assume different values on varying of the wave-length of the radiation, we imagine an ideal surface which absorbs all the solar radiation \dot{E}_s and which does not emit radiation \dot{E}_e . In this way it is possible to determine the



Figure 3. Italian location analyzed : AG, AL, AN, AO, AP, AQ, BA, BL, BN, BO, BR, BZ, CA, CB, CL, CO, CS, CZ, EN, FE, FG, FI, FO, FR, GR, GE, GO, LI, MC, ME, MI, MN, NA, OR, PE, PG, PR, PT, PZ, RI, RM, RN, SO, SP, TA, TO, TN, TP, TR, VA, VE, VI

exergy of the solar radiation independently from the device surface. The characteristics of the device surface should be taken into account in a subsequent step.

Then, we have utilized the expression for the specific exergy flux of Eq. (1). For the calculation of \dot{E}_s and \dot{S}_s , we have followed the approach proposed by Pons [7]: the direct and the diffuse components have been considered separately by means of the DBR model of Landsberg and Tonge [10, 11], and the χ_{dr} and χ_{df} functions have been calculated respectively by means of Eq. (17) and Eq. (18).

For the solar energy \dot{E}_s , we have started from the data reported in the UNI EN 10349 standard [14]. The standard [14] reports the monthly day average air temperature, the monthly daily average of specific direct and diffuse solar radiation on a horizontal surface E_{drh} and E_{df} , for all the Italian provincial capitals. We have chosen a subgroup of location shown in Fig. 3, in order to cover all ranges of latitude, longitude and altitude relative to Italy.

Data reported in the standard [14] are the average of ten years of measurements: the influence of any daily weather condition (for example cloudy sky) was spread on a large number of measurements.

In order to apply the approach proposed by Pons [7] we needed to spread the daily average monthly specific radiation during the day. The diffuse radiation can be considered constant during the day, but this is not possible for the direct radiation on a horizontal surface. Therefore we have represented the specific direct radiation on a horizontal surface by means of a sine function, whose area below is equal to the daily average monthly

direct radiation. The sine function is the following

$$\dot{E}_{drh} = \left(\frac{\pi E_{drh}}{2 h_s} \right) \sin \left(t \frac{\pi}{h_s} \right) \quad (23)$$

where h_s represents the monthly average of the daylight duration in the considered location and t is the time interval from sunrise up to the instant considered. We have determined the specific direct radiation flux on horizontal surface every hour.

In order to calculate the dilution factors, we have determined the specific direct radiation that reaches the Earth every hour considering the angle θ between the direct radiation and the vertical direction. For computing the angle θ , first we have calculated the solar declination δ for each month

$$\delta = 0.40928 \sin \left[2\pi \left(\frac{284 + n}{365} \right) \right] \quad (24)$$

where n is the number of the considered day. δ is the angle between incident radiation and the equatorial plane at noon on the considered meridian. Then we have calculated the hour angle h , which is the angular distance between the sun and its position at noon, along its apparent trajectory: h is zero at noon and varies of $\pi/12$ per hour (positive values in the morning hours and negative in the afternoon hours). The angle α between direct radiation and the horizontal surface, that is the complementary to θ angle, has been calculated as follows

$$\sin \alpha = \sin L \sin \delta + \cos L \cos \delta \cosh \quad (25)$$

where L is the latitude of the given location. The angle α has been calculated for each time instant and for each month. Direct radiation \dot{E}_{dr} , that is the radiation that would be captured by a sun tracking device, has been calculated as follows

$$\dot{E}_{dr} = \frac{\dot{E}_{drh}}{\cos(\pi/2 - \alpha)} \quad (26)$$

Solar radiation reaches the Earth surface only for a certain number of hours per day depending on the location and on the day. We have calculated daylight length average h_s for each month. The dawn time h_a and the sunset time h_t were calculated as follows:

$$h_a = -h_t = \text{acos}(-\tan L \tan \delta) \quad (27)$$

and the difference between h_a and h_t represents the daylight length h_s . From the monthly average air temperatures reported in [14], we have calculated the yearly average air temperature T_0 . For each location, we have considered the same temperature in order to obtain comparable exergies.

As done by Pons [7], we have assumed the sun temperature T_s equal to 5770 K, the sun solid angle ω_s equal to $6.79 \cdot 10^{-5}$ sr and we have applied Eq. (15) - Eq. (22).

We have calculated the exergy factors of direct and diffuse solar radiation

$$\eta_{dr} = \frac{Ex_{dr}}{E_{drh}} \quad (28)$$

$$\eta_{df} = \frac{Ex_{df}}{E_{df}} \quad (29)$$

η_{dr} represents the ratio of the exergy of the direct radiation and the vertical component of the direct radiation. η_{df} represents the ratio of the exergy of the diffuse radiation and the diffuse radiation. As can be seen in Fig. 4 and Fig. 5, η_{dr} ranges

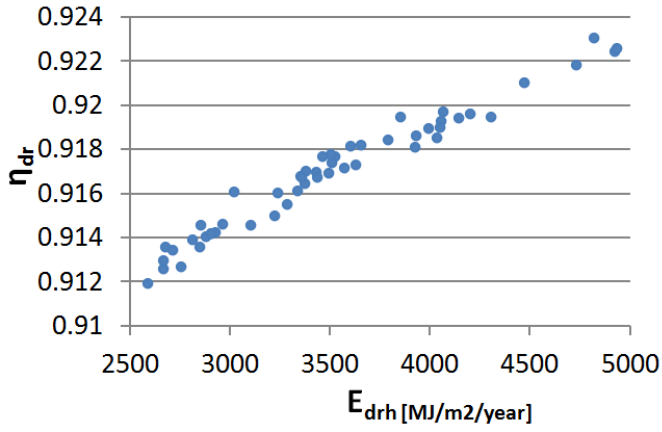


Figure 4. Exergy factor of direct solar radiation

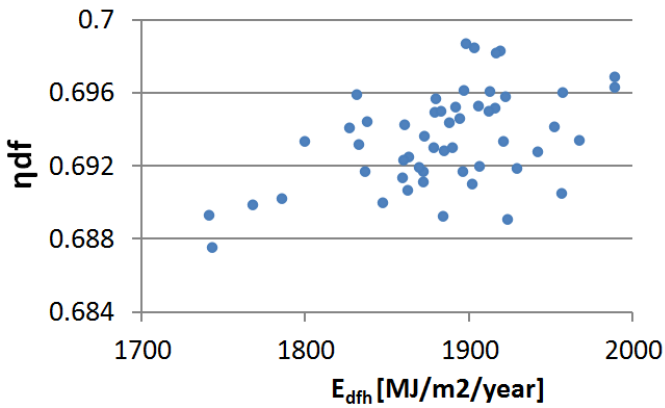


Figure 5. Exergy factor of diffuse solar radiation

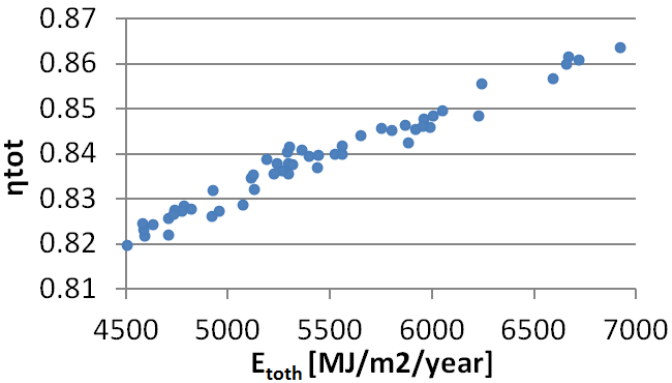


Figure 6. Exergy factor of total solar radiation

between 0.912 and 0.923, while η_{df} ranges between 0.688 and 0.699. We have calculated the total exergy factor for each considered location as follows

$$\eta_{tot} = \frac{Ex_{tot}}{E_{totth}} \quad (30)$$

where $Ex_{tot} = Ex_{dr} + Ex_{df}$ is the yearly solar radiation exergy and $E_{totth} = E_{drh} + E_{dfh}$ is the yearly solar radiation that reaches an horizontal surface. In Fig. 6, η_{tot} is shown and it ranges between 0.820 and 0.864.

Fig. 7 shows the trend of total exergy factor as a function of altitude (without distinction for latitude). The more the altitude, the lower the thickness of the atmospheric layer that solar radiation has to pass through for reaching the Earth surface (latitude

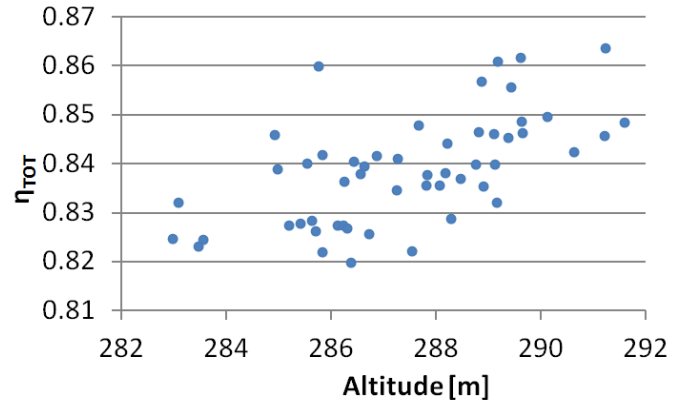


Figure 7. Total exergy factor as function of altitude

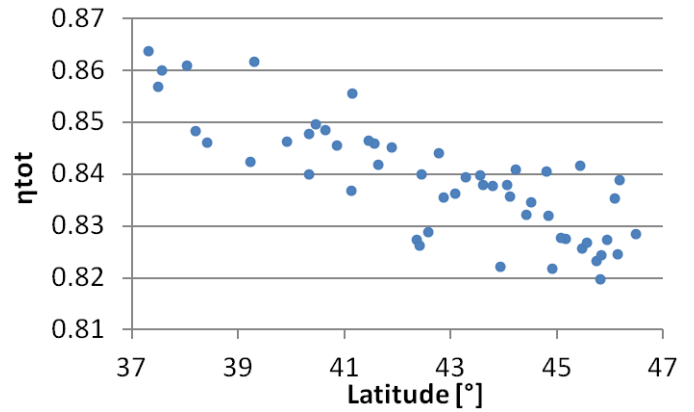


Figure 8. Total exergy factor as function of latitude

being equal). In Fig. 7 there is no any identifiable trend: latitude does not affect the exergy factor predominantly.

Fig. 8 shows the trend of total exergy as function of latitude. Increasing latitude increases the thickness of the atmospheric layer that solar radiation has to pass through for reaching the Earth surface. It is noted that with increasing latitude, the total exergy factor decreases.

The exergy calculation involves the environment temperature T_0 as shown in Eq. (1) and, if the latitude increases, the average annual temperature T_0 decreases: for example, in Messina (latitude $38^\circ 11'$) T_0 is equal to 291.55 K, while in Belluno (latitude $46^\circ 08'$) T_0 is equal to 282.96 K. Fig. 9 shows the total exergy factor as function of the yearly air temperature average. Increasing T_0 , total exergy factor increases. This is probably due to the fact that in locations with high temperature the radiation is stronger. This indicates that solar radiation exergy is more affected by the quantity of solar radiation than by the environment temperature.

Fig. 10 shows that increasing the ratio between direct and diffuse solar radiation, the total exergy factors increases.

We have also applied our procedure on the three location analyzed by Pons [7] (Ouagadougou, Odeillo and Saint Pierre de la Reunion), using direct and diffuse solar radiations on horizontal surface calculated by means of a software. We have calculated the ratio Ex_{dr}/E_{totth} and $\eta_{tot} = Ex_{tot}/E_{totth}$: Tab. 1 shows that we have found different, but comparable data.

It is also interesting to see the trend of the total exergy factor as function of the ratio of specific vertical direct radiation and specific diffuse radiation. In Fig. 10 it can be noted that increas-

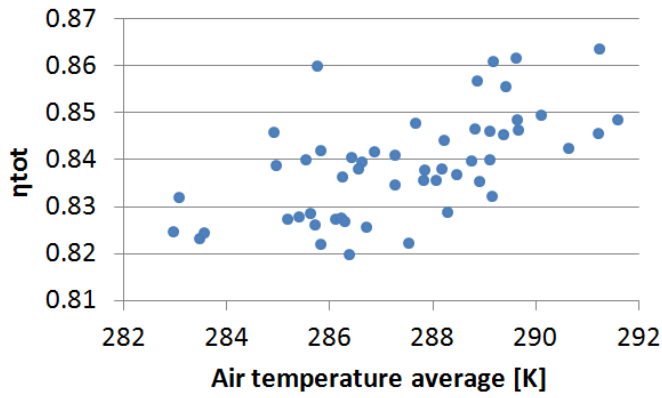


Figure 9. Total exergy factor as function of yearly air temperature average

Table 1. Total exergy factor: comparison between data calculated by Pons and data that we calculated

	Location	Pons	Our computing
Ex_drh/E_toth	St Pierre Reunion	0.63	0.67
	Ouagadougou	0.58	0.66
	Odeillo	0.62	0.56
Ex_tot/E_toth	St Pierre Reunion	0.86	0.86
	Ouagadougou	0.84	0.84
	Odeillo	0.85	0.83

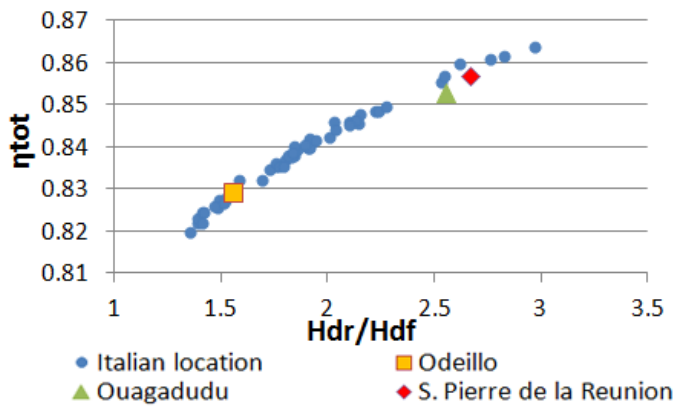


Figure 10. Total exergy factors as function of the ratio between direct and diffuse radiation

ing the percentage of this ratio the total exergy factor increases. This trend is also followed by the three locations analyzed by Pons [7].

At the end, as η_{tot} values are very similar for all the Italian locations, it was decided to determine a single value η_{IT} valid for Italy, by means of which to determine the solar radiation exergy. This factor has been determined as average of the values obtained for the analyzed locations and it is

$$\eta_{IT} = 0.839 \quad (31)$$

In this way, it is possible to calculate solar radiation exergy multiplying this factor for the total solar radiation measured in an Italian location.

CONCLUSIONS

The aim of this work has been the evaluation of the exergy of the solar radiation on the Italian area: this value should represent the maximum obtainable work and it should not be dependent on the characteristics of the device surface. Then we have imagined an ideal surface which absorbs all the solar radiation \dot{E}_s and which does not emit radiation \dot{E}_e . Following the analysis proposed by Pons, we have analyzed real radiation data and we have treated direct and diffuse radiation separately. We have proposed a single exergy factor valid on the Italian area, which is to be applied to the total radiation measured on horizontal surface.

REFERENCES

- [1] G.P. Beretta, P. Iora, A.F. Ghoniem, Allocating electricity production from a hybrid-fossil renewable power plant among its multi primary resources consumption, submitted
- [2] S.M. Jeter, Maximum conversion efficiency for the utilization of direct solar radiation, *Solar Energy*, vol 26, pp. 231-236 (1981)
- [3] C. Zamfirescu, I. Dincer, How much exergy one can obtain from incident solar radiation?, *J. Appl. Phys.* 105, (2009)
- [4] G. P. Beretta, E. P. Gyftopoulos, Electromagnetic radiation: a carrier of energy and entropy, in *Fundamentals of Thermodynamics and Exergy Analysis*, Edited by G. Tsatsaronis, R.A.Gaggioli, Y.M. El-Sayed, M.K. Drost, ASME Book G00566, AES, Vol. 19, pp. 1-6 (1990)
- [5] R. Petela, Exergy of undiluted thermal radiation, *Solar Energy* 74, pp. 469-488 (2003)
- [6] D.C. Spanner, *Introduction to thermodynamics*. Academic Press, London (1964)
- [7] M. Pons, 'Exergy analysis of solar collectors, from incident radiation to dissipation', *Renewable Energy* 47, pp. 194-202 (2012)
- [8] R. Petela, Exergy of heat radiation. *J. Heat Trnsfer* 86, pp. 187-192 (1964)
- [9] A. Bejan, Unification of three different theories concerning the idea conversion of enclosed radiation, *J. Solar Energy Eng.* 109, pp. 46-51 (1987)
- [10] P.T. Landsberg, G. Tongue, Thermodynamics of the conversion of diluted radiation, *J. Phys.A: Math.Gen.* 12, pp. 551-562 (1979)
- [11] P.T. Landsberg, G. Tongue, Thermodynamics energy conversion efficiencies, *J. Appl. Phys.* 51, pp. R1-R20 (1980)
- [12] S.X. Chu, L.H. Liu, 'Analysis of terrestrial solar radiation exergy', *Solar Energy* 83, pp.1390-1404 (2009)
- [13] M. Pons, 'On the reference state for exergy when ambient temperature fluctuates', *International Journal of Thermodynamics* 12, pp. 113-21 (2009)
- [14] UNI EN 10349, Riscaldamento e raffreddamento degli edifici - Dati climatici, UNI, Milano 1997

DETAILED THERMODYNAMIC ANALYSIS OF FUEL CELL EFFICIENCY

Michal Pavelka^{abc}, František Maršík^{ad}

^a New Technologies - Research Centre, University of West Bohemia,
Univerzitní 8, 306 14 Plzeň, Czech Republic

^b Mathematical Institute, Faculty of Mathematics and Physics, Charles University in Prague,
Sokolovská 83, 186 75 Prague, Czech Republic

^c Corresponding author's e-mail: michal.pavelka@email.cz

^d E-mail: marsik@it.cas.cz

ABSTRACT

Efficiency of hydrogen fuel cells is analyzed using a non-equilibrium theory of mixtures based on classical irreversible thermodynamics. The efficiency is expressed in terms of processes taking place inside the fuel cells revealing which processes are responsible for efficiency losses. This provides a new method of optimization. It is shown that efficiency losses are not only given by entropy production rate but also by some additional terms, which become important if steep gradients of temperature are present. Consequently, we compare the new theory with the standard entropy production minimization approach. Finally, we discuss effects of the additional terms in polymer electrolyte membrane fuel cells and in solid oxide fuel cells showing that the new theory gives the same results as the standard theory in the former case while it becomes important in the latter case.

1 INTRODUCTION

In this work we present a method of evaluation of fuel cell efficiency which is alternative to the approach of entropy production rate minimization based on the Gouy-Stodola theorem, see Refs. [4, 13, 34, 19]. The method has already been published in Ref. [28], and it is, from a point of view, more suitable for fuel cells than the standard approach, see section 4.

Our analysis is formulated within classical irreversible thermodynamics (CIT), which is very well presented for example in Refs. [29, 10, 24, 17, 18]. CIT has already proven very useful in fuel cell modelling. For example, Kjelstrup and Røsjorde developed in article [20] a comprehensive non-isothermal model of polymer electrolyte membrane fuel cells (PEMFC) based on CIT, where even coupling effects between heat flux and diffusion fluxes were taken into account. Sciacovelli used the method of entropy production rate minimization to optimize a solid oxide fuel cell (SOFC), see Refs. [31, 32].

2 CLASSICAL IRREVERSIBLE THERMODYNAMICS

The analysis of efficiency is formulated within the framework of CIT. Since the system we consider is composed of multiple species, it is necessary to use a theory of mixtures. Many theories of mixtures have been published so far, see Refs. [10, 35, 26, 36, 6, 8, 15, 7, 25, 21, 16, 17, 28]. We chose the theory presented by Jou et al. in chapter 1 of book [17] in the form introduced in paper [28]. We also have to mention that the theory is quite limited since it can be rigorously justified only for a mixture of fluids in local thermodynamic equilibrium while various parts of fuel cells are usually porous media. However, Lebon et al. in article [23] and del Río et al. in article [11] showed that porous media can be described by means of Extended Irreversible Thermodynamics (EIT), see Ref. [17],

which can be seen as a direct extension of CIT. Therefore, we take the theory of mixtures formulated within CIT as the first approximation of a more complex model formulated within EIT. However, probably the most promising approach is the framework of GENERIC, see Refs. [12, 14, 27], since it is capable to take into account the complexity of multi-level description necessary in modeling mixtures containing polymers, see for example Ref. [1]. Let us now turn to the theory of mixtures itself.

Balance of mass can be formulated as

$$\frac{\partial \rho_\alpha}{\partial t} = -\text{div}(\rho_\alpha \mathbf{v}_\alpha) + \hat{\rho}_\alpha, \quad \sum_\alpha \hat{\rho}_\alpha = 0 \quad (1)$$

where ρ_α , \mathbf{v}_α and $\hat{\rho}_\alpha$ are density, velocity and production of species α , respectively. Mass fractions are denoted by $w_\alpha = \frac{\rho_\alpha}{\rho}$ where ρ is the total density $\rho = \sum_\alpha \rho_\alpha$. Diffusive velocity and diffusive flux of the species are defined as

$$\mathbf{v}_{D\alpha} = \mathbf{v}_\alpha - \mathbf{v}, \quad \mathbf{j}_{D\alpha} = \rho_\alpha \mathbf{v}_{D\alpha} \quad (2)$$

respectively where \mathbf{v} stands for the center of mass or barycentric velocity $\mathbf{v} = \sum_\alpha \mathbf{v}_\alpha w_\alpha$.

Balance of linear momentum of species α can be formulated as

$$\frac{\partial \rho_\alpha \mathbf{v}_\alpha}{\partial t} = -\text{div}(\rho_\alpha \mathbf{v}_\alpha \otimes \mathbf{v}_\alpha) + \text{div} \mathbf{t}_\alpha^T + \rho_\alpha \mathbf{F}_\alpha + \hat{\rho}_\alpha \quad (3)$$

where \mathbf{t}_α , \mathbf{F}_α and $\hat{\rho}_\alpha$ stand for partial Cauchy stress tensor of species α , external force exerted on species α and internal transfer of momentum from other species, also called momentum

production rate, respectively. Since no momentum is created by interactions between species, we have $\sum_{\alpha} \hat{p}_{\alpha} = 0$. We suppose that external forces are potential, i.e. $\mathbf{F}_{\alpha} = -\nabla\varphi_{\alpha}$. The total Cauchy stress tensor and the total force are defined as

$$\mathbf{t} = \sum_{\alpha} \mathbf{t}_{\alpha} - \sum_{\alpha} \rho_{\alpha} \mathbf{v}_{D\alpha} \otimes \mathbf{v}_{D\alpha}, \quad \mathbf{F} = \sum_{\alpha} w_{\alpha} \mathbf{F}_{\alpha} \quad (4)$$

respectively. Partial Cauchy stress tensors are assumed to be symmetric, i.e. $\mathbf{t}_{\alpha}^T = \mathbf{t}_{\alpha}$. Dissipative part of the Cauchy stress tensor is defined as $\mathbf{t}_{dis} = \mathbf{t} + p\mathbf{I}$ where p is pressure.

Balance of total energy can be formulated as

$$\begin{aligned} \frac{\partial}{\partial t} \sum_{\alpha} \rho_{\alpha} \left(\frac{\mathbf{v}_{\alpha}^2}{2} + \varepsilon_{\alpha} + \varphi_{\alpha} \right) = \\ - \operatorname{div} \left(\sum_{\alpha} \rho_{\alpha} \mathbf{v}_{\alpha} \left(\frac{\mathbf{v}_{\alpha}^2}{2} + \varepsilon_{\alpha} + \varphi_{\alpha} \right) \right) - \\ - \operatorname{div} \left(\mathbf{j}_q - \sum_{\alpha} \mathbf{t}_{\alpha}^T \cdot \mathbf{v}_{\alpha} \right) + \sum_{\alpha} \rho_{\alpha} \frac{\partial \varphi_{\alpha}}{\partial t} \end{aligned} \quad (5)$$

where ε_{α} is internal energy of species α in the frame of reference of the species itself. The last term in the latter equation represents the change of energy of the material point caused by variation of external force fields. Flux of total energy is then

$$\mathbf{j}_{en} = \mathbf{j}_q + \sum_{\alpha} \rho_{\alpha} \mathbf{v}_{\alpha} \cdot \left(\left(\frac{1}{2} \mathbf{v}_{\alpha}^2 + \varepsilon_{\alpha} + \varphi_{\alpha} \right) \mathbf{I} - \frac{\mathbf{t}_{\alpha}}{\rho_{\alpha}} \right) \quad (6)$$

Internal energy is defined as

$$\rho u = \sum_{\alpha} \rho_{\alpha} \varepsilon_{\alpha} - \frac{1}{2} \rho \mathbf{v}^2 - \sum_{\alpha} \rho_{\alpha} \varphi_{\alpha} \quad (7)$$

and it's balance equation can be obtained straightforwardly from the previous balance equations, see Ref. [28] for details.

Gibbs relation can be expressed as

$$\frac{Ds}{Dt} = \frac{1}{T} \frac{Du}{Dt} + \frac{p}{T} \frac{D}{Dt} \frac{1}{\rho} - \sum_{\alpha} \frac{\mu_{\alpha}}{T} \frac{Dw_{\alpha}}{Dt} \quad (8)$$

where temperature, pressure and chemical potentials were identified as the corresponding derivatives of local equilibrium entropy.

Combining Eq. (8), balance of internal energy and some equilibrium thermodynamic relations following from the assumption of local thermodynamic equilibrium, see Ref. [28] for details, we arrive at the balance of entropy

$$\frac{\partial \rho s}{\partial t} = -\operatorname{div} \mathbf{j}_{s,tot} + \sigma_s \quad (9)$$

where entropy flux and entropy production rate are

$$\mathbf{j}_{s,tot} = \rho s \mathbf{v} + \mathbf{j}_s \quad (10)$$

$$\mathbf{j}_s = \frac{\mathbf{j}_q}{T} + \sum_{\alpha} \mathbf{j}_{D\alpha} s_{\alpha} - \frac{1}{T} \sum_{\alpha} (\mathbf{t}_{\alpha}^T + p v_{\alpha} \rho_{\alpha} \mathbf{I}) \cdot \mathbf{v}_{D\alpha} \quad (11)$$

$$\begin{aligned} \sigma_s = & -\frac{1}{T} \mathbf{j}_s \cdot \nabla T - \sum_{\alpha} \frac{1}{T} \mathbf{j}_{D\alpha} \cdot \nabla \tilde{\mu}_{\alpha} + \\ & + \frac{1}{T} \mathbf{t}_{dis} : \mathbf{d} + \sum_r \frac{1}{T} \dot{\xi}_r \tilde{A}_r \end{aligned} \quad (12)$$

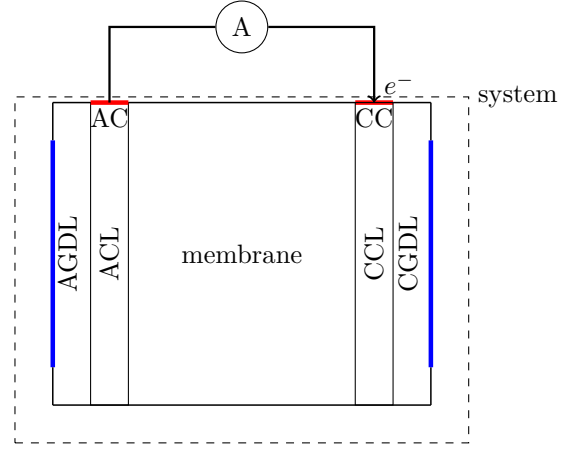


Figure 1. A scheme of a PEM fuel cell for better understanding of the acronyms.

where $\tilde{\mu}_{\alpha}$ and \tilde{A}_r are electrochemical potential of species α and electrochemical affinity of reaction r , respectively, defined as

$$\tilde{\mu}_{\alpha} = \mu_{\alpha} + \varphi_{\alpha} \quad \tilde{A}_r = -\sum_{\alpha} v_{\alpha r} \tilde{\mu}_{\alpha} \quad (13)$$

where $v_{\alpha r}$ is the stoichiometric coefficient of species α in reaction r . $\dot{\xi}_r$ in Eq. (12) is the rate of reaction r . The second law of thermodynamics is expressed as

$$\sigma_s \geq 0 \quad (14)$$

For a mixture of ideal gases subject to external forces and for a single-species non-viscous continuum the total flux of energy (6) can be simplified to

$$\mathbf{j}_{en} = \mathbf{j}_q + \sum_{\alpha} \rho_{\alpha} \mathbf{v}_{\alpha} \left(\frac{1}{2} \mathbf{v}_{\alpha}^2 + h_{\alpha} + \varphi_{\alpha} \right) \quad (15)$$

where h_{α} is partial specific enthalpy¹. Moreover, for such mixtures entropy flux (11) simplifies to

$$\mathbf{j}_s = \frac{\mathbf{j}_q}{T} + \sum_{\alpha} \mathbf{j}_{D\alpha} s_{\alpha} \quad (16)$$

From the assumption of local thermodynamic equilibrium it follows that

$$h_{\alpha} = \left(\frac{\partial H}{\partial m_{\alpha}} \right)_{T,p,m_{\beta \neq \alpha}} = u_{\alpha} + p v_{\alpha} = T s_{\alpha} + \mu_{\alpha} \quad (17)$$

3 EFFICIENCY OF FUEL CELLS

For clarity of terminology the thermodynamic analysis is formulated for PEMFC. The results, however, hold also for other kinds of fuel cells, e.g. SOFC. In figure 1 we show a scheme of a PEM fuel cell. The fuel cell is composed of the following parts: anode gas diffusion layer (AGDL), through which

¹Of course, in case of single-species continuum the summation is not present.

hydrogen and water flow, cathode gas diffusion layer (CGDL), through which oxygen and water flow, an anode, where hydrogen splits into protons and electrons, a cathode, where oxygen reacts with protons and electrons forming water, and a membrane, through which protons are transported from the anode to the cathode. Hereafter, these parts together, represented by the area enclosed in the dashed frame in figure 1, are referred to as the system. The system is denoted by V and its boundary by ∂V . We assume that the fuel cell is in a stationary state.

In order to evaluate efficiency of the fuel cell, fluxes of energy and entropy into and out of the system are analyzed. Energy and entropy flow into and out of the system through AGDL, CGDL, through the conductive part of the anode (CA) from which electrons leave the system and through the conductive part of the cathode (CC) where electrons re-enter the system.

Fluxes of enthalpy, Gibbs energy and conductive heat into the system are defined as

$$\Delta H = - \int_{\partial V} \sum_{\alpha \neq e^-} h_{\alpha} \rho_{\alpha} \mathbf{v}_{\alpha} \cdot d\mathbf{S} \quad (18)$$

$$\Delta G = - \int_{\partial V} \sum_{\alpha \neq e^-} \mu_{\alpha} \rho_{\alpha} \mathbf{v}_{\alpha} \cdot d\mathbf{S} \quad (19)$$

$$\Delta Q = - \int_{\partial V} \mathbf{j}_q \cdot d\mathbf{S} \quad (20)$$

respectively. The fluxes are positive when flowing into the system. Note that electrons are excluded from the fluxes. They are analyzed separately since they are closely related to electrical work.

Electrical work extracted from the fuel cell ΔW_{el} is the flux of total energy carried by electrons through boundary of the system, i.e. through AC and CC. Therefore, from Eqs. (15) and (17) it follows² that the electrical work can be expressed as

$$\Delta W_{el} = \frac{I}{F} M_{e^-} (\mu_{e^-}^a - \mu_{e^-}^c) + I(\Phi^c - \Phi^a) + \frac{I}{F} (T^a s_{e^-}^a - T^c s_{e^-}^c) \quad (21)$$

where I denotes the total electric current flowing from the cathode to the anode. Obviously, the first two terms on the right hand side of the latter equation represent the standard electrical work. The last term is related to thermoelectric power caused by possibly different temperatures at AC and CC. However, it was shown in Ref. [28] that the term is usually quite negligible.

Stationary balance of total energy³ gives

$$0 = \int_{\partial V} \mathbf{j}_{en} \cdot d\mathbf{S} \quad (22)$$

Using definitions (18), (20) and (21) and expression for energy flux in Eq. (15), we obtain

$$\Delta W_{el} = \Delta Q + \Delta H \quad (23)$$

which is a well known formula, used for example in Ref. [3].

In the stationary state local balance of entropy (9) gives

$$\text{div} \mathbf{j}_{s,tot} = \sigma_s \quad (24)$$

Flux of entropy can be generally expressed, according to Eq. (11), as

$$\mathbf{j}_s = \frac{1}{T} \mathbf{j}_q + \sum_{\alpha} s_{\alpha} \mathbf{j}_{D\alpha} + \mathbf{j}'_s \quad (25)$$

where \mathbf{j}'_s disappears at ∂V in our case. Therefore, Eq. (16) describes entropy flux at the boundary. Hence, we get for the flux of heat into the system

$$\begin{aligned} \Delta Q &= \int_{\partial V} \left(-T \mathbf{j}_{s,tot} + T \sum_{\alpha} \rho_{\alpha} \mathbf{v}_{\alpha} s_{\alpha} \right) \cdot d\mathbf{S} \\ &= \Delta G - \Delta H + \int_{\partial V} -T \mathbf{j}_{s,tot} \cdot d\mathbf{S} + \\ &\quad + \frac{I}{F} (T^a s_{e^-}^a - T^c s_{e^-}^c) \end{aligned} \quad (26)$$

where Eq. (17) was used. From the stationary balance of entropy (24) we get

$$\begin{aligned} \int_{\partial V} -T \mathbf{j}_{s,tot} \cdot d\mathbf{S} &= - \int_V \text{div}(T \mathbf{j}_{s,tot}) dV = \\ &= \int_V -\mathbf{j}_{s,tot} \cdot \nabla T dV - \Pi \end{aligned} \quad (27)$$

where dissipation in the system was introduced as

$$\Pi = \int_V T \sigma_s dV \quad (28)$$

Using relations (23), (26) and (27), we obtain the final formula for electrical work

$$\begin{aligned} \Delta W_{el} &= \Delta G - \Pi + \frac{I}{F} M_{e^-} (T^a s_{e^-}^a - T^c s_{e^-}^c) - \\ &\quad - \int_V \mathbf{j}_{s,tot} \cdot \nabla T dV \end{aligned} \quad (29)$$

The first term on the right hand side of the latter equation expresses that electrical work is produced from flux of Gibbs energy into the system. The second term expresses that entropy production rate inevitably lowers the electrical work produced. The next to last term shows a direct contribution of thermoelectric effects and the last term contains dissipation due to temperature gradient, see the formula for entropy production rate (12),

$$\int_V -\mathbf{j}_s \cdot \nabla T dV \quad (30)$$

Therefore, this part of entropy production rate does not reduce the produced electrical work since it cancels with the same term in the dissipation term.

Efficiency of fuel cells is defined as, see for example Ref. [3],

$$\eta = \frac{\Delta W_{el}}{\Delta H} \quad (31)$$

²We assume that electrons can be described with the electron gas approximation, see §57 in book [22].

³We neglect kinetic energy since it is negligible compared to other kinds of energy flowing into the system.

Therefore, using the formula for electrical work (29), we obtain

$$\begin{aligned}
\eta &= \frac{\Delta G}{\Delta H} \frac{\Delta W_{el}}{\Delta G} = \\
&= \eta_c \left(1 - \frac{\Pi}{\Delta G} \right) - \frac{\eta_c}{\Delta G} (T^c s_{e^-}^c - T^a s_{e^-}^a) \frac{I}{F} \\
&\quad - \frac{\eta_c}{\Delta G} \int_V \mathbf{j}_{s,tot} \cdot \nabla T dV = \\
&= \eta_c \left(1 - \eta_{e^-} - \frac{1}{\Delta G} \int_V \left(\rho_{sv} \cdot \nabla T - \right. \right. \\
&\quad \left. \left. - \sum_{\alpha} \mathbf{j}_{D\alpha} \cdot \nabla \tilde{\mu}_{\alpha} + \mathbf{t}_{dis} : \mathbf{d} + \sum_r \dot{\xi}_r \tilde{A}_r \right) dV \right) \quad (32)
\end{aligned}$$

where the conversion efficiency and change of efficiency due to entropy of electrons were defined as

$$\eta_c = \frac{\Delta G}{\Delta H}, \quad \eta_{e^-} = \frac{(T^a s_{e^-}^a - T^c s_{e^-}^c) \frac{I}{F}}{\Delta G} \quad (34)$$

respectively.

Conversion efficiency η_c can be calculated from definitions (19) and (18) using thermodynamic tables, see for example book [33]. It can be approximated as 80% at 80°C and standard pressure as shown in Barbir's book [3]. The last three terms in Eq. (32) are not standard and they are referred to as the new terms later in this work. Their effects on efficiency are discussed in section 5.

The second law of thermodynamics, see Eq. (14), dictates that $\Pi \geq 0$. Therefore, dissipation inevitably reduces efficiency of fuel cells.

4 COMPARISON OF THE STANDARD AND THE PROPOSED THEORY

The standard theory is based on the Gouy-Stodola theorem as has been already said in the introduction. The purpose of this section is to clarify the possible advantages of the new theory.

What does optimization of fuel cells mean, in fact? Recalling the definition of efficiency (31), the optimization is a way of maximization of the electrical work obtained from conversion of the fuel to the exhausts, i.e. in hydrogen fuel cells from combustion of hydrogen. From the thermodynamic point of view, the conversion can be characterized by ΔH and ΔG . Therefore, the optimization means maximizing the gained electrical work for given ΔH and ΔG or, recalling Eq. (32), maximizing η keeping ΔH and ΔG constant.

Let us now have a closer look at formula (32). Obviously, entropy production rate reduces the efficiency since if it were zero everywhere in the system, the dissipation term, which is always non-negative, would disappear. This is a common point of both the standard and the new theory.

However, as has been said above the optimization means maximizing η while keeping ΔG and η_c constant⁴. If we set the dissipation to zero, there is still the last term in (32), which affects the efficiency. Hence, the efficiency could be further enhanced by optimization of this term. Moreover, the same holds for the next to last term in Eq. (32) as well but since it is negligible, we do not take it into account.

Hence, from Eq. (33) it follows that if we neglect the η_{e^-} term and the term with barycentric velocity, we should minimize the functional

$$\int_V - \sum_{\alpha} \mathbf{j}_{D\alpha} \cdot \nabla \tilde{\mu}_{\alpha} + \mathbf{t}_{dis} : \mathbf{d} + \sum_r \dot{\xi}_r \tilde{A}_r dV \quad (35)$$

rather than entropy production rate itself.

Of course, this functional should be understood as the first approximation of a more precise expression since we are restricted to the area of validity of CIT and the theory of mixtures formulated within. More microscopic levels of description should be, therefore, taken into account to obtain more accurate results for the efficiency. Hence, optimization of fuel cells is an area where a more precise framework, for example the GENERIC framework in Ref. [1], is needed.

5 POSSIBLE ENHANCEMENTS OF EFFICIENCY

In this section we analyze influence of the new terms on efficiency of PEMFC and SOFC. To avoid repetition we only summarize results of a previous analysis provided in Ref. [28], where details can be found. Estimates of effects of the new terms in Eq. (32) on efficiency of fuel cells are based on the thermodynamic analysis of Kjelstrup and Røsjorde in article [20]. We also evaluate the effects for a concrete set of conditions considered in the paper. For SOFC our analysis is based on works of Sciacovelli [31, 32].

5.1 PEM FC

The first new term in formula for efficiency (32)

$$- \eta_c \frac{\frac{I}{F} (T^c s_{e^-}^c - T^a s_{e^-}^a)}{\Delta G} \quad (36)$$

describes contribution of entropy of electrons transported along when electric current leaving and re-entering the fuel cell. It's contribution to the final efficiency is, however, negligible⁵ as has been shown in Ref. [28].

The second new term⁶ in (32) is

$$- \frac{\int_V \frac{\mathbf{j}_q}{T} \cdot \nabla T dV}{\Delta G} - \frac{\int_V \sum_{\alpha} \rho_{\alpha} s_{\alpha} \mathbf{v}_{\alpha} \cdot \nabla T dV}{\Delta G} \quad (37)$$

Conductive heat flux affects the efficiency by 0.2%. Calculating partial specific entropy of gaseous oxygen, hydrogen, water and protons at 80°C, the effect of flux of entropy in gradient of temperature in Eq. (37) to the efficiency can be estimated as 0.1%, see Ref. [28] for details.

In summary, the new terms in (32) are quite negligible in PEM fuel cells compared to the dissipation term. Therefore, entropy production rate is the main cause of efficiency losses in PEM fuel cells and the new method and the standard method are equivalent in this case. This is not true for SOFC anymore as we show in section 5.2.

⁴Recall that η_c is a function of ΔG and ΔH , see Eq. (34).

⁵approximately 10⁻³%

⁶For simplicity, the additional entropy flux \mathbf{j}'_s is neglected.

5.2 SOFC

In this section we summarize effects of the new terms in Eq. (32) on efficiency of SOFC. Generally, the effect is higher than in PEMFC because temperature gradients are steeper in SOFC. Thermodynamic quantities will be evaluated at temperature 880°C to correspond with [31]. At that temperature the corresponding conversion efficiency becomes approximately $\eta_c \approx 74\%$.

Usually, the biggest part of a SOFC is the anode. Let us now summarize effects of the new terms in the anode. Contribution of oxygen to the last term in Eq. (37) was estimated as 2%. The analogical contribution of hydrogen was estimated as 3% and the contribution of water vapor as 4%. Moreover, oxygen anions diffuse through the solid part of the anode. Partial molar entropy of oxygen anions in the anode was estimated using Refs. [9, 2, 18, 30]. Effect of oxygen anions on the efficiency was then estimated as 0.7%. The effect of conductive heat flux in Eq. (37) was estimated using Refs. [5, 31] as 0.1%. See Ref. [28] for details.

As well as in PEMFC the effect of entropy of electrons η_{e^-} is negligible in SOFC.

In summary, the new terms in (32) affect the total efficiency by several per cent. Therefore, the new method of evaluation of fuel cell efficiency differs from the standard method in case of SOFC, and we suggest that the new method should be used instead of the standard method in that case, i.e. functional (35) should be minimized instead of entropy production rate.

6 CONCLUSIONS

In this work we discussed the meaning of optimization of hydrogen fuel cells, see section 4. A formula for efficiency compatible with the meaning of optimization, which has been derived in Ref. [28] using classical irreversible thermodynamics of mixtures, was presented in sections 2 and 3. The formula was then compared with the standard theory based on the Gouy-Stodola theorem, which leads to the procedure of entropy production rate minimization.

The new theory gives different results than the standard theory in case of solid oxide fuel cells while it is equivalent to the standard theory in case of polymer electrolyte membrane fuel cells, see section 5. In summary, we propose that the new theory should be used in optimization of solid oxide fuel cells instead of the standard theory. In other words, functional (35) should be minimized instead of entropy production rate in the fuel cells.

ACKNOWLEDGEMENT

The result was developed within the CENTEM project, reg. no. CZ.1.05/2.1.00/03.0088, co-funded by the ERDF as part of the Ministry of Education, Youth and Sports OP RDI programme.

Author M.P. was partially supported by the student project of the Faculty of Mathematics and Physics of Charles University in Prague No. 267310.

NOMENCLATURE

A cross section area of the anode [m^2]
 \tilde{A}_r electrochemical affinity of reaction r [J kg^{-1}]
 \mathbf{d} symmetric velocity gradient [s^{-1}]
 \mathbf{F} total external body force [N kg^{-1}]

F Faraday constant [C mol^{-1}]
 \mathbf{F}_α external body force exerted on species α [N kg^{-1}]
 h_α partial specific enthalpy [J kg^{-1}]
 I total electric current passing through the system [A]
 $\mathbf{j}_{D\alpha}$ diffusion flux of species α [$\text{kg m}^{-2} \text{s}^{-1}$]
 \mathbf{j}_{en} flux of total energy [$\text{J m}^{-2} \text{s}^{-1}$]
 \mathbf{j}_s flux of entropy [$\text{JK}^{-1} \text{m}^{-2} \text{s}^{-1}$]
 $\mathbf{j}_{s,tot}$ total flux of entropy [$\text{JK}^{-1} \text{m}^{-2} \text{s}^{-1}$]
 \mathbf{j}_q conductive heat flux [$\text{J m}^{-2} \text{s}^{-1}$]
 $\frac{D_\bullet}{Dt}$ material time derivative [s^{-1}]
 p pressure [Pa]
 p_α partial pressure of species α [Pa]
 \hat{p}_α production of momentum of species α due to interactions with other species [$\text{kg m}^{-2} \text{s}^{-2}$]
 s specific entropy [$\text{JK}^{-1} \text{kg}^{-1}$]
 s_α partial specific entropy of species α [$\text{J kg}^{-1} \text{K}^{-1}$]
 $s_{e^-}^a$ partial specific entropy of electrons in the anode [$\text{JK}^{-1} \text{mol}^{-1}$]
 $s_{e^-}^c$ partial specific entropy of electrons in the cathode [$\text{JK}^{-1} \text{mol}^{-1}$]
 V total volume [m^3]
 \mathbf{v}_α velocity of species α [m s^{-1}]
 \mathbf{v} barycentric velocity [m s^{-1}]
 v_α partial specific volume of species α [$\text{m}^3 \text{kg}^{-1}$]
 $\mathbf{v}_{D\alpha}$ diffusive velocity of species α [m s^{-1}]
 T temperature [K]
 \mathbf{t} total Cauchy stress tensor [J m^{-3}]
 \mathbf{t}_{dis} dissipative part of the Cauchy stress tensor [Pa]
 \mathbf{t}_α partial Cauchy stress tensor of species α [J m^{-3}]
 u total specific internal energy [J kg^{-1}]
 u_α partial specific internal energy of species α [J kg^{-1}]
 w_α mass fraction of species α [1]
 ΔG total flux of Gibbs free energy into the system [J s^{-1}]
 ΔH total flux of enthalpy into the system [J s^{-1}]
 ΔQ total flux of heat into the system [J s^{-1}]
 ΔW_{el} electrical work extracted from the system [J s^{-1}]
 ε_α specific internal energy of species α with respect to its own frame of reference [J kg^{-1}]
 ε_F Fermi energy [J]
 η total efficiency [1]
 η_c conversion efficiency [1]
 η_{e^-} change of efficiency due to entropy of electrons [1]
 μ_α chemical potential of species α [J kg^{-1}]
 $\tilde{\mu}_\alpha$ electrochemical potential of species α [J kg^{-1}]
 $\nu_{\alpha r}$ stoichiometric coefficient of species α in reaction r [1]
 ξ_r rate of chemical reaction r [$\text{kg m}^{-3} \text{s}^{-1}$]
 Π total dissipation [J s^{-1}]
 ρ overall density [kg m^{-3}]
 ρ_α density of species α [kg m^{-3}]
 $\hat{\rho}_\alpha$ production of species α [$\text{kg s}^{-1} \text{m}^{-3}$]
 \sum_α sum over all species
 σ_s entropy production rate [$\text{JK}^{-1} \text{m}^{-3} \text{s}^{-1}$]
 Φ electric potential [V]
 φ_α potential of external force \mathbf{F}_α [J kg^{-1}]
 χ_g characteristic function of gas phase [1]
 χ_l characteristic function of liquid phase [1]

REFERENCES

- [1] A. El Afif and M. Grmela. Non-fickian mass transport in polymers. *Journal of Rheology*, 46(3):591–628, 2002.
- [2] E. Ahlgren and F. W. Poulsen. Thermoelectric power of

- ysz. *Solid State Ionics*, 70-71, Part 1(0):528 – 532, 1994.
- [3] F. Barbir. *Pem Fuel Cells: Theory And Practice*. Academic Press Sustainable World Series. Elsevier Acad. Press, 2005.
- [4] A. Bejan. Method of entropy generation minimization, or modeling and optimization based on combined heat transfer and thermodynamics. *Revue Générale de Thermique*, 35(418-419):637 – 646, 1996.
- [5] R. Bove and S. Ubertini. *Modeling Solid Oxide Fuel Cells: Methods, Procedures and Techniques*. Fuel Cells and Hydrogen Energy Series. Springer Science+Business Media B.V., 2008.
- [6] R. M. Bowen. The thermochemistry of a reacting mixture of elastic materials with diffusion. *Archive for Rational Mechanics and Analysis*, 34:97–127, 1969.
- [7] R. M. Bowen. *Continuum Physics*, volume 3. Academic Press, New York, 1976.
- [8] R.M. Bowen and J.C. Wiese. Diffusion in mixtures of elastic materials. *International Journal of Engineering Science*, 7(7):689 – 722, 1969.
- [9] V. N. Chebotin, S. L. Fridman, and S. F. Pal'ghev (translated from Russian). *Elektrokhimiya*, 6:1300–1304, 1970.
- [10] S. R. de Groot and P. Mazur. *Non-equilibrium Thermodynamics*. Dover Publications, New York, 1984.
- [11] J. A. del Río and M. L. de Haro. Extended irreversible thermodynamics as framework for transport phenomena in porous media. *Transport in Porous Media*, 9(3):207–221, 1992.
- [12] I. E. Dzyaloshinskii and G.E. Volovick. *Phys. (NY)*, 125:67–97, 1980.
- [13] G. Gouy. *J. Phys.*, 8(501), 1889.
- [14] M. Grmela and H. C. Öttinger. Dynamics and thermodynamics of complex fluids. i. development of a general formalism. *Phys. Rev. E*, 56:6620–6632, Dec 1997.
- [15] M. E. Gurtin. On the thermodynamics of chemically reacting fluid mixtures. *Archive for Rational Mechanics and Analysis*, 43:198–212, 1971.
- [16] K. Hutter and K. Jöhnk. *Continuum Methods of Physical Modeling: Continuum Mechanics, Dimensional Analysis, Turbulence*. Physics and Astronomy Online Library. Springer, 2004.
- [17] D. Jou, J. Casas-Vázquez, and G. Lebon. *Extended Irreversible Thermodynamics*. Springer-Verlag, New York, 4th edition, 2010.
- [18] S. Kjelstrup and D. Bedeaux. *Non-Equilibrium Thermodynamics of Heterogeneous Systems*. Series on Advances in Statistical Mechanics. World Scientific, 2008.
- [19] S. Kjelstrup, D. Bedeaux, and E. Johannessen. *Non-Equilibrium Thermodynamics for Engineers*. Science and culture series (Singapore).: Physics. World Scientific, 2010.
- [20] Signe Kjelstrup and Audun Røsørde. Local and total entropy production and heat and water fluxes in a one-dimensional polymer electrolyte fuel cell. *The Journal of Physical Chemistry B*, 109(18):9020–9033, 2005. PMID: 16852075.
- [21] V. Klika. A guide through available mixture theories for applications. *Critical Reviews in Solid State and Material Science*, 2013. Accepted Manuscript.
- [22] L.D. Landau and E.M. Lifschitz. *Statistical physics*. Number pt. 1 in Course of theoretical physics. Pergamon Press, 1969.
- [23] G. Lebon, T. Desaive, and P. Dauby. A unified extended thermodynamic description of diffusion, thermodynamic diffusion, suspensions, and porous media. *Journal of Applied Mechanics*, 73(1):16–20, 2006.
- [24] G. Lebon, D. Jou, and J.C. Vázquez. *Understanding Non-Equilibrium Thermodynamics: Foundations, Applications, Frontiers*. SpringerLink: Springer e-Books. Springer London, Limited, 2008.
- [25] J. Málek and K.R. Rajagopal. A thermodynamic framework for a mixture of two liquids. *Nonlinear Analysis: Real World Applications*, 9(4):1649 – 1660, 2008.
- [26] I. Müller and T. Ruggeri. *Rational extended thermodynamics*. Springer tracts in natural philosophy. Springer, 1998.
- [27] H. C. Öttinger and M. Grmela. Dynamics and thermodynamics of complex fluids. ii. illustrations of a general formalism. *Phys. Rev. E*, 56:6633–6655, Dec 1997.
- [28] M. Pavelka and F. Maršík. Detailed thermodynamic analysis of polymer electrolyte membrane fuel cell efficiency. *International Journal of Hydrogen Energy*, 38:7102–7113, 2013.
- [29] I. Prigogine. *Thermodynamics of Irreversible Processes*. Thomas, 1955.
- [30] S. K. Ratkje and Y. Tomii. Transported entropy in zirconia with 3 to 12 mole percent yttria. *Journal of The Electrochemical Society*, 140(1):59–66, 1993.
- [31] A. Sciacovelli. Entropy generation analysis in a monolithic-type solid oxide fuel cell (sofc). *Energy*, 34(7):850 – 865, 2009.
- [32] A. Sciacovelli. Thermodynamic optimization of a monolithic-type solid oxide fuel cell. *International Journal of Thermodynamics*, 13(3):95–103, 2010.
- [33] J.M. Smith, H. Van Ness, and M. Abbott. *Introduction to Chemical Engineering Thermodynamics*. McGraw-Hill chemical engineering series. McGraw-Hill Companies, Incorporated, 2004.
- [34] A. Stodola. *Steam and Gas Turbines*. McGraw-Hill, New York, 1910.
- [35] C. Truesdell. *Rational thermodynamics: a course of lectures on selected topics*. McGraw-Hill series in modern applied mathematics. McGraw-Hill, 1969.
- [36] K. Wilmański. *Continuum Thermodynamics, Part 1: Foundations*. Series on Advances in Mathematics for Applied Sciences. World Scientific, 2008.

EXERGY BASED METHODS FOR ECONOMIC AND ENVIRONMENTAL ANALYSIS APPLIED TO A 320 MW COMBINED CYCLE POWER PLANT

Matteo Rocco*, Claudia Toro°

*Politecnico di Milano, Department of Energy, via Lambruschini 4, Milan, Italy

°Università di Roma "Sapienza", Department of Mechanical and Aerospace Engineering, via Eudossiana 18, Rome, Italy

ABSTRACT

In the last decades, the growing scarcity of non-renewable resources led analysts and researchers to sharpen Second Law analysis methods in order to understand how to minimize the consumption of natural resources on the part of energy conversion systems. Thermoeconomics demonstrates to be a proper and promising framework to evaluate and optimize exergetic and economic costs of energy systems products. Understanding the relation between the economic cost and its natural resource counterpart is likely to be a key factor in future research activities.

This paper presents an Exergy and Thermoeconomic analysis of a 320 MW Dual Pressure Combined Cycle Plant, aimed to identify the optimal design configurations of the system with respect to its specific objective functions: second law efficiency, economic cost and natural resource consumption cost of the generated unit of electric energy. The natural resource consumption of the system is computed according to the Cumulative Exergy Consumption (CExC) method.

The CCPP plant simulations have been performed by using CAMEL-Pro™ Process Simulator and the sensitivity study of the plant behaviour and its optimization as a function of the selected parameters have been developed by using the Proper Orthogonal Decomposition procedure. Our results confirm that the optimal design configuration is strictly dependent on the considered objective function, and helps to investigate the relationship between the thermodynamics, the economics and the resource consumption of the system, thus giving a more comprehensive understanding of its performance from different perspectives.

INTRODUCTION

Combined Cycle Power Plants (CCPPs) are well proven and reliable technology for electricity production. CCPPs are widely used in the Italian grid network and their design and optimization are today more and more relevant.

This paper presents an original implementation of the Thermoeconomics framework for the optimal design analysis of a 320 MW Dual Pressure CCPP. The purpose of the study is to identify the possible optimal design configuration of this system, including thermodynamic, economic and environmental perspectives.

As a first step, modelling and simulation of the system is performed. Secondly, economic and environmental perspectives are assessed performing exergy based specific analyses. Exergy analysis (EA) is used to determine the second law efficiency of the system, whereas Thermoeconomic framework is used to assess both the economic and the environmental costs of the product. In the case study electricity is considered as the unique product of the system. Economic optimal cost of product is assessed with the Thermoeconomic analysis (TA-ECO), finding the best trade-off between investment and operative economic costs [1]. On the other hand, Thermoeconomic analysis is also used to assess, in an environmental cost perspective, the primary exergy consumed in order to produce the system product (TA-EXER). The primary exergy may represent the natural resources consumed [2].

As will be shown, the optimal design configuration is strictly dependent on the considered objective cost function. The paper shows how changing the objective function of the analysis

(efficiency, monetary cost or primary exergy cost) can influence the optimal design of the system, and proposes a key to understanding the relationship between economic and environmental costs of energy systems.

CASE STUDY: DUAL PRESSURE COMBINED CYCLE POWER PLANT

Plant layout and simulation

As a case study, the *Neka* CCPP power plant operative data have been used [3]. The main components of this combined plant are two gas turbines, two air compressors, two HRSGs with a supplementary fired unit (duct burner), one steam turbine and one surface condenser with a seawater cooling system. The total output power is 320 MW, 130MW produced by the steam turbine and 190 MW two gas turbines.

Table 1. CCPP fixed operative parameters.

Parameter	u. m.	Value
Outlet Power	MW	160
Gas Turbine Adiabatic Efficiency	%	87.7
Compressor Adiabatic Efficiency	%	88.0
Steam Turbine Efficiency	%	78.0
Condenser inlet pressure	kPa	14
HRSG Low Pressure	kPa	1029
HRSG High Pressure	kPa	11425
Turbine Inlet Temperature	K	1383
Plant Availability	h/y	2628

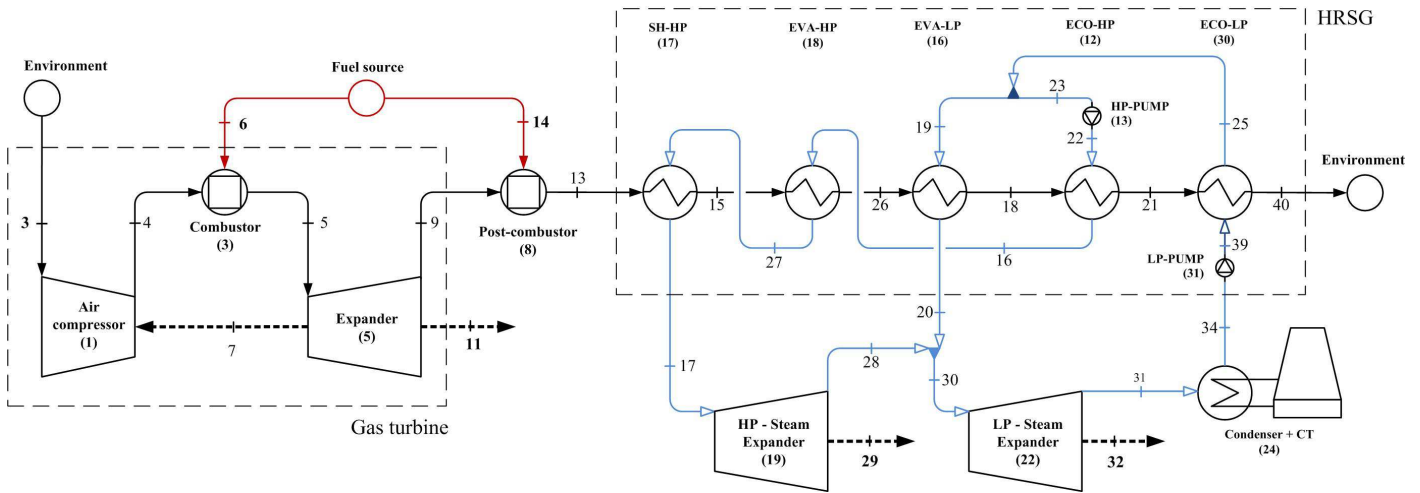


Figure 1. Plant layout.

The power plant was modeled with CAMEL-Pro™ process simulator [4]; its layout consist in two identical blocks, each generating half of the total output: all simulations were performed accordingly for one single block with an output net power of 160 MW. The layout of the simulated plant is reported in Figure 1 and the operative conditions (steady state operation being assumed throughout) are reported in Table 1. The low Load Factor (2628 hours per year) reflects the actual operative conditions of the average Italian CCPPs.

Table 2. Selected design variables and their respective ranges.

Process variables	Symbol [u. m.]	Min. value	Max. value
Air pressure ratio	β_C [-]	10	21
Post-Firing fuel	\dot{m}_{14} [kg/s]	1	2

To proceed with the optimization of the plant, two process variables have been selected: the gas turbine pressure ratio β_C and the duct burner fuel mass flow rate $\dot{m}_{NG,pf}$ (\dot{m}_{14}). Their respective possible ranges of variation are reported in Table 2.

Determination of the plant behavior: Proper Orthogonal Decomposition method (POD)

The sensitivity study of the plant behavior and the optimization with respect to the selected process variables and the objective functions have been developed by using the Proper Orthogonal Decomposition mathematical procedure (POD – RBF). The POD Method is a statistical method that aims to provide a compact representation of the data by projecting the data set into a lower dimensional space. The POD-RBF procedure has been previously tested on the optimization of a simple MSF desalination plant [5] and of a single pressure CCGT [6] plant and the very satisfactory results obtained for these plants suggested extending its application to more complex configurations and to different processes. Moreover, the POD enables designers to extrapolate functions linking the variables to be optimized with the selected process variables.

More details about POD as well as an introductory mathematical explanation of its conceptual basis are provided in [7]. In the case study here presented the objective functions are minimized considering the constraints listed in Table 3.

Table 3. Constraints for plant operation.

Parameter [u. m.]	Device / Pipe no.	Lower limit	Higher limit
$\Delta T_{pp,LP}$ [°C]	16	5	35
$\Delta T_{pp,HP}$ [°C]	18	5	35
$\Delta T_{ap,LP}$ [°C]	16,30	10	-
$\Delta T_{ap,HP}$ [°C]	17,18,12	10	-
T_{40} [°C]	40	100	-

EXERGY BASED METHODS ANALYSES AND OPTIMIZATION

Thermodynamic evaluation: exergy analysis

As stated in [2], in order to perform the exergy analysis for a generic energy system, it is convenient to set up its productive structure, or functional diagram. Using the physical model of the system as reference and grouping all the energy and material flows for every component of the system, and therefore for the whole system, the productive structure is completed according to the Resources–Product–Wastes (R/P/I) criterion. For the generic j -th system component, exergy balance is:

$$\dot{\mathbf{E}}_{R,j} = \dot{\mathbf{E}}_{P,j} + \dot{\mathbf{E}}_{I,j} + \dot{\mathbf{E}}_{D,j} \quad (1)$$

For every system consisting of n components connected by m streams, the exergy balance system can be expressed in matrix form by (2), where \mathbf{A} is the $n \times m$ incidence matrix of the system, defined in [2]:

$$\mathbf{A}_{(n \times m)} \cdot \mathbf{E}_{(m \times 1)} = \mathbf{E}_{D,(n \times 1)} \quad (2)$$

For each component of the system, exergy efficiency is defined as the ratio between exergy of products over exergy of the resources and it represents a criterion for evaluating the thermodynamic performance of the component. The objective of the exergy analysis is to find the combination of the selected process variables β_C and \dot{m}_{14} that provides the highest exergy efficiency for the whole system, defined as (3).

$$\eta_{II,tot} = \frac{\dot{\mathbf{E}}_{P,tot}}{\dot{\mathbf{E}}_{F,tot}} = \frac{\dot{W}_{el,net}}{(\dot{m}_6 + \dot{m}_{14}) \cdot \mathbf{e}_{NG}} \quad (3)$$

This goal has been reached applying the POD procedure on simulated plant results, which allows extrapolating the exergy efficiency (3) as a function of the selected process variables β_C and \dot{m}_{14} . Figure 2 shows the exergy efficiency as function of these process variables, normalized within their own range.

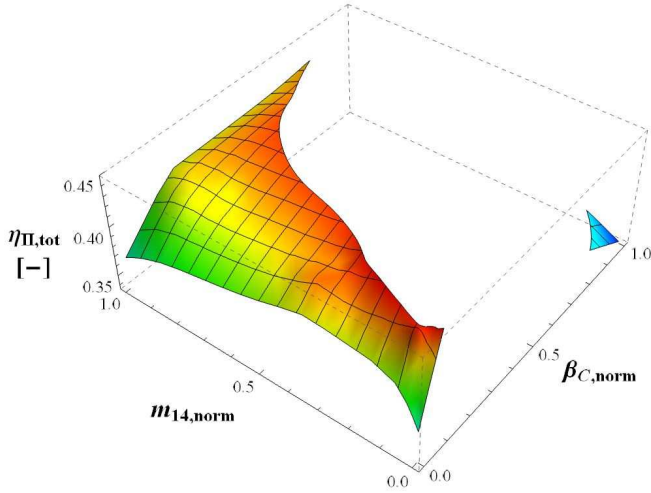


Figure 2. Overall plant exergy efficiency map.

For the plant given in the case study, the best exergy efficiency results around 44.8 %, corresponding to $\beta_C = 14.36$ and $\dot{m}_{14} = 1.6$ kg/s.

Thermoeconomic design analysis for Economic cost evaluation and optimization (TE-ECO)

According to productive structure adopted for exergy analysis, the economic cost rate balances for the i -th plant component is:

$$\dot{C}_{eco,R,i} + \dot{Z}_{eco,i} = \dot{C}_{eco,P,i} + \dot{C}_{eco,I,i} \quad (4)$$

Where $\dot{C}_{eco,i}$ represent the economic cost rate associated with each exergy transfer, and $\dot{Z}_{eco,i}$ represents the sum of capital investment, operating and maintenance cost rates for the i -th system component. Exergy costing principle (5) allows to compute the economic cost rate of every j -th material or energy flow entering the i -th system component as the product between its average monetary cost per unit of exergy $c_{eco,j}$ (in €/kJ) and its exergy content:

$$\dot{C}_{eco,j} = c_{eco,j} \cdot \dot{\mathbf{E}}_j \quad (5)$$

The complete thermoeconomic system can be rewritten in matrix form as follows:

$$\mathbf{A}_{(n \times m)} \cdot \mathbf{C}_{eco,(m \times 1)} + \mathbf{Z}_{eco,(n \times 1)} = \mathbf{0}_{(n \times 1)} \quad (6)$$

If the considered system has n components and m streams, \mathbf{C}_{eco} is the $m \times 1$ economic cost rates vector and \mathbf{Z}_{eco} is the $n \times 1$ investment cost rates vector of system components. In order to close the equations system, it is therefore necessary to write

other $m-n$ auxiliary monetary costs equations [1]: some of them depends on the adopted branchings and cost allocation criteria [2], whereas the others are defined by the boundary conditions, such as market prices. In the case study the following auxiliary equations were adopted:

$$c_{eco,6} = c_{eco,14} = c_{eco,NG} \quad (7)$$

$$c_{eco,3} = 0 \quad (8)$$

$$c_{eco,40} = 0 \quad (9)$$

The specific cost of the natural gas (7) was computed on the base of the Italian market average price, and it was considered constant for the entire lifetime of the plant. With the auxiliary equation (9) it comes out that all the economic costs of exiting flue gases are charged to the HRSG, thus on the cost of the product. Other standard assumptions have been made to distribute costs among internal streams [8].

Table 4. Economic parameters.

Parameter	Symbol [u. m.]	Max. value
Interest rate	i [%]	5
Plant lifetime	t [years]	30
Natural gas cost	$c_{eco,NG}$ [€/Nm ³]	0.35

The main parameters of the economic analysis are reported in Table 3. To calculate equipment costs as a function of the main plant operation parameters, the Frangopoulos capital costing equations have been used: values obtained with these equations could be considered acceptable approximations of real values which usually are not given by industry as a function of components parameters [9].

The main result of the thermoeconomic plant optimization, obtained by the application of the POD-RBF procedure, is the combination of the process variables which lead to the attainment of the most convenient compromise between plant efficiency and economic costs.

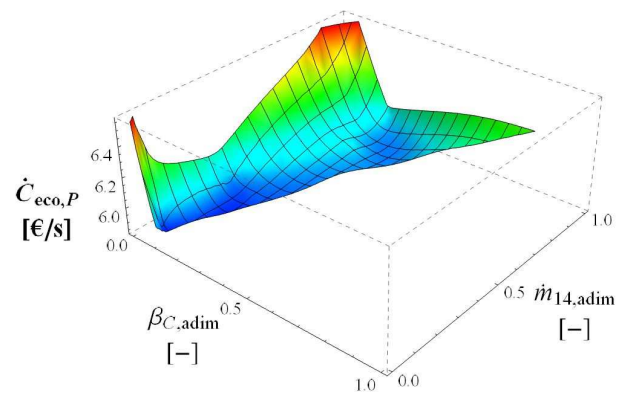


Figure 3. Economic cost map of the system product.

Figure 3 shows the economic cost map of electricity as a function of the normalized selected process variables β_C and \dot{m}_{14} . For this plant, the minimum cost results 5.90 €/s, corresponding to values of $\beta_C = 13.32$ and $\dot{m}_{14} = 1.84$ kg/s.

Thermoeconomic design analysis for Environmental cost evaluation and optimization (TA-EXER)

According to literature [10], the impact of energy systems on environment is mainly related to: natural resource consumption in the whole life cycle of the system (a) and polluting effect of all the waste emissions in water, atmosphere and soil (b).

Exergy is widely accepted as a common measure of natural resources consumption and it can be therefore used as an indicator for the environmental impact [11, 12]. Indeed, several attempts have been made to combine exergy analysis and Life Cycle Assessment (LCA) to quantify the natural resources consumption (a) of industrial processes [13, 14]: such as Cumulative Exergy Consumption (CExC) [15], Thermo - Ecological Cost (TEC) [16], Exergetic Life Cycle Analysis (ELCA) [17], Cumulative Exergy Extraction From Natural Environment (CEENE) [18] and so on. All these indicators are development of the “embodied energy” paradigm, well explained in [19]: they differ from each other in the definition of the resource cost factors included into the accounting and in the analysis time window.

On the other hand, one of the main weakness of exergy analysis is that the exergy of waste emissions hardly reflects the magnitudes of the environmental impact [20]. For this reason, some authors propose to evaluate the waste emissions polluting effect (b) as the additional natural resource consumption needed to reduce the exergy content of the effluents to zero: CExC_T [21], Zero-ELCA [22] and Extended Exergy Accounting [14] are examples of this approach.

In this paper the authors propose the adoption of the Cumulative Exergy Consumption (CExC) indicator for evaluating the natural resource consumption of the system as partial evaluation of the environmental cost of energy systems. This approach accounts only for energy and materials resources (renewables and non-renewables), as well as human labour, involved in the production of a unit of energy or material products [16]; it does not includes other externalities.

The thermoeconomic cost rate balance (4) for each i -th plant component is rewritten according to the same productive structure and input data adopted in 0, replacing economic costs rates of Resources, Products, Wastes and Plant components with their respective exergetic costs:

$$\dot{C}_{ex,R,i} + \dot{Z}_{ex,i} = \dot{C}_{ex,P,i} + \dot{C}_{ex,I,i} \quad (10)$$

Where $\dot{C}_{ex,i}$ represent the resource cost rate embodied in each exergy transfer, and $\dot{Z}_{ex,i}$ represents the resource cost embodied in the i -th system component. Exergy costing principle (11) allows to compute the resource cost rate for every j -th material or energy flow entering the i -th system component as the product between its exergy content and its CExC (represented here by $c_{ex,j}$, in kJ/kJ):

$$\dot{C}_{ex,j} = c_{ex,j} \cdot \dot{\mathbf{E}}_j \quad (11)$$

In a dual way of paragraph 0, the complete thermoeconomic system can be rewritten in matrix form (12).

$$\mathbf{A}_{(n \times m)} \cdot \mathbf{C}_{ex,(m \times 1)} + \mathbf{Z}_{ex,(n \times 1)} = \mathbf{0}_{(n \times 1)} \quad (12)$$

Where \mathbf{C}_{ex} is the $m \times 1$ thermoeconomic costs vector and \mathbf{Z}_{ex} is the $n \times 1$ investment cost rates vector of system components.

Here, the same rules for branchings and cost allocations adopted in 0 were used, and auxiliary relations necessary to close the equation system were computed relying to Simapro 7.3.3 software [23] and Szargut database [15].

$$c_{ex,6} = c_{ex,14} = c_{ex,NG} \quad (13)$$

$$c_{ex,3} = 0 \quad (14)$$

$$c_{ex,40} = 0 \quad (15)$$

CExC of the Ecoinvent unit process “Natural gas, high pressure, at consumer/RER U” is 1.069 MJ/MJ and was adopted as specific exergy cost of the natural gas (13). Like TE-ECO analysis, with the auxiliary equation (15) comes out that all the exergetic costs are charged to the HRSG, thus on the cost of the product. Exergy cost functions for plant and O&M costs ($\dot{Z}_{ex,i}$) have been extrapolated from Ecoinvent database as a function of the size, weight and the operative parameters of the plant components [24]. In case of data scarcity, average value for primary exergy consumption of European Machinery and Equipment production sector have been extrapolated from European Input-Output tables (year 2003) and result to be 50.21 MJ/kg [25]. Like the investment economic cost functions, the exergy cost functions could be considered acceptable approximations of real values.

Exergy costs of system product were obtained as a function of the selected process variables β_C and \dot{m}_{14} by applying the POD-RBF procedure.

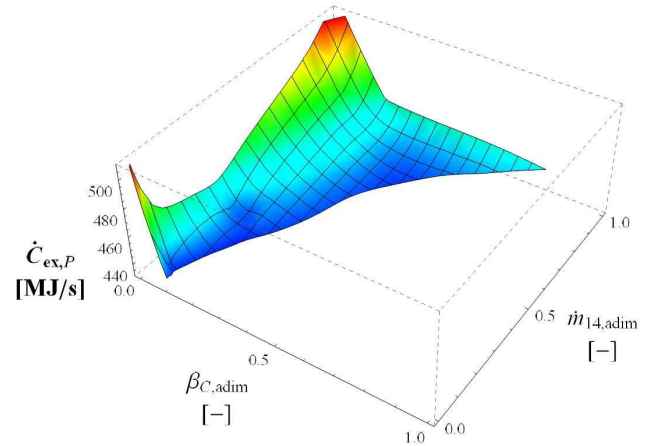


Figure 4. Exergetic cost map of the system product. Values in x and y axes are normalized between 0 and 1.

Figure 4 shows the exergetic cost map of electricity as a function of normalized process variables β_C and \dot{m}_{14} . For this plant, the minimum resources consumption results to be 434.5 MJ/s, corresponding to values of $\beta_C = 14.29$ and $\dot{m}_{14} = 1.75$ kg/s. It is noteworthy that, starting from this thermoeconomic analysis, an extension of the traditional second law efficiency can be introduced:

$$\eta_{CExC,tot} = \frac{\dot{\mathbf{E}}_{P,tot}}{\dot{C}_{ex,R,tot} + \dot{Z}_{ex,tot}} \quad (16)$$

Since it takes into account also for the production processes of the fuel and the plant equipment, efficiency defined in (16) is an extended insight of the overall energy conversion process. For this plant, best CExC-efficiency is about 0.36, obtained in

correspondence with the minimum resource consumption as previously described.

RESULTS AND DISCUSSION

Exergy based methods results

As previously explained, three different exergy based optimization criteria have been applied to the specific case study. For each identified optimal configuration, it is therefore possible to calculate all the corresponding process variables, summarized in Table 5. As expected, the three couples of β_C and \dot{m}_{14} variables that define each optimal configuration are different; therefore, also the other operative parameters such as efficiency, exergetic and economic costs differ.

Considering a plant availability of 2628 hours per year, the minimization of the economic cost of electricity ($\dot{C}_{eco,opt}$) allows to reduce the annual cost of electricity by 336 k€/year with respect to the optimal efficiency configuration ($\eta_{II,opt}$), and by 219 k€/year with respect to the optimal exergy cost configuration ($\dot{C}_{ex,opt}$).

On the other hand, considering as design point the optimal exergy cost of electricity ($\dot{C}_{ex,opt}$), the global resource consumption of the plant is reduced by 84,5 toe/year and 1070 toe/year if compared respectively with the optimal efficiency ($\eta_{II,opt}$) and economic ($\dot{C}_{eco,opt}$) configurations.

Table 5. Results of CCPP exergy based optimizations.

Parameter	u. m.	$\eta_{II,opt}$	$\dot{C}_{eco,opt}$	$\dot{C}_{ex,opt}$
β_C	-	14.36	13.32	14.29
$\dot{m}_{NG,pf}$	kg/s	1.60	1.84	1.75
$\dot{m}_{NG,tot}$	kg/s	9.24	9.41	9.25
\dot{m}_{Air}	kg/s	282.76	280.47	282.70
η_{II}	-	0.448	0.438	0.449
η_{CEXC}	-	0.358	0.353	0.36
$\dot{C}_{eco,el}$	€/h	21373	21245	21328
\dot{Z}_{eco}	€/h	6149	5712	6106
$\dot{C}_{eco,NG}$	€/h	15305	15586	15315
$\dot{C}_{ex,el}$	toe/h	37.39	37.76	37.36
\dot{Z}_{ex}	toe/h	4.27	3.97	4.24
$\dot{C}_{ex,NG}$	toe/h	33.51	34.12	33.53

To comprehensively evaluate the relationship between the three optimisation functions it is therefore necessary to investigate the relation between thermodynamic, economic and environmental costs of the product.

Coupling procedure for global optimization

Figure 5 depicts a general simplified 2-D representation of this optimization problem: the economic optimization of the plant design (**Eco,opt**) leads to an additional consumption of resources ($\Delta\dot{C}_{ex,P} = 0.41$ toe/h) while the resource cost optimization (**Ex,opt**) causes an increment of the economic cost of the product ($\Delta\dot{C}_{eco,P} = 83.63$ €/h).

The subsequent question that arises is whether it is possible to link these two aspects. Referring to Table 5 data, and assuming an average oil barrel market price of 623 €/toe (2011) [26] as a proxy for the primary exergy market price, the CCPP operating in the optimal economic cost design absorbs 0.407 toe/h more with respect to the exergy optimal design. This primary energy surplus purchased by society at its market price would result in 253.76 €/h which is greater than the difference of costs between the economic optimal design and the exergy

optimal design ($\Delta\dot{C}_{eco,P} = 83.63$ €/h). Therefore, this CCPP plant “pays” the primary exergy less than the commercial price: for the societal niche in which this CCPP operates, it is convenient to invest (perhaps by means of a specifically aimed incentive policy) in systems designed to minimize the exergetic primary resources rather than the economic costs: saving resources costs globally less than producing them.

Even if today we still live in world where the objective function is the monetary cost, and therefore the most probable configuration chosen at the end of the process would be the optimal economic cost configuration (**Eco,opt**), the current analysis opens a window over a new chance for evaluating resource consumption as an environmental cost for the society. The evaluation of the optimal exergy cost configuration (**Ex,opt**) adds another set of information to Decision Makers for having a more comprehensive understanding of the overall impact of the total system for the whole society.

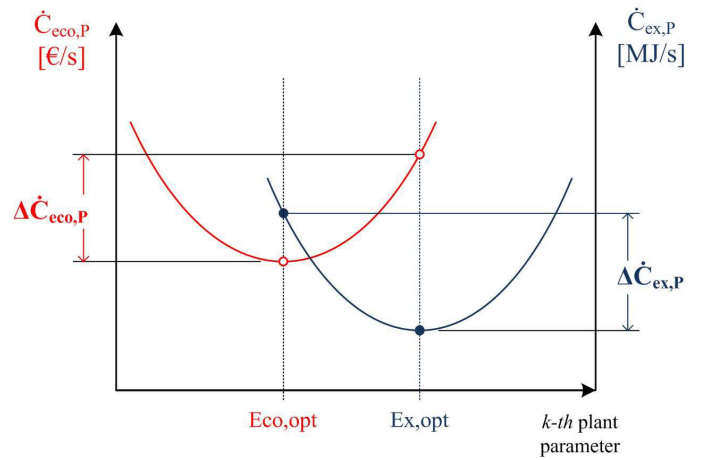


Figure 5. 2-D schematic comparison among economic and exergetic cost function of product.

CONCLUSION

Results of the presented exergy based analyses confirm the existence of substantial differences in designing the CCPP plant considering the optimization of second law efficiency, economic or exergy costs of system product.

Thermoeconomics proved to be an appropriate framework to evaluate both economic and exergy cost of system product. In particular, exergy cost evaluation was expanded in order to include the embodied exergy of resources and equipment into the analysis, as shown by eq. (12), according to CExC method. This improvement gives a better insight of the overall energy conversion process with respect to a standard exergy analysis. Moreover, it has been proposed a criterion for determining the relation between the economic and the environmental costs of the product linked to the consumption of resources (i.e. cost of the primary exergy), giving therefore different perspectives to Decision Makers. In the current economic asset, the optimal economic cost configuration will be probably selected but a number of information can be obtained by comparing the optimal efficiency configuration and the optimal exergy cost configuration.

On the other hand, some drawbacks can be identified and they indicate possible further research directions to improve Thermoeconomic analysis from practical point of view. They fall under two major categories: need for standardization, refinement and extension of the CExC database, and a more

accurate socio-economic model to compute the primary exergy market price.

NOMENCLATURE

Symbol	Quantity	SI Unit
c	Specific cost	€/J – J/J
\dot{C}	Cost rate	€/s – J/s
e	Specific exergy	J/kg
\dot{E}	Exergy rate	J/s
i	Interest rate	%
m	Total system streams	-
\dot{m}	Mass flow rate	kg/s
n	Total plant components	-
T	Temperature	°C
t	Plant lifetime	years
\dot{W}	Work	J/s
\dot{Z}	Investment cost rate	€/s – J/s
β_C	Air pressure ratio	-
η	Efficiency	-

Subscripts

adim	Adimensional
D	Destruction
eco	Economic
el	Electricity
ex	Exergetic
i	Plant component no.
I	Waste
II	Second Law
j	Material / Energy flow no.
P	Product
pf	Post-firing
R	Resource
tot	total

REFERENCES

[1] A. Bejan, G. Tsatsaronis, M.J. Moran. Thermal Design and Optimization: Wiley, 1996.

[2] E. Querol, B. González-Regueral, J.L.P. Benedito. Practical Approach to Exergy and Thermo-economic Analyses of Industrial Processes: Springer, 2012.

[3] P. Ahmadi, I. Dincer. Thermodynamic analysis and thermo-economic optimization of a dual pressure combined cycle power plant with a supplementary firing unit. *Energy Conversion and Management*. 2011;52(5):2296-308.

[4] Università di Roma "La Sapienza", CAMEL-Pro Users Manual, v.4. www.turbomachinery.it. 2008.

[5] R. Melli, E. Sciubba, C. Toro, A. Zoli-Porroni. An Improved POD technique for the optimization of MSF processes. *International Journal of Thermodynamics*. 2012;15(4):231-8.

[6] R. Melli, E. Sciubba, C. Toro, A. Zoli-Porroni. An example of Thermo-Economic optimization of a CCGT by means of the Proper Orthogonal Decomposition Method. *Proceedings of the ASME IMECE2012 November 9-15, 2012, Houston, TEXAS, USA*.

[7] V. Buljak. Proper Orthogonal Decomposition and Radial Basis Functions for Fast Simulations. Inverse Analyses with Model Reduction: Springer Berlin Heidelberg; 2012. p. 85-139.

[8] A.a.T. Lazzaretto, G. . On the quest for objective equations in exergy costing. in *ML Ramalingam, JG Lage, Vc Mei, and JN Chapman (eds), Proceedings of the ASME Advanced Energy Syrems Devision, 37, ASME, New York, 197-210*. 1997.

[9] C.A. Frangopoulos. Comparison of thermo-economic and thermodynamic optimal design of a combined-cycle plant. in: *DA Kouremenos (Ed), Proceedings of the International Conference on the Analysis of Thermal and Energy Systems, Athens*. 1991.

[10] S.E. Jorgensen, B. Fath. Encyclopedia of Ecology, Five-Volume Set: Elsevier Science, 2008.

[11] G. Wall. Conditions and tools in the design of energy conversion and management systems of a sustainable society. *Energy Conversion and Management*. 2002;43(9–12):1235-48.

[12] M.A. Rosen, I. Dincer. On Exergy and Environmental Impact. *International Journal of Energy Research*. 1997;21(7):643-54.

[13] J.-F. Portha, S. Louret, M.-N. Pons, J.-N. Jaubert. Estimation of the environmental impact of a petrochemical process using coupled LCA and exergy analysis. *Resources, Conservation and Recycling*. 2010;54(5):291-8.

[14] E. Sciubba. Can an Environmental Indicator valid both at the local and global scales be derived on a thermodynamic basis? *Ecological Indicators*. 2013;29(0):125-37.

[15] J. Szargut, D.R. Morris, F.R. Steward. Exergy analysis of thermal, chemical, and metallurgical processes: Hemisphere, 1988.

[16] J. Szargut. Exergy Method: Technical And Ecological Applications: WIT Press, 2005.

[17] R.L. Cornelissen, G.G. Hirs. The value of the exergetic life cycle assessment besides the LCA. *Energy Conversion and Management*. 2002;43(9–12):1417-24.

[18] B. De Meester, J. Dewulf, S. Verbeke, A. Janssens, H. Van Langenhove. Exergetic life-cycle assessment (ELCA) for resource consumption evaluation in the built environment. *Building and Environment*. 2009;44(1):11-7.

[19] S. International Federation of Institutes for Advanced. IFIAS Workshop Report, energy analysis and economics. *Resources and Energy*. 1978;1(2):151-204.

[20] R.U. Ayres, L.W. Ayres, K. Martínás. Exergy, waste accounting, and life-cycle analysis. *Energy*. 1998;23(5):355-63.

[21] P. Zhu, X. Feng, R.J. Shen. An Extension to the Cumulative Exergy Consumption Applied to Environmental Impact Analysis of Industrial Processes. *Process Safety and Environmental Protection*. 2005;83(3):257-61.

[22] G. Hirs. Thermodynamics applied. Where? Why? *Energy*. 2003;28(13):1303-13.

[23] Simapro 7.3.3, site: <http://www.pre.nl/simapro/>. Pré Consultants.

[24] X. Feng, G. Zhong, P. Zhu, Z. Gu. Cumulative exergy analysis of heat exchanger production and heat exchange processes. *Energy & fuels*. 2004;18(4):1194-8.

[25] S. Suh. Handbook of Input-output Analysis Economics in Industrial Ecology: Springer London, Limited, 2009.

[26] B. Petroleum. Statistical Review of World Energy. 2012.

PHASE TRANSITIONS IN MULTICOMPONENT SYSTEMS AT THE NANO-SCALE: THE EXISTENCE OF A MINIMAL BUBBLE SIZE

Øivind Wilhelmsen*, Dick Bedeaux*, Signe Kjelstrup*, David Reguera **

* Department of Chemistry, Norwegian University of Science and Technology, Trondheim, Norway

** Department of Fundamental Physics, University of Barcelona, Barcelona, Spain

ABSTRACT

The formation of nanoscale droplets/bubbles from a metastable bulk phase is still connected to many unresolved scientific questions. In this work, we analyze the stability of multicomponent liquid droplets and bubbles in closed $N_{\text{tot},i}$, V_{tot} , T systems (total mass of components, total volume and temperature). To investigate this problem, square gradient theory combined with an accurate equation of state is used. To give further insight into how the state of the fluid affects the formation of droplets and bubbles, we compare the results from the square gradient model to a modified bubble/drop model which gives a macroscopic capillary description of the system. We discuss under which conditions the square gradient model or the modified bubble models predict a finite threshold size for bubbles and their stability in terms of the reversible work of bubble formation. The work reveals a metastable region close to the minimal bubble radius. We find that the liquid compressibility is crucial for the existence of this minimum threshold size for bubble formation in $N_{\text{tot},i}$, V_{tot} , T systems.

INTRODUCTION

Small systems receive now increasing attention, not only in academia, but also in industry. Fabrication of novel nano materials for instance, requires insight into phase transitions such as condensation, evaporation and crystallization at the nanoscale [1; 2]. The first and important step in a typical phase transition is the formation of a nucleus from a metastable bulk phase. Recent experimental developments have made it possible to observe formation of tiny droplets and crystals consisting of only a few molecules. The experiments have evidenced the limitations of current theories, including classical nucleation theory, to describe some of the observations [3]. These systems challenge our current understanding and they motivate the development and use of new tools. In this work, we will give insight into the stability of multicomponent bubbles/droplets in systems with constant $N_{\text{tot},i}$, V_{tot} , T (total mass of components, total volume and temperature). Special attention will be given to the conditions under which very small stable or critical-sized bubbles cannot be formed [4].

For nanoscale bubbles or droplets, the thickness of their interfaces can be of the same order of magnitude as their size. Models which do not specifically take into account surface gradients, such as classical nucleation theory and discontinuous excess formulations, might then be insufficient. We will thus use a square gradient theory for curved systems coupled with a qualitatively accurate cubic equation of state [5; 6] to investigate the system. In the square gradient theory, the Helmholtz energy density has contributions up to second order in the gradients of the densities. The functional minimization of the total Helmholtz energy keeping $N_{\text{tot},i}$ and T constant, gives the equilibrium density and concentration distributions in the canonical ensemble [7]. The advantage of this approach is that continuous profiles across the interface can be found. Square gradient theory combined with an accurate equation of state and suitable models for the pure components has been able to reproduce ex-

perimental results for the surface tension of planar interfaces of multicomponent mixtures [8]. We will use it here to describe the formation of bubbles and liquid droplets. To give further insight into how the size of the system and the composition of the fluid affect the formation of small bubbles and drops, we will compare the results from the square gradient model to a modified bubble model which gives a macroscopic capillary description for different models of the bulk phases [9]. While previous work on this topic has focused on single-component systems [4], we formulate our problem for several components. In addition, we show that a thermodynamic stability analysis is crucial to capture the behavior of the system near the threshold size, an asset which was not discussed in detail earlier [4].

The paper is structured as follows. First, the theoretical framework used will be presented. A short introduction will be given to the use of a quantitatively accurate cubic equation of state coupled with either the square gradient theory (mesoscopic approach), or the capillary approach (macroscopic approach) to describe the formation of bubbles and liquid droplets of interest for nucleation processes. We will then show that the capillary approach is able to reproduce results from the square gradient theory remarkably well for a binary mixture, using hexane-cyclohexane as an example. This observation is used to explain the behavior of very small bubbles, based on a thermodynamic stability analysis. Both approaches will be used to analyze the stability of small bubbles and the existence of a threshold size below which no stable or critical-sized bubbles can be formed. Finally, some concluding remarks are provided.

THEORY

We consider a spherical container with volume, V_{tot} , temperature T and a fixed number of molecules of each component i , $N_{\text{tot},i}$. We assume that a perfectly spherical bubble or droplet is placed at the center of the container. At equilibrium, we know that the state of this system should be at a global minimum in the

total Helmholtz energy. Both the square gradient model and the capillary approach rely on an equation of state which is capable of capturing the thermodynamic behavior of both the liquid and the vapor at different compositions. In this work, we will use the cubic equation of state, Peng Robinson, which has proven to give accurate predictions of the density in both gas and liquid regions for non-polar mixtures. In addition, it captures the vapor-liquid equilibrium behavior of multicomponent mixtures, if proper interaction parameters are used, as demonstrated for CO₂-rich fluids by several authors [5; 6]. In general, most two-parameter cubic equation of state may be represented as:

$$P = \frac{R_g T}{v-b} + \frac{a\alpha(T)}{(v-bm_1)(v-bm_2)} \quad (1)$$

Here, P is the pressure, R_g the universal gas constant, v the molar volume, and a , α , and b are parameters of the equation of state. The constants m_1 and m_2 represent the biggest difference between the various two-parameter cubic equations of state. For the Peng-Robinson equation of state, $m = -1 \pm \sqrt{2}$. Provided that $m_1 \neq m_2$, Eq. 1 can be integrated with respect to the volume to give the residual Helmholtz energy (i.e. the difference between the Helmholtz energy of the homogeneous phase and that of an ideal gas) :

$$\frac{F_{\text{eos, res}}}{R_g T} = N \ln \left(\frac{v}{v-b} \right) - \frac{a\alpha(T)}{(m_1 - m_2)bR_g T} \ln \left(\frac{v - m_2 b}{v - m_1 b} \right) \quad (2)$$

This expression can be differentiated to give the first and second order derivatives of the Helmholtz energy, which are the building blocks for residuals of the other thermodynamic variables such as the chemical potentials, the entropy, the enthalpy and the internal energy. To obtain a complete thermodynamic description of the system, the residual values must be linked to the ideal gas state. Accurate heat capacity polynomials for each component, standard values for enthalpy of formation and entropy have been used to create a thermodynamic framework which gives values for the state functions that follow SI-standards. To verify that the framework is indeed thermodynamically consistent and correctly implemented, a comprehensive consistency check as described by Michelsen and Mollerup was applied [10].

The square gradient model

A rigorous introduction to the square gradient model both at equilibrium and outside equilibrium has been given by Glavatskiy [7]. The functional minimization of the total Helmholtz energy of the square gradient model keeping the total mass of each component constant gives the equilibrium molar concentration distributions, c_i , in the canonical ensemble. The local specific Helmholtz energy is given by:

$$F_{\text{sgm}} = F_{\text{eos}} + \sum_{i,j}^{N_c} \frac{\kappa_{ij}}{c_i} \nabla c_i \cdot \nabla c_j \quad (3)$$

Where the subscript "sgm" refers to the square gradient model. Assuming that the square gradient parameters κ_{ij} are constant and symmetrical, the chemical potentials of the multicomponent

square gradient model are:

$$\begin{aligned} \mu_{\text{sgm},k} &= \mu_{\text{eos},k} - \sum_{i=1}^{N_c} \kappa_{ik} \nabla \cdot \nabla c_i \\ &= \mu_{\text{eos},k} - \sum_{i=1}^{N_c} \kappa_{ik} \left(\frac{2}{r} \frac{\partial c_i}{\partial r} + \frac{\partial^2 c_i}{\partial r^2} \right) \end{aligned} \quad (4)$$

Here, the second line is a simplified expression valid for a system with spherical symmetry around the center, N_c is the number of components and r is the distance from the center. This can be rewritten in matrix form:

$$\mathbf{M}_\kappa \nabla \cdot \nabla \mathbf{c} = \boldsymbol{\mu}_{\text{eos}} - \boldsymbol{\mu}_{\text{sgm},k} \quad (5)$$

The matrix \mathbf{M}_κ is such that each index (i,j) equals κ_{ij} . Bold face variables refer to tensors of rank > 0 . If the mixing rule for the square gradient constants is defined according to the most common expression $\kappa_{ij} = \sqrt{\kappa_i \kappa_j}$, the matrix is singular with row rank 1, since row i equals row j times $\sqrt{\kappa_i / \kappa_j}$. This allows us to define the variables from the multicomponent square gradient model using the structure parameters κ , ε_i and q . We then define the following variables:

$$\kappa = \kappa_s \quad (6)$$

$$\varepsilon_i = \sqrt{\frac{\kappa_i}{\kappa}} \quad (7)$$

$$q = \sum_{i=1}^{N_c} \varepsilon_i c_i \quad (8)$$

We choose the component with subscript s , as the one with the largest $N_{\text{tot},i}$. Moreover, by introducing the definitions of κ , ε and q in Eq. 5 one obtains the following system of partial differential equations:

$$\mu_{\text{eos},k} - \mu_{\text{sgm},k} = \kappa \varepsilon_k \nabla \cdot \nabla q \quad (9)$$

Since the coefficient matrix \mathbf{M}_κ has row rank 1, the system of differential equations above can be reduced to one second order differential equations and (N_c-1) algebraic equations:

$$(\boldsymbol{\mu}_{\text{eos}} - \boldsymbol{\mu}_{\text{sgm}}) - \boldsymbol{\varepsilon} (\mu_{\text{eos},s} - \mu_{\text{sgm},s}) = 0 \quad (10)$$

In terms of the new order parameter, q , the state functions and pressures can be represented as follows:

$$F_{\text{sgm}} = F_{\text{eos}} + \frac{\kappa}{2c} (\nabla q)^2 \quad (11)$$

$$U_{\text{sgm}} = U_{\text{eos}} + \frac{\kappa}{2c} (\nabla q)^2 \quad (12)$$

$$S_{\text{sgm}} = S_{\text{eos}} \quad (13)$$

$$H_{\text{sgm}} = H_{\text{eos}} - \frac{\kappa q}{c} \nabla^2 q \quad (14)$$

$$G_{\text{sgm}} = G_{\text{eos}} - \frac{\kappa q}{c} \nabla^2 q \quad (15)$$

$$P_{\text{sgm}} = P_{\text{sgm},\parallel} = P_{\text{eos}} - \frac{1}{2} \kappa (\nabla q)^2 - \kappa q \nabla^2 q \quad (16)$$

$$P_{\text{sgm},\perp} = P_{\text{eos}} + \frac{1}{2} \kappa (\nabla q)^2 - \kappa q \nabla^2 q \quad (17)$$

Details in derivations of the state functions will not be provided in this paper. A more detailed discussion of for instance the parallel and perpendicular pressures can be found in [7]. In addition to the second order partial differential equation, Eq. 9, which can be represented as two first order differential equations, the cumulative mass, $\overline{N_{\text{tot},i}}(r)=4\pi\int_0^r r^2 c_i dr$, is used as additional variable, satisfying:

$$\frac{\partial \overline{N_{\text{tot},i}}}{\partial r} = 4\pi r^2 c_i \quad (18)$$

The combined system of differential and algebraic equations was solved using the "bvp4c" solver in Matlab, coupled with a multidimensional Newton-Raphson approach to solve the system of algebraic equations at each iteration. The Jacobian matrix of the Newton-Raphson approach was constructed based on the Hessian matrix of the Helmholtz energy. In addition to the temperature and the total volume, the following $(2+N_c)$ boundary conditions are necessary to fully specify the boundary value problem:

$$\left. \frac{\partial q}{\partial r} \right|_{r=R_{\text{tot}}} = \left. \frac{\partial q}{\partial r} \right|_{r=0} = 0 \quad (19)$$

$$\overline{N_{\text{tot},i}} \Big|_{r=R_{\text{tot}}} = N_{\text{tot},i} \quad (20)$$

The capillary model

Based on previous work on small bubbles and droplets described in Refs. [9; 11] we define a modified bubble/droplet model, also called the capillary model, to be able to compare the square gradient model to a macroscopic approach. Assuming that the bubble/droplet and the exterior both have homogeneous thermodynamic properties separated by a discontinuous interface at the radius, R , the changes in the Helmholtz energies of the gas and the liquid phases are:

$$dF_g = -P_g dV_g + \sum_{i=1}^{N_c} \mu_{g,i} dN_{g,i} \quad (21)$$

$$dF_l = -P_l dV_l + \sum_{i=1}^{N_c} \mu_{l,i} dN_{l,i} + \sigma d\Omega \quad (22)$$

Here, the surface has been assigned to the liquid phase. In addition, the total number of moles of each component and the total volume are constant. This means that $dV_l = -dV_g$ and that $dN_{g,i} = -dN_{l,i}$. We will use the subscript "n" to denote both a liquid droplet and a bubble at the center of the container, and "e" for the exterior. Assuming that the bubbles/droplets are perfectly spherical, $d\Omega = 2dV_n/R$, is the link between the surface area, Ω and their radius. The change in the Helmholtz energy valid for both the liquid droplet and the bubble is then:

$$dF_{\text{sys}} = - \left(P_n - P_e - \frac{2\sigma}{R} \right) dV_n + \sum_{i=1}^{N_c} (\mu_{n,i} - \mu_{e,i}) dN_{n,i} \quad (23)$$

Equilibrium at constant mole numbers and volume is characterized by a global minimum in the Helmholtz energy, at which a necessary condition is $dF_{\text{sys}} = 0$. This leads to equality of

the chemical potentials of both phases and the famous Laplace relation:

$$P_n - P_e = \frac{2\sigma}{R} \quad (24)$$

The Laplace relation and equality of the chemical potentials are necessary conditions for a minimum, but maxima and saddle points satisfy the same conditions, since they are also extrema of the Helmholtz energy of the system. We have to investigate the second derivative matrix, H , namely the Hessian of the Helmholtz energy to resolve whether the solution is thermodynamically stable, i.e. a minimum. A minimum is characterized by a positive definite Hessian matrix (positive eigenvalues), a maximum by a negative definite matrix (negative eigenvalues) and a saddle point is characterized by a non-singular Hessian matrix which is neither positive nor negative definite. A singular Hessian means that higher derivatives have to be investigated. The component mass balances for the system give additional algebraic equations to be satisfied:

$$\frac{4\pi}{3} (c_{n,i} R^3 + c_{e,i} (R_{\text{tot}}^3 - R^3)) = N_{\text{tot},i} \quad (25)$$

Equality of the chemical potential for each component through the system, together with the mass balances and the Laplace equation gives a total of $2N_c+1$ equations, which fully specify the composition in the interior and exterior of the bubble/droplet together with the unknown radius. We will investigate two different models in the capillary approach:

Capillary Model 1: Here, we assume that the liquid is compressible and its pressure and volume are given by the cubic equation of state.

Capillary Model 2: In this approach, we assume that the liquid is incompressible and behaves as an ideal mixture. The gas is ideal.

For an incompressible ideal mixture, the chemical potential of component i is given by:

$$\mu_i(T, P) = \mu_i(T, P_{i,\text{sat}}) + RT \ln x_i + v_{i,\text{sat}} (P - P_{i,\text{sat}}) \quad (26)$$

Here, subscript "sat" refers to a saturated quantity, x_i is the mole fraction, and v_i is the partial molar volume. The two different capillary models will be used to investigate the role of compressibility of the liquid in the stability of bubbles in a multi-component system.

RESULTS AND DISCUSSION

Results are presented for the binary system, hexane-cyclohexane, since it has been a popular mixture in the literature [7; 12]. Parameters used in the models can be found in Tab. 1. Here, the square gradient parameters, κ_1 and κ_2 , were chosen such that they reproduce exactly the surface tension reported for the single-component systems hexane and cyclohexane at 300 K [13]. The surface tension used in the capillary models, reported in Tab. 1, is the one predicted by the square gradient model for a planar surface. The overall composition for the simulations was constant, and close to the liquid phase composition. It was thus not necessary to consider a composition dependent surface

tension in the capillary models. We will first show how the capillary models compare with the square gradient model in terms of quantitative results for key-parameters, such as composition and pressure. Given that the surface tension is calculated by the excess of the parallel pressure in the square gradient model, both capillary models reproduce well results from the square gradient model for small bubbles and droplets (Fig. 1. and 2) From the

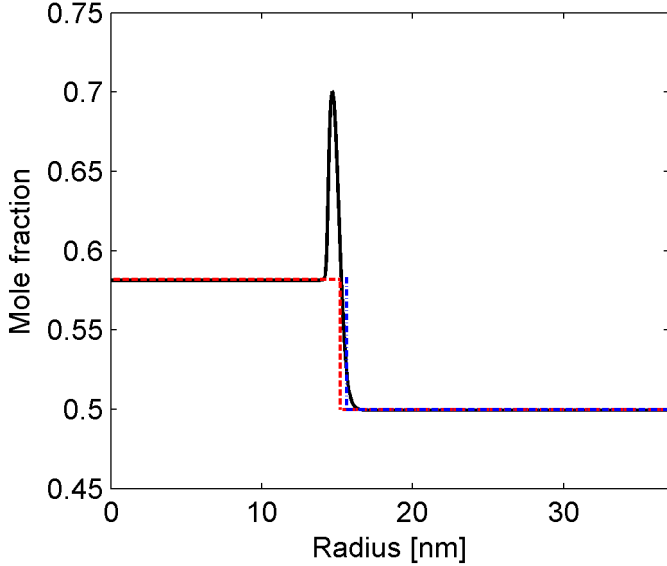


Figure 1. Bubble; mole fraction of hexane, predicted by the square gradient model (solid line), Capillary Model 1 (red dashed line) and Capillary Model 2 (blue dash-dot line)

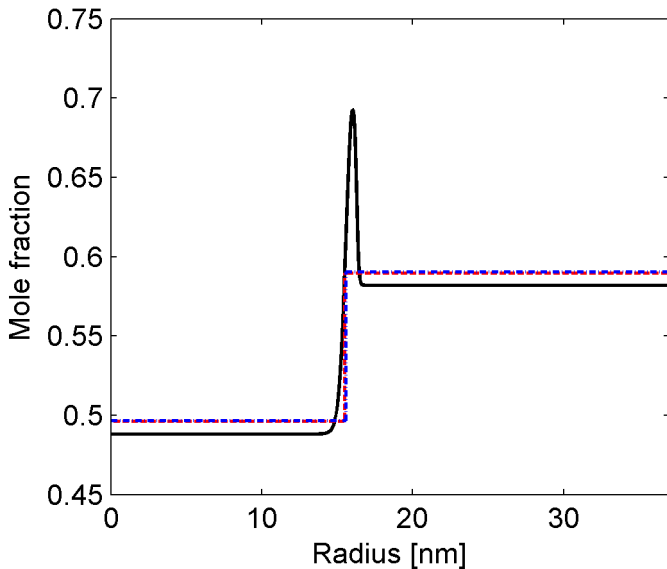


Figure 2. Droplet; Mole fraction of hexane, predicted by the square gradient model (solid line), Capillary Model 1 (red dashed line) and Capillary Model 2 (blue dash-dot line)

figures, one can see that the thickness of the surface, coarsely defined as the zone where the composition deviates from those of the two homogeneous phases, is significant compared to the

Table 1. Data used in the simulations. Component 1 is hexane, component 2 is cyclohexane. Surface tension is calculated by the square gradient model for a flat surface, for the mixture at the temperature and composition considered

Variable	Value
Temperature	330 K
κ_1	$4.2 \cdot 10^{-13} \text{ Jm}^5/\text{kmol}^2$
κ_2	$3.4 \cdot 10^{-13} \text{ Jm}^5/\text{kmol}^2$
Mole fractions	0.5
Surface tension	0.162 N/m
Container radius	38 nm

radius. Even if the capillary models are obviously not capable of reproducing the behavior of the square gradient model at the surface, the compositions, pressures and densities in the homogeneous regions are reproduced well, both for the single component systems, and for the binary system. This is surprising since the excess of mass of both components is 0 in the capillary models, when it is clearly different from 0 in the square gradient model. The location of the equimolar surface (overall density) in the square gradient model gives the radius of the bubble/droplet. The radii predicted by the capillary models deviate from this by less than one percent. The difference between the gas and the liquid pressure in the two cases, also known as the Laplace pressure, is even less. These observations are true, even if the liquid is assumed to be incompressible. This shows that a capillary model can be used as a tool to understand the behavior of the more detailed square gradient model, and to reveal the behavior and stability of bubbles and droplets at small sizes, as we shall see.

The minimal bubble radius

In this section, we discuss how assumptions about the liquid-phase will affect the smallest possible bubble-size in a system in the canonical ensemble. We also discuss the stability of the different extrema of the Helmholtz energy in terms of the Hessian and of the work of formation. The difference in Helmholtz energy between a system with a bubble or a droplet and a super-saturated gas or undersaturated liquid is known as the reversible work of formation, ΔW [9; 14]. If this quantity is positive, it indicates that the bubble is unstable or metastable with respect to the homogeneous liquid solution. In particular, one can show that there exists a region where a bubble is metastable, which means that the total Helmholtz energy of the system is at a local minimum, but ΔW is positive. We define the minimal radius of a bubble as the smallest radius for which it will form spontaneously, i.e. the state where $\Delta W = 0$, $dF_{\text{sys}}=0$ and F_{sys} is convex (positive eigenvalues of the Hessian matrix). Fig 3 shows how the radii corresponding to the extrema of the Helmholtz energy of the system change with the scaled total mass. The reference point for mass is the mass corresponding to the homogeneous liquid at the equilibrium density. It is evident that with a specified total mass in the system, Capillary model 1 predicts two possible bubble radii, one large and one small, both representing extrema of the Helmholtz energy in the capillary models. The radii of the large bubbles in both capillary models

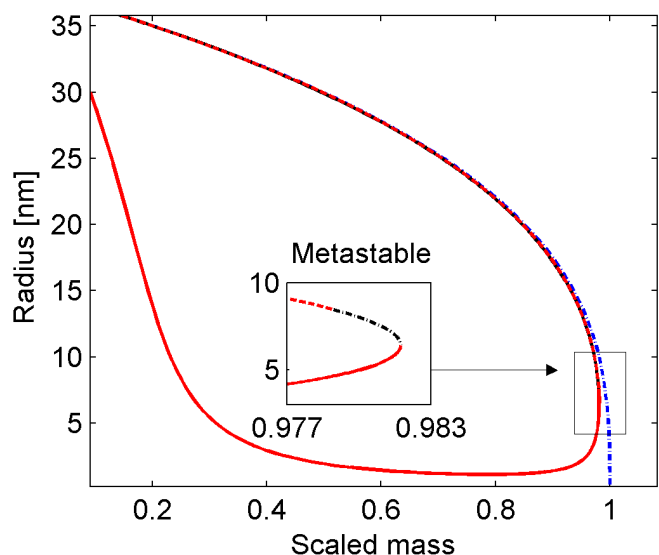


Figure 3. The square gradient model (black solid line) compared with Capillary Model 1 in the stable (dashed line) and the unstable (solid line) region, and Capillary Model 2 (dash-dot lines) for two component bubbles at 330 K.

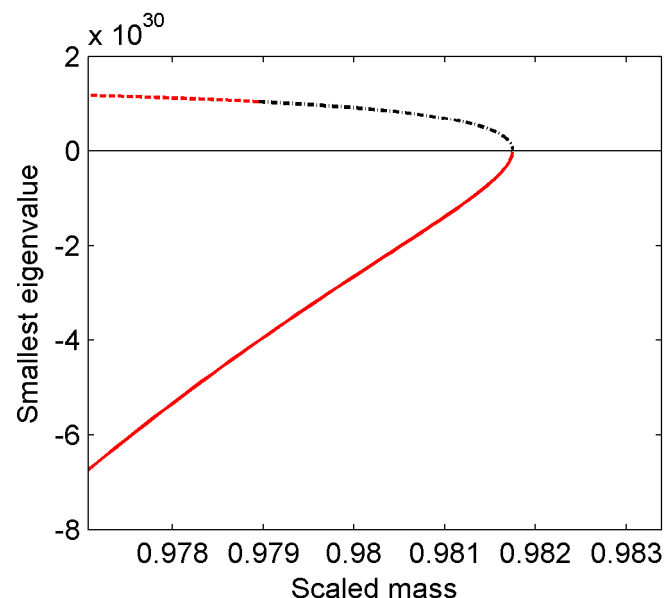


Figure 4. The smallest eigenvalue of the hessian, $H_{m,n}$, in the Capillary Model 1 describing two component bubbles at 330 K, for the stable (dashed line), the unstable (solid line) and the metastable region (dash-dot line). The solid line corresponds to small bubbles, and the upper line is the large bubbles.

are almost identical to the radii predicted by the square gradient model. In fact, they are so similar that they can hardly be distinguished from each other in Fig. 3. Since we have two components in this system, there are three possible eigenvalues of the Hessian, associated with the number of moles of the components and the volume of the bubble. Fig. 4 shows that the large bubbles give only positive eigenvalues of the Hessian, which proves that these solutions are minima, and locally stable bubbles. The small bubbles (dot-dashed lines) have one negative and two positive eigenvalues. This means that these solutions are unstable saddle-points of the Helmholtz energy, corresponding to the critical bubble of interest for nucleation. The same behavior was observed for the single-component systems, hexane and cyclohexane (not shown here).

We would like to give some attention to the region close to where the stable and unstable solutions of Capillary Model 1 merge. From Fig. 5 we observe that there exists locally stable minima of the Helmholtz energy of the bubbles, where it is energetically favorable for the system to have a homogeneous density and no bubble. We make this observation for both Capillary Model 1 and the square gradient model, and refer to this region as metastable. The minimal radius for a stable bubble is reached at 8.4 nm, but it is actually possible to have a metastable bubble down to 6.5 nm in this system (see Fig. 3). The minimal stable radius is found by identifying the radius at which $\Delta W = 0$, and the minimal metastable radius is found by locating the point where the smallest eigenvalue is close to zero. We have done the same analysis for the single-components, hexane and cyclohexane and found the same behavior. Metastable behavior can also be observed for hexane-cyclohexane droplets near the minimum density, as already discussed in Ref. [11]. These observations show that one should be careful to distinguish between metastable and unstable bubbles, since they are all extremal states of the total Helmholtz energy.

Another interesting observation is that Capillary Model 2, where the liquid surrounding the bubble is incompressible, has only one possible bubble solution at a specified total mass of

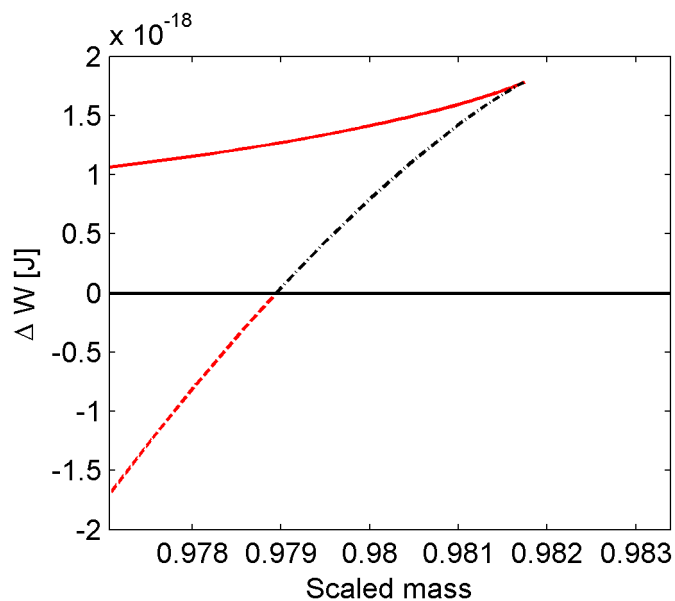


Figure 5. The reversible work of formation of Capillary Model 1 for two component bubbles at 330 K for the stable (dashed line), the unstable (solid line) and the metastable region (dash-dot line)

the system (Fig. 3). This means that assumptions about the compressibility of the liquid will have a large impact on estimates of minimal radii. In the limiting case of an incompressible liquid, there is no minimal radius of the bubble, but when the liquid is compressible there is a minimal radius. We can address the stability of Capillary Model 2, through evaluation of ΔW , with homogeneous ideal gas as the only possible reference state. Then the bubbles are always stable. A more detailed analysis is needed to see if the minimal radius decreases monotonically with the compressibility. For small drops, the assumption of an incompressible liquid did not change the minimal radius of the drop to a significant extent (not shown).

CONCLUSION

In this paper, we have investigated how the formation of nanoscale bubbles are limited by a minimal size in systems with constant $N_{\text{tot},i}$, V_{tot} , T (total mass of components, total volume and temperature). We used the square gradient model for curved systems combined with the cubic equation of state, Peng Robinson, to analyze the system from a mesoscopic point of view, and compared the results to those obtained from the capillary model, which addresses the problem from a macroscopic point of view. For the hexane-cyclohexane mixture, we observed that the capillary model was able to reproduce the results from the square gradient model in the homogeneous regions well, if the value for the surface tension obtained from the square gradient model was used. The minimal radius for a stable bubble in a 38 nm container in this binary system was found to be 8.4 nm, but a thermodynamic stability analysis showed that it was possible to have metastable bubbles down to 6.5 nm. No threshold radius, and only one possible bubble solution corresponding to a stable bubble was found using the capillary model with the liquid assumed to be incompressible. The assumption of incompressible liquid had little effect on the minimal droplet radius. This indicates that a more detailed analysis should be done regarding the role of the compressibility in determining the stability and size of nano bubbles in binary systems.

ACKNOWLEDGMENT

Øivind Wilhelmsen would like to thank the Faculty of Natural Sciences and Technology at the Norwegian University of Science and Technology for the PhD-grant. He would also like to thank Kirill Glavatskiy for explanations of his work on the square gradient model.

NOMENCLATURE

α	Parameter in EoS
a	Parameter in EoS [Pam^6]
b	Parameter in EoS [m^3/mol]
c	Concentration [mol/m^3]
\mathbf{c}	Concentration vector [mol/m^3]
ε	Structure parameter
F	Helmholtz energy [J/mol]
H	Hessian matrix of Helmholtz energy
κ	Square gradient parameter [Jm^5/mol^2]
\mathbf{M}	Matrix with kappas [Jm^5/mol^2]
m	Constants in EoS
μ	Chemical potential [J/mol]
N	Number of moles, capillary model [mol]
\mathbf{n}	Composition vector [mol]
n_i	Moles of component i [mol]
Ω	Surface area [m^2]
P	Pressure [Pa]
q	Order parameter
r	Radial position in container [m]
σ	Surface tension [N/m]
R	Radius bubble/droplet [m]
R_{tot}	Radius of container [m]
R_g	Universal gas constant [$\text{J}/\text{K mol}$]
U	Internal energy [J/mol]
v	Molar volume [m^3/mol]
V	Volume [m^3]
x_i	Mole fractions

References

- [1] U. Gasser, E.R. Weeks, A. Schofield, P.N. Pussey and D.A. Weitz, "Real-Space Imaging of Nucleation Growth in Colloidal Crystallization", *Science* 292(5515), pp. 258-262, 2001.
- [2] S.T. Yau and P.G. Vekilov, "Quasi-Planar Nucleus Structure in Apoferritin Crystallization", *Nature* 406, pp. 494-497, 2000.
- [3] H. Vehkamäki, "Classical Nucleation Theory in Multi-component Systems", Springer, Berlin, 2006.
- [4] K. Glavatskiy, D. Reguera and D. Bedeaux, "Effect of compressibility in bubble formation in closed systems", *Submitted, 2013*.
- [5] H. Li, J.P. Jakobsen, Ø. Wilhelmsen, J. Yan, "PVTxy properties of CO₂-mixtures relevant for CO₂ capture, transport and storage", *Applied Energy* 88(11), pp. 3567-3579, 2011.
- [6] Ø. Wilhelmsen, G. Skaugen, O. Jørstad and H. Li, "Evaluation of SPUNG and other Equations of State for Use in Carbon Capture and Storage Modelling", *Energy Procedia* 23, pp. 236-245, 2012.
- [7] K. Glavatskiy, "Multicomponent Interfacial Transport Described by the Square Gradient Model during Evaporation and Condensation", Springer PhD-thesis, Springer, 2011.
- [8] H. Lin, Y.Y. Duan, Q. Min, "Gradient Theory Modelling of surface tension for pure fluids and binary mixtures", *Fluid Phase Equilibria* 254, pp. 75-90, 2007.
- [9] D. Reguera, R.K. Bowles, Y. Djikaev and H. Reiss, "Phase transitions in systems small enough to be clusters", *Journal of Chemical Physics*, 118, pp. 340-353, 2003.
- [10] M.L. Michelsen and J.M. Møllerup, "Thermodynamic models: Fundamentals & Computational Aspects", Tie-Line Publications, Denmark, 2007.
- [11] D. Reguera and H. Reiss, "Nucleation in confined ideal binary mixtures: The Renninger-Wilemski problem revisited", *The Journal of Chemical Physics*, 119(1533), 2003.
- [12] I. Inzoli, S. Kjelstrup, D. Bedeaux, K. Kjelstrup, "Transfer coefficients for the liquid-vapour interface of a two-component mixture", *Chemical Engineering Science*, 66(20), 2011.
- [13] J. Jasper, "The Surface Tension of Pure Liquid Compounds", *J. Phys. Chem. Ref. Data*, 1(4), pp. 841-1008 1972.
- [14] J.M. Yang, "The thermodynamic stability of the heterogeneous system with a spherical interface", *J. Chem. Phys.*, 82(4), pp. 2082-2085, 1985.

STRUCTURAL AND POLARIZATION PROPERTIES OF AQUEOUS NONPOLAR SOLUTE MIXTURES

Igor Shvab, Richard Sadus

Centre for Molecular Simulation, Swinburne University of Technology,
Hawthorn, Victoria 3122, Australia.

EXTENDED ABSTRACT

The microscopic structure and polarization properties of aqueous solutions of Ne, Ar, CH₄, Kr, and Xe over the wide range of state points have been investigated via molecular dynamic simulation. The use of a polarizable MCYna potential [1, 2] for water and Lennard-Jones potential for water-solute and solute-solute interactions allows us to study the system over the temperature range 278-750 K and solute molar fractions up to 30%. A combined MCYna + LJ potential was chosen for these systems with Lorentz-Berthelot combining rules. The MCYna + LJ model reproduces the experimentally observed homogeneous phase region of both water-methane and water-noble gas systems more accurately than the SPC/E + LJ model.

The effect of the solute size and concentration on solubility of system, shell structure, hydrogen bonding, static dielectric constant and dipole moment has been investigated. It is found that even at low concentrations and high temperature solute particles affect structure of water, resulting in the compression of oxygen-oxygen (O-O) and oxygen-hydrogen (O-H) radial distribution functions [3,4]. Coordination numbers of aqueous solutions of nonpolar solutes appear to be proportional to the size of solute particles. Our study shows that at the solute molar fractions $x_s \leq 30\%$ some strengthening of vicinal water structure has been observed. It manifests mainly in increasing of the number of water molecules in the 1st solvation shell around central solute particle and consequent increase in O-O and O-H coordination numbers. At the same time at solute concentration $x_s > 30\%$ nonpolar solute plays clearly destructive role on tetrahedral water structure and the formation of hydrogen bonds (H-bonds).

The dielectric constant ϵ_r and average dipole moment μ_m of water-nonpolar solute systems have been calculated. The calculations confirmed the gradual decrease of dielectric constant and average dipole moment with temperature and solute concentration. At high temperatures, this trend is caused by the reduction of polarizability of the system, which in turn is caused by the collapse of the H-bond network and resulting thermal fluctuations that oppose dipole alignment by an electrostatic field. In case of high solute concentration, the trend is caused by the "negative" influence of solute particles on cooperative response of water molecules on the external field. Dielectric constants ϵ_r calculated in the given MD simulation are in good agreement with the analytical approach of calculating ϵ_r of aqueous solutions at small solute concentrations x_s and temperatures up to the boiling temperature of water. At higher temperatures and solute concentrations, analytical calculations underestimate ϵ_r compared to MD results. ϵ_r and μ_m do not show any clear dependence from solute particles size.

REFERENCES

- [1] I. Shvab and Richard J. Sadus, *J. Chem. Phys.*, **137**, 124501 (2012).
- [2] I. Shvab and Richard J. Sadus, *Phys. Rev. E*, **85**, 051509 (2012).
- [3] R. J. Sadus, *Molecular Simulation of Fluids: Theory, Algorithms and Object-Oriented* (Elsevier, Amsterdam, 1999).
- [4] P. Cristofori, P. Gallo, and M. Rovere, *Molecular Physics*. **103**, 501 (2005).

HIGH TEMPERATURE THERMODYNAMIC PROPERTIES OF THE (U, AM)O₂ SOLID SOLUTIONS

Octavian S. Vălu*^o, Ondřej Beneš*, Rudy J. M. Konings*^o

* European Commission, Joint Research Centre, Institute for Transuranium Elements, Karlsruhe, 76125, Germany

^o Delft University of Technology, Faculty of Applied Sciences, Mekelweg 15, 2629 JB Delft, The Netherlands

EXTENDED ABSTRACT

Studies on oxides of actinide elements such as thorium, uranium, plutonium and americium are of great interest in nuclear industry since most of these oxides are used or are planned to be used as nuclear fuels in various types of reactors [1] in the form of mixed oxides. The thermodynamic properties such as enthalpy and heat capacity of these materials are needed for reactor safety calculations. Furthermore studies of the temperature dependence of vapour pressure are essential in calculation of the thermodynamic functions in order to predict stable phases in any multi-component system.

The most abundant transuranium elements found in the high level waste of nuclear power reactor fuels are Am and Np [2]. Because the two elements can be transformed by fast neutrons into shorter-lived fission products, recycling these elements in fast reactors would improve the efficiency and reduce the long-term hazard. The solid solution of the uranium and americium oxides is a possible chemical form for recycling americium. To understand the stability of the system with respect to the temperature the thermodynamic properties of mixed oxides needs to be investigated.

One of the objectives of this study is to investigate the heat capacity of the (U, Am)O₂ solid solution system. In this purpose we are using a Setaram multi detector high temperature calorimeter (MDHTC), operated in drop mode and the heat capacity is obtained by derivation of the measured enthalpy increments over temperature [3]. The enthalpy increments of (U_{1-y}, Am_y)O₂ solid solutions were measured in the temperature range 400 – 1800 K and fitted using the least squares method.

The results of this study will be used to clarify if uranium and americium dioxides that form a continuous solid solution show an ideal behavior of the heat capacity (i.e. can be calculated by summing the proportional weights of their end-members) or if some excess contributions appear. The derived C_p curves of (U_{1-y}, Am_y)O₂ solid solutions, in the temperature range 298 – 1800 K, and the origin of the behavior will be discussed.

A Knudsen cell coupled with a mass spectrometer was used to perform vapour pressure measurements [4]. The vaporisation behaviour of (U_{1-y}, Am_y)O₂ solid solution samples has been studied in vacuum at high temperatures up to 2400 K. The evolution of the uranium and americium bearing species was also determined as a function of time, in order to evaluate the congruent vapour composition. Appearance potentials of the key molecular species were determined by varying the energy of the ionising electrons at constant temperature. The partial and the total vapour pressures of the oxides have been measured as a function of temperature. The dissociative ionisation contribution was evaluated with respect to the composition of the gaseous phase which under Knudsen conditions is in equilibrium with the condensed phase. The results on the vapour pressure of the (U_{1-y}, Am_y)O₂ samples will be discussed.

All the thermodynamic results obtained in this study are used for a consistent description of the ternary U-Am-O system and optimisation of the phase diagram.

REFERENCES

- [1] C. Ganguly *IAEA-TECDOC*, 352, pp. 107-127 (1985).
- [2] W. Bartscher and C. Sari, *Journal of Nuclear Materials*, 118, pp. 220-223 (1983).
- [3] O. Beneš et al., *J. Chem.*, 49, pp. 651-655 (2011).
- [4] P. Gotcu-Freis et al., *J. Chem. Thermodynamics*, 43, pp. 492-498 (2011).

THERMODYNAMIC STABILITY AND KINETIC ASPECTS OF CH₄ - CO₂ HYDRATE EXCHANGE

K. S. Glavatskiy*, M. H. Waage*, T. J. H. Vlught**, T. S. van Erp*, S. Kjelstrup*

*Department of Chemistry, Norwegian University of Science and Technology, NO 7491 Trondheim, Norway, E-mail: magnus.h.waage@ntnu.no.

**Delft University of Technology, Process & Energy Laboratory, Leeghwaterstraat 44, 2628 CA Delft, The Netherlands

EXTENDED ABSTRACT

Hydrates are ice-like, crystalline structures, occurring at high pressures and temperatures around 5°C, in which gas molecules are trapped in water-cages[1]. Research on hydrate formation has become increasingly popular since it became evident that large reserves of naturally occurring methane hydrates exist. As the total amount of methane trapped in hydrates exceeds the collected amount of conventionally available gas, research on harvesting of methane hydrates becomes imperative.

By exchanging CH₄ with CO₂, two things can be accomplished. We harvest natural gas for energy production, and we store a greenhouse gas. We thus have an elegant solution to two problems of paramount importance.

In previous work, the thermodynamic properties of an sI hydrate filled with CO₂, CH₄, and a mixture of the two has been studied[2] using semi-Grand Canonical Monte Carlo simulations. An empty hydrate lattice, with a specified amount of water molecules, was filled with CO₂ and CH₄ while maintaining constant volume and temperature. The Helmholtz energy difference between an occupied hydrate and an empty hydrate with isolated gas molecules was computed. Thus, a potential thermodynamic pathway for exchanging CH₄ for CO₂ hydrates was found. In that work, calculations for the Helmholtz energy associated with the formation of the empty hydrate structure were not reported. Now, we will present precisely those results[3]. In addition, we will report values for the Gibbs energy associated with this process. Those values are relevant for applications where one operates at a constant pressure, rather than at a constant volume.

The kinetic aspects of the CO₂ - CH₄ exchange are also important. In order to establish a model of guest molecules swapping cages, we first investigate H₂ molecules diffusing into empty cages in an sII hydrate. We expect the H₂ molecules to have an easier time swapping cages, due to their smaller size. It will be necessary to introduce flaws in the hydrate lattice, by removing some water molecules[4]. A fraction of the hydrate is filled with H₂, such that a gradient of the filling fraction arises along one of the axes. By artificially maintaining this gradient, we will obtain a flow along the direction of the gradient. By calculating the average flow for different gradients, we can thus establish the diffusion constant for one total fractional filling.

With the model for cage swapping established, we consider pure CO₂ and CH₄ diffusing in an otherwise empty lattice. We then consider a mixture of CO₂ and CH₄. Results from these simulations will be presented.

REFERENCES

- [1] Sloan, E. D.; Koh, C. A.; Clathrate Hydrates of Natural Gases, 3d Edition
- [2] Glavatskiy, K. S.; Vlught, T. J. H.; Kjelstrup, S. J. Phys. Chem. B, 2012, 116(12), pp 3745-3753
- [3] Glavatskiy, K. S.; Vlught, T. J. H.; Kjelstrup, S. in preparation
- [4] Peters, B. et al.; J. Am. Chem. Soc., 130 17342 (2008)

STUDY OF THERMODYNAMIC AND STRUCTURAL PROPERTIES OF A FLEXIBLE HOMOPOLYMER CHAIN USING MULTICANONICAL MONTE CARLO METHOD

Chahrazed Meddah*, Sid Ahmed Sabeur**, Amine Bouziane Hammou***

*LAAR, Département de Physique, Faculté des Sciences, USTOMB,
BP 1505 El M'naouer, Oran 31000 Algérie, E-mail: chahrazedmeddah@gmail.com

**LPPMCA, Département de Physique, Faculté des Sciences, USTOMB,
BP 1505 El M'naouer, Oran 31000 Algérie, E-mail: sidsabeur@gmail.com

***LEPM, Département de Physique, Faculté des Sciences, USTOMB,
BP 1505 El M'naouer, Oran 31000 Algérie, E-mail: aminebh@yahoo.fr

ABSTRACT

We study the thermodynamic and structural properties of a flexible homopolymer chain by means of multi-canonical Monte Carlo method. In this work, we focus on the coil-globule transition. Starting from a completely random chain, we have obtained a globule for different sizes of the chain. The implementation of these advanced Monte Carlo method allowed us to obtain a flat histogram in energy space and calculate various thermodynamic quantities such as the density of states, the free energy and the specific heat. Structural quantities such as the radius of gyration were also calculated.

INTRODUCTION

Monte Carlo methods are very efficient to study the behavior of complex systems. However, the Metropolis method[1] in the canonical ensemble is not able to sample all possible conformations. Especially at low temperatures, the system will be trapped in local energy minima. The simulation in generalised ensemble[2] is the best way to avoid such problems. Recently, the multicanonical Monte Carlo method[3; 4], the Wang-Landau and the parallel tempering methods[5; 6] became very popular in statistical physics. Their approaches allow the system to visit all possible energy states in a single simulation in order to produce a flat histogram in the energy landscape.

In this work, we present a multicanonical Monte Carlo study to understand the coil-globule transitions in homopolymer systems. The model and the simulation method are described in Sec. II and III respectively. The results are given in Sec. IV and we conclude in Sec. V.

MODEL AND SIMULATION METHOD

The polymer chain is described by a coarse grained off lattice flexible homopolymer model that contains N identical monomers (the same model used in references[7; 8; 9]). The non bonded monomers interact pairwise via a truncated shifted Lennard Jones potential given by

$$U_{LJ}(r) = 4\epsilon \left[\left(\frac{\sigma}{r} \right)^{12} - \left(\frac{\sigma}{r} \right)^6 \right] - U_{LJ}(r_c) \quad (1)$$

here r denotes the relative distance between the monomers. ϵ is set to 1, $r_c = 2.5\sigma$ and $\sigma = r_0 2^{-\frac{1}{6}}$ with the minimum potential distance $r_0 = 0.7$, and the bonded interaction between nearest

neighbors is given by the FENE potential,

$$U_{FENE}(r) = -\frac{k}{2} R^2 \ln \left\{ 1 - \left[\frac{r-r_0}{R} \right]^2 \right\} \quad (2)$$

k is a spring constant set to 40 and $R = 0.3$.

The total energy is given by

$$E_{tot} = \sum_{i=1}^N \sum_{j=i+1}^N U_{LJ}(r_{ij}) + \sum_{i=1}^{N-1} U_{FENE}(r_{ii+1}) \quad (3)$$

The curves of the potentials as a function of the distance between two monomers are shown in figure 1.

In the present work, we employ the multicanonical Monte Carlo algorithm[3; 4] that consists of performing a random walk in energy space. The Boltzmann energy distribution $P_{can}(E) = g(E) \exp(-\beta E)$ is deformed by introducing weight factors $W(E)$ which are unknown a priori and have to be determined iteratively. Thereby, the multicanonical energy distribution will be $P_{muca}(E) = g(E) \exp(-\beta E) W(E) = H(E)$. Where $H(E)$ denotes the multicanonical histogram.

Initially, the weight factors $W^0(E) = 1$ are set to unit. We start by performing a simulation at infinite temperature under canonical distribution which yields an estimate histogram $H^0(E)$. The estimation $W^1(E)$ is given by $W^1(E) = \frac{W^0(E)}{H^0(E)}$. Then, in the next run yield an estimate of $H^1(E)$ and $W^2(E) = \frac{W^1(E)}{H^1(E)}$ and so on. The iterative procedure is continued until the multicanonical histogram is flat.

After having estimated the appropriate weights $W(E)$, a long production run is performed to determine different statistical quantities which can be obtained by the following equation

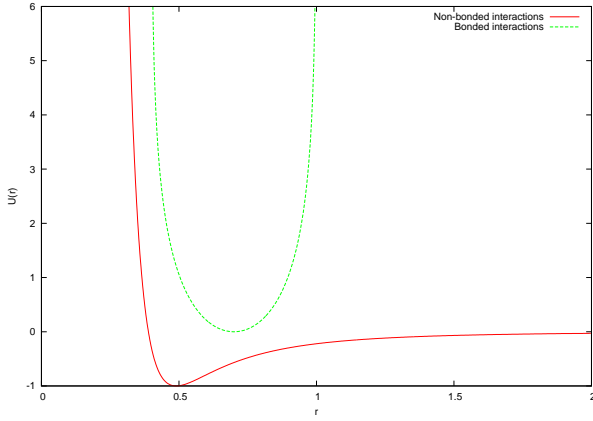


Figure 1. Bonded and Non-bonded potentials versus the distance between two monomers

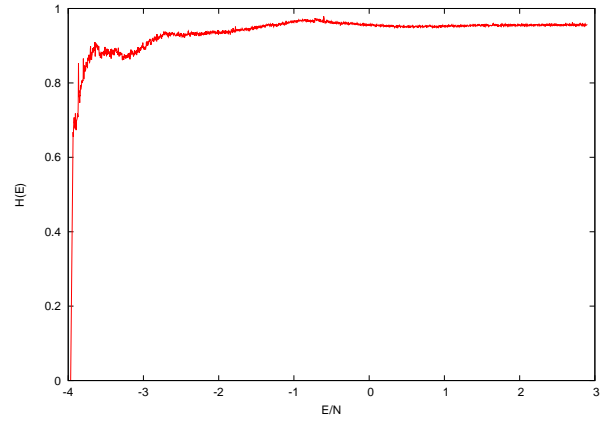


Figure 2. Flat multicanonical histogram obtained for a homopolymer chain with $N=43$ monomers.

$$\langle A \rangle_T = \frac{\sum_E A_E H(E) / W(E) e^{-E/k_B T}}{\sum_E H(E) / W(E) e^{-E/k_B T}} \quad (4)$$

RESULTS

In the following, we present results of the multicanonical simulation for homopolymer chains for $N = 19, 43$ and 51 . to obtain the multicanonical weights we performed 300 iterations with 10^5 sweeps at each iteration. One sweep is N displacements updates. The simulation has been performed over an energy range in $E/N \in [-3, 4]$ which is divided in bins with bin resolution $dE = 0.1$ and temperature range in $[0.01; 5]$ A long simulation with 3×10^8 sweeps is performed to obtain thermodynamic and structural quantities.

In figure 2 we show the multicanonical histogram obtained at the end of simulation for homopolymer chain with $N = 43$ monomers. In figure 3, we plot the specific heat obtained for different length of the chain. The coil-globule transition is characterized by a peak that appears at approximately $T \simeq 0.5$.

In our simulation we used the shift monomer update, that type of displacement does not allow the detection of the transition signatures at low temperatures. More sophisticated moves are required such as crankshaft move, end bridging move, reptation move[10] and the bond exchange move[11]. We are implementing these types of displacements.

The radius of gyration (structural quantity) is shown in figure 5 for the different lengths of the chain.

CONCLUSION

The coil-globule transition for homopolymer systems is studied by means of multicanonical Monte Carlo simulation for $N = 19, 43$ and 51 chain sizes. To improve our results, It would be more efficient to use more sophisticated displacement algorithm. Especially at low temperature, where transition signatures are still difficult to detect.

Our code was validated for $N = 30$ with the results of another group[8].

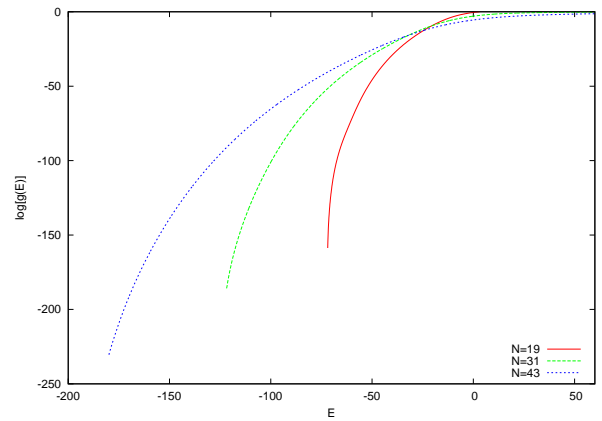


Figure 3. Density of states obtained for homopolymer chains with different length of the chains $N=19, 43$ and 51 .

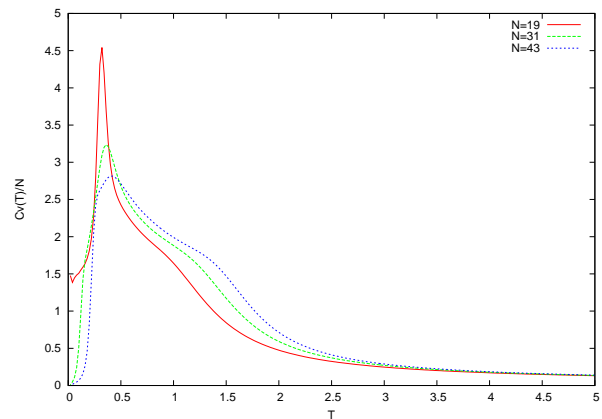


Figure 4. Specific heat per monomers with different lengths $N=19, 43$ and 51 versus temperature in range $[0, 5]$.

ACKNOWLEDGMENT

We would like to thank Prof. Michael Bachmann for helpful discussions.

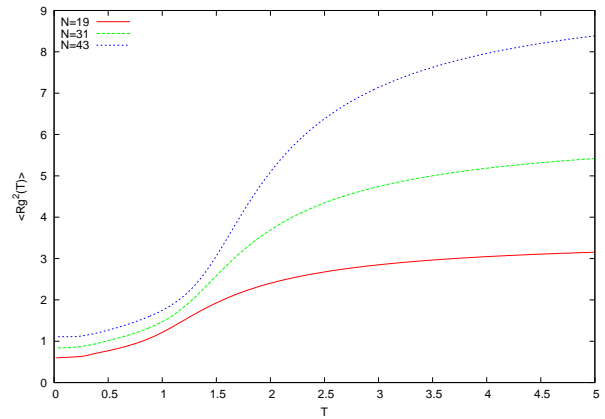


Figure 5. Radius of gyration obtained for $N = 19, 43$ and 51 vs temperature.

REFERENCES

- [1] N. Metropolis, Arianna W. Rosenbluth, Marshall N. Rosenbluth, Augusta H. Teller and E. Teller, *J. Chem. Phys.*, vol. 21, pp 1087,1953.
- [2] M. Mezei, *J. Comput. Phys.*, vol. 68, pp 237248,1987.
- [3] B. A. Berg, T. Neuhaus, *phys. Lett. B*, vol. 267, pp 249,1991.
- [4] B. A. Berg, *J. Stat. Phys.*, vol. 82,1995.
- [5] F. Wang and D. P. Landau, *Phys. Rev. E*, vol. 64, pp 056101,2001.
- [6] R. H. Swendsen, J. S. Wang, *Phys. Rev. Lett.*, vol. 57, pp 2607,1986.
- [7] S. Schnabel, M. Bachmann and W. Janke, *Elastic Lennard-Jones polymers meet clusters: Differences and similarities*, *J. Chem. Phys.*, vol. 131, pp 124904,2009.
- [8] S. Schnabel, T. Vogel, M. Bachmann and W. Janke, *Surface effects in the crystallisation process of elastic flexible polymers*, *Chem. Phys. Lett.*, vol. 476, pp 201,2009.
- [9] D. T. Seaton, T. Wüst and D. P. Landau, *Collapse transitions in a flexible homopolymer chain: application of the Wang-Landau algorithm*, *Phys. Rev. E*, vol. 81, pp 011802,2010.
- [10] F. A. Escobedo and J. J de Pablo, *J. Chem. Phys.*, vol. 102, pp 2636,1995.
- [11] S. Schnabel, W. Janke, and M. Bachmann, *Advanced Multicanonical Monte Carlo Methods for Efficient Simulations of Nucleation Processes of Polymers*, *J. Comput. Phys.*, vol. 230, pp 4454-4465,2011.

INNOVATIVE THERMODYNAMICAL CYCLES BASED ON ENHANCEMENT MASS, MOMENTUM, ENTROPY AND ELECTRICITY TRANSPORT DUE TO SLIP, MOBILITY, TRANSPARATION, ENTROPY AND ELECTRIC JUMPS AS WELL AS OTHER NANO-FLOWS PHENOMENA.

Paweł Ziółkowski*, Witold Zakrzewski*, Janusz Badur*

*Department of Energy Conversion, Institute of Fluid Flow Machinery PAS-ci, Gdańsk, POLAND
E-mail: pawel.ziolkowski@imp.gda.pl

ABSTRACT

In our work, a further development of the authors model of thermo-chemical flow of fuel, air, oxygen, steam water, species, ionic and electron currents within nano channels and nano-structures of novel devices is presented. Different transport enhancement models are taken into account -among them the most important are: the velocity slip connected with complex external friction, the Darcy mobility and the Reynolds transpiration. Increasing gas path to the triple-phase-boundary (TPB) enhances mass and electricity fluxes due to the concentration jump and the electron resistivity jump. Enhancement of heat transport due to the von Smoluchowski jump is considered within the frame of generalized model of Navier-Stokes slip boundary condition. Particular elements of the model have been tested and calibrated on the literature benchmark experiments concerning nano-flows, nano-combustion, nano-condensation and separation. Integrated geometrical characteristics of working fluids and canal materials such as: porosity, tortuosity and mean radii are finally involved into a macroscopic continuum model, and implemented into the standard CFD code. As a result of analysis the production characteristics have been examined and compared with the benchmark data.

MOTIVATION OF OUR STUDY

Standing within the current clean coal technologies, the coal-fired power plants using carbon capture equipment becomes an expensive source of electricity in Poland. Other power sources, such as wind, nuclear, geothermal are in a starting level and cannot be taken to be a serious candidate to repowering of polish energy market. One of contra-candidate to the clean coal power plants are, at the moment, the plants based on natural and shale gases ei. the combined cycle with CO₂ capture technology that currently appear to be more economical [17].

Due to recent possibility, growing after discovery of Polish natural and unconventional gas sources, a new possibility of realistic huge cleaner than coal heat energy source will be obtainable in a few years. In this new chance for modern repowering of Polish energy system, as we assume, the steam turbines technologies should be widely used, firstly, for combined heat and power plants [16; 17]. The new candidates to repowering are plants based on the gas-steam combined cycles erragemed within innovative thermodynamical cycle based, generally, on using of different nanoflow phenomena. But in innovative combined cycle the role a steam turbine change radically. Now, unlike a gas turbine, in a steam turbine heat is only a byproduct of power, therefore in cogeneration, steam turbines generate reduced amount of electricity as a byproduct of heat contained in flue gases. Recall, that usually about 10 kg/s of flux of flue gases is needed for generating of 1 kg/s of fresh steam [4; 5; 15; 16]. In conventional combined cycle, a steam turbine is captive only to a separate heat source and does not directly convert fuel to electric energy. The energy is transferred from flue gasses to the turbine through a multi-pressure steam generator

(HRSG) [14; 15], and steam such produce, in turn, powers the turbine and generator. This separation of functions enables steam turbines to operate independently from the gas turbine. Therefore some advantages of steam turbines as for instance, unusually high drop of pressure from 22 MPa to 500 Pa cannot be fully explored in the whole conversion process¹.

In the following paper, one of innovative cycle is a compact combined cycles which turns combined heat and power plants to a power plant dedicated only to clean electricity production. It can be done by removing of the HRSG from a role of heat exchanger between the flue gases and working water, and to replace the combustion chamber on a internal direct steam producer [17]. Such combined gas and steam turbines can keep their main performance specifications like the high pressure (22 MPa) and high temperature (1100°C) - it is quite a new situation - up to now there is no steam turbine with such high temperature of working medium, and, vice versa, there is no gas turbines with such extremely high pressure. Since this concept can be simply and naturally connected with concept of oxy combustion there is a thermodynamical base for a zero-emission gas-steam turboset.

Especially, in next chapter, the particular analysis of gas-

¹Now, The basic question is - does clean gas technologies shall be economically substantial? The leading factor is the gas price due to Gasprom monopole. The hope on cheaper gas comes from the recent searches of the shale gas in the Pomerania district. The ability to economically produce natural gas from unconventional shale gas reservoirs in Poland, has been made possible recently through the application of horizontal drilling technology and so-called "hydraulic fracturing" (e.i. fracking, fracturing). Concerns like: Chevron, Exxon Mobil, ConocoPhillips, Marathon Oil, have already prepared this drilling technique which has revolutionized gas production in the United States. [17]

steam turbine within a zero-emission cycle will be presented. In that case, the working fluid contains only the mixture of CO_2 and H_2O what leads to direct separation of CO_2 [11; 12; 13].

Innovative cycles, concerned here, leading to high-efficient, zero-emission energy production and there are combined from simple cycles ordered in a conversion cascades [10; 8]. Typical for these cycles the enhancement of efficiency and power are to be obtained via compactification of devices dimensions and using of the so-called direct conversion. For instance, fuel cells are profitable modern devices being the best examples of a useful machinery where complex conversion of energy at nano-scale takes place. Especially, we observe such conversion at the high temperature solid oxide fuel cell (SOFC) that is built from ceramic nanomaterials. Anode supported fuel cell consist mainly of two nanoporous electrodes (cermets, lanthanum strontium manganite) separated by a thin, very dense solid electrolyte (yttria-stabilized zirconia or perovskite-type material). Finding of a mathematical model of an acting SOFC at temperatures as high as 1000°C is a serious challenge as well for nanomechanics as for nano-thermo-chemistry [10; 8].

ZERO-EMISSION CYCLE VIA A STEAM-GAS TURBINE

Concept of cycle based on enhancement energy transport

In principle the oxycombustion and capture of CO_2 can be accomplished more easily and cheaply than post-combustion removal of CO_2 from the exhaust gases emitted by a conventional coal plant. The promise of more efficient carbon capture is one of the primary rationales for clean gas technology (CGT). Ziólkowski et al. [17] has recently been prepared a concept of repowering of GT8C cycle. Their concept is based on introducing of compact nanotechnology devices leading to removing large-scale devices like Heat Recovery Steam Generator (HRSG) and Low Pressure Condenser (Fig. 1). The first is to exchange the combustion diffusional mode from the classical one into a one based on oxygen nano-enriched air. In this same place (MKS), phenomena of nano-removing of heat revised form oxygen-hydrocarbon combustion process occur which is governed by adequate steam injection (water-nano-jets) into the combustion zone. It leads directly to high enthalpy flue gases that contain only CO_2 and steam. The second novel element is a Dual Brayton Cycle used for steam condensation and compression of CO_2 . The enhanced condensation is based on nano-injection of cold water condensate and a jet compression of CO_2 (in SNS). Due to compactness of process within turbine low part and exhaust hood, as well as the heat recuperation high efficiency is obtained.

CFM simulation

By introducing enhancement transport and conversion integral-like coefficients into zero-dimensional model of thermodynamical cycle, it is possible to simulate the work of an innovative zero-emission power plant. A starting point for conversion of GT8C into zeroemission-GT8C has been taken as normal operating condition for PGE Gorzów. Data for numerical analysis of traditional GT8C have taken from literature [16]. Two different modernization of GT8C have been considered. Both modernizations are based on oxy combustion,

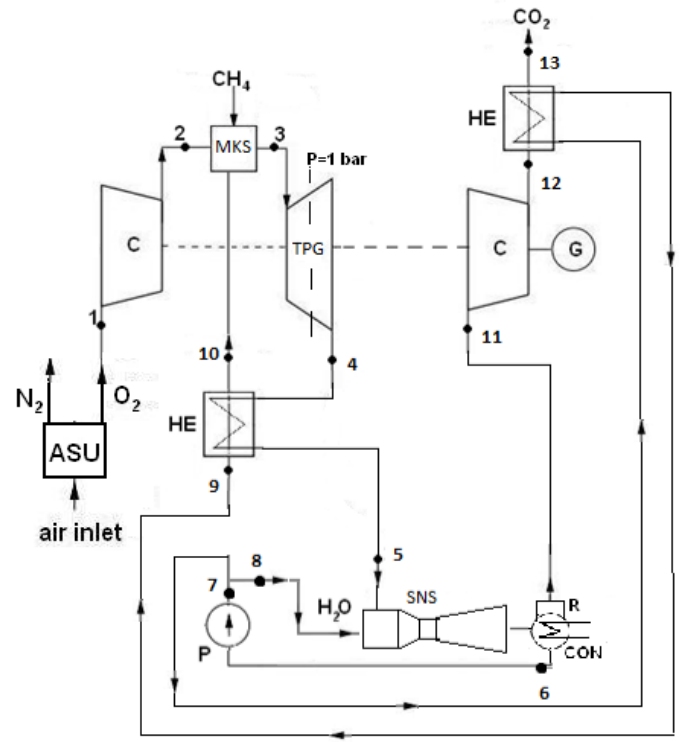


Figure 1. IFFM cycle to the compact, high efficiency and zero-emissions power plant, where the MKS - Wet Combustion chamber, TPG - Paro-Gas Turbine and SNS - Condenser spray-ejector, C - compressor, HE - heat exchanger, G - generator, P - pump and R - a gas-water separator, CON - condenser

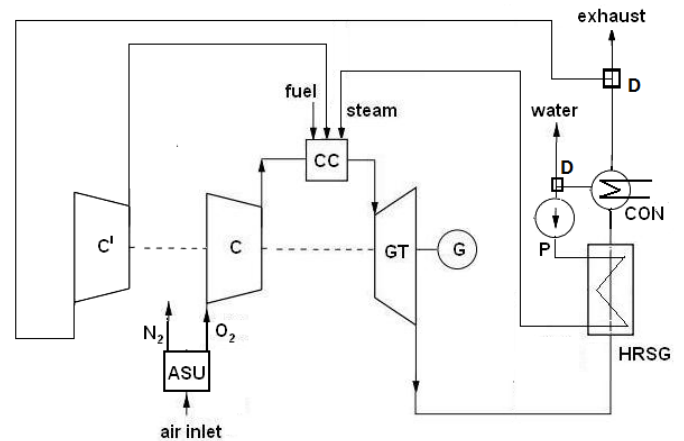


Figure 2. PGE Gorzów plant scheme of a gas-steam turbosets with oxy combustion and flue gases recirculation (ASU - air separation unit, C - compressor, C' - additional compressor, CC - combustion chamber, GT - gas-steam turbine, HRSG - heat recovery steam generator, P - pump, CON - condenser, D - dividing elements).

steam/water injection and steam from exhaust gases condensation (Fig. 1 and Fig. 2). The basic original cycle contains: 12-stage compressor (C); silo-combustion chamber (CC), and three stage gas turbine (GT). Modernized cycle presented on(Fig. 2) contains also; an air separation unit (ASU); heat recovery steam generator (HRSG), condenser of water vapor (CON), additional compressor (C') for recirculation flue gases, a pump (P) and dividing elements (D).

The station ASU products ca. 14,8kgO₂/s and its power consuming ratio is 0,248kWh/kgO₂ [6]. From HRSG one obtains mass flux of steam $\dot{m}_{st}=28\text{kg/s}$, what together with the combustion steam flux (ca. 8kg/s) gives 0,2 mass fraction in steam-gas working fluid. This H₂O - CO₂ mixture expands in a gas turbine from pressure 16,2 bar to ambient pressure, and next, after cooling down in HRSG, goes into a steam condenser. The excess of CO₂ after compressing to the pressure of liquidation is removed from the cycle [6; 7].

Comparison of solutions

The principal differences in both modifications lead on the treatment of amount of injected fuel and amount of components working medium. In the second modification (Fig. 2) the fuel mass flow rates \dot{m}_f becomes the same like in original GT8C. In the first one (Fig. 1), the fuel mass rate becomes higher. We noted that together with increasing of \dot{m}_f the temperature at combustion chamber t_{KS} grow. The netto efficiency of IFFM cycle with oxy combustion and capture CO₂, at the level of $\eta_{el-netto} = 43.67\%$. The decrease of the efficiency is caused by the oxygen producing (6.38%) and capture the CO₂(2.28%). The indubitable advantage of this cycle with oxy combustion and CO₂ capture is lack of pollution such as NO_x and CO₂ (Fig. 2). Essential results are shown in (Tab. 1).

Table 1. Comparison of two conversions of GT8C into the gas-steam turbine.

Parameters	dimension	Original GT8C	I modification Fig1	II modification Fig2
t_{0t}	[°C]	15	15	15
p_{0t}	[bar]	1,013	1,013	1,013
t_f	[°C]	15	15	15
p_f	[bar]	40,5	40,5	40,5
\dot{m}_f	[kg/s]	3,21	12,83	3,41
\dot{m}_{sp}	[kg/s]	182,3	182,3	182,5
\dot{m}_{st}	[kg/s]	-	-	28
t_{st}	[°C]	-	-	580
t_{GT}	[°C]	520	272	591
t_{KS}	[°C]	1100	1274	1032
η_{el}	[%]	34,8	43,66	32,55
N_{el}	[MWe]	54,5	281,3	54,1
\dot{m}_{spot}	[kg/s]	182,3	35,8	11,0
CO ₂	[kg/MWh]	592	0	610
NO _x	[kg/MWh]	0,3670	0,0003	0,0079
[O ₂]	[-]	0,139	0,002	0,181
[H ₂ O]	[-]	0,076	0,001	0,017
[N ₂]	[-]	0,745	0,014	0,027
[CO ₂]	[-]	0,031	0,987	0,775
[NO _x]	[ppm]	30	0,6	15

The electrical efficiency of the conventional GT8C is calculated to be $\eta_{el} = 34,8\%$. The GT8C conversion to the gas-steam cycle with oxy combustion results and recirculation in decreasing of efficiency to the level of $\eta_{el} = 32,6\%$. But simultaneously, the significant decreasing of NO_x emission to the level of

8g/MWh have been observed. Yet other advantage is reduction of the flue gases rates that is rejected into ambient air: 11kg/s, since the flux 136 kg/s flue gases undergo recirculation connected with condensation of 35kg/s steam water. It is also observed the increase of CO₂ emission to ca. 18kg/MWh In comparison with the original cycle GT8C. On the other hand in both modification, simultaneously, the grow of mole fraction [CO₂] from level 0,03 to 0,987 (I modification - CO₂ is captured in the end) to 0,78 (II modification) is observed (Tab. 1). It appears that one obtain the better conditions to carbon capture from the flue gases.

ZERO-EMISSION CYCLE WITH SOFC AND GAS TURBINE

Nano-phenomena within SOFC

Within the context of mounting pressures on zero emission technologies fuel cell systems will play a major role. Since a fuel cell, like SOFC is working without the Carnot limit of efficiency, the systems build on the fuel cells can approach more effective, then conventional, energy conversion processes. On known system combining SOFC and gas turbine working with power 300 kW, has been developed by Siemens Westinghouse. Yet another system leading to advance zero emission power plants has been prepared and tested by Lemański [10]. Their concept is to combine high-temperature solid oxide fuel cells (SOFC) with gas shifting and post-combustion of a rest fuel within a one chamber. Since the efficiency of pSOFC/GT system depends mainly form a level used pressure, Lemański has research a system with double levels of pressure and double SOFC; one working in the higher and one in lower pressure (Fig. 3). The ratio of both pressures change from $\Pi = 1 \div 3.8$ and it depends on additional heat exchange between high and low pressure parts. The electrical efficiency of double pressure pSOFC/GT system is calculated - with increase of Π the electrical efficiency both SOFC becomes lower, but tie total efficiency of system increse mainly due to higher inlet parameters for gas turbine. To be included is delving into the impact fuel cell-CO₂ capture technology from hydrocarbon sources might have in terms of energy economics, as well as on our evolving energy resource mix and on renewable energy development.

CFD simulation

The high temperature solid oxide fuel cell is build mainly from nanomaterials. It consists of two porous electrodes separated by a dence solid electrolyte. Finding of a solid-state material that operate at temperatures as high as 1000°C is a serious challenge. Especially, porous ceramics, being double phase electrodes, needs advanced mathematical modeling [3; 8] which include some nano-flow effects. The phenomenological description of a combination of a huge number of a single nano-channel can be given by two geometrical parameters of porous body: porosity factor, the mean pore radius, and tortuosity. Tortuosity is defined as the ratio of the porous channel length to the straight distance between the end surfaces of the control volume. Tortuosity together with porosity indicates the ratio of the active surface to the volume electrodes. Mean radius of pores is the basic parameter determining nano-flows. All these parameters are involved mainly in description of parameters of 3D model like the diffusive transport of species throughout a fuel cell. The main diffusion mechanism i.e. molecular dif-

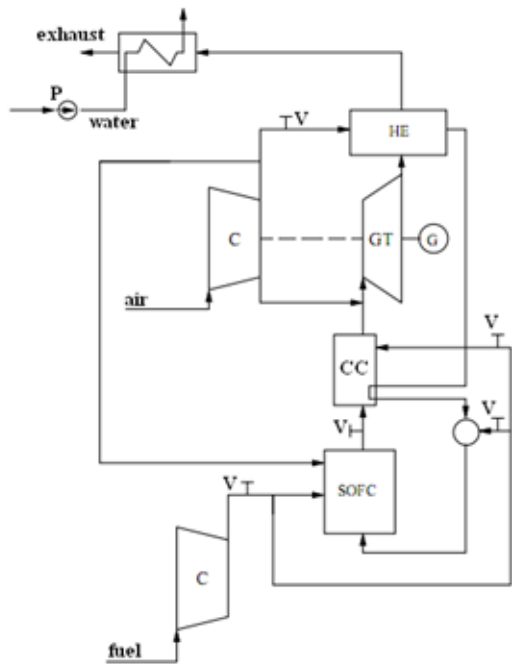


Figure 3. The scheme of hybrid pSOFC/GT used in commercial application by Siemens Westinghouse (SOFC - solid oxide fuel cells, CC - combustion chamber, C - compressor, GT - gas turbine, HE -heat exchanger, V - valve, P - pump) [10; 9].

fusion, Knudsen diffusion and Darcy's pressure diffusion, Pelat electrical diffusion are, generally, a function of above nano-geometrical parameters [2; 3; 1].

On (Fig4) solution domain of a tubular fuel cell is presented. In present paper, a tubular geometry examined by Siemens and Westinghouse was employed with basic dimensions given elsewhere [4]. The model has been implemented into commercial solver using user subroutine technique (UDF) and validated.

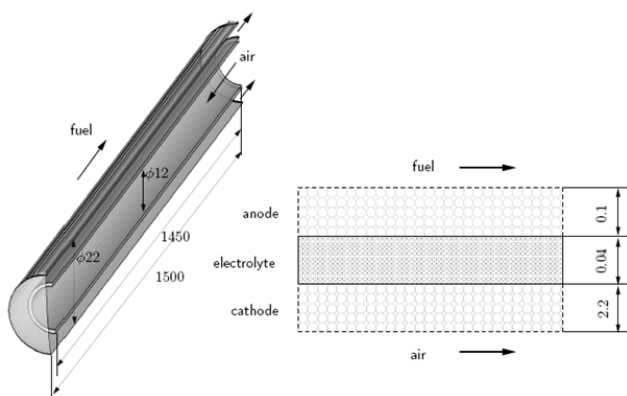


Figure 4. 3D Computational domain for a SOFC tubular [8].

Local solution based on slip velocity, thermal, mass and electric potential mobility forces has been adopted in average manner to transcription of phenomenological coefficients in function of porosity, tortuosity and mean pore size. Finally the mean pore radii has been taken to be equal 300 nm. In Fig5 dependence of generated voltage on current at various porosities are presented. When lower porosities are assumed the concentration polarization is higher. However, a higher tortuosity explicitly disturb the mass diffusion process (Fig6).

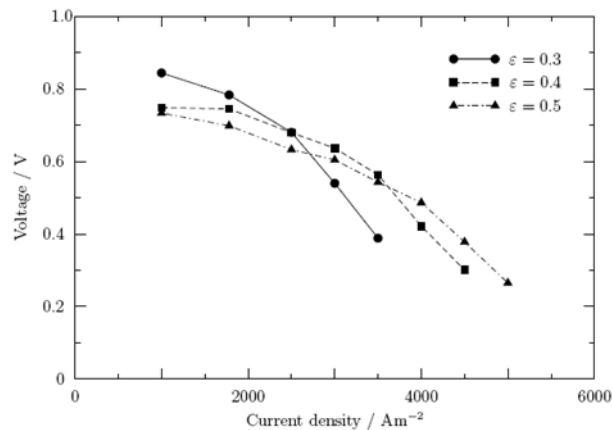


Figure 5. Influence of porosity nano parameter on SOFC performance [8].

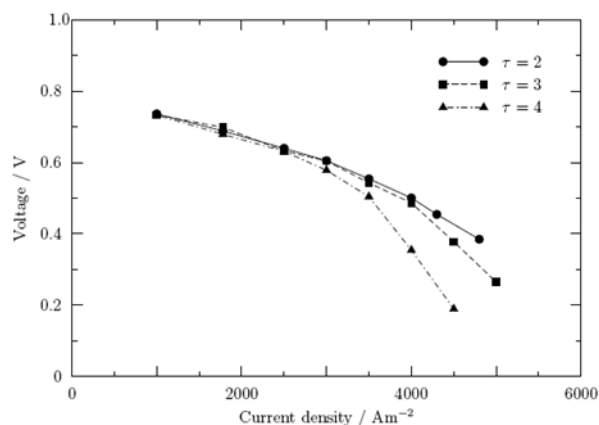


Figure 6. Influence of nano tortuosity parameter on SOFC performance [8].

Yet other novel concept is to use instead of air some oxygen enriched mixture. It can be done if one exchange of ASU unit for oxygen separation by modern technique called the Mixed Conducting Membranes (MCM) which produce pure oxygen from air which produce pure oxygen from air [2]. These membranes acts similarly to the cathode in a SOFC which can conduct ions via non-porous, metallic oxides that operate at high temperatures, i.e. $> 700^{\circ}\text{C}$. In comparison to cathode material it has high oxygen flux and selectivity. Utilization of the MCM reactor instead of ASU means its integration into conventional gas turbine combustion. Similarly to SOFC, the classical chamber in an ordinary gas turbine is replaced by the MCM-reactor, which includes a combustion chamber, a 'low' temperature heat exchanger, an MCM membrane and a high temperature heat exchanger. The concept allows 100% CO_2 capture, increase of cycle efficiency to 50%, and will in this case have less than 1 ppm v/v NO_x in the oxygen depleted outlet air.

ROLE OF NANO-FLOWS PHENOMENA

Despite the achieved fluency in experiment design, there is an apparent lack of understanding of the energy conversion enhancement in it's theoretical background. This is revealed with the numerical prediction discrepancy compared to measurement. Usually, the discrepancy grows with the growth of a medium rarefaction, and the channel hydraulic diameter [2; 3]. That is, when the channel's diameter is comparable with the mean free path of molecules (which is defined as Knudsen

number), acquired either through increased rarefaction or decreased channel diameter, the flow slip seems to occur. This rule also stands for other phenomena, when their influence on the bulk flow is not negligible. By the last statement it is understood, that although the phenomena may be present in a large scaled devices, they seem to be of insignificant importance. When the boundary layer however, extends to the bulk, as it takes place in micro and nano channels, the wall effects alter the entire flow field.

Boundary friction forces

In nano-flow boundary friction appear as a generalization of Young's form of boundary condition:

$$\vec{f} + \vec{\tau}_w = 0. \quad (1)$$

which stay that the boundary friction force is equal to the fluid "wall stress". It is a very neat representation, and to some extent complete. If one considers a simple flow of a fluid in contact with the solid wall we must to add a condition that the solid "wall stress" should be equal the fluid "wall stress" and the friction force. However, in a more general case, as Poisson has shown, the condition requires further extension for the inclusion of capillary forces, most important in case of multi-phase flows. The capillary forces may have a strong influence on friction and velocity slip. The Cauchy boundary condition is hence supplemented with an additional term by Poisson, and has a form:

$$\vec{f} + \vec{\tau}_w + \text{div}_s (\gamma \overleftrightarrow{I}_s) = 0 \quad (2)$$

According to Duhem and Roy the friction forces must be based on the velocity slip in the following form :

$$\vec{f} = \left(v_0 \frac{1}{|\vec{v}_s|} + v_1 + v_2 |\vec{v}_s| \right) \vec{v}_s \quad (3)$$

governed by three slip coefficients v_0, v_1, v_2 and where \vec{v}_s - surface velocity. On the other hand, in the boundary condition definition Eq.(1), there is the wall stress vector, which is, in accordance with Cauchy definition, defined to be $\vec{\tau}_w = \overleftrightarrow{t} \cdot \vec{n}$, where \overleftrightarrow{t} is the Cauchy tensor of momentum flux.

Transpiration effects

Graham and Reynolds transpiration effect manifests itself as a countercurrent at the wall to the main flow. That is, while the gradient between the inlet and the outlet of a microtube generates the flow in the opposite to the gradient direction, the transpiration occurs as the counter flow at the fluid - solid interface. When spoken of Graham observed transpiration, we speak of concentration transpiration. The "wall flow" occurs from the region of a lower concentration to the region of a higher concentration of a given constituent. When spoken of Reynolds observed transpiration, we speak of thermal transpiration, i.e. the flow from region of a lower temperature to the region of a higher temperature, also at the fluid - solid interface. Taking into account the transpiration effects, and also accounting for

the pressure transpiration we achieve a more general form of the friction force definition as:

$$\vec{f} = v_1 (\vec{v}_s - \vec{v}_{wall}) - (c_{s,\varpi} \text{grad}_s \varpi + c_{s,c} \text{grad}_s c + c_{s,\theta} \text{grad}_s \theta + c_{s,\phi} \text{grad}_s \phi) \quad (4)$$

Where appears Navier's slip coefficient and the pressure ($c_{s,\varpi}$), concentration ($c_{s,c}$), thermal transpiration ($c_{s,\theta}$) and electro-mobility $c_{s,\phi}$ coefficients, respectively.

Temperature jump model

Proposed by von Smoluchowski temperature jump model introduces a characteristic length scale It defined as the jump length, which is connected with the heat boundary condition:

$$h(\theta - \theta_{wall}) + \vec{q} \cdot \vec{n} = 0, \quad (5)$$

where heat flux is defined by Fourier law $\vec{q} = \lambda \text{grad} \theta$; h - coefficient of thermal conduction, θ_{wall} - temperature on the wall, λ - thermal conductivity coefficient

Temperature jump length was defined by Smoluchowski to be:

$$l_\theta = \frac{\lambda}{h}. \quad (6)$$

Now if one postulate of Navier-Stokes layer temperature then a generalized form of the boundary condition has a form:

$$\begin{aligned} & \partial_t (c_{p,s} \theta_s) + \text{div} (c_{p,s} \theta_s \vec{v}_{s||}) - \theta_s \overleftrightarrow{I}_s \vec{v}_s \vec{n} \\ & + \text{div}_s (\lambda_s \text{grad}_s \theta_s) + h(\theta - \theta_{wall}) + \vec{q} \cdot \vec{n} = 0 \end{aligned} \quad (7)$$

where $\overleftrightarrow{I}_s = \overleftrightarrow{I} - \vec{n} \otimes \vec{n}$, \vec{n} - normal vector, γ - surface stress, div_s - surface divergence, grad_s - surface gradient, $c_{p,s}$ - specific heat of thermal layer, θ_s - temperature of thermal layer $\vec{v}_{s||}$ tangent component of \vec{v}_s .

Concentration jump model

In case of the flow of a fluid mixture an effect of concentration jump may occur, particularly when the reactin mixture is considered, and channel walls have catalytic properties. Thus the discontinuity of concentration may take place in the direction normal to the wall. The model proposed by Lewis defines the concentration boundary condition as follows:

$$\alpha(c - c_{wall}) + \vec{j} \cdot \vec{n} = 0, \quad (8)$$

where constituent flux is defined according to Fick diffusion law $\vec{j} = D \text{grad} c$.

The closure for a corresponding concentration jump was proposed in literature, to be defined as:

$$l_c = \frac{D}{\alpha} \approx 0.03 \text{mm}. \quad (9)$$

Postulating the layer concentration the generalized form of the concentration boundary condition is:

$$\begin{aligned} & \partial_t (\rho_s c_s) + \text{div} (\rho_s c_s \vec{v}_{s||}) - c_s \overleftrightarrow{I}_s \vec{v}_s \vec{n} \\ & + \text{div}_s (D_s \text{grad}_s c_s) + \alpha(c - c_{wall}) + \vec{j} \cdot \vec{n} = 0, \end{aligned} \quad (10)$$

Electric current jump

Numerous researcher on jonic electric current have been shown [8; 10] that enhancement flow of electricity is observed due to nanostructure of the electrolyte medium. Therefore, according to [8] we propose to replace the classical condition of disappearance of electric current on a boundary $\mathbf{j} \cdot \mathbf{n} = 0$, where the jonic current $\mathbf{j} = \sigma \text{grad} \phi$ is described by the Ohm law based on bulk conductivity constant σ – by the following condition of "electric jump":

$$\mathbf{j} \cdot \mathbf{n} + \text{div}(\sigma_s \text{grad}_s \phi) = 0. \quad (11)$$

The surface gradient of electric potential is very important now. It can be treated as a "mobility" surface force. If this force is added to general friction force (4) some additional surface flow appears which is known to be the Pellat effect.

SUMMARY

In the paper the different effects coming from generalized boundary condition model derived in IFFM PASci has been described and numerically implemented 3D as well 0D model. It was shown, that more than velocity slip may account for the enhanced flow phenomenon, i.e. the concentration, thermal, pressure, electric charge or phase progress may have considerable impact on the flow, efficiency, power performance increase. Aside from co-current and counter-current velocity profile influences observed in the micro and nano flows, there exist phenomena enacting on the temperature or concentration continuity occurring in the temperature and concentration jumps in the normal to the fluid-solid interface direction. These discontinuities are non-negligible due to strong wall domination in the micro and nano flows. Further experimental and theoretical investigation in this field is also required to establish the form and value of the model parameters. Along with the mentioned merits, the model provides a good physical interpretation of all the terms, however experimental research is required for further confirmation of the model assumptions.

REFERENCES

- [1] J. Badur. *Development of Energy Concept*. Wyd. IMP PAN w Gdańsku, Gdańsk, 2009.
- [2] J. Badur, M. Karcz, and M. Lemański. On the mass and momentum transport in the navier-stokes slip layer. *Microfluidics and Nanofluidics*, 11:439 – 449, 2011.
- [3] J. Badur, M. Karcz, M. Lemański, and L. Nastałek. Enhancement transport phenomena in the navier-stokes shell-like slip layer. *Computer Modeling In Engineering and Science*, 73:299–310, 2011.
- [4] R. Carapellucci and A. Milazzo. Repowering combined cycle power plants by a modified stig configuration. *Energy Conversion and Management*, 48, 2007.
- [5] D.Y. Cheng. The distinction between cheng and stig cycle. In *Proceedings of ASME EXPO 2006, GT-2006-90382*, 2006.
- [6] C. Gou1, R. Cai, and H. Hong. An advanced oxy-fuel power cycle with high efficiency. *Proc. IMechE Part A: J. Power and Energy*, 220:315–324, 2006.
- [7] M. Jonson and J. Yan. Humidified gas turbine - a review of proposed and implemented cycles. *Energy*, 30:34–39, 2005.
- [8] M. Karcz, S. Kowalczyk, and J. Badur. On the influence of geometric nanostructural properties of porous materials on the modelling of a tubular fuel cell. *Chem. Proc. Eng.*, 31:489–503, 2010.
- [9] M. Lemański. *Analyses of thermodynamic cycles with fuel cells and gas-steam turbine(in Polish)*. Phd thesis, IF-FM PAS, Gdańsk, 2007.
- [10] M. Lemański and J. Badur. Parametrical analysis of a tubular pressurized sofc. *Archives of Thermodynamics*, 25:53–72, 2004.
- [11] F. Normann, K. Andersson, B. Leckner, and F. Johnson. Emission control of nitrogen oxides in the oxy-fuel process. *Progress in Energy and Combustion Science*, 35:343–361, 2009.
- [12] A. Poullikkas. An overview of current and future sustainable gas turbine technologies. *Renewable and Sustainable Energy Reviews*, 9:34–54, 2005.
- [13] M.A. Saad and D.Y. Cheng. The new lm2500 cheng cycle for power generation and cogeneration. *Energy Conversion and Management*, 38, 1997.
- [14] T. Srinivas, A.V.S.S.K.S. Gupta, and B.V. Reddy. Sensitivity analysis of stig based combined cycle with dual pressure hrsg. *International Journal of Thermal Sciences*, 47, 2008.
- [15] J. Topolski and J. Badur. Efficiency of hrsg within a combined cycle with gasification and sequential combustion at gt26 turbine. In *Proc. COMPOWER.2000*, pages 291–298, 2000.
- [16] P. Ziółkowski, M. Lemański, J. Badur, and L. Nastałek. Power augmentation of pge gorzów gas turbine by steam injection thermodynamic overview. *Rynek Energii*, 98:161–167, 2012.
- [17] P. Ziółkowski, W. Zakrzewski, D. Sławiński, and J. Badur. Clean gas technology opportunity for pomerania. *Rynek Energii*, 104:79–85, 2013.

POSTER PRESENTATIONS

OPTIMIZATION CRITERIA AND EFFICIENCIES OF ISOTHERMAL MOLECULAR MACHINES

R. E. González-Narváez*, N. Sánchez-Salas*, A. Calvo Hernández** and M.A. Barranco-Jiménez***

*Depto. de Física, Escuela Superior de Física y Matemáticas del IPN, UP Zacatenco,
México D.F. CP 07738, E-mail: norma@esfm.ipn.mx

**Departamento de Física Aplicada, Universidad de Salamanca, 37008 Salamanca, Spain, E-mail: anca@usal.es

*** Escuela Superior de Cómputo del IPN, UP Zacatenco, México D.F. CP 07738, mbarrancoj@ipn.mx

ABSTRACT

In this work we present the efficiency performance for an isothermal molecular machine under maximum conditions for a figure of merit representing a compromise between useful energy and lost energy (the Ω criterion). This represents the best compromise between energy benefits and losses for a specific job and neither an explicit evaluation of entropies nor the consideration of environmental parameters are required. Such a regime has been invoked as optimum not only in macroscopic heat engines but also in some molecular motors. We compared our results with previous ones for the same model obtained by Van den Broeck, *et al.* PRL 108, 210602 (2012), where the efficiency is considered at maximum power conditions. The motion of a molecule, is very different from a macroscopic heat engine; to understand how molecular motors operate requires mechanical concepts such as force, elasticity, damping and work but it is necessary to consider special events such as highly damped and diffusive effects. In this work we studied a protein machine managed by a chemical force, where two chemical reaction rate theories were considered: the Eyring rate theory, where the reaction is assumed to correspond to the break-down of a single quantum-mechanical vibration of the protein, and the Kramers rate theory, where a global protein conformational changes, and the more physically realistic model is this rate theory. Then, we investigated the asymptotic behaviour of efficiencies at small global reaction chemical potential gap (ϵ), expanding them up to the third-order term of ϵ . This points to a number of revealing observations: the three first expansion terms are the prediction of linear irreversible thermodynamics of efficiency for the same optimization criteria under certain conditions. We also derive upper and lower bounds for the efficiency of an isothermal molecular machine operating at Omega function. The upper bound is reached when the activated state is close to the fuelling or reactant state (Eyring-like), while the lower bound is reached when the activated state is close to the product state (Kramers-like).

INTRODUCTION

Molecular motors [1] are biological molecular machines being the essential agents of movement in living organisms. In general terms, a motor may be defined as a device that consumes energy in one form and converts it into motion or mechanical work; for example, motor proteins are molecular machines that convert the chemical energy derived from the hydrolysis of ATP into a mechanical work used to power cellular motility [2; 3]. Molecular motors are an assembly of mechanical parts-springs, levers, swivels, and latches- that move in a coordinate fashion and as ATP is hydrolyzed a directed motion is produced. However, proteins and other biomolecules are so tiny that the inertial forces are comparatively small and can usually be ignored, whereas the viscous forces from the surrounding fluid, at constant temperature, are usually large and dominate the mechanical responses. In contrast with heat engines limited by Carnot's theorem [4], the upper value of thermodynamic efficiency of isothermal motors is 1. Similar to heat engines, however, operating at the upper bound comes at the price of zero power, since it requires infinitely slow driving. Searching the efficiency at maximum power (EMP) is most interesting [5; 6].

For heat engines this issue has been profoundly studied since the publication of the Curzon and Ahlborn paper [7], opened the perspective of establishing more real theoretical bounds for a real heat engine. The Curzon and Ahlborn paper gave rise

to the birth and development of finite-time thermodynamics (FTT), a branch of thermodynamics devoted to extend classical reversible thermodynamics to include more realistic finite-time and finite-size (irreversible) processes [8; 9; 10; 11; 12; 13; 14; 15; 16].

The main goal of FTT is to ascertain the best operating mode of heat devices with finite-time cycles. Basically, finite-rate constraints arising from several sources of irreversibility are modelled and then a suitable function is optimized with respect to the involved parameters. In principle, one has the freedom to choose such a function. This has led to the proposal of a great variety of criteria based on thermodynamic, economic, compromise, and sustainability considerations [17; 18; 19] in this context the so-called Ω criterion was presented by [20] and this represents a compromise between energy benefits and losses for a specific job. It is easy to apply in any energy converter (isothermal or non-isothermal) because it does not require the explicit evaluation of the entropy generation and it is independent of environmental parameters. It follows then that we present this criterion applied to isothermal molecular machine in this present work.

Already the efficiency of molecular motors has been discussed [21; 22; 23; 24], the problem of EMP or under other optimum condition, has received much less attention for machines working under isothermal conditions [25; 26]. For molecular motors, a case study has shown values well above the linear re-

sponse result 1/2 [27]

In this work we address the issue of efficiency under Omega criterion for a model of molecular motor, the work is organized in the following way, in the section 1 the theoretical model of a molecular motor is presented, in section 2 we present the efficiencies of molecular motor in optimum conditions (EMP and Omega), finally in section 3 some discussions are enunciated.

1 MODEL FOR A MOLECULAR MOTOR

We first consider a generic model for a molecular motor, presented in [5], namely, a two-state machine operating along a one-dimensional reaction coordinate, see Fig. 1. The states correspond to two minima of an appropriate free energy landscape. While a physical energy landscape is expected to be very complicated and high dimensional, the thermally activated transitions between the two states will typically follow a preferred pathway that connects these states via the lowest lying saddle point, the so-called activated state. One can project the motion on this pathway and introduce a one-dimensional reaction coordinate x with corresponding effective free energy potential $G(x)$. The two rest states of the machine, that is, the minima in the absence of external forces, correspond to, say, locations

$$x = 0 \text{ and } x = L$$

The activated state lies at an intermediate position

$$x_a = \lambda L \ni \lambda \in [0, 1]$$

In the unperturbed phase there are no net transitions, and the states 1 and 2 have the same baseline potential value,

$$G_0(x=0) = G_0(x=L) = 0$$

The potential has a maximum

$$G(x = \lambda L) = G_a$$

at the activated state, whose value is typically much larger than the thermal energy $\beta^{-1} = k_B T$ (T being the temperature and k_B the Boltzmann constant).

In this rest state, the rates, when potential is minimum, k_0^+ from 1 to 2 and k_0^- from 2 to 1, are equal and given by

$$k_0^+ = k_0^- \equiv k_0 = \kappa \exp(-\beta G_a),$$

where the pre-exponential factor κ is considered constant.

In the presence of external forces, states 1 and 2 can be identified as fuel and product states, respectively. To transform fuel into product, the machine is subject to a driving force F_1 which allows it to overcome an opposing but weaker loading force $-F_2$, with $F_2 \leq F_1$. These forces can be of various physical origins, including chemical, electrical or mechanical. The combined effect of driving and loading is a tilting of the potential towards the product state 2, that is,

$$G(x) = G_0(x) - Fx$$

with $F = F_1 - F_2 \geq 0$.

In a transition from state 1 to state 2, a input energy $\varepsilon_1 = \varepsilon_2 L$ is transformed into a output energy $\varepsilon_2 = \beta F_2 L$.

The efficiency of this conversion of energy is given by

$$\eta = \frac{\varepsilon_2}{\varepsilon_1} = \frac{F_2}{F_1}. \quad (1)$$

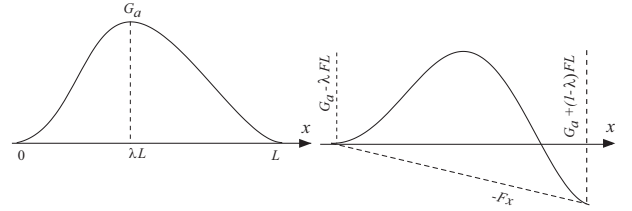


Figure 1. Schematic free energy potential $U_0(x)$ for a two-state molecular engine described by a reaction coordinate x under the net load force $F = F_1 - F_2 \geq 0$.

Equation (1) indicates how efficiently the energy is converted in the system in the process of doing work against the load. The maximum value of efficiency is $\eta = 1$, this is reached when the loading force F_2 approaches to the driving force F_1 , and the transition from 1 to 2 is taken in infinity time, that is, in a reversible manner and therefore with zero power.

1.1 Rate Theories of Chemical Reactions

The Eyring and Kramers rate theories [1] represent two extreme views of the mechanism of global conformational changes of proteins. In the **Eyring** model, the transition state is like the initial state. A sudden, local chemical change creates a highly strained protein that then relaxes into a new stable conformation. The activated state is very close to the fuel state 1; *i.e.*, λ is close to zero. The perturbation $-Fx$ barely affects the height of the activation barrier that needs to be crossed to go from state 1 to 2. The rate also remains essentially unaffected, $k^+ \approx k_0$. However, a maximum barrier increase of FL occurs for the backward transition, resulting in a rate $k^- \approx k_0 \exp(-\beta FL)$ (assuming $FL \ll G_a$). In the **Kramers** view, a protein undergoes a global diffusion into the activated state. When a sufficiently large conformational change has been achieved, the protein converts to the final state, at this scenario scenario $\lambda \approx 1$, $k_0^+ \exp(\beta FL)$, while $k^- \approx k_0$ remains essentially unaffected. For a barrier at $x_a = \lambda L$, one has $k^+ = k_0 \exp(\lambda \varepsilon)$ and $k^- = k_0 \exp[-(1-\lambda)\varepsilon]$, where $\varepsilon = \varepsilon_1 - \varepsilon_2 = \beta FL$ is the energy loss. βF is a proper thermodynamics force that appears in the entropy production and is thus a measure of the distance from equilibrium.

2 MAXIMUM POWER AND OMEGA CRITERION

2.1 Maximum power output

With the explicit expressions for the rates, it is possible to write the output power P , given by the output energy ε_2 multiplied by its net rate of productions, that is, $P = k\varepsilon_2$, with $k = k^+ - k^- = k(\varepsilon) = k_0[e^{\lambda\varepsilon} - e^{-(1-\lambda)\varepsilon}]$. To specify the condition of maximum power it is necessary to solve next equation

$$\frac{\partial P}{\partial \varepsilon_2} = 0,$$

which yields the solution

$$\varepsilon_2 = \frac{1 - e^{-\varepsilon}}{\lambda(1 - e^{-\varepsilon}) + e^{-\varepsilon}}. \quad (2)$$

Substituting this expression in Eq.(1), it is possible to get the EMP, given by,

$$\eta_{MP} = \frac{e^\varepsilon - 1}{(\lambda\varepsilon + 1)(e^\varepsilon - 1) + \varepsilon} \quad (3)$$

or,

$$\eta_{MP} = \frac{1}{2} + \frac{1 - 2\lambda}{8}\varepsilon + \frac{1 - 12\lambda + 12\lambda^2}{96}\varepsilon^2 + O(\varepsilon^3) \quad (4)$$

written in an expansion of Taylor series. In the next subsection we present the same procedure but under Omega criterion.

2.2 Omega function

Now we present the analysis of efficiency for the model of isothermal molecular engine, under the so-called Ω function, which represents a compromise between energy benefits and losses for a specific job; it is easy to apply in any energy converter, and it is independent on environmental parameters. The details of this optimization criterion is presented in [20].

For isothermal engine the Ω criterion reads as

$$\Omega = \frac{2\eta - 1}{\eta}P. \quad (5)$$

To find the efficiency under condition of maximum Omega we get,

$$\frac{d\Omega}{d\varepsilon_2} = 0, \quad (6)$$

this equation is solved where,

$$\varepsilon_2 = \frac{(e^\varepsilon - 1)(2 + \lambda\varepsilon) + \varepsilon}{\lambda(e^\varepsilon - 1) + 1}. \quad (7)$$

Substituting this expression in the expression for the efficiency eq. (1), we get the efficiency under Omega criterion condition, that is,

$$\eta_\Omega = \frac{\varepsilon_2}{\varepsilon_2 + \varepsilon} = \frac{(2 + \lambda\varepsilon)(e^\varepsilon - 1) + \varepsilon}{2[(1 + \lambda\varepsilon)(e^\varepsilon - 1) + \varepsilon]}. \quad (8)$$

Expanding this in a Taylor series around zero we get,

$$\eta_\Omega = \frac{3}{4} + \frac{1}{16}(1 - 2\lambda)\varepsilon + \frac{1}{192}(1 - 12\lambda + 12\lambda^2)(\varepsilon)^2 + O((\varepsilon)^3) \quad (9)$$

3 CONCLUSIONS

In this work we presented the efficiency of a model of molecular motor, under maximum power output conditions previously found by Broeck *et al.*, We also presented a new result, the efficiency under Omega criterion, we can note that the behaviour observed for thermal heat engines, working between two heat reservoir [28], is similar for this isothermal model presented here. It could be interesting to check with experimental verification if molecular motors works closer to EMP or any other regime, like Omega criterion.

ACKNOWLEDGMENT

We would like to thanks CONACYT, EDI-IPN, and COFAA-IPN, México for supporting this work. N.Sánchez-Salas and A. Calvo Hernández thank for financial support from Ministerio de Educación y Ciencia of Spain under Grant No. FIS2010-17147 FEDER.

REFERENCES

- [1] J. Howard, *Mechanics of Motor Proteins and the Cytoskeleton* Sinauer, New York, 2001, 1st ed.
- [2] D. McQuarrie and J. Simon, *Physical Chemistry: A Molecular Approach*, U.S.A, 1997, 10th ed.
- [3] D. Nelson and M. Cox, *Principles of Biochemistry*, New York, 2008, 5th ed.
- [4] H. Callen, *Thermodynamics and an Introduction to Thermostatistics*, New York, 1985, 2nd ed.
- [5] C. Van del Broeck, N. Kumar and K. Lindenberg, Efficiency of Isothermal Molecular Machines at Maximum Power, *Phys. Rev. Lett.*, vol. 108, pp.210602, 2012.
- [6] U. Seifert, Efficiency of Autonomous Soft Nanomachines at Maximum Power, *Phys. Rev. Lett.*, vol. 106, pp.020601, 2011.
- [7] F. Curzon and B. Ahlborn, Efficiency of a Carnot engine at maximum power output, *Am. J. Phys.* vol. 43, pp.22, 1975.
- [8] C. Van den Broek, Thermodynamic Efficiency at Maximum Power, *Phys. Rev. Lett.*, vol. 95, pp.190602, 2005.
- [9] T. Schmiedl and U. Seifert, Efficiency at maximum power: An analytically solvable model for stochastic heat engines, *Europhys. Lett.*, vol. 81, pp. 20003, 2008.
- [10] Z. Tu, Efficiency at maximum power of Feynman's ratchet as a heat engine, *J. Phys. A*, vol. 41, pp. 312003, 2008.
- [11] A. Allahverdyan, R. Johal, and G. Mahler, Work extremum principle: Structure and function of quantum heat engines, *Phys. Rev. E*, vol. 77, pp. 041118, 2008.
- [12] Y. Izumida and K. Okuda, Molecular Kinetic analysis of a finite-time Carnot cycle, *Europhys. Lett.*, vol. 83, pp. 60003, 2008.
- [13] M. Esposito, K. Lindenberg and C. Van den Broeck, Thermoelectric efficiency at maximum power in a quantum dot, *Europhys. Lett.*, vol.85, pp. 60010, 2009.
- [14] M. Esposito, R. Kawai, K. Lindenberg, and C. Van den Broeck, Quantum-dot Carnot engine at maximum power, *Phys. Rev. E*, vol. 81, pp. 041106, 2010.
- [15] M. Esposito, K. Lindenberg, and C. Van den Broeck, Universality of Efficiency at Maximum Power, *Phys. Rev. Lett.*, vol. 102, pp. 130602, 2009.
- [16] M. Esposito, R. Kawai, K. Lindenberg, and C. Van den Broeck, Efficiency at Maximum Power of Low-Dissipation Carnot Engines, *Phys. Rev. Lett.*, vol. 105, pp.150603, 2010.
- [17] F. Angulo-Brown, Ecological optimization criterion for finite-time heat engines, *J. Appl. Phys.*, vol. 69, pp.7465, 1991.
- [18] C. Wu, L. Chen, J. Chen, and F. Sun, Advances in Finite Time Thermodynamics, *Nova Science Publishers, Inc (US)*, 2004.
- [19] A. de Vos, Endorreversible Thermoeconomics, *Energy Conversion and Management*, vol. 36, pp.1, 1995.
- [20] A. Calvo Hernández, A. Medina, J. M. M. Roco, J. A.

- White, and S. Velasco, Unified optimization criterion for energy converters, *Phys. Rev. E*, vol. 63, pp.037102, 2001.
- [21] O. Dudko, T. Graham, and R. Best, Locating the barrier for folding of single molecules under an external force. *Phys. Rev.Lett.*, vol. 107, pp. 208301, 2011.
- [22] R. L. Stratonovich, *Topics in the Theory of Random Noise*, New York, 1963, Vol. 1.
- [23] N. Golubeva, A. Imparato, and L. Peliti, Efficiency of molecular machines with continuous phase space, *Europhys. Lett.*, vol. 97, pp. 60005, 2012.
- [24] P. Reimann, Brownian motors: noisy transport far from equilibrium, *Phys. Rep.*, vol. 361, pp. 57, 2002.
- [25] N. Sánchez Salas and A. Calvo Hernández, Adiabatic rocking ratchets: optimum-performance regimes, *Phys. Rev. E Stat Nonlin Soft Matter Phys.*, vol. 68, pp. 046125, 2003.
- [26] O. Díaz-Hernández, R. Páez-Hernández, M. Santillán, Thermodynamic performance vs. dynamic stability in an enzymatic reaction model, *Physica A*, vol.389, pp. 3476, 2010.
- [27] T. Schmiedl and U. Seifert, Efficiency of molecular motors at maximum power, *Europhys. Lett.*, vol. 83, pp. 30005, 2008.
- [28] N. Sánchez-Salas, and L. López-Palacios, and S. Velasco and A. Calvo Hernández, *Phys. Rev. E*, vol 82, pp. 051101, 2010

FREE-ENERGY CALCULATION OF A PROTEIN AS A FUNCTION OF TEMPERATURE AND PRESSURE: MULTIBARIC-MULTITHERMAL MOLECULAR DYNAMICS SIMULATIONS

Hisashi Okumura*,**

*Institute for Molecular Science, Okazaki, Aichi 444-8585, Japan, E-mail: hokumura@ims.ac.jp

**The Graduate University for Advanced Studies, Okazaki, Aichi 444-8585, Japan

ABSTRACT

Free-energy calculation is one of the main topics in thermodynamics. However, biomolecules such as proteins have complicated free energy surfaces with many local minima. Conventional molecular dynamics (MD) and Monte Carlo (MC) simulations in physical ensembles, such as the canonical and isobaric-isothermal ensemble, tend to get trapped in these local-minimum states and cannot give the correct free-energy difference between different-conformational states. In order to avoid this difficulty, generalized-ensemble algorithms such as the multicanonical algorithm are frequently employed. However, because the multicanonical simulation is performed in a fixed volume, neither the pressure dependence nor temperature dependence at certain pressure can be investigated as in experiments. To overcome this difficulty, the author recently proposed multibaric-multithermal MD and MC algorithms. In this ensemble, two-dimensional random walks in the potential-energy space and in the volume space are realized. In this paper, the multibaric-multithermal molecular dynamics algorithm is reviewed and application to a 10-residue protein, chignolin is presented.

INTRODUCTION

Molecular dynamics (MD) simulation is a standard tool to calculate free-energy landscape and to investigate the conformational changes for biomolecules such as proteins at atomic level. However, biomolecules have complicated free energy surfaces with many local minima. Thus, conventional MD simulations in physical ensembles, such as the canonical [1; 2; 3] and isobaric-isothermal [4] ensemble, tend to get trapped in these local-minimum states. One of the powerful techniques to avoid this difficulty is generalized-ensemble algorithms [5; 6; 7; 8; 9] such as the multicanonical algorithm [10; 11; 12; 13]. In the multicanonical ensemble, a free one-dimensional random walk is realized in the potential-energy space and a simulation does not get trapped in free-energy-minimum states.

However, because the multicanonical simulation is performed in a fixed volume, neither the pressure dependence nor temperature dependence at certain pressure can be investigated as in experiments. To overcome this difficulty, the author have proposed the multibaric-multithermal algorithm [14; 15; 16; 17; 18; 19; 20]. In this algorithm, two-dimensional random walks are realized both in the potential-energy space and in the volume space, so that the temperature and pressure dependence can be discussed. This algorithm can be also used for Monte Carlo (MC) simulations. In this paper, the multibaric-multithermal algorithm is reviewed and applications of this algorithm to chignolin in explicit water is presented.

METHOD

In the isobaric-isothermal ensemble [4], the distribution $\mathcal{P}_{NPT}(E, V)$ of potential energy E and volume V is given by

$$\mathcal{P}_{NPT}(E, V) = n(E, V)e^{-\beta_0 H}, \quad (1)$$

where $n(E, V)$ is the density of states as a function of E and V and H is the “enthalpy” (without the kinetic energy contributions): $H = E + P_0 V$. Here, P_0 is the pressure at which simulations are performed. This ensemble has bell-shaped distributions both in the potential-energy space and in the volume space, as shown in Fig. 1(a). In order to obtain the isobaric-isothermal ensemble, the combination of the Nosé thermostat [1; 2] and the Andersen barostat [4] is frequently employed.

In the multibaric-multithermal ensemble [14; 15; 16; 17; 18], every state is sampled with a weight factor $W_{\text{mbt}}(E, V) \equiv \exp\{-\beta_0 H_{\text{mbt}}(E, V)\}$ so that a uniform distribution of both E and V , as shown in Fig. 1(b), may be obtained:

$$\mathcal{P}_{\text{mbt}}(E, V) = n(E, V)W_{\text{mbt}}(E, V) = \text{constant}. \quad (2)$$

Here, $W_{\text{mbt}}(E, V)$ and H_{mbt} are referred to as the multibaric-multithermal weight factor and the multibaric-multithermal enthalpy, respectively. The difference between H_{mbt} and H is written as $\delta H(E, V)$: $H_{\text{mbt}}(E, V) = H + \delta H(E, V)$. The difference $\delta H(E, V)$ is therefore characteristic of the multibaric-multithermal simulation. The case of $\delta H(E, V) = 0$ gives the regular isobaric-isothermal ensemble.

The equations of motion in the multibaric-multithermal ensemble based on the Nosé thermostat [1; 2] and the Andersen barostat [4] are given by

$$\dot{r}_i = \frac{p_i}{m_i} + \frac{\dot{V}}{3V} r_i, \quad (3)$$

$$\dot{p}_i = \left(1 + \frac{\partial \delta H}{\partial E}\right) F_i - \left(\frac{\dot{V}}{3V} + \frac{\dot{s}}{s}\right) p_i, \quad (4)$$

$$\dot{V} = s \frac{P_V}{W}, \quad (5)$$

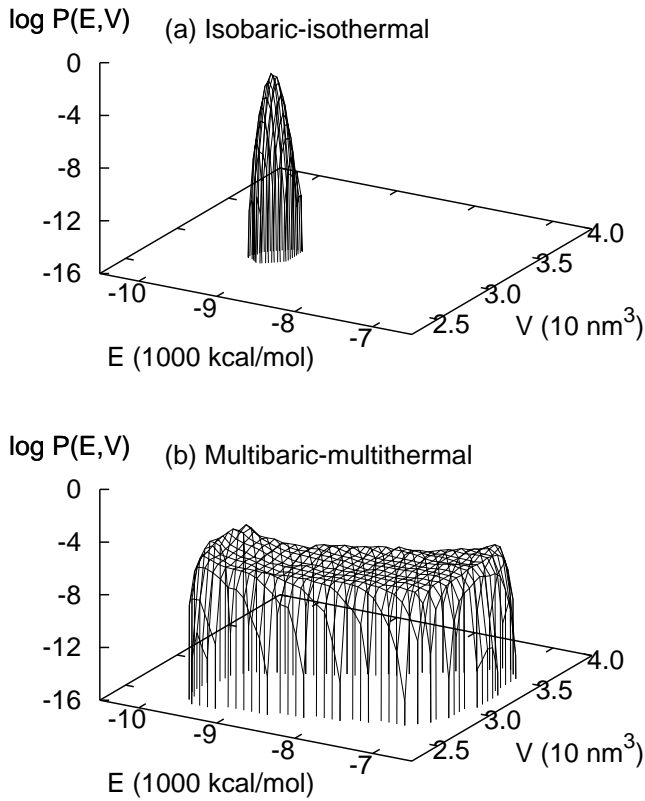


Figure 1. Distributions $\mathcal{P}(E, V)$ of potential energy E and volume V of an chignolin in explicit water (a) by the isobaric-isothermal MD simulation at $T = 298$ K and $P = 0.1$ MPa and (b) by the multibaric-multithermal MD simulation.

$$\dot{P}_V = s \left[\frac{1}{3V} \left\{ \sum_{i=1}^N \frac{p_i^2}{m_i} + \left(1 + \frac{\partial \delta H}{\partial E} \right) \sum_{i=1}^N F_i \cdot r_i \right\} - \left(P_0 + \frac{\partial \delta H}{\partial V} \right) \right], \quad (6)$$

$$\dot{s} = s \frac{P_s}{Q}, \quad (7)$$

$$\dot{P}_s = \sum_{i=1}^{N+M} \frac{p_i^2}{m_i} - g k_B T_0, \quad (8)$$

where r_i is the coordinate, p_i is the momentum, s is the additional degree of freedom for the Nosé thermostat, the dot ($\dot{\cdot}$) stands for the real time derivative d/dt , and F_i stands for the force acting on atom i . The variables P_V and P_s are the conjugate momenta for V and s , respectively. The constant m_i is the mass of atom i . The constants W and Q are the artificial “mass” related to V and s , respectively. Performing the MD simulation by the equations of motion, the multibaric-multithermal distribution $\mathcal{P}_{\text{mbt}}(E, V)$ in Eq. (2) is obtained.

After an optimal weight factor $W_{\text{mbt}}(E, V)$ is determined, for example, by the iterations of short simulations [21; 22] or by the Wang-Landau techniques [23], a long production run is performed for data collection. The reweighting techniques [24] are used for the results of the production run to calculate the isobaric-isothermal-ensemble averages. The expectation value of a physical quantity A at the desired temperature T and pressure P is given by

$$\langle A \rangle_{NPT} = \frac{\langle A(r, V) W_{\text{mbt}}^{-1}(E(r, V), V) e^{-\beta\{E(r, V) + PV\}} \rangle_{\text{mbt}}}{\langle W_{\text{mbt}}^{-1}(E(r, V), V) e^{-\beta\{E(r, V) + PV\}} \rangle_{\text{mbt}}}, \quad (9)$$

where $\langle \dots \rangle_{\text{mbt}}$ is the multibaric-multithermal ensemble average. Because of the random walks both in the potential-energy space and in the volume space, physical quantities can be calculated in wide ranges of T and P .

In order to calculate free-energy landscape, we should calculate first an unnormalized histogram as a function of reaction coordinates (ξ_1, ξ_2, \dots) by the reweighting techniques. In the case of two reaction coordinates (ξ_1, ξ_2) , it is given by

$$\begin{aligned} & \langle N(\xi_1, \xi_2) \rangle_{NVT} \\ &= \frac{\langle N(\xi_1(r), \xi_2(r)) W_{\text{mbt}}^{-1}(E(r, V), V) e^{-\beta\{E(r, V) + PV\}} \rangle_{\text{mbt}}}{\langle W_{\text{mbt}}^{-1}(E(r, V), V) e^{-\beta\{E(r, V) + PV\}} \rangle_{\text{mbt}}}. \end{aligned} \quad (10)$$

Probability distribution $P(\xi_1, \xi_2)$ is calculated by normalizing $\langle N(\xi_1, \xi_2) \rangle_{NVT}$:

$$P(\xi_1, \xi_2) = \frac{\langle N(\xi_1, \xi_2) \rangle_{NVT}}{\int d\xi_1 d\xi_2 \langle N(\xi_1, \xi_2) \rangle_{NVT}} \quad (11)$$

The free-energy landscape then can be calculated by

$$F(\xi_1, \xi_2) = -k_B T \log P(\xi_1, \xi_2). \quad (12)$$

APPLICATION TO CHIGNOLIN

Application to chignolin in explicit water solvent [25] is now presented. Chignolin is a 10 residue protein (GYDPETGTWG) of which the native state is a β -hairpin structure [26]. The N and C termini of the protein were left uncapped as in the experiment by Honda et al. [26]. That is, the N terminus and C terminus have a positive and negative electric charge, respectively. The system is consisting of one chignolin molecule, 902 water molecules, and two sodium ions Na^+ as counter ions. The initial values of the chignolin backbone dihedral angles were $\phi = \psi = 180^\circ$ except for proline. The initial dihedral-angle values of PRO4 were set to $\phi = -60^\circ$ and $\psi = 180^\circ$.

AMBER parm99SB force field [27] was used for the chignolin molecule and the TIP3P [28] rigid-body model was used for the water molecules. A cubic unit cell was employed with periodic boundary conditions. The electrostatic potential was calculated by the Ewald method. Cutoff distance was $r_c = 12$ Å for both electrostatic and Lennard-Jone potential. The combination [29] of the Nosé-Hoover thermostat [1; 2; 3], the Andersen barostat [4], and the symplectic quaternion scheme [30; 31] was used for the rigid-body water molecules. Reversible multiple time scale molecular dynamics techniques [32] were also applied. The time step was taken to be $\Delta t = 0.5$ fs for the protein atoms and $\Delta t = 4.0$ fs for the water molecules. Because the symplectic rigid-body algorithm was used for the water molecules here, Δt was able to be taken as long as 4.0 fs [29].

During this MD simulation, the root mean square deviation (RMSD) decreased and increased repeatedly. It mean that folding and unfolding events occurred. the unfolding events occurred four times.

Temperature and pressure dependences of the fraction of the folded chignolin f_{fold} are shown in Fig. 2. The fraction of the folded protein f_{fold} decreases as temperature and /or pressure

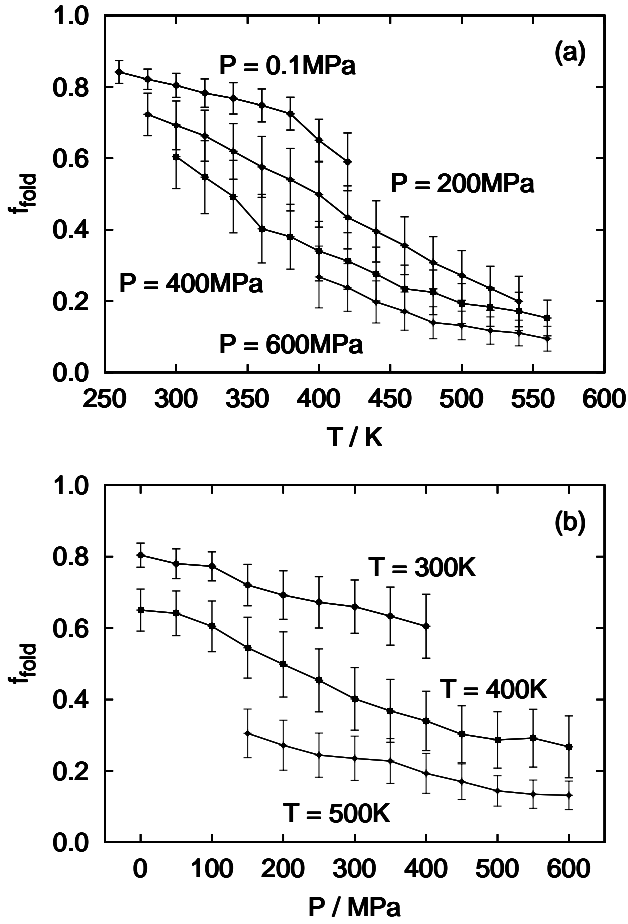


Figure 2. (a) Temperature dependence of fraction of the folded protein f_{fold} at $P = 0.1, 200, 400,$ and 600 MPa and (b) pressure dependence of f_{fold} at $T = 300, 400,$ and 500 K obtained by the reweighting techniques from the results of the multibaric-multithermal MD simulation.

increases. The partial molar enthalpy change ΔH and the partial molar volume change ΔV on unfolding is calculated by

$$\Delta H = R \left[\frac{\partial \log \{ f_{\text{fold}} / (1 - f_{\text{fold}}) \}}{\partial (1/T)} \right]_P, \quad (13)$$

$$\Delta V = RT \left[\frac{\partial \log \{ f_{\text{fold}} / (1 - f_{\text{fold}}) \}}{\partial P} \right]_T. \quad (14)$$

Interpolating or extrapolating the temperature dependence of f_{fold} , the derivatives in Eqs. (13) and (14) were calculated. The partial molar enthalpy change ΔH was determined that $\Delta H = 24.1 \pm 4.9$ kJ/mol at $P = 0.1$ MPa, as listed in Table 1. Honda et al. determined ΔH by the CD spectroscopy and NMR experiments and their data distribute between 25.9 kJ/mol and 32.2 kJ/mol. The partial molar enthalpy change ΔH by the present multibaric-multithermal MD simulation is slightly lower than the experimental data, but shows a reasonably good agreement.

The partial molar volume change ΔV was determined that $\Delta V = -5.6 \pm 1.5$ cm³/mol at $T = 298$ K, as listed in Table 1. Imamura and Kato obtained $\Delta V = -8.8$ cm³/mol by their Fourier transform infrared spectrometer (FT-IR) experiments [33]. The absolute value of the present multibaric-multithermal MD result is slightly lower than their experimental data, but still agrees well.

The lower absolute values of ΔH and ΔV mean that chignolin

Table 1. Difference in the Gibbs free energy ΔG between the unfolded state and the folded state, difference in the partial molar enthalpy ΔH at $P = 0.1$ MPa, and difference in the partial molar volume ΔV at $T = 298$ K calculated by the multibaric-multithermal (MUBATH) MD simulation. Experimental data are taken from Refs. [26; 33].

Method	ΔG /(kJ/mol)	ΔH /(kJ/mol)	ΔV /(cm ³ /mol)
MUBATH	3.5 ± 0.5	24.1 ± 4.9	-5.6 ± 1.5
Exp.	$1.07 - 1.87$	$25.9 - 32.2$	-8.8

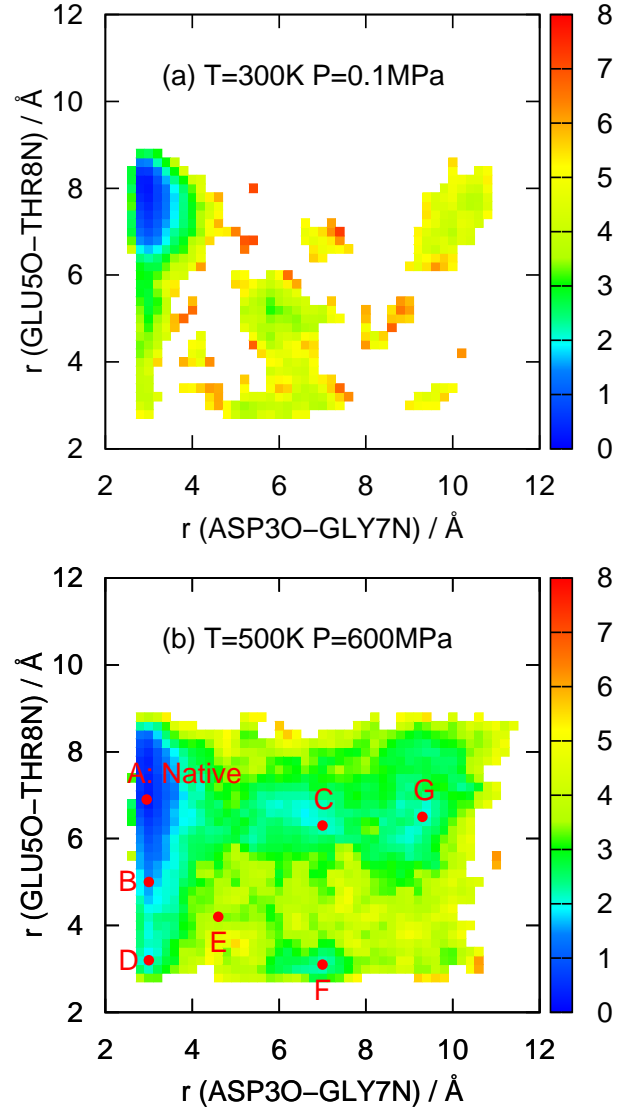


Figure 3. Potential of mean force (PMF) as a function of $r(\text{ASP30-GLY7N})$ and $r(\text{GLU50-THR8N})$ (a) at $T = 300$ K and $P = 0.1$ MPa and (b) at $T = 500$ K and $P = 600$ MPa obtained by the reweighting techniques from the results of the multibaric-multithermal MD simulation.

does not unfold with the increasing temperature or pressure in the MD simulation as fast as in the experiment. A possible reason is that the Coulomb potential parameter or the electrostatic charge in the classical force field is too large. Reducing the absolute value of the electrostatic charge may evaluate the hydrogen bonds weaker so that the simulational temperature/pressure

dependence of f_{fold} and ΔG may agree better with the experiment.

The present multibaric-multithermal MD simulation sampled not only the β -hairpin structure but also a 3_{10} -helix structure. Figure 3 shows potential of mean force as a function of $r(\text{ASP30} - \text{GLY7N})$ and $r(\text{GLU50} - \text{THR8N})$, which are the distance between ASP30 and GLY7N atoms and that between GLU50 and THR8N atoms, respectively. ASP30 and GLY7N atoms make a hydrogen bond at the β -hairpin structure and GLU50 and THR8N atoms make a hydrogen bond at the 3_{10} -helix structure. The potential of mean force has a global minimum state at $r(\text{ASP30} - \text{GLY7N}) = 3.0 \text{ \AA}$ and $r(\text{GLU50} - \text{THR8N}) = 7.8 \text{ \AA}$ at $T = 300 \text{ K}$ and $P = 0.1 \text{ MPa}$, as shown in Fig. 3(a). This state is the native state, at which the chignolin folds into the β -hairpin structure. There also exists other states, which correspond to unfolded states. We can see blue and green distribution in a wide area at $T = 500 \text{ K}$ and $P = 600 \text{ MPa}$, which means that the unfolded states increase, as shown in Fig. 3(b). There are several local-minimum free-energy states besides the global-minimum state. The state E is not a local-minimum states but a transition state between the states B and F or the states D and C.

Typical conformations obtained by the multibaric-multithermal MD simulation at these states are illustrated in Fig. 4. At the global-minimum state A, chignolin forms the native β -hairpin structure. The local-minimum state B is obtained from the state A by bending the C terminus of the β -hairpin structure. The local-minimum state C is obtained from either state A or state B by bending both N and C terminus of the β -hairpin structure. This conformation looks like a Greek letter " Ω ". If the N terminus of the state B does not bent like the state C, but make a turn, an α -helix structure is obtained at the state D. The transition state E is obtained by breaking some of the hydrogen bonds of the α -helix structure at the state D. It can be obtained also from the state B or C. The local-minimum state F, a 3_{10} -helix structure, is obtained from the state E by forming hydrogen bonds in a different way from the α -helix structure at the state D. This 3_{10} -helix structure can also be attained from the Ω -like structure at the state C by making turn structures. Finally an extended structure is obtained at the state G if all hydrogen bonds are broken from the state C or F. Following these pathways, the native β -hairpin structure at the state A unfolds to the extended structure at the state G. When chignolin folds, it follows the reverse process to the native structure.

CONCLUSION

The multibaric-multithermal ensemble algorithm is reviewed. The multibaric-multithermal MD or MC simulation performs a two-dimensional random walk both in the potential-energy space and in the volume space so that one can obtain various isobaric-isothermal ensemble averages at different temperatures and pressures from only one simulation run. The multibaric-multithermal algorithm will thus be a powerful simulation technique to study the temperature and pressure dependences of biomolecules like proteins.

REFERENCES

[1] S. Nosé, A molecular-dynamics method for simulations in the canonical ensemble, *Mol. Phys.* vol. 52, pp. 255-268, 1984.

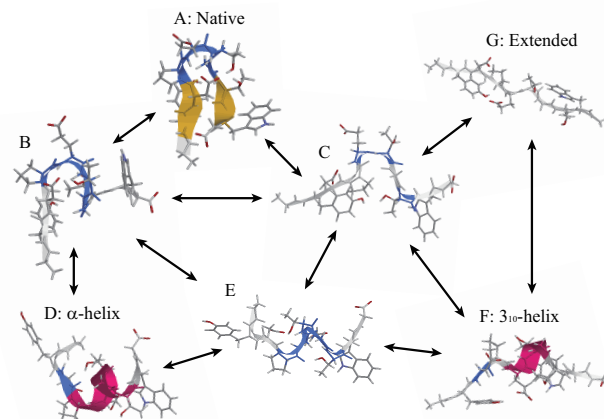


Figure 4. Folding and unfolding pathways of chignolin from the state A to G. These conformations are obtained by the multibaric-multithermal MD simulation. The N terminus and the C terminus are on the left-hand side and on the right-hand side, respectively. The figures were created with RasMol [34].

- [2] S. Nosé, A unified formulation of the constant temperature molecular-dynamics methods, *J. Chem. Phys.* vol. 81, pp. 511-519, 1984.
- [3] W.G. Hoover, Canonical dynamics: Equilibrium phase-space distributions, *Phys. Rev. A* vol. 31, pp. 1695-1697, 1985.
- [4] H.C. Andersen, Molecular dynamics simulations at constant pressure and/or temperature, *J. Chem. Phys.* vol. 72, pp. 2384-2393, 1980.
- [5] U. H. E. Hansmann and Y. Okamoto, The generalized-ensemble approach for protein folding simulations, in D. Stauffer (ed.), *Ann. Rev. Comput. Phys.* VI, pp. 129-158, World Scientific, Singapore, 1999.
- [6] A. Mitsutake, Y. Sugita, Y. Okamoto, Generalized-ensemble algorithms for molecular simulations of biopolymers, *Biopolymers (Pept Sci)* vol. 60, pp. 96-123, 2001.
- [7] B. A. Berg, Biased metropolis sampling for rugged free energy landscapes, *Comp. Phys. Commun.* vol. 104, pp. 52-57, 2002.
- [8] H. Okumura, Partial multicanonical algorithm for molecular dynamics and Monte Carlo simulations, *J. Chem. Phys.* vol. 129, 124116, 2008.
- [9] H. Okumura, Optimization of partial multicanonical molecular dynamics simulations applied to an alanine dipeptide in explicit water solvent, *Phys. Chem. Chem. Phys.* vol. 13, pp. 114-126, 2011.
- [10] B. A. Berg, T. Neuhaus, Multicanonical algorithms for first order phase transitions, *Phys. Lett. B* vol. 267, pp. 249-253, 1991.
- [11] B. A. Berg, T. Neuhaus, Multicanonical ensemble: a new approach to simulate first-order phase transitions, *Phys. Rev. Lett.* vol. 68, pp. 9-12, 1992.
- [12] U. H. E. Hansmann, Y. Okamoto, and F. Eisenmenger, Molecular dynamics, Langevin and hybrid Monte Carlo simulations in a multicanonical ensemble, *Chem. Phys. Lett.* vol. 259, pp. 321-330, 1996.
- [13] N. Nakajima, H. Nakamura, and A. Kidera, Multicanonical ensemble generated by molecular dynamics simula-

- tion for enhanced conformational sampling of peptides, *J. Phys. Chem. B* vol. 101, pp. 817-824, 1997.
- [14] H. Okumura and Y. Okamoto, Monte Carlo simulations in multibaric-multithermal ensemble, *Chem. Phys. Lett.* vol. 383, pp. 391-396, 2004.
- [15] H. Okumura and Y. Okamoto, Monte Carlo simulations in generalized isobaric-isothermal ensembles, *Phys. Rev. E* vol. 70, 026702, 2004.
- [16] H. Okumura and Y. Okamoto, Liquid-gas phase transitions studied by multibaric-multithermal Monte Carlo simulations, *J. Phys. Soc. Jpn.* vol. 73, pp. 3304-3311, 2004.
- [17] H. Okumura and Y. Okamoto, Molecular dynamics simulations in the multibaric-multithermal ensemble, *Chem. Phys. Lett.* vol. 391, pp. 248-253, 2004.
- [18] H. Okumura and Y. Okamoto, Multibaric-multithermal ensemble molecular dynamics simulations, *J. Comput. Chem.* vol. 27, pp. 379-395, 2006.
- [19] H. Okumura and Y. Okamoto, Multibaric-multithermal molecular dynamics simulation of alanine dipeptide in explicit water, *Bull. Chem. Soc. Jpn.* vol. 80 pp. 1114-1123, 2007.
- [20] H. Okumura and Y. Okamoto, Temperature and pressure dependence of alanine dipeptide studied by multibaric-multithermal molecular dynamics simulations, *J. Phys. Chem. B* vol. 112 pp. 12038-12049, 2008.
- [21] B. A. Berg and T. Celik, New approach to spin-glass simulations, *Phys. Rev. Lett.* vol. 69, pp. 2292-2295, 1992.
- [22] U. H. E. Hansmann and Y. Okamoto, Thermodynamics of helix-coil transitions studied by multicanonical algorithms, *J. Phys. Chem.* vol. 99, pp. 11276-11287, 1995.
- [23] F. Wang and D. P. Landau, Efficient, multiple-range random walk algorithm to calculate the density of states, *Phys. Rev. Lett.* vol. 86, pp. 2050-2053, 2001.
- [24] A. M. Ferrenberg and R. H. Swendsen, Optimized Monte Carlo data analysis, *Phys. Rev. Lett.* vol. 61, pp. 2635-2638, 1988. *ibid.* vol. 63, p. 1658(E), 1989.
- [25] H. Okumura, Temperature and pressure denaturation of chignolin: Folding and unfolding simulation by multibaric-multithermal molecular dynamics method, *Proteins* vol. 80, pp. 2397-2416, 2012.
- [26] S. Honda, K. Yamasaki, Y. Sawada, H. Morii, 10 residue folded peptide designed by segment statistics, *Structure* vol. 12, pp. 1507-1518, 2004.
- [27] V. Hornak, R. Abel, A. Okur, B. Strockbine, A. Roitberg, and C. Simmerling, Comparison of multiple amber force fields and development of improved protein backbone parameters, *Proteins* vol. 65, pp.712-725, 2006.
- [28] W. L. Jorgensen, J. Chandrasekhar, J. D. Madura, R. W. Impey, and M. L. Klein, Comparison of simple potential functions for simulating liquid water, *J. Chem. Phys.* vol. 79, pp. 926-925, 1983.
- [29] H. Okumura, S. G. Itoh, and Y. Okamoto, Explicit symplectic integrators of molecular dynamics algorithms for rigid-body molecules in the canonical, isobaric-isothermal, and related ensembles, *J. Chem. Phys.* vol. 126, 084103, 2007.
- [30] H. Yoshida, Construction of higher order symplectic integrators, *Phys. Lett. A* vol. 150, pp. 262-268, 1990.
- [31] T. F. Miller, M. Eleftheriou, P. Pattnaik, A. Ndirango, D. Newns, and G. J. Martyna, Symplectic quaternion scheme for biophysical molecular dynamics, *J. Chem. Phys.* vol. 116, pp. 8649-8659, 2002.
- [32] M. Tuckerman, B. J. Berne, and G. J. Martyna, Reversible multiple time scale molecular dynamics, *J. Chem. Phys.* vol. 97, pp. 1990-2001, 1992.
- [33] H. Imamura and M. Kato, Unfolding of β -hairpin peptides by pressure : FT-IR and FRET studies, *The 48th Annual Meeting of the Biophysical Society of Japan*, 3P066, 2010.
- [34] R. A. Sayle and E. J. Milner-White, RASMOL: biomolecular graphics for all, *Trends Biochem. Sci.* vol. 20, pp. 374-376, 1995.

A POSSIBLE APPLICATION OF THE MECHANICS OF FLUIDS AND THE NONLINEAR DYNAMICS OF BEHAVIOR OF THE HEART

M. Zamora-Gómez*, R. Páez-Hernández°, P. Portillo-Díaz°, D. Ladino-Luna°,

*Hospital General "Dr. Gaudencio González Garza" CMN La Raza, IMSS, Calz. Vallejo S/n, Col. La Raza, CP 02990,
Azcapotzalco, México DF

°Área de Física de Procesos Irreversibles, Departamento de Ciencias Básicas, Universidad Autónoma Metropolitana
Azcapotzalco, Av. San Pablo No. 180, Col. Reynosa Tamps. CP02200 México DF
corresponding author (phrt@correo.azc.uam.mx)

ABSTRACT

In this work, we use some results from mechanics of fluids and the thermodynamics of finite time to calculate, the efficiency of the heart, considering the heart like a mechanics pump. We also study the model of the heartbeat. We find results of the efficiency to heart far away from the real values, i.e. the model to heart like a mechanics pump is too oversimplified, the above is because the heart is a complex system. However using the nonlinear dynamics considering the time delays inherent of the system, we obtain two fixed points which sustained oscillations, and these could be the Diastole and Systole, these parameters are associated with blood flow in human body called pressure arterial and are very important in the cardio-vascular problems. We have to point out that our work is from point view academic, and pretend to the students taking in account that the theory can be immediately applied to many real systems, but also has very limitations.

INTRODUCTION

Mathematically modeling physical phenomena, such as a rigid body dynamics of the deformation of an elastic material or the propagation of an electromagnetic wave in the atmosphere, our best scientific knowledge about the laws of physics. So for the first case we used Newton's laws, the continuum mechanics and Maxwell's laws.

These laws are the result of centuries of experimentation, observation and inspiration of the scientists involved in the creation of knowledge of nature.

In biology and life sciences in general, the interaction between the observed phenomena and their mathematical description, are still in the early stages of development and apart from the Hardy-Weinberg equilibrium. The philosophy is to develop mathematical models that can describe in a qualitative manner observed biological processes.

There is a lot of work in the literature of complex systems, which consider its efficiency analysis and even related to probable heart heartbeat analyzed as time series, others show dynamic and thermodynamic models. Our the study subject is the heart, so we give a brief description about its operation.

The heart is one of the most important organs of the human body and it has as principal task, maintain circulation the blood, so the function of the heart is to pump blood. The blood carries oxygen (O_2) from the lungs to the various tissues of the body and it carries carbon dioxide (CO_2) from these tissues back to the lungs. Since the circulation forms a closed loop, its description can begin anywhere. We will begin on the left side of the heart. The left heart side receives blood rich in O_2 and pumps this blood into the systemic arteries. These form a tree of progressively smaller vessels that supply fully oxygenated (and hence bright red) blood to all of the organs and tissues of the body. From the smallest of the systemic arteries, blood flows into the systemic capillaries, which are roughly the diameter of a single red

blood cell. It is in capillaries that the actual exchange of O_2 and CO_2 takes place. The blood that leaves the systemic capillaries carries less O_2 and more CO_2 than the blood that entered. (The loss of O_2 causes a change in the color so that the blood is now more bluish than before.)

Leaving the systemic capillaries, the blood enters *systemic veins* through which it flows in vessels of progressively increasing size toward the right side of the heart.

The right heart pumps blood into the *pulmonary arteries* which form a tree that distributes the blood to the tissues of the lung. The smallest branches of this tree give rise to the *pulmonary capillaries* where CO_2 leaves the blood stream and O_2 enters from the air space of the lungs. Leaving the pulmonary capillaries, the oxygenate blood is collected in the pulmonary veins through which it flows back to the left heart. This complete the circulation, F. C. Hoppensteadt [1].

BLOOD FLOW

The circulatory blood system

If we consider for a moment a simplified concept of the circulatory blood system in man, we can imagine that we have a pump delivering blood to a complicates networks of pipes, which has innumerable connections. To develop an appropriate mathematical model of this system and its behavior is an almost impossible task. Thus, in order to make any progress, we attempt to model parts of system separately. Here we concentrate on a small section of this circuit, say in the region of the aorta as shown in Fig. 1. Indeed we shall consider the relative straight section between A and B. One can imagine that the blood flow in this section behaves in much the same way a water in a cylindrical tube. This, however, is a gross oversimplification of the situation. To see this, let us consider some salient facts regarding blood flow. First of all unlike water, blood does not have constant

viscosity and this vary with the velocity. Thus blood may be claimed to be non-Newtonian; indeed the properties of blood change rapidly if removed from the system and so it is extremely difficult to perform experiments on it under laboratory conditions .

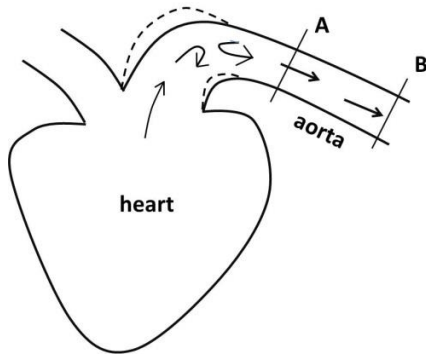


Fig. 1 Schematic description of an aorta

If we now consider the type of flow in an artery, it is apparent that because the heart delivers blood in short bursts during contraction into systole, the flow is pulsatile and not uniform. Furthermore, we do not know the velocity profile of the flow entering A in Fig. 1 and consequently the velocity profile at B is also unknown. This observation is of fundamental importance in the mathematical description of blood flow. On the other hand, the hydrodynamic problem of considering the change of an initial velocity profile a Newtonian fluid in a rigid pipe is fairly well understood and is based on the fundamental theory of Poiseuille (1846). One should remark here that Poiseuille whose contributions to hydrodynamics are well known to engineers and mathematicians, was in fact a physician and his interest was precisely the problem we are considering here, namely, the study of the blood flow.

Let us now focus on the arteries themselves. We know them to be elastic and a typical cross section may change significantly with time due to pulsating nature of the flow of blood. Thus once again it may be unreasonable to treat the arteries as rigid tubes. Nevertheless we find it necessary to assume this as first approximation.

In Fig. 1 consider the flow of blood delivered into an aorta. The blood is pumped in an asymmetrical fashion and there large cross-channel components of velocity in the arch region and consequently large thoracic surgery on animals. However, away from the arch itself, say in section A-B, the cross-channel components of velocity are considerably reduced and the flow is almost entirely longitudinal but, of course, still pulsatile. In the arc region it is found thoracic surgery that the arc pliant and yields easily to the cross-channel pressure gradients. Thus it is reasonable to assume changes and the “general give” radially of all cross sections of the aorta cause changes in pressure to be dampened, especially the radial components. We radial velocity components may be neglected. This assumption is known to physiologists as the Windkessel effect assumption, an idea introduced by the German physiologist Otto Frank, D. S. Jones [2].

Mechanics of Fluids

We define a fluid as a substance which must continue to change shape as long as there is a shear stress, however small, present. By contrast a solid undergoes a definite displacement

(or breaks completely) when subjected to a shear stress. In fluid mechanics study different types of fluids such as compressible, incompressible, Newtonian and non-Newtonian. In the previous section studied that blood flow can be considered as a non-Newtonian fluid, as this does not satisfy the conditions to be studied as incompressible and Newtonian fluid. A. Bejan [3] was obtained an expression to calculate the efficiency for a piston and cylinder apparatus for extracting mechanical power from the flow of a fluid between two pressure reservoirs, given as

$$\eta_{max} = \frac{1}{2} \left(1 - \frac{P_2}{P_1} \right) \quad (1)$$

where η_{max} is the maximum efficiency, P_1 is the reservoir pressure, P_2 is the reservoir pressure with $P_1 > P_2$. The Fig.11-28 of A. Vander et al [4] shows that the initial pressure reaches a value more than 110 mmHg before going through the aorta.

Now as we saw in the physiology of the left side of the heart, we can assume in a first approximation that this can be represented as proposed in [3], this is shown in Fig.2.

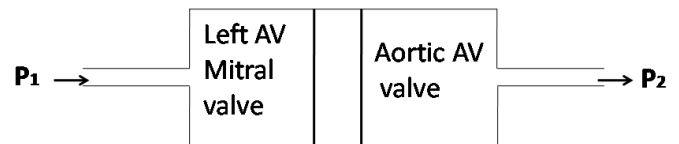


Fig. 2 Piston and cylinder apparatus for extracting mechanical power from the flow of a fluid between two pressure reservoirs.

On the other hand, the maximum pressure supported by a vein is 140 mmHg, also the normal arterial pressure in person without hypertension is 120 mmHg, moreover the biological systems have good efficiency, then we can suppose that the heart's efficiency is around 30%, i.e. $\eta_{max} = 0.3$, so from Eq. (1) we obtain that $P_1 = 300$ mmHg, with $P_2 = 120$ mmHg, these result cannot be real. Therefore our approximation of the heart like mechanics pump is far from the reality. And we have to propose a model that takes in account more details of the blood flow.

NON- LINEAR DYNAMICS

As is known, the heart muscle is an autonomous system and has an intermittent dynamic, i.e. its operation is periodic. Then we use Non-linear Dynamics considering the time delays inherent to the heart to study the model heart's dynamics proposed by E. C. Zeeman [5].

Times Delays

In real life situations when the value of a variable is modified the effect in the dynamic response of the system is not observed immediately. A certain time must elapse until the system begins to respond or "feel" the effect of the changes made. Suppose we modify the concentration of a reactor feed. Our experience, and common sense tells us that time passes until the variables that characterize the dynamic behavior of the reactor (eg concentration) begin to modify its value relative to their pre-change. These systems are known as dynamical systems. Delayed systems appear naturally in Medicine, Biology and Engineering. These systems have been

studied since before the last century. Studies in Medicine and Biology begin with Ross' epidemiology models (1911) and others in the early twentieth century, which were studied by Lotka, Volterra and Kostitzin, N. McDonald [6]. A distinctive feature of these systems is that their rate of evolution is described by differential equations that include information about the history of the system. The effects of delays are of great interest, since their presence may include complex behavior (oscillations, instability, bad system performance). R. Páez-Hernández et al [7] studied the effect time delays produced in a mathematical model for the stretch reflex regulatory pathway. A. Rojas-Pacheco et al [8] studied time-delay effects on dynamics of a two-actor conflict model.

Fixed points and linearisation system with delays

Consider a dynamic system which has a single variable with time delays ξ ,

$$\frac{dx}{dt} = f(x, y_\xi) \quad (2)$$

$$\frac{dy}{dt} = g(x_\xi, y) \quad (3)$$

where subscript ξ is a time delay variable. Following step to H. S. Strogatz [9] to obtain a linear system,

$$\dot{u} = f(x^*, y^* + v_\xi), \quad \dot{v} = g(x^* + u_\xi, y^* + v), \quad (4)$$

where u and v represent a small perturbation of the system and (x^*, y^*) is a fixed point, now we do a Taylor's series expansion to Eq. (2) and we consider negligible the terms of two on ward, and evaluate in the steady-state and we obtain

$$\dot{u} = \left. \frac{\partial f}{\partial x} \right|_{(x^*, y^*)} u + \left. \frac{\partial f}{\partial y} \right|_{(x^*, y^*)} v_\xi \quad (5)$$

$$\dot{v} = \left. \frac{\partial g}{\partial x} \right|_{(x^*, y^*)} u_\xi + \left. \frac{\partial g}{\partial y} \right|_{(x^*, y^*)} v. \quad (6)$$

Now we assume that u and v are of the form

$$u = A_1 e^{\lambda t} \quad (7)$$

$$u_\xi = A_1 e^{\lambda t} e^{-\lambda \xi} \quad (8)$$

$$v = A_2 e^{\lambda t} \quad (9)$$

$$v_\xi = A_2 e^{\lambda t} e^{-\lambda \xi} \quad (10)$$

where λ is a complex number, A_1 and A_2 are constant.

Substituting Eqs. (7)-(10) into Eqs. (5) and (6) leads to the following set of homogeneous linear system for A_1 and A_2 :

$$(f_x - \lambda)A_1 + f_{y_\xi} e^{-\lambda \xi} A_2 = 0 \quad (11)$$

$$f_{x_\xi} e^{-\lambda \xi} A_1 + (g_y - \lambda)A_2 = 0. \quad (12)$$

This system of equations has non-trivial solutions only if the determinant of the matrix of coefficients equals zero, i.e.

$$(f_x - \lambda)(g_y - \lambda) - f_{x_\xi} g_{y_\xi} e^{-2\lambda \xi} = 0. \quad (13)$$

This equation is also called the transcendental characteristic equation, and can be written as

$$H(z) + K(z)e^{-z\xi} = 0, \quad (14)$$

with z an eigenvalue, and $H(z)$ and $K(z)$ are polynomials of second and zero order, respectively.

The solutions to this equation are not obvious because has an infinite number of roots [6]. One way to overcome this situation is to consider the fact a common effect of time delays to destabilize stable fixed points or to stabilize unstable fixed points by sustained oscillations. If we assume that $(z = i\omega)$, and substitute in (14), we obtain a complex variable equation.

$$P(\omega) + iQ(\omega) = e^{-i\omega\xi} \quad (15)$$

where $P(\omega)$ and $Q(\omega)$ are second and first order polynomials, respectively. We observe that the right hand side of this equation represents the unitary circle whereas the left hand side describes a parabola. The intersection of these two curves could represent a change in the stability of the system. The analysis of intersection between the parabola and the unitary circle leads to the following classification:

- If the parabola does not intersect the unitary circle, and the system is stable to $\xi = 0$, then the system is stable independent of delay.
- If the system is stable for $\xi = 0$ and the parabola intersects the unit circle, then the system can be affected by delays.

Non-Linear Dynamic Model of Heart

A mathematical model that describes the behaviour of the heartbeat was developed in [5], where it was suggested that such a model contain three basic features:

- a stable equilibrium state representing diastole;
- the threshold for triggering the electrochemical wave causing the heart to go into systole; and
- the return of the heart into the diastolic state.

The resulting model is given by

$$\dot{x} = -\frac{1}{\epsilon}(x^3 - Tx + y) \quad (16)$$

$$\dot{y} = x + x_d \quad (17)$$

where $x(t)$ represents the length of the muscle fiber, $y(t)$ is a variable related to electrochemical activity; the parameter ϵ is a small positive constant associated with the fast eigenvalue of the system, x_d is a scalar quantity representing a typical length of muscle fiber in the diastolic state, and T represents tension in the muscle fiber. Now we use the result for linearization systems, for the case $\xi = 0$,

$$f(x, y) = -\frac{1}{\epsilon}(x^3 - Tx + y) \quad (18)$$

and

$$g(x, y) = x + x_d \quad (19)$$

this yields,

$$f_x|_{(x^*, y^*)} = \frac{T}{\epsilon} \quad (20)$$

$$f_y|_{(x^*, y^*)} = -\frac{1}{\epsilon} \quad (21)$$

$$g_x|_{(x^*, y^*)} = 1 \quad (22)$$

$$g_y|_{(x^*, y^*)} = 0 \quad (23)$$

now substituting Eqs.(20)-(23) into Eq. (13), we obtain the eigenvalues $\lambda_1 = 3.62$ and $\lambda_2 = 1.38$ for $T = 1$, $\epsilon = 0.2$ and $x_d = 0$. Therefore, the origin is unstable since both eigenvalues are real and positive. In Fig. 3 we show the phase portrait of Eqs. (2) and (3), with the same values for the parameters, the cubic line (red curve) represents the steady state of Eq.(18), A and B may be represent the systole and diastole points.

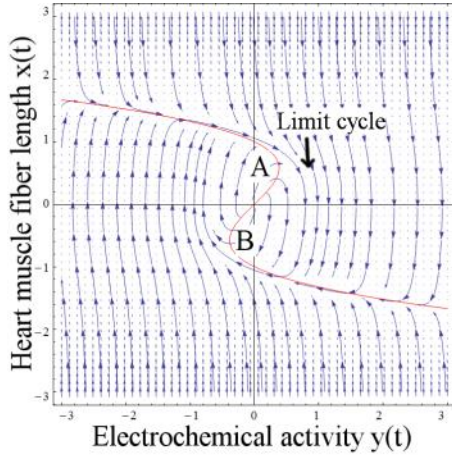


Fig.3 Phase portrait of the heartbeat model.

Dynamic effects of time delays

Consider again the systems of delay differential equations given by Eqs. (2) and (3), but now $\xi = \frac{\pi}{2}$. They can rewritten as

$$\begin{aligned} \frac{dx}{dt} &= f(x, y_{\pi/2}) \\ \frac{dy}{dt} &= g(x_{\pi/2}, y) \end{aligned}$$

with f and g as defined in Eqs. (18) and (19). Following section 2.1, the time course of small perturbations from the steady state is determined; we can write Eq. (13) as

$$(f_x - \lambda)(g_y - \lambda) - f_y g_x e^{-\lambda\pi} = 0. \quad (24)$$

The stability analysis of a dynamic system involving time delays can be quite complicated due to the fact that, in general, the characteristic equation has an infinite number of solutions. On the other hand, it is known that a common effect of time delays is to destabilize formerly stable steady states by inducing sustained oscillations. To test whether this happens, assume that λ is imaginary ($\lambda = i\omega$) and substitute into the characteristic equation to obtain

$$(-E\omega^2 + F) + iD\omega = e^{(-i\omega\pi)}, \quad (25)$$

wit

$$E = \frac{1}{f_y g_x}, \quad F = \frac{f_x g_y}{f_y g_x} \quad \text{and} \quad D = \frac{f_x + g_y}{f_y g_x}.$$

It follows from Eqs. (20)-(23) that $f_x > 0$, $f_y < 0$, $g_x > 0$ and $g_y = 0$. This further implies that $E < 0$, $F=0$, and $D > 0$.

The left-hand side of Eq. (25) determines the lower branch of a horizontal parabola in the complex plane. This parabola opens to the to the right and its vertex is located in the point (0,0). On the other hand, the right-hand side of Eq. (25)

determines a unitary circle in the complex plane. The points where these curves cross correspond to values of ω and π at which sustained oscillations appear due to a destabilization of the steady state, or vice versa. Let ρ and σ real variables along the real and the imaginary axes of the complex plane, respectively. In terms of these variables, the equation for the parabola can be written as

$$\rho = -\frac{E}{D^2} \sigma^2, \quad (26)$$

While the equation for the circle is

$$\rho^2 + \sigma^2 = 1. \quad (27)$$

To find the points where both curves cross, solve for σ in Eq. (26) and substitute into Eq. (27) to obtain

$$\rho^2 - \frac{D^2}{E} \rho = 0. \quad (28)$$

The solutions to this last equation give the real coordinates of the crossing points. The corresponding imaginary coordinates can then calculated as $\sigma = -\sqrt{1 - \rho^2}$. The solutions of Eq. (28) are

$$\rho_1 = \frac{L}{2} + \frac{1}{2} \sqrt{L^2 - 4K}, \quad (29)$$

$$\rho_2 = \frac{L}{2} - \frac{1}{2} \sqrt{L^2 - 4K}, \quad (30)$$

with $L = D^2/E$ and $K = -1$. From its definition and the fact that E is negative and D is positive, L is negative. Notice that ρ_1 and ρ_2 have common points. Therefore, the parabola of Eq. (26) crosses the unitary circle in the points $(-0.19, \pm 0.98)$, this indicating that there a two points which induce oscillations, i.e., those points can be destabilize the system. In Fig. 4 shows these points.

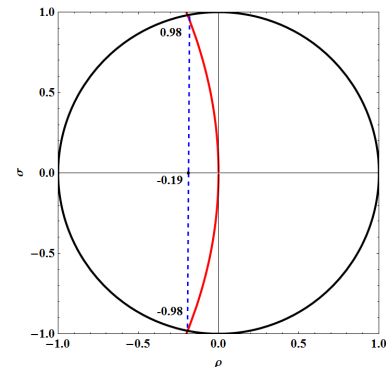


Fig. 4 Plot shows the intersections between unit circle and the parabola given in Eqs.(26) and Eqs.(27).

COMMENTS

From the result obtained with mechanics of fluids we can assert, that our approximation of the heart like mechanics pump is far from the reality. We will looking another model that takes in account more details of the blood flow, and probably we can get an expression, that gives values more realist. Finally we have to remark that Non-linear dynamics is an useful and powerful tool to tackle system with time delays, because it was possible to get two points which destabilizes the system, and assume that the intersection of these points could be associated with both arterial pressure the called Systole and Diastole, important parameters of pressure in blood flow.

ACKNOWLEDGMENT

This work was partially supported by CONACYT (SNI). We appreciate the valuable review of the manuscript in English to F. Miranda the English review.

NOMENCLATURE

Symbol	Quantity	SI Unit
x	length of muscle fiber	(m)
x_d	typical length of muscle fiber in the diastolic state	(m)
y	variable related to electrochemical activity	(J)
δx	small disturbances from the corresponding fixed point values	(m)
δy	small disturbances from the corresponding fixed point values	(m)
λ_1	eigenvalue 1	(Hz)
λ_2	eigenvalue 2	(Hz)
ξ	time delay	(s)
ω	frequency	(Hz)
P_1	constant high pressure reservoir	(Pa)
P_2	constant low pressure reservoir	(Pa)
T	tension in the muscle fiber	(N)
\vec{u}_1	eigenvector corresponding to eigenvalue λ_1	(m)
\vec{u}_2	eigenvector corresponding to eigenvalue λ_2	(m)

Dimensionless Quantity

ϵ	is a small positive constant
η_{max}	efficiency
A	systole
B	diastole
E	constant
F	constant
D	constant
i	imaginary unit
A_1	arbitrary constant 1
A_2	arbitrary constant 2
B_1	arbitrary constant 1
B_2	arbitrary constant 2

REFERENCES

- [1] Frank C. Hoppensteadt and Charles C. Peskin, Mathematics in Medicine and the Life Sciences, chap. 5, Springer-Verlag, New York, Inc. 1992.
- [2] D. S. Jones and B.D. Sleeman, Differential Equations and Mathematical Biology, chap. 6, Chapman & Hall/CRC 2003.
- [3] A. Bejan and N. Dan Analogy between electrical machines and heat transfer-irreversible heat engines, Int. J. Heat Mass Transfer. Vol. 39, No. 17, pp. 3659-3666, 1996.
- [4] A. Vander, J. Sherman and L. Dorothy, Human Physiology, The Mechanisms of Body Function, chap. 2, Mc Graw Hill 1970.
- [5] E.C. Zeeman, Differential Equations for heartbeat and nerve impulse, Toward a Theoretical Biology, Vol. 4, pp. 8-67, 1972.
- [6] N. McDonald, Biological Delay Systems: Linear Stability Theory, Cambridge, UK: Cambridge University Press;1989.
- [7] R. Páez-Hernández and M. Santillán, Comparison of the energetic properties and the dynamical stability in a mathematical model of the stretch reflex. Physica A 387, pp. 3574-3582, 2008.
- [8] A. Rojas-Pacheco, B. Obregón-Quintana, L.S. Liebovitch, L. Guzmán-Vargas. Time-delay effects on dynamics of a two-actor conflict model. Physica A 392, pp. 458-467, 2013.
- [9] H.S. Strogatz. Non Linear Dynamics and Chaos: With Applications to Physics, Chemistry and Engineering. chap. 6, Perseus, Cambridge MA, 1994.

EFFECTS OF THE TIME DELAYS IN AN ENDOREVERSIBLE AND NONENDOEVERSIBLE THERMAL ENGINES WORKING AT DIFFERENT REGIMES

Páez-Hernández R.*, Portillo-Díaz P.°, Ladino-Luna D.*

*Área de Física de Procesos Irreversibles, °Departamento de Ciencias Básicas, Universidad Autónoma Metropolitana-Azcapotzalco, Av. San Pablo No. 180 Col. Reynosa Tamps. CP02200 MÉXICO
Corresponding Author: phrt@correo.azc.uam.mx

ABSTRACT

In this work we analyze engine implicit time delays of an endoreversible Curzon-Ahlborn engine using a van der Waals gas working at maximum power regime, we obtain relaxation times, and system phase portrait. When comparing the phase portrait with an endoreversible Curzon-Ahlborn engine using a van de Waals gas working at maximum ecological regime, we observe that eigenvectors have a counter clockwise rotation, as can be seen in the corresponding phase portrait. We find that the total time delay does not destabilize the system steady-state, regardless of this length, and thus it does not seem to play a role in the dynamic-thermodynamic properties trade-off. This result is in accordance with previous studies of endoreversible and non-endoreversible Curzon-Ahlborn engines. Finally we can conclude that it is a fact that the engine dynamic properties are different when the work regimes and working substance change.

INTRODUCTION

There are many previous works on Finite Time Thermodynamics (FTT), several of them focus on the steady-state energetic properties of the systems. Nevertheless, it is worthwhile to consider the local stability of the system. Santillán et al [1] first studied the local stability of a Curzon-Ahlborn-Novikov (CAN) engine working in a maximum-power-like regime considering the heat resistance and the equal high and low temperature heat transfer coefficients with Newton's heat transfer law. Chimal-Eguia et al. [2] analyzed the local stability of an endoreversible heat engine working in a maximum-power-like regime with Stefan-Boltzman law. Guzman-Vargas et al. [3] studied the effect of heat transfer law and heat transfer coefficients on the local stability of an endoreversible heat engine operating in a maximum-power-like regime. Barranco-Jimenez et al [4] investigated the local stability of a thermo-economic model of a Novikov-Curzon-Ahlborn heat engine. Páez-Hernandez et al. [5] studied the dynamic properties in an endoreversible Curzon-Ahlborn (CA) engine using a Van der Waals gas working substance at maximum power regime. Páez-Hernandez et al. [6] studied the Local stability analysis of a Curzon-Ahlborn engine considering the Van der Waals equation state in the maximum ecological regime. Chimal-Eguia et al. [7] analyzed the local stability of an endoreversible heat engine working in an ecological regime. Páez-Hernández et al [8] studied the dynamic robustness of a non-endoreversible engine working at maximum power output. Sanchez-Salas et al. [9] studied the dynamic robustness of a non-endoreversible engine working in an ecological regime. Huang et al [10] studied the local analysis of an endoreversible heat pump operating at minimum input power for a given heating load with Newton's heat transfer law. Huang [11] analyzed the local asymptotically stability of an irreversible heat pump subject to total thermal conductance constraint. Wu et al [12] studied the

local stability of an endoreversible heat pump with Newton's heat transfer law working at the maximum ecological function.

TIME DELAYS

In real life situations when the value of a variable is modified, the effect in the dynamic response of the system is not observed immediately. A certain time must elapse until the system begins to respond or "feel" the effect of the changes made. Suppose we modify the concentration of a reactor feed. Our experience and common sense tell us that time passes until the variables that characterize the dynamic behavior of the reactor (e.g. concentration) begin to modify its value relative to their pre-change. These systems are known as dynamical systems. Delayed systems appear naturally in Medicine, Biology and Engineering. These systems have been studied before the last century. Studies in Medicine and Biology begin with Ross' epidemiology models (1911) and others in the early twentieth century, which were studied by Lotka, Volterra and Kostitzin [13]. A distinctive feature of these systems is that their rate of evolution is described by differential equations that include information about the history of the system. The effects of delays are of great interest, since their presence may include complex behavior (oscillations, instability, bad system performance). Páez-Hernández et al [14] studied the effect time delays produced in a mathematical model for the stretch reflex regulatory pathway. Guzmán-Vargas et al [15] studied time-delay effects on dynamics of a two-actor conflict model.

FIXED POINT AND LINEARIZED SYSTEM WITH DELAYS

Consider a dynamic system which has a single variable with time delays ξ ,

$$\begin{aligned}\frac{dx}{dt} &= f(x, y_\xi) \\ \frac{dy}{dt} &= g(x_\xi, y)\end{aligned}\quad (1)$$

where subscript ξ is a time delay variable. Following step by step Strogatz [16] to obtain a linear system,

$$\dot{u} = f(x^* + u, y^* + v_\xi), \quad \dot{v} = g(x^* + u_\xi, y^* + v), \quad (2)$$

where u and v represent a small perturbation of the system and (x^*, y^*) is a fixed point, now we do a Taylor series expansion to Eq. (2) and we consider negligible the terms of two onward, and evaluate the steady-state and we obtain

$$\dot{u} = \left. \frac{\partial f}{\partial x} \right|_{(x^*, y^*)} u + \left. \frac{\partial f}{\partial y_\xi} \right|_{(x^*, y^*)} v_\xi \quad (3)$$

$$\dot{v} = \left. \frac{\partial g}{\partial x_\xi} \right|_{(x^*, y^*)} u_\xi + \left. \frac{\partial g}{\partial y} \right|_{(x^*, y^*)} v. \quad (4)$$

Now we assume that u and v are of the form

$$u = A_1 e^{\lambda t} \quad (5)$$

$$u_\xi = A_1 e^{\lambda t} e^{-\lambda \xi} \quad (6)$$

$$v = A_2 e^{\lambda t} \quad (7)$$

$$v_\xi = A_2 e^{\lambda t} e^{-\lambda \xi} \quad (8)$$

where λ is a complex number, A_1 and A_2 are constant.

Substituting (5)-(8) in (3) and (4) leads to the following set of homogeneous linear system for A_1 and A_2 :

$$(f_x - \lambda)A_1 + f_{y_\xi} e^{-\lambda \xi} A_2 = 0 \quad (9)$$

$$f_{x_\xi} e^{-\lambda \xi} A_1 + (g_y - \lambda)A_2 = 0. \quad (10)$$

This system of equations has non-trivial solutions only if the determinant of the matrix of coefficients equals zero, i.e.

$$(f_x - \lambda)(g_y - \lambda) - f_{x_\xi} g_{y_\xi} e^{-2\lambda \xi} = 0. \quad (11)$$

This equation is also called the transcendental characteristic equation, and can be written as

$$H(z) + K(z)e^{-z\xi} = 0, \quad (12)$$

with z an eigenvalue, and $H(z)$ and $K(z)$ are polynomials of second and zero order, respectively.

The solutions to this equation are not obvious because has an infinite number of roots [13]. One way to overcome this situation is to consider the fact a common effect of time delays to destabilize stable fixed points or to stabilize unstable fixed points by sustained oscillations. If we assume that $(z = i\omega)$, and substitute in (12), we obtain a complex variable equation.

$$P(\omega) + iQ(\omega) = e^{-i\omega\xi} \quad (13)$$

where $P(\omega)$ and $Q(\omega)$ are second and first order polynomials, respectively. We observe that the right hand side of this equation represents the unitary circle whereas the left hand side describes a parabola. The intersection of these two curves could represent a change in the stability of the system. The analysis of intersection between the parabola and the unitary circle leads to the following classification:

- If the parabola does not intersect the unitary circle, and the system is stable to $\xi = 0$, then the system is stable and independent of delay.
- If the system is stable for $\xi = 0$ and the parabola intersects the unit circle, then the system can be affected by delays.

THE STEADY-STATE CURZON-AHLBORN ENGINE USING A VAN DER WAALS GAS AS WORKING SUBSTANCE

Consider the endoreversible CA heat engine (Figure 1). This engine works between the heat reservoirs T_1 and T_2 ($T_1 > T_2$). The working temperatures at steady state are \bar{x} , and \bar{y} ($T_1 > \bar{x} > \bar{y} > T_2$). Heat flows from T_1 to \bar{x} and from \bar{y} to T_2 through thermal resistances, with a thermal conductance denoted by α .

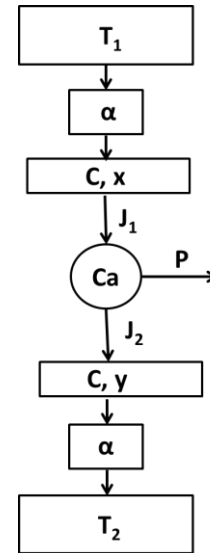


Figure 1: Schematic representation of a CA engine which consists of a Carnot engine (Ca) and the heat reservoirs T_1 and T_2 . The heat exchanges J_1 and J_2 take place through both thermal conductors with the same conductance α .

Using the endoreversibility hypothesis, an engine working between the reservoir \bar{x} and \bar{y} acts like a Carnot engine, although it works in finite time cycles, i.e.

$$\bar{J}_1 = \frac{\bar{x}}{\bar{x} - \bar{y}} \bar{P} \quad (14)$$

and

$$\bar{J}_2 = \frac{\bar{y}}{\bar{x} - \bar{y}} \bar{P} \quad (15)$$

\bar{J}_1 and \bar{J}_2 are the steady-state heat flows from \bar{x} to the engine, and from the engine to \bar{y} respectively. \bar{P} is the engine power output.

The CA engine works usually in steady state, so that the heat flux from T_1 to \bar{x} is \bar{J}_1 , and the heat flux from \bar{y} to T_2 is \bar{J}_2 ,

$$\bar{J}_1 = \alpha(T_1 - \bar{x}) \quad (16)$$

and

$$\bar{J}_2 = \alpha(\bar{y} - T_2). \quad (17)$$

From equations (14)–(17), and from the definition of efficiency given as,

$$\bar{\eta} = \frac{\bar{P}}{J_1}. \quad (18)$$

it follows that

$$\bar{x} = \frac{T_1}{2} \left(1 + \frac{T_2/T_1}{1-\bar{\eta}} \right) \quad (19)$$

$$\bar{y} = \frac{T_1}{2} (1 - \bar{\eta}) \left(1 + \frac{T_2/T_1}{1-\bar{\eta}} \right). \quad (20)$$

The efficiency of a Curzon-Ahlborn engine working at maximum power output using a van der Waals gas as working substance η_{vW} , was found by Ladino-Luna [17] and it is given as,

$$\eta_{vW} = 1 - \left\{ \sqrt{\tau} + 1/2 (1 - \sqrt{\tau})^2 \lambda_{vW} + \frac{1}{4} (1 - \sqrt{\tau})^2 \left[\frac{(1-\sqrt{\tau})^2}{2\sqrt{\tau}} - \ln \tau \right] \lambda_{vW}^2 + O(\lambda_{vW}^3) \right\}, \quad (21)$$

with: $\tau = T_2/T_1$, and

$$\lambda_{vW} = \frac{1}{\gamma-1} \left(\ln \frac{v_{max}-b}{v_{min}-b} \right)^{-1}, \quad (22)$$

where b is a constant which depends on the gas, γ is the ratio of the constant-pressure and constant-volume heat capacities $\gamma = C_p/C_v$, v_{max} and v_{min} are the subtended volumes maximum and minimum respectively by the gas in a cycle. Now if we consider that b is smaller than v_{max} and v_{min} , table 13.1 [18], then the ratio $(v_{max} - b)/(v_{min} - b)$ is approximately v_{max}/v_{min} , this ratio is called volumetric compression ratio r_c , for Diesel cycle the typical values are 12-15, table 10.1 [19], so we do the calculus using (22) and obtain $\lambda_{vW} = 1.006$, which shows that we can use for calculus purposes $\lambda_{vW} = 1$, equation (22) gives more values to λ_{vW} , but do not have physical meaning, in accordance with [20].

So we use only the linear approximations of (21), and supposing a value $\lambda_{vW} = 1$, and we obtain the approximate expression,

$$\eta_{vW} = 1 - \sqrt{\tau} - \frac{1}{2} (1 - \sqrt{\tau})^2 = \frac{1-\tau}{2} = \frac{\eta_C}{2}. \quad (23)$$

In this approximation we observe a relation between Carnot's efficiency (η_C) and van der Waals's efficiency (η_{vW}) at maximum power, which is $\eta_{vW} = \eta_C/2$. It is reasonable because η_{vW} is smaller than η_C , so the efficiency of a CA engine working in the maximum power regime using a van der Waals gas working substance is given by (21), with $\tau = T_2/T_1$. Now, substituting this efficiency (23), into equations (19) and (20) renders

$$\bar{x} = \frac{T_1 (1+3\tau)}{2 (1+\tau)} \quad (24)$$

and

$$\bar{y} = \frac{T_1}{4} (1 + 3\tau). \quad (25)$$

From (14), and (18)-(20) we can write the power output of the steady- state in terms of T_1 and T_2 (T_1 and τ) and it becomes

$$\bar{P} = \frac{T_1 \alpha (1-\tau)^2}{4 (1+\tau)}. \quad (26)$$

Solving T_1 and T_2 , from equations (19) and (20) results in

$$T_1 = - \frac{2\bar{x}\bar{y}}{\bar{x}-3\bar{y}} \quad (27)$$

and

$$T_2 = \frac{2}{3} \left(2\bar{y} + \frac{\bar{x}\bar{y}}{\bar{x}-3\bar{y}} \right). \quad (28)$$

Finally substituting (27) and (28) in (26) we obtain the power output in steady-state \bar{P} as function of \bar{x} and \bar{y} ,

$$\bar{P} = - \frac{\alpha(\bar{x}-\bar{y})}{\bar{x}-3\bar{y}}. \quad (29)$$

LOCAL STABILITY OF AN ENDOREVERSIBLE CURZON-AHLBORN ENGINE

Following Santillán et al [1], a system of differential equations is constructed, which provides information about of the stability engine. Santillán et al. developed a system of coupled differential equations to model the rate of change of intermediate temperature.

Assuming that the temperatures x and y correspond to macroscopic objects with heat capacity C , the differential equations for x and y are given by [1]

$$\frac{dx}{dt} = \frac{1}{C} [\alpha(T_1 - x) - J_1] \quad (30)$$

and

$$\frac{dy}{dt} = \frac{1}{C} [J_2 - \alpha(y - T_2)], \quad (31)$$

Both derivatives cancel when x, y, J_1 and J_2 take their steady state values. Under the endoreversibility assumption, the heat flux from x to the working fluid is J_1 and the heat flux from the Carnot engine to y is J_2 , so J_1 and J_2 are given in terms of x and y , and the power output P as,

$$J_1 = \frac{x}{x-y} P \quad (32)$$

and

$$J_2 = \frac{y}{x-y} P. \quad (33)$$

It seems reasonable to assume that the power output produced by the CA engine is related to temperature x and y in the same way that the power output at steady state \bar{P} depends on \bar{x} and \bar{y} in the maximum power regime (see equation (26)), i.e.,

$$P = \frac{\alpha(x-y)^2}{3y-x}. \quad (34)$$

The substitution (32)-(34) in (30) and (31) leads to the following set of differential equations for temperatures x and y of a CA engine performing in maximum-power regime and using a van der Waals gas as working substance.

$$\frac{dx}{dt} = \frac{\alpha[T_1(x-3y)+2xy]}{C(x-3y)} \quad (35)$$

and

$$\frac{dy}{dt} = \frac{\alpha[T_2(x-3y)-2y(x-2y)]}{C(x-3y)}. \quad (36)$$

To analyze the system stability near to the steady state, we proceed by following the steps described in section stability with $\xi = 0$. First we define

$$f(x, y) = \frac{\alpha[T_1(x-3y)+2xy]}{C(x-3y)} \quad (37)$$

and

$$g(x, y) = \frac{\alpha[T_2(x-3y)-2y(x-2y)]}{c(x-3y)}. \quad (38)$$

The matrix $A = \begin{pmatrix} f_x & f_y \\ g_x & g_y \end{pmatrix}$, A is called the jacobian matrix.

Now using Eqs. (37) and (38), we obtain

$$f_x = -\frac{6\alpha(1-\tau)^2}{c(1+3\tau)^2} \quad (39)$$

$$f_y = \frac{8\alpha}{c(1+3\tau)^2} \quad (40)$$

$$g_x = \frac{2\alpha(1+\tau)^2}{c(1+3\tau)^2} \quad (41)$$

$$g_y = -\frac{4\alpha(1+\tau(2+3\tau))}{c(1+3\tau)^2} \quad (42)$$

with $\tau = T_2/T_1$.

By substitution of (39)-(42) in Eq. (11) with $\xi = 0$, we find that both eigenvalues λ_1 and λ_2 have real parts, then we can conclude that any perturbation decays exponentially with time and thus that steady-state is stable for every value of α , C and $\tau = T_2/T_1 > 0$. The above permit us establish the relaxation times, in [5] was studied the dynamic properties for this engine and is shown that energetic properties of an endoreversible Curzon-Ahlborn engine using a Van der Waals gas working at maximum power output regime (MP) worsens as τ decrease to zero, and there is an interval for the Curzon-Ahlborn engine which has efficiency and power output subject to compromise with τ , as it has been shown in [1,3,8]. In [6] was studied the dynamic properties for this engine and is shown that energetic properties of an endoreversible Curzon-Ahlborn engine using a van der Waals gas working at maximum ecological regime (ME). This engine has the same characteristic as the maximum power output regime, now our interest is show the behavior for both regimes; in Fig. 2 we compare the relaxation times for both regimes, we observe that relaxation times exhibit approximately the same stability interval.

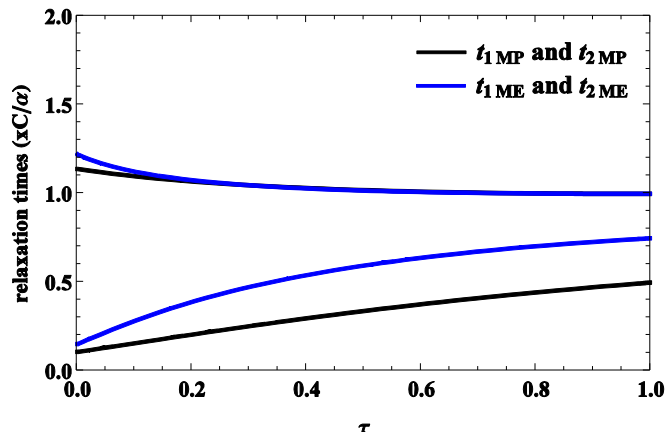


Fig. 2 Plots of relaxation times t_1 and t_2 , in units of C/α , vs. τ

However when we compare the portrait phase for both maximum power output and maximum ecological regimes, there is a small difference between the eigenvectors, i.e., there is a rotation for both eigenvectors, this can see in the Fig.3.

DYNAMIC EFFECTS OF TIME DELAYS

Consider again the systems of delay differential equations given by Eqs. (1) and (2), but now $\xi = \frac{\pi}{2}$. They can rewritten as

$$\begin{aligned} \frac{dx}{dt} &= f(x, y_{\pi/2}) \\ \frac{dy}{dt} &= g(x_{\pi/2}, y) \end{aligned}$$

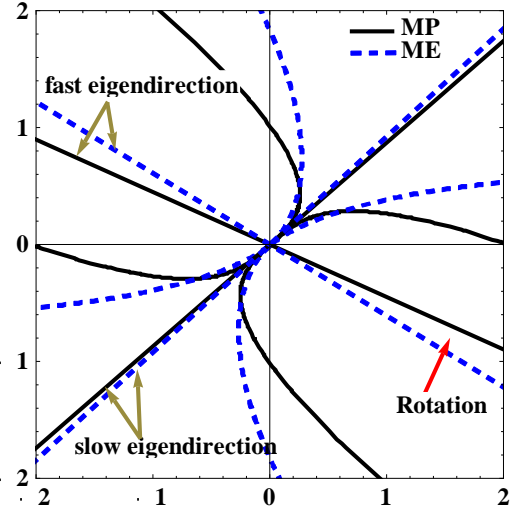


Figure 3. Phase portrait of a Curzon-Ahlborn engine working at two different regimes

with f and g as defined in Eqs. (30) and (31). From the fixed points theory with time delays, the time course of small perturbations from the steady state is determined; we can write Eq. (11) as

$$(f_x - \lambda)(g_y - \lambda) - f_y g_x e^{-\lambda\pi} = 0. \quad (43)$$

The stability analysis of a dynamic system involving time delays can be quite complicated due to the fact that, in general, the characteristic equation has an infinite number of solutions. On the other hand, it is known that a common effect of time delays is to destabilize formerly stable steady states by inducing sustained oscillations. To test whether this happens, assume that λ is imaginary ($\lambda = i\omega$) and substitute into the characteristic equation to obtain

$$(-A\omega^2 + B) + iD\omega = e^{(-i\omega\pi)}, \quad (44)$$

with

$$A = \frac{1}{f_y g_x}, \quad B = \frac{f_x g_y}{f_y g_x} \quad \text{and} \quad D = \frac{f_x + g_y}{f_y g_x}.$$

It follows from Eqs. (39)-(42) that $f_x, g_y < 0$, while $f_y, g_x > 0$. This further implies that constants A , B , and D are all positive.

The left-hand side of Eq. (44) determines the lower branch of a horizontal parabola in the complex plane. This parabola opens to the left and its vertex is located in the point $(B, 0)$. On the other hand, the right-hand side of Eq. (44) determines a unitary circle in the complex plane. The points where these curves cross correspond to values of ω and π at which sustained oscillations appear due to a destabilization of the steady state, or vice versa. If both curves never cross, the steady state cannot be destabilized by the total delay π , no matter how long it is. Let ρ and σ real variables along the real

and the imaginary axes of the complex plane, respectively. In terms of these variables, the equation for the parabola can be written as

$$\rho = B - \frac{A}{D^2} \sigma^2, \quad (45)$$

While the equation for the circle is

$$\rho^2 + \sigma^2 = 1. \quad (46)$$

To find the points where both curves cross, solve for σ in Eq. (45) and substitute into Eq. (46) to obtain

$$\rho^2 - \frac{D^2}{A} \rho + \frac{BD^2 - A}{A} = 0. \quad (47)$$

The solutions to this last equation give the real coordinates of the crossing points. The corresponding imaginary coordinates can then be calculated as $\sigma = -\sqrt{1 - \rho^2}$. The solutions of Eq. (47) are

$$\rho_1 = \frac{L}{2} + \frac{1}{2} \sqrt{L^2 - 4K}, \quad (48)$$

$$\rho_2 = \frac{L}{2} - \frac{1}{2} \sqrt{L^2 - 4K}, \quad (49)$$

with $L = D^2/A$ and $K = (BD^2 - A)/A$. From its definition and the fact that A and D are positive, L is also positive and so $\rho_1 > \rho_2$. In Fig. 4, the plot of ρ_1 , ρ_2 and τ is shown. Notice that ρ_1 and ρ_2 there are no common points. Therefore, the parabola of Eq. (41) never crosses the unitary circle given by Eq. (45), because $\rho_1, \rho_2 >$ implies that σ takes imaginary values and the endoreversible Curzon-Ahlborn engine using a Van der Waals gas working at maximum power output regime cannot be destabilized by any time delay. In Fig.4 is shown this result, it is important to remark that there are no common points on both surfaces.

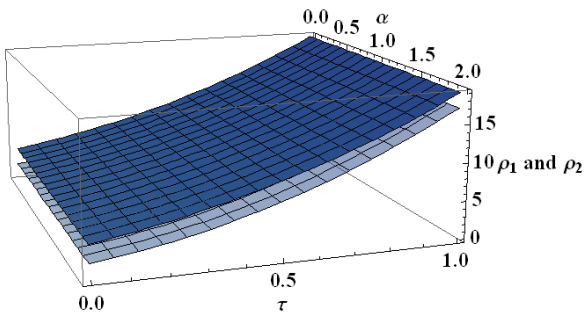


Figure 4. Plot of (ρ_1, ρ_2) , as given by Eqs. (48) and (49), vs. α and τ , for an endoreversible Curzon-Ahlborn engine using a Van der Waals working at maximum power output regime.

Analogously we can do the same calculus for an endoreversible Curzon-Ahlborn engine using a Van der Waals gas working at maximum ecological regime, and we find a similar behavior and this is shown in Fig. 5.

NON-ENDOREVERSIBLE CURZON-AHLBORN ENGINE

Following Páez-Hernández et al. [8], we obtain the relaxation times, the phase portrait diagram and also investigate the effect of delays in time, for reasons of space, here we only show in Fig. 6 the behavior of the effects of delays for a non-endoreversible Curzon-Ahlborn engine using

a Van der Waals gas working at maximum power output regime

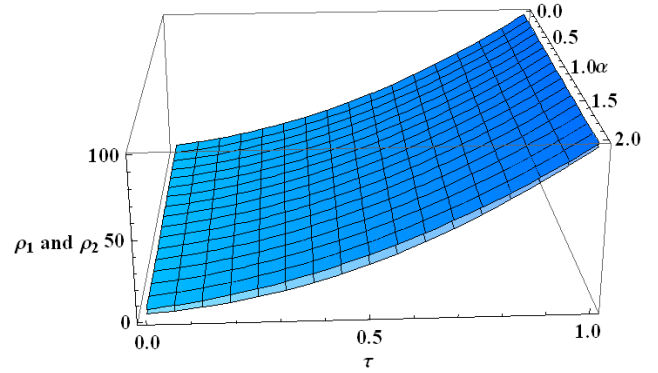


Figure 5. Plot of (ρ_1, ρ_2) , as given by Eqs. (48) and (49), vs. α and τ , for an endoreversible Curzon-Ahlborn engine using a Van der Waals working at maximum ecological regime.

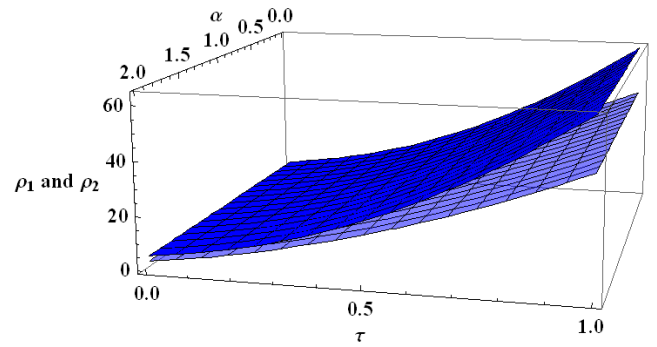


Figure 6. Plot of (ρ_1, ρ_2) , as given by Eqs. (48) and (49), vs. α and τ , for a non-endoreversible Curzon-Ahlborn engine using a Van der Waals working at maximum power output regime.

CONCLUDING REMARKS

In this paper we have extended a previous work by R. Páez-Hernández et al. [5,6] in which the local stability of an endoreversible Curzon-Ahlborn engine working in both maximum power output and maximum ecological regimes. Here, we have considered a Curzon-Ahlborn engine using a Van der Waals gas working at maximum power output regime, also we present the analysis to a non-endoreversible Curzon-Ahlborn in the maximum power regime, taking into account the engine inherent time delays.

Our results indicate that the only effect of different regimes is a rotation in the corresponding eigenvectors in the phase portrait.

Time delays are present in many systems subject to dynamic regulation. In the endoreversible and non-endoreversible Curzon-Ahlborn engine, the inherent time delays are not capable of destabilizing the steady state; thus, they not to play a role in the trade-off between energetic and dynamic properties. This does not have to be true for all energetic-converting systems, though. For instance, time delays are essential to understand the origin of clonus (sustained oscillations in muscle contraction).

ACKNOWLEDGMENT

This work was partially supported by CONACYT (SNI). We appreciate the valuable review from F. Miranda Maldonado of the manuscript in English.

NOMENCLATURE

Symbol	Quantity	SI Unit
b	constant which depend on the gas	(m ³ /kg mol)
C	Heat capacity	(J/K)
\bar{P}	steady-state power output	(W)
t	time	(s)
\bar{x}	steady-state working hot temperature of the Carnot cycle	(K)
\bar{y}	steady-state working cool temperature of the Carnot cycle	(K)
α	thermal conductance	(W/K·m)
δx	small disturbances from the corresponding fixed point values	(m)
δy	small disturbances from the corresponding fixed point values	(m)
λ_1	eigenvalue 1	(Hz)
λ_2	eigenvalue 2	(Hz)
ξ	time delays	(s)
\bar{J}_1	steady-state heat flow from hot to the engine	(W)
\bar{J}_2	steady-state heat flow from the engine to cold	(W)
t_1	relaxation time 1	(s)
t_2	relaxation time 2	(s)
T_1	reservoir at temperature hot	(K)
T_2	reservoir at temperature cold	(K)
\vec{u}_1	eigenvector corresponding to eigenvalue λ_1	(m)
\vec{u}_2	eigenvector corresponding to eigenvalue λ_2	(m)
v_{max}	maximum subtended volume by the gas in a cycle	(m ³ /kg mol)
v_{min}	minimum subtended volumes by the gas in a cycle	(m ³ /kg mol)

Dimensionless Quantities

γ	the ratio of the constant-pressure and constant-volume heat capacities
$\bar{\eta}$	steady-state efficiency
τ	ratio of the hot and cold temperatures
η_{vw}	efficiency of a Curzon-Ahlborn engine working at maximum power output using a van der Waals gas as working substance
A_1	arbitrary constant 1
A_2	arbitrary constant 2
B_1	arbitrary constant 3
B_2	arbitrary constant 4
r_C	volumetric compression ratio

REFERENCES

[1] M. Santillán, G. Maya-Aranda and F. Angulo-Brown Local stability analysis of an endoreversible Curzon-Ahlborn engine working in maximum-power-like regime. *J. Phys. D: Appl. Phys.* 34 (13), pp. 2068-2072, 2001.

[2] J.C. Chimal-Eguia, M.A. Barranco-Jimenez and F. Angulo-Brown, Stability analysis of an endoreversible heat engine with Stefan-Boltzmann heat transfer law working in maximum-power-like regime. *Open Syst. Inf. Dyn.*, 13(1), pp. 43-54, 2006.

[3] L. Guzmán-Vargas, I. Reyes-Ramírez and N. Sanchez-Salas, The effect of heat transfer laws and thermal

conductances on the local stability of an endoreversible heat engine. *J. Phys. D: Appl. Phys.* 38(8), pp. 1282-1291, 2005.

[4] M.A. Barranco-Jimenez, R. Páez-Hernández, I. Reyes-Ramírez and L. Guzmán-Vargas, Local stability analysis of a thermo-economic model of a Novikov-Curzon-Ahlborn engine, *Entropy*, 13(9), pp. 1584-1594, 2011.

[5] R. Páez-Hernández, D. Ladino-Luna and P. Portillo-Díaz. Dynamic properties in an endoreversible Curzon-Ahlborn engine using a van der Waals gas as working substance. *Physica A*, 390(20), pp. 3275-3282, 2011.

[6] R. Páez-Hernández, P. Portillo-Díaz, D. Ladino-Luna, M.A. Barranco-Jiménez. Local stability analysis of a Curzon-Ahlborn engine considering the van der Waals equation state in the maximum ecological regime. *ECOS2012. Proceedings of the 25th International Conference on Efficiency, Costs, Optimization, Simulation and Environmental Impact of Energy Systems*; June 26-29, Perugia, Italy.

[7] J.C. Chimal-Eguia, I. Reyes-Ramírez and L. Guzmán-Vargas. Local stability of an endoreversible heat engine working in an ecological regime. *Open Syst. Inf. Dyn.*, 14(4), pp. 411-424, 2005.

[8] R. Páez-Hernández, F. Angulo-Brown and M. Santillán. Dynamic Robustness and Thermodynamic Optimization in a Non-endoreversible Curzon-Ahlborn engine. *J. Non-Equilib. Thermodyn.* 31, pp. 173-188, 2006.

[9] N. Sanchez-Salas, J.C. Chimal-Eguia and F. Guzmán-Aguilar. On the dynamic robustness of a non-endoreversible engine working in different operation regimes, *Entropy*, 13(2), pp. 422-436, 2011.

[10] Y.W. Huang, D.X. Sun and Y.M. Kang. Local stability analysis of a class of endoreversible heat pumps. *J. Appl. Phys.* 102(3), pp. 034905, 2007.

[11] Y.W. Huang. Local asymptotic stability of an irreversible heat pumps subject to total thermal conductance constraint. *Energy Convers. Manage.* 50(6). Pp. 1444-1449, 2009.

[12] X. H. Wu, L. G. Chen and F.R. Sun. Local stability of an endoreversible heat pump working at the maximum ecological function, *Chinese J. Eng. Thermophys.* 32(11), pp. 1811-1815 (in Chinese) 2011.

[13] McDonald, N., *Biological Delay Systems: Linear Stability Theory*, Cambridge, UK: Cambridge University Press; 1989.

[14] Ricardo Páez-Hernández and Moisés Santillán, Comparison of the energetic properties and the dynamical stability in a mathematical model of the stretch reflex. *Physica A* 387, pp. 3574-3582, 2008.

[15] A. Rojas-Pacheco, B. Obregón-Quintana, L.S. Liebovitch, L. Guzmán-Vargas. time-delay effects on dynamics of a two-actor conflict model. *Physica A* 392, pp. 458-467, 2013.

[16] H.S. Strogatz. *Non Linear Dynamics and Chaos: With Applications to Physics, Chemistry and Engineering*, Perseus, Cambridge MA, 1994.

[17] D. Ladino-Luna *Rev. Mex. Fis.* 48, pp 575, 2002.

[18] F.F. Huang, *Engineering Thermodynamics an Applications*, 2nd. ed., McMillan Publishing Company. New York, 1989.

[19] J.B. Heywood, *Internal Combustion Engine*, Mc Graw Hill Publishing Company, 1988.

[20] D. Ladino-Luna *J. Energy Institute* 81, (2) 114, 2008.

STIRLING ENGINE AS SIMPLE AS POSSIBLE

P. Županović*, I. Sorić **, T. Sorić***

*University of Split, Faculty of Science, Teslina 12, 21000 Split Croatia, E-mail: pasko@pmfst.hr

**University of Split, FESB, Boškovićeve b.b. 21000 Split, Croatia, E-mail: suri@fesb.hr

***University of Split, Faculty of Science, Teslina 12 21000 Split Croatia, E-mail: tomsor@pmfst.hr

ABSTRACT

Within isothermal analysis of Stirling engine analytical expressions for a pressure as a function of crank angle and for a work are found. The efficiency is numerical calculated for a wide range of temperatures. In contrast to the efficiency of the Carnot cycle, which is monotonically increasing function of the ratio of temperatures of heat baths, the efficiency of the Stirling engine has its maximum. The value of this maximum, as well as the corresponding ratio of heat baths temperatures, depends on a molar heat capacity of the working substance.

INTRODUCTION

In 1816 Stirling brothers patented an engine known as the Stirling engine. Stirling brothers patented five different kinds. Although there are several different kinds of Stirling engines they all have two major things in common. A gas as working substance never leave the engine. This engine uses an external heat source of any kind like, Sun, geothermal water, fossil resources, biomass or nuclear reactor.

BASIC ASSUMPTIONS

In this paper we consider α type of Stirling engine. It consists of two power pistons situated in mutually perpendicular cylinders. Pistons are interconnected via flying wheel as it is shown in Fig. 1.

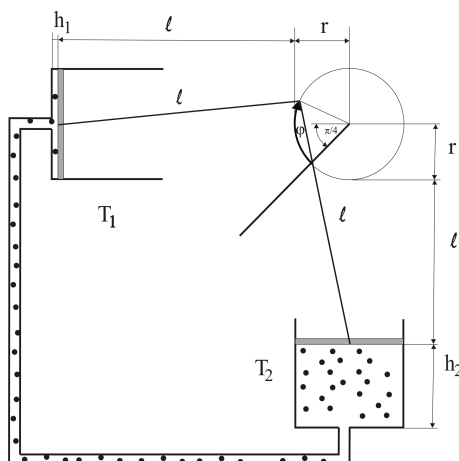


Figure 1. α Stirling engine.

We assume isothermal process between gas and heat baths. This assumption is in common with the Schmidt theory [1; 2] of Stirling engine. The basic difference between Schmidt analysis and one in this paper is the method of calculation of absorbed

heat. Schmidt theory assumes that gas absorbs heat in expansion part of the cycle. In contrary to this, rather arbitrary assumption, we keep track of sign of infinitesimal heat exchange between gas and hot cylinder. In this way the regions of heat absorption is clearly determined. This allow us to find the efficiency as a function of ratio of bath temperatures. Parameters is the gas molar heat capacity.

CYCLE

The speed of pressure transmission is equal to the sound speed. Pistons speeds are much less than speed of sound, Neglecting viscous effects pressures in both cylinders are practically equal. For the sake of simplicity the following assumptions are made:

There is no dead volume. Pistons move from the bottom of cylinders.

A lengths of shafts (l) are much longer than radius (r) of circle described by shafts ends, $r/l \ll 1$.

Working substance is an ideal gas.

From the mechanical point of view Stirling engine has one degree of freedom, the crank angle. A branch of crank angle is defined with radius of flying wheel that ends at shafts ends. The coincidence of this radius with the line of symmetry of Stirling engine, depicted in Fig. 1, at minimum value of the total gas volume defines the zero angle.

Taking into account above mentioned assumptions volumes of the gas in cylinders are,

$$V_1 = Ar \left[1 - \cos \left(\varphi - \frac{\pi}{4} \right) \right], \quad (1)$$

$$V_2 = Ar \left[1 + \sin \left(\varphi + \frac{\pi}{4} \right) \right], \quad (2)$$

where A is the area of the cross section of cylinders. The total volume is

$$V = Ar \left(2 - \sqrt{2} \cos \varphi \right). \quad (3)$$

Assuming isothermal processes in cylinders and using ideal gas equation of state we find the dependence of the pressure on the crank angle,

$$p = \frac{nRT_1 B}{Ar \left(1 + B - \sqrt{1 + B^2} \cos(\varphi - \delta)\right)}. \quad (4)$$

Here n is the total number of moles, $B = T_2/T_1$ where T_1 and T_2 are bath temperatures, and

$$\delta = \arctg B - \frac{\pi}{4} \quad (5)$$

is delay angle. It shows how many degrees a maximum of pressure follows after the total volume has achieved its minimum value. In the case of equal bath temperatures these extrema occurs at the same value of the crank angle ($\varphi = 0$), as it should be. The delay angle tends to its maximum value, $\pi/4$, when ratio of bath temperatures goes to infinity.

The cycle of Stirling engine in the (p, V) diagram is depicted in Fig. 2. Note that points in this (p, V) diagram do not represent a state of working substance. Within isothermal approach, gas is in equilibrium state only within cylinders while gas as a whole is in nonequilibrium state.

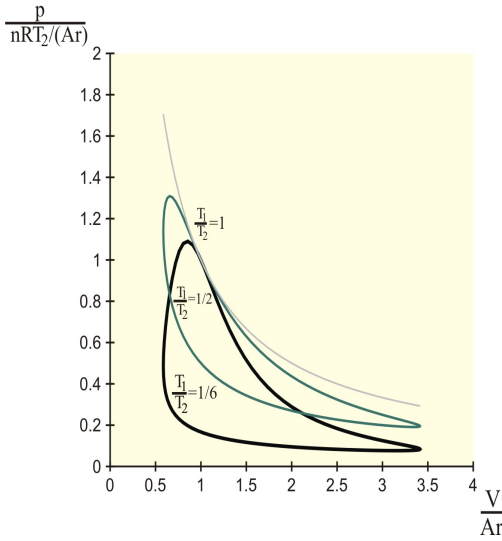


Figure 2. Cycle of Stirling engine for a different values of the ration of bath temperatures.

WORK

Work done by working substance within one cycle is equal to the surface within cycle in (p, V) diagram (Fig. 2),

$$W = \int_0^{2\pi} p dV. \quad (6)$$

Inserting pressure from Eq. (4) into above expression work becomes,

$$W = \sqrt{2} n R T_1 \pi (B - 1) \sqrt{B} \frac{1 + B - \sqrt{2B}}{1 + B^2}. \quad (7)$$

The dependence of work on the bath temperatures ratio, B , is shown in the Fig. 3.

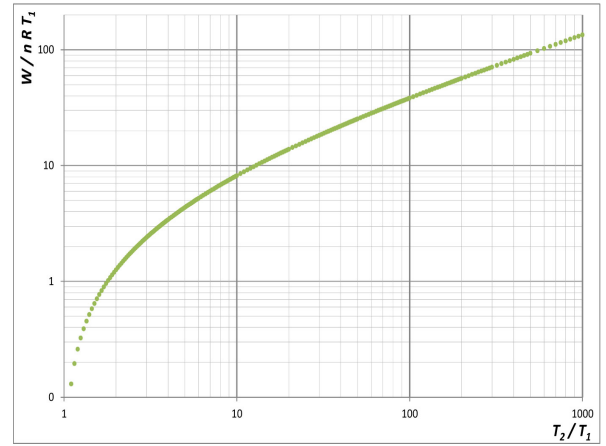


Figure 3. Work done by the Stirling engine as a function of the ratio of bath temperatures.

ABSORBED HEAT

Only the working substance that enters into warm cylinder absorbs heat. Infinitesimal heat exchanged between hot bath and working substance is, according to the first law of thermodynamics,

$$dQ = dn_2 C_V (T_2 - T_1) + p dV. \quad (8)$$

In order to find absorbed heat we have to find out the angle interval characterised with $dQ > 0$. Using the principle of mass conservation (fixed number of moles of working substance) and Eq.(3), after lengthily, but otherwise straightforward calculations we get,

$$dQ = BnRT_1 \left[\frac{\frac{C_V}{R} (B - 1) \left[\cos\left(\varphi - \frac{\pi}{4}\right) - \sin\left(\varphi - \frac{\pi}{4}\right) - 1 \right]}{\left(1 + B - \sin\left(\varphi - \frac{\pi}{4}\right) - B \cos\left(\varphi - \frac{\pi}{4}\right)\right)^2} + \frac{\sqrt{2} \sin \varphi \left\{ 1 + \sin\left(\varphi - \frac{\pi}{4}\right) + B \left[1 - \cos\left(\varphi - \frac{\pi}{4}\right) \right] \right\}}{\left(1 + B - \sin\left(\varphi - \frac{\pi}{4}\right) - B \cos\left(\varphi - \frac{\pi}{4}\right)\right)^2} \right] d\varphi. \quad (9)$$

Equation $dQ = 0$ defines the region of heat absorption. We have found numerically solutions of following equation,

$$\frac{C_V}{R} (B - 1) \left[\cos\left(\varphi - \frac{\pi}{4}\right) - \sin\left(\varphi - \frac{\pi}{4}\right) - 1 \right] + \sqrt{2} \sin(\varphi) \left\{ 1 + \sin\left(\varphi - \frac{\pi}{4}\right) + B \left[1 - \cos\left(\varphi - \frac{\pi}{4}\right) \right] \right\} = 0 \quad (10)$$

The results are shown in Fig. 4.

As it has been expected gas absorbs heat during expansion ($0 < \varphi < \pi$) and releases it during compression for $B = 1$. As ratio of temperatures goes to infinity gas absorbs heat within interval $-\pi/6 < \varphi < \pi/4$.

Absorbed heat is

$$Q^+ = \int_{\varphi_1}^{\varphi_2} dE + \int_{\varphi_1}^{\varphi_2} p dV, \quad (11)$$

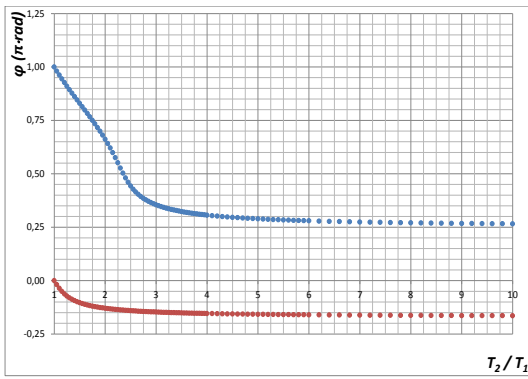


Figure 4. Points of zero absorbed heat ϕ_1 i ϕ_2 as a function of ratio of bath temperatures.

where limits of integrations are the zero points of infinitesimal change of heat.

Heat absorbed and released by working substance and work are shown as a function of ratio of bath temperatures in the Fig. 5.

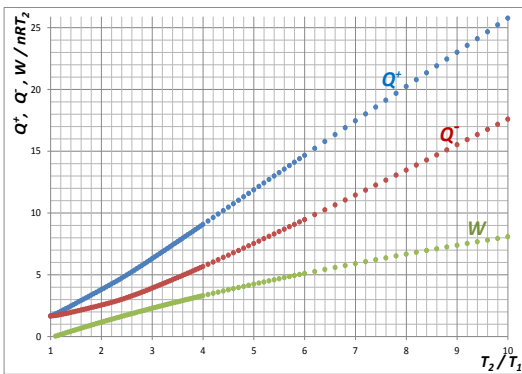


Figure 5. Absorbed, released heat and work as a function of the ratio of bath temperatures.

EFFICIENCY

The most important parameter of any engine is efficiency. Having calculated absorbed heat and work it is easy to determine efficiency of the Stirling engine. Efficiency is compared with the efficiency of the Carnot cycle as it is shown in Fig. 6.

In contrast to the efficiency of Carnot cycle that is increasing function of the temperature ratio the efficiency of Stirling engine exhibits its maximum. The position of maximum and its value are functions of working gas heat capacity (see Fig. 7). One gets the highest possible efficiency achieves for monoatomic gases at $\approx T_2/T_1 = 3,4$.

DISCUSSION AND CONCLUSION

The efficiency of Stirling engine is calculated within isothermal approach. The basic assumption is isothermal process be-

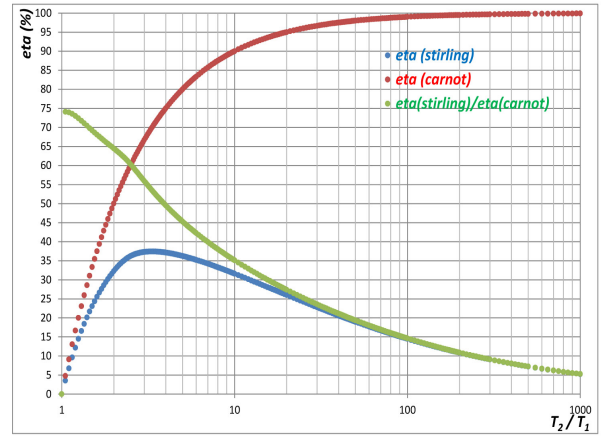


Figure 6. The efficiency of the Stirling engine compared to the efficiency of the Carnot cycle as a function of ratio of temperatures.

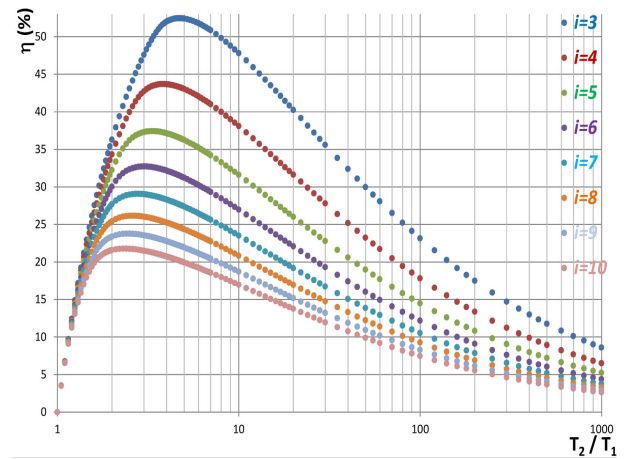


Figure 7. The efficiency of the Stirling engine. A parameter is the molar heat capacity, $C_V = i \cdot R/2$.

tween gas and heat baths. Most cylinders are closed with disc-like pistons. This design does not ensure isothermal process. An adiabatic process better describes gas state then isothermal ones. In order to ensure absorption of heat one have to add thermal regenerator which is in fact heat exchanger. Heat exchanger introduce dead volume. Dead volume as well as adiabatic process cause the reduction of efficiency. Regenerator keeps a part of working gas that does not exchange heat between hot and cold cylinder. Due to the adiabatic process there is reduced heat exchange between working gas and he baths.

According to analysis exposed in this paper efficiency of the Stirling engine can be even higher than 50% in the case of monoatomic gas as a working substance. The fact that monoatomic gas gives higher efficiency then polyatomic gases is in accordance with kinetic theory of gases. Namely, only translation degrees of freedom contributes to work.

NOMENCLATURE

Symbol	Quantity	SI Unit
l	Length of shaft	m
r	Radius of circle described by shafts ends	m
φ	Crank angle	rad
A	Area of piston basis	m^2
V_1	Volume of working substance in cold cylinder	m^3
V_2	Volume of working substance in hot cylinder	m^3
V	Total Volume of working substance	m^3
p	Pressure	Pa
n	Amount of substance	mol
R	Gas constant	$J/(mol K)$
T_1	Temperature of the cold bath	K
T_2	Temperature of the hot bath	K
W	Work	J
Q	Heat	J
E	Internal energy	J
C_V	Molar heat capacity	J/mol
η	Efficiency	

REFERENCES

- [1] I. Urieli and D. Berchowitz, *Stirling Cycle Engine Analysis*, Adam Hilger, Bristol, 1984.
- [2] J. Škorpk, The Amount of Regenerated Heat Inside the Regenerator of a Stirling Engine, *Acta Polytechnica*, vol. 48, pp. 10-14, 2008

SIMULATING CO₂ ADSORPTION AND DIFFUSION ON A GRAPHITE SURFACE

T.T. Trinh*, T. J. H. Vlugt^o, M.-B. Hägg[§], D. Bedeaux*, S. Kjelstrup^o *

* Department of Chemistry, Norwegian University of Science and Technology, Trondheim, Norway

^o Process and Energy Laboratory, Delft University of Technology, Delft, The Netherlands

[§] Department of Chemical Engineering, Norwegian University of Science and Technology, Trondheim, Norway

ABSTRACT

We performed classical molecular dynamics (MD) simulation to understand the mechanism of CO₂ adsorption and transport on graphite surface. The temperature of the system in our simulation was in the range 300-500K. The simulation data show that there are two layers of CO₂ molecules adsorbed on the surface. These two layers have a different behavior. The first CO₂ layer is isolated as it does not exchange molecules with the second layer and is liquid-like, while the second layer exchanges molecules with the gas phase. The layers are separate thermodynamic systems. We use the simple Langmuir model to fit the adsorption isotherm for the second layer. The enthalpy of adsorption is calculated $\Delta H^0 = -16$ kJ/mol. This value is in good agreement with experimental data of adsorption of CO₂ on activated carbon. Along the graphite surface, the diffusion coefficient of CO₂ in the first layer and the second layer are roughly of 10^{-11} m²/s, 10^{-10} m²/s respectively. These values are much smaller than for H₂.

INTRODUCTION

The production of cheap membranes for CO₂ separation is of primary importance for the realization of carbon capture and sequestration technologies.¹ Nano-porous, fibrous, carbonaceous materials are promising candidates from an experimental point of view. In order to make further progress to produce molecular sieve membranes, better knowledge of several issues is needed. Central for good membrane functionality are pore size, surface binding, surface wall transport, pore inlet control, carbon structure and composition.

There are many experimental works and simulations devoted to understand the adsorption of CO₂ on carbon based material such as activated carbon and graphite.²⁻⁵ The adsorption isotherm of CO₂ on active carbon is well described by several models such as Langmuir,² Tóth,⁶ Dubinin-Astakhov (D-A),^{3,7} Reported values for iso-steric enthalpy of adsorption differ a lot and depend on the sorbent used and the condition of adsorption. Saha *et al.* reported that heats of adsorption of CO₂ in Maxsorb II and ACF (A-20) material were around -20 kJ/mol.³ If one uses another untreated activated carbon C3345 material, the heat of adsorption was -14 kJ/mol.² Guo *et al.* reported that the heat of adsorption can vary in the range of (-10 – -28 kJ/mol) depending on the modification condition of the activated carbon material.⁵ Himeno *et al.* also reported an adsorption enthalpy which was in range -16 – -25 kJ/mol) of pure CO₂ on five different commercial activated carbons.⁶

Several theories have motivated the adsorption isotherm of CO₂ on graphite surface and in the slit pores of graphite. Lim *et al.* presented a Langmuir adsorption model and diffusion coefficient ($D_s = 10^{-9} - 10^{-10}$ m²/s) of CO₂ in a narrow pore width ($H = 0.65 - 0.75$ nm) and for temperatures $T = 298 - 318$ K.⁸ While Zhou *et al.* reported these value in wider range of

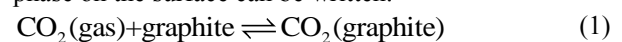
slit pore size ($H = 0.7 - 3.4$ nm) and the values were comparable with Lim *et al.*, Levesque *et al.* calculated the heat of CO₂ adsorption on activated carbon using Monte-Carlo simulations.⁴ The authors discussed the dependence of adsorption enthalpy on the distribution of pore sizes. These works had no distinct CO₂ layers in the pores or on the surface.

This work aims to establish a thermodynamic model for the layers of CO₂ on the graphite surface and find diffusion coefficient for the surface. We use molecular dynamics simulation (see Figure 1) for wide range of temperatures ($T = 300 - 550$ K)

THEORY AND MODEL

Isotherm adsorption

The reaction between the gas phase and the adsorbed phase on the surface can be written:



At equilibrium, the gas chemical potential is equal to the surface chemical potential:

$$\mu_g = \mu_s \quad (2)$$

$$\mu_g = \mu_g^0 + RT \ln \left(\frac{p}{p_0} \right) \quad (3)$$

where μ_g^0 is the standard chemical potential of the gas phase, *i.e.*, the chemical potential at the reference pressure p_0 .

We may also write the chemical potential for surface as

$$\mu_s = \mu_s^* + RT \ln a_s \quad (4)$$

where a_a is the activity of the adsorbed phase:

$$a_s = \gamma \frac{C_s}{C_s^*} \quad (5)$$

where μ_a^* is the standard state chemical potential at standard state. It follows from equation 2 that

$$\mu_a^* - \mu_g^0 = RT \ln \left(\frac{p}{p^0 a_s} \right) \quad (6)$$

Hence the adsorption equilibrium constant is given by

$$K = \left(\frac{p^0 a_s}{p} \right) \quad (7)$$

If we choose the standard state such that $p^0 = 1 \text{ atm}$,

$C_s^* = C_s^{\text{max}}$ then we obtain the Langmuir model isotherm

$$\frac{C_s}{C_s^{\text{max}}} = \frac{Kp}{1 + Kp} \quad (8)$$

K is the Langmuir equilibrium constant. The van't Hoff relationship to describe the temperature dependence of K

$$K = K_0 \exp \left(\frac{-\Delta H^0}{RT} \right) \quad (9)$$

where K_0 is the pre-exponential factor, and ΔH^0 is the constant iso-steric enthalpy of adsorption. Plotting K semi logarithmically versus $1/T$ gives a linear fit from which the slope $-\Delta H^0 / R$ is extracted.

Surface Excess Densities

In a thermodynamic description, the surface excess concentration C_s is determined. From that we can describe the adsorption isotherm by plotting the surface excess density versus the gas pressure. We use the Gibbs surface excess for systems in global equilibrium as described in the book of Kjelstrup and Bedeaux.⁹ An interface is considered as a thin layer between phases. We restrict ourselves to surfaces parallel to the graphite surface, so

$$C_s = \int_{\alpha}^{\beta} (C^{2nd} - C^{gas}) dz \quad (10)$$

where C_s is the surface excess concentration, and C^{gas} , C^{2nd} are the concentration of CO_2 in the gas and in the second layer, respectively. (See Figure 2)

Simulation details

We performed classical molecular dynamic (MD) simulation with the DL_POLY classic package¹⁰ to understand the mechanism of CO_2 adsorption and transport on the graphite surface. The system consists of a sheet of crystalline graphite and CO_2 molecules. The graphite has hexagonal structure with P63/mmc without any defects. The crystal is constructed from 5 sheets of graphene and contains 4284 carbon atoms. We orient graphene sheets in our simulation box such that the surfaces of the sheets are perpendicular to the z direction. The size of the box is around $42 \times 51 \times 84 \text{ \AA}^3$. We use periodic boundary conditions in all directions. At least ten systems with different number of CO_2 molecules ranging from $N_{\text{CO}_2} = 50 - 700$ were

simulated. For each N_{CO_2} , simulations were performed at different 10 temperatures in the range 300-500K.

The MD simulation had time steps of 0.001ps. The initial configuration was constructed by randomly distributing of CO_2 molecules above the graphite surface. The system was stabilized during 1000 ps by NVT runs with the Nosé-Hoover thermostat.¹¹ When the system was in the thermal equilibrium, we performed another 1000 ps run with microcanonical ensemble (NVE) to study adsorption and transport properties. The trajectory is printed every 100 time step and stored for further analysis.

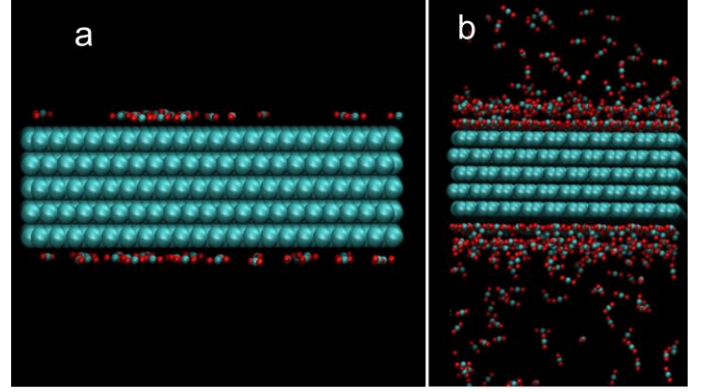


Figure 1. Typical snapshot of CO_2 adsorption on graphite surface at $T=350\text{K}$ with $N_{\text{CO}_2}=50$ (a) and $N_{\text{CO}_2}=600$ (b). In the time scale of simulation there is no CO_2 molecule in the gas phase at low concentration (a). At high concentration, there are two layers of CO_2 forming on the surface (b). The green, red are represented carbon and oxygen atom, respectively.

Potential energy interaction

We fix the graphite layer and use the rigid body model TraPPE for CO_2 .¹² The intermolecular potential consist of the long range Columbic interactions handled using the Ewald sum technique¹³ and the shifted and truncated 12-6 Lennard-Jones (LJ) potential.¹³

$$V_{ij}^{nb} = V_{ij}^{LJ} + V_{ij}^{columbic} \quad (11)$$

$$V_{ij}(r_{ij}) = 4\epsilon_{ij} \left[\left(\frac{\sigma_{ij}}{r_{ij}} \right)^{12} - \left(\frac{\sigma_{ij}}{r_{ij}} \right)^6 \right] \quad (12)$$

$$V_{ij}^{LJ}(r_{ij}) = \begin{cases} V_{ij}(r_{ij}) - V_{ij}(r_c) & r_{ij} < r_c \\ 0 & r_{ij} > r_c \end{cases} \quad (13)$$

where r_{ij} is the distance between atoms i and j , ϵ_{ij} and σ_{ij} are LJ potential parameters, and r_{ij} is the cutoff radius. The LJ interaction parameters between different types of atoms are calculated from the Lorentz-Berthlot mixing rules¹³

$$\epsilon_{ij} = \sqrt{\epsilon_{ii}\epsilon_{jj}} \quad (14)$$

$$\sigma_{ij} = \frac{1}{2}(\sigma_{ii} + \sigma_{jj}) \quad (15)$$

The parameters is taken from the DREIDING¹⁴ and TraPPE¹² force field are listed on table 1.

Table 1. LJ potential parameters used in simulation

Atom	σ (Å)	ϵ/k_B (K)	charge (e)
C (in CO ₂)	2.80	27	0.7
O (in CO ₂)	3.05	79	-0.35
C (graphite)	3.34	26	0

RESULTS AND DISCUSSION

Two distinct CO₂ surface layers

Figure 2 depicts the distribution of CO₂ molecules along the surface of graphite with system $N_{\text{CO}_2}=700$ at different temperatures. It is shown that there are different regions of CO₂ on the surface. The first adsorption layer is located around 0-5Å, the second adsorption layer is located around 5-12Å and the CO₂ gas above 12 Å. The first layer is well separable from the second, see bar indicated with α . The separation between the second layer and the gas β is less precise. In the first layer, there are two peaks, the higher one is big and corresponds to the CO₂ molecule that are parallel to the surface. The second small peak corresponds CO₂ molecules that do not touch completely the surface (the angle surface-C-O is around 30°).

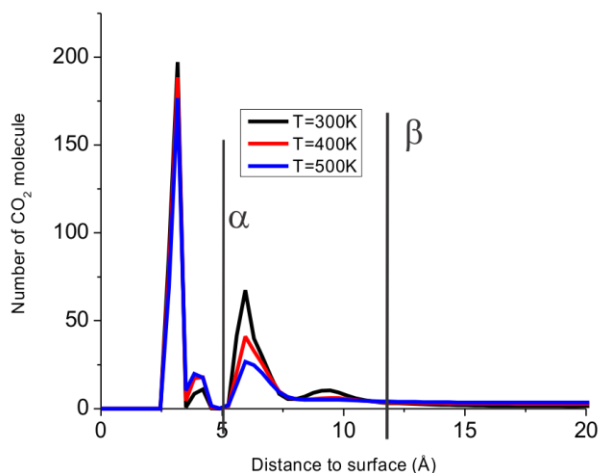


Figure 2. The distribution of CO₂ molecules along the surface in different layer with $N_{\text{CO}_2}=700$ at selected temperatures. There are three zones, from 0- α : first adsorbed layer, α - β : second adsorbed layer, above β : gas phase.

The radial distribution function (RDF) of CO₂-CO₂ molecules of the different layers along is reported in Figure 3. In the first adsorption layer (Nad1) the RDF of CO₂ has a liquid like form. Molecules are more organized than in the second layer (Nad2) and the gas phase (Ngas). The position of maximum RDF of the first layer is slightly below that of the second layer and the gas.

Figure 4 depicts the trajectories of CO₂ molecules during 100 ps. The lines indicate the motion of CO₂ during the trajectory. The first layer (dark color in Figure 4) does not exchange molecules with the second layer. Only CO₂ from the second layer go in and out of the gas phase (the blue lines in Figure 4). This behavior occurs during the whole simulation of 1000 ps.

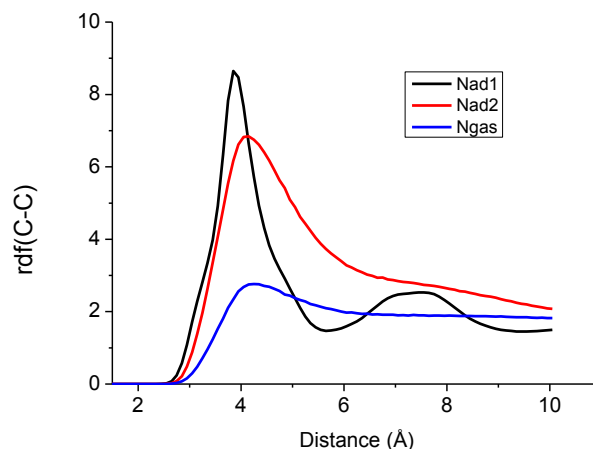


Figure 3. Radial distribution function of CO₂-CO₂ in different layers

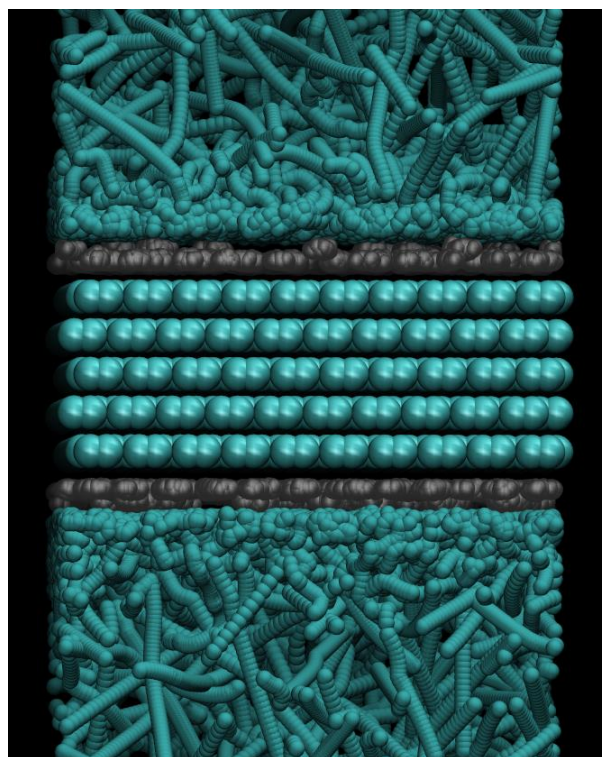


Figure 4. Trajectory plot of CO₂ movement in different layers in time scale of 100ps. Only carbon atom is shown. The dark color is the adsorbed first layer. There is only the second layer exchange molecule with gas phase.

The Langmuir model for the adsorption isotherm

In the previous section we have shown that the first layer and the second layer of adsorbed CO₂ show very different behavior. So we only use the second layer to construct the adsorption isotherm.

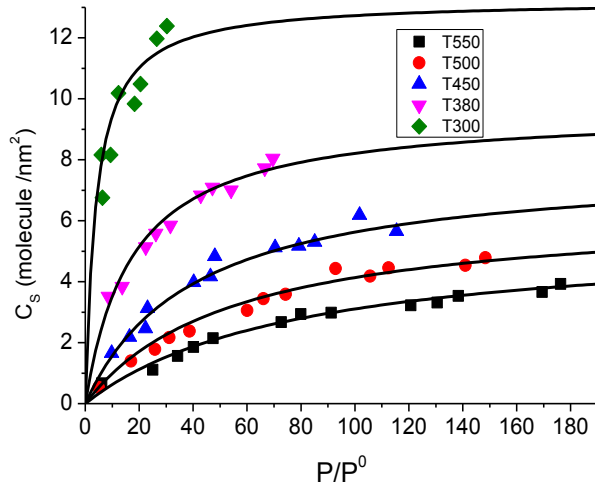


Figure 5. CO₂ adsorption isotherm on graphite surface at selected temperatures. The continuous line is the fitted Langmuir model.

Table 2. Langmuir parameters isotherm of CO₂ on graphite

T (K)	C_s^{\max} (molecule/nm ²)	K
300	13.2	2.48×10^{-1}
320	12.2	1.53×10^{-1}
350	10.5	1.08×10^{-1}
380	9.6	5.74×10^{-2}
400	9.1	4.57×10^{-2}
420	8.7	3.65×10^{-2}
450	7.9	2.49×10^{-2}
480	6.8	2.06×10^{-2}
500	6.4	1.82×10^{-2}
550	5.6	1.27×10^{-2}

The Langmuir model can be fitted quite well to experimental adsorption isotherms for CO₂ on activated carbon.² We extended the number of CO₂ molecules to 2000 in an additional calculation to see if we could obtain more than two adsorbed layers. However the system formed only two layers as in Figure 2. The Langmuir model was chosen to fit our data. The isotherms are presented in Figure 5. The excess surface adsorption of the second layer reaches a plateau when the pressure increases. This type of adsorption is typically for a CO₂ isotherm not only on graphite, activated carbon but also on other material such as zeolite, MOF, COF, etc.

The parameters for Langmuir equation 8 are presented in Table 2. The maximum excess adsorption decreases when the temperature increases (Figure 6).

A plot of the logarithm of the equilibrium constant K versus the inverse temperature is given in Figure 7. The dependence is linear and from the slope, a value of the isosteric enthalpy of adsorption $\Delta H^0 = -16$ kJ/mol is obtained. This value is typical for physisorption and in the range (-10.5, -28.4 kJ/mol) of experimental data of adsorption of CO₂ on activated carbons.^{3,7,15}

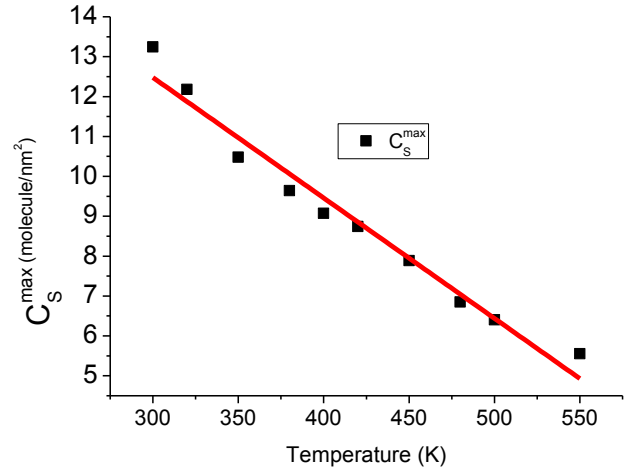


Figure 6. Maximum excess surface adsorption as a function of temperature

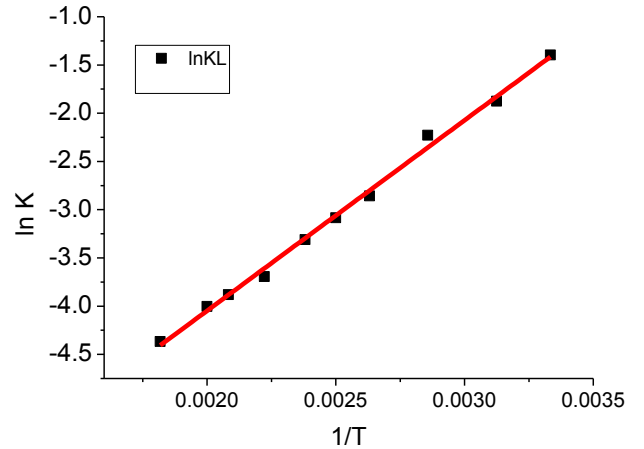


Figure 7. Logarithm of the adsorption equilibrium constants versus the inverse temperature for adsorption of CO₂ on graphite

Surface self-diffusion

We limited our study to the self-diffusion of adsorbed CO₂ on the surface. This gives an important contribution to the transport of CO₂ inside the slit pores. The self-diffusion coefficient of molecule can be obtained from:

$$D_{||}^s = \lim_{t \rightarrow \infty} \left[\frac{1}{2dNt} \sum_{i=1}^N \left\langle \left| \vec{r}_i(t) - \vec{r}_i(0) \right|^2 \right\rangle \right] \quad (16)$$

where d is the dimensionality (for surface $d = 2$), N is the total molecules, $\vec{r}_i(t)$ and $\vec{r}_i(0)$ is the position of molecule at time t and time initial.

By plotting the logarithm of the diffusion coefficients found versus the inverse of temperature, we obtained an Arrhenius plot. This was used to estimate the temperature dependence of the diffusion coefficient according to

$$D(T) = D_0 \exp\left(\frac{-E_{\text{act}}}{k_B T}\right) \quad (17)$$

where D_0 is the pre-exponential factor, k_B is the Boltzmann constant, and E_{act} is the activation energy.

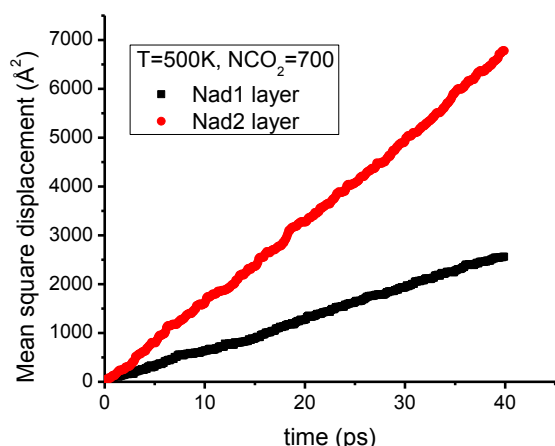


Figure 8. The mean-squared displacement of CO₂ in the first and second layer at T=500K and NCO₂=700

Figure 8 shows an example of mean-squared displacement of CO₂ in the first layer and in the second layer. It is clearly shown that CO₂ in the first layer also mobile but slower.

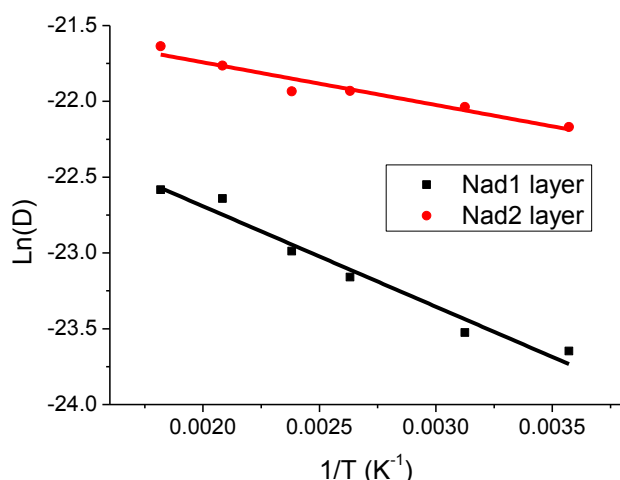


Figure 9. Natural logarithm of the self-diffusion coefficients as a function of inverse temperature.

The activation barrier for self-diffusion is obtained by calculating the slope of linear relationship between the natural logarithm of self-diffusion and $1/T$ (Figure 9). We found that for the activation barriers of the first and second layer were $E_{act1}=5.5$ and $E_{act2}=2.3$ kJ/mol, respectively.

Along the graphite surface, the diffusion coefficient of first and second layers of CO₂ on graphite surface is roughly 10^{-11} m²/s and 10^{-10} m²/s, respectively which are in good agreement with previous simulations.^{8,16} The value is much smaller than for diffusion of H₂ on graphite (10^{-7} m²/s). It is interesting that the first layer of adsorbed CO₂ is mobile along the surface. The mobility is less than that of the second layer because the first layer is confined between graphite surface and the second layer and has a strong interaction with the graphite surface. The figure is comparable with the picture of mobile H₂ molecule on graphite by Simon *et al.*^{17,18}

CONCLUSION

In this work, we have used Equilibrium Molecular Dynamics to study the adsorption isotherm and diffusion of CO₂ on a graphite surface. The results show that there are two CO₂ adsorbed layers. The two layers have very different diffusion and exchange possibilities with the gas phase. A simple Langmuir model was used to fit the isotherm of the second layer. The heat of adsorption was estimated ($\Delta H^0 = -16$ kJ/mol). The rate of self-diffusion of CO₂ on graphite ($\sim 10^{-10}$ m²/s) is small compared to H₂ adsorbed ($\sim 10^{-7}$ m²/s) and CO₂ dense gas ($\sim 10^{-9}$ m²/s). These results of the equilibrium system form the basis for further studies of non-equilibrium properties of pure CO₂ and mixture CO₂/H₂ systems.

ACKNOWLEDGMENT

The authors acknowledge The Research Council of Norway NFR project no 209337 and The Faculty of Natural Science and Technology, Norwegian University of Science and Technology (NTNU) for financial support. The calculation power is granted by The Norwegian Metacenter For Computational Science (NOTUR).

REFERENCES

- (1) He, X.; Arvid Lie, J.; Sheridan, E.; Hägg, M.-B. *Energy Procedia* **2009**, *1*, 261.
- (2) Jin, Y.; Lee, D.; Lee, S.; Moon, W.; Jeon, S. *Analytical Chemistry* **2011**, *83*, 7194.
- (3) Saha, B. B.; Jribi, S.; Koyama, S.; E-Sharkawy, I. I. *J. Chem. Eng. Data* **2011**, *56*, 1974.
- (4) Levesque, D.; Lamari, F. D. *Mol. Phys.* **2009**, *107*, 591.
- (5) Guo, B.; Chang, L.; Xie, K. *Journal of Natural Gas Chemistry* **2006**, *15*, 223.
- (6) Himeno, S.; Komatsu, T.; Fujita, S. *J. Chem. Eng. Data* **2005**, *50*, 369.
- (7) Sevilla, M.; Fuertes, A. B. *J. Colloid Interface Sci.* **2012**, *366*, 147.
- (8) Lim, Y.-I.; Bhatia, S. K.; Nguyen, T. X.; Nicholson, D. J. *Membr. Sci.* **2010**, *355*, 186.
- (9) Kjelstrup, S.; Bedeaux, D. *Non-equilibrium thermodynamics of heterogeneous systems*; World Scientific Singapore, 2008; Vol. 16.
- (10) Smith, W.; Yong, C.; Rodger, P. *Mol. Simul.* **2002**, *28*, 385.
- (11) Martyna, G. J.; Klein, M. L.; Tuckerman, M. *The Journal of chemical physics* **1992**, *97*, 2635.
- (12) Potoff, J. J.; Siepmann, J. I. *AIChE J.* **2001**, *47*, 1676.
- (13) Allen, M. P.; Tildesley, D. J. *Computer simulation of liquids*; Oxford university press, 1989.
- (14) Mayo, S. L.; Olafson, B. D.; Goddard, W. A. *J. Phys. Chem.* **1990**, *94*, 8897.
- (15) Gavrilov, V.; Zakharov, R. *Kinetics and Catalysis* **2010**, *51*, 609.
- (16) Zhou, J.; Wang, W. *Langmuir* **2000**, *16*, 8063.
- (17) Simon, J. M.; Haas, O. E.; Kjelstrup, S. *The Journal of Physical Chemistry C* **2010**, *114*, 10212.
- (18) Haas, O.-E.; Simon, J. M.; Kjelstrup, S. *The Journal of Physical Chemistry C* **2009**, *113*, 20281.

EXPERIMENTAL ASPECTS OF HEAT CONDUCTION BEYOND FOURIER

P. Ván^{1,2,3}, B. Czél², T. Fülöp^{1,2,3}, Gy. Gróf², Á. Gyenis² and J. Verhás³

¹Dept. of Theoretical Physics, Institute for Particle and Nuclear Physics, Wigner Research Centre for Physics, HAS,
H-1525 Budapest, P.O.Box 49, Hungary;

²Dept. of Energy Engineering, Budapest Univ. of Technology and Economics,
H-1111, Budapest, Műegyetem rkp. 3-9, Hungary;

³Montavid Thermodynamic Research Group
Email: van.peter@wigner.mta.hu

ABSTRACT

Heat conduction experiments are performed in order to identify effects beyond Fourier. Two experimental setups are discussed. First, a simple experiment by a heterogeneous material is investigated from the point of view of generalized heat conduction, then the classical laser flash method is analysed.

INTRODUCTION

The theory of heat conduction is the parade ground of testing and developing generalized thermodynamic theories [1; 2; 3]. Recently, a linear irreversible thermodynamic framework of heat conduction was introduced, where the deviation from local equilibrium is characterized by a single internal variable and by the generalization of the entropy current density via a current intensity factor [4; 5; 6]. A general constitutive evolution equation of the current density of internal energy was derived via introducing linear relationship between the thermodynamic forces and fluxes. The Fourier, Maxwell-Cattaneo-Vernotte, Guyer-Krumhansl, Jeffreys type and Green-Naghdi type equations of heat conduction were obtained as special cases [7]. This constitutive equation incorporates memory effects and weak nonlocality at the same time, however, only a local entropy function is assumed, that does not depend on the space derivatives of the internal energy, the basic state variable.

The balance of internal energy is written as

$$\rho \frac{\partial e}{\partial t} + \partial^i q^i = 0, \quad (1)$$

where ρ is the density, e is the specific internal energy and q^i is the conductive current density of the internal energy, the heat flux. For the internal energy we assume a constant specific heat c in the equation of state $e = cT$, where T is the temperature. The above evolution equation is written in a substantial form, assuming negligible production of internal energy. ∂_t denotes the substantial time derivative, the partial time derivative of the corresponding scalar quantity on the material manifold [8]. The heat flux is interpreted accordingly. The space derivative ∂^i is used for the gradient in the material framework.

Then one may introduce two kind of irreversibilities. A vectorial internal variable together with the assumption that the heat is not parallel to the entropy current density, $j_s^0 = B^{ij}q_j$, leads to the following nonlocal, relaxation type constitutive evolution

equation of heat flux q^i is obtained in the following form [7]:

$$\tau \frac{\partial}{\partial t} q^i + q^i = \lambda_1 \partial^i \frac{1}{T} + \lambda_2 \frac{\partial}{\partial t} \left(\partial^i \frac{1}{T} \right) + a_1 \partial^{ij} q^j + a_2 \partial^{jj} q^i + b_1 \frac{\partial}{\partial t} (\partial^{ij} q^j) + b_2 \frac{\partial}{\partial t} (\partial^{jj} q^i). \quad (2)$$

The material parameters $\tau, \lambda_1, \lambda_2, a_1, a_2, b_1, b_2$ are nonnegative and not independent, because

$$a_1 \lambda_2 = b_1 \lambda_1, \quad a_2 \lambda_2 = b_2 \lambda_1. \quad (3)$$

Based on these theoretical considerations, the universality of the theory was demonstrated by showing that various heat conduction mechanisms and material structures lead to the above form of the constitutive relation. For example, material heterogeneity, with the possibility of two temperatures, is one such possible substructure. Therefore, (2) is interpreted as a universal, effective approach to heat conduction beyond Fourier.

This rendering leads to a new point of view for the experimental investigations. Phonon propagation is not the only possibility of non-Fourier heat conduction, but new, mesoscopic structural effects can also play a role. The question is whether and under what conditions we can observe these deviations. One may think, and can also partially show, that in (2) the additional terms have the effect of driving the solution toward the solution of the Fourier equation. Therefore, suppressing the dissipation – as it was performed in the classical experiments of phonon based low temperature heat conduction (see e.g. [9]) – is not an option.

We show some results of the analysis of two experimental setups in order to identify possible deviations from the Fourier heat conduction:

1. *Simple heterogeneous materials.* In these experiments, a layered periodical heterogeneous structure is the subject of abrupt temperature jump at one of the boundaries. The heat transfer properties of the layers (paper and air) are different. The additional material parameters of the equation are

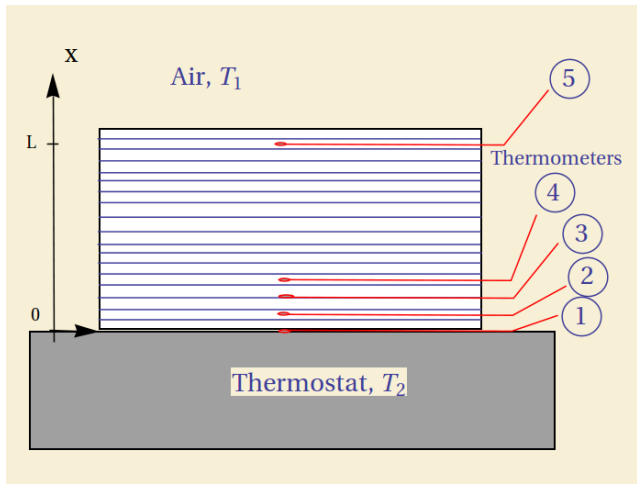


Figure 1. Experimental setup. The position of the thermometers is indicated by the numbers.

determined by the experiments, fitting the solutions of different models of heat conduction.

2. *Heat conduction measurements with flash method.* Here, we analyse models of ordinary flash experiments from the point of view of beyond-Fourier heat conduction. Some benchmarks are established for the parameters of the material, the device and the operation for the identification of non-Fourier effects.

BOOK EXPERIMENT

In this simple measurement we constructed a layered structure of 200 paper sheets, initially at ambient temperature $T_L = 29.9^\circ\text{C}$. At the beginning of the measurement, the structure has been contacted to a thermostat, while measuring the temperature at 5 different points of the structure. The experimental setup is sketched in Fig 1. The sample contained 200 layers of $19\text{cm} \times 15\text{cm}$ sheets that were fastened at one of the shorter sides. The total thickness of the sample was $L = 20\text{mm}$. The pages were 0.09mm thick and the air between them initially 0.01mm , an estimation based on the difference of the total and compressed thickness. The density of the paper is $800\text{kg}/\text{m}^3$ and the isobaric specific heat $1340\text{J}/\text{kgK}$. The temperature was measured by a K-type thermometer at the thermostat and by copper-constantan thermocouple wires with diameter $d = 0.1\text{mm}$ between the papers. The first thermometer was built in at the copper plate surface of the thermostat, and the second, third and fourth thermometers were 1mm , 2mm and 3mm distant from the surface of the sample at the side of the thermostat, respectively. The position of the fifth thermometer was 19mm from the thermostat surface. The thermometers were positioned 7.5cm from the free, not fastened sides.

The measured temperatures are shown in Fig 2 as a function of time. One can see that the thermostat cannot be considered homogeneous at the beginning, the temperature of the first thermometer drops by some centigrades in the first seconds of the measurement. The temperature of the farthest thermometer, number 5, increases only a few centigrades during the measurement. We have introduced two effective models for the evaluation of the data. In both cases, the thickness of the thermocouple wires was neglected and the problem was considered as one dimensional, the x axis being perpendicular to the surface

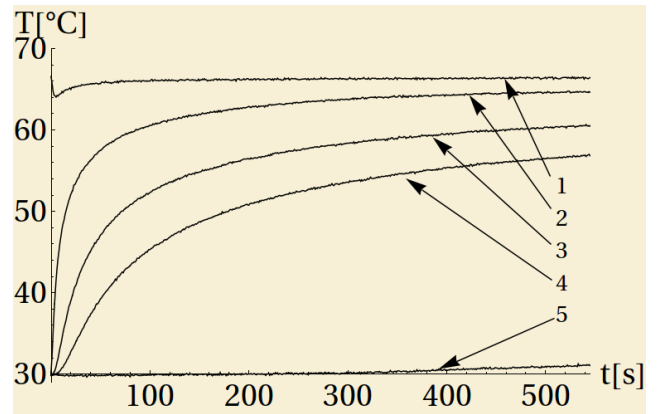


Figure 2. Temperatures of the thermometers 1-5, the serial numbers are increasing downward.

of the layers. The thermometers were comoving with the material, therefore the heat conduction models were interpreted in a material, i.e. first Piola-Kirchhoff framework.

Effective nonlinear Fourier equation

Here, we introduced the Fourier equation with linearly temperature dependent heat conductivity,

$$q = -\lambda_F [1 + b(T - T_{ref})] \frac{\partial T}{\partial x}. \quad (4)$$

where q is the x component of the heat flux and the space derivative is a material one at the x direction. λ_F is the Fourier heat conduction coefficient at $T_{ref} = 0^\circ\text{C}$, and b characterizes the linear temperature dependence of the thermal conductivity.

The initial temperature of the sample was uniform $T(t = 0, x) = T_L = 29.9^\circ\text{C}$. The boundary condition in the free surface was constant, at the ambient temperature $T(t, x = L) = T_L$. At the side of the thermostat we have assumed a constant thermal conductance α , therefore, the corresponding boundary condition is

$$\lambda_F [1 + b(T(t, x = 0) - T_{ref})] \frac{\partial T}{\partial x}(t, x = 0) = \alpha [T(t, x = 0) - T_0].$$

The free parameters of the model were the heat conduction coefficient λ_F , the thermal conductance α , the parameter b , and the temperature of the thermostat T_0 . In order to determine the best effective model parameters we considered the measured temperature data of thermometers 2, 3, 4 in every 5s to be fitted by the following partial differential equation, subject to the above boundary and initial conditions:

$$\rho c \frac{\partial T}{\partial t} - \lambda_F \frac{\partial}{\partial x} \left([1 + b(T - T_{ref})] \frac{\partial T}{\partial x} \right) = 0. \quad (5)$$

The best fit parameters are the following:

	$\lambda_F [\text{W}/\text{mK}]$	$b [1/\text{K}]$	$T_2 [^\circ\text{C}]$
Values	0.140	-0.008	69.65
Stand. err.	0.006	0.0003	0.15

Table 1. Fitted parameters of the nonlinear Fourier model

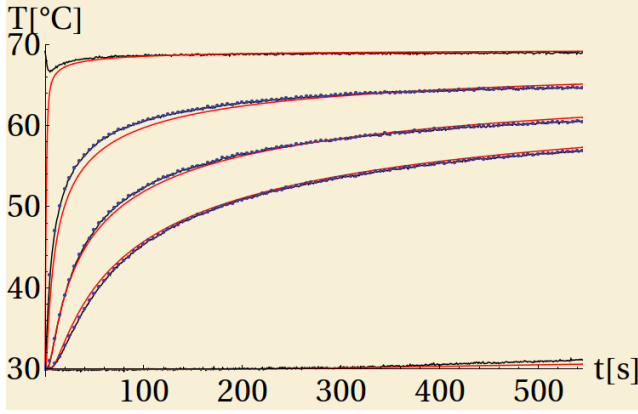


Figure 3. Fitted nonlinear Fourier equation. Black, uncertain line: thermometer data, blue dots: data points of the fit, red smooth line: fitted model.

The calculations resulted in a high and uncertain value of the thermal conductance α , indicating that the boundary can be considered at a constant temperature, and that the fit is not sensitive to this parameter. The negative b may indicate the role of the weight on the top of the sheets. The goodness of the fit can be characterised by $R^2 = 0.9992$. We have plotted the data and the fit together in Fig 3. The red lines denote the fitted function, the blue dots indicate the data points used for the fit from thermometers 2, 3 and 4, and the black lines show the complete measurement data according to Fig 2.

Effective Guyer-Krumhansl equation

Our second model introduces the same number of fit parameters with a reduced version of the generalized constitutive heat conduction, where $\lambda_2 = 0$, therefore, $b_1 = b_2 = 0$. The one dimensional form of (2) can be written as

$$\tau \frac{\partial}{\partial t} q + q = -\lambda_F \frac{\partial T}{\partial x} + a \frac{\partial^2 q}{\partial x^2}. \quad (6)$$

The Jeffreys type heat conduction could be a similar simplification, with a similar number of parameters. The role of the nonlocal terms with these boundary and initial conditions is probably similar [7].

In this case, the initial temperature distribution in the sample is the same as in the nonlinear Fourier case $T(t=0, x) = T_1 = 29.9^\circ\text{C}$ and the boundary conditions are similar: $T(t, x=L) = T_L$ and $q(t, x=0) = -\alpha_0[T(t, x=0) - T_0]$. However, this model requires an additional initial and also a further boundary condition. We assume that in case of uniform temperature distribution the initial heat flux was zero $q(t=0, x) = 0$ and at the free side of the sample we assume constant thermal conductance, with a large constant coefficient $q(t, x=L) = -\alpha_L[T(t, L) - T_L]$ in order to ensure approximately constant boundary temperature. The thermal conductances were chosen $\alpha_0 = \alpha_L = 50000 \pm 40000 \text{ W/m}^2\text{K}$. The error estimate is based on sensitivity calculations, the heat conduction model is not sensitive in these parameters, similarly to the previous nonlinear Fourier one. The free parameters of the model are the heat conduction coefficient λ_F , the relaxation time τ , the Guyer-Krumhansl parameter a and the temperature of the thermostat T_0 .

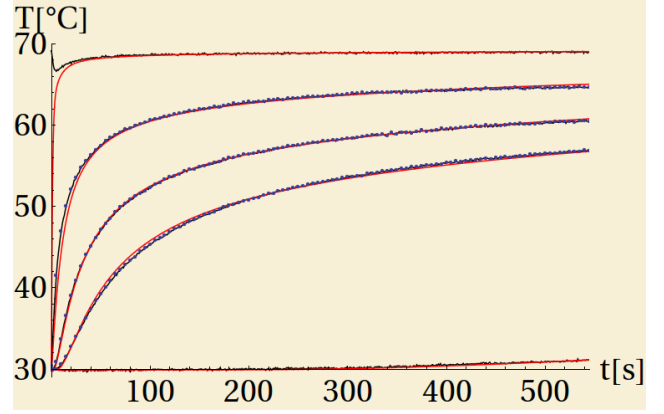


Figure 4. Fitted Guyer-Krumhansl equation. Black, uncertain line: thermometer data, blue dots: data points of the fit, red smooth line: fitted model.

In order to determine the best effective model parameters, we considered the same temperature data as in the case of the nonlinear Fourier model. The model introduces the following system of partial differential equations:

$$\rho c \frac{\partial T}{\partial t} + \frac{\partial q}{\partial x} = 0, \quad (7)$$

$$\tau \frac{\partial}{\partial t} q + q = -\lambda_F \frac{\partial T}{\partial x} + a \frac{\partial^2 q}{\partial x^2}. \quad (8)$$

The best fit parameters are the following:

	λ [W/mK]	τ [s]	a [m ²]	T_0 [°C]
Values	0.05243	194.9	1.415×10^{-5}	69.52
Stand. err.	0.00003	0.1	9×10^{-8}	0.05

Table 2. Fitted parameters of the Guyer-Krumhansl model.

The goodness of the fit can be characterised by $R^2 = 0.99997$. We have plotted the data and the fit together in Fig 4. The red lines denote the fitted function, the blue dots indicate the data points used for the fit from thermometers 2, 3 and 4, and the black lines show the complete measurement data according to Fig 2.

The Guyer-Krumhansl equation seems to fit the data slightly better than the nonlinear Fourier model. The thermostat temperatures are approximately the same. However, neither fits are perfect, there are visible deviations. Remarkable is the large difference of the Fourier heat conduction coefficients in case of the different models. The heat conduction of paper is $\lambda_{\text{paper}} = 0.11 - 0.13 \text{ W/mK}$, and that of air is $\lambda_{\text{air}} = 0.024 \text{ W/mK}$. In our evaluation, the temperature dependent heat conduction coefficient is $\lambda_F(T = T_L) = 0.11 \text{ W/mK}$ at air temperature and $\lambda_F(T = T_0) = 0.063 \text{ W/mK}$ at the thermostat.

FLASH SIMULATIONS

The laser flash method is a common method to measure the thermal diffusivity (D , see its definition below) of solid materials having medium and high thermal conductivity (λ_F). During the measurement, a small disk-shaped specimen (with 1-3mm thickness and 10-30mm diameter) is subjected to a short and high intensity laser pulse on the front face, and the temperature

response is recorded on the rear face. D is then calculated based on the time to reach half of the maximum temperature rise of the rear face. The method was originally proposed by Parker et al. [10] in 1961, then further improved by applying corrections for finite pulse time [11] and heat loss effects [12; 13]. Since the 1960s, numerous extensions of the original method have been introduced including e.g., the application for liquids, heterogeneous materials, and two- or three-layered specimens. Recently, the ultrafast laser flash method has been proposed by Baba et al. [14] for the measurement of thin films attached to a substrate. The thickness of the film can be less than 100nm, for which the laser pulse duration should be in the order of magnitude of picoseconds. In this parameter domain, the application of hyperbolic heat conduction models might be necessary. (It should be noted that the ultrafast laser flash method has significant differences in the way of temperature measurement compared to the classical laser flash method.) In the present study the Maxwell-Cattaneo-Vernotte (MCV) type heat conduction model was applied to simulate laser flash experiments. Our aim was to find the parameters for which the relaxation effect of the MCV equation can be observed via the measurement.

The laser flash experiment was simulated for a single layer specimen that is solid, homogeneous and material properties are constant. One-dimensional heat conduction through the thickness of the specimen was assumed; heat losses were neglected. Heat conduction was modeled according to the MCV equation:

$$\tau \frac{\partial}{\partial t} q + q = \lambda_F \frac{\partial T}{\partial x}, \quad (9)$$

which is identical to (6) when $a = 0$. With the help of (1), one can obtain the following partial differential equation for the temperature:

$$\tau \frac{\partial^2 T}{\partial t^2} + \frac{\partial T}{\partial t} = D \frac{\partial^2 T}{\partial x^2}, \quad (10)$$

where $D = \frac{\lambda_F}{\rho c}$ is the thermal diffusivity. We solve the differential equation with the following initial conditions $T(t = 0, x) = T_0$, $\frac{\partial T}{\partial t}(t = 0, x) = 0$. At the front boundary, $x = 0$, a heat pulse is introduced, with the following form (Fig 5):

$$q_0(t) = \begin{cases} \frac{1}{2} q_{max} [1 - \cos(2\pi t/t_p)], & 0 < t \leq t_p, \\ 0, & t > t_p. \end{cases} \quad (11)$$

The front boundary condition itself can be given with the help of the MCV equation (9)

$$\tau \frac{d}{dt} q_0 + q_0 = -\lambda_F \frac{\partial T}{\partial x}(t, x = 0). \quad (12)$$

At the rear face, the boundary condition is required to be $\frac{\partial T}{\partial x}(t, x = L) = 0$.

In order to find the parameters, for which the relaxation effect of the MCV equation can be observed, we introduced the

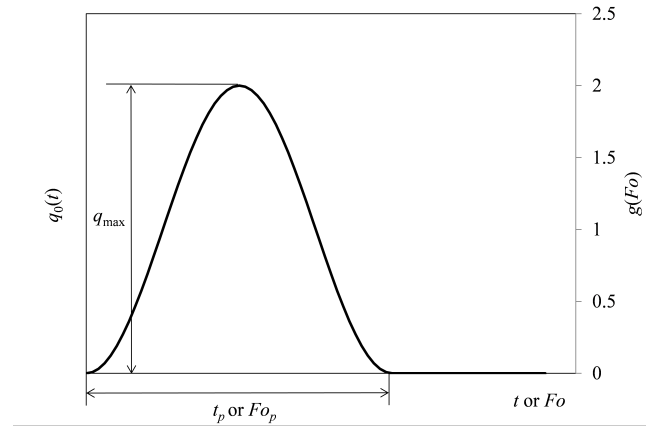


Figure 5. The shape of the applied pulse.

following dimensionless variables and parameters:

$$\theta = \frac{T - T_0}{T_L - T_0}, \quad \text{where } T_L = T_0 + \frac{1}{\rho c L} \int_0^{t_p} q_0(t) dt, \quad (13)$$

$$Fo = \frac{Dt}{L^2}, \quad (14)$$

$$\xi = \frac{x}{L}, \quad \text{therefore } 0 \leq \xi \leq 1, \quad (15)$$

$$\Pi^2 = \frac{D\tau}{L^2}, \quad (16)$$

$$g(Fo) = \frac{q_0(Fo)}{\bar{q}}, \quad \text{where } \bar{q} = \frac{1}{Fo_p} \int_0^{Fo_p} q_0(Fo) dFo. \quad (17)$$

Then we obtain the differential equation (10) in a dimensionless form as follows:

$$\Pi^2 \frac{\partial^2 \theta}{\partial Fo^2} + \frac{\partial \theta}{\partial Fo} = \frac{\partial^2 \theta}{\partial \xi^2}, \quad (18)$$

The initial conditions are $\theta(Fo = 0, \xi) = 0$ and $\frac{\partial \theta}{\partial Fo}(Fo = 0, \xi) = 0$. The heat pulse is

$$g(Fo) = \begin{cases} 1 - \cos\left(2\pi \frac{Fo}{Fo_p}\right), & 0 < Fo \leq Fo_p, \\ 0, & Fo > Fo_p. \end{cases} \quad (19)$$

and the front boundary condition

$$\Pi^2 \frac{d}{dt} g + g = -Fo_p \frac{\partial \theta}{\partial \xi}(Fo, \xi = 0). \quad (20)$$

The rear face boundary condition is $\frac{\partial \theta}{\partial \xi}(Fo, \xi = 1) = 0$.

The problem was solved numerically, using a simple explicit finite difference method. The key for obtaining a stable numerical solution was to keep the Courant number, $Cou = \frac{\delta t}{\delta x} \sqrt{\frac{D}{\tau}}$ close to but less than 1. ($Cou = 0.99$ was applied.)

The shape of the laser pulse $q(t)$ is shown in Fig 5. This function was chosen because it starts with 0 derivative, its derivative is finite everywhere, and it has finite height and length. (Starting with non-zero derivative and/or a jump in the function can

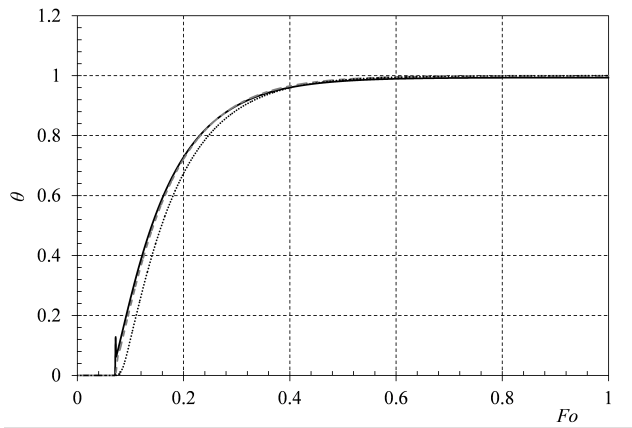


Figure 6. Rear side temperature history, $\Pi^2 = 0.005$. Black solid lines $Fo_p = 0.5\Pi^2$, grey dashed lines $Fo_p = 2\Pi^2$, black dotted lines $Fo_p = 8\Pi^2$

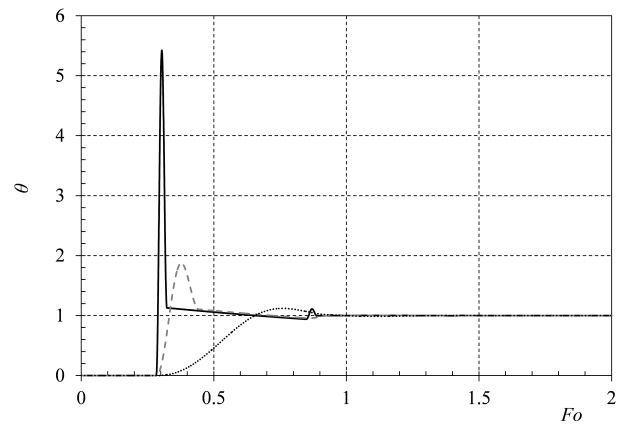


Figure 8. Rear side temperature history, $\Pi^2 = 0.08$. Black solid lines $Fo_p = 0.5\Pi^2$, grey dashed lines $Fo_p = 2\Pi^2$, black dotted lines $Fo_p = 8\Pi^2$

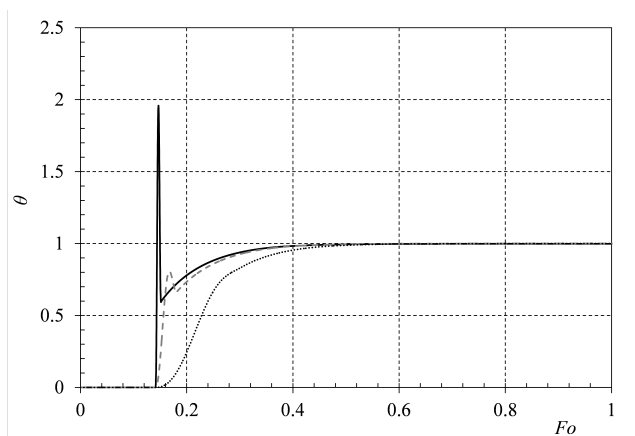


Figure 7. Rear side temperature history, $\Pi^2 = 0.02$. Black solid lines $Fo_p = 0.5\Pi^2$, grey dashed lines $Fo_p = 2\Pi^2$, black dotted lines $Fo_p = 8\Pi^2$

cause instability in the numerical solution.) Looking at the dimensionless equations we can conclude that the problem can be fully characterized by two dimensionless parameters: Π^2 and Fo_p . In a laser flash experiment, the rear face temperature history, $\theta(Fo, \xi = 1)$, is recorded. Hence, the effect of these two parameters on the rear face temperature history is to be examined.

Results of the numerical solution of the dimensionless problem are shown in Figs 6-8 for various values of Π^2 and Fo_p . In Fig 6, where $\Pi^2 = 0.005$, only a slight relaxation effect can be seen for $Fo_p = 0.5\Pi^2$. For longer pulses, waves are not present in the temperature histories. The main difference in these temperature histories compared to the ones calculated using the classical Fourier model is that the temperature remains 0 for a specified time before it starts increasing. In real measurements, it is difficult to detect this because of the noise in the temperature measurement, and applying a finite pulse time correction might appear to fix the deviance from the Fourier model. In Fig 7, where $\Pi^2 = 0.02$, a wave can be clearly seen in the temperature history for $Fo_p = 0.5\Pi^2$ and $Fo_p = 2\Pi^2$, which is a clear and easily detectable sign of the MCV equation. Increasing Π^2 further (see Fig 8 where $\Pi^2 = 0.08$), a second wave can be seen in the temperature history for the shortest pulse. This means

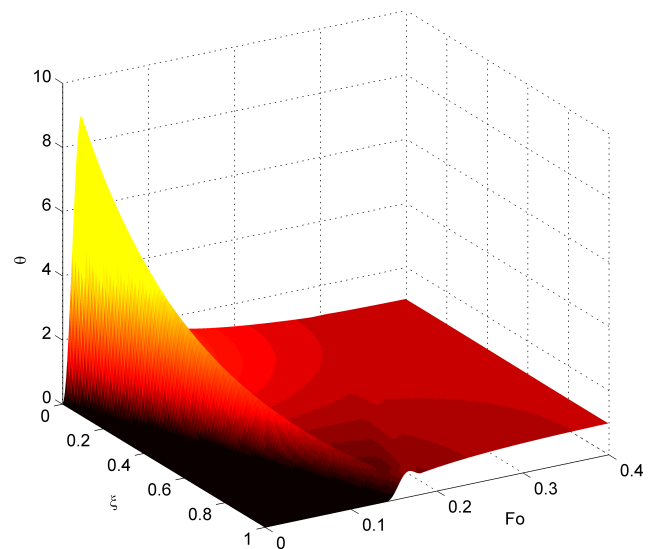


Figure 9. Dimensionless temperature distribution for $\Pi^2 = 0.02$ and $Fo_p = 2\Pi^2$.

that the wave bounces back from the front side and reaches the rear side for the second time. The temperature histories for all three Fo_p values rise above the steady state value, which is again a detectable sign of the MCV equation. The length of the pulse (Fo_p) has a significant effect on the temperature history. When Fo_p is much less than Π^2 then the wave is very sharp, which causes high maximum temperature on the front side. When Fo_p is much more than Π^2 then the wave might disappear from the temperature history. This effect can be understood by comparing the two terms on the left hand side of equation (20). We found that the optimal value of Fo_p is around $2\Pi^2$, because in this case the two terms have the same order of magnitude.

The value of Π^2 in case of the classical laser flash measurements is very low. In order to obtain higher values, special conditions are necessary. This is why it is desirable to find the smallest value of Π^2 for which the relaxation effect of the MCV equation can be reliably observed. Considering the results of the

numerical calculations, we suggest $\Pi^2 = 0.02$ and $Fo_p = 2\Pi^2$ as target values for the detection of the relaxation effect with the laser flash method. The complete temperature distribution in time and space for this case is shown in Fig 9. The propagation of the wave caused by the laser pulse can be followed along the thickness. The wave bounces back from the rear side but does not reach the front side again. The maximum temperature on the front side is about 9 times higher than the steady state temperature.

	Al @293K	NaF @15K
$D [m^2/s]$	$9.2 \cdot 10^{-5}$	2.6
$\tau [s]$	$2.6 \cdot 10^{-12}$	$6.8 \cdot 10^{-7}$
$L [m]$	$1.1 \cdot 10^{-7}$	$9.4 \cdot 10^{-3}$
$t_p [s]$	$5.2 \cdot 10^{-12}$	$1.4 \cdot 10^{-6}$

Table 3. Parameters according to $\Pi^2 = 0.02$ and $Fo_p = 2\Pi^2$ for aluminium at 293K and for NaF at 15K (NaF properties are based on [9]).

Finally, we calculated the recommended thickness (L) and pulse time (t_p) according to $\Pi^2 = 0.02$ and $Fo_p = 2\Pi^2$ for aluminium at 293K and NaF at 15K. The results are summarized in Table 3. For aluminium at 293K the recommended thickness is about 110nm, and the pulse time is about 5.2ps. With this thickness, the measurement cannot be performed on a standalone sample, however, measurements on two-layer configurations might be possible [14]. This, naturally needs the modification of the mathematical model, and the target values of the dimensionless parameters must be revised. Regarding NaF at 15K, the recommended thickness is 9.4mm, and the pulse time is 1.4μs. These are close to the experimental values in [9] and not extreme, customised laser flash instruments are able to perform measurements with these parameters. The big challenge is to perform the measurement at 15K. The second difficulty is that the thermal conductivity of NaF around 15K changes rapidly with temperature, which has to be considered in the mathematical model. Another option is to keep the temperature change caused by the pulse very small, which makes the temperature measurement very challenging.

In conclusion, the detection of the relaxation effect of the MCV equation by the laser flash method in the classical configuration might be possible only for materials with extremely high conductivity and very sophisticated instrumentation. However, the possibility of detecting the relaxation effect seems to be open for a wider range of materials applying a modified multilayer configuration of the classical method like in [14]. For this the mathematical model must be modified to match the multilayer configuration, and the target values of the dimensionless parameters must be revised.

DISCUSSION

The book experiment can be modeled reasonably well by both a nonlinear Fourier equation, with time dependent heat conductivity and by a linear Guyer-Krumhansl equation. *These results are not conclusive, one cannot decide which model is better.* Especially, the high value of the relaxation time in the GK model should be handled by care. First, because there are uncertainties in the fitting, and in the modeling of the contact with the thermostat. Moreover, here the special qualitative phenomena of the Maxwell-Cattaneo-Vernotte equation may be

suppressed by the higher order dissipation due to the last term of (7).

The analysis of the laser flash method highlighted the experimental parameters where qualitative effects due to the MCV equation can be identified. When dissipation beyond the Fourier equation cannot be suppressed, a similar analysis of the Guyer-Krumhansl and the Jeffreys type model is necessary.

ACKNOWLEDGEMENT

The work was supported by the grants OTKA K81161 and K104260.

REFERENCES

- [1] D. D. Joseph and L. Preziosi. Heat waves. *Reviews of Modern Physics*, 61:41–73, 1989.
- [2] D. D. Joseph and L. Preziosi. Addendum to the paper "heat waves". *Reviews of Modern Physics*, 62:375–391, 1990.
- [3] V. A. Cimmelli. Different thermodynamic theories and different heat conduction laws. *Journal of Non-Equilibrium Thermodynamics*, 34(4):299–332, 2009.
- [4] B. Nyíri. On the entropy current. *Journal of Non-Equilibrium Thermodynamics*, 16:179–186, 1991.
- [5] P. Ván. Weakly nonlocal irreversible thermodynamics – the Guyer-Krumhansl and the Cahn-Hilliard equations. *Physics Letters A*, 290(1-2):88–92, 2001.
- [6] V. A. Cimmelli and P. Ván. The effects of nonlocality on the evolution of higher order fluxes in non-equilibrium thermodynamics. *Journal of Mathematical Physics*, 46(11):112901–15, 2005.
- [7] P. Ván and T. Fülöp. Universality in heat conduction theory: weakly nonlocal thermodynamics. *Annalen der Physik*, 524(8):470–478, 2012.
- [8] T. Fülöp and P. Ván. Kinematic quantities of finite elastic and plastic deformations. *Mathematical Methods in the Applied Sciences*, 35:18251841, 2012.
- [9] H. E. Jackson and C. T. Walker. Thermal conductivity, second sound and phonon-phonon interactions in NaF. *Physical Review Letters*, 3:1428–1439, 1971.
- [10] W. J. Parker, R. J. Jenkins, C. P. Butler, and G. L. Abbott. Flash method of determining thermal diffusivity, heat capacity, and thermal conductivity. *Journal of Applied Physics*, 32(9):1679, 1961.
- [11] J. A. Cape and G. W. Lehman. Temperature and finite pulsetime effects in the flash method for measuring thermal diffusivity. *Journal of Applied Physics*, 34(7):1909, 1963.
- [12] R. D. Cowan. Pulse method of measuring thermal diffusivity at high temperatures. *Journal of Applied Physics*, 34(4):926, 1963.
- [13] L. M. Clark III and R. E. Taylor. Radiation loss in the flash method for thermal diffusivity. *Journal of Applied Physics*, 46(2):714, 1975.
- [14] T. Baba, N. Taketoshi, and T. Yagi. Development of ultrafast laser flash methods for measuring thermophysical properties of thin films and boundary thermal resistances. *Japanese Journal of Applied Physics*, 50(11):RA01, 2011.

ELASTICITY, PLASTICITY, RHEOLOGY AND THERMAL STRESS — AN IRREVERSIBLE THERMODYNAMICAL THEORY

Tamás Fülöp^{1,2,4,5}, Péter Ván^{1,2,4}, Attila Csatár^{3,4}

¹ Wigner Research Centre for Physics, P. O. Box 49, H-1525 Budapest, Hungary

² Dept. of Energy Engineering, Budapest Univ. of Technology and Economics, Bertalan L. u. 4-6, H-1111 Budapest, Hungary

³ Hungarian Institute of Agricultural Engineering, Tessedik S. u. 4, H-2100 Gödöllő, Hungary

⁴ Montavid Thermodynamic Research Group, Igmándi u. 26, H-1112 Budapest, Hungary

⁵ E-mail: fulop.tamas@wigner.mta.hu

ABSTRACT

We present a thermodynamical formulation of elastic, plastic, rheological and thermal stress phenomena of solids that is based on two pillars. One of them is a recent novel definition of kinematic quantities that enables the description of finite deformation elastic, plastic and thermal expansion changes in an automatically objective way. In parallel, the other pillar is irreversible thermodynamics. We show how naturally the well-known aspects of plasticity, as well as the inclusion of rheology, meet the requirement of positive definite entropy production. The general framework is illustrated via a simulation example and an experimental example.

INTRODUCTION

In nonquantitative/heuristic terms, objectivity may be formulated as the requirement that the physical content of a theory must be independent from the description used for the formulation of the theory. It might be expected that it is nontrivial to ensure objectivity for a theory, and paradoxes, controversies and errors indicate that indeed this is the case.

Motivated by the need for a safely objective formulation of continuum physics, in a recent work, we have introduced a novel definition of kinematic quantities [1; 2]. By working on Galilean spacetime directly, it was possible to avoid the use of any auxiliary element—reference frame, reference time, reference configuration etc.—, which are sources of possible violation of objectivity in the conventional approaches. In our framework, all kinematic quantities and equations are automatically objective.

The logical continuation of this program is to reformulate the mechanical and thermodynamical theories in terms of these quantities, as well as to look for possible improvements and possibly emerging new opportunities for theory building. The present work reports on results obtained in this direction. We show here a small deformation thermodynamical framework for elastic, plastic, thermal expansion and rheological phenomena of solids. Our original aim was an illustration of that, with the spacetime-based quantities, one can express anything that is needed in continuum physics. In parallel, it has gradually turned out that these quantities enable and suggest some such improvements and possibilities in continuum physics that have not been apparent before.

To see how our thermodynamical theory performs in practice, we provide here two illustrations, a numerical calculation of a concrete example process and an experiment, where the results demonstrate the features of the theoretical framework.

KINEMATIC QUANTITIES

Based on Matolcsi's reference frame free approach to theoretical physics [3; 4; 5], the problems of objectivity and material frame indifference [6; 7; 8; 9; 10] have been investigated in a series of papers [11; 12; 13; 14; 1]. In particular, in [1], the kinematic quantities for elastic and plastic processes of solids have been presented in a way that is free from any auxiliary elements like reference frame, reference time and reference configuration. During the birth of [1], it has been realized that this new approach incorporates thermal expansion also in a natural way and reveals some nontrivial kinematic and dynamical consequences of thermal expansion [2].

This kinematic background of the subsequent thermodynamical framework can be summarized as follows.

The motion of the continuum

The continuum is considered as a three dimensional smooth manifold. Each material point of it moves along a smooth world line in spacetime—which we will take here as a Galilean (“non-relativistic”) spacetime—, at time t , the spacetime location of P is $r_t(P)$. Its material gradient $\tilde{\nabla}$, *i.e.*, the derivative with respect to the variable P ,

$$\mathbf{J}_t(P) := (r_t \otimes \tilde{\nabla})(P), \quad (1)$$

is the world line gradient (and is the spacetime compatible generalization of the traditional deformation gradient) [spatial derivatives will act to the left or to the right according to the context, always to indicate the correct tensorial order]. This tensor maps tangent vectors of the material manifold to spacelike spacetime vectors, which form a three dimensional Euclidean vector space with Euclidean scalar product \mathbf{h} . At any instant t , the current spatial distance of two material points P, Q is the

distance of $r_t(P)$ and $r_t(Q)$ with respect to the spatial Euclidean metric \mathbf{h} ,

$$d_t(P, Q) = \|r_t(Q) - r_t(P)\|_{\mathbf{h}}. \quad (2)$$

This induces a current metric

$$\tilde{\mathbf{h}}_t := \mathbf{J}_t^T \mathbf{h} \mathbf{J}_t \quad (3)$$

on the material manifold (T standing for transpose), a scalar product for the tangent vectors at each material point.

The spacetime velocity of material point P at t is the time derivative $\dot{r}_t(P) = v_t(P)$. If we change from the Lagrangian/material/comoving variable to the Eulerian/spacetime variable then the material gradient $\tilde{\nabla}$ is mapped to the spatial spacetime derivative ∇ via \mathbf{J}_t , and we find

$$\mathbf{L}_t = \dot{\mathbf{J}}_t \mathbf{J}_t^{-1} \quad (4)$$

for the velocity gradient

$$\mathbf{L}_t(P) := (v_t \otimes \tilde{\nabla})(P). \quad (5)$$

(Naturally, the substantial/comoving time derivative coincides with the partial time derivative in the Lagrangian picture.)

Elasticity

So far, our continuum could have been a solid as well as a liquid (and even a laminarly flowing gas). What could be the mathematical formulation of the distinction between a solid and a liquid? Expressing that ‘a solid has a structure’, we can say that a solid possesses a self-metric (natural metric) structure, with which its current metric coincides when the solid is under no external influence. Namely, we assign to a solid a certain metric $\tilde{\mathbf{g}}$ on the material manifold. This metric tells the distances of material points—*i.e.*, coincides with the current metric $\tilde{\mathbf{h}}_t$ —when the solid is relaxed.

Our intention with an elastic kinematic quantity is to be the variable on which elastic stress depends, which, under classical mechanical experience, may be expected to depend on the distances between nearby material points. Taking into account that $\tilde{\mathbf{g}}$ describes the distances in unstressed state, the elastic kinematic quantity could measure the deviation of the current metric $\tilde{\mathbf{h}}_t$ from the self-metric $\tilde{\mathbf{g}}$. To this end, we can define

$$\tilde{\mathbf{A}}_t := \tilde{\mathbf{g}}^{-1} \tilde{\mathbf{h}}_t \quad (6)$$

(elastic shape tensor), which proves to be the spacetime compatible generalization of the ‘right’ Cauchy-Green tensor, and

$$\tilde{\mathbf{D}}_t := \ln \sqrt{\tilde{\mathbf{A}}_t} = \frac{1}{2} \ln \tilde{\mathbf{A}}_t \quad (7)$$

(elastic deformedness tensor), which is the generalization of the ‘right’ Hencky strain.

These tensors have been defined on the material manifold—acting on material tangent vectors—but can be transported to spacetime via \mathbf{J} . For the spacetime version (the ‘left’ version), we can derive the evolution equation

$$\dot{\mathbf{A}} = \mathbf{L}\mathbf{A} + \mathbf{A}\mathbf{L}^T. \quad (8)$$

Thermal expansion

As far as elasticity is concerned, the relaxed metric can be regarded as a constant tensor. However, we are aware of physical phenomena where the structure of a solid changes, where its relaxed distances change. One such phenomenon is thermal expansion. Restricting ourselves to isotropic solids, if $l(T)$ denotes a characteristic length (edge length of a cube, or radius of a sphere) of a unit amount (mass, or molar number) of the material at temperature T then, for the temperature dependence of the relaxed metric, we have

$$\tilde{\mathbf{g}}(T_2) = \left(\frac{l(T_2)}{l(T_1)} \right)^2 \tilde{\mathbf{g}}(T_1) \quad (9)$$

[in accord with that the metric expresses squared distances]. The usual definition of the linear thermal expansion coefficient is

$$\alpha(T) := \frac{dl(T)/dT}{l(T)}. \quad (10)$$

When temperature changes in time at a material point, we have

$$\dot{\tilde{\mathbf{g}}} = \left(\frac{d}{dT} \tilde{\mathbf{g}} \right) \dot{T} = 2\alpha(T) \dot{T} \tilde{\mathbf{g}} \quad (11)$$

following from Eq. (9), implying

$$\dot{\mathbf{A}} = \mathbf{L}\mathbf{A} + \mathbf{A}\mathbf{L}^T - 2\alpha\mathbf{A}. \quad (12)$$

Let us note that, in a theory, $l(T)$, and thus $\alpha(T)$, must be given constitutively.

Plasticity

Another phenomenon where the structure of a solid changes is plasticity. Therefore, plasticity is another source of $\dot{\tilde{\mathbf{g}}} \neq \mathbf{0}$. Putting elasticity, thermal expansion and plasticity together, we have

$$\dot{\mathbf{A}} = \mathbf{L}\mathbf{A} + \mathbf{A}\mathbf{L}^T - 2\alpha\mathbf{A} - 2\mathbf{Z}, \quad (13)$$

where \mathbf{Z} , the plastic change rate tensor is responsible for the additional change rate of $\tilde{\mathbf{g}}$, and is also to be given constitutively.

Remarks

We can see that, actually, $\tilde{\mathbf{g}}$ is not purely a kinematic quantity. Still, since elastic, plastic and thermal expansion deformations are traditionally considered as kinematic, we must speak about it here, where these kinematic definitions are given. Also, $\tilde{\mathbf{g}}$ is not purely dynamical, either.

As another remark, useful for the applications, strain can be defined only with respect to a reference time t_0 , as

$$\mathbf{E}_{t_0 \rightarrow t} := \int_{t_0}^t \mathbf{L}^S \tilde{\mathbf{g}} dt, \quad (14)$$

where $\overset{\text{S}}{\mathbf{D}}$ denotes symmetric part and $\widetilde{d}t$ indicates comoving integration. In parallel, the conventional deformation gradient can be expressed in the present formalism as

$$\mathbf{F}_{t_0 \rightarrow t} = \mathbf{J}_t \mathbf{J}_{t_0}^{-1}, \quad (15)$$

and satisfies

$$\mathbf{A}_t = \mathbf{F}_{t_0 \rightarrow t} \mathbf{A}_{t_0} \mathbf{F}_{t_0 \rightarrow t}^T. \quad (16)$$

Small deformation

From now on, we restrict our treatment to the small deformation regime, where (i) \mathbf{A} is near to \mathbf{I} , thus also satisfying $\mathbf{A} \approx \mathbf{I} + 2\mathbf{D}$, (ii) \mathbf{J} does not change considerably during the time scale on which we consider a process, and (iii) α can also be regarded as a constant. Then Eq. (13) simplifies, in leading order, to

$$\dot{\mathbf{A}} = \mathbf{L} + \mathbf{L}^T - 2\alpha\mathbf{I} - 2\mathbf{Z}, \quad (17)$$

rearrangeable as

$$\mathbf{L}^S = \dot{\mathbf{D}} + \alpha\dot{T}\mathbf{1} + \mathbf{Z}. \quad (18)$$

A consequence of the small deformation approximation is that we do not have to pay attention to the difference between ‘right’ and ‘left’, *i.e.*, material and spacetime tensorial quantities.

MECHANICS AND THERMODYNAMICS

Stress

Let us start building the dynamical theory by choosing what we expect on the mechanical side: let our elastic constitutive equation be the simple linear one:

$$\boldsymbol{\sigma} = U^d \mathbf{D}^d + U^s \mathbf{D}^s \quad (19)$$

with

$$\mathbf{D}^s = \frac{1}{3}(\text{tr}\mathbf{D})\mathbf{1}, \quad \mathbf{D}^d = \mathbf{D} - \mathbf{D}^s, \quad U^s = 3K, \quad U^d = 2G. \quad (20)$$

Actually, a nonlinear choice could also be incorporated, but let us now pursue a simple, yet interesting, setting.

At this point, we can already observe that the classic Duhamel-Neumann formula for thermoelasticity [15] is recovered as a special case. To see this, we must assume what are assumed there: that, at an initial time t_0 , the temperature is T_0 and elastic deformedness is considered zero ($\mathbf{D}_{t_0} = \mathbf{0}$, $\mathbf{A}_{t_0} = \mathbf{I}$), that is, we start with an unstressed, relaxed, natural initial state. We also stay in the small deformation regime, and neglect plastic changes. Then, at time t , in the leading order approximation,

$$\begin{aligned} \mathbf{D}_t &= \frac{1}{2}(\mathbf{A}_t - \mathbf{I}) = \frac{1}{2}(\mathbf{F}_{t_0 \rightarrow t} \mathbf{F}_{t_0 \rightarrow t}^T - \mathbf{I}) \\ &= \mathbf{E}_{t_0 \rightarrow t} - \alpha(T - T_0)\mathbf{I}. \end{aligned} \quad (21)$$

Inserting this into Eq. (19) yields

$$\boldsymbol{\sigma}_t \approx 2G\mathbf{E}_{t_0 \rightarrow t} + (K - \frac{2}{3}G)(\text{tr}\mathbf{E}_{t_0 \rightarrow t})\mathbf{I} - 3K\alpha(T - T_0)\mathbf{I}, \quad (22)$$

which is precisely the Duhamel-Neumann expression.

Thermodynamical quantities for elasticity, thermal expansion and plasticity

Our first step towards thermodynamics is that we expect the first law to be satisfied:

$$\rho\dot{u} = -\mathbf{j}_u \cdot \nabla + \boldsymbol{\sigma} : \mathbf{L}^S \quad (23)$$

for the specific internal energy u and its current \mathbf{j}_u , both to be specified constitutively later (and the density ρ being constant in the small deformation regime) [tr denotes trace]. Let us then construct the rest of the thermodynamical build-up as follows: our aim is to rewrite Eq. (23) assuming $\mathbf{j}_s = \mathbf{j}_u/T$ for the entropy current \mathbf{j}_s , and with an appropriate specific entropy $s(\mathbf{D}, T)$, as

$$T\rho\dot{s} = T(-\mathbf{j}_s \cdot \nabla + \boldsymbol{\sigma}_s), \quad (24)$$

where the positive definiteness of the entropy production, $\boldsymbol{\sigma}_s \geq 0$ is also to be ensured constitutively.

If we choose again a simple internal energy function, *i.e.*, consisting of an elastic energy part and a thermal term corresponding to a constant specific heat c ,

$$u = cT + \frac{U^d}{2\rho} \mathbf{D}^d : \mathbf{D}^d + \frac{U^s}{2\rho} \mathbf{D}^s : \mathbf{D}^s + \frac{U^s}{\rho} T \alpha \text{tr} \mathbf{D}^s, \quad (25)$$

then, omitting the straightforward details, that appropriate entropy function proves to be

$$s = c \ln \frac{T}{T_0} + \frac{U^s}{\rho} \alpha \text{tr} \mathbf{D}^s + s_0 \quad (26)$$

with any temperature value T_0 and constant s_0 , and the corresponding entropy production is found to be

$$\boldsymbol{\sigma}_s = \nabla \frac{1}{T} \cdot \mathbf{j}_u + \frac{1}{T} \boldsymbol{\sigma} : \mathbf{Z} = \nabla \frac{1}{T} \cdot \mathbf{j}_u + \frac{U^d}{T} \mathbf{D}^d : \mathbf{Z} + \frac{U^s}{T} \mathbf{D}^s : \mathbf{Z}. \quad (27)$$

Our remaining task is to ensure the positive definiteness of the latter.

One simple choice guaranteeing this is when we take the standard constitutive formula for heat conduction,

$$\mathbf{j}_u = \lambda \nabla \frac{1}{T} \quad (28)$$

(with, say, a constant positive λ), and prescribe the plastic constitutive equation as

$$\mathbf{Z} = \Gamma \dot{\mathbf{D}}^d \quad \text{with} \quad \Gamma = \gamma H \left(\mathbf{D}^d : \mathbf{D}^d - B \right) H \left(\mathbf{D}^d : \dot{\mathbf{D}}^d \right), \quad (29)$$

where γ and B are positive constants, and H is the Heaviside function.

The choice Eq. (29) is fairly plausible from the plasticity point of view: the plastic change rate is deviatoric and is proportional to the elastic change rate, the first Heaviside term describes a von Mises yield criterion (recall that stress is in a linear relationship with \mathbf{D}), and the second Heaviside term expresses the natural expectation that plastic change is switched off during unloading.

On the other, thermodynamical, side, the second Heaviside term ensures that entropy production is positive definite. One may actually dare to put this reversely: plasticity must be switched off during unloading, as otherwise positive definiteness of entropy production would be violated.

We remark that it poses no difficulty to incorporate temperature dependent coefficients U^s , U^d , α , c .

Adding rheology

The thermodynamical formulation of rheological models is possible with the aid of internal variables (dynamical degrees of freedom [16]). The details [17] of this derivation cannot be given here, but the outline is similar to what happens in [18].

Namely, we assume the presence of an additional internal variable, a symmetric tensor ξ , and extend our previous entropy function as

$$s = s_{\text{previous}} - \frac{1}{2} \xi : \xi. \quad (30)$$

If plasticity and thermal expansion are neglected then the positive definiteness of entropy production leads to, in the linear Onsagerian setting, after eliminating the internal variable, a linear rheological model with σ , $\dot{\sigma}$, \mathbf{D} , $\dot{\mathbf{D}}$, $\ddot{\mathbf{D}}$ terms. Therefore, we arrive at a common generalization of the Poynting–Thomson–Zener and the Jeffreys models, which we may call the inertial Poynting–Thomson–Zener model.

A SIMULATION

The evolution equations Eq. (18), Eq. (23), together with the approximate mechanical equation of motion

$$\sigma \cdot \nabla = 0 \quad (31)$$

and the constitutive prescriptions Eq. (19), Eq. (25), Eq. (28), Eq. (29), form a closed set of equations, thus being capable to calculate a concrete process. To demonstrate this, we have performed a numerical calculation for a cylindrical rod uniaxially stretched by an increasing force, linear in time.

Figure 1. shows the strains and the temperature as the function of time. Plastic change (blue line) begins only above the critical stress. Below this, temperature decreases, similarly to what happens for an adiabatically expanded gas. Therefore, the total strain (black line) runs a bit below the elastic strain (green line), the difference caused by the nonzero thermal expansion coefficient. When the plastic change also appears, the total strain increases faster, and, due to the dissipative power term $\sigma : \mathbf{Z}$, temperature also starts to increase.

Figure 2. shows the modification of the setup, where the rod has slightly nonconstant cross section: then plasticity (blue

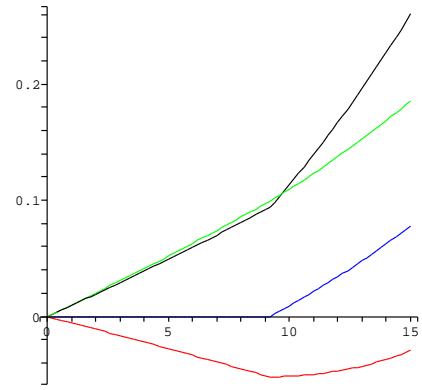


Figure 1. Uniaxially stretched rod. The temperature (red line) first decreases and then increases, the elastic strain (green line) increases following the increased stress, the plastic strain (blue line) appears only above the critical stress, causing that the total strain (black line) starts to increase faster.

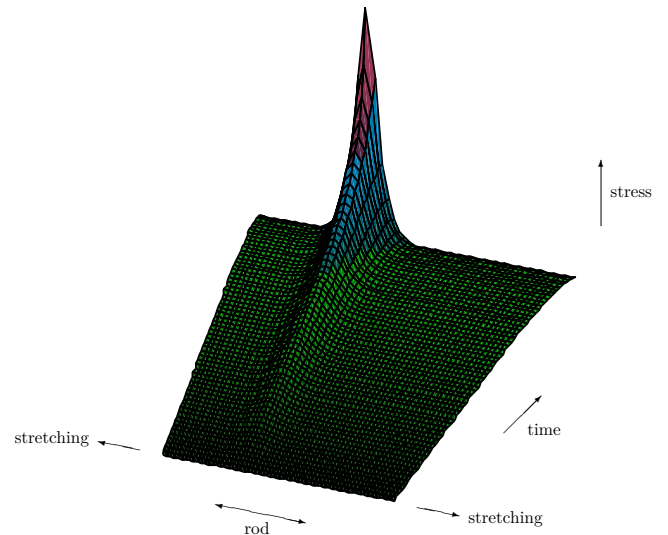


Figure 2. Stretching a rod with slightly nonconstant cross section. Plastic change (blue region) starts where the rod is the thinnest, and failure (red region) also occurs there, the remaining part of the rod has only elastic and thermal expansion deformations (green region).

region) appears first at the location where the sample is thinner, and failure (red region) would also appear there, if a simple stress failure criterion is added for illustration and for the sake of the following Section.

AN EXPERIMENT

We have carried out the above stretching example not only in simulation but also as an experiment on a plastic (“Docamid 6G-H”) polyamide) sample. In addition to measuring the extensions, a thermal camera has measured the surface temperature of the sample during the process. We can observe on the snapshots in Fig. 3 the initial decrease of temperature and then its increase, observable where plastic change has already started.

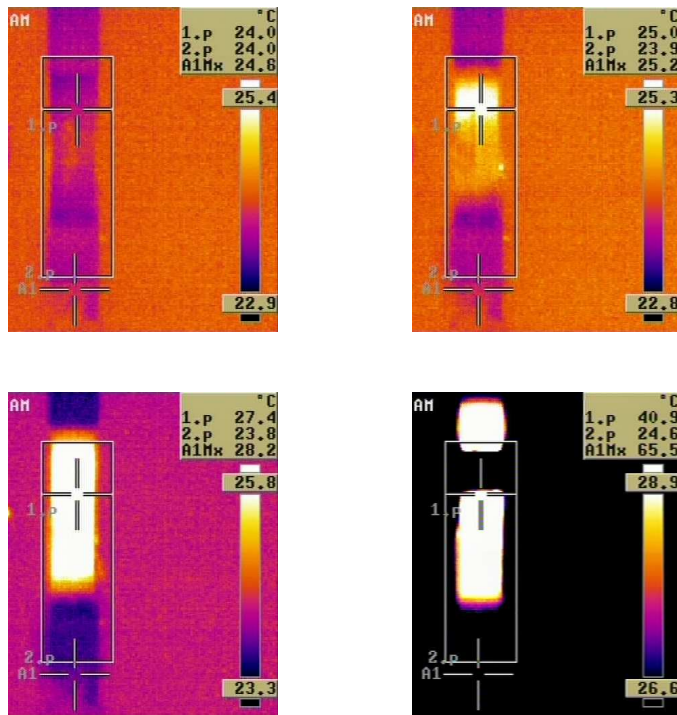
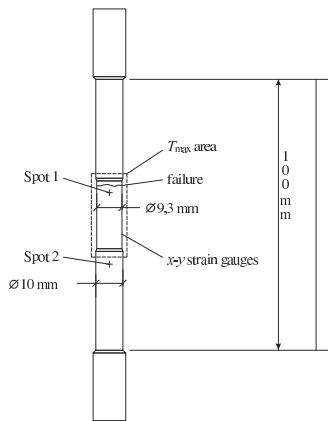


Figure 3. Stretching a rod with slightly nonconstant cross section — experiment. The outline (upper left figure) displays the two spots whose temperature was not only recorded by the thermal camera but also numerically displayed, together with the maximal temperature in the rectangle area. The subsequent five figures are snapshots taken by thermal camera. The first shows the initial state, then the quasi-adiabatic cooling is observable, then heat dissipation appears due to plastic change, then the plastic change reaches the whole thinner part of the sample, and finally failure occurs.

CONCLUSION

We intended to illustrate that our recent kinematic formulation can be incorporated in mechanical and thermodynamical theories, with thermal expansion and plastic processes described naturally and realistically, even when considering only simple constitutive choices and small deformations. Rheology can also be added—when plasticity and thermal expansion are also kept then interesting cross effects are expected to emerge, offering new theoretical possibilities for explaining experimental observations.

The finite deformation version of the presented theory is also possible, though some formulae become nontrivial due to the

fact that the multiplication of tensors is not commutative. This work is in progress currently. Finally, we wish to strengthen the connection between theory and experiment, evaluating quantitatively the already performed experiments and to devise new ones.

ACKNOWLEDGMENT

This work was supported by the grant OTKA K81161.

REFERENCES

- [1] T. Fülöp and P. Ván, Kinematic Quantities of Finite Elastic and Plastic Deformation, *Math. Meth. Appl. Sci.*, vol. 35, pp. 1825–1841, 2012.
- [2] T. Fülöp, Thermal Expansion, Elastic Stress and Finite Deformation Kinematics, in: Proceedings of the 10th HEEP International Conference, 23–25 May 2011, Balatonfüred, Hungary. Published by: Budapest University of Technology and Economics, Department of Energy Engineering, 2011, pp. 227–232.
- [3] T. Matolcsi, *A Concept of Mathematical Physics: Models for SpaceTime*, Akadémiai Kiadó (Publishing House of the Hungarian Academy of Sciences), Budapest, 1984.
- [4] T. Matolcsi, *A Concept of Mathematical Physics: Models in Mechanics*, Akadémiai Kiadó (Publishing House of the Hungarian Academy of Sciences), Budapest, 1986.
- [5] T. Matolcsi, *Spacetime Without Reference Frames*, Akadémiai Kiadó Publishing House of the Hungarian Academy of Sciences), Budapest, 1993.
- [6] G. Ryskin, Misconception Which Led to the "Material Frame Indifference" controversy, *Physical Review E*, vol. 32(2), pp. 1239–1240, 1985.
- [7] M. E. Gurtin, E. Fried, and L. Anand, *The Mechanics and Thermodynamics of Continua*, Cambridge University Press, 2010.
- [8] A. I. Murdoch, Objectivity in classical continuum physics: a rationale for discarding the 'principle of invariance under superposed rigid body motions' in favour of purely objective considerations, *Continuum Mechanics and Thermodynamics*, vol. 15, pp. 309–320, 2003.
- [9] W. Noll, A Frame Free Formulation of Elasticity, *Journal of Elasticity*, vol. 83, pp. 291–307, 2006.
- [10] M. Frewer, More Clarity on the Concept of Material Frame-indifference on Classical Continuum Mechanics, *Acta Mechanica*, vol. 202, pp. 213–246, 2009.
- [11] T. Matolcsi, On Material Frame-indifference, *Archive for Rational Mechanics and Analysis*, vol. 91(2), pp. 99–118, 1986.
- [12] T. Matolcsi and T. Gruber, Spacetime Without Reference Frames: An Application to the Kinetic Theory, *International Journal of Theoretical Physics*, vol. 35(7), pp. 1523–1539, 1996.
- [13] T. Matolcsi and P. Ván, Can Material Time Derivative Be Objective? *Physics Letters A*, vol. 353, pp. 109–112, 2006.
- [14] T. Matolcsi and P. Ván, Absolute Time Derivatives, *Journal of Mathematical Physics*, vol. 48, No. 053507–19, 2007.
- [15] V. A. Lubarda, On Thermodynamic Potentials in Linear Thermoelasticity, *International Journal of Solids and Structures*, vol. 41(7), pp. 7377–7398, 2004.
- [16] J. Verhás, *Thermodynamics and Rheology*, Akadémiai Kiadó and Kluwer Academic Publisher, Budapest, 1997.

[17] P. Ván and T. Fülöp, Classic and New Rheological Models in the Framework of a Thermodynamical Internal Variable Theory, in preparation.

[18] P. Ván and T. Fülöp, Universality in Heat Conduction Theory: Weakly Nonlocal Thermodynamics, *Annalen der Physik*, vol. 524, 470–478, 2012.

MAXIMUM ENTROPY PRODUCTION IN BOILING SHOCKS

Oleg Ivashnyov, Marina Ivashneva

Moscow MV Lomonosov State University, Vorobyovi Gori 1, Moscow 119899, Russia

ABSTRACT

Experimental studies of hot water depressurization have shown that liquid boiling proceeds in a shock which moves at a speed of approximately 10 m/s from the open end deep into the tube. The ‘boiling shock’ was obtained in a numerical experiment using the flow model that considered temperature and velocity non-equilibrium of phases. To analyse the mechanism of an instantaneous evaporation, the wave structure was described with model’s stationary version in the moving frame linked with the wave front. From the numerical experiment there were taken all the parameters of nonequilibrium mixture ahead of the wave front but the velocity of the oncoming flow. The velocity was varied to see if a stationary wave-type solution could be obtained. Among the integral curves there was a series of regimes in which the flow velocity went over on a steady level and the mixture reached an equilibrium state. Their analysis showed that an instantaneous transformation of the non-equilibrium boiling mixture into an equilibrium state was caused by a chain bubble fragmentation which led to a sharp increase in the interfacial area, intensification of the vaporization process and loss of liquid’s excess heat. Each of stationary wave-type regimes was characterized by a definite meaning of the entropy increase in the shock. It occurred that, in a numerical experiment using a full, non-stationary, system of model equations that was in good agreement with a physical experiment, there realized the regime with a maximum entropy production.

INTRODUCTION

Boiling shocks are formed in flows with accelerations of tens-hundreds metres per second. Such flows are most of interest since they are realized under loss-of-coolant nuclear power stations accidents.

In a classic experiment on a high-pressure vessel depressurization of Edwards and O’Brien [1], the vessel was a 4 m length horizontal tube with 7.3 cm internal diameter. The tube initially contained hot water with temperature 515 K. The pressure in the tube, $P_0=6.9$ MPa, was twice the pressure of saturation and the water did not boil. The right-hand end of the tube was closed with a glass disc. On destroying the disc, the liquid efflux accompanied by boiling started. A uniform pressure of 2.7 MPa, which was less than the pressure of saturation (3.5 MPa) but greater than an atmospheric one, settled all over the vessel.

In large-scale experimental pressure oscillograms (figure 1), the first waves crossing the channel within 3 ms looked like an instant pressure drop up to $P=2.7$ MPa at zero time. The pressure remained constant for a long time: only after 0.2 s did it start to decrease rapidly at the 3rd point, and then at the 4th and 5th points. This was the second wave of rarefaction, a ‘slow wave’, moving with the speed of only 10 m s⁻¹. The experimental oscillograms of the pressure and volumetric vapor fraction measured at the 4th point (solid lines in figure 3a,b) showed that the pressure drop in the ‘slow wave’ was accompanied by the increase in the volumetric vapour content from 0.2 to 0.9.

Slow waves of boiling were observed in Edwards and O’Brien’s experiments at different initial parameters of water and in the experiments with the other fluids: CO₂ [2] and dichlorodifluoromethane [3].

HIGH-PRESSURE VESSEL DECOMPRESSION IN THE FRAMES OF AN EQUILIBRIUM MODEL

An equilibrium model [4] includes the equations of conservation for mixture mass, momentum and entropy:

$$\frac{\partial \rho}{\partial t} + \frac{\partial(\rho u)}{\partial x} = 0, \quad (1)$$

$$\frac{\partial(\rho u)}{\partial t} + \frac{\partial(\rho u^2 + P)}{\partial x} = 0, \quad (2)$$

$$\frac{\partial S}{\partial t} = 0. \quad (3)$$

The equation of state for an equilibrium mixture is a sectionally continuous dependence between the mixture density, pressure and entropy. It consists of two parts. At the point of their intersection (the point of boiling inception) the derivative of density with respect to pressure breaks:

$$\rho = \begin{cases} \rho_l(P, S_l), & \text{if } P \geq P_s(T_0), \\ \left(\frac{1}{\rho_l} + \varphi(P)(S - S_l) \right)^{-1}, & \text{if } P < P_s(T_0), \end{cases} \quad (4)$$

$$\varphi(P) = \left(\frac{\partial T}{\partial P} \right)_S.$$

The first part of (4) is the equation of state for a pure liquid and the second one is that for an equilibrium mixture.

The isoentropic curve for an equilibrium mixture expansion is shown by a dashed line in figure 3c.

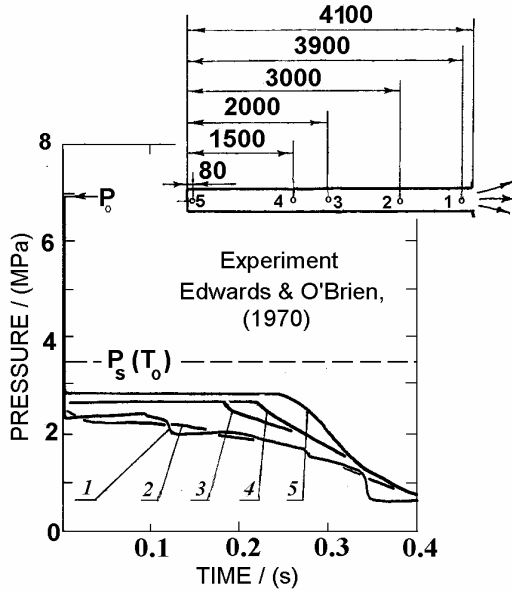


Figure 1. Experimental pressure oscillograms at five different tube cross-section locations (shown in the insert).

It follows from the equation of state (4) that at $P=P_s(T_0)$, the speed of sound

$$a_e = \left(\frac{\partial P}{\partial \rho} \right)_{S=\text{const}}^{-1/2}$$

changes instantaneously from the speed of sound in a pure liquid, 1100 m s^{-1} , down to the speed of sound in an equilibrium two-phase mixture

$$a_e = \left\{ \frac{\rho}{\rho_l^2 a_l^2} + \rho \left[\left(1 - \frac{\rho}{\rho_l} \right) \frac{1}{\varphi} \left(\frac{\partial^2 T}{\partial P^2} \right)_s - \frac{\rho \varphi}{\rho_l T} \left(\rho_l \left(\frac{\partial i_l}{\partial P} \right)_s - 1 \right) \right] \right\}^{-1/2},$$

which is much less, 26 m s^{-1} (at 515 K). Therefore the wave of rarefaction is split into two waves moving with different velocities. The first wave where the pressure drops down to the pressure $P_s(T_0)$ spreads with the speed 1100 m s^{-1} . The second wave, where further diminishing of the pressure occurs, moves with the speed of 26 m s^{-1} . These two waves are separated by a zone of constant pressure.

The calculations using the equilibrium model are shown in figure 2 and by dashed lines in figure 3. The two parts of the rarefaction wave are seen (in multi-scale oscillograms, the first one looks like a vertical pressure drop at zero time). According to calculations the pressure behind the first wave of rarefaction is equal to the pressure of saturation, 3.5 MPa , while in the experiment it is much less, 2.7 MPa .

Using experimental oscillograms of pressure and volumetric vapour content the curves of the mixture expansion in P-V (pressure-specific volume) coordinates have been built (figure 3c). Their comparison with curves for an adiabatic expansion of an equilibrium mixture have shown that the 1st rarefaction wave converts the mixture into a metastable, overheated, state and the 2nd one turns it back to equilibrium.

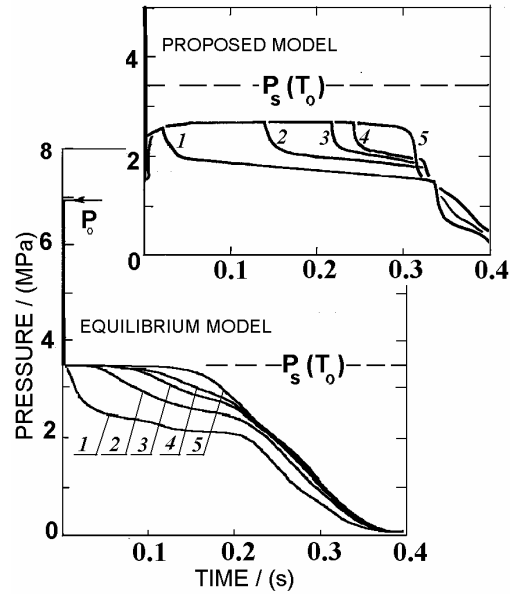


Figure 2. Calculations using an equilibrium and nonequilibrium models of boiling.

DECOMPRESSION IN THE FRAMES OF THE MODEL ACCOUNTING FOR TEMPERATURE AND VELOCITY NON-EQUILIBRIUM OF PHASES

In the model, the boiling is considered to start up at centers of nucleation. The pressures in the phases are assumed to be equal; the parameters in a bubble are uniform and equal to the parameters on the line of saturation; the vapour density is much less than the liquid density; the phase slip is much less than the flow velocity.

Along with the equations (1), (2) for mixture mass and momentum conservation, the model comprises the equations of conservation for internal energy, vapour mass, bubble number, and the equation of motion of an individual bubble:

$$\frac{\partial i}{\partial t} - \frac{1}{\rho} \frac{dP}{dt} = 0, \quad (5)$$

$$\frac{\partial(\rho_g \alpha)}{\partial t} + \frac{\partial(\rho_g \alpha u)}{\partial x} = j n, \quad (6)$$

$$\frac{\partial n}{\partial t} + \frac{\partial(nu)}{\partial x} = \rho \psi, \quad (7)$$

$$\begin{aligned} (\rho_g + C_{vm} \rho_l) \frac{d_g u_g}{dt} &= \rho_l \frac{Du}{Dt} + C_{vm} \rho_l \frac{Du}{Dt} - \\ &- \frac{3}{a} C_{vm} \rho_l (u_g - u) \frac{d_g r}{dt} - \left(\frac{3}{2a} C_{\mu} \rho_l |u_g - u| \right) (u_g - u) \end{aligned}, \quad (8)$$

$$\rho = (1 - \alpha) \rho_l + \alpha \rho_g, \quad (9)$$

$$i = (1 - \chi) i_l + \chi i_g, \quad \chi = \frac{\rho_g \alpha}{\rho},$$

$$\frac{D}{Dt} = \frac{\partial}{\partial t} + u \frac{\partial}{\partial x}, \quad \frac{d_g}{dt} = \frac{\partial}{\partial t} + u_g \frac{\partial}{\partial x}.$$

Virtual mass coefficient C_{vm} is equal to $1/2$ for spherical bubbles. D/Dt is the material derivative following the mixture and d_g/dt is that following the bubbles.

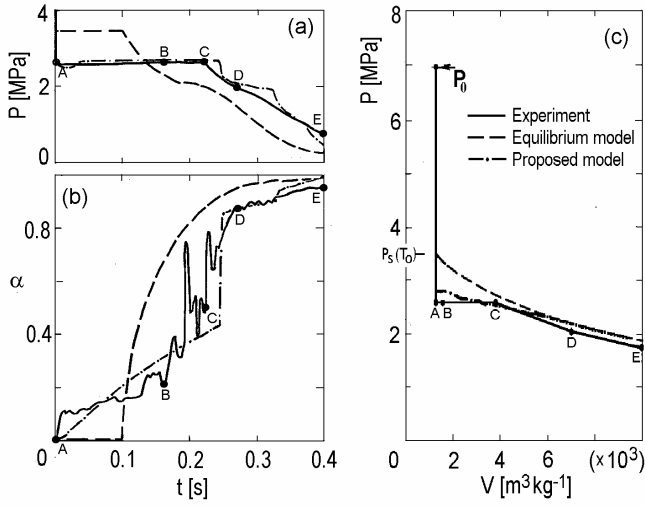


Figure 3. (a,b) A comparison of experimental and theoretical oscillograms of pressure and volumetric vapour content for point 4 (see figure 1). (c) Experimental (built using parameters' values at points ABCDE marked in a,b) and theoretical pressure-specific volume dependencies.

Neglecting the dependence of liquid density on temperature, and considering that, nearby the saturation line, the isotherms built in P - V coordinates are strait lines, we used the equation of the liquid state in the following form:

$$\frac{1}{\rho_l} = k - \frac{P}{\beta^2},$$

$$\beta = \beta(T_0) = \text{const}, \quad k(T_0) = \frac{1}{\rho_{ls}(T_0)} + \frac{P_s(T_0)}{[\beta(T_0)]^2} = \text{const} \quad (10)$$

Then thermal-energy equation for the liquid state is:

$$i_l(P, T_l) = i_{ls}(T_l) + k(P - P_s(T_l)) - \frac{P^2 - P_s^2(T_l)}{2\beta^2}, \quad (11)$$

$$i_{ls} = B(T_l - D)$$

where i_{ls} is the liquid enthalpy on the line of saturation, $B=5000 \text{ m}^2/(\text{c}^2 \text{ K})$, $D=305 \text{ K}$ are approximation parameters.

Differentiating (11) we obtain specific isobaric thermal capacity of the liquid h

$$h = \left(\frac{\partial i_l}{\partial T_l} \right)_P = B - \frac{1}{\varphi(P_s(T_l))} \left(k - \frac{P_s(T_l)}{\beta^2} \right), \quad (12)$$

where $\varphi(P)$ is the derivative taken along the line of saturation.

For the wide range of temperatures, $450 \text{ K} \leq T_s \leq 590 \text{ K}$, the approximation $\rho_g = P_g/A$, $A = 2 \cdot 10^5 \text{ m}^2/\text{s}^2$ describes the vapour state on the line of saturation with a relative error of 2%.

The intensity of bubble breakup ψ is defined with a relaxation ratio:

$$\psi = \frac{c^* - c}{\tau^*}, \quad (13)$$

where c^* is the number of bubbles that would be formed if the fragmentation were instantaneous, and τ^* is the characteristic fragmentation time which are specified using the solution of the problem about the rise in amplitude of a small harmonic

perturbation with wavelength λ arising on a plane interphase boundary [5]:

$$\xi = K \exp \left[I(\lambda)t - i \frac{2\pi}{\lambda} x \right],$$

$$I(\lambda) = \pm \sqrt{\frac{4\pi^2 \rho_g (u_g - u_l)}{\lambda^2 \rho_l} - \frac{8\pi^3 \sigma}{\lambda^3 \rho_l}}$$

From the condition that a bubble is divided by the wave with the fastest growing amplitude,

$$\lambda^* = \frac{3\pi \sigma}{\rho_g (u_g - u_l)^2},$$

the number of fragments appeared as a result of a bubble breakup (c^*/c) is determined as the ratio of the bubble diameter to the length of the wave λ^* . A characteristic time of breakup is adopted to be the time of e-time ($e=2.7\dots$) rise in amplitude of the perturbation with wavelength λ^* . From an evident condition: $\lambda^* \leq 2r$, one obtains the criterion of the surface stability of the bubble overflowing by fluid, the Weber number:

$$We = \frac{2r \rho_g (u_g - u_l)^2}{\sigma}, \quad (14)$$

and the evaluation of its critical value, $We^* = 3\pi$.

$$\frac{c^*}{c} = \frac{2r}{\lambda^*} = \frac{We}{We^*}, \quad \tau^* \sim \sqrt{\frac{\rho_l r^3}{\sigma} \left(\frac{We}{We^*} \right)^3} \quad (15)$$

Δu in the equation (14) is determined from the equation for motion of an individual dispersed unit (8) by:

$$\frac{D}{Dt} \left(\frac{u_g - u}{\rho_g} \right) =$$

$$= \frac{2}{\rho_g} \frac{Du}{Dt} - \frac{3}{4r} \left[C_\mu |u_g - u| + \frac{j}{\pi r^2 \rho_g} \right] \frac{u_g - u}{\rho_g} \quad (16)$$

Where D/Dt is the material derivative following the mixture which substitutes the material derivative following the bubbles d_g/dt taking into account the assumption about the smallness of the phase slip, $|u_g - u_l| \ll u_l$.

The expression for the interfacial drag coefficient C_μ is:

$$C_\mu = \begin{cases} \frac{16}{\text{Re}}, & \text{Re} \leq 10.9, \\ \frac{48}{\text{Re}} \left(1 - \frac{2.2}{\sqrt{\text{Re}}} \right), & 10.9 < \text{Re} \leq 1000, \\ 4.466 \times 10^{-2}, & \text{Re} > 1000, \end{cases}$$

$$\text{Re} = 2r \rho_l \frac{|u_g - u_l|}{\mu}$$

Following [6] the intensity of liquid evaporation into a bubble j is defined using an automodel solution about a motionless bubble growth in an overheated liquid [7] as:

$$j = \frac{2\pi\gamma}{l} r Nu [T_l - T_s(P)].$$

$$Nu = 2 + \left(\frac{6Ja}{\pi}\right)^{1/3} = \frac{12Ja}{\pi}, \quad Ja = \frac{h\rho_l(T_l - T_s)}{\rho_g l}$$

From (16), it follows that the liquid acceleration is the only reason of the disturbance of the equality in the phase velocities.

The number of initial bubbles and the critical Weber number are specified as: $c_0 = 4 \times 10^5 \text{ kg}^{-1}$, $We^* = 1$.

The numerical results obtained using the model (for more details one may see [8]) correspond to experimental ones: the pressure level (2.7 MPa) remains constant for a long time and then suddenly drops (figure 2, upper section); the decrease of pressure is accompanied by the increase in the volumetric vapour content (dashed-dotted lines in figure 3). Thus the shock of boiling has been obtained in the numerical experiment.

THE STRUCTURE OF THE BOILING SHOCK

The width of the 'boiling wave' is small and does not increase in time that allows us to suppose that it can be described by stationary equations in the coordinate system linked with it:

$$G = \rho u = \text{const}, \quad (17)$$

$$Gu + P = \text{const}, \quad (18)$$

$$i + \frac{u^2}{2} = \text{const}, \quad (19)$$

$$\frac{\partial u}{\partial z} = \frac{c j \rho (1/\rho_g - 1/\rho_l)}{1 - u^2/a_f^2}, \quad (20)$$

$$\frac{d}{dz} [\alpha \Delta u] = 2\alpha \frac{du}{dz} - \frac{3C_\mu |\Delta u|}{4ru} [\alpha \Delta u], \quad (21)$$

The frozen speed of sound a_f , the velocity of high-frequency indignations spread in the absence of interphase transfer processes, is determined as:

$$a_f = \left[\rho \left(\frac{(1-\alpha)\rho_l}{\beta^2} + \frac{\alpha}{P} \right) \right]^{-1/2}.$$

All the parameters at $z=0$ but the velocity of the oncoming flow u^* are taken from the numerical experiment given in figure 2 (upper section): $P=2.7 \text{ MPa}$, $T=513 \text{ K}$, $\alpha = 0.2$, $c=c_0=4 \times 10^5 \text{ kg}^{-1}$ and $We=We^*$.

Parameters profiles obtained at different u^* values are presented in figure 4. At a starting point of the wave, the Weber number reaches its critical value and bubbles begin to break-up. Due to the fragmentation the interfacial area increases and boiling intensifies. The pressure decreases (since the bubble number c is in the numerator of 20). The increase in velocity gradient du/dz causes an increase in the difference of phase velocities Δu (see 21). The increase in Δu is why the Weber number (14) does not decrease after breakup in spite of the diminishing of bubble radius and so breakup is repeated. Thus, it proceeds like a chain reaction, i.e. one breakup creates the conditions for the next one. That leads to the great increase in bubble number. The bubble fragmentation comes to an end when the mixture reaches an equilibrium state ($T_l = T_g$). Then, the intensity of the

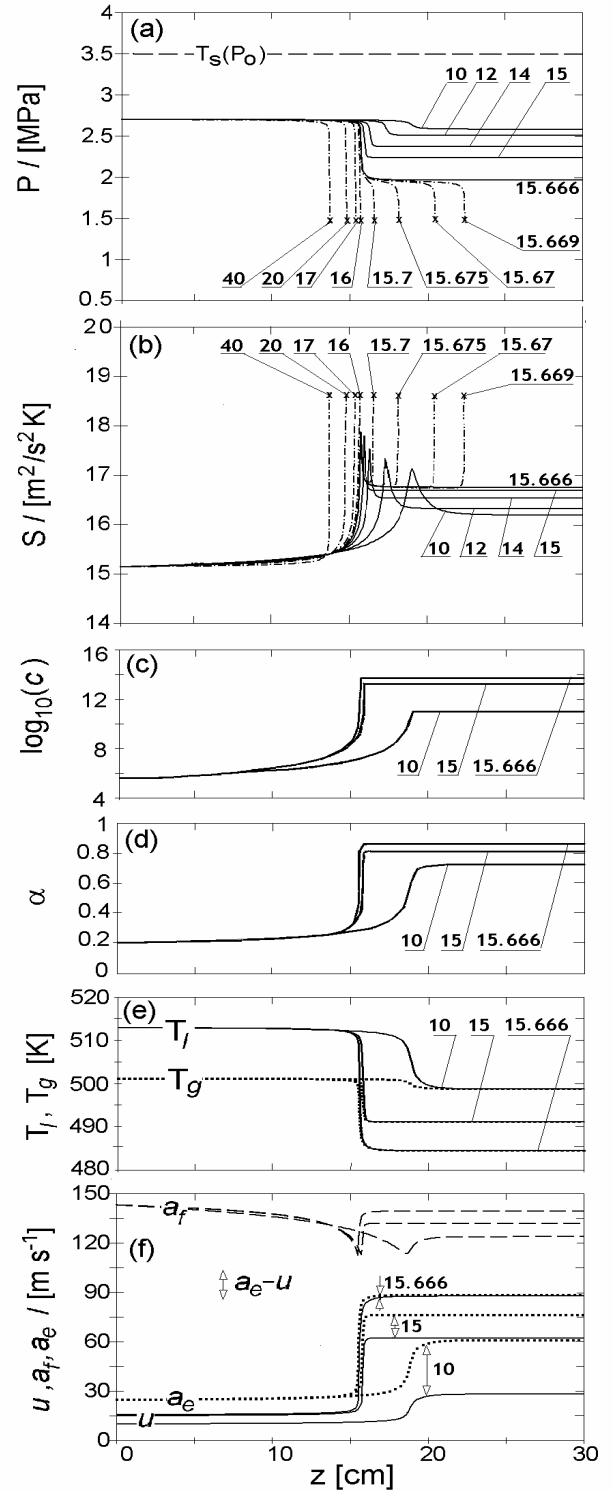


Figure 4. The structure of the boiling wave calculated using stationary model equations. The parameters at $z=0$ (except for the velocity of the oncoming flow) are specified being equal to that ahead of the wave front obtained in the numerical experiment using nonstationary model version. The curves correspond to different values of the flow velocity in front of the wave (shown in m s^{-1}). (a,b) The distribution of the pressure and entropy along the channel for different regimes. (c,d,e,f) The distribution of the other parameters for 3 wave-type regimes.

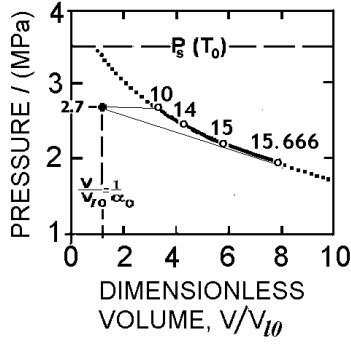


Figure 6. The Hugoniot curve with energy release, the dependence of the specific mixture volume on the pressure behind the wave. Points marked correspond to regimes with different velocities of the flow ahead of the wave's front (shown in m s^{-1}).

interphase heat exchange j approaches to zero, $du/dz \rightarrow 0$ and the chain fragmentation is switched off. $dP/dz \rightarrow 0$ as well. As a result, 'step like' solutions (solid lines in figure 4a) are obtained. The regimes of this type are realized under the oncoming velocity $10\text{m/s} \leq u^* \leq 15.666\text{m/s}$. Entropy distribution along the channel shows entropy peak in the coordinate of the wave front. (The explanation why the entropy increase in a rarefaction wave does not contradict the 2nd law of thermodynamics may be found in the next paragraph.) The entropy value in the peak corresponds to the pressure wave amplitude, the greater the pressure fall the greater the rise in the entropy. Maximum entropy production is attained under a limit oncoming velocity value $u^* = 15.666\text{m s}^{-1}$ when the flow accelerates up to the equilibrium sonic speed a_e (figure 4f). This is the regime that is realized in the calculations with the full model, as the condition $u = a_e$ ensures the 'linkage' of the wave of boiling with the waves following it.

At u^* greater than 15.666m s^{-1} , the flow velocity increases up to the sonic one $u = a_e$ earlier than the phases come to equilibrium. The denominator in right part of (20) becomes equal to zero, parameters' gradients tend to infinity and the solutions break off (the regimes under $u^* > 15.666\text{m s}^{-1}$ are shown by dashed-dotted lines in figure 4a). Broken-off solutions are of two types: with the pressure break-down behind the wave front section ($15.666 < u^* < 16$), and with the pressure tearing off at once ($u^* \geq 16\text{m/s}$). The 'broken' entropy distributions are of two types as well (figure 4b).

INTEGRAL RATIOS IN FRONT OF THE BOILING SHOCK

Let us now explain why the regime with the flow velocity behind the wave equal to the equilibrium sonic speed is the one realised in a numerical experiment using a full, non-stationary, model.

The state with parameters fixed ahead of the wave front in the numerical experiment will be considered to be an initial one. For the terminal state, we claim boiling to be equilibrium: $T_l = T_s(P)$. We will link the states by the laws of the mass, impulse and energy conservation (17-19).

Let us build the dependence of the specific mixture volume on the pressure behind the wave (the Hugoniot curve).

Excluding velocities from (17-19) we obtain:

$$i_e(P, V) - i(P_0, V_0, \Delta T_{l0}) = \frac{1}{2}(V + V_0)(P - P_0) \quad (22)$$

Where the 1st and the 2nd terms in the left-hand part are the enthalpies of an equilibrium and nonequilibrium (ahead of the wave) mixture, correspondingly; ΔT_{l0} is the liquid's overheat. Inserting

$$i(P_0, V_0, \Delta T_{l0}) - i_e(P, V) = Q_l(P_0, V_0, \Delta T_{l0}), \quad (23)$$

we obtain the equation for an equilibrium Hugoniot curve from (22):

$$i_e(P, V) - i_e(P_0, V_0) - \frac{1}{2}(V + V_0)(P - P_0) = Q_l(P_0, V_0, \Delta T_{l0}) \quad (24)$$

Since $\chi = \chi(P, V)$, $i_g = i_g(P)$, the only component of mixture enthalpy (9) depending on the mixture overheats is the liquid enthalpy. In correspondence with (11), (12) this dependence may be presented as follows:

$$i_{l0}(P_0, \Delta T_{l0}) = i_{le}(P_0) + c_l \Delta T_{l0}, \quad i_{le}(P_0) = i_{ls}(T_s(P_0)).$$

Having substituted this equation for i_{l0} into (9) we obtain the expression for the inequilibrium mixture enthalpy in the form:

$$i(P_0, V_0, \Delta T_{l0}) = i_e(P_0, V_0) + (1 - \chi_0)c_l \Delta T_{l0}. \quad (25)$$

The second term in the right-hand part of this expression is the energy of an initial liquids' overheat. Comparing (23) with (25) we see that

$$Q_l(P_0, V_0, \Delta T_{l0}) = (1 - \chi_0)h \Delta T_{l0}.$$

That is Q_l is positive. For waves with $Q_l > 0$, it has been shown that the entropy increases across the wave front for both compression and rarefaction waves, in contrast to waves with $Q_l \leq 0$. Thus the entropy increase in a rarefaction wave (figure 4a,b) does not contradict the second law of thermodynamics.

The equation for the equilibrium sonic speed may be obtained by differentiating of the equation for the equilibrium mixture state:

$$\begin{aligned} \frac{1}{a_e^2} &= \left(\frac{\partial \rho}{\partial P} \right)_{S=\text{const}} = \\ &= \frac{\rho^2}{\rho_l^2 a_l^2} + \rho \left[\left(1 - \frac{\rho}{\rho_l} \right) \frac{1}{\varphi} \left(\frac{\partial^2 T}{\partial P^2} \right)_S - \frac{\rho \varphi}{\rho_l T} \left(\rho_l \left(\frac{\partial i_l}{\partial P} \right)_S - 1 \right) \right]. \end{aligned}$$

Under the analysis usually carried for Hugoniot curves with heat release [9], it has been shown that a maximal flow rate through the shock wave front is attained when the flow rate behind the wave front is equal to the equilibrium sonic speed since the flow is equilibrium behind the wave.

Among the wave-type stationary regimes there is one with the flow speed equal to the equilibrium sonic speed behind the wave front (under $u^* = 15.666\text{m/s}$ in figure 4f), this regime being just the one obtained in a numerical experiment using full, nonstationary, boiling flow model equations. The realization of the regime with a maximum mass flow rate may be regarded as the implementation of Jouguet's hypothesis set up for combustion waves for the waves of boiling.

CONCLUSIONS

The phenomenon of shock boiling under a high-pressure-vessel decompression has been simulated using boiling flow model which considers phases to be non-equilibrium in temperatures and velocities.

The shock wave structure investigation using stationary equations in the moving frame linked with the wave's front has shown that a quick boiling mixture transformation into an equilibrium state is caused by a chain bubble fragmentation which led to a fast loss of liquid's excess heat by means of a sharp increase in the interfacial area.

For the stationary model system solution, all the parameters ahead of the wave front but the velocity of the oncoming flow were taken from the numerical experiment using a full, non-stationary, system of model equations. There were obtained a set of wave-type regimes each characterizing by a definite meaning of the entropy increase in a shock. It occurred that, in a numerical experiment on depressurization that was in good agreement with the physical one there realized the regime with the maximum entropy production.

ACKNOWLEDGMENT

The work was supported by the Russian Foundation for Basic Research (grant no. 12-08-162a).

NOMENCLATURE

Symbol	Quantity	SI Unit
a	Speed of sound	m s^{-1}
A	Approximation parameter	$\text{m}^2 \text{s}^{-2}$
c	Bubble number per unit mixture mass	kg^{-1}
B	specific heat of the liquid on saturation curve	$\text{m}^2 \text{s}^{-2} \text{K}^{-1}$
C_{vm}	Virtual mass coefficient	dimensionless
C_μ	Interfacial drag coefficient	dimensionless
D	Constant in the approximation dependence for liquid enthalpy on a saturation curve	K
G	Mass flow rate	$\text{kg m}^{-2} \text{s}^{-1}$
h	Specific heat capacity of the liquid	$\text{m}^2 \text{s}^{-2} \text{K}^{-1}$
i	Specific enthalpy	$\text{m}^2 \text{s}^{-2}$
$I(\lambda)$	Decrement of a wave	s^{-1}
j	Intensity of liquid evaporation into a bubble	kg s^{-1}
Ja	Jacob number	dimensionless
k	Constant in the equation for the liquid state	$\text{m}^3 \text{kg}^{-1}$
K	Constant number symbol	dimensionless
l	Specific heat of liquid vaporization	$\text{m}^2 \text{s}^{-2}$
n	Bubble number per unit mixture volume	m^{-3}
Nu	Nusselt number	dimensionless
P	Pressure	$\text{kg m}^{-1} \text{s}^{-2}$
r	Bubble radius	m
Re	Bubble Reynolds number	dimensionless
S	Entropy	$\text{m}^2 \text{s}^{-2} \text{K}^{-1}$

t	time	s
T	Temperature	K
u	Velocity	m s^{-1}
V	Specific volume	$\text{m}^3 \text{kg}^{-1}$
We	Weber number	dimensionless
x	Coordinate	m
z	Coordinate in a moving frame	m
α	Volumetric vapour fraction	dimensionless
β	Coefficient of the liquid compressibility	$\text{kg m}^{-2} \text{s}^{-1}$
χ	Mass vapour fraction	dimensionless
γ	Coefficient of the thermal conductivity for the liquid	$\text{kg m s}^{-3} \text{K}$
λ	Wavelength	m
μ	Dynamic viscosity coefficient	$\text{kg m}^{-1} \text{s}^{-1}$
ρ	Mixture density	kg m^{-3}
σ	Coefficient of the surface tension	kg s^{-2}
τ	Fragmentation time	s
ξ	Perturbation amplitude	m
ψ	Intensity of bubble fragmentation	$\text{kg}^{-1} \text{s}^{-1}$
e	Refers to the 'equilibrium' mixture characteristic	
f	Refers to the 'frozen' mixture characteristic	
g	Refers to the vapour phase	
l	Refers to the liquid phase	
s	Refers to a saturation condition	
0	Refers to an initial condition	
$*$	Refers to a critical condition	

REFERENCES

- [1] A.R. Edwards and T.P. O'Brien, Studies on phenomena connected with the depressurization of water reactors, *J. Brit. Nucl. Engng Soc.*, vol. 9, pp. 125–135, 1970.
- [2] O.A. Isaev, Liquid boiling under a fast pressure fall in an adiabatic unsteady stream, Ph.D. thesis, Sverdlovsk, 1980 (in Russian).
- [3] W.S. Jr. Winters and H.Jr. Merte, Experiments and nonequilibrium analysis of pipe blowdown, *Nucl. Sci. Engng.*, vol 69 (3), pp. 411–429, 1979.
- [4] A.I. Ivandaev and A.A. Gubaidullin, The investigation of an unsteady efflux of boiling liquid in a thermodynamically equilibrium approximation, *Teplofiz. Vys. Temp.*, vol 16 (3), pp. 556–562, 1978 (in Russian).
- [5] G. Lamb, *Hydrodynamics*, Cambridge University Press, Cambridge, 1957.
- [6] R.I. Nigmatulin and K.I. Soplentkov, The study of an unsteady efflux of boiling liquid from channels in the thermodynamically non-equilibrium approximation, *Teplofiz. Vys. Temp.*, vol. 18 (1), pp. 118–131, 1980 (in Russian).
- [7] L.E. Scriven, On the dynamics of phase growth, *Chem Engng Sci.*, vol. 10, pp. 1–13.
- [8] O.E. Ivashnyov and K.I. Soplentkov, A model involving break-up to explain peculiarities of boiling liquid efflux process, *Intl J. Multiphase Flow*, vol. 18 (5), pp. 727–738, 1992.
- [9] N.N. Smirnov and I.N. Zverev, *Heterogeneous burning*, Moscow University Press, Moscow, 1992 (in Russian).

THE THERMODYNAMIC STATES OF A FLUID IN A JOULE-THOMSON PROCESS INVOLVING PHASE CHANGES AT INTERFACES WITH LARGE CURVATURE

Thomas Loimer

Institute of Fluid Mechanics and Heat Transfer, Vienna University of Technology,
Resselgasse 3, 1040 Wien, Austria
E-mail: thomas.loimer@tuwien.ac.at

ABSTRACT

In the classical experiment of Joule and Thomson, a gas passes through a porous plug. The pressure difference between the upstream and the downstream side of the porous plug causes a temperature difference. Here, the flow process is described for the case that the fluid may condense, and the pressure loss is caused by a thin capillary. The process is calculated assuming local thermodynamic equilibrium and one-dimensional temperature and pressure distributions, respectively.

A vapor far from saturation does not condense, and the temperature and pressure distribution for the common Joule-Thomson process is recovered. A vapor close enough to saturation may condense partially or completely, and a liquid or a two-phase mixture flows through a part of the capillary. The thermodynamic path of the fluid is presented in temperature-entropy and pressure-temperature diagrams.

INTRODUCTION

In an adiabatic throttling or Joule-Thomson process, the contribution of the kinetic energy to the energy balance is negligible. The enthalpies of the fluid are the same upstream and downstream of the region where a pressure loss occurs. For gases, the Joule-Thomson coefficient, i.e., the change of temperature with respect to pressure at constant enthalpy, $\mu_{JT} = (\partial T / \partial p)_h$, may be positive or negative. Vapors, i.e., fluids in a gaseous state below the critical temperature, always have a positive Joule-Thomson coefficient. Hence, a vapor undergoing a Joule-Thomson process always has a downstream temperature which is smaller than the upstream temperature.

The temperature difference causes the transport of heat, usually by conduction, in downstream direction. However, a vapor at or close to saturation upstream of the tube may not be able to release a sufficient amount of heat by cooling down. Instead, the vapor must condense, either partially or completely. The heat released by condensation is consumed further downstream by evaporation of the partially or fully condensed fluid.

The temperature field of the flow through a long, thin capillary may be approximated by a one-dimensional temperature distribution, and a one-dimensional description of the flow becomes possible. A one-dimensional description is also applicable to the flow through a porous medium, if the porous medium is modeled as a bundle of equivalent capillaries. Hence, results obtained for the flow through a porous medium may also be applied to the flow of a fluid through a capillary.

Schneider [1] described the one-dimensional flow of a fluid that is in an upstream state of a saturated vapor through a porous medium. Schneider did not account for effects of capillarity, such as capillary condensation or the pressure difference across curved menisci, but assumed that phase changes occur at plane interfaces. He observed that, due to the Joule-Thomson effect, a saturated vapor that flows through a porous medium must condense.

A critical permeability was given for the porous medium. With respect to the flow through a capillary, this is equivalent to a critical radius. For a radius of the capillary below the critical value, the vapor condenses completely. For a radius of the capillary larger than the critical radius, the fluid condenses partially, and a two-phase mixture flows through a part of the capillary. The value of the critical radius depends on the properties of the fluid and on the thermal conductivity in the flow region. For common substances, the critical radius is of the order of 10 nm. The critical radius may be much larger for very good heat conductors.

The, usually, very small value of the critical radius may be the reason that the Joule-Thomson effect did not receive much attention under conditions where phase changes occur. Confer, for instance, the remark of Tien [2], who stated, with respect to the flow of vapors through porous media, that 'Another basic thermodynamic phenomenon that may play an interesting role in heat-pipe performance under certain conditions has never been mentioned or analyzed in the literature. This is the Joule-Thomson effect of real gas flow.'

Capillary effects, which dominate the flow, were investigated more thoroughly. Rhim and Hwang [3] investigated the flow of vapors near saturation through porous Vycor glass. They did not account for the Joule-Thomson effect, but for capillary condensation, adsorption and the large capillary pressure across curved interfaces between the liquid and the vapor phase. They found that the mass flow of a fluid under conditions where condensation occurs is greatly enhanced with respect to the mass flow of a vapor that does not condense. They also observed that, because a large amount of heat is evolved due to condensation and evaporation within the porous medium, the fluid can not stay isothermal. However, later, in their seminal work Lee and Hwang [4] described the flow of a vapor through a porous medium as an isothermal process.

Based on the approach of Schneider [1], the Joule-Thomson process of a vapor was analyzed, including also the effects of

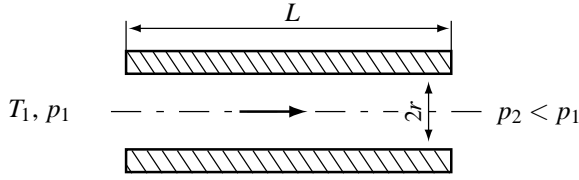


Figure 1. Sketch of the flow.

capillarity [5; 6]. A modified expression for the critical permeability [6] or for the critical radius of a capillary [7] was given. It was found that the mass flow rates calculated by applying an isothermal description were an order of magnitude larger than the mass flow rates calculated from an adiabatic, non-isothermal description [8]. Experimentally measured mass flow rates were still smaller than those obtained from the adiabatic description [8].

These results suggest that capillary forces may dominate the flow. However, in turn, the capillary forces are notably influenced by the small variation due to the Joule-Thomson effect. Consider a situation where a liquid plug is located inside a capillary. At both ends of the liquid plug curved interfaces are formed. The pressure differences across the curved interfaces are large, and large forces are exerted on the liquid on both ends of the liquid plug. However, because these forces act in opposite directions, they sum up to zero. If the thermodynamic equilibrium at one end of the plug changes, e.g., by heating up one end, a large force equal to the difference of the capillary forces remains and acts on the liquid plug. This perception is somehow supported by the observation that, over a wide range of contact angles, the mass flow rate is independent of the contact angle [7].

The states of a fluid that flows through a small capillary, with and without phase changes, are presented further below.

THEORETICAL DESCRIPTION

The flow configuration is sketched in Fig. 1. A vapor is in a state p_1, T_1 upstream of the end of a tube. The pressure p_2 downstream of the tube is smaller than the pressure at the upstream side, $p_2 < p_1$. Due to the Joule-Thomson effect, the temperature T_2 at the downstream side is also smaller than the temperature T_1 upstream of the tube. The length of the capillary is L , which is large compared to the inner diameter $2r$. The walls of the tube contribute to the heat transfer in longitudinal direction. However, there is no heat transfer in radial direction, which can be achieved either by isolating the tube adiabatically against the surrounding or by placing a large number of the same tubes in parallel.

Governing equations

The flow is governed by the balances of mass, momentum and energy,

$$\dot{m} = \text{constant}, \quad (1)$$

$$\dot{m} = -\frac{r^4 \pi}{8\nu} \frac{dp}{dz}, \quad (2)$$

$$\dot{m}h + r^2 \pi \dot{q} / \varepsilon = \text{constant}. \quad (3)$$

Here, \dot{m} denotes the mass flow rate, ν refers to the viscosity of the fluid, p is the pressure, z the spatial coordinate, h refers to

the specific enthalpy of the fluid and \dot{q} denotes the heat flux. The ratio of the inner to the outer cross-sectional area of the tube is given by ε . The Reynolds-number is small, hence the law of Hagen-Poiseuille is applied, Eq. (2). The heat flux is given by Fourier's law of heat conduction,

$$\dot{q} = -k_{mf} \frac{dT}{dz}, \quad (4)$$

where T is the absolute temperature and k_{mf} is the effective thermal conductivity of the fluid-filled tube,

$$k_{mf} = (1 - \varepsilon)k_m + \varepsilon k_f. \quad (5)$$

Here, k_m and k_f refer to the thermal conductivities of the solid tube material and the fluid, respectively.

Two-phase flow within the membrane is modeled as homogeneous flow,

$$x = \frac{\alpha v_{2ph}}{v_g}, \quad \dot{x} = x, \quad (6)$$

$$v_{2ph} = \left(\frac{1 - \alpha}{v_l} + \frac{\alpha}{v_g} \right)^{-1}. \quad (7)$$

Here, x and \dot{x} are the mass fraction and the mass flow fraction of the vapor, respectively, α is the vapor volume fraction and v_l, v_g and v_{2ph} refer to the specific volumes of the liquid phase, the gaseous phase and the two-phase mixture of the fluid, respectively. The effective kinematic viscosity and the effective thermal conductivity of the two-phase mixture, ν_{2ph} and k_{2ph} , are given by

$$\nu_{2ph} = (\alpha \mu_g + (1 - \alpha) \mu_l) \nu_{2ph}, \quad (8)$$

$$k_{2ph} = \alpha k_g + (1 - \alpha) k_l. \quad (9)$$

Here, μ_g and μ_l refer to the dynamic viscosities and k_g and k_l to the thermal conductivities of the gaseous and the liquid phase, respectively.

At interfaces between the liquid and the gaseous phase of the fluid within the tube, the pressure difference is given by the Young-Laplace equation,

$$p_{cap} = \frac{2\sigma \cos \theta}{r}, \quad (10)$$

where σ refers to the surface tension and θ is the contact angle. The pressure of the vapor phase of the fluid at a front of phase change, p_K , is given by Kelvin's equation,

$$\ln \left(\frac{p_K}{p_{sat}} \right) = -\frac{2\sigma \cos \theta}{r} \frac{v_l}{RT}. \quad (11)$$

Here, p_{sat} is the saturation pressure at a plane interface and R refers to the specific gas constant. Within the tube, a phase change occurs if the pressure of a vapor rises to $p = p_K(T)$, or if the pressure in the liquid falls below $p = p_K(T) - 2\sigma(T) \cos \theta / r$. With respect to the condition at a plane interface, the pressures at a curved interface are different in the

gaseous and the liquid phase. On both sides of the interface work is done on the fluids to bring them from their states at a plane interface to their respective states at a curved interface. These works must be added to the enthalpy of vaporization at a plane interface. Therefore, the specific enthalpy of vaporization at fronts of phase change within the porous membrane, $h_{\text{vap,K}}$, is given by

$$\Delta h_{\text{vap,K}} = \Delta h_{\text{vap}} + (p_{\text{K}} - p_{\text{sat}}) \times \left(\left(\frac{\partial h_{\text{g}}}{\partial p} \right)_T - \left(\frac{\partial h_{\text{l}}}{\partial p} \right)_T \right) + \left(\frac{\partial h_{\text{l}}}{\partial p} \right)_T \frac{2\sigma \cos \theta}{r}. \quad (12)$$

Here, Δh_{vap} is the specific enthalpy of vaporization at a plane interface and h_{l} and h_{g} denote the specific enthalpies of the liquid and the gaseous phase, respectively.

For the flow of a single phase of a fluid, Eqs. (1) to (3) and (4) yield, together with, e.g., initial conditions for \dot{m} , $\dot{m}h + \dot{q}$, T and p , a well-posed initial value problem for the variables T and p in dependence of z . For two-phase flow, pressure and temperature are not independent of each other. Instead, two independent variables are, e.g., T and α , and the dependence between T and p must be formulated. To determine the gradient $(dp/dT)_{2\text{ph}}$ in a two-phase region in dependence of T and α , the marginal cases of $\alpha \rightarrow 1$ and $\alpha \rightarrow 0$ are considered. The first case is equivalent to the state of a vapor that is in equilibrium with its liquid phase at a curved meniscus, hence, $(dp/dT)_{\alpha \rightarrow 1} = dp_{\text{K}}/dT$. The second case is equivalent to the state of the liquid at the other side of the meniscus, $(dp/dT)_{\alpha \rightarrow 0} = d(p_{\text{K}} - 2\sigma \cos \theta / r) / dT$. For homogeneous two-phase flow the pressure gradient is put as the volume-averaged mean of the pressures in the liquid and the gaseous phases, respectively,

$$\left(\frac{dp}{dT} \right)_{2\text{ph}} = \frac{dp_{\text{K}}}{dT} - (1 - \alpha) \frac{2 \cos \theta}{r} \frac{d\sigma}{dT}. \quad (13)$$

The boundary conditions complete the governing system of equations. They are

$$T = T_1, p = p_1, \dot{q} = 0 \quad \text{at } z \rightarrow -\infty, \quad (14)$$

$$p = p_2, \dot{q} = 0 \quad \text{at } z = L. \quad (15)$$

The system of governing equations is solved numerically. A shooting method is used to solve the boundary value problem. First, the downstream state of the fluid is completely determined. With $h_2 = h_1$, the downstream temperature T_2 is calculated by integration along an isenthalpic line,

$$T_2 = T_1 + \int_{p_1}^{p_2} \left(\frac{\partial T}{\partial p} \right)_h dp. \quad (16)$$

Applying the initial conditions $T = T_2$, $p = p_2$ and $\dot{q} = 0$ at $z = L$, the governing equations are integrated in negative z -direction. Integration is iteratively repeated, each time changing the value of \dot{m} , until the condition $p(z=0) = p_1$ is fulfilled within a tolerance of $(p_1 - p_2)/1000$.

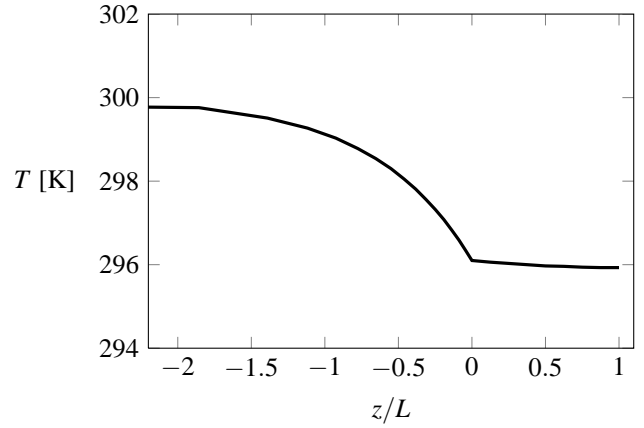


Figure 2. Temperature distribution in a Joule-Thomson process of a vapor without phase change. The tube extends from $z/L = 0$ to $z/L = 1$.

RESULTS

Results are presented for the flow of butane through a glass capillary. The thickness of the wall is half the inner radius, hence $\varepsilon = 0.44$. The thermal conductivity of glass is 0.5 W/m K . At a temperature of 300 K , the saturation pressure of butane is $p_{\text{sat}}(300 \text{ K}) = 2.57 \text{ bar}$. For a vapor that does not condense, the temperature-entropy and the pressure-temperature diagram is shown in Fig. 3. In this case, the upstream pressure is $p_1 = 2.1 \text{ bar}$ and the downstream pressure is $p_2 = 0.5 \text{ bar}$. The vapor cools down isobarically in front of the tube. Within the tube, the vapor expands nearly isothermally until it reaches the downstream pressure p_2 . Figure 2 shows the temperature distribution. The vapor expands nearly isothermally within the tube because the thermal conductivity of the tube material is much larger than the thermal conductivity of the vapor, 0.5 W/m K vs. 0.016 W/m K .

The path of the process in the temperature-entropy diagram in Fig. 3 shows that, even though the upstream state 1 and the downstream state 2 are both unsaturated vapors, condensation must occur if the path of the process crosses the line $p = p_{\text{K}}$. The line $p = p_{\text{K}}$ is depicted as a dotted line close to the line of saturated vapor in the T - s diagram. In the p - T diagram, the dashed line refers to $p = p_{\text{K}}$.

The states of a fluid when partial condensation occurs are shown in Fig. 4. With respect to the case shown in Fig. 3, the only condition which is changed is the upstream pressure, from $p_1 = 2.1$ to $p_1 = 2.3 \text{ bar}$. The two-phase mixture that flows through a part of the tube has a vapor mass fraction and also a liquid mass fraction of order unity. Hence, because the density of the liquid phase of the fluid is much larger than the density of the vapor phase, the volume fraction of the vapor is very close to one. The p - T diagram shows that the pressure in the two-phase mixture within the tube is close to p_{K} , the pressure of a vapor in the tube.

ACKNOWLEDGMENT

Financial support by Androsch International Management Consulting GmbH and by the OeAd-GmbH (Austrian Agency for International Cooperation in Education and Research), grants no. CZ 08/2012 and 09/2006, is gratefully acknowledged.

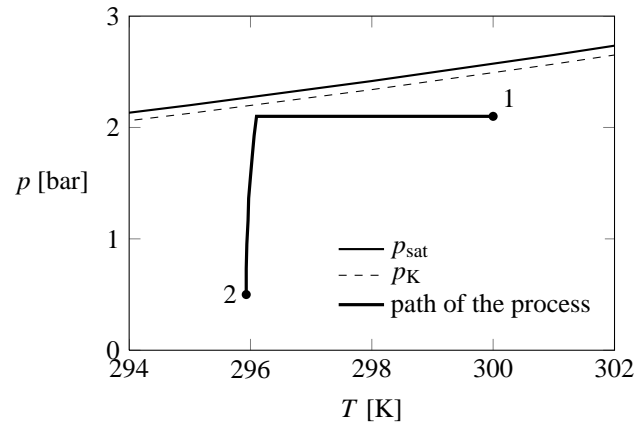
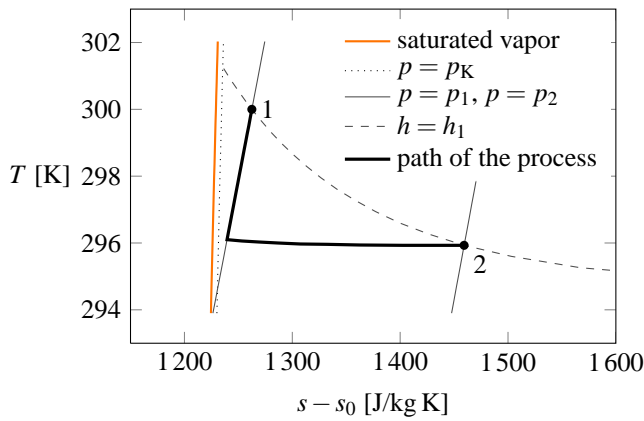


Figure 3. Joule-Thomson process of a vapor without phase change. States of the fluid in a temperature-entropy and a pressure-temperature diagram.

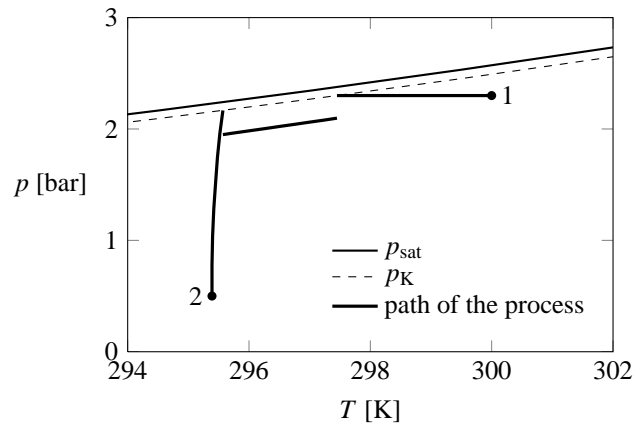
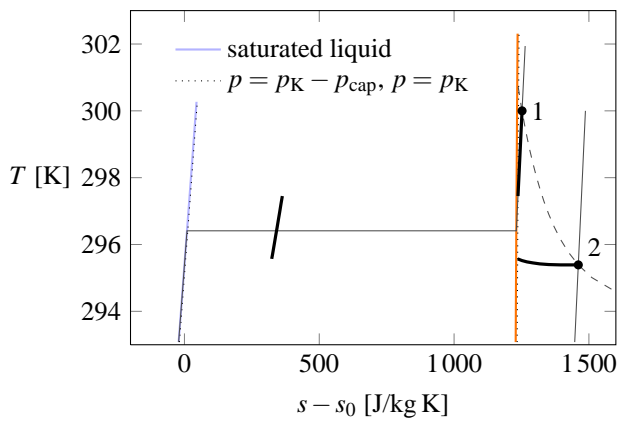


Figure 4. States of the fluid when partial condensation occurs. Temperature-entropy and pressure-temperature diagram. For remaining legend labels, see Fig. 3.

NOMENCLATURE

h	Specific enthalpy [J/kg]
k	Thermal conductivity [W/m K]
\dot{m}	Mass flow rate [kg/s]
p	Pressure [Pa]
\dot{q}	Heat flux [W/m ²]
R	Specific gas constant [J/kg K]
r	Radius [m]
T	Absolute temperature [K]
ν	Specific volume [m ³ /kg]
x	Vapor mass fraction
\dot{x}	Vapor mass flow fraction
z	Spatial coordinate [m]
α	Greek letters to follow
α	Vapor volume fraction [-]
ε	Void fraction [-]
θ	Contact angle [-]
μ	Dynamic viscosity [Pa s]
ν	Kinematic viscosity [m ² /s]
σ	Surface tension [N/m]

Subscripts

0	Reference state
1	Upstream state
2	Downstream state
2ph	Two-phase

cap	Capillary pressure, cf. Eq. (10)
f	Fluid
g	Gaseous
l	Liquid
K	Vapor pressure at a curved interface, cf. Eq.(11)
m	Solid material
sat	Saturation pressure

REFERENCES

- [1] W. Schneider. Vapor Flow Through a Porous Membrane — a Throttling Process with Condensation and Evaporation. *Acta Mech.*, vol. 47, pp. 15–25, 1983.
- [2] C. L. Tien. Fluid Mechanics of Heat Pipes. *Ann. Rev. Fluid Mech.* vol. 7, pp. 167–185, 1975.
- [3] H. Rhim and S.-T. Hwang. Transport of Capillary Condensate. *J. Colloid Interf. Sci.* vol. 52, pp. 174–181, 1975.
- [4] K.-H. Lee and S.-T. Hwang. The Transport of Condensable Vapors Through a Microporous Vycor Glass Membrane. *J. Colloid Interf. Sci.* vol. 110, pp. 544–555, 1986.
- [5] T. Loimer. Linearized Description of the Non-isothermal Flow of a Saturated Vapor Through a Micro-porous Membrane. *J. Membr. Sci.* vol. 301, pp. 107–117, 2007.
- [6] T. Loimer, P. Uchytíl, R. Petrickovic, and K. Setnickova. The Flow of Butane and Isobutane Vapors near Saturation Through Porous Vycor Glass Membranes. *J. Membr. Sci.* vol. 383, pp. 104–115, 2011.
- [7] T. Loimer. The Effect of the Contact Angle on a Flow with Condensation and Evaporation Through a Microchannel.

Proc. 6th International ASME Conference on Nanochannels, Microchannels and Minichannels, Darmstadt, Germany, June 23–25, Paper ICNMM2008-62167, pp. 321–326, 2008.

- [8] T. Loimer, P. Uchytíl, R. Petrickovic, and K. Setnicková. Isothermal and Adiabatic Flow of Vapors near Saturation Through Porous Membranes. *Eurotherm Seminar Nr. 84, Thermodynamics of Phase Changes, Namur, Belgium, May 24–27, 2009.*

ON THE LAGRANGE MULTIPLIERS METHOD IN EXTENDED THERMODYNAMICS OF IRREVERSIBLE PROCESSES

S.I. Serdyukov

Department of Chemistry, Moscow State University, 119992 Moscow, Russia
serdkv@tech.chem.msu.ru

ABSTRACT

In this paper we consider extended thermodynamic theory based on the postulate that entropy density is a function of the internal energy density and its time derivative. Using fundamental equation and the balance equation for the internal energy density, we can write the entropy balance equation and obtain expressions for the entropy flux and the entropy source. Further we consider tools of the rational thermodynamics, namely Lagrange multipliers method. We start from the entropy balance equation (entropy inequality) and suppose that entropy flux and entropy production are functions of the heat flux and heat flux rate. Definitions of the generalized temperature and new intensive quantity as functions of the Lagrange multipliers lead to the fundamental equation (generalized Gibbs equation) and explicit expressions for the entropy flux and entropy production.

INTRODUCTION

Conventional version of extended irreversible thermodynamics [1-5] is based on the postulate that entropy density s is function of the dissipative fluxes. Let us consider the heat conduction in a rigid isotropic body at rest without source term. For the system under consideration

$$s = s(u, \mathbf{q}), \quad (1)$$

where u is the internal energy density, \mathbf{q} the heat flux. In this paper, we consider extended thermodynamic theory [6-9] based on the postulate that the entropy density s is a function of the internal energy density u and time derivative \dot{u} :

$$s = s(u, \dot{u}), \quad (2)$$

where $\dot{u} = \partial u / \partial t$ and t is the time. The total differential of the entropy density has the form

$$ds = \frac{\partial s}{\partial u} du + \frac{\partial s}{\partial \dot{u}} d\dot{u}. \quad (3)$$

Let us define generalized temperature θ and new intensive quantity Λ in analogy with the classical theory:

$$\theta^{-1} = \frac{\partial s}{\partial u}, \quad \theta^{-1}\Lambda = \frac{\partial s}{\partial \dot{u}}, \quad (4)$$

where $\theta = \theta(u, \dot{u})$ and $\Lambda = \Lambda(u, \dot{u})$ depend on the additional variable \dot{u} . Then, the fundamental equation is given by

$$\theta ds = du + \Lambda d\dot{u},$$

and

$$\frac{\partial s}{\partial t} = \theta^{-1} \frac{\partial u}{\partial t} + \theta^{-1} \Lambda \frac{\partial \dot{u}}{\partial t}. \quad (5)$$

The second differential of the entropy density has the form

$$d^2 s = d\theta^{-1} du + d(\theta^{-1}\Lambda) d\dot{u}. \quad (6)$$

Further, let us postulate the convexity of s as function of u and \dot{u} . Then, we have inequality

$$\frac{\partial \theta^{-1}}{\partial t} \frac{\partial u}{\partial t} + \frac{\partial(\theta^{-1}\Lambda)}{\partial t} \frac{\partial \dot{u}}{\partial t} \leq 0. \quad (7)$$

GENERAL THEORY

The balance equations for the variable u ,

$$\rho \dot{u} = -\nabla \cdot \mathbf{q}, \quad (8)$$

(ρ is the mass density) relates the extra variables \dot{u} and \mathbf{q} . Differentiating equation (8) with respect to time leads to the balance equation for the variable \dot{u} :

$$\rho \frac{\partial \dot{u}}{\partial t} = -\nabla \cdot \dot{\mathbf{q}}, \quad (9)$$

where $\dot{\mathbf{q}} = \partial \mathbf{q} / \partial t$. Using balance equations (8), (9), from the fundamental equation (5), we obtain the entropy balance equation:

$$\rho \frac{\partial s}{\partial t} = -\nabla \cdot (\theta^{-1} \mathbf{q} + \theta^{-1} \Lambda \dot{\mathbf{q}}) + \mathbf{q} \cdot \nabla \theta^{-1} + \dot{\mathbf{q}} \cdot \nabla (\theta^{-1} \Lambda). \quad (10)$$

We can see that equation (10) is written in the standard form

$$\rho \dot{s} = -\nabla \cdot \mathbf{J}^s + \sigma, \quad (11)$$

where

$$\mathbf{J}^s = \theta^{-1} \mathbf{q} + \theta^{-1} \Lambda \dot{\mathbf{q}} \quad (12)$$

is the entropy flux,

$$\sigma = \mathbf{q} \cdot \nabla \theta^{-1} + \dot{\mathbf{q}} \cdot \nabla (\theta^{-1} \Lambda) \geq 0 \quad (13)$$

is the entropy source. According to the second law of thermodynamics, the entropy production is non-negative. Expression (13) shows that, to the heat flux \mathbf{q} , the thermodynamic force $\nabla \theta^{-1}$ corresponds, and to the time derivative $\dot{\mathbf{q}}$, the thermodynamic force $\nabla (\theta^{-1} \Lambda)$ corresponds.

As in classical irreversible thermodynamics we consider total entropy production

$$P = \int \sigma dV = \int [\mathbf{q} \cdot \nabla \theta^{-1} + \dot{\mathbf{q}} \cdot \nabla(\theta^{-1} \Lambda)] dV, \quad (14)$$

where V is the volume of the system. A part of the time derivative of the entropy production, $d_X P/dt$, has the form

$$\frac{d_X P}{dt} = \int \left[\mathbf{q} \cdot \frac{\partial}{\partial t} \nabla \theta^{-1} + \dot{\mathbf{q}} \cdot \frac{\partial}{\partial t} \nabla(\theta^{-1} \Lambda) \right] dV. \quad (15)$$

Let us transform (15) into

$$\begin{aligned} \frac{d_X P}{dt} = & - \int \left[\frac{\partial \theta^{-1}}{\partial t} \nabla \cdot \mathbf{q} + \frac{\partial(\theta^{-1} \Lambda)}{\partial t} \nabla \cdot \dot{\mathbf{q}} \right] dV + \\ & + \oint \left[\frac{\partial \theta^{-1}}{\partial t} \mathbf{q} + \frac{\partial(\theta^{-1} \Lambda)}{\partial t} \dot{\mathbf{q}} \right] \cdot \mathbf{n} d\Sigma, \end{aligned} \quad (16)$$

where \mathbf{n} is a unit vector directed outside along the normal to the surface, $d\Sigma$ is a surface element. When time-independent boundary conditions take place (θ and Λ are given), the surface integral becomes zero. Using equations (8), (9) and inequality (7), we obtain from (16) that

$$\frac{d_X P}{dt} = \int \rho \left[\frac{\partial \theta^{-1}}{\partial t} \frac{\partial u}{\partial t} + \frac{\partial(\theta^{-1} \Lambda)}{\partial t} \frac{\partial \dot{u}}{\partial t} \right] dV \leq 0 \quad (17)$$

Inequality (17) is extended evolution criterion, which is generalization of the Glansdorff-Prigogine criterion.

LINEAR THEORY

To a first approximation, the thermodynamic forces are linearly related to the corresponding fluxes and flux rates. Therefore, from expression (13), we have

$$\nabla \theta^{-1} = R_{11} \mathbf{q} + R_{12} \dot{\mathbf{q}}, \quad (18)$$

$$\nabla(\theta^{-1} \Lambda) = R_{21} \mathbf{q} + R_{22} \dot{\mathbf{q}}. \quad (19)$$

Thus, for a single irreversible process, we have obtained two phenomenological equations. According to the Onsager-Casimir principle, the matrix of the coefficients R_{ij} is antisymmetric, i.e.,

$$R_{12} = -R_{21}. \quad (20)$$

Using phenomenological equations (18) and (19), we replace the thermodynamic forces in expression (13) for the entropy production and obtain expression

$$\sigma = R_{11} \mathbf{q} \cdot \mathbf{q} + R_{22} \dot{\mathbf{q}} \cdot \dot{\mathbf{q}} \geq 0, \quad (21)$$

from which it follows that the diagonal coefficients are positive: $R_{11} > 0$, $R_{22} > 0$.

Let us transform phenomenological equation (18) in the form

$$\frac{R_{12}}{R_{11}} \frac{\partial \mathbf{q}}{\partial t} + \mathbf{q} = -\frac{1}{R_{11} \theta^2} \nabla \theta, \quad (22)$$

and consider Maxwell-Cattaneo law

$$\tau \frac{\partial \mathbf{q}}{\partial t} + \mathbf{q} = -\lambda \nabla T, \quad (23)$$

where T is the local-equilibrium temperature, τ is the relaxation time, λ is the thermal conductivity. Comparing

equations (22) and Maxwell-Cattaneo law (23), we find the expression for generalized temperature,

$$\theta = T, \quad (24)$$

and relationship between the coefficients: $R_{11} = 1/\lambda T^2$, $R_{12} = \tau/\lambda T^2$.

However, if heat conduction is governed by the dual-phase-lag equation,

$$\tau \frac{\partial \mathbf{q}}{\partial t} + \mathbf{q} = -\lambda \left(\nabla T + \varepsilon \frac{\partial \nabla T}{\partial t} \right), \quad (25)$$

then the comparison of the equation (22) with equation (25) gives a more complex linear approximation for the generalized temperature:

$$\theta = T + \varepsilon \frac{\partial T}{\partial t}. \quad (26)$$

Thus, in the proposed theory the generalized temperature is defined by the form of the constitutive equation.

LAGRANGE MULTIPLIES METHOD

In the previous sections the methods of classical irreversible thermodynamics was used. Further let us consider tools of the rational thermodynamics, namely Lagrange multipliers method proposed by Liu [10]. We start from the entropy balance equation which we write in the form

$$\rho \dot{s} + \nabla \cdot \mathbf{J} = \sigma \geq 0. \quad (27)$$

Apart from we suppose that entropy flux and entropy production are functions of the heat flux \mathbf{q} and heat flux rate $\dot{\mathbf{q}}$. So that constitutive relations are

$$s = s(u, \dot{u}), \quad \mathbf{J}^s = \mathbf{J}^s(\mathbf{q}, \dot{\mathbf{q}}), \quad \sigma = \sigma(\mathbf{q}, \dot{\mathbf{q}}). \quad (28)$$

Within this theory the constraints are given by the energy balance equation and time derivative of the energy balance equation which can be written in the form

$$\rho \dot{u} + \nabla \cdot \mathbf{q} = 0, \quad \rho \ddot{u} + \nabla \cdot \dot{\mathbf{q}} = 0. \quad (29)$$

Multiplication of the balance equations by Lagrange multipliers λ_1 , λ_2 and insertion this terms to the left-hand side of the entropy inequality (27) give more general expression:

$$\rho \dot{s} + \nabla \cdot \mathbf{J}^s - \lambda_1 (\rho \dot{u} + \nabla \cdot \mathbf{q}) - \lambda_2 (\rho \ddot{u} + \nabla \cdot \dot{\mathbf{q}}) \geq 0. \quad (30)$$

Let us represent time derivative of u and divergence of \mathbf{J}^s in the form

$$\dot{s} = \frac{\partial s}{\partial u} \dot{u} + \frac{\partial s}{\partial \dot{u}} \ddot{u}, \quad (31)$$

$$\nabla \cdot \mathbf{J}^s = \frac{\partial \mathbf{J}^s}{\partial \mathbf{q}} : \nabla \mathbf{q} + \frac{\partial \mathbf{J}^s}{\partial \dot{\mathbf{q}}} : \nabla \dot{\mathbf{q}}. \quad (32)$$

Using (31) let us make substitution in (30). After rearrangement we obtain inequality

$$\begin{aligned} \left(\frac{\partial s}{\partial u} - \lambda_1 \right) \rho \dot{u} + \left(\frac{\partial s}{\partial \dot{u}} - \lambda_2 \right) \rho \ddot{u} + \left(\frac{\partial \mathbf{J}^s}{\partial \mathbf{q}} - \lambda_1 \mathbf{U} \right) : \nabla \mathbf{q} + \\ + \left(\frac{\partial \mathbf{J}^s}{\partial \dot{\mathbf{q}}} - \lambda_2 \mathbf{U} \right) : \nabla \dot{\mathbf{q}} \geq 0, \end{aligned} \quad (33)$$

where we used equalities

$$\nabla \cdot \mathbf{q} = \mathbf{U} : \nabla \mathbf{q}, \quad \nabla \cdot \dot{\mathbf{q}} = \mathbf{U} : \nabla \dot{\mathbf{q}}. \quad (34)$$

Since inequality (33) becomes valid for completely arbitrary variation of the values \dot{u} , \ddot{u} , $\nabla \mathbf{q}$, $\nabla \dot{\mathbf{q}}$ (time derivatives of the independent variables u , \dot{u} and gradients of the flux \mathbf{q} and flux rate $\dot{\mathbf{q}}$), we have

$$\frac{\partial s}{\partial u} - \lambda_1 = 0, \quad \frac{\partial s}{\partial \dot{u}} - \lambda_2 = 0, \quad (35)$$

$$\frac{\partial \mathbf{J}^s}{\partial \mathbf{q}} - \lambda_1 \mathbf{U} = 0, \quad \frac{\partial \mathbf{J}^s}{\partial \dot{\mathbf{q}}} - \lambda_2 \mathbf{U} = 0. \quad (36)$$

Further, let us define generalized temperature θ and new intensive quantity Λ corresponding to variable \dot{u} by the equalities

$$\lambda_1 = \theta^{-1}, \quad \lambda_2 = \theta^{-1} \Lambda. \quad (37)$$

The first supposition of the classical approach is definitions of the intensive quantities (4). Within proposed theory, based on the Lagrange multipliers methods, definitions of the generalized temperature θ and new intensive quantity Λ (37) are last supposition.

Then, (31), (35) and (37) lead to the expression for \dot{s} :

$$\dot{s} = \theta^{-1} \dot{u} + \theta^{-1} \Lambda \ddot{u}. \quad (38)$$

We can see that Lagrange multipliers are functions of u and \dot{u} . From (36) we obtain that entropy flux \mathbf{J}^s is linear function of \mathbf{q} and $\dot{\mathbf{q}}$:

$$\mathbf{J}^s = \theta^{-1} \mathbf{q} + \theta^{-1} \Lambda \dot{\mathbf{q}}. \quad (12a)$$

Entropy balance equation (27) and equalities (38), (12a) lead to expression for the entropy production:

$$\sigma = \mathbf{q} \cdot \nabla \theta^{-1} + \dot{\mathbf{q}} \cdot \nabla (\theta^{-1} \Lambda) \geq 0. \quad (13a)$$

Linear theory on the basis of the expression (13a) can be obtained as in the previous section (see formulas (18)-(26)).

Equations (38), (12a) and (13a) are final result of the general theory. Using classical approach, we started from

the fundamental equation (5) and obtained the entropy balance equation (11). Lagrange multipliers method permits us to obtain fundamental equation (38) from the entropy balance equation (27).

REFERENCES

- [1] D. Jou, J. Casas-Vázquez and G. Lebon, *Extended Irreversible Thermodynamics*, 3rd edn., Springer, Berlin, 1996.
- [2] D. Jou, J. Casas-Vázquez and G. Lebon, *Extended Irreversible Thermodynamics Revisited (1988-98)*, Rep. Prog. Phys. vol. 62, pp. 1035-1142, 1999.
- [3] I. Müller and T. Ruggeri, *Extended Thermodynamics*, Springer, New York, 1993.
- [4] L.S. Garsia-Cólin and F.J. Uribe, *Extended irreversible thermodynamics beyond the linear regime: A critical overview*, J. Non-Equilib. Thermodyn., vol. 16, pp. 89-128, 1991.
- [5] R.E. Nettleton and S.L. Sobolev, *Applications of extended thermodynamics to chemical, rheological and transport processes. Part I. Approaches and scalar rate processes*, J. Non-Equilib. Thermodyn. vol. 20, pp. 205-229, 1995.
- [6] S.I. Serdyukov, *A new version of extended irreversible thermodynamics and dual-phase-lag model in heat transfer*, Phys. Lett. A, vol. 281, pp. 16-20, 2001.
- [7] S.I. Serdyukov and N.M. Voskresenskii, *Behavior of entropy in non-classical heat conduction of incompressible media*, J. Non-Equilib. Thermodyn., vol. 35, pp. 323-335, 2010.
- [8] S.I. Serdyukov, *Dual-phase-lag equations and entropy behavior in relaxation hydrodynamics*, Physica A., vol. 391, pp. 5871-5882, 2012.
- [9] S.I. Serdyukov, *Generalized temperature and non-classical heat conduction in rigid bodies*, J. Non-Equilib. Thermodyn., vol. 38, pp. 81-96, 2013.
- [10] I.-S. Liu, *Method of Lagrange multipliers for exploitation of the entropy principle*, Arch. Rat. Mech. Anal., vol. 46, pp. 131-148, 1972.

MULTITEMPERATURE MIXTURE OF PHONONS AND ELECTRONS AND NONLOCAL THERMOELECTRIC TRANSPORT IN NANOSYSTEMS

V. A. Cimmelli*, A. Sellitto**, D. Jou†

*University of Basilicata, Department of Mathematics, Computer Science and Economics, Potenza (Italy), E-mail: vito.cimmelli@unibas.it

**University of Basilicata, Department of Mathematics, Computer Science and Economics, Potenza (Italy), E-mail: ant.sellitto@gmail.com

†Autonomous University of Barcelona, Department of Physics, Bellaterra, Catalonia (Spain), E-mail: david.jou@uab.cat

EXTENDED ABSTRACT

In the past decades the need for more efficient materials for electronic refrigeration and power generation has driven a heightening interest in the field of thermoelectricity. Different thermoelectric materials are currently under investigation by many research groups. Some of them are focusing their efforts on minimizing the lattice thermal conductivity and others on getting large power factors.

Usually, the analysis is especially focused on computer simulations, or statistical mechanical analyses, while scant attention is paid to continuous models which may give strong physical grounds to practical research and to investigate new frontiers.

In this poster we present a mesoscopic model of thermoelectric effects in rigid bodies, leading to a system of enhanced thermoelectric balance equations, accounting for different phonon and electron temperatures and mutual energy exchanges. In particular, following the way drawn in recent papers [1; 2], we assume that the overall heat flux \mathbf{q} has two different contributions: the electron heat-flux contribution $\mathbf{q}^{(e)}$ and the phonon heat-flux one $\mathbf{q}^{(p)}$, such that

$$\mathbf{q} = \mathbf{q}^{(e)} + \mathbf{q}^{(p)}.$$

We regard the phonons and electrons as a mixture of gases flowing through the crystal lattice, each of which is endowed with its own temperature. Accounting for two different temperatures may be important, for instance, in

1. **Time-dependent situations: fast laser pulses.** When a laser pulse hits the surface of a system, initially the electrons capture the main amount of the incoming energy, with respect to the phonons. Subsequently, through the electron-phonon collisions, they give a part of it to the phonons. This may be of interest, for example, in the Raman thermometry (which is often utilized to measure the temperature in small electronic devices) or in information recording on optical discs (CD, DVD, Blu-Ray).
2. **Steady-state situations: nonequilibrium temperatures.** As the electron mean-free path ℓ_e is usually shorter than the phonon mean-free path ℓ_p , in heat propagation and when the longitudinal distance z is such that $\ell_e < z < \ell_p$, it is expected a very high number of electron collisions, and only scant phonon collisions. This yields that the electron temperature may reach its local-equilibrium value, whereas the phonon temperature is still far from its own local-equilibrium value.

Our goal will be pursued in the framework of Extended Irreversible Thermodynamics, the theory in which the dissipative fluxes are updated to the rank of thermodynamic variables and the gradients of the unknown fields are allowed to enter the state space [3; 4]. We also take advantage from the theory of mixtures of fluids with different temperatures, recently proposed in the literature [5; 6].

REFERENCES

- [1] D. Jou, V. A. Cimmelli and A. Sellitto, Nonlocal heat transport with phonons and electrons: Application to metallic nanowires, *Int. J. Heat Mass Transfer*, vol. 55, pp. 2338-2344, 2012.
- [2] A. Sellitto, V. A. Cimmelli and D. Jou, Thermoelectric effects and size dependency of the figure-of-merit in cylindrical nanowires, *Int. J. Heat Mass Transfer*, vol. 57, pp. 109-116, 2013.
- [3] G. Lebon, D. Jou and J. Casas-Vázquez, *Understanding nonequilibrium thermodynamics*, Berlin: Springer, 2008.
- [4] D. Jou, J. Casas-Vázquez and G. Lebon, *Extended Irreversible Thermodynamics*, Berlin: Springer, fourth revised ed., 2010.
- [5] H. Gouin and T. Ruggeri, Identification of an average temperature and a dynamical pressure in a multitemperature mixture of fluids, *Phys. Rev. E*, vol. 78, pp. 016303, 2008.
- [6] T. Ruggeri, Multi-temperature mixture of fluids, *Theoret. Appl. Mech.*, vol. 36, pp. 207-238, 2009.

DISSIPATION FLOW-FRAMES: PARTICLE, ENERGY, THERMOMETER

P. Ván^{1,2,3} and T.S. Biró¹

¹Dept. of Theoretical Physics, Wigner Research Centre for Physics, Institute for Particle and Nuclear Physics,
H-1525 Budapest, Konkoly Thege Miklós út 29-33, Hungary;

²Dept. of Energy Engineering, Budapest Univ. of Technology and Economics,
H-1111, Budapest, Műegyetem rkp. 3-9, Hungary;

³Montavid Thermodynamic Research Group

Email: van.peter@wigner.mta.hu

ABSTRACT

We associate the following physical co-mover conditions of to different frame choices: i) Eckart: particle flow, ii) Landau-Lifshitz: energy flow, iii) Jüttner: moving thermometer frame. The role of fixing a flow-frame is analysed with respect to local equilibrium concentrating on dissipative currents and forces in single component relativistic fluids. The special role of a "Jüttner frame" is explored and contrasted to the more common Eckart and Landau-Lifshitz choices.

INTRODUCTION

In dissipative theories of relativistic fluids we deal with four fundamental questions.

The first considers *causality*. Only divergence type theories are, in general, causal because there the symmetric hyperbolicity of the system of nonlinear evolution equations is established by construction [1; 2; 3; 4; 5; 6]. The weaker version of causality requires for the symmetric hyperbolicity only for the linearized equations, and allows for characteristic speeds less than the speed of light [7]. This weak causality was studied in the Israel-Stewart theory; numerous resulting inequalities are given in [8]. From a physical point of view the causality of theories with parabolic differential equations should also be possible. In this case the validity of the continuum description is restricted by the characteristic maximal speeds [9; 10; 11; 12]. A necessary condition for this type of restrictions requires the damping of the perturbations, equivalent to the linear stability of the theory [13].

The second question deals with *generic stability*. Generic stability is the linear stability of the homogeneous equilibrium solutions. The simplest relativistic generalization of the nonrelativistic Fourier-Navier-Stokes equations was proved to be unstable by Hiscock and Lindblom [14]. In the sequel they formulated mathematical conditions of generic stability of the Israel-Stewart theory [8] specified to the Eckart frame. However, due to the overwhelming complexity of these conditions they are not connected to reasonable properties of equations of state or transport coefficients. Since then several different propositions arose suggesting a first order theory, mostly motivated by the restoration of the generic stability [15; 16; 12; 17; 18; 19; 20; 21].

The third question is the correct *distinction between ideal and dissipative fluids*, especially in a relativistic context. It is customary to assume that perfect, nondissipative fluids are characterized by a special form of the energy-momentum tensor and the particle current density vector [22; 23]. On the other hand physical dissipation is accompanied by nonzero entropy produc-

tion. From this point of view there is a more extended family of perfect fluids beyond the customarily treated ones [24]. These distinctions are technically addressed by the so called matching conditions [25; 20; 21; 26].

Finally the proper choice of *flow-frames* continues to be an unsettled question [16]. One generally believes that in relativistic fluids the flow field u^a can be chosen arbitrarily, since it is a somewhat vaguely defined physical property, belonging to the flow of volatile quantities, once the energy, once the conserved charge. In this situation it is customary to fix the flow either to the motion of particles (Eckart frame) [27], or that of the energy density (Landau-Lifshitz frame) [28]. The flow fixing determines a continuous set of local rest frames in the fluid: we shall refer to the different choices of fixing the flow as *flow-frames or frames*. Contrary to the belief in a free choice of the flow-frame we point out that this may not be completely arbitrary, as one associates a given physical content of the dissipation to each. Further choices than the two classical ones should be preferred by demanding a given form of local Gibbs relations.

In this paper we present the general flow-frame, the separation of perfect and dissipative parts of energy-momentum and particle number current density and their relation to generic stability. The key theoretical aspect connecting these problems is relativistic thermodynamics. Our most important observation is that the usual assumption of kinetic equilibrium by introducing the velocity field parallel to the local thermometer and Lagrange multiplier field β^a also appearing in the collision invariant $\psi = \alpha + \beta_a k^a$, already acts as a flow-frame fixing. This choice we tag as thermometer frame or Jüttner frame, distinguishing from the Eckart, Landau-Lifshitz and other conventions.

GENERAL ONE COMPONENT DISSIPATIVE RELATIVISTIC FLUIDS

In this paper the Lorentz form is given as $g^{ab} = \text{diag}(1, 1, 1, 1)$ and all indexes a, b, c, \dots run over 0, 1, 2, 3. We use natural units, $\hbar = k = c = 1$.

THERMODYNAMICS OF RELATIVISTIC FLUIDS – EQUILIBRIUM

A single component fluid is characterized by the particle number four-vector N^a and the symmetric energy-momentum density tensor T^{ab} . The velocity field of the fluid, the flow-frame u^a , introduces a local rest frame and the basic fields N^a and T^{ab} can be expanded by their local rest frame components parallel and perpendicular to the flow:

$$N^a = nu^a + j^a, \quad (1)$$

$$T^{ab} = eu^a u^b + q^a u^b + u^a q^b + P^{ab}. \quad (2)$$

Here n is the flow-frame particle number density, j^a is in this frame the non-convective particle number current density, e is the energy density, q^a is the momentum density and P^{ab} is the pressure tensor. These components are flow-frame dependent, in particular $j^a u_a = 0$, $q^a u_a = 0$ and $P^{ab} u_b = 0$. Introducing the substantial time derivative $\frac{d}{dt} := u^a \partial_a$ denoted by and over-dot, the balances of the particle current density and energy-momentum are expressed by the local rest frame quantities:

$$\partial_a N^a = \dot{n} + n \partial_a u^a + \partial_a j^a = 0, \quad (3)$$

$$\begin{aligned} \partial_b T^{ab} &= \dot{e} u^a + e \dot{u}^a + e u^a \partial_b u^b + \dot{q}^a + q^a \partial_b u^b + \\ &u^a \partial_b q^b + q^b \partial_b u^a + \partial_b P^{ab} = 0^a. \end{aligned} \quad (4)$$

The energy and momentum balances are the time and space-like components of the energy-momentum balance projected in the flow-frame:

$$u_a \partial_b T^{ab} = \dot{e} + e \partial_b u^b + u_a \dot{q}^a + \partial_b q^b - P^{ab} \partial_b u_a = 0, \quad (5)$$

$$\Delta_c^a \partial_b T^{cb} = e \dot{u}^a + \Delta_b^a \dot{q}^b + q^a \partial_b u^b + q^b \partial_b u^a + \Delta_c^a \partial_b P^{cb} = 0^a \quad (6)$$

The frame related quantities are important in the separation of the ideal and dissipative parts of the basic fields. This separation is best performed by analyzing the thermodynamical relations. In order to achieve this one postulates the existence of an additional vector field, the entropy current as a function of the basic fields $S^a(N^a, T^{ab})$. It must not decrease by fulfilling the condition of the balances (3) and (4). That conditional inequality can be best represented by introducing the Lagrange-Farkas multipliers¹ α and β^a , respectively:

$$\Sigma := \partial_a S^a + \alpha \partial_a N^a - \beta_b \partial_a T^{ba} \geq 0. \quad (7)$$

The left hand side of this inequality shows, that the definition of the entropy production is done before specifying the flow-frame. However, the separation of ideal and dissipative parts of basic physical quantities, is a consequence to the choice of that flow-frame. Citing the authors of [32], when arguing about the uniqueness of the Landau-Lifshitz frame “The uniqueness of the energy frame comes from ... the physical assumption that the dissipative effect comes from only the spatial inhomogeneity“. However, what is spacelike is a frame dependent question and one hopes only that physical systems may reveal by their internal dynamics a physical ground for such a separation. A possible candidate for this separation can be the thermometer vector, β^a , reconstructable from observations of a multiparticle spectra stemming from a relativistic fluid.

The concept of perfect fluids deals with the absence of dissipation, the entropy production vanishes:

$$\Sigma_0 = \partial_a S_0^a + \alpha \partial_a N_0^a - \beta_b \partial_a T_0^{ba} = 0. \quad (8)$$

The equilibrium entropy density S_0^a is connected to the equilibrium particle number density N_0^a and equilibrium energy-momentum density T_0^{ab} by the following definition of the isotropic pressure:

$$p_0 \beta^a = S_0^a + \alpha N_0^a - \beta_b T_0^{ab}. \quad (9)$$

Standard kinetic theory definitions and calculations satisfy the above expressions. Then α and β^a are coefficients in the collision invariant of the equilibrium distribution function, $\psi = \alpha + \beta_a k^a$, and the pressure is that of an ideal gas $p_0 = n_0 T$.

Kinetic theory describes a perfect fluid by the detailed balance requirement. Out of equilibrium dissipation can occur. In a dissipative fluid all physical quantities in principle deviate from their local equilibrium values. There also may exist non-dissipative currents (presumably driven by non-dissipating forces, like the Lorentz force in magnetic fields). The thermodynamic approach aims at the separation of dissipative and non-dissipative local currents, in order to ensure the positivity of the expression (7). Physical freedom in the choice of a flow-frame should be restricted to different handlings of non-dissipative currents.

It is natural to introduce the *Jüttner frame* u_J^a defined by the direction of β^a (thermometer motion):

$$u_J^a = \frac{\beta^a}{\sqrt{\|\beta^a \beta_a\|}}. \quad (10)$$

In that frame the equilibrium fields are decomposed as:

$$N_0^a = n_J u_J^a, \quad (11)$$

$$T_0^{ab} = e_J u_J^a u_J^b - p \Delta_J^{ab}, \quad (12)$$

$$S_0^a = (\beta_J h_J - \alpha n_J) u_J^a, \quad (13)$$

where $h_J = e_J + p_0$ is the equilibrium enthalpy density in the Jüttner frame, and $\beta_J = \beta_a u_J^a = 1/T_J$ is the reciprocal Jüttner temperature. α , β_a and p_0 do not carry a frame index, because they are introduced before specifying the flow-frame. On the other hand the representations (11)-(13) are frame dependent. In case of a general flow-frame u^a , that is not parallel to β^a , one can characterize this difference by introducing $w^a = \beta^a / (\beta^b u_b) - u^a$. Then w^a is orthogonal to u^a ($w^a u_a = 0$) and spacelike ($w_a w^a = -w^2$). The Lagrange multiplier four-vector, β^a , can be splitted as

$$\beta^a = \beta_J u_J^a = \beta(u^a + w^a), \quad (14)$$

where $\beta = \beta^a u_a$ is the reciprocal temperature in a general frame

¹Lagrange multipliers are introduced for conditional extrema. For conditional inequalities Gyula Farkas suggested analogous quantities and proved the corresponding theorem of linear algebra, called Farkas' lemma [29; 30; 31].

defined by u^a . The equilibrium fields in this frame are given as

$$N_0^a = n_0 u^a + j_0^a, \quad (15)$$

$$T_0^{ab} = e_0 u^a u^b + q_0^a u^b + q_0^b u^a - p \Delta^{ab} + \frac{q_0^a q_0^b}{h_0}, \quad (16)$$

$$S_0^a = (\beta h_0 + \beta w_b q_0^b - \alpha n_0) u^a + \beta q_0^a - \alpha j_0^a. \quad (17)$$

Here $\beta = \beta_J / \sqrt{1-w^2}$, $n_0 = n_J / \sqrt{1-w^2}$, $e_0 = (e_J + p w^2) / (1-w^2)$, α and p_0 does not change, $j_0^a = n_0 w^a$, $q_0^a = h_0 w^a$ [24]. (15)-(17) and (11)-(13) are the forms of the same equilibrium fields in the Jüttner and in the general frames respectively. In the specific equilibrium the Jüttner, Eckart and Landau-Lifshitz frames coincide, the different choices lead to the same condition: $w_a = 0$.

THERMODYNAMICS OF RELATIVISTIC FLUIDS – OUT OF EQUILIBRIUM

In classical non-equilibrium thermodynamics, without internal variables, one assumes that the gradients of the equilibrium fields characterize the deviation from local kinetic equilibrium. In that case the concept of local equilibrium is not modified. The internal variable theories, like the Israel-Stewart theory [33; 34; 25; 35; 36] or GENERIC [37; 38], choose a different characterization: local equilibrium is modified, some *formerly dissipative currents appear among the state variables and as a consequence their contribution may reduce the entropy production*. The relativistic theories revealed that the flow-frame fixing plays a special role in the specification of local equilibrium. It has been an observation of Planck and Einstein, that the momentum density (energy current density) is not purely dissipative and therefore in relativistic theories it has to be taken into account even in local equilibrium [39; 40].

Our starting point is the fundamental inequality of the second law (7). We introduce the following relation of the fields out of equilibrium, as a generalization of (9):

$$S^a + \alpha N^a - \beta_a T^{ab} = \Phi^a. \quad (18)$$

With a general Φ^a this relation is valid without any restriction. In a general flow-frame, u^a , we define the thermostatic pressure as:

$$p = \frac{u_a \Phi^a}{\beta}. \quad (19)$$

Therefore the general form of the potential Φ^a can be written as

$$\Phi^a = \beta p (u^a + g^a), \quad \text{where } u^a g_a = 0. \quad (20)$$

The parallel and perpendicular components of (18) to the flow u^a are

$$s + \alpha n - \beta(h + w_b q^b) = 0, \quad (21)$$

$$J^a + \alpha j^a - \beta(q^a + w_b \Pi^{ab}) + \beta p (w^a - g^a) = 0^a, \quad (22)$$

where $h = e + p$ and $\Pi^{ab} = P^{ab} + p \Delta^{ab}$ is the viscous pressure. Then we rewrite the entropy production (7) with flow related

quantities:

$$\begin{aligned} \Sigma = \partial_a S^a + \alpha \partial_a N^a - \beta_a \partial_b T^{ab} = & -N^a \partial_a \alpha + T^{ab} \partial_a \beta_b + \partial_a \Phi^a = \\ & -n \dot{\alpha} + h \dot{\beta} + q^a (\beta w_a) + \beta \dot{p} + \Pi^{ab} \partial_a \beta_b - j^a \partial_a \alpha + q^a \partial_a \beta + \\ & \beta \dot{u}_b (q^b - h w^b) + \beta q^a u^b \partial_a w_b + p (g^a - w^a) \partial_a \beta + \\ & p \beta \partial^a (g^a - w_a) + g^a \beta \partial_a p. \end{aligned} \quad (23)$$

Thermodynamics is taken into account by the following two postulates.

1) *The underlined part in the above expression with proper time derivatives (total differentials) is zero.*

$$\beta \frac{d}{dt} p = n \frac{d}{dt} \alpha - h \frac{d}{dt} \beta - q^a \frac{d}{dt} (\beta w_a). \quad (24)$$

This is the relativistic Gibbs-Duhem relation. Considering this together with the vanishing differential of (21), we obtain the Gibbs relation [41]:

$$\beta (de + w_a dq^a) = ds + \alpha dn. \quad (25)$$

Based on this result we conclude that the entropy has to be given by a functional relationship between the local densities (but certainly including the momentum density q^a), i.e. the proper relativistic and local equation of state is a function $s(e, q^a, n)$. It has the following partial derivatives:

$$\left. \frac{\partial s}{\partial e} \right|_{q^a, n} = \beta, \quad \left. \frac{\partial s}{\partial n} \right|_{e, q^a} = -\alpha, \quad \left. \frac{\partial s}{\partial q^a} \right|_{e, n} = \beta w_a, \quad (26)$$

identifying the thermodynamical entropic intensive parameters as being β , $\alpha = \beta \mu$ and βw^a . The four-vector w^a is constrained by its orthogonality to the local flow, so it contains independent information on a spatial three-vector only. In isotropic media this degree of freedom is reduced to the length of this vector, w^2 . In cases containing radiation it appears as a velocity parameter of the Doppler shift [41].

By utilizing the above functional form of the equation of state one derives that the pressure, the intensive parameter associated to mechanical work, satisfies the following four-vector generalized Gibbs-Duhem relation, now written by the traditional differentials:

$$\beta \partial_a p = n \partial_a \alpha - h \partial_a \beta - q^b \partial_a (\beta w_b). \quad (27)$$

2) *Our second postulate is $g^a = w^a$.* By doing so we spell out the fundamental compatibility of non-equilibrium (18) with the equilibrium (9) definitions of pressure. In this way we treat the non-dissipative part of the thermodynamical potential, and with that the influence of the pressure gradient on the entropy production rate possibly closest to the ideal gas behavior. This is a special matching condition known from kinetic theory ($\delta n = 0$, $\delta e = 0$): in this case the pressure four-vector Φ^a is parallel to the thermometer vector β^a .

Now a short calculation reduces (23) to a form collecting terms according to the gradients of intensives. A chemical diffusion part is associated to $\partial_a \alpha$, a heat diffusion (Fourier-) part

to the gradient of β , and finally a viscosity term with the symmetric gradient tensor of the full four-vector $\partial_a \beta_b$. We also gain one further term containing the gradient of the difference between u^a and w^a . The antisymmetry of the multiplier enforces the antisymmetry of this velocity related gradient, therefore this term we tag as "vorticity". We arrive at the following expression:

$$\begin{aligned} \Sigma &= (nw^a - j^a)\partial_a \alpha + (q^a - hw^a)(\partial_a \beta + \beta \dot{u}_a) \\ &+ (\Pi^{ab} - q^{(a} w^{b)})\partial_a \beta_b + q^{[b} w^{a]}\partial_a (\beta(u_b - w_b)) \geq 0. \end{aligned} \quad (28)$$

Here $q^{(a} w^{b)}$ and $q^{[a} w^{b]}$ denotes the symmetric and antisymmetric parts of $q^a w^b$ respectively. (28) is the entropy production rate without fixing the flow-frame. For a perfect fluid, characterized by (15)-(16), the local entropy production is zero. Now it is straightforward to identify thermodynamic fluxes and forces and establish functional relationships, that are strictly linear in the first approximation²:

	Diffusive	Thermal	Viscous	Vortical
Fluxes	$nw^a - j^a$	$q^a - hw^a$	$\Pi^{ab} - q^{(a} w^{b)}$	$q^{[b} w^{a]}$
Forces	$\nabla^a \alpha$	$\nabla^a \beta + \beta \dot{u}^a$	$\Delta^{(bc} \nabla^a) \beta_c$	$\Delta^{[bc} \nabla^a] (\beta(u_c - w_c))$

Table 1. Thermodynamic fluxes and forces in a general flow frame

Here $\nabla_a = \Delta_a^b \partial_b$. The corresponding linear response relations for isotropic continua are:

$$nw^a - j^a = D \nabla^a \alpha + \sigma (\nabla^a \beta + \beta \dot{u}^a), \quad (29)$$

$$q^a - hw^a = \sigma \nabla^a \alpha + \lambda (\nabla^a \beta + \beta \dot{u}^a), \quad (30)$$

$$\Pi^{ab} - q^{(a} w^{b)} = \zeta \Delta^{ab} \partial^c \beta_c + 2\eta \Delta^{(bc} \nabla^a) \beta_c, \quad (31)$$

$$q^{[b} w^{a]} = \chi \Delta^{[bc} \nabla^a] (\beta(u_c - w_c)). \quad (32)$$

Here $\langle \rangle$ denotes the symmetric traceless part in the bracketed indices, λ is the heat conduction coefficient, D is the diffusion coefficient, σ is the Soret-Dufour coefficient of thermal diffusion. ζ is the bulk viscosity, η is the shear viscosity, and χ is the vortical viscosity coefficient. Because of the nonnegative entropy production (28) the linear transport coefficients must fulfill the following inequalities:

$$D \geq 0, \quad \lambda \geq 0, \quad \lambda D - \sigma^2 \geq 0, \quad \zeta \geq 0, \quad \eta \geq 0, \quad \chi > 0. \quad (33)$$

Here the first three inequalities are coupled channel conditions for stability, while the last three are independent ones.

The procedure described here ensures the existence of a homogeneous flow field as a time independent solution of the equations of motion of the fluid. *That is why deviation from local equilibrium is best characterized by gradients of the basic fields in the first approximation.*

In the following we study some important particular choices for the flow-frame.

THERMOMETER FRAME

The thermometer or Jüttner frame is the natural choice in kinetic theory calculations. In this case the direction of β^a defines the flow-frame similarly to the natural frame in perfect fluids:

²Since dissipative fluxes are orthogonal to u^a , only the projected gradient terms, $\Delta_a^c \partial^b$, constitute thermodynamical forces.

$\beta = \sqrt{\|\beta_b \beta^a\|}$ and $u^a = \beta^a / \beta$. In this section we apply this definition of the flow-frame. Then the local equilibrium relations are:

$$s + \alpha n - \beta h = 0, \quad ds + \alpha dn - \beta de = 0. \quad (34)$$

The entropy current density, J^a satisfies

$$J^a + \alpha j^a - \beta q^a = 0^a, \quad (35)$$

and the entropy production rate fulfills the inequality,

$$\Sigma = -j^a \partial_a \alpha + q^a (\partial_a \beta + \beta \dot{u}_a) + \beta \Pi^{ab} \partial_a u_b \geq 0. \quad (36)$$

This form of the entropy production was derived originally by Eckart restricting to the case $g^a = w^a = 0$.

Eckart identified the following thermodynamic fluxes and forces

	Diffusive	Thermal	Mechanical
Fluxes	$-j^a$	q^a	$\beta \Pi^{ab}$
Forces	$\nabla^a \alpha$	$\nabla^a \beta + \beta \dot{u}^a$	$\Delta^{(bc} \nabla^a) u_c$

Table 2. Thermodynamic fluxes and forces by Eckart.

Unfortunately in this case a generic instability occurs, the linear instability of the homogeneous equilibrium, as it was proved by Hiscock and Lindblom in [14]. Nonnegative entropy production is established only if considering the basic balance equations (for energy, momentum and further conserved Noether-charges) as constraints. However, by deriving (36) the balance of momentum does not enter the calculations. Therefore the linear relation between the thermal part of the fluxes and forces with the acceleration term, $\beta \dot{u}^a$, connects changes in these quantities irrespective to the momentum balance equation (6). A correct treatment of thermodynamic forces and fluxes on the other hand should introduce the momentum balance into the above entropy production formula. A short calculation leads to:

$$\begin{aligned} \Sigma &= \left(\frac{n}{h} q^a - j^a \right) \partial_a \alpha - \frac{\beta}{h} q^a \left(\dot{q}_a + q_a \partial_b u^b + q^b \partial_b u_a + \partial_b \Pi^b_a \right) \\ &+ \beta \Pi^{ab} \partial_a u_b \geq 0. \end{aligned} \quad (37)$$

This step makes an important difference with respect to stability properties of the homogeneous equilibrium of a fluid. The corresponding thermodynamic fluxes and forces in the Jüttner frame are

	Diffusive	Thermal	Mechanical
Fluxes	$\frac{n}{h} q^a - j^a$	$-\frac{\beta}{h} q^a$	$\beta \Pi^{ab}$
Forces	$\nabla^a \alpha$	$X^a = \Delta^{ab} \dot{q}_b + q^a \partial_b u^b + q^b \partial_b u^a + \Delta^{ac} \partial_b \Pi_c^b$	$\Delta^{(bc} \nabla^a) u_c$

Table 3. Thermodynamic fluxes and forces in Jüttner frame providing generic stability

Here X^a is a convenient abbreviation for the thermal force, the thermodynamical force associated to the dissipative current of the heat. Linear transport relations for isotropic continua in the Jüttner frame can now be easily established:

$$\frac{n}{h} q^a - j^a = D \nabla^a \alpha + \sigma X^a, \quad (38)$$

$$-\frac{\beta}{h} q^a = \sigma \nabla^a \alpha + \lambda X^a, \quad (39)$$

$$\beta \Pi^{ab} = \zeta \Delta^{ab} \partial_c u^c + 2\eta \Delta_c^{(b} \nabla^a) u^c. \quad (40)$$

With this modification the generic stability of the theory in Jüttner frame is established: the heat transfer vector q^a receives a positive relaxation factor, $\beta/h\lambda > 0$. It is easy to realize that by ignoring viscosity, component diffusion and cross effects, in homogeneous equilibrium, where all spacelike projected gradients of the velocity field vanish, the only surviving term in the thermal force is that with the total time derivative of the heat vector:

$$\lambda X^a = \lambda \Delta^{ab} \dot{q}_b = -\frac{\beta}{h} q^a. \quad (41)$$

Multiplied by q^a this leads to a relaxation equation for the length of the vector, $Q = -q_a q^a$ as follows

$$\dot{Q} = -2 \frac{\beta}{h\lambda} Q. \quad (42)$$

This means a relaxation towards the $q^a = 0$ value of the energy current density.

An important property of these equations is the expected generic stability of the homogeneous equilibrium. Without the detailed calculations (to be shown elsewhere) we want to emphasize that the conditions of generic stability are purely thermodynamic. Namely, it is fulfilled whenever the transport coefficients $\lambda, \tilde{\eta}$ are nonnegative and the following inequalities for thermodynamic stability i.e. the concavity of the entropy $s(e, n, q^a)$ are satisfied:

$$\partial_e T > 0, \quad \partial_n \frac{\mu}{T} > 0, \quad \partial_e T \partial_n \frac{\mu}{T} - \left(\frac{\partial_n T}{T} \right)^2 \geq 0. \quad (43)$$

OTHER FLOW-FRAMES

The other flow frames can be conveniently defined in our general framework.

The Eckart frame is defined by the direction of the particle current density vector $u^a = N^a / \sqrt{\|N^b N_b\|}$. One realizes that in case of dissipative fluids the Jüttner and Eckart frames do not coincide.

In case of a Landau-Lifshitz frame the flow field is defined by the direction of the momentum density vector $u^a = u^b T_b^a / \|u^c T_c^d\|$, therefore $q^a = 0^a$. In case of dissipative fluids the Jüttner and Landau-Lifshitz frames also do not coincide. However, in the absence of q^a , the thermodynamic relations are similar to the ones in a Jüttner frame

$$s + \alpha n - \beta h = 0, \quad ds + \alpha dn - \beta de = 0, \quad nd\alpha - hd\beta - \beta dp = 0. \quad (44)$$

In principle there are several further possibilities of frame fixing. One of them introduces $w^a = \beta^a/h$. This choice fixes the velocity field compatible to some kinetic theory calculations [24; 18].

Once a choice of the linear response has been made, one can transform the description in one frame to the other. The different transport coefficients are not equivalent, a constant invariant coefficient may become flow-frame dependent in other frames. Whether the primary flow-frame independent choice is preferred or not requires further investigations.

SUMMARY

Thermodynamic relations in relativistic fluids adhere to flow-frames, while dividing spacial homogeneous changes from the forces enforcing this homogeneity. It is made transparent in the train of thoughts from (18) to (23), where we calculated entropy production separating comoving time derivatives and spacial gradients. *We have seen, that α, β^a and p are flow-frame independent.* Then local equilibrium was postulated by the thermodynamic relation (25), containing homogeneous thermodynamics. In [41], presenting a different reasoning, we have shown that the different transformation formulas of the relativistic temperature, due to Planck-Einstein, Blanuša-Ott, Landsberg and Doppler, can be unified and reasonably explained in exactly this thermodynamic framework.

We propose that the thermometer frame, defined in (10), should be a preferred choice. In general β^a can be divided into parts orthogonal and parallel to the flow u^a : $\beta^a = \beta(u^a + w^a)$, where $u^a w_a = 0$. We have revealed how far this choice differs from the Eckart and Landau-Lifshitz frames. There are arguments, that the widely used Landau-Lifshitz frame should be preferred [10; 42]. However, these studies do not distinguish the thermometer frame.

The entropy production in a general frame (28) helps to recognize

- that viscous pressure is damps the inhomogeneities in β^a ,
- that there are perfect fluids with zero entropy production but $j^a/n = q^a/h = w^a \neq 0$ and $\Pi^{ab} = hw^a w^b \neq 0$,
- there is a vorticity related dissipative term.

Furthermore we have mentioned, that generic stability is properly derived if the momentum balance constraint is also considered in the calculation of the entropy production (36).

In our previous works we have shown further examples of flow-frames. In [12; 17; 43; 41] the $w^a = q^a/e$ case was explored and in [24] and [18] we have analyzed the kinetic theory compatibility and thermodynamics when $w^a = q^a/h$. Thermodynamic considerations show, that the coupling of the momentum balance to the entropy production cannot be avoided [43]. It was proven independently of the Eckart or Landau-Lifshitz frame for $w^a = q^a/e$ in [17], for the $w^a = q^a/h$ case a partial proof was given in [18].

ACKNOWLEDGEMENT

The work was supported by the grants Otká K81161, K104260 and TT 10-1-2011-0061/ZA-15-2009. The authors thank Etele Molnár for valuable discussions.

REFERENCES

- [1] R. Geroch. On hyperbolic "theories" of relativistic dissipative fluids. 2001. arXiv:gr-qc/0103112.
- [2] R. Geroch. Relativistic theories of dissipative fluids. *Journal of Mathematical Physics*, 36(8):4226–4241, 1995.
- [3] R. Geroch and L. Lindblom. Dissipative relativistic fluid theories of divergence type. *Physical Review D*, 41:1855–1861, 1990.
- [4] R. Geroch and L. Lindblom. Causal theories of dissipative relativistic fluids. *Annals of Physics*, 207:394–416, 1991.
- [5] I-S. Liu, I. Müller, and T. Ruggeri. Relativistic thermodynamics of gases. *Annals of Physics*, 169:191–219, 1986.

- [6] J. Peralta-Ramos and E. Calzetta. Divergence-type non-linear conformal hydrodynamics. *Physical Review D*, 80:126002, 2010.
- [7] Shi Pu, Tomoi Koide, , and Dirk H. Rischke. Does stability of relativistic dissipative fluid dynamics imply causality? *Physical Review D*, 81:114039, 2010.
- [8] W. A. Hiscock and L. Lindblom. Stability and causality in dissipative relativistic fluids. *Annals of Physics*, 151:466–496, 1983.
- [9] G. Fichera. Is the Fourier theory of heat propagation paradoxical? *Rediconti del Circolo Matematico di Palermo*, XLI:5–28, 1992.
- [10] P. Kostädt and M. Liu. On the causality and stability of the relativistic diffusion equation. *Physical Reviews D*, 62:023003, 2000.
- [11] V. A. Cimmelli. On the causality requirement for diffusive-hyperbolic systems in non-equilibrium thermodynamics. *Journal of Non-Equilibrium Thermodynamics*, 29(2):125–139, 2004.
- [12] P. Ván and T. S. Bíró. Relativistic hydrodynamics - causality and stability. *The European Physical Journal - Special Topics*, 155:201–212, 2008.
- [13] G. S. Denicol, T. Kodama, T. Koide, and Ph. Mota. Stability and causality in relativistic dissipative hydrodynamics. *Journal of Physics G - Nuclear and Particle Physics*, 35(11):115102, 2008.
- [14] W. A. Hiscock and L. Lindblom. Generic instabilities in first-order dissipative relativistic fluid theories. *Physical Review D*, 31(4):725–733, 1985.
- [15] K. Tsumura and T. Kunihiro. Stable first-order particle-frame relativistic hydrodynamics for dissipative systems. *Physics Letters B*, 668(5):425–428, 2008.
- [16] K. Tsumura and T. Kunihiro. First-principle derivation of stable first-order generic-frame relativistic dissipative hydrodynamic equations from kinetic theory by renormalization-group method. *Progress of Theoretical Physics*, 126(5):761–809, 2011.
- [17] P. Ván. Generic stability of dissipative non-relativistic and relativistic fluids. *Journal of Statistical Mechanics: Theory and Experiment*, page P02054, 2009.
- [18] P. Ván and T.S. Bíró. First order and generic stable relativistic dissipative hydrodynamics. *Physics Letters B*, 709(1-2):106–110, 2012.
- [19] A. L. Garcia-Perciante, L. S. Garcia-Colin, and A. Sandoval-Villalazo. On the nature of the so-called generic instabilities in dissipative relativistic hydrodynamics. *General Relativity and Gravitation*, 41(7):1645–1654, 2009.
- [20] T. Osada. Relativistic hydrodynamical model in the presence of long-range correlations. *Physical Review C*, 81:024907, 2010.
- [21] T. Osada. Modification of Eckart theory of relativistic dissipative fluid dynamics by introducing extended matching conditions. *Physical Review C*, 85:014906, 2012.
- [22] S.R. de Groot, W. A. van Leeuwen, and Ch. G. van Weert. *Relativistic Kinetic Theory*. North Holland, Amsterdam, 1980.
- [23] Csernai L. *Introduction to relativistic heavy ion physics*. John Wiley and Sons, Chicester-etc., 1994.
- [24] P. Ván. Kinetic equilibrium and relativistic thermodynamics. *EPJ WEB of Conferences*, 13:07004, 2011.
- [25] W. Israel and J. M. Stewart. On transient relativistic thermodynamics and kinetic theory. *Annals of Physics*, 118:341–372, 1979.
- [26] A. Monnai and T. Hirano. Effects of bulk viscosity at freezeout. *Physical Review C*, 80:054906, 2009.
- [27] Carl Eckart. The thermodynamics of irreversible processes, III. Relativistic theory of the simple fluid. *Physical Review*, 58:919–924, 1940.
- [28] L. D. Landau and E. M. Lifshitz. *Fluid mechanics*. Pergamon Press, London, 1959.
- [29] Gy. Farkas. A Fourier-féle mechanikai elv alkalmazásai. *Mathematikai és Természettudományi Értesítő*, 12:457–472, 1894. in Hungarian.
- [30] H. Minkowski. *Geometrie der Zahlen*. Teubner, Leipzig und Berlin, 1896.
- [31] A. Schriver. *Theory of linear and integer programming*. John Wiley and Sons, Chicester-etc., 1998.
- [32] K. Tsumura and T. Kunihiro. Derivation of relativistic hydrodynamic equations consistent with relativistic Boltzmann equation by renormalization-group method. *The European Physical Journal A*, 48:162, 2012.
- [33] I. Müller. Toward relativistic thermodynamics. *Archive for Rational Mechanics and Analysis*, 34(4):259–282, 1969.
- [34] W. Israel. Nonstationary irreversible thermodynamics - causal relativistic theory. *Annals of Physics*, 100(1-2):310–331, 1976.
- [35] W. Israel and J. M. Stewart. On transient relativistic thermodynamics and kinetic theory. II. *Proceedings of Royal Society London A*, 365:43–52, 1979.
- [36] J. M. Stewart. On transient relativistic thermodynamics and kinetic theory. *Proceedings of Royal Society London A*, 357:59–75, 1977.
- [37] H. C. Öttinger. General projection operator formalism for the dynamics and thermodynamics of complex fluids. *Physical Review E*, 57(2):1416–1420, 1998.
- [38] H. C. Öttinger. *Beyond equilibrium thermodynamics*. Wiley-Interscience, 2005.
- [39] M. Planck. Zur Dynamik bewegter Systeme. *Annalen der Physik*, 331(6):1–34, 1908.
- [40] A. Einstein. Über das Relativitätsprinzip und die aus demselben gezogenen Folgerungen. *Jahrbuch der Radioaktivität und Elektronik*, 4:411–462, 1907.
- [41] T. S. Bíró and P. Ván. About the temperature of moving bodies. *EPL*, 89:30001, 2010.
- [42] K. Tsumura and T. Kunihiro. Uniqueness of Landau-Lifshitz energy frame in relativistic dissipative hydrodynamics. *Physical Review E*, 87:053008, 2013.
- [43] P. Ván. Internal energy in dissipative relativistic fluids. *Journal of Mechanics of Materials and Structures*, 3(6):1161–1169, 2008.

ADVANCED EXERGY ANALYSIS OF THE STEAM TURBINE OPERATIONS OPTIMISATION

Dilek Celenk*, Zehra Ozcelik^o, Sadi Senocak*

*PhD Student at Chemical Engineering Department, Ege University, Bornova – Izmir /Turkey, Senior R&D Engineer / Energy, Petkim Petrochemicals Inc. Office I, 35800 Aliaga – Izmir/Turkey
^oAss.Prof. Dr., Chemical Engineering Department, Ege University, Bornova – Izmir /Turkey
* Energy Manager, Petkim Petrochemicals Inc. Office I, 35800 Aliaga – Izmir/Turkey

ABSTRACT

Petkim Petrochemical Inc. is one of the most important companies in Turkey. The Petkim Complex consists of 14 production plants and 7 utility plants to supply the production plants. Petrochemical processing has a high energy requirement, especially plants with the complex technology that is used at the Petkim Complex. This means that Petkim is a large energy consumer, with a total consumption of 913.000 TEO in 2009.

Following privatization of Petkim in 2008, an energy management system was introduced and several energy saving studies were initiated. In 2012, after implementation of energy saving projects, the energy consumption at Petkim was 813.000 TOE. This means that from 2009 to 2012, there was a reduction of 100.000 TEO, which is equal to a financial saving 50.8 M USD, and represents a saving 232.000 tons CO₂e.

To enable the Power Plant efficiencies in Petkim complex to be improved, the advanced exergetic analysis of the system were studied on some what-if scenarios which were studied by using simulation and optimisation software. In this article, how steam turbine operations were optimized will be explained in detail and the results of the advanced exergetic analysis will be given.

INTRODUCTION

The energy requirement of industry is supplied mainly by fossil and nuclear fuels. According to New Policies Scenario, global primary energy demand rises by over one-third in the period to 2035. Oil demand reaches 99.7 mb/d in 2035, up from 87.4 mb/d in 2011. Coal demand rises by 21% and natural gas by a remarkable 50%. Renewables are deployed rapidly, particularly in the power sector, where their share of generation increases from around 20% today to 31%. Growth in nuclear power is revised down relative to our previous projections, in large part due to policy moves following Fukushima Daiichi. These trends call for \$37 trillion of investment in the world's energy supply infrastructure to 2035. All those projections show that energy demand is growing up by coming years besides policy makers confronted with the twin challenges of ensuring reliable and affordable energy supplies and dealing with climate change have consistently identified energy efficiency as an essential means of moving to a more sustainable energy future. Energy and economic analysis point to the same conclusion: improving energy efficiency in energy-importing countries reduces import needs or slows their growth; measures can be implemented quickly compared with often lengthy projects to expand production; it is among the cheapest of the large-scale carbon dioxide (CO₂) abatement options; and it can play a role in spurring economic growth and reducing energy bills, both of particular importance during this period of economic uncertainty and persistently high energy prices [1].

For this reason, the studies on alternative energy resources and new techniques in order to utilize the energy resources more efficiently have increased. The optimization of energy conversion systems becomes one of the most important subjects in the industry. Engineers and scientists dealing with the design

and operation of an energy conversion system want to improve or optimize it by maximizing efficiency, and minimizing product cost and environmental impact associated with this plant [2]. In order to optimize such systems, firstly the real mechanism should be understood according to which thermodynamic inefficiencies, costs, and environmental impacts are formed within the system.

In 2011 all major energy-consuming countries introduced new legislation on energy efficiency, making provisions for a 16% reduction in energy intensity by 2015 in China, new fuel-economy standards in the United States and a cut of 20% in energy demand in the European Union in 2020. Japan also aims to achieve a 10% reduction in electricity demand by 2030 in its new energy strategy. Implementation of those policies and of those under discussion in many other countries, at the level assumed in our New Policies Scenario, would result in annual improvements in energy intensity of 1.8% over 2010-2035, a very significant increase compared with 1.0% per year achieved over 1980-2010. In the absence of those gains, global energy demand in 2010 would have been 35% higher, almost equivalent to the combined energy use of the United States and China. According to the New Policies Scenario of WEO 2012, efficiency accounts for about 70% of the reduction in projected global energy demand in 2035, compared with the Current Policies Scenario [3].

The performance of energy conversion systems is reduced by the presence of irreversibilities. Entropy is used as a quantitative measure of irreversibilities associated with a process, and can also be used to determine the performance of process and its equipment. For this purpose a technique called exergy analysis is used. Exergy analysis is a thermodynamic tool for assessing and improving the efficiency of processes and their equipment, and for increasing environmental and economic performance. The exergy analysis is used to identify

the location, the magnitude, and the causes of thermodynamic inefficiencies in systems, which are exergy loss and exergy destruction [2]. The sum of exergy destruction and exergy loss within an energy conversion system represents the real thermodynamic inefficiencies of this system. The exergy loss in a component is caused by the transfer of thermal exergy to the environment. When the boundaries for the component analysis are drawn at the ambient temperature, the exergy loss is zero and the thermodynamic inefficiencies consist exclusively of exergy destruction [3].

The exergy destruction is caused chemical reaction, heat transfer, mixing of matter at different compositions or states, unrestrained expansion, and friction. At any given state of technological development, some exergy destruction within a system component will always be unavoidable due to physical and economic constraints [4].

A conventional exergetic analysis does not evaluate the mutual independencies among the system components nor the potential for improving a component [2]. This can be achieved by an advanced analysis, in which the exergy destruction in each component is split into endogenous and exogenous parts; also avoidable and unavoidable parts, and a combination of these two splitting approaches. Such an approach can provide an energy conversion system with valuable detailed information in order improve the overall efficiency of a system.

After investments of plants in Petkim, power generation and utility operations in the petrochemical complex had had a complicated structure. Optimisation of the big sized and complicated power generation operations was getting higher importance.

After investments of plants in Petkim, power generation and utility operations in the petrochemical complex had had a complicated structure.

Optimisation of the big sized and complicated power generation operations was getting higher importance. It was really too important to monitor and to optimise the energy consumption and power generation operations in order to perform energy saving studies. By optimising energy consumption of the complex continuously it is possible to save 2 – 5 % of energy consumption of the complex.

In this study advanced exergy analysis of the steam turbines which are running in the power plant of a petrochemical complex, operations optimisation was performed. At the initial state two backpressure turbines having 64 MW power output each, and two condensing turbines having 20 and 22 MW power outputs were running in the power plant. After making some what – if scenarios by using HSPO (Heat – Steam – Power – Optimisation software), one of the backpressure steam turbine was shut down. What – if study and the exergy analysis results will be examined in coming section.

POWER PLANT

Petkim has its own Power Plant to generate steam at different pressure and temperature levels and electricity to use its processes. There are 4 steam boilers having 350 tons/h capacity to generate XHS (extra high pressure steam) and two backpressure turbines to generate HS (high pressure steam), MS (medium pressure steam), and LS (low pressure steam) and electricity and two condensing turbines for electricity generation using LS. Depending on the complex demand steam and electricity generation is changed. 420.000 TOE fuel is consumed annually to produce 4.400.000 tons XHS and 920.000 MW electricity in the Power Plant. Steam and power system have a dynamic structure and it brings on to optimize the generation and consumption of the complex.

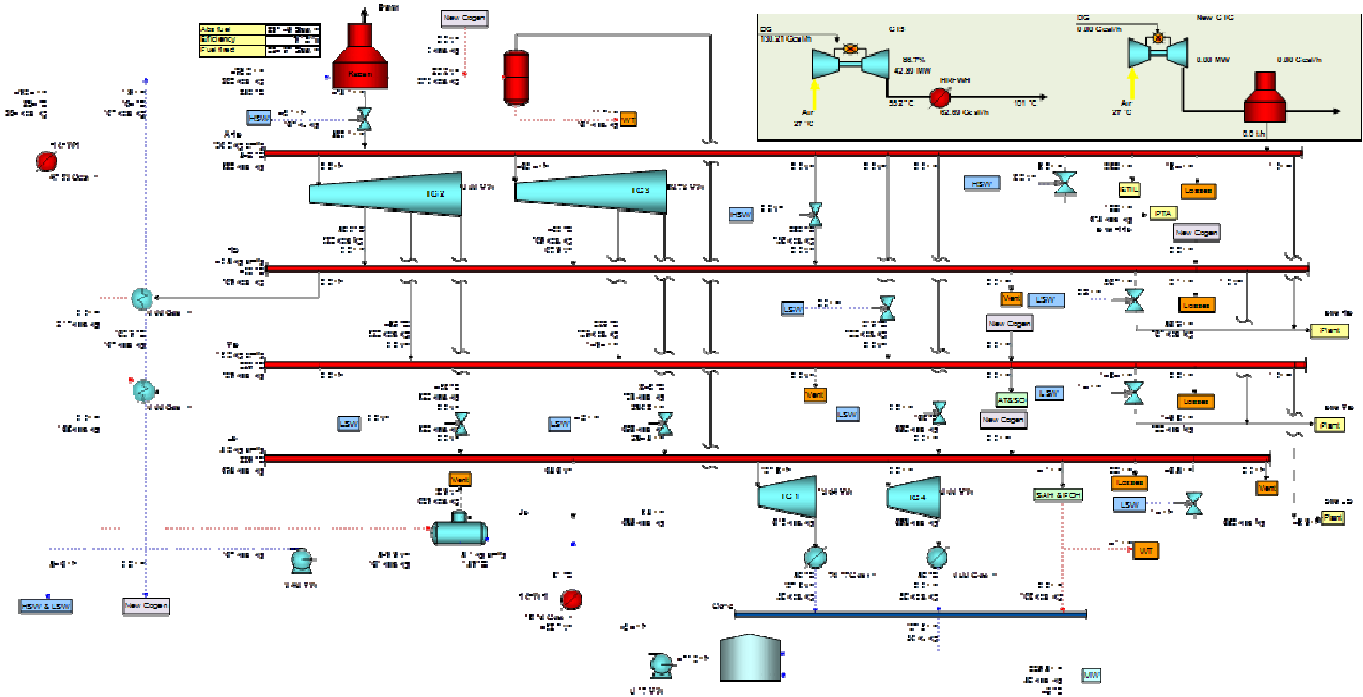


Figure 1. General Scheme of the Steam and Power Generation

Fuel oil, natural gas, fuel gas, aromatic oil, hydrogen and ethylene oxide plant vent gas are used as primary energy sources to produce XHS and electricity in Petkim Power Plant. It has 4 steam boilers (B1, B2, B3, and B4) having maximum capacity of 350 tons/h XHS; two backpressure turbines (TG2, and TG3) having 64 MWh capacity for each; two condensing turbines having capacity of 20 MWh (TG1) and 22 MWh (TG4); and one gas turbine (TG5) having capacity of 58 MWh, (Figure 1). 500 t/h steam and 130 MWh electricity is used by plants in the complex given in Table 1.

Table 1. Steam Levels Generated by Power Plant

STEAM LEVELS	PRESSURE (kg/cm ² g)	TEMPERATURE (°C)
XHS	134	540
HHS	84	310
HS	42	390
MS	18	300
LS	5.5	190

WHAT – IF STUDY

Electricity is generated by passing XHS through backpressure turbines and HS, MS, and LS which are used in processes are taken from different sections of each turbine. For supplying the complex demand for steam and electricity at least three boilers, two backpressure turbines and two condensing turbines had been running. Depending on the complex demand steam and electricity generation is changed. By performing what – if scenario by using HSPSO software, it was seen that instead of two running backpressure turbines at lower loads, one backpressure turbine at higher loads and one condensing turbine could supply the complex demand. All analysis showed that three boilers, one backpressure turbine, and one condensing turbine could supply the complex demand for steam and electricity without any disturbances on the system and complex.

Table 2. What – if Scenario Complex Application Results

		TG2	TG3	Total	Difference
XHS Consumption of Turbines (tons/h)	Before Application	279	188	467	-11(tons/h)
	After Application	456	0	456	
Power Generation (MW)	Before Application	26	15	41	+12 (MW)
	After Application	53	0	53	

At the beginning the capacity of the backpressure turbines were 35 – 45% and this caused big losses in efficiency. To prevent this, one of the back pressure turbine was stopped and other backpressure turbine was loaded twice than before. At this condition the running backpressure turbine is run 80 – 90% of its capacity. The what – if scenario was studied in software firstly and then it was applied in the complex gave results that XHS consumption was decreased by 11 tons/h and the electricity generation was increased by 12 MWh as seen in Table 2.

EXERGY ANALYSIS

Exergy of a thermodynamic system is the maximum theoretical useful work (shaft work or electrical work) obtainable as the system is brought into complete thermodynamic equilibrium with the thermodynamic environment while the system interacts with this environment only. [5] A conventional exergy analysis can highlight the main components having high thermodynamic inefficiencies, but cannot consider the interactions among components or the true potential for the improvement of each component. By splitting the exergy destruction into endogenous/exogenous and avoidable/unavoidable parts, the advanced exergy analysis is capable of providing additional information to conventional exergy analysis for improving the design and operation of energy conversion systems [6].

Like mass, energy, and entropy, exergy is an extensive property, so it too can be transferred into or out of a control volume where streams of matter enter and exit. The general form of such exergy transfer can be expressed as:

$$\frac{dE_{ex}}{dt} = \sum_j \left(1 - \frac{T_0}{T_j}\right) Q_j - \left(W_{cv} - p_0 \frac{dV_{cv}}{dt}\right) + \sum_i \dot{m}_i e_i - \sum_e \dot{m}_e e_e - \dot{E}_D \quad (1)$$

The first term denotes rate of exergy change, the term \dot{E}_D denotes rate of exergy destruction and the rest of the terms on the right side of the equation denote rates of exergy transfer.

In the absence of nuclear, magnetic, electrical, and surface tension effects the total exergy of a system E can be expressed as:

$$E = E^{PH} + E^{KN} + E^{PT} + E^{CH} \quad (2)$$

where E^{PH} is physical exergy, E^{KN} is kinetic exergy, E^{PT} is potential exergy, and E^{CH} is chemical exergy.

The physical exergy can be expressed as:

$$E^{PH} = (U - U_0) + p_0(V - V_0) - T_0(S - S_0) \quad (3)$$

Where U , V , and S denote, respectively, the internal energy, volume, and entropy of the specified state, and U_0 , V_0 , and S_0 are the values of the same properties when the system is at the restricted dead state.

The chemical exergy per mole of mixture is,

$$\bar{e}^{CH} = \sum x_k \bar{e}_k^{CH} + \bar{R}T_0 \sum x_k \ln x_k \quad (4)$$

and x_k is the mole fraction of gas k in the environmental gas phase and \bar{e}_k^{CH} is the chemical exergy per mole of kth component.

Exergy rate balance at steady – state can be expressed as:

$$\dot{E}_i = \dot{E}_e + \dot{E}_D + \dot{E}_L \quad (5)$$

where \dot{E}_i denotes exergy rate at the inlet, \dot{E}_e denotes exergy rate at the outlet, \dot{E}_D denotes exergy destruction, and \dot{E}_L denotes exergy loss.

The exergetic efficiency ε is the ratio between product and fuel and is expressed as [7]:

$$\varepsilon = \frac{\dot{E}_P}{\dot{E}_F} = 1 - \frac{\dot{E}_D + \dot{E}_L}{\dot{E}_F} \quad (6)$$

RESULTS

In this paper the advanced exergy analysis of the steam turbine operations optimisation were studied. Firstly the what – if analysis of the turbine operations were examined and then the action which was defined in the what – if scenario was applied to Power Generation in the complex. According to the scenario applied one of the backpressure turbine TG2 and one of the condensing turbine TG4 had been shut down. Before the application HS only was taken from TG2 and this amount of HS could be supplied to complex HS demand. So, before application there was no HS section data to calculate exergy and efficiency of the HS section of TG3. After application HS is started to be taken from TG3. Before and after application of the scenario the exergetic efficiency of the backpressure turbines and condensing turbines had been calculated and all results are given in Table 3. It is clear that for backpressure turbine operation all efficiencies of the turbine sections was increased at least 5%.

Table 3. Exergy and Efficiency Results of the Steam Turbines Operation

	Before Application		After Application	
	Exergy (kW)	Efficiency %	Exergy (kW)	Efficiency %
TG1	13591.9	70.3	24838.4	52.7
TG2-HS	4122.3	85.3		
TG2-MS	9031.6	80.6		
TG2-LS	33139.9	79.0		
TG3-HS			5457.8	80.3
TG3-MS	10228.5	77.1	21600.7	82.5
TG3-LS	30456.6	68.1	51781.6	75.4
TG4	16091.9	43.8		

NOMENCLATURE

Symbol	Quantity	SI Unit
XHS	Extra High Pressure Steam	tons/h
HHS	High High Pressure Steam	tons/h
HS	High Pressure Steam	tons/h
MS	Medium Pressure Steam	tons/h
LS	Low Pressure Steam	tons/h
TOE	Tonnes Oil Equivalent	-
HSPO	Heat – Staem – Power – Optimisation Boilers	-
B1, B2, B3, B4	Boilers	-
TG2, TG3	Backpressure Turbines	-
TG1, TG4	Condensing Turbines	-
TG5	Gas Turbine	-
E _D	Rate of Exergy Destruction	
E	The Total Exergy of A System	kJ/kmol
E ^{PH}	Physical Exergy	kJ/kmol
E ^{KN}	Kinetic Exergy	kJ/kmol
E ^{PT}	Potential Exergy	kJ/kmol
E ^{CH}	Chemical Exergy	kJ/kmol
U	The Internal Energy	kJ/kmol
V	Volume	m ³
S	Entropy	kJ/kmolK
U ₀	The Internal Energy at the Restricted Dead State	kJ/kmol
V ₀	Volume at the Restricted Dead State	m ³
S ₀	Entropy at the Restricted Dead State	kJ/kmolK
\bar{e}^{CH}	The Chemical Exergy Per Mole of Mixture	kJ/kmol
x_k	The Mole Fraction Of Gas k in the Environmental Gas Phase	-
\bar{e}_k^{CH}	The Chemical Exergy Per Mole of k th Component	kJ/kmol
\dot{E}_i	Exergy Rate at the Inlet	MW
\dot{E}_e	Exergy Rate at the Outlet	MW
\dot{E}_D	Exergy Destruction	MW
\dot{E}_L	Exergy Loss	MW
ε	The Exergetic Efficiency	MW

\dot{E}_p	Exergy Rate of Product	MW
\dot{E}_f	Exergy Rate of Fuel	MW

REFERENCES

- [1] World Energy Outlook, International Energy Agency, France, 2012.
- [2] G. Tsatsaronis, T. Morosuk, Understanding and Improving Energy Conversion Processes with the Aid of Exergy – Based Methods, ELCAS, Nisyros, Greece, 2009.
- [3] G. Tsatsaronis, M.-H. Park, On Avoidable and Unavoidable Exergy Destructions and Investment Costs In Thermal Systems, Energy Conversion and Management, 43, pp, 1259-1270, 2002.
- [4] F. Czesla, G. Tsatsaronis, Z. Gao, Avoidable Thermodynamic Inefficiencies and Costs in an Externally Fired Combined Cycle Power Plant, Energy, 31, pp. 1472–1489, 2006.
- [5] G. Tsatsaronis, Definitions and Nomenclature in Exergy Analysis and Exergoeconomics, Energy 32, pp. 249 – 253, 2007.
- [6] L. Wang, Y. Yang, T. Morosuk, and G. Tsatsaronis, Advanced Thermodynamic Analysis and Evaluation of a Supercritical Power Plant, Energies 5, pp. 1850 – 1863, 2012.
- [7] A. Bejan, G. Tsatsaronis, M. Moran, Thermal Design & Optimization, John Wiley & Sons Inc., USA, 1996.

CALCULATION OF POLYTHERMAL SECTIONS OF TERNARY PHASE DIAGRAMS BY THE CONVEX HULL METHOD

Alexander V. Dzuban*, Alexey L. Voskov°

*Department of Materials Science, Lomonosov Moscow State University, Moscow, Russia

°Department of Chemistry, Lomonosov Moscow State University, Moscow, Russia

ABSTRACT

An algorithm for ternary phase diagrams polythermal sections assessment based on the convex hull method has been suggested. It is based on p, T -sections set calculation in the needed temperature interval with step between them depending on required accuracy and its subsequent analysis. Improvements of existing technique of ternary isobaric-isothermal sections construction implemented in TernAPI software complex also have been proposed and successfully tested. Suggested modifications improve reliability of diagram regions discrimination near the singular points such as eutectic or peritectic and greatly increase the performance of p, T -sections construction. Polythermal sections of Au-Bi-Sb, Al-Mg-Zn, LiF-LiCl-LiI and another ternary systems have been calculated.

INTRODUCTION

Phase diagrams assessment is an actual part of modern theoretical materials science. Most of modern programs for calculating multicomponent diagrams are based on the conditional minimization of Gibbs energy of the system. The sensitivity of this method to the initial approximation and to features of used minimization algorithm significantly complicates its practical application. Such situation makes a development of alternative methods for phase equilibria assessment, e.g. geometric, an actual problem. A rather new convex hull method belongs to them.

The convex hull method is based on the fact that equilibrium Gibbs energy (G) surface of the system in extensive thermodynamic coordinates (e.g. amounts of components n_i , volume V , etc.) is the convex hull of G functions of all set of phases. It has a number of advantages: doesn't require specifying initial conditions, applicable for wide range of thermodynamic models, doesn't use explicit minimization of thermodynamic potentials [1]. It should be noted that convex hull method allows direct calculations of phase diagrams in extensive variables only (n_i , volume V , etc.).

For isobaric-isothermal sections of ternary systems this method is implemented in the TernAPI program developed at the Laboratory of Chemical Thermodynamics of MSU Chemistry Department [2]. However in the practical, e.g. industrial, applications an assessment and visualization of polythermal sections and surfaces (i.e. diagrams in extensive coordinates that cannot be obtained by the convex hull method directly) are often required.

So the technique of making polythermal sections of ternary phase diagrams using convex hull method was suggested and implemented into TernAPI package.

POLYTHERMAL SECTIONS CONSTRUCTION METHOD

The proposed method of polythermal sections construction is based on the assessment of the p, T -sections set within specified range of temperatures with their subsequent analysis and consists of the next steps:

- (1) The set of phase diagram p, T -sections in the temperature range from T_{\min} to T_{\max} with user defined step ΔT is constructed. All sections have the same resolution in components molar fractions coordinates (x_2, x_3).
- (2) The cutting plane parallel to T axis and intersecting AB (A and B are the points inside the Gibbs-Rosebom triangle) interval in each composition triangle is plotted.
- (3) The rasterization of each p, T -section obtained in item 1 is carried out. Points situated on the interval AB are selected from each rasterized section. Phase composition of every point is stored in the matrix, in which every row corresponds to one temperature T_i and a column – to a definite composition ξ_i .
- (4) Based on the matrix from item 3 coordinates of boundaries between diagram areas are determined.
- (5) Using obtained data array the phase diagram polythermal section in the T - ξ coordinates (temperature-composition) is plotted.

Suggested algorithm is implemented as the computer program in MATLAB programming language and uses the TernAPI kernel to calculate single p, T -sections. It comprise four modules – PolyTSection, CalcPolyTDiagram, BuildPolyTSection and ShowPolyTSection, which perform next functions:

- (1) First one (PolyTSection) is designed to setup user input data (path to the source file with information about system, temperature interval for section calculation, composition and temperature step, geometrical parameters of required polythermal section) and to call other three modules.
- (2) Second one (CalcPolyTDiagram) calculates the set of p, T -sections and determines phase composition and boundaries inside each of them.
- (3) Third module (BuildPolyTSection) performs rasterization of each p, T -section and builds up the matrix as described in item 3 of algorithm, then receives information about boundaries of diagram phase fields from previous module.
- (4) Last one (ShowPolyTSection) makes graphical construction of obtained polythermal section.

Such modularization was made to divide the procedure of p, T -sections calculations and their analysis as well as to facilitate further modernization, addition of another functionality and integration with TernAPI.

It should be emphasized that quality of built polythermal section is essentially depends on defined temperature step ΔT . It was emerged during program testing that optimal value of ΔT is about 1% of temperature interval for diagram construction. Such ΔT allows to find adequately most of existing phase fields of section and make the representation of obtained T - x -diagrams in a user-friendly style.

Concerning operating time of the algorithm we can say that primary rate-controlling factor is the calculation of the isobaric-isothermal sections set. Depending on temperature and composition step it can take from a few minutes to hours on modern personal computer and amount to about 80% of program working time, where almost 2/3 of calculation time goes to the construction of convex hull and the remainder – to the determination of their phase compositions and boundaries. Remaining availability is taken by construction of the final T - x -diagram (usually 5-60 seconds). Therefore we recommend begin with calculation and saving the set of p, T -sections for chosen system to improve the time for construction of arbitrary polythermal section loading it from outside.

Suggested algorithm tested on the next groups of systems:

- (1) Systems with ternary eutectic (model, LiF-LiCl-LiI etc.)
- (2) Systems with splitting solutions (model, CdTe-HgTe-ZnTe, Au-Pt-Pd etc.)
- (3) Systems with a large number of phases with non-permanent composition (Au-Bi-Sb, Al-Mg-Zn etc.)

An agreement between calculated diagrams and literature data confirms the applicability of the developed technique of polythermal sections assessment for a wide range of ternary systems. As an example the comparison between calculated and reference sections of ternary Au-Bi-Sb diagram with is shown on the Figure 1. Model descriptions for all phases in this system were taken from [3] and reference plotted polythermal section was taken from [4]. As can be seen calculated polythermal section contains phase fields boundaries of different colors. The reason for that will be described below.

During the algorithm testing a necessity to upgrade TernAPI program for improving accuracy in determination of phase boundaries around singular points of phase diagram (eutectic, peritectic, critical points etc.) was clearly shown.

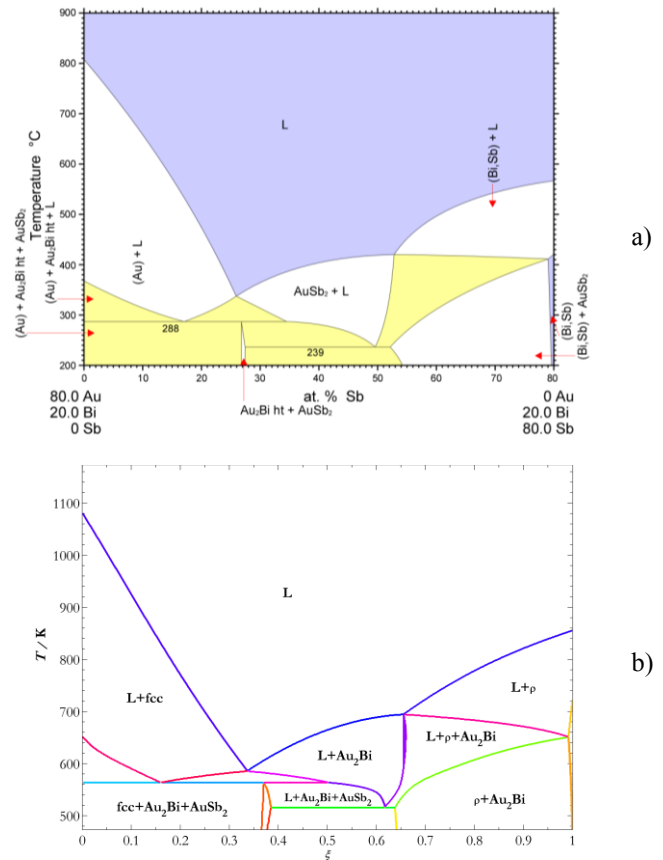


Figure 1. Polythermal section of Au-Bi-Sb phase diagram with constant molar fraction of Bi $x_{Bi} = 0.2$: a – from [4], b – calculated using suggested algorithm.

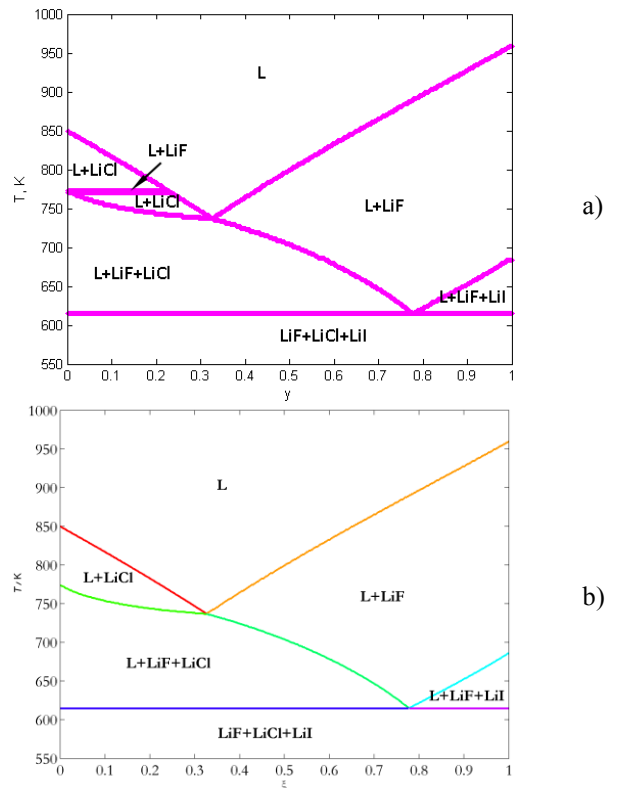


Figure 2. Polythermal section of LiF-LiCl-LiI phase diagram (0.9;0)-(0;0.5). Coordinates are given as $(x_2^{start}, x_3^{start})-(x_2^{final}, x_3^{final})$. a – first version of program, b – calculated using refined algorithm.

To illustrate this an arbitrary polythermal section in the ternary LiF-LiCl-LiI diagram is shown on Figure 2a. Model description for this system was taken from [5] and [6]. One can see the splitting of one whole two-phase region L+LiCl into two due to “wedging” between them of narrow two-phase band L+LiF. Such inaccuracy is caused by the problems of discrimination between three- and two-phase diagram regions. As can be seen on the Figure 3, narrow three-phase triangle near the eutectic point is incorrectly recognized as two-phase. Such error distorts the view of polythermal section; it is caused by the convex hull projection analysis algorithm features (which is based on geometrical principles) used in TernAPI.

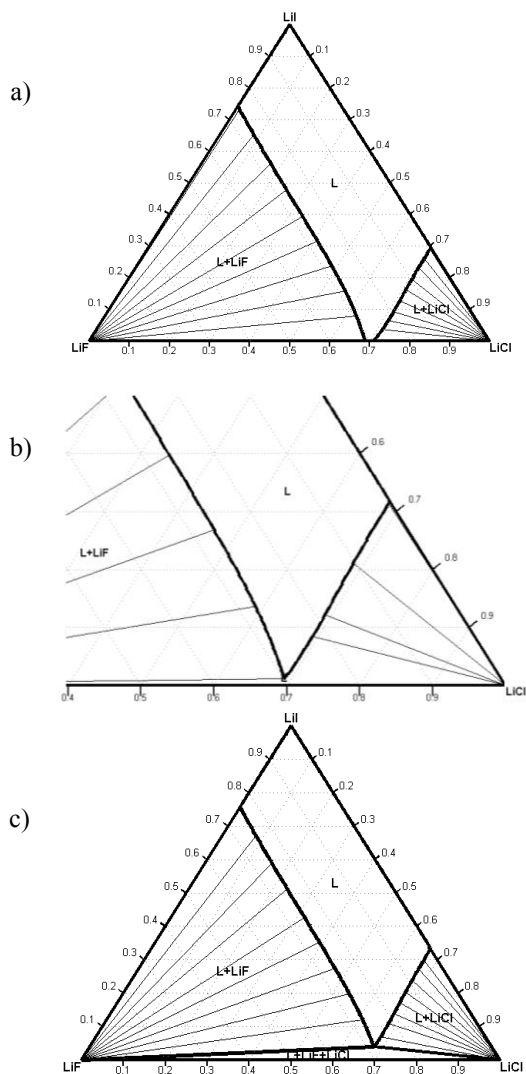


Figure 3. Calculated isothermal sections of LiF-LiCl-LiI phase diagram at: a – 779 K, b – 771 K, c – 765 K.

It can be avoided by decreasing composition step that results in increasing of the section calculation and visualization time. Another possible way is in comparing two p, T -sections differed from each other by the value of ΔT in temperature with further recognition and automatic repairing the “artefacts”, but this method takes additional investigations and significant sophistication of the algorithm. We used different approach.

This one and other corrections of algorithm implementation drawbacks mentioned above are described in the next section of this article.

ALGORITHM REFINEMENT

In the new version of algorithm some its parts were significantly improved. The most important features are the follows:

- (1) Inaccuracy in determination of phase boundaries around singular points of phase diagram was eliminated by the modification of TernAPI kernel.
- (2) Combining of single points dividing phase diagrams into a solid lines of phase boundaries was added.
- (3) Time of polythermal section construction from precalculated set of p, T -sections was reduced to one-tenth as much (now it is less than 10 sec on a typical modern personal computer).

Elimination of errors in phase boundaries determination near singular points was achieved by addition of extra procedure of phase number assessment inside the triangles of the convex hull projection to the (x_2, x_3) plane. It was made by the modification of TernAPI kernel. Old version of algorithm includes only one method of its assessment based on geometrical properties of the triangles [2]. Extra procedure contains two steps:

- (1) Calculate number of phases by counting the number of Gibbs energy functions (points, lines, surfaces) touched by the triangle.
- (2) Use obtained number of phases if it is greater that calculated by the geometrical method

In this technique geometrical method allows to detect miscibility gaps generated by the one phase (e.g. liquid) and non-geometrical method can discriminate between three and two-phase region near such singular points as eutectic and peritectic.

New feature of program to determine phase regions boundaries not as dotted but solid improves the visual appearance of phase diagrams and makes its automatic analysis easier (e.g. during thermodynamic model parameters optimization based on an experimental data set). It can be seen on Figures 2b and 3b, where boundaries dividing different fields have distinct colours. Comparing Figures 3a and 3b one can see also developments of the algorithm in second version vs first one.

Algorithm performance improvement was achieved by means of program code optimization that includes MATLAB code refactoring and rewriting of its critical parts (from the viewpoint of performance) to the C programming language. Comparison of two program versions performance is shown in the Table 1.

Table 1. Comparison of the algorithm performance before and after optimization.

Section assessment stage	Time elapsed, relative units ^a	
	Before optimization	After optimization
Convex hulls construction	1	1
p, T -sections analysis	0.64	0.42
Polythermal section construction	0.05	0.0035

^a “Relative unit” is time elapsed on the convex hull construction that was not changed after optimization

DISCUSSION OF THE RESULTS

The algorithm of ternary systems polythermal sections calculation has been proposed and refined in the present work; and its efficiency and robustness during testing was clearly shown. Its key feature is preliminary calculation of p, T -sections array by the convex hull method with the fixed step ΔT between them. Although such procedure requires a lot of time (about 5-60 minutes on the modern personal computers) it allows further rapid (in several seconds) polythermal section construction that can be useful for the phase diagram exploration. The process of calculation can be easily parallelized on the multicore/multiprocessor computer. Obtained p, T -sections array also makes possible a fast visualization of three-dimensional boundaries (i.e. surfaces) between regions of polythermal phase diagram (e.g. liquidus or solidus surface).

The geometrical approach that is the basis of the developed algorithm (see “polythermal sections construction method” section) can be generalized to the isothermal and polythermal sections of the multicomponent systems (e.g. quaternary). Another way of improvement is the minimization of convex hull construction elapsed time. It may be achieved by an adaptation of existing convex hull building algorithms for a phase diagram assessment task. For the case of binary systems such approach been described in the literature [7].

CONCLUSIONS

In the present work an effective algorithm for the ternary phase diagrams polythermal sections assessment based on the convex hull method has been proposed and successfully tested. Although it's significantly slower than the algorithms based on the Gibbs energy minimization in the case of single polythermal section calculation, it has an important advantage over it: after assessment of one polythermal section the next ones can be obtained almost instantly.

Possible ways of further development of the proposed algorithm are its generalization for the multicomponent system case and increasing its performance by the optimization of p, T -sections array assessment.

ACKNOWLEDGMENT

This work was supported by the Russian Foundation for Basic Research, projects Nos. 11-03-00499-a and 12-03-31069-mol_a.

NOMENCLATURE

Symbol	Quantity	SI Unit
G	Gibbs energy	J·mol ⁻¹
n_i	Amount of i-th component	mol
V	Volume	m ³
p	Pressure	bar
T	Temperature	K
x_i	Mole fraction of i-th component	
ξ, y	Coordinate on section line proportional to mixture composition	

REFERENCES

- [1] G. F. Voronin, Convex functions in the thermodynamics of heterogeneous substances, *Russ. J. Phys. Chem. A*, vol. 79, no. 12, pp. 1890–1902, 2005.
- [2] A. L. Voskov and G. F. Voronin, A universal method for calculating isobaric-isothermal sections of ternary system phase diagrams, *Russ. J. Phys. Chem. A*, vol. 84, no. 4, pp. 525–533, 2010.
- [3] J. Wang, F. G. Meng, H. S. Liu, L. B. Liu, and Z. P. Jin, Thermodynamic Modeling of the Au-Bi-Sb Ternary System, *J. Electron. Mater.*, vol. 36, no. 5, pp. 568–577, 2007.
- [4] A. Prince, G. V. Raynor, and D. S. Evans, Phase diagrams of ternary gold alloys, Institute of Metals, London, 1990.
- [5] J. Sangster and A. D. Pelton, Phase Diagrams and Thermodynamic Properties of the 70 Binary Alkali Halide Systems Having Common Ions, *J. Phys. Chem. Ref. Data.*, vol. 16, no. 3, p. 509, 1987.
- [6] J. Sangster and A. D. Pelton, Thermodynamic calculation of phase diagrams of the 60 common-ion ternary systems containing cations Li, Na, K, Rb, Cs and anions F, Cl, Br, I, *J. Phase Equilib.*, vol. 12, no. 5, pp. 511–537, 1991.
- [7] S.-L. Chen, J.-Y. Zhang, X.-G. Lu, K.-C. Chou, and Y. A. Chang, Application of Graham Scan Algorithm in Binary Phase Diagram Calculation, *J. Phase Equilib. Diffus.*, vol. 27, no. 2, pp. 121–125, 2006.

QUANTUM CONFINEMENT EFFECTS ON SEEBECK COEFFICIENT

Z.Fatih Ozturk, Altug Sisman* and Sevan Karabetoglu

Istanbul Technical University, Energy Institute, 34469, Istanbul/Turkey

*Corresponding Author: sismanal@itu.edu.tr

ABSTRACT

Seebeck coefficient is analytically derived for Fermi gas by considering quantum size effects to investigate the dependencies of Seebeck coefficient on domain size and quantum degeneracy. Under the relaxation time approximation, particle flux equation is expressed in terms of external potential, chemical potential and temperature gradient. The summations in the expression of particle flux are replaced by the Poisson summation formula to consider quantum size effects. Since the system size considered here is comparable to the thermal de Broglie wavelength, the contribution of zero correction term of the Poisson summation formula is included. In order to obtain an analytically solvable problem, rectangular domain geometry is considered. The results show that quantum size effects cause a significant improvement on Seebeck coefficient when the system size in one direction approach to thermal de Broglie wave length. This improvement is due to transition from bulk to quantum well behaviour. Variation of quantum size effects with quantum degeneracy, which is represented by dimensionless chemical potential, is also examined. It is seen that the chemical potential value for the maximum dimensionless Seebeck coefficient decreases with decreasing system size while the Seebeck coefficient increases.

INTRODUCTION

Since the low dimensional behaviours of the thermoelectric materials are different than the bulk ones, higher thermoelectric efficiencies can be achieved by using low dimensional structures like quantum wells, wires and dots [1-3]. The conversion efficiency of thermoelectric devices depends on the properties of the materials and determined by the well known figure of merit relation, $Z = S^2\sigma/\kappa$, where S is the Seebeck coefficient, σ is the electrical conductivity and κ is the thermal conductivity. Since the all variables in the figure of merit relation are dependent, they adversely affect each other so that the figure of merit does not vary significantly for the bulk thermoelectric materials. However, in the literature, it is proposed that quantum confinement plays an important role to enhance the figure of merit by using low dimensional nanostructures [4-8].

In contrast to the macroscopic approaches, transport properties of materials become size and shape dependent when the domain size is comparable to the characteristic length scale of the problem. Therefore, size and shape of the system are considered as additional control parameters on transport properties of nanoscale devices [9, 10]. In sufficiently small structures, the wave character of particles significantly changes the transport properties by modifying probability density distribution, the smallest values of the momentum components and momentum spectrum of particles [9, 11]. Some contributions arise when the thermal de Broglie wavelength of particles are not negligible in comparison with the size of the domain. These contributions are called as quantum size effects (QSE) in general [9, 11].

In the calculations here, free electrons in the conduction band of conductors and semi-conductors are considered as an

ideal Fermi gas and Seebeck coefficient is analytically derived by considering QSE. Through the confinement, sizes of the domain are smaller than the mean free path of the particles but equal to or greater than the thermal de Broglie wave length. Therefore conventional definitions of particle flux and transport coefficients are used. Dependencies of Seebeck coefficient on domain size and quantum degeneracy are investigated. Particle flux equation is derived in terms of external potential, chemical potential and temperature gradients. Relaxation time approximation is used to obtain non-equilibrium distribution function. Furthermore, relaxation time is assumed to be equal to the inverse of the collision frequencies of the particles. The summations inside the particle flux expression are replaced by the Poisson summation formula to consider QSE. Since the system size in at least one direction is comparable to the thermal de Broglie wavelength, the contribution of zero correction term of the Poisson summation formula is included. On the other hand, discreteness correction term is neglected since all the sizes are equal to or larger than the thermal de Broglie wavelength of particles. In order to obtain an analytically solvable problem, rectangular domain geometry is considered.

DERIVATION OF PARTICLE FLUX AND SEEBECK COEFFICIENT

Transport domain is a rectangular structure with dimensions of L_x, L_y, L_z and the domain is strongly confined through the direction x . The particle flux in direction x is written as,

$$J_x^N = \sum_{ijk} v_{w,x} f \quad (1)$$

where $v_{w,x}$ is the x component of velocity of the carrier at quantum state w and f is non-equilibrium distribution function. The equilibrium distribution function for Fermi-Dirac statistics is given by,

$$f_0 = \frac{1}{V} \frac{1}{\exp\left[\frac{\epsilon_w - \mu}{k_b T}\right] + 1} \quad (2)$$

where ϵ_w is the translational energy of the carriers, μ is the chemical potential, T is temperature, V is the domain volume, k_b is the Boltzmann's constant. Under the relaxation time approximation, the non-equilibrium distribution function in direction x can be determined as,

$$f = f_0 - \tau v_{w,x} \frac{\partial f_0}{\partial x} \quad (3)$$

where τ is the relaxation time which is expressed by using the particle-boundary mean free path (geometric mean free path, $L_g = V/2A$ where A is the surface area of the domain) and the particle velocity v as $\tau(v) = L_g/v$. Inserting Eq.(3) into Eq.(1), the particle flux in direction x for the particle-boundary collision dominated transport is derived as [9, 12],

$$J_x^N = \frac{L_g}{k_b T V} \left(\frac{2k_b T}{m} \right)^{1/2} (g_0 F_x^{\Phi T} + g_2 F_x^T) \quad (4)$$

where $F_x^{\Phi T} = F_x^\Phi - (\mu/k_b T) F_x^T$ and m is the mass of the carrier. Driving forces are defined by the gradients of the chemical and electrical (electrochemical) potentials and temperature as $F_x^\Phi = -(\partial\mu/\partial x + \partial\phi/\partial x)$, $F_x^T = -k_b(\partial T/\partial x)$ respectively. In Equation.(4), g function is a dimensionless quantity given by,

$$g_a = \sum_w \frac{m v_{w,x}^2 / 2k_b T}{(\epsilon_w / k_b T)^{\frac{1-a}{2}}} \frac{\exp(B_w)}{[\exp(B_w) + 1]^2} \quad (5)$$

where $B_w = (\epsilon_w - \mu)/k_b T$ [9, 12]. By using the parabolic dispersion relation, translational kinetic energy of the particles is easily written as,

$$\epsilon_{ijk} = \frac{\hbar^2}{8m} \left[\left(\frac{i}{L_x} \right)^2 + \left(\frac{j}{L_y} \right)^2 + \left(\frac{k}{L_z} \right)^2 \right] \quad (6)$$

where $i, j, k = 1, 2, 3, \dots, \infty$. By using Eq.(6), $\epsilon_w/k_b T$ is written as,

$$\frac{\epsilon_w}{k_b T} = \frac{\epsilon_{ijk}}{k_b T} = (\alpha_x i)^2 + (\alpha_y j)^2 + (\alpha_z k)^2 \quad (7)$$

where $\alpha_x = L_c/L_x$, $\alpha_y = L_c/L_y$, $\alpha_z = L_c/L_z$ and the length $L_c = \hbar/\sqrt{8mk_b T}$ is half of the most probable de Broglie wavelength of the particles.

In macroscale, sums may be replaced by integrals with a negligible error. However, since the system size approaches to thermal de Broglie wavelength at nanoscale this replacement causes a considerable error. Therefore, instead of replacing sum with an integral, Poisson summation formula is used to have more accurate result to calculate the sum in Eq.(5). For an even function, Poisson summation formula is written in the form of,

$$\sum_{i=1}^{\infty} f(i) = \int_0^{\infty} f(i) di - \frac{f(0)}{2} + 2 \sum_{s=1}^{\infty} \int_0^{\infty} f(i) \cos(2\pi s i) di \quad (8)$$

where the first term is the bulk term, the second term is the zero correction term which is important when the system size approach to the thermal de Broglie wavelength, and the third term is the discreteness correction term. Although it is possible to calculate sums exactly with Poisson summation formula, the third term of the Poisson summation formula is negligible compared with the others since the domain sizes here are always larger than the thermal de Broglie wavelength [9]. Inserting Eq.(7) into Eq.(5) and by using Poisson summation formula given in Eq.(8), g_a function is analytically obtained as,

$$g_a = -\frac{2\pi}{3\alpha_x \alpha_y \alpha_z} \Gamma\left(\frac{4+a}{2}\right) Li_{\frac{2+a}{2}} \left[1 - \frac{3(\alpha_x + \alpha_y + \alpha_z)}{4} \frac{\Gamma\left(\frac{3+a}{2}\right) Li_{\frac{1+a}{2}}}{\Gamma\left(\frac{4+a}{2}\right) Li_{\frac{2+a}{2}}} + \frac{3(\alpha_x \alpha_y + \alpha_y \alpha_z + \alpha_z \alpha_x)}{2\pi} \frac{\Gamma\left(\frac{2+a}{2}\right) Li_{\frac{a}{2}}}{\Gamma\left(\frac{4+a}{2}\right) Li_{\frac{2+a}{2}}} \right] \quad (9)$$

where Γ is Gamma function and Li_n is the Polylogarithm function with the degree of n and argument of $-\exp(\mu/k_b T)$. In Eq.(9), the first term is the bulk term which could be obtained by replacing sum with the integral and the other terms in the square bracket come from the second term of Poisson summation formula and arise due to wave character of particles. Inserting Eq.(9) into Eq.(4), size dependent particle flux is obtained. It is clear that the size dependency of particle flux appears for the confined directions only since the value of α is zero for other directions.

Seebeck coefficient is defined as the ratio of the electrochemical gradient to temperature gradient under zero particle flux condition and given by,

$$S = \frac{k_b}{q} \left(\frac{F_x^\Phi}{F_x^T} \right)_{J_N=0} \quad (10)$$

where q is the charge of the particle. By using Eqs.(9) and (10), Seebeck coefficient is obtained in term of g_a function as,

$$S = \frac{k_b}{q} \left(\frac{g_2}{g_0} - \Lambda \right) \quad (11)$$

where $\Lambda = \mu/k_b T$.

RESULTS

To show the deviations from the macroscopic picture, Seebeck coefficients derived with and without QSE (S and S_o) versus dimensionless chemical potential are plotted for a Fermi gas in Fig.1. Transport domain is confined only in x direction ($\alpha_y = \alpha_z \approx 0$, $\alpha_x = 1$).

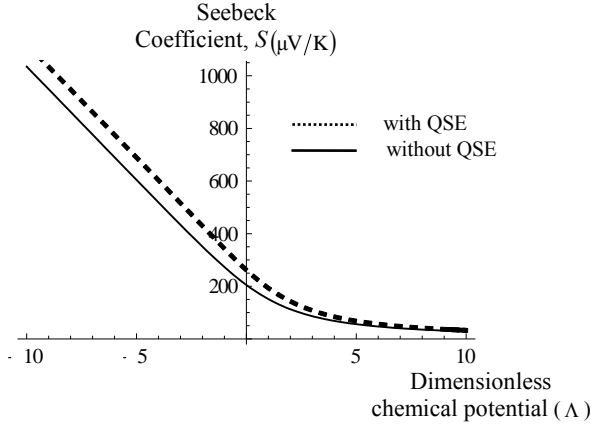


Fig.1: Variation of S and S_o with $\Lambda = \mu/k_bT$.

Fig.1 shows that increasing chemical potential (increasing degeneracy) decreases the contribution of the quantum size effects on Seebeck coefficient due to decreasing of mean de Broglie wave length. Therefore the difference between the curves becomes smaller for the higher values of Λ . The dimensionless form of the Seebeck coefficient is defined by dividing S to S_o and given by,

$$\tilde{S} = \frac{S}{S_o} \quad (12)$$

In Fig.2, \tilde{S} versus Λ is given for different values of domain size in x direction. The results show that QSE cause a significant improvement (as high as %30) on Seebeck coefficient when the system size approaches to thermal de Broglie wave length, ($\alpha_x \rightarrow 1$). Variation of quantum size effects with dimensionless chemical potential shows that there is a maximum value for \tilde{S} which increases with decreasing system size or increasing de Broglie wavelength.

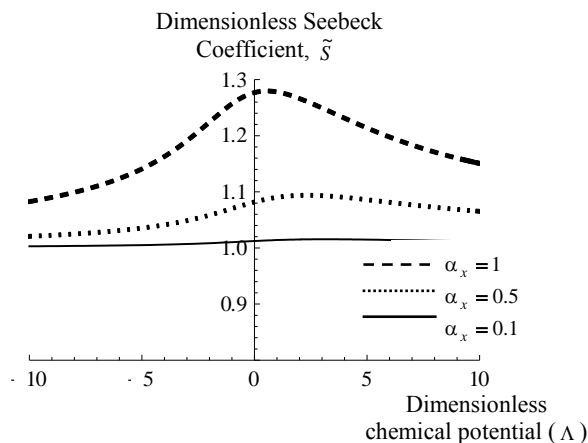


Fig.2: Variation of \tilde{S} with Λ for different values of α_x .

In Fig.3, variation of the maximum value of dimensionless Seebeck coefficient with dimensionless inverse scale factor in x direction is given. The effect of domain size on Seebeck coefficient is clearly seen. It is possible to improve Seebeck coefficient only by decreasing the domain size without making any change in the composition of the material. Therefore, size itself becomes a control parameter on material properties. This is due to the transition from bulk to quantum well behavior. Similarly, size itself play an important role during the transition from quantum well to quantum wire and from quantum wire to quantum dot behaviors.

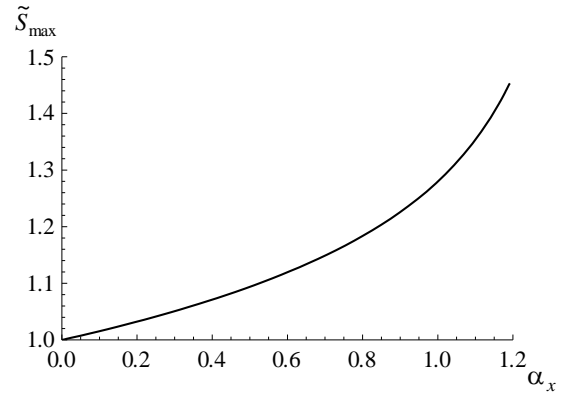


Fig.3: Variation of maximum dimensionless Seebeck coefficient with α_x for $\alpha_y = \alpha_z \approx 0$.

NOMENCLATURE

Symbol	Quantity	SI Unit
A	Surface area of the domain	m^2
f	Nonequilibrium distribution function	<i>dimensionless</i>
f_0	Equilibrium distribution function	<i>dimensionless</i>
F_x^Φ	Driving force due to electrochemical potential gradient	J / m
F_x^T	Driving force due to temperature gradient	J / m
h	Planck's constant	$J s$
i, j, k	Quantum numbers	<i>dimensionless</i>
k_b	Boltzman's constant	J / K
L_c	Half of the most probable de Broglie wave length	m
L_g	Geometric mean free path	m
Li	Polylogarithm function	<i>dimensionless</i>
L_x, L_y, L_z	Sizes of domain	m
m	Mass of particle	kg
q	Charge of particle	C
S	Seebeck coefficient	V / K
\tilde{S}	Dimensionless Seebeck coefficient	<i>dimensionless</i>
S_o	Seebeck coefficient without QSE	V / K
\tilde{S}_{max}	Dimensionless maximum Seebeck coefficient	<i>dimensionless</i>
T	Temperature	K

V	Volume	m^3
Z	Figure of merit	$1/K$
$\alpha_x, \alpha_y, \alpha_z$	Inverse scale factors	<i>dimensionless</i>
σ	Conductivity	$1/\Omega m$
Γ	Gamma function	<i>dimensionless</i>
ϵ_w	Translational energy	J
κ	Thermal conductivity	W/mK
Λ	Dimensionless chemical potential ($\mu/k_b T$)	<i>dimensionless</i>
μ	Chemical potential	J
τ	Relaxation time	s
φ	External potential	J

REFERENCES

- [1] M.S. Dresselhaus, G. Chen, M.Y. Tang, R. Yang, H. Lee, D. Wang, Z. Ren, J.P. Fleurial and P. Gogna, New Directions for Low Dimensional Thermoelectric Materials, *Advanced Materials*, vol.19, 1043-1053, 2007.
- [2] P. Pichanusakorn and P. Bandaru, Nanostructured Thermoelectrics, *Materials Science and Engineering R*, vol.67, pp.19-63, 2010.
- [3] C.J. Vineis, A. Shakouri, A. Majumdar and M.G. Kanatzidis, Nanostructured Thermoelectrics: Big Efficiency Gains from Small Features, *Advanced Materials*, vol.22, pp.3970-3980, 2010.
- [4] L.D. Hicks and M.S. Dresselhaus, Effects of Quantum-Well Structures on the Thermoelectric Figure of Merit, *Physical Review B*, vol.47, pp.12727-12731, 1993.
- [5] T.E. Huber, A. Nikolaeva, D. Gitsu, L. Konopko and C.A. Foss, Confinement Effects and Surface Induced Charge Carriers in Bi Quantum Wires, *Applied Physics Letters*, vol. 84, pp.1326-1328, 2004.
- [6] A.I Boukai, Y. Bunimovich, J.T. Kheli, J.K. Yu, W.A. Goddard and J.R. Heath, Silicon Nanowires as Efficient Thermoelectric Materials, *Nature*, vol.451, pp.168-171, 2008.
- [7] L.D. Hicks, T.C. Harman, X. Sun and M.S. Dresselhaus, Experimental Study of the Effect of Quantum-Well Structure on the Thermoelectric Figure of Merit, *Physical Review B*, vol.53, pp. 10493-10496, 1996.
- [8] P. Pichanusakorn and P.R. Bandaru, The Optimal Seebeck Coefficient for Obtaining the Maximum Power Factor in Thermoelectrics, *Applied Physics Letters*, vol.94, pp.223108, 2009.
- [9] Z.F. Ozturk and A. Sisman, Quantum Size Effects on the Thermal and Potential Conductivities of Ideal Gases, *Physica Scripta*, vol. 80, 065402, 2009.
- [10] R. Kim, S. Datta and M.S. Lundstorm, Influence of Dimensionality on Thermoelectric Device Performance, *Journal of Applied Physics*, vol.105, pp.034506, 2009.
- [11] A. Sisman, Z.F. Ozturk and C. Firat, Quantum Boundary Layer: Non-uniform Density Distribution of an Ideal Gas in Thermodynamic Equilibrium, *Physics Letters A*, vol.362, pp.16-20, 2007.
- [12] Z.F. Ozturk, Quantum Size Effects on Nano Gas Transport, Ph.D. Thesis, Istanbul Technical University, Istanbul, 2008.

THERMOELECTRIC EFFECTS AND SIZE DEPENDENCY OF THE FIGURE-OF-MERIT IN CYLINDRICAL NANOWIRES

A. Sellitto*, V. A. Cimmelli**, D. Jou†

*University of Basilicata, Department of Mathematics, Computer Science and Economics, Potenza (Italy), E-mail: ant.sellitto@gmail.com

**University of Basilicata, Department of Mathematics, Computer Science and Economics, Potenza (Italy), E-mail: vito.cimmelli@unibas.it

†Autonomous University of Barcelona, Department of Physics, Bellaterra, Catalonia (Spain), E-mail: david.jou@uab.cat

EXTENDED ABSTRACT

The conversion of heat current into electric current through thermoelectric effects, i.e., the direct conversion of temperature differences to electric voltage and vice-versa, offers a promising avenue in energy management. From the practical point of view, one of the most explored possibilities is the junction of two nanostructured crystals of different type, in which the heat is carried by phonons and electrons, whose efficiency may be evaluated through the parameter ZT , being T the absolute temperature, and Z the so-called figure-of-merit, defined as

$$Z = \frac{\varepsilon^2 \sigma_e}{\lambda_e + \lambda_p},$$

ε being the Seebeck coefficient, σ_e the electrical conductivity, and λ_e and λ_p the thermal conductivities due to electrons and phonons, respectively.

An interesting aspect of nanosystems is the possibility of an additional control of the transport coefficients by getting sizes comparable to the mean-free path (MFP) ℓ of the different heat carriers (phonons, electrons, holes, etc.). For instance, in nanowires it is expected that whenever the radius of the transversal section is comparable to (or smaller than) the phonon MFP, the phonon contribution to the thermal conductivity λ_p will be reduced, leading to an increase of Z .

Thus, incorporating explicitly the effects of the several MFPs is useful to study new strategies for the optimization of these effects.

In the present poster we explore phenomenologically the size dependency of Z in nanowires. To achieve that task we use a phonon-hydrodynamic approach [1; 2] and a simple thermodynamic model [3], which is developed in the framework of Extended Irreversible Thermodynamics, the theory in which the dissipative fluxes are updated to the rank of thermodynamic variables and the gradients of the unknown fields are allowed to enter the state space [1; 2]. Our aim is to bridge the gap between the much detailed microscopic approaches (i.e., kinetic theory or numerical simulations) and the classical nonequilibrium-thermodynamic approaches lacking the explicit presence of the MFP.

In the particular case of a nanosample made by Bi_2Te_3 interesting results are also obtained.

REFERENCES

- [1] G. Lebon, D. Jou and J. Casas-Vázquez, *Understanding nonequilibrium thermodynamics*, Berlin: Springer, 2008.
- [2] D. Jou, J. Casas-Vázquez and G. Lebon, *Extended Irreversible Thermodynamics*, Berlin: Springer, fourth revised ed., 2010.
- [3] A. Sellitto, V. A. Cimmelli and D. Jou, Thermoelectric effects and size dependency of the figure-of-merit in cylindrical nanowires, *Int. J. Heat Mass Transfer*, vol. 57, pp. 109-116, 2013.

HEAT CAPACITIES AND TRANSPORT PROPERTIES OF AQUEOUS NONPOLAR SOLUTE MIXTURES

Igor Shvab, Richard Sadus

Centre for Molecular Simulation, Swinburne University of Technology,
Hawthorn, Victoria 3122, Australia.

EXTENDED ABSTRACT

Heat capacity, diffusion coefficients, and velocity autocorrelation functions for water mixtures with different nonpolar solutes (methane and noble gases) have been studied using molecular dynamics at constant volume and temperature. A combined SPCE + Lennard-Jones potential was chosen for these systems with Lorentz-Berthelot combining rules. The use of such a potential for water-solute and solute-solute interactions allows us to study the system in a single phase region over the wide pressure-temperature range and solute molar fractions up to 15%. The heat capacities were calculated using the formalism developed in works of Lustig [1] for NVT ensemble. Comparison with experimental data for pure water [2] in the temperature range 298 - 650 K has been done. Simulations show good agreement of bulk water C_v with experimental data in the high temperature region, and slight overestimation at ambient temperatures.

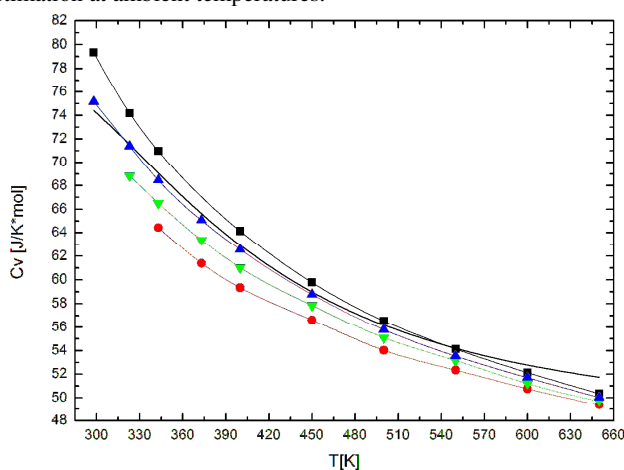


FIG. 1. Isochoric heat capacity as a function of temperature at 0.998 g/cm^3 : water + 0% CH_4 (black ■), water + 6% CH_4 (blue ▲), water + 10% CH_4 (red ●), water + 15% CH_4 (green ▼), and IAPWS-95 reference data[2] for water (—). The lines through the data points are given only for guidance.

The first MD simulations of heat capacity changes in water induced by the solvation of nonpolar solutes (methane, krypton) at solute molar fractions up to 15% are reported (see Fig. 1). Heat capacities of aqueous nonpolar solute mixtures are smaller than that of pure water, and proportional to the solute concentration. This is in agreement with the previous results for very dilute aqueous nonpolar solute mixtures [3] and aqueous solutions of alcohols in wide concentration range [4]. Difference between heat capacities of pure water and water-solute mixtures gradually decreases with temperature, completely converging at critical temperature.

Self-diffusion constants of water are in fairly good agreement with experimental data almost up to the boiling temperature. Diffusion coefficients of the given aqueous nonpolar solute mixtures decrease with solute concentration and show the following temperature-mass dependence $D \propto T / \mu^\beta$. Self-diffusion coefficients of water molecules in the mixture are smaller than that of pure water. Degree to which D of water in the mixture is smaller than in the pure water appears to be proportional to the solute concentration.

Solvation of nonpolar groups in water is accompanied by specific changes in structure and transport properties which appear to be proportional to particles mass and size, and are very different from the changes in water structure induced by solvation of polar and ionic groups.

REFERENCES

- [1] R. Lustig, *Molecular Simulation*, **37**, 457 (2011)
- [2] W. Wagner. See <http://www.thermo.rub.de/en/prof-w-wagner/software/iapws-95.html>. The IAPWS-95 software used to obtain reference data for water is available from this website.
- [3] K. Sharp, B. Madan, *J. Phys. Chem. B* **101**, 4343 (1997)
- [4] T. Kuroki, N. Kagawa, H. Endo, S. Tsuruno, and J. W. Magee, *J. Chem. Eng. Dat.* **46**, 1101 (2001).

INTRINSIC QUANTUM THERMODYNAMIC PREDICTION OF THE NON-EQUILIBRIUM ATOMISTIC-LEVEL BEHAVIOUR OF CHEMICALLY REACTIVE SYSTEMS

Omar Al-Abbasi*, Gian Paolo Beretta^o, Michael R. von Spakovsky*

* Mechanical Engineering Department, Virginia Tech, Blacksburg, Virginia, 24061, USA

^o Department of Mechanical and Industrial Engineering, Università di Brescia, Brescia, 25123, Italy

ABSTRACT

This paper presents an application of a fundamentally new approach called Intrinsic Quantum Thermodynamic (IQT) to the prediction of the kinetics of chemically reactive systems at small scales. The IQT framework satisfies the laws of quantum mechanics as well as thermodynamics and provides an alternative, comprehensive, and reasonable means for modeling non-equilibrium processes even far from equilibrium. It does so without the need for any of the a priori limiting assumptions common to most conventional methods in the literature such as that of stable equilibrium via a specific choice of temperature or of pseudo-equilibrium between reactants and activated complex. The IQT framework assumes time evolution along the steepest entropy ascent path in state space and is, in fact, able to predict a unique non-equilibrium path, which the system takes in relaxing from a state of non-equilibrium to that of stable equilibrium, and in so doing, dynamically provides a plausible complete picture of the changes occurring in key thermodynamic properties (e.g., the instantaneous species concentrations, entropy and entropy generation, reaction coordinate, chemical affinities, reaction rate, etc.) throughout the reaction process. In this paper, the IQT framework is applied to a chemically reactive system governed by the reaction mechanism

INTRODUCTION

This paper discusses the use of a relatively new theory known as intrinsic quantum thermodynamics (IQT) [1-4] to predict the reaction kinetics at atomistic levels of chemically reactive systems in the non-equilibrium realm. IQT has emerged over the last three decades as the theory that not only unifies two of the three theories of physical reality, namely, quantum mechanics (QM) and thermodynamics, but as well provides a physical basis for both the entropy and entropy production. The IQT framework is able to describe the evolution in state of a system undergoing a dissipative process based on the principle of steepest entropy ascent or locally maximal entropy generation [5]. The dynamical postulate of this theory was formulated originally to predict the evolution dynamics of closed, isolated systems composed of a single particle, an assembly of indistinguishable particles, or a field [6] or a set of distinguishable particles, fields, or some combination of these [7]. More recently some preliminary attempts have been made to extend the IQT equation of motion so as to model a larger class of systems, namely, those involving heat [8-10] and/or mass interactions [10].

The work presented in this paper demonstrates for the first time the use of the IQT framework to model the evolution in state of a chemically reactive system as its state relaxes to stable equilibrium. This framework brings a number of benefits to the field of reaction kinetics. Among these is the ability to predict a unique, non-equilibrium (kinetic), thermodynamic path, i.e., unique cloud of trajectories, which the state of the system follows in relaxing to stable equilibrium. As a consequence, the reaction rate kinetics at every instant of time is known as are the chemical affinities, the reaction coordinates, the direction of reaction, the activation energies, the entropy, the entropy production, etc. All is accomplished without any a priori limiting assumption of stable equilibrium via a specific choice of temperature nor of pseudo-equilibrium

between reactant and activated complex. This is fundamentally different from all conventional methods (e.g., Transition State Theory [11,12], Trajectory Calculations [13], Quantum Scattering Theory [14, 15], etc.), which envision the reaction as a process driven only by collisions (i.e., the laws of mechanics, whether classical or quantum). In contrast, IQT envisions the same problem driven by both the laws of mechanics and thermodynamics. It is, thus, able to provide detailed information about the so-called state-to-state reaction channels and is not only able to predict the thermal reaction rate constant but its instantaneous details as well. As a consequence, this rate constant is transformed into a variable rate of the reaction process.

To illustrate the IQT approach, the



reaction mechanism, which for decades has been under intensive investigation both theoretically and experimentally [16,17], is used to benchmark the IQT results and illustrate the IQT reaction kinetics in the non-equilibrium realm.

IQT MODEL

The application of the general IQT framework for chemically reactive systems at small scales developed by Beretta and von Spakovsky [18] to the chemical kinetics of these systems is consistent with the idea put forward by Ziegler [19] concerning the thermodynamic consistency of the standard model of chemical kinetics. In modeling the non-equilibrium time evolution of state of these systems, both the system energy and particle number eigenvalue problems as well as the non-linear IQT equation of motion must be solved. The former establish the so-called energy and particle number eigenstructure of the system, i.e., the landscape of quantum eigenstates available for the system, while the latter determines the unique non-equilibrium thermodynamic path taken by the

system, showing how the density operator ρ , which represents the thermodynamic state of the system at every instant of time, evolves from a given initial non-equilibrium state to the corresponding stable chemical equilibrium state. For this framework, the thermodynamic system is defined as an isolated system consisting of r different reacting species contained in a tank.

In the present paper, only the principal IQT model equations are presented. For complete details of the model, the reader is referred to [18]. To begin with, the system energy and particle occupation number eigenvalue problems, which must be solved to establish the landscape of quantum eigenstates available for the system, are the following:

$$H|\xi_{sq_s}\rangle = E_{sq_s}|\xi_{sq_s}\rangle \quad s=1,\dots,C \quad q_s=1,\dots,L_s \quad (2)$$

where H is the system-level Hamiltonian, E_{sq_s} the system-level energy eigenvalue, ξ_{sq_s} the system-level eigenvector, C the number of subspaces of compatible compositions, and L_s the dimension of subspace s . The dimension of the overall Hilbert space \mathcal{H} of the system is $L = \sum_{s=1}^C L_s$. A Hilbert as opposed to Fock space is assumed since the framework presented is based on the assumption that, consistent with the earlier assumption of an isolated system, the number of atoms is fixed (i.e., is conserved) and always known [18]. The corresponding system-level particle occupation number eigenvalue problem is expressed as

$$N_{A_i j_i}|\xi_{sq_s}\rangle = \alpha_{ij_i}^{sq_s}|\xi_{sq_s}\rangle \quad s=1,\dots,C \quad q_s=1,\dots,L_s \quad (3)$$

$$i=1,\dots,r \quad j_i=1,\dots,M_i$$

$$N_{A_i} = \sum_{j_i=1}^{M_i} N_{A_i j_i} \quad (4)$$

where A_i is the i^{th} species, N_{A_i} the A_i -particles number operator, $N_{A_i j_i}$ the A_i -particles-in-the- j_i^{th} -internal-level occupation number operator, and $\alpha_{ij_i}^{sq_s}$ the A_i -particles-in-the- j_i^{th} -internal-level eigenvalue for the q_s^{th} combination in the s^{th} compatible composition. M_i is the number of eigenvectors of the one- A_i -particle internal Hamiltonian operator associated with the internal degrees of freedom (i.e., vibrational, rotational, etc. energy levels).

Defining the Hilbert space and the set of eigenvectors that span that space requires that the initial amounts n_{ia} for each species A_i in the reacting mixture be related to the set of compatible amounts via the proportionality relations [20], namely,

$$n_{is} = n_{ia} + \sum_{l=1}^{\tau} \nu_{il} \varepsilon_{ls} = n_{ia} + \mathbf{v}_i \cdot \boldsymbol{\varepsilon}_s \geq 0 \quad (5)$$

where n_{is} is the eigenvalue of the amount of the A_i species for the subspace s , ν_{il} the stoichiometric coefficient for species A_i in reaction mechanism " l ", \mathbf{v}_i the set of stoichiometric coefficients for species A_i in each of the τ reaction mechanisms, ε_{ls} the eigenvalue of the reaction coordinate operator of reaction " l " that corresponds to the s^{th} compatible composition, and $\boldsymbol{\varepsilon}_s$ the set of reaction coordinate eigenvalues identifying the s^{th} compatible composition. This set of inequality equations determines the number of compatible solutions (i.e., subspaces s). Note that the n_{is} are related to the $\alpha_{ij_i}^{sq_s}$ via

$$n_{is} = \sum_{j_i=1}^{M_i} \alpha_{ij_i}^{sq_s} \quad \text{for every } q_s=1,\dots,L_s \quad (6)$$

Equations (2) and (3) are not solved directly due to their complexity but instead related to a set of one-particle

eigenvalue problems, which can be solved. For details of how this is done, the reader is referred to [18]. The result is that, the one-particle A_i energy eigenvalues and eigenvectors for the internal degrees of freedom are made to correspond to the system-level ones via the following relations:

$$\left| \xi_{sq_s}^{int} \right\rangle = \left(\bigotimes_{i=1}^r \left(\bigotimes_{j_i=1}^{M_i} \left| \varepsilon_{j_i}^{A_i} \right\rangle \right)^{\otimes \alpha_{ij_i}^{sq_s}} \right) \quad (7)$$

$$E_{sq_s}^{int} = \sum_{i=1}^r \sum_{j_i=1}^{M_i} e_{j_i}^{A_i} \alpha_{ij_i}^{sq_s} \quad (8)$$

and for the translational degrees of freedom via the following:

$$\left| \xi_{sq_s}^{tr} \right\rangle = T^{-1} \left(\bigotimes_{j_s=1}^{n_s} \left| \hat{\varepsilon}_{k_{j_s}}^{s j_s} \right\rangle \right) \quad (9)$$

$$E_{sq_s}^{tr} = e_{k_{s1}}^{s1} + \dots + e_{k_{s j_s}}^{s j_s} + \dots + e_{k_{s n_s}}^{s n_s} \quad (10)$$

where the $q_s^{tr} = (k_{s1}, \dots, k_{s j_s}, \dots, k_{s n_s})$, each $k_{s j_s} = 1, \dots, K_{s j_s}$, and $K_{s j_s}$ corresponds to some practical truncation of what is an infinite dimensional problem. In addition, T^{-1} in Eq. (9) signifies an inverse unitary transformation from the center-of-mass coordinate frame in which the one-particle translational eigenvalue problems are solved. The system-level energy eigenvalues and eigenvectors are now found from those for the various degrees of freedom via

$$\left| \xi_{sq_s} \right\rangle = \left| \xi_{sq_s}^{tr} \right\rangle \otimes \left| \xi_{sq_s}^{int} \right\rangle \quad (11)$$

$$\text{and } E_{sq_s} = E_{sq_s}^{tr} + E_{sq_s}^{int} \quad (12)$$

The system-level Hamiltonian is next constructed according to the following expression:

$$H = \sum_{s=1}^C \sum_{q_s=1}^{L_s} E_{sq_s} P_{\mathcal{H}_{sq_s}} \quad (13)$$

where the projector $P_{\mathcal{H}_{sq_s}}$ is given by

$$P_{\mathcal{H}_{sq_s}} = \left| \xi_{sq_s} \right\rangle \left\langle \xi_{sq_s} \right| \quad (14)$$

In a like manner, the particle number operator for each species is written as

$$N_{A_i} = \sum_{s=1}^C \sum_{j_i=1}^{M_i} \sum_{q_s=1}^{L_s} \alpha_{ij_i}^{sq_s} P_{\mathcal{H}_{sq_s}} \quad (15)$$

The preceding quantities provide the basis for determining the set of occupation probabilities y_{sq_s} , which correspond to the density operator ρ at any given instant of time and in turn are used to calculate the expectation values of properties or observables of interest. Thus,

$$y_{sq_s} = \text{Tr}(\rho P_{\mathcal{H}_{sq_s}}) = \left\langle \xi_{sq_s} \left| \rho \right| \xi_{sq_s} \right\rangle \quad (16)$$

and the expectation energy of the system is given by

$$\langle H \rangle = \text{Tr}(\rho H) = \sum_{s=1}^C \sum_{q_s=1}^{L_s} y_{sq_s} E_{sq_s} \quad (17)$$

The expectation value for the number of particles of species A_i is found from

$$\langle N_{A_i} \rangle = \sum_{j_i=1}^{M_i} \langle N_{A_i j_i} \rangle = \sum_{s=1}^C \sum_{q_s=1}^{L_s} y_{sq_s} \sum_{j_i=1}^{M_i} \alpha_{ij_i}^{sq_s} \quad (18)$$

while that for the reaction coordinate is given by

$$\langle \boldsymbol{\varepsilon} \rangle = \sum_{s=1}^C \boldsymbol{\varepsilon}_s \sum_{q_s=1}^{L_s} y_{sq_s} \quad (19)$$

or on a rate basis by

$$\langle \dot{\mathcal{E}} \rangle = \sum_{s=1}^C \varepsilon_s \sum_{k=1}^{L_s} \dot{y}_{sq_s} \quad (20)$$

Now, the IQT equation of motion governing the reaction kinetics for the system considered here is the following:

$$\frac{d\rho}{dt} = -\frac{i}{\hbar} [H, \rho] + \frac{1}{2k_B\tau} \{ \Delta M, \rho \} \quad (21)$$

where the first term on the right governs the linear Hamiltonian dynamics of the state evolution and the second, the so-called dissipation term, the nonlinear non-Hamiltonian steepest-entropy-ascent dynamics. In this equation, τ is the internal-relaxation time for the dissipation, $\{ \}$ the anti-commutator operator, k_B Boltzmann's constant, and $\Delta M = M - \langle M \rangle$ the deviation from the mean of the non-equilibrium Massieu operator defined as

$$M = S - H/\theta_H \quad (22)$$

where S and H are the entropy and Hamiltonian operators, respectively, and θ_H is a constant-energy, nonequilibrium temperature given in terms of the variance of the entropy and Hamiltonian operators by

$$\theta_H(\rho) = \langle \Delta H \Delta H \rangle / \langle \Delta S \Delta H \rangle \quad (23)$$

The entropy operator S is expressed by one of two equivalent forms, namely,

$$S = -k_B \ln(\rho + P_o) = -k_B B \ln \rho \quad (24)$$

with P_o and B , respectively, the projection operators onto the range and the kernel of ρ .

ONE-PARTICLE ENERGY EIGENVALUES

It is assumed that the reacting mixture considered here behaves as a Gibbs-Dalton mixture of ideal gases. For that reason, the energy eigenvalues for translation, vibration, and rotation for the species involved are given by a set of closed-form relations. For translation,

$$\varepsilon_k^{tr} = \frac{h^2}{8m} \left(\frac{\pi n_x}{L_x} + \frac{\pi n_y}{L_y} + \frac{\pi n_z}{L_z} \right)^2 \quad (25)$$

where ε_k^{tr} is the one-particle translational energy eigenvalue; h Planck's constant; m the mass of the particle; n_x , n_y and n_z are the quantum numbers in the x , y and z directions, respectively; and L_x , L_y , and L_z the dimensions for the system volume in the x , y , and z directions, respectively.

For vibration, the expression is

$$\varepsilon_v^{vib} = \nu(\nu + \frac{1}{2}) \omega \hbar^2 \quad (26)$$

where ν is the vibrational quantum number which takes values of $\nu=0,1,2, \dots$, ω is the vibrational frequency, and \hbar Planck's modified constant. A wide range of wavenumbers from which ω can be calculated are reported in the literature [21, 22]. In the present paper, the wavenumber values used are 4401 cm^{-1} for H_2 and 4000 cm^{-1} for FH .

Finally, for rotation, the following expression is used:

$$\varepsilon_J^{rot} = \frac{J(J+1)\hbar^2}{2\mu r^2} \quad (27)$$

where J is the rotational quantum number that takes values of $J=0,1,2, \dots$, μ is the reduced mass, and r the distance between two atoms.

NUMERICAL APPROACH

For purposes of this paper and the preliminary comparisons given below, the system considered here initially consists of 1

particle of F and 1 of H_2 and is governed by the reaction mechanism of Eq. (1). The degrees of freedom for each of the molecules and atoms in the IQT model are given in Table 1.

To apply the IQT equation of motion to this IQT model, the density operator for an initial non-equilibrium state is required. Such a state far from equilibrium is found by first finding the density operator or matrix ρ^{pe} for a partially canonical state

Table 1. Quantum numbers considered for each of the molecules and atoms in the IQT model.

Species	Translational quantum nos.	Vibrational quantum nos.	Rotational quantum nos.
F	$k=1, \dots, 5$		
H_2	$k=1, \dots, 5$	$\nu=0$	$J=0, 1$
FH	$k=1, \dots, 5$	$\nu=0, 1, 2, 3$	$J=0, 1, \dots, 7$
H	$k=1, \dots, 5$		

and then perturbing it. To determine ρ^{pe} , the following set of equations for the occupation probabilities y_j^{pe} must be solved:

$$y_j^{pe} = \frac{\delta_j e^{(-\beta E_j)}}{\sum_{k=1} \delta_k e^{(-\beta E_k)}} \quad (28)$$

subject to the constraints

$$\text{Tr}(\rho^{pe} H) = \sum_j y_j^{pe} E_j = \langle H \rangle \quad (29)$$

$$\text{Tr}(\rho^{pe} N_{A_i}) = \sum_j y_j^{pe} (n_j)_i = \langle N_{A_i} \rangle \quad i=1, \dots, r \quad (30)$$

The E_j in these equations are the system-level energy eigenvalues and the $(n_j)_i$ the system-level particle number eigenvalues for the i^{th} species. The values for the δ_j for each reactant species are set to either 0 or 1. As long as at least one of the δ_j has a value of 0, Eq. (28) describes the occupation probabilities for the density operator or matrix of a partially canonical state.

To find the initial non-equilibrium density operator or matrix, ρ^{pe} is perturbed as follows:

$$f_j = 1 - \lambda + \lambda \frac{y_j^{pe}}{y_j^{se}} \quad (31)$$

$$y_j = \frac{f_j y_j^{se}}{\sum_{i=1} f_i y_i^{se}} \quad (32)$$

where λ is an arbitrary perturbation parameter constrained by $0 < \lambda < 1$ and the y_j^{se} are the occupation probabilities for the stable equilibrium density matrix given by

$$y_j^{se} = e^{\left(\frac{-E_j}{k_b T} \right)} / \sum_{k=1} e^{\left(\frac{-E_k}{k_b T} \right)} \quad (33)$$

Here T is the stable equilibrium temperature.

Once the initial density operator or matrix is found, Eq. (21) is solved for the evolution in state of the system. This equation has been solved here using a fourth order Runge-Kutta explicit scheme with the relative tolerance error set to $1e-5$.

RESULTS AND DISCUSSION

Predicting the value of the entropy and the entropy generation at each instant of time are direct outcomes of the IQT framework since the 1st and 2nd laws of thermodynamics are explicitly built into the equation of motion. Figures 1 and 2 show how both the entropy and the rate of entropy generation of the system evolve in time. A state of stable equilibrium is

reached when the entropy plateaus out. In addition, the peak in the rate of entropy generation occurs quite early in the process and then quickly decreases as stable equilibrium is approached.

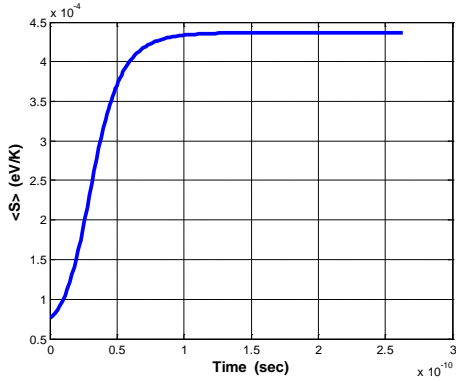


Figure 1. The instantaneous entropy of the reaction processing system.

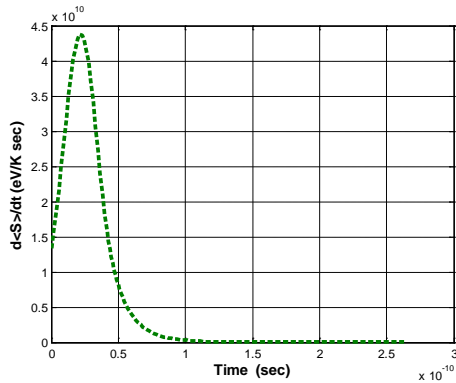


Figure 2. The instantaneous entropy generation during the reaction process.

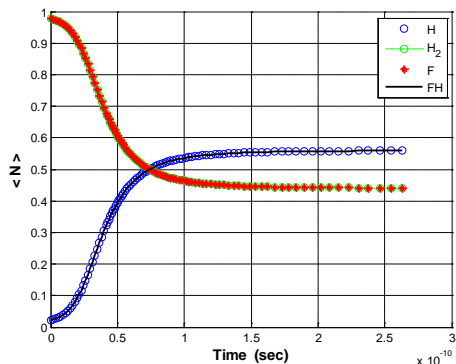


Figure 3. The expectation values of the particle number operator for each species.

A key feature of the IQT framework is that it is able to dynamically predict the concentration of reactive species as the reaction evolves in time. Figure 3 shows how the reactive species are depleted and created throughout the entire reaction process. Indeed the availability of these instantaneous values for the species concentrations indicates that the reaction rate constant $k(T)$, which in the literature is usually referred to as the thermal rate constant¹, may in fact not be a constant but rather a parameter changing in time. In Figure 3, the identical amounts for the reactants F and H_2 as well as for the products H and FH is a direct consequence of the proportionality relations, Eq. (5), and the initial amounts chosen for the reactants and products.

For the bimolecular reaction mechanism of Eq. (1), the net reaction rate as a function of time t is given by

$$r(t) = r_f(t) - r_b(t) \quad (34)$$

$$r(t) = k_f(t, T)[F(t)][H_2(t)] - k_b(t, T)[FH(t)][H(t)] \quad (35)$$

where r_f and r_b are the forward and backward reaction rates, k_f and k_b the forward and backward reaction rate “constants”, and $[A(t)]$ the concentrations of the various species. The reaction orders for the species F , H_2 , FH , and H coincide here with the stoichiometric coefficients for each species for this reaction mechanism although it is noted that this is not generally the case [23]. Based on the initial amounts of species chosen and the proportionality relations, it follows that the net reaction rate r for this reaction mechanism coincides with the expectation value of the rate of the reaction coordinate $\langle \dot{\mathcal{E}} \rangle$ given by Eq. (20). Numerically, it can also be found by calculating the slope of the expectation value of the particle number operator of either one of the product species using a second order accurate finite difference scheme. Once known, Eq. (35) along with the zero rate condition at stable equilibrium and the assumption that the detailed balance condition holds also for the time-dependent rate constants, i.e.,

$$\frac{k_f(t, T)}{k_b(t, T)} = \frac{k_f(t_{se}, T)}{k_b(t_{se}, T)} = \frac{[F]_{se}[H_2]_{se}}{[FH]_{se}[H]_{se}} \quad (36)$$

can be used to determine $k_f(t, T)$ and $k_b(t, T)$ at every instant of time along the entire kinetic path determined by the equation of motion.

Figure 4 shows these instantaneous values as well as the equilibrium constant $K(T)$ given by the ratio of k_f to k_b for the case of a system expectation energy which corresponds at stable equilibrium to a temperature of 298 K. The instantaneous values for the corresponding net, forward, and backward reaction rates are seen in Figure 5. Clearly, as expected, the forward reaction dominates at the beginning of the reaction with the reverse reaction growing in importance as stable equilibrium is approached. Note that the time scale seen in these two figures and the previous ones is based on a value of τ in the equation of motion which has been fitted to the value of k_f at 298 K reported in Heidner *et al.* [24] and shown in Table 2. This table also includes the values of k_f from Heidner *et al.* [24] for a number of other stable equilibrium temperatures as well as values for k_f from a number of other researchers.

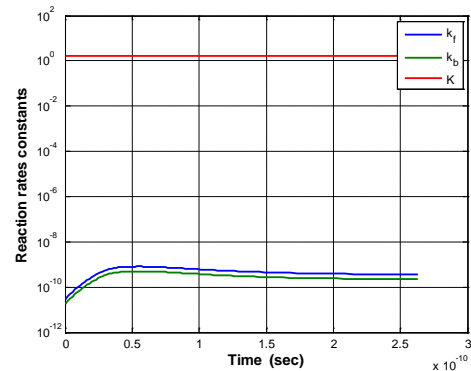


Figure 4. The forward and reverse reaction rate constants as well as the equilibrium constant as a function of time for a system expectation energy, which at stable equilibrium corresponds to a temperature of 298 K.

For a value of τ based on the value for k_f in Table 2 from Heidner *et al.* [24] corresponding to a stable equilibrium temperature of 700 K, a similar evolution of the reaction rate constants and reaction rates is given in Figures 6 and 7. The trends are the same as in Figures 4 and 5 with the forward

¹ In fact, this reaction rate constant is that for the forward reaction found at the start of the reaction when the backward reaction rate is negligible [22].

reaction dominating initially and the backward reaction growing in importance as stable equilibrium is approached. However, the reaction rate magnitudes are clearly much greater and the difference between the forward and backward reaction rate constants is significantly larger.

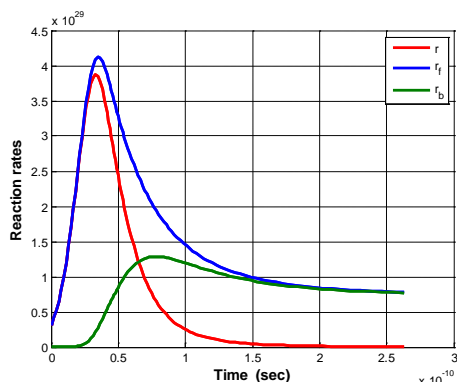


Figure 5. The forward, reverse and net reaction rates for a system expectation energy, which at stable equilibrium corresponds to a temperature of 298 K.

Table 2. Values of the forward reaction rate constant reported in the literature for the reaction mechanism of Eq. (1) [16].

T (K)	$k_f(T)/10^{-11}$ (cm ³ /molecule-sec)				
	WH ^a	SBA ^b	HBGM ^c	RHPB ^d	WTM ^e
298	2.33	2.48	2.93	2.81	2.26
350	2.89	3.14	3.94	3.35	
400			4.88	3.80	
450			5.76		
500			6.57		
600			8.01		5.68
700			9.23		

^aWurzberg and Houston [25]; ^bStevens, Brune, and Anderson [26]; ^cHeidner, Bott, Gardner, and Melzer [24]; ^dRosenman, Hochman-Kowal, Persky, and Baer [27]; ^eWang, Thompson and Miller [16]

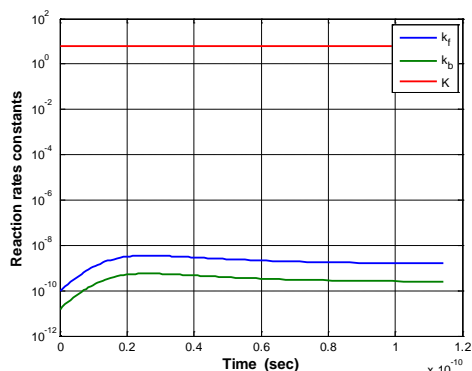


Figure 6. The forward and reverse reaction rate constants and the equilibrium constant as a function of time for a system expectation energy, which at stable equilibrium corresponds to a temperature of 700 K.

Although all the previous figures are referred to some stable equilibrium temperature, the use of such a temperature in the IQT simulations for the reaction kinetics of the reacting system is not required. In fact, it is a result and not an input to the model. Instead, it is the non-equilibrium temperature θ_H defined by Eq. (23), which plays a role in the IQT simulations. As seen in Figure 8, this temperature evolves towards that at stable equilibrium for three different expectation energies, i.e., those corresponding to 298 K (blue curve), 500 K (red curve), and 700 K (green curve) at stable equilibrium.

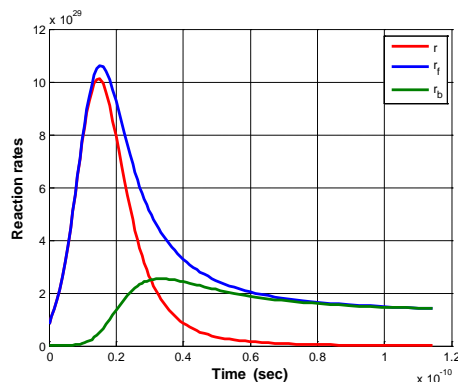


Figure 7. The forward, reverse and net reaction rates for a system expectation energy, which at stable equilibrium corresponds to a temperature of 700 K.

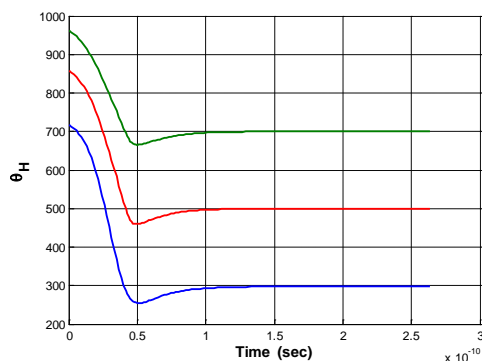


Figure 8. Time evolution of θ_H for system expectation energies corresponding to 298 K, 500 K, and 700 K at stable equilibrium.

SOME FURTHER RESULTS

A fundamental difference between the results for the reaction rate constant obtained by theories based on quantum mechanics to those based on classical mechanics is the divergence from linear behaviour at low temperatures as illustrated in Figure 9. For the system considered here and within the IQT framework, Figure 10 shows the behaviour of the forward reaction rate constant as a function of stable equilibrium temperature. Clearly, the deviation from linear behaviour at low temperatures seen in this figure provides confirmation that the predictions being made with IQT follow what would be expected from a quantum mechanically based model. Of course, additional validation of the IQT predictions is needed. In principle, it would be interesting to see if it is possible to identify a fixed, physically meaningful functional $\tau(\rho)$ such that (1) $k_f(t, T)$ and $k_b(t, T)$ as computed above from the assumption of the detailed balance result are effectively independent of time and (2) the reaction rates match the data of

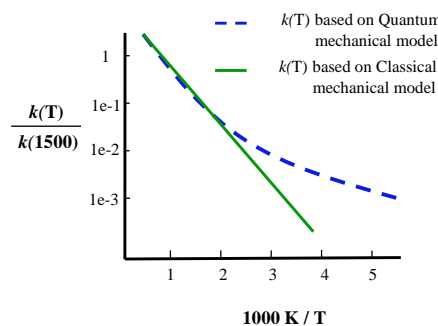


Figure 9. Depiction of the temperature dependence of the forward reaction rate constant with and without quantum mechanical effects taken into account.

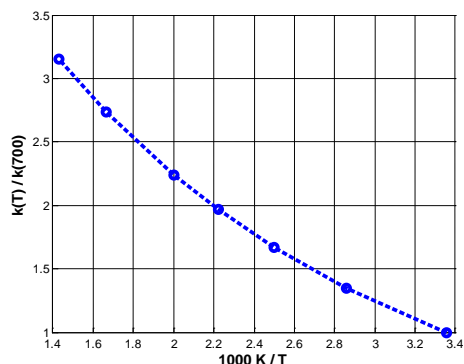


Figure 10. Temperature dependence of the forward reaction rate constant for various stable equilibrium temperatures.

Table 2 without the need for adjusting any parameter. This validation has not yet been done. Instead the values used for τ are those as mentioned earlier, which simply fit the values in column four of Table 2. Figure 15 is a plot of these values as a function of stable equilibrium temperature. The authors are presently working on a functional for τ , and Figure 11 provides a basis for understanding at least some part of the behaviour, which such a functional must reflect. Knowing the expected behaviour of τ should help in identifying a unique functional $\tau(\rho)$ capable of capturing the dynamics of the reaction without the use of adjustable parameters.

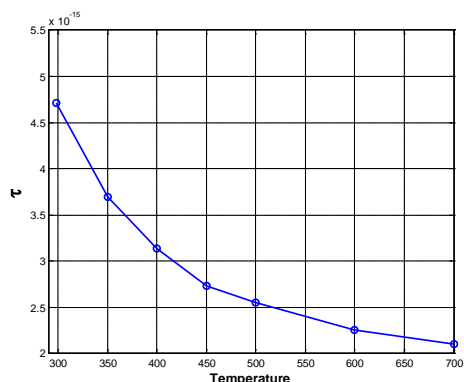


Figure 11. Relaxation time constant for the various stable equilibrium temperatures found in Table 2.

CONCLUSIONS

The IQT framework provides a comprehensive and reasonable approach for predicting the chemical kinetics of small scale reactive systems that could become a valid alternative to conventional approaches. Because IQT unifies quantum mechanics and thermodynamics into a single theory with a single internally consistent kinematics and dynamics, the laws of both are automatically satisfied when modeling reactive or non-reactive systems at the atomistic level. The consequence is that unlike conventional methods that use hybrid approaches to try to predict details of the kinetics of a change in state, IQT holds the promise to provide a full set of thermodynamically consistent, time-dependent features of the chemical kinetics of an atomistic-scale, chemically reactive system.

Finally, the preliminary data presented in this paper demonstrates that the predictions of IQT appear consistent with what the best conventional methods in the literature are able to predict. For very few particle systems and by considering a small set of energy levels the computational burden is not large at all.

ACKNOWLEDGMENTS

The second author gratefully acknowledges the Cariplo-UniBS-MIT-MechE faculty exchange program co-sponsored by UniBS and the CARIPLO Foundation, Italy, under grant 2008-2290, EOARD (European Office of Aerospace R&D) grant FA8655-11-1-3068, and Italian MIUR grant PRIN-2009-3JPM5Z-002.

REFERENCES

- [1] Hatsopoulos, G. N. and Gyftopoulos, E. P., *Foundations of Physics*, **6**(1), 15-31, 1976.
- [2] Hatsopoulos, G. N. and Gyftopoulos, E. P., *Foundations of Physics*, **6**(2), 127-141, 1976.
- [3] Hatsopoulos, G. N. and Gyftopoulos, E. P., *Foundations of Physics*, **6**(4), 439-455, 1976.
- [4] Hatsopoulos, G. N. and Gyftopoulos, E. P., *Foundations of Physics*, **6**(5), 561-570, 1976.
- [5] Beretta, G. P., *On the general equation of motion of Quantum Thermodynamics and the distinction between quantal and nonquantal uncertainties*, Sc.D. dissertation, (advisor: E. P. Gyftopoulos, MIT, Cambridge, MA), 1981.
- [6] Beretta, G. P., Gyftopoulos, E. P., Park, J. L., Hatsopoulos, G. N., *Il Nuovo Cimento B*, **82**, 169-191, 1984.
- [7] Beretta, G. P., Gyftopoulos, E. P., and Park, J. L., *Nuovo Cimento B*, **87**, 77, 1985.
- [8] Beretta, G. P., *Rep. on Math. Phys.*, **64**(1), 139-168, 2009.
- [9] Beretta, G. P., *J. Phys.: Conf. Ser.* **237**, 012004, 2010.
- [10] Smith, C. E., *Intrinsic Quantum Thermodynamics: Application to Hydrogen Storage on a Carbon Nanotube and Theoretical Consideration of Non-Work Interactions*, (advisor: M. R. von Spakovsky, Virginia Tech), 2012.
- [11] Laidler, K. J. and King, M. C., *Journal of Physical Chemistry*, **87**(15), 2657-2664, 1983.
- [12] Truhlar, D. G., Garrett, B. C., Klippenstein, S. J., *Journal of Physical Chemistry*, **100**(31), 12771-12800, 1996.
- [13] Aoiz, F. J., Bañares, L., Díez-Rojo, T., Herrero, V. J., Sáez Rábanos, V., *J. of Phys. Chem.*, **100**(10), 4071-4083, 1996.
- [14] Schatz, G. C., *Journal of Physical Chemistry*, **100**(31), 12839-12847, 1996.
- [15] Althorpe, S. C. and Clary, D. C., *Annual Review of Physical Chemistry*, **54**(1), 493-529, 2003.
- [16] Wang, H., Thompson, W. H. and Miller, W. H. *Journal of Physical Chemistry A*, **102**(47), 9372-9379, 1998.
- [17] Aquilanti, V., Cavalli, S., De Fazio, D., Volpi, A., Aguilar, A., Lucas, J. M., *Chem. Phys.*, **308**(3), 237-253, 2005.
- [18] Beretta G. P. and von Spakovsky, M. R., in preparation.
- [19] Ziegler, H., *J of Appl. Math. and Phys. (ZAMP)* **34** 832-844, 1983.
- [20] Gyftopolous, E. P., Beretta, G. P., *Thermodynamics: Foundations and Applications*, 2nd ed. (NY: Dover), 2005.
- [21] Borysow, A., *Astr. and Astrophys.*, **390**(2), 779-782, 2002.
- [22] Levine, R. D., *Molecular Reaction Dynamics*, Cambridge University Press, N.Y., 2005.
- [23] Carr, R. W., *Modeling of Chem. Reactions*, Elsevier, 2007.
- [24] Heidner, R. F., Bott, J. F., Gardner, C. E., Melzer, J. E., *The Journal of Chemical Physics*, **72**(9), 4815-4821, 1980.
- [25] Wurzburg, E. and Houston, P. L., *The Journal of Chemical Physics*, **72**(9), 4811-4814, 1980.
- [26] Stevens, P. S., Brune, W. H. and Anderson, J. G., *The Journal of physical chemistry*, **93**(10), 4068-4079, 1989.
- [27] Rosenman, E., Hochman-Kowal, S., Persky, A. and Baer, M., *Chemical Physics Letters*, **257**(5-6), 421-428, 1996.

MOLECULAR SIMULATION STUDY OF KAOLINITE INTERCALATION

Zoltán Ható*, Éva Makó^o and Tamás Kristóf*

*Institute of Chemistry, Department of Physical Chemistry, University of Pannonia,
P.O. Box 158, H-8201 Veszprém, Hungary
E-mail address: kristoft@almos.vein.hu

^oInstitute for Materials Engineering, University of Pannonia,
P.O. Box 158, H-8201 Veszprém, Hungary

EXTENDED ABSTRACT

Kaolinite is a common 1:1 type clay mineral, consisted of layers which are built up from one tetrahedral silica sheet and one octahedral aluminium hydroxide sheet. The layers are held together by hydrogen bonds forming a distinct space between the layers and this causes the cleavage and softness of the mineral. The equilibrium basal spacing of kaolinite is around 0.72 nm. Depending upon the application, kaolinite is often modified from its natural state by physical or chemical treatments to enhance the properties of the material. Kaolinite can intercalate various molecules in their interlayer space. Strong polar molecules can expand the basal spacing by disturbing the intermolecular hydrogen bonds between the layers. The obtained mechanically stable complexes have well defined basal spacings. The separation of kaolinite layers by reactive guest molecules (e.g. dimethyl sulfoxide, urea, formamide, potassium acetate) has been studied both experimentally and theoretically. In this work, molecular simulations and X-ray diffraction experiments were used to investigate the properties of kaolinite/urea and kaolinite/potassium acetate complexes. Urea has the earliest practical application in synthesis of organocomplexes of kaolinite, and potassium acetate is the substance by which one of the largest basal spacings can be achieved in direct kaolinite intercalation. Molecular simulations are suitable tools to study the adsorption and intercalation of molecules in clays. In our simulations the kaolinite model was constructed according to its experimental crystal structure [1] using a recently published thermodynamically consistent force field (INTERFACE [2]) to describe its intramolecular and intermolecular interactions. The INTERFACE force field operates as an extension of common harmonic force fields (AMBER, CHARMM, GROMACS, OPLS, etc.) by employing the same functional form and combination rules to enable accurate simulations of inorganic-organic (as well as inorganic-biomolecular) interfaces. According to the literature [2], the INTERFACE force field performs well in comparison to experimental data and alternative force fields. The validity of the force field parameters has been tested for several materials, such as layered silicates and fcc metals. For the guest molecules standard force fields (CHARMM for urea and potassium acetate, and SPCE for water) were applied. The simulations were performed using the GROMACS [3] program suit. The basal spacings were determined by series of NpT (fixed number of molecules, constant pressure and temperature) Molecular Dynamics (MD) simulations.

In control experiments, high-grade Zettlitz kaolin was used and a dry manual or a mechanical grinding technique was employed for intercalation. The basal spacings were determined by X-ray diffraction analysis based on the well-defined 001 reflections.

We investigated the hypothetical loading vs. basal spacing diagrams obtained from the simulations for the kaolinite/guest molecule complexes: the results are in agreement with the expectations, the basal spacing increases with the content of the guest molecules. Stable regions were identified, where the calculated distance is almost constant in function of the intercalated molecule content. The Gibbs free energy for the simulated systems with kaolinite was also calculated, where possible, to locate more precisely the loading in the stable structures. The simulated basal spacing data for the kaolinite/urea and kaolinite/potassium acetate complexes are in good agreement with our experimental X-ray diffraction results and other experimental data available in the literature. From the two types of stable kaolinite/potassium acetate intercalate complexes identified in this study, the one with larger basal spacing is formed with incorporating water into the interlayer space (only this complex can be produced by the basic synthesis procedure in air atmosphere).

The structure of interlayer molecules of the complexes was characterized by density profiles and molecular orientation distributions of the guest molecules obtained from simulation data. Our examinations validated the supposed (single- or double- layered) arrangements of guest molecules and revealed the character of the hydrogen bonds between the guest molecules and the layer surfaces.

REFERENCES

- [1] D.L. Bish, Rietveld refinement of the kaolinite structure at 1.5 K, *Clays Clay Miner.* 41 (1993) 738.
- [2] Hendrik Heinz, Tzu-Jen Lin, Ratan Kishore Mishra, and Fateme S. Emami, Thermodynamically Consistent Force Fields for the Assembly of Inorganic, Organic, and Biological Nanostructures: The INTERFACE Force Field, *Langmuir*, 2013, 29 (6), pp 1754–1765.
- [3] D. van der Spoel, E. Lindahl, B. Hess, G. Groenhof, A. E. Mark and H. J. C. Berendsen, GROMACS: Fast, Flexible and Free, *J. Comp. Chem.* 26 (2005) pp. 1701-1719

COMPUTER SIMULATION OF A RECTIFYING ION CHANNEL

Zoltán Ható*, Dirk Gillespie^o, Tamás Kristóf* and Dezső Boda*

*Institute of Chemistry, Department of Physical Chemistry, University of Pannonia,
P.O. Box 158, H-8201 Veszprém, Hungary
E-mail address: kristoft@almos.vein.hu

^o Department of Molecular Biophysics and Physiology, Rush University Medical Center,
Chicago, Illinois 60612, United States

EXTENDED ABSTRACT

Miedema et al. [1] modified the OmpF ion channel by point mutation and changed the amino acids lining the pore so that a p-n junction was formed inside the channel. They showed with electrophysiological experiments that this channel shows rectification; the current at positive voltage is much smaller than at negative voltage. The goal of this work is to build models for the rectifying ion channel and study them with computer simulation methods thus trying to reproduce the phenomenon and to explain the mechanism behind it. In modelling, we used two limiting approaches. In one approach, we used an all-atom model based on the known crystal structure of the OmpF porin and on well-established classical force fields and studied this model with the GROMACS molecular dynamics simulation package [2]. In this approach, we found selectivity, but we did not find rectification. Therefore, we also used a reduced model, in which we approached the problem from the other end; only the important degrees of freedom are built into this model. We model the ions and the charged protein side chains explicitly, while water, the rest of the protein, and the membrane is averaged into a dielectric background. We have studied this model with the Nernst-Planck transport equation coupled to the Local Equilibrium Monte Carlo method (NP+LEMC) [3]. In this model, we found clear rectification behavior.

REFERENCES

- [1] H. Miedema, M. Vrouenraets, J. Wierenga, W. Meijberg, G. Robillard, B. Eisenberg, A biological porin engineered into a molecular, nanofluidic diode. *Nano Letters* 10/2007; 7(9):2886-91.
- [2] D. van der Spoel, E. Lindahl, B. Hess, G. Groenhof, A. E. Mark and H. J. C. Berendsen, GROMACS: Fast, Flexible and Free, *J. Comp. Chem.* 26 (2005) pp. 1701-1719
- [3] D. Boda and D. Gillespie, Steady-State Electrodifffusion from the Nernst-Planck Equation Coupled to Local Equilibrium Monte Carlo Simulations, *J. Chem. Theor. Comput.* 8, 824 (2012)

FURTHER REMARKS ON THE SURFACE *VIS IMPRESSA* CAUSED BY A FLUID-SOLID CONTACT

Janusz Badur*, Paweł Ziółkowski*,

*Department of Energy Conversion, INSTITUTE OF FLUID-FLOW MACHINERY Gdańsk, Poland
E-mail: pziolkowski@karol.imp.gda.pl

ABSTRACT

It is well-known that, nano-mechanics should take into account not only physical phenomena occurring within the bulk but, first of all, the physical phenomena appropriate for a surface of two materials contact. The huge volume density of internal surfaces as well as contours lines located within the nanomaterial results in our interest in, apart from classical form of mass, momentum and entropy transport, those modes of transportation where a carrier of physical property follows a free path having of a dimension greater than nanostructure characteristic dimension. The mode of transport dominated by mechanical, thermal and electrical slip of carried bounding off walls (a surface of separation) is called usually in physics "a ballistic mode". In the paper the appropriate Newtonian surface *vis impressa* responsible for the ballistic mode of transport is defined, classified and explained. We postulate that generally surface *vis impressa* can be additively splitted onto friction and mobility forces.

MOVING SHELL-LIKE CONTACT

We assume that the fluid-solid contact layer (denoted as $\mathcal{M}^+\mathcal{M}^-$) can be treated as thin domain moving in a space with a geometrical, migration velocity \mathbf{w} . This shell-like domain divides the continuum into a continuum \mathcal{A} - that is a fluid under consideration, and a continuum \mathcal{B} which can be a free surface, solid body or second fluid, as in Fig. 1. If both \mathcal{A} and \mathcal{B} are fluids then it is the fluid-solid contact layer represents the moving interfacial region, where physical properties change in a radical manner. For instance in a thin transition layer between liquid and vapor, the change of density is so noticeable, that it looks like a jump throughout the layer thickness. Therefore, we assume that in the layer we observe so-called „apparent” material properties, quite different than in bulk continuum \mathcal{A} and \mathcal{B} . Thus we define an excess of layer density ρ_s [kg m⁻²], the layer particle velocity \mathbf{v}_s [m s⁻¹], an excess of layer momentum density $\rho_s \mathbf{v}_s$, and a surface excess of momentum flux \mathbf{p}_s , [1; 6; 7; 20].

In general, this layer moves with the geometrical velocity \mathbf{w} that differs from material velocity \mathbf{v}_A in \mathcal{A} , velocity \mathbf{v}_B in \mathcal{B} , and velocity \mathbf{v}_s in $\mathcal{M}^+\mathcal{M}^-$. In particular case, the velocity \mathbf{w} denotes the rate of changing a phase transition surface within the fluid being at rest. Usually, the component w_n normal to moving middle surface \mathcal{M} , differs from normal components of \mathbf{v}_A , \mathbf{v}_B and \mathbf{v}_s . It practically means that there is also a mass transport across the layer. Indeed, the geometrical velocity field is not *a priori* known, and can be determined from a special evolution equation, [1; 19]. If $\mathbf{w} = \mathbf{v}_s$ then the moving layer is material, if $\mathbf{w} = \mathbf{v}_s \mathbf{I}_s + w_n \mathbf{n}$ the surface is semi-coherent (Fig. 1). Navier and Stokes have assumed, that the surface layer density is equal to zero. Apparently, we want to determine the slip velocity \mathbf{v}_s from an independent balance of the layer momentum. In special cases however, it simplifies to the well-known Cauchy balance of the boundary traction forces. For immiscible liquids being in contact, the tangential components $\mathbf{v}_s \mathbf{I}_s$ can be approximately described to be $\frac{1}{2} (\mathbf{v}_A + \mathbf{v}_B) \mathbf{I}_s$. Quite similarly,

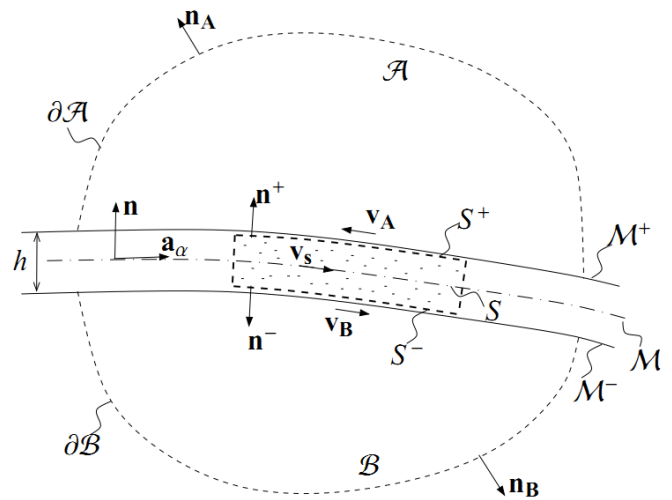


Figure 1. Outline of the fluid-solid contact layer

only in a special case is $\rho_s = \frac{1}{2} (\rho_A + \rho_B) h$, where h is a finite thickness of the layer¹.

We introduce a new concept of an „excess of momentum flux” within the fluid-solid contact layer, which is described by a surface symmetrical diade \mathbf{p}_s . It governs the momentum transport within the layer, and therefore it has a tangential and normal components. We postulate the surface momentum flux in a following form:

$$\mathbf{p}_s(\xi) = p^{\alpha\beta} \mathbf{a}_\alpha \otimes \mathbf{a}_\beta + p^{n\alpha} \mathbf{n} \otimes \mathbf{a}_\alpha + p^{\alpha n} \mathbf{a}_\alpha \otimes \mathbf{n} + p^{nn} \mathbf{n} \otimes \mathbf{n}, \quad (1)$$

where ξ^α , $\alpha = 1, 2$ are a local surface curvilinear coordinates

¹We are based on a general surface kinematics elaborated by [20]. The general form of the surface balances of mass, momentum, angular momentum, energy, entropy, etc. is given by [16; 9; 21].

on \mathcal{M} , and $\mathbf{a}_\alpha, \mathbf{n}$ ($\alpha = 1, 2$) are the base vectors on the middle surface of the layer \mathcal{M} . Since the physical properties of the layer are unknown *a priori*, they depend on the resulting apparent properties in both continua \mathcal{A} and \mathcal{B} . For example, elastic recoverable properties of \mathbf{p}_s depend on an actual shape of the surface \mathcal{M} . Many authors postulate, that due to strong induced elasticity of the fluid layer, it changes from the elastic fluid (only recoverable spherical deformations) into an elastic fluid with recoverable shape deformations [7]. Similarly, owing to induced strong anisotropy, the internal viscosity of the fluid layer can be described by four apparent viscosity coefficients, [3; 11].

Let us now recall a few mathematical relations required for establishing of balance of the layer mass and momentum. At first the Weatherburn surface fundamental diades can be introduced, [17]:

$$\mathbf{I}_s = \mathbf{I} - \mathbf{n} \otimes \mathbf{n} = \text{grad}_s \mathbf{x}_s = a^{\alpha\beta} \mathbf{a}_\alpha \otimes \mathbf{a}_\beta, \quad (2)$$

$$\mathbf{II}_s = -\text{grad}_s \mathbf{n} = b^{\alpha\beta} \mathbf{a}_\alpha \otimes \mathbf{a}_\beta, \quad (3)$$

which are called the first and second fundamental form of the surface \mathcal{M} . As far as the surface gradient acts also on the coordinate dependent base $\mathbf{a}_\alpha, \mathbf{n}$, then the surface gradient of velocity is calculated to be:

$$\begin{aligned} \text{grad}_s \mathbf{v}_s &= (v^\alpha \mathbf{a}_\alpha + v_n \mathbf{n}) \otimes \nabla_\beta \mathbf{a}^\beta \\ &= (v_{\alpha|\beta} - v_n b_{\alpha\beta}) \mathbf{a}^\alpha \otimes \mathbf{a}^\beta \\ &\quad + (v^\alpha b_{\alpha\beta} + v_{n,\beta}) \mathbf{n} \otimes \mathbf{a}^\beta, \end{aligned} \quad (4)$$

and the surface divergence of velocity vector is based on the contraction $C_{1,2}$:

$$\begin{aligned} \text{div}_s \mathbf{v}_s &= C_{1,2} \text{grad}_s \mathbf{v}_s = (v_{\alpha|\beta} - v_n b_{\alpha\beta}) a^{\alpha\beta} \\ &= v^\alpha{}_{|\alpha} - v_n b^\alpha{}_\alpha = \text{div}_s (\mathbf{v}_{s||}) - v_n \mathbf{I}_b. \end{aligned} \quad (5)$$

where the invariants of the second fundamental form of the curvature diade are: $\mathbf{I}_b = \text{tr} \mathbf{II}_s = b^\alpha{}_\alpha = b^1{}_1 + b^2{}_2 = \left(\frac{1}{r_1} + \frac{1}{r_2} \right)$, $\mathbf{II}_b = \det \mathbf{II}_s = \det (b_{\alpha\beta})$ and $C_{1,2}$ denotes contraction of first and second base. In analogy to the three-dimensional case, the rate of surface deformation is defined as a symmetric part of the surface gradient of velocity:

$$\begin{aligned} \mathbf{d}_s &= \frac{1}{2} (\text{grad}_s \mathbf{v}_s + \text{grad}_s^T \mathbf{v}_s) \\ &= \left[\frac{1}{2} (v_{\alpha|\beta} + v_{\beta|\alpha}) - v_n b_{\alpha\beta} \right] \mathbf{a}^\alpha \otimes \mathbf{a}^\beta \\ &\quad + \frac{1}{2} (v^\alpha b_{\alpha\beta} + v_{n,\beta}) (\mathbf{n} \otimes \mathbf{a}^\beta + \mathbf{a}^\beta \otimes \mathbf{n}). \end{aligned} \quad (6)$$

The first invariant of \mathbf{d}_s is in analogy to 3D:

$$\mathbf{I} \mathbf{d}_s = \text{tr} \mathbf{d}_s = C_{1,2} \mathbf{d}_s = v^\alpha{}_{|\alpha} - v_n \mathbf{I}_b. \quad (7)$$

Similarly, the surface gradient of the flux of momentum is:

$$\text{grad}_s \mathbf{p}_s = \mathbf{p}_s \otimes (\nabla_\gamma \mathbf{a}^\gamma) = p^{\alpha\beta}{}_{|\gamma} \mathbf{a}_\alpha \otimes \mathbf{a}_\beta \otimes \mathbf{a}^\gamma$$

$$\begin{aligned} &+ p^{\alpha\beta} b_{\alpha\gamma} \mathbf{n} \otimes \mathbf{a}_\beta \otimes \mathbf{a}^\gamma + p^{\alpha\beta} b_{\beta\gamma} \mathbf{a}_\alpha \otimes \mathbf{n} \otimes \mathbf{a}^\gamma \\ &\quad + p^{n\alpha}{}_{|\gamma} (\mathbf{n} \otimes \mathbf{a}_\alpha \otimes \mathbf{a}^\gamma + \mathbf{a}_\alpha \otimes \mathbf{n} \otimes \mathbf{a}^\gamma) \\ &\quad + \left(2p^{n\alpha} b_{\alpha\gamma} + p^{nn}{}_{|\gamma} \right) \mathbf{n} \otimes \mathbf{n} \otimes \mathbf{a}^\gamma \\ &\quad - p^{n\alpha} b^\epsilon{}_\gamma (\mathbf{a}_\epsilon \otimes \mathbf{a}_\alpha \otimes \mathbf{a}^\gamma + \mathbf{a}_\alpha \otimes \mathbf{a}_\epsilon \otimes \mathbf{a}^\gamma) \\ &\quad - p^{nn} b^\epsilon{}_\gamma (\mathbf{a}_\epsilon \otimes \mathbf{n} \otimes \mathbf{a}^\gamma + \mathbf{n} \otimes \mathbf{a}_\epsilon \otimes \mathbf{a}^\gamma), \end{aligned} \quad (8)$$

and its divergence:

$$\begin{aligned} \text{div}_s \mathbf{p}_s &= C_{2,3} \text{grad}_s \mathbf{p}_s \\ &= \left(p^{\alpha\beta}{}_{|\beta} - p^{n\beta} b^\alpha{}_\beta - \mathbf{I}_b p^{n\alpha} \right) \mathbf{a}_\alpha \\ &\quad + \left(p^{\alpha\beta} b_{\alpha\beta} + p^{n\alpha}{}_{|\alpha} - \mathbf{I}_b p^{nn} \right) \mathbf{n}. \end{aligned} \quad (9)$$

where $C_{2,3}$ means scalar multiplication second & third vector of base (operation of contraction $C_{2,3}$).

MOMENTUM BALANCES WITHIN A CONTACT THIN LAYER

The local form of the momentum balance can be finally written as² [2]:

$$\partial_t (\rho \mathbf{v}) + \text{div} (\rho \mathbf{v} \otimes \mathbf{v} + \mathbf{p}) = \rho \mathbf{b} \quad \text{for } \mathcal{A} \cup \mathcal{B}, \quad (10)$$

$$\begin{aligned} \partial_t (\rho_s \mathbf{v}_s) + \text{div}_s (\rho_s \mathbf{v}_s \otimes \mathbf{v}_{s||}) - w_n \mathbf{I}_b \rho_s \mathbf{v}_s + \text{div}_s \mathbf{p}_s \\ + \partial_n (\mathbf{p}_s \mathbf{n}) + [\mathbf{p}_A \mathbf{n}_A + \mathbf{p}_B \mathbf{n}_B + \mathbf{f}_{SA} + \mathbf{f}_{SB}] = \rho_s \mathbf{b}_s \\ + \dot{m}_A (\mathbf{v}_A - \mathbf{v}_s) + \dot{m}_B (\mathbf{v}_B - \mathbf{v}_s) \quad \text{on } \mathcal{M}. \end{aligned} \quad (11)$$

Repeating now the reasoning of d'Alembert and Euler, we can define a surface d'Alembert-Euler acceleration vector to be:

$$\mathbf{a}_s = \frac{d_s}{dt} \mathbf{v}_s = \partial_t \mathbf{v}_s + (\text{grad}_s \mathbf{v}_s) \mathbf{v}_{s||}. \quad (12)$$

Employing the surface identity, instead of divergence of the convective flux of surface momentum we obtain:

$$\rho_s \mathbf{a}_s = \partial_t (\rho_s \mathbf{v}_s) + \text{div}_s (\rho_s \mathbf{v}_s \otimes \mathbf{v}_{s||}) \quad (13)$$

The fluid-solid contact layer in generalized form is described now by the layer balances of mass and momentum. These are two additional nonlinear differential equations for two additional fields of unknowns, i.e. the surface mass density ρ_s and the layer slip velocity \mathbf{v}_s . These equations are both geometrically and physically nonlinear, and should be solved using any discretization method (FEM, FVM), under assumption that the surface \mathcal{M} possesses an independent from the bulk space discretization. In the case when \mathcal{M}^- is a fixed solid surface, the geometrical velocity $\mathbf{w} = 0$, and then discretization mesh could be fixed in the marching time of numerical solution. Apparently, if $\mathbf{w} \neq 0$, then a moving, self deforming mesh should be resolved together with surface mass and surface momentum equations, and the appropriate set of equations for bulk. There are

²An example how to define \mathbf{p}_B for the deformable wall is given in the paper by dell'Isola et al. [8], eq.(40)

different cases of using the Navier-Stokes layer balances in the literature. For instance, when \mathcal{A} and \mathcal{B} are ideal, non-viscous Euler fluids, and the surface density is equal to zero $\rho_s = 0$, and the layer momentum flux is omitted $\mathbf{p}_s = 0$, then the surface mass and momentum equations reduce to the generalized form of the Rankine-Hugoniot jump conditions:

$$\begin{cases} \dot{m}_A = \dot{m}_B \\ \dot{m}_A \mathbf{v}_A + p_A \mathbf{n}_A = \dot{m}_B \mathbf{v}_B + p_B \mathbf{n}_B \end{cases}, \quad (14)$$

where p_A, p_B are thermodynamic pressure in the Euler fluids \mathcal{A} and \mathcal{B} , respectively. If, additionally $\mathbf{w} = 0$, and there is an additional contribution to the surface diade $\mathbf{p}_s = \gamma \mathbf{I}_s$, then the layer momentum balance leads to the generalized Young-Laplace equation:

$$\begin{aligned} & \text{div}_s (\gamma \mathbf{I}_s) + p_A \mathbf{n}_A + p_B \mathbf{n}_B \\ &= \left[\gamma \left(\frac{1}{r_1} + \frac{1}{r_2} \right) + p_A - p_B \right] \mathbf{n} = 0. \end{aligned} \quad (15)$$

If an interfacial density is omitted i.e. $\rho_s = 0$, the difference between the external friction forces \mathbf{f}_{SA} and \mathbf{f}_{SB} simply vanishes then, and a single layer friction force exists:

$$\mathbf{f}_{AB} = \mathbf{f}_{SA} + \mathbf{f}_{SB} = \nu (\mathbf{v}_A - \mathbf{v}_B), \quad (16)$$

where ν is an external viscosity coefficient. It is an exact form of an external friction force proposed by Navier ($\mathbf{v}_B = 0$) and Stokes ($\mathbf{v}_B = \mathbf{v}_{wall}$). Assuming, that the continuum \mathcal{A} is an incompressible viscous fluid: $\mathbf{p}_A = p \mathbf{I} - 2\mu \mathbf{d}$, and the continuum \mathcal{B} is a rigid, fixed solid body: $\mathbf{p}_B = 0$, $\mathbf{v}_B = 0$, we obtain the Navier slip boundary condition:

$$\mathbf{f}_{AB} + \mathbf{p}_A \mathbf{n}_A = \nu \mathbf{v}_A + (p \mathbf{I} - 2\mu \mathbf{d}) \mathbf{n} = 0 \quad \text{on } \mathcal{M}, \quad (17)$$

where $\mathbf{v}_s = \mathbf{v}_{A|\mathcal{M}}$ is identified with the slip velocity. Let note that the layer flux of momentum is responsible for recoverable and viscous transport: $\mathbf{p}_s = \mathbf{p}_s^{(c)} + \mathbf{p}_s^{(\nu)}$. The first most important part of the elastic recoverable diade $\mathbf{p}_s^{(c)}$, that is known as the capillarity diade, can be described by the surface tension γ . This quantity was introduced to the process of mathematical modeling by Young, Laplace and Poisson. The second contribution comes from the recoverable stresses called the surface bending C_1, C_2 , introduced by Gibbs. There is also a layer „normal pressure” ϖ , introduced by Stokes. These altogether lead to the following definition of the capillarity diade:

$$\mathbf{p}_s^{(c)} = \varpi \mathbf{n} \otimes \mathbf{n} + \gamma \mathbf{I}_s + C \mathbf{II}_s, \quad \partial_n (\mathbf{p}_s \mathbf{n}) = \varpi \mathbf{n}, \quad (18)$$

where $2C = C_1 + C_2$, and $\text{div}_s \mathbf{p}_s^{(c)} = \gamma \mathbf{I}_b \mathbf{n} + C (\mathbf{I}_b^2 - 2\mathbf{II}_b) \mathbf{n}$. A quite general form of the capillarity diade has been proposed recently [1] as:

$$\mathbf{p}_s^{(c)} = \gamma_0 - \mathbf{II}_s \gamma_1 + \mathbf{n} \otimes \mathbf{I}_s \text{div}_s (\gamma_1 - \mathbf{II}_s \gamma_2), \quad (19)$$

where the surface capillary measures can be defined to be spherical:

$$\gamma_0 = \gamma \mathbf{I}_s, \quad \gamma_1 = C \mathbf{II}_s, \quad \gamma_2 = K \mathbf{III}_s. \quad (20)$$

These capillary measures are expressed in terms of the first, second and third fundamental surface forms, and γ, C, K are the surface tension, bending and torque, respectively.

The viscous properties of the Navier-Stokes layer depend on the so-called „apparent viscosity” which, in general, possesses a transversal anisotropy, [11]. One can define the viscous surface stresses by using the surface diade of the rate of deformation and a normal change $v_{n,n}$:

$$\begin{aligned} \mathbf{p}_s^{(\nu)} &= \lambda' (\text{trd}_s) \mathbf{I}_s + \lambda'' v_{n,n} \mathbf{n} \otimes \mathbf{n} \\ &+ 2\mu' \mathbf{I}_s \mathbf{d}_s \mathbf{I}_s + 2\mu'' (\mathbf{d}_s - \mathbf{I}_s \mathbf{d}_s \mathbf{I}_s). \end{aligned} \quad (21)$$

This diade does not undergo the classical 3D de Saint-Venant condition, saying that the viscous stresses must be traceless. For a special case when $\lambda'' = \mu'' = 0$, this constitutive relation was proposed by B.M.J. Boussinesq (1913), [4; 19]:

$$\mathbf{p}_s^{(\nu)} = (\lambda' - \mu') (\text{trd}_s) \mathbf{I}_s + 2\mu' \mathbf{I}_s \mathbf{d}_s \mathbf{I}_s. \quad (22)$$

The formula for surface viscosity coefficients λ', μ' needs extended investigations.

SURFACE FRICTION VIS IMPRESSA CLASSIFICATION

Let us consider now a more consistent velocity slip boundary conditions that should be consistent with the Newton postulate stating, that a friction phenomenon depends on three components: the pressure dependent part, the relative velocity part, and the square velocity dependent part. Let the Newton postulate be true for a fluid in the bulk as well as for the thin layer on a boundary surface realizing a contact with a solid surface. Then taking into account, we have more consistent definition of the surface friction force:

$$\begin{aligned} \mathbf{f}_{AB}^f &= f_{SS'} N \frac{\mathbf{v} - \mathbf{v}_{wall}}{|\mathbf{v} - \mathbf{v}_{wall}|} + \nu (\mathbf{v} - \mathbf{v}_{wall}) \\ &+ f_\kappa (\mathbf{v} - \mathbf{v}_{wall})^2 \frac{\mathbf{v} - \mathbf{v}_{wall}}{|\mathbf{v} - \mathbf{v}_{wall}|}. \end{aligned} \quad (23)$$

where $f_{SS'}, \nu, f_\kappa$ are cohesive, external friction and kinematic friction coefficients and $N = \mathbf{n} \cdot (\mathbf{p}_A - \mathbf{p}_B) \mathbf{n}$ is contact normal force. Some consistencies of this condition can be simply recognized if we compare the internal and external coefficients that appear in the model. This consistency can even be extended on reversible properties of the model i.e. the internal (Euler) and the external (Stokes) pressures p and ϖ , respectively. In the Table1 the comparison of these properties is shown .

The better consistency of the above model results from the fact that it needs three coefficients of internal friction (k_{vis}, μ_1, μ_2) and three coefficients of external friction ($f_{SS'}, \nu, f_\kappa$), respectively. Therefore, we can define a ratio between the internal and external friction by a dimensionless coefficient λ_{vis} , and two lengths of velocity slip: $l_{1\nu}$ and $l_{2\nu}$ (see: table 1). Having a measure of internal properties of friction, one can connect the external properties of friction at the fluid-solid contact layer by appropriate closures written for $\lambda_{vis}, l_{1\nu}$ and $l_{2\nu}$, respectively.

Table 1. Comparison of a concise model of internal and external friction, according to Newton's postulate. The model (\dagger) of a viscous bulk pressure has been proposed by Natanson [15].

	Internal (bulk)	External (boundary)	Characteristic ratio
Elastic pressure	p [Nm^{-2}]	ϖ [Nm^{-2}]	$\lambda_{\text{press}} = p/\varpi$
frictional pressure	$p_{\text{vis}} = k_{\text{vis}} J^\dagger$ [Pa]	$f_{SS'}$	$\lambda_{\text{vis}} = k_{\text{vis}}/f_{SS'} N$
linear slip velocity	μ_1 [Nsm^{-2}]	ν [Nsm^{-3}]	$l_{1\nu} = \mu_1/\nu$
square slip velocity	μ_2 [Ns^2m^{-2}]	f_k [Ns^2m^{-3}]	$l_{2\nu} = \mu_2/f_k$

SURFACE MOBILITY VIS IMPRESSA CLASSIFICATION

Here, we must note that the previous literature statements of the phenomena of surface mobility, called transpiration, should be taken into account to the proper definition of surface friction. Yet another mobility force, other than the difference of pressure or temperature, was discovered by Graham in 1849. He found a new kind of transpiration called „atomism” [18; 14]. This phenomena is nowadays called „diffusional transpiration” or „diffusionphoresis”. It is quite different kind of flow than the classical transpiration flow induced by difference of the normal surface pressures, i.e. „pressure transpiration”. The diffusion transpiration deals with a flow of gas mixture by a long capillary pipe, where there is another interaction of every mixture component with a surface. It leads to the mixture separation. In this case the most important is a coefficient of diffusion mobility c_{vN} . Another type of induced motion is due to the difference of an electric potential ϕ on a surface. This phenomenon is called „electrophoresis” and is governed by an electro-mobility coefficient³ $c_{v\phi}$. Other mobility mechanism is connected with the phase transition change, [2] and the surface gradient of the phase order parameter x .

Let us note that these all types of mobility, i.e., pressure, thermal, diffusional, phase, and electrical define only an external mobility force in the fluid-solid contact layer. This force, partially given by Reynolds [18] and Maxwell [14], can be generalized to:

$$\mathbf{f}_{AB}^m = -c_{v\varpi} \text{grad}_s \varpi - c_{v\theta} \text{grad}_s \theta - c_{vN} \text{grad}_s N - c_{v\phi} \text{grad}_s \phi - c_{vx} \text{grad}_s x, \quad (24)$$

where $c_{v\theta}$ - the thermo-mobility coefficient, c_{vN} - the concentration-mobility coefficient, $c_{v\phi}$ - electro-mobility coefficient, $c_{v\varpi}$ - the pressure-mobility coefficient, c_{vx} - the phase mobility coefficient.

In a special case, when gas is at rest, we can observe a motion of the particle induced by different surface *vis impressa*. This kind of motion is called in the literature the „phoretic motion” [5]. In general, any nano-particle immersed in the fluid may undergo simultaneously five types of motions which are shown in Table 2⁴.

Table 2. Five kinds of motions connected with the surface mobility of a particle immersed in a fluid at rest. Here: $c_{v\theta}$ - the thermo-mobility coefficient, c_{vN} - the concentration-mobility coefficient, $c_{v\phi}$ - electro-mobility coefficient, $c_{v\varpi}$ - the pressure-mobility coefficient, c_{vx} - the phase mobility coefficient.

Phenomena	Corresponding velocity	Driving potential
thermophoresis	$\mathbf{v}_{wall} = c_{v\theta} \text{grad}_s \theta$	temperature θ
diffusionphoresis	$\mathbf{v}_{wall} = c_{vN} \text{grad}_s N$	concentration N
electrophoresis	$\mathbf{v}_{wall} = c_{v\phi} \text{grad}_s \phi$	electric potential ϕ
pressurephoresis	$\mathbf{v}_{wall} = c_{v\varpi} \text{grad}_s \varpi$	pressure ϖ
phasephoresis	$\mathbf{v}_{wall} = c_{vx} \text{grad}_s x$	order parameter x

COMBINED SURFACE FRICTION AND MOBILITY

Let postulate surface *vis impressa* to be:

$$\mathbf{f}_{AB} = \nu (\mathbf{v} - \mathbf{v}_{wall} - c_{v\theta} \text{grad}_s \theta). \quad (25)$$

The thermo-mobility coefficient $c_{v\theta}$ should be formulated, according to Maxwell's slip formula [14], as a coefficient that is not dependent on the property of the solid surface:

$$c_{v\theta} = \frac{3}{4} \frac{\mu}{\rho \theta}. \quad (26)$$

Equation (25) is called the „Maxwell slip boundary layer”. Let us note that in this equation very particular role plays the gradient of temperature θ . It is a completely external surface effect which is not connected with any form of stress tensor. It means that the motion of the gas close to a solid surface, in general is governed by two kinds of forces. The first is a mechanical one, which is connected with the external viscosity, and the second one is a temperature gradient which drives of gas particle close to the surface from colder to hotter part. Therefore the coefficient of thermal mobility $c_{v\theta}$ is independent from mechanical layer properties and should be experimentally verified⁵.

Finally, let us recall Maxwell solution for a flow of a gas in a long capillary tube having inner radius a , which occurs under

³Electrophoresis was discovered by von Smoluchowski in 1916 [22]. See also: H.J. Keh, J.L. Anderson, Boundary effects on electrophoretic motion of colloidal sphere, *J. Fluid Mech.* 153,417-439(1985)

⁴These phenomena must be distinguished from the motion-less phenomena like: „temperature jump”, „concentration jump”, „potential jump” related with the external heat conductivity, external mass diffusivity, and external electric

conductivity coefficients, respectively. Recently the phenomenon of jump concentration of salt in a gel mixture has been discovered by [12].

⁵There are numerous modern papers that mention about the proper experiments. The impressive electrokinetic properties predicted for a carbon nanotube channels have not yet been measured in careful experiments, [10].

two kind of driving forces. These forces are a bulk pressure transpiration due to difference of pressure at the ends of the tube, and the surface thermal transpiration due to difference of temperature at the same ends of the tube. Since the gas is flowing from higher to lower pressure and, simultaneously, from the colder to the hotter end, then these effects can be summarized. In a particular case, where the driving forces are opposite and equal themselves, there is no net outflow of gas from the capillary. Then an enhancement of mass flux due to the Maxwell slip is⁶:

$$\frac{Q_{Maxwell}}{Q_{Poiseuille}} = \left(1 + 4 \frac{l_s}{a}\right) - \frac{8}{\pi} c_{v\theta} \frac{\mu}{\rho a^4} \frac{d\theta}{dz} \left(\frac{dp}{dz}\right)^{-1}. \quad (27)$$

This enhancement is essential only if the inner radius a is small in comparison with the slip length l_s and thermal mobility $c_{v\theta}$ is small. Thermal contribution to the slip is important when the gas is rarefied. Both driving forces (per unit of length of the pipe): dp and $d\theta$, can be in opposition. In a particular case there is no flow in the pipe $Q = 0$. Then we have⁷:

$$\frac{dp}{d\theta} = 6 \frac{\mu^2}{\rho \theta} \frac{1}{a^2 + 4l_s a}. \quad (28)$$

For given temperature difference $d\theta = 100$ K, under the pressure of 40 mm of mercury, and assuming $l_s = 0.00016$ cm, this formula leads to the resulting pressure at the hot end which exceed that at the cold end by about 1.2 millionth of the atmosphere. Modern numerical techniques allowed us to reconstruct this experiment by means of Finite Volume Method. Obtained results are however slightly different - see Fig. 2, b) for which $\dot{m} = 0$.

CONCLUSION

In the paper the applications of the extended solid-fluid contact equations, including the different surface mobility mechanisms are presented in order to explain the enhanced flow in micro-channels.

Boundary force is a sum of friction and mobility force: $\mathbf{f}_{\partial V} = v(\mathbf{v} - \mathbf{v}_{wall}) + (-c_{s,\omega} \mathbf{grad}_s \varpi - c_{s,\theta} \mathbf{grad}_s \theta - c_{s,c} \mathbf{grad}_s c)$ where $c_{s,\omega}$ - pressure transpiration; $c_{s,\theta}$ - thermal transpiration; $c_{s,c}$ - concentration transpiration.

Generalization of the fluid-solid contact boundary slip layer, formulated in the present paper, supplements the original Navier-Stokes model by additional surface quantities like the surface mass and the surface momentum flux. In the present case the slip velocity \mathbf{v}_s is determined from the solution of the complete balance of momentum (11) written within the layer. Since the stress tensors \mathbf{p}_A , \mathbf{p}_B are determined in the bulk and cannot be arbitrarily changed at the boundary, such an approach leads to the separation for those constitutive relations which

⁶Another objective for analytical study lies in exploring the underlying physics of the so called Knudsen paradox. Explanations of this paradox cannot be given by model of Navier slip layer, and needs more advanced method of modeling, [1; 13]. Let recall, that the Knudsen paradox relates to the presence of a minimum of mass flow rate in a function of the Knudsen number. Thus, the exploration of Knudsen paradox and its full understanding also require a considerations on the limit of continuum approaches. It is fact, that the Knudsen-Gaede flow should be a fundamental benchmark for nano-flows of rarefied gases like the Pouiselle or Couette flow at macro-scale.

⁷See: ([14],Appendix,eq.(81))

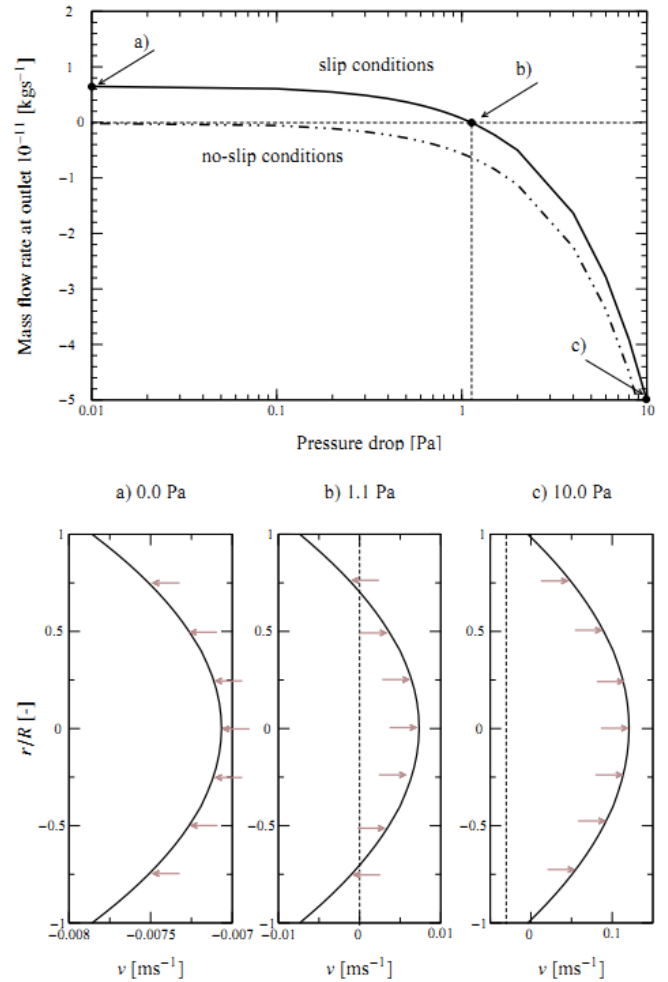


Figure 2. The calculated mass flow rate and relevant velocity profiles in the Maxwell capillary tube for given constant temperature difference $d\theta = 100$ K, and for different dp : a) 0 Pa, b) 1.1 Pa and c) 10 Pa. The case a) describes pure thermal transpiration (no pressure driven flow), where slip velocity $v_s = 0.0077$ m/s drives the bulk flow of a gas.

can be imposed to fulfill the surface balance of momentum. There is still an open place for the modeling of the surface momentum diade \mathbf{p}_s and the surface friction force \mathbf{f}_{AB} , where indeed a second gradient of surface velocity can be postulated.

REFERENCES

- [1] J. Badur and M. Karcz. On evolution of the notion of a capillarity tensor. In W. Pietraszkiewicz and I. Kreja, editors, *Shell Structures: Theory and Applications*, volume 2, pages 159 – 162. CRC Press Taylor & Francis Group, London, 2010.
- [2] J. Badur, M. Karcz, and M. Lemański. On the mass and momentum transport in the navier-stokes slip layer. *Microfluid Nanofluid*, 11:439 – 449, 2011.
- [3] Z. Bilicki and J. Badur. A thermodynamically consistent relaxation model for turbulent binary mixture undergoing phase transition. *J. Non-Equilibrium Thermodynamics*, 28:311 – 340, 2003.
- [4] M.J. Boussinesq. Sur l'existence d'une viscosité superficielle, dans le mince couche de transition separant un liquide d'une autre fluide contigu. *Ann. Chim. Phys.*, 29:349 – 357, 1913.
- [5] H. Brenner. Navier-stokes revisited. *Physica*, A349:60 –

- 132, 2005.
- [6] P. Cermelli, E. Fried, and M.E. Gurtin. Transport relations for surface integrals arising in the formulation of balance laws for evolving fluid interfaces. *J. Fluid Mech.*, 544:339 – 351, 2005.
- [7] F. dell’Isola and W. Kosiński. Deduction of thermodynamic balance laws for bidimensional nonmaterial directed continua modelling interphase layers. *Arch. Mech.*, 45:333 – 359, 1993.
- [8] F. dell’Isola, A. Madeo, and P. Seppecher. Boundary conditions at fluid-permeable interfaces in porous media: A variational approach. *Int. J. Solid Structures*, 46:3150 – 3164, 2009.
- [9] E. Fried and M.E. Gurtin. Traction, balances and boundary conditions for nonsimple materials with application to liquid flow at small-length scales. *Arch. Ration. Mech. Anal.*, 182(3):513 – 554, 2005.
- [10] H. Gardeniers and A. Van den Berg. Micro- and nanofluidic devices for environmental and biomedical applications. *Int. J. Environ. Anal. Chem.*, 84:809 – 819, 2004.
- [11] F.C. Goodrich. Surface viscosity as a capillary excess transport property. In F.C. Goodrich and A.I. Rusanov, editors, *The Modern Theory of Capillarity*, pages 19 – 34. Akademie-Verlag, 1981.
- [12] M. Kaczmarek and K. Kazimierska-Drobny. Simulation of reactive materials in column and reservoir test. Sensitivity analysis of a linear coupled model. *Computers and Geotechnics*, 34(4):247 – 253, 2007.
- [13] M. Knudsen. Eine Revision der Gleichgewichtsbedingung der Gase. Thermische Molekularströmung. *Ann. Phys.*, 31:205 – 229, 1910.
- [14] J.C. Maxwell. On stresses in rarefied gases arising from inequalities of temperature. *Phil. Trans. Royal Soc. London*, 170:231 – 256, 1879.
- [15] L. Natanson. On the laws of viscosity. *Phil. Mag*, 2:342 – 356, 1901.
- [16] H. Petryk and Z. Mróz. Time derivatives of integrals and functionals defined on varying volume and surface domain. *Arch. Mech.*, 38:694 – 724, 1986.
- [17] W. Pietraszkiewicz. Introduction to the non-linear theory of shells. *Ruhr-Univ. Inst. f. Mech. Mitt*, Nr 10, 1977.
- [18] O. Reynolds. On certain dimensional properties of matter in the gaseous state. *Phil. Trans. Royal Soc. London*, 170:727 – 845, 1879.
- [19] L.E. Scriven. On the dynamics of phase growth. *Chem. Eng. Sci.*, 10(1-2):1 – 13, 1959.
- [20] L.E. Scriven. Dynamics of fluid interfaces. *Chem. Eng. Sci.*, 12(2):98 – 108, 1960.
- [21] H. Stumpf and J. Badur. On objective surface rate. *Quart. Appl. Math.*, 51:161 – 181, 1993.
- [22] M. von Smoluchowski. Drei Vorträge über Diffusion, Brownsche Molekularbewegung und Koagulation von Kolloidteilchen. *Phys. Z.*, 17:557 – 571, 1916.

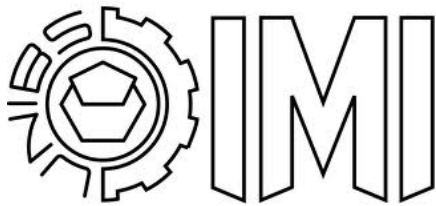
AUTHOR INDEX

- Abe S., 334
Al-Abbasi O., 573
Altamura E., 73
Andresen B., 2, 93
Asinari P., 188
Aydın A., 425
Babac G., 353, 421
Badur J., 482, 581
Baelmans M., 410
Barranco-Jiménez M.A., 490
Bedeaux D., 34, 162, 470, 514
Bejan A., 4
Beneš O., 477
Beretta G.P., 100, 152, 430, 573
Berkache A., 552
Biró T.S., 546
Boda D., 580
Bozorg Bigdeli M., 188
Brauner N., 370
Bresme F., 54
Browarzik C., 436
Browarzik D., 436
Caccin M., 284
Cafaro C., 110
Calvo Hernández A., 490
Camiola V.D., 217
Cano-Andrade S., 430
Caputo M., 73
Celenk D., 558
Chamberlin R.V., 189
Chaturvedi S., 337
Chiavazzo E., 188
Chong S., 82
Cimmelli V.A., 208, 545, 571
Constales D., 330
Correra S., 377
Csatár A., 525
Czél B., 519
Daivis P.J., 35, 447
Daniotti S., 251
De Luca S., 447
Deiters U.K., 383
Demirel Y., 55
Dizene R., 552
Dzuban A.V., 563
Enders S., 436
Essex C., 2
Evans D.J., 40, 206
Fasano M., 188
Favrat D., 10
Feidt M., 16
Firat C., 353
Fischer A., 22
Fülöp T., 519, 525
Gaggioli R.A., 236
Gammaitoni L., 190
Gaspard P., 191
Gemmer J., 338
Getzlaff J., 22
Ghoniem A.F., 21
Gielen R., 410
Glavatskiy K.S., 162, 478
González-Narváez R.E., 490
Gorban A.N., 292
Grmela M., 41
Gróf Gy., 519
Gyenis Á., 519
Hägg M.-B., 514
Hammou A.B., 479
Hansen J.S., 447
Ható Z., 579
Ható Z., Gillespie D., 580
Hoffmann K.H., 22, 93
Hütter M., 210
Issa K.M., 201
Ivashneva M., 531
Ivashnyov O., 531
Janbozorgi M., 313

Jaubert J.N., 388
 Johannessen E., 24
 Johnston B.M., 206
 Jou D., 43, 211, 545, 571
 Juretić D., 94
 Karabetoglu S., 416, 567
 Kjelstrup S., 24, 34, 470, 478, 514
 Kleidon A., 61
 Klimenko A.Y., 294, 304
 Kona A., 284
 Konings R.J.M., 477
 Kosloff R., 344
 Kowalski G.J., 25
 Kristóf T., 579, 580
 Kruse K., 91
 Kurzynski M., 67
 Ladino-Luna D., 499, 504
 Lambert T., 22
 Langenbach K., 436
 Latella I., 437
 Lazzaretto A., 244
 Leng K., 133
 Lervik A., 54
 Levi A., 344
 Lezzi A.M., 140
 Liu Y., 133
 Llovell F., 169
 Loimer T., 537
 Luscietti D., 452
 Maas U., 294, 304
 Makó É., 579
 Margaretti P., 442
 Marin G.B., 330
 Maršík F., 458
 Mascali G., 217
 Mauri R., 175
 Mavelli F., 73
 Meddah C., 479
 Mehnert J., 22
 Metghalchi H., 313
 Michel G., 206
 Modaresifar M., 25
 Moroz A., 82
 Najm H.N., 319
 Naudts J., 42
 Neri M., 452
 Nicolas G., 313
 Niro A., 140
 Niven R.K., 119
 Noack B.R., 119
 Okumura H., 494
 Ott A., 91
 Ozawa H., 121
 Ozcelik Z., 558
 Ozturk Z.F., 353, 421, 567
 Páez-Hernández R., 499, 504
 Pagonabarraga I., 442
 Paolucci S., 323
 Pavelka M., 458
 Pérez-Madrid A., 200, 437
 Pilotelli M., 140, 452
 Pinna M., 402
 Plapp M., 176
 Poesio P., 201
 Poletini M., 404
 Portillo-Díaz P., 499, 504
 Privat R., 388
 Radulescu O., 292
 Reggiani L., 219
 Reguera D., 470
 Reid J.C., 206
 Reini M., 251
 Restuccia L., 43
 Rocco M., 464
 Romano V., 217
 Rondoni L., 206
 Rosen M.A., 259
 Rousseau B., 394
 Rubi J.M., 49, 442
 Ruggeri T., 218
 Sabeur S.A., 479
 Sadus R., 476
 Sadus R., 572
 Sagis L.M.C., 177
 Salamon P., 93
 Sánchez-Salas N., 490
 Santamaria-Holek I., 200
 Scherer S., 91

Schneider W., 178
 Sciubba E., 268
 Searles D.J., 40, 206
 Sellitto A., 545, 571
 Senocak S., 558
 Serdyukov S.I., 542
 Shacham M., 370
 Shimokawa S., 121
 Shvab I., 476, 572
 Sisman A., 353, 416, 421, 425, 567
 Sorić I., 510
 Sorić T., 510
 Stano P., 73
 Svendsen B., 210
 Theodorou D.N., 396
 Thess A., 148
 Todd B.D., 447
 Tondeur D., 149
 Toro C., 464
 Trinh T.T., 514
 Trovato M., 219
 Tsatsaronis G., 276
 Valero Al., 277
 Valero An., 277
 Valorani M., 323
 Vălu O.S., 477
 van Erp T.S., 478
 Ván P., 228, 519, 525, 546
 Vaziri Sereshk M.R., 188
 Vedovato F., 404
 Vega L.F., 169
 Verda V., 284
 Verhás J., 127, 519
 Vilaseca O., 169
 Vlugt T.J.H., 478, 514
 von Spakovsky M.R., 359, 430, 573
 Voskov A.L., 563
 Waage M.H., 478
 Wilhelmsen Ø., 24, 470
 Williams S.R., 40
 Wollrab E., 91
 Worst E., 91
 Yablonsky G.S., 330
 Yang Q., 133
 Yngvason J., 151
 Zakrzewski W., 482
 Zamora-Gómez M., 499
 Zanchini E., 152
 Zenouzi M., 25
 Zimmer P., 91
 Zinovyev A., 292
 Ziólkowski P., 482, 581
 Županović P., 94, 510
 Zvelindovsky A.V., 402

ORGANIZED BY:



Dipartimento di Ingegneria
Meccanica e Industriale



of the Università degli Studi
di Brescia

WITH THE PATRONAGE OF:



the Brescia Municipality

AND CONTRIBUTIONS FROM:



WWW.FONDAZIONECARIPLO.IT



a group company of  MITSUBISHI HEAVY INDUSTRIES, LTD.

WWW.TURBODEN.EU



WWW.MDPI.COM/JOURNAL/ENTROPY